Punching Shear capacity of Flat Slab-column Junctions

(A study by 3-D Non-linear Finite Element Analysis)

by

Boon Tiong, Lim

UNIVERSITY
of
GLASGOW

A thesis submitted for the degree of

Doctor of Philosophy

Department of Civil Engineering

University of Glasgow

March 1997

TABLE OF CONTENTS

ACKNOWLEDGEMENTS i

SUMMARY ii

CHAPTER 1 : INTRODUCTION

1.1 Problem Statement 1

1.2 Scope of the study 2

1.3 Layout of the thesis 3

CHAPTER 2 : PUNCHING SHEAR IN REINFORCED CONCRETE SLABS

2.1 Introduction 4

2.2 Behaviour of slabs failing by punching 4

2.3 Theoretical approach (Kinnunen and Nylander model) 9

2.3.1 Model for symmetrical punching 9

2.3.2 Model for unsymmetrical punching 12

2.3.3 Model for symmetrical punching with known inplane restraint 14

2.4 Parameters governing shear strength of solid slabs 17

2.4.1 Concrete strength 17

2.4.2 Reinforcement 17

2.4.3 In-plane Restraints 19

2.4.4 Size of loaded Area 20

2.4.5 Column shape 21

2.4.6 Size effect 21

2.4.7 Concrete cover 22

2.5 Slabs with shear reinforcement 25

2.6 Failure Mechanisms 26
2.6.1 Symmetrical punching 27
2.6.2 Punching with unbalanced moment 27
2.7 Modes of failure for Slabs without shear reinforcement 29
2.7.1 Pure flexural failure 29
2.7.2 Flexural punching failure 30
2.7.3 Pure punching failure 30
2.8 Treatment of punching shear by BS8110 30
2.8.1 Shear strength for slabs without shear reinforcement 30
2.8.2 Shear strength for slabs with moment transfer 31
2.8.3 Shear strength for slabs with shear reinforcement 34

CHAPTER 3 : FINITE ELEMENT AND MATERIAL MODELLING

3.1 Introduction 37
3.2 Finite Element Method 37
3.2.1 Discretisation by Finite Elements 37
3.2.2 Element choice 39
3.2.3 Solid isoparametric element representing concrete 40
3.2.4 Embedded line element representing reinforcement 45
3.2.5 Numerical Integration 48
3.3 Material Modelling 49
3.3.1 Modelling of concrete 49
3.3.2 Kotsovos's concrete model 54
3.3.3 Failure criteria for concrete 59
3.3.4 Modelling of post cracking behaviour of concrete 60
3.3.5 Material properties of concrete 68
3.4 Non-linear Analysis 69
3.4.1 Solution technique 69
3.4.2 Convergence criterion 70

CHAPTER 4 : KOTSOVOS' MODEL AND ABAQUS' MODEL - A COMPARISON

4.1 Introduction 71

4.2 ABAQUS concrete model 71

4.3 Material Properties 73

4.4 Numerical modelling of slab 76

4.5 Validation of numerical results 78

4.5.1 Kotsovos' concrete model 78

3.4.2 ABAQUS' concrete model 79

4.6 Discussions 79

4.7 Conclusions 80

CHAPTER 5 : PARAMETRIC STUDY

5.1 Introduction 91

5.2 Determination of modes of failure 91

5.2.1 Load-deflection response 92

5.2.2 Strain in flexural steel 92

5.2.3 Principal compressive stress and strain in concrete 93

5.2.4 Crack pattern 93

5.2.5 Notations 93

5.3 Conventional slab-column specimens tested by Rankin 94

5.4 Numerical parameters 96

5.4.1 Effect of convergence tolerance 96

5.4.2 Effect of the size of load increment 102

5.4.3 Mesh size 106

5.4.4 Number of elements through the thickness of slab 111

5.4.5 Simulation of boundary conditions 115

5.4.6 Conclusions 117

5.5 Material parameters 118

5.5.1 Tensile strength of concrete 118

5.5.2 Tension stiffening Factor 126

5.5.3 Shear Retention Factor 133

5.5.4 Confinement effect 143

5.5.4 Conclusions 149

CHAPTER 6 : SIMPLY SUPPORTED SLABS

6.1 Introduction 150

6.2 Calculation of ultimate load of slabs according to BS8110 151

6.3 Slabs without shear reinforcement 152

6.3.1 Coventional slab-column specimens tested by Rankin 152

6.3.2 Simply supported slabs tested by Regan 160

6.4 Slabs with shear reinforcement 175

6.4.1 Full scale slabs tested by Chana and Desai 175

6.4.2 Interior slab-column connections tested by Gomes 177

6.4.3 Interior slabs tested by Yamada et al 181

6.4.4 Slabs with preassembled shear reinforcing units 184

6.5 Numerical model and Comparisons with K&N model and BS8110 188

6.6 Conclusions 194

CHAPTER 7 : SLAB-COLUMN CONNECTIONS WITH SHEAR AND MOMENT TRANSFER

7.1 Introduction 195

7.2 Interior slabs 195

7.2.1 Interior column-slab connections reported in CIRIA 220 195

7.2.2 Interior column-slab connections with shear steel 199

7.3 Edge column-slab connections 205

7.3.1 Edge column-slab connections tested by Zakaria 205

7.3.2 Edge column-slab connections with shear steel 216
7.4 Corner column-slab connections 221
7.4.1 Corner column-slab connections without shear reinforcement 221
7.4.2 Corner column-slab connections with shear steel 226
7.5 Predictions by BS8110 233
7.5.1 Interior column-slab connections 234
7.5.2 Edge column-slab connections 236
7.5.3 Corner column-slab connections 239
7.6 Conclusions 241

CHAPTER 8 : RESTRAINED SLABS

8.1 Introduction 243
8.2 Full panel slab-column specimens tested by Rankin 243
8.3 Slab-beam panels 249
8.4 Fully restrained Slab 253
8.5 Punching with in-plane restraint 257
8.6 Conclusions 260

CHAPTER 9 : CONCLUSIONS AND RECOMMENDATIONS

9.1 General conclusions 262
9.2 Recommendations for future work 264

References 266
Appendix A : Samples calculation using BS8110 274
Appendix B : Flow chart for the computer program for Kinnunnen and Nylander's model 280
Appendix C : Numerical results 281

ACKNOWLEDGEMENTS

I wish to express my deepest gratitude to my supervisor Dr. P. Bhatt for his invaluable guidance and endless encouragement. His energy and foresight have been the driving forces behind this work.

I would also like to thank Dr. J.G. Herbertson, Head of the Department of Civil Engineering for making the facilities available.

Many thanks are also due to Professor N. Bicanic, Dr. T. J. A. Agar and Dr. D. V. Philips for their interest and fruitful discussions.

Thanks also go to Mr. K. McColl, Computer Manager of the department for his valuable support in computational matter.

I am also grateful to my friends at Glasgow, especially Dr. B. Zhang, Mr. Y.P. Lee, Mr. A. Nicol, Dr. Iain Logan, Mr F. Basile, Mr. A.Cuthbertson, Dr. C.J. Pearce, Mr. H. Chen, Mr. X.W. Gao and Mr. A. Al-Muzahmi for their friendship and discussions.

This work was made possible by the award of postgraduate scholarship by University of Glasgow and Overseas Research Scholarship (ORS) by the Committee of Vice Chancellors and Principals of the Universities of the United Kingdom. I am grateful to these bodies.

Finally, my special thanks go to my parents for their understanding, support and encouragement throughout the years.

SUMMARY

This thesis presents a study of punching shear capacity of flat slab-column junctions. A three dimensional nonlinear finite element program based on 20 node isoparametric solid element was used for the investigation. The non-linear 3-D elastic isotropic model proposed by Kotsovos was used to describe the behaviour of concrete before cracking or crushing. After cracking, an yield criteria for 2-D model similar to Kupfer-Hilsdorf was used and concrete was assumed to be anisotropic. No softening in compression is assumed. Smeared crack approach with simple tension stiffening and shear retention equations were employed to mimic the post-cracking behaviour of concrete. Reinforcing bars were represented by one dimensional element embedded in the solid elements and for both tension and compression, linear elastic-plastic behaviour is assumed.

A comparison was first made between the predictions of slab behaviour using Kotsovos' model (In-house program) and plasticity based model used in the commercial package ABAQUS. From this it was concluded that Kotsovos' concrete model is a good model for the three dimensional analysis of punching shear problem but ABAQUS model was unsuitable.

In order to achieve an accurate and economical solution for the non-linear analysis, a parametric study was carried out to choose a suitable analytical model. After having chosen the "best" concrete model, over 175 slabs from different sources were analysed using a constant set parameters. The analysis includes various types connections (interior, edge and corner) with and without shear reinforcement, subjected to shear force alone or to a combination of shear force and unbalanced moment. These slabs cover most of the factors affecting punching shear strength, such as slab thickness, flexural reinforcement ratios, concrete strength, and column size. This study also includes the effect of in-plane restraint on punching shear strength of slabs.

This study placed particular emphasis on the predicted mode of failure and other responses to load being in agreement with observed values. The classification of modes of failure was based on the structural response (deflection, crack pattern, strain in steel and concrete) which agree with experimental observations. The finite element predictions show good agreement with available test data. It was concluded that the present finite element model is capable of simulating realistically the structural behaviour of slab-column junctions. Hence, this program can be confidently used to obtain good lower bound predictions in actual design practice.

Chapter 1

INTRODUCTION

1.1 Problem statement

Flat slab is an ideal structural form for architects and contractors. Its flush soffit makes the formwork construction, wiring and ducting work easy. Without using beams, flat slab provides more headroom or lower storey height. It can thus allow for more storeys than other types of slab systems within the same building height. But flat slab has inherent weaknesses. The connections between the floor slab and column in a flat slab structure are generally the most critical part as far as the strength is concerned because it is a region where large moments and shear forces are concentrated.

Despite an extensive amount of experimental research work on shear strength of reinforced concrete slab, there is still no single theory that can accurately predict the shear strength of a reinforced concrete slab and the corresponding mode of failure. With the advancement in computing technology and numerical modelling of constitutive relationship of reinforced concrete, many features have been implemented into the finite element model to describe the behaviour of reinforced concrete rationally. Therefore, the time has come to use the finite element method for studying the behaviour of reinforced concrete flat slabs and see how well it can predict the actual behaviour. A brief review of the research on the prediction of shear strength of slab using finite element in the literature includes the following :-

Jofriet and McNeice (1971) studied experimentally and numerically a slab where the corners were prevented from lifting and subjected to a point load at the centre. They used plate element for their numerical analysis. This slab was subsequently analysed by many other investigators. The main emphasis was on predicting behaviour in flexure.

de Borst and Nauta (1984) using axisymmetric element with smeared crack model analysed two simply supported slabs subjected to concentrated load which were tested at Delft University.

Gonzalez, Kotsovos and Palvovic (1988) used 8 node axisymmetric elements with smeared crack model to investigate reinforced concrete slabs under symmetric punching loads. They analysed two series of slabs. The first series comprised of four circular slabs tested by Kinnunen et al (1978); the second series consists of five square slabs tested by Elstner and Hognestad (1956).

Gonzalez, Kotsovos and Palvovic (1991) used 20 node solid elements with smeared crack model to investigate a plain concrete prism, a reinforced concrete beam and a reinforced concrete slab.

Malvar (1992) used 8 node solid element with smeared crack model to simulate a reinforced concrete pier deck subjected to a patch load. He analysed only one bridge deck tested by himself.

Abbasi et al (1992) investigated the effect of flexural reinforcement ratios and edge restraints on punching capacity of reinforced concrete slabs. They used a multilayered plate element with smeared crack to analyse slabs tested by Taylor and Hayes (1965).

Marzouk and Chen (1993), used shell element with layered approach to study the behaviour of high strength concrete slab. The post-cracking behaviour of concrete was represented by smeared crack model. They analysed fourteen slabs tested by Marzouk and Hussein (1991a).

The brief literature reviews shows that :-

- Some investigators used two dimensional analysis as the aim was to understand flexural behaviour. Punching shear is a three dimensional problem, and three dimensional analysis is necessary;
- only a small number of slabs from one source were analysed;
- Analysis included only simply supported slabs without shear reinforcement. The applicability of the model to slabs with shear reinforcement is thus in doubt.
- emphasis was on the prediction of ultimate load only;
- Specimens chosen did not cover all the important parameters governing punching shear capacity;
- No attempt was made to study whether there is agreement between experimental and computed modes of failure and other structural responses.

1.2 Scope of the study

Non-linear finite element has been used to predict the experimentally observed behaviour. But, the prediction from numerical analysis can vary over a wide range depending on the "tuning factors " such as concrete strength, tension stiffening factor, shear retention factor, etc. In addition, only a small number of experimental tests from one resource which do not cover all the factors influencing the behaviour of reinforced concrete slab have been analysed. In other words, the generality of anyone of these

models has not been established and it is difficult to judge which model gives best predictions for any kind of structure.

The purpose of this study is to attempt to find out the features of a finite element model which is able to predict, with reasonable accuracy, the ultimate load and the correct mode of failure for a large number of slabs which cover all factors affecting the behaviour of reinforced concrete slabs. The study will use three dimensional element with Kotsovos' concrete model (1979a & 1979b) to study the behaviour of slabs with different types of column-slab connections (i.e., Interior column-slab connections, Corner column-slab connections and Edge column-slab connections).

1.3 Layout of the thesis

Chapter 2 focuses on the Punching shear in reinforced concrete slabs. Chapter 3 describes the features available in the program used in the study. This includes the finite element method and material modelling (steel and concrete).

Chapter 4, describes a study of three dimensional finite element analysis using two different concrete constitutive models, namely the non-linear elastic isotropic model proposed by Kotsovos (1979a & 1979b) and the plasticity-based concrete model proposed by Chen and Chen (1975) used in the commercial package ABAQUS.

In Chapter 5, a parametric study of the major factors affecting the prediction of shear strength of interior slab-column connections is presented. The purpose of the parametric study is to "calibrate" the parameters used in the study, in order that a set of "constant " parameter can be used for the analysis of a large number of slabs.

The following two chapters present the analysis results for different types of slab-column connections from different sources. Chapters 6 presents the results of analysis for interior column-slab connections subjected to shear only. Chapters 7 presents the results of analysis for column-slab connections subjected to a combination of shear and unbalanced moment. This study includes interior slab-column junctions with moment transfer, edge column-slab connections and corner column-slab connections. Only typical results are presented in these chapters, results and details of all the specimens are included in Appendix C.

Chapter 8 is presents an investigation of the effect of inplane restraint on the punching shear strength of reinforced concrete slabs. Finally, conclusions and recommendations for future research are given in Chapter 9.

Chapter 2

PUNCHING SHEAR IN REINFORCED CONCRETE SLABS

2.1 Introduction

This chapter will first briefly describe the parameters which influence the behaviour and shear strength of slabs as studied from experimental observations and theoretical model. Later on, it discusses how these parameters govern punching shear strength of solid slabs. It is followed by a review of the failure mechanism of different types of slab-column connections and classification of the mode of failure of slab based on experimental observations. Finally, design against punching shear failure as presented in BS8110 is reported.

2.2 Behaviour of slabs failing by punching

In experimental work on punching shear failure of interior slab-column junction, the slabs are loaded at the centre through steel plates or column stubs and are simply supported around their edges. This section describes the observed behaviour of slab with this type of configuration.

When the load is applied to the slab, the first crack to form is roughly a circular crack around the perimeter of the loaded area due to negative bending moments in the radial direction. Radial cracks, due to negative bending moments in the circumferential direction, then extend from that perimeter (see Fig 2.1a). After a significant increase in load, tangential cracks form around the loaded area at some distance out from the column in the slab. And at about the same time, inclined or shear cracks form on the truncated surface (Figure 2.1b).

The critical sections of the slab for moment and shear are both at or close to the perimeter of the loaded area, and hence it would be expected that moment-shear interaction would occur. This complicates the classification of the modes of failure at the connection. However, there is a change in the characteristic of the failure mode and load-deflection curves measured for slabs with different reinforcement ratios. Figure 2.2 is taken from Criswell (1974b) illustrates the situation. Curves 1-3 show brittle behaviour which clearly represent the behaviour of slabs failing by primary punching while curves 6-8 display large ductility which is basically flexural behaviour. The slabs represented by curves 4 and 5 reached their yield line strengths but must be regarded as having failed in punching in view of lack of ductility.

If the shear strength of the slab is reached, punching shear failure occurs along a truncated cone caused by the diagonal tension crack around the column. The failure surface runs through the slab at a mean inclination of about 25 to 30 degrees to the horizontal. All rotations in the compression region of the slab are virtually within a hinge adjacent to the column. The deflected profiles of the compression side are practically linear while those on the tension face generally show a slight discontinuity in the region where the shear crack intersects the reinforcement. The discontinuity becomes more significant if the shear crack is not crossed by flexural reinforcement (i.e. if the steel is arranged in the rings around the column as shown in Figure 2.3c). The work by Kinnunen and Nylander (1960) in Figure 2.3d illustrates the difference. It can be seen from this figure that the discontinuity across the shear crack can be considered a consequence of the rotation of the outer slab portion about its centre of rotation CR.

The strains in concrete at the compressed surface reach their highest values adjacent to the column. The strain in the radial direction decreases very rapidly with increasing distance from the column (Figures 2.4-2.6). For circular slabs on round columns the tangential strain seems always to be higher than the radial strain, and the radial strain near the column often decrease before failure, sometimes changing from compression to tension (Figure 2.4 & 2.5).

The distribution of strains at the faces of rectangular columns show concentrations of stress at corner as illustrated in Figure 2.7 (Moe, 1961). The concentration generally increases with larger square or rectangular column but is absent in slabs with circular column (Figure 2.8).

Experimental observations clearly show that the behaviour of slabs is influenced by reinforcement ratios, arrangement of reinforcement and column shape. The influence of these parameters on the load carrying capacity of slab will be discussed in section 2.4.

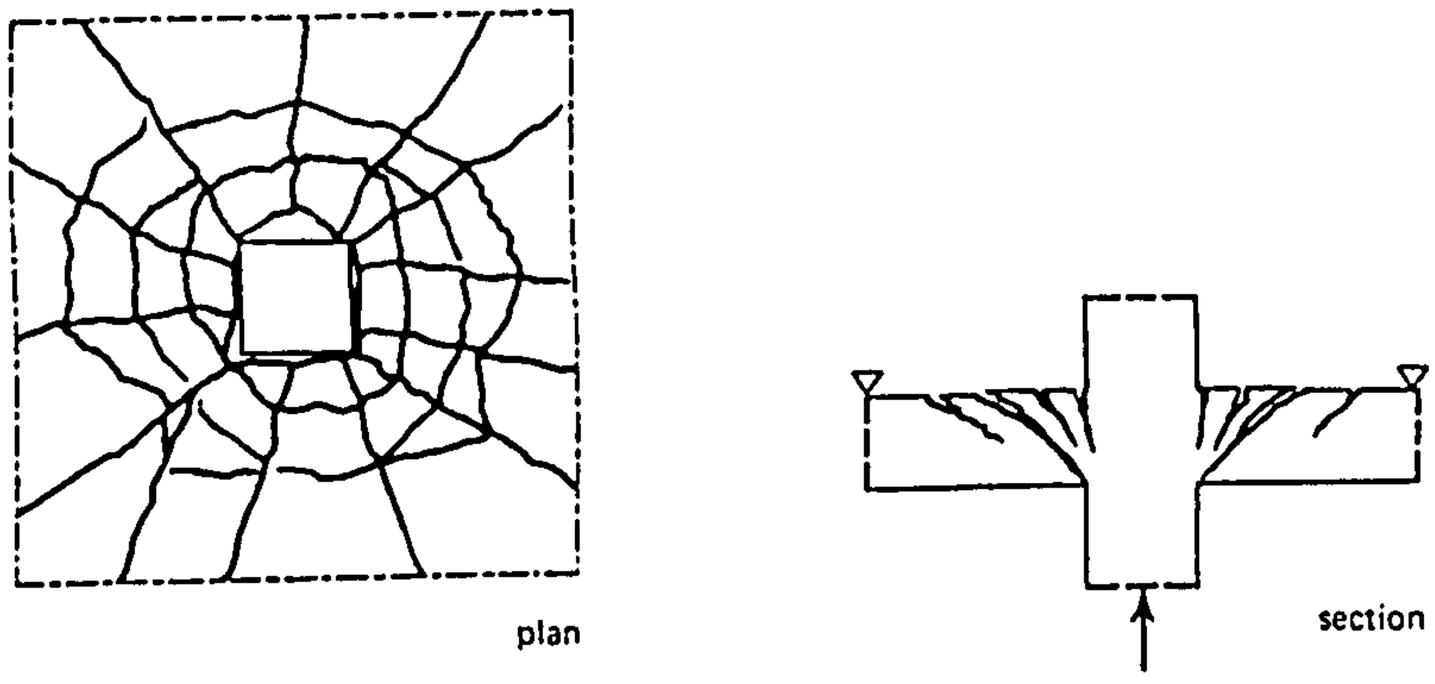

(a) (b)

Figure 2.1 Cracks of slab subjected to concentrated load

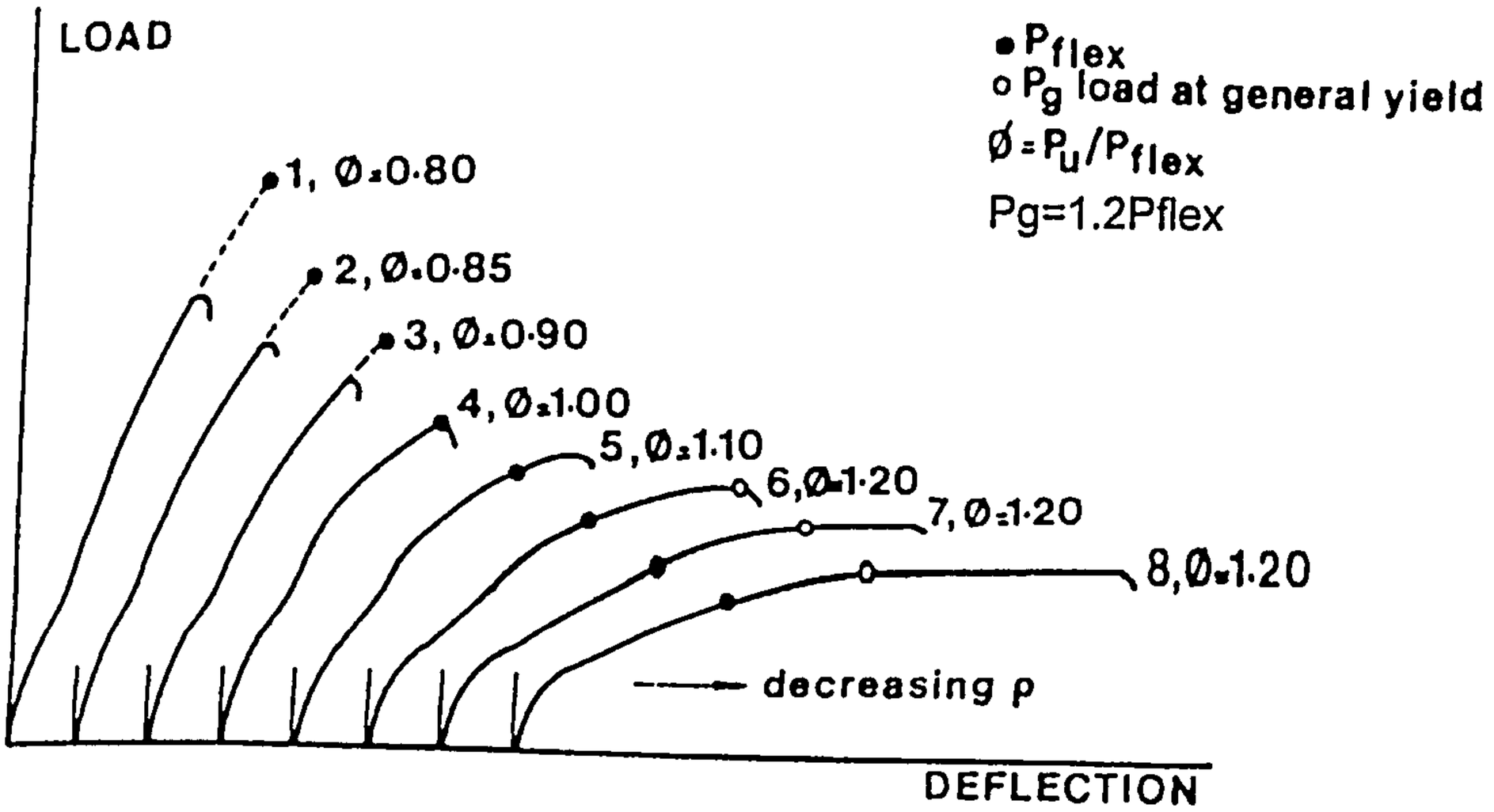

Figure 2.2 Effect of flexural reinforcement ratio on load-deflection response (Criswell, 1974)

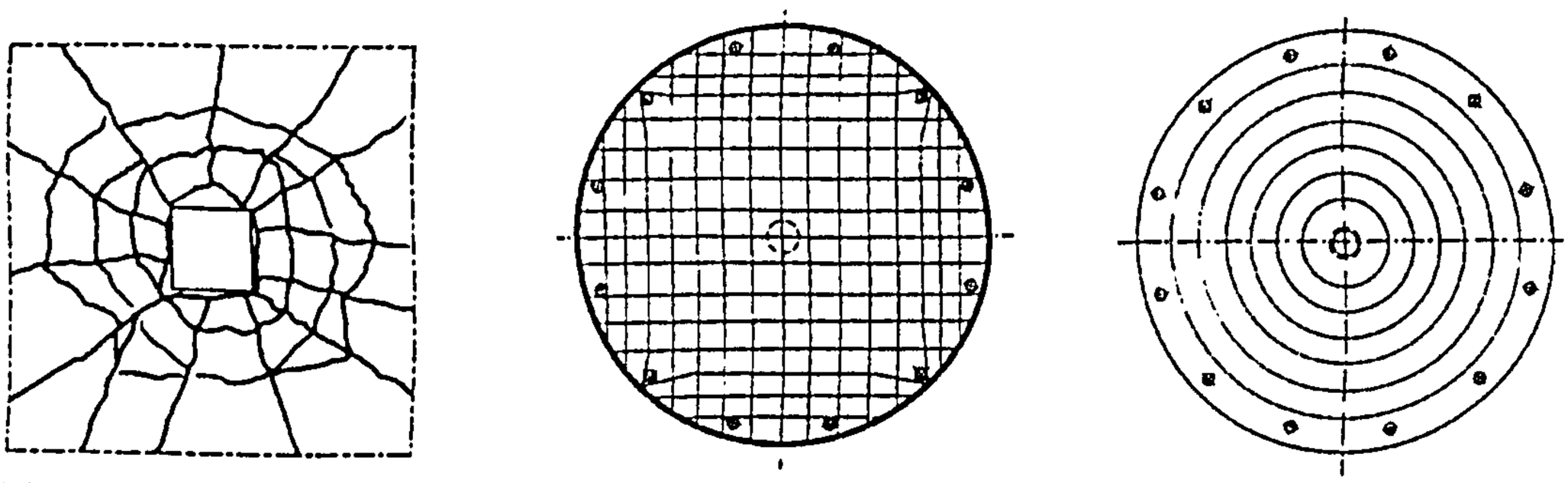

(a) crack pattern (b) two way reinforcement (c) ring reinforcement

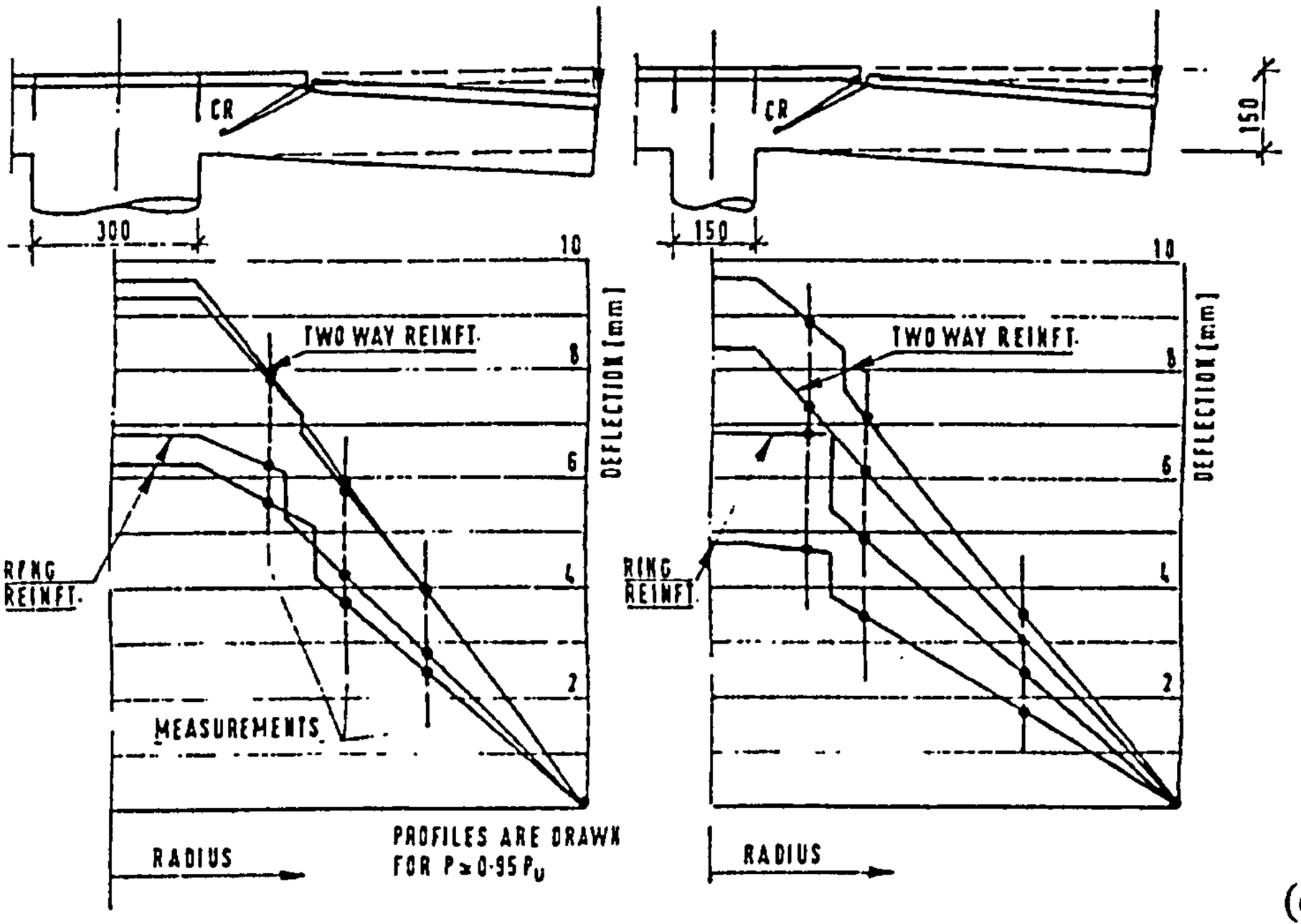

(d)

Figure 2.3 Deflected profiles at the top surface along the radius of slabs (Kinnunen and Nylander, 1960)

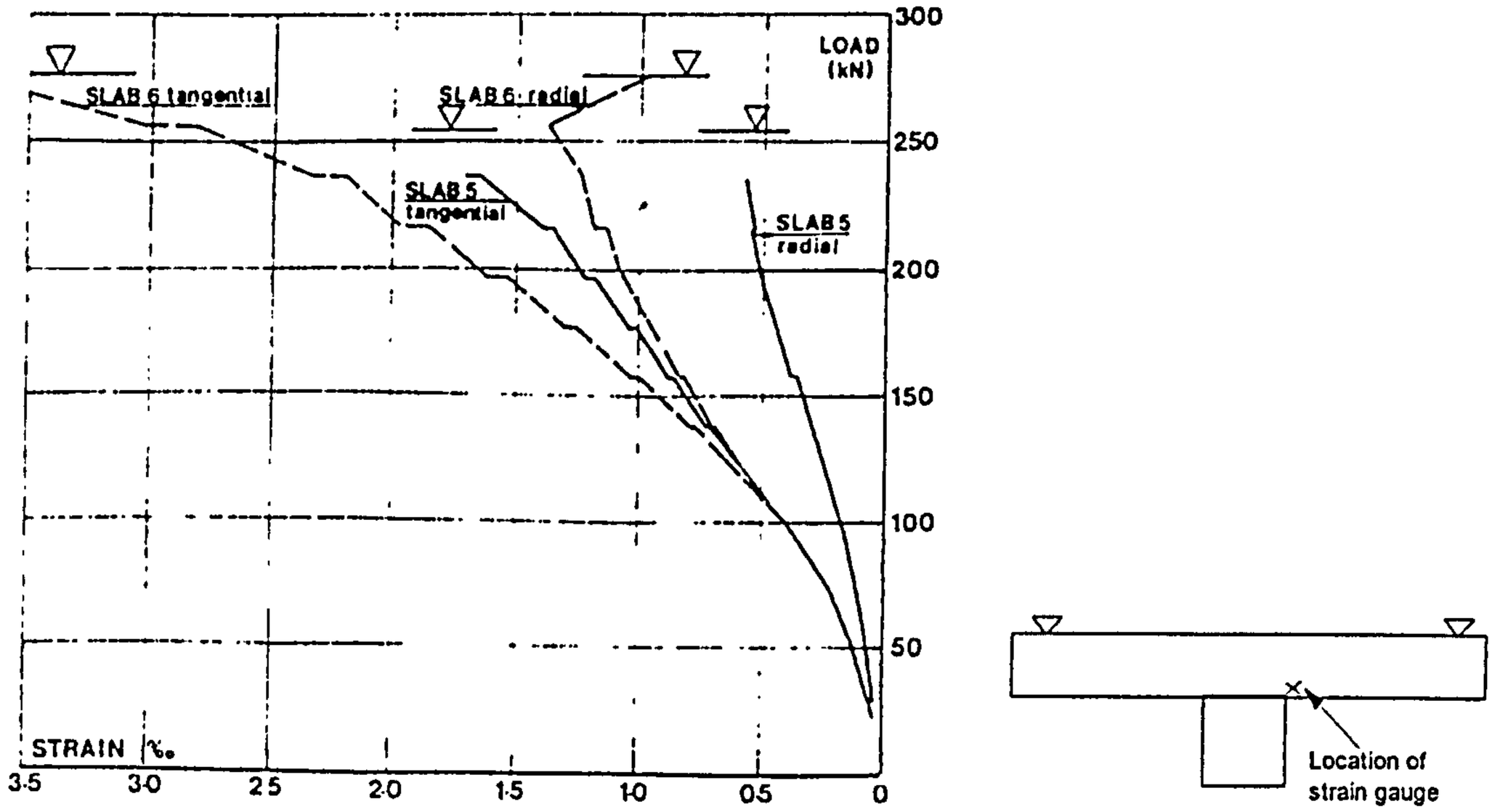

Figure 2.4 Radial and tangential strains on the compression side for slabs with two way reinforcement (Kinnunen and Nylander, 1960)

**Note: $^{0}/_{oo} = {}^{1}/_{1000}$

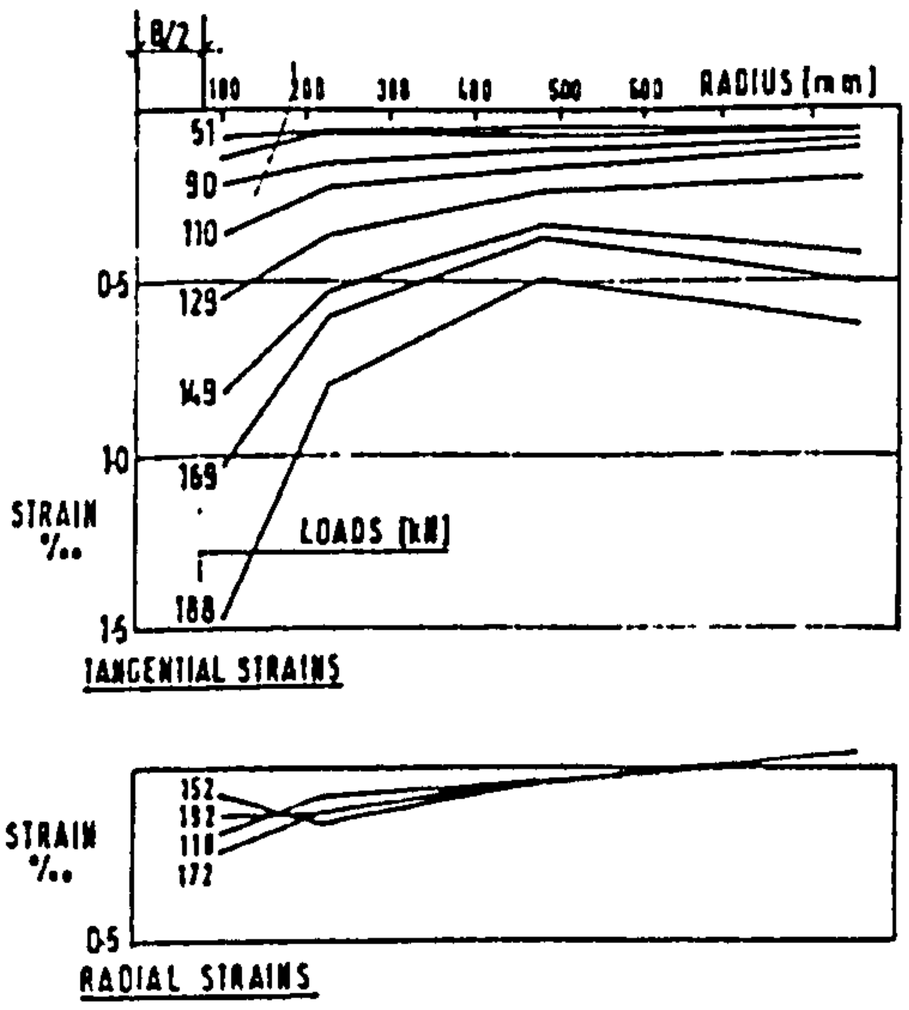

Slab 15,

Column diameter, B=150mm.

(Kinnunen and Nylander, 1960)

Figure 2.5 Radial distributions of strains in a slab with only ring reinforcement

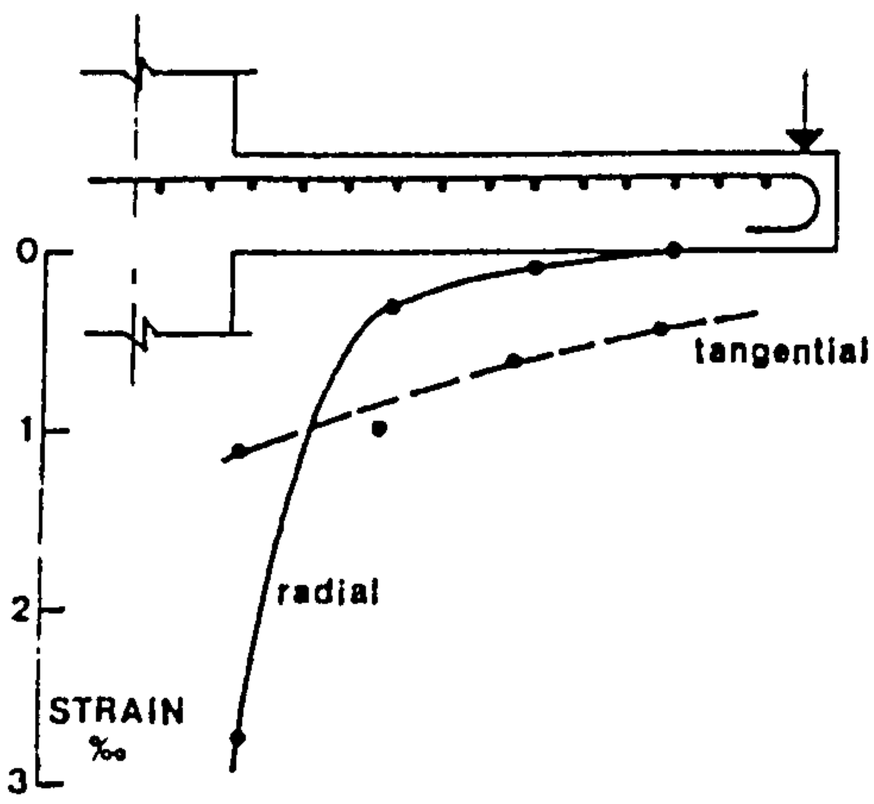

(Anis, 1970, Slab B3)

Figure 2.6 Distribution of radial and tangential strains in the compressed surface

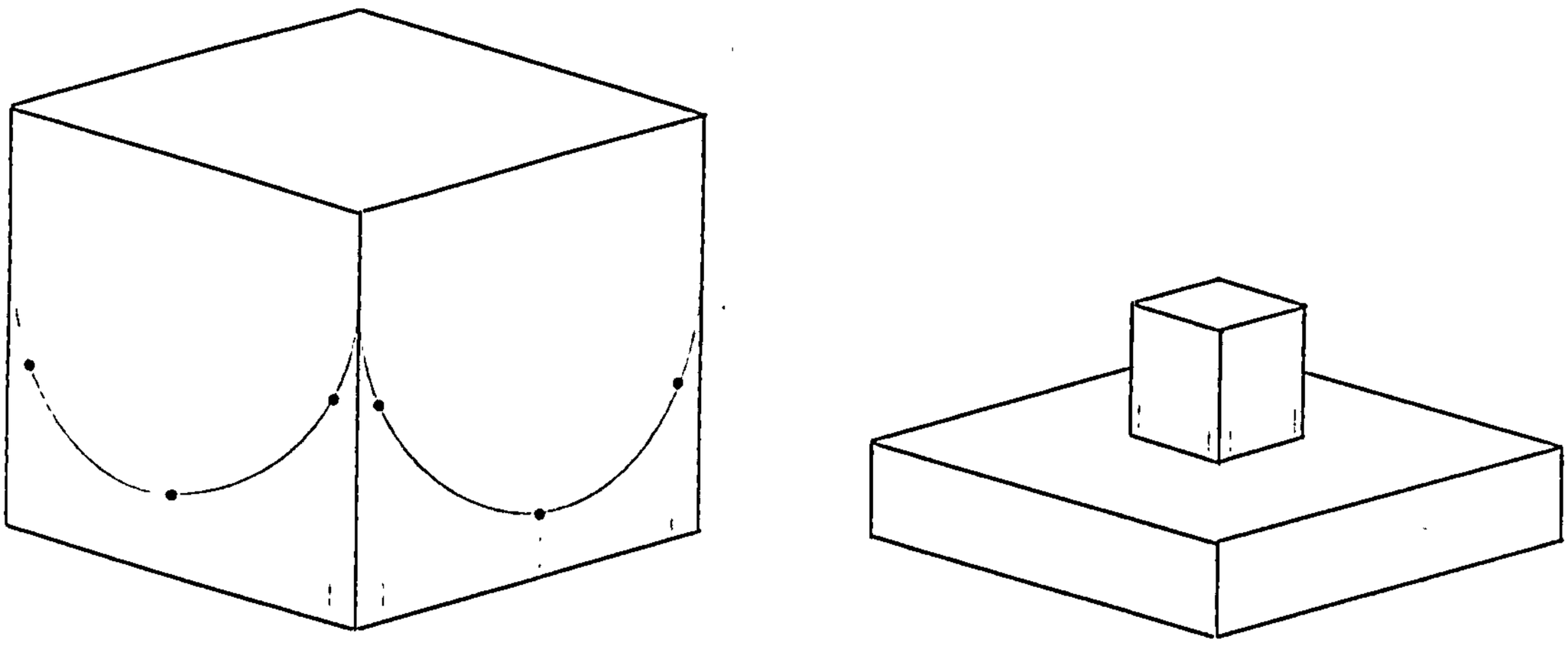

Figure 2.7 Vertical strains at a column face (Moe,1961)

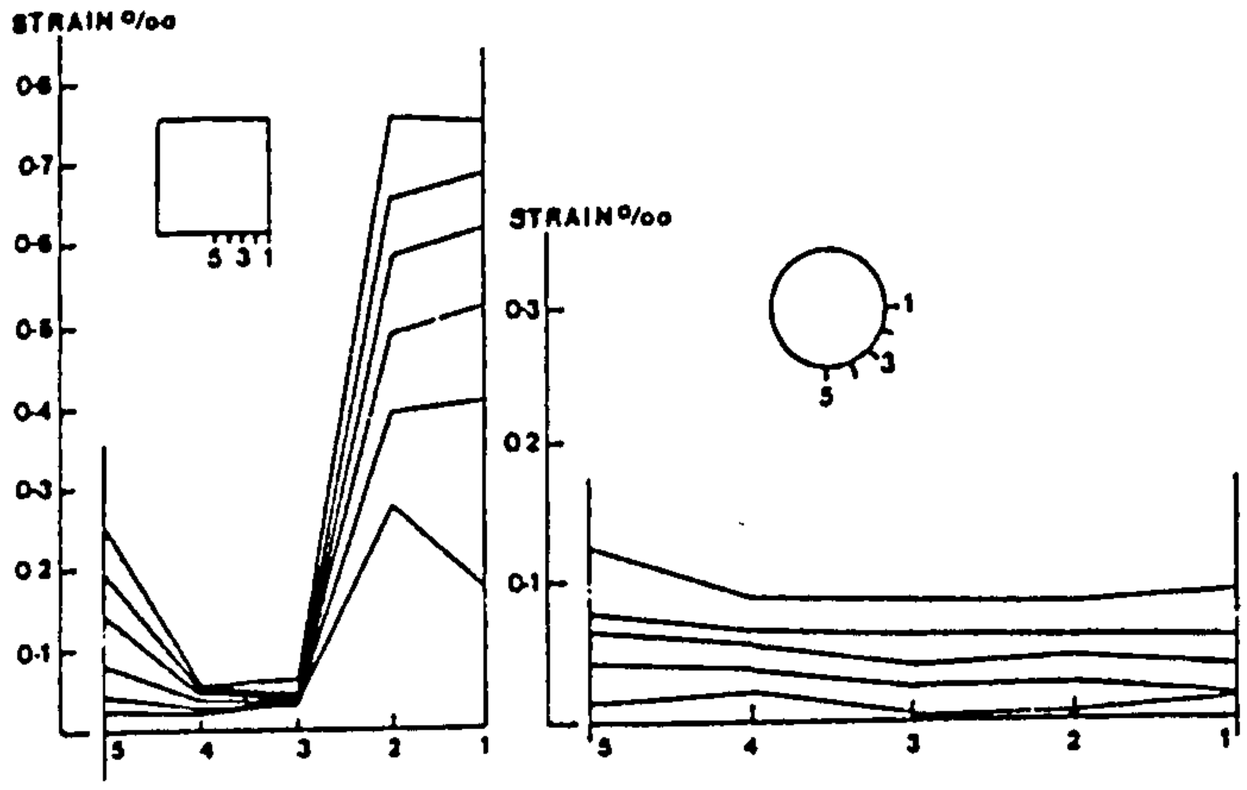

(Vanberbilt, 1972)

Figure 2.8 Vertical strains at column faces (square & circular column) at different load levels

2.3 Theoretical approach (Kinnunen and Nylander Model)

To date, Kinnunen and Nylander model seems to be the most rational model for predicting the punching shear failure of slabs. This model has been used by many investigators. They modified it to cater for different types of situations. For example; Broms (1990) modified it to include unsymmetrical punching, Marzouk et al (1991b) modified it to analyse high-strength reinforced concrete slabs. Different versions of Kinnunen and Nylander model will be discussed to illustrate the dependence of the theoretical punching resistance on the influential parameters.

2.3.1 Model for symmetrical punching

The following models treated punching failure in a similar manner and used same parameters for predicting punching capacity, although the definition of the failure criteria are different. So, only the equations for Kinnunen and Nylander's model are listed below.

2.3.1.1 Kinnunen-Nylander Model (K&N model)

The model discussed here is the original model developed by Kinnunen and Nylander (1960). This model is based upon observations of tests on circular slabs, centrally supported on circular columns, and loaded at the free edges. It consists of a central truncated cone confined by the shear crack and segmental slab parts, divided by radial cracks. Each segment is assumed act as a rigid body supported by an imaginary compressed conical shell between the column and the root of the shear crack (Figure 2.9c&2.9d).

When subjected to load, each rigid segment rotates about CR the centre of rotation, and is acted upon by the resultant forces. The internal forces are functions of the angle of rotation and the mechanical properties of the concrete and steel. The equations of equilibrium of the segment and a criterion of failure determine the ultimate load. Failure is assumed to occur when the circumferential concrete strain at the bottom surface of slab, at a point located vertically under the root of the shear crack, reaches a critical value. At the same time, the concrete stress in the tangential direction at the same point and the stress in the conical shell reach its critical stress at failure.

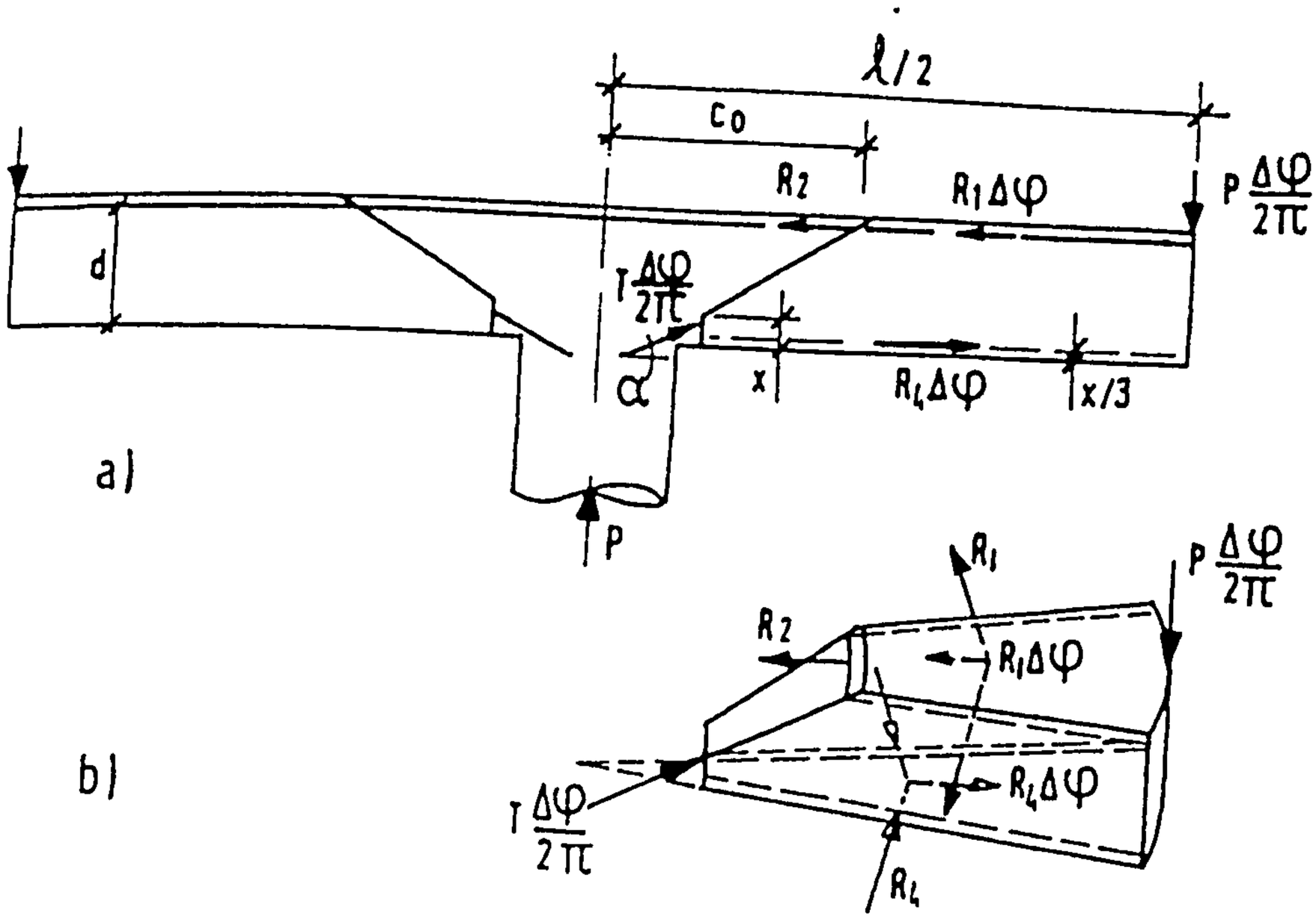

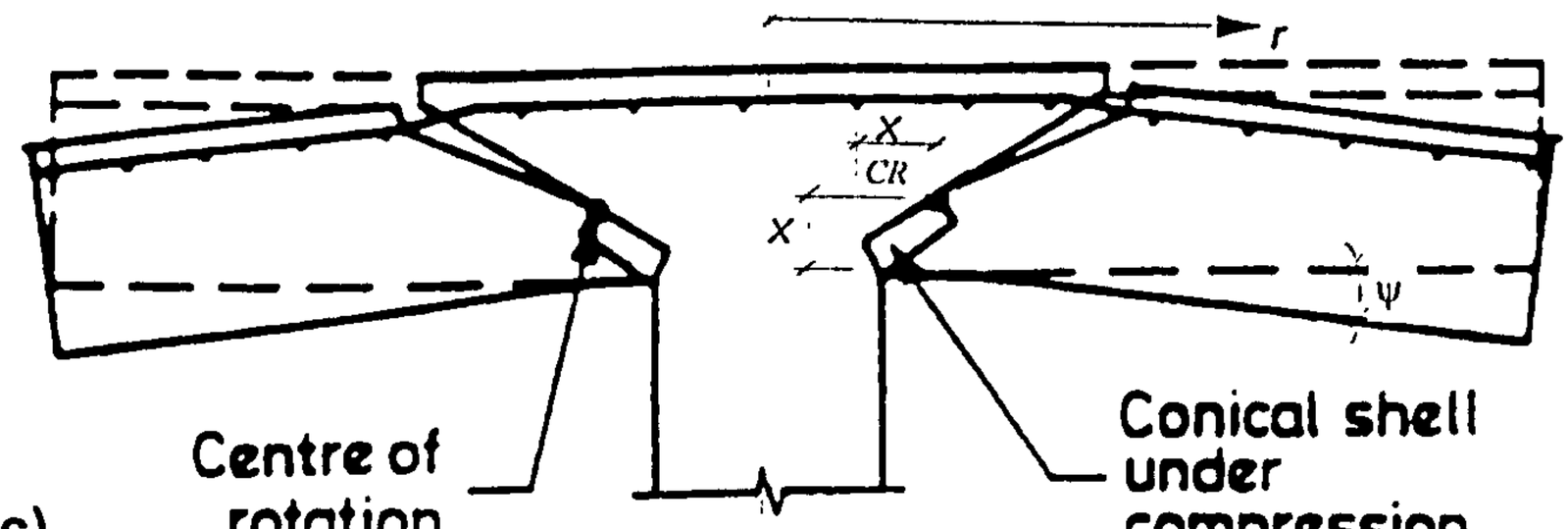

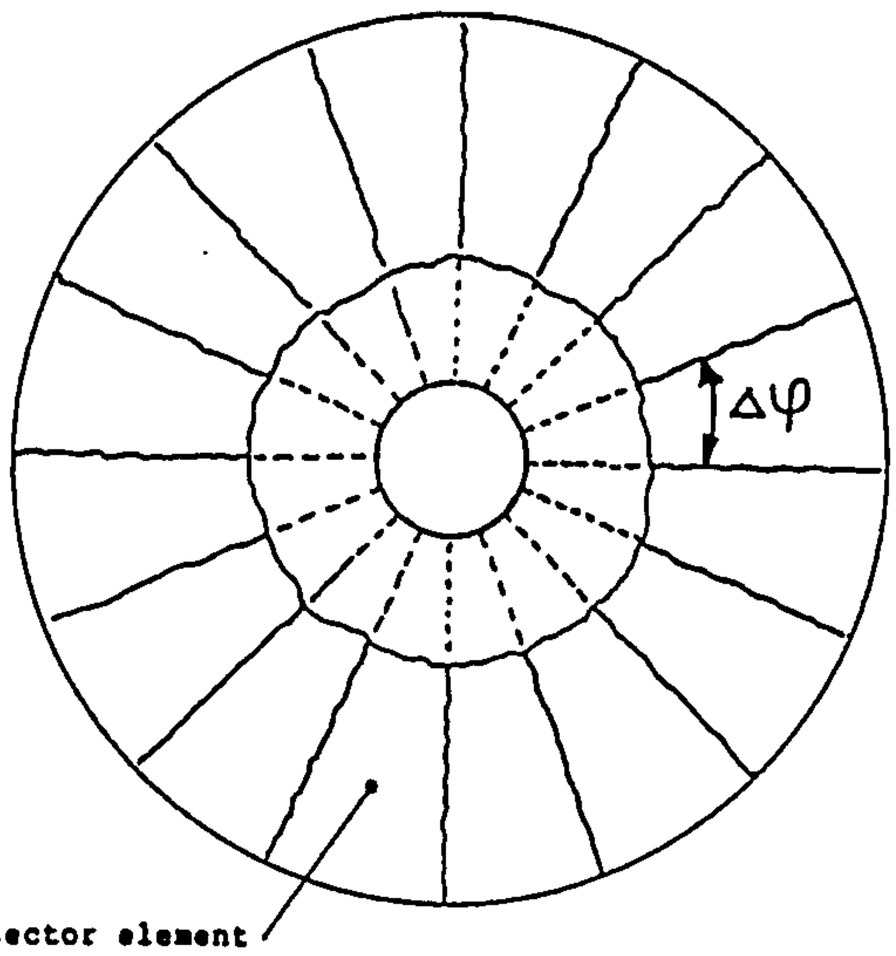

Figure 2.9 Kinnunen-Nylander punching model

At failure, the flexural reinforcement within a slab area of radius r_s is yielded. Outside this area, the reinforcement is in elastic state. If the ratio of reinforcement, ρ, is low then $r_s > l/2$ at failure, yielding is reached in all the reinforcement, and the ultimate load is equal to the flexural failure load. If the ratio of reinforcement, ρ, is high then $r_s < l/2$ at failure, i.e., reinforcement within r_s is yielded and reinforcement outside r_s is in elastic state, and the ultimate load is less than the flexural failure load.

The theoretical punching load is calculated from equations (2.3) and (2.4) given below. Equation 2.3 indicates that punching shear resistance of a slab is highly dependent on the ratio of column width to effective depth of slab i.e. (*c/d*). These equations are based on stress and the strain criteria mentioned. The calculation involves iterative process on the value of the neutral axis depth (*x*) until the predicted load by the two failure criteria coincide. This model was originally formulated for the slab with ring reinforcement where the dowel effect is not signicant. For two way orthogonal reinforcement, dowel effect was taken into consideration by multiplying the calculated load by a factor of 1.1.

From vertical equilibrium (see Figure 2.9),

$$P = T\sin\alpha \qquad (2.1)$$

$$T = \sigma_{cs} \cdot A_{cs} \qquad (2.2)$$

where P = *Punching Load;*

T = Compressive force in conical shell

α = *angle of the compressive force in the conical shell*

σ_{CS} = *stress in the conical shell;*

A_{CS} = *cross-section area of the conical shell;*

$$P = \pi\left(\frac{c}{d}\right)\left(\frac{x}{d}\right)\left(\frac{c+2x}{c+x}\right)\sigma_{cs} f(\alpha) d^2 \qquad (2.3)$$

Taking moments about the point of intersection of $T\Delta\varphi/(2\pi)$ in the conical shell and the resultant of the forces, R_4 (see Figure 2.9), gives

$$P = \frac{2\pi}{K_y}[C_1 + C_2]\rho f_y d \qquad (2.4)$$

where

$$f(\alpha) = \frac{\tan\alpha(1-\tan\alpha)}{(1+\tan^2\alpha)} \qquad (2.5)$$

$$K_y = \frac{3(l-c)}{2(3d-x)} \qquad (2.6)$$

if $r_S \geq C_O$ $\quad C_1 = (r_s - C_o) + r_s \ln\left(l/2r_s\right), \quad C_2 = C_o \Delta\varphi$

if $r_S \leq C_O$ $\quad C_1 = r_s \ln\left(l/2C_o\right), \quad C_2 = r_s \Delta\varphi$

c	=	*diameter or equivalent diameter of column;*
d	=	*effective depth of slab;*
f_y	=	*yield stress of flexural steel;*
l	=	*diameter (span) or equivalent diameter of slab;*
x	=	*neutral axis depth;*
C_o	=	*radius of shear crack*
r_s	=	*radius of the area of yielded reinforcement;*
$\Delta\varphi$	=	*angle of sector element;*
ρ	=	*flexural reinforcement ratio.*

Kinnunen and Nylader model shows that punching load of slab is governed by the compressive strength of concrete, column size, slab thickness and flexural reinforcement ratio. The influence of these parameters on the failure load of slab will be discussed in section 2.4.

2.3.1.2 Modified Model by Shehata (1989)

This model treated punching failure in a manner similar to Kinnunen and Nylander but utilised the generally recognised values for concrete properties and different failure criteria. Punching failure is considered to take place either by splitting under principal tensile stresses or by crushing in the radial or tangential direction. The failure criteria are defined as follows :

- Failure by splitting of concrete is assumed to occur when the angle α of the compressive force at the column face reaches 20°.
- If the average radial strain on the compressed face reaches a value of 0.0035 in the plastic length starting from the column face, there is radial crushing of the concrete. Based on the experimental ultimate rotations, Shehata assumed the plastic length as 150mm.
- If the tangential strain of the compressed face reaches a value of 0.0035 at a distance x from the column face, there is tangential crushing of the concrete. This criterion is expressed by the equation $0.0035 = \psi\left[x/150\right]$ (see Figure 2.9c for the definition of ψ).

This model basically used the same parameters in the equations for the punching resistance as K&N model. The main differences between this model and K&N model can be summarised as follows :

- This model allows deformation of the part of the slab on top of the column which is assumed remain underformed in Kinnunen and Nylander model.
- The slab may fail in diagonal tension.
- The compression failure is controlled by strain.
- The contributions by dowel effect are calculated from equilibrium conditions.

This model indicates that punching failure is caused not only by the destruction of the conical shell, but it may also be initiated by a diagonal tension crack. Thus punching shear strength may be controlled by the tensile strength of concrete.

2.3.1.3 Model for high strength concrete

Marzouk and Hussein (1991b) adopted the model modified by Shehata, but excluded the failure criterion for tensile splitting. They made this assumption probably due to the following reasons:

- They observed that the angle of failure surface for high strength concrete slabs varied between 32° and 38°. This indicated that the contribution of tensile stress to the punching strength is less than the punching strength based on α=20°. i.e. the effect of tensile strength is less significant.
- Although the ratio of tensile strength to f_c' for high strength concrete is smaller than for normal strength concrete, still the absolute value can be large.

This model indicates that the influence of tensile strength on punching capacity is less important for high strength concrete.

2.3.2 Model for unsymmetrical punching

Broms (1990) modified K&N model by assuming different compression zone heights for tangential (Figure 2.10) and radial directions strain failure mechanisms (Figure 2.11) and using normal value for concrete ultimate stress and strain. This model was then extended to include unsymmetrical punching for interior slab with moment transfer.

Punching is assumed to occur either when the radial compressive stress reaches 1.1 f_c' or tangential compressive strain reaches 0.008. This strain value is assumed to be valid for thick slabs with a concrete strength of f_c'=25MPa. It can be modified according to the concrete grade and height of the equivalent rectangular

stress block at flexure in tangential direction when punching occurs (refer to equation 2.10).

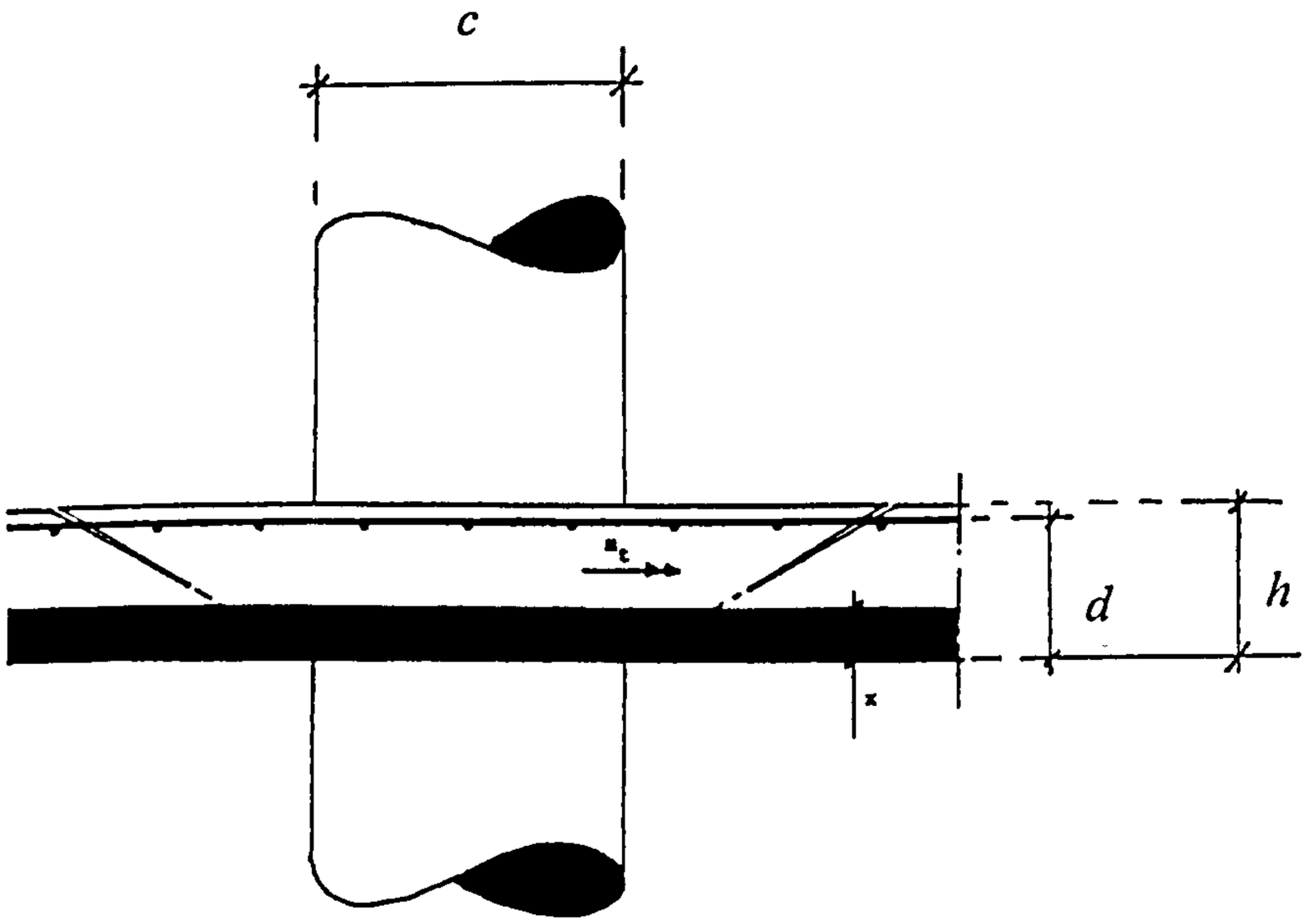

Figure 2.10 High tangential compression strain failure mechanism (Broms, 1990)

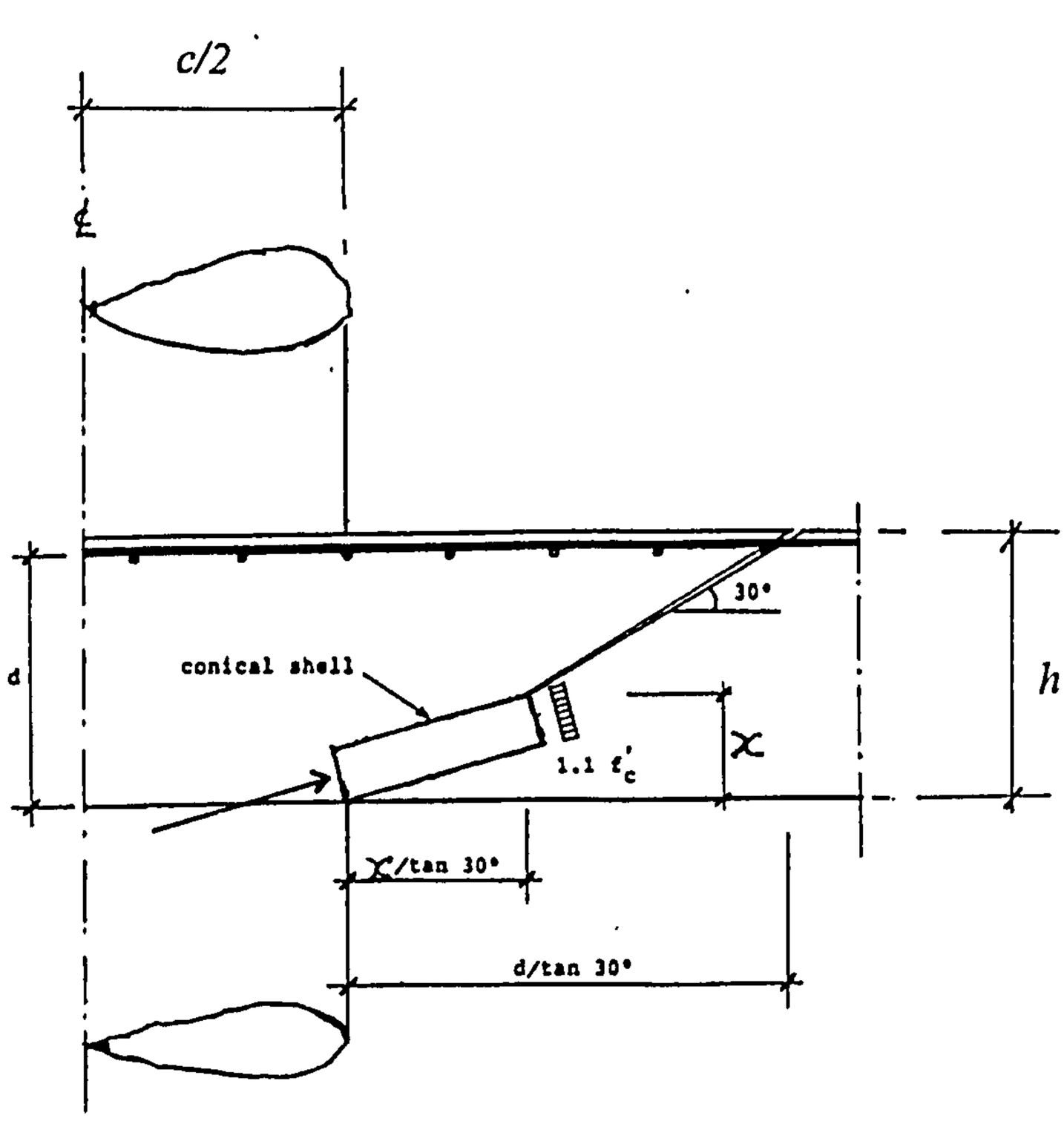

Figure 2.11 High radial compression stress failure mechanism (Broms, 1990)

When there is a moment transferred between the column and the slab, the effect of the unbalanced moment was included by the shear-moment interaction relationship as illustrated in equation (2.7). The contributions to the punching capacity by torsional moment was considered to be negligible.

$$\frac{V}{V_R}+\frac{M}{M_R}\leq 1 \qquad (2.7)$$

where V_R = *lesser of* V_ε *and* V_σ (see equations 2.8, 2.11)

M_R = *lesser of* M_ε *and* M_σ (see equations 2.9, 2.12)

M = *unbalanced moment*

The shear and moment capacities of the slab are calculated separately according to the failure mechanisms. The punching load of slab is the smaller of the two calculated values (V_ε *and* V_σ).

High tangential compression strain failure mechanism (Refer to Figure 2.10)

$$V_\varepsilon=\frac{4\pi M_\varepsilon}{\ln\frac{l}{c}+\frac{1}{2}\left(1-\frac{c^2}{l^2}\right)} \qquad (2.8)$$

The flexural capacity M_ε of the slab (see figure 2.12) by the expression

$$M_\varepsilon=\rho\sigma_s d^2\left(1-\beta\frac{x}{d}\right) \qquad (2.9)$$

$$\varepsilon_c\leq 0.0008\left(\frac{150}{\gamma x}\cdot\frac{25}{f_c'}\right)^{0.333} \qquad (2.10)$$

High radial compressive stress failure mechanism (Refer to Figure 2.11)

$$V_\sigma\approx 0.46(c+3.5x)xf_c'\left(\frac{300}{x}\right)^{0.333} \qquad (2.11)$$

$$M_\sigma=1.1f_c'\left(\frac{150}{0.5h}\right)^{0.333}\cdot W \qquad (2.12)$$

$$W = \gamma\beta\frac{h^2}{2}(c+1.75h) \qquad (2.13)$$

$$\varepsilon_c = 0.002\left(\frac{150}{0.5h}\cdot\frac{25}{f_c'}\right)^{0.333} \qquad (2.14)$$

where $$\beta = \frac{1}{\gamma}\left[\gamma - 0.5 + \frac{2}{3}(1-\gamma)^2\right] \qquad (2.15)$$

$$\gamma = 1 - \frac{\varepsilon_{cy}}{\varepsilon_c} \qquad \left(\gamma = 0.5 \;\; if \;\; \varepsilon_c \le \varepsilon_{cy}\right) \qquad (2.16)$$

ε_C= *strain of concrete at the extreme fibre of compression zone*

$$\varepsilon_{cy} = \frac{f_c'}{E_c}$$

$$\sigma_s = E_s\varepsilon_s \le f_y$$

h = overall thickness of slab

Failure criteria for this model are similar for both symmetrical and unsymmetrical punching. It includes the influence of unbalanced moment by the interaction formula for unsymmetrical punching.

2.3.3 Model for symmetrical punching with known inplane restraints

The collapse in punching shear mode involves rotations and in-plane deformation of the slab edge. Such movement occur freely without restraint in the circular test slabs. However, they will normally be resisted in the flat slab, because of the restraints imposed by the surrounding structure. Restraining forces induced lead to enhancement of the failure load. The magnitude of the restraining forces depends highly on the stiffness of the surrounding structure and are usually not exactly known. If the restraining forces are known, they can be incorporated into this mechanical model as boundary forces. This theory yields good agreement with the test results as shown by Hewitt and Batchelor (1975).

2.4 Parameters governing shear strength of solid slabs

Kinnunen and Nylander model shows that strength of concrete, ratio of reinforcement, column size, thickness of slab and surrounding restraints will affect the theoretical failure load of slab. This section reviews, based on the experimental evidence, the influence of these parameters on the punching shear strength for solid slabs without shear reinforcement.

2.4.1 Concrete strength

Moe (1961) believed that shear failures are controlled primarily by concrete tensile splitting. He assumed that the shear strength is dependent on $\sqrt{f_c'}$ because tensile strength of concrete is generally assumed to be proportional to $\sqrt{f_c'}$. However, based on the tests for interior slab with moment transfer, Hawkins (1971a) concluded that the shear strength of concrete is more likely to be proportional to the cubic root of concrete strength. The ratio of nominal ultimate shear stress to $\sqrt{f_c'}$ shows significant scatter in practice due to the scatter in tensile strength of concrete.

From Section 2.3, Kinnunen/Nylander model assumed that the punching failure occurs due to the crushing of concrete. This implies that compressive strength of concrete influences the shear strength of reinforced concrete slab.

2.4.2 Reinforcement

2.4.2.1 Ratio of flexural reinforcement

Percentage of flexural reinforcement is often used as an index for the dowel effect. Shear strength is expected to increase with increasing flexural reinforcement ratios and increasing concrete strength. However, according to the work on dowel action in reinforced concrete beam (Baumann et al, 1970), the rate of increase of shear strength decreases at higher concrete strengths and flexural reinforcement ratios.

Kinnunen and Nylander (1960) tested a number of slabs with ring reinforcement in which steel ratios was equal to those in other tests with two way reinforcement (Figure 2.12). By comparisons, they concluded that dowel action carries about 30% of the total shear. However, Criswell (1974a) (quoting Moe's (1961) results) concluded that this effect is not important.

The failure modes of the dowel mechanism defined by Vintzeleou and Tassios (1986) might explain the reason for the contradiction noted above. They stated that there are two possible failures model of dowel mechanisms:

(1) yield of the steel bar and concrete crushing under the dowel;
(2) concrete splitting.
Concrete cover is the main parameter upon which dowel mechanism depends. For small cover (less than 6 to 7 times the bar diameter), the mechanism is governed by splitting of concrete.

In view of the above statement, because of the small cover in slabs, concrete splitting and the lack of stirrup reinforcement decrease the dowel force which can be developed in any given bar (see Figure 2.14). However, if the cover is thick enough, concrete splitting is unlikely to occur. In comparison with the situation in a beam, the width (circumference) of concrete involved in the dowel action is large resulting in a large number of bars passing through the inclined crack. This probably results in the dowel forces carrying a greater proportion of the shear in slabs than in beams.

2.4.2.2 Arrangement of flexural reinforcement

Elstner and Hognestad (1956) and Moe (1961) conducted tests on slabs with flexural reinforcement concentrated in the column region. The dimensions of the slabs tested by Elsner and Hognestad were 254mm thick with side length of 1830mm. The square column stubs at the centre were 254mm and 356mm. The tensile reinforcement was uniformly spaced and with 50% concentrated within a distance *d* (effective depth) of the column. Moe (1961) conducted tests in which the total amount of steel was held constant and the spacing varied between uniform spacing and an arrangement in which 82% of the total steel was placed within a distance d of the column. Both tests indicated that the concentration of reinforcement does not increase the ultimate load of slab. In some slabs, concentration of reinforcement even reduced the ultimate load of slab. The results are not suprising because the concentration leaves large radial sector almost unreinforced (Figure 2.13). From these tests results, Hawkins (1974a) concluded that concentration causes a slight decrease in strength and a reduction of ductility.

Alexander and Simmonds (1992) studied the effects of concentration of reinforcement by adding extra reinforcement placed over the column strip of 450mm (i.e. different amount of steel) resulting in spacings of 50mm, 75mm and 150mm at the column region. Considering the densities of reinforcement, decreasing the spacing increases the load capacity but decreases ductility. Although all slabs failed in punching, but the bar force profiles indicate that anchorage failure occurred in the centre bar in slab with a spacing of 50mm. From this observation, they suggested that in those slabs tested by Elstner and Hognestad (1956) and Moe (1961) failure was actually anchorage failure. They concluded that the above observation may explain

why the concentrating of reinforcement through the column region does not increase punching capacity.

However, concentration of flexural reinforcement in the column region (critical perimeter) is to be encouraged because it improves the behaviour of the slab in the service load range. Concentration increases the stiffness of the slab, increases the load for the first yielding of the flexural reinforcement, and consequently results in smaller maximum crack widths for a given loading.

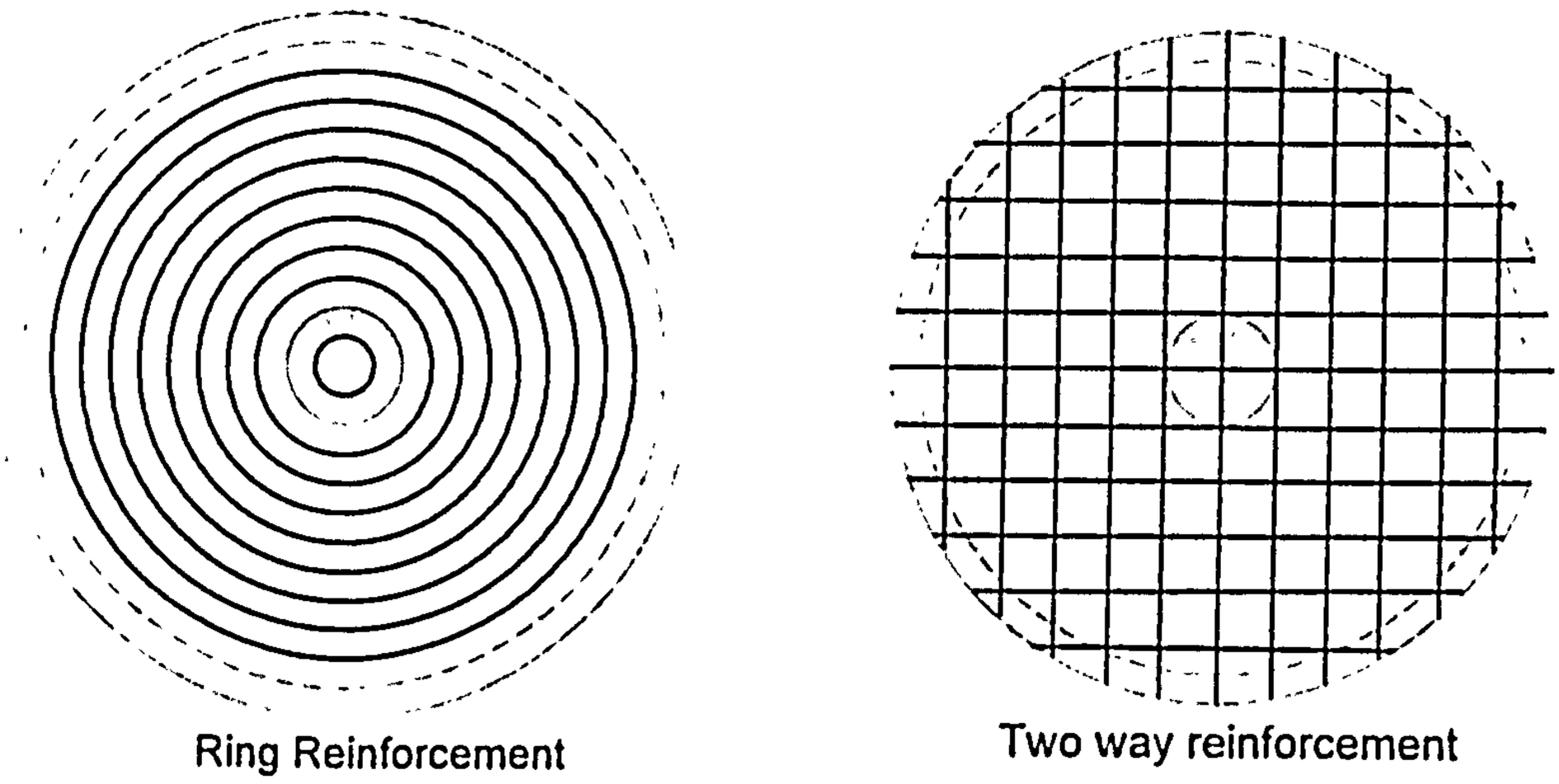

Figure 2.12 Ring reinforcement and two way reinforcement

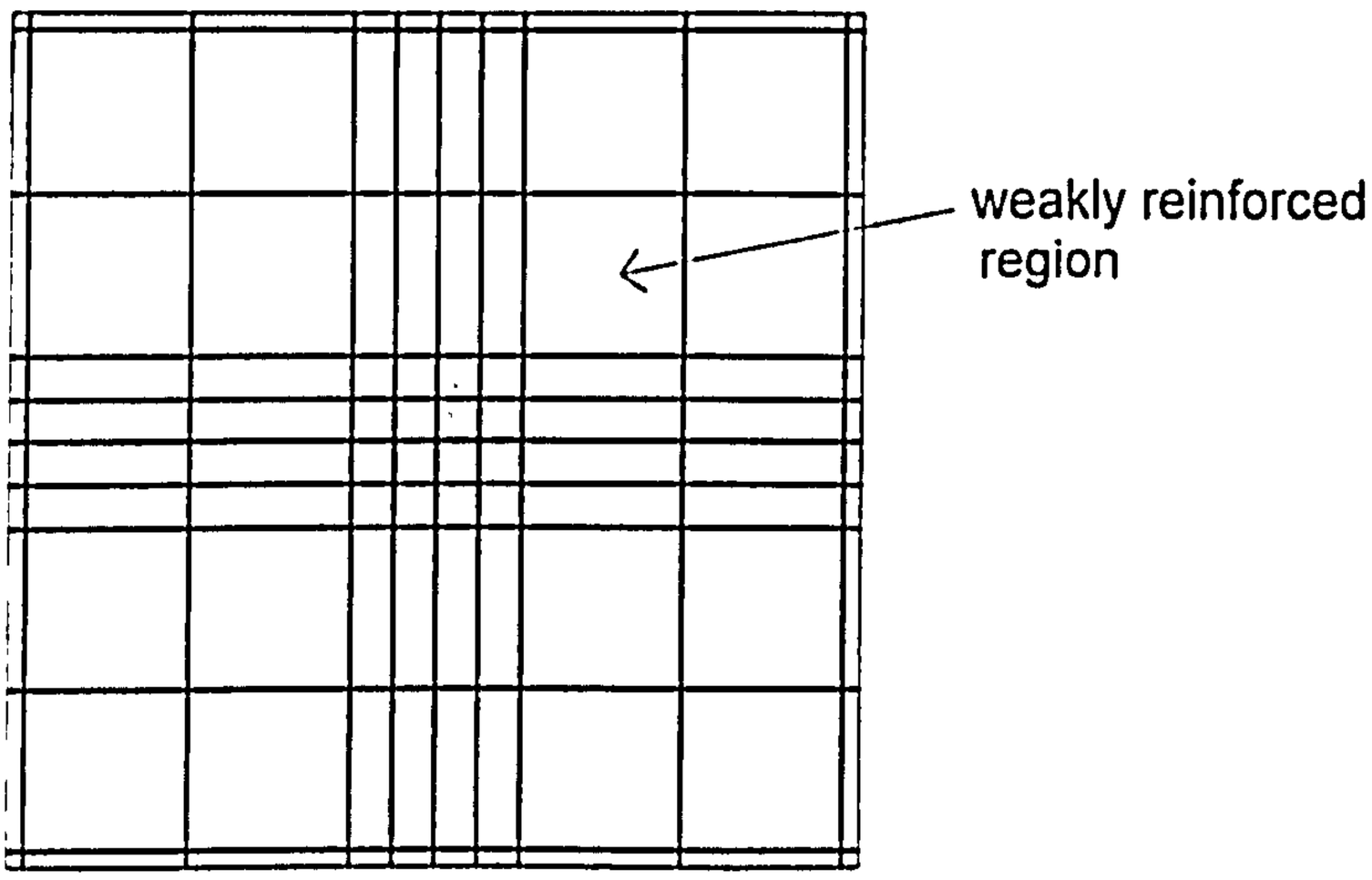

Figure 2.13 Concentration of flexural reinforcement

2.4.2.3 Compression reinforcement

Manterola (1966) tested a series of twelve slabs in which the ratio of compression steel to tension reinforcement was zero, 0.5 and 1.0. He reported that the compression reinforcement had negligible effect on ultimate strength of the slab when the ratio of tension reinforcement is small. However, when the ratio of tension reinforcement is large enough to make a doubly reinforced section, increasing the compression area from zero to an equal amount to the tension reinforcement increased the ultimate capacity of the slab by about 30%. The test results indicated that compression reinforcement may increase the flexural capacity of slabs and there is no direct evidence as to how the compression reinforcement will affect the shear strength of slab.

Pan and Moehle (1992) tested slabs under combined gravity and lateral loads. They observed that if the compression reinforcement (bottom bar) in the slab continues through the column, then it can act as a suspension net holding the slab to the column and thus support some load after punching failure occurred (Figure 2.14). Top steel is not effective in providing post punching resistance because it tends to tear out of the slab when punching occurs due to concrete cover over this steel splitting off. Therefore, properly detailed bottom reinforcement in the slab may prevent catastrophic failure.

2.4.3 Inplane Restraints

Taylor and Hayes (1965) carried out a series of tests on the effect of edge restraint. The slabs were divided into three groups depending on the amount of tension reinforcement which was zero, 1.57% and 3.14%. The restraint was imposed by a heavy welded steel frame which surrounded the slabs, i.e. the edges of slab were restrained against lateral movement. All slabs without reinforcement were tested in the restrained condition. For pairs of slab with reinforcement, one of each pair was tested in the simply supported condition and the other in the restrained condition.

The test results indicated that for slab with low percentage of reinforcement, the restraint significantly increased the ultimate load up to 60%. This group of slabs exhibited high ductility and were more likely to fail in flexural mode. The ductile behaviour allowed compressive membrane forces (Figure 2.15a) to fully develop. The flexural capacity was thus significantly increased as observed by other researchers (Roberts 1969, Kuang and Morley 1992). However, for slabs with high reinforcement ratio, the enhancement by restraint was less significant and in some cases there was virtually no increase in strength. Punching shear failure is critical for this group of slabs and the slabs suddenly rupture. It is possible that the slab fails

before the membrane action has developed. Others (Aoki and Seki 1971, Tong and Batchelor 1971, Rankin and Long 1987) observed that restraint will enhance punching shear strength of slab in all cases.

Kuang and Morley (1992) tested a total twelve slabs which were supported and restrained on all four sides by edge beams. Different degrees of edge restraint was provided by different sizes of edge beam. They observed that a restrained slab with low percentage of steel failed in punching shear mode when subjected to concentrated loading. This indicated lateral restraint may also change the mode of failure because the membrane forces developed enhances the shear and flexural capacity of the slab and at the same time reduces the ductility of the slab.

It is apparent that from the above test results that the restraint can considerably enhance the load carrying capacity of slab, but reduce the ductility of the slab. However, the degree of the enhancement in strength due to the membrane action is difficult to quantify since it depends on the in-plane restraint provided by the surrounding structure.

2.4.4 Size of Loaded area (column)

Moe (1961) assumed a linear variation in shear strength with side dimension of the column based on test data when the side length of loaded area was between 0.75d and 3.0d, where d is the slab thickness. Regan (1986) tested five slabs where the loaded area is the only significant variable. The shapes of loaded area are : circular with diameters of 54mm, 110, 150 170mm and 102×102mm square. The test results confirmed the linear relationship for the loaded dimension provided that it exceeds 0.75d. When the loaded area is very small (side dimension less than about 0.75d) , the slab failed in local crushing and therefore the strength of slab is far below that predicted by the linear relationship.

In view of the above, if the loaded dimension is greater than 0.75d, the length of critical section become greater as the loaded area increases, resulting in an increase in shear strength of slab. Therefore it is very common in practice to provide drop panels or capitals (Figure 2.16) to increase the punching shear resistance rather than increasing the column size.

2.4.5 Column shape

The majority of available test data from literature indicate that slab loaded through a circular area are stronger than those loaded through square areas with the same perimeter. The improved shear strength is apparently a result of the absence of

stress concentrations which occurs at the corners of rectangular column (see Figures 2.7 & 2.8).

Hawkins et al (1971b) carried out a series of tests on nine slabs in which the length of the perimeter was held constant but the aspect ratio was varied. He found that if the aspect ratio is increased, the shear strength of slab decreases because the behaviour of slab transform form two way bending to one-way bending. Therefore beam action shear tends to develop at the long faces of the loaded area. This also reflects the tendency for the shear force to be concentrated at the end of a wide column (Figure 2.17) as observed in the experiment. He concluded that when the aspect ratio for a rectangular column is greater than two, strength can be lower than that for a square column.

2.4.6 Size effect (span-depth ratio)

Regan (1986) tested six specimens where the main variable was the thickness of slab. The effective depths were 80mm, 160mm and 250mm. Test results show that nominal shear strength increased as d decreased (Figure 2.18). These results also agree reasonably well with the size factor ($\sqrt[4]{1/d}$) used in the BS8110. Regan quoted that the range of the slab depth in his test is limited but the tests carried out by Kinnunen et al (1978) with effective depth up to 619mm further confirmed the fourth root relationship.

John and David (1990) tested a series of slabs of constant thickness (100mm) with varying span-depth ratios. They concluded that the punching shear strength was significantly increased for the span-depth ratio below six (Figure 2.19). The strength enhancement may be due to the development of compression struts forming an arch mechanism in the slabs and in plane compressive forces resulting from friction at the support.

2.4.7 Concrete cover

Alexander and Simmonds (1992) tested a series of eight isolated interior column-slab connections where three specimens were used to study the effect of the clear cover to tension reinforcement. The clear covers were 11mm, 19mm and 38mm. The experimental load-deflection relationship is shown in Figure 2.20. Slabs with 11mm and 19mm cover exhibit stiffer response due to the higher value of flexural depth (Figure 2.20), but the slab with 38mm cover failed at a load which was 3% higher than the rest. They observed that slab with smaller cover suffered larger bond deformation. From the test results, they concluded that for a given slab thickness, the elevation of the flexural reinforcement does not greatly affect the punching shear of

the connection since a change in the flexural depth is offset by a corresponding change in the cover. Thus the cover of the reinforcement is as significant to punching shear as the effective depth.

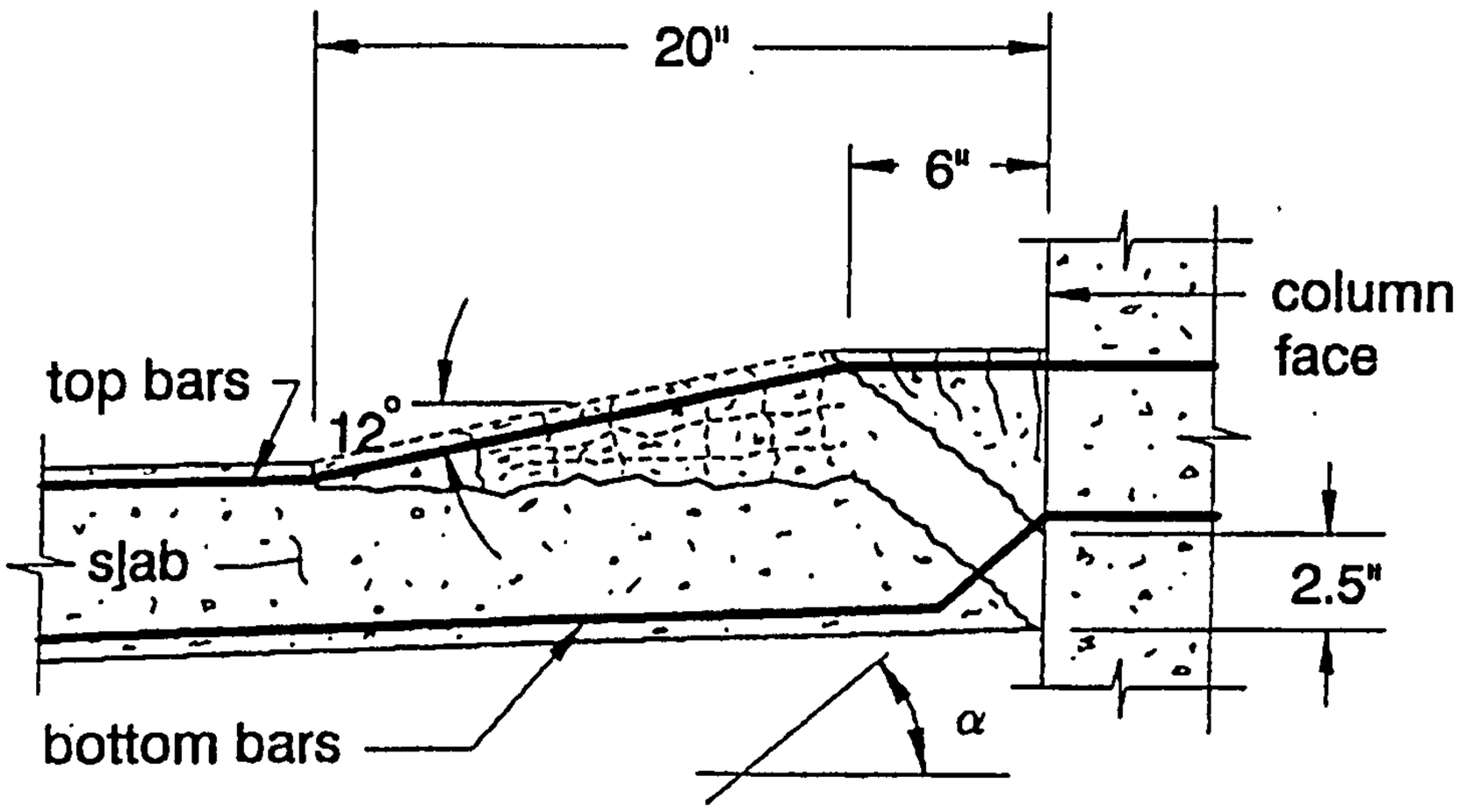

Figure 2.14 Post-punching behaviour of slab-column connections

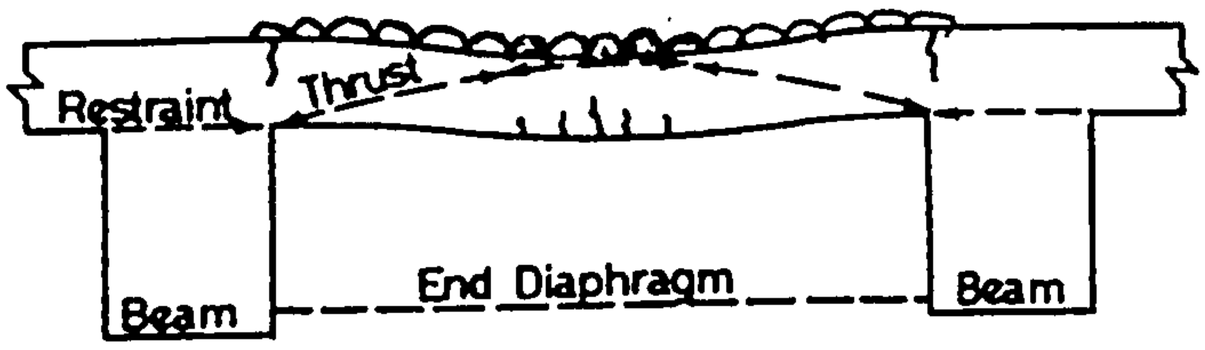

(a) Compressive membrane action

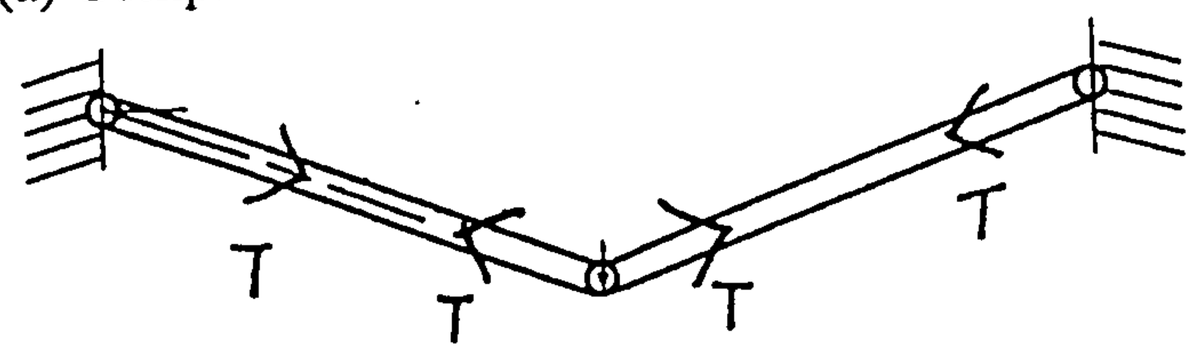

(b) Tensile membrane action

Figure 2.15 Membrane action

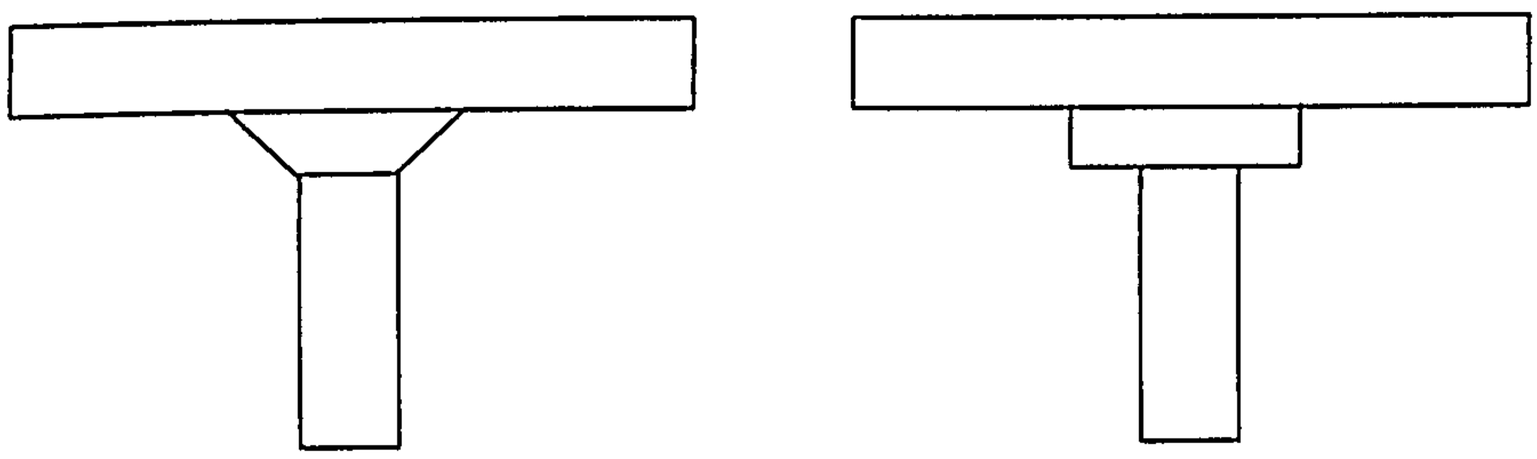

Figure 2.16 Capital and drop panel

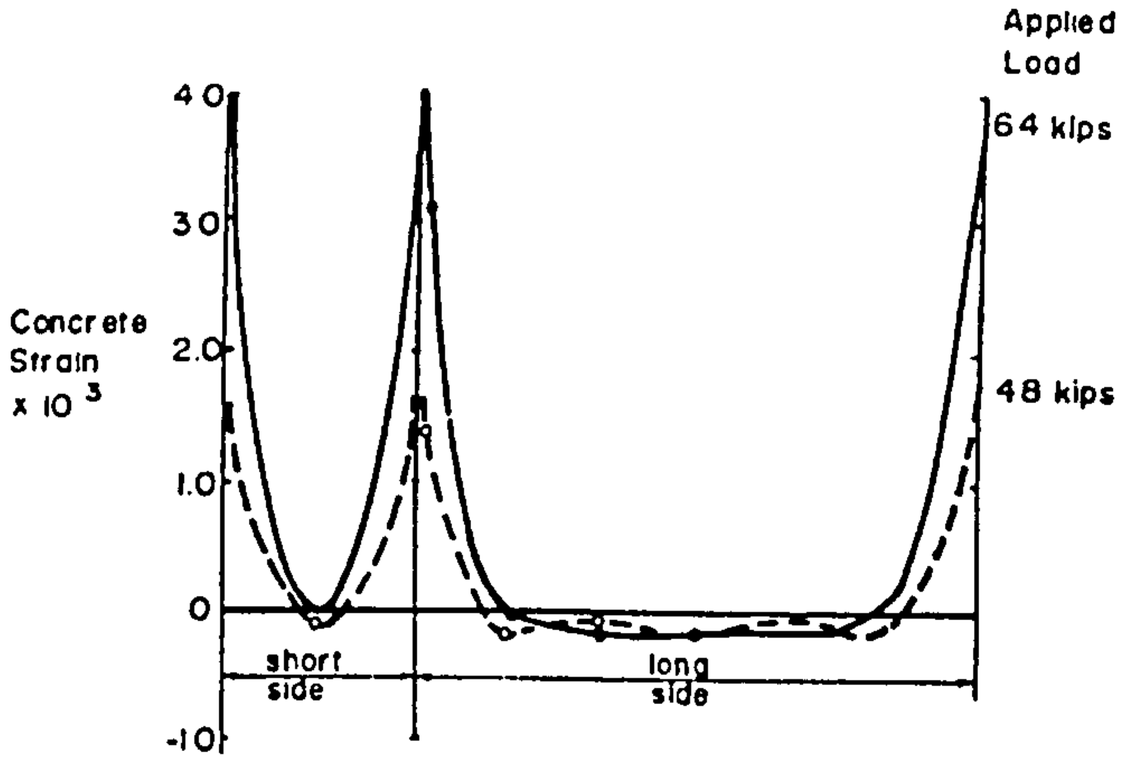

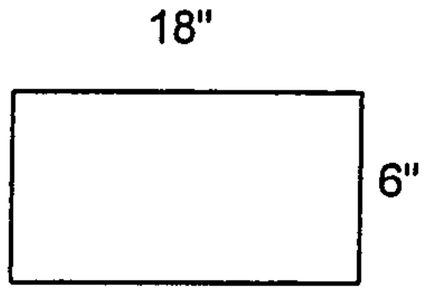

1 kip = 4.45 kN

50 kips = 222.5 kN

(Hawkins et al, 1971b)

Figure 2.17 Concrete strain on column (specimen 7, Aspect Ratio=3)

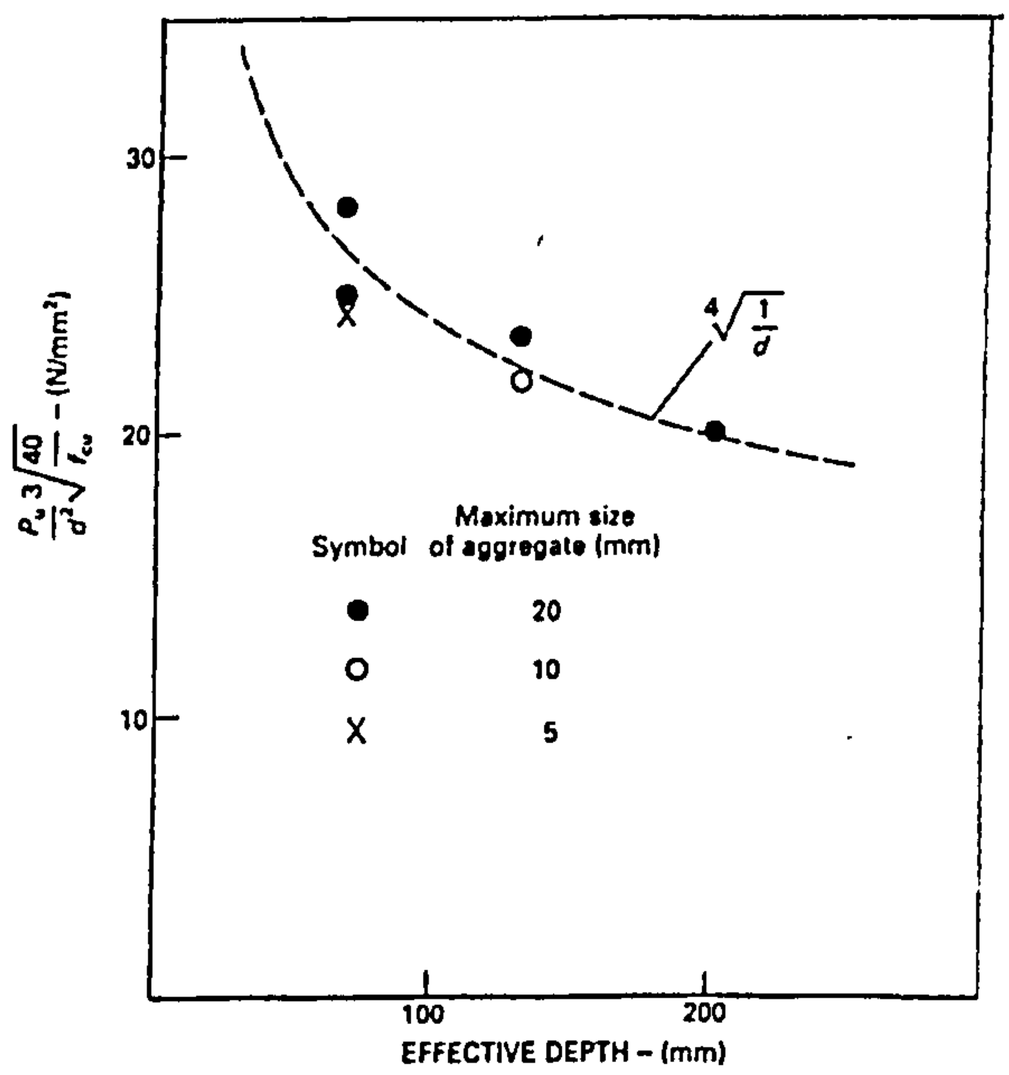

Regan (1986)

Figure 2.18 Influence of effective depth on unit resistance

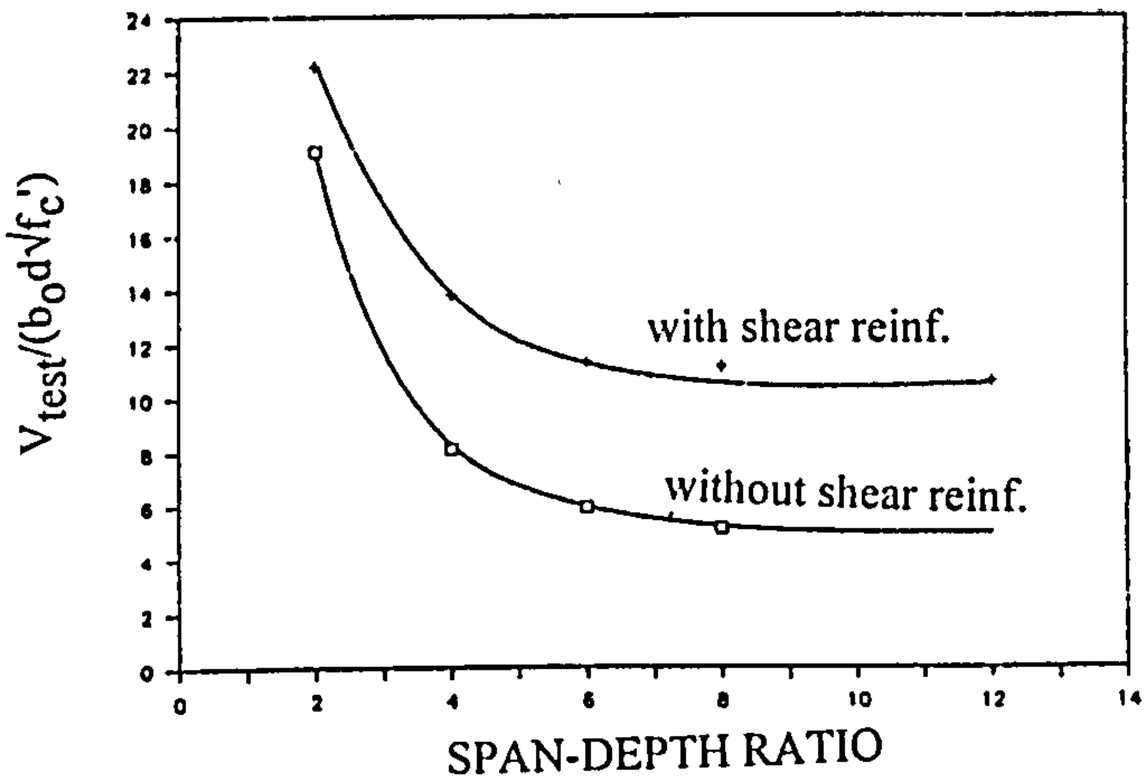

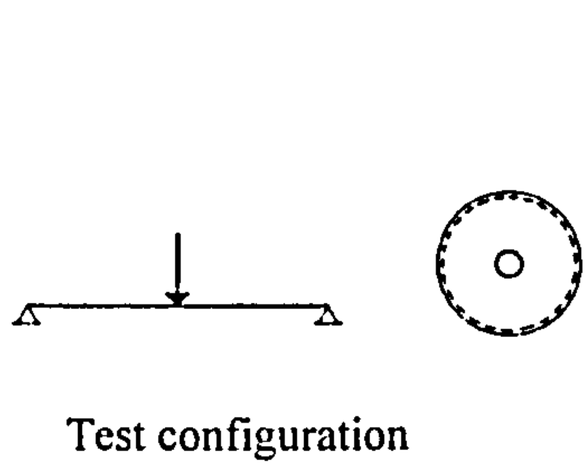

John and David (1990)

Figure 2.19 Effects of span-depth ratio on punching shear strength

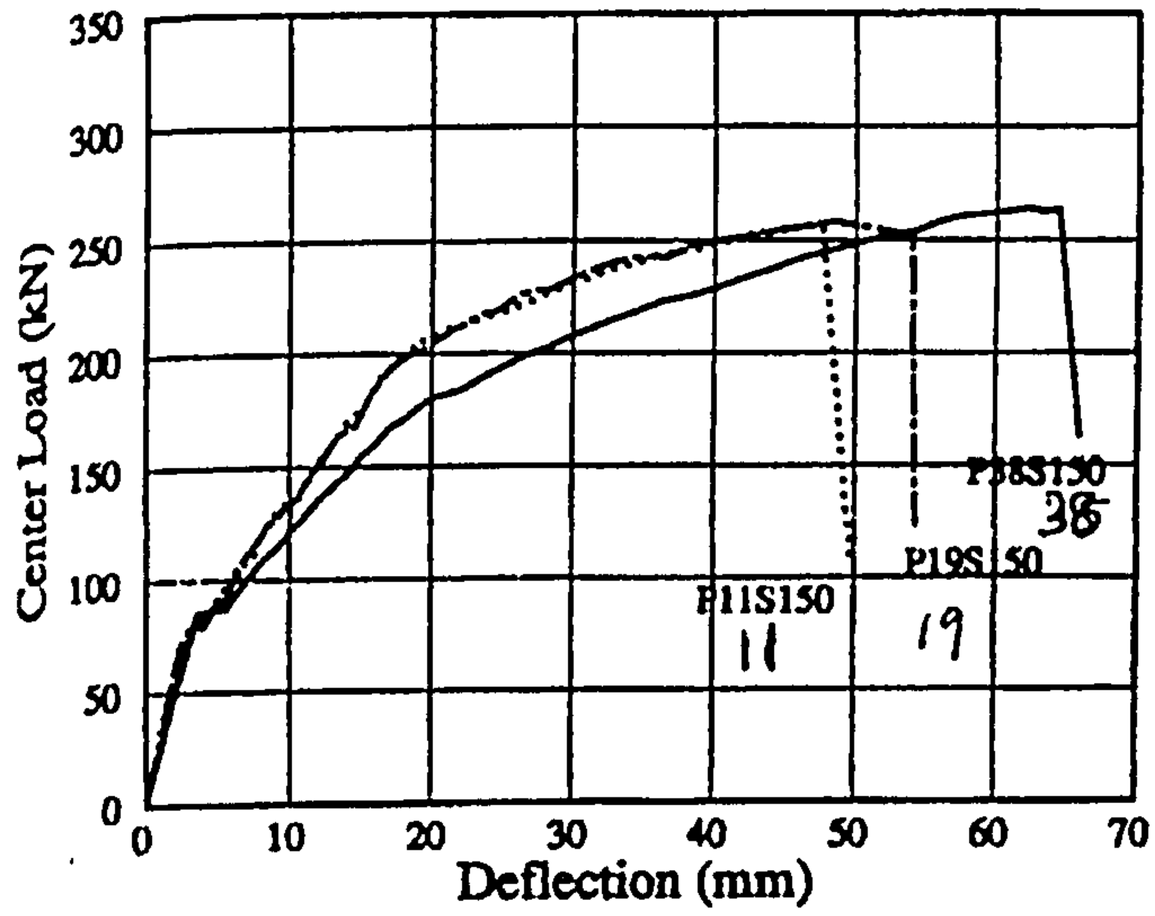

P11S150
cover = 11 mm

P19S150
cover = 19 mm

P38S150
cover = 38 mm

Figure 2.20 Effects of clear cover

2.5 Slabs with shear reinforcement

Building structures should be designed in such a way that they exhibit ductile failure mode when subjected to catastrophic loading. Large deformations (large deflection and excessive cracking) give clear warning of impending failure. Shear reinforcement not only increases the load carrying capacity of the flat slab, but it also improves the ductility of slab. Shear reinforcement not only provides resistance to the tensile stress across the shear crack, but it also provides confinement to concrete. However, this tensile stress cannot develop unless the shear reinforcement is effectively anchored (Figure 2.21). The importance of anchorage of shear reinforcement has been confirmed experimentally by John and David (1990) and Broms.C.E. (1990). Due to the difficulty of achieving effective anchorage in thin slab, the use of shear reinforcement is generally not recommended for slab with overall thickness less than 200mm.

Another important factor is the spacing of shear reinforcement. The resistance to punching is provided by shear steel and concrete and according to truss mechanism, the shear resistance contributed by concrete is less for lower inclination of concrete strut. Thus, if shear links are too widely spaced in the tangential direction, it is ineffective in enhancing shear strength of slab as reported by Langhor et al (1976). In order to ensure that there is a shear resistance contribution from the concrete between shear links, it is required to limit the spacing of shear links (e.g. a spacing of 0.75d proposed by BS8110).

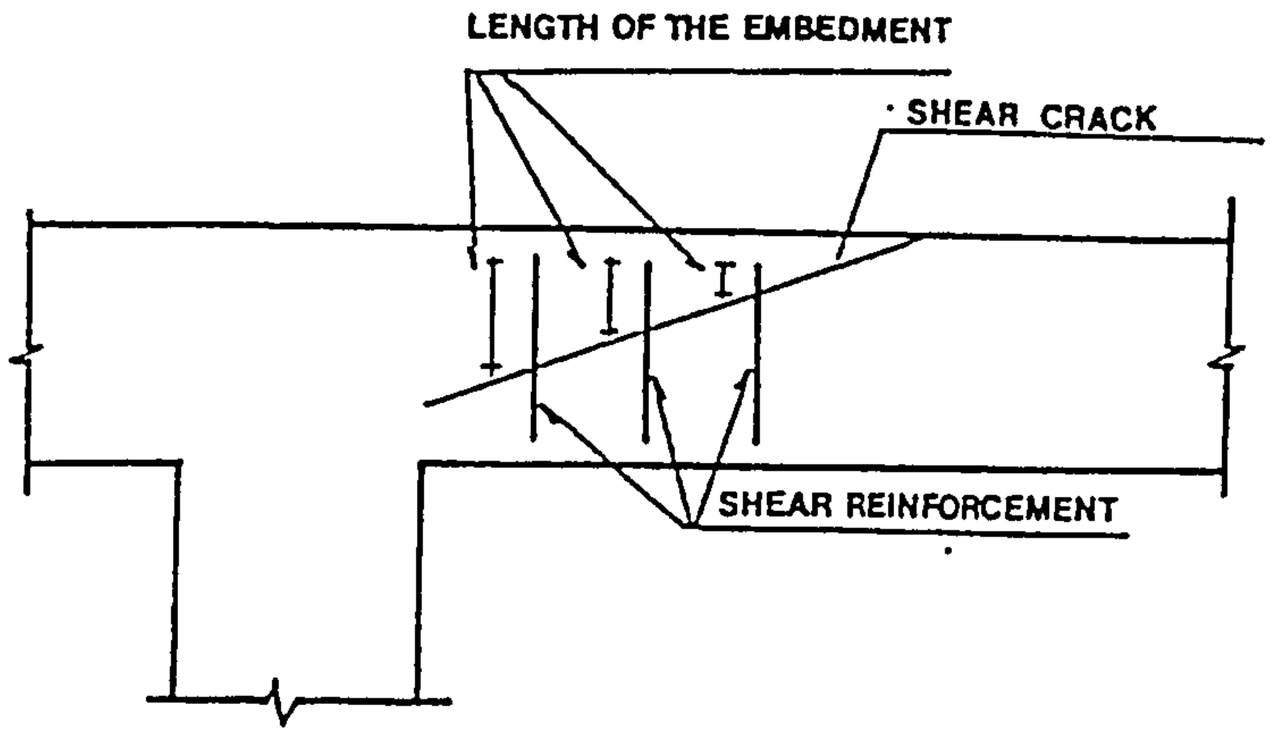

Figure 2.21 Length of the embedment of shear reinforcement

2.6 Failure mechanisms

Most research on the shear strength of slab has concentrated on generating experimental data to develop empirical equations for design. Very little work has been done on understanding the mechanisms of shear failure in slabs. This deficiency is largely due to the difficulties of observing the development of failure mechanism which takes place inside the slab and is generally not visible on an exposed surface.

A two-way slab may fail in shear as a wide beam (Beam action) or due to punching. In beam action or one-way shear (Figure 2.22a), the slab fails as a wide beam (diagonal crack forming across the full width of the slab). This type of shear failure can be treated by beam shear theories and will not be discussed further here. Punching shear or two-way shear failure occurs around the column (concentrated load). The failure is caused by diagonal tension crack around the column in the shape of a truncated cone (Figure 2.22b).

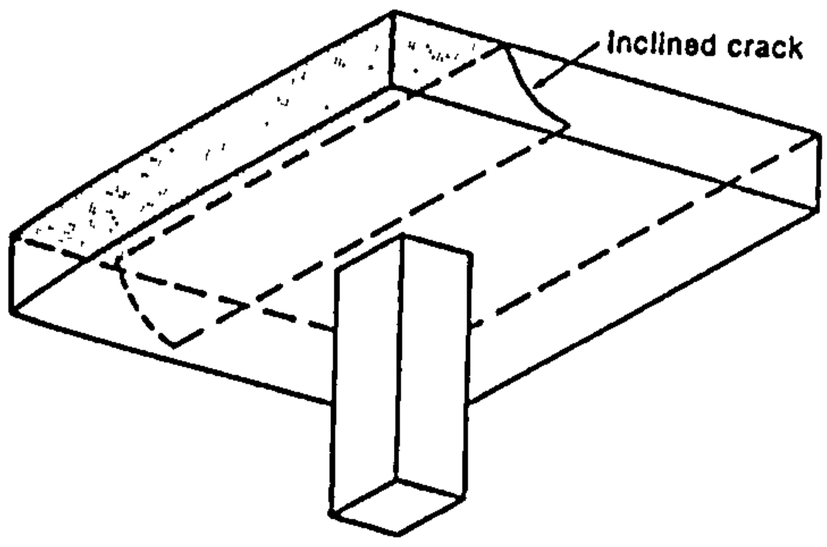

(a) One-way shear

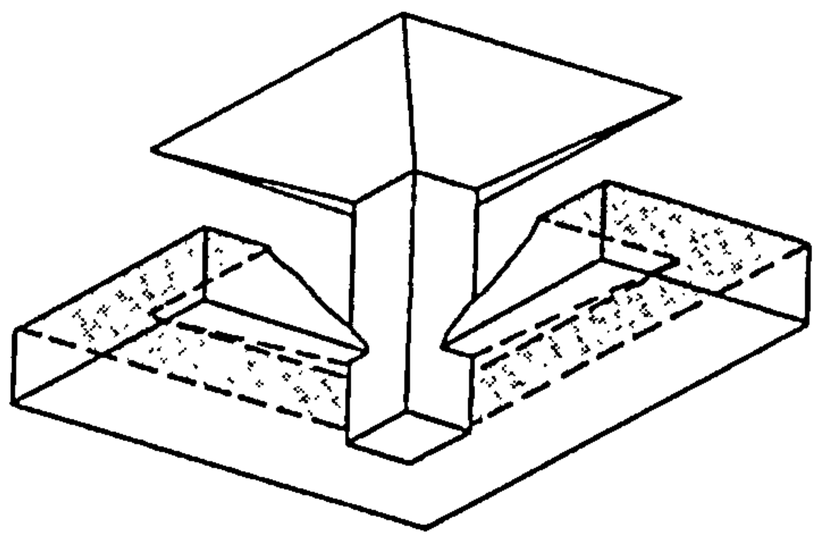

(b) Punching shear

Figure 2.22 Shear failure in a slab

2.6.1 Symmetrical punching

This section will discuss mechanisms of symmetrical punching around the critical section. Symmetrical punching occurs when the load is applied without eccentricity with respect to the critical section of the slab.

Before cracking, the shear force is carried by the entire depth of the slab. After diagonal tension cracking has occurred in the vicinity of the critical section of the slab around the column, the slab carries the shear force by shear across the compression zone, aggregate interlock and dowel action.

When the load is applied to the slab, the first crack appears as a roughly circular crack around the perimeter of the loaded area due to negative bending moments in the radial direction. Radial cracks, due to negative bending moments in the tangential direction, then extended from the critical perimeter. Because the radial moment decreases rapidly away from the loaded area, a significant increase in load is necessary before the tangential cracks form around the loaded area at some distance out in the slab. At about half of the failure load, the diagonal tension crack develop in the slab and this crack is thought to tend to originate near the mid-depth of the slab. The stiffness of the slab surrounding the cracked region tends to control the opening of the diagonal tension cracks, thus preserving the shear transfer by aggregate interlock at higher loads. Punching shear failure eventually occurs with or without the yielding of reinforcement.

2.6.2 Punching with unbalanced moment

In a flat slab floor carrying only gravity loading, there will in general be transfer of both shear and a small amount of unbalanced moment. However when flat slab structures are subjected to horizontal loading due to wind or earthquake, there is substantial unbalanced moment to be transferred at every connection. The transfer of unbalanced moment causes the distribution of shear stress around the column to become non-uniform. This reduces the shear strength of the connections. The shear force and unbalanced moment are transferred by combined bending, torsion and shear at the faces of the critical section in the slab around the column.

Figure 2.23 illustrates the situation near an edge column. M_u and V_u are the unbalanced bending moment and shear force transferred to the column. Let us look at the free body diagram at the slab's critical section. The shear force is transferred partly by V_1 at the front face and the remainder by V_2 at each side face. The moment transfer occurs partly as the moment M_1 at the front face of the critical section, and the remainder as torsional moment T_2 at each side face. At an interior column,

transfer of forces also occurs at a back face of the critical section (Figure 2.24). At a corner column, there is only one side face (Figure 2.25).

If the shear strength of the slab is reached, the slab will fail in diagonal tension on the side of the column where the vertical shear stress is highest (e.g. if V_1 exceeded shear strength of the slab, failure will take place in front face of the critical section) as shown in Figure 2.26, resulting in the column punching through the slab and the top reinforcing bar splitting off the cover concrete.

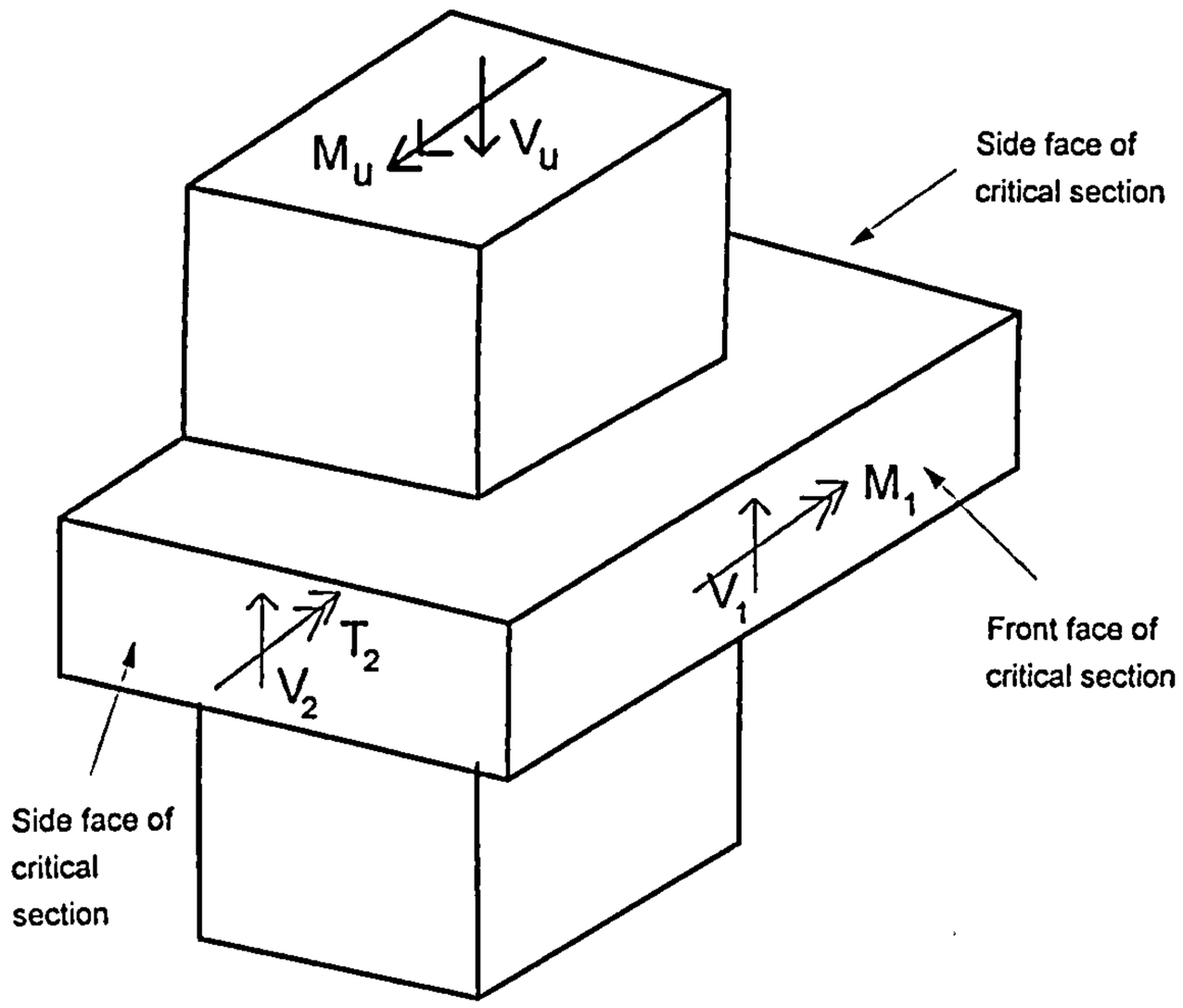

Figure 2.23 : Transfer of forces between floor and edge column

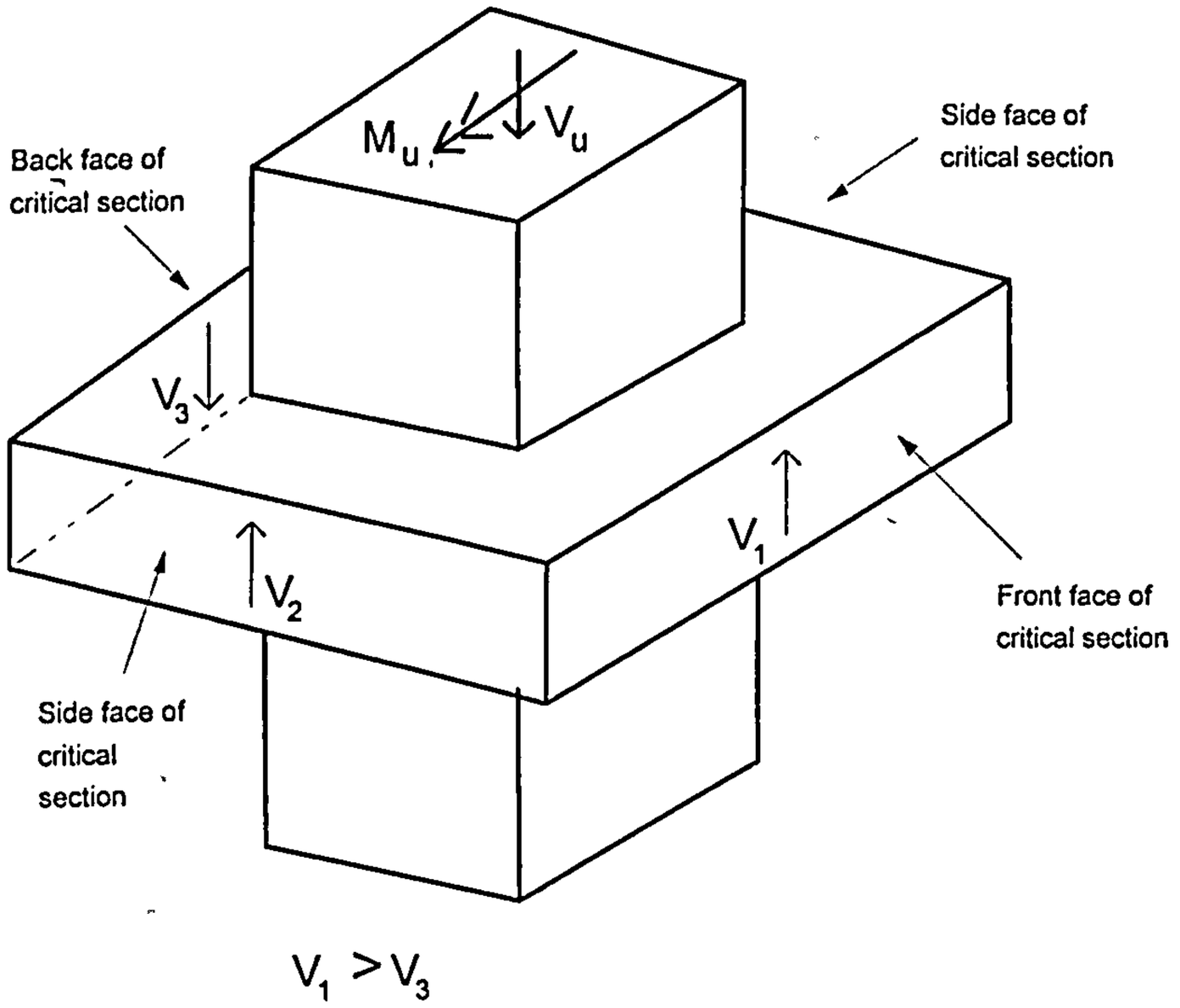

Figure 2.24 : Transfer of forces between floor and interior column

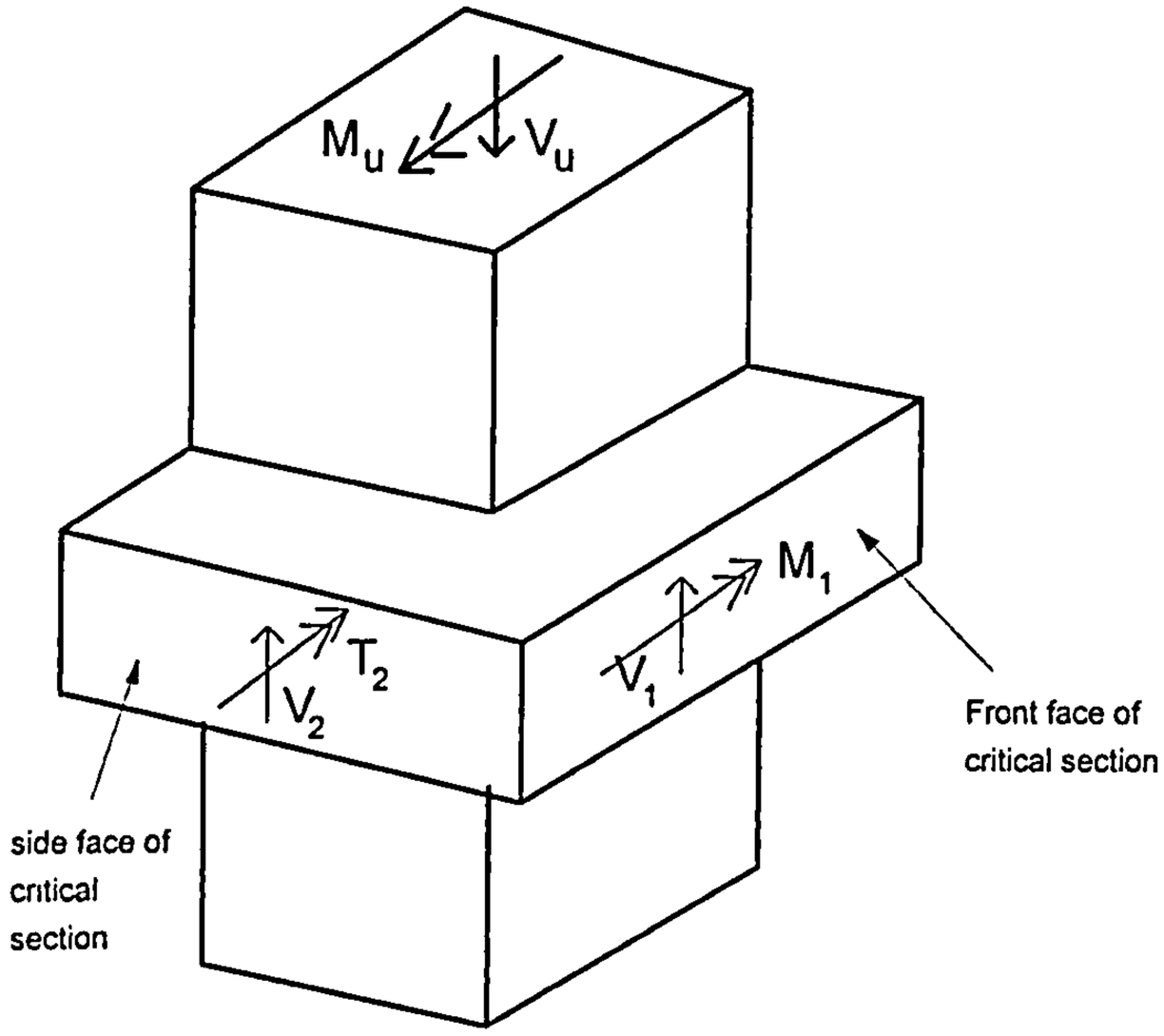

Figure 2.25 : Transfer of forces between floor and corner column

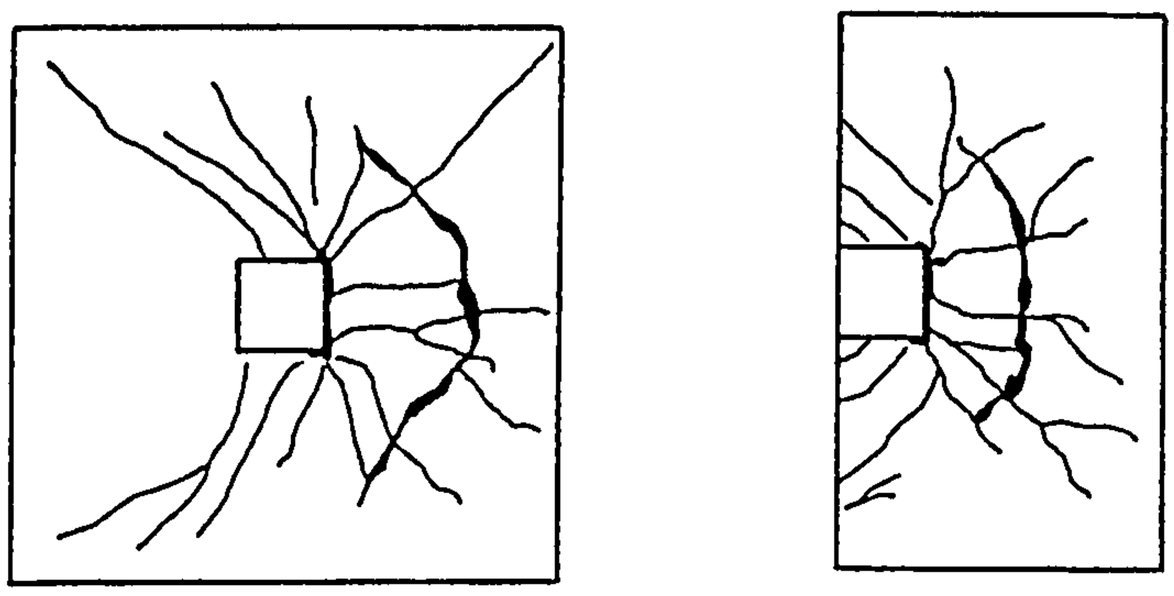

Figure 2.26 : Punching shear failure under combined shear and unbalanced moment

2.7 Modes of failure for slabs without shear reinforcement

The observed modes of failure of slabs can be classified into three categories, depending on whether failure was initiated by the yielding of the reinforcement (flexure), crushing of concrete or by internal diagonal cracking (shear punching) or a combination of both (flexural punching).

2.7.1 Pure flexural failure

For slabs which fail in flexural mode, a small number of large flexural cracks develop before failure. The crack pattern might approach the full yield line pattern as shown in Figure 2.27(a). This type of failure often occurs in slabs with a small amount of reinforcement. The slab fails in a ductile mode with large deflection developing

prior to failure. The flexural reinforcement yields before final failure and yielding spreads over a wide area of slab at failure.

2.7.2 Flexural Punching failure

This type of failure is somewhere between the pure flexural failure and pure punching failure as shown in Figure 2.27(b). Yield line pattern is not fully developed and ultimate failure is by punching accompanied by yielding of steel. The yielding of reinforcement takes place only locally around the column.

2.7.3 Pure Punching failure

For slabs failing in shear mode, a large number of fine flexural cracks (radial and tangential) develope before failure but without the yielding of reinforcement. This type of failure often occurs in heavily reinforced slab. The large amount of reinforcement will increase the flexural capacity of slab substantially. The large bi-axial compression due to bending plus the vertical applied load cause the slab to more likely fail in crushing of concrete than yielding in flexural steel. Finally the slab fails in a local area around the column in the shape of truncated cone. For slab with large amount shear reinforcement or small column size, the slab may fails in local compression failure as shown in Figure 2.27(c). This type of failure is brittle in nature and take place with small deflection.

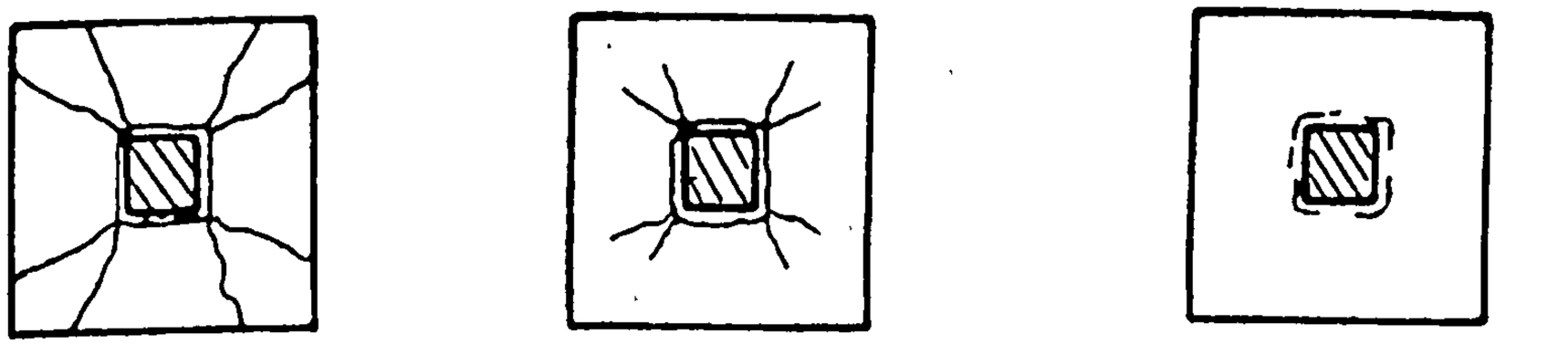

a) Full yield line pattern b) Partial yield failure mode c) Compression failure mode

Figure 2.27 Modes of Failure

2.8 Treatment of punching shear by BS8110

2.8.1 Shear strength for slab without shear reinforcement

With no single theory of punching failure being generally accepted, code recommendations are empirical and are expressed in term of nominal shear stress. British standard BS8110 determines punching shear strength from equation(2.18). The

critical shear perimeter is taken as a rectangle at a distance of 1.5d from column faces regardless of whether the columns are rectangular or circular in section (Figure 2.28). This nominal shear stress is very sensitive to the location of the critical section. The nominal stress decreases rapidly with increasing distances from the loaded area.

$$v_{nom} = \frac{V}{ud} \leq v_c \qquad (2.17)$$

$$v_c = const \times (\rho \times f_{cu})^{1/3} \times (400/d)^{1/4} \qquad (2.18)$$

where V = *Shear force due to the ultimate load*
d = *Effective depth of the slab* $\left({}^{400}/_{d} \not< 1.0\right)$
u = *perimeter at 1.5d from the column face*
f_{cu} = *characteristic cube strength of concrete*
ρ = *percentage of flexural steel* $(\rho \leq 3)$
v_c = *concrete shear stress*

Equation (2.18) implies that the shear capacity of concrete is influenced by the strength of concrete, ratio of flexural reinforcement and size effect. BS8110 recommends that ρ be calculated for a width equal to those of columns plus $1.5d$ to each side. Thus for a given total amount of steel, the code predicts an increase of punching resistance if the reinforcement is heavily concentrated toward the column lines. Section 2.4.2.2 shows that test results do not entirely support this.

No matter with or without shear reinforcement , maximum shear capacity at the column face should not exceed $0.8\sqrt{f_{cu}}$ or 5 N/mm^2 whichever is smaller. The limitation is to prevent local crushing. It also implies that the size of loaded area is taken into consideration. But the code does not take into account the reduction in shear resistance for rectangular or wall shaped supports. In such cases, there is shear stress concentration in the corners as explained in section 2.4.5.

As discussed in section 2.4.6, the punching shear strength is significantly increased for the span-depth ratio below 6. BS8110 allows enhancement of strength for perimeters at a distance less than $1.5d$ from the face of the loaded area, v_c can be increased by a factor of $1.5d/a_v$, where a_v is the shear span of the slab.

2.8.2 Shear strength for slab with moment transfer

If a slab transmits an unbalanced moment M to a column, the distribution of shear is uneven and the load capacity is reduced. In BS8110, this effect is expressed by determining a maximum nominal shear stress.

$$v_{\max} = \frac{V_{eff}}{ud} \leq v_c \qquad (2.19)$$

(i) The effective shear force, V_{eff} required for interior slab-column connections at the critical section is :

$$V_{eff} = V + \frac{1.5M}{X} \qquad (2.20)$$

where X = *The side length of the perimeter considered parallel to the axis of bending.*

M = *Moment transmitted from the column to the slab*

V = *Shear force transferred to the column.*

In the absence of calculations, for internal column in braced structures with approximately equal spans, it will be satisfactory to take V_{eff} as :

$$V_{eff} = 1.15V \qquad (2.21)$$

where V is calculated on the assumption that the maximum design load is applied to all panels adjacent to the column considered.

(ii) At edge and corner column connections where bending about an axis parallel to the free edge is being considered, as shown in Figure 2.29, the effective shear strength is calculated from :

$$V_{eff}^{\neg} = 1.25V \qquad (2.22)$$

For edge column connections when bending about an axis perpendicular to the free edge is being considered, the effective shear strength should be calculated using the following equation :

$$V_{eff} = 1.25V + \frac{1.5M}{X} \qquad (2.23)$$

Alternatively , V_{eff} may be taken as $1.4V$ for approximately equal spans.

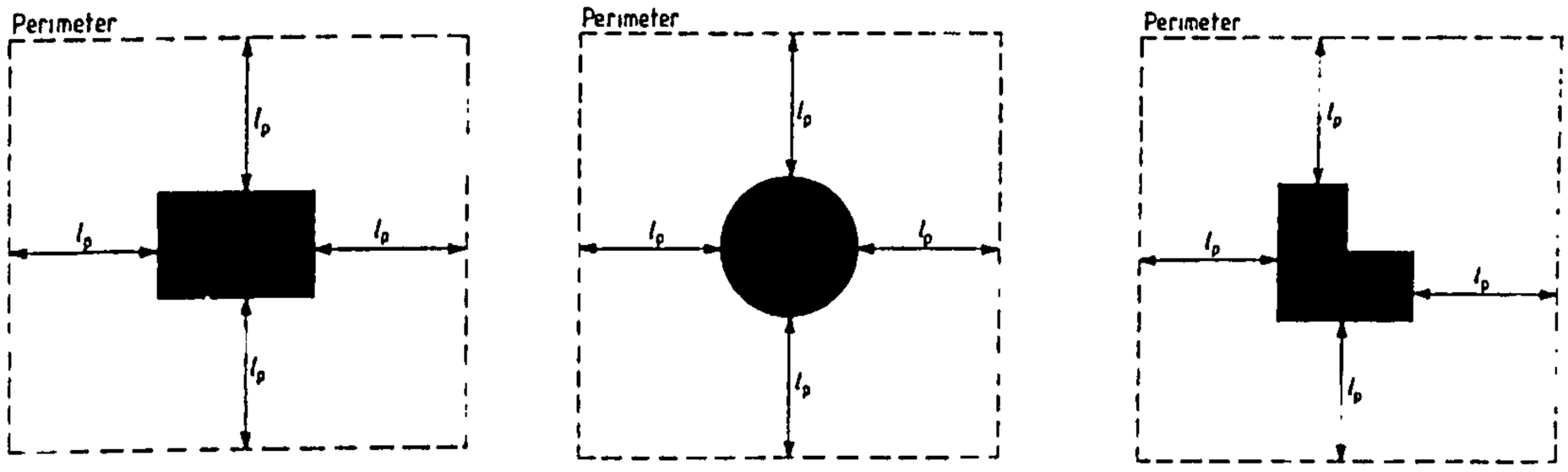

lp= Multiple of 0.75d (where d is the effective depth of slab)

Figure 2.28 Definition of perimeter

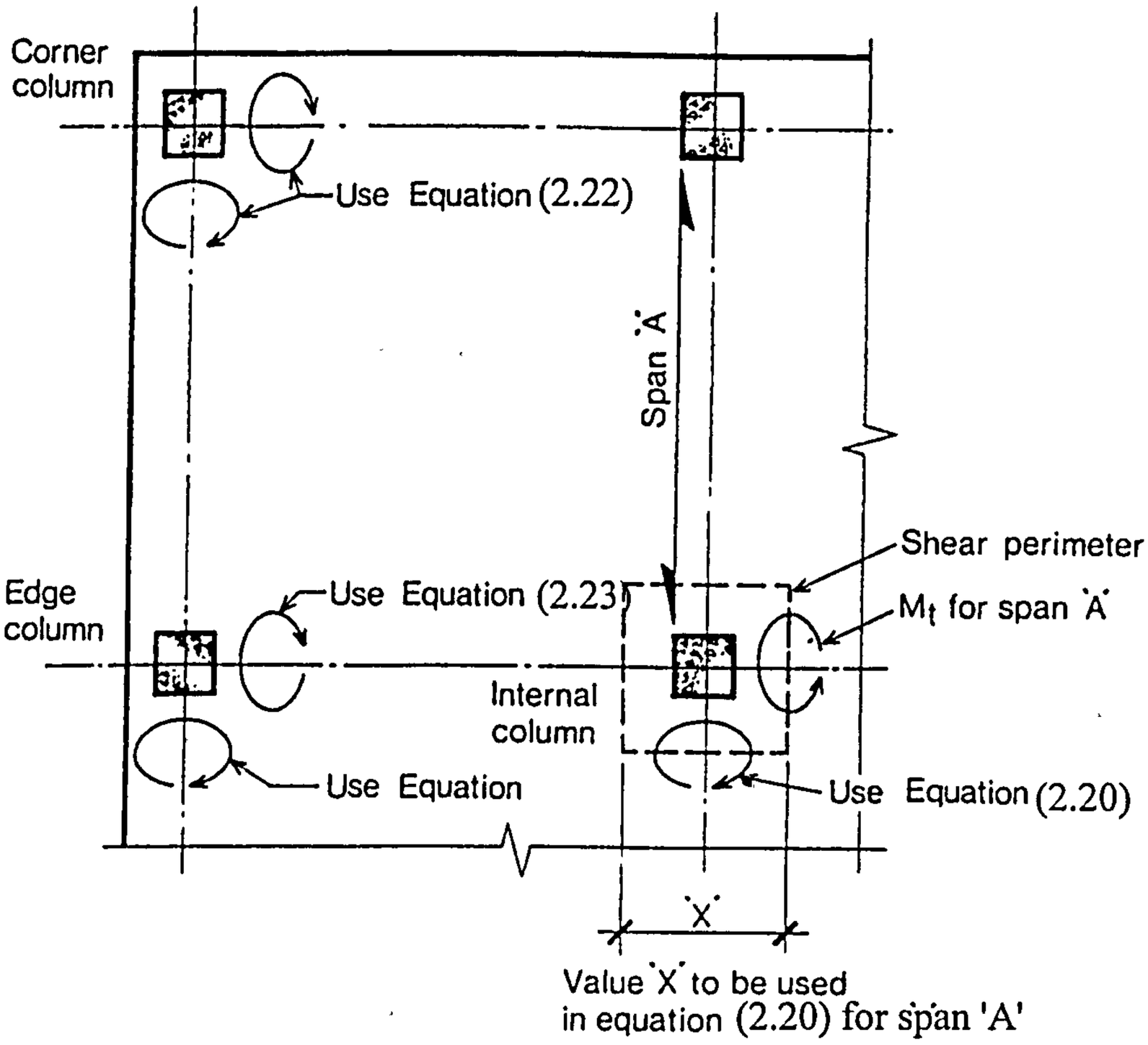

Figure 2.29 Use of effective shear equations for various cases

2.8.3 Shear strength for slab with shear reinforcement

If the shear stress exceeds v_c, shear reinforcement should be provided if the slab thickness is not less than 200mm. Shear reinforcement is to be provided at at-least two perimeters, one close to the control parameter and one not more than 0.5d from the column (Figure 2.30). The shear resistance V_s provided by shear steel is equal to the difference between the applied shear, V and the resistance of concrete alone V_c (i.e. V-V_c). V_s must be greater than (ud×0.4 N/mm^2). Further layers of shear reinforcement are to be provided to reinforce zone further from the column until the applied load is less than the shear resistance calculated from equation 2.18. It is recommended that the calculation should be made in steps with the distance from the column to the control perimeter augmented by 0.75d at each increment as shown in Figure 2.31.

It is helpful to relate the design and detailing of shear links to the various modes of failure in slab with shear reinforcement. In general, there are three types of shear failure as shown in Figure 2.32. These are :-

- failure between the column and the innermost shear reinforcement;
- failure through some or all of the shear reinforcement;
- failure outside the shear reinforcement.

Punching between column and the innermost shear reinforcement : This is generally prevented by positioning the first shear link at a distance of 0.5d from the column face. This forces a steep inclined crack which will enhance the shear resistance.

Failure within the shear reinforcement region : In this region, the shear strength is provided by a combination of component V_c from the concrete and V_s from the shear steel. i.e. $V=V_c + V_s$

V_c = the resistance of a slab without shear reinforcement;

V_s = the resistance of two layer shear steel crossing the inclined surface.

Failure outside shear reinforcement zone : This can be treated by applying equation 2.18 to a control perimeter outside the shear reinforcement region.

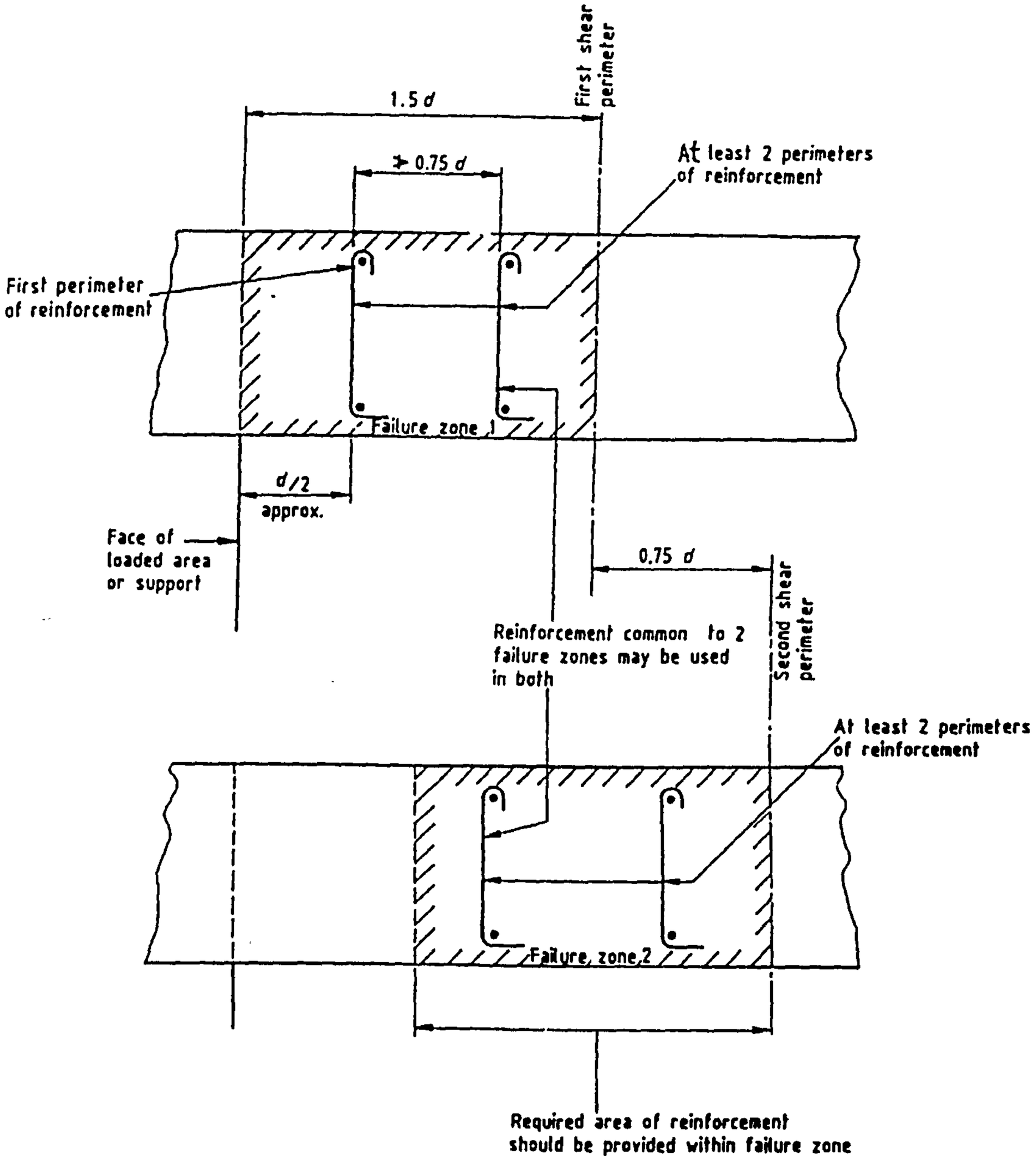

Figure 2.30 Zones for punching shear reinforcement

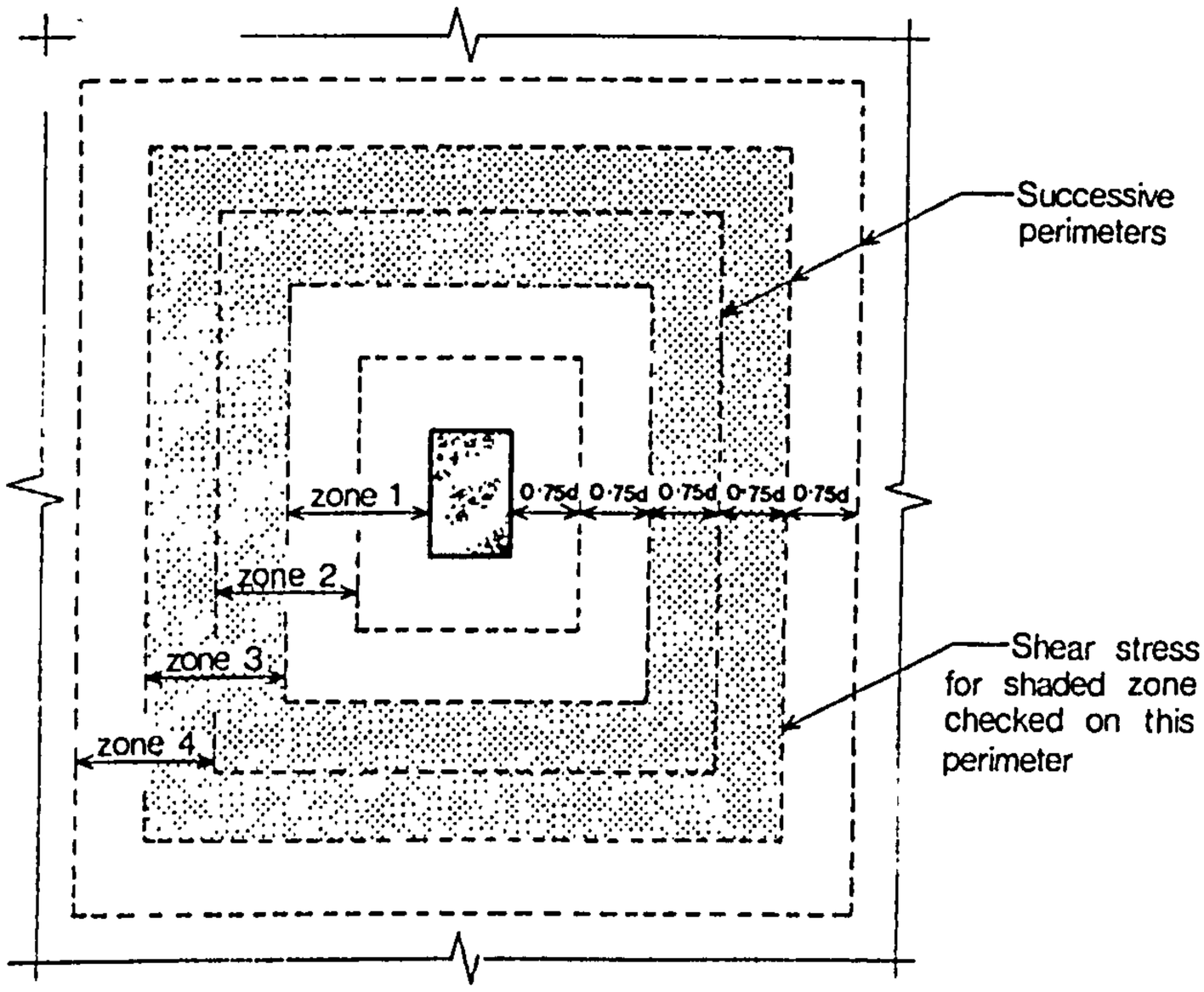

Figure 2.31 Punching shear zone

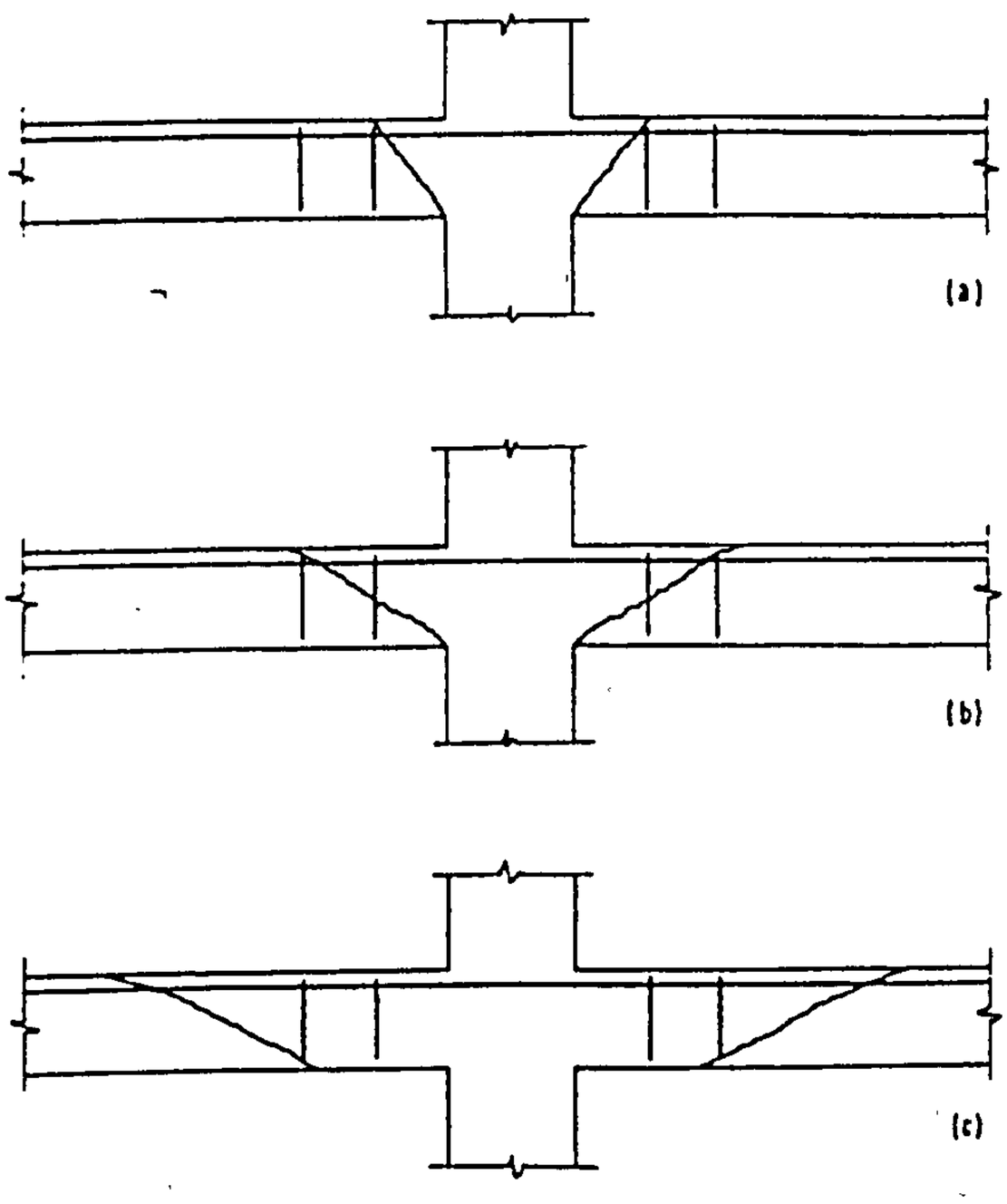

Figure 2.32 Punching in slabs with shear reinforcement

Chapter 3

FINITE ELEMENT AND MATERIAL MODELLING

3.1 Introduction

Finite element method is the most widely used numerical technique in the engineering field. With the advancement in the understanding of material properties of concrete, various constitutive laws and failure criteria have been developed to model the behaviour of concrete. Therefore, an increasing number of researchers are using finite element to study the response of reinforced concrete structures.

Finite element method and material modelling of concrete has been extensively covered in many books (Zienkiewicz O.C. and Taylor R.L. 1989, Bathe K-J. 1996, Hinton E, and Owen D.R.J. 1989, Bangash M.Y.H. 1989, Kotsovos M.D. and Palvlovic M.N. 1995, Chen W.F. 1982), and it is not the purpose of this chapter to review the vast literature in this field. Instead, the objective of this chapter is to describe the features available in the program used in the study.

3.2 Finite Element Method

3.2.1 Discretisation by Finite Elements

In any continuum, the actual number of degrees of freedom is infinite and, unless a closed form solution is available, an exact analysis is impossible. In finite element method, the continuum is divided by imaginary boundaries into elements, the elements are then assumed to be inter-connected at a finite number of nodal points at element corners or on element boundaries. There is no unique way of discretizing a structure. The analyst will have to rely on his experience to choose an appropriate finite element mesh.

For structural applications, the governing equilibrium equations can be obtained by minimising the total potential of the system. The total potential, π, can be expressed as :

$$\pi = 0.5\int_{v} \{\sigma\}^T \{\varepsilon\} dv - \int_{v} \{\delta\}^T \{p\} dv - \int_{s} \{\delta\}^T \{q\} ds - \{P\}\{\delta\}^T \qquad (3.1)$$

where σ and ε are the stress and strain vectors respectively, δ is the displacement at any point, p is the body force per unit volume, q is the applied surface tractions, and P is the concentrated nodal force vector. Integration is carried over the volume v of the

structure and loaded surface area ***s***. The first term on the right hand side of equation (3.1) represents the internal strain energy and the remaining terms are the work contributions of the external forces ***p***, ***q*** and ***P*** respectively.

In the displacement method, the displacement is assumed to have unknown values only at the nodal points so that the variation within any element is described in terms of the nodal values by means of interpolation functions. Thus

$$\{\delta\} = [N].\{\delta^e\} \tag{3.2}$$

where N is the vector of interpolation functions termed as shape functions, and δ^e is the vector of nodal displacements of the element. The strains within the element can be expressed in terms of the element nodal displacement as :

$$\{\varepsilon\} = [B].\{\delta^e\} \tag{3.3}$$

where ***B*** is the strain matrix generally composed of derivatives of shape functions. If the material is elastic, stress, σ may be related to the strains by use of an elasticity matrix ***D*** as :

$$\{\sigma\} = [D]\{\varepsilon\} \tag{3.4}$$

The total potential energy of the continuum will be the sum of the energy contributions of the individual elements. Thus

$$\pi = \sum \pi_e \tag{3.5}$$

where π_e represents the total potential energy of an element ***e***. By using equation (3.1), π_e can be written as follow:

$$\pi_e = 0.5\int_{V_e} \{\delta^e\}^T [B]^T [D]^T [B]\{\delta^e\} dv - \int_{V_e} \{\delta^e\}^T [N]^T \{p\} dv - \int_{S_e} \{\delta^e\}^T [N]^T \{q\} ds \tag{3.6}$$

where V_e is the element volume, s_e is the loaded element surface area. Minimisation of π_e for element ***e*** with respect to the element nodal displacement δ^e results in :

$$\frac{\partial \pi_e}{\partial \delta^e} = \int_{V_e} [B]^T [D]^T [B]\{\delta^e\} dv - \int_{V_e} [N]^T \{p\} dv - \int_{S_e} [N]^T \{q\} ds$$
$$= [K^e]\{\delta^e\} - \{F^e\} = 0 \tag{3.7}$$

where $$\{F^e\} = \int_{V_e} [N]^T \{p\} dv + \int_{S_e} [N]^T \{q\} ds \quad (3.8)$$

are the equivalent nodal forces for the element, and

$$[K^e] = \int_{V_e} [B]^T [D]^T [B] dv \quad (3.9)$$

is termed the element stiffness matrix. The summation of the terms in equation (4.7) over all the elements, when equated to zero, results in a system of equilibrium equations for the complete continuum, i.e.

$$\{F\} = [K].\{\delta\} \quad (3.10)$$

where $\{F\}$ is the equivalent nodal forces for the continuum, $[K]$ is the stiffness matrix of continuum and $\{\delta\}$ is the nodal displacement of the continuum.

These equations are then solved by any standard technique to yield the nodal displacements. Once the displacements are determined, the strains and thereafter the stresses in each element can be evaluated by using equations (3.3) and (3.4) respectively.

3.2.2 Element Choice

The selection of element type is always related to the type of problem to be analysed. As mentioned in section 1.1, some investigators have used two dimensional analysis (plate and shell elements) to study punching shear problem. The plate and shell elements are very attractive on account of both simplicity and economy, but are these elements suitable for the study of punching shear problem the nature of whose behaviour is three dimensional ?.

The main differences between plate element and solid element are as follows:

- The formulation of plate/shell is based on the two principal stress (σ_1 and σ_2), i.e. without σ_3 in the yield criteria (Figure 3.1). This implies that there is no triaxial effect. Punching failure often occurs at location where large bending moment and shear forces are concentrated. The effect of σ_3 could be significant.
- The formulation of plate/shell elements assume that the distribution of strain through the thickness is linear (Figure 3.2). The actual distribution of strain through the thickness of plate is not necessarily linear, and solid element allows non-linear distribution of strain.

Apart from the differences in the formulations, it is difficult to simulate shear reinforcement (steel in z-direction) and column in plate/shell elements. Therefore it is recommended that the study of punching shear problem use three dimensional solid element.

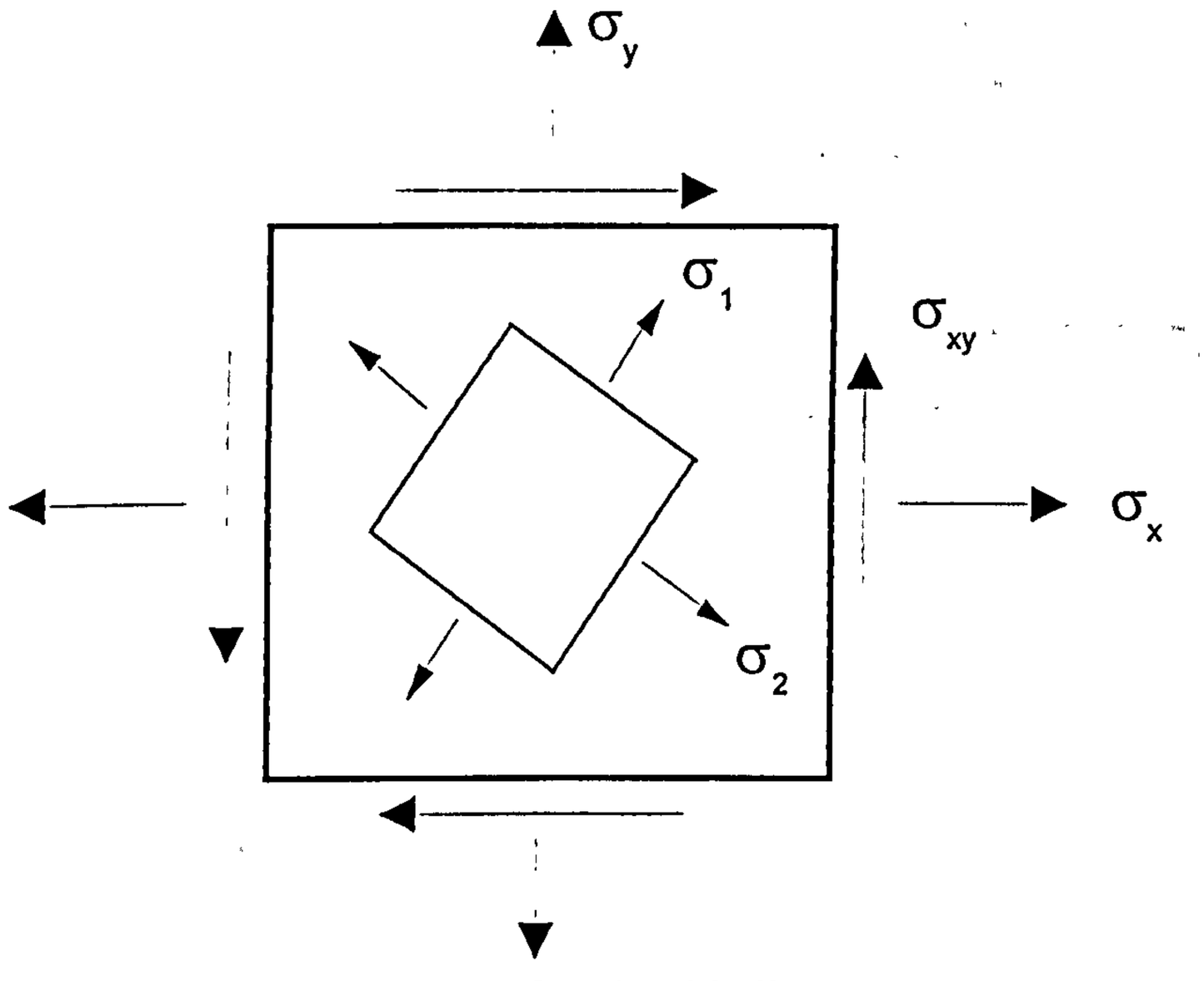

Figure 3.1 Stress resultants for plate/shell

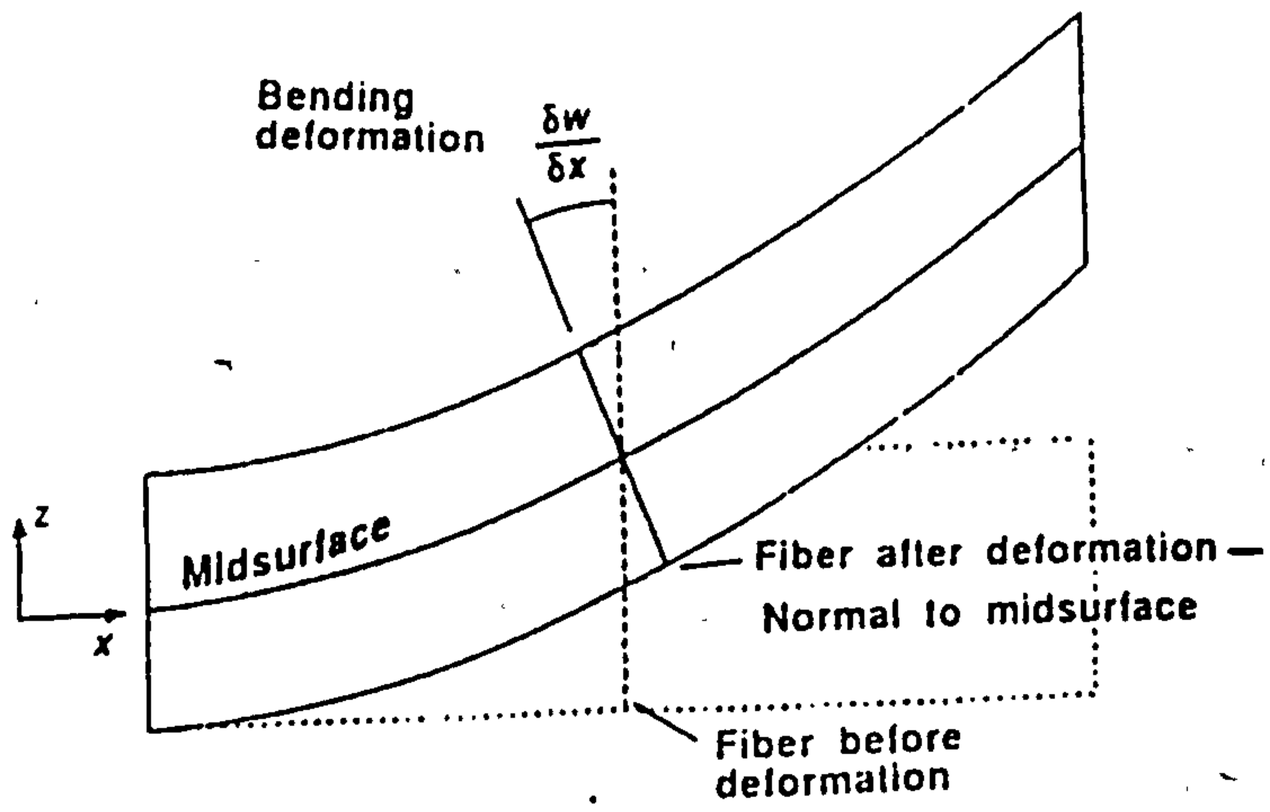

Figure 3.2 Assumption Regarding deformation of a plate/shell

3.2.3 Solid isoparametric element representing concrete

Three most commonly used solid elements are shown in the Figure 3.3. It has been recognised that 8 noded solid elements produce very stiff response and have shear locking problem. While the 32 noded solid element can be quite expensive to

use, involving 96 degrees of freedom and a fairly high order of integration for the element stiffness matrix. Therefore the 20 noded solid isoparametric element is used to represent concrete. Each node has three degrees of freedom. In order to cope with curved boundaries, this program uses an isoparametric element.

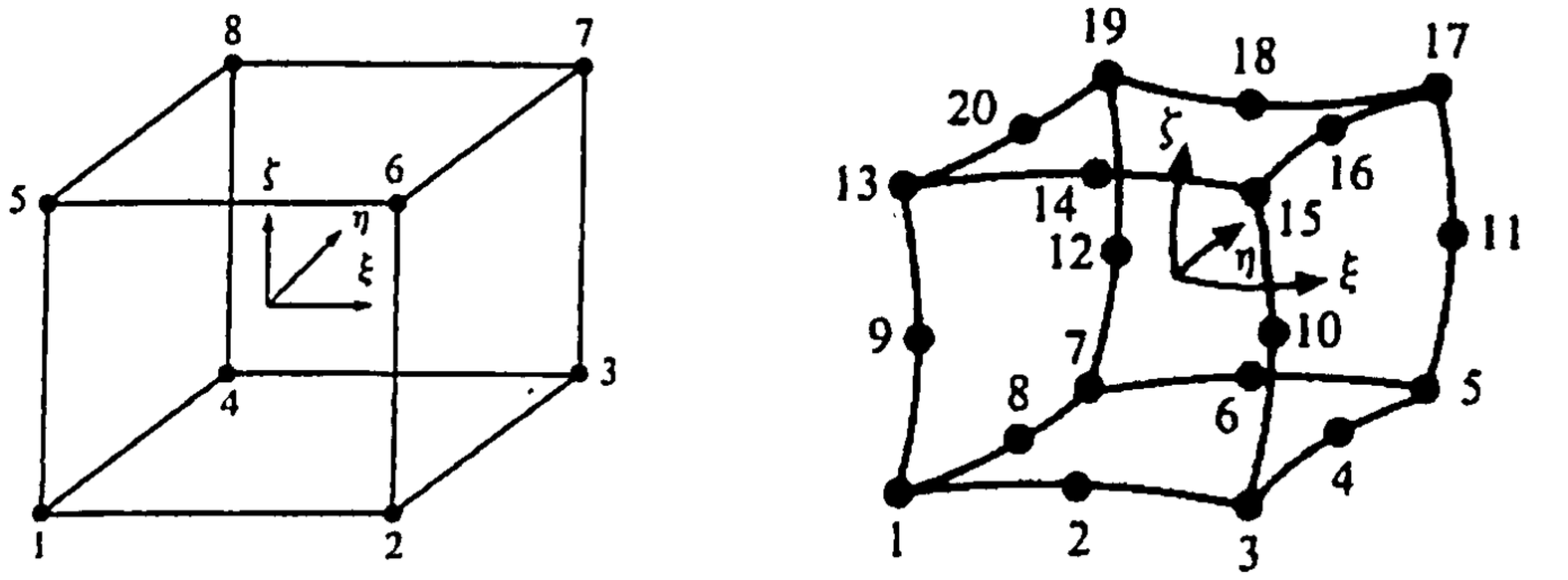

(a) 8 noded

(b) 20 noded

(c) 32 noded

Figure 3.3 Solid isoparametric elements

3.2.3.1 Shape functions

The fundamental property of the shape (interpolation) function N_i is that its value in the natural co-ordinate system is unity at node i and is zero at all other nodes. The shape functions define the variation of the displacement within the element in terms of the nodal displacement.

The efficiency of any particular element type will depend on the how well shape function are capable of representing the true displacement field. Polynomials are often selected as shape functions because they are relatively easy to manipulate mathematically, particularly with regard to integration and differentiation. However, the degree of polynomial chosen will clearly depend on the number of nodes and the degree of freedom associated with the element. The shape function for 20-noded solid element are given by the following equations in curvilinear co-ordinate ξ, η and ζ :

For corner nodes $\xi_i = \pm 1$, $\eta_i = \pm 1$ $\zeta_i = \pm 1$:

$$N_i(\xi,\eta,\zeta) = \frac{1}{8}(1+\xi\xi_i)(1+\eta\eta_i)(1+\zeta\zeta_i)(\xi\xi_i + \eta\eta_i + \zeta\zeta_i - 2) \quad (3.11)$$

For mid-side nodes $\xi_i = \pm 0$, $\eta_i = \pm 1$ $\zeta_i = \pm 1$:

$$N_i(\xi,\eta,\zeta) = \frac{1}{4}(1-\xi^2)(1+\eta\eta_i)(1+\zeta\zeta_i) \quad (3.12)$$

For mid-side nodes $\xi_i = \pm 1$, $\eta_i = \pm 0$ $\zeta_i = \pm 1$:

$$N_i(\xi,\eta,\zeta) = \frac{1}{4}(1+\xi\xi_i)(1-\eta^2)(1+\zeta\zeta_i) \quad (3.13)$$

For mid-side nodes $\xi_i = \pm 1$, $\eta_i = \pm 1$ $\zeta_i = \pm 0$:

$$N_i(\xi,\eta,\zeta) = \frac{1}{8}(1+\xi\xi_i)(1+\eta\eta_i)(1-\zeta^2) \quad (3.14)$$

where ξ, η and ζ are the intrinsic co-ordinates of any point within the element:
The displacement at any point inside the element, namely u, v and w, can be expressed in terms of these shape functions as follows :

20

$$u = \sum_{i=1} N_i(\xi,\eta,\zeta).u_i \quad (3.15)$$

$$v = \sum_{i=1}^{20} N_i(\xi,\eta,\zeta).v_i \quad (3.16)$$

$$w = \sum_{i=1}^{20} N_i(\xi,\eta,\zeta).w_i \quad (3.17)$$

It should be noted that the displacements u, v and w are parallel to the x, y and z, and not to the ξ, η and ζ axis. Similarly, the position at any point within the element in global co-ordinates is given by :

$$x = \sum_{i=1}^{20} N_i(\xi,\eta,\zeta).x_i \quad (3.18)$$

$$y = \sum_{i=1}^{20} N_i(\xi,\eta,\zeta).y_i \quad (3.19)$$

$$z = \sum_{i=1}^{20} N_i(\xi,\eta,\zeta).z_i \quad (3.20)$$

3.2.3.2 Strain Matrix

For the three dimensional element, the strain-displacement relationships in matrix form are given below :

$$[\varepsilon]=\begin{bmatrix}\varepsilon_x\\ \varepsilon_y\\ \varepsilon_z\\ \gamma_{xy}\\ \gamma_{yz}\\ \gamma_{zx}\end{bmatrix}\begin{bmatrix}\partial/\partial x & 0 & 0\\ 0 & \partial/\partial y & 0\\ 0 & 0 & \partial/\partial z\\ \partial/\partial y & \partial/\partial x & 0\\ 0 & \partial/\partial z & \partial/\partial y\\ \partial/\partial z & 0 & \partial/\partial x\end{bmatrix}\begin{bmatrix}u\\ v\\ w\end{bmatrix} \tag{3.21}$$

where ε_x, ε_y, ε_z are the normal strain components and γ_{xy}, γ_{yz}, γ_{zx} are the shear strain components. Using the finite element idealisation, matrix (3.21) can written as :

$$[\varepsilon]=\sum_{i=1}^{20}\begin{bmatrix}\partial N_i/\partial x & 0 & 0\\ 0 & \partial N_i/\partial y & 0\\ 0 & 0 & \partial N_i/\partial z\\ \partial N_i/\partial y & \partial N_i/\partial x & 0\\ 0 & \partial N_i/\partial z & \partial N_i/\partial y\\ \partial N_i/\partial z & 0 & \partial N_i/\partial x\end{bmatrix}\begin{bmatrix}u_i\\ v_i\\ w_i\end{bmatrix} \tag{3.22}$$

or simply expressed as

$$[\varepsilon]=\sum_{i=1}^{20}[B_i].[\delta_i] \tag{3.23}$$

where $[B_i]$ is the 6 x 3 strain matrix in equations (3.22) which contains the cartesian derivatives of the shape functions. Since the shape functions N_i are defined in terms of the local co-ordinates of the element (ξ, η, ζ), a transformation from local to global co-ordinates is required to obtain the $[B]$ matrix in equation (3.22). This is done through the well known Jacobian matrix which is written as :

$$[J]=\begin{bmatrix}\partial x/\partial\xi & \partial y/\partial\xi & \partial z/\partial\xi\\ \partial x/\partial\eta & \partial y/\partial\eta & \partial z/\partial\eta\\ \partial x/\partial\zeta & \partial y/\partial\zeta & \partial z/\partial\zeta\end{bmatrix} \tag{3.24}$$

thus

$$[J]=\sum_{i=1}^{20}\begin{bmatrix}\frac{\partial N_i}{\partial \xi}.x_i & \frac{\partial N_i}{\partial \xi}.y_i & \frac{\partial N_i}{\partial \xi}.z_i\\ \frac{\partial N_i}{\partial \eta}.x_i & \frac{\partial N_i}{\partial \eta}.y_i & \frac{\partial N_i}{\partial \eta}.z_i\\ \frac{\partial N_i}{\partial \zeta}.x_i & \frac{\partial N_i}{\partial \zeta}.y_i & \frac{\partial N_i}{\partial \zeta}.z_i\end{bmatrix} \tag{3.25}$$

the inverse of the Jacobian matrix will be

$$[J]^{-1}=\begin{bmatrix}\frac{\partial \xi}{\partial x} & \frac{\partial \eta}{\partial x} & \frac{\partial \zeta}{\partial x}\\ \frac{\partial N_i}{\partial y} & \frac{\partial N_i}{\partial y} & \frac{\partial \zeta}{\partial y}\\ \frac{\partial N_i}{\partial z} & \frac{\partial N_i}{\partial z} & \frac{\partial \zeta}{\partial z}\end{bmatrix} \tag{3.26}$$

therefore the cartesian derivatives are given by

$$\begin{bmatrix}\frac{\partial N_i}{\partial x}\\ \frac{\partial N_i}{\partial y}\\ \frac{\partial N_i}{\partial z}\end{bmatrix} = [J]^{-1}\begin{bmatrix}\frac{\partial N_i}{\partial \xi}\\ \frac{\partial N_i}{\partial \eta}\\ \frac{\partial N_i}{\partial \zeta}\end{bmatrix} \tag{3.27}$$

3.2.3.3 Stress-Strain Relationship

For the linear analysis of uncracked concrete, the stress-strain relationship may be expressed in the following form :

$$\{\sigma\}=[D].\{\varepsilon\} \tag{3.28}$$

where [D] is the elasticity matrix given by :

$$[D]=\frac{E(1-\nu)}{(1+\nu)(1-2\nu)}\begin{bmatrix}1 & \frac{\nu}{(1-\nu)} & \frac{\nu}{(1-\nu)} & 0 & 0 & 0\\ & 1 & \frac{\nu}{(1-\nu)} & 0 & 0 & 0\\ & & 1 & 0 & 0 & 0\\ & \textit{symmetry} & & \frac{(1-2\nu)}{2(1-\nu)} & & \\ & & & & \frac{(1-2\nu)}{2(1-\nu)} & \\ & & & & & \frac{(1-2\nu)}{2(1-\nu)}\end{bmatrix} \tag{3.29}$$

where E is the Young's modulus of elasticity, and ν is the Poisson's ratio. The cracking and crushing of concrete are the major sources of nonlinearity in most reinforced concrete structures. All changes in material properties due to cracking and crushing are taken into account in a new elasticity matrix. This will be discussed later in section 3.3.4.

3.2.4 Embedded line element representing reinforcement

Steel bars are simulated by line elements embedded in the concrete element at specified locations in the structure. A three -noded line element corresponds to the 20 noded solid element used in the present study. This line element can carry axial load only. The line element must lie parallel to one of the curvilinear axis (ξ,η,ζ) of the solid element as shown in Figure 3.4. This line element can be anywhere in the solid element with maximum curvilinear co-ordinates ξ=±1, η=±1 and ζ =±1.

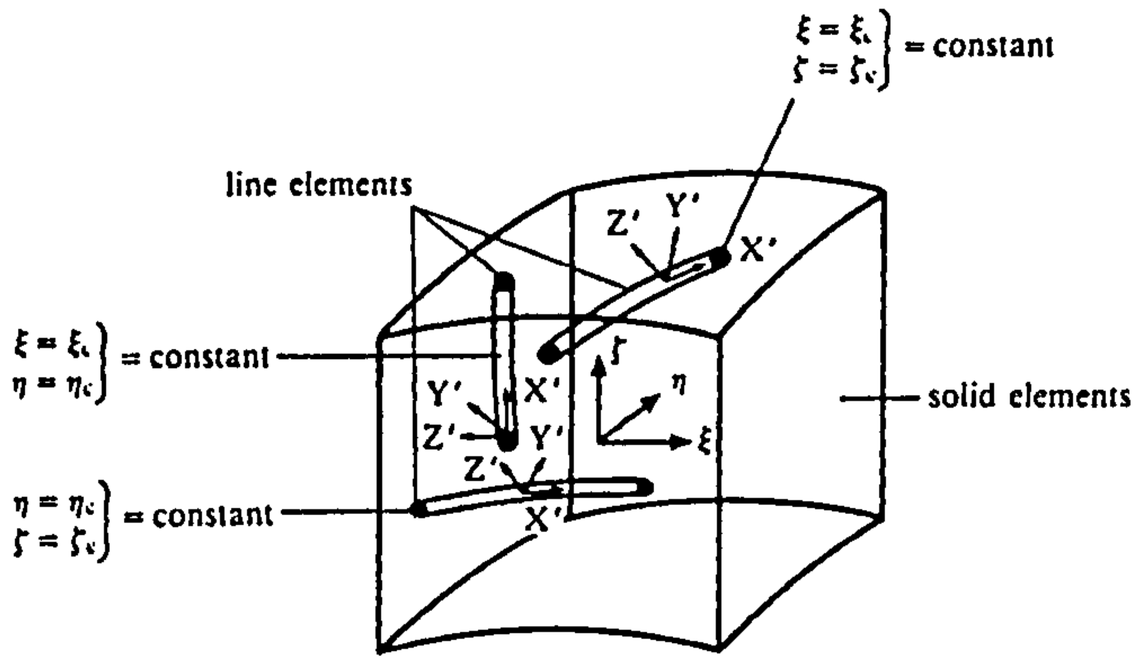

Figure 3.4 : Embedded reinforcement in 3D concrete element

The displacement {u} of any point on the bar is written as :

$$\{u\} = [\bar{N}]\{\delta\}^e$$

$$[\bar{N}] = [N(\xi, \eta_c, \zeta_c)] \qquad (3.30)$$

such that

$$\eta = \eta_c \,, \qquad \zeta = \zeta_c \text{ (constant)}$$

where N is the shape function of concrete element and $\{\delta\}^e$ is the nodal displacement vector.

The virtual work of the line element (steel bar) can be written as :

$$\delta U = A_s \int_l \delta\varepsilon_l . \sigma_l . dl \qquad (3.31)$$

where dU = internal virtual work in the steel bar;

A_S = cross-sectional area of steel bar;

dl = line segment along the steel bar; and

σ_l, ε_l = the longitudinal stress and strain along line segment, respectively.

For a horizontal bar parallel to the x-axis,

$$\sigma_l = \sigma_x$$
$$\varepsilon_l = \varepsilon_x$$
$$dl = dx$$

Equation (3.31) becomes

$$\delta U = A_s \int_x \delta\varepsilon_x . \sigma_x . dx \qquad (3.32)$$

At any point in the line element, the local Cartesian axis X' is tangential to the curvilinear axis. The local strain in the steel bar can be calculated as follows:

$$\varepsilon_x = \frac{\partial u'}{\partial X'}$$

where X', Y' and Z' are local co-ordinates at a point, and u', v' and w' are the corresponding displacements.

Using the displacement transformation,

$$\varepsilon_x = \frac{1}{L}\left(l_1 \frac{\partial u}{\partial \xi} + m_1 \frac{\partial v}{\partial \xi} + n_1 \frac{\partial w}{\partial \xi}\right)$$

where l_1, m_1, n_1 are the direction cosines of the X' axis and are written as

$$l_1 = \frac{\partial x}{\partial \xi} \Big/ L$$

$$m_1 = \frac{\partial y}{\partial \xi} \Big/ L$$

$$m_1 = \frac{\partial z}{\partial \xi} \Big/ L$$

$$L = \sqrt{(\partial x/\partial \xi)^2 + (\partial y/\partial \xi)^2 + (\partial z/\partial \xi)^2}$$

In terms of the shape function deriatives is written as

$$\{\varepsilon_x\} = \frac{1}{L}\sum_{1}^{n} \left[l_1 \frac{\partial N_i}{\partial \xi}, m_1 \frac{\partial N_i}{\partial \xi}, n_1 \frac{\partial N_i}{\partial \xi} \right] \begin{Bmatrix} u_i \\ v_i \\ w_i \end{Bmatrix}$$

The strain in steel can be written as

$$\varepsilon = B\delta^e$$

$$\delta\varepsilon = B\delta(\delta^e)$$

where B is the nodal displacement-strain matrix. The relation between the stress and strain in the steel bar is :

$$\sigma = E_s\varepsilon$$

And the stiffness of the embedded bar can be expressed as :

$$K_s = A_s E_s \int_x B^T B dx$$

$$dx = \frac{dx}{d\xi} d\xi = J_s . d\xi$$

$$K_s = A_s E_s \int_{-1}^{1} B^T B \frac{d\xi}{J_s} \qquad (3.33)$$

where E_S is the Young's modulus of steel bar and J_S is the Jacobian for steel element. The same steps can be repeated for bars parallel to y and z axis.

The final expression for the composite element stiffness is simply evaluated by adding the stiffness matrices for concrete and steel together, as follows :

$$K_e = K_c + K_s \qquad (3.34)$$

where K_e is the stiffness matrix for the composite element, K_C and K_S are the element concrete and steel stiffness matrices respectively.

3.2.5 Numerical Integration

The element stiffness matrix, $[K^e]$, in equation (3.9) is given by :

$$[K^e] = \int_{V_e} [B]^T [D][B] dv$$

Since it is difficult or perhaps impossible to perform the closed form integration, some form of numerical integration is essential. In this study, Gauss-Legendre quadrature rules have been used because of their higher efficiency over other forms of quadrature. These rules are particularly suitable for isoparametric elements since the limits of integration are ±1 which coincide with the local co-ordinate system ±1 on element boundary. A 3×3×3 gauss rule is adopted in the present study.

3.3 Material modelling

In this study, the behaviour of concrete is assumed to be non-linear-elastic isotropic while the current state of stress does not violate the strength envelope based on the concrete model developed by Kotsovos (1979a & 1979b). After cracking, smeared crack approach with simple tension stiffening and shear retention equations are employed to mimic the post-cracking behaviour of concrete. Standard elastic-plastic (with/without hardening) material model is used to describe the behaviour of the steel reinforcement. The stress-strain relationships for steel in compression and tension are assumed to be identical and only uniaxial behaviour is assumed.

3.3.1 Modelling of concrete

Modelling of reinforced concrete in non-linear finite element analysis is not straight forward, because of the complexities involved in the behaviour of concrete. Experimental evidence shows that the behaviour of concrete is non-linear even for low stress levels. The significant non-linear behaviour of concrete is mainly due to various forms of softening behaviour, especially cracking because it occurs at a low level of loading. So, an appropriate finite element model of cracking is essential to get satisfactory results.

A concrete structure is generally under the action of multiaxial stress state. Under certain stress combinations, concrete can carry loads that are considerably in excess uniaxial cube crushing strength. However, under other stress combinations, it is possible that the concrete will fail even though the stress acting is lower than uniaxial cube crushing strength. Thus, a proper description of the multiaxial behaviour of concrete is a key factor for a successful analysis. A brief summary of multi-axial behaviour of concrete is given in this section.

3.3.1.1 Uni-axial stress

Typical stress strain curves of concrete in uniaxial compression under monotonic short term loading are shown in Figure 3.6. Under this condition, concrete has a nearly linear-elastic behaviour up to some fraction of the compressive strength. There after, the strain increases rapidly with stress up to cylinder compressive strength at a strain of about 0.002, beyond which the stress-strain curve has a descending part until crushing failure occurs at some ultimate strain. Thus concrete has limited ductility in compression. The higher the concrete strength, the steeper are both the ascending and the descending portions of the curve.

The ratio of the uniaxial tensile strength to compressive strength may vary considerably but usually ranges from 0.05 to 0.1. The uniaxial tensile stress-strain relationship is almost linear up to a relatively high level (See Figure 3.5). The shape of curve shows many similarities to the uniaxial-compression curve.

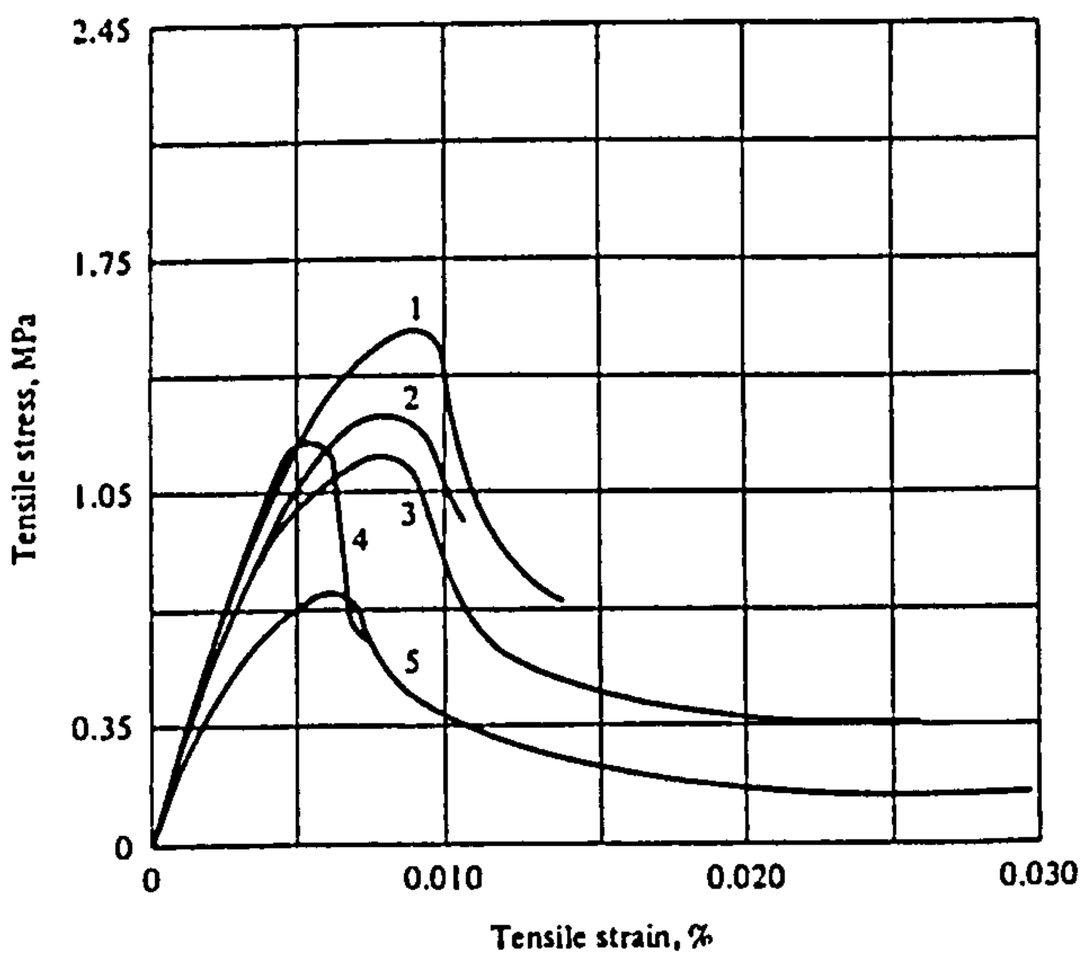

Figure 3.5 Uniaxial tensile stress-strain curves

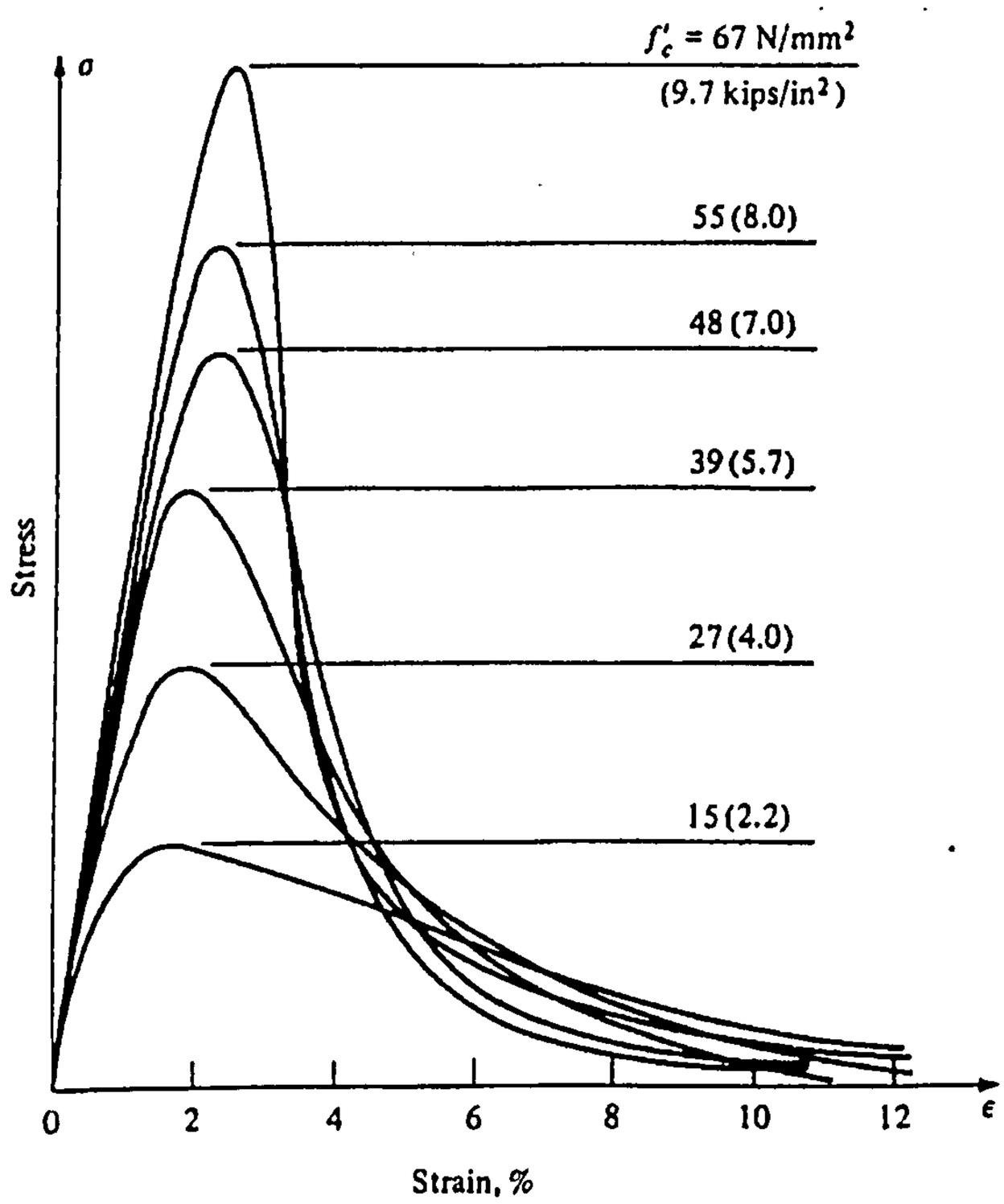

Figure 3.6 Uniaxial compressive stress-strain curve for different strength of concrete

3.3.1.2 Bi-axial stress

Under biaxial stresses, the work by Kupfer et al (1969) is often employed to describe the behaviour of concrete. Figure 3.7 shows the strength in the principal directions compared with the uniaxial strength. One of the conclusions of Kupfer et al is that the strength of concrete subjected to biaxial compression may be up to 27% higher than the uniaxial compressive strength. The compressive strength of concrete however decreases with the applied tensile stress under biaxial compression-tension as shown in Figure 3.8b. Under bi-axial tension, the tensile strength is not much different from uniaxial tensile strength (Figure 3.8c).

3.3.1.3 Tri-axial stress

Although many triaxial test results are available in the literature, most of them are test results for tri-axial compression and little information exists for the stress state in which at least one stress is tensile.

In triaxial state of stress, the strength of concrete can increase considerably above the uniaxial strength, in particular under hydrostatic stress conditions. Figures 3.9 and 3.10 show stress-strain curves from tests by Hobbs et al (1977) and Attard and Setunge (1996). The tests were conducted under different confining pressures. All the stress-strain curves basically followed a similar pattern. The initial tangent modulus was approximately the same for all confining pressure, with linear portion of the ascending curve extended with increasing confining pressure. The peak strength increased with increasing confining pressure. These two graphs also show that different stress states can affect the ultimate strains of the test specimens.

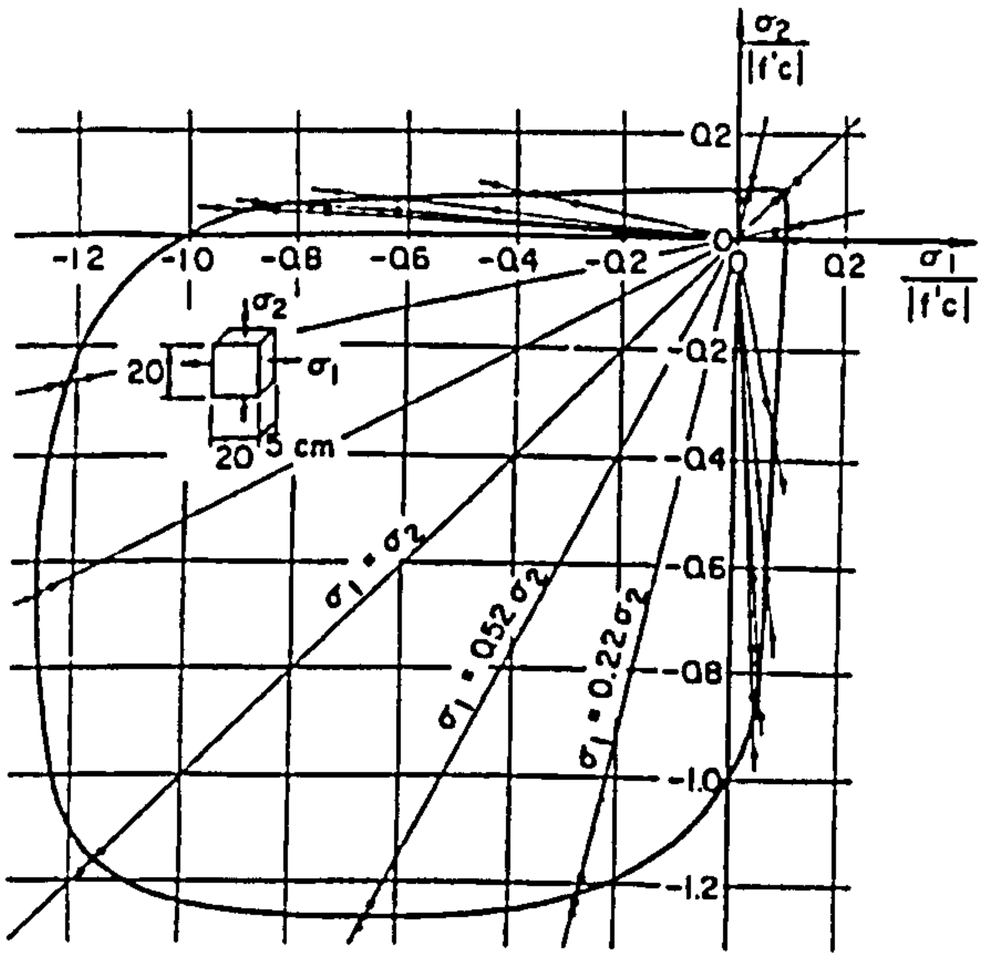

Figure 3.7 Biaxial strength envelope of concrete (Kufer and Hilsdorf, 1969)

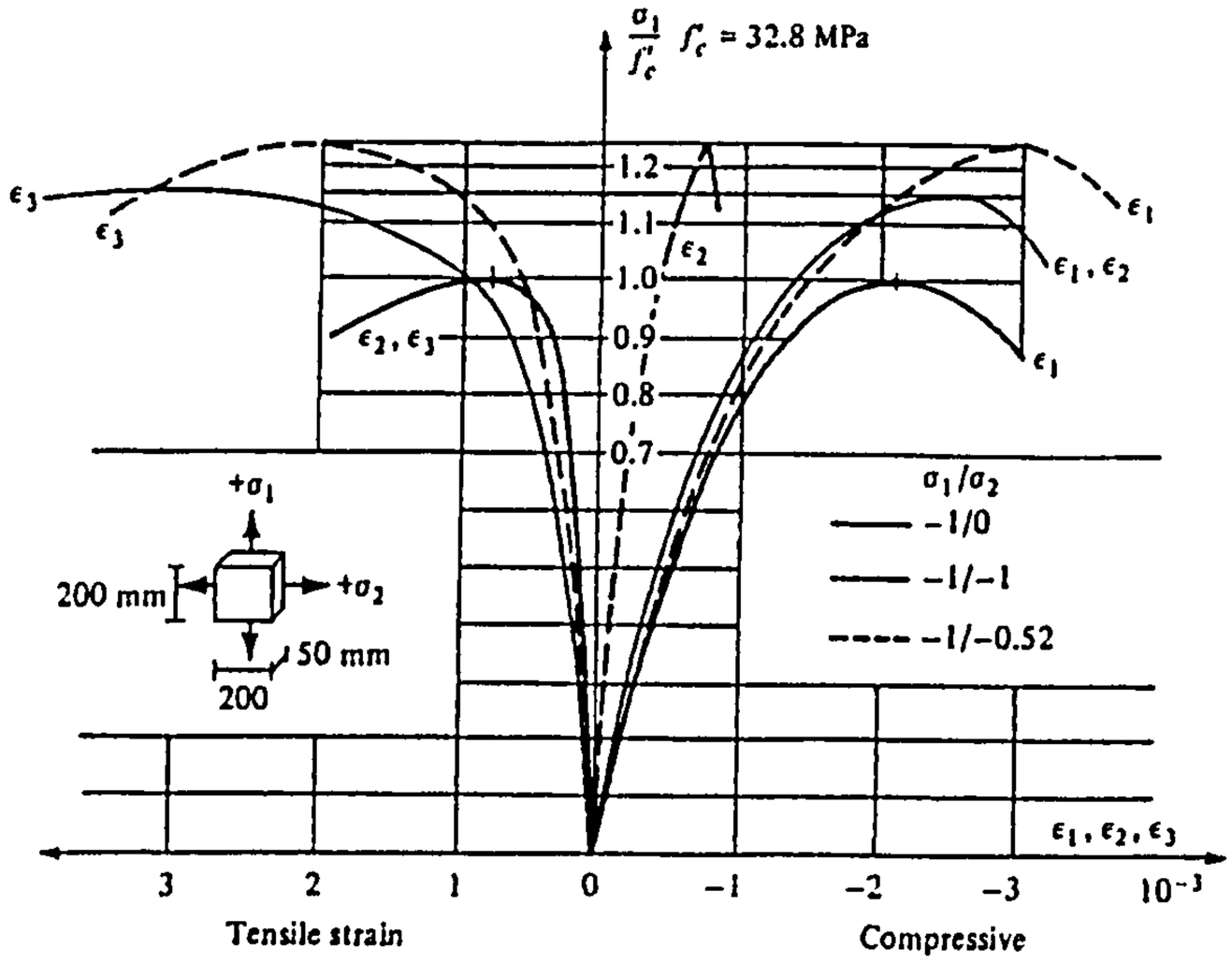

(a) Compression-compression

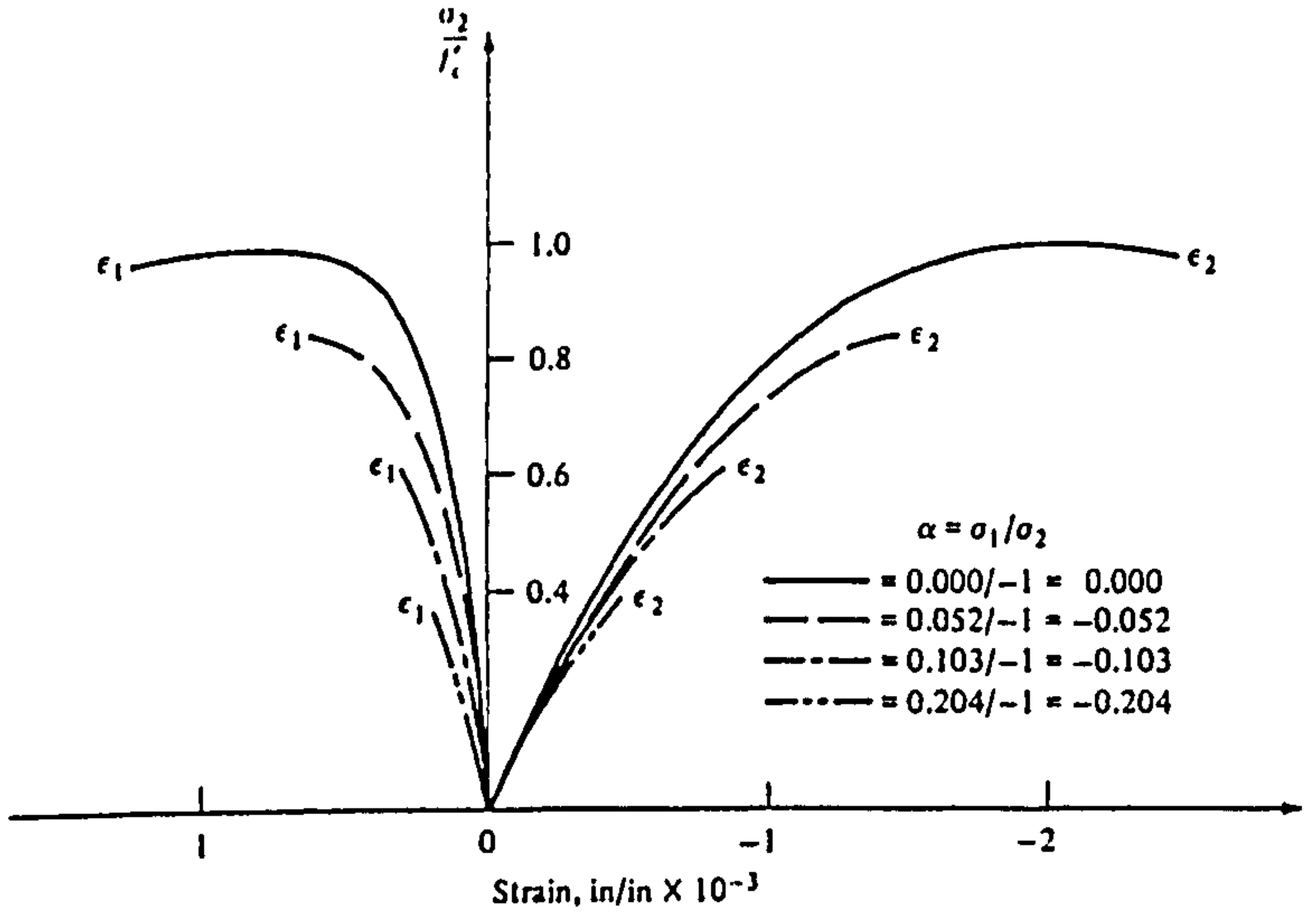

(b) Compression-tension

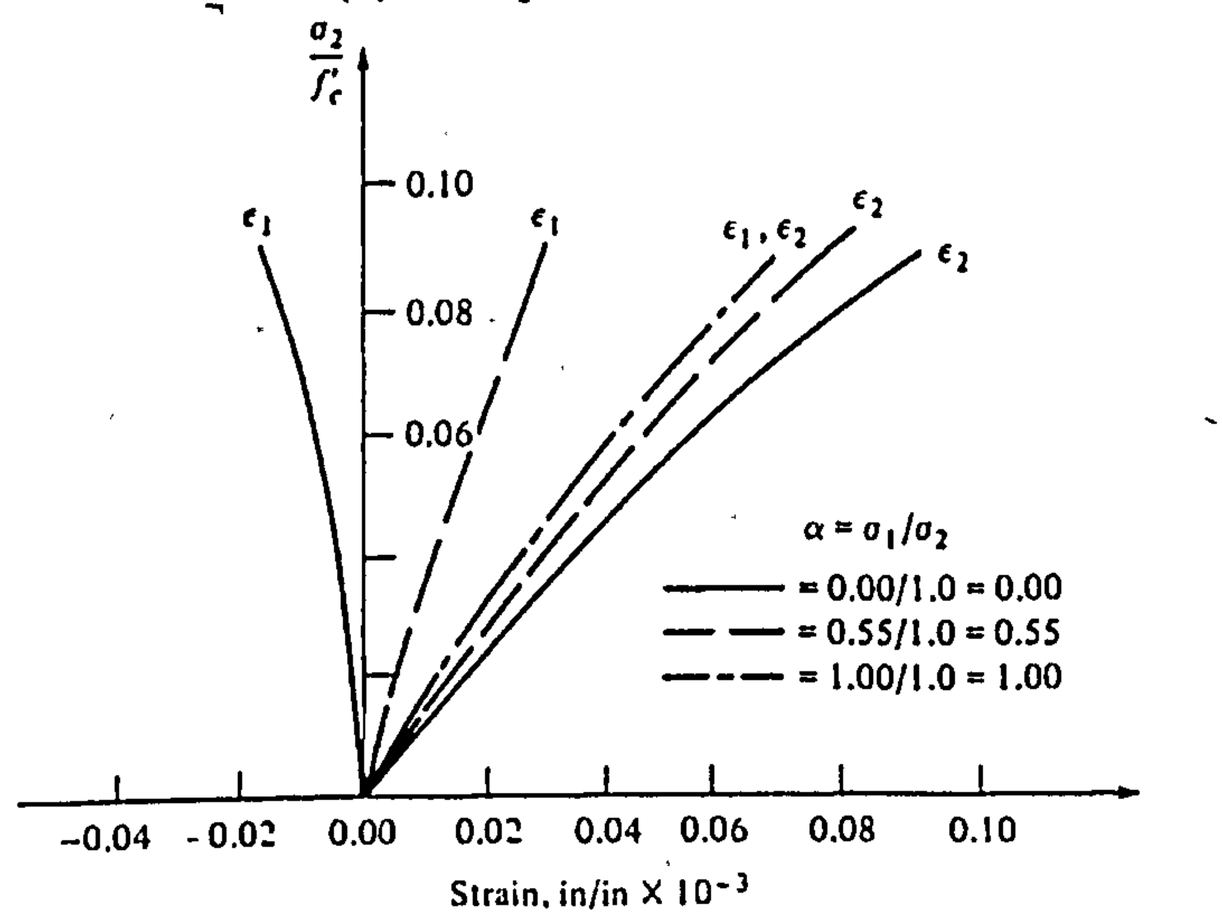

(c) Tension-tension

Figure 3.8 Stress-strain curve of concrete for biaxial stress

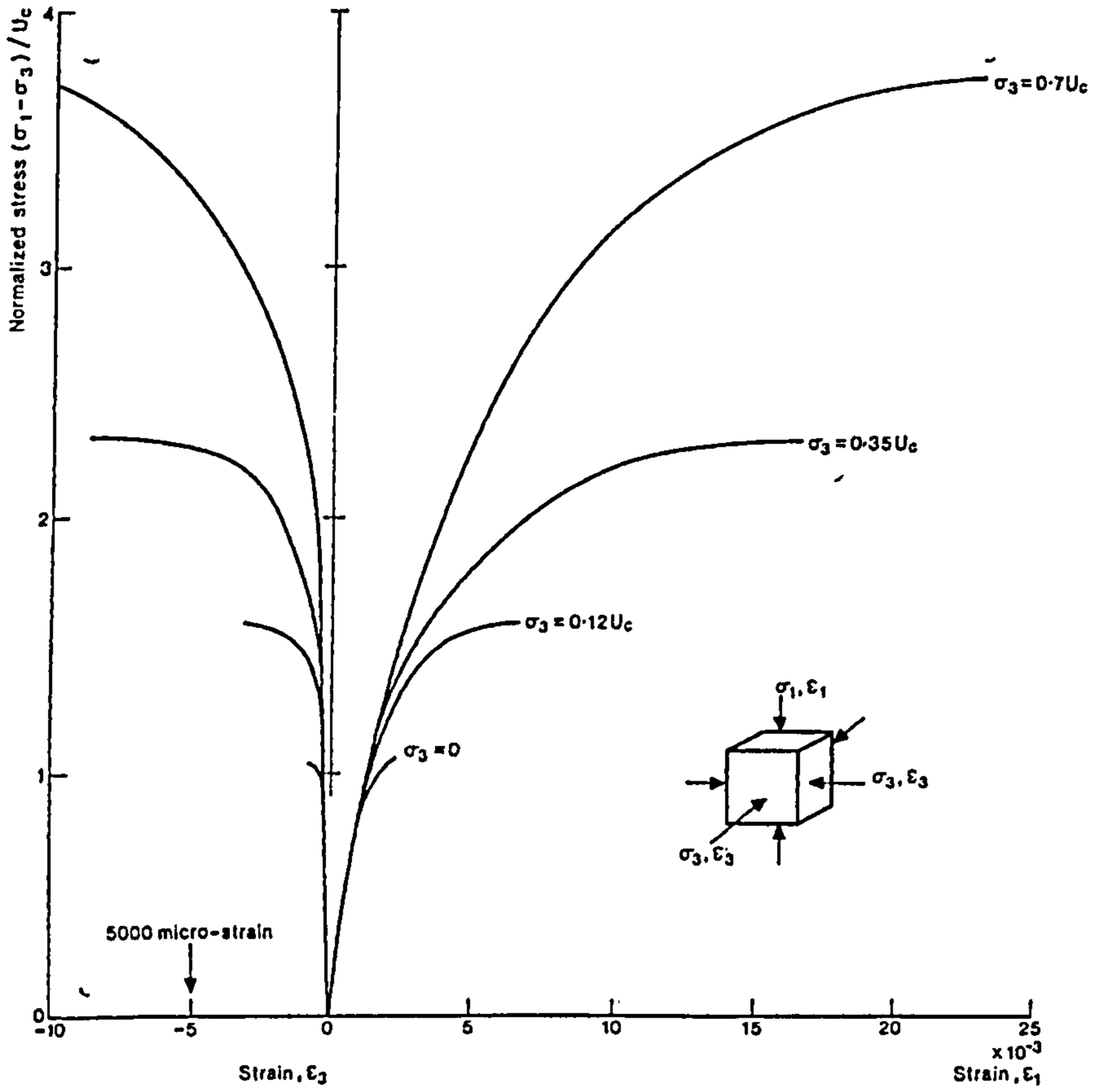

Figure 3.9 Stress-strain curve of concrete under triaxial compression ($U_c=f_{cu}$)

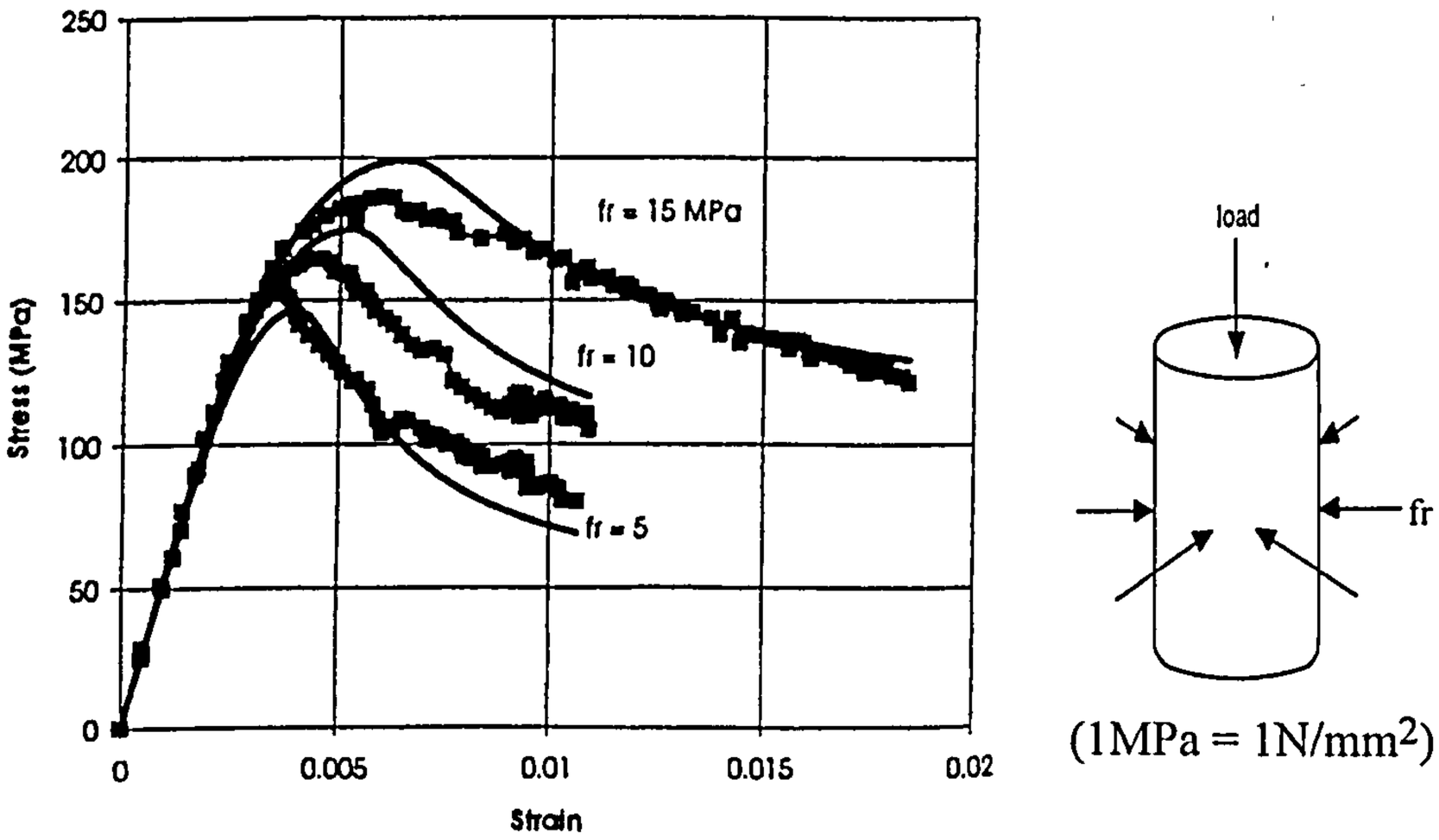

(1MPa = 1N/mm^2)

Figure 3.10 Stress-strain curve of concrete for different confining pressures

3.3.2 Kotsovos' Concrete model

The mechanical properties of the non-linear elastic isotropic model proposed by Kotsovos was based on experimental data obtained at Imperial College London from tests on the behaviour of concrete under complex stress states (Kotsovos, 1979a&197b). The testing techniques used to obtain this data, have been validated by comparing them with those obtained in an international co-operative programme of research into the effect of different test methods on the behaviour of concrete. The main reason why this model is chosen for this study is because it shows good correlation with the experimental data and its capability to describe the behaviour of concrete under uniaxial, biaxial and triaxial stress conditions. This model is intended for concrete subjected to monotonic short-term loading and applicable to concrete with unixial cylinder compressive strength (f_c') range from 15 to 65 N/mm^2.

The main features of this model are as follows:

- it needs only one parameter to define the behaviour of the concrete under different stress states;
- it consists only of ascending branch in compression (i.e no softening in compression);
- it considers the effect of volume dilation of concrete just before the peak stress level.

3.3.2.1 State of stress at a point

The state of stress at a point is expressed in terms of the principal stresses σ_1, σ_2, σ_3. If the orthogonal co-ordinate system $\sigma_1,\sigma_2,\sigma_3$ is transformed into a cylindrical co-ordinate system q, r, θ such that q coincides with the space diagonal ($\sigma_1=\sigma_2=\sigma_3$) of the original system, r and θ are the radius and rotational variables respectively on the plane perpendicular to the axis q (octahedral plane). The two co-ordinate systems are related by the following equations:

$$q = \frac{(\sigma_1+\sigma_2+\sigma_3)}{\sqrt{3}} \tag{3.35a}$$

$$r = \frac{1}{\sqrt{3}}\sqrt{(\sigma_1-\sigma_2)^2+(\sigma_2-\sigma_3)^2+(\sigma_3-\sigma_1)^2} \tag{3.35b}$$

$$\cos\theta = \frac{1}{r\sqrt{6}}(\sigma_1+\sigma_2-2\sigma_3) \tag{3.35c}$$

The variable q and r are related to the hydrostatic and deviatoric components respectively, where as the variable θ defines the direction of the deviatoric component on the octahedral plane. The q and r components can be expressed in terms of the normal (σ_o) and shear (τ_o) octahedral stresses, which are defined as follows:

$$\sigma_o = \frac{(\sigma_1 + \sigma_2 + \sigma_3)}{3} = \frac{q}{\sqrt{3}} \qquad (3.36a)$$

$$\tau_o = \frac{1}{3}\sqrt{(\sigma_1 - \sigma_2)^2 + (\sigma_2 - \sigma_3)^2 + (\sigma_3 - \sigma_1)^2} = \frac{r}{\sqrt{3}} \qquad (3.36b)$$

Similarly, the octahedral normal (ε_o) and shear (γ_o) strains are defined as follows :

$$\varepsilon_o = \frac{(\varepsilon_1 + \varepsilon_2 + \varepsilon_3)}{3} \qquad (3.37a)$$

$$\gamma_o = \frac{1}{3}\sqrt{(\varepsilon_1 - \varepsilon_2)^2 + (\varepsilon_2 - \varepsilon_3)^2 + (\varepsilon_3 - \varepsilon_1)^2} \qquad (3.37b)$$

where ε_1, ε_2, ε_3 are the principal strains.

For the deformational properties, use has been made of the secant bulk (K_S) and secant shear (G_S) moduli expressed as follows :

$$K_s = \frac{\sigma_o}{3\varepsilon_o} \qquad (3.38a)$$

$$G_s = \frac{\tau_o}{2\gamma_o} \qquad (3.38b)$$

3.3.2.2 Deformational Properties

The deformational behaviour of concrete under increasing stress can be completely described by the relationship between:

(a)- hydrostatic stress ,σ_o, and volumetric strain ,ε_{oh},

(b)- deviatoric stress ,τ_o, and deviatoric strain , γ_o,

(c)- deviatoric stress ,τ_o, and volumetric strain ,ε_{od}, (under deviatoric stress).

(Note that for metals, ε_{od} is not affected by τ_o, but this may not be so for other materials which exhibit volume dilation under shear stress)

The σ_o - ε_{oh} and τ_o, - γ_o relationship can be described by the mechanical properties of the model as follows:

$$\frac{K_s}{K_o} = \frac{1}{1 + A\left(\frac{\sigma_o}{f_c'}\right)^{b-1}} \quad \text{for } \frac{\sigma_o}{f_c'} < 2, \text{ or}$$

$$\frac{K_s}{K_o} = \frac{1}{1 + 2^{b-1}bA - 2^b(b-1)A\left(\frac{\sigma_o}{f_c'}\right)^{-1}} \quad \text{for } \frac{\sigma_o}{f_c'} \geq 2 \tag{3.39}$$

$$\frac{G_s}{G_o} = \frac{1}{1 + C\left(\frac{\tau_o}{f_c'}\right)^{d-1}} \tag{3.40}$$

where K_O and G_O (in kN/mm^2) are the initial values of the moduli K_S and G_S, and A, b, C, d are parameters which depend on the material properties such that:

$$K_o = 11.0 + 0.0032(f_c')^2$$

$$G_o = 9.224 + 0.136 f_c' + 3.296 \times 10^{-15}(f_c')^{8.273}$$

$$A = 0.516 \qquad \text{for } f_c' \leq 31.7 \, N/mm^2, \text{ and}$$

$$A = \frac{0.516}{1.0 + 0.0027(f_c' - 31.7)^{2.397}} \qquad \text{for } f_c' > 31.7 \, N/mm^2$$

$$b = 2.0 + 1.81 \times 10^{-8}(f_c')^{4.461} \tag{3.41}$$

$$C = 3.573 \qquad \text{for } f_c' \leq 31.7 \, N/mm^2, \text{ and}$$

$$C = \frac{3.573}{1.0 + 0.0134(f_c' - 31.7)^{1.414}} \qquad \text{for } f_c' > 31.7 \, N/mm^2$$

$$d = 2.12 + 0.0183 f_c' \qquad \text{for } f_c' > 31.7 \, N/mm^2, \text{ and}$$

$$d = 2.7 \qquad \text{for } f_c' \leq 31.7 \, N/mm^2$$

In order to evaluate the effect of internal stresses on deformation, use is made of the artificial concept that the volumetric strain (ε_{od}) under deviatoric stress is due to the hydrostatic component of such stresses so that

$$\sigma_{int} = 3K_s\varepsilon_{od} \tag{3.42}$$

the τ_o - ε_{od} relationship was expressed in a non-dimensionalised form as follows:

$$\frac{\sigma_{int}}{f_c'} = M\left(\frac{\tau_o}{f_c'}\right)^{d_1} \tag{3.43}$$

where

$$M = \frac{k}{1+d_2\left(\sigma_o/f_c'\right)^{d_3}} \tag{3.44}$$

$$k = \frac{4.0}{1.0+1.087(f_c'-15.0)^{0.23}}$$

$d_1 = 1.0$ for $f_c' \le 31.7\ N/mm^2$, and

$d_1 = 0.3124 + 0.0217 f_c'$ for $f_c' > 31.7\ N/mm^2$

$$d_2 = 0.222 + 0.01086 f_c' - 0.000122(f_c')^2 \tag{3.45}$$

$d_3 = -2.415$ for $f_c' \le 31.7\ N/mm^2$, and

$d_3 = -3.5308 + 0.0352 f_c'$ for $f_c' > 31.7\ N/mm^2$

The hydrostatic component (σ_{int}) is equivalent to the three principal stresses, $\sigma_1 = \sigma_2 = \sigma_3 = \sigma_{int}$, and its effect on deformation will be the deformational response of the model under these principal stresses.

Equations (3.41) and (3.42) when used with equation (3.40), the total octahedral normal strain will be

$$\varepsilon_o = \varepsilon_{oh} + \varepsilon_{od} \tag{3.46}$$

3.3.2.3 Strength properties of concrete

The strength of concrete under multiaxial stresses is a function of the state of stress consisting of six components. Based on an analysis of strength data, Kotsovos derived mathematical expressions to described the strength properties of concrete under biaxial or triaxial stress states which can be presented as follows:

τ_{oe} is the value of τ_o at the ultimate strength level for $\theta = 0°$

τ_{oc} is the value of τ_o at the ultimate strength level for $\theta = 60°$

the value of τ_{ou} at the ultimate strength level for any values θ such that $0° < \theta < 60°$, is given by the following expression:

$$\tau_{ou} = \frac{2\tau_{oc}(\tau_{oc}^2 - \tau_{oe}^2)\cos\theta + \tau_{oc}(2\tau_{oe} - \tau_{oc})\sqrt{4(\tau_{oc}^2 - \tau_{oe}^2)\cos^2\theta + 5\tau_{oe}^2 - 4\tau_{oc}\tau_{oe}}}{4(\tau_{oc}^2 - \tau_{oe}^2)\cos^2\theta + (\tau_{oc} - 2\tau_{oe})^2} \quad (3.47)$$

This expression describes in the deviatoric plane a smooth convex curve with tangents perpendicular to the directions of τ_{oe} and τ_{oc} at rotational angle θ=0° and 60° respectively (see Figure 3.11).

As the concrete is assumed to be initially isotropic, equation (3.47) will define a six-fold symmetric ultimate strength surface, provided the variations of τ_{oe} and τ_{oc} with σ_o are established.

Figure 3.12 shows the normalised combinations of octahedral stresses (with respect to the uniaxial cylinder compressive strength ,f_c') at the ultimate strength level obtained from triaxial tests. The envelopes in Figure 3.12 are considered to describe adequately the strength of most normal strength concretes likely to be encountered in practice. For a given value of octahedral normal stress σ_o, the value of ultimate octahedral shear stresses are calculated from the following equations;

$$\frac{\tau_{oe}}{f_c'} = 0.633\left(\frac{\sigma_o}{f_c'} + 0.05\right)^{0.857}$$

$$\frac{\tau_{oc}}{f_c'} = 0.944\left(\frac{\sigma_o}{f_c'} + 0.05\right)^{0.724} \quad (3.48)$$

Equation (3.48) represents two open ended convex envelops whose slope tends to become equal to that of the diagonal as σ_o tends to infinity. These expressions together with equation (3.47) are used in this work to define an ultimate strength surface which conforms with the generally accepted shape requirement such as six-fold symmetry, convexity with respect to the space diagonal, and open ended shape which tends to become cylindrical as σ_o tends to infinity.

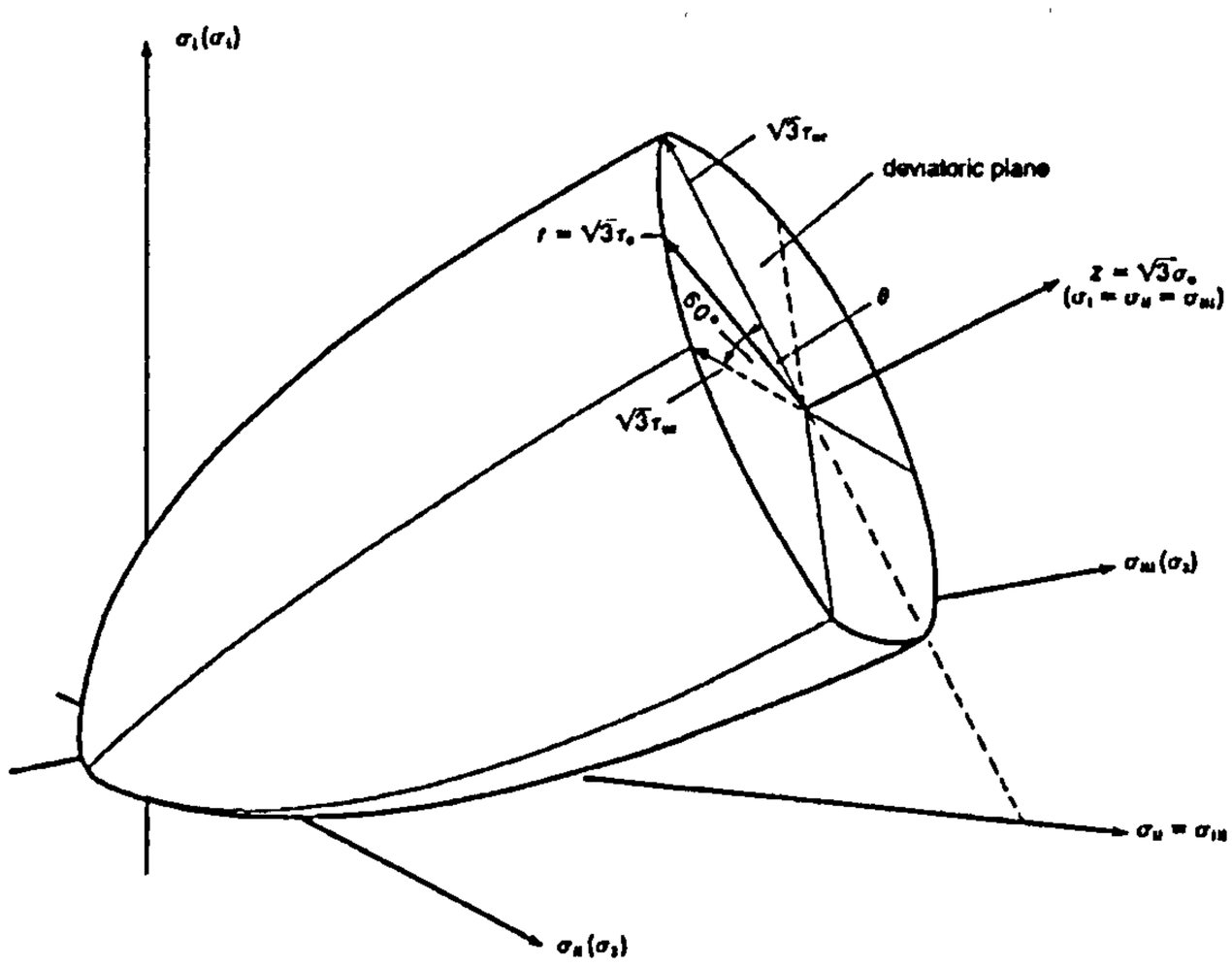

Figure 3.11 Strength Envelope of Concrete

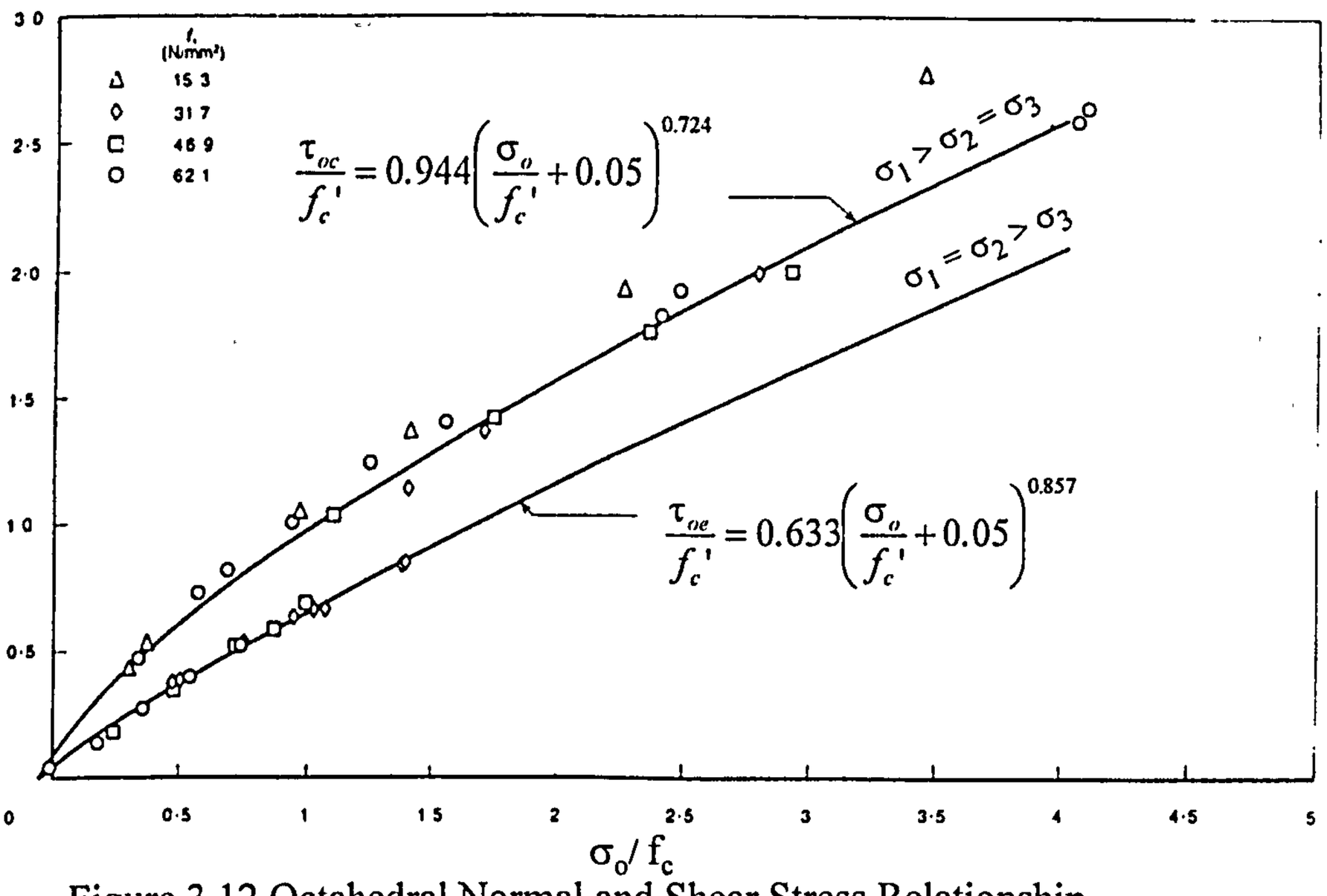

Figure 3.12 Octahedral Normal and Shear Stress Relationship

3.3.3 Failure Criteria of Concrete

In general, concrete failures are divided into two types, tensile type and compressive type. Tensile and compressive types of failure are generally characterised by brittleness and ductility, respectively. With respect to the present definition of failure, tensile type of failure is defined by the formation of cracks and compressive type of failure is due to crushing of concrete. After the state of stress reaches the strength envelope, the material stiffness matrix is modified to account for cracking or crushing.

3.3.3.1 Concrete Compressive Failure Criteria

In this study, it is assumed that the crushing of concrete occurs when :

(a) the current state of stress reaches the strength envelope presented in section 3.3.2.3 and all the principal stress components are compressive, or

(b) the maximum compressive strain is greater than the specified value (which is taken as 0.0035 according to BS8110)

Condition (a) holds for isotropic (uncracked) concrete material, and it is found that condition (b) will never be satisfied prior to condition (a) as long as the material is isotropic. But when a crack exists, condition (a) is not applicable thus only condition (b) is valid.

After crushing, a complete loss of load carrying capacity occurs. Therefore the rigidity matrix [D] becomes a null matrix.

3.3.3.2 Concrete Tensile Failure Criteria

In this study, it is assumed that the cracking of concrete occurs when :

(a) the current state of stress reaches the strength envelope presented in section 3.3.2.3 and at least one of the principal stresses is tensile, or

(b) the maximum tensile principal stress is greater than the specified value. A value equal to $f_t/2$, is approximately the value on the failure surface for uniaxial tensile stress state (f_t is ultimate uniaxial tensile strength of concrete obtained from split cylinder test)

Condition (a) holds for isotropic (uncracked) concrete material. Under multiaxial stress state, condition (b) will never be satisfied prior to condition (a) as long as the material is uncracked. When at least one crack exists at any point due to condition (a), only condition (b) is applicable to check against a second or third crack.

After cracking, the tensile stress across the crack is simulated by tension stiffening. However, material parallel to the crack is assumed to carry stress according to the uniaxial or biaxial conditions prevailing parallel to the crack. Further detail of modelling of post-cracking behaviour is discussed later in this chapter.

3.3.4 Modelling of post-cracking behaviour of concrete

In finite element analysis of reinforced concrete structures, two basic approaches have been employed for crack modelling namely discrete cracks at element nodes and smeared crack within the element with fixed or variable directions. The discrete model (Figure 3.13) introduces extra nodes on the crack faces where

tensile stresses exceed the limit of the strength envelope of concrete in tension. In the smeared crack model (Figure 3.14), the isotropic behaviour of concrete before cracking is replaced by orthotropic behaviour when the current state of stress violates the failure surface in tension. Since the discrete model requires changing the mesh topology, it is not easy to program and needs much effort, so the smeared crack model is adopted in the present study.

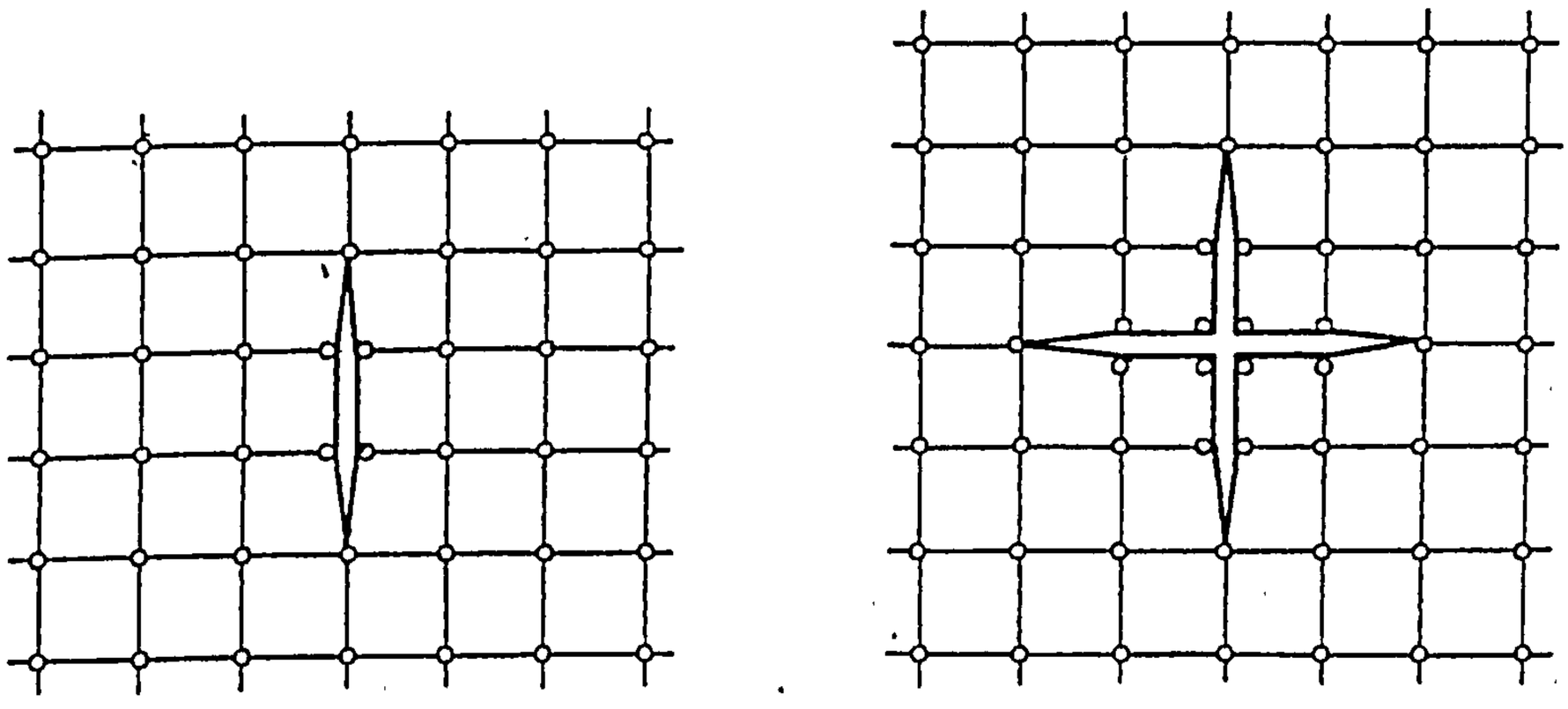

(a) One-directional cracking (b) Two-directional cracking

Figure 3.13 Discrete cracking model

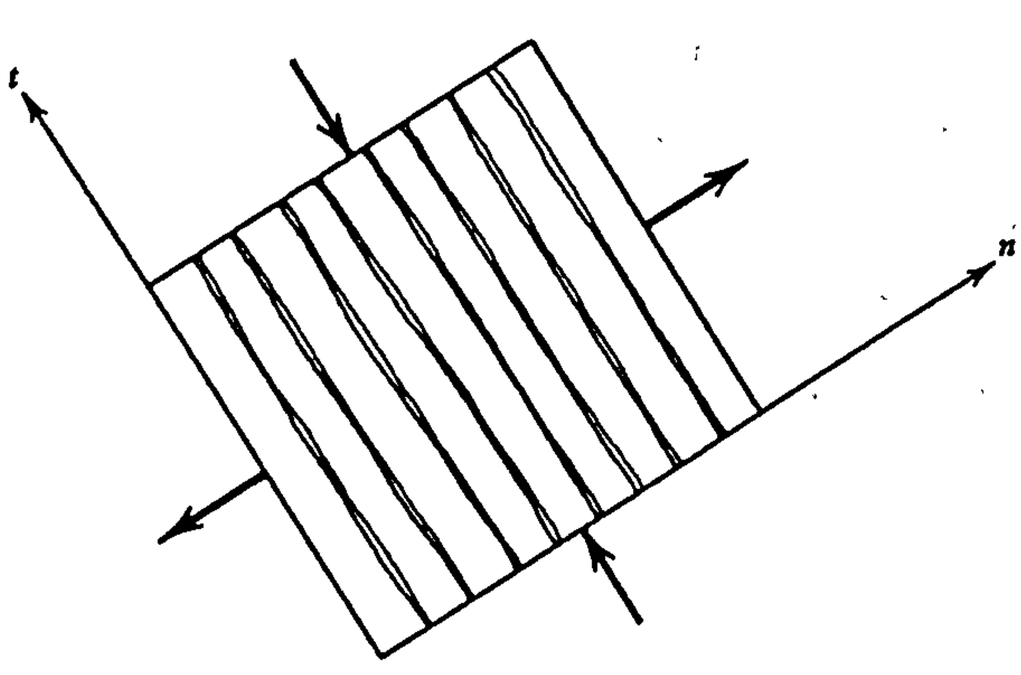

Figure 3.14 Smeared cracking model

3.3.4.1 Smeared crack model

Smeared crack model assumes that the cracked concrete remains a continuum, i.e., the cracks are smeared out in a continuous fashion. In this study, the fixed crack direction approach is used. Once a crack occurs, the crack's direction is fixed and remains constant throughout the analysis. The direction of the crack is assumed to be perpendicular to the direction of the maximum principal stress. However, the crack is allowed to close or reopen again depending on the current value of strain across the crack. A second or third crack at the same Gauss point occurs when the tensile failure

criterion is reached again. These new crack directions must be orthogonal to the first crack and to one another as shown in Figure 3.15.

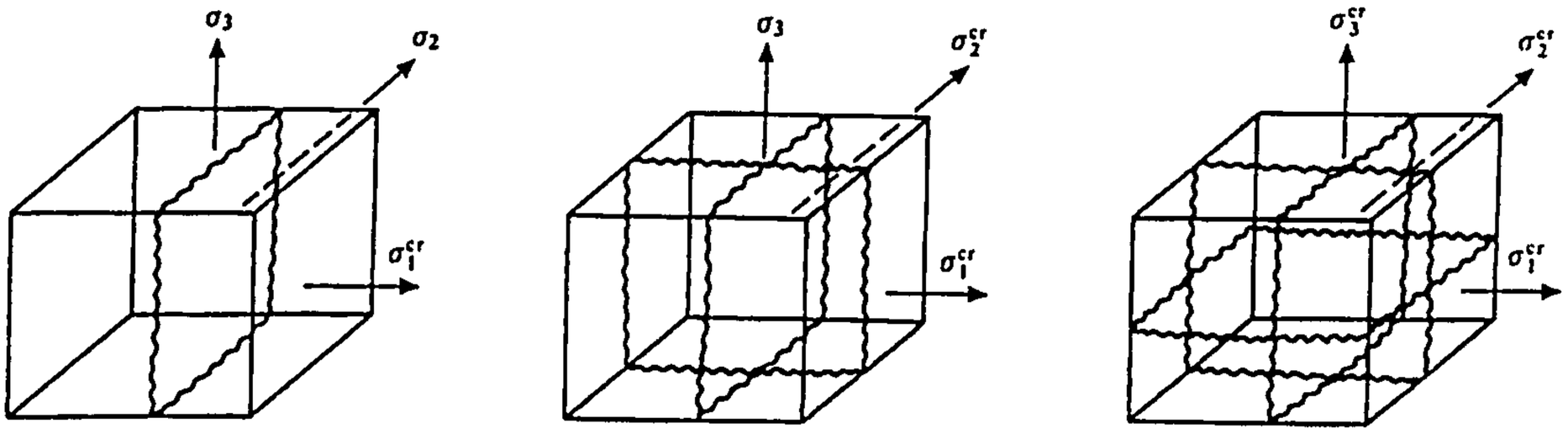

Figure 3.15 Cracks in concrete

Since smeared crack approach is employed to simulate concrete cracking, the cracked concrete is assumed to remain as a continuum when a crack occurs at the Gauss point. Before cracking, the isotropic incremental constitutive matrices are used. After cracking has occurred, the cracked concrete becomes an orthotropic material and new incremental relationship must be derived. The presence of cracks are taken into account by modifying material stiffness matrix [D]. This can be done by reducing the modulus of elasticity 'E' (by tension stiffening) and shear modulus 'G' (by shear retention) across the crack.

In order to improve the realism of the present model, the possibility of closing of a crack is considered. This behaviour may take place due to the redistribution of stresses during an iteration or upon further loading. In the present work, the possibility of cracking at any Gauss point is re-examined within each iteration until the numerical solution converges. After convergence, the direction of crack is fixed. The fictitious principal strain normal to the crack is monitored to assess the state of the cracks in the cracked concrete. If this strain is a negative value, then the crack is assumed to close and the modulus of elasticity normal to the crack is restored to the initial value 'E'.

3.3.4.2 Material Stiffness Matrix for Cracked Concrete

It has been mentioned earlier in the finite element method that the material stiffness matrix [D] for uncracked concrete is given by

$$[D]=\frac{E(1-\nu)}{(1+\nu)(1-2\nu)}\begin{bmatrix} 1 & \frac{\nu}{(1-\nu)} & \frac{\nu}{(1-\nu)} & 0 & 0 & 0 \\ & 1 & \frac{\nu}{(1-\nu)} & 0 & 0 & 0 \\ & & 1 & 0 & 0 & 0 \\ & symmetry & & \frac{(1-2\nu)}{2(1-\nu)} & 0 & 0 \\ & & & & \frac{(1-2\nu)}{2(1-\nu)} & 0 \\ & & & & & \frac{(1-2\nu)}{2(1-\nu)} \end{bmatrix} \quad (3.49)$$

In principal stress space, and with reference to the adopted cracking criterion, if the concrete is cracked in direction 1, the material matrix will be :

$$[D_c]_1 = \begin{bmatrix} D_{11}^* & D_{12}^* & D_{13}^* & 0 & 0 & 0 \\ & D_{22} & D_{23} & 0 & 0 & 0 \\ & & D_{33} & 0 & 0 & 0 \\ & \textit{symmetry} & & \beta G & 0 & 0 \\ & & & & D_{55} & 0 \\ & & & & & \beta G \end{bmatrix} \qquad (3.50)$$

where D_{ij} are the corresponding values in the [D] matrix. For D_{ij}^*, the Young modulus 'E' will be adjusted according to tension stiffening model depending on the strain across the cracks. β is the shear retention factor, $0 \leq \beta \leq 1$ and 'G' is the shear modulus which is obtained from constitutive laws prior to cracking.

If the concrete is cracked in direction 2, then the material matrix will be

$$[D_c]_2 = \begin{bmatrix} D_{11} & D_{12}^* & D_{13} & 0 & 0 & 0 \\ & D_{22}^* & D_{23}^* & 0 & 0 & 0 \\ & & D_{33} & 0 & 0 & 0 \\ & \textit{symmetry} & & \beta G & 0 & 0 \\ & & & & \beta G & 0 \\ & & & & & D_{66} \end{bmatrix} \qquad (3.51)$$

and if the concrete is cracked in direction 3, then the material matrix will be

$$[D_c]_3 = \begin{bmatrix} D_{11} & D_{12} & D_{13}^* & 0 & 0 & 0 \\ & D_{22} & D_{23}^* & 0 & 0 & 0 \\ & & D_{33}^* & 0 & 0 & 0 \\ & \textit{symmetry} & & D_{44} & & \\ & & & & \beta G & \\ & & & & & \beta G \end{bmatrix} \qquad (3.52)$$

Depending on the stress situation, cracks may occur in more than one direction at a single Gauss point. In this case combination between $[D_c]_1$, $[D_c]_2$ and $[D_c]_3$ may be necessary as follows:

a) If cracks occurr in direction 1 and 2, then [D] matrix is given by

$$[D_c]_{1,2} = \begin{bmatrix} D_{11}^* & D_{12}^* & D_{13}^* & 0 & 0 & 0 \\ & D_{22}^* & D_{23}^* & 0 & 0 & 0 \\ & & D_{33} & 0 & 0 & 0 \\ & \textit{symmetry} & & \beta G & 0 & 0 \\ & & & & \beta G & 0 \\ & & & & & \beta G \end{bmatrix} \quad (3.53)$$

b) If cracks occurr in direction 2 and 3, then [D] matrix is given by

$$[D_c]_{2,3} = \begin{bmatrix} D_{11} & D_{12}^* & D_{13}^* & 0 & 0 & 0 \\ & D_{22}^* & D_{23}^* & 0 & 0 & 0 \\ & & D_{33}^* & 0 & 0 & 0 \\ & \textit{symmetry} & & \beta G & 0 & 0 \\ & & & & \beta G & 0 \\ & & & & & \beta G \end{bmatrix} \quad (3.54)$$

c) If cracks occurr in direction 3 and 1, then [D] matrix is given by

$$[D_c]_{3,1} = \begin{bmatrix} D_{11}^* & D_{12}^* & D_{13}^* & 0 & 0 & 0 \\ & D_{22} & D_{23}^* & 0 & 0 & 0 \\ & & D_{33}^* & 0 & 0 & 0 \\ & \textit{symmetry} & & \beta G & 0 & 0 \\ & & & & \beta G & 0 \\ & & & & & \beta G \end{bmatrix} \quad (3.55)$$

and finally if cracks occurred in all three directions, it is assumed that at this Gauss point [D] matrix is a null matrix.

$$[D_c]_{1,2,3} = [0] \quad (3.56)$$

3.3.4.3 Tension stiffening

When a reinforced concrete member is subjected to a sufficiently high tensile stress, concrete cracks at discrete sections. Concrete between cracks continues to carry tensile stress and the stiffness of the member is therefore larger than that of a fully cracked section. This effect is known as "tension stiffening". Tension stiffening has been studied by many researchers. Several models have been developed; Scanlon and Murray (1974) proposed a stepped stress-strain curve as shown in Figure 3.16a. In 1975, Lin and Scordelis used a gradual unloading curve , Figure 3.16b. Gilbert and

Warner (1978) used several variations of Scanlon-Murray and Lin-Scordelis curves. In addition, they employed a new curve consisting of a small drop in strength immediately after cracking followed by piecewise linear unloading, which is shown in Figure 3.16c. Gupta and Maestrini (1990) have studied in detail a concrete member reinforced by a single bar allowing for bond-slip. They concluded that the tensile stress carried by concrete is a function of bond, area of bar and strength (tensile strength of concrete and yield strength of steel) parameters which is not used by other tension stiffening relationships. Even so, the model developed by Gupta and Maestrini has a trend similar to that of others (Figure 3.16d).

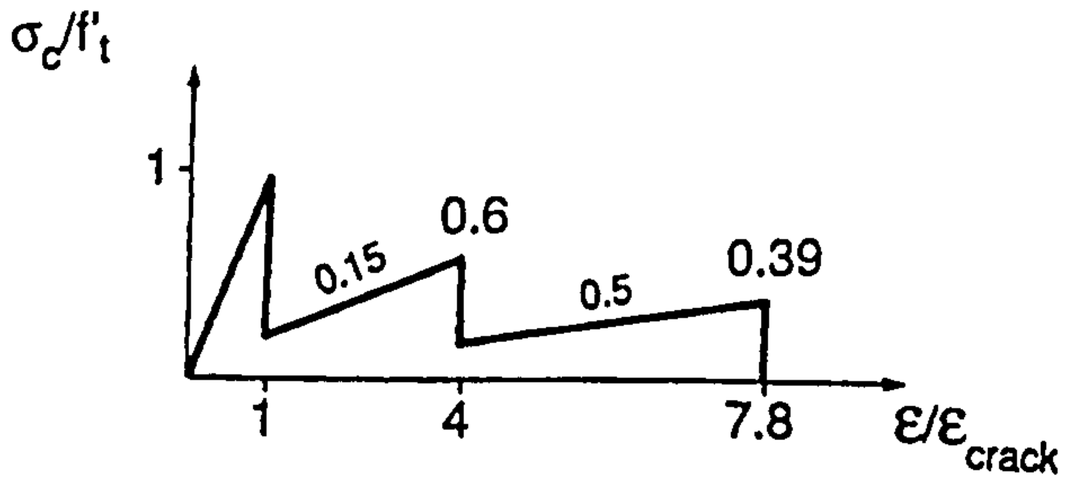

(a) Stepped response after cracking (Scanlon and Murray 1974)

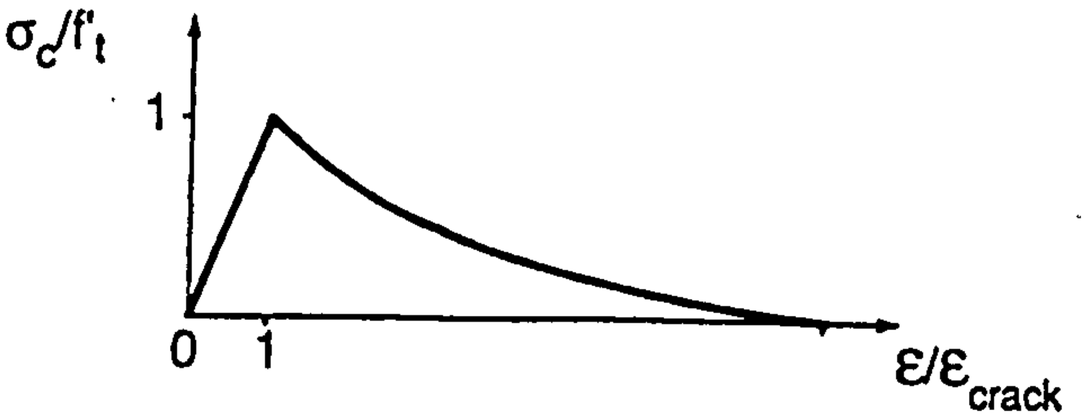

(b) Gradual unloading after cracking (Lin and Scordelis 1975)

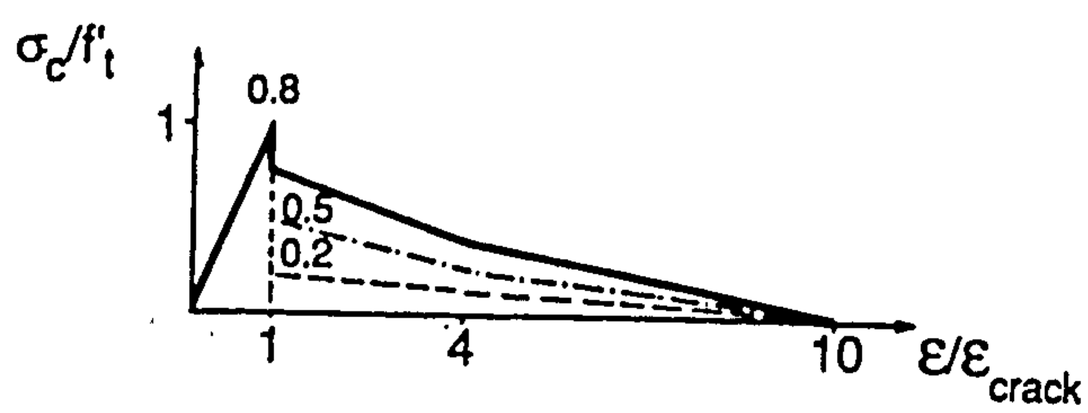

(c) Discontinuous unloading after cracking (Gilbert and Warner 1978)

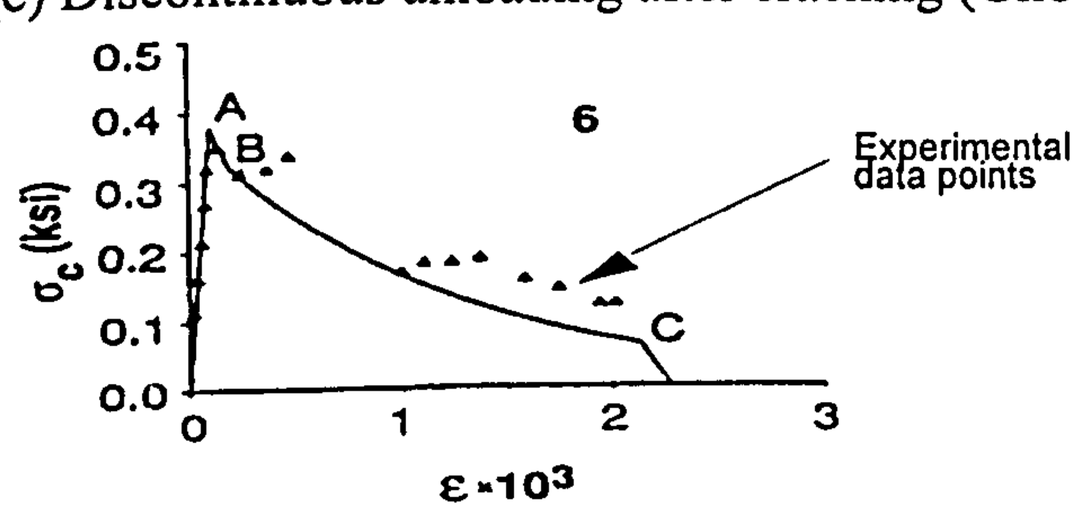

(d) Simplified effective tensile stress-strain curve (Gupta and Maestrini 1990)

Figure 3.16 Concrete Tensile stress-strain curves

Experimental data shows that strain softening can exist in plain concrete subjected to tensile stress. The term "tension stiffening" is used here to denote the tensile stress carried by the cracked concrete for both plain and reinforced concrete. Therefore a unique tension stiffening curve will be used for a structure regardless of the amount of reinforcement in the element.

In the present study, a tensile stress-strain curve as shown in Figure 3.17 is used. The ascending part is assumed to be linear elastic until cracking occurs. The descending part is taken as a linear function of principal strain normal to the crack direction and, the resistance becomes zero when the principal strain exceeds a certain maximum strain. The tensile strength immediately after cracking is defined as a fraction "*A*" of the tensile strength of concrete before cracking.

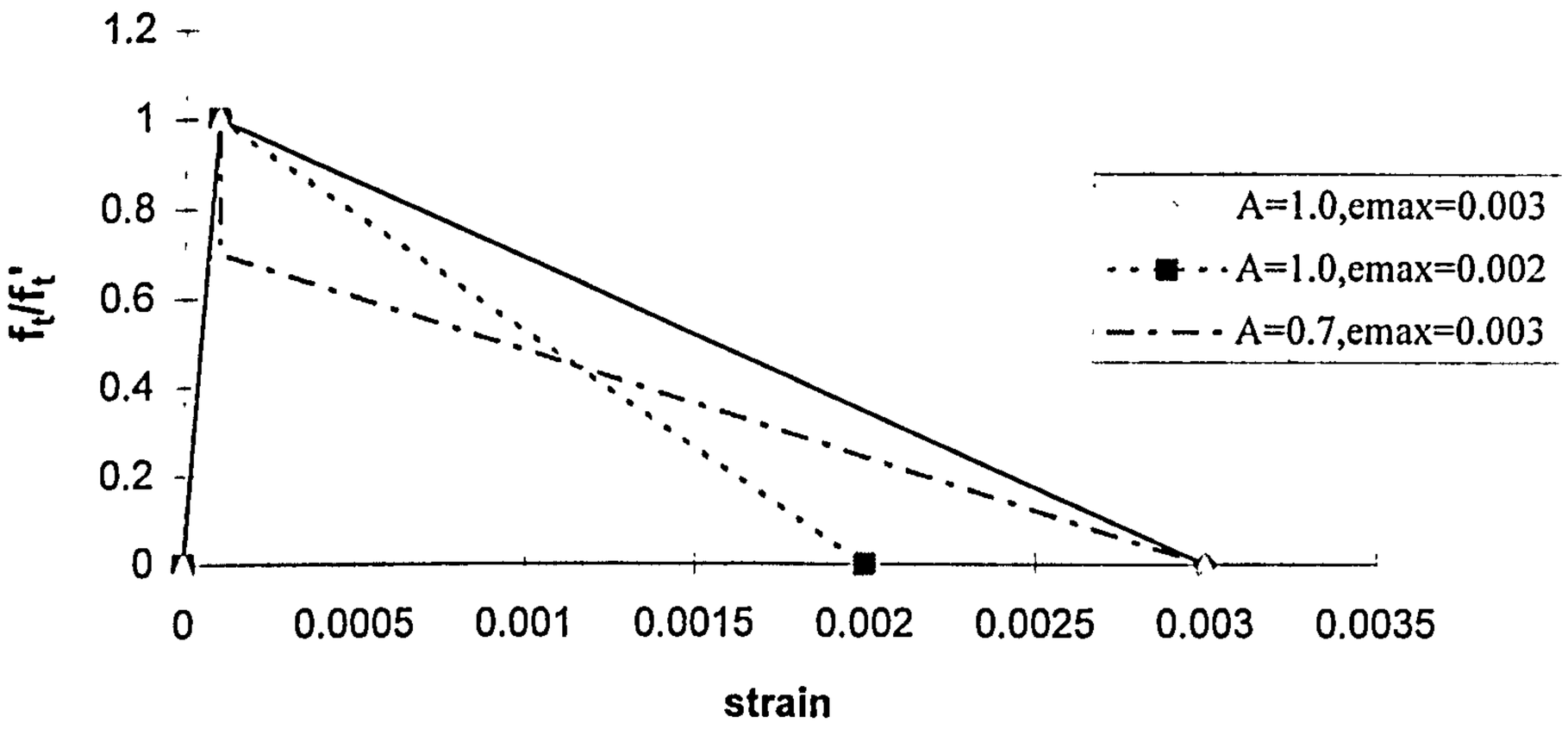

Figure 3.17 Tension stiffening curves

3.3.4.4 Shear Retention

Experimental results indicate that both plain and reinforced cracked concrete can exhibit significant shear stiffness. A considerable amount of shear stress can be transferred across the rough and irregular surfaces of cracked concrete by aggregate interlocking and friction forces. Also, the dowel action of steel bars contributes to the shear stiffness across cracks. Experimental evidence shows that the primary variable in the shear transfer mechanism is the crack width (Figure 3.18 & 3.19), although aggregate size, reinforcement ratio and bar size also have a certain influence.

A common procedure to account for aggregate interlock and dowel action in a smeared crack model is to use an appropriate value to the cracked shear modulus (G').

In this study, the transfer of the shear stresses across cracks is modelled by means of the 'shear retention' factor, β, which defines the shear modulus of cracked concrete as $G_c=\beta G$, where G is the elastic shear modulus of the uncracked concrete. β taken as a function of the average of the three principal strains at any cracked point as follows

$$\beta = B\frac{\varepsilon_{cr}}{\varepsilon_n} \qquad (3.57)$$

where $\varepsilon_{cr} = \frac{f_{sp}}{E_c} \approx 0.0001$

f_{sp} = *splitting cylinder tensile strength* = $0.53\sqrt{f_c'}$

E_c = *Young's modulus of concrete* = $4730\sqrt{f_c'}$

$\varepsilon_n = \frac{\varepsilon_1 + \varepsilon_2 + \varepsilon_3}{3}$

B = numerical constant

Three values of B will be used in this study as shown in Figure 3.20.

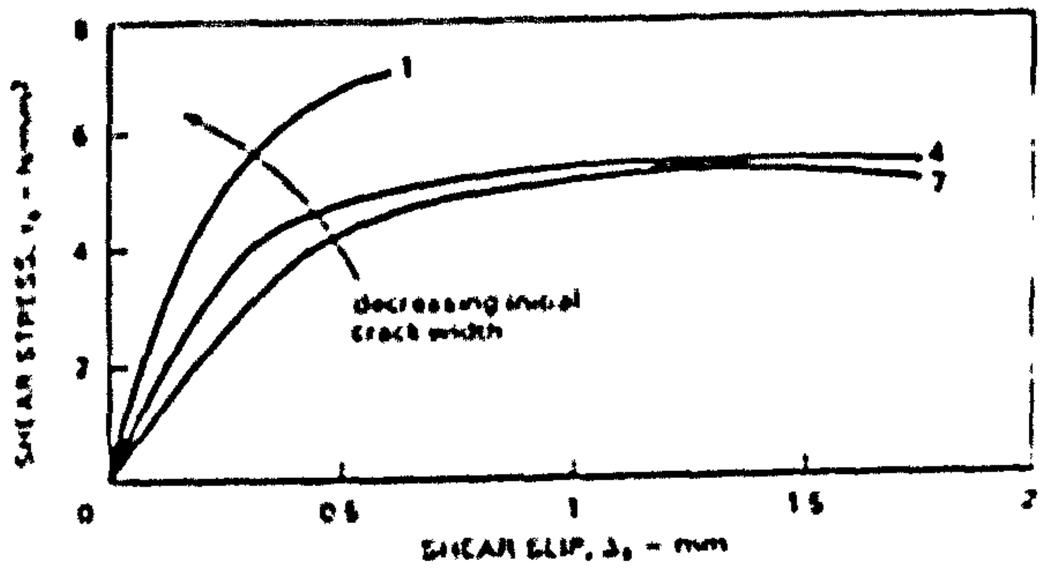

Initial crack width

specimen 1 = 0.125mm

specimen 4 = 0.250 mm

specimen 7 = 0.350 mm

(a) Test results for specimens with 12mm bars and different initial crack widths

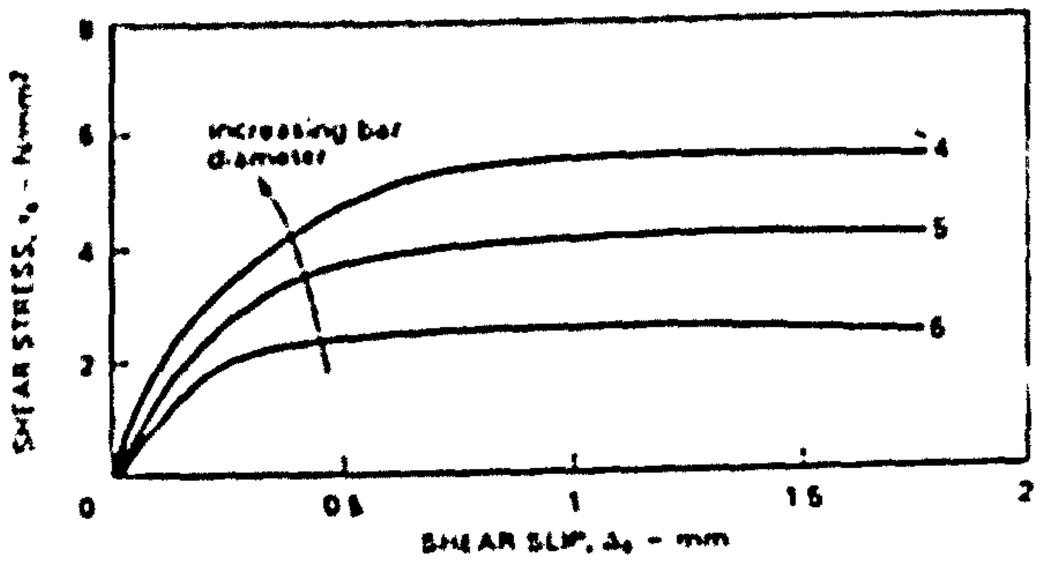

Reinforcement

specimen 4 = 2 nos 16 mm ϕ bar

specimen 5 = 2 nos 12 mm ϕ bar

specimen 6 = 2 nos 8 mm ϕ bar

(b) Test results for specimens with 0.25mm initial crack width and different reinforcement

Figure 3.18 Shear transfer in cracked reinforced concrete (Millard and Johnson 1985)

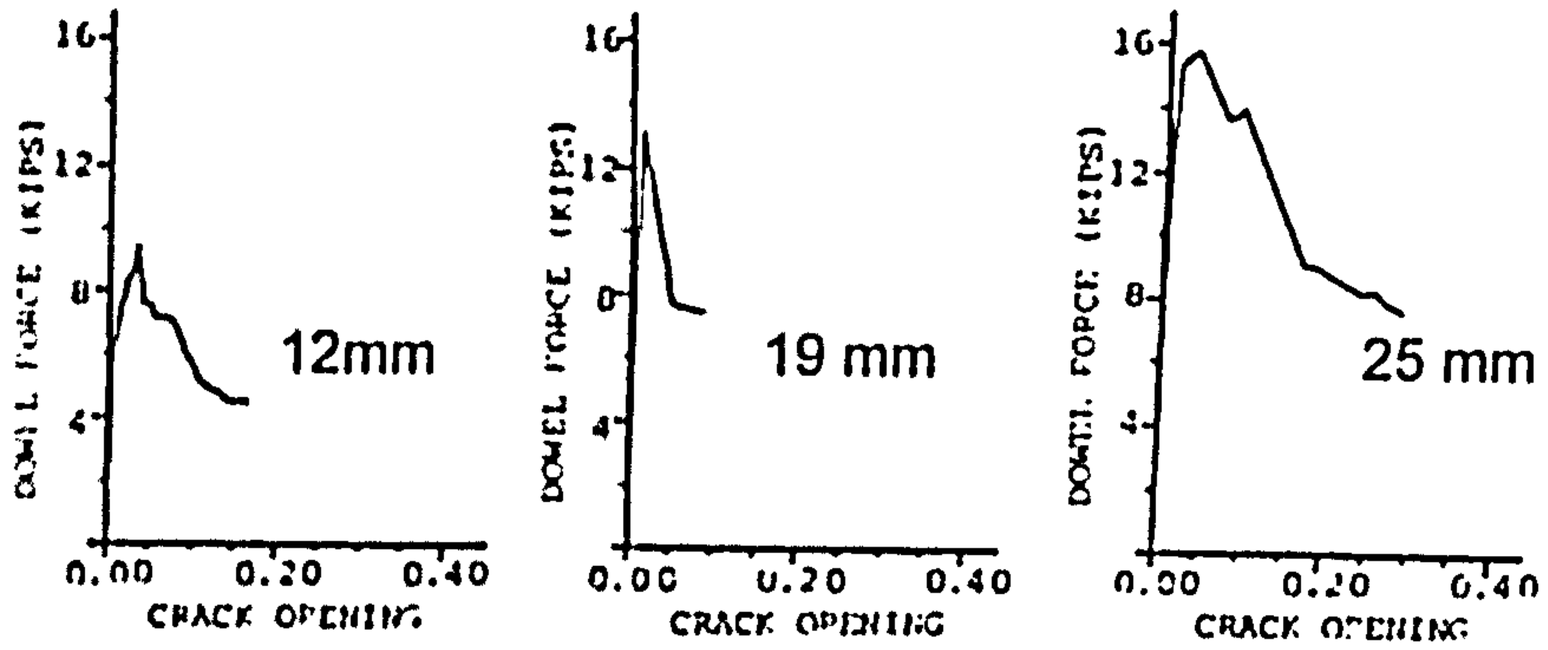

Figure 3.19 Dowel load -crack opening relationship (Soroushian et al, 1986)
(f_y=416 N/mm^2, f_c' = 44N/mm^2, Bar perpendicular to crack)

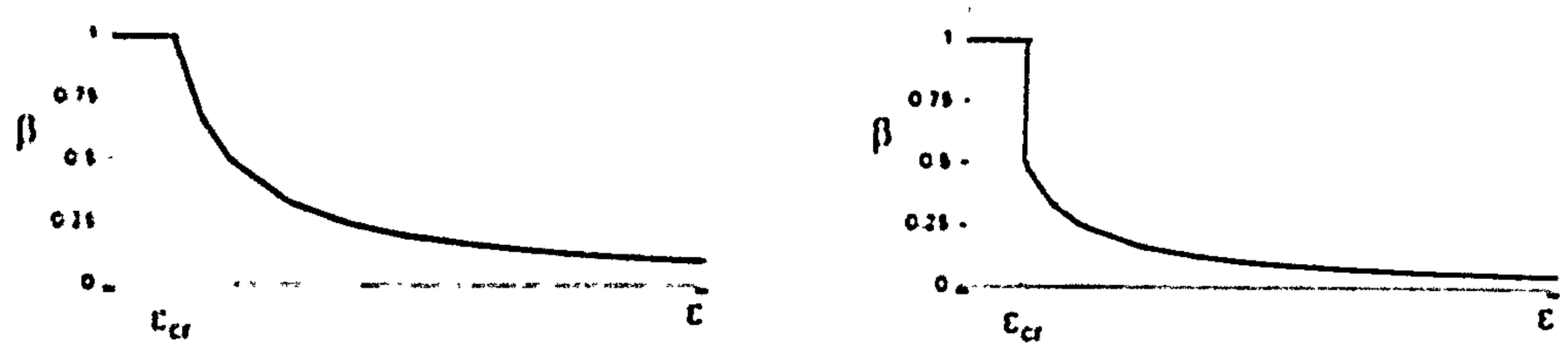

(a) $\beta = \varepsilon_{cr}/\varepsilon_n$ (B=1) (b) $\beta = 0.5\varepsilon_{cr}/\varepsilon_n$ (B=0.5)

(c) $\beta = 0.25\varepsilon_{cr}/\varepsilon_n$ (B=0.25)

Figure 3.20 Shear Retention curves

3.3.5 Material properties of concrete

Although Kotsovos' concrete model requires only cylinder compressive strength to define the behaviour of concrete, the program also requires other parameters such as elastic Young's modulus (E_c) and Poisson's ratio (ν) of concrete as a starting value for the analysis. The material properties of concrete required for input data are taken as follows :-

- Young's modulus (E_c) of concrete obtained from $E_c = 4730\sqrt{f_c'}$ N/mm^2
- Poisson's ratio of concrete set at constant value as 0.2
- the cylinder compressive strength (f_c') of concrete was taken as 0.8 f_{cu}, where f_{cu} is cube strength of concrete.
- The splitting cylinder tensile strength $f_{sp} = 0.53\sqrt{f_c'}$ N/mm^2

3.4 Non-linear Analysis

3.4.1 Solution technique

As pointed out in section 3.3, the behaviour of concrete structure is highly non-linear. A non-linear problem is often tackled on the basis of linearly-elastic concept, i.e. solving a series of linear equation such that the appropriate nonlinear conditions are satisfied. Unlike linear analyses, nonlinear systems cannot be solved directly but rely on repeated solutions (iterative) of linear systems until a specified degree of accuracy (convergence tolerance) is achieved. In this study, modified "Newton-Raphson" method has been used in conjunction with frontal method to solve the equations mentioned earlier. The main feature of the frontal method is that, it assembles the equations and eliminates the variables at the same time. Hence the complete structural stiffness is never formed, and this reduces computer storage significantly. The stiffnesses are evaluated using a secant rigidity matrix and it was updated at the second iteration in each increment.

The solution of non-linear problems by finite element method are usually attempted by one of the following basic techniques:

- incremental method
- Iterative method
- Incremental-iterative (mixed procedure)

The details of these methods are described in many books (Zienkiiewicz O.C. and Taylor R.L. 1989, Bathe K-J. 1996, Hinton E, and Owen D.R.J. 1989, Kotsovos M.D. and Palvlovic M.N. 1995). The mixed incremental/iteration procedure is adopted in the study. In this method, the load is applied in increments and the solutions are obtained iteratively until equilibrium is achieved to an acceptable level of accuracy. The stiffness is calculated by using secant modulus approach (because the concrete constitutive law requires the use of secant modulus) as a starting value for the iterative process. The stiffness is then updated at the second iteration of each increment.

The equilibrium conditions are checked by evaluating "residual forces". The basic technique of this method is that, at any stage, a load system evaluated from the stress in the structure, is checked against the applied load system. The difference between these two will result in a set of residuals. These residuals are then applied to the structure to restore equilibrium. The process is then continued to dissipate the residual forces to a sufficiently small value.

3.4.2 Convergence criterion

It is important to include reliable convergence criteria which will ensure the gradual elimination of the residual forces and terminate the iterative process when the desired accuracy has been achieved. However, it is difficult and expensive to check the decay of residual forces for every degree of freedom, therefore an overall evaluation is preferable. This is achieved by out-of-balance force (or residual) norms as follows :

$$\frac{\sqrt{R_i^*}}{\sqrt{\Delta F_i^*}} \times 100 \leq Toler \tag{3.58}$$

where

$$\Delta F_i^* = \sum_{i=1}^{N} (F_{ai}')^2$$

$$\Delta R_i^* = \sum_{i=1}^{N} (R_i)^2$$

N = total number of nodal points in the system

R_i = the residual force at node i at r^{th} iteration

F_{ai}' = the total external applied load at node i

Finally, it should be noted that the rate of convergence very much depends on the method used in the solution. For example, the constant stiffness will lead to slow convergence and this leads to many iterations, which is without doubt a very costly operation.

Chapter 4

KOTSOVOS' MODEL AND ABAQUS' MODEL - A COMPARISON

4.1 Introduction

Finite element method is often used to predict the response of reinforced and prestressed concrete structures. The results from Finite Element analysis are very much dependent on the constitutive model used for concrete and its failure criteria, simulation of steel and interaction between the steel and concrete. In order to obtain a reliable prediction, a suitable constitutive model should be used in the analysis. However, there are a large number of three dimensional concrete constitutive models available in the literature. The question is which model is most suitable for the study of punching shear problem in slabs? In this work, two widely used concrete models have been selected for detailed study. They are :

1. Non-linear elastic isotropic model proposed by Kotsovos (1979a & 1979b).
2. Plasticity-based concrete model proposed by Chen and Chen (1976) used in the commercial package ABAQUS.

The validity of the models is verified against experimental results of 27 interior slab-column junctions tested by Rankin (1982). This study covered models with variations in the important parameters such as: thickness of slab, flexural reinforcement ratios and concrete strengths (Table 4.1).

Kotsovos' concrete constitutive law has been described in the previous chapter, so only the concrete model and numerical method used in the ABAQUS package are briefly described here.

4.2 ABAQUS concrete model

ABAQUS is a well established commercial finite element code. Its constitutive model treats concrete as a continuous isotropic linearly elastic-plastic strain hardening-fracture material. The stress-strain characteristics of this model can best be described by the idealised uniaxial stress-strain curve shown Figure 4.1. Iniatially, the concrete is assumed to be linear-elastic for both tensile and compressive stress state. At stress levels $-f_c$ (point A) and f_t, concrete yields. Strain hardening takes

place until the stresses reach $-f_c'$ (point *B*) and f_t', respectively. At stress level $-f_c'$, the concrete becomes perfectly plastic until crushing occurs (point *C*) at a compressive strain of $-\varepsilon_u$ and the stress drops suddenly to zero. The concrete is assumed to have a limited tensile strength of f_t' and limited tensile strain ε_t.

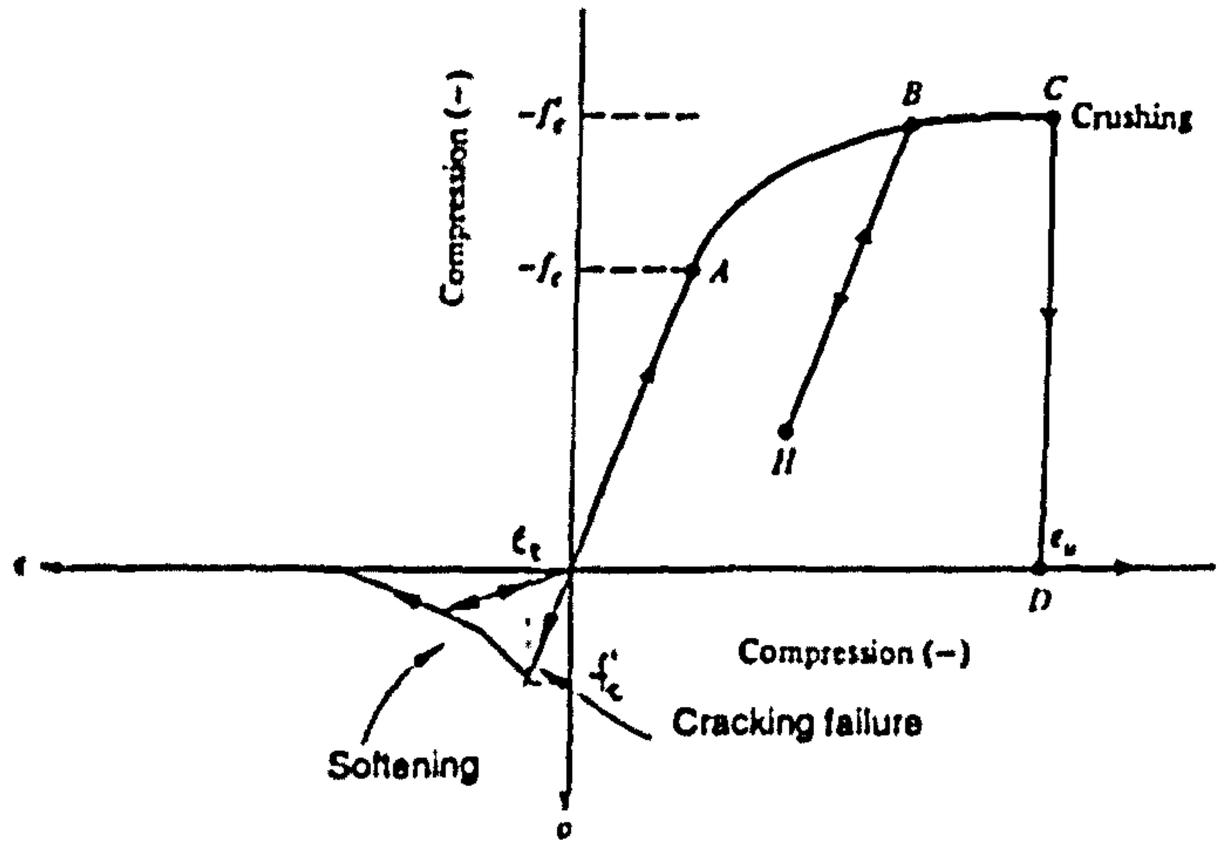

Figure 4.1 Idealised uniaxial stress-strain curve for concrete

The initial yield surface (point *A*) is assumed to take the same form as failure surface, thus this surface and the subsequent loading surfaces are of similar shape as the failure surface (Figure 4.2). The failure surfaces can be expressed in terms of first and second stress invariants, p and q, as shown in the figure 4.3.

where
$$p = -\frac{1}{3} I_1 \qquad (4.1)$$

$$q = \sqrt{\frac{3}{2} J_2} \qquad (4.2)$$

I_1 = first invariant of the stress tensor
$= \sigma_1 + \sigma_2 + \sigma_3$
J_2 = second invariant of the deviatoric stress tensor.
$$= \frac{1}{6}\left[(\sigma_1 - \sigma_2)^2 + (\sigma_2 - \sigma_3)^2 + (\sigma_3 - \sigma_1)^2\right]$$

and σ_1, σ_2, σ_3 are the principal stresses.

Cracking is assumed to occur when the stress reaches a failure surface, which is called the "crack detection surface". Once a crack has been detected its orientation is stored. Subsequent cracking at the same point is assumed to be orthogonal to this direction. Smeared crack model is used to represent cracking. After cracking, the

behaviour of concrete is modelled by tension stiffening and shear retention factors. The tension stiffening model used in the ABAQUS concrete model is similar to the tension stiffening used in the in-house program, which is linear for both the ascending and the descending portions of the curve (Figure 4.4). However, the equations for shear retention are slightly different in these two models (the definition of β is different). The β for ABAQUS concrete model defined as

$$\beta = B\left(1 - \frac{\varepsilon_n}{\varepsilon_{max}}\right) \qquad (4.3)$$

In order to make comparisons valid, 20 noded solid element was chosen to represent concrete as in the in-house program. Steel bars were represented by one dimensional element embedded in the solid elements(concrete). Standard elastic-plastic (with/without strain hardening) material model was used to describe the behaviour of the reinforcing steel.

The computation is performed by incremental loading, with iterations in each increment. Modified Riks algorithm (Arc-length method) is used to perform the non-linear analysis. The fundamental concept of this method is that the solution is viewed as the discovery of a single equilibrium path in a space defined by the nodal variables, and the loading parameter (Figure 4.6). This is done by moving a given distance (ρ_1) along the tangent line to the current solution point (A^0). Once the point A^1 is found (distance between A^1 and equilibrium surface equal to ρ_1), then the next point (A^2) which passes through equilibrium surface is obtained by projecting a line perpendicular to the same tangent line at point (A^1). A detailed description of this method is given in ABAQUS manual (1989).

4.3 Material Properties

Although two different material models were used, most of the material properties were kept identical, and were defined using the uniaxial cylinder compression strength f_c' in N/mm^2. If the compressive strength of concrete for the test is measured by the cube test, the corresponding cylinder compressive strength f_c' was taken to be 0.8 of cube strength (f_{cu}). Initial Young's modulus (E_c) of concrete was taken as $E_c = 4730\sqrt{f_c'}$ N/mm^2 and Poisson's ratio of 0.2 was assumed. The splitting cylinder tensile strength (f_{sp}) was calculated as $f_{sp} = 0.53\sqrt{f_c'}$ N/mm^2. The stress-strain relationship in tension was assumed to be linear up to f_{sp} and afterwards the stress decreased linearly with strain and was zero at the maximum strain of 0.002 (i.e. A=1.0 and ε_{max}=0.002) as shown in Figure 4.4. In order to match the two curves for

shear retention factor as closely as possible, the values for B and ε_{max} were taken as 0.4 and 0.0012 respectively for ABAQUS code. While for the in-house program, B was taken as 1.0 (Figure 4.5). For steel, the measured values of the elastic modulus and yield stress were used and a perfectly elastic-plastic behaviour was assumed.

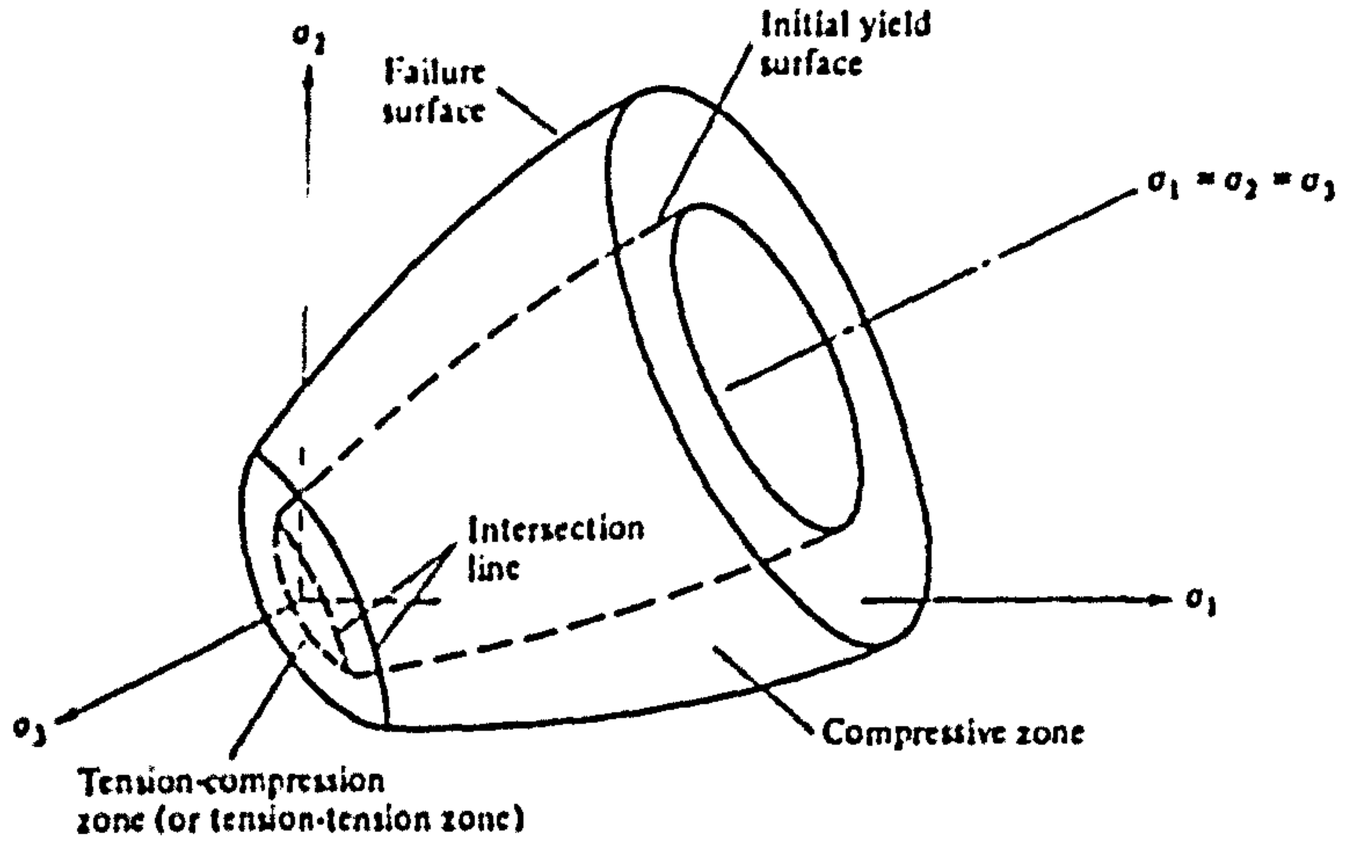

Figure 4.2 Failure and initial yield surfaces in principal stress space

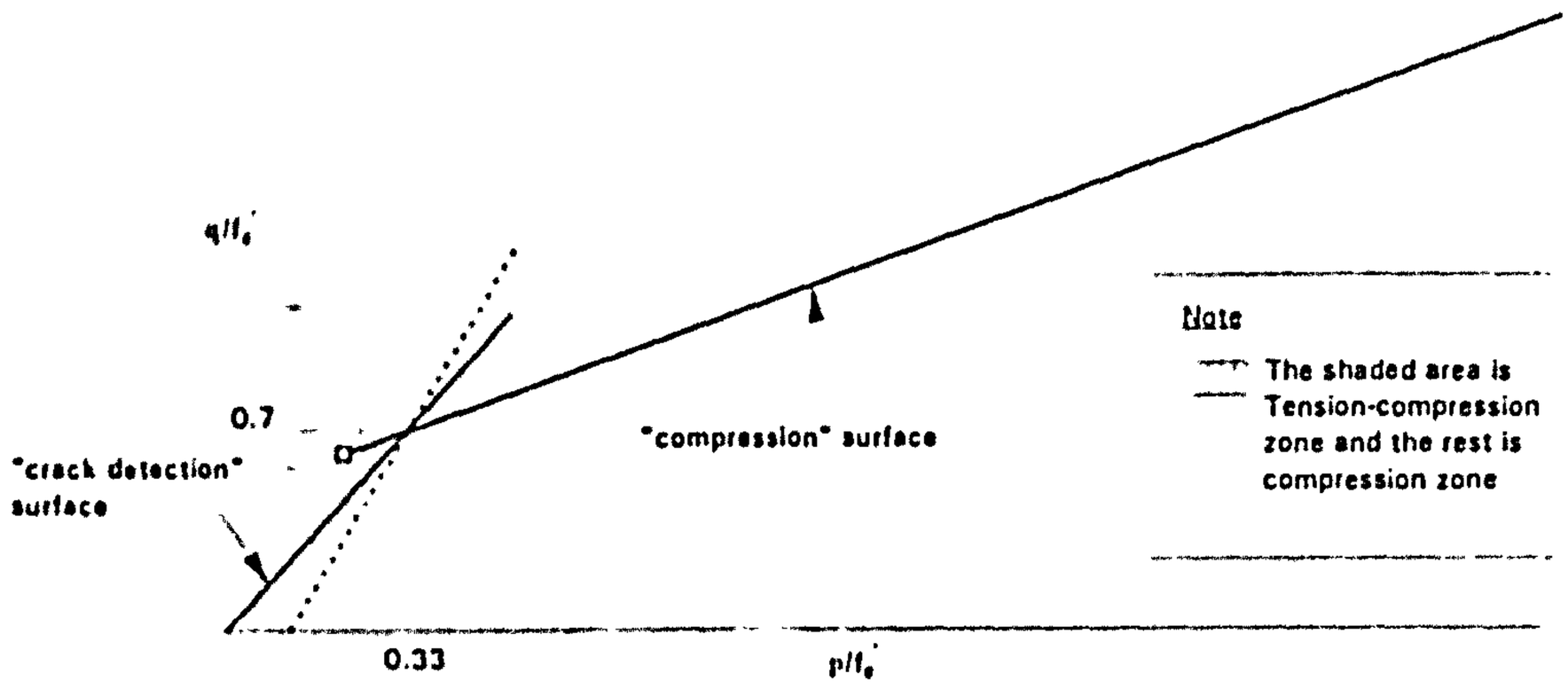

Figure 4.3 -Concrete failure surfaces in the p-q plane

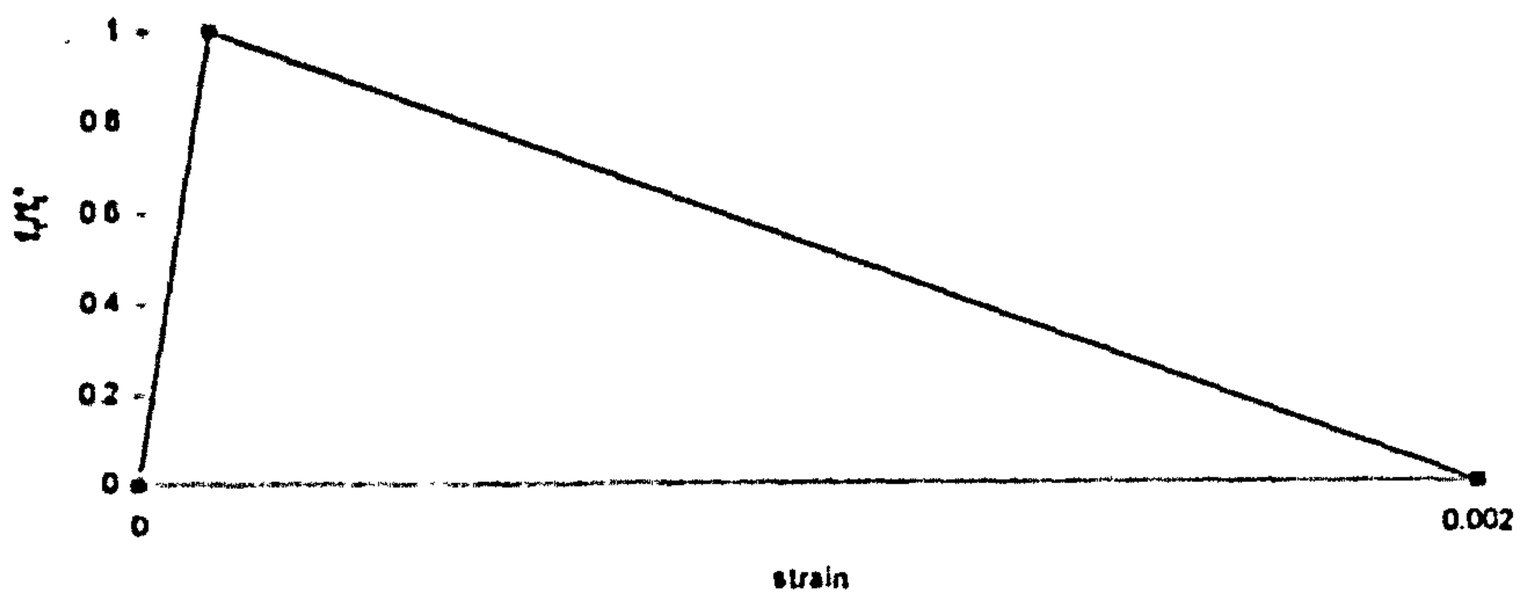

Figure 4.4 -Tension Stiffening curve

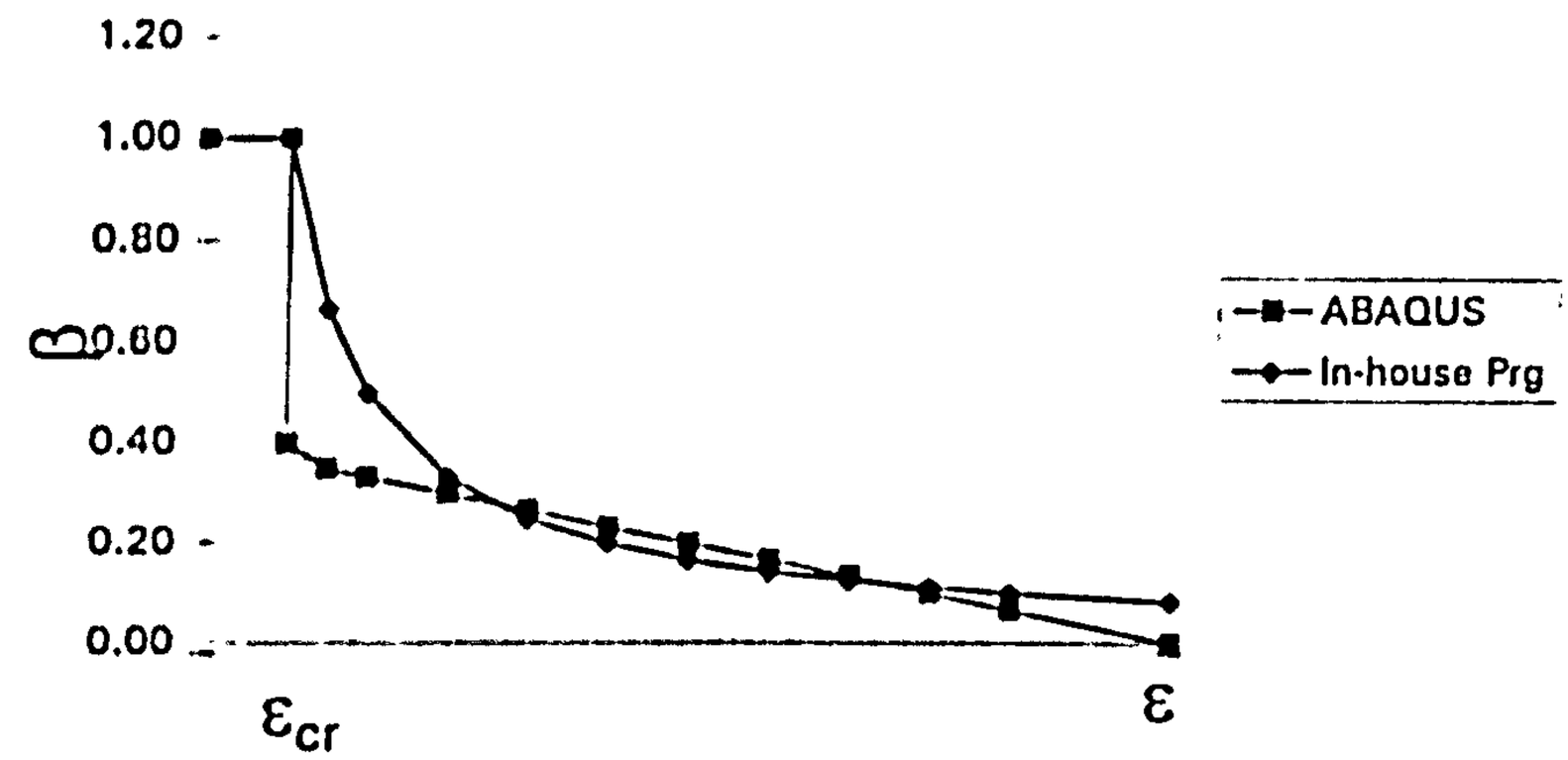

(In-house Program) $\beta = \varepsilon_{cr}/\varepsilon_n$ (ABAQUS) $\beta = 0.4(1-\varepsilon_n/0.0012)$

Figure 4.5 Shear Retention curves

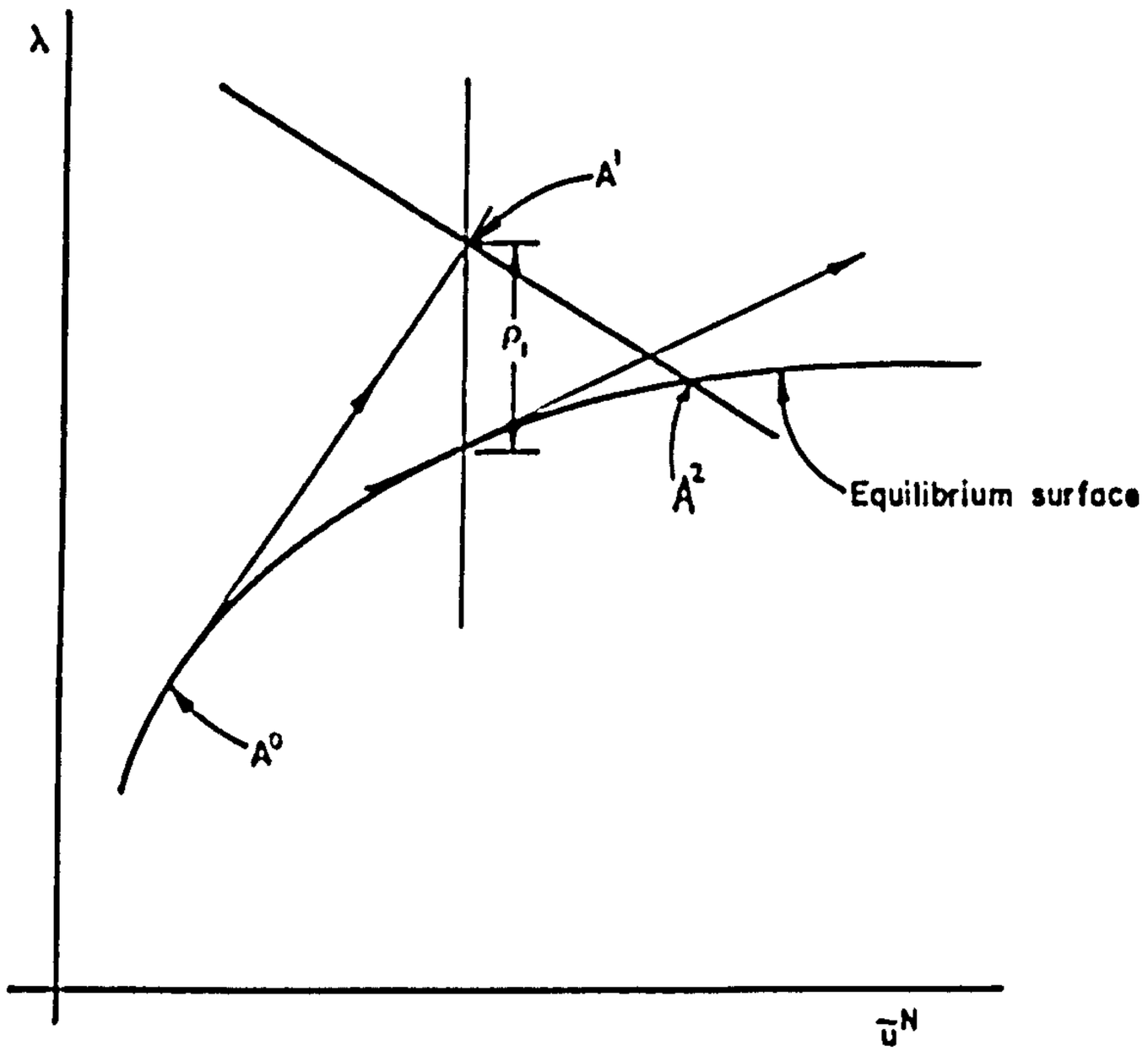

Figure 4.6 Modified Riks algorithm

4.4 Numerical modelling of slab

The tested slabs were simply supported along the four edges with corners free to lift and subjected to a concentrated load at the centre as shown in Figure 4.7. Owing to symmetry, only one-quarter of the slab was modelled (see Figure 4.8a). The applied load was simulated by uniformly distributed load over the element representing the loading stub, and vertical restraint for corner node was released to mimic corner lifting. Concrete slab was discretised by using one layer of solid elements.

At the beginning of the study, only a 5x5 mesh (Figure 4.8a) was used, but later it was found that the solid element using ABAQUS concrete model gave very poor predictions. In an attempt to find out why ABAQUS predicted such poor results, coarser meshes were used to re-analyse the same batch of slabs. For the sake of simplicity, these meshes do not include the portion of slab beyond the support and the applied load was simulated by a concentrated load (Figure 4.8b & 4.8c).

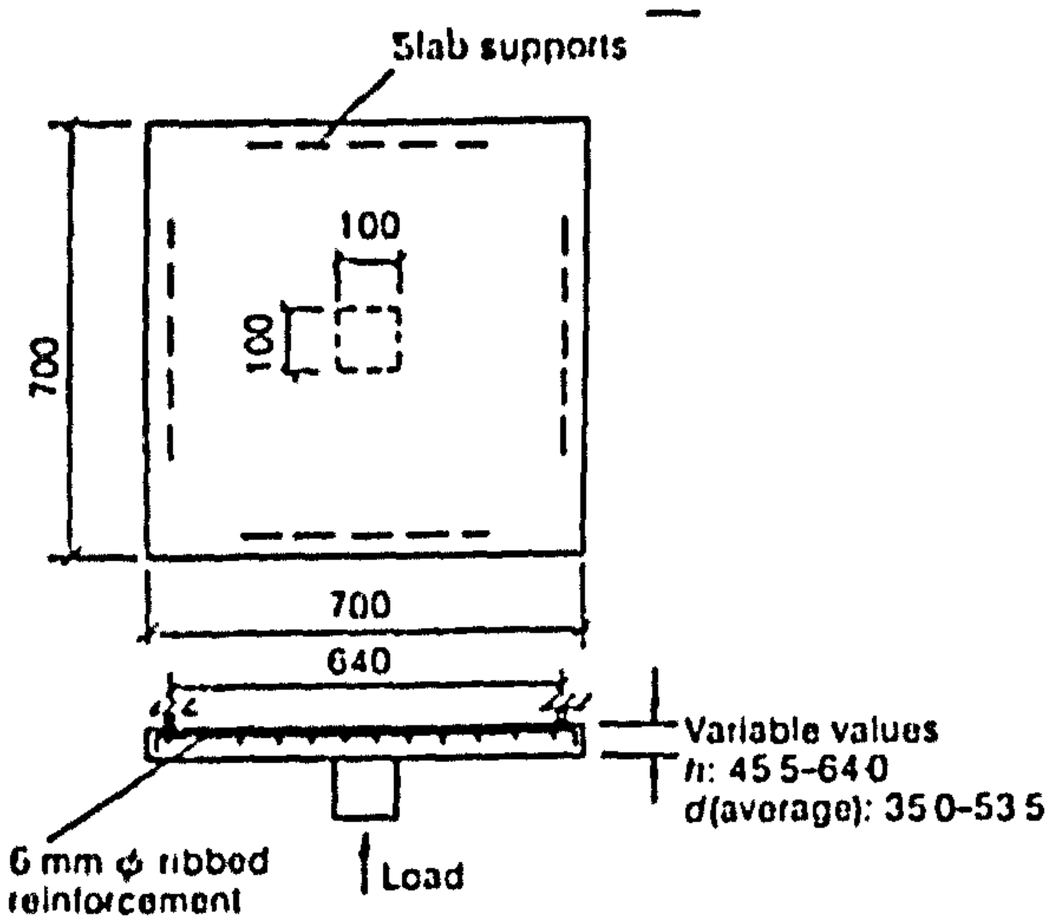

Figure 4.7 :Rankin's slab-column models

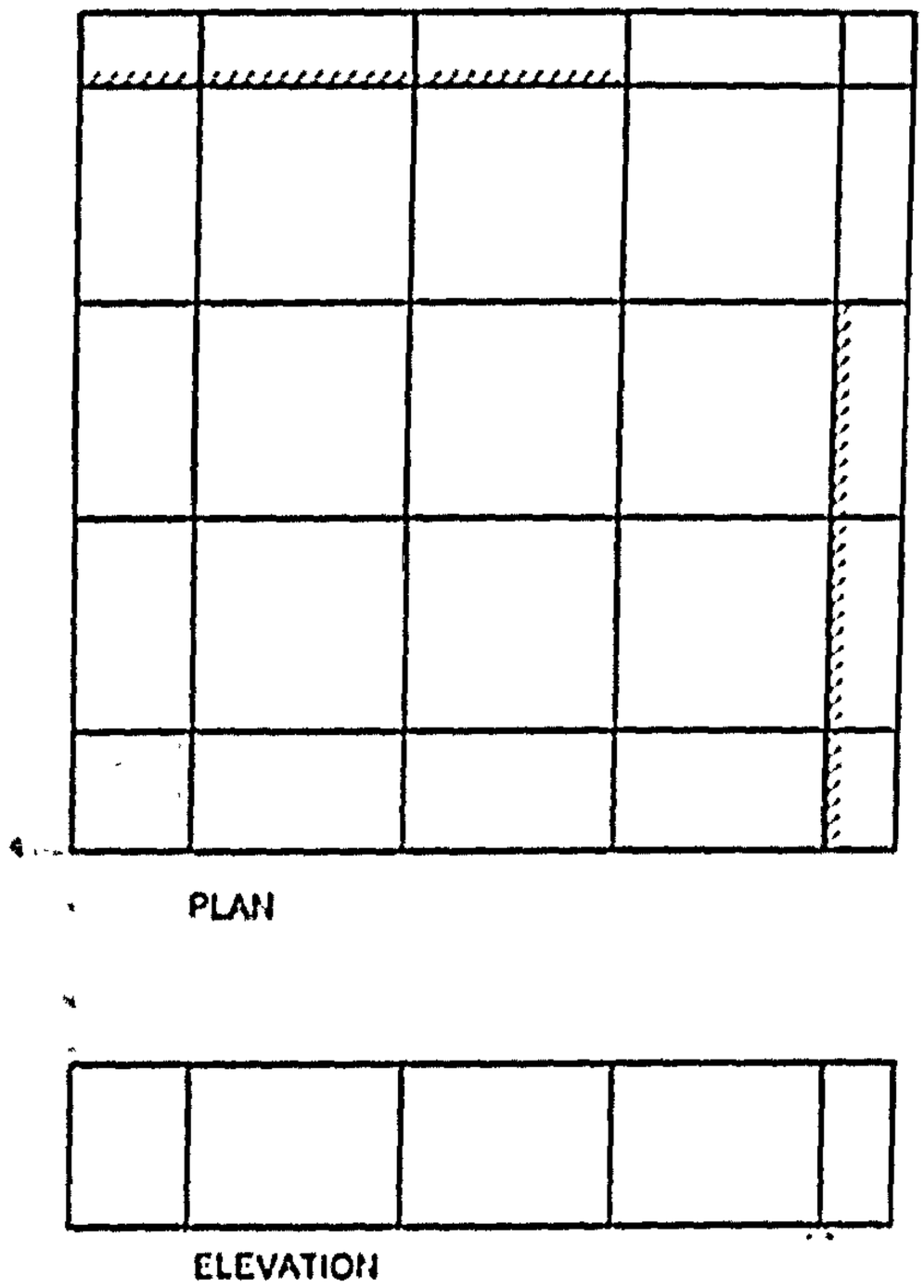

(a) 5×5 mesh

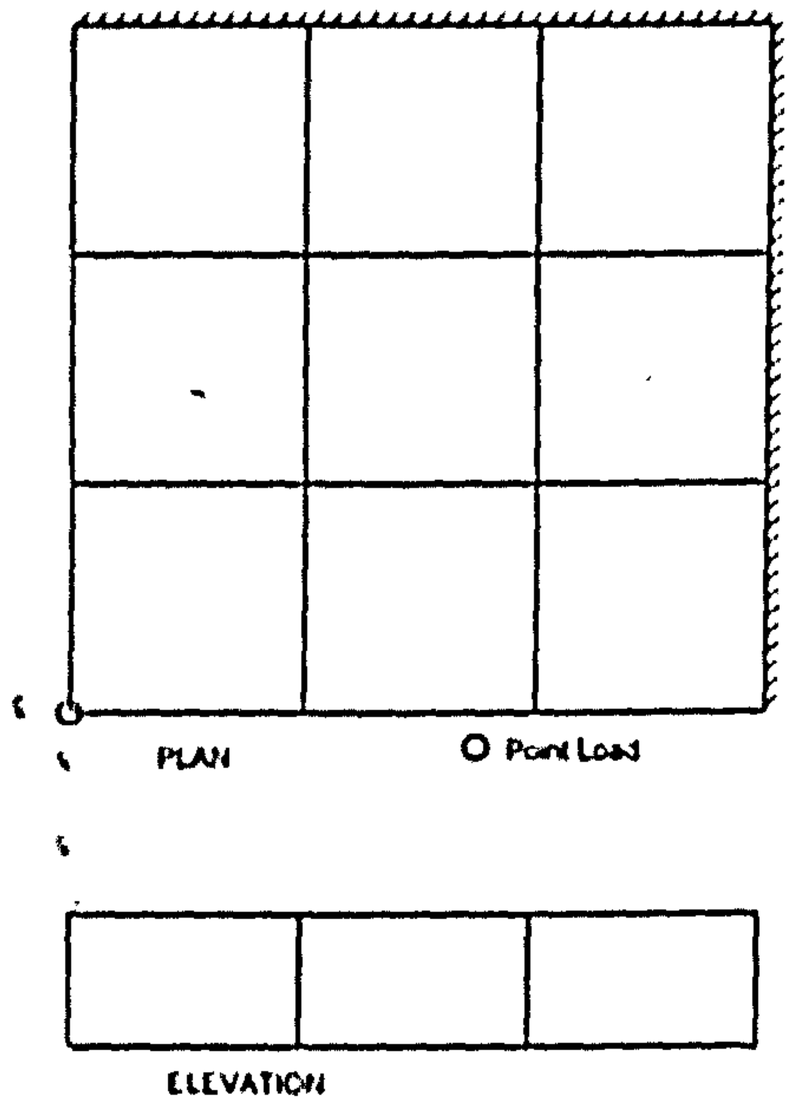

(b) 3×3 mesh

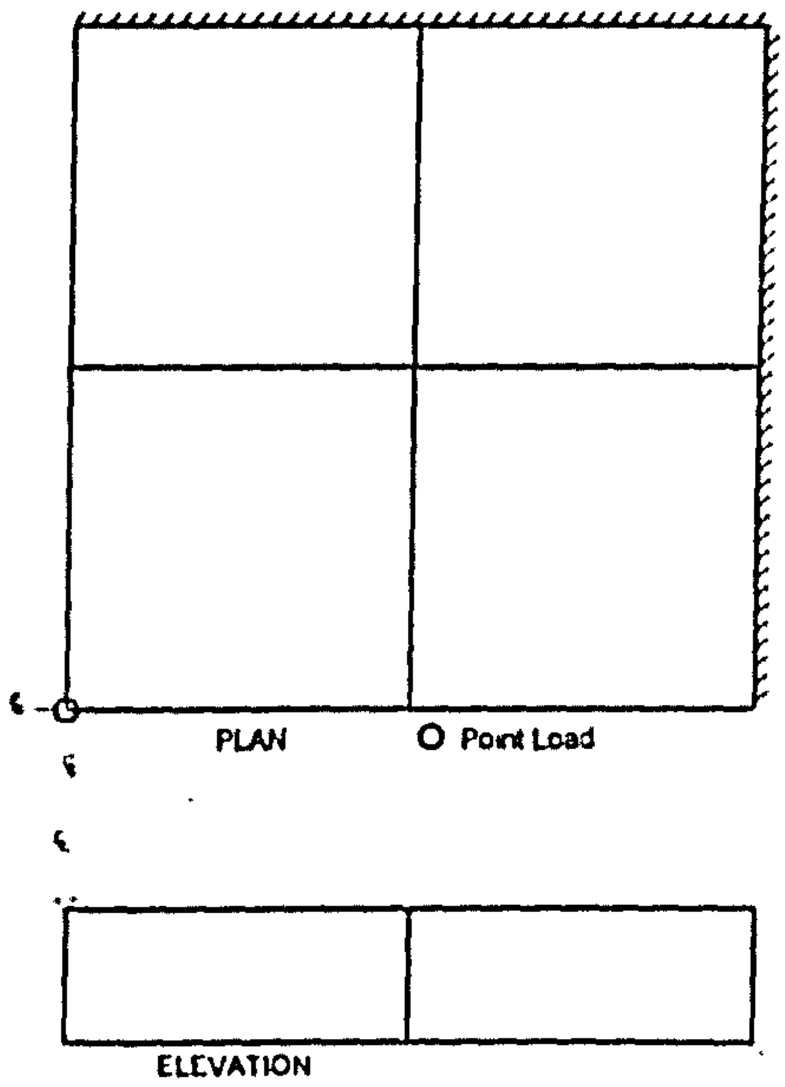

(c) 2×2 mesh

Figure 4.8 : Typical finite element mesh

4.5 Validation of numerical results

This section will briefly look into the predicted behaviour and mode of failure to validate the mathematical model. The validation was based on the correlation between the experimental and predicted values on three aspects of observed structural behaviour :

1.) The ultimate load capacity of slab.
2.) The load-deflection response.
3.) Strains in steel and concrete near the loading stub.

The mode of failure was classified in a simplistic manner as follows:

Flexural mode

- Ductile
- Steel yields

Shear mode

- Brittle
- Steel does not yield

4.5.1 Kotsovos' concrete model (In-house Program)

The computed ultimate load of slabs using Kotsovos' concrete model are given in Table 4.1. The ratio of predicted to measured ultimate load ranged from 0.65 to 1.02, with an average value of 0.89 and a standard deviation of 0.08.

For the slabs with low reinforcement ratio ($\rho<0.7\%$), pure flexural failure is expected. The predicted load-deflection response before cracking follows experimental results very closely. After cracking, the numerical load-deflection response is stiffer than the experimental results, but the gradient of the load-deflection response prior to failure is very low (Figure 4.9). Although no experimental measurement of strain in steel and concrete for lightly reinforced concrete slab is available, the predicted steel strains reach yield values (0.0024) and steel strain in some slabs was as high as 5% (Table 4.1). All these indications show that these slabs failed in a flexural mode.

This concrete model is particularly suitable for heavily reinforced slabs with steel ratio ($\rho > 1.5\%$). Computed variation of deflection, steel and concrete strain with load followed the test measurements closely. The gradient of load-deflection response is steep (Figure 4.10). The predicted strains in the flexural steel remain below the yield value (Figure 4.11) and the predicted concrete strain approaches crushing strain

(0.0035) as shown in Figure 4.12. All these indications shows that the slab failed in shear mode.

As shown in Figure 4.13, mesh size has little effect on the numerical response and ultimate load of slab. A detailed study of effect of mesh size will be given in the next chapter.

From the predicted ultimate load and structural response, it can be seen that Kotsovos' concrete model gives reasonably good results.

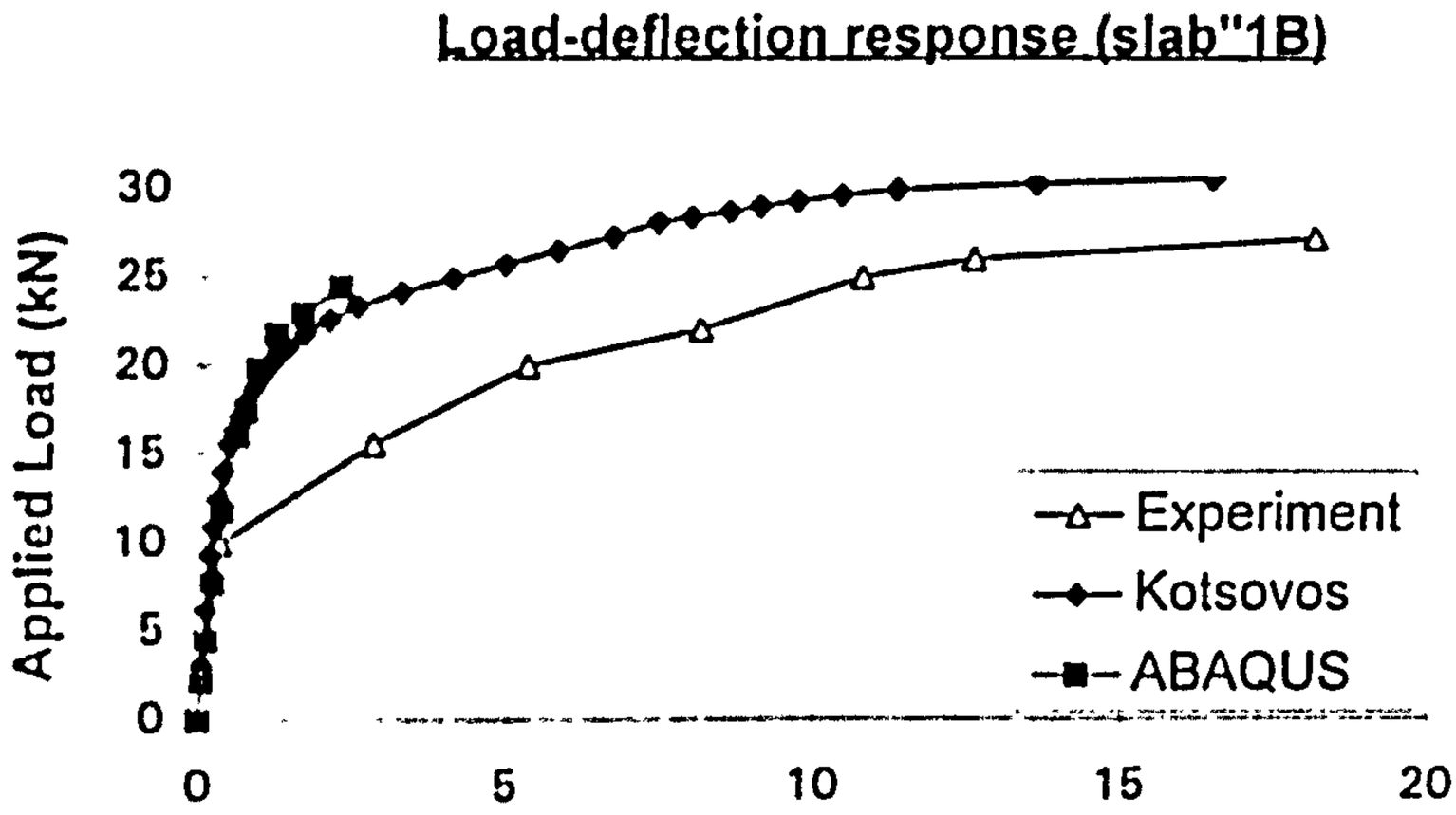

Figure 4.9 : Load-deflection response for slab failed in flexural mode

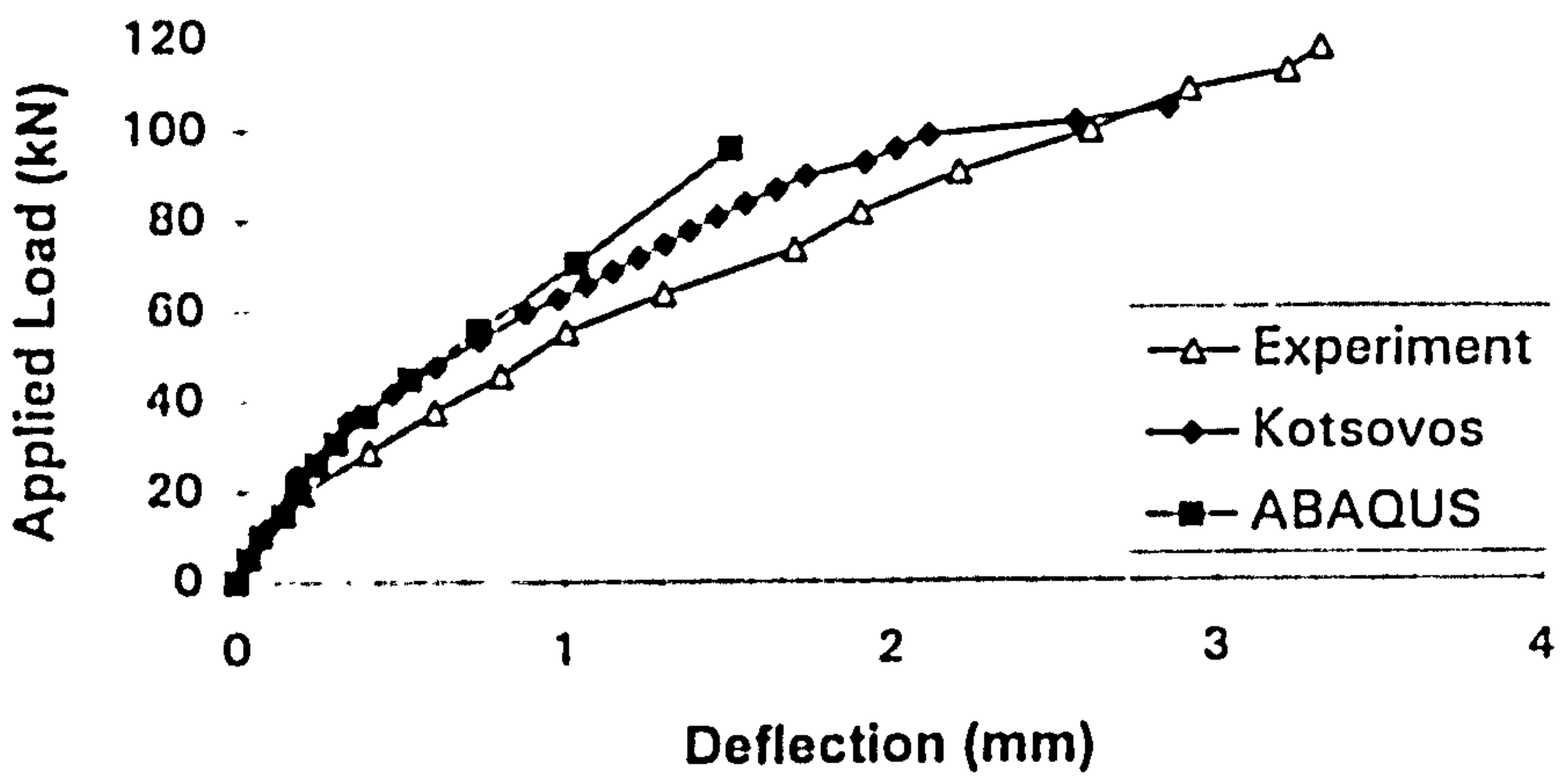

Figure 4.10 : Load-deflection response for slab failed in shear mode

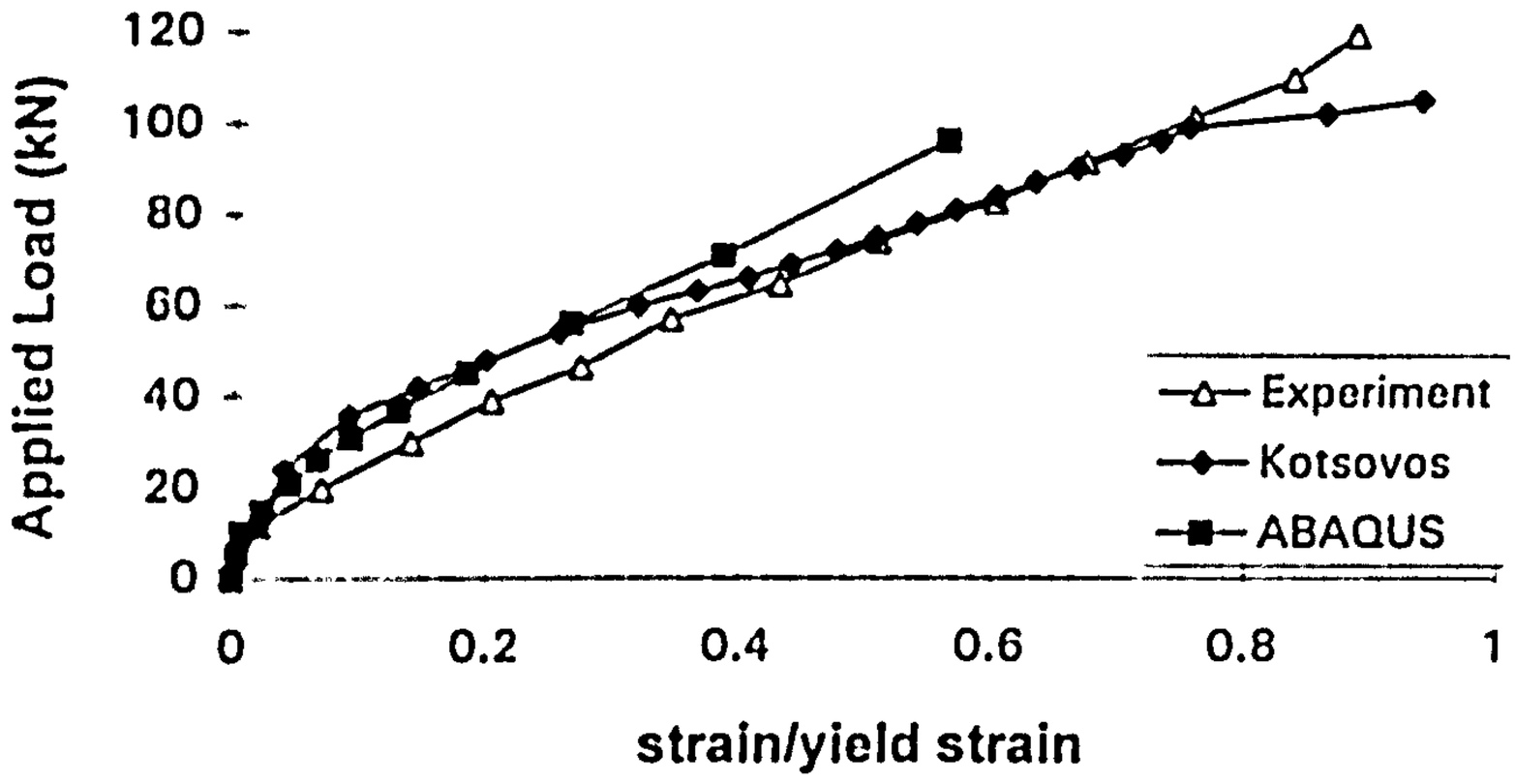

Figure 4.11 : Strain in flexural steel for slab failed in shear mode

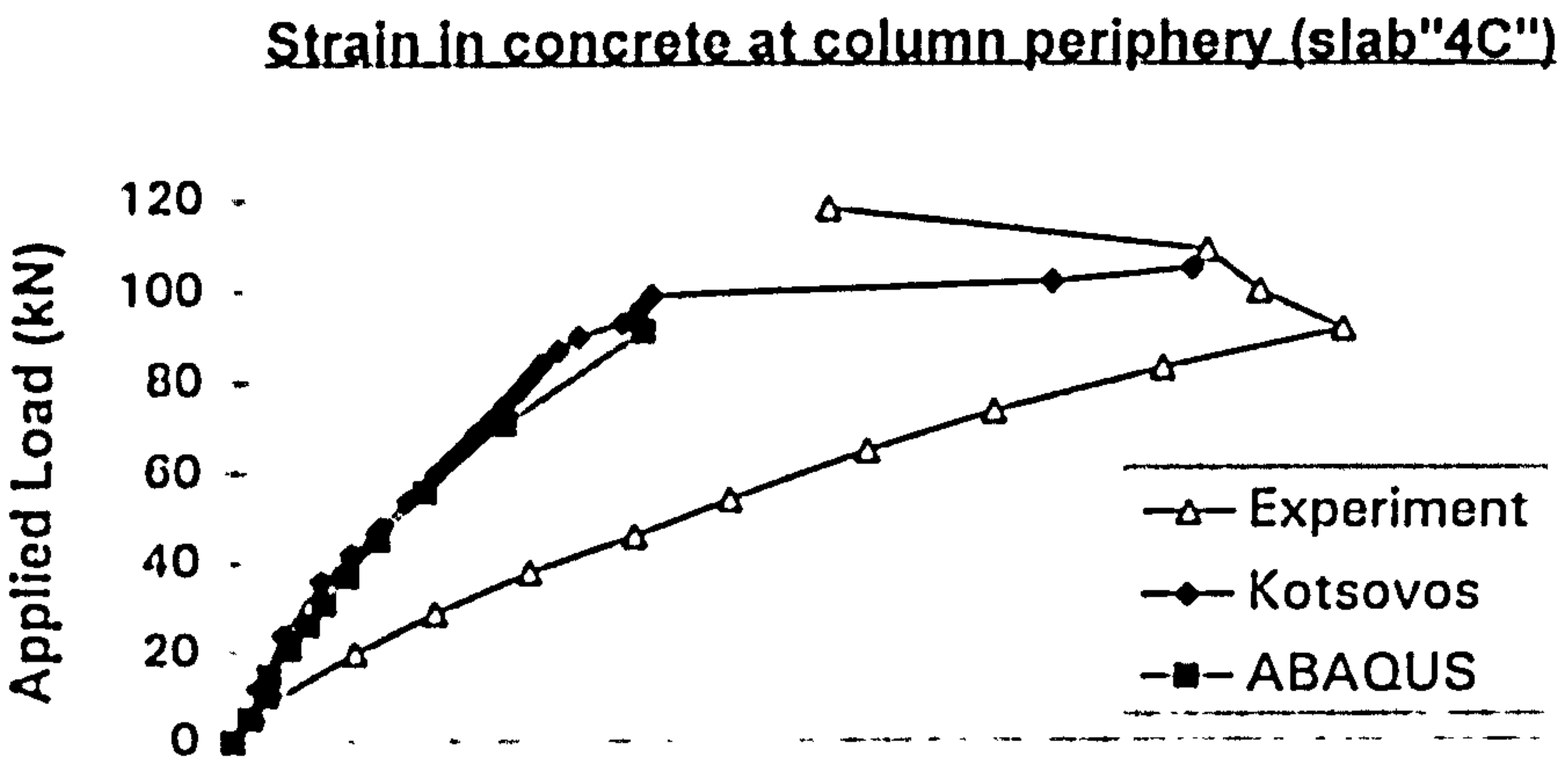

Figure 4.12 : Strain in concrete for slab failed in shear mode

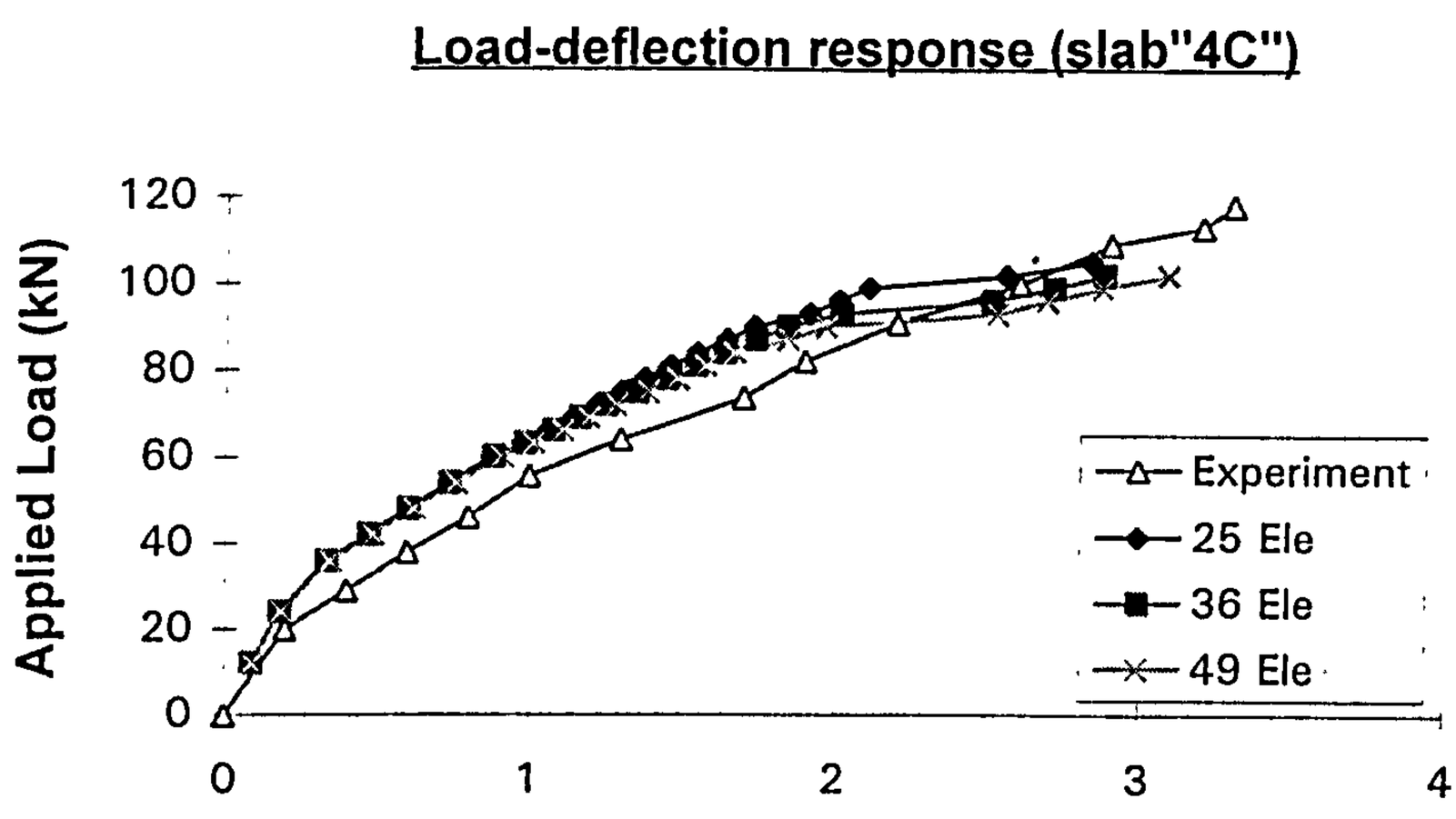

Figure 4.13 : Effect of mesh size (**In-house Program**)

4.5.2 ABAQUS Concrete model

The ultimate load predicted by ABAQUS concrete model is much lower than the experimental results (Table 4.2). These results show that the finer the mesh, the lower the predicted ultimate load which indicates that ABAQUS concrete model is highly mesh dependent. A very coarse mesh (2x2) gave a reasonably good prediction in which the predicted average ratio and standard deviation were 0.76 and 0.14 respectively. Marzouk and Jiang (1996) used a very coarse mesh in their 3D analysis using ABAQUS to study punching shear problem for high strength concrete slabs. Their results showed that very coarse mesh gave reasonably good prediction.

Due to the poor prediction by finer mesh, only structural response for very coarse mesh (2x2) is discussed here. The load-deflection response is stiffer than experimental measurement (Figures 4.9 & 4.10). Furthermore, the predicted strain in steel is far lower than the measured value (Table 4.2). Marzouk and Jiang (1996) also predicted a much stiffer load-deflection response when compared to the test results. However, they did not show any predicted strain in steel. So, it is not clear how well the strain in steel was predicted in their analysis.

Although a very coarse mesh predicted a reasonably accurate ultimate load of slabs, there is no clear indication of mode of failure (see Table 4.2). From this study, it can be concluded that at present three dimensional analysis using ABAQUS concrete model is not suitable for the study of punching shear problem.

Table 4.1: Prediction of Ultimate Load and mode of failure by In-house Program

(Rankin)

Slab No	f_{cu} (N/mm^2)	ρ (%)	Experimental		Numerical Prediction			
			P_{test} (kN)	Failure Mode	N/E	deflection	Steel (strain/ys)	Failure Mode
1	38.40	0.423	36.42	y	0.949	y	5.54	y
2	38.40	0.558	49.08	y	0.831	y	3.12	y
3	38.40	0.691	56.55	y	0.683	y	2.00	y
4	43.50	0.821	56.18	y	0.688	y	0.91	s/y
5	43.50	0.883	57.27	y	0.654	s	0.70	s/y
6	43.50	1.026	65.58	s	0.743	s	1.25	s/y
7	37.10	1.163	70.94	s	0.660	s	0.94	s
8	37.10	1.292	71.09	s	0.709	s	1.32	s/y
9	37.10	1.454	78.60	s	0.756	s	0.96	s
10	37.40	0.517	43.50	y	0.842	y	2.04	y
11	37.40	0.802	55.00	y	0.648	y	0.95	s/y
12	37.40	1.107	67.06	s	0.676	y	1.2	y
13	42.50	0.601	49.39	y	0.842	y	1.39	y
14	42.50	0.691	52.45	y	0.789	s	1.17	s/y
15	42.50	1.994	84.84	s	0.792	s	0.89	s
1A	36.00	0.422	45.19	y	0.918	y	2.67	y
2A	36.00	0.691	66.24	y	0.786	y	1.71	y
3A	36.00	1.293	89.72	s	0.762	s	0.94	s
4A	38.60	1.992	97.43	s	0.838	s	0.85	s
1B	47.10	0.423	28.85	y	1.027	y	2.38	y
2B	47.10	0.690	37.63	y	0.867	y	2.17	y
3B	47.10	1.292	56.67	y	0.711	s	0.98	s
4B	38.60	1.994	72.52	s	0.720	s	0.95	s
1C	34.80	0.423	62.74	y	0.845	y	1.51	y
2C	40.50	0.690	87.86	s	0.713	s	1.06	s/y
3C	40.50	1.288	124.14	s	0.749	s	0.97	s
4C	34.80	1.993	125.94	s	0.834	s	0.95	s
				Average	0.892			
				STDEV	0.081			

Note
N/E=Predicted/Experimental load
y = flexure failure mode
s = shear failure mode
ys=yield strain of steel

Table 4.2: Prediction of Ultimate Load by ABAQUS
(Rankin's slabs)

	Experimental		Numerical				
Slab	P_{test} (kN)	Failure Mode	*Steel strain/ys	*Failure Mode	Numerical/Exp. failure Load		
					4 solids	9 solids	25 solids
1	36.42	y	0.71	s	0.865	0.457	0.220
2	49.08	y	0.55	s	0.683	0.375	0.212
3	56.55	y	0.53	s	0.698	0.352	0.186
4	56.18	y	0.83	s	0.731	0.374	0.214
5	57.27	y	0.71	s	0.762	0.372	0.236
6	65.58	s	0.30	s	0.725	0.352	0.233
7	70.94	s	0.36	s	0.641	0.265	0.228
8	71.09	s	0.30	s	0.656	0.264	0.253
9	78.60	s	0.30	s	0.619	0.261	0.254
10	43.50	y	1.00	y	0.721	0.399	0.202
11	55.00	y	0.28	s	0.676	0.313	
12	67.06	s	0.35	s	0.657	0.268	
13	49.39	y	0.55	s	0.762	0.436	
14	52.45	y	0.59	s	0.777	0.360	
15	84.84	s	0.35	s	1.162	0.287	
1A	45.19	y	0.19	s	0.883	0.429	
2A	66.24	y	0.32	s	0.725	0.337	
3A	89.72	s	0.39	s	0.559	0.267	
4A	97.43	s	0.34	s	0.857	0.298	
1B	28.85	y	0.53	s	1.004	0.605	
2B	37.63	y	0.90	s	0.813	0.714	
3B	56.67	y	0.69	s	0.793	0.639	
4B	72.52	s	0.56	s	1.046	0.243	
1C	62.74	y	0.59	s	0.627	0.431	
2C	87.86	s	0.38	s	0.717	0.331	
3C	124.14	s	0.82	s	0.708	0.303	
4C	125.94	s	0.60	s	0.762	0.295	
				Average	0.764	0.371	0.224
				STDEV	0.136	0.119	0.022

Note
*strain and mode of failure here are for 4 solid element model
ys=yield strain of steel

4.6 Discussion

In order to find out why ABAQUS concrete model gave such a poor prediction for punching shear problem, a concrete element subjected to tri-axial (Figure 4.14) and pure shear loading was examined. The compressive cylinder strength of the element was assumed to be 45N/mm^2 and the tensile strength as 3.6N/mm^2.

From Figure 4.15, it can be seen that when the state of stress is dominantly compressive (I_1 is high), the allowable tensile stress in the third direction goes up to 30% of compressive strength. This value is far too high compared to actual tensile strength of concrete. This implies that when stresses in the element is compressive dominant (high I_1), the third direction will never crack due to the high allowable tensile stress. From table 4.3, ABAQUS concrete model is stronger than Kotsovos' concrete model in both tension and compression under multiaxial stress. Clearly, this is not the reason why ABAQUS code predicted such a low ultimate load.

Figure 4.16 shows the results of a study into strength envelope of concrete in term of octahedral stresses for both constitutive models. This figure shows that Kotsovos' model gives higher shear strength than ABAQUS model under large octahedral stress ($\sigma_o/f_c>0.9$). But stress combination for a slab is unlikely to reach this region. For small octahedral stress ($\sigma_o/f_c<0.1$), Kotsovos' model gave higher shear resistance than ABAQUS model (Figure 4.17) for certain combination of stress. From the results of slabs analysed (octahedral stress for every Gauss point) from both models (Figures 4.18-4.21) confirmed that octahedral stress for slab structure subjected to concentrated load have a tendency to lie in this region. Test of single element subjected to pure shear loading (Table 4.4) also show that Kotsovos' model have higher shear resistance. The above finding may be the reason for the analysis using solid element with ABAQUS concrete model, predicted such a low ultimate load. Unfortunately, there is no source code available for ABAQUS program to check where the error lies.

4.7 Conclusion

From a comparison between the predictions by Kotsovos' and ABAQUS' concrete model, the following conclusions can be drawn:

- Kotsovos' concrete model is more suitable for three dimensional analysis because its prediction proved to be very close to experimental observation in terms of ultimate load, structural response and mode of failure.

- The prediction by ABAQUS concrete model is not reliable, even though very coarse mesh predicted reasonably good results for ultimate load of slabs. The prediction does not give a clear indication of mode of failure and for some slabs even wrong mode of failure was given.
- The behaviour of concrete under triaxial loading simulated by Kotsovos is closer to experimental results (see figure 3.12).
- ABAQUS concrete model cannot mimic the true tri-axial effect of concrete.

The comparison, between the predictions of Kotsovos and ABAQUS models leads to the conclusion that non-linear elastic isotopic model proposed by Kotsovos is a good model for predicting the behaviour of reinforced concrete slab. Therefore Kotsovos concrete model will be used for the later study.

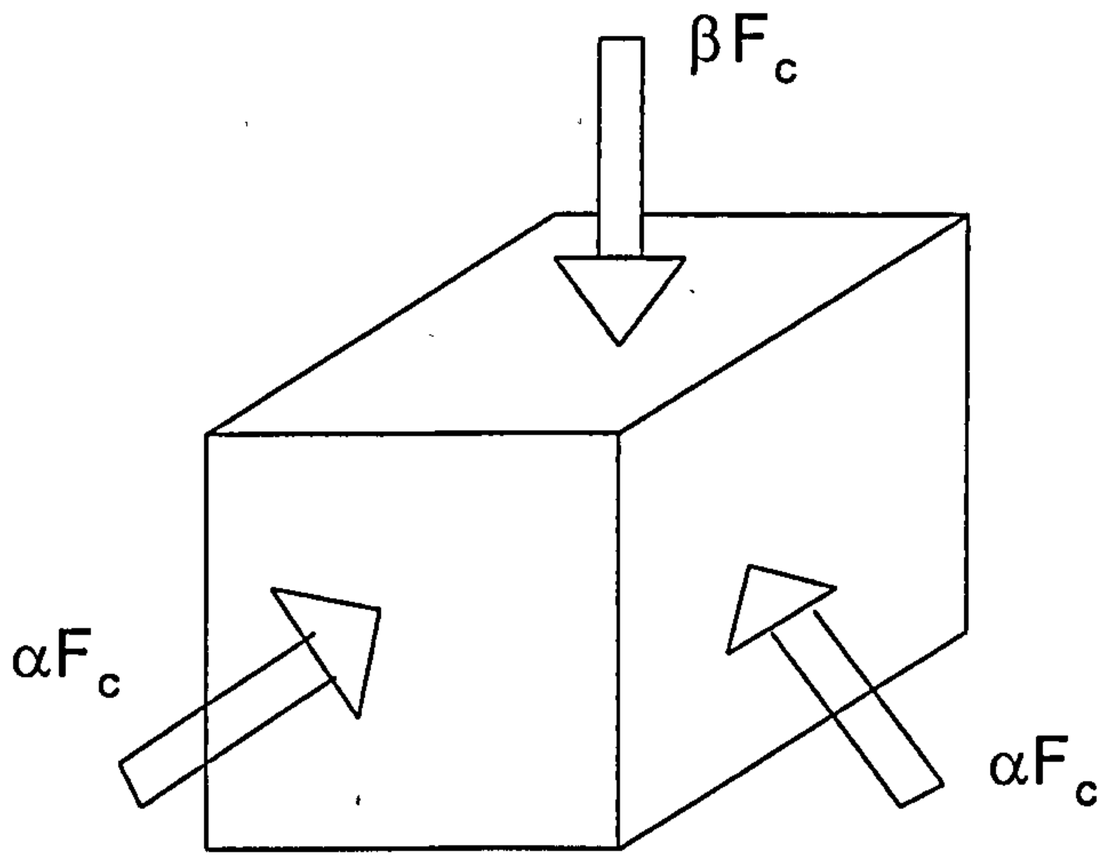

Figure 4.14 : An element subjected to Triaxial loadings

Table 4.3 Allowable stress under triaxial loading

Loadings	Maximum Allowable stress (N/mm^2)	
	ABAQUS	*Kotsovos
Tri-axial Tension	+2.964	+1.575
Bi-axial Tension	+2.763	+1.800
Uni-axial Tension	+3.600	+1.980
Tri-axial compression	infinity	-72.000
Bi-axial compression	-54.520	-49.200
Uni-axial compression	-45.000	-45.000
Bi-axial compression & Tension	see Figure 4.12	see Figure 4.12

* Kotsovos' model use $f_{sp}/2$ for tensile strength

Table 4.4 Allowable stress under pure shear loading

Loadings	Maximum Allowable stress (N/mm^2)	
	ABAQUS	Kotsovos
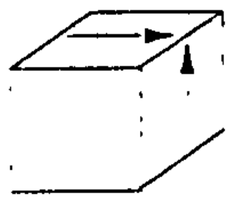	2.23	2.61
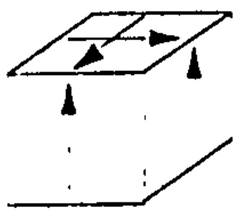	+1.22	1.56
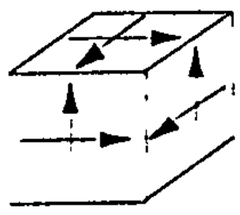	0.82	1.20

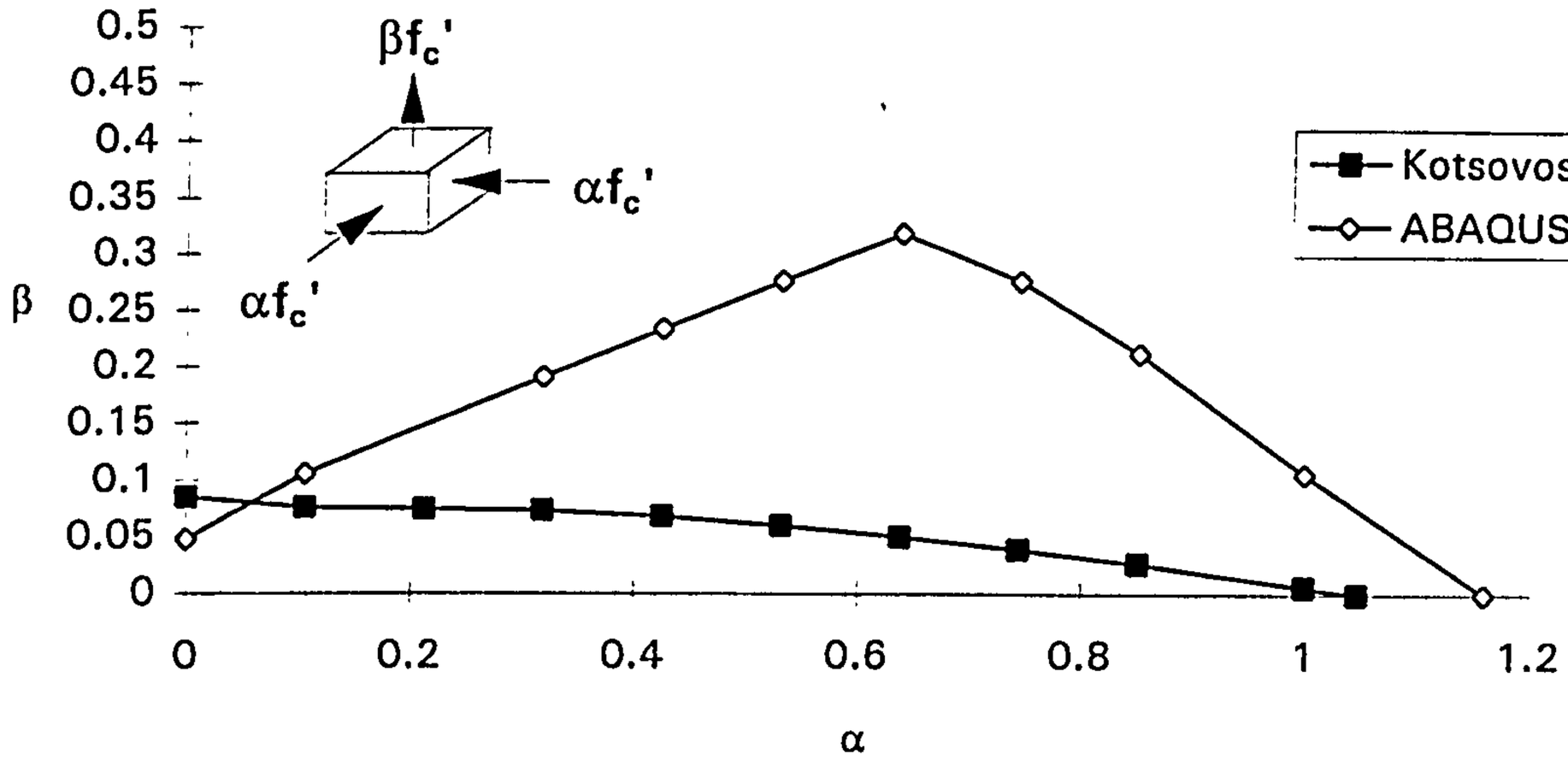

Figure 4.15 : Maximun tensile stress under Triaxial loadings

Note. $\alpha f_c' > \beta f_c'$

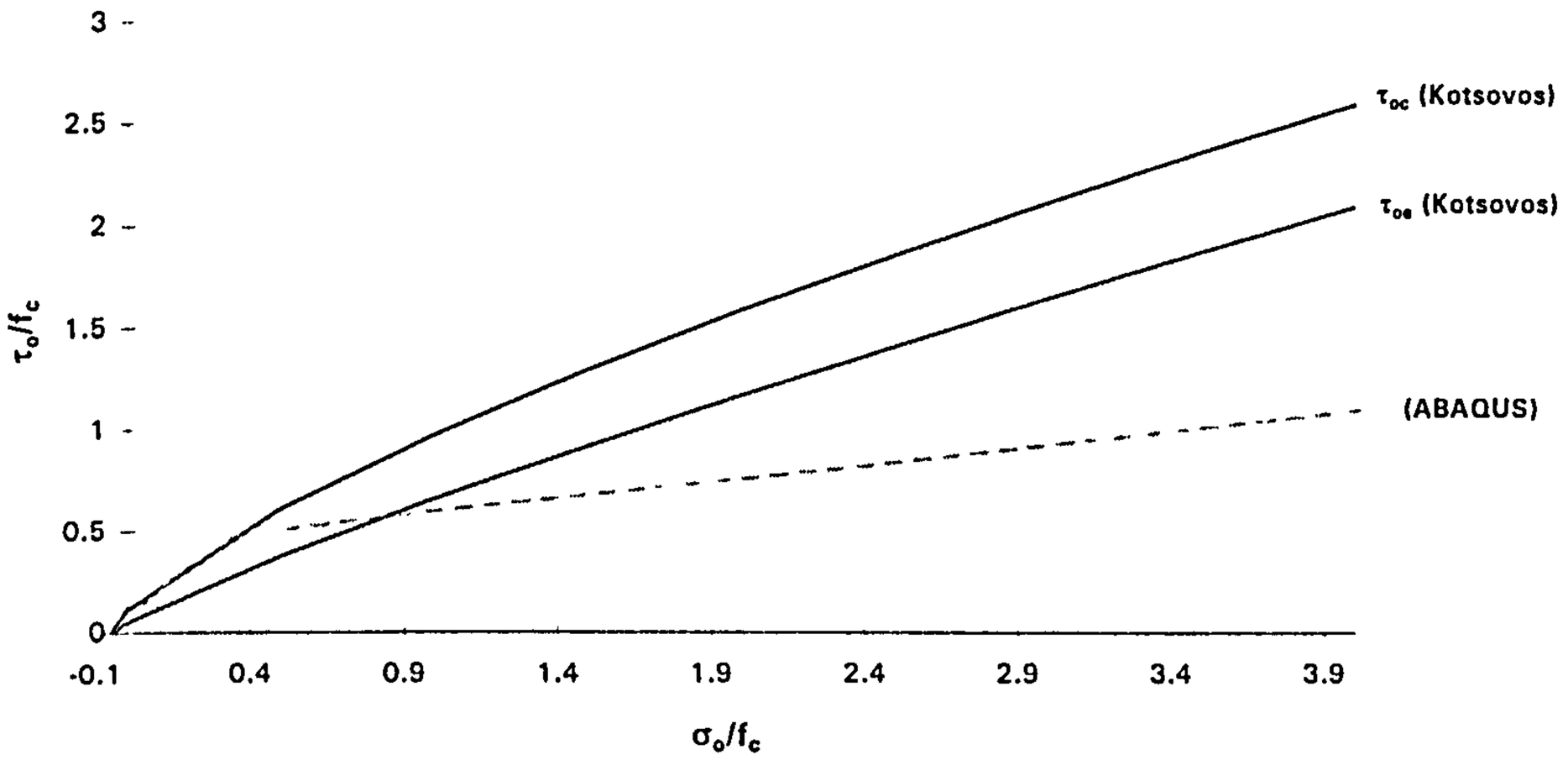

Figure 4.16 : Strength envelope of concrete

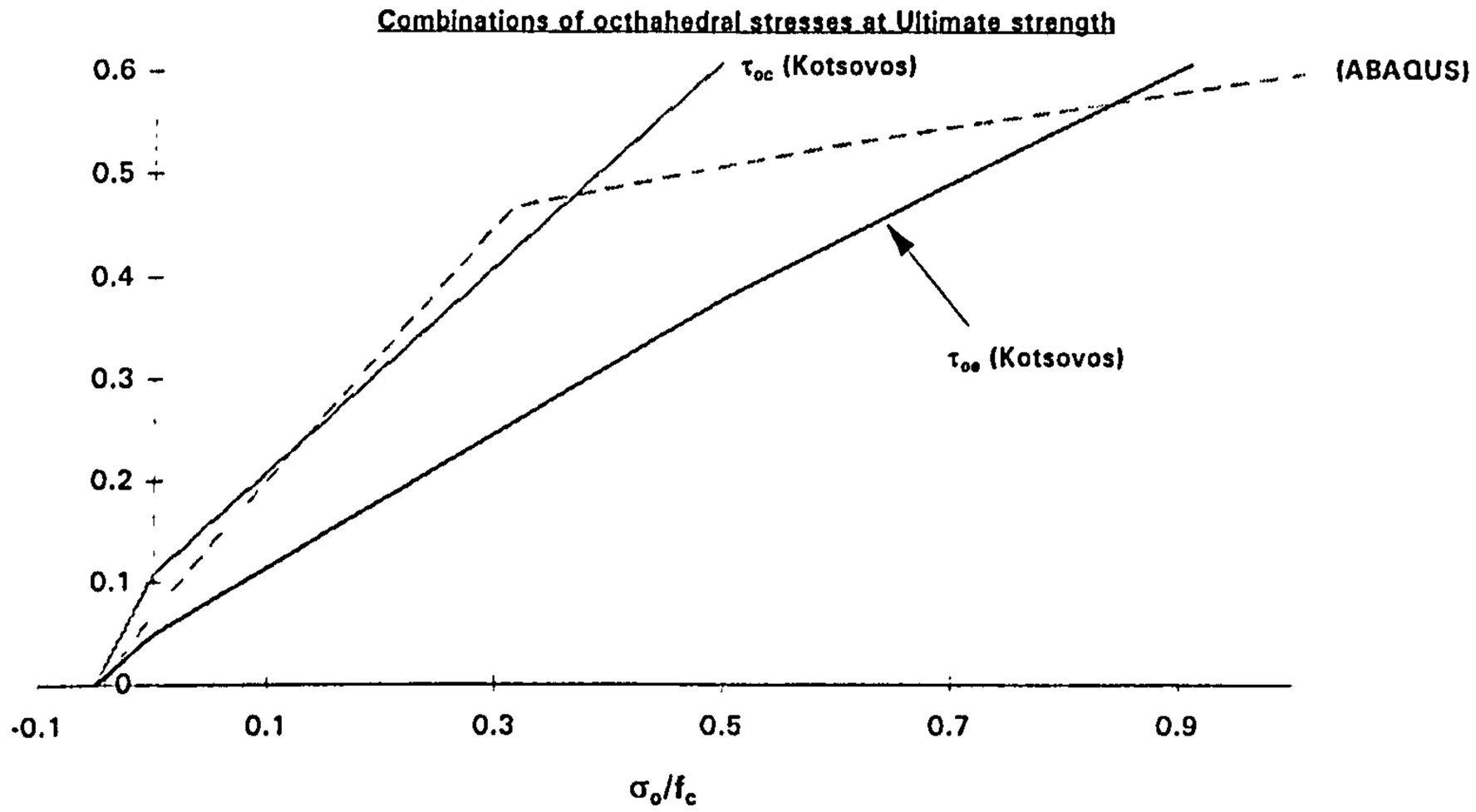

Figure 4.17 : Strength envelope of concrete (Magnified for $\sigma_o/f_c \leq 1.0$)

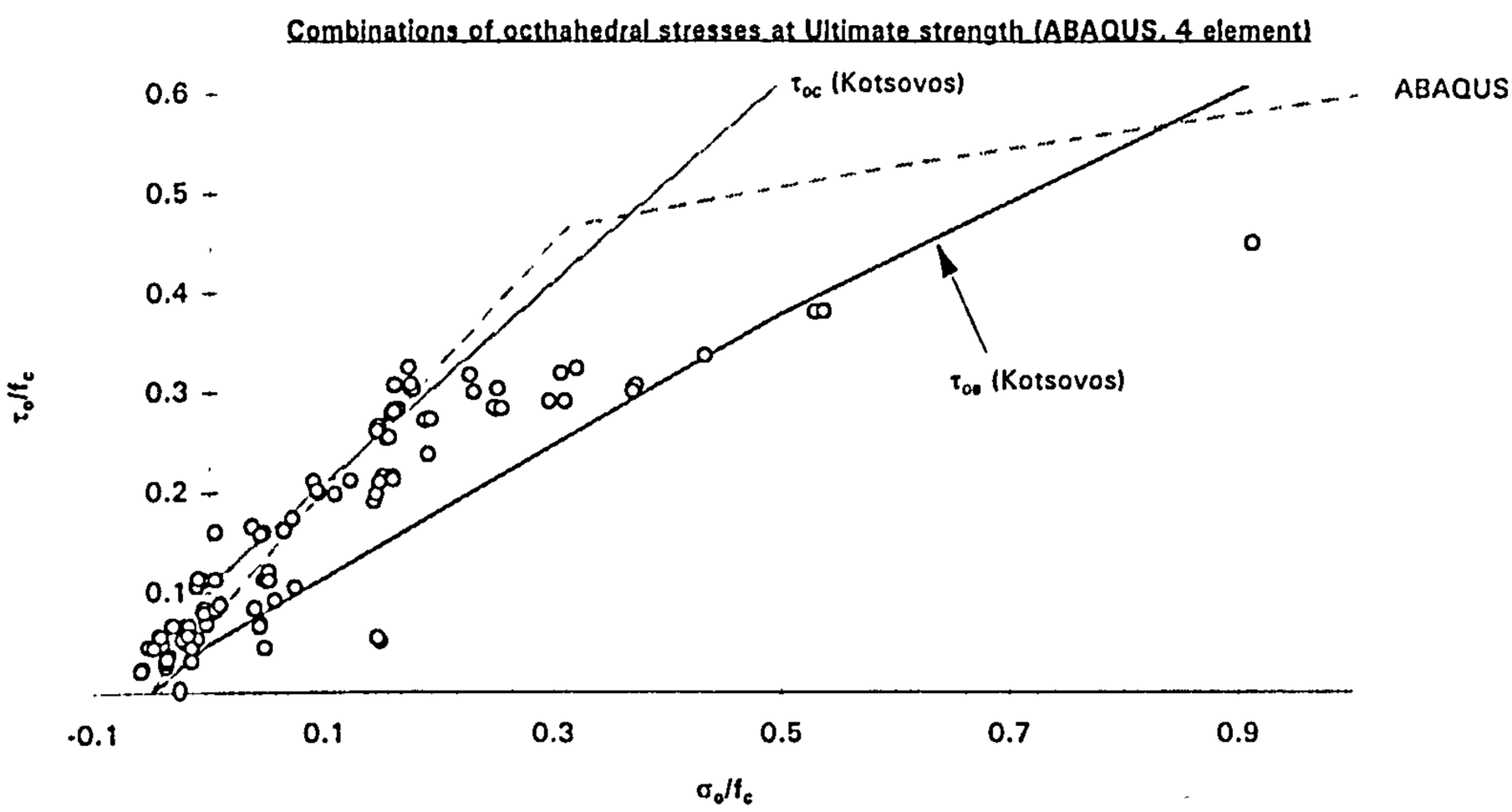

Figure 4.18 : Stress combinations for 2x2 mesh analysed by ABAQUS

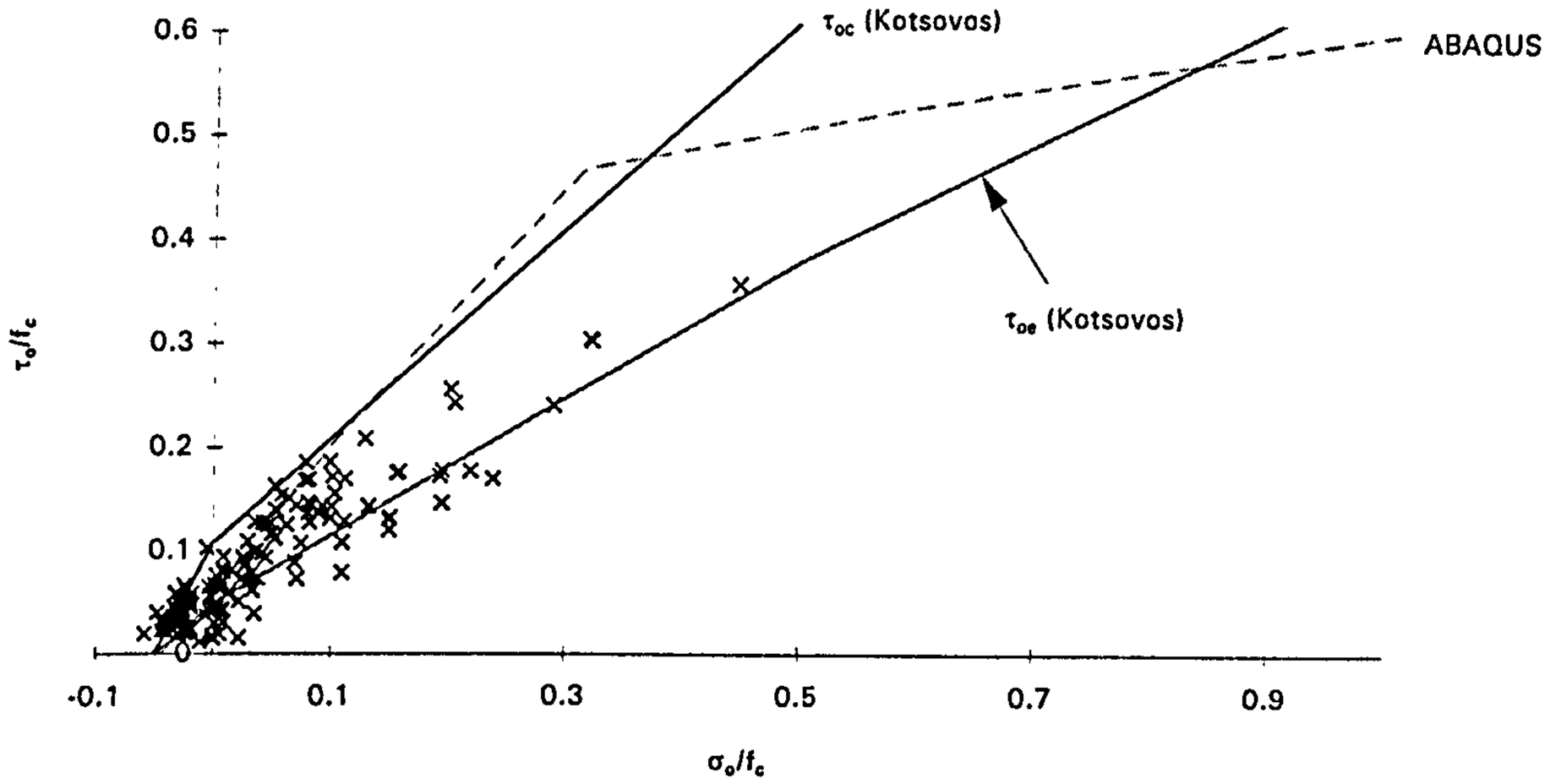

Figure 4.19 : Stress combinations for 3x3 mesh analysed by ABAQUS

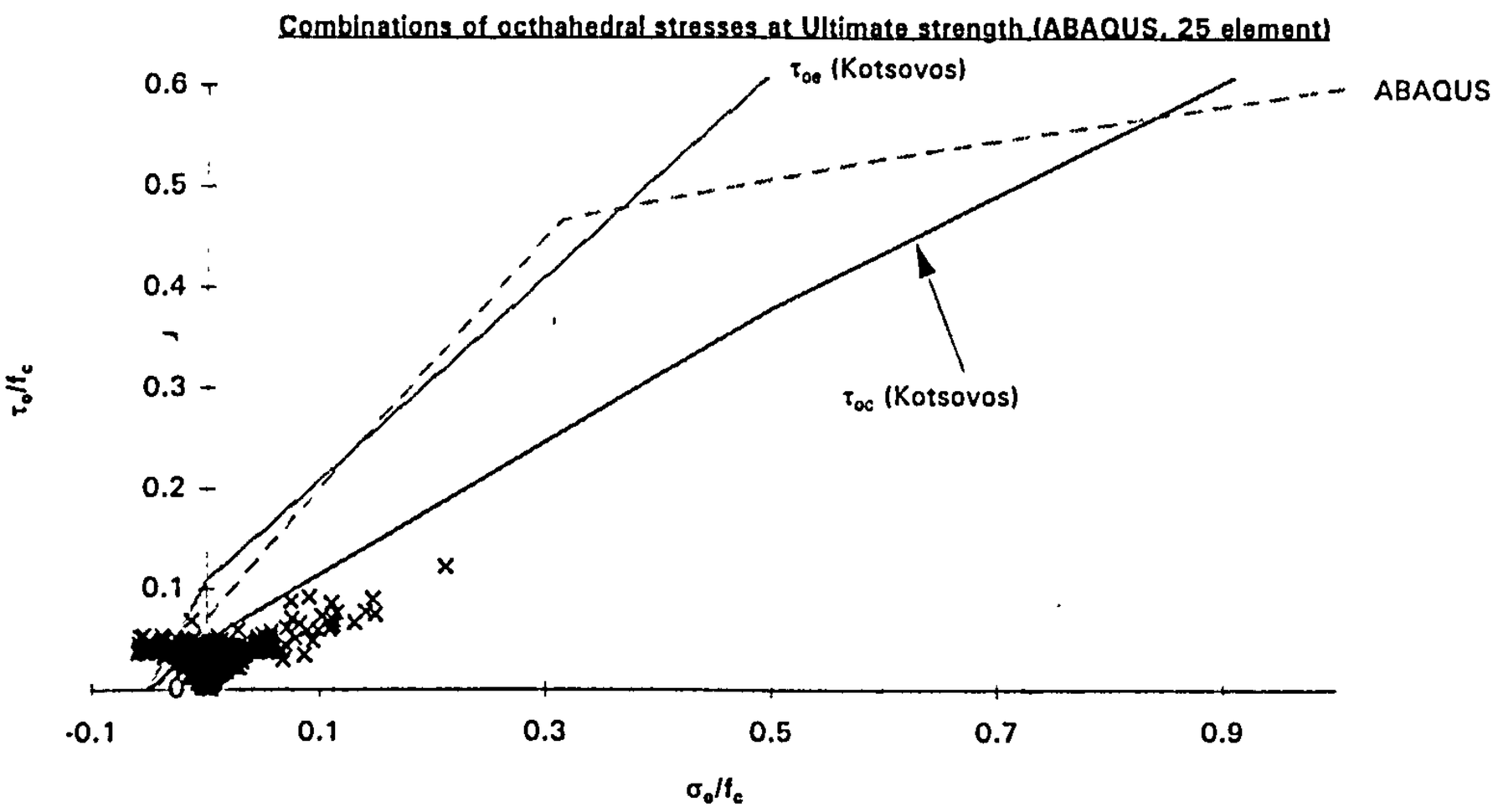

Figure 4.20 : Stress combinations for 5x5 mesh analysed by ABAQUS

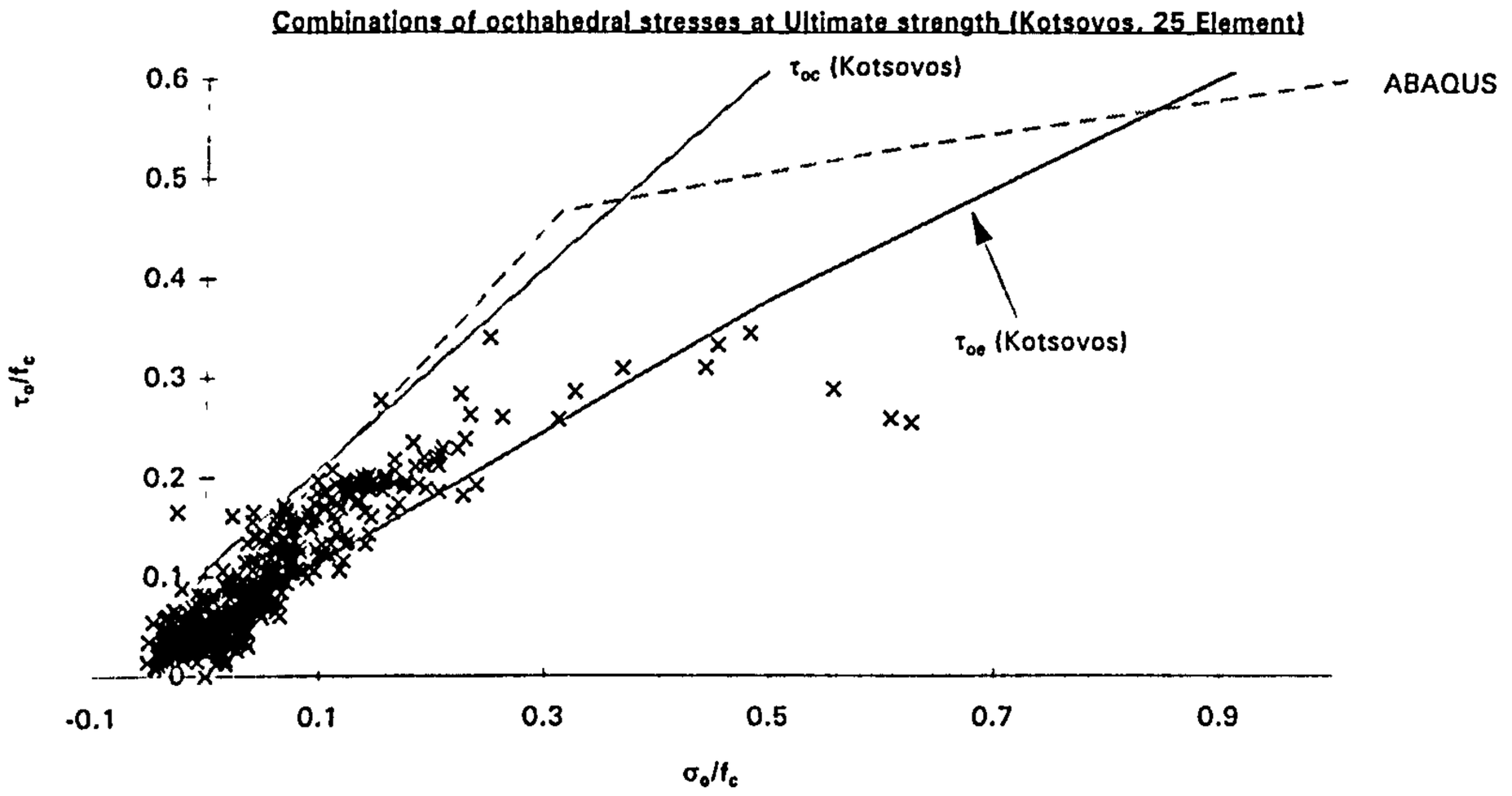

Figure 4.21 : Stress combinations for 5x5 mesh analysed by Kotsovos' model

Chapter 5

PARAMETRIC STUDY

5.1 Introduction

There are many parameters which affect the finite element prediction of the behaviour of slabs. Generally these parameters can be classified into two categories. The first category contains numerical parameters such as solution procedure, size of load increment, maximum number of iteration per increment, the convergence tolerance, mesh size, type of element, order of numerical integration, simulation of boundary conditions and applied loads. The second category contains material parameters such as compressive and tensile strengths of concrete, Young's modulus, Poisson's ratio, tension stiffening factor, shear retention factor and yield strength of reinforcement.

The objective of the parametric study is to see how these parameters affect the behaviour of the slab. In this section, the parameters are varied one at a time. As the number of variations is large, the computation will be confined to a small number of typical slabs. The final values of the parameters chosen is based upon those giving the best comparison with the experimental results. The comparison between the experiments and predicted values was based on the following aspects of structural behaviour :-

- The ultimate load capacity of the slab;
- The load-deflection response;
- Strains in flexural reinforcement;
- Distribution of strains and stresses in concrete within the compressive zone;
- Crack pattern;
- The mode of failure.

After having chosen the "best" concrete model, all the analysis will use this set parameters for the analysis of a large number of slabs from different sources.

5.2 Determination of modes of failure

A set of general rules were laid down for the classification of modes of failure based on following structural responses from experimental observations:-

- Load-deflection response;
- Strain in flexural reinforcement;
- Principal compressive stress and strain in concrete;
- Crack pattern.

5.2.1 Load deflection response/Load-rotation response

Section 2.2 stated that slabs which display large ductility, basically fail in flexural mode, while brittle behaviour represents slabs failing by primary punching. However, this is only rough classification. From the experimental load-deflection curve (Figure 5.1), it can be observed that lightly reinforced slab have three stages of behaviour:

1.) Stiffness for uncracked concrete;
2.) After flexural cracks have formed, there is an obvious decrease in the stiffness of the slab.
3.) Yielding of flexural reinforcement leading to a further decrease in stiffness.

For slabs which fail in brittle (shear) mode, the load-deflection curve consists of first two stages only because very often steel does not yield.

Experimental load-deflection response also shows that the gradient of the curve prior to failure is low for slabs which fail in flexure mode and is steep for slabs which fail in shear mode. Therefore, if the gradient prior to failure is low, the slab is said to have failed in flexure mode. Conversely, if the slope is very steep the slab is said to have failed in shear mode.

For corner and edge column-slab connections, the failures are more likely to occur at the column-slab junction. Because of lack of symmetry, there is considerable rotation involved. Thus, judging of mode of failure for these two types of connections will include rotation of slab at the junction.

5.2.2 Strain in flexural reinforcement

Judging of modes of failure from strain in flexural reinforcement is done as follows :-

Flexural failure

If flexural steel yields well before failure and yielding spreads over a wide area of the slab at failure, the slab is said to have failed in pure flexural mode.

Flexural punching failure

If the flexural steel yields at failure and the yielding of reinforcement is confined to a small area locally around the column, the slab is said to have failed in flexure punching mode.

Pure punching failure

If there is no yielding of reinforcement, the slab is said to have failed in punching shear mode.

5.2.3 Principal compressive stress and strain of concrete in compression zone

Kinnunen-Nylander's model indicates that slabs failing in punching shear mode are highly stressed. It assumes that punching occurs when the stress and strain in the conical shell reaches critical values (see section 2.3.1.1). In the present study, concrete crushing is assumed to occur when the maximum compressive strain exceeded 0.0035 (see section 3.3.1.1). Therefore, when either principal compressive stress greater than f_c'.or principal compressive strain reaches or exceeds 0.0035, the slab is said to fail in punching.

5.2.4 Crack Pattern

Fixed crack model (section 3.3.4) is used in the present study. Once a crack occurs, its direction is fixed and remains constant during subsequent loadings. Crack direction is perpendicular to the direction of first principal strain and in the vector plot diagram, the crack length is plotted as proportional to the magnitude of first principal strain.

From experimental observation, pure bending action produces vertical cracks and pure shear action will produces inclined cracks. Thus, if the cracks in the vicinity of the column are vertical, it indicates that the slab has failed in flexure mode (Figure 5.2a). Conversely, if the cracks are inclined, it indicates that the slab failed in shear mode (Figure 5.2b).

5.2.5 Notations

The notations used to represent different modes of failure are defined as follows:

y = pure flexural failure

fp = flexural punching

s = punching failure

c = crushing of concrete

For slabs with shear reinforcement, shear failure is defined as

out = punching occurs outside shear reinforcement region

in = punching occurs within shear reinforcement region

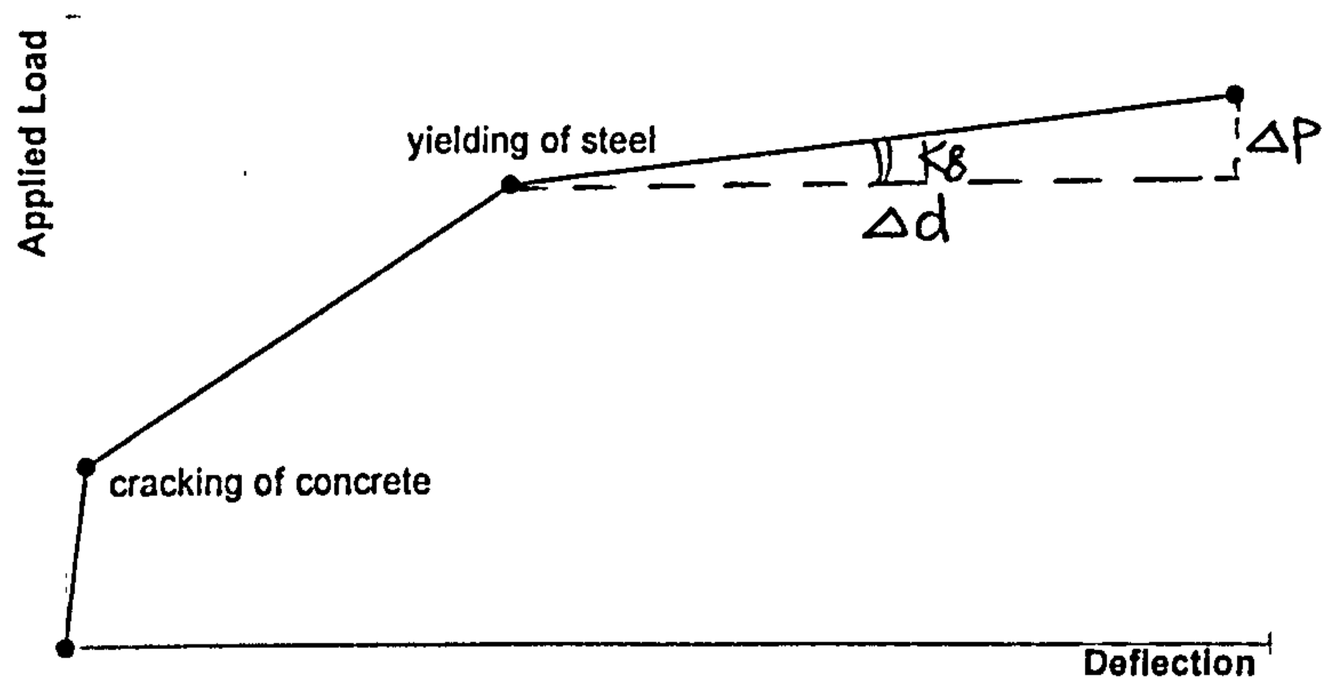

Flat $\Rightarrow K_\delta$=small

Steep $\Rightarrow K_\delta$=large

where $K_\delta = \Delta P / \Delta d$

Figure 5.1 Load-deflection curve for slab failing in ductile mode

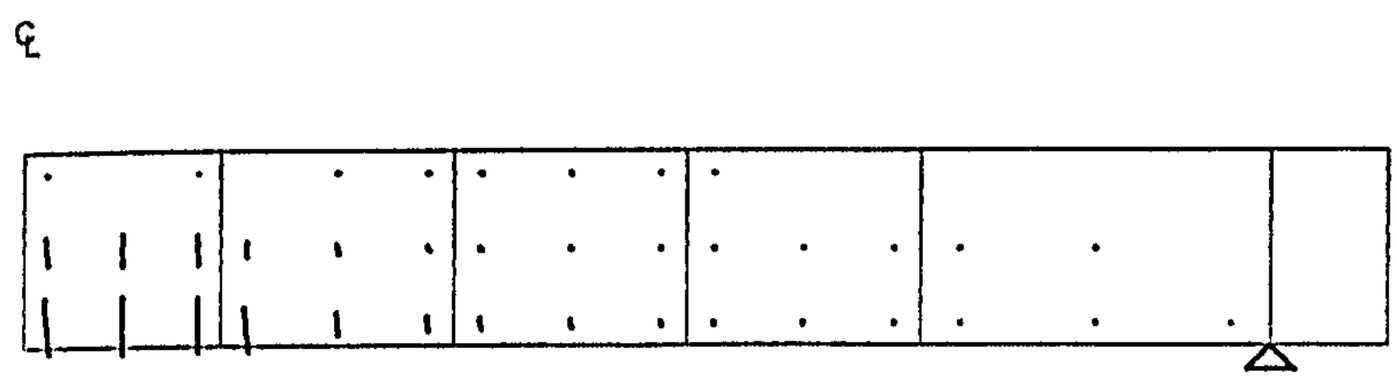

(a) Flexure mode

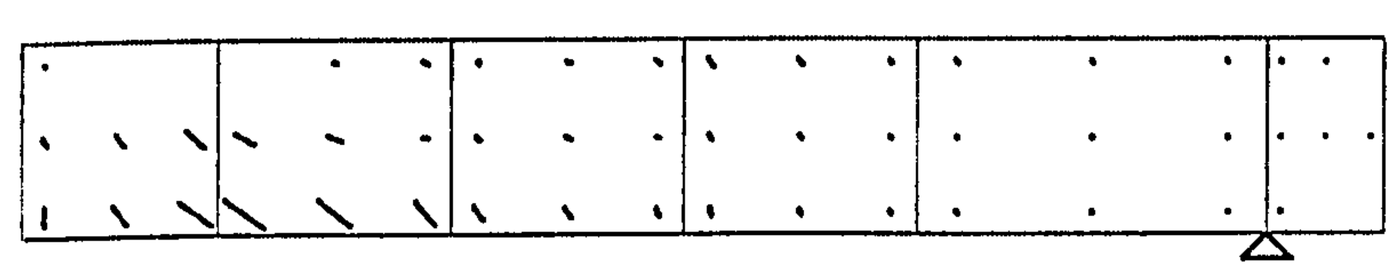

(b) Shear mode

Figure 5.2 Crack pattern (elevation)

5.3 Conventional slab-column specimens tested by Rankin

Rankin (1982) tested 27 conventional slab-column specimens without shear reinforcement. These slabs cover most of the important parameters (thickness of slab, flexural reinforcement ratio, concrete strength, etc.) governing punching shear strength. A parameteric study was done on five slabs only. These slabs are models "1B", "1C", "2C", "3C" and "4C". These slabs are chosen because they failed in different failure modes (i.e. flexural failure and punching shear failure) and experimental data is available to verify the proposed concrete model (Table 5.1).

These slabs were simply supported along the four edges with corners free to lift and subjected to a concentrated load at the centre of slab as shown in Figure 5.3. Concrete strength ranged from 36-47 N/mm^2. Flexural reinforcement only was included in the models and this varied over the range of 0.4-2.0%. The span/depth

(L/h) ratios varied over a range of 25-35. The reinforcement had a well defined yield point with no strain hardening (f_y = 530 N/mm^2). A summary of details of these slabs is presented in Table 5.1.

Owing to symmetry, only one-quarter of the slabs was modelled. The applied load was simulated by uniformly distributed load over the element representing the loading stub. The slab was generally discretised by using one layer of twenty node solid elements.

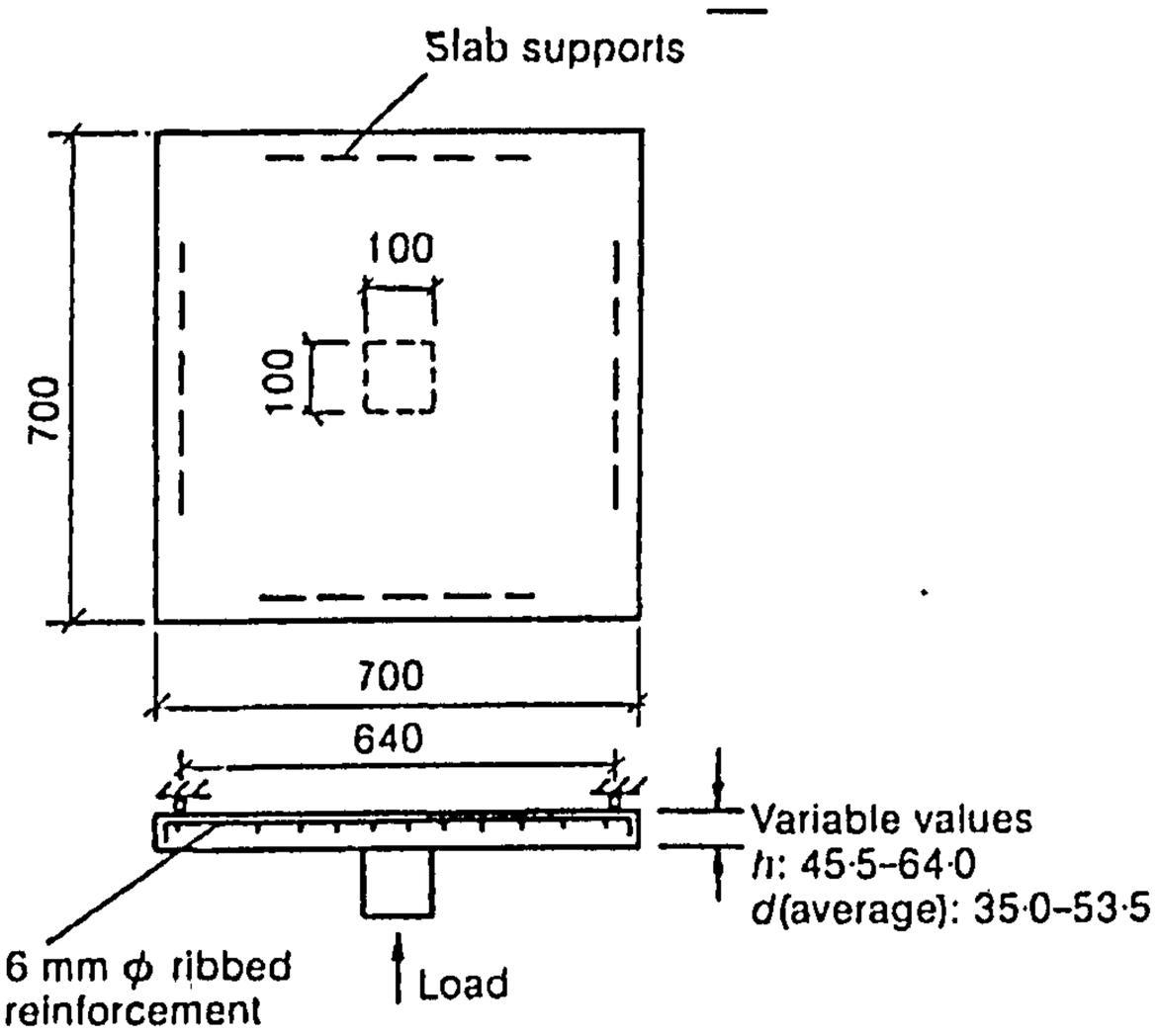

Figure 5.3 :Rankin's slab-column models

Table 5.1 : Details of slabs, 1B, 1C-4C (Rankin, 1982)

Slab	f_{cu} (N/mm^2)	d (mm)	ρ (%)	P_{test} (kN)	Failure Mode
1B	47.10	35.00	0.423	28.850	y
1C	34.80	53.50	0.423	62.740	y
2C	40.50	53.50	0.690	87.860	s
3C	40.50	53.50	1.288	124.140	s
4C	34.80	53.50	1.993	125.940	s

where d = effective depth

$$\rho = \frac{100 A_s}{bd}$$

5.4 Numerical Parameters

The main purpose of the study of the effect of numerical parameters on slabs behaviour is to choose the values of parameters to achieve an accurate, and at the same time economical solution for the non-linear analysis. Five parameters which have significant effect on the computational cost and Finite Element prediction was studied. These parameters are :

i) Convergence tolerance,
ii) Size of load increment,
iii) Mesh size,
iv) Number of elements through the thickness of slab,
v) simulation of boundary conditions.

For this study, material parameters were kept constant as follows :

- the cylinder compressive strength of concrete (f_c') was taken to be 0.8 f_{cu}, where f_{cu} is the compressive cube strength of concrete
- Young's modulus of concrete, $E_c = 4730\sqrt{f_c'}$ N/mm^2
- Poisson's ratio 0.2
- Tensile strength of concrete, $f_t = f_{sp}/2$ and the splitting cylinder tensile strength, $f_{sp} = 0.53\sqrt{f_c'}$ N/mm^2
- The tension stiffening is taken as a linear function of the principal strain. There is no reduction of tensile strength immediately after cracking. Maximum strain ε_{max} was kept constant at 0.003 (Refer to Figure 3.17).
- The shear retention factor is kept constant as $\beta=0.5\ \varepsilon_{cr}/\varepsilon_n$ (Refer to Figure 3.20).
- For steel, the measured values of the elastic modulus and yield stress were used. An elastic perfectly plastic behaviour was assumed.

5.4.1 Effect of convergence tolerance

A 6x6 mesh on plan, with one layer of solid element to represent the thickness of slab as shown in Figure 5.4 was used in this study. For this study, the size of load increment was kept constant as 5% of experimental failure load for all the increments. The tolerance factors studied were 1%, 5% and 10%.

In the numerical procedure, convergence tolerance is used to monitor the gradual elimination of the out-of-balance residual forces until desired accuracy is achieved. Theoretically, small tolerance is required but it can be very expensive because it requires a large number of iterations. Figures 5.5-5.11 show that the results

for load-deflection and strain in steel, the structural response are exactly similar for different values of tolerance factor except that smaller value of tolerance predicted lower ultimate load. Table 5.3 shown the number of iterations per increment required for different slabs analysed. Table 5.3 shows the variation of the ratio of predicted/experimental failure load with the tolerance limits. The predicted ultimate load for tolerance of 1% is about 82% of the ultimate load predicted by tolerance of 10%, but the number of iterations increased by 300%. However, the ultimate load predicted for tolerance of 5% and 10% are almost same (see table 5.2), but using tolerance of 5% will increase computational cost by 60% as measured by the solution time (see table 5.3). The above study indicates that smaller tolerances do not show much difference in the structural behaviour other than increasing the computational cost. Therefore, a 5% tolerance will be used throughout the present investigation.

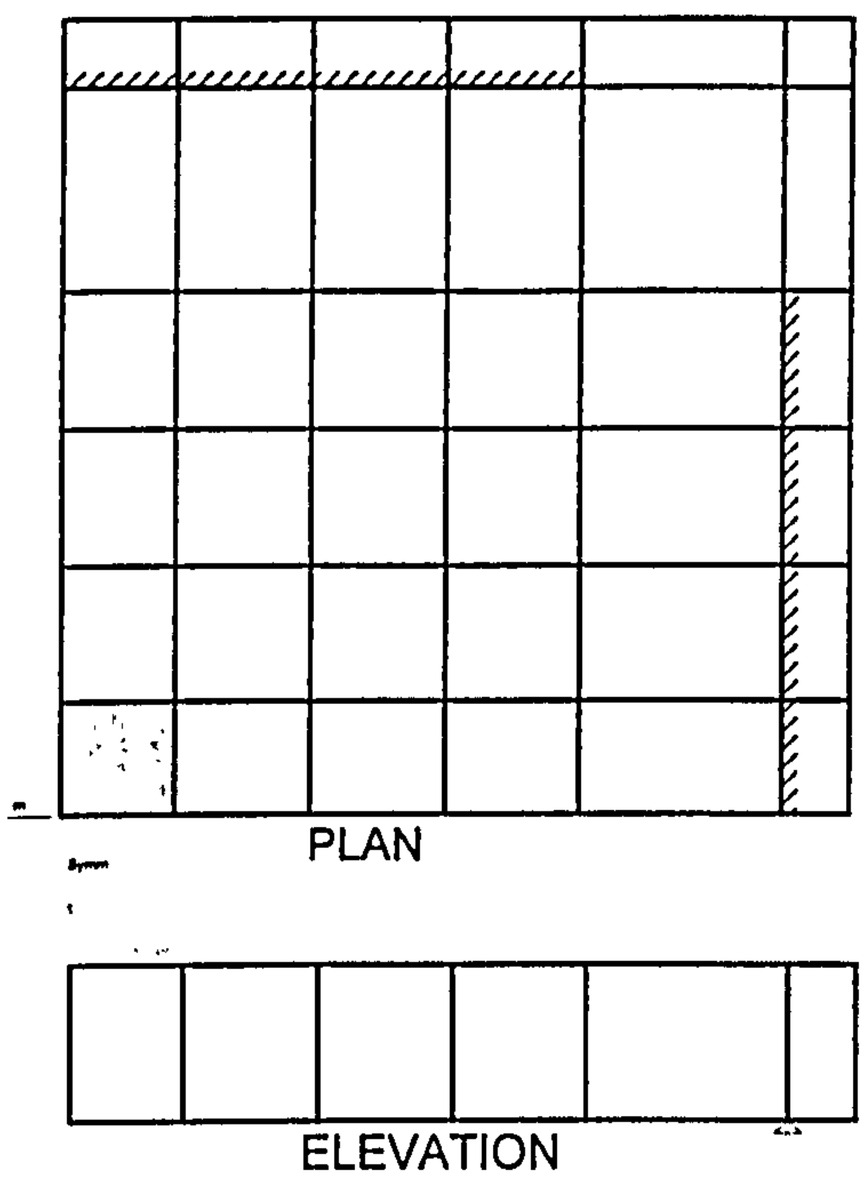

Figure 5.4 : Finite Element Mesh

Table 5.2 : Effect of convergence tolerance on Ultimate Load

Slab	P_{test} (kN)	Numerical/Exp. failure Load		
		TOL=1%	TOL=5%	TOL=10%
1B	28.850	0.865	1.027	1.027
1C	62.740	0.696	0.895	0.945
2C	87.860	0.738	0.787	0.836
3C	124.140	0.532	0.822	0.822
4C	125.940	0.858	0.858	0.858
Average		0.738	0.878	0.897
STDEV		0.137	0.093	0.087

Table 5.3: Effect of convergence tolerance on Numbers of Iterations

Inc	Numbers of iterations														
	Slab "1B"			Slab "1C"			Slab "2C"			Slab "3C"			Slab "4C"		
	1%	5%	10%	1%	5%	10%	1%	5%	10%	1%	5%	10%	1%	5%	10%
1	2	2	2	2	2	2	2	2	2	2	2	2	2	2	2
2	1	1	1	1	1	1	1	1	1	2	1	1	2	1	1
3	2	1	1	1	1	1	2	1	1	2	2	2	2	2	2
4	2	2	1	2	2	2	4	2	2	3	2	2	3	2	2
5	2	4	2	2	2	2	3	2	2	4	2	2	3	2	2
6	2	2	2	3	2	2	4	2	2	4	2	2	4	2	2
7	3	2	2	4	2	2	4	3	2	4	2	2	4	2	2
8	4	2	2	4	2	2	4	2	2	6	3	2	6	3	2
9	4	2	2	4	2	2	5	3	2	8	4	2	7	3	2
10	3	2	2	5	3	2	7	4	2	11	5	3	8	4	2
11	7	2	2	7	4	2	9	5	3	13	6	3	10	5	2
12	5	3	2	9	5	3	10	6	4	50	7	4	27	5	3
13	7	4	3	13	7	4	13	8	5	-	31	4	30	23	3
14	10	5	3	20	9	5	18	10	6	-	10	9	12	7	3
15	17	9	6	50	19	6	23	12	7	-	30	7	14	6	4
16	29	15	7	-	27	9	50	19	10	-	27	14	23	8	4
17	50	22	10	-	22	16	-	50	50	-	22	21	40	11	4
18	-	29	15	-	29	17	-	-	-	-	50	50	15	21	4
19	-	50	35	-	50	32	-	-	-	-			50	50	50
20	-	-	50	-	-	50	-	-	-	-					
$\sum$	152	159	150	127	191	162	159	132	103	109	208	132	262	159	96
ST	57	62	56	45	76	62	70	60	43	41	68	43	75	64	36

Note : ST denote Solution Time in minutes

Total no of iteration for 5 analysis (*at similar number of increments)

1 % of convergence tolerance = 809 (ST=288 minutes)

4 % of convergence tolerance = 422 (ST=164 minutes)

10 % of convergence tolerance = 264 (ST= 98 minutes)

* ST is not a good criterion to judge the computational cost, because the number of people using the computer at the same time will affect the solution time. Total number of iterations is, perhaps, a better indication of cost of solution.

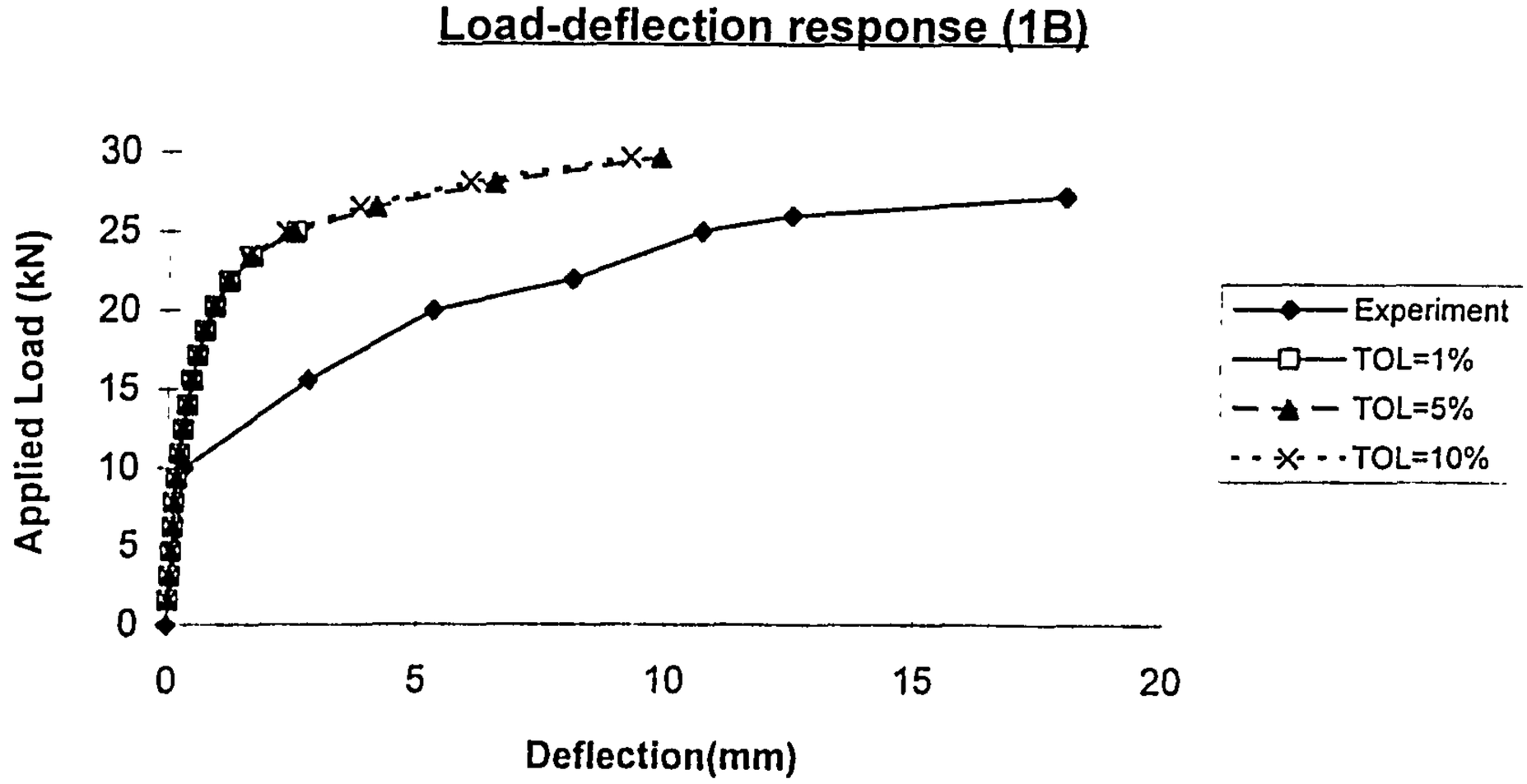

Figure 5.5: Effect of convergence tolerance (Slab "1B")

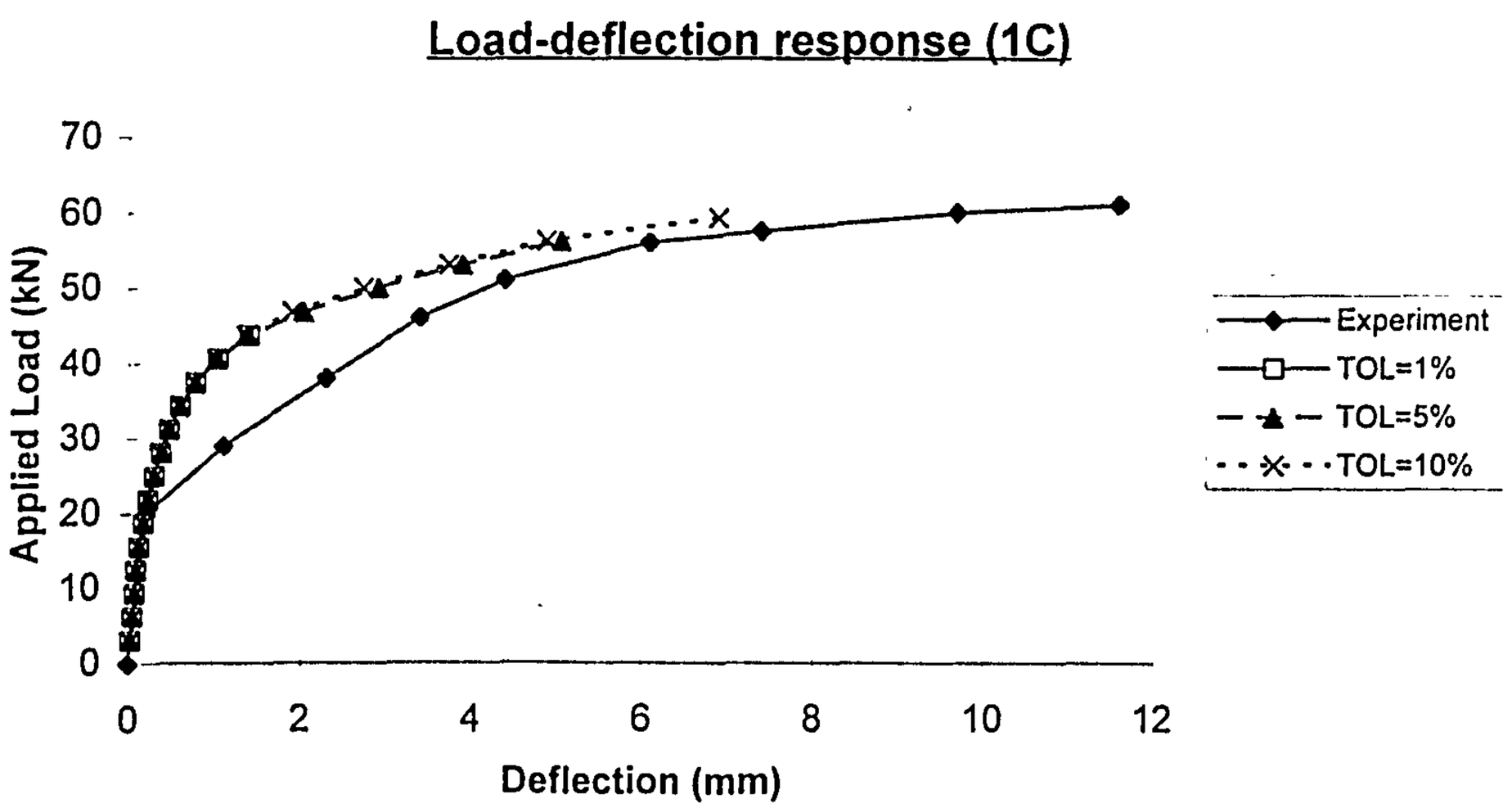

Figure 5.6 Effect of convergence tolerance (Slab "1C)

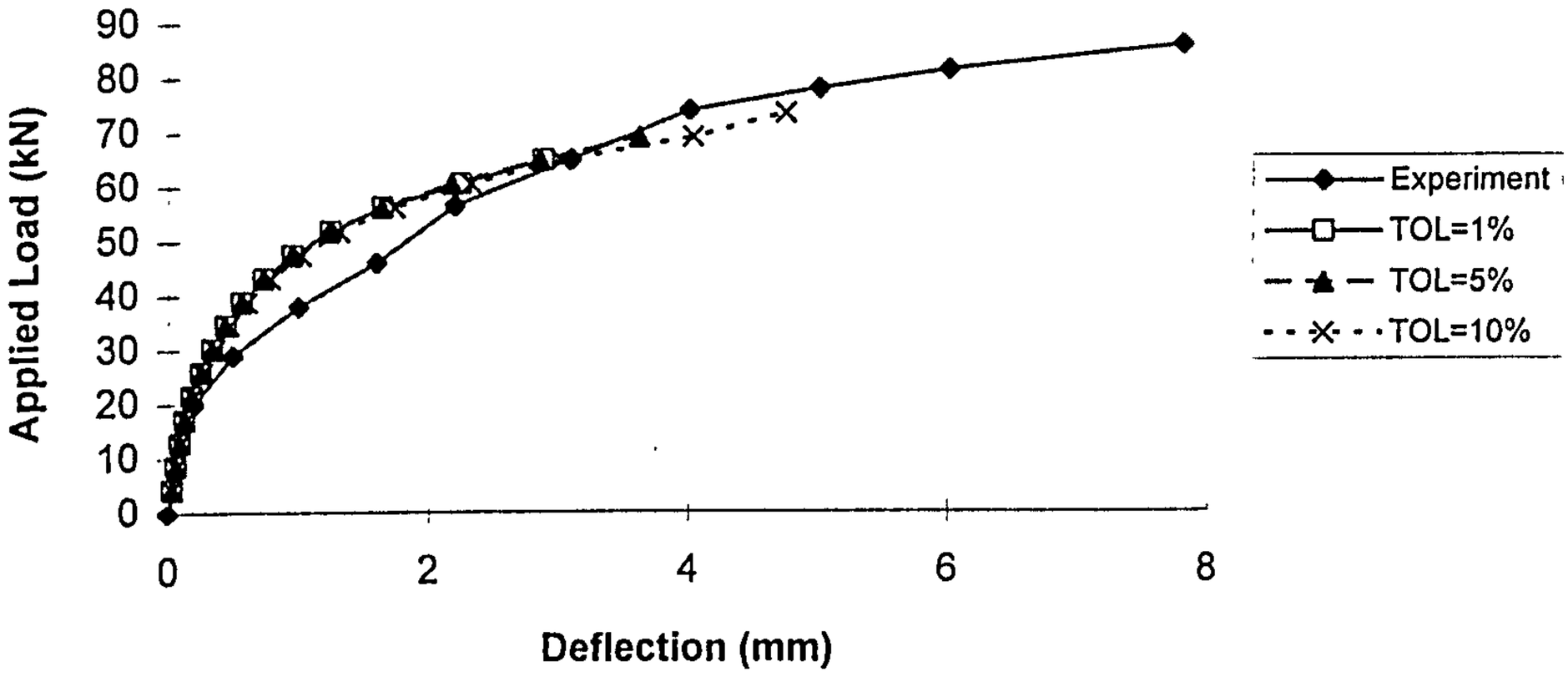

Figure 5.7 Effect of convergence tolerance (Slab "2C)

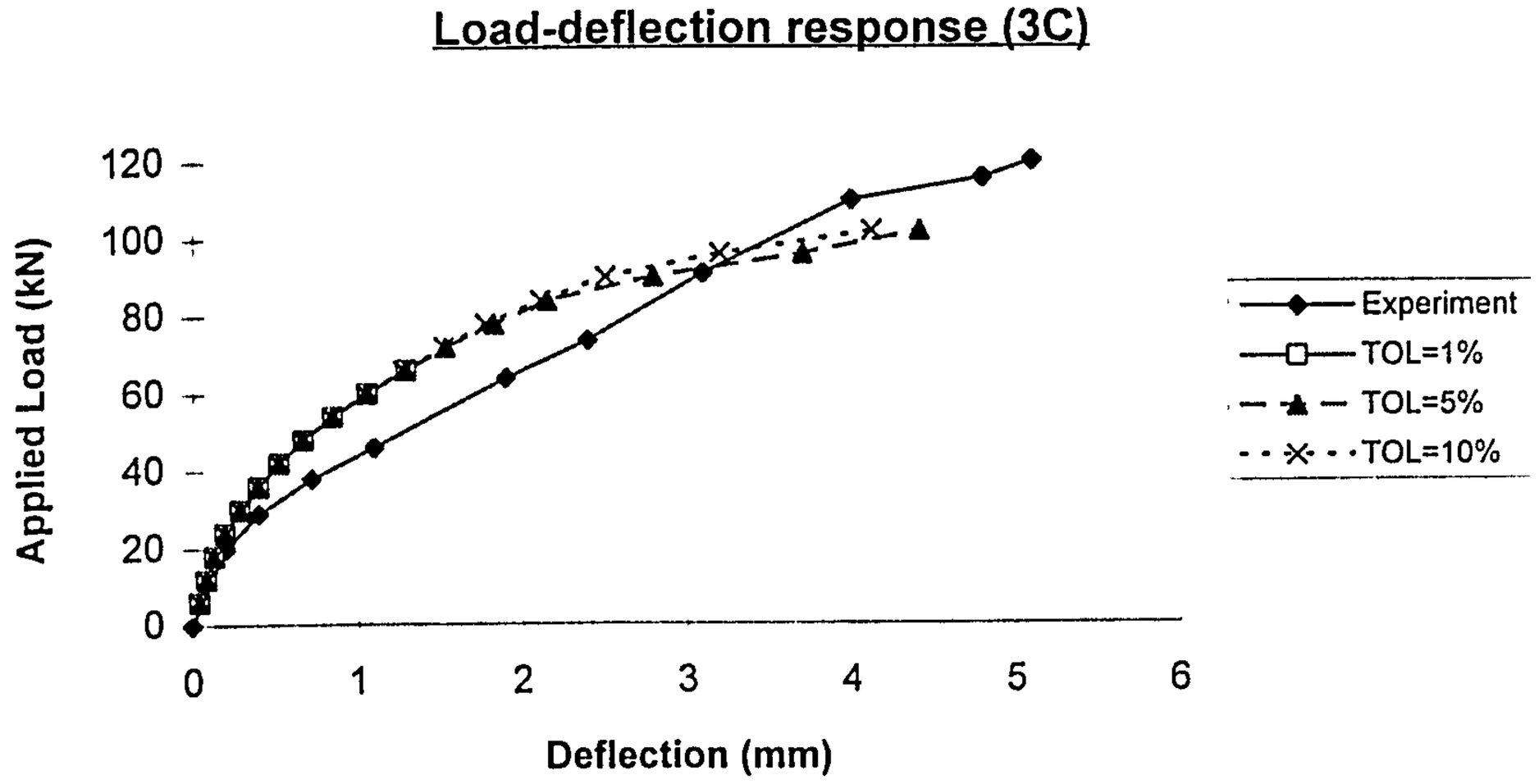

Figure 5.8 Effect of convergence tolerance (Slab "3C)

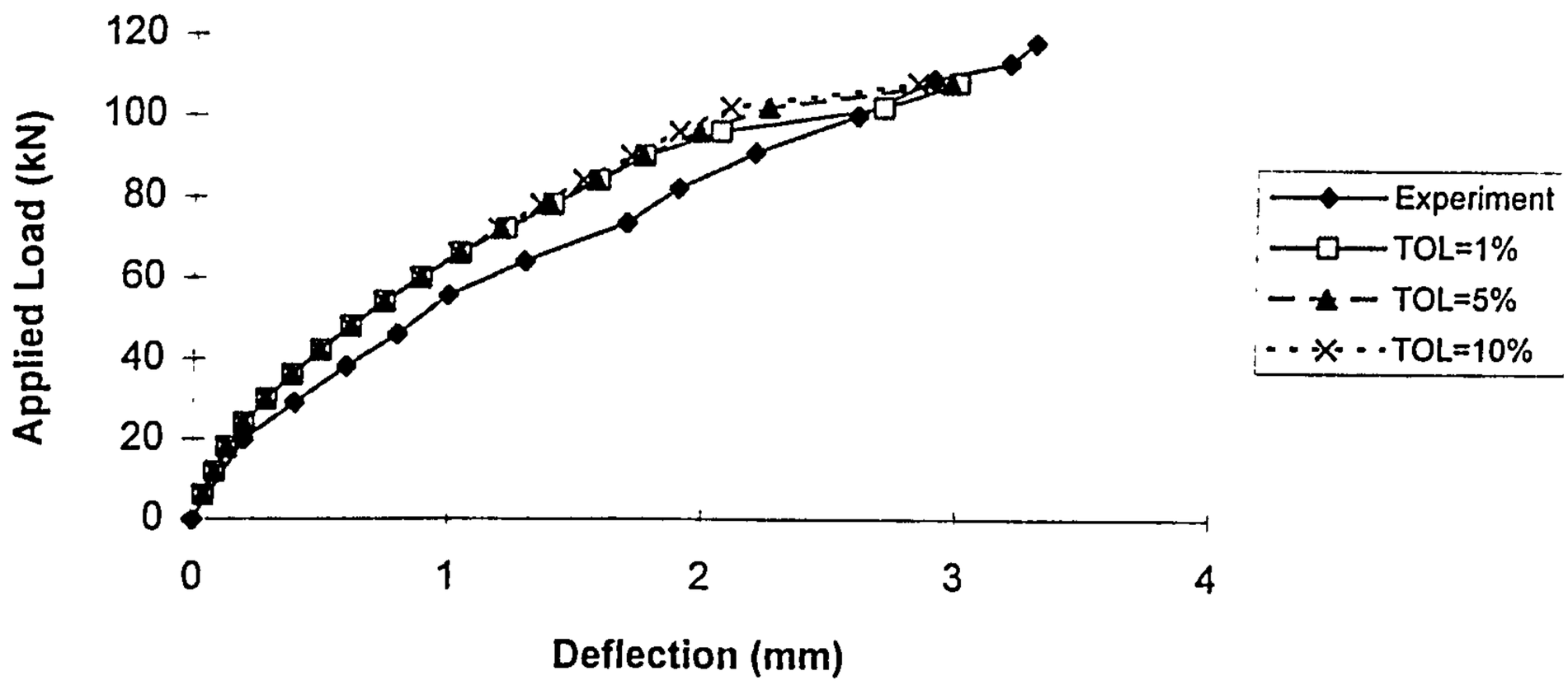

Figure 5.9 : Effect of convergence tolerance (Slab "4C")

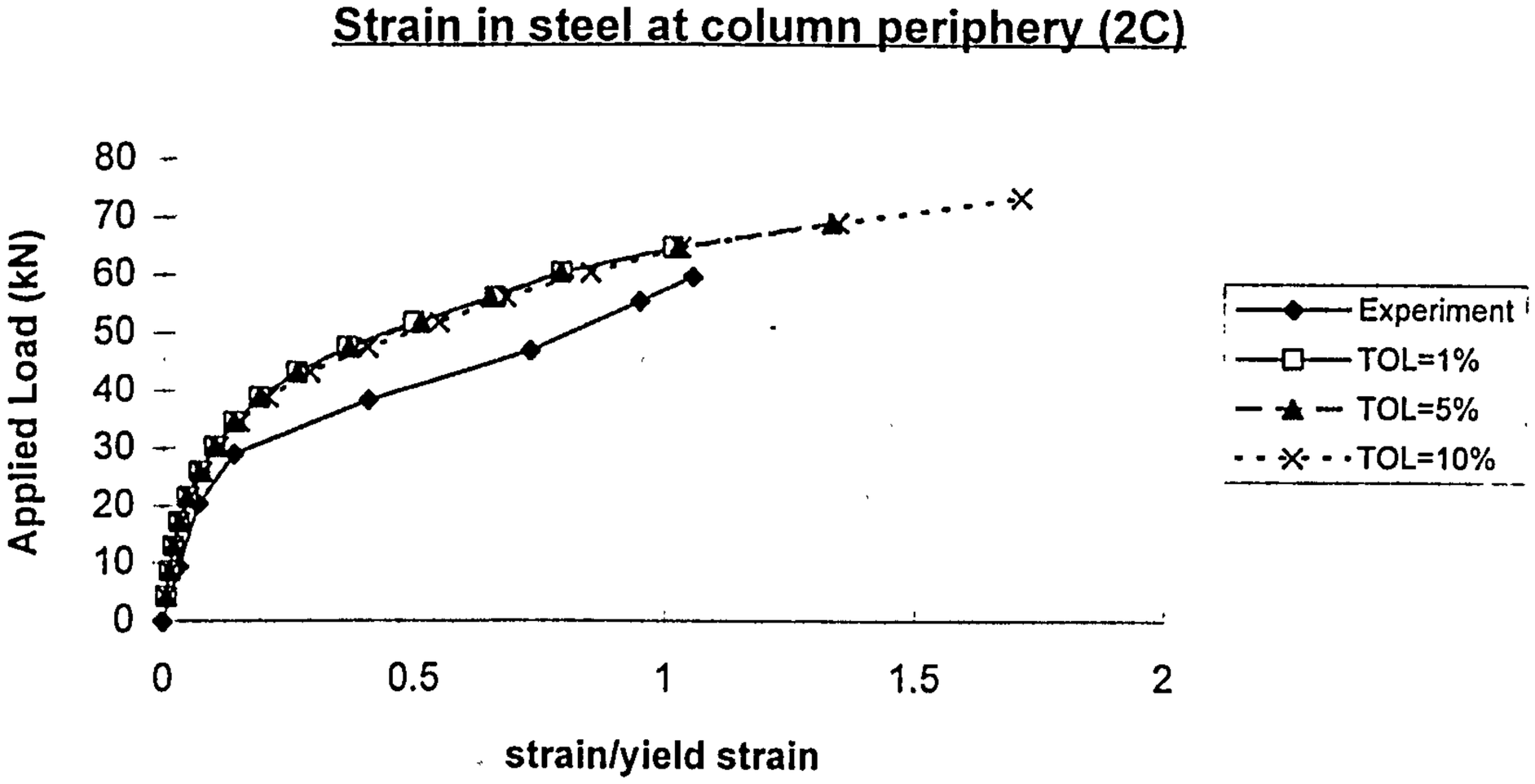

Figure 5.10 Effect of convergence tolerance (Slab "2C)

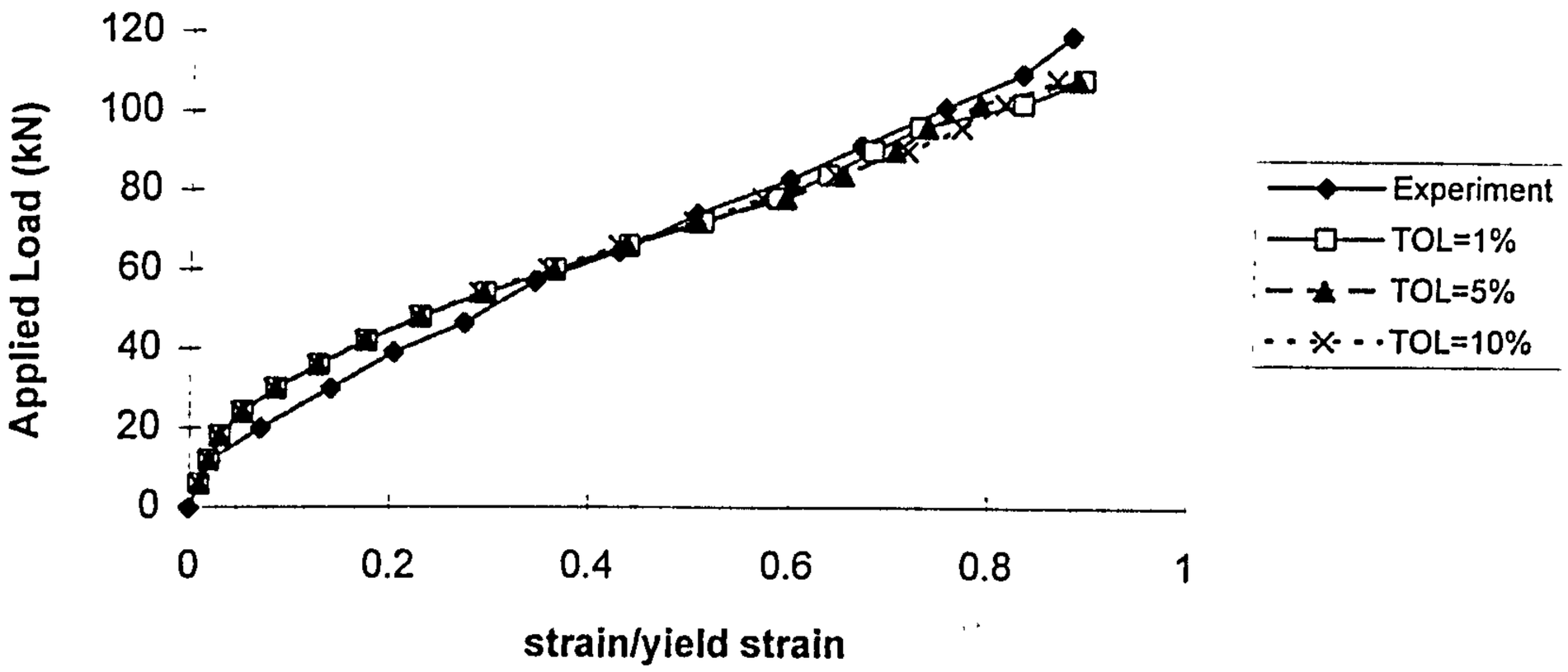

Figure 5.11 Effect of convergence tolerance (Slab "4C)

5.4.2 Effect of the size of load increment

In order to keep the computational cost at a reasonable level, three different load increment sizes were studied : 10%, 5% and 2.5% of experimental failure load. This study adopted 6×6×1 mesh as shown on Figure 5.4.

From table 5.4, load increment size of 10% predicted the highest average value of ratio of numerical to experimental ultimate load along with the highest standard deviation, STDEV (i.e. less consistent). However there is not much difference in the numerical ultimate load between load increment sizes of 5% and 2.5%. Larger value of load increment also produced stiffer response (refer to figures 5.9-5.15). Load increment size of 10% predicted overstiff response when compared to experimental results (deflection and strain in steel) especially for slabs with low amount of reinforcement. Load increment sizes of 5% and 2.5% predicted response that matched very well with experimental results for all slabs no matter what the amount of reinforcement in the slab was. From figures 5.9-5.15, it can be observed that at low load level (around 20% of experimental failure load), there is not much difference in response for all the three load increment sizes.

From the above analysis, it can be concluded that applying small load increment for highly non-linear parts and large load increment whenever nonlinearity is not significant will give reasonably good results. In order to reduce the computational cost, it was decided to use in the present work load increment size of 10% for the first two increments and of 5% for the remaining increments.

Table 5.4 : Effect of load Increment size on Ultimate Load

Slab	P_{test} (kN)	Numerical/Experimental failure Load		
		10%	5%	2.5%
1B	28.850	1.190	1.027	1.000
1C	62.740	0.995	0.945	0.845
2C	87.860	0.885	0.836	0.738
3C	124.140	0.870	0.822	0.870
4C	125.940	0.858	0.858	0.834
Average		0.960	0.898	0.857
STDEV		0.140	0.087	0.094

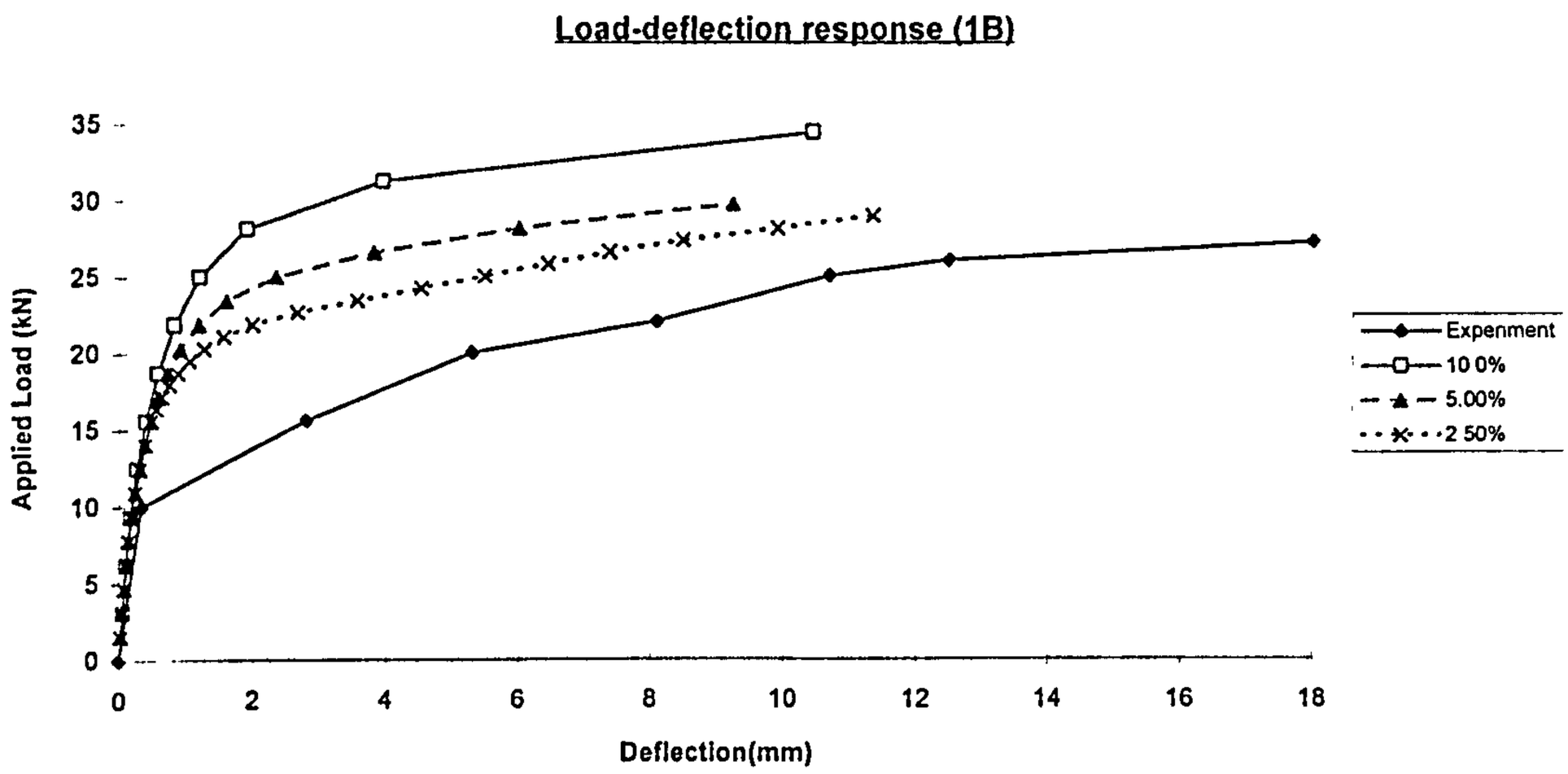

Figure 5.12 : Effect of load increment size (Slab "1B")

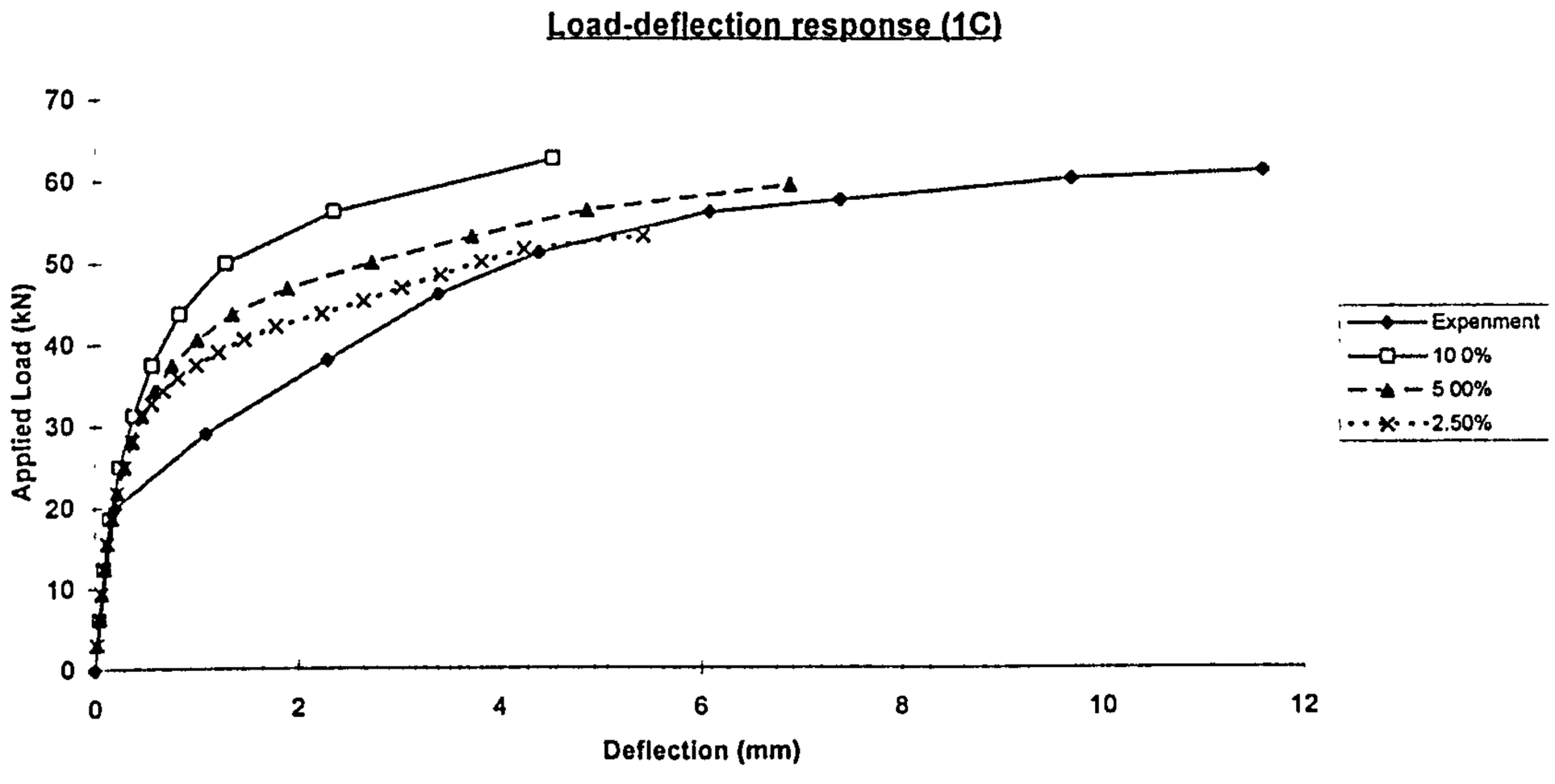

Figure 5.13 : Effect of load increment size (Slab "1C")

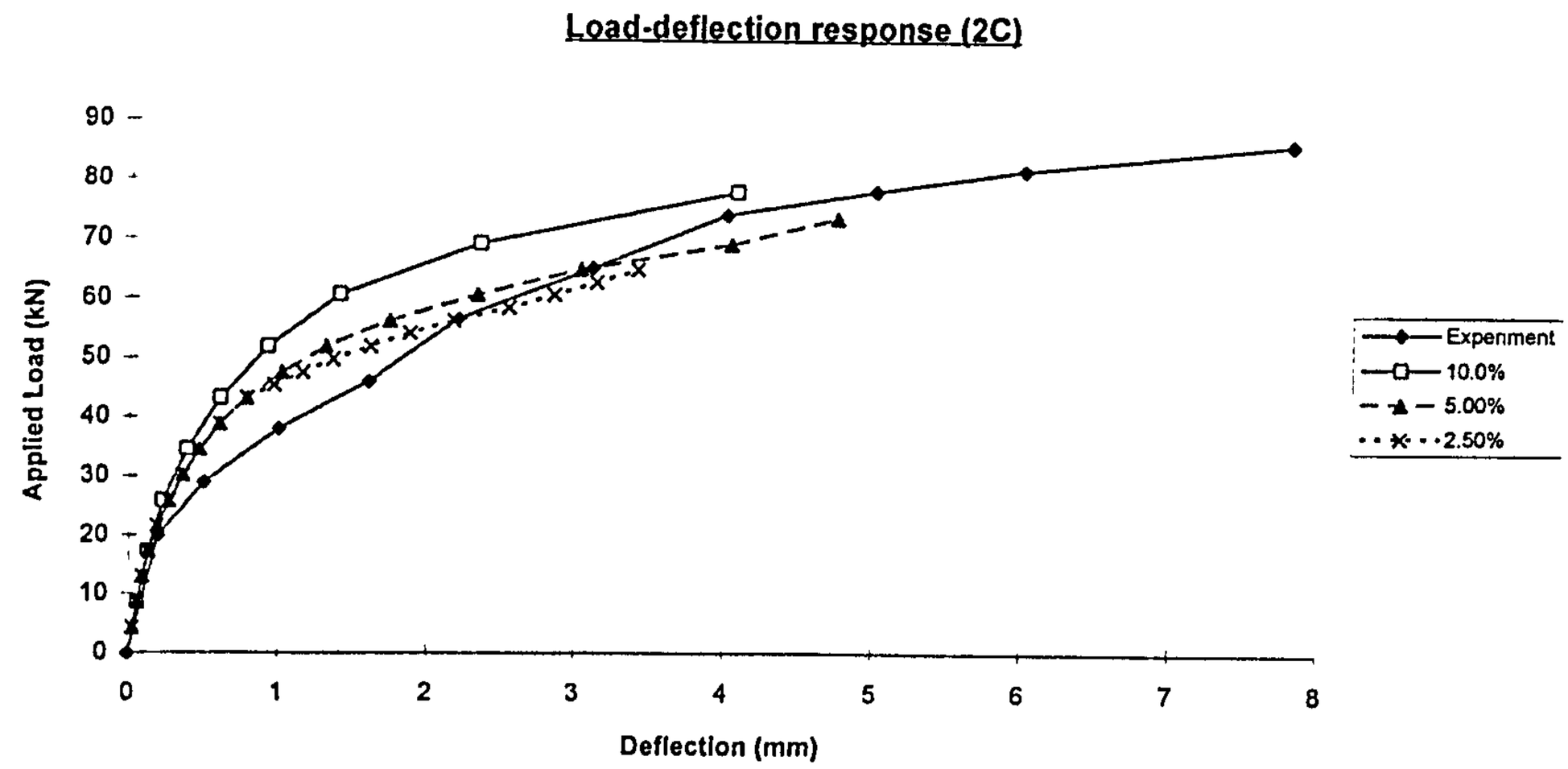

Figure 5.14 : Effect of load increment size (Slab "2C")

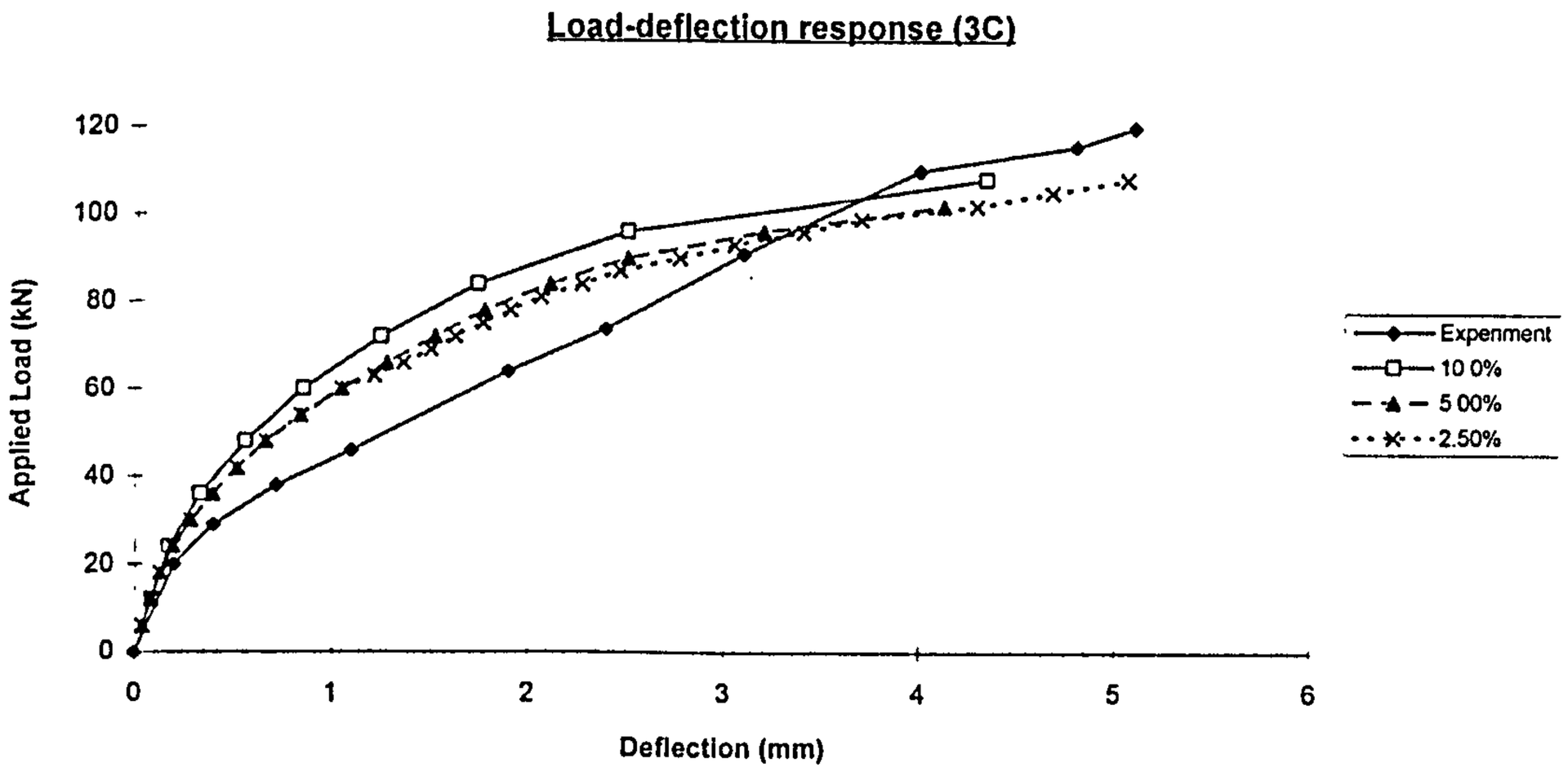

Figure 5.15 : Effect of load increment size (Slab "3C")

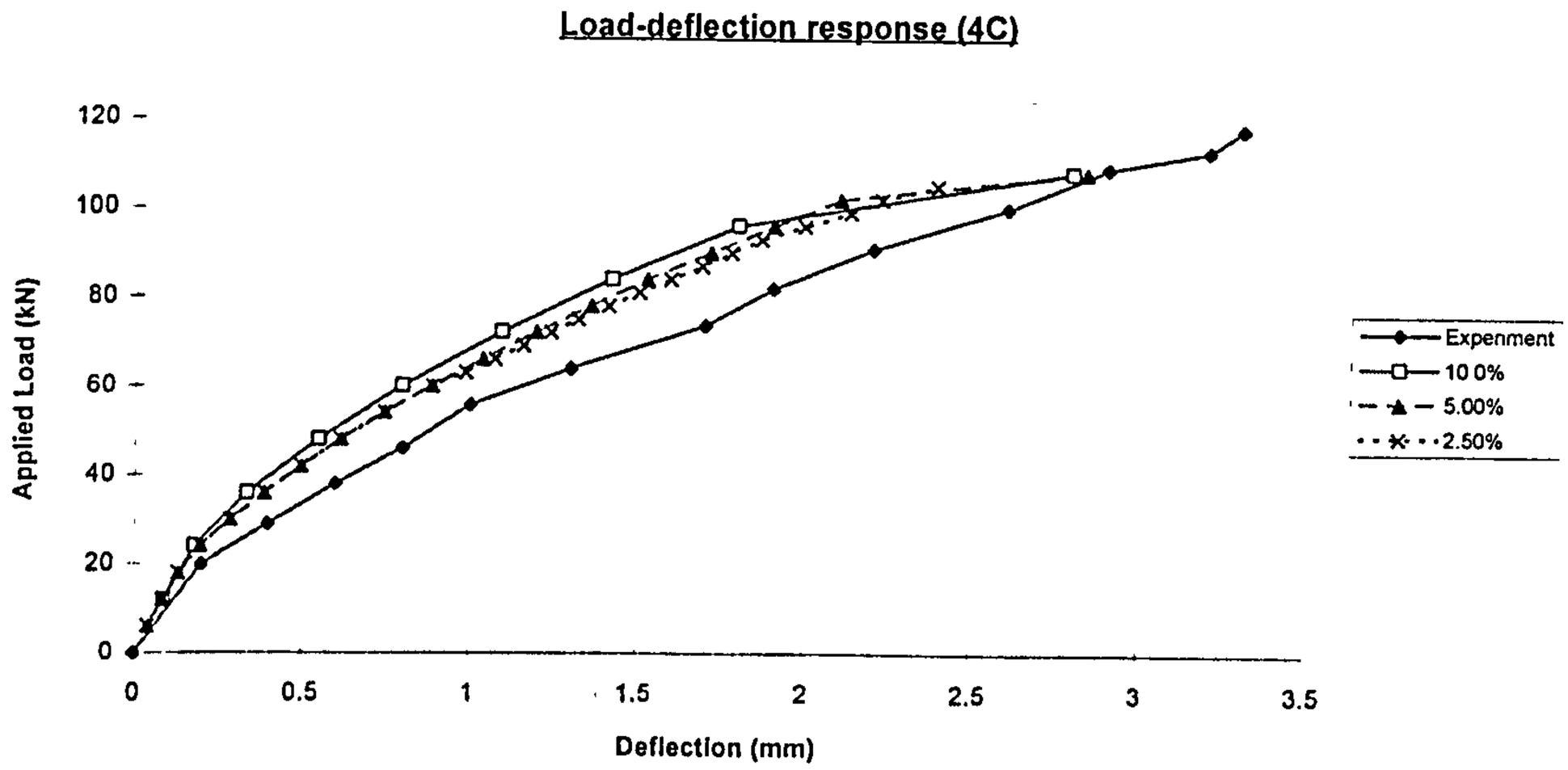

Figure 5.16: Effect of load increment size (Slab "4C)

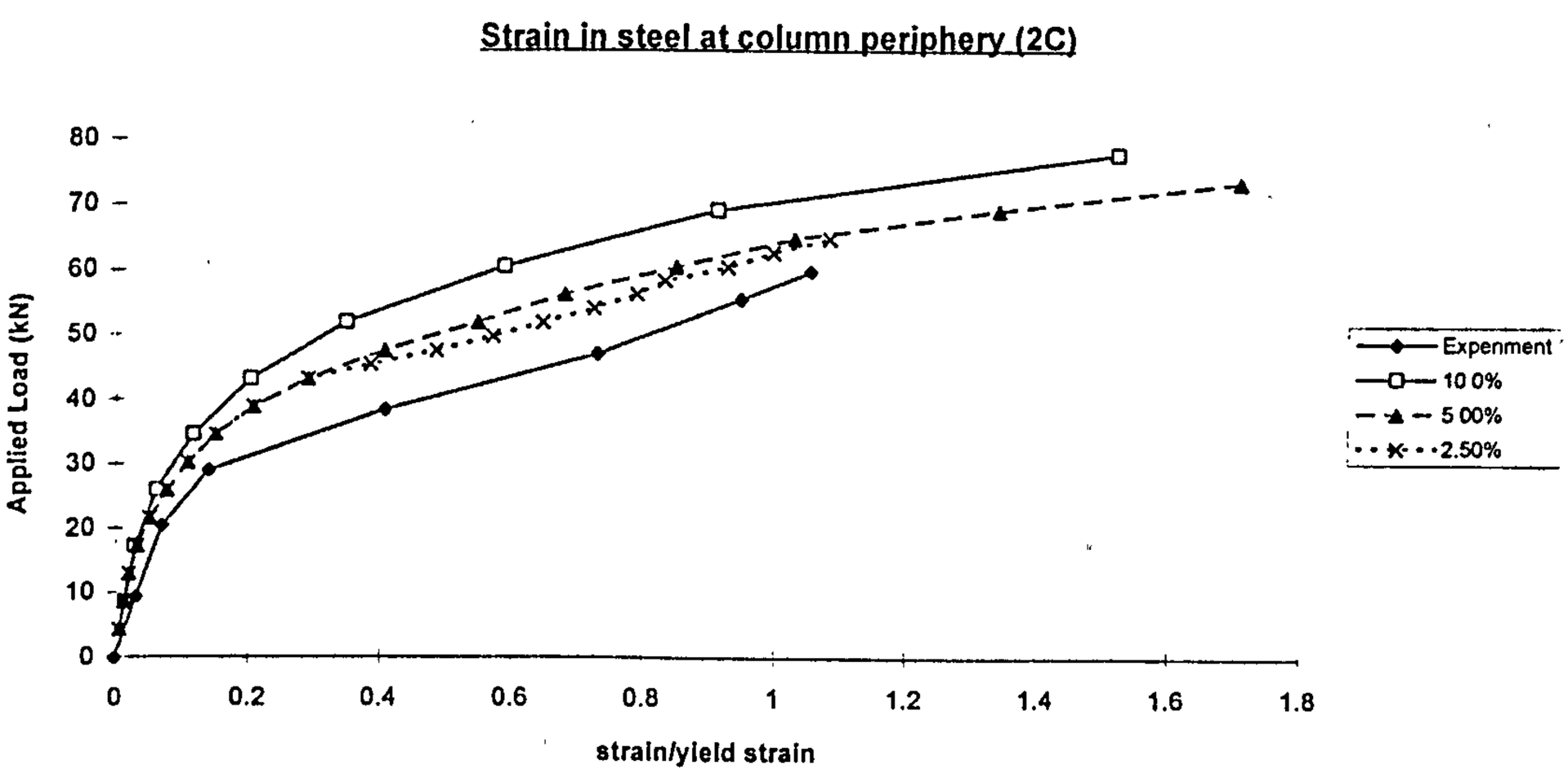

Figure 5.17 : Effect of load increment size (Slab "2C")

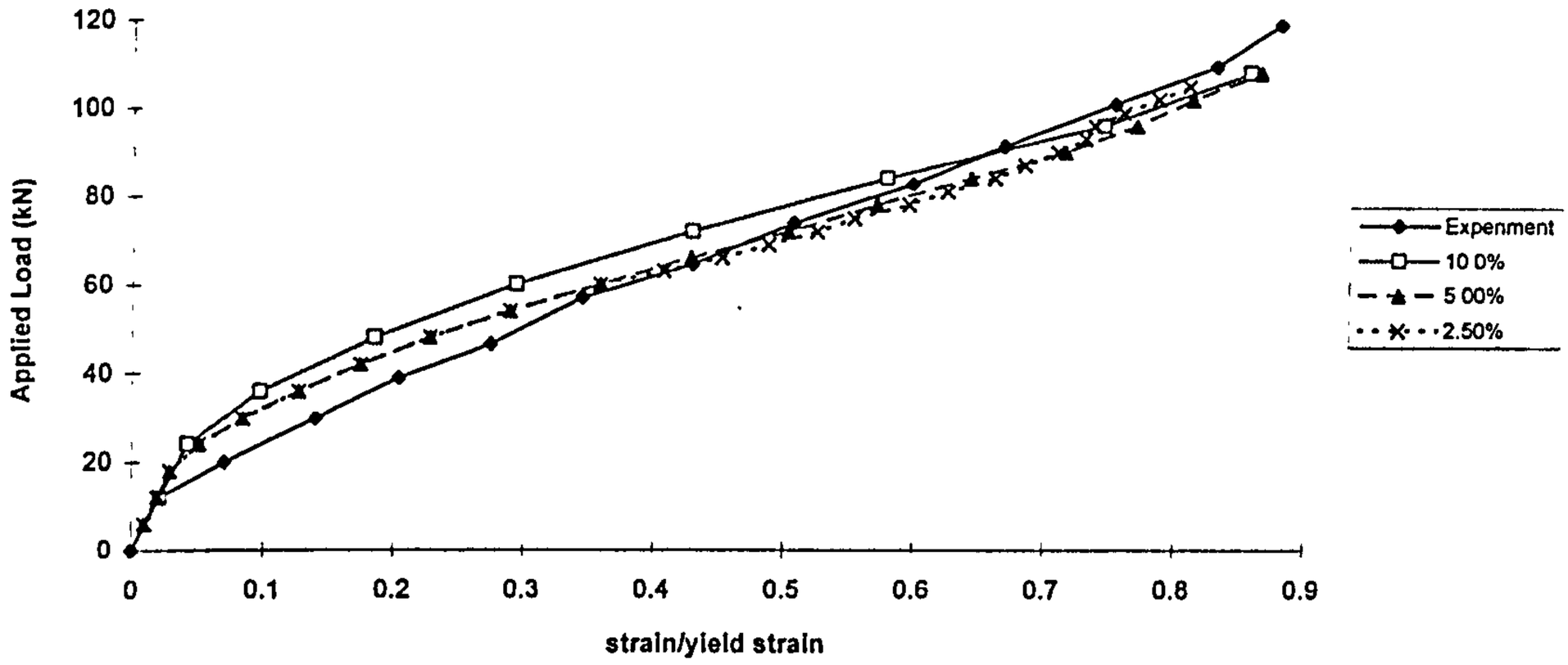

Figure 5.18 : Effect of load increment size (Slab "4C)

5.4.3 Mesh size

For slabs subjected to a concentrated load at the middle, the element representing the loading stub will be the smallest element. In order to reduce computational cost, elements further away from loading stub should be larger. The study of mesh refinement was conducted mainly for the elements within and near the failure region (i.e. element representing the loading stub and elements beside the loading stub). Three different mesh arrangement with number of elements of 25, 36 and 49 respectively (Figure 5.19) were used to study the effect on predicted structural response from slabs.

The results of analysis are shown in Table 5.5, it can be seen that the finest mesh (49 elements) predicted results with lowest standard deviation (i.e. consistent results). While the analysis using coarse mesh (25 elements) predicted results with highest standard deviation (i.e. less consistent). The aspect ratios for 49 and 36 elements mesh were 1.2 and 1.0 respectively, and the aspect ratio for 25 elements mesh was 1.8. This indicates that large aspect ratio produced less consistent results. Comparing the load deflection response and strain in steel (Figures 5.20-5.26), the mesh size has little effect on the ultimate load and behaviour of the slabs.

The results of this mesh size study show that mesh size (within the range of the chosen meshes) have a little effect on the ultimate load and behaviour of the slab, i.e. the results are not particularly mesh dependent. But elements with large aspect ratio give less consistent predictions. Therefore, it was concluded that if a mesh is reasonably fine, further refinement will not improve the prediction but only increase computational cost. In order to achieve a consistent, accurate and economical solution,

the aspect ratio for element beside loading stub should not be more than 1.5 and element size can be gradually increased when it is further away from loading stub.

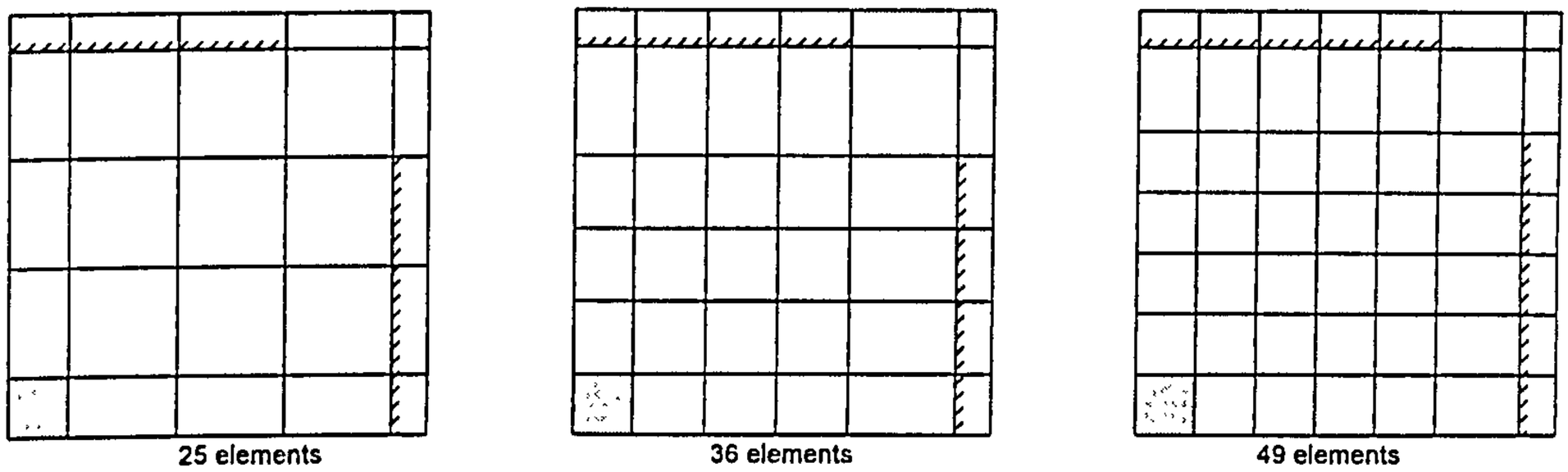

Figure 5.19 Finite Element meshes

Table 5.5 : Effect of mesh size

Slab	P_{test} (kN)	Numerical/Experimental failure Load		
		25 elements	36 elements	49 elements
1B	28.850	1.081	1.027	1.027
1C	62.740	0.995	0.945	0.895
2C	87.860	0.788	0.836	0.885
3C	124.140	0.773	0.822	0.822
4C	125.940	0.905	0.858	0.858
	Average	0.908	0.898	0.897
	STDEV	0.132	0.087	0.078

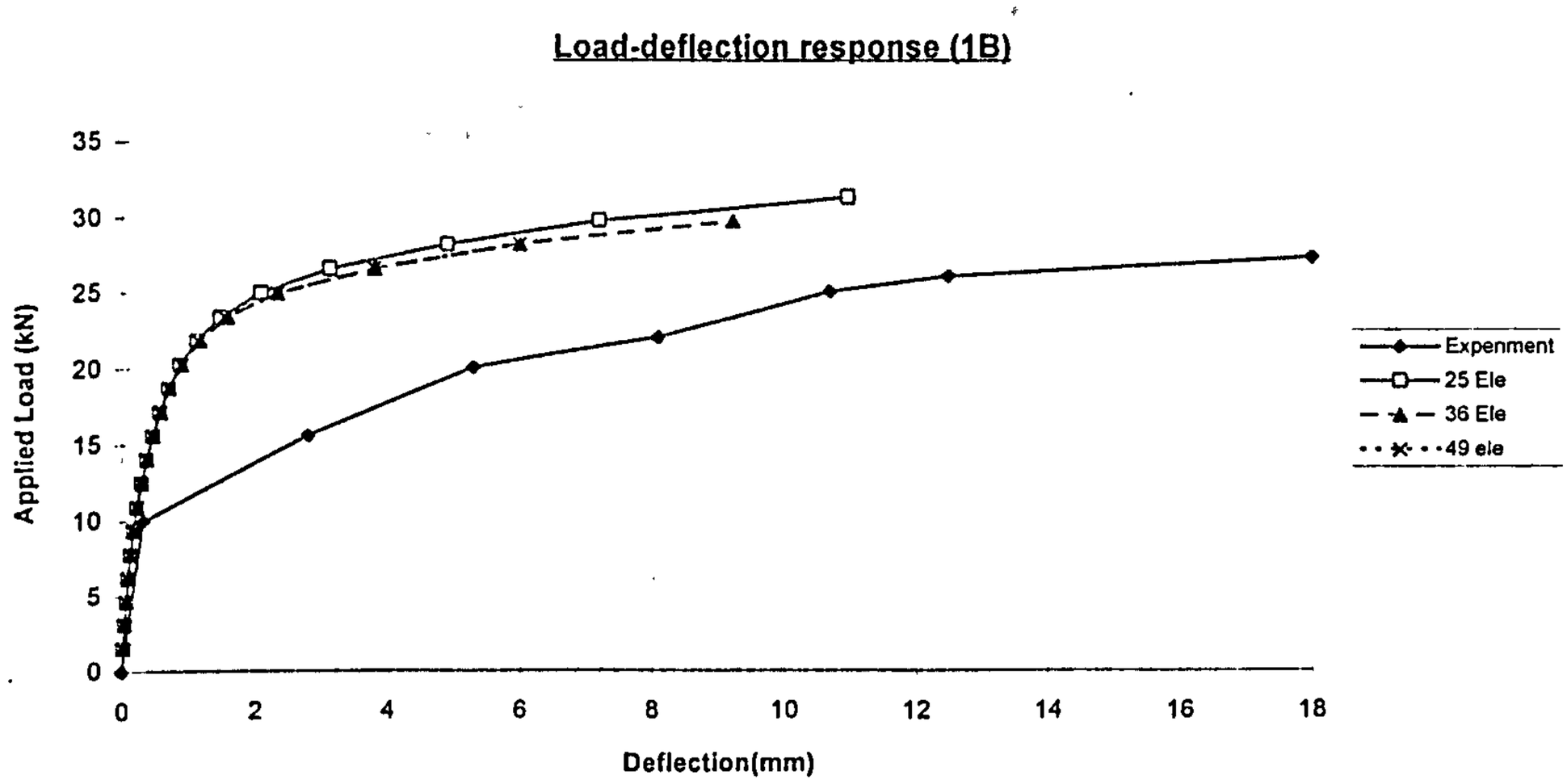

Figure 5.20 : Effect of mesh size Ratio (Slab "1B")

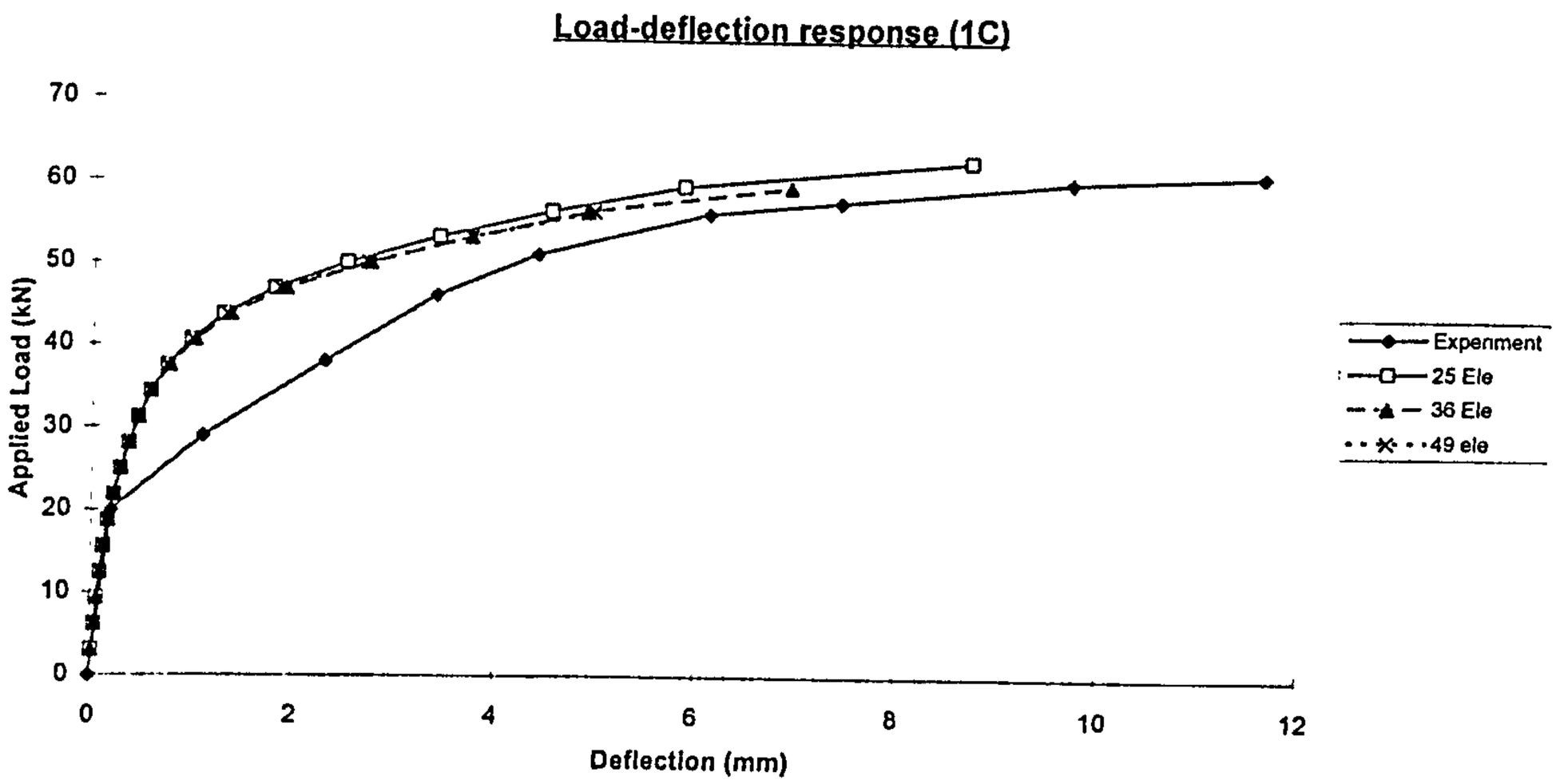

Figure 5.21 : Effect of mesh size (Slab "1C")

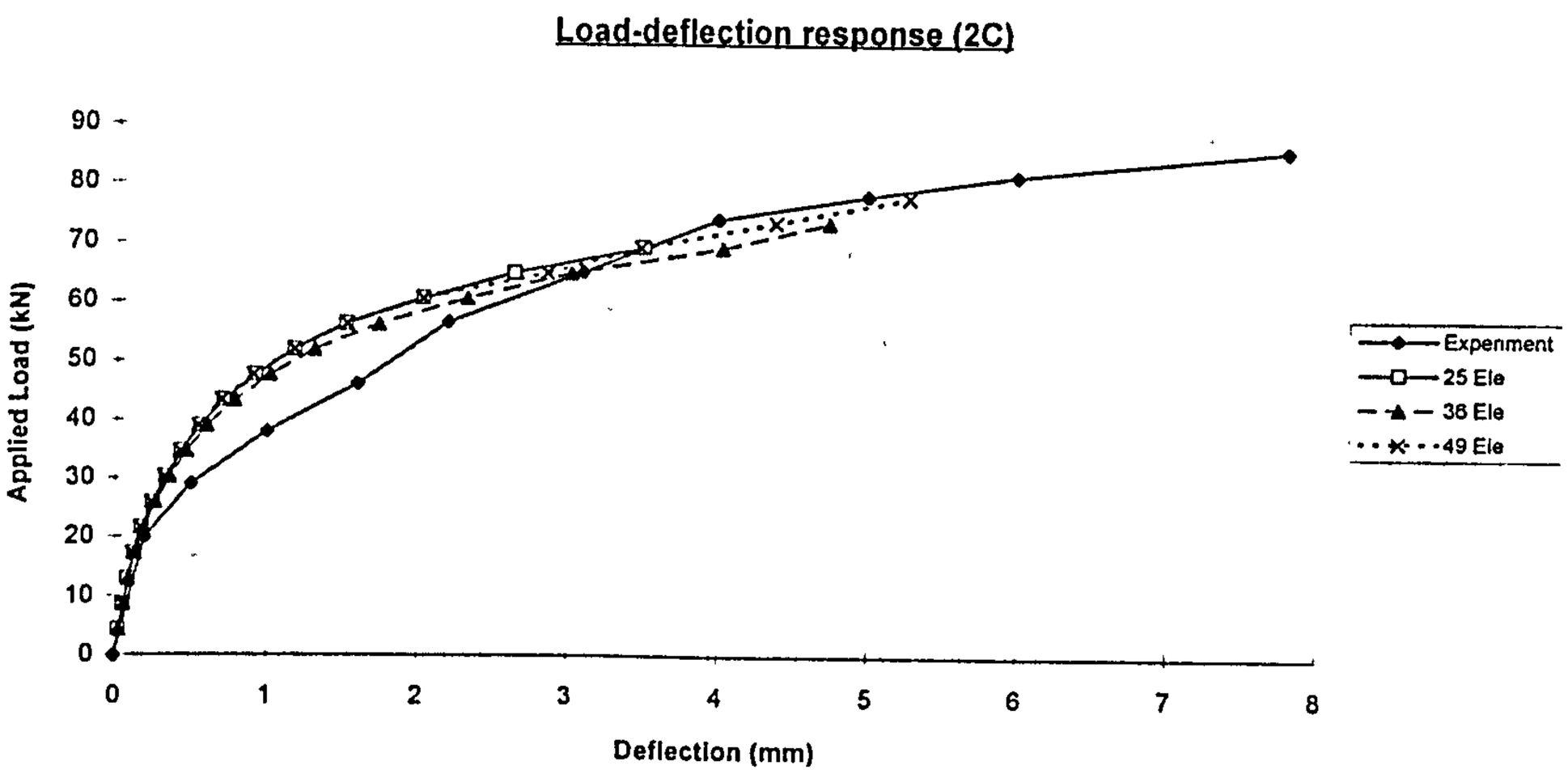

Figure 5.22 : Effect of mesh size (Slab "2C")

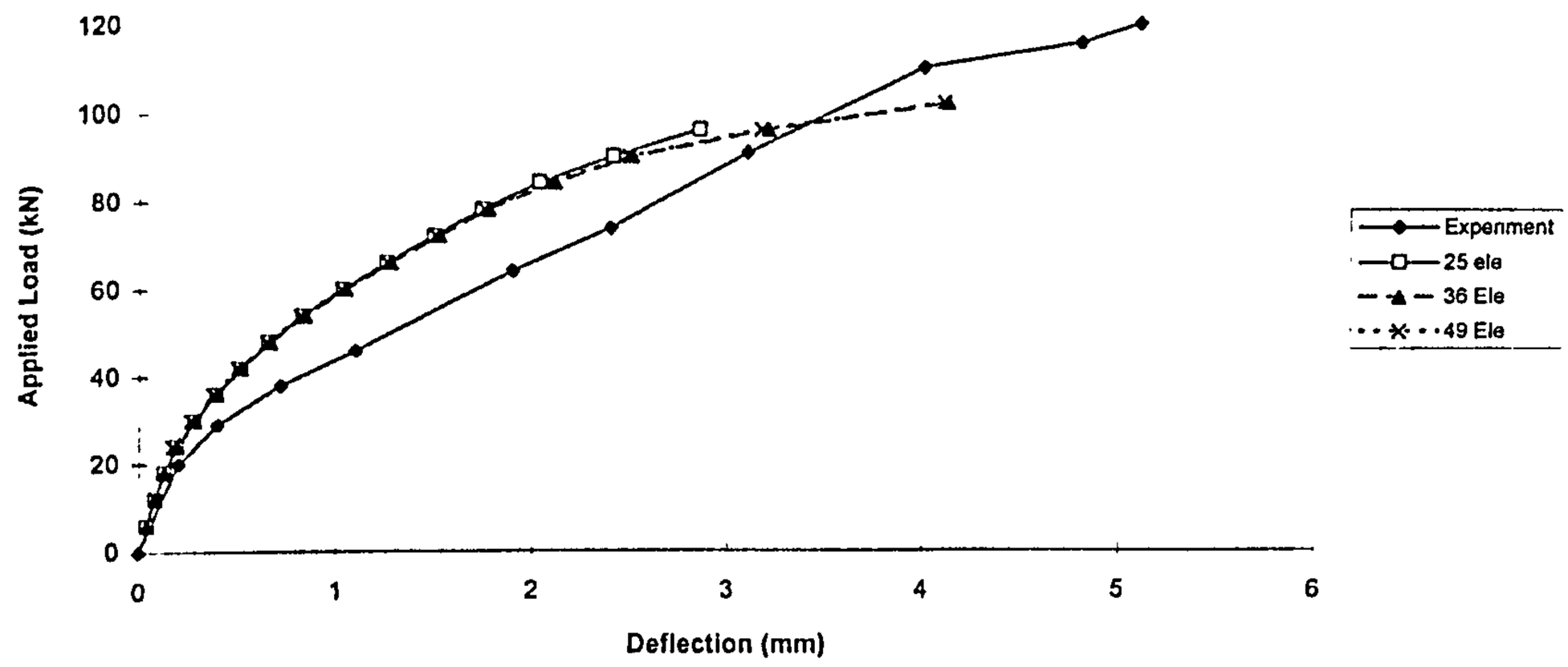

Figure 5.23 : Effect of mesh size (Slab "3C")

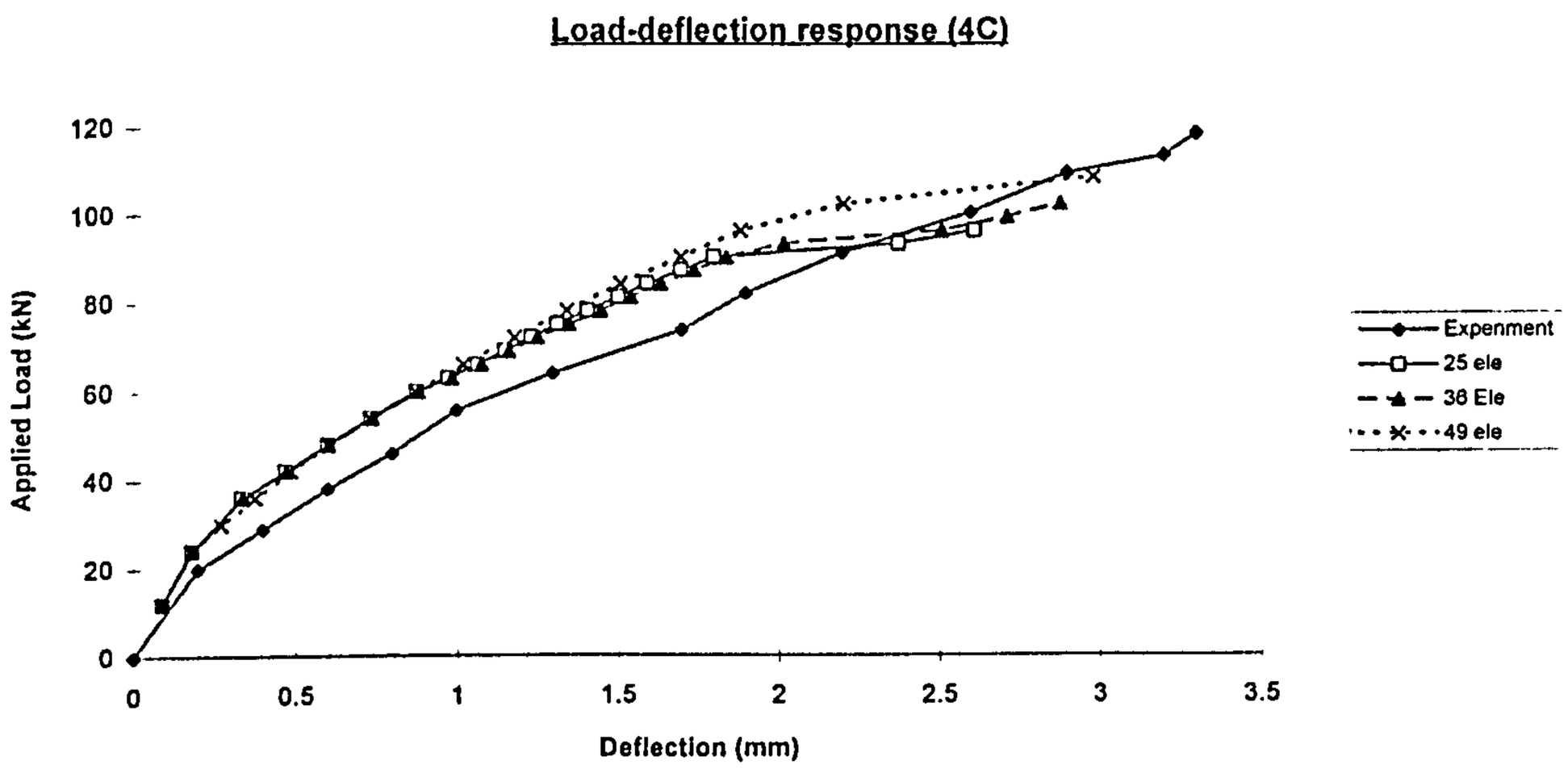

Figure 5.24 : Effect of mesh size (Slab "4C")

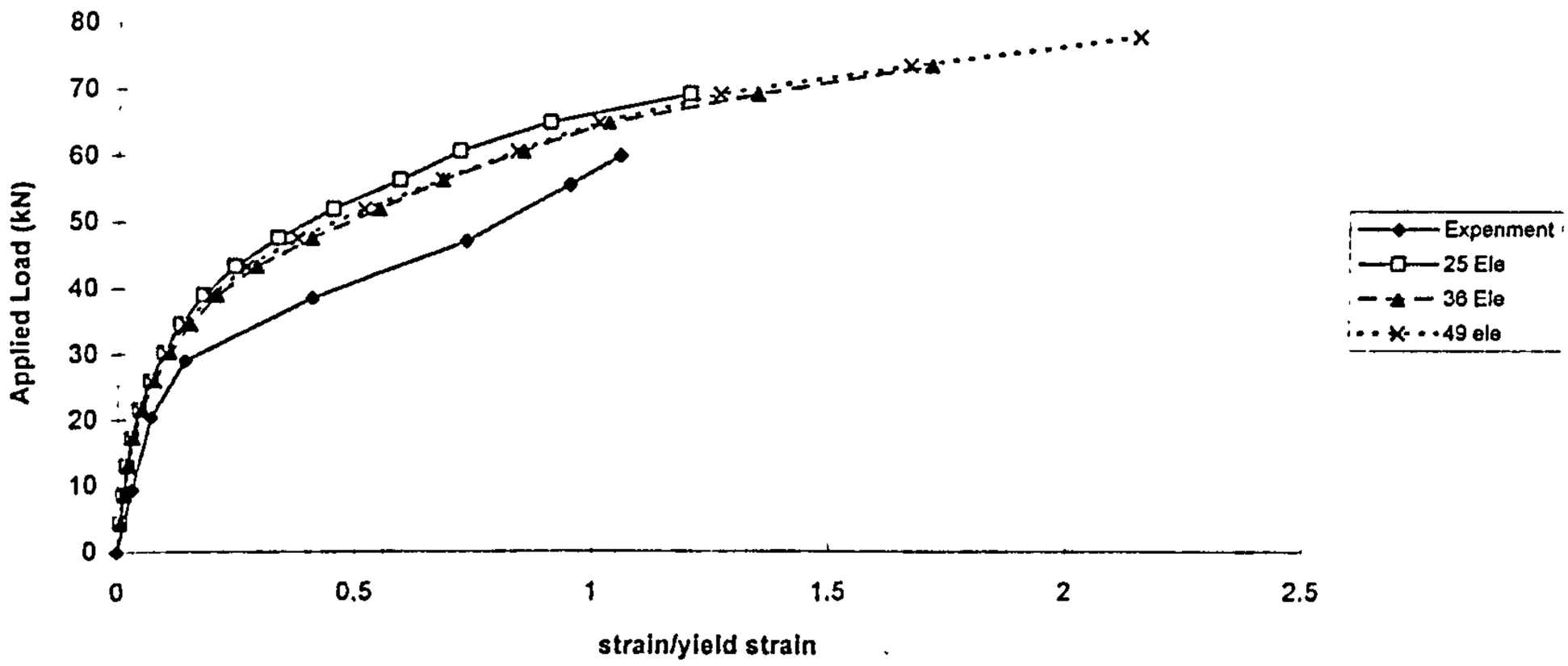

Figure 5.25 : Effect of mesh size (Slab "2C")

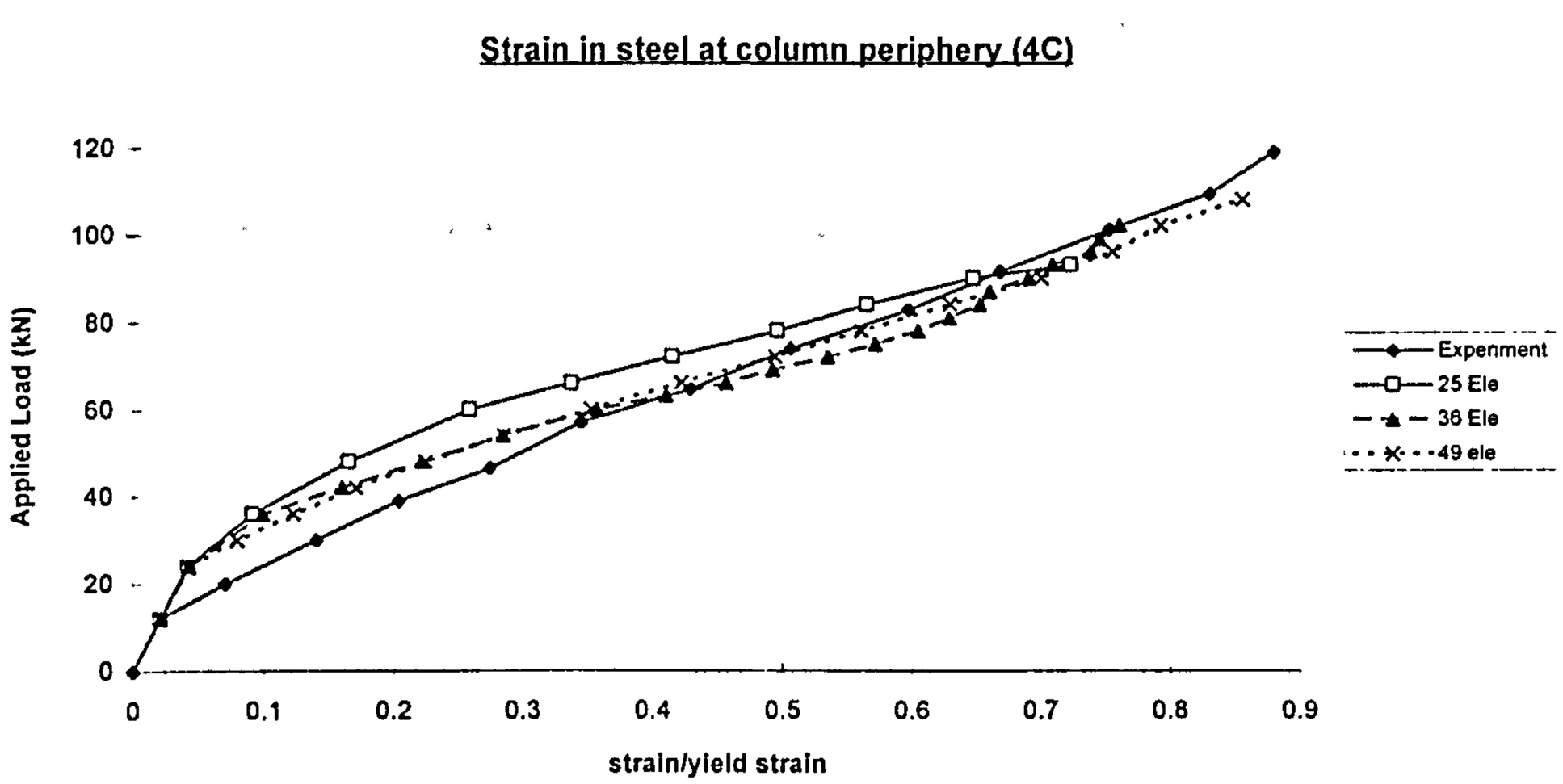

Figure 5.26 : Effect of mesh size (Slab "4C")

5.4.4 Number of elements through the thickness of slab

Increasing the stress calculation points (Gauss points) through the thickness to cater for nonlinearity of concrete as cracks propagate through the thickness of slab, is done by increasing number of elements through the thickness. But slab is a very thin member and increasing number of elements through the thickness will also increase the aspect ratio of the element. This might result in inconsistent prediction as shown in the previous study.

Three types of arrangement (1,2,3 elements through the thickness) were analysed using the layout of the mesh shown in Figure 5.4. Analysed results show that increasing the number of element through the thickness has little effect on the load vs. strain and deflection of the slabs (Figures 5.27-5.33), but it had significant effect on the ultimate load of heavily reinforced slab (e.g. slabs 3C & 4C). Generally, the analysis terminated because it could not achieve the prescribed limit of convergence tolerance. However, the analysis for specimens 3C (2 layers) and 4C (3 layers) terminated due to the divergence of the solution.

This study shows that increasing the number of elements through the thickness did not improve the prediction but doubled (or trebled) the computational cost and in some cases caused the solution to diverge. It is very important in the numerical analysis to prevent divergence of the solution and by comparing with the experiment results, one element through the thickness of slab predicted reasonably accurate results. Therefore, generally one element through the thickness of slab was used for the later study. Two or more elements through the thickness of slab will be use only when it required to limit the aspect ratio of the element near critical region to about 1.5 (see section 5.4.3).

Table 5.6 : Effect of Number of element through the thickness

Slab	P_{test} (kN)	Numerical/Experimental failure Load		
		1 Layer	2 Layer	3 Layer
1B	28.850	1.027	1.027	0.973
1C	62.740	0.945	0.995	0.995
2C	87.860	0.836	0.836	0.787
3C	124.140	0.822	0.677	0.773
4C	125.940	0.858	0.762	0.572
Average		0.898	0.860	0.820
STDEV		0.087	0.150	0.172

Note : 1 Layer=1 element through the thickness, Aspect Ratio=1.02
2 Layer=2 elements through the thickness, Aspect Ratio=2.04
3 Layer=3 elements through the thickness, Aspect Ratio=3.06

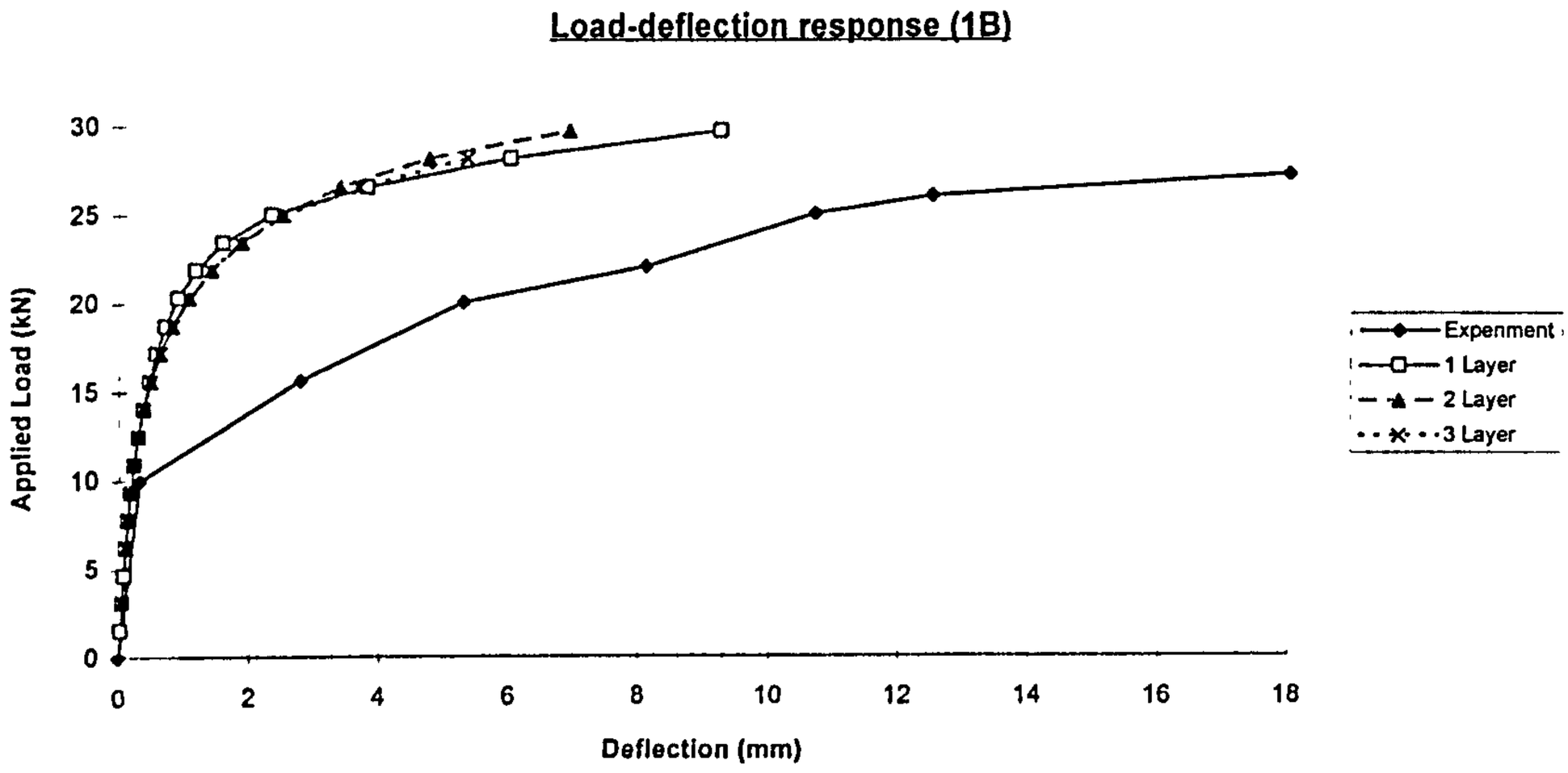

Figure 5.27 : Effect of layer

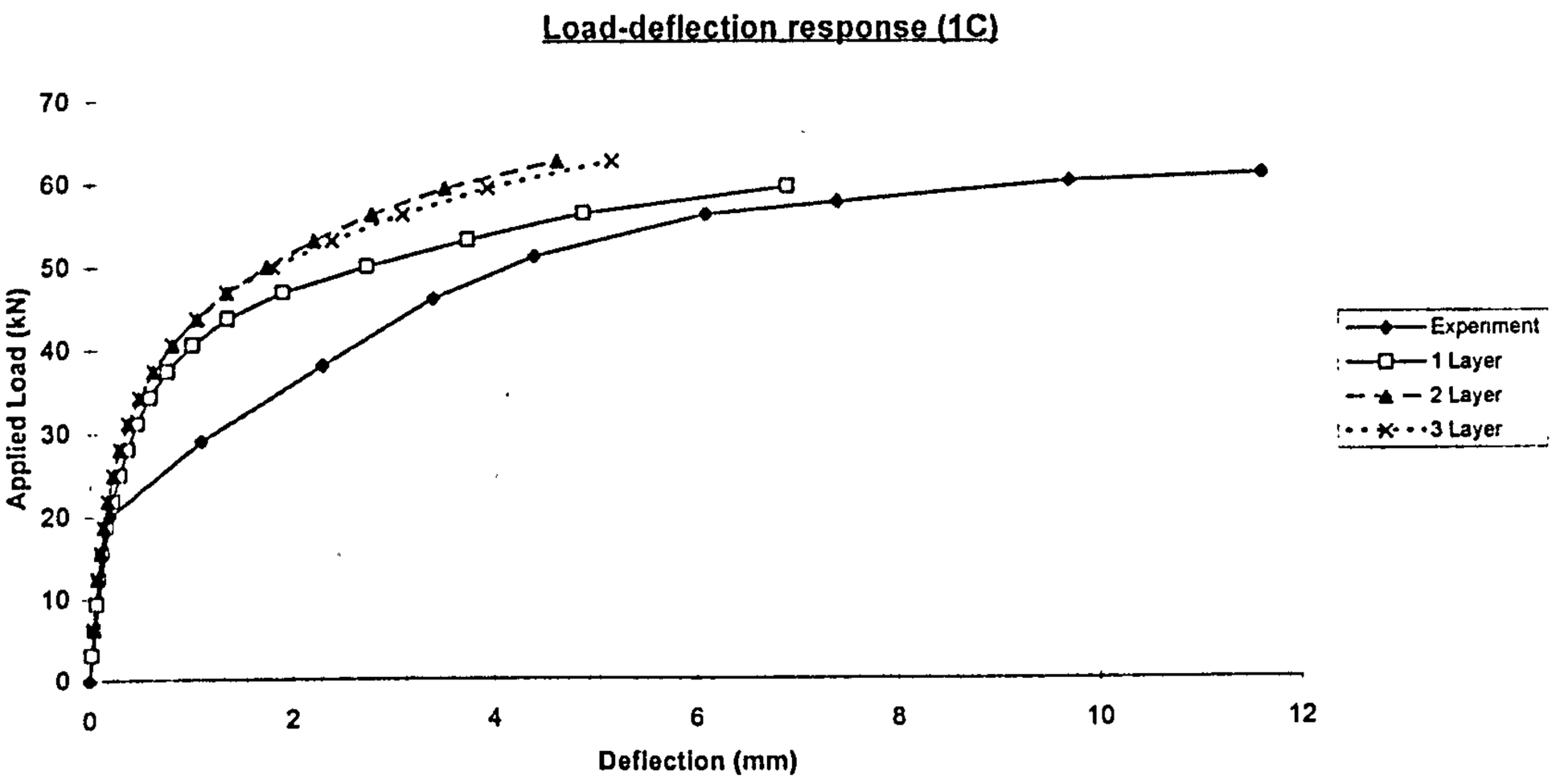

Figure 5.28 : Effect of layer

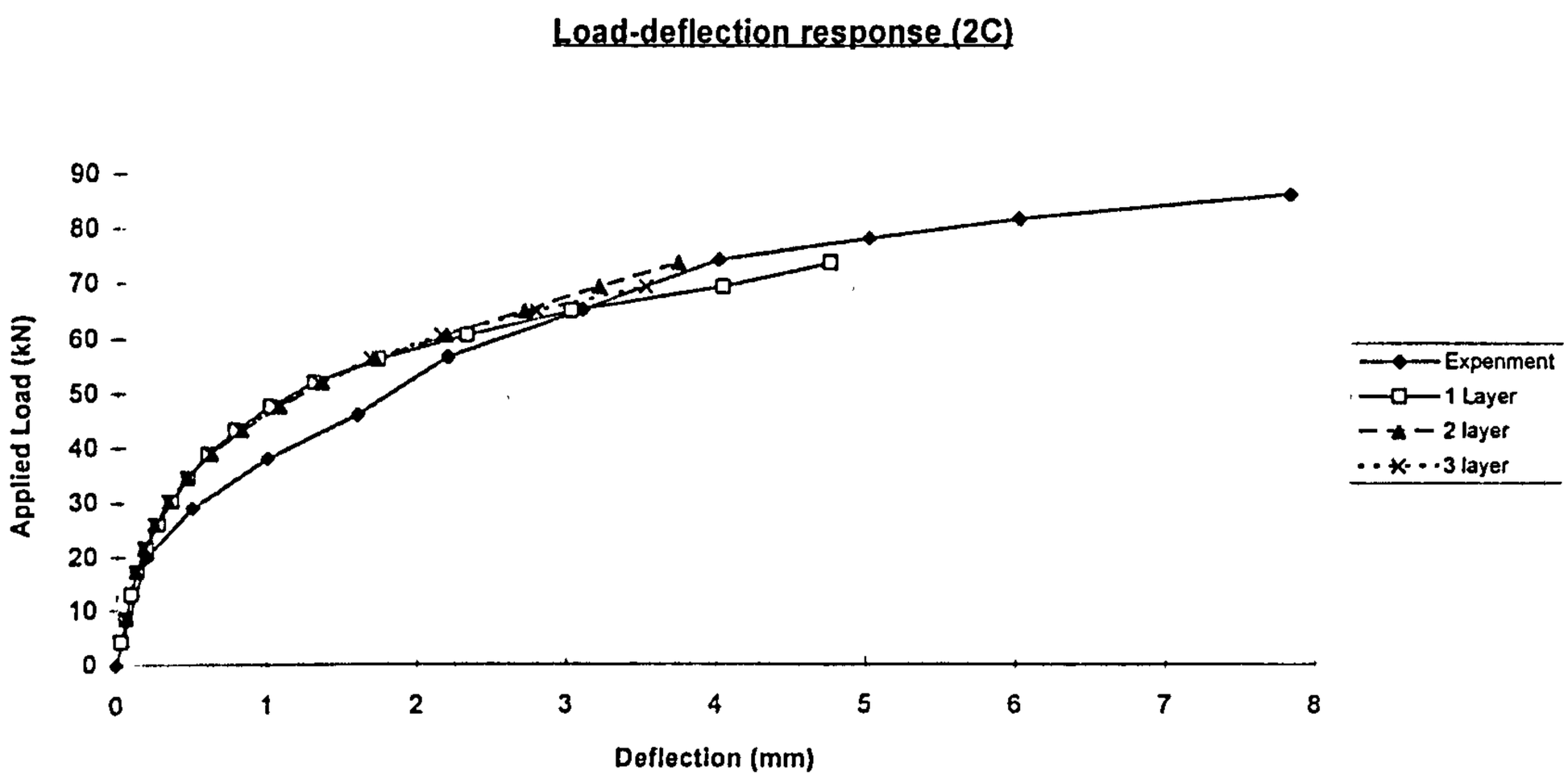

Figure 5.29 : Effect of layer

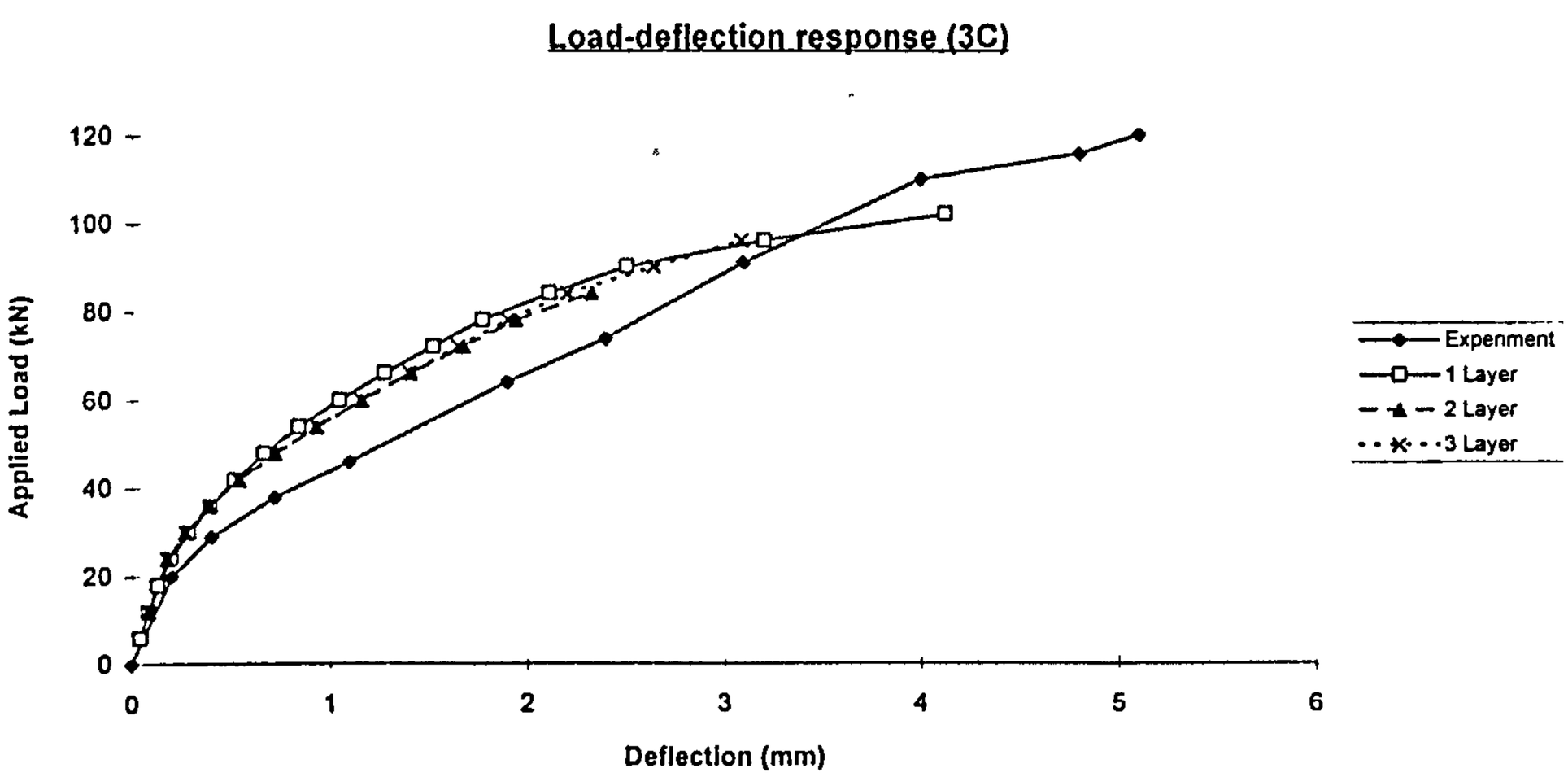

Figure 5.30 : Effect of layer

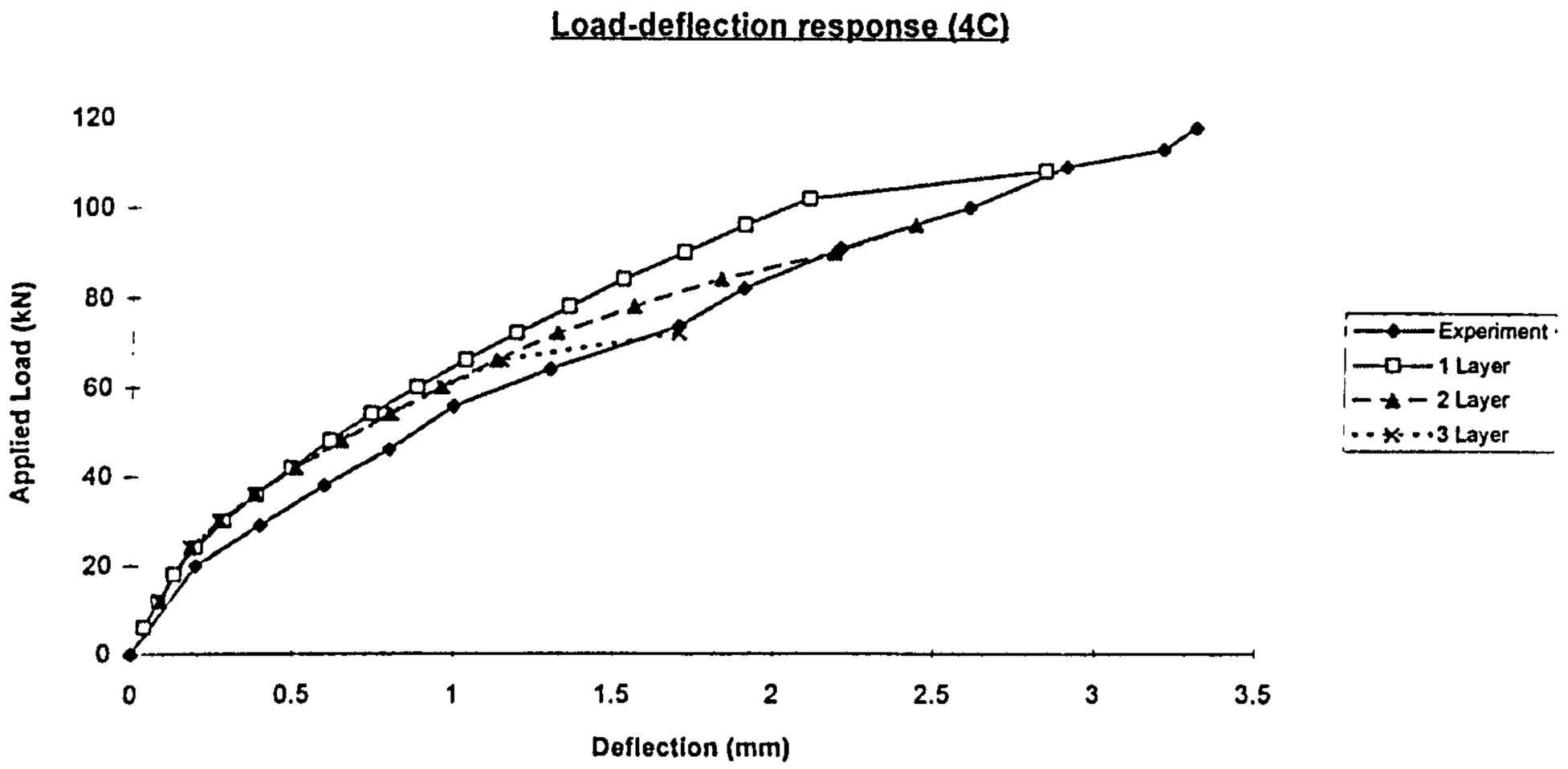

Figure 5.31 : Effect of layer

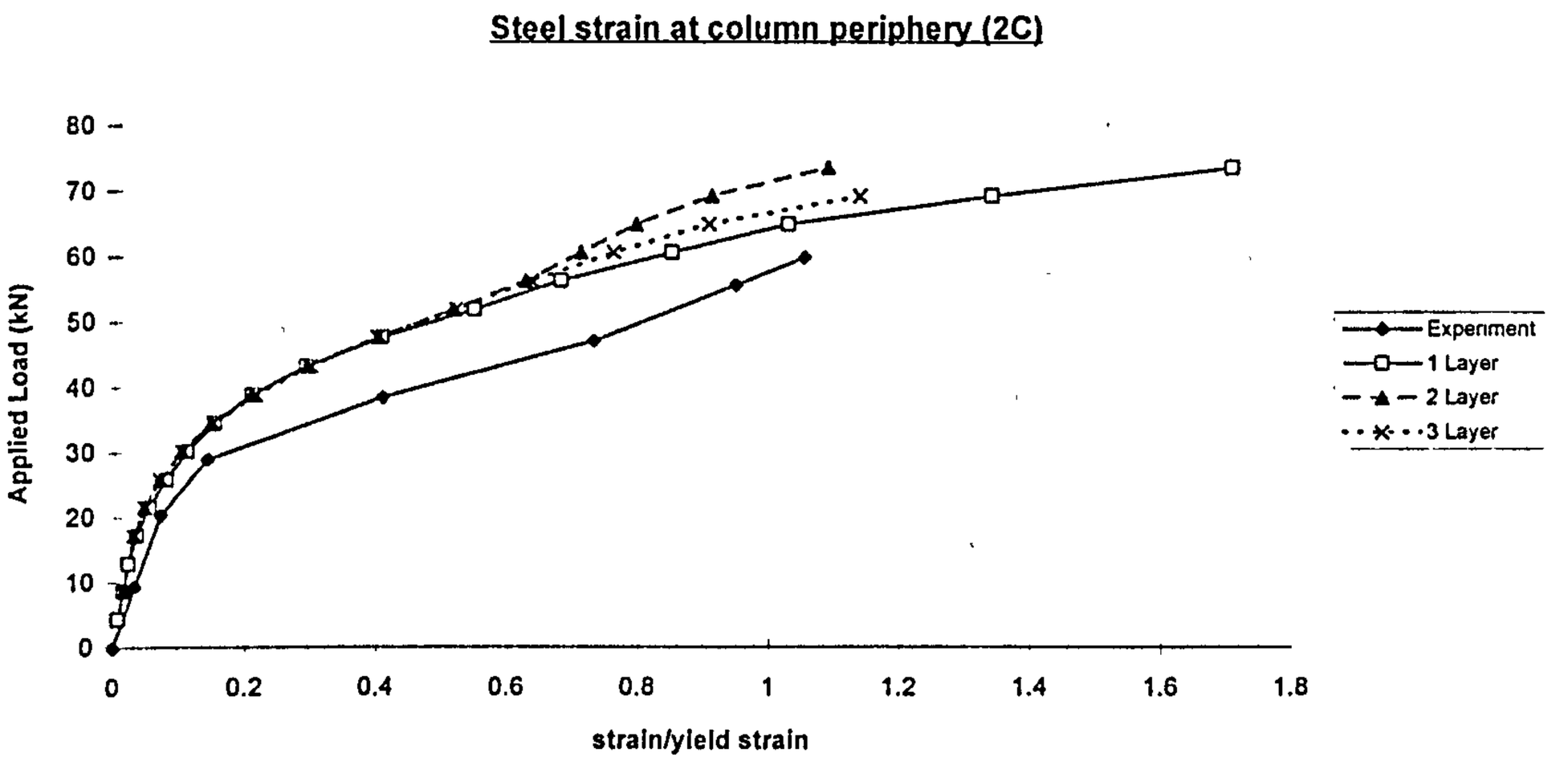

Figure 5.32 : Effect of layer

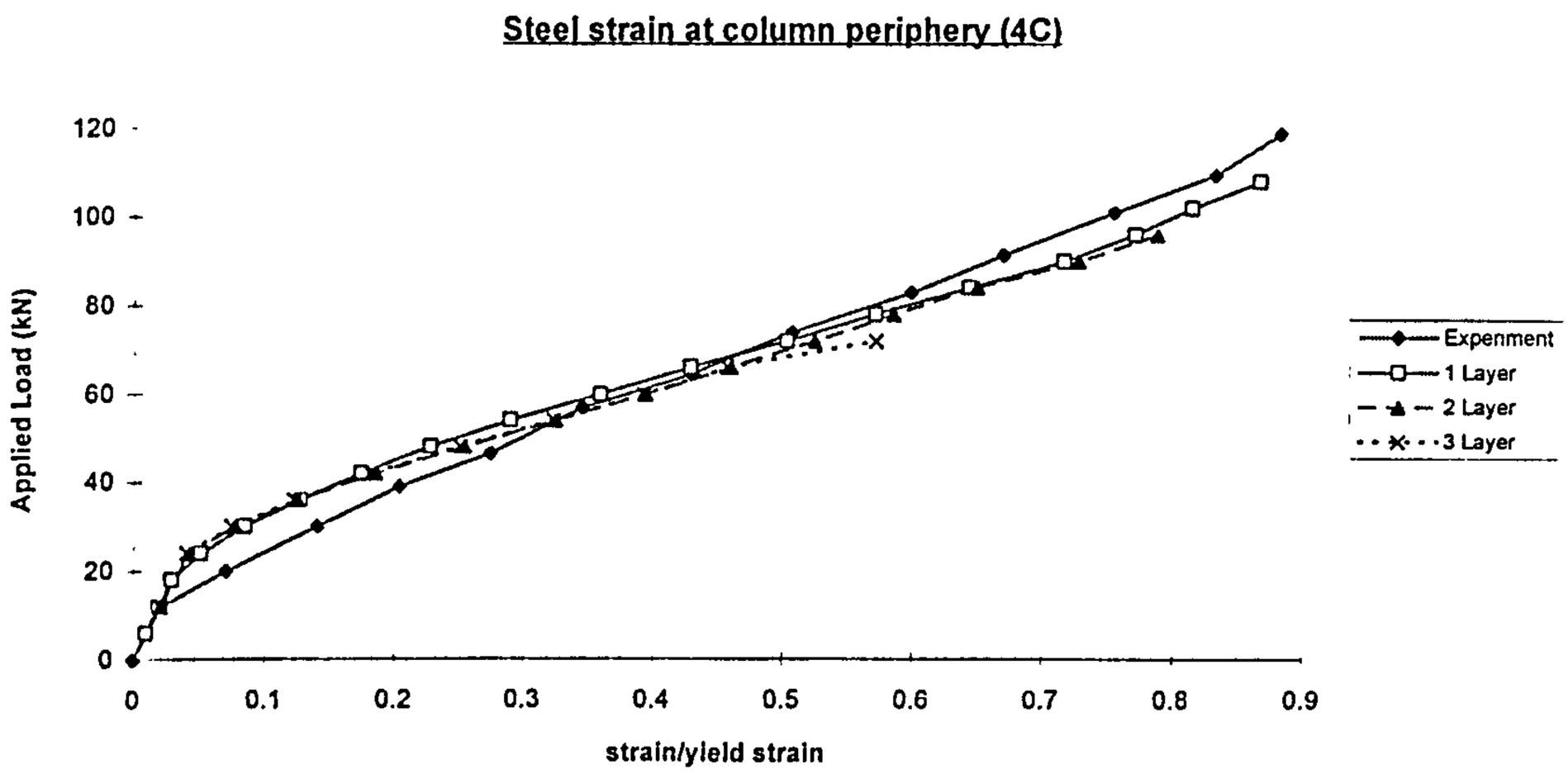

Figure 5.33 : Effect of layer

5.4.5 Simulation of boundary conditions (vertical restraint)

As mentioned earlier, the corners of slabs are free to lift when subjected to a concentrated load at the middle, but we do not know exactly which portion of slab will lift. In order to find out the effect of vertical restraint, the vertical restraint for support nodal point was released node by node from the corner of the slab (Refer to Figure 5.34).

Figures 5.35 and 5.36 show that the effect of vertical restraint is insignificant for both the ultimate load and response of slab. Therefore it was decided that in all analysis only nodal points for corner element will be released (e.g. Res=22).

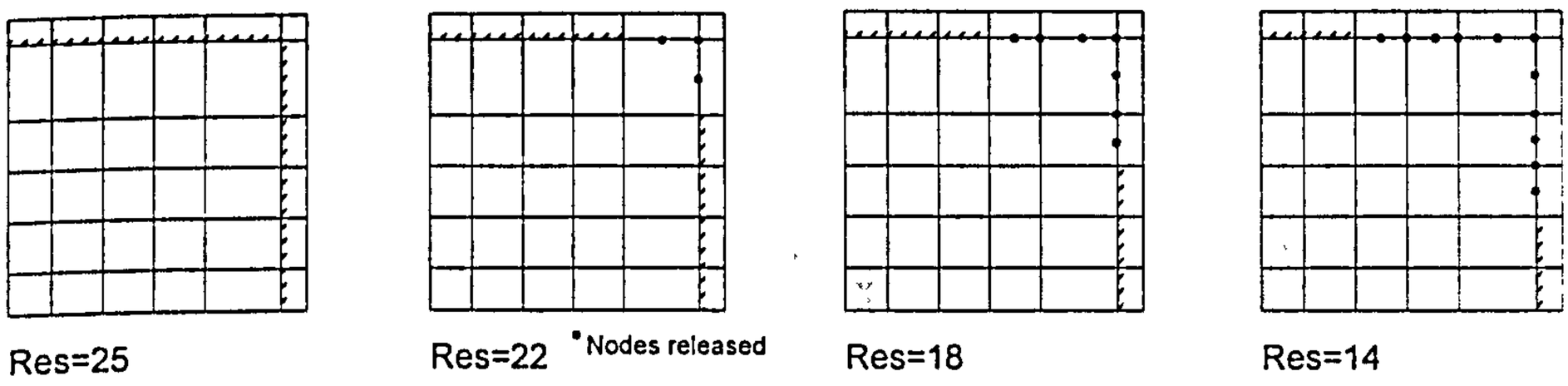

*Res=number of nodes where the vertical movement is restrained

Figure 5.34 : Slabs with various number of vertical restraint

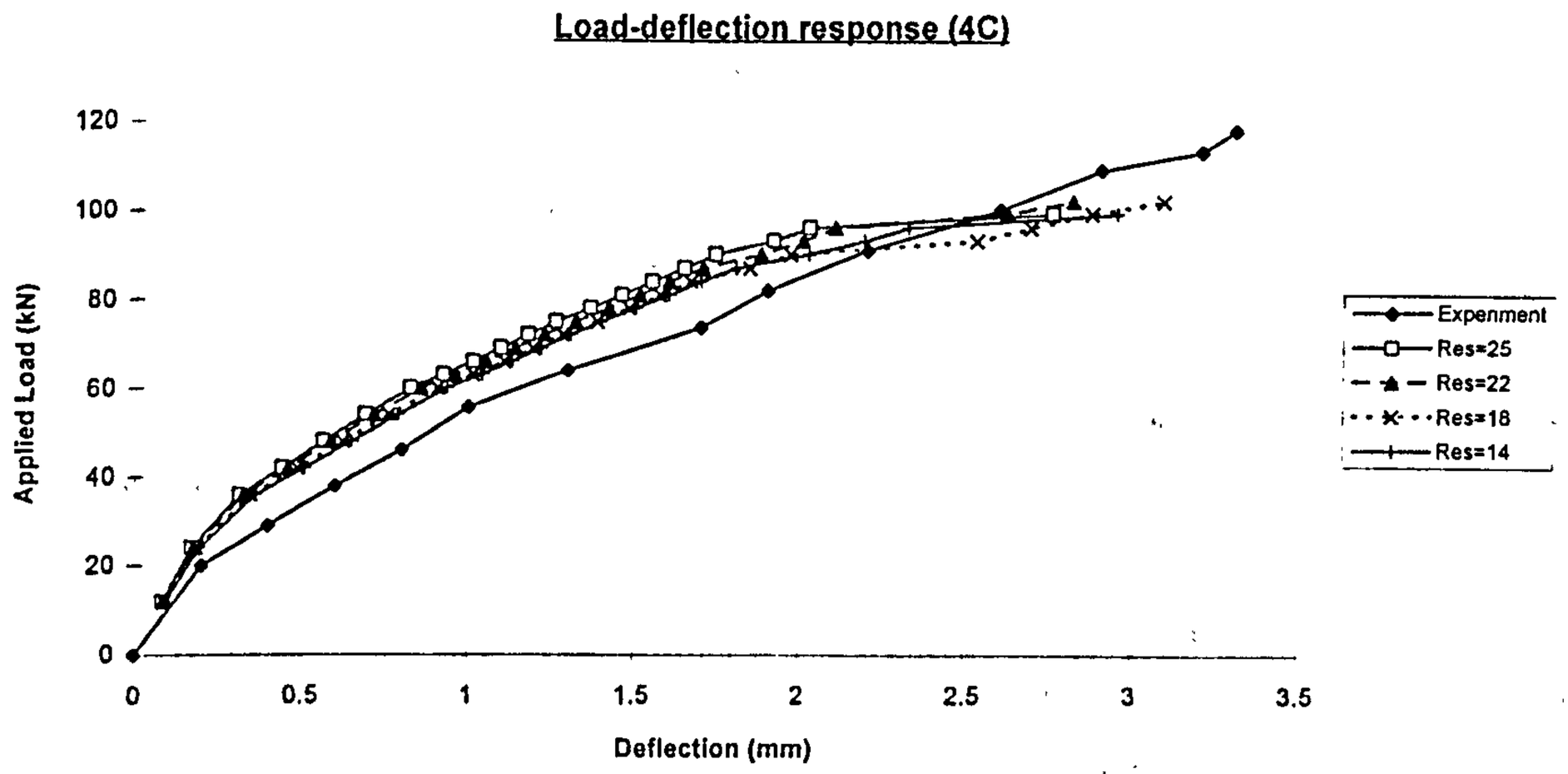

Figure 5.35 : Load-deflection response (Effect of vertical restraint)

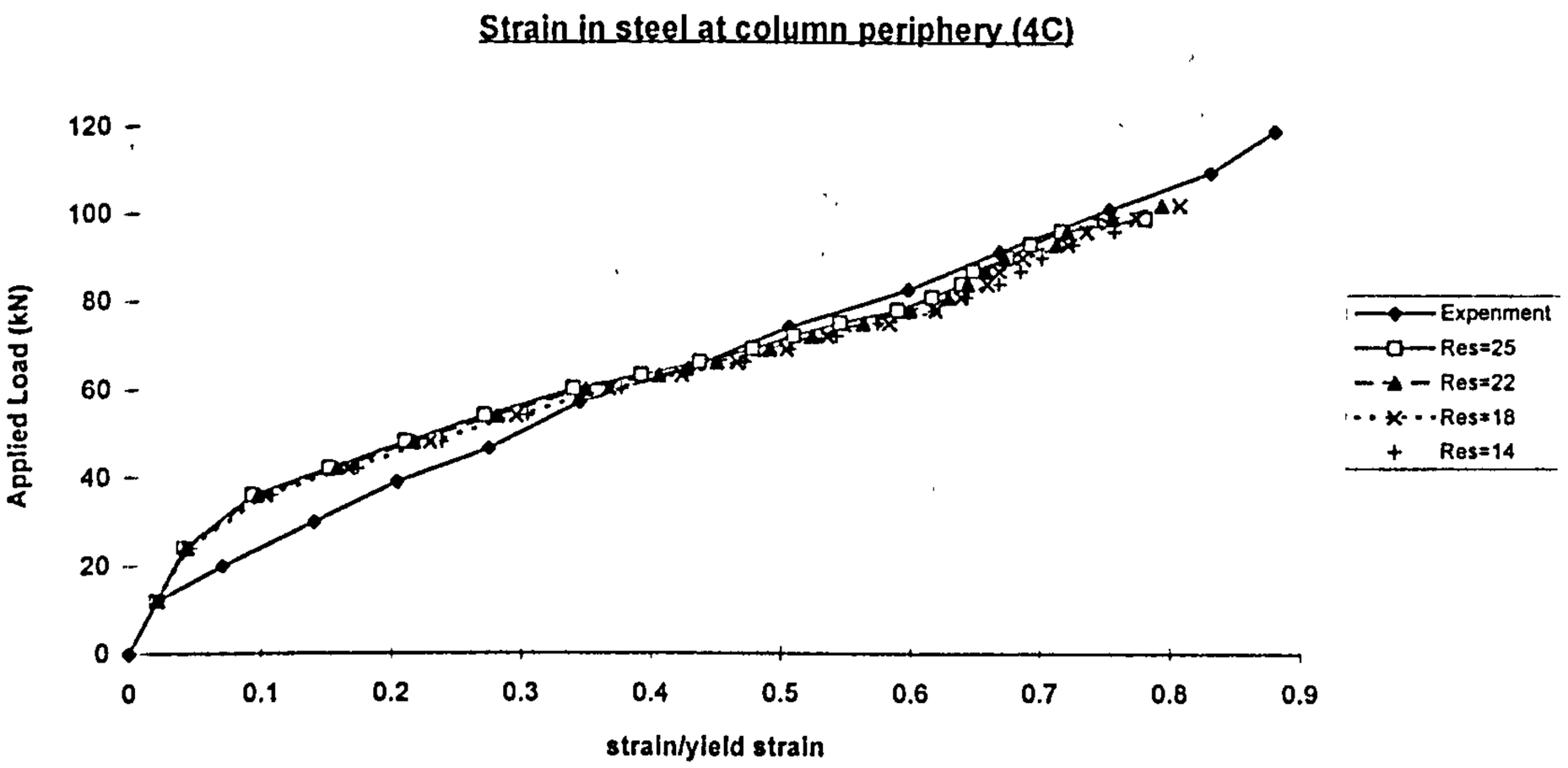

Figure 5.36 : Strain in steel at column periphery (Effect of vertical restraint)

5.4.6 Conclusions

From the parametric study for the numerical parameters, the following conclusions can be drawn :-

- Convergence tolerance generally does not greatly affect the predicted structural response, but smaller value of tolerance will increase the computational cost tremendously. From this study, 5% tolerance predicted good results with relatively low computational cost. Therefore, 5% tolerance was deemed acceptable for use in later study.
- Load increment size will affect the predicted ultimate load and structural response. Larger load increment size predicted higher ultimate load and stiffer structural response. In order to reduce the computational cost, it was decided to apply large load increment at the initial stages and small load increment for highly non-linear part. Thus, load increment size of 10% for the first two increments and 5% for the remaining increments is suitable.
- Within limits, mesh size has little affect on the ultimate load and structural response of the slab. But large aspect ratio may cause the divergence of the analysis and finer mesh is very costly. Therefore, finer mesh arrangement (aspect ratio close to unity) is needed for elements within and near the failure zone and coarser mesh for the elements further away from the failure region is recommended.
- Number of elements through the thickness of slab has little affect on structural response. But increasing the number of elements through the thickness of slab will greatly increase the computational cost and may cause divergence of the solution. Therefore, generally one element through the thickness of slab was used in the later study.
- Number of vertical restraint released had little affect on the ultimate load and structural response of the slab. Therefore only support nodes for the corner element will be released.

5.5 Material Parameters

Four parameters which may have significant effect on the ultimate load, mode of failure and behaviour of slab was studied. These parameters are :

1. Tensile strength of concrete,
2. Tension stiffening factor,
3. Shear Retention factor.
4. Confinement effect (for slabs with shear reinforcement only)

For this study, the following parameters were kept constant for all slabs analysed.

- The load steps for the first two increments was 10% of experimental failure load and 5% of the experimental failure load for the remaining increments.
- The convergence criteria based on the residual forces tolerance of 5%.
- The maximum number of iterations per increment is 50.
- The study was based on the mesh arrangement of 36 elements, aspect ratio for the element beside loading stub of 1.2, and only the support nodal point for corner element being released (see Figure 5.4).
- The predicted failure load is the load at the last converged increment.
- The Poisson's ratio is kept constant at 0.2
- Young's modulus, $E_c = 4730\sqrt{f_c'}$ N/mm^2.
- For steel, the measured values of the elastic modulus and yield stress were used, assuming a perfectly elastic-plastic material behaviour.

5.5.1 Tensile strength of concrete

For this part of study, tension stiffening curve corresponding to A=0.7, $\varepsilon_{max} = 0.003$ i.e. immediately after cracking, tensile strength drops to 70% of the strength at the time of cracking (see Figure 3.17) and the shear retention factor $\beta = 0.5$ $\varepsilon_{cr}/\varepsilon_n$ were kept constant. Three types of tensile strength of concrete versus f_c' was studied :

i) Denoted as f_t1, the splitting tensile strength obtained from equation $f_{sp} = 0.53\sqrt{f_c'}$ (value recommended by Rankin, 1982).

ii) Denoted as f_t2, the splitting tensile strength obtained from equation $f_{sp}=1.4(f_{cu}/10)^{2/3}$ (tensile strength recommended in CEB-FIP Model Code, 1990).

iii) Denoted as f_t3, the splitting tensile strength obtained from equation $f_{sp} = 0.33\sqrt{f_c'}$ (value recommended in ACI code for direct tension test).

Figure 5.37 shows f_{sp} as a function of f_c'.

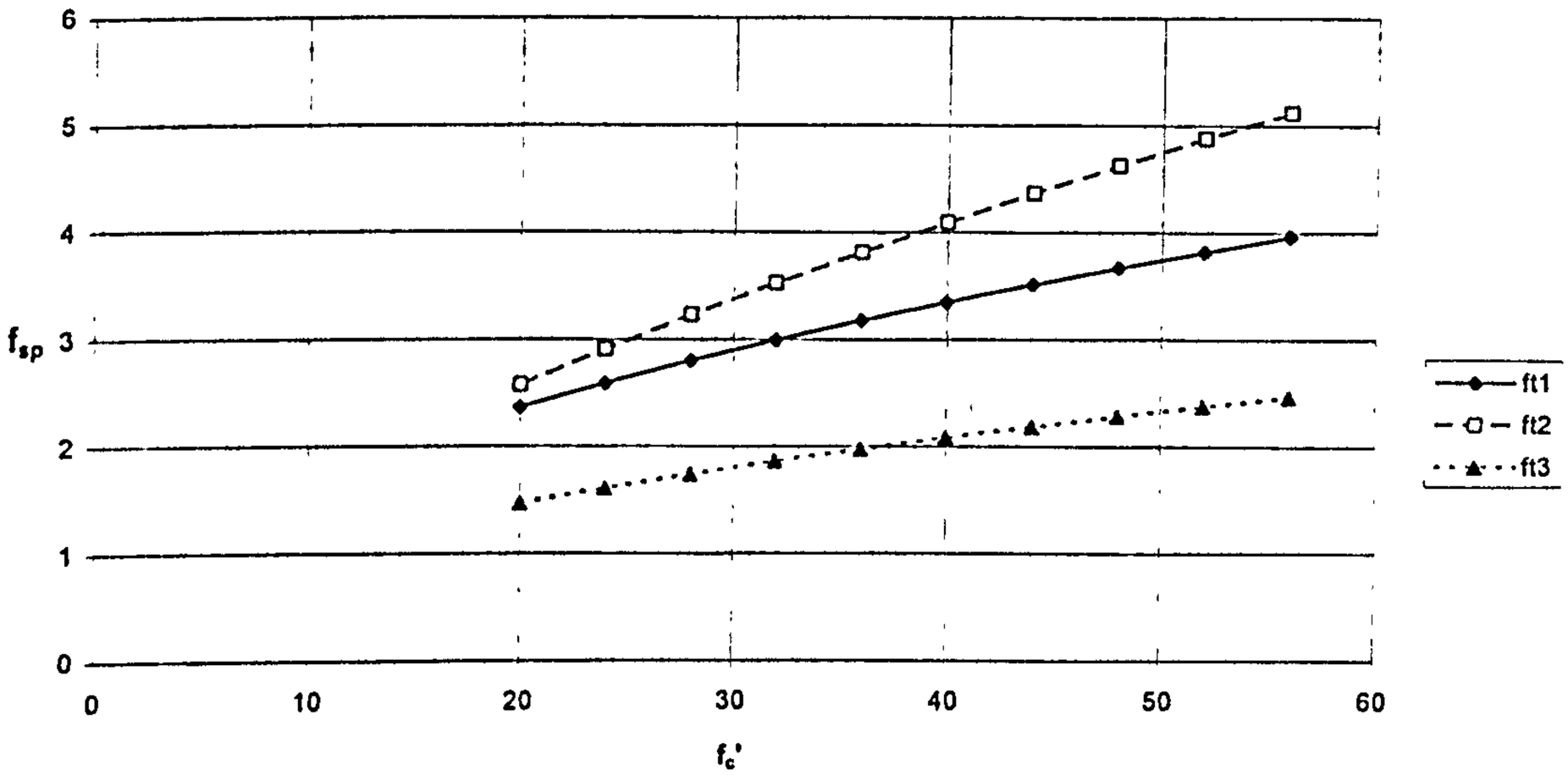

Figure 5.37 Estimating tensile strength from compressive strength

Results in Table 5.7 show that the effect of tensile strength of concrete on the ultimate load of slab is insignificant. Taking f_t1 as a reference, increasing the tensile strength of concrete by 20% (f_t2), increased the ultimate load by 3% and reducing tensile strength of concrete by 40% (f_t3), reduced the ultimate load by 5% (If we ignore model "2C", the reduction of ultimate load is not significant). But too low a tensile strength might cause divergence of the solution, like for example analysis of model "2C" which diverged at a relatively low load level. Figures 5.37-5.44 show that the magnitude of tensile strength affects the stiffness of the slab. This effect is more significant in slabs with low amount of reinforcement than in slabs with high amount of reinforcement. In order to achieve consistent results, the divergence of the solution at low load level must be avoided. Therefore, when the tensile strength is not given, f_t1 ($f_{sp} = 0.53\sqrt{f_c'}$) was used in the later study and tensile strength from experiment was used if available.

The fact that changes in the values of tensile strength did not affect the ultimate of "heavily" reinforced slabs, was a bit suprising. In order to make sure that the result was reliable, three more slabs (slabs 9, 15 and 4B) all failing in shear were analysed. The results are presented in Figures 4.44a to 4.44f. The results clearly indicate that the conclusion is justified.

Table 5.7 : Effect of tensile strength of concrete

Slab	f_{cu} (N/mm^2)	Tensile strength(N/mm^2)			P_{test}	Num/Exp failure Load		
		f_t1	f_t2	f_t3	(kN)	f_t1	f_t2	f_t3
1B	47.10	3.253	3.934	2.026	28.850	0.973	0.973	0.919
1C	34.80	2.796	3.215	1.741	62.740	0.845	0.895	0.845
2C	40.50	3.017	3.557	1.878	87.860	0.787	0.836	0.639
3C	40.50	3.017	3.557	1.878	124.140	0.773	0.822	0.773
4C	34.80	2.796	3.215	1.741	125.940	0.905	0.905	0.858
					Average	0.857	0.886	0.807
					STDEV	0.084	0.061	0.107

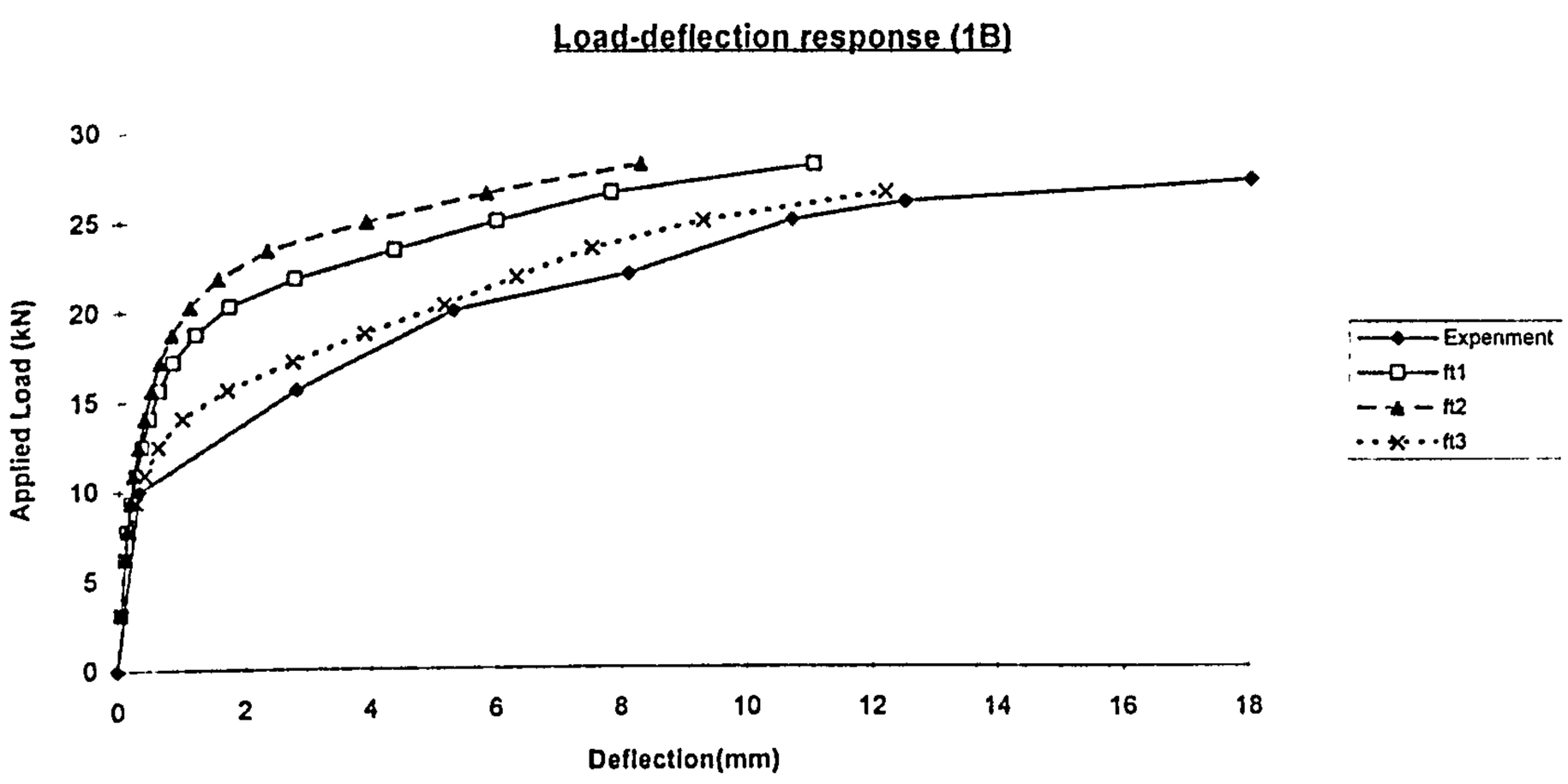

Figure 5.38 Effect of tensile strength of concrete ("1B")

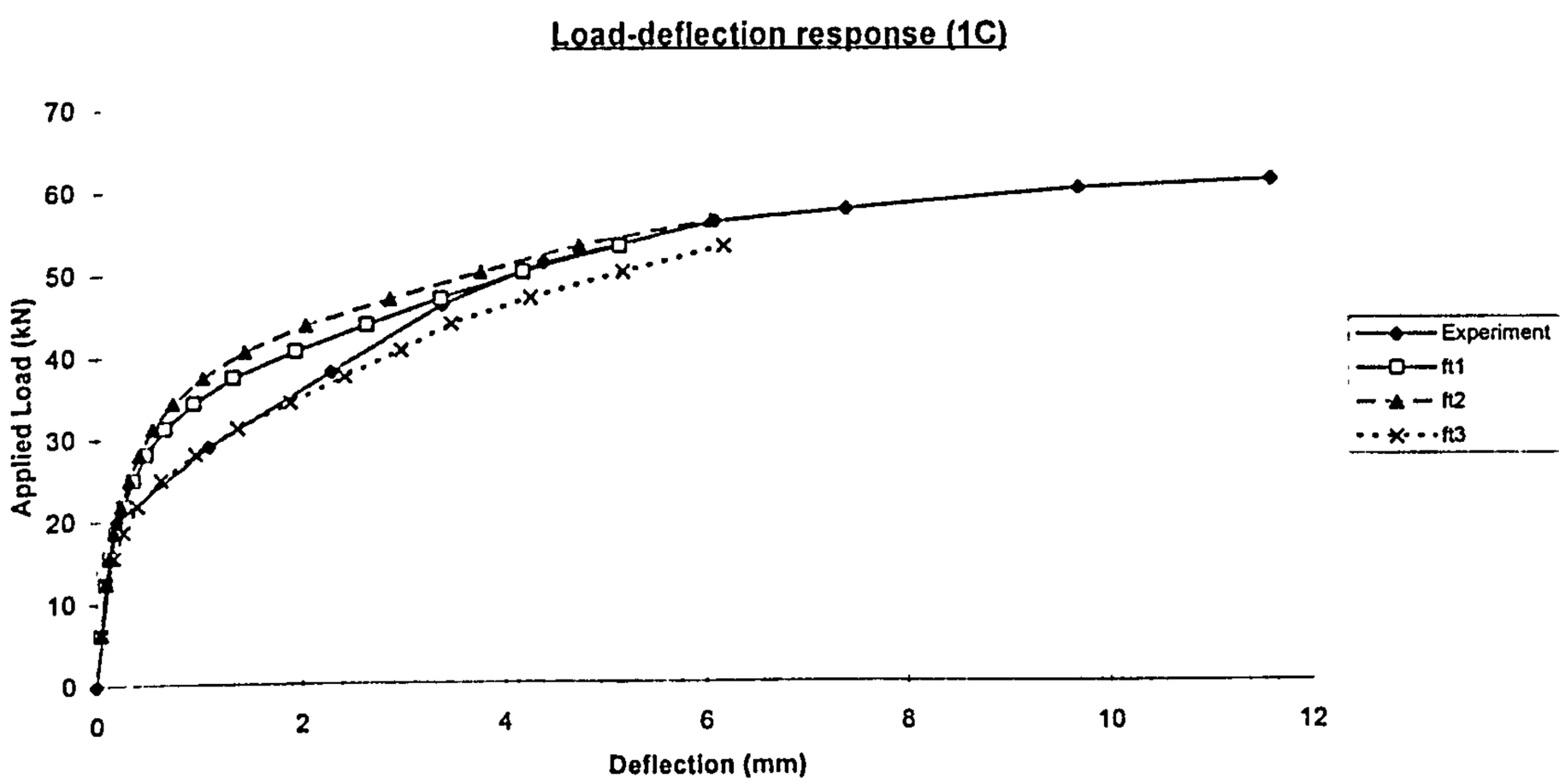

Figure 5.39 Effect of tensile strength of concrete ("1C")

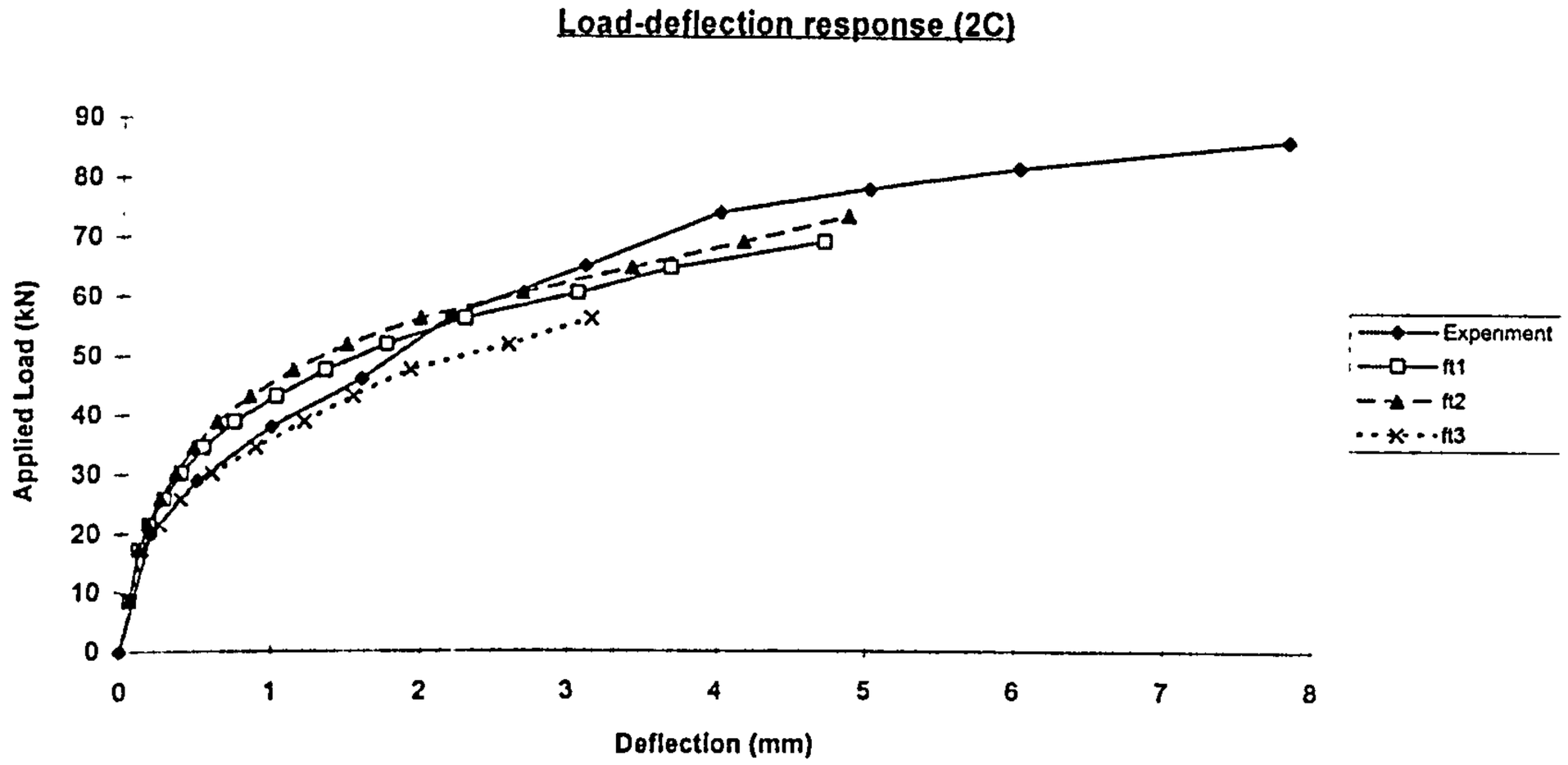

Figure 5.40 Effect of tensile strength of concrete ("2C")

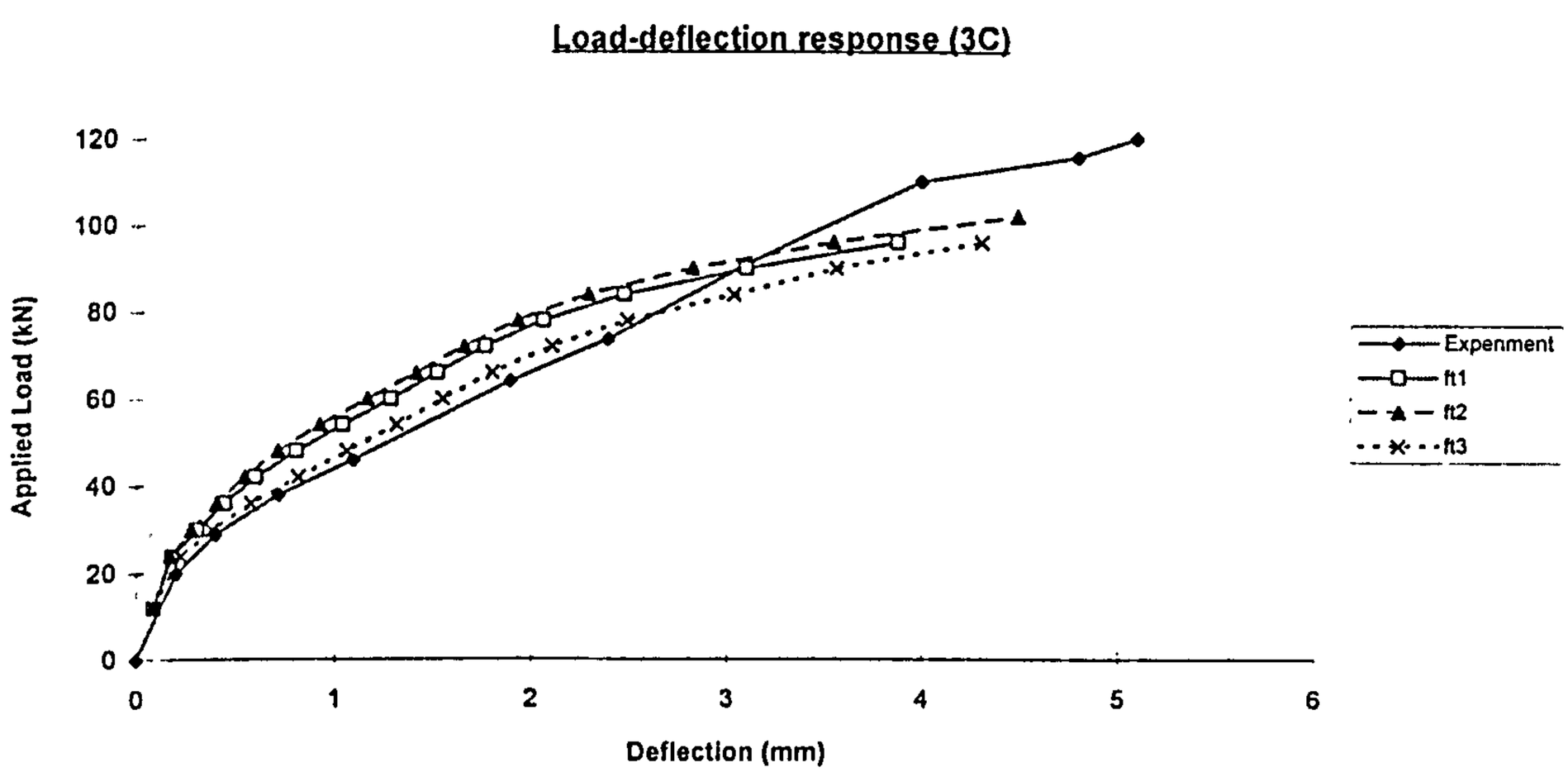

Figure 5.41 Effect of tensile strength of concrete ("3C")

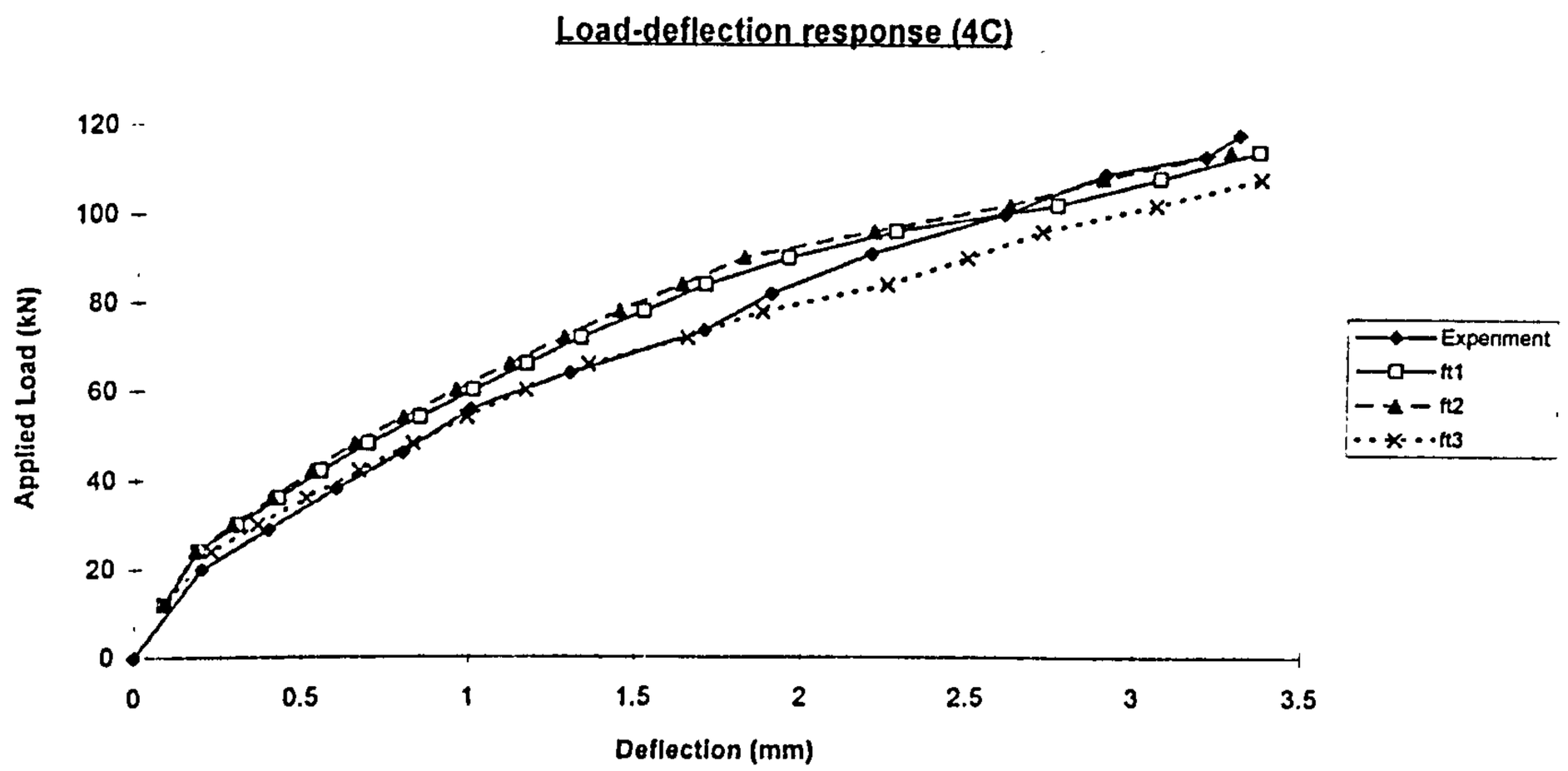

Figure 5.42 Effect of tensile strength of concrete ("4C")

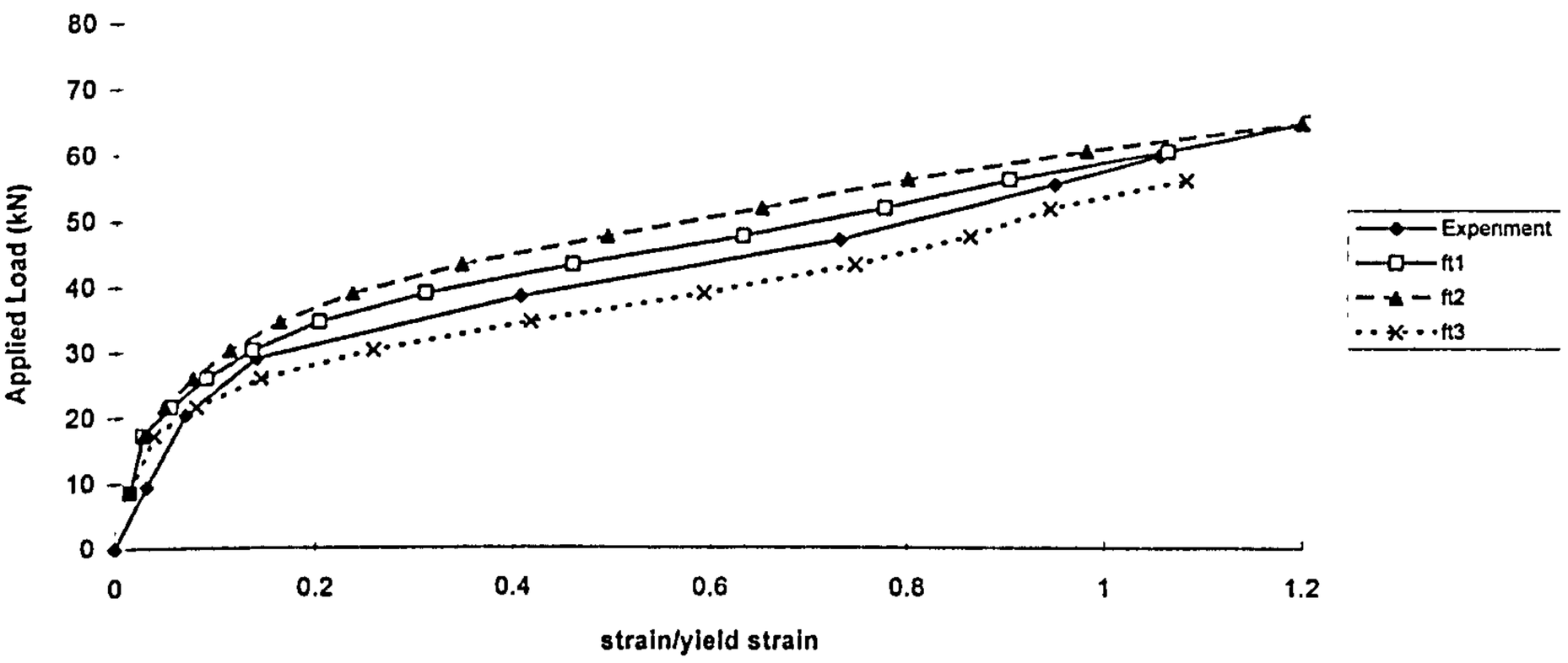

Figure 5.43 Effect of tensile strength of concrete ("2C")

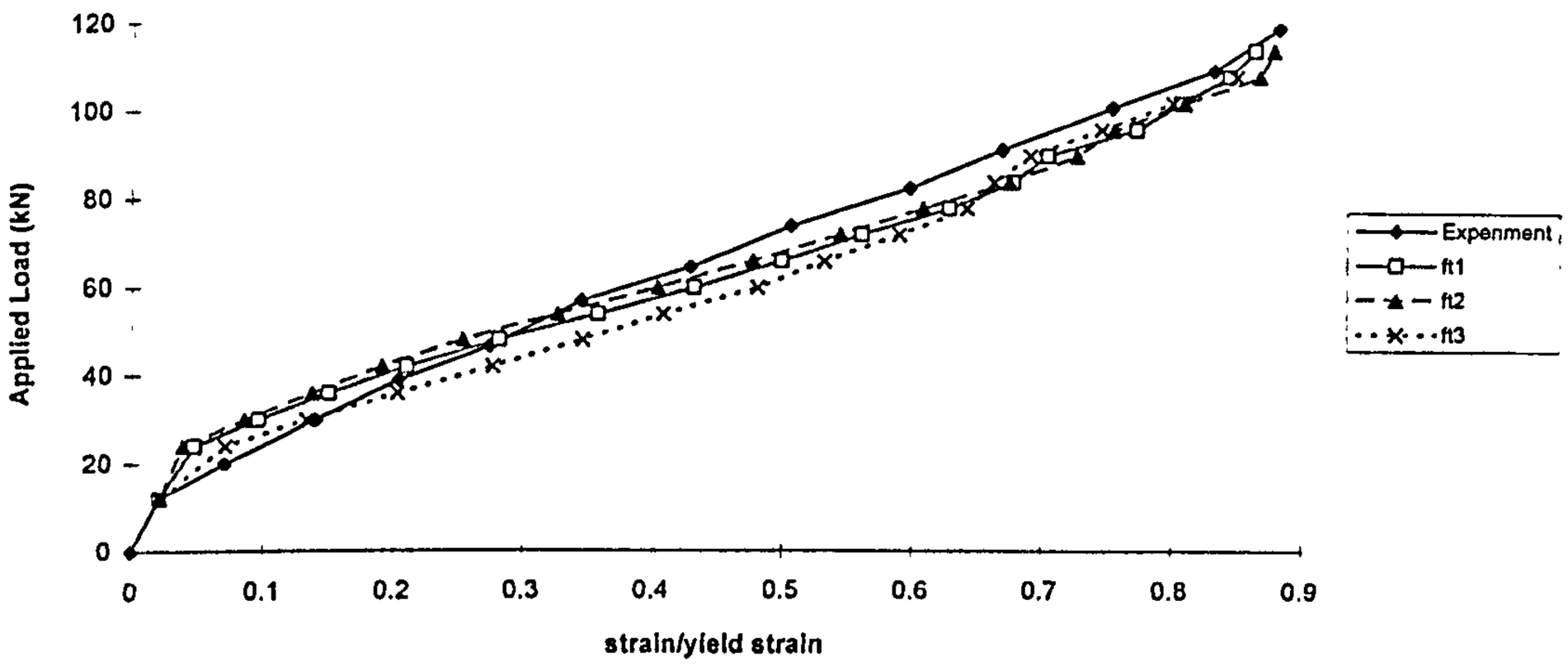

Figure 5.44 Effect of tensile strength of concrete ("4C")

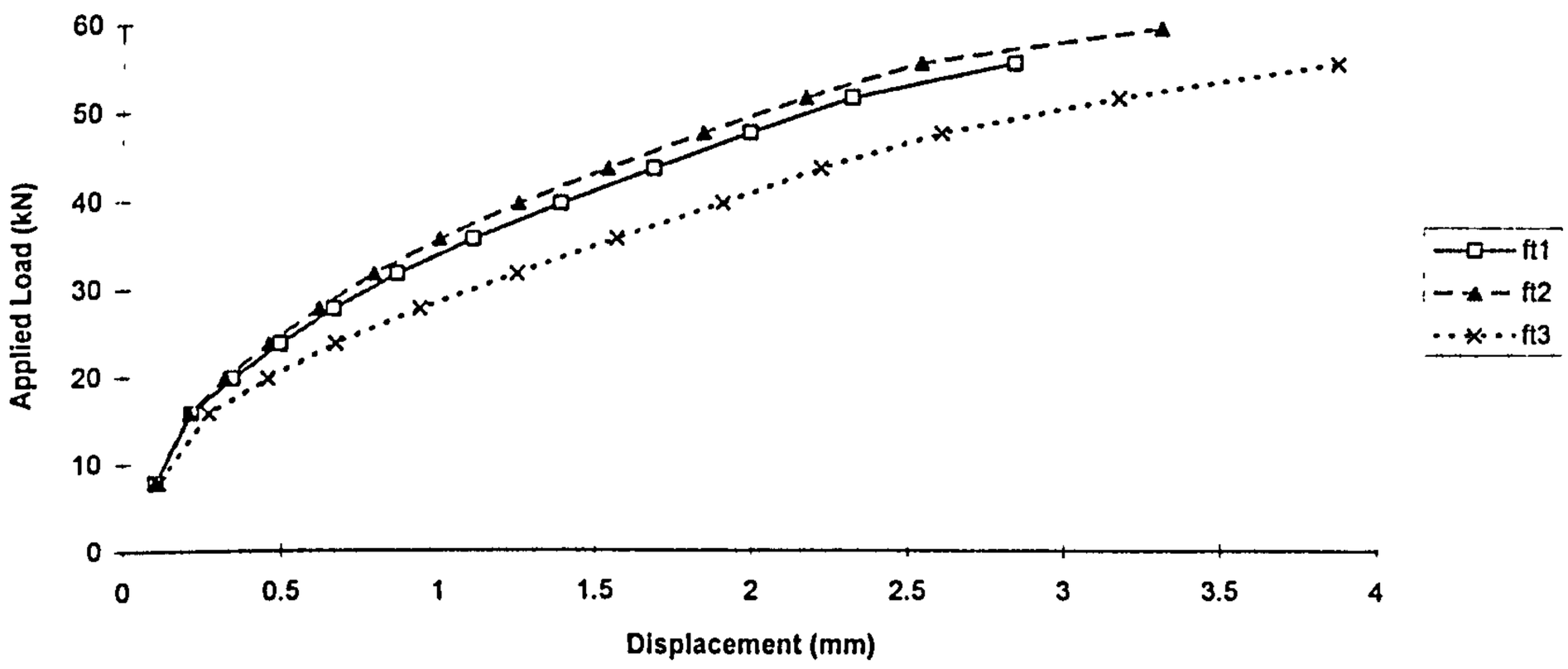

Figure 5.44a Effect of tensile strength of concrete ("9")

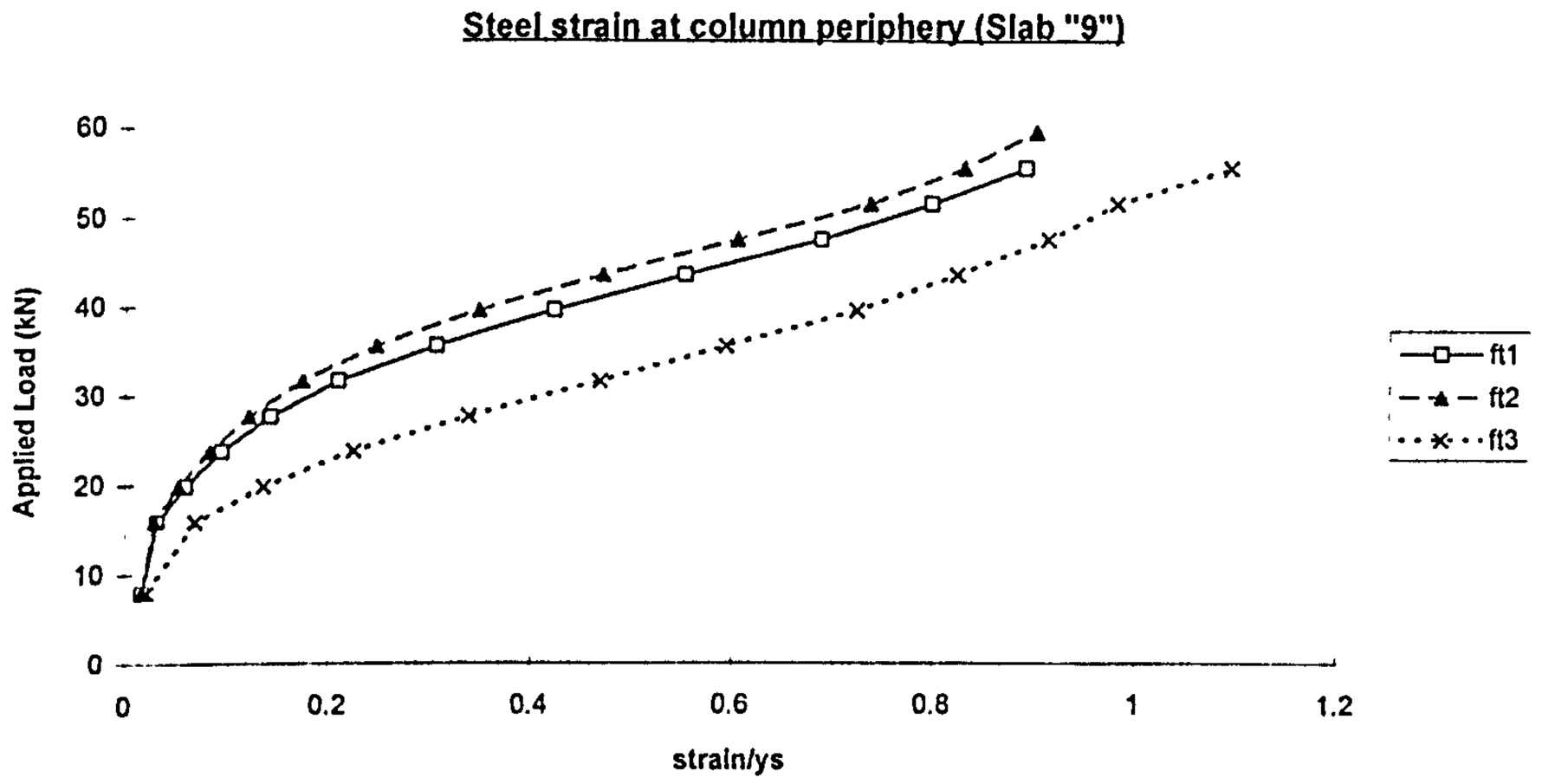

Figure 5.44b Effect of tensile strength of concrete ("9")

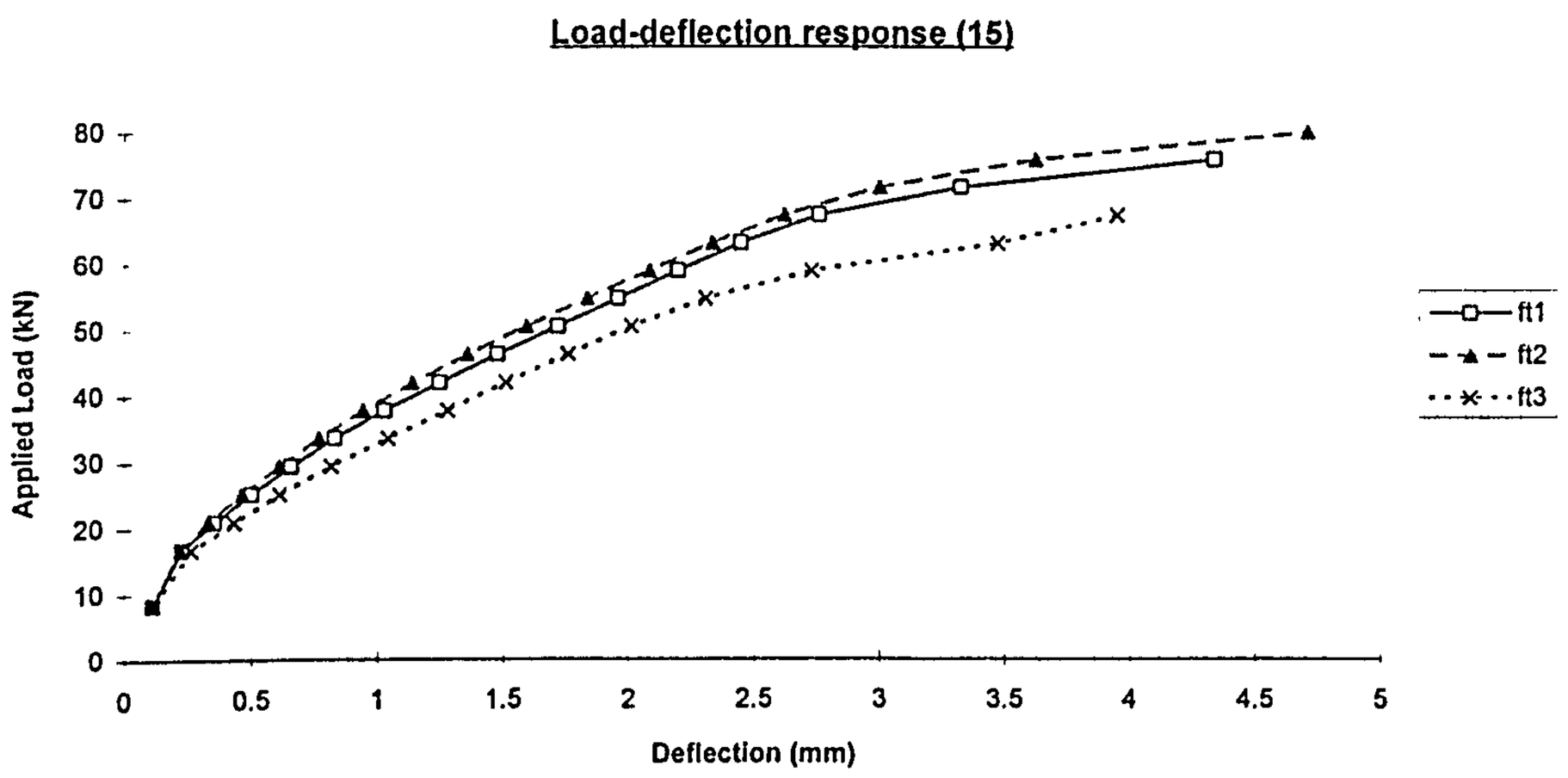

Figure 5.44c Effect of tensile strength of concrete ("15")

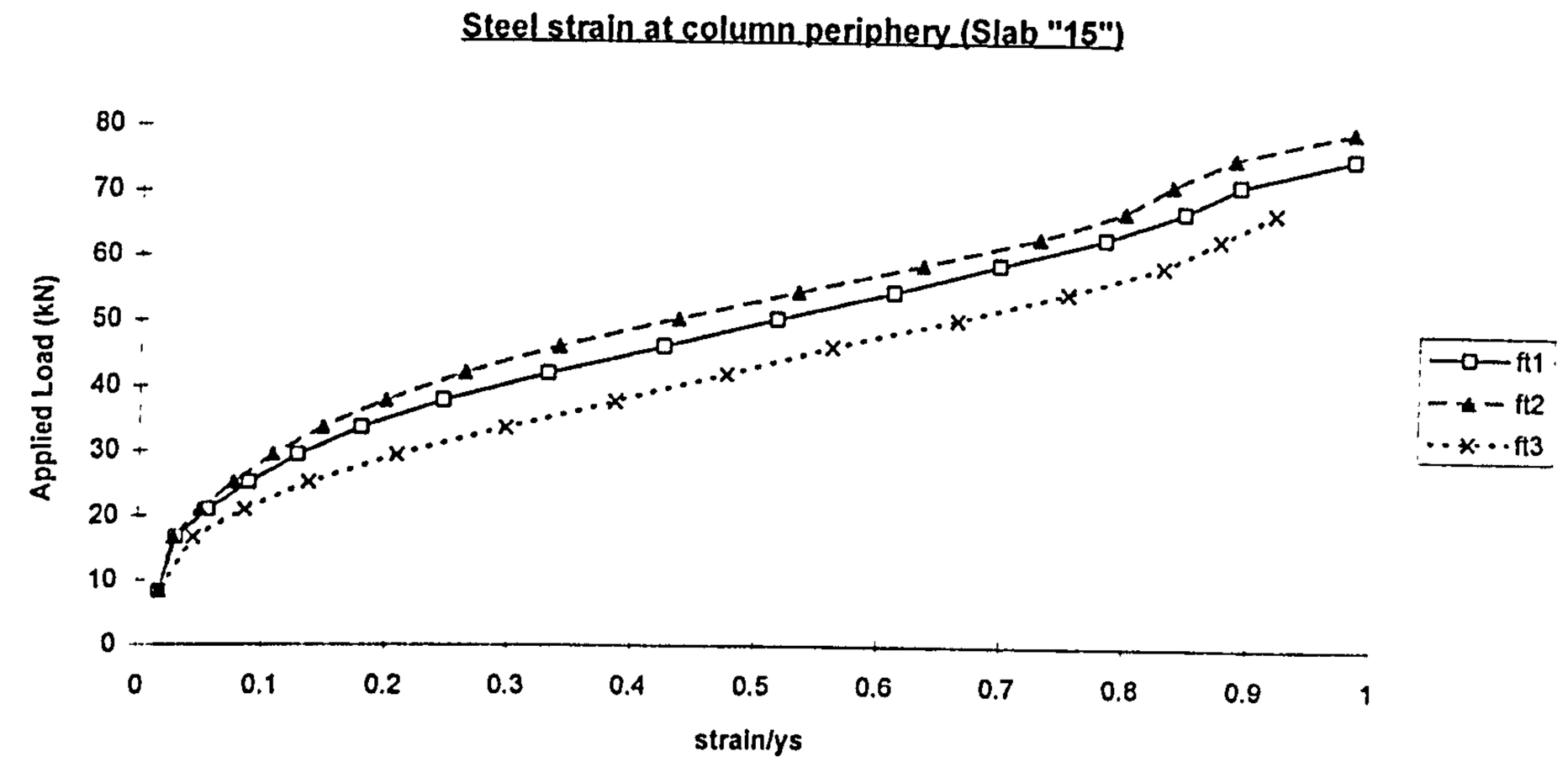

Figure 5.44d Effect of tensile strength of concrete ("15")

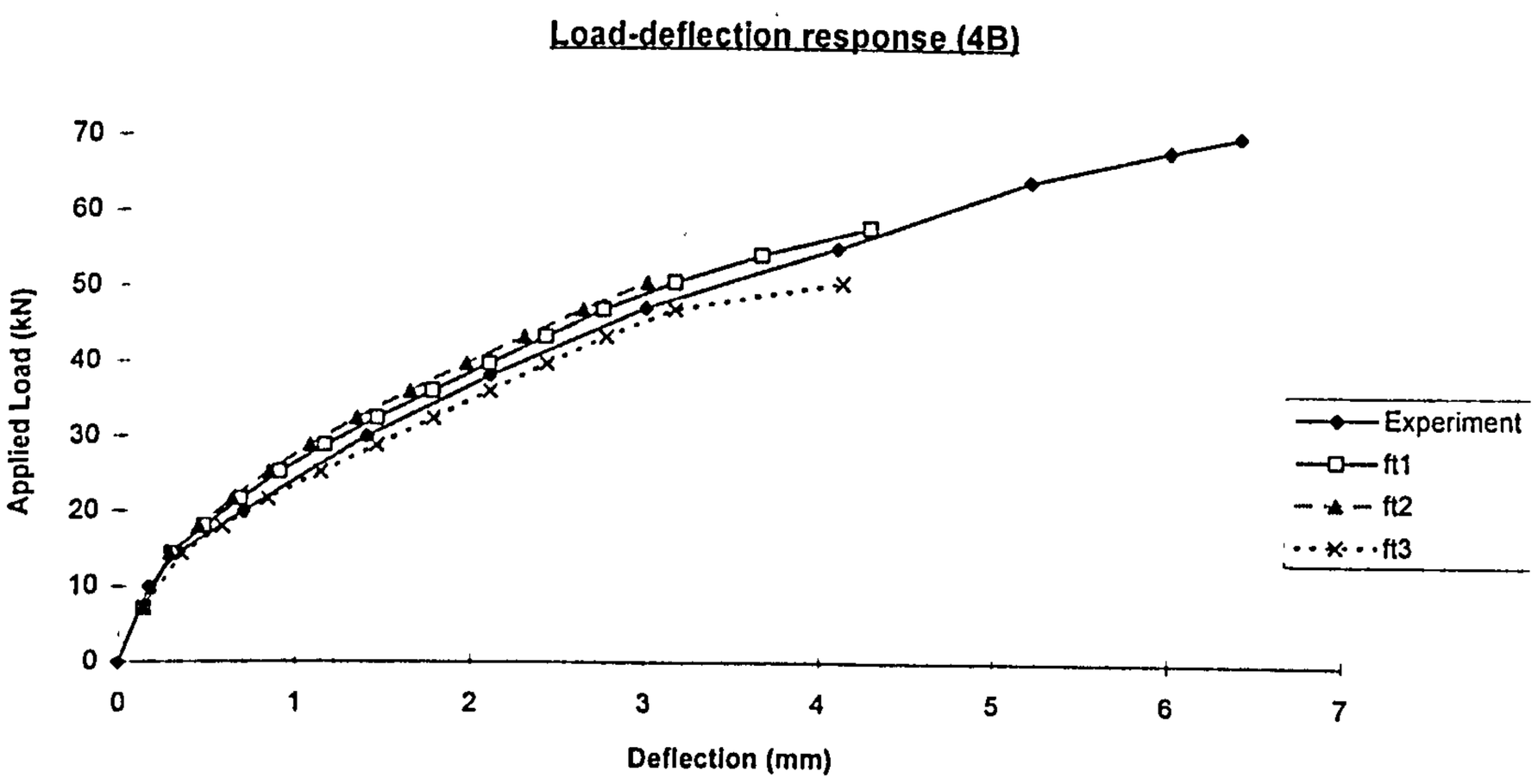

Figure 5.44e Effect of tensile strength of concrete ("4B")

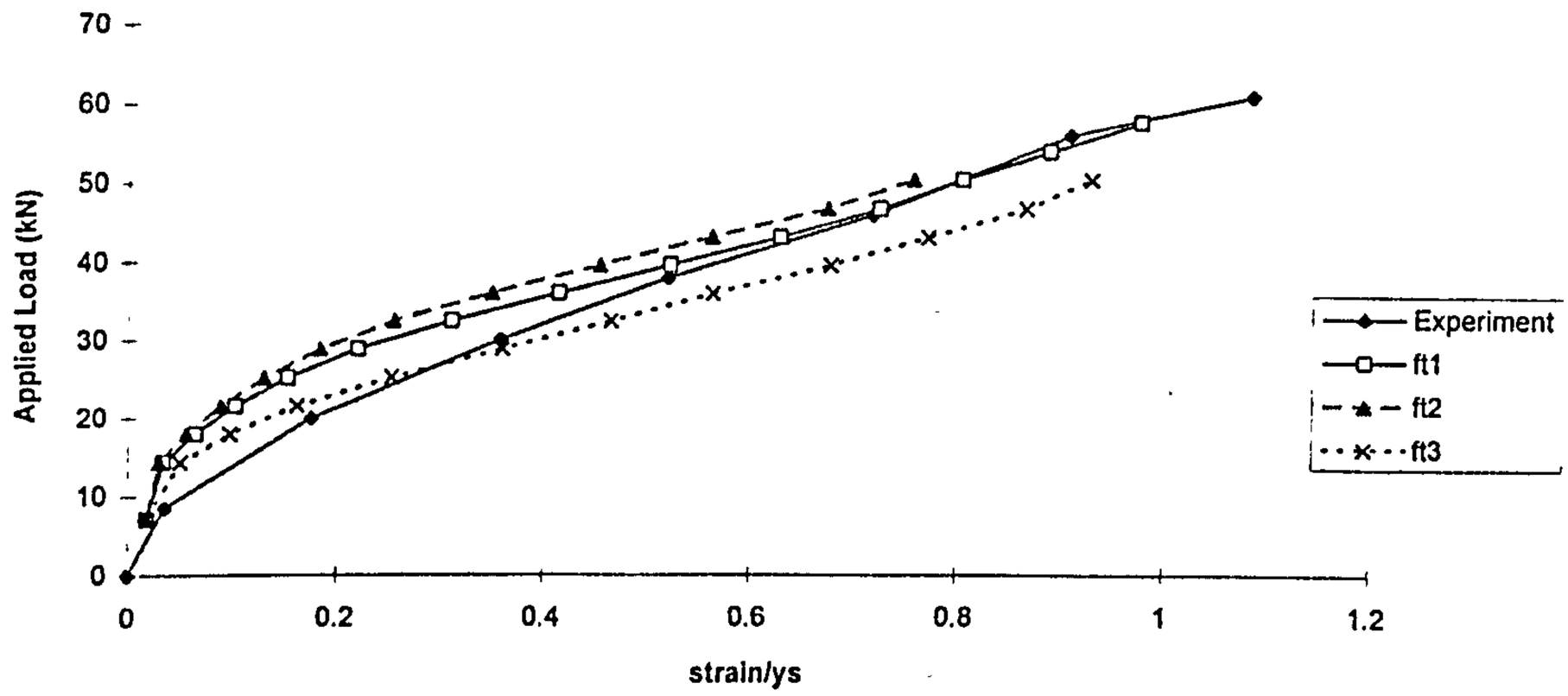

Figure 5.44f Effect of tensile strength of concrete ("4B")

5.5.2 Effect of Tension Stiffening

The objective of this section is to see the effect of tension stiffening on the behaviour of slabs and mode of failure. The shear retention factor is kept constant as $\beta = 0.5\varepsilon_{cr}/\varepsilon_n$ and cylinder splitting strength of concrete is obtained from $f_{sp} = 0.53\sqrt{f_c'}$.

Three types tension stiffening variation as shown in Figure 5.45 were studied:

i) There is no reduction of tensile strength of concrete immediately after cracking and maximum strain ε_{max} taken as 0.003 (A=1.0, emax=0.003).

ii) There is no reduction of tensile strength of concrete immediately after cracking but maximum strain ε_{max} taken as 0.002 (A=1.0, emax=0.002).

iii) Tensile strength of concrete immediately after cracking is reduced to $0.7f_t$ and maximum strain ε_{max} taken as 0.003 (A=0.7, emax=0.003).

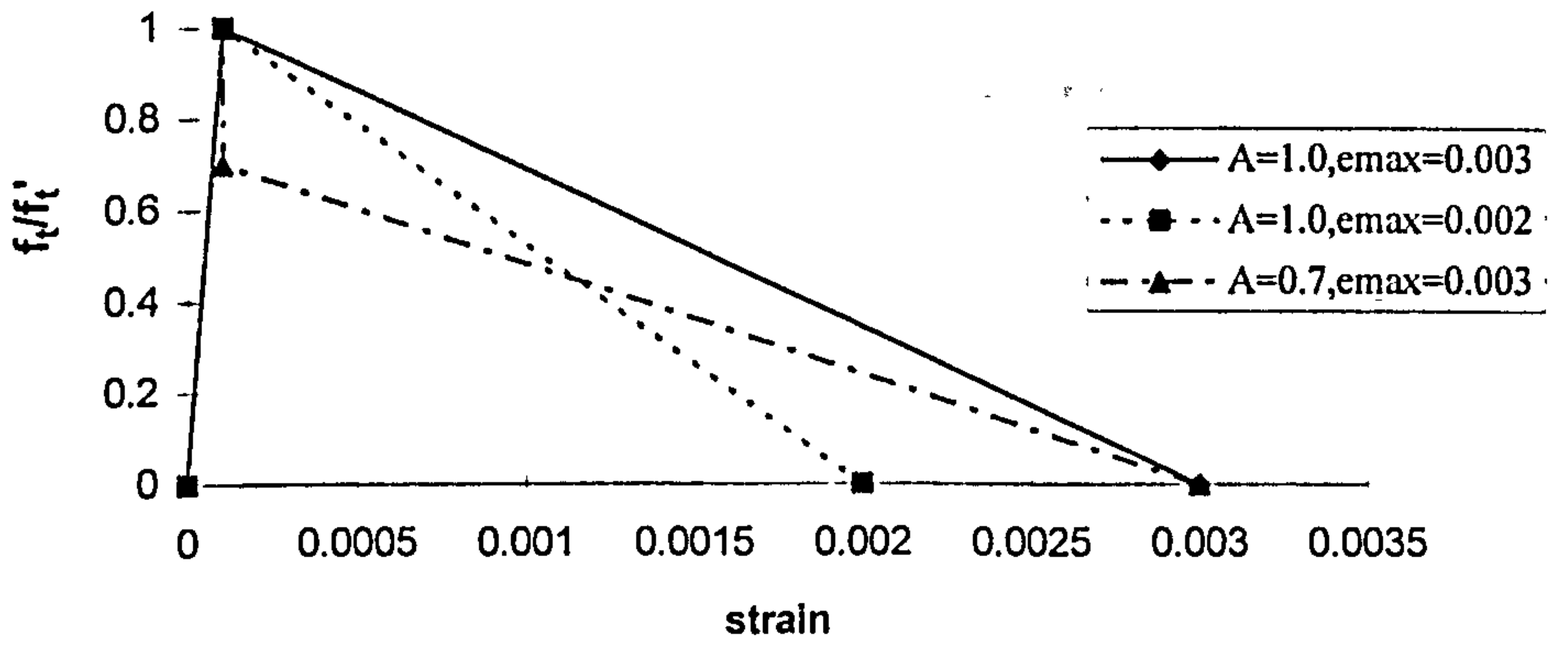

Figure 5.45 Tension stiffening curves

The effect of tension stiffening model used on the results can be summarised as follows :

- It has significant effect on the behaviour of slabs with low percentage of steel (Figures 5.46-5.47) but less significant effect on the behaviour of slabs with high percentage of steel (Figures 5.48-5.52). The predicted load-deflection response by tension stiffening curves (A=1.0, emax=0.003 and A=1.0, emax=0.002) for slabs with low percentage of steel are overstiff immediately after cracking occurs. Thus, loss of stiffness due to cracking of concrete is not shown. However, reducing the tensile strength immediately after cracking (i.e. A=0.7, emax=0.003) reflected the loss of stiffness due to cracking of concrete.
- Tension stiffening does not affect the strain in concrete at early stage of loading. However, it affects the concrete strain prior to failure of slab (Figure.5.53)
- Generally, tension stiffening does not affect the crack pattern (Figure 5.54).
- The influence of tension stiffening on the load versus strain in steel is insignificant. However, it affected the load at first yield (Tables 5.9) and the ultimate load of slab. Tension stiffening model (A=1.0, emax=0.003) predicted highest failure load in all cases. It allowed yielding of steel develop. Compared to experimental results, it predicted incorrect mode of failure for slabs "2C" and "4C" (Figure 5.55).
- Generally, reducing the tensile strength immediately after cracking or reducing maximum strain at which tensile strength becomes zero, reduced the ultimate load of the slab.

From the above observation, tension stiffening curve (A=0.7, emax=0.003) was deemed to be the best model because it can reflect the loss of stiffness due to cracking of concrete and predicted reasonably accurate results (standard deviation=8.4% and correct mode of failure). Therefore this tension stiffening curve was chosen for use in later study.

Table 5.8 : Effect of Tension Stiffening on failure load

Slab	P_{test} (kN)	Num/Exp failure load		
		A=1.0, emax=0.003	A=1.0, emax=0.002	A=0.7, emax=0.003
1B	28.850	1.027	0.973	0.973
1C	62.740	0.945	0.895	0.845
2C	87.860	0.885	0.787	0.787
3C	124.140	0.822	0.725	0.773
4C	125.940	0.858	0.858	0.905
Average		0.907	0.848	0.857
STDEV		0.081	0.096	0.084

Table 5.9 : Effect of tension stiffening on mode of failure

	Test	Numerical Predictions					
		A=1.0, emax=0.003		A=1.0, emax=0.002		A=0.7, emax=0.003	
Slab	Failure Mode	Load at 1st yield (kN)	Failure Mode	Load at 1st yield (kN)	Failure Mode	Load at 1st yield (kN)	Failure Mode
1B	y	25.0	y	23.4	y	21.8	y
1C	y	43.7	y	43.7	y	40.6	y
2C	s	60.5	y	56.2	y	51.8	y
3C	s	84.0	y	78.0	fp	78.0	s
4C	s	108.0	s	108.0	s	108.0	s

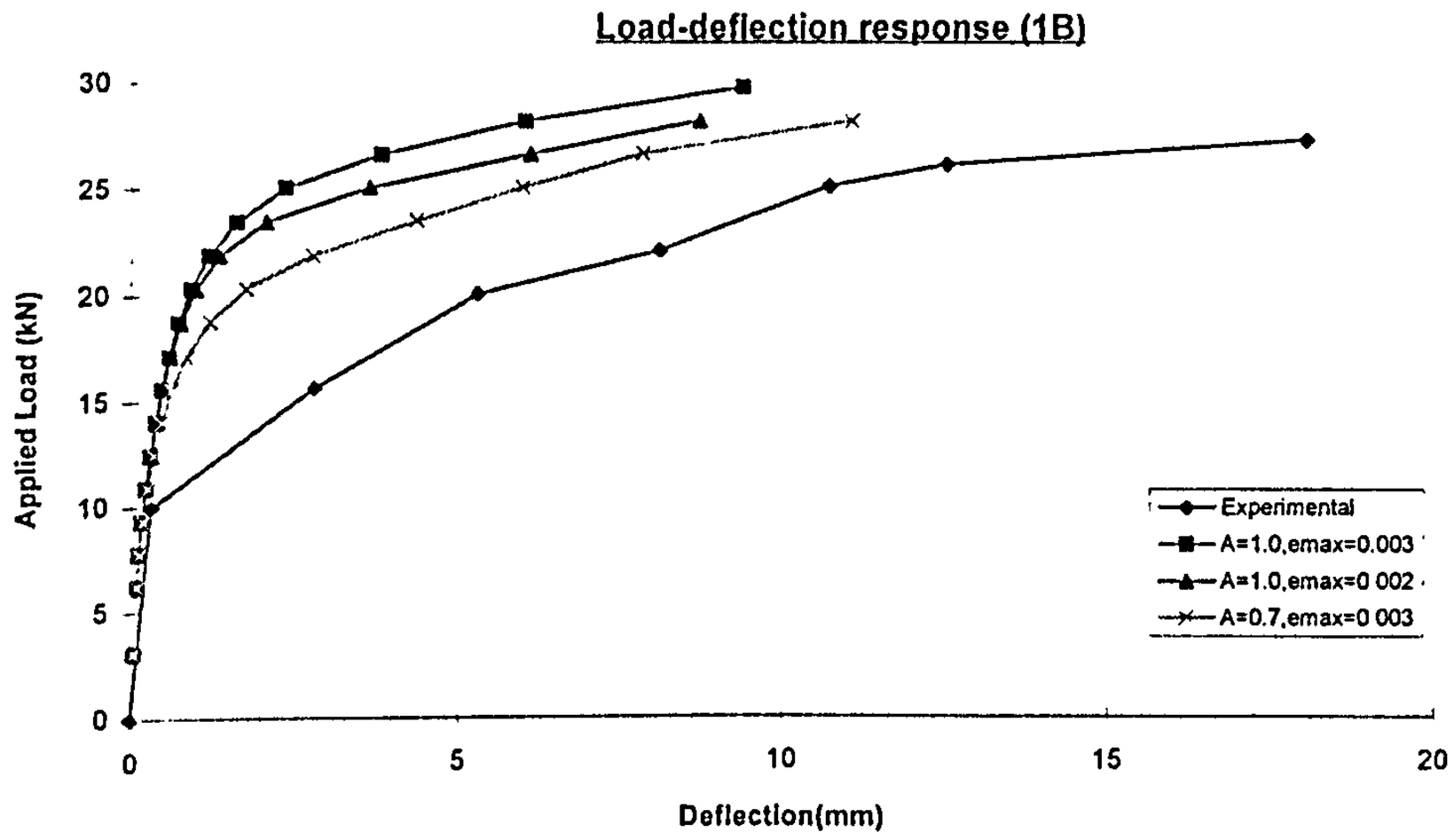

Figure 5.46 Effect of tension stiffening ("1B")

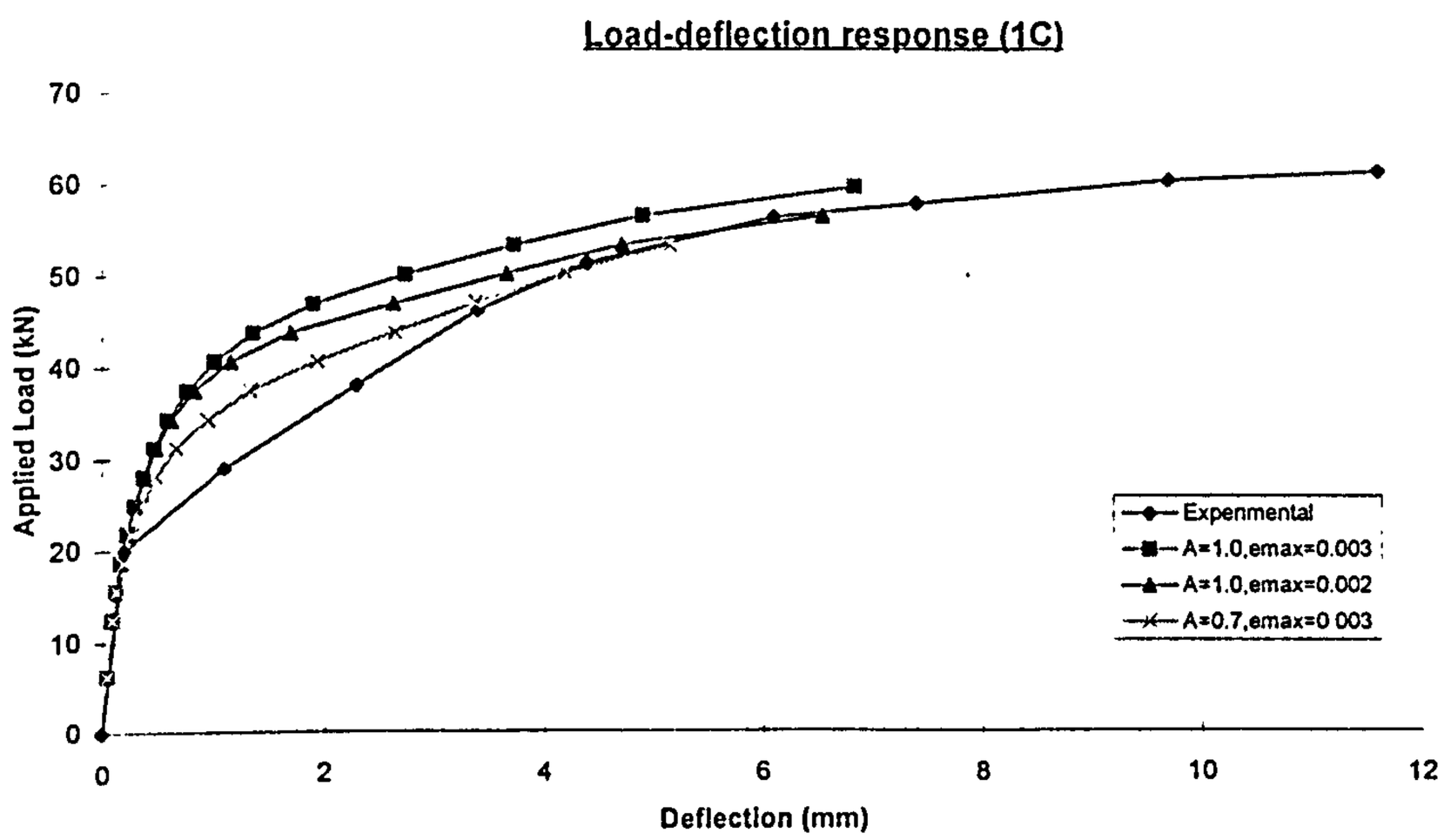

Figure 5.47 Effect of tension stiffening ("1C")

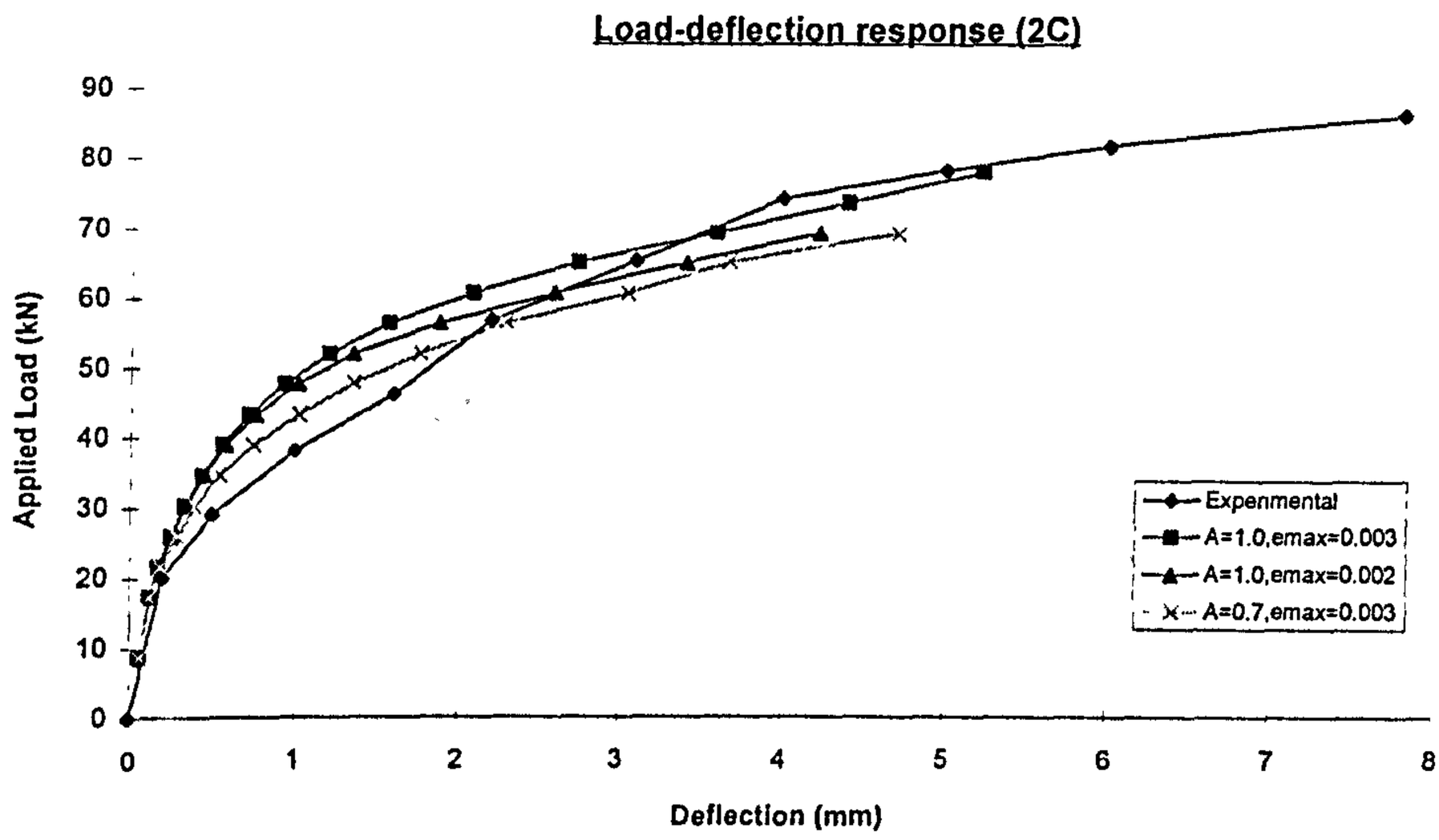

Figure 5.48 Effect of tension stiffening ("2C")

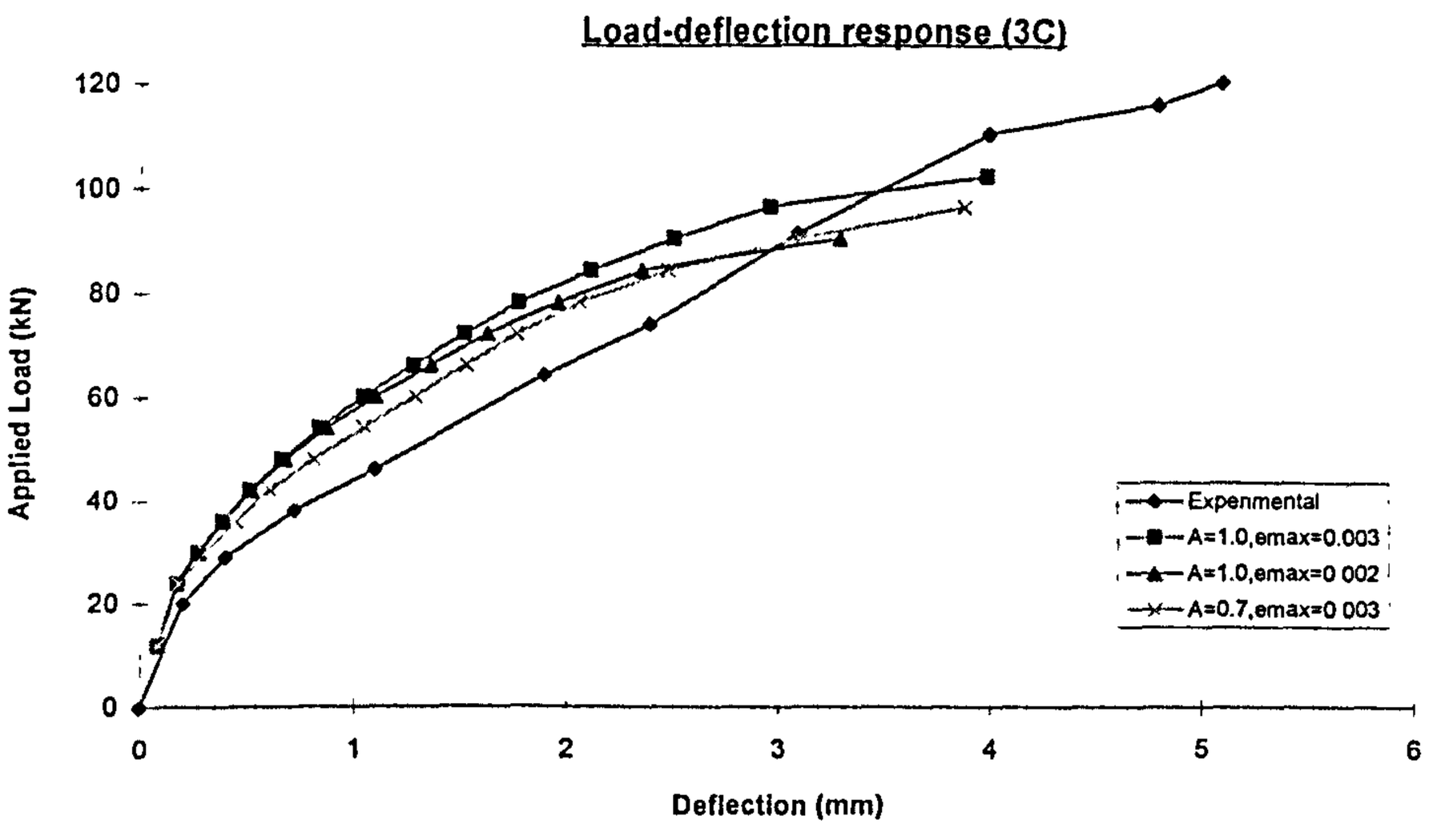

Figure 5.49 Effect of tension stiffening ("3C")

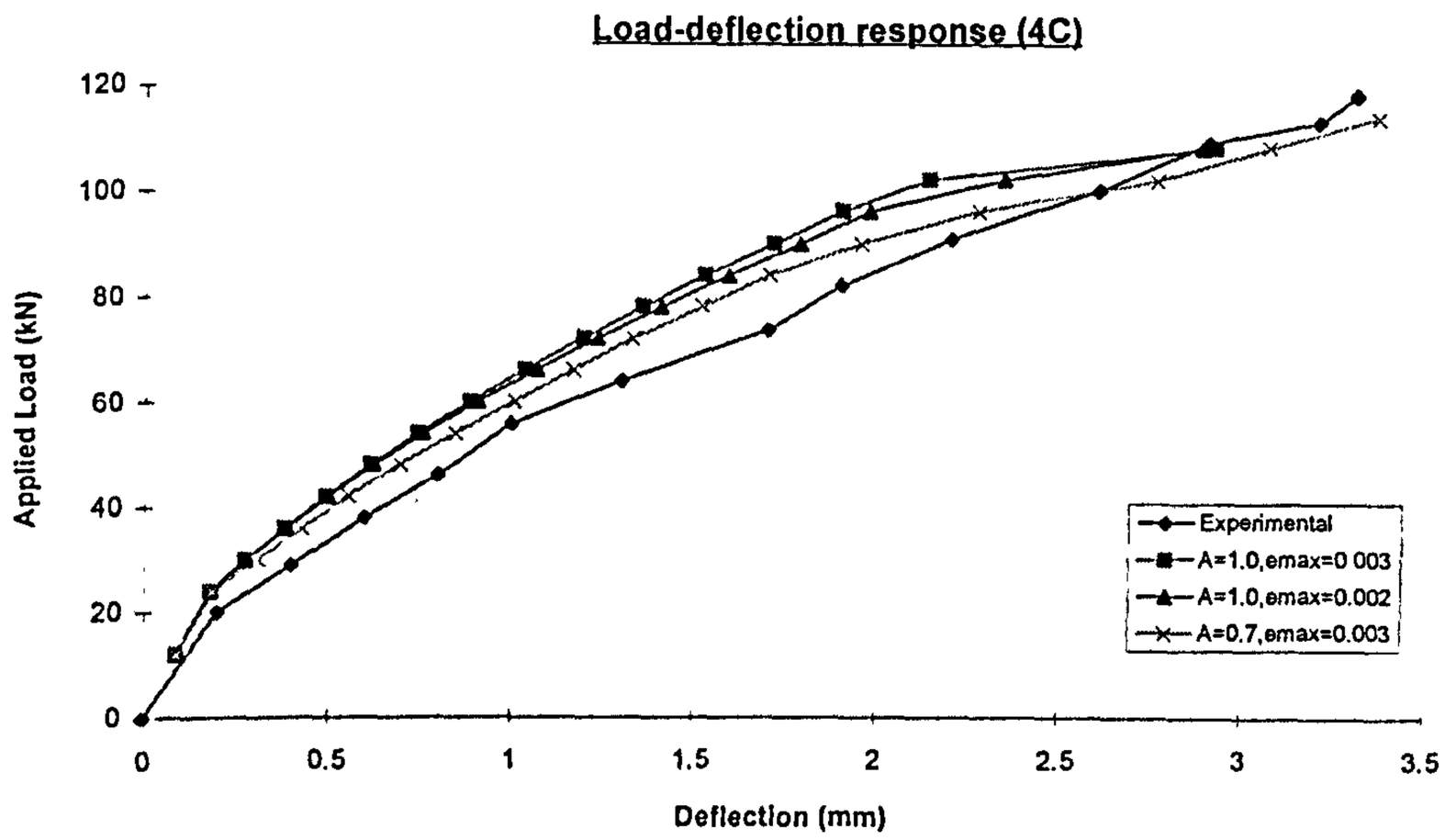

Figure 5.50 Effect of tension stiffening ("4C")

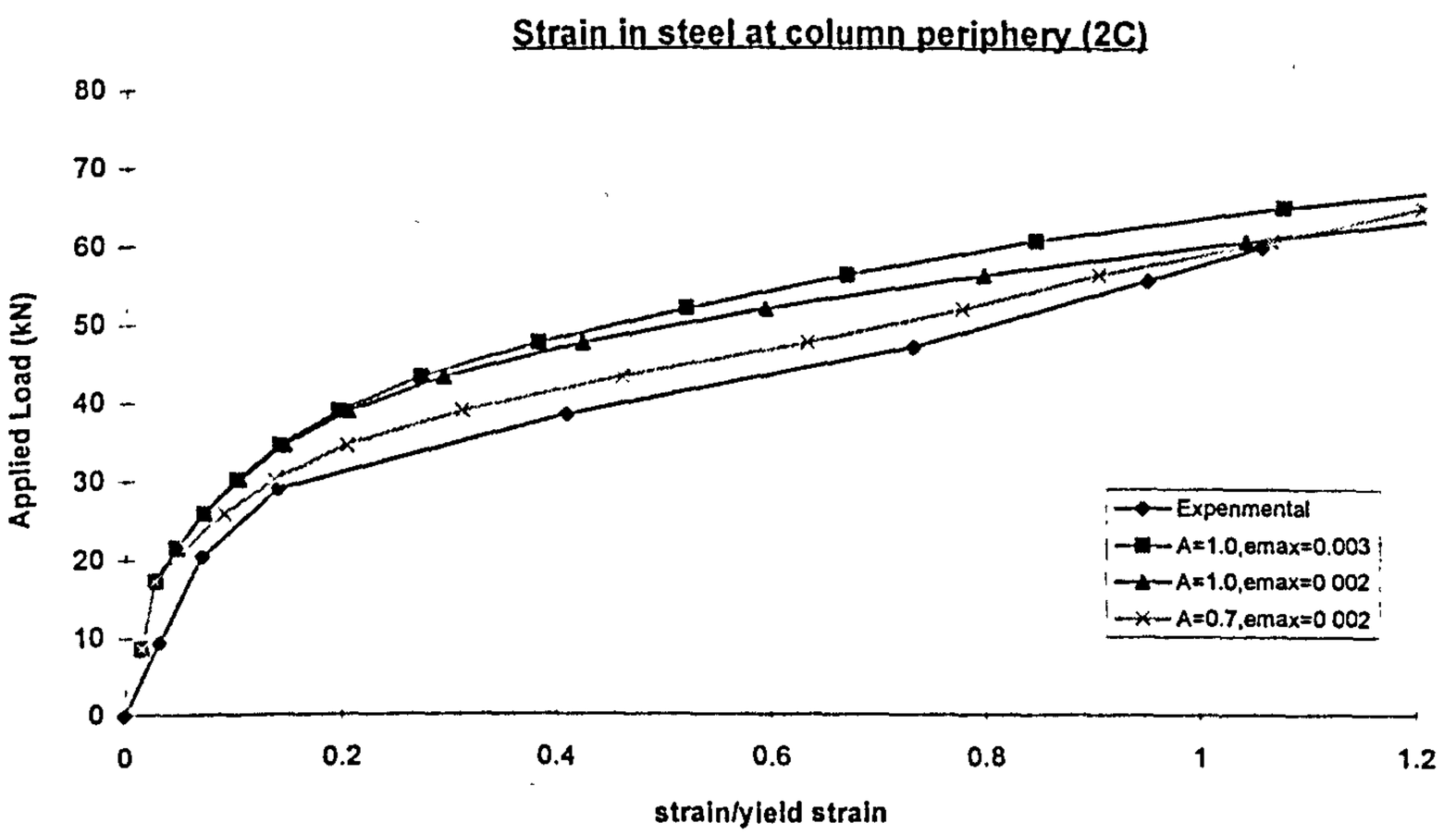

Figure 5.51 Effect of tension stiffening ("2C")

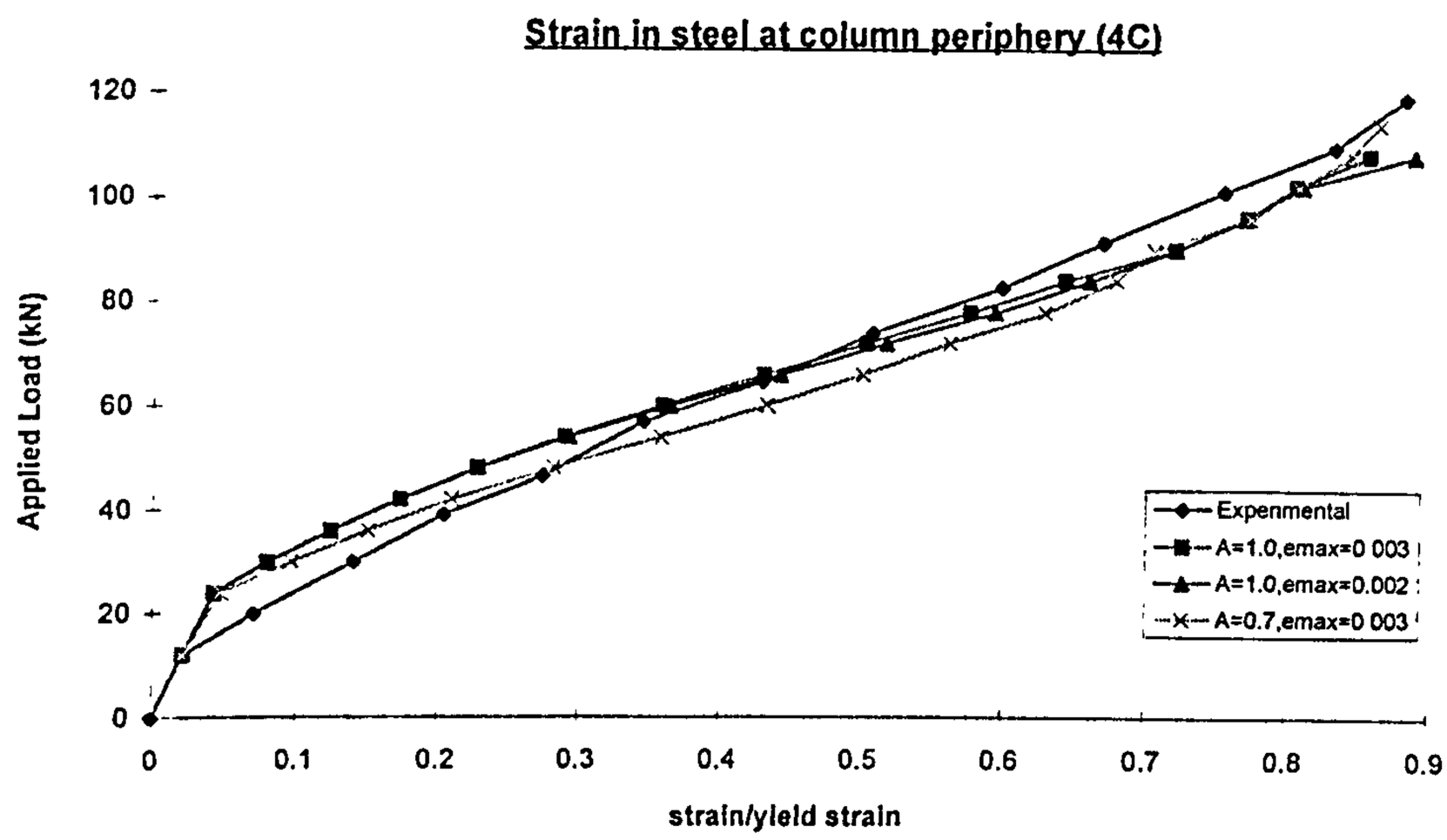

Figure 5.52 Effect of tension stiffening ("4C")

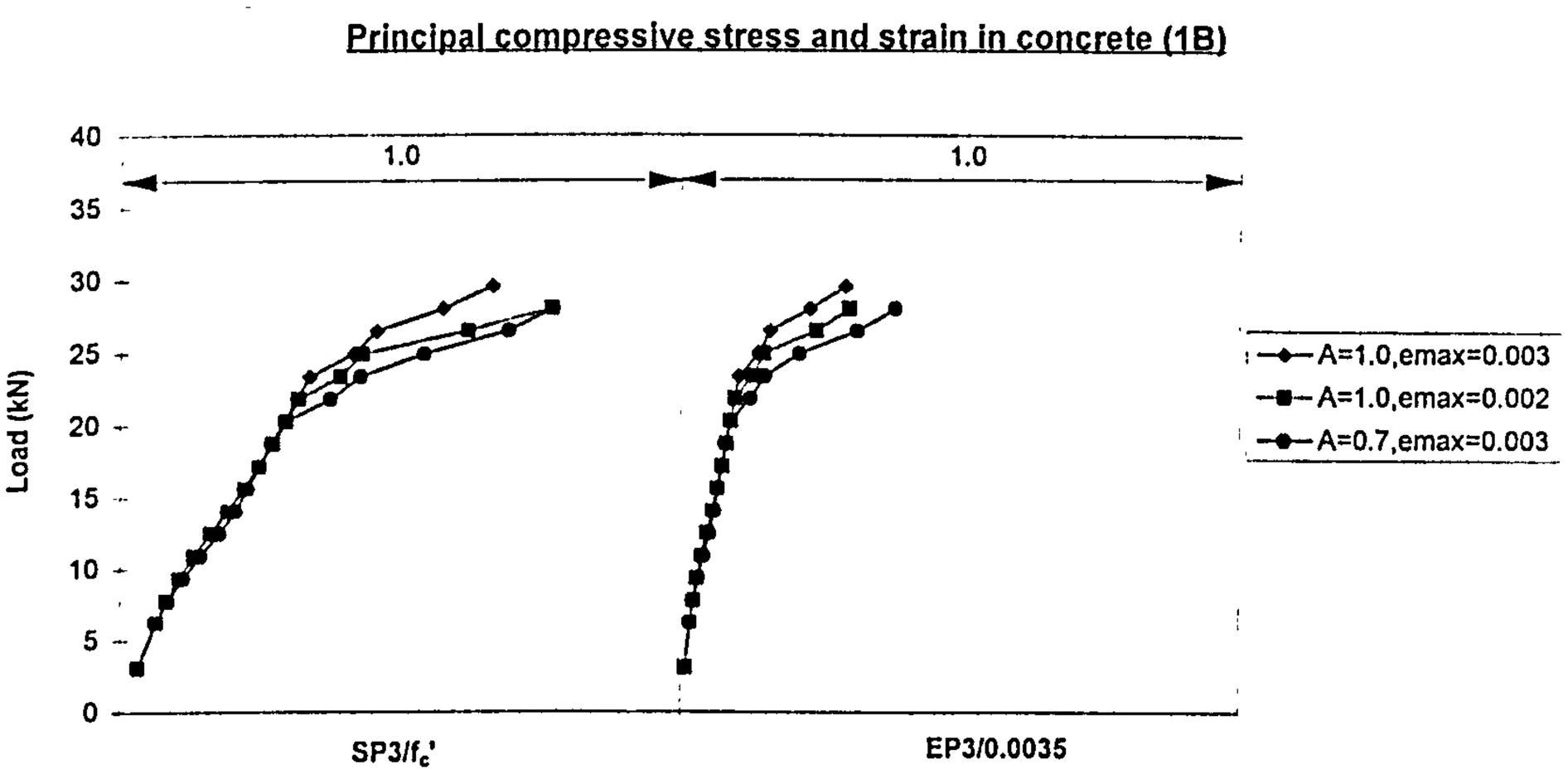

Note: SP3=σ_3=maximum compressive principal stress

EP3=ε_3=maximum compressive principal strain

Figure 5.53 Effect of tension stiffening on concrete stress and strain ("1B")

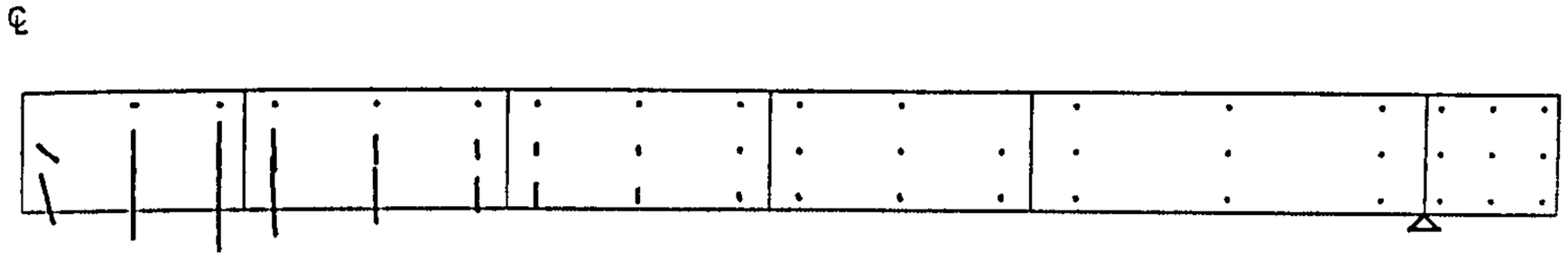

(a) A=1.0, emax=0.003

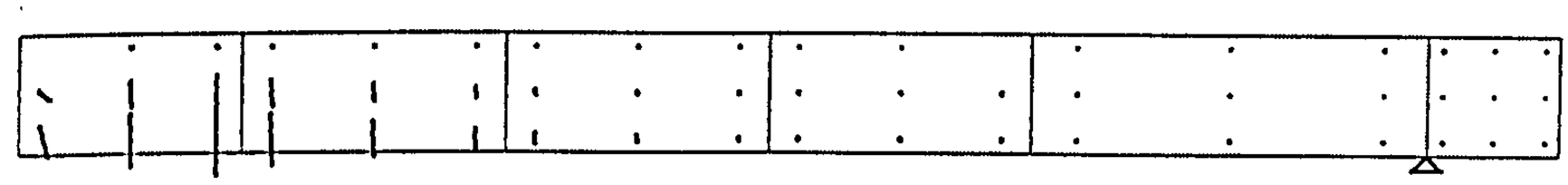

(b) A=1.0, emax=0.002

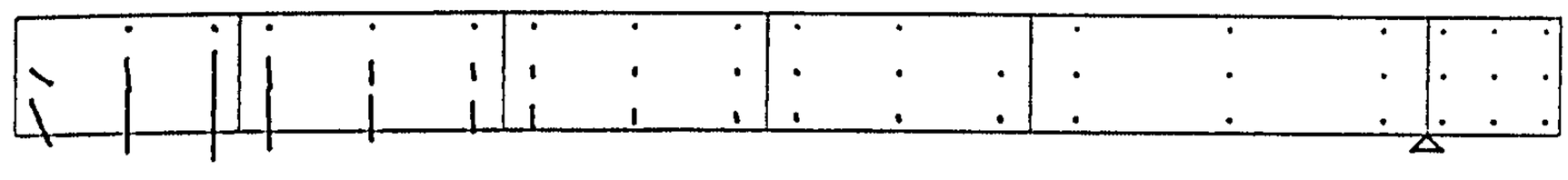

(c) A=0.7, emax=0.003

Figure 5.54 Crack pattern of slab "1B"

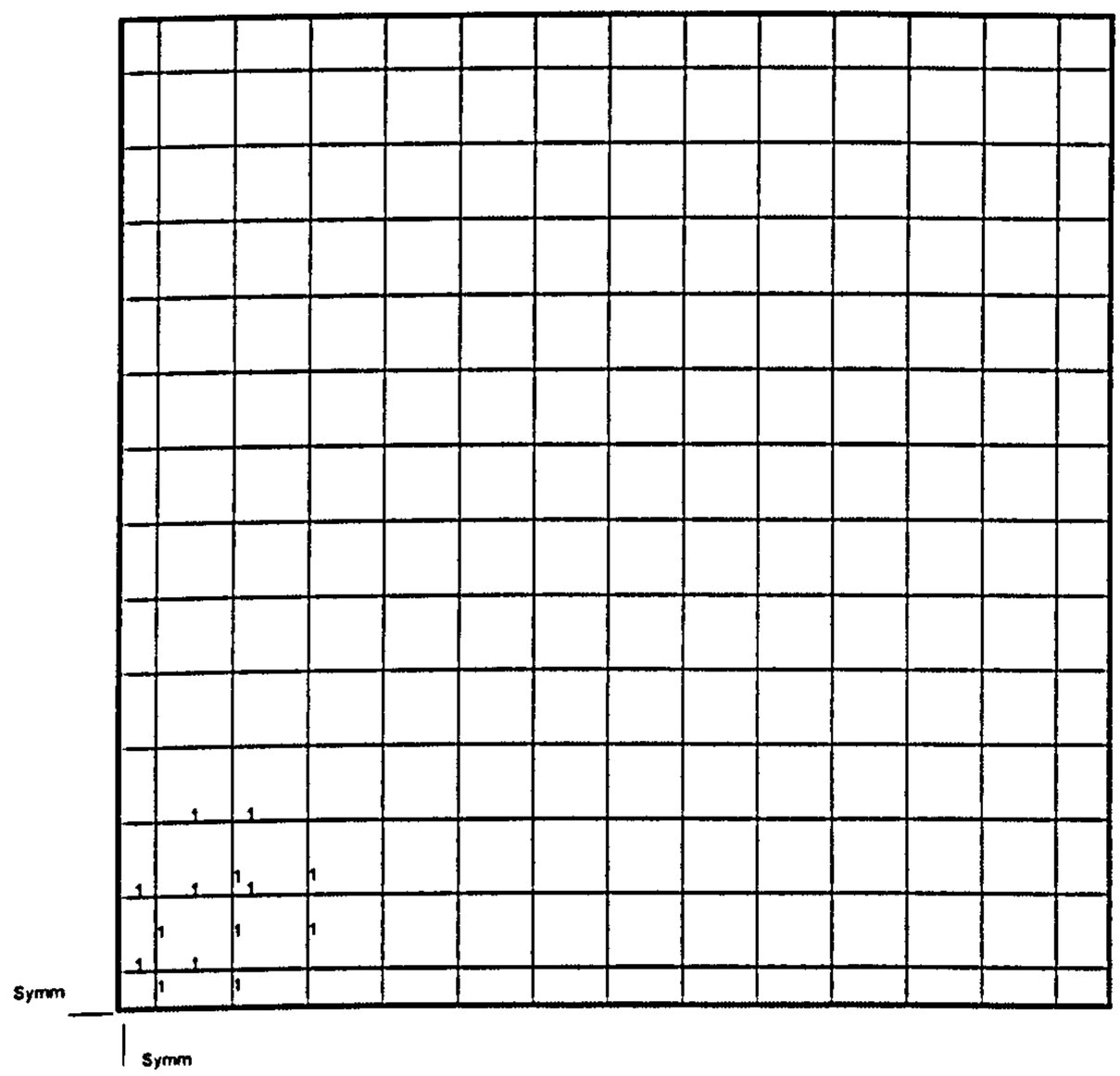

NB. : The numbers on the drawing indicate strain in steel at collapse expressed as a ratio of yield strain

Figure 5.55 Yielding of flexural reinforcement for specimen "4C" predicted by using (A=1.0, emax=0.003)

5.5.3 Effect of Shear retention factor

For this part of study, tension stiffening curve (A=0.7, ε_{max}=0.003) is used and splitting tensile strength of concrete is obtained from $f_{sp} = 0.53\sqrt{f_c'}$. Three types of shear retention variations was studied, that is

$$\frac{G_{crack}}{G_{uncrack}} = \beta = B\frac{\varepsilon_{cr}}{\varepsilon_n}$$

B=1.0, 0.5, 0.25

where $\varepsilon_{cr} = 0.0001$

ε_n = normal strain to perpendicular to crack

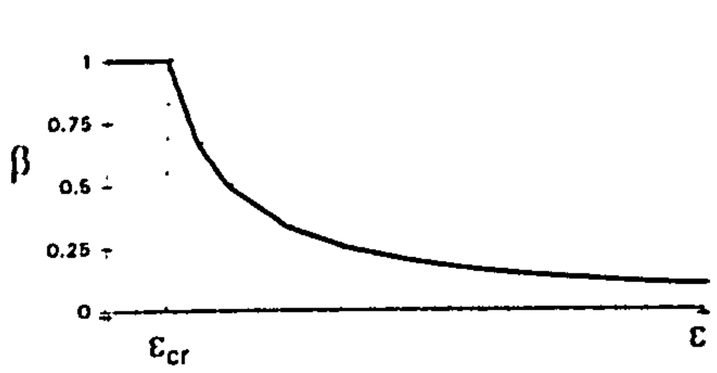

(a) $\beta = \varepsilon_{cr}/\varepsilon_n$ (B=1.00)

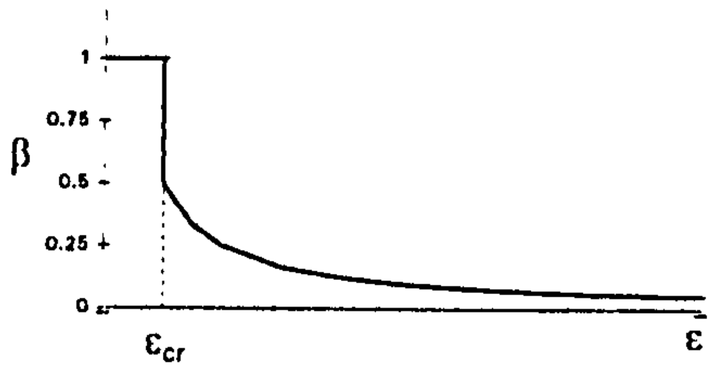

(b) $\beta = 0.5\varepsilon_{cr}/\varepsilon_n$ (B=0.50)

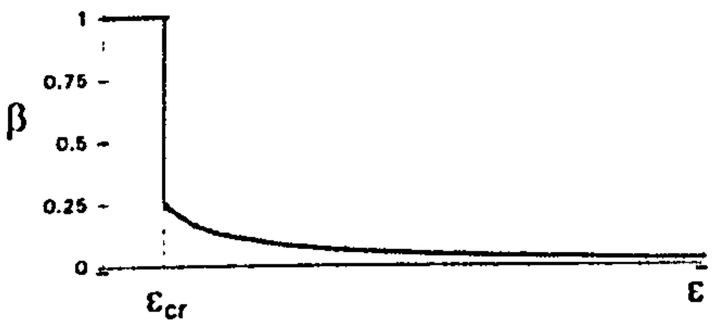

(c) $\beta = 0.25\varepsilon_{cr}/\varepsilon_n$ (B=0.25)

Figure 5.56 Shear Retention curves

Table 5.10 : Effect of shear retention factor on ultimate load

Slab	P_{test} (kN)	Numerical/Experimental failure load		
		B=0.25	B=0.50	B=1.00
1B	28.850	0.865	0.973	0.973
1C	62.740	0.845	0.845	0.895
2C	87.860	0.738	0.787	0.885
3C	124.140	0.773	0.773	0.822
4C	125.940	0.810	0.905	0.858
Average		0.806	0.857	0.887
STDEV		0.052	0.084	0.056

Table 5.11 : Effect of shear retention factor on mode of failure

Slab	Exp F. Mode	Numerical Failure Mode		
		B=1.00	B=0.50	B=0.25
1B	y	y	y	y
1C	y	y	y	y
2C	s	y	y	fp
3C	s	fp	s	s
4C	s	s	s	s

The effect of shear retention on behaviour of slabs (ultimate load, load-deflection response, strain in steel, concrete strain and crack pattern) and modes of failure can be summarised as follows:

- The effect of shear retention factor on deflection of slabs (Figures 5.57-5.61) and strain in flexural steel (Figures 5.62-5.63) are insignificant.
- Figures 5.64-5.68 show that shear retention factor does not affect concrete strain at early stage because its comes into operation only after cracking occurs. However, it affects the subsequent response of concrete.
- It affects the failure load of slabs (Table 5.12). The higher the "B" value, the higher failure load predicted and vice-versa. But high "B" value might predict incorrect mode of failure especially for slabs failing in shear mode. For example, from test observation, specimen "2C" failed in shear mode. Analysed results using B=1.0 show that yielding of flexural reinforcement spread over a wide area of slab (Figure 5.71) which indicates that this slab failed in flexure mode. With B=0.5, the area of where steel has yielded was smaller (Figure 5.72) and when B=0.25, the yielding was concentrated over the column only (Figure 5.73). Obviously, B=0.25 predicted the correct mode of failure.
- Generally, the shear retention factor does not affect the crack pattern of lightly reinforced concrete slabs. However, too large a shear retention factor (B=1.00) might change the crack pattern for the slabs with large amount of reinforcement (Figure 5.70).

From the predicted load-deflected response, area of slabs where steel yielded, concrete strain and crack pattern, the modes of failure were determined (based on general rule described in section 5.2) as shown in table 5.11. Compared to experimental results, it shows that too large the shear retention factor (B=1.0) may over estimate the failure

load. It may also lead to the mode of failure for slabs (especially heavily reinforced slab) which fail in shear being predicted as flexural. This comparison leads to the conclusion that small value of shear retention factor (B=0.25) is preferable because the correct of mode of failure is predicted.

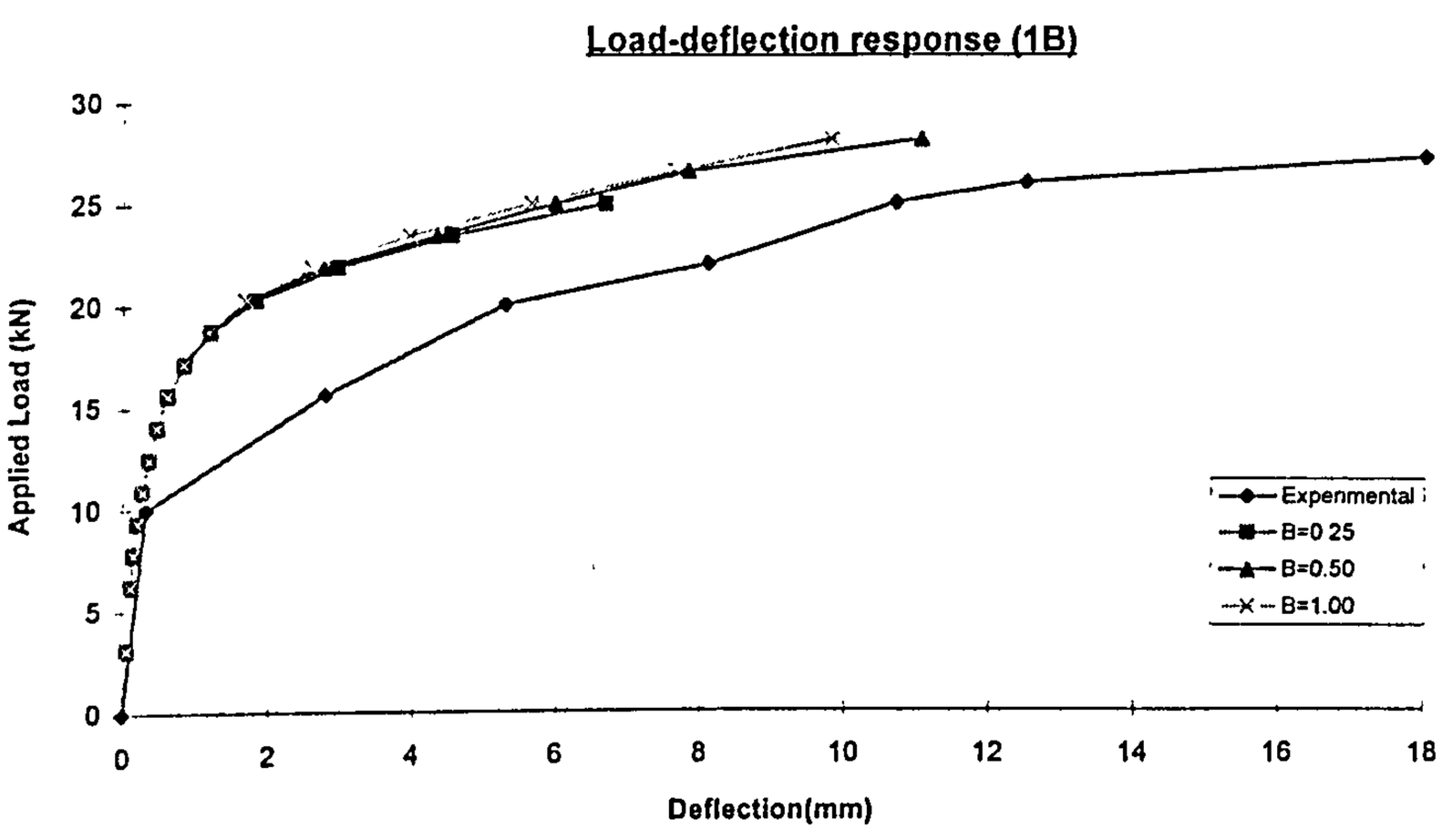

Figure 5.57 Effect of shear retention factor ("1B"), flexure failure

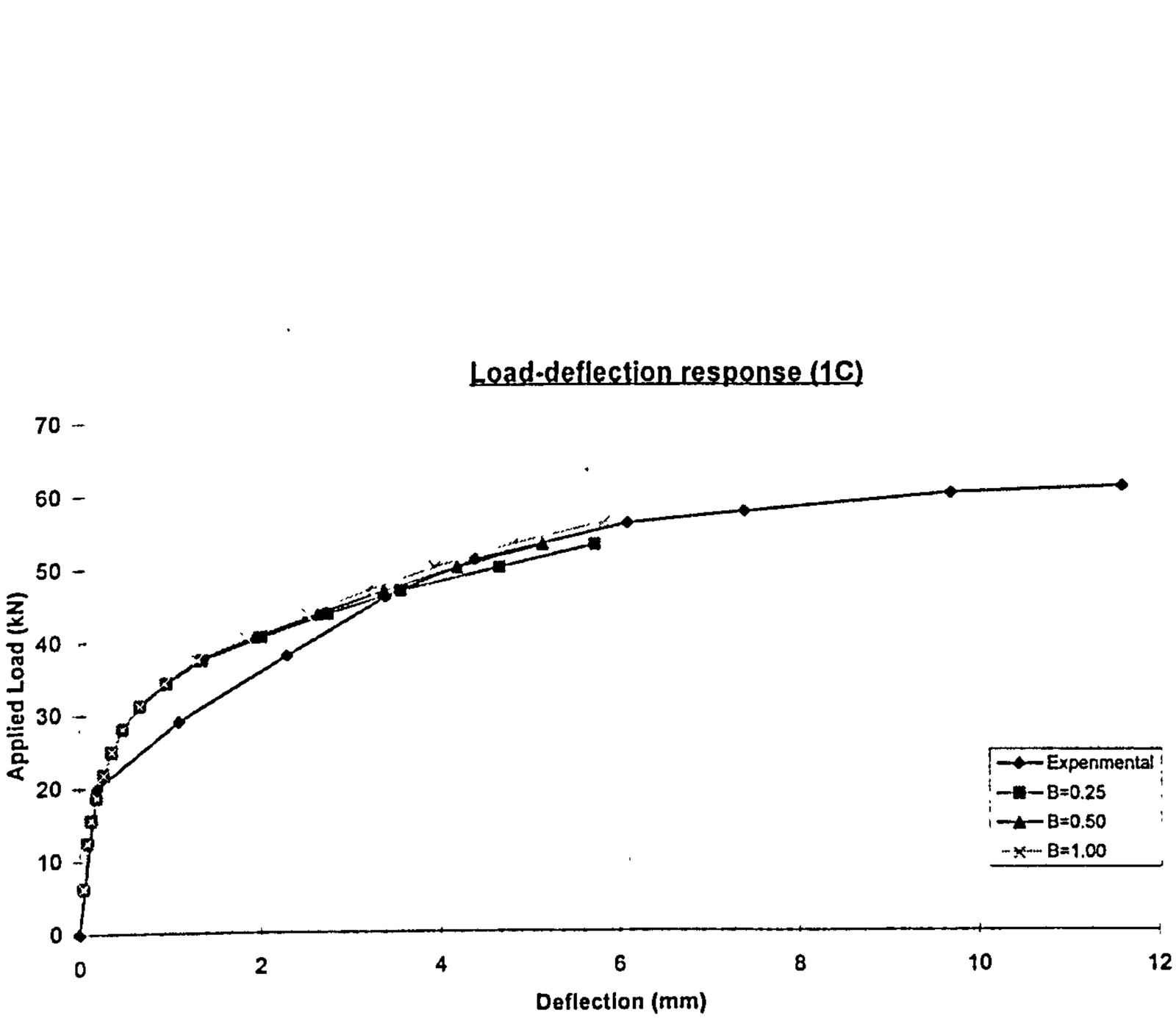

Figure 5.58 Effect of shear retention factor ("1C"), flexure failure

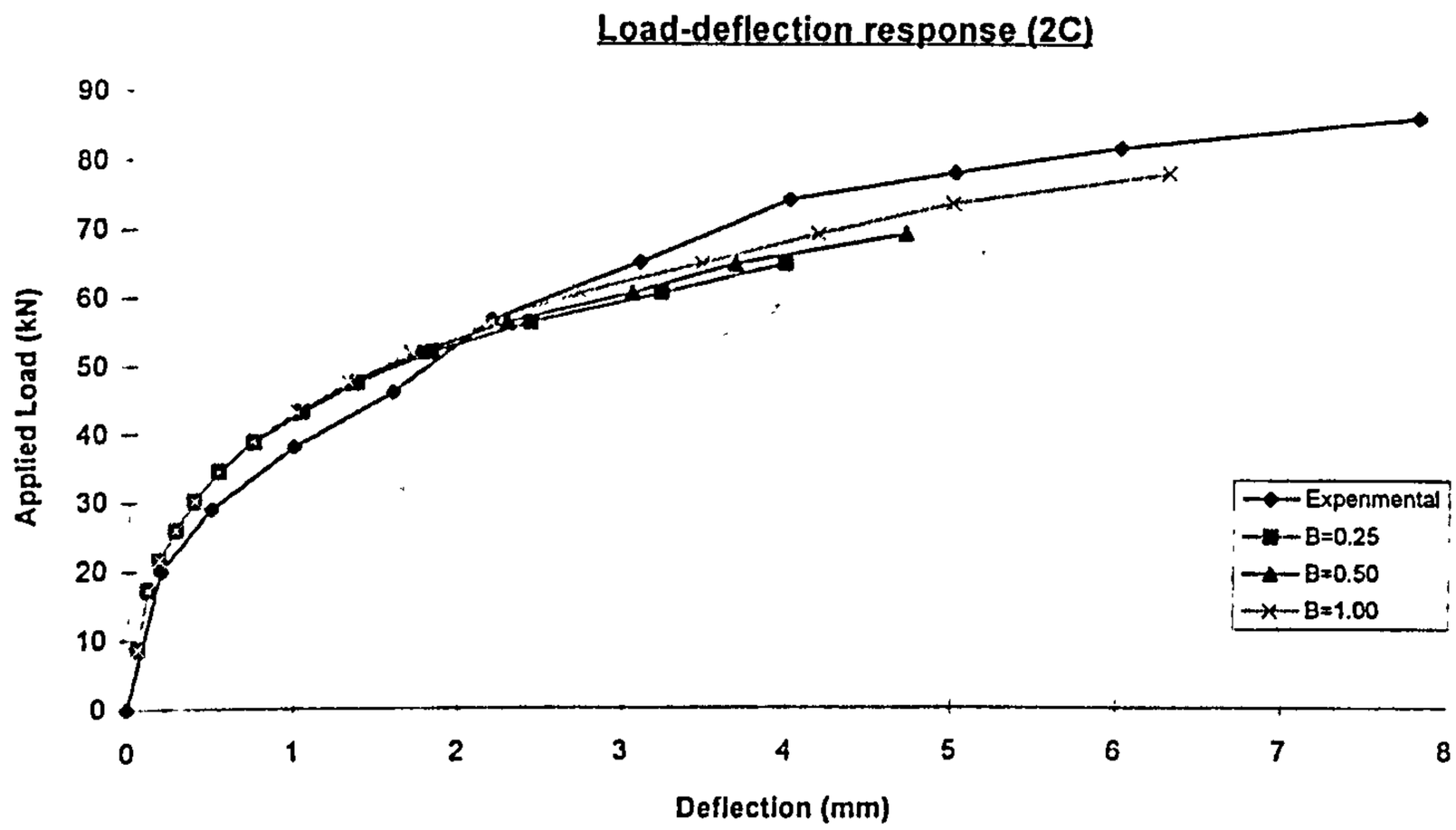

Figure 5.59 Effect of shear retention factor ("2C"), flexure failure

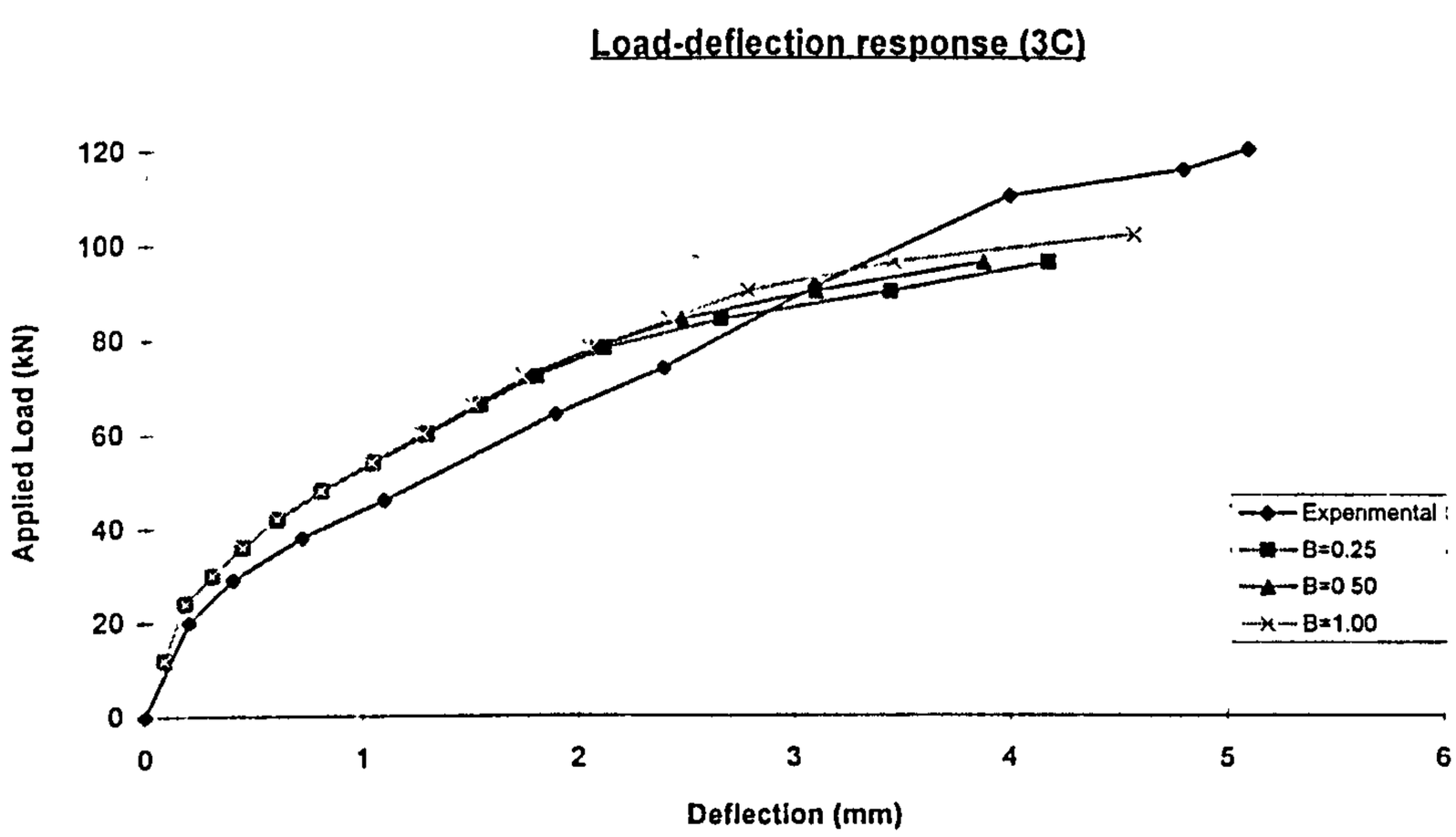

Figure 5.60 Effect of shear retention factor ("3C"), shear failure

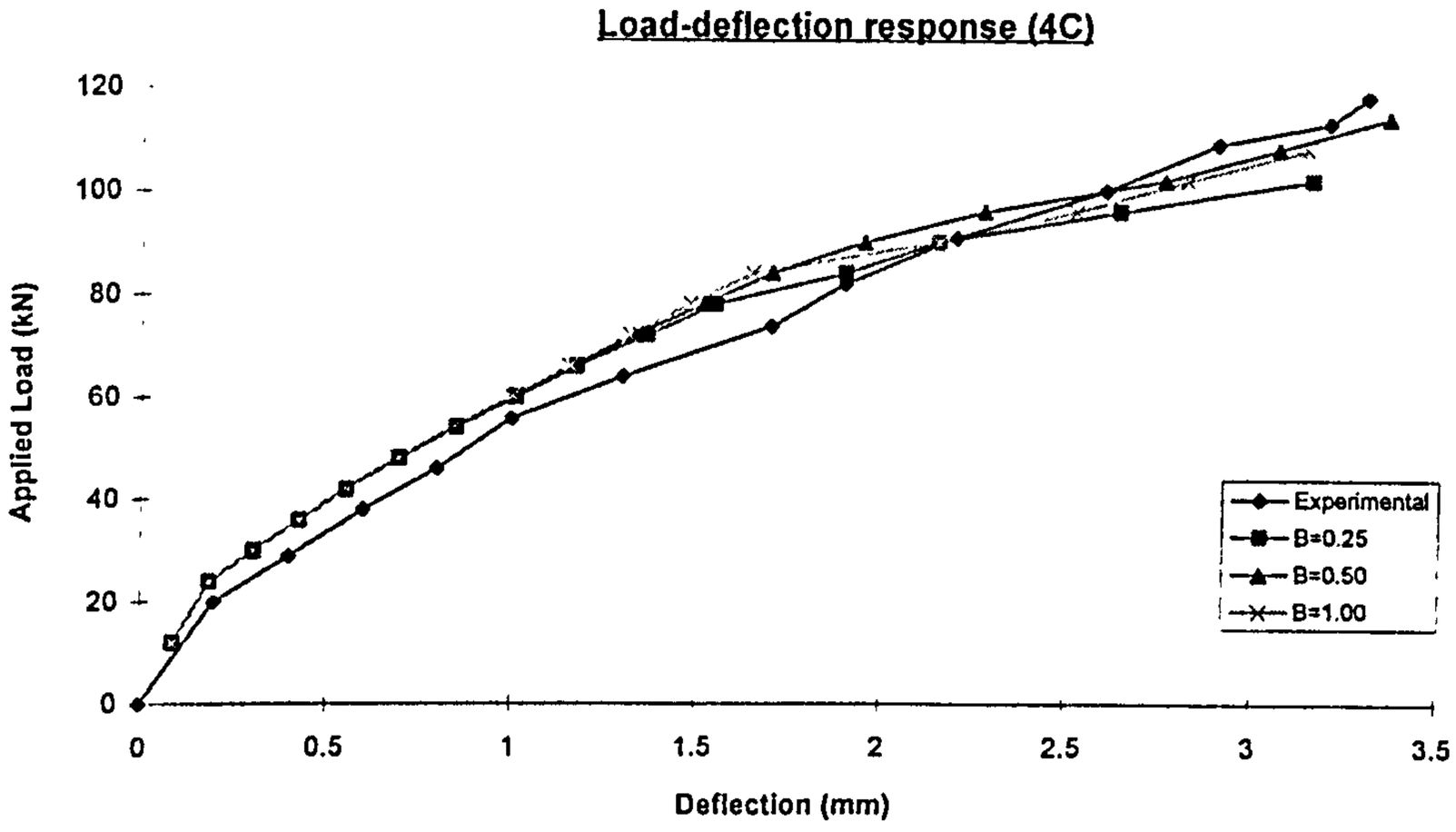

Figure 5.61 Effect of shear retention factor ("4C"), shear failure

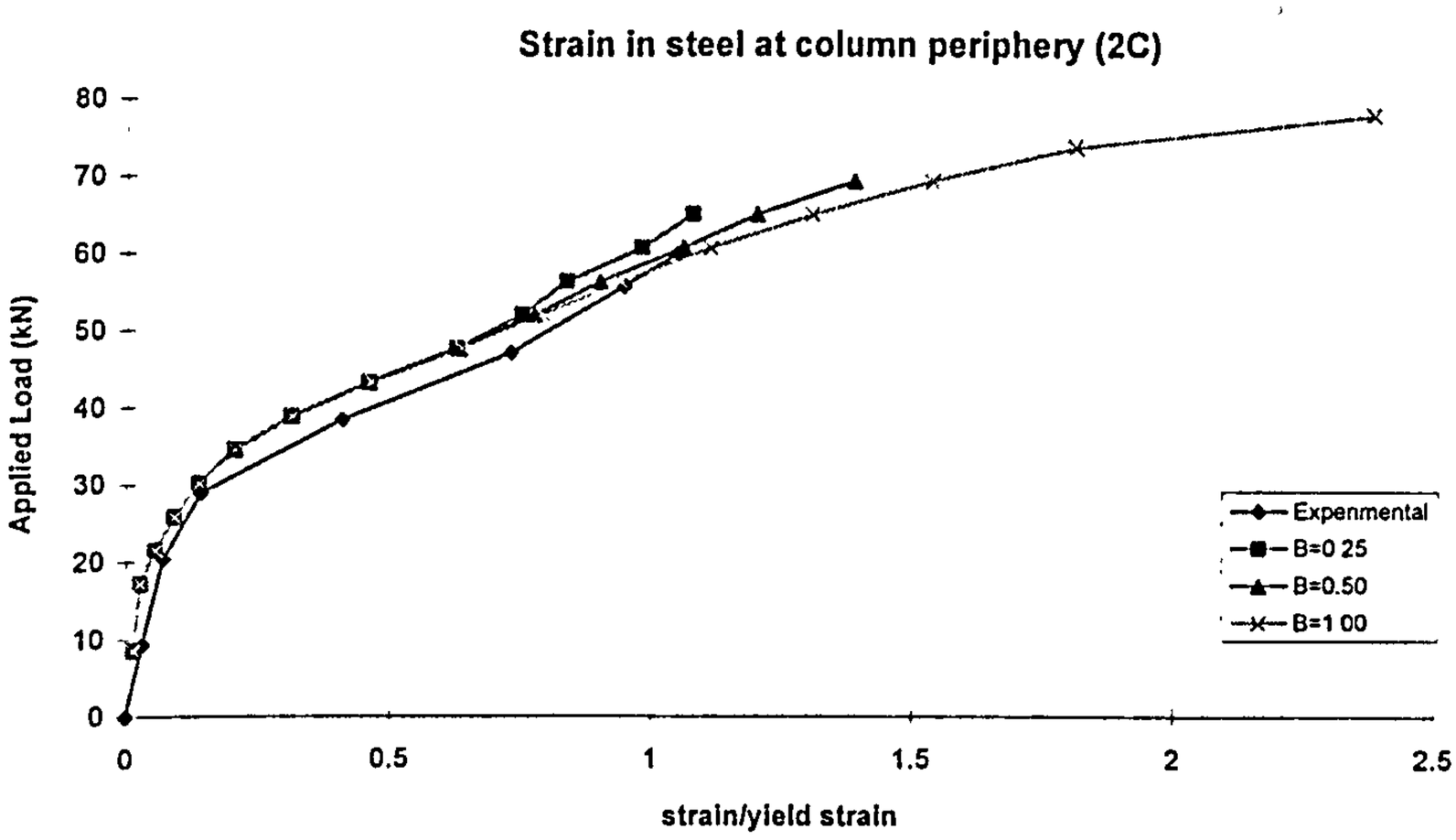

Figure 5.62 Effect of shear retention factor ("2C"), **shear failure (test)**

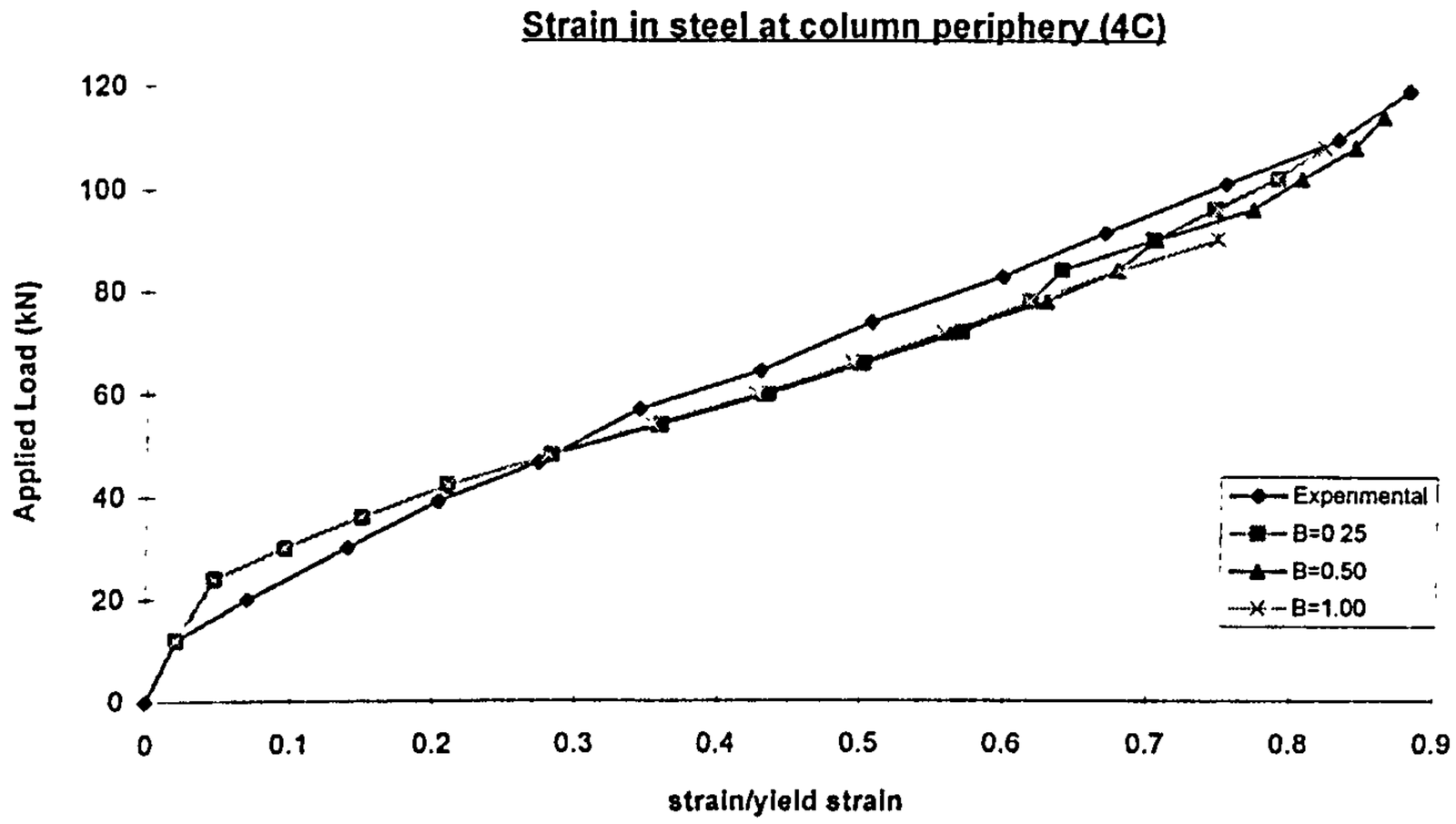

Figure 5.63 Effect of shear retention factor ("4C"), shear failure (test)

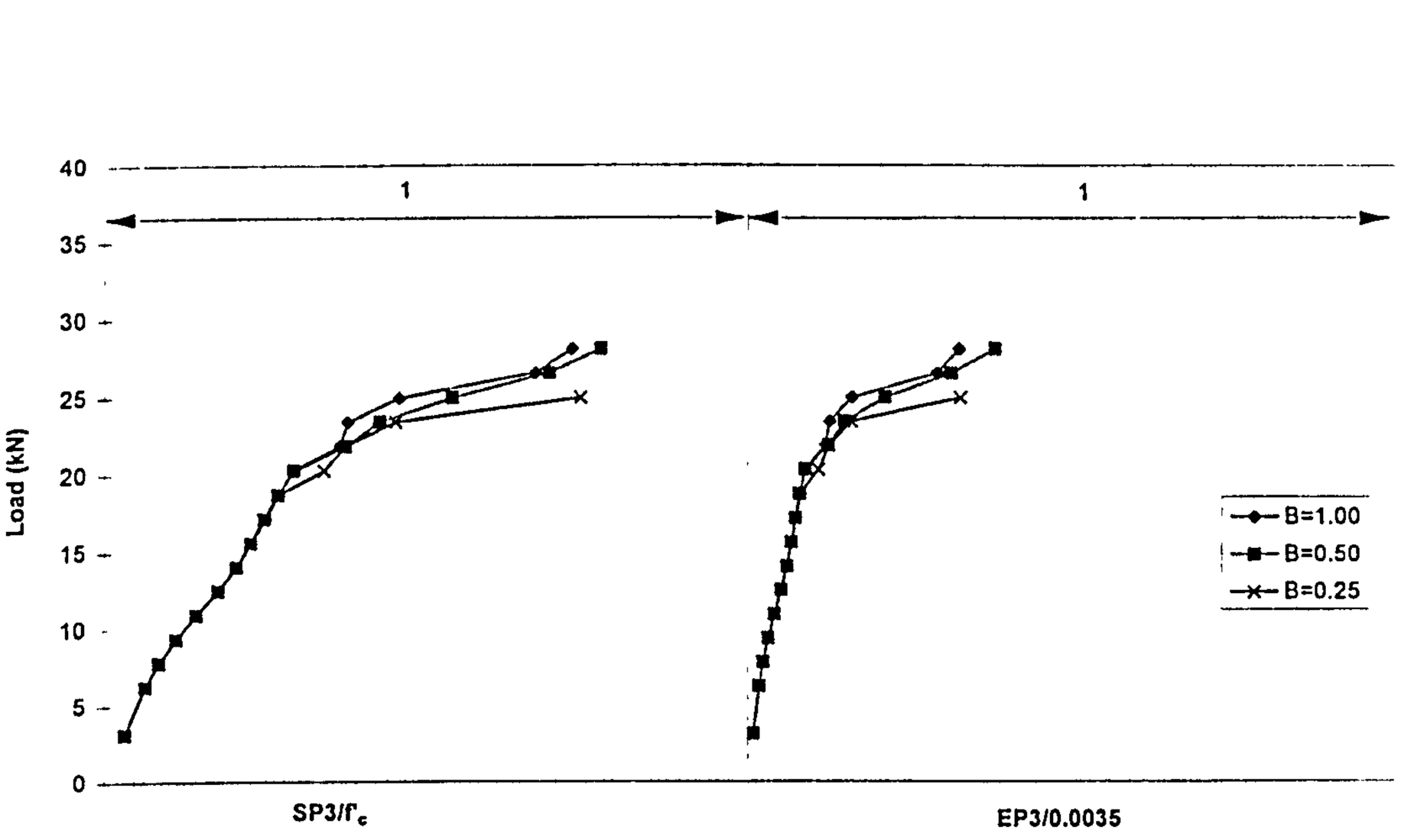

Note: SP3=σ_3=maximum compressive principal stress

EP3=ε_3=maximum compressive principal strain

Figure 5.64 Principal compressive stress and strain of concrete ("1B")

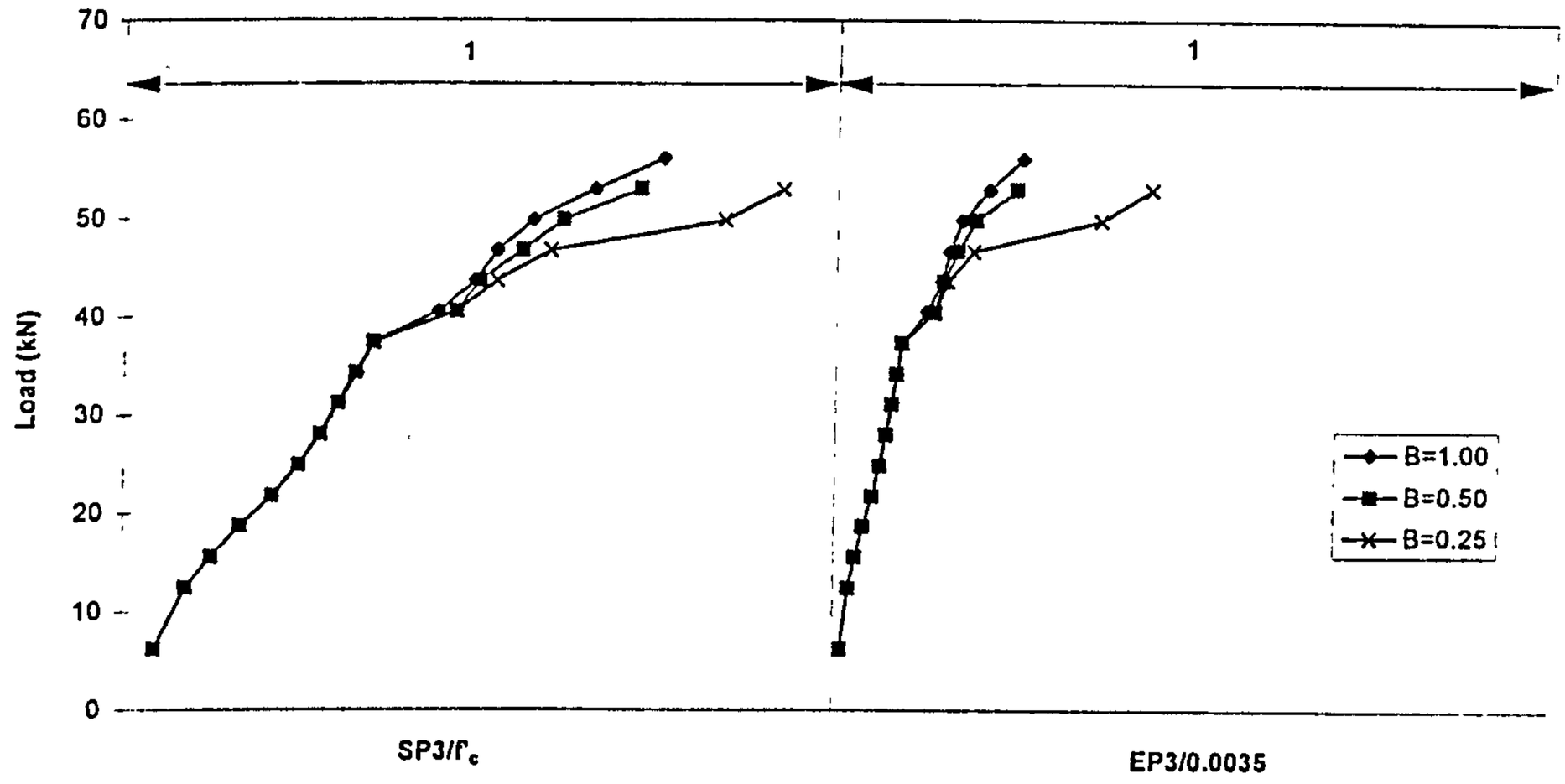

Note: SP3=σ_3=maximum compressive principal stress

EP3=ε_3=maximum compressive principal strain

Figure 5.65 Principal compressive stress and strain of concrete ("1C")

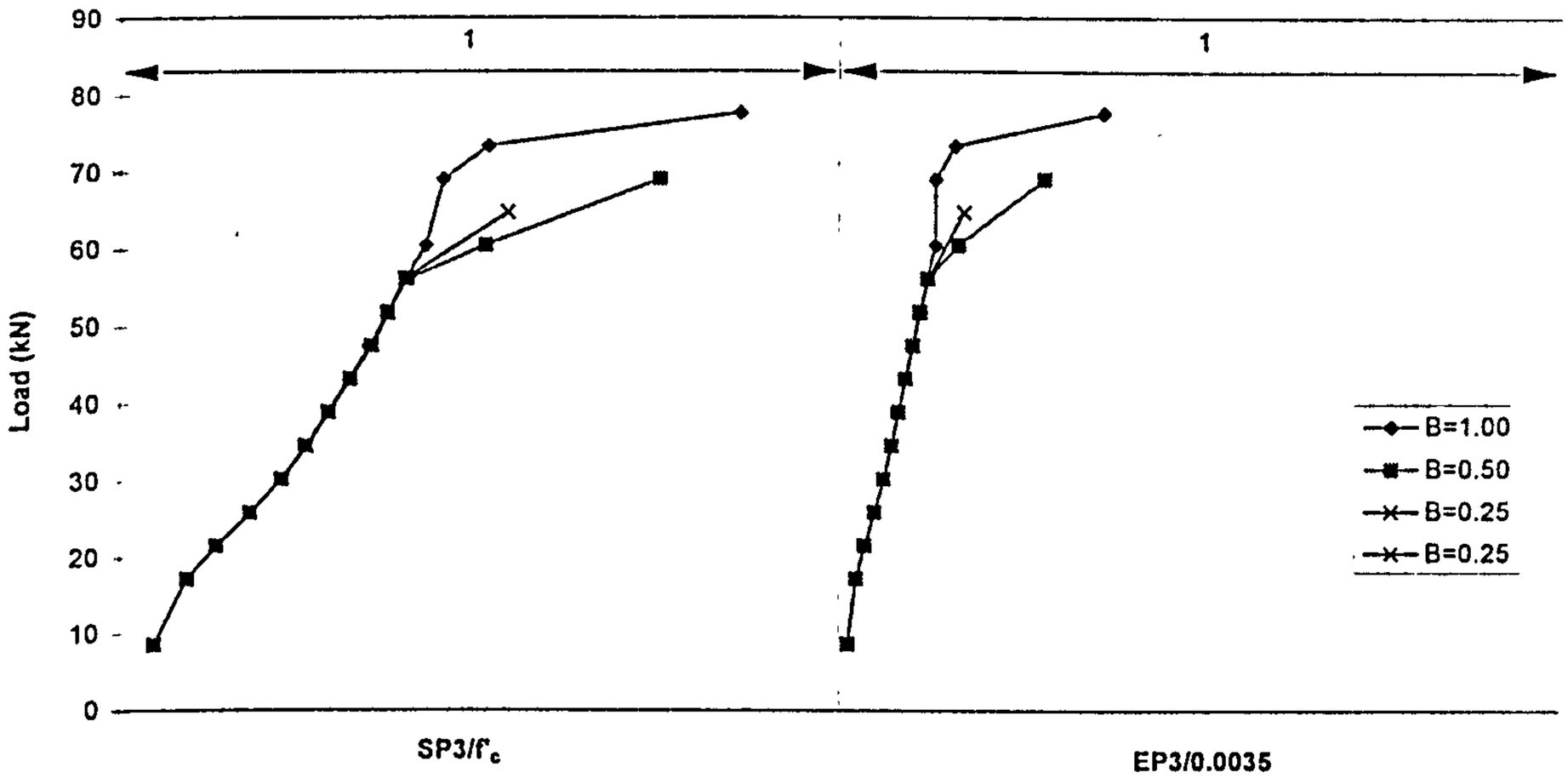

Note: SP3=σ_3=maximum compressive principal stress

EP3=ε_3=maximum compressive principal strain

Figure 5.66 Principal compressive stress and strain of concrete ("2C")

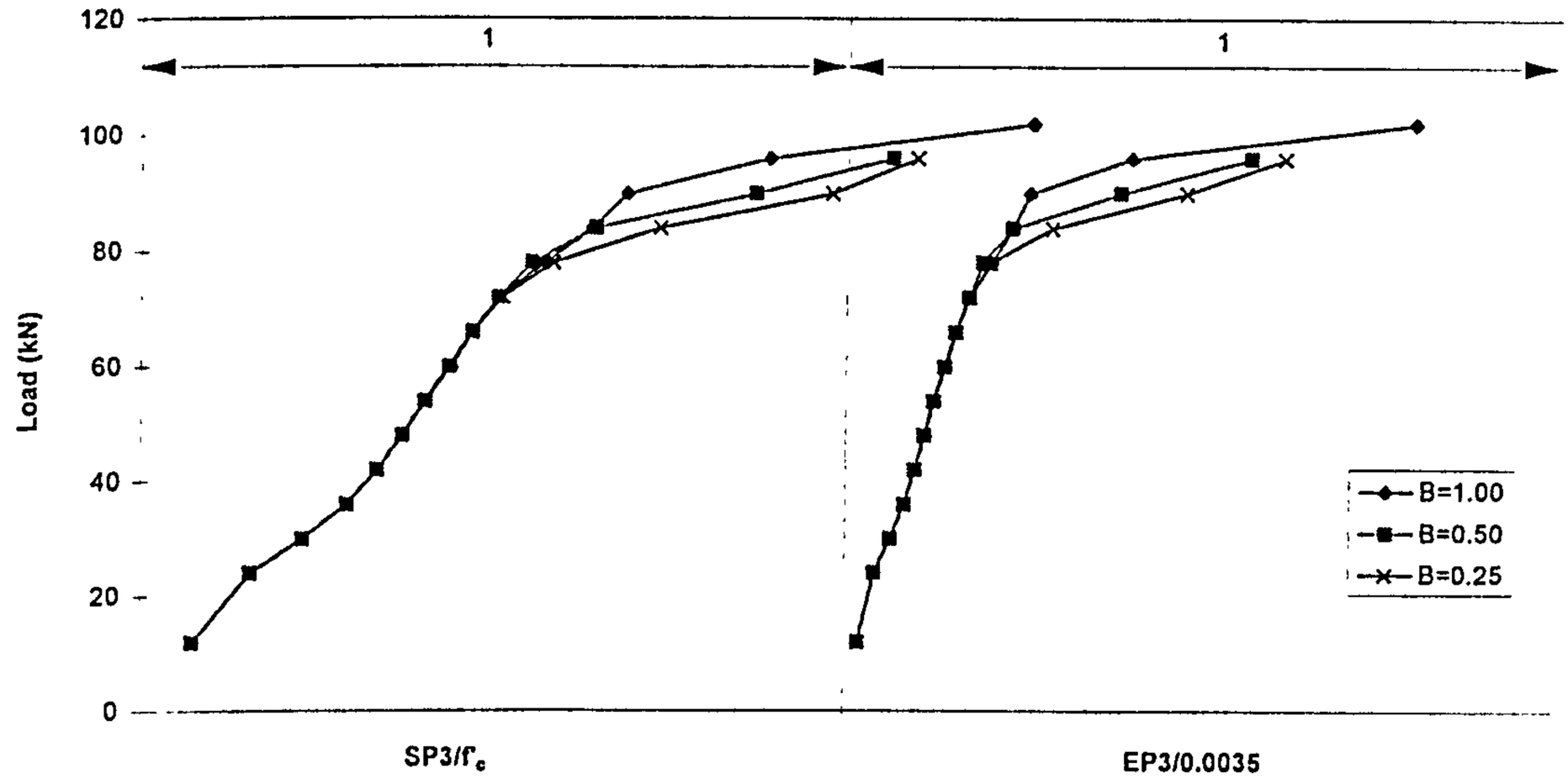

Note: SP3=σ_3=maximum compressive principal stress

EP3=ε_3=maximum compressive principal strain

Figure 5.67 Principal compressive stress and strain of concrete ("3C")

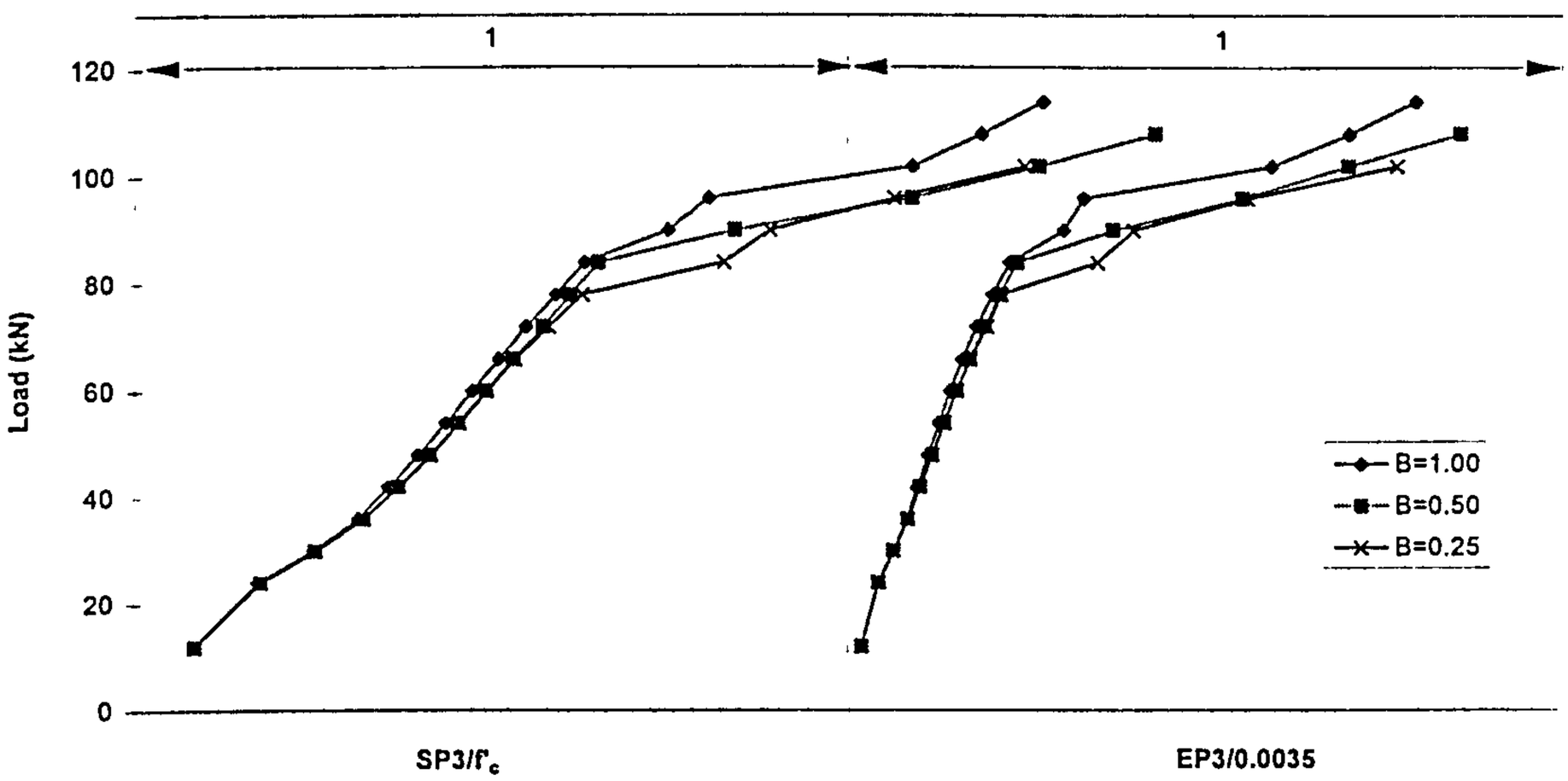

Note: SP3=σ_3=maximum compressive principal stress

EP3=ε_3=maximum compressive principal strain

Figure 5.68 Principal compressive stress and strain of concrete ("4C")

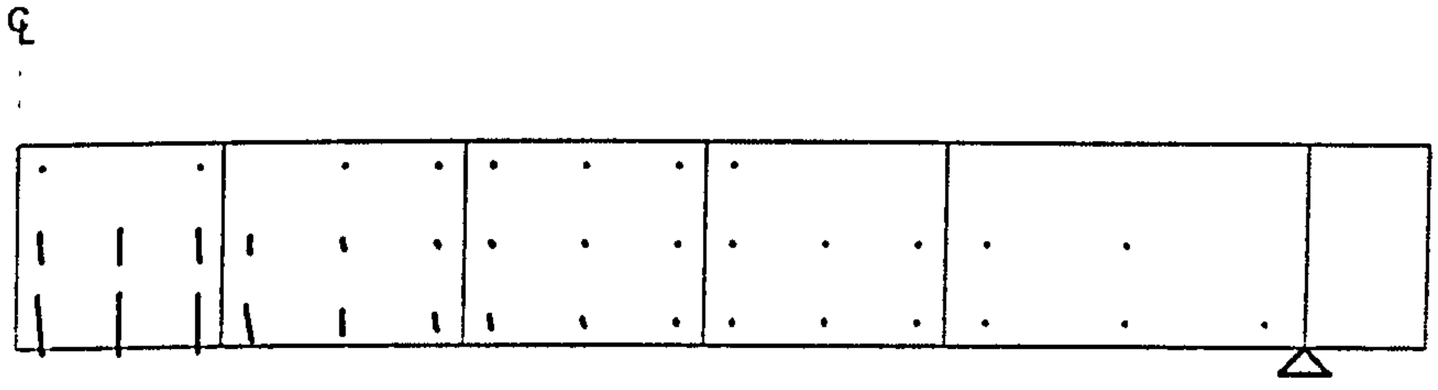

Figure 5.69 Crack pattern (elevation) for slab "1C"

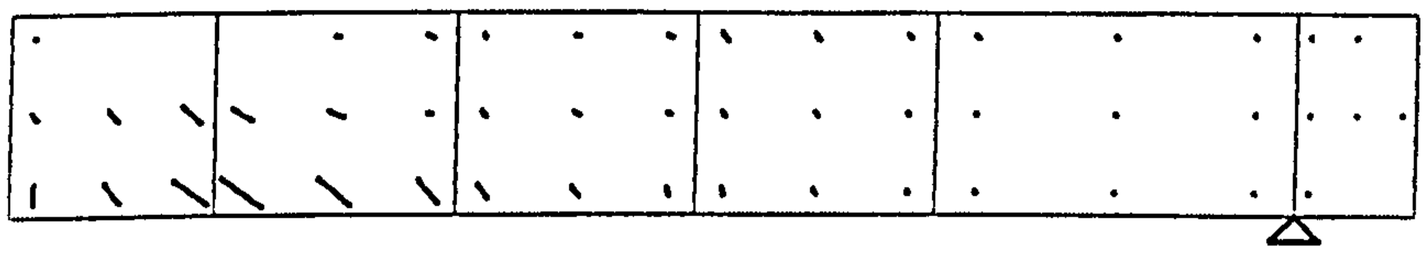

(a) Elevation (B=0.50)

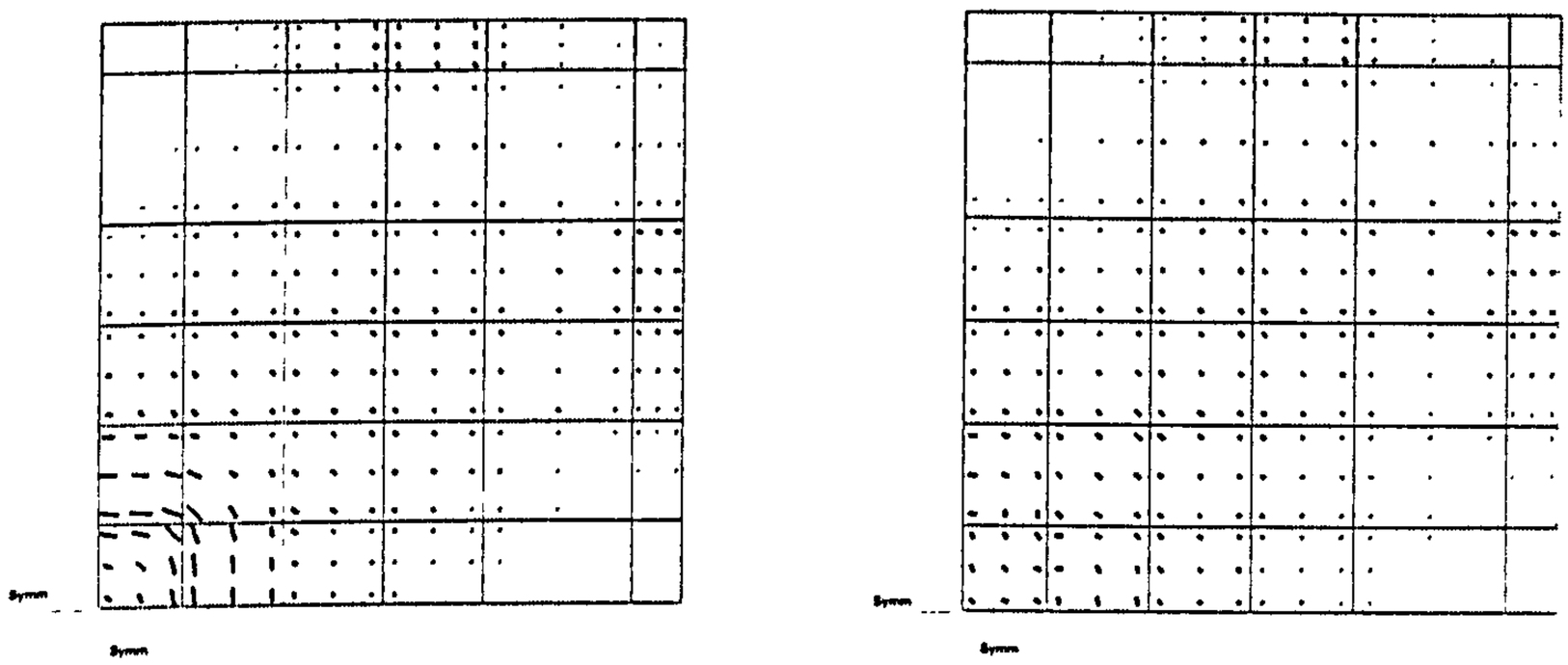

(b)Plan (B=0.50) (c)Plan (B=1.0)

Figure 5.70 : Crack pattern for slab "4C"

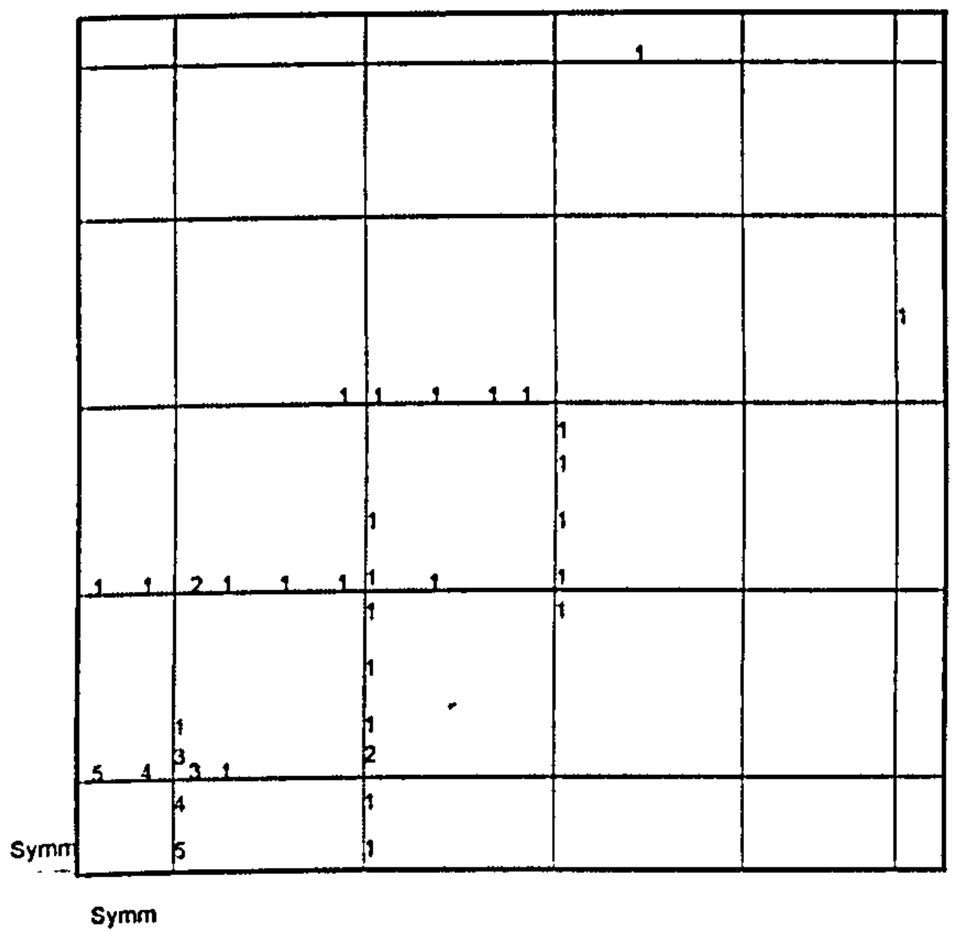

NB. : The numbers on the drawing indicate strain in steel at collapse expressed as a ratio of yield strain

Figure 5.71 : Yielding of flexural steel , specimen "2C" (B=1.00)

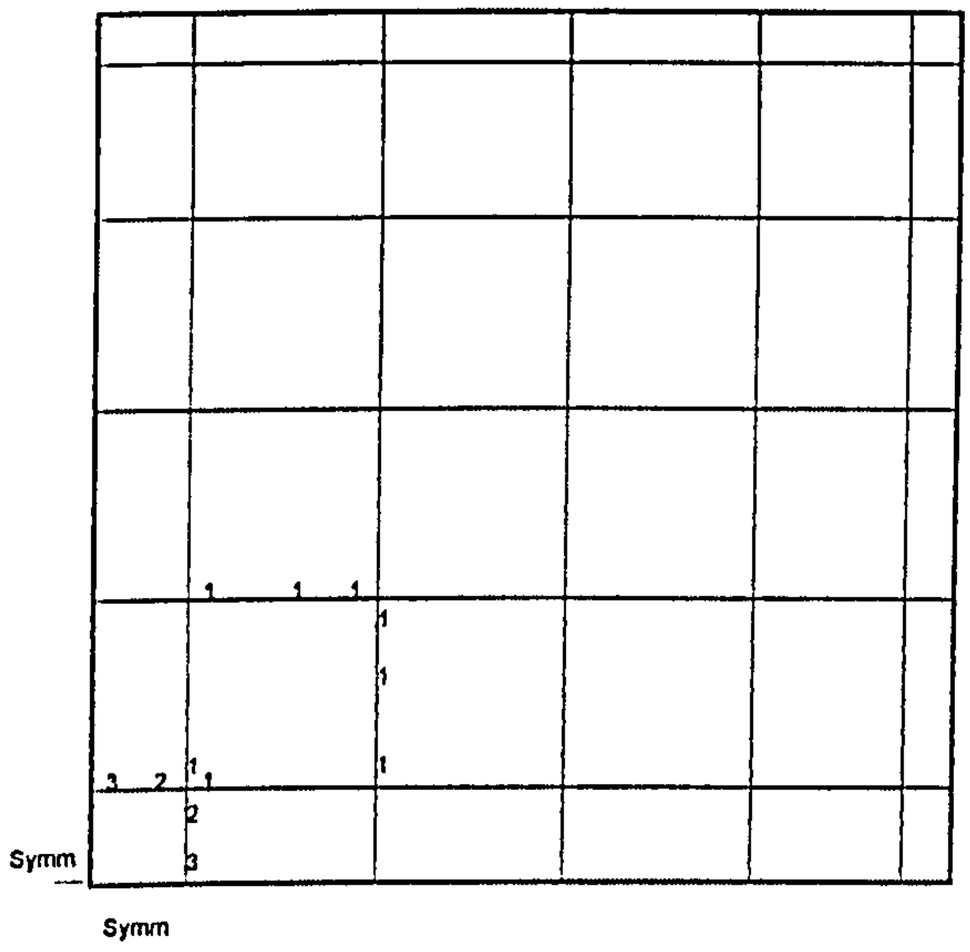

NB. : The numbers on the drawing indicate strain in steel at collapse expressed as a ratio of yield strain

Figure 5.72 : Yielding of flexural steel , specimen "2C" (B=0.50)

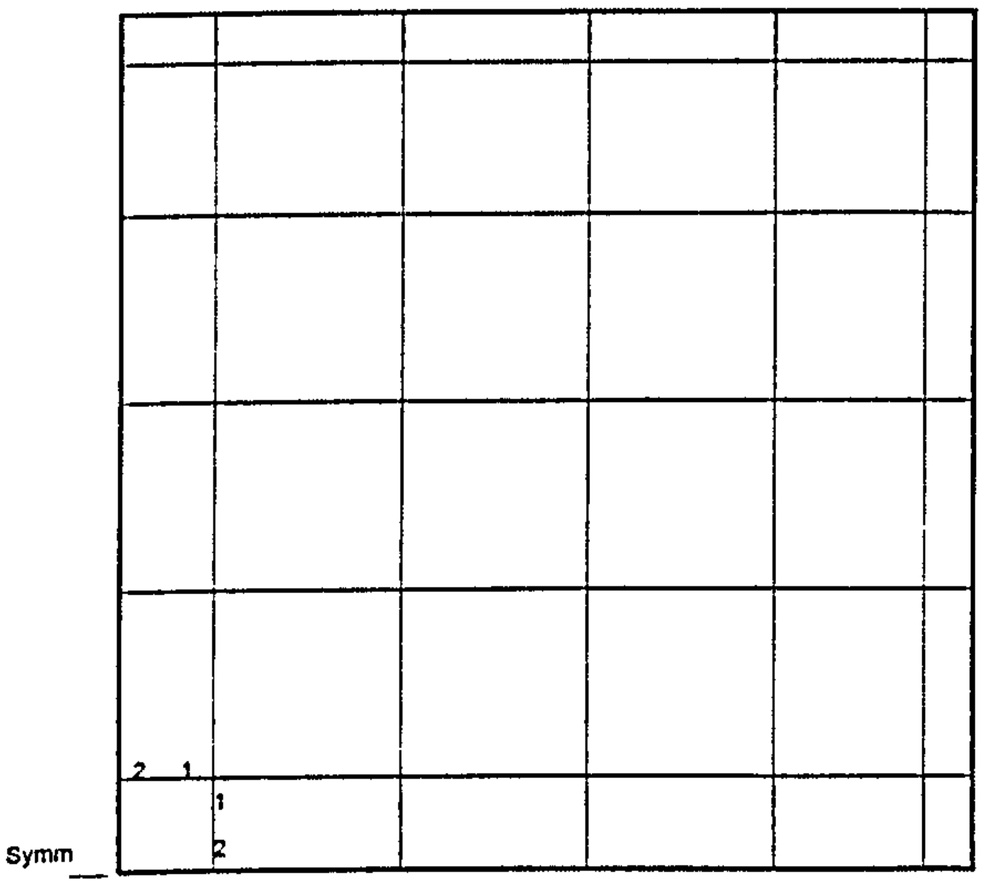

NB. : The numbers on the drawing indicate strain in steel at collapse expressed as a ratio of yield strain

Figure 5.73 : Yielding of flexural steel , specimen "2C" (B=0.25)

5.5.4 Confinement effect

The purpose of this section is to study the effect of confinement of concrete due to the presence of shear links in the slab. Many investigators have assumed allowable uniaxial compressive strength higher than f_c' due to this effect (for example Steven, et al. 1991; Vecchio 1992 and Abdel Kader 1993). In the present study, this was done by either increasing the compressive strength f_c' by 28% or increasing both the compressive strength f_c' by 28% and maximum compressive strain to 0.007 for the elements within the shear reinforcement region. Three cases were studied :

i) Case 1, no confinement effect; i.e. $f_c=f_c'$ and maximum compressive strain equal to 0.0035;
ii) Case 2, $f_c=1.28f_c'$ and maximum compressive strain equal to 0.0035;
iii) Case 3, $f_c=1.28f_c'$ and maximum compressive strain equal to 0.007.

The material parameters in the previous section were kept constant as follows :-
Tension stiffening curve corresponding to (A=0.7, ε_{max}=0.003), shear retention factor as $\beta= 0.25\varepsilon_{cr}/\varepsilon_n$ and the splitting tensile strength of concrete is obtained from $f_{sp} = 0.53\sqrt{f_c'}$.
Two types of shear reinforcement were studied:-

- Stirrup as shear reinforcement;
- Universal beam off cut section as shear reinforcement.

Slabs tested by Chana and Desai (1992) which used stirrup as shear reinforcement and slabs tested by Gomes (1991) which used off-cut sections of universal I beam as shear reinforcement were chosen for study of confinement effect. The details of these slabs are summarised as follows:

Chana and Desai's slabs
These specimens were 3 m square, and the thicknesses were 228mm , 240mm and 250mm. The loading was applied at points equally spaced along the circumference of a circle of 2.4 m diameter and supported by a square column at the centre of slab. The shear reinforcements for these slab were located at perimeters of 0.5d or 1.25d. The finite element mesh used is shown in Figure 5.74.

Gomes' slabs
These specimens have the same amount of flexural steel of diameter 16mm bar at spacing of 100mm and compression steel of T8 @ 140 c/c. These specimens were 200mm thick with side length of 3000 mm, the central columns (or loaded areas) were

200mm square. Load was applied through either a column stub or a steel plate at the centre of the slab. The reactions were provided by four high tensile steel bars at each edge. In order to prevent local failure at support nodal points, the vertical restraint along the edges were restrained as shown in Figure 5.75. The shear reinforcement was of off-cut sections of universal I beam arranged either radially or in a cross shape on plan (refer to Figure 6.24).

Shear reinforcement was simulated by line element in the transverse direction (i.e. z-direction). For the properties of shear reinforcement, measured values of the elastic modulus and yield stress were used, a perfectly elastic-plastic behaviour was assumed.

Analysed results for slabs reinforced by stirrups (referred to Table 5.12) show that Case 1 (no confinement effect) cannot reflect the presence of shear reinforcement and generally predicted lower ultimate loads than the experiments ultimate load. Increasing only the compressive strength of concrete by 28% (Case 2), reflected better the presence of shear reinforcement (i.e. higher ultimate load for slab with more shear reinforcement and vice-versa). Increasing both the compressive strength of concrete by 28% and the maximum compressive strain to 0.007 (Case 3), also reflected the presence of shear reinforcement but overestimated the ultimate load for some slabs.

Result of analysis for slabs reinforced by Universal beam off cut section showed that the failure load predicted by Case 1 (no confinement effect) were less than the actual failure load. Increasing only the compressive strength of concrete by 28% (Case 2) reflected the presence of shear reinforcement for slabs with a low amount of shear reinforcement only. Increasing both the compressive strength of concrete by 28% and maximum compressive strain to 0.007 (Case 3) reflected the presence of shear reinforcement for all the slabs (i.e. higher ultimate load for the slab with more shear reinforcement and vice-versa) and the predicted structural response agreed well with the experiment results (Figures 5.76-5.78). From these figures, it is obvious that the structural response for all three cases follow similar path. This indicates that considering the confinement effect does not change the structural response. It only prevents the slab from failing in local crushing. Consequently it yielded higher ultimate load for the slab. The predicted ultimate load of slabs are summarised in Table 5.13.

Two important conclusions can be drawn from the above observations.

- It is necessary to include the confinement effect due to the presence of shear reinforcement.
- Universal I beam (with flange) provide a higher degree of confinement than stirrup (without flange).

Table 5.12 shows that Case 2 predicted a more consistent result for slabs reinforced by stirrups. While Table 5.13 shows that Case 3 is more suitable for slabs reinforced by shear reinforcement with flange (such as I beam off cut section and shear stud). Therefore, for slab with shear reinforcement, the compressive strength of concrete for the elements within shear reinforcement region was increased depending on the type of the shear links in the slab. For slabs with stirrup as shear reinforcement, use $f_c=1.28f_c'$, maximum compressive strain=0.0035. And for slabs with universal I beam off-cut sections as shear reinforcement, use $f_c=1.28f_c'$, maximum compressive strain=0.007 is recommended.

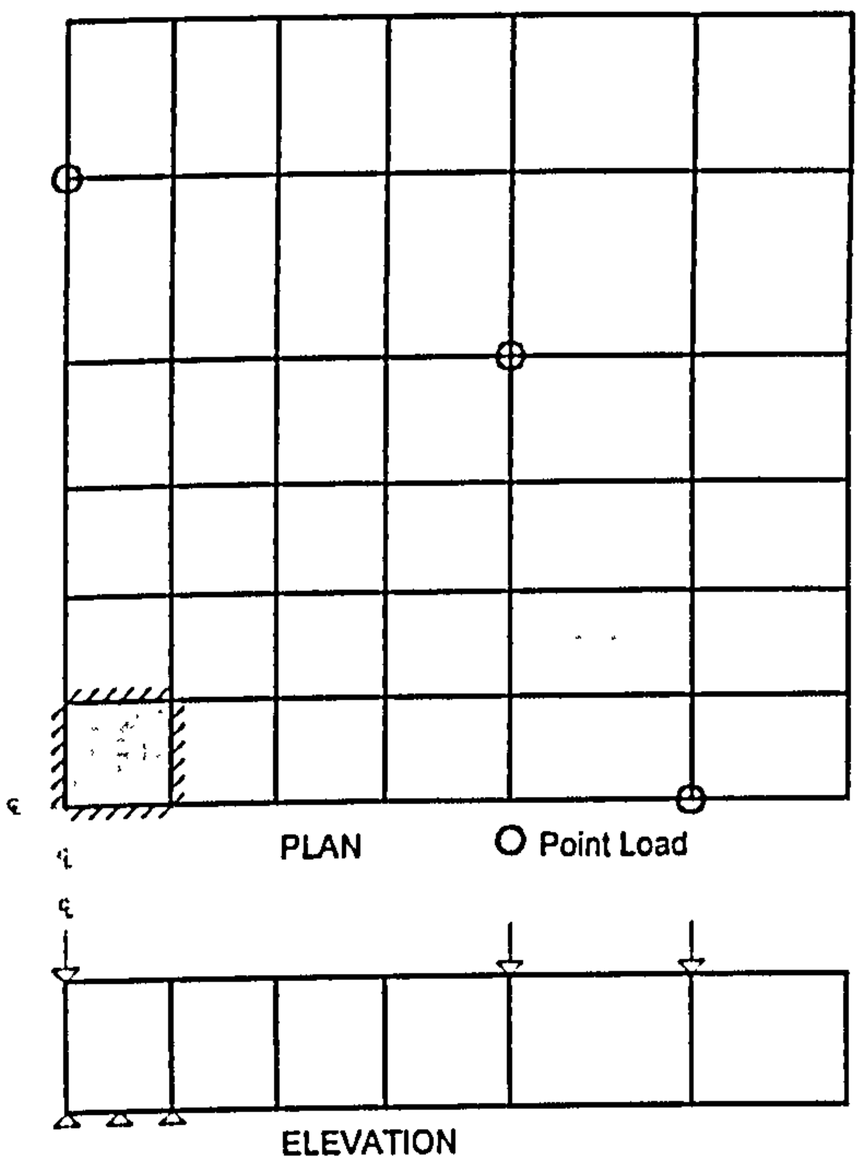

Figure 5.74 Arrangement of mesh for slabs C2-C9

Table 5.12 : Predictions for slab C2-C9 (Chana and Desai)

Slab	P_{test} (kN)	Num/Exp failure load		
		Case 1	Case 2	Case 3
C2	1094.0	0.709	0.858	1.082
C4	1302.0	0.595	0.877	0.971
C5	1382.0	0.790	0.903	1.016
C6	1283.0	1.013	1.094	1.094
C7	1492.0	0.788	0.826	0.826
C8	1324.0	0.689	0.870	0.870
C9	1135.0	0.775	0.804	0.804
Average		0.766	0.890	0.952
STDEV		0.130	0.096	0.120

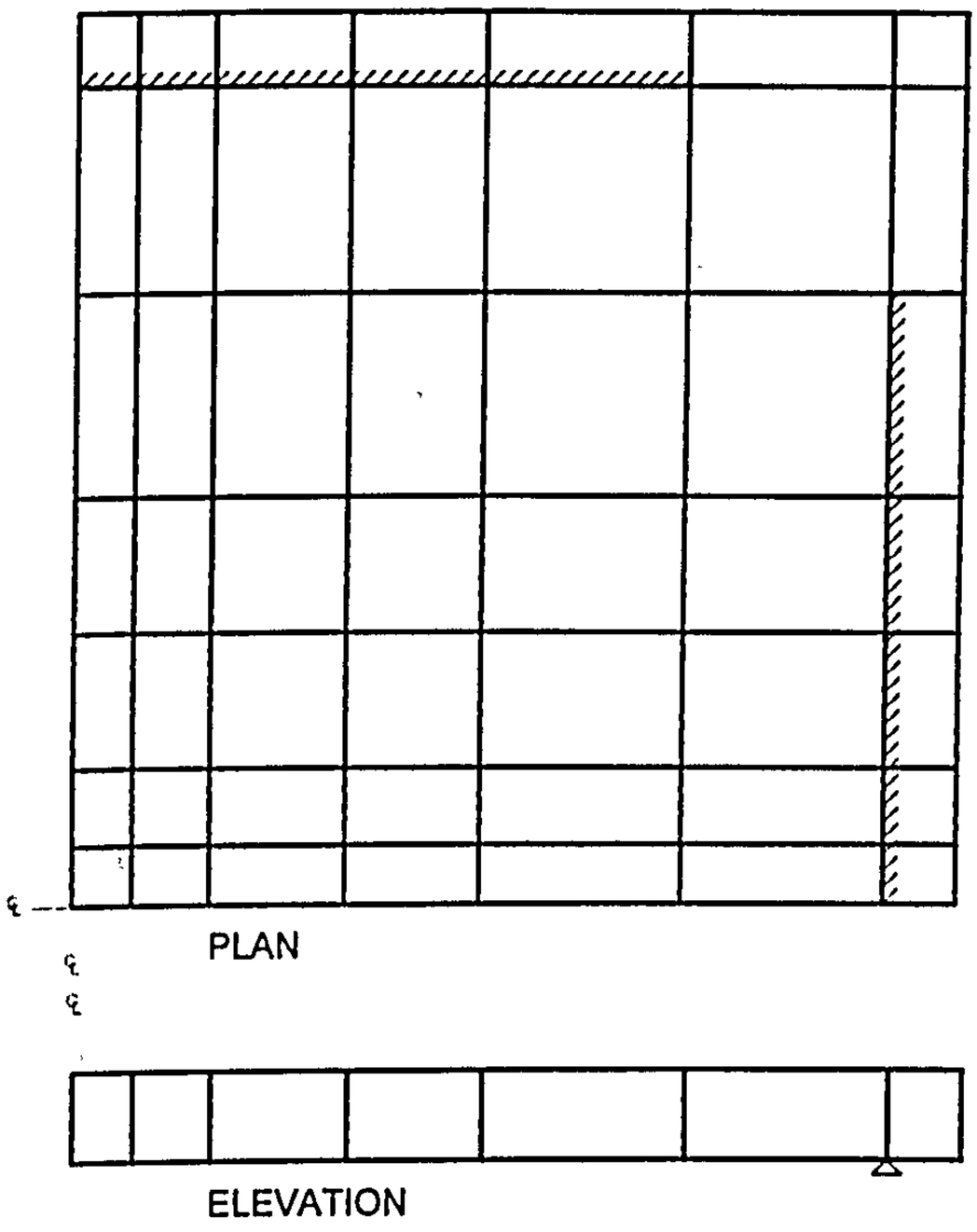

Figure 5.75 Arrangement of mesh for slabs G2-G8

Table 5.13 : Predictions of specimens G2-G8 (Gomes)

Slab	Ptest (kN)	Num/Exp failure load		
		Case 1	Case 2	Case 3
G2	693.0	0.909	0.952	0.952
G3	773.0	0.854	0.893	0.893
G4	853.0	0.774	0.809	0.949
G5	853.0	0.809	0.949	0.949
G6	1040.0	0.727	0.727	0.831
G7	1120.0	0.739	0.739	0.804
G8	1200.0	0.594	0.660	0.810
Average		0.772	0.818	0.884
STDEV		0.101	0.116	0.068

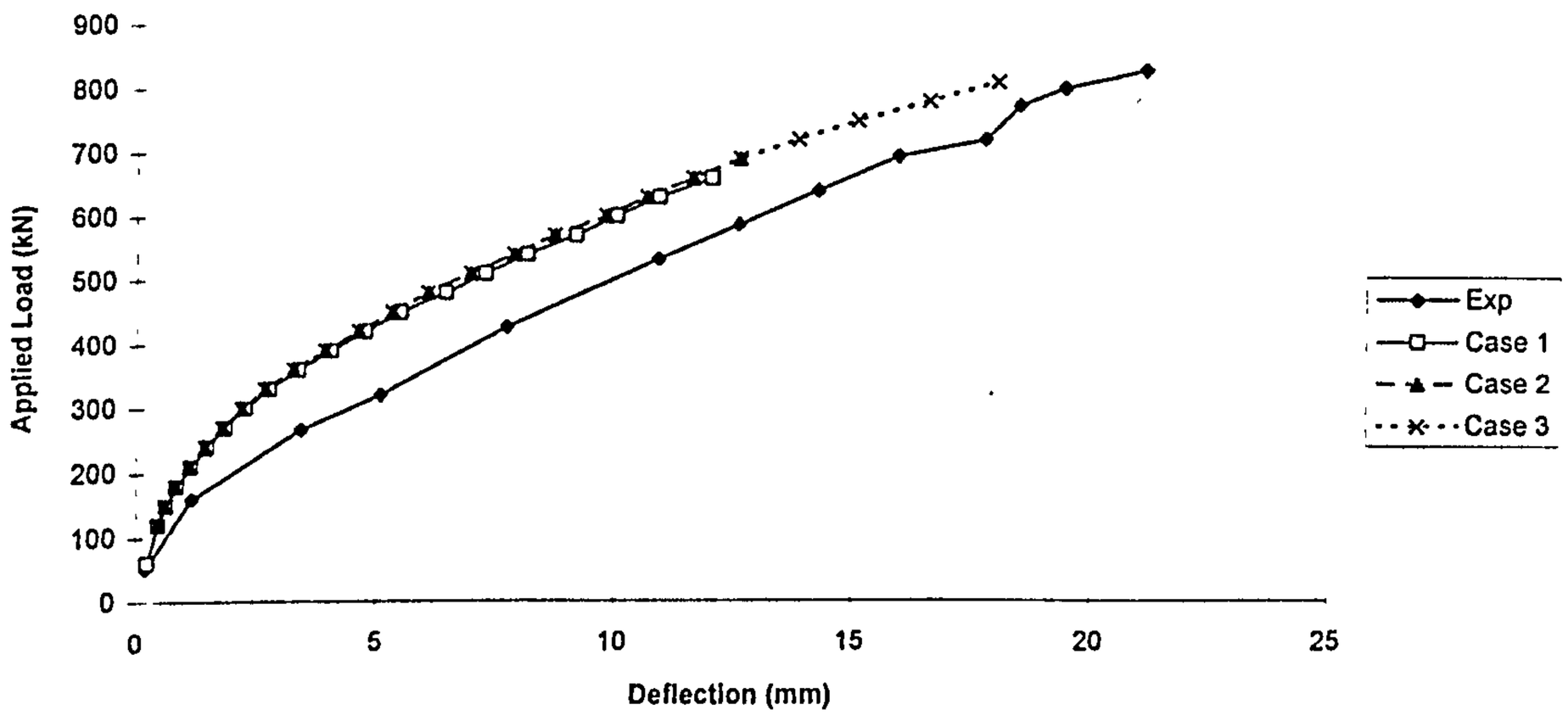

Figure 5.76 Confinement effect on load-deflection response for slab G4

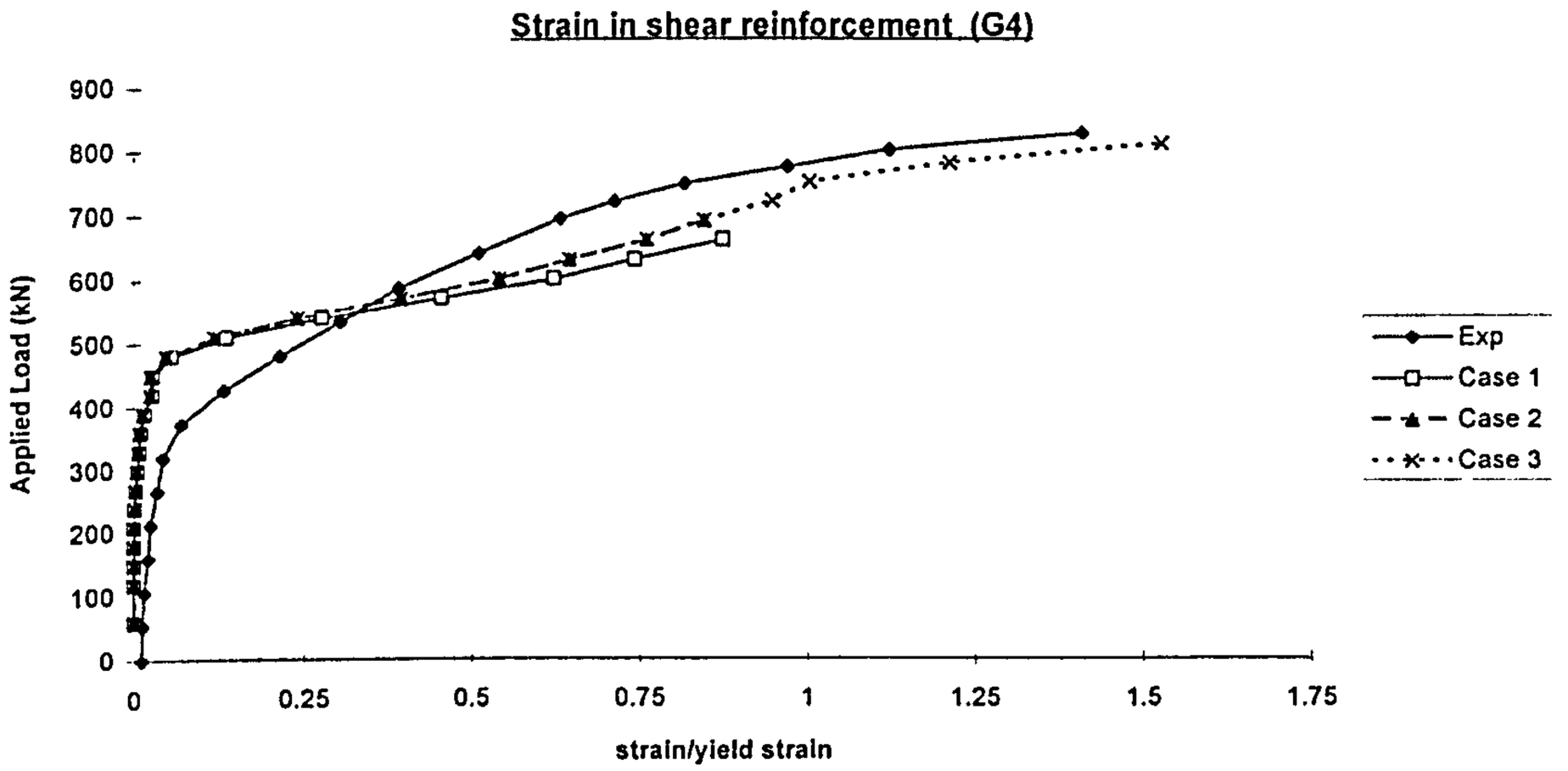

Figure 5.77 Confinement effect on strain in shear reinforcement for slab G4

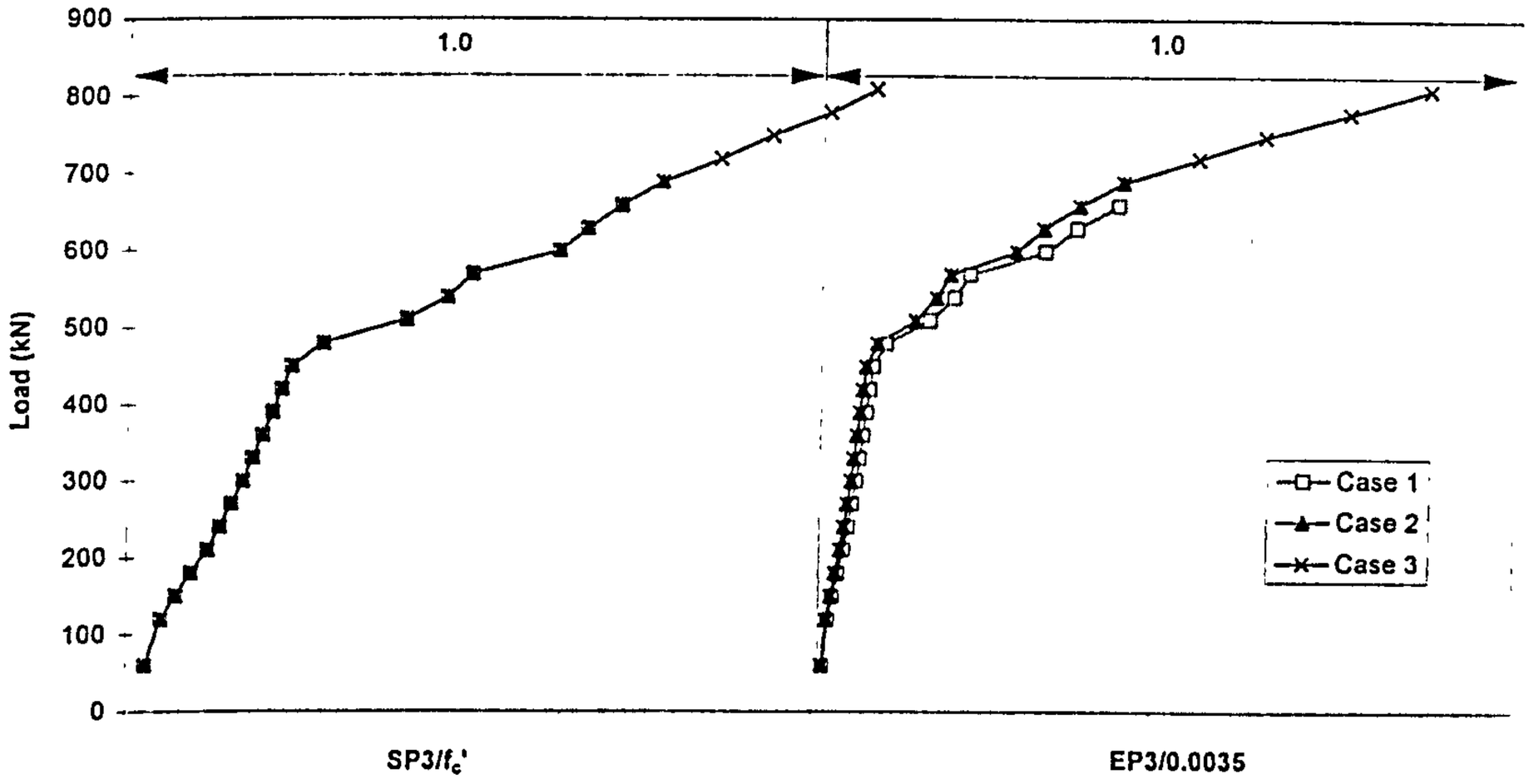

Note: SP3=σ_3=maximum compressive principal stress

EP3=ε_3=maximum compressive principal strain

Figure 5.78 Confinement effect on stress and strain in concrete (slab G4)

5.5.5 Conclusions

From the parametric study for the material parameters, the following conclusions can be drawn :-

- The effect of tensile strength of concrete on the ultimate load is insignificant. It is more significant to the structural response of lightly reinforced slab and less significant for heavily reinforced slab. Low tensile strength of concrete may cause divergence of the solution at low load levels. This should be avoided.
- Tension stiffening has more significant effect on the structural response for thin slabs with low percentage of reinforcement and less significant effect on slabs with high percentage of steel. Generally, reducing the tensile strength immediately after cracking or reducing maximum strain at which tensile strength becomes zero, reduced the ultimate load of the slab. Reducing the tensile strength immediately after cracking can reflect better the loss of stiffness due to cracking of concrete for lightly reinforced concrete
- The effect of the shear retention factor on the structural response is insignificant. The difference in structural behaviour is more likely to be caused by reinforcement ratio, span/depth ratio, concrete strength etc. But higher value of shear retention factor predicted higher ultimate load. Small value of shear retention factor (B=0.25 or 0.50) predicted good lower bound to ultimate load and correct mode of failure. Too large a shear retention factor (B= 1.0) may over predict the ultimate load and change the mode of failure from shear to flexure.
- For slab with shear reinforcement, it is necessary to include the confinement effect of concrete due to the presence of shear links in the slab. Considering confinement effect does not change the structural response of the slab. It only prevents the slab from failing in local crushing. Different types of shear reinforcements provide different degrees of confinement. For example off cuts of universal I beam provide higher degree of confinement than stirrup. To reflect the different degrees of confinement, for slabs with stirrup as shear reinforcement, in the analysis use $f_c=1.28f_c'$ and maximum compressive strain equal to 0.0035. For slabs with universal I beam off-cut sections as shear reinforcement, in the analysis use $f_c=1.28f_c'$ and maximum compressive strain equal to 0.007.

Chapter 6

SIMPLY SUPPORTED SLABS

6.1 Introduction

This chapter presents the results of analysis of internal slab-column junctions without moment transfer from different sources. The chosen slabs were with and without shear reinforcement, and these slabs cover the important parameters governing punching shear strength such as : thickness of slabs, flexural reinforcement ratios, concrete strength and size of loaded area. The analysis used the same parameters held constant as follows:

Numerical parameters

- The load step for the first two increments was 10% of experimental failure load and 5% of the experimental failure load for the remaining increments.
- The convergence criterion was based on the residual forces with a tolerance of 5%.
- The maximum number of iterations per increment is 50.
- The aspect ratio for the element within and near the failure region (i.e. element representing the loading stub and element beside the loading stub) should not be more than 1.5 and element size was gradually increased when it is further away from loading stub.
- only support nodal points for corner element was released.

Material parameters

- the cylinder compressive strength of concrete (f_c') was taken to be $0.8f_{cu}$, where f_{cu} is the compressive cube strength of concrete
- Young's modulus for concrete, $E_c = 4730\sqrt{f_c'}$ N/mm^2
- Poisson's ratio 0.2
- Tensile strength of concrete, $f_t = f_{sp}/2$ and the splitting cylinder tensile strength, $f_{sp} = 0.53\sqrt{f_c'}$ N/mm^2
- The tension stiffening is taken as a linear function of the principal strain, tensile strength of concrete immediately after cracking is reduced to $0.7f_t$, maximum strain ε_{max} is taken as 0.003 i.e. A=0.7, emax=0.003 (Refer to Figure 5.43).
- The shear retention factor β taken as 0.25 $\varepsilon_{cr}/\varepsilon_n$ ie. **B=0.25** (Refer to Figure 5.56).
- For steel, the measured values of the elastic modulus and yield stress were used directly. Perfectly elastic-plastic behaviour was assumed.

- For slabs with shear reinforcement, the compressive strength of concrete for the elements within shear reinforcement region was increased depending on the type of the shear links in the slab. For slabs with stirrup as shear reinforcement, $f_c=1.28f_c'$ and maximum compressive strain=0.0035 were used. For slabs with universal I beam off-cut sections or shear stud as shear reinforcement, $f_c=1.28f_c'$ and maximum compressive strain=0.007 were used.

The analysis took into account the following observed structural behaviour for deciding on the mode of failure (section 5.2):-

- The ultimate load capacity of the slab;
- The load-deflection response;
- Strains in flexural reinforcement;
- Distribution of strains and stresses in concrete within the compressive zone;
- Crack pattern;

6.2 Calculation of ultimate load of slabs according to BS8110

The study also used British Code BS8110 to see how well it can predict the load carrying capacity of slabs and the mode of failure. The ultimate load of slabs without shear reinforcement are calculated as follows :

- P_c is the shear force at column face; given by
  P_c=column perimeter × d × ($\sqrt{f_{cu}}$ or 6.25 N/mm^2 whichever is smaller)
- P_v is the shear force at 1st perimeter; given by
  P_v=(perimeter at 1.5d from column face) × d × v_c
- P_f is the flexural capacity of the slab, calculated by using equation in clause 3.4.4.4 BS8110.
- P_u is the ultimate load of the slab = smallest of [P_c, P_v, and P_f].

For slabs with shear reinforcement, the possibility of punching taking place outside shear region was included. Thus the P_v was calculated for two perimeters;

- $P_{v(in)}$ is the shear force at 1st perimeter; calculated by
  $P_{v(in)} = P_v + P_s$
  P_s = shear strength provided by the shear reinforcement within the 1st perimeter
- $P_{v(out)}$ is the shear force at a perimeter outside of shear reinforcement region;
  $P_{v(out)}$ = (perimeter just outside shear reinforcement zone) × d × v_c

where $v_c=0.79(100As/(bd))^{1/3}(400/d)^{1/4}(f_{cu}/25)^{1/3}$

d = effective depth of slab

The above analysis was calculated based on the safety factor = 1.0. Sample calculations are presented in Appendix A.

6.3 Slabs without shear reinforcement

6.3.1 Conventional slab-column specimens tested by Rankin

Rankin (1982) tested a series of 27 conventional slab-column specimens without shear reinforcement. These slabs cover most of the important parameters (thickness of slab, flexural reinforcement ratio, concrete strength) governing punching shear strength.

These slabs were simply supported along the four edges with corners free to lift and subjected to a concentrated load at midspan as shown in Figure 5.3. Concrete strength ranged from 36-47 N/mm^2. Flexural reinforcement only was included in the models and this varied over the range 0.4-2.0%. The span/depth (L/h) ratios varied over a range of 25-35. The reinforcement had a well-defined yield point with no strain hardening (f_y = 530 N/mm^2). A summary of slabs' details is presented in Table 6.1.

Owing to symmetry, only one-quarter of the slabs was modelled (Refer to Figure 5.2). The applied load was simulated by uniformly distributed load over the element representing the loading stub. Concrete slab was discretised by using one layer of twenty node solid elements.

Predicted ultimate load is presented in Table 6.2. It ranges from 66% to 97% of the experimental values. The average of predicted ultimate load is 81% of experimental ultimate load with 8.3% standard deviation. The predicted load gives a good lower bound value. Table 6.4 shows that the present model can predict more accurate ultimate load for slabs which failed in flexure mode (Average 84.5%, SD=6.1%) than slabs which failed in shear mode (Average 76.7%, SD=8.9%).

The predicted mode of failure is presented in Table 6.2. 25 out of 27 slabs were predicted with correct mode of failure. The two slabs for which predicted mode of failure was incorrect are slabs "6" and "2C". These slabs failed in shear mode from experiment observation, but numerical model does not give a clear indication of mode of failure (the predicted load-deflection response and steel strain show that these slabs failed in shear mode, but concrete strain and crack pattern show that these slabs failed in flexure mode). The percentage of reinforcement was such that the failure mode could be either flexural or shear. In the case of thin slabs, slabs with steel percentage of less than 0.8% failed in pure flexural failure and slabs with steel percentage of more than 1.2% failed in pure punching shear mode. Specimen "6" is a thin slab (l/d=16) and contains a moderate amount of reinforcement (1.026%). It lies in the region between flexure and shear failure. However, specimen "2C" is a thick slab (l/d=12) with a relatively low amount of reinforcement (0.69%). Rankin (1982) mentioned that the punching strength of the thick slabs levels off at a lower

reinforcement ratio than for the thin slabs (for slabs with constant steel ratio, an increase in the thickness of slab will increase its flexural capacity), so it changes from the flexural to the shear mode of punching failure. This table also shows that compression failure of concrete only occurs for the slabs with extremely heavy reinforcement (15, 4A, 3B, 3C, 4C) as observed by Rankin in the experiment. For the remaining slabs which failed in shear mode, failure was more likely initiated by internal diagonal cracking because the concrete had not failed in compression. The spread of yielding of flexural reinforcement is shown in Figures 6.4 & 6.5. For slab which failed in flexure mode, yielding of steel was spread over a large area of slab (Figure 6.4). However, for slabs which failed in shear mode, the flexural steel either did not yield or yielding was confined to an area around the loading stub (Figure 6.5).

Figure 6.1 shows that lightly reinforced slabs displayed large ductility while a brittle behaviour was shown by heavily reinforced slabs. The strain profile of flexural steel for lightly reinforced slab has a shape similar to the bending moment diagram (Figure 6.2) indicating that flexure is dominant. Conversely, strain profile for heavily reinforced slab within a certain distant was similar to the shape of shear force diagram (Figure 6.3).

The predicted ultimate load and mode of failure by using BS8110 are presented in Table 6.3. The average of predicted ultimate load is 86.3% of experimental ultimate load with 6.4% standard deviation. Although BS8110 predicted reasonably accurate ultimate load, it often predicted incorrect mode of failure for slabs with moderate amount of reinforcement (0.8% to 1.2%).

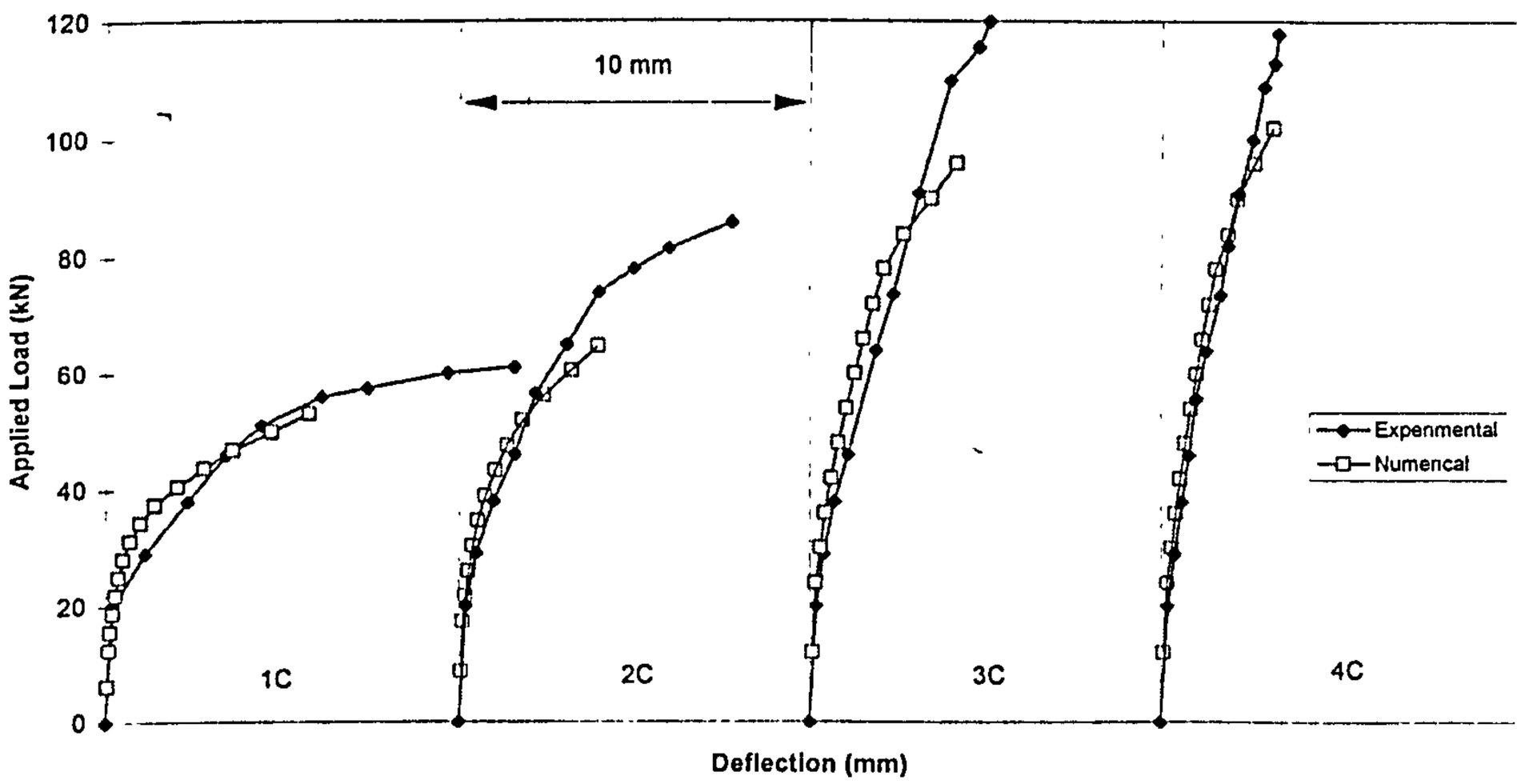

Figure 6.1 The influence of reinforcement ratio on the ductility of slabs

Table 6.1 : Details of Rankin's conventional slabs

Slab	h (mm)	d (mm)	f_{cu} (N/mm^2)	ρ (%)	P_{test} (kN)
1	51.00	40.50	38.40	0.423	36.42
2	51.00	40.50	38.40	0.558	49.08
3	51.00	40.50	38.40	0.691	56.55
4	51.00	40.50	43.50	0.821	56.18
5	51.00	40.50	43.50	0.883	57.27
6	51.00	40.50	43.50	1.026	65.58
7	51.00	40.50	37.10	1.163	70.94
8	51.00	40.50	37.10	1.292	71.09
9	51.00	40.50	37.10	1.454	78.60
10	51.00	40.50	37.40	0.517	43.59
11	51.00	40.50	37.40	0.802	55.00
12	51.00	40.50	37.40	1.107	67.06
13	51.00	40.50	42.50	0.601	49.39
14	51.00	40.50	42.50	0.691	52.45
15	51.00	40.50	42.50	1.994	84.84
1A	57.00	46.50	36.00	0.422	45.19
2A	57.00	46.50	36.00	0.691	66.24
3A	57.00	46.50	36.00	1.293	89.72
4A	57.00	46.50	38.60	1.992	97.43
1B	45.50	35.00	47.10	0.423	28.85
2B	45.50	35.00	47.10	0.690	37.63
3B	45.50	35.00	47.10	1.292	56.67
4B	45.50	35.00	38.60	1.994	72.52
1C	64.00	53.50	34.80	0.423	62.74
2C	64.00	53.50	40.50	0.690	87.86
3C	64.00	53.50	40.50	1.288	124.14
4C	64.00	53.50	34.80	1.993	125.94

Table 6.2 : Ultimate load and mode of failure for Rankin's conventional slabs

Slab	Experimental results		Numerical Predictions		P_{num}/P_{test}
	P_{test} (kN)	Failure Mode	P_{num} (kN)	Failure Mode	
1	36.42	y	32.40	y	0.890
2	49.08	y	40.79	y	0.831
3	56.55	y	44.90	y	0.794
4	56.18	y	42.14	y	0.750
5	57.27	y	51.83	y	0.905
6	65.58	s	53.78	fp	0.820
7	70.94	s	46.82	s	0.660
8	71.09	s	46.78	s	0.658
9	78.60	s	55.41	s	0.705
10	43.59	y	35.52	y	0.815
11	55.00	y	42.24	y	0.768
12	67.06	s	47.08	s	0.702
13	49.39	y	42.82	y	0.867
14	52.45	y	44.16	y	0.842
15	84.84	s	75.60	s	0.891
1A	45.19	y	41.03	y	0.908
2A	66.24	y	50.41	y	0.761
3A	89.72	s	72.94	s	0.813
4A	97.43	s	91.20	s	0.936
1B	28.85	y	24.96	y	0.865
2B	37.63	y	36.50	y	0.969
3B	56.67	y	49.00	s	0.864
4B	72.52	s	50.40	s	0.695
1C	62.74	y	34.80	y	0.845
2C	87.86	s	53.02	fp	0.738
3C	124.14	s	95.96	s	0.773
4C	125.94	s	102.10	s	0.810
				Average	0.810
				STDEV	0.083

y=flexural failure, s=shear failure

* Appendix C presents full details of result of analysis.

Table 6.3 : Ultimate Load and Mode of failure predicted by using BS8110

(Rankin's slab)

Slab	Test results		Predictions by BS8110		P_u/P_{test}
	P_{test} (kN)	Failure Mode	P_u (kN)	Failure Mode	
1	36.42	y	29.15	y	0.800
2	49.08	y	38.15	y	0.777
3	56.55	y	46.55	y	0.823
4	56.18	y	55.04	s	0.980*
5	57.27	y	56.39	s	0.985*
6	65.58	s	59.28	s	0.904
7	70.94	s	60.28	s	0.850
8	71.09	s	62.43	s	0.878
9	78.60	s	64.94	s	0.826
10	43.59	y	35.45	y	0.815
11	55.00	y	53.24	y	0.968
12	67.06	s	59.46	s	0.887
13	49.39	y	41.16	y	0.833
14	52.45	y	46.90	y	0.894
15	84.84	s	73.98	s	0.872
1A	45.19	y	40.15	y	0.888
2A	66.24	y	60.17	s	0.908*
3A	89.72	s	74.15	s	0.826
4A	97.43	s	87.65	s	0.900
1B	28.85	y	21.77	y	0.755
2B	37.63	y	35.21	y	0.936
3B	56.67	y	53.10	s	0.937*
4B	72.52	s	60.65	s	0.836
1C	62.74	y	50.86	y	0.811
2C	87.86	s	75.27	s	0.857
3C	124.14	s	92.67	s	0.747
4C	125.94	s	102.33	s	0.813
				Average	0.802
				STDEV	0.170

y=flexural failure, s=shear failure

* wrong mode of failure predicted

Table 6.4 : Comparison between slabs which failed in different modes

(Rankin's slab)

Slabs failed in flexure mode		Slabs failed in shear mode	
Slab	Num/Exp	Slab	Num/Exp
1	0.890	6	0.820
2	0.831	7	0.660
3	0.794	8	0.658
4	0.750	9	0.705
5	0.905	12	0.702
10	0.815	15	0.891
11	0.768	3A	0.813
13	0.867	4A	0.936
14	0.842	4B	0.695
1A	0.908	2C	0.738
2A	0.761	3C	0.773
1B	0.865	4C	0.810
2B	0.969		
3B	0.864		
1C	0.845		
Average	0.845	Average	0.767
STDEV	0.061	STDEV	0.089

Strain profile for steel along mid-span ("1C")

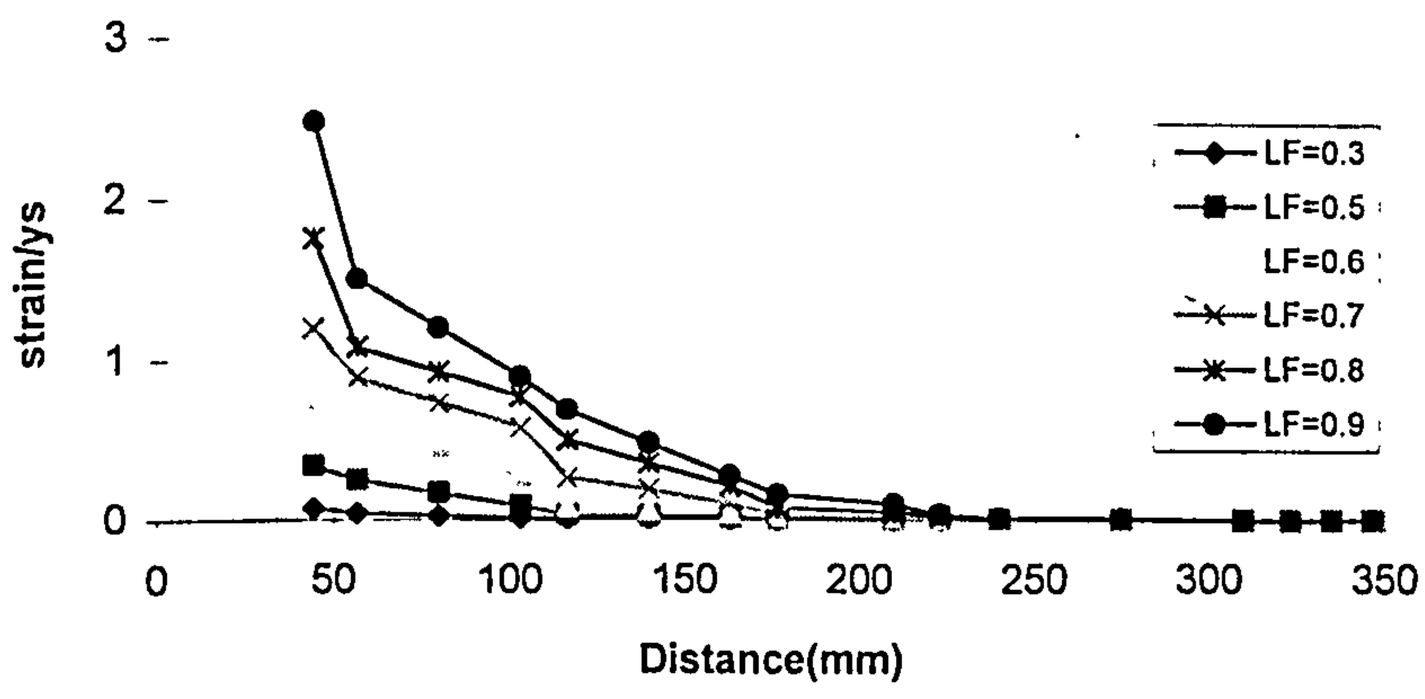

Figure 6.2 Strain variation for flexural steel along mid-span ("1C"), **Flexural failure**

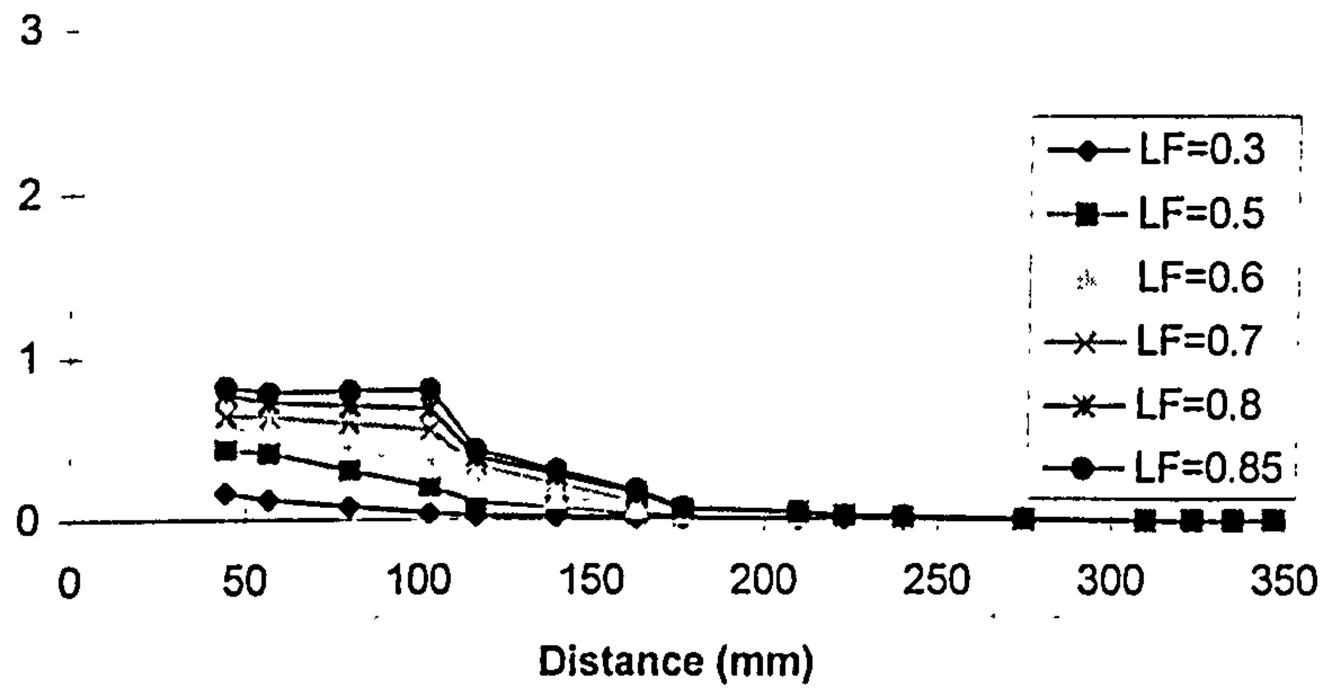

Figure 6.3 Strain variation for flexural steel along mid-span ("4C"), **Shear failure**

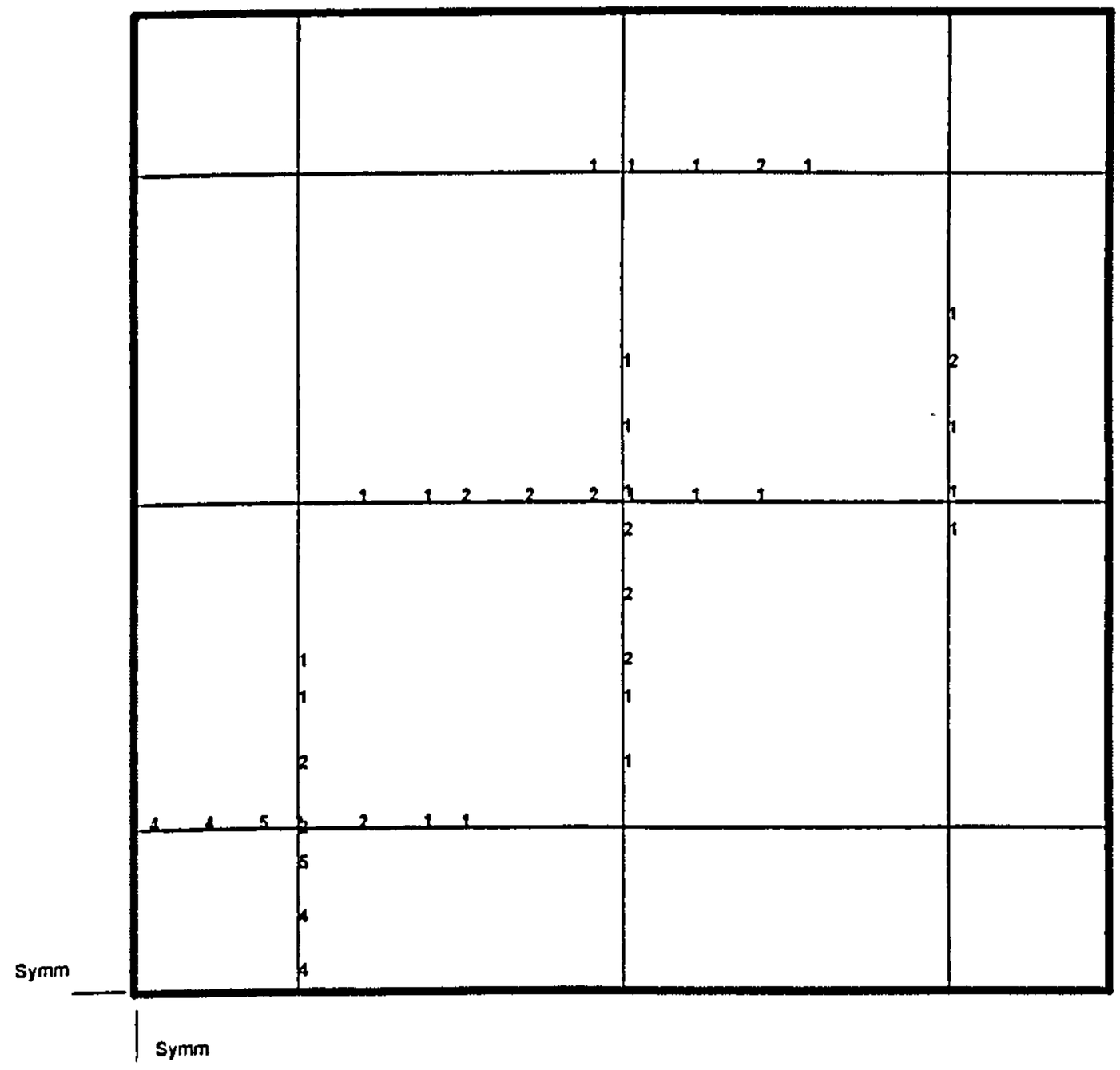

NB. : The numbers on the drawing indicate strain in steel at collapse expressed as a ratio of yield strain (e.g. 5=5 times yield strain of steel)

Figure 6.4 : Yielding of flexural reinforcement for Slab "2B" (**Flexural failure**)

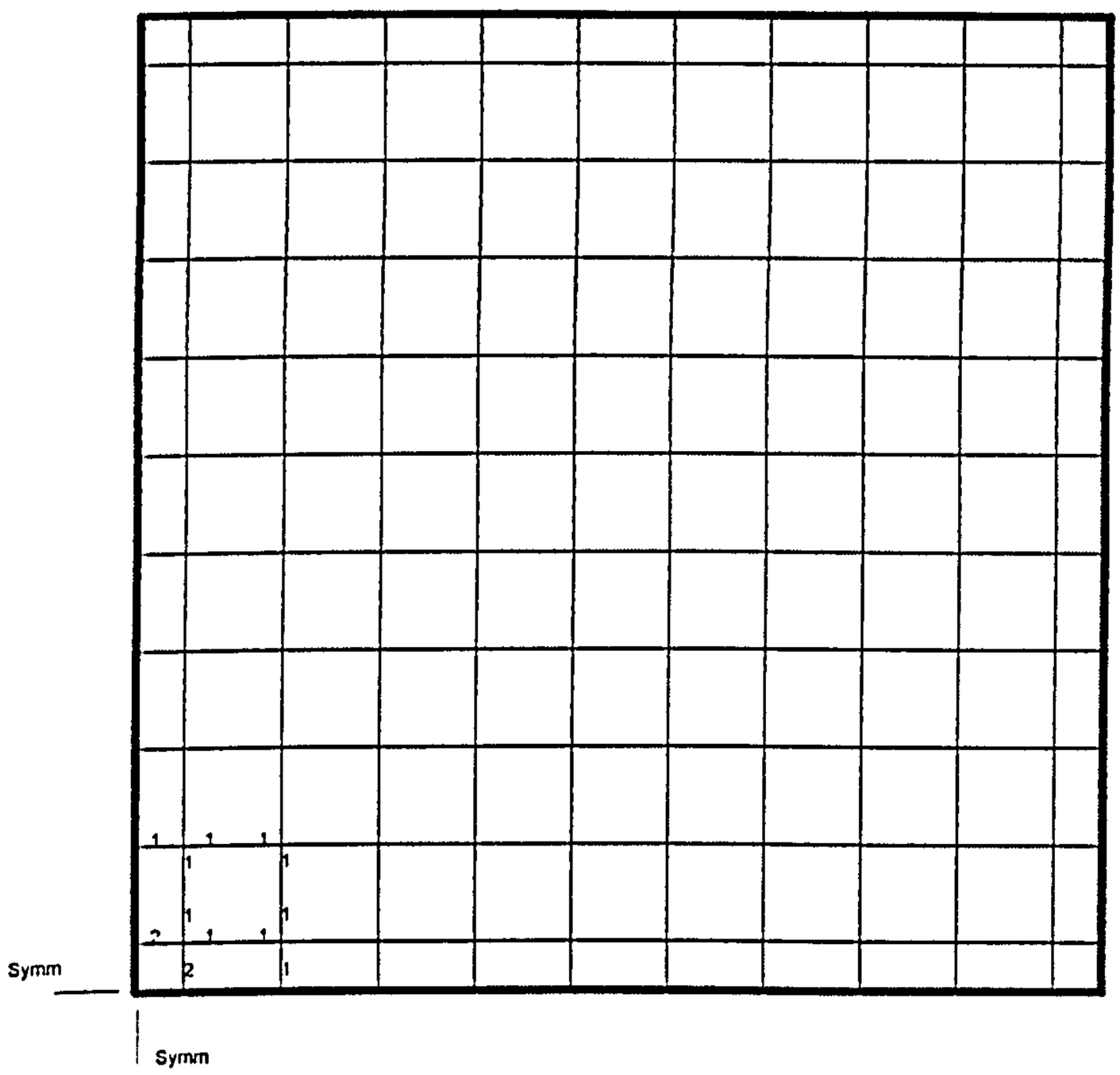

NB. : The numbers on the drawing indicate strain in steel at collapse expressed as a ratio of yield strain

Figure 6.5 : Yielding of flexural reinforcement for Slab "15" (**Shear failure**)

6.3.2 Simply supported slabs tested by Regan

This section deals with the analysis of a number of slabs (31 specimens) tested by Regan. These slabs were simply supported along the four edges with corners free to lift and subjected to a concentrated load at the slab centre. They were divided into four groups:

1. SS1-SS7 (CIRIA 220)

The variables in these slabs were the amount and the arrangement of flexural reinforcement.

2. SS8-SS11 (CIRIA 220)

These tests are concerned with scale effects. Three sizes of slab were tested.

3. V1-V5 (Regan, 1986)

The only significant variable in these tests was the size of the loaded area.

4. SP1-SP18 (Regan, 1984)

The main variable of this series was the shear span/depth ratio of the slab.

6.3.2.1 Arrangement of flexural reinforcement (SS1-SS7)

These seven slabs were 2.0 m square and 100mm thick with central column stubs 200mm square projecting on both faces. The clear span of the slabs was 1.83m. The finite element mesh used is shown in Figure 6.6. The variables of this series were the amount and arrangement of flexural reinforcement. The arrangement was either of uniform spacing or varied in accordance with the theoretical elastic distribution of moments. The first six slabs formed three pairs, with the slabs of a pair having the same total amount of reinforcement but detailed either uniformly or according to the elastic field. The seventh slab was almost similar to the sixth except for the addition of compression bars passing through the column.

Table 6.5 : Details and Predictions for slabs SS1-SS7 (Regan)

Slab	f_{cu} (N/mm^2)	d (mm)	ρ (%)	Detailing	P_{test} (kN)	Failure Mode	Load at 1st yield	Num/Exp failure load
SS1	32.30	77.00	1.200	elastic	194.00	s	No yield	0.841
SS2	29.30	77.00	1.200	uniform	176.00	s	70%	0.764
SS3	34.30	77.00	0.920	elastic	194.00	s	75%	0.792
SS4	40.40	77.00	0.920	uniform	194.00	s	60%	0.742
SS5	35.20	79.00	0.750	elastic	165.00	s	80%	0.890
SS6	27.40	79.00	0.750	uniform	165.00	s	60%	0.791
SS7	38.00	79.00	0.800	uniform	186.00	s	65%	0.877
							Average	0.814
							STDEV	0.057

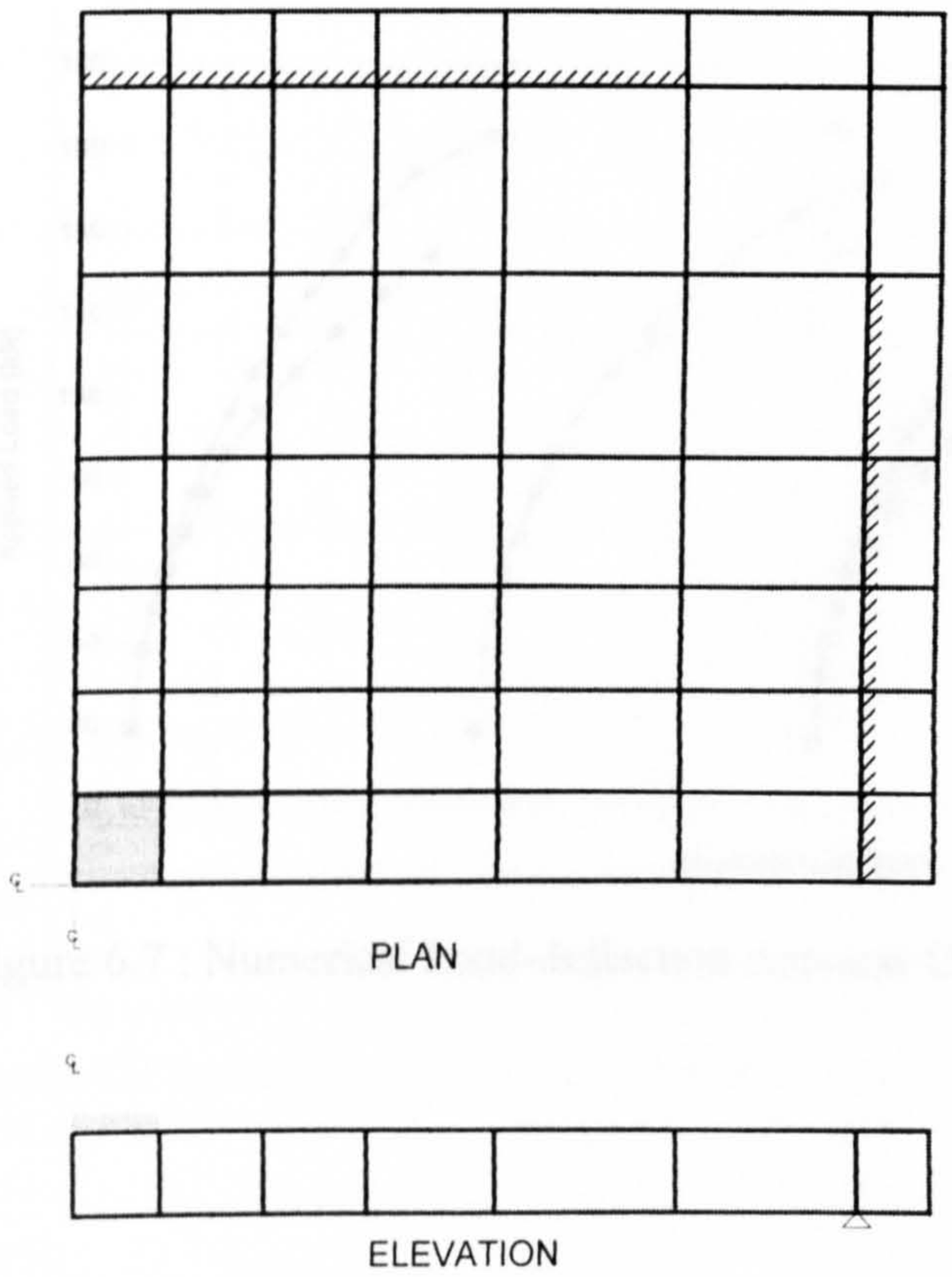

Figure 6.6 : Arrangement of mesh for specimens SS1-SS7

Figure 6.7 shows that the predicted load-deflection response has a trend similar to the experimental observation, i.e. the response was generally less stiff for slabs where the flexural reinforcement was detailed uniformly. This is because the slabs detailed uniformly yielded much earlier than slabs detailed elastically (refer to Table 6.5). Present model generally predicted a slightly higher load for slabs detailed elastically. This may be due to the finite element method dividing the slab into elements, leading to the elements at critical region having more reinforcement in slabs detailed elastically than slabs spaced uniformly. For slabs which failed in shear mode (SS1-SS6) regardless of the arrangement of steel, generally yielding was confined to a small area around the column (Figures 6.8 & 6.9). For slabs which failed in flexure mode, yielding of flexural steel was spread over a wide area of slab (Figure 6.10).

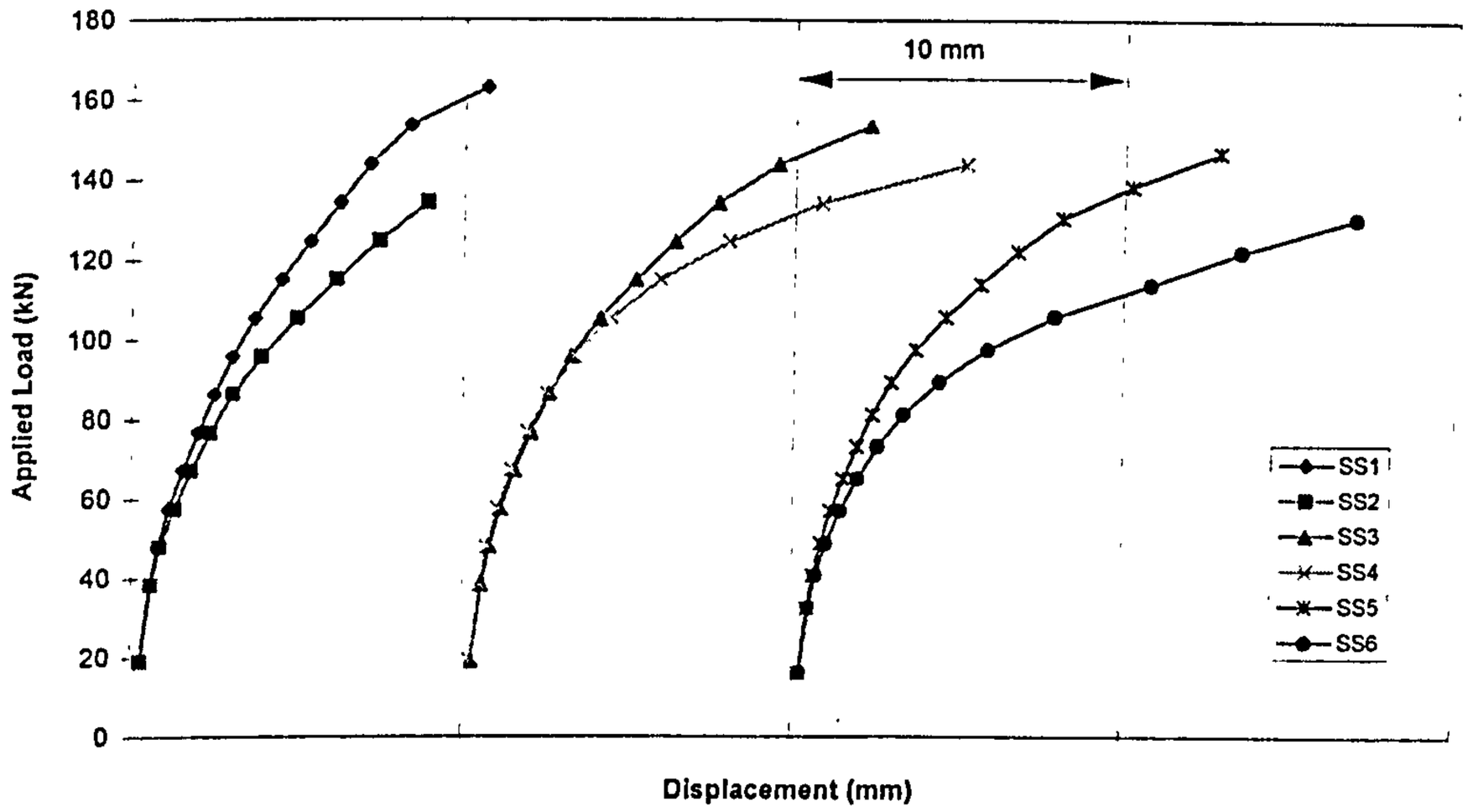

Figure 6.7 : Numerical Load-deflection response (SS1-SS6)

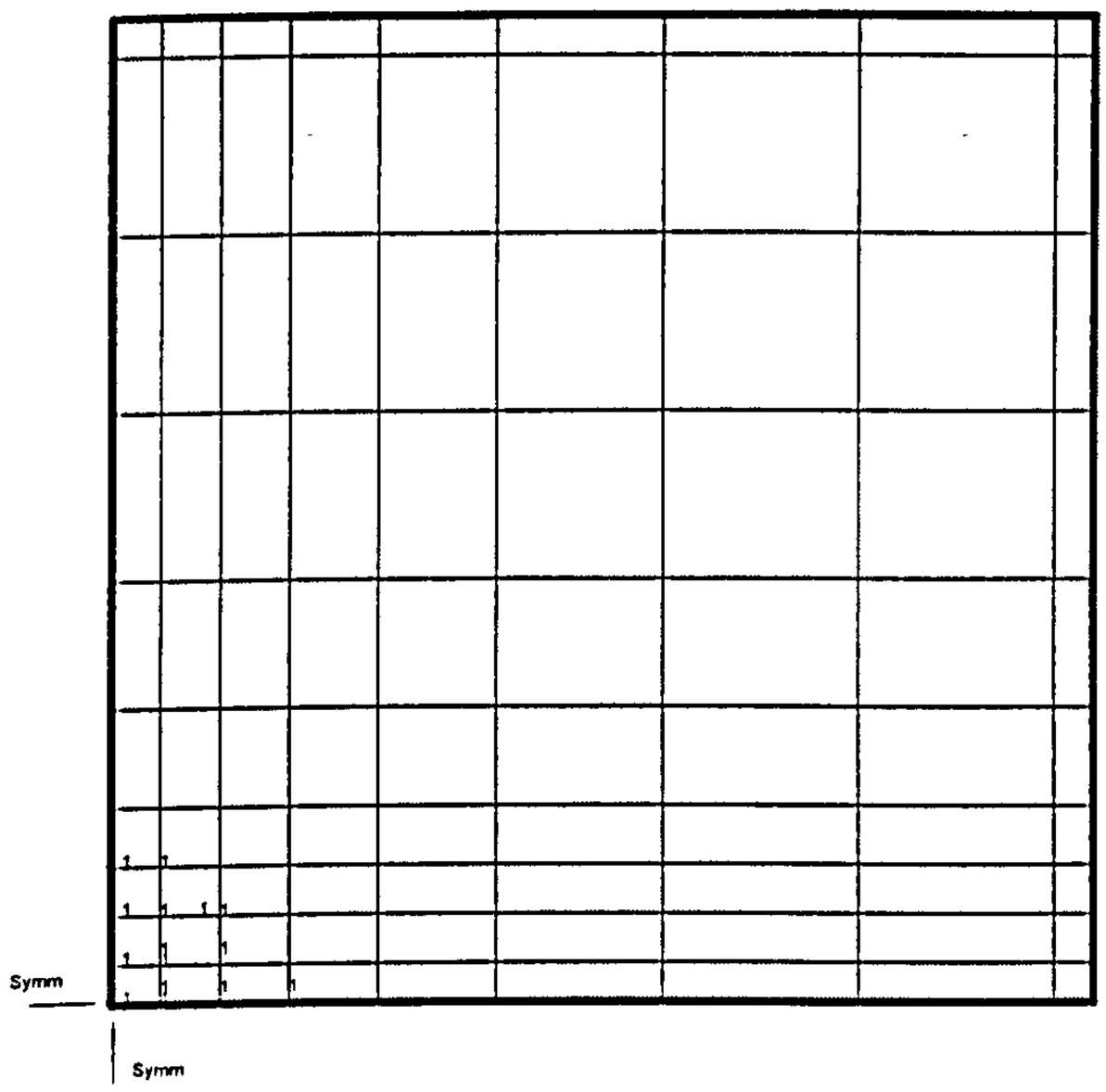

Figure 6.8 Spreading of yielding of flexural reinforcement (SS3); **shear failure**

NB. : The numbers on the drawing indicate strain in steel at collapse expressed as a ratio of yield strain

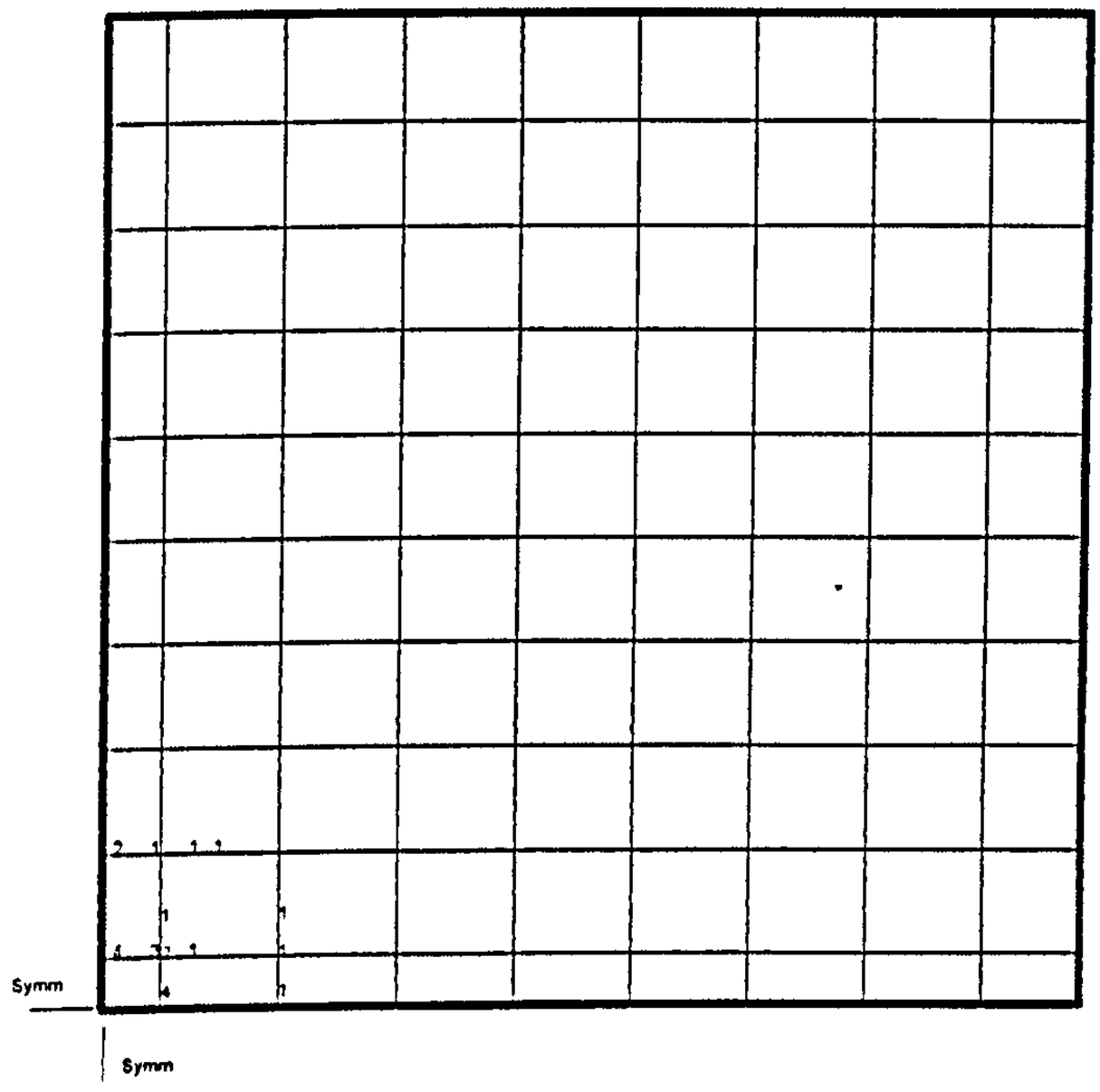

NB. : The numbers on the drawing indicate strain in steel at collapse expressed as a ratio of yield strain

Figure 6.9 Spreading of yielding of flexural reinforcement (SS4); **shear failure**

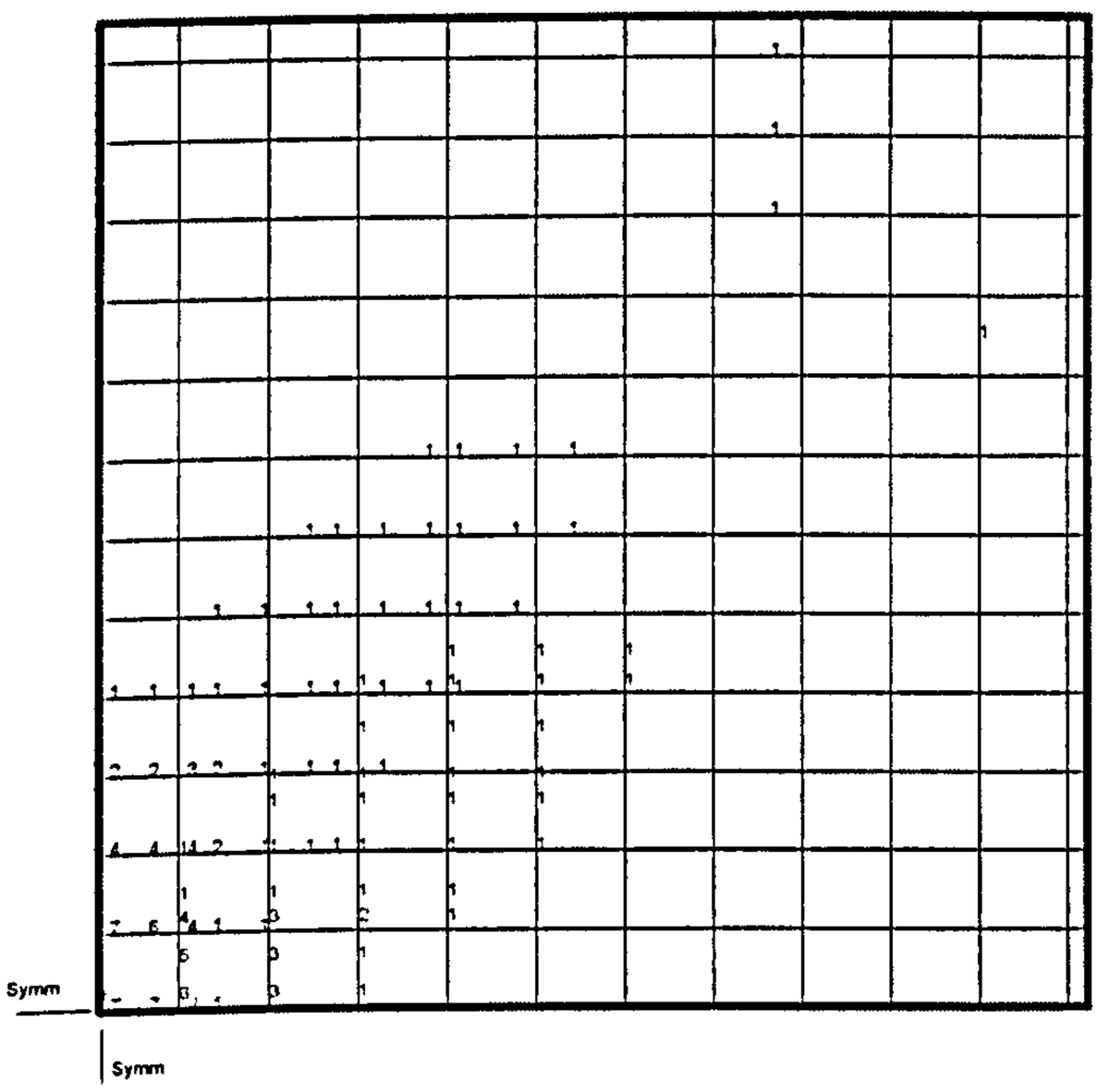

NB. : The numbers on the drawing indicate strain in steel at collapse expressed as a ratio of yield strain

Figure 6.10 Spreading of yielding of flexural reinforcement (SS7); **flexural failure**

6.3.2.2 Scale effects (SS8-SS13)

This series consisted of six slabs of three different overall thicknesses in millimetre of 250 (20mm aggregate), 160 (20 and 10mm aggregate) and 80mm (20, 10 and 5mm aggregate). The slabs were made from concrete of different maximum size of aggregate as indicated above. Since the experimental results show that size of aggregate does not affect the cube strength of concrete and punching shear strength of slabs, only specimens cast from concrete with maximum aggregate size of 20mm are chosen for analysis, i.e. SS8, SS9 and SS11. As in the previous group, the slabs were simply supported at four edges and centrally loaded. The loads were applied through a circular steel plate. Since the diameter of loaded area is similar to the thickness of slabs, the slab was discretised by two layers of solid elements to avoid large aspect ratio (Figure 6.11). The dimensions such as bar sizes and spacings were scaled linearly (i.e. all slabs have almost the same percentage of reinforcement as shown in table 6.6.)

The predicted mode of failure of all three slabs was punching shear. In order to compare the structural response, numerical predictions were plotted in non-dimensional format. All three slabs predicted almost exactly similar response (Figures 6.12-6.17) regardless of the scale of slab.

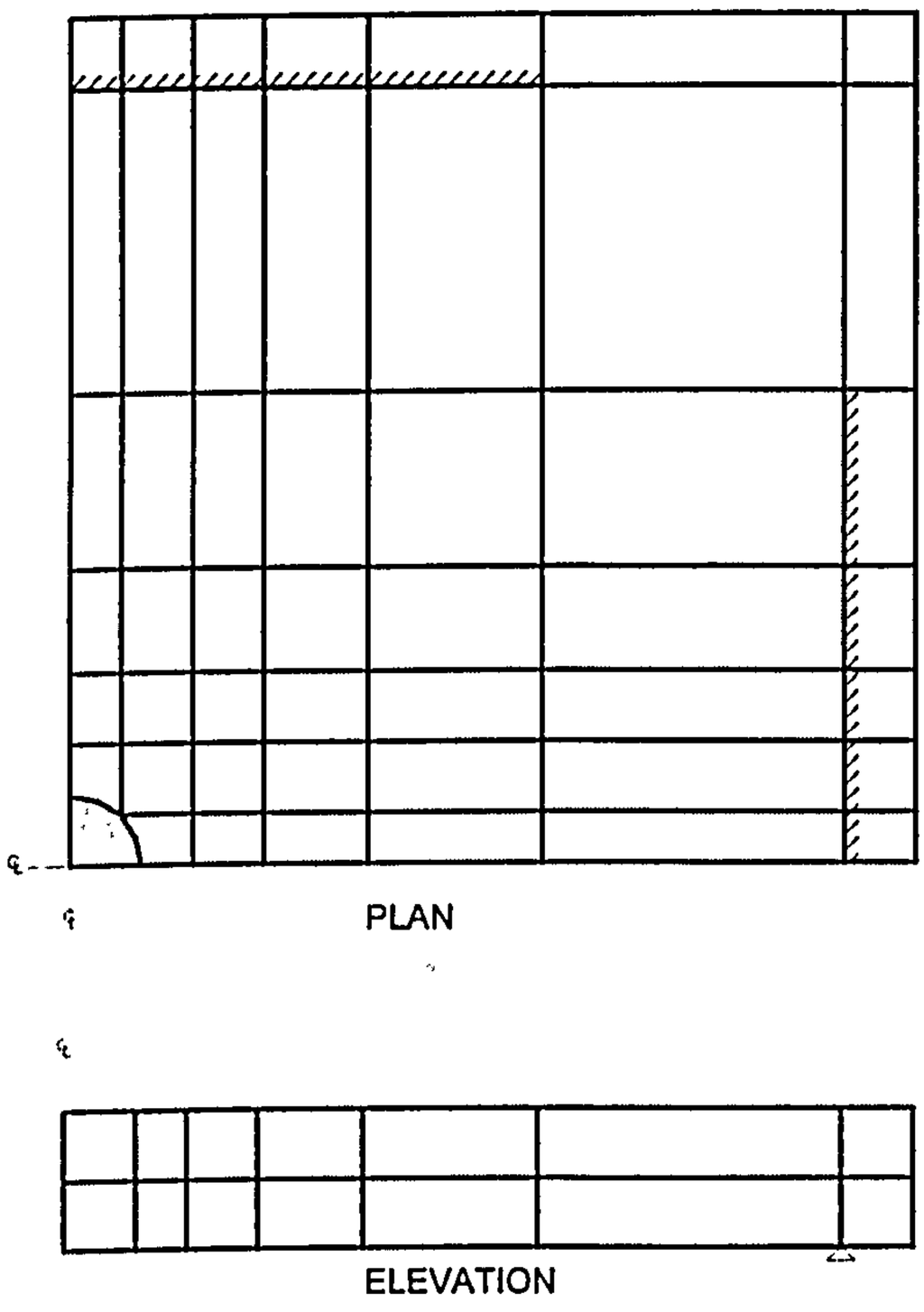

Figure 6.11 : Arrangement of mesh for SS8-SS11 (and V1-V5)

Table 6.6 : Details and Predictions for slabs SS8-SS11 (Regan)

Slab	f_{cu} (N/mm^2)	Dimensions				Flexural steel	P_{test} (kN)	Num/Exp failure load
		h(mm)	d(mm)	D(mm)	l(mm)			
SS8	43.6	250	200	250	2745	Y25@250	825.0	1.038
SS9	41.6	160	128	160	1800	Y16@160	390.0	0.886
SS11	41.6	80	64	80	900	Y8 @ 80	117.0	0.769

D = size of loaded area, ρ=0.90% for all the slabs.

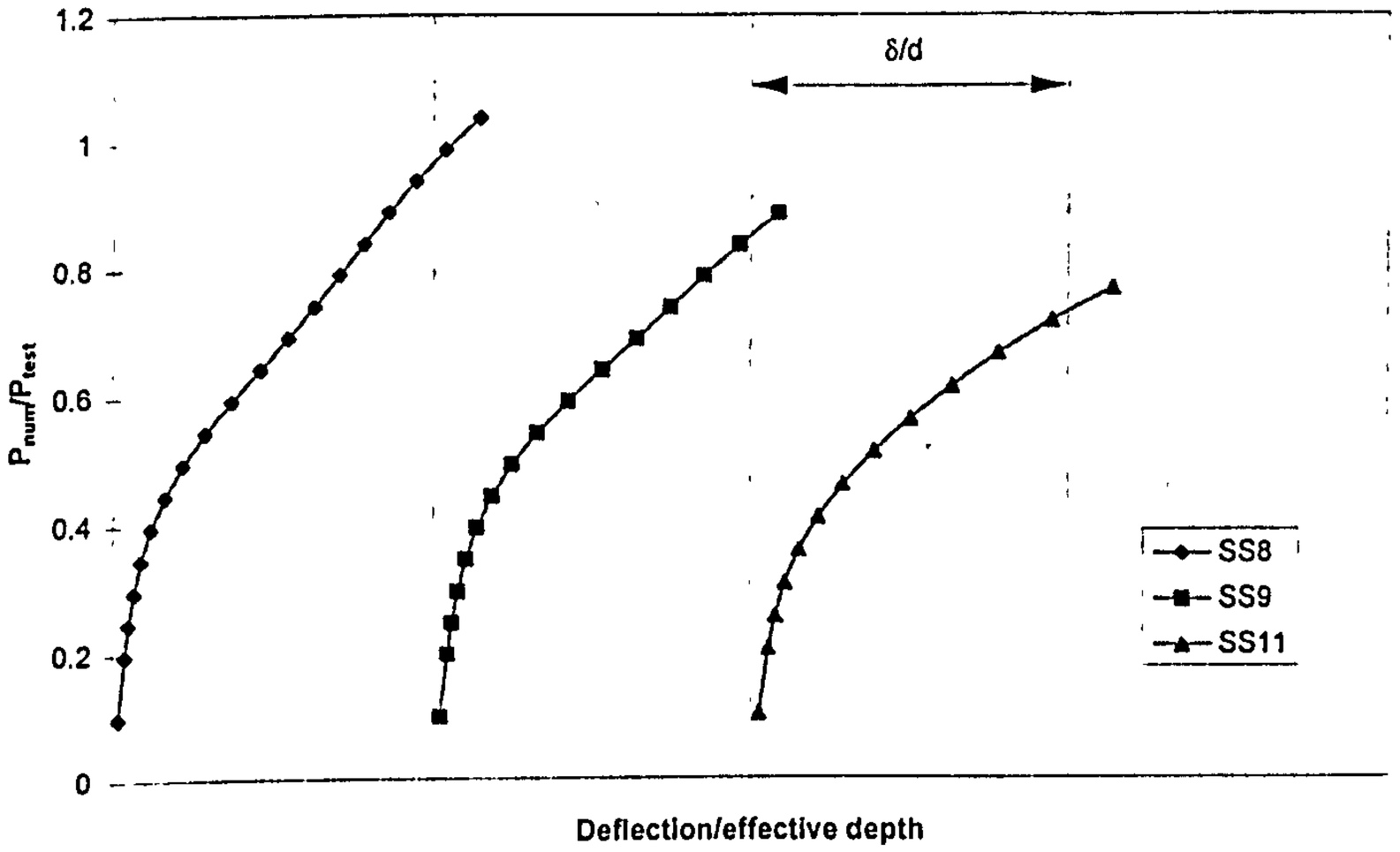

Figure 6.12 : Numerical load-deflection response (SS8, SS9 and SS11)
P_{num} = Numerical ultimate load

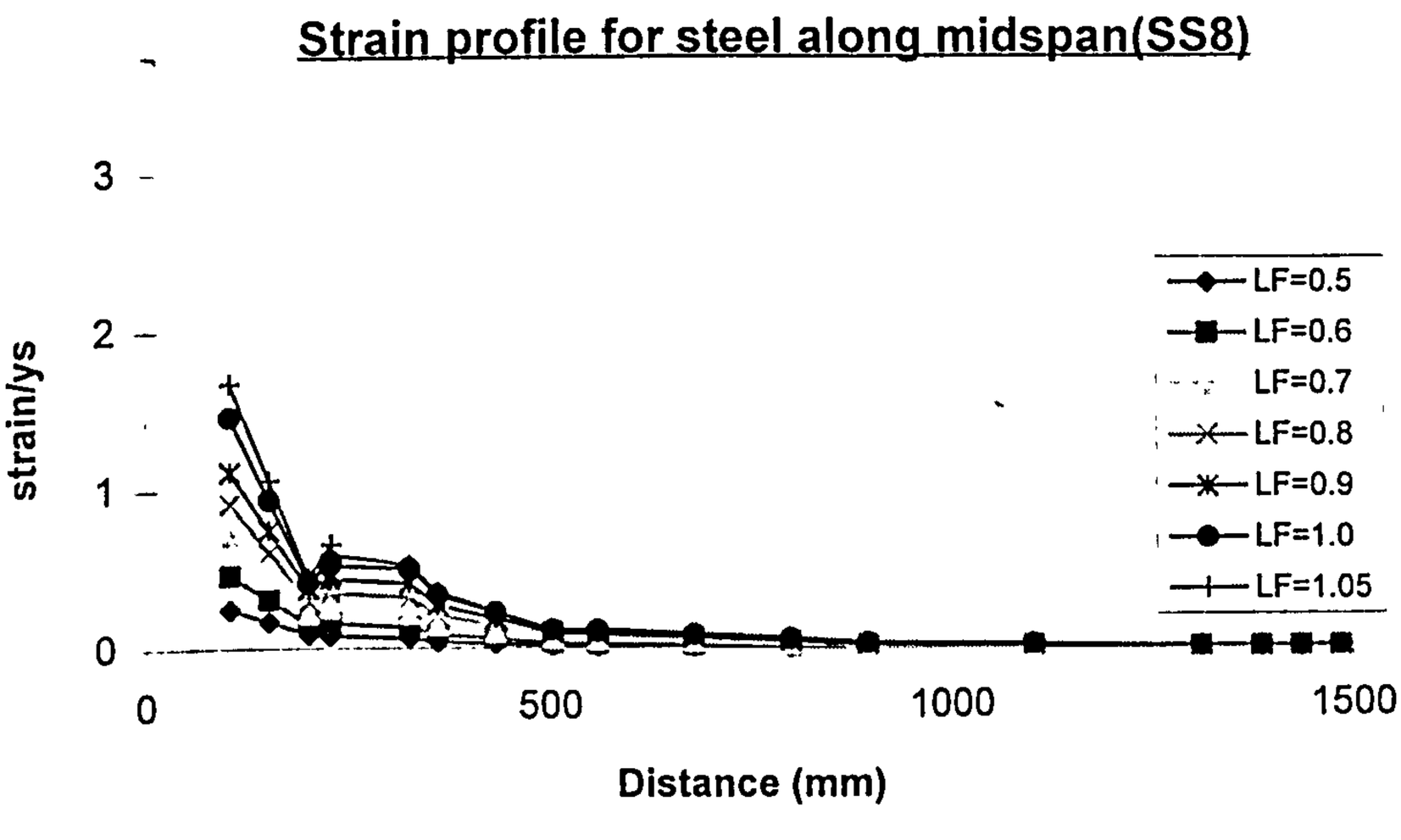

Figure 6.13 : Predicted strain-profile for flexural steel along mid-span (SS8)

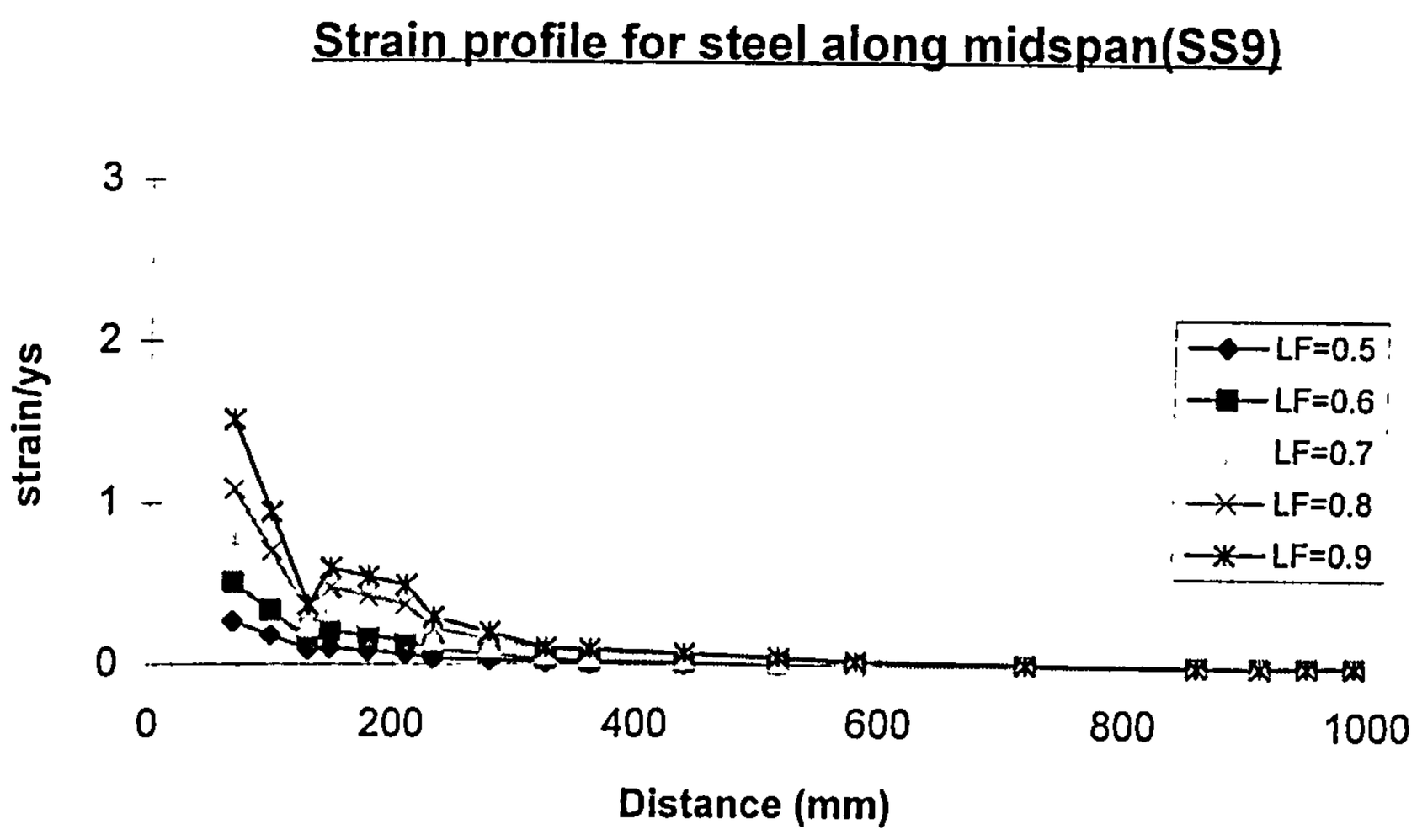

Figure 6.14 : Predicted strain-profile for flexural steel along mid-span (SS9)

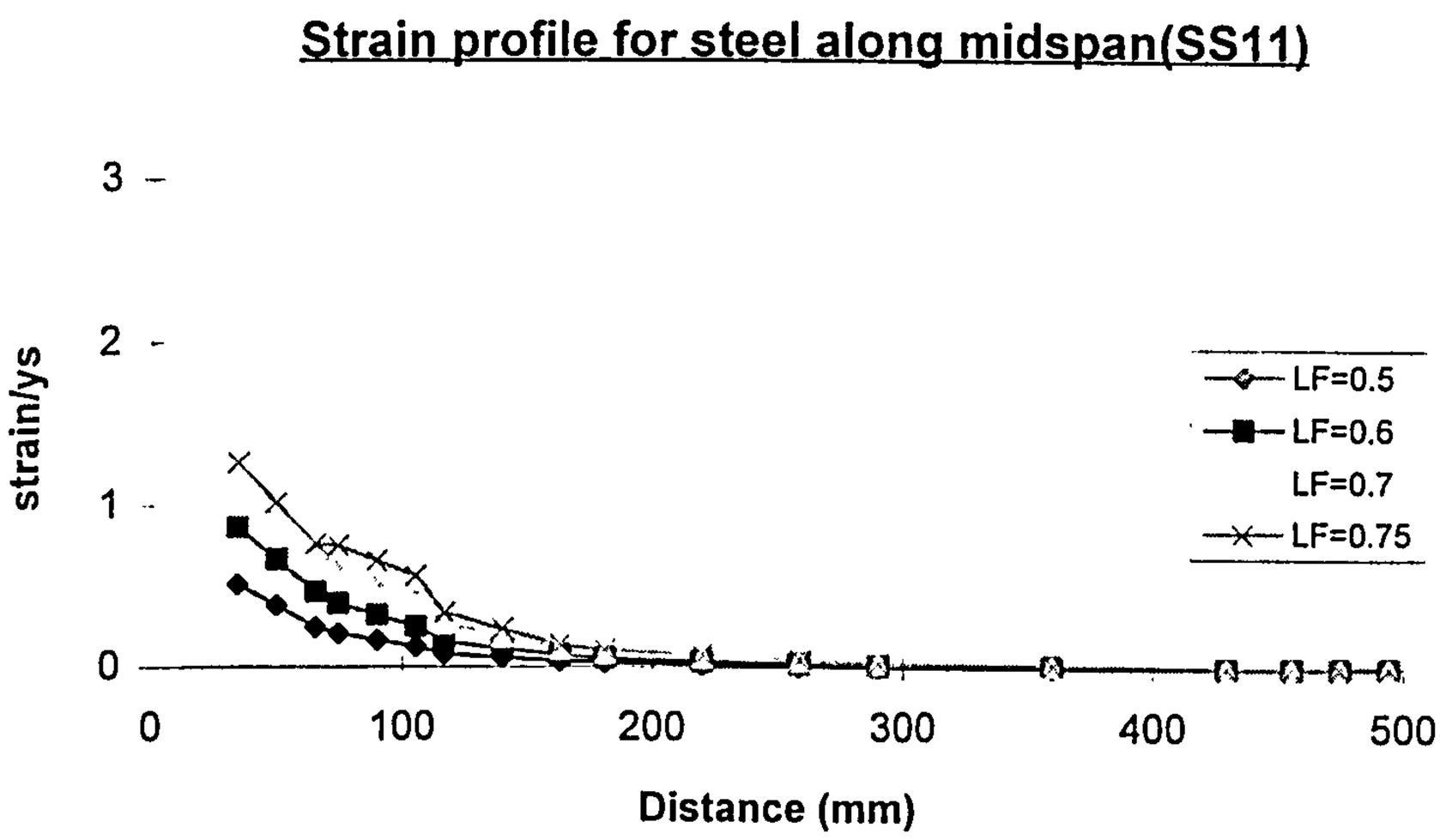

Figure 6.15 : Predicted strain-profile for flexural steel along mid-span (SS11)

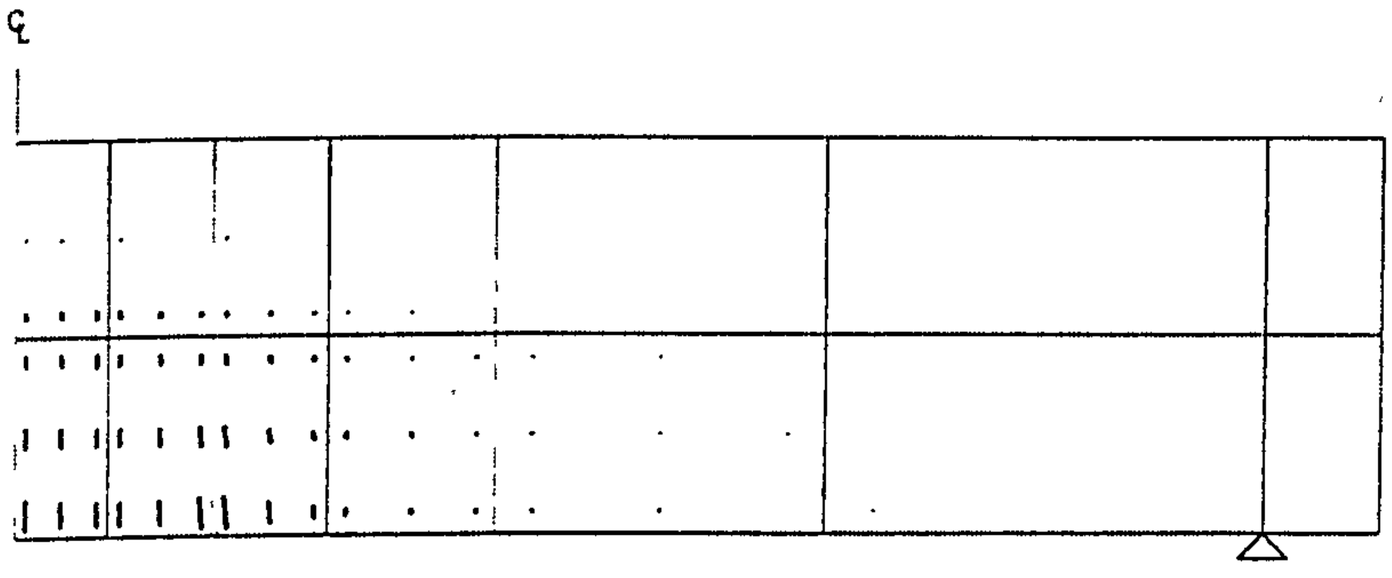

LF=0.70

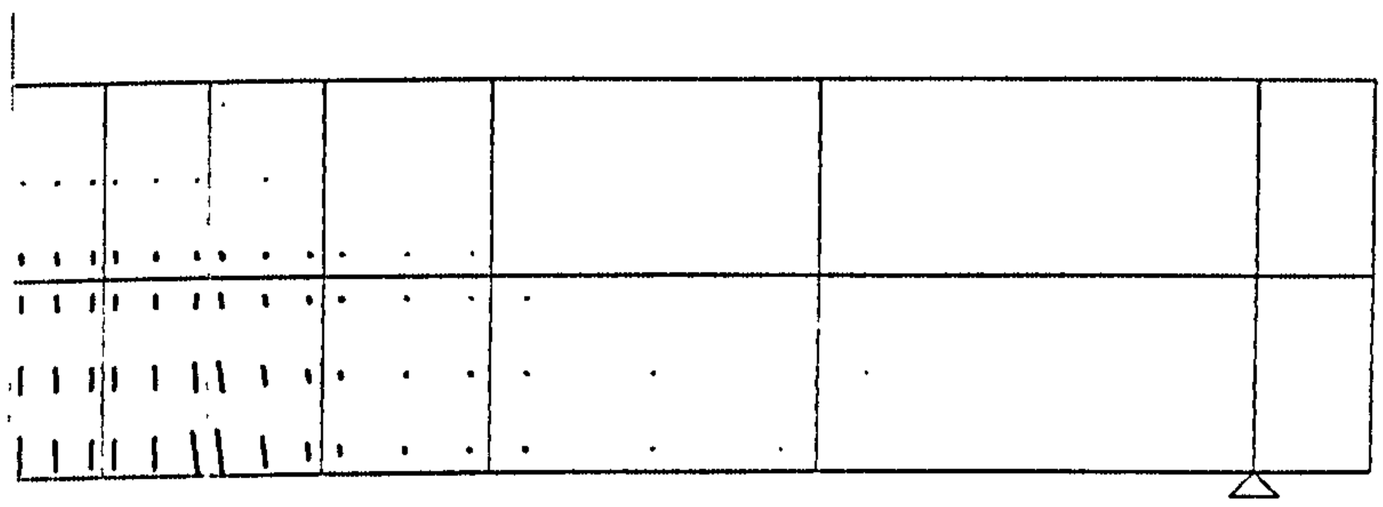

LF=0.80

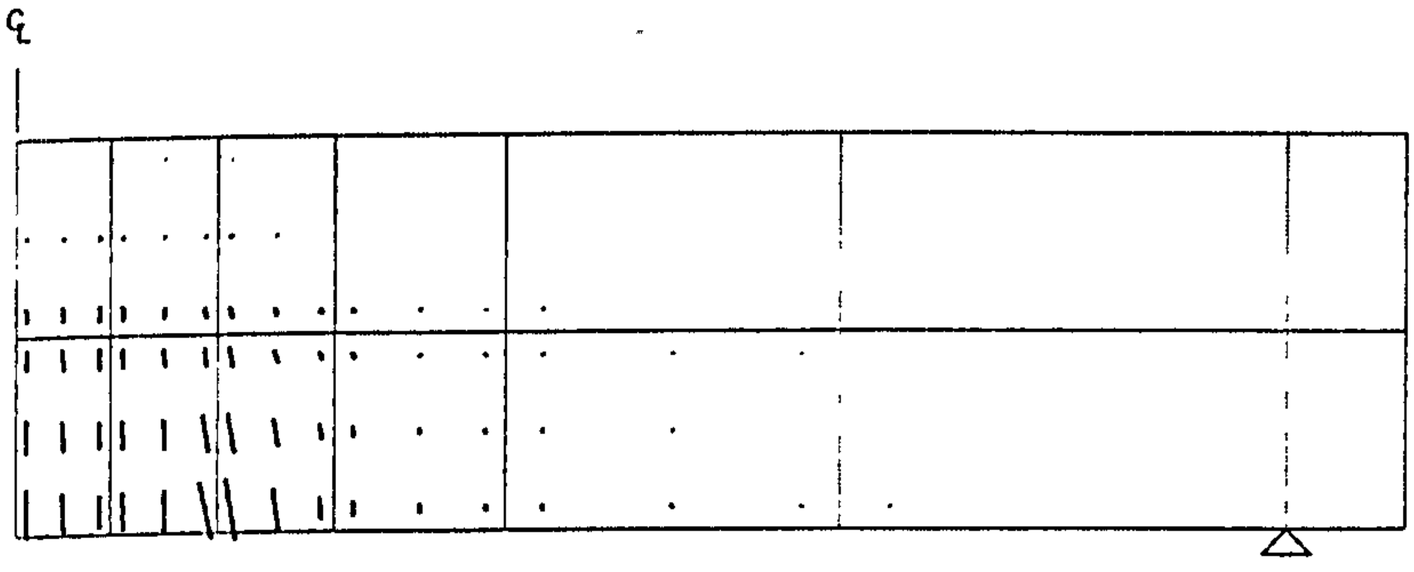

LF=0.90

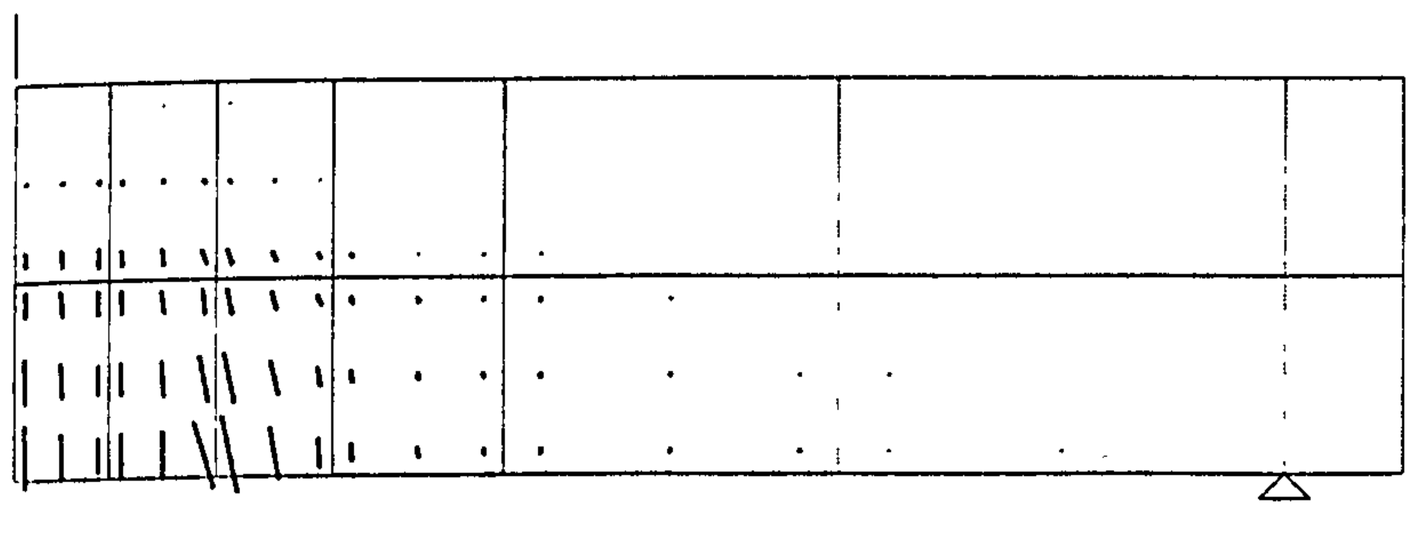

LF=1.00

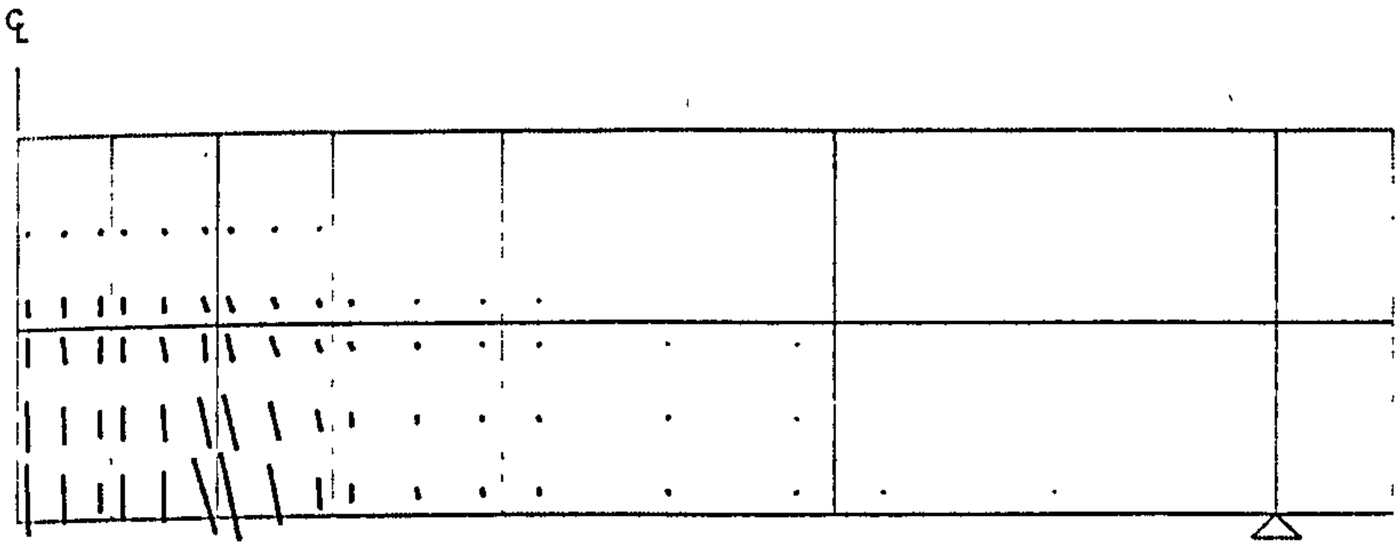

LF=1.05(ultimate Load)

Figure 6.16 Crack Pattern for slab "SS8"

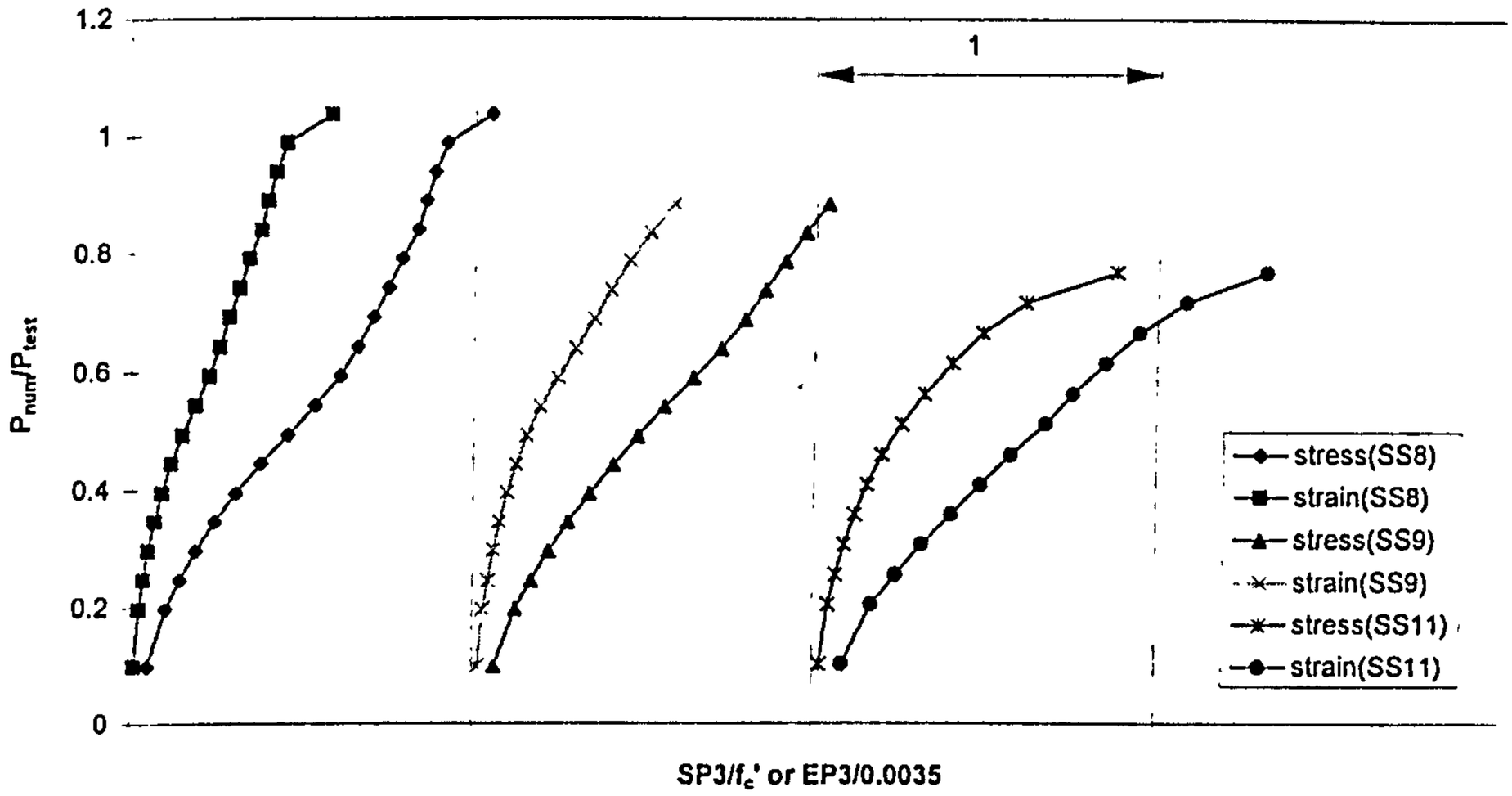

Figure 6.17 : Principal compressive stress and strain variation in concrete

6.3.2.3 Size of loaded area (V1-V5)

The thickness of these slabs was 150mm. The overall dimensions was 1.6x1.6m and the slabs were simply supported on all four edges giving an effective span of 1.5m. They were reinforced with 12mm bars at 120mm centres both ways (ρ=0.80%). The mean effective depth was 118mm. The only significant variable in these slabs was the detail of loaded area. In slabs V1-V4 the size of loading plate are varied, while slab V5 the load was applied through a precast concrete cylinder cast into the slab. In the present analysis, the applied load was simulated by uniformly distributed load over an element representing the loading stub (Figure 6.11).

The predicted mode of failure of all the slabs was punching shear. Figure 6.19 shows that the size of loaded area does not affect the deflection of the slabs, but small size of loaded area reduced the failure load of the slab due to the local crushing (Figure 6.18, slab V1 shows high compressive stress at a relatively low load level). It can be seen that present model predicted reasonably accurate ultimate loads for these slabs (Table 6.7).

Table 6.7 : Details and Predictions for specimens SS1-SS7 (Regan)

Slab	f_{cu} (N/mm^2)	Loaded area (mm)	P_{test} (kN)	Failure Mode	Num/Exp failure load
V1	32.30	diameter 54	170.0	s	0.939
V2	29.30	diameter 170	280.0	s	0.874
V3	34.30	diameter 110	265.0	s	0.996
V4	40.40	102 x 102	285.0	s	0.960
V5	35.20	diameter 150	285.0	s	1.010

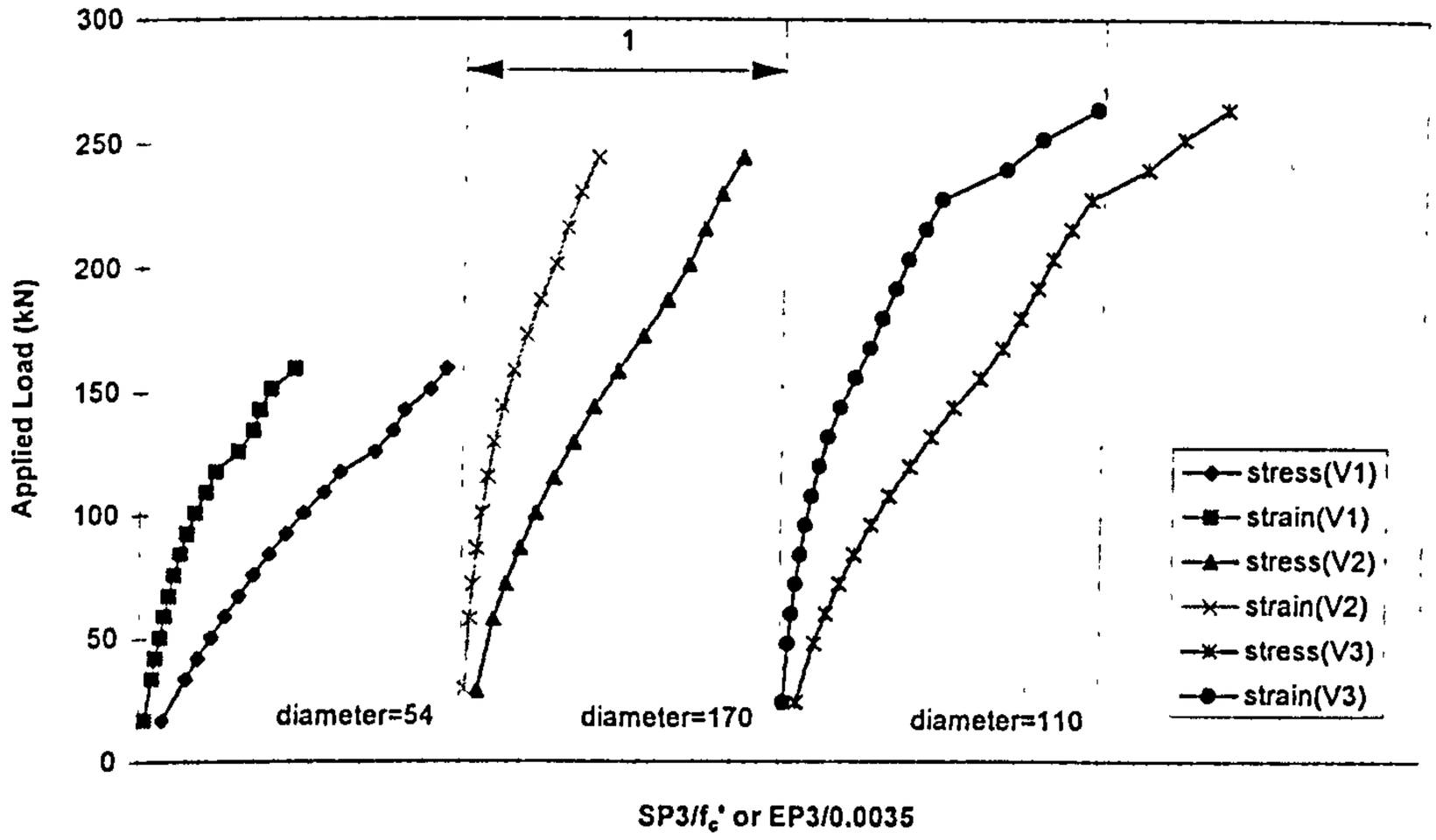

Note: SP3=σ_3=maximum compressive principal stress

EP3=ε_3=maximum compressive principal strain

Figure 6.18 : Principal compressive stress-strain relationship of concrete (Effect of size of loaded area)

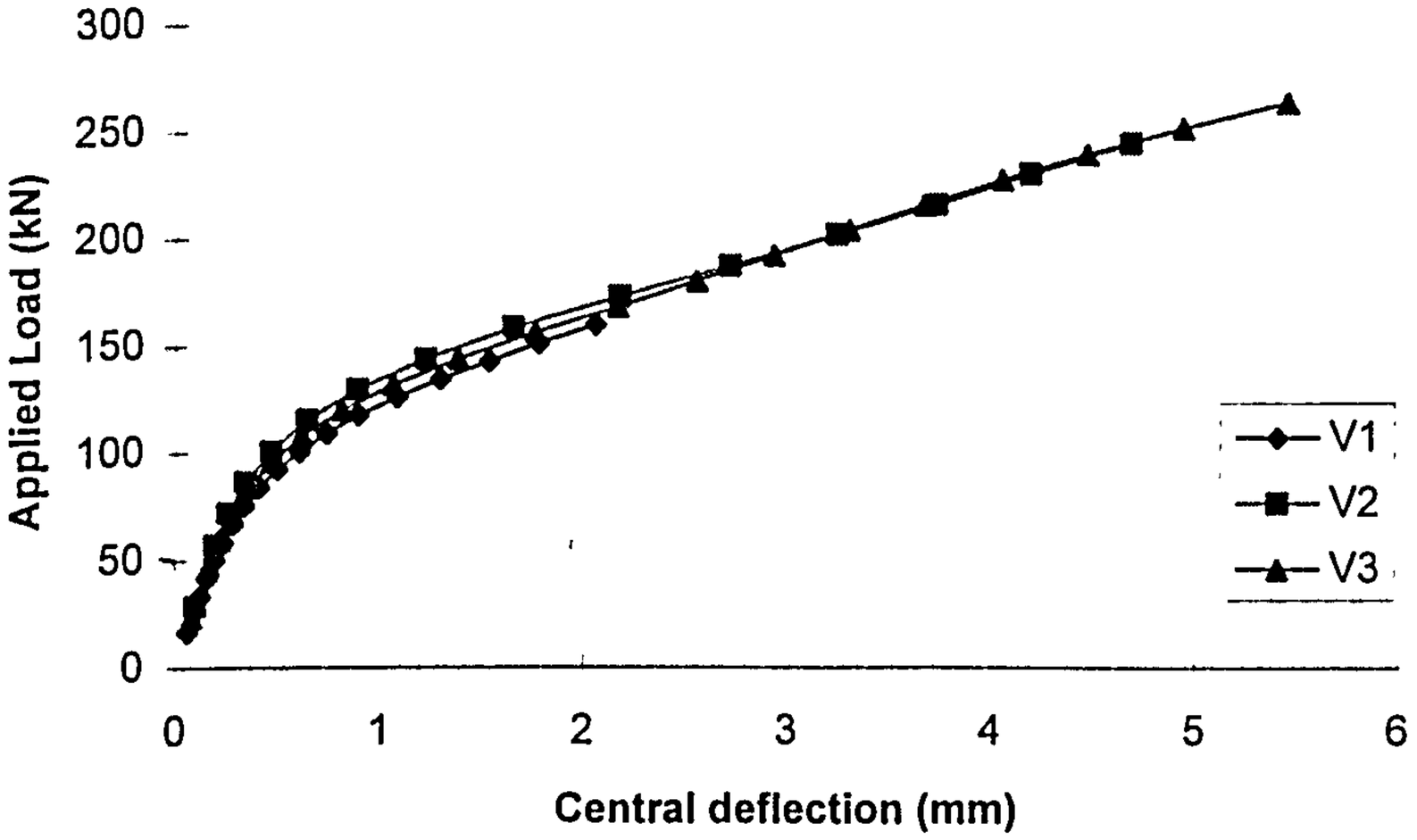

Figure 6.19 : Load-deflection response for specimens V1, V2 and V3

6.3.2.4 Shear span (SP1-SP18)

The specimens in this series were square slabs with uniformly distributed reinforcement in two directions and loaded by square columns. Six types of meshes were used depending on the loaded area, span, and thickness of slab as shown in Figure 6.20. The cube strength of concrete for slabs SP12 and SP13 was 15.40 N/mm^2

which is very low indeed (concrete strength for Kotsovos' model ranges from 18.75 N/mm^2 to 81.25 N/mm^2 in terms of cube strength). Therefore, the cube strength of concrete for these two slabs was taken as 18.75 N/mm^2. This has perhaps lead to some inaccuracy.

Numerically, all slabs failed in punching shear. From the results of this analysis, it can be seen that for slabs with a span-depth ratio of 4.67 or less (a_v/d less than 1.7), present model over predicted the ultimate load of the slabs except for model SP17. This may be due to the fact that for slabs with low span/depth ratio are subjected to low bending and high shear, and this results in lower principal strain in the slabs (Figure 6.21). Since the tension stiffening in present model is taken as a linear function of principal strain, low principal strain means that the concrete can carry relatively high tensile stress after cracking occurs. Consequently the stiffness deteriorates at a slower rate than what happen in real structure. Figure 6.22 shows that when span-depth ratios are low, the behaviour of slabs will be shear dominant.

Table 6.8 : Details and Predictions for slabs SP1-SP18 (Regan)

Slab	f_{cu} (N/mm^2)	d (mm)	a_v (mm)	a_v/d	l/d	ρ (%)	P_{test} (kN)	Failure Mode	Num/Exp failure load
SP1	28.70	75.0	350	4.67	11.33	1.00	197.0	s	0.827
SP2	31.60	75.0	225	3.00	8.00	1.00	227.0	s	0.894
SP3	36.00	75.0	100	1.33	4.67	1.00	235.0	s	1.226
SP4	35.20	75.0	125	1.67	4.67	1.00	185.0	s	1.035
SP5	35.20	75.0	75	1.00	4.67	1.00	338.0	s	1.193
SP8	44.60	75.0	125	1.67	4.67	0.50	172.0	s	1.005
SP9	44.60	75.0	75	1.00	4.67	0.50	284.0	s	1.014
SP10	48.10	75.0	75	1.00	4.67	1.00	421.0	s	1.204
SP11	48.10	75.0	125	1.67	4.67	1.00	182.0	s	1.302
SP12*	15.40*	75.0	75	1.00	4.67	1.00	221.0	s	1.213
SP13*	15.40*	75.0	125	1.67	4.67	1.00	109.0	s	1.064
SP14	47.80	75.0	50	0.67	4.00	1.00	623.0	s	1.102
SP15	47.80	75.0	100	1.33	4.67	1.00	368.0	s	1.041
SP16	47.80	75.0	50	0.67	2.67	1.00	451.0	s	1.053
SP17	37.60	160.0	100	0.63	2.50	0.75	1099.0	s	0.955
SP18	37.60	75.0	50	0.67	2.67	0.75	142.0	y	1.318
								Average	1.090
								STDEV	0.142

d=effective depth, a_v=shear span, l=effective span

* Analysis used f_{cu}=18.75 N/mm^2

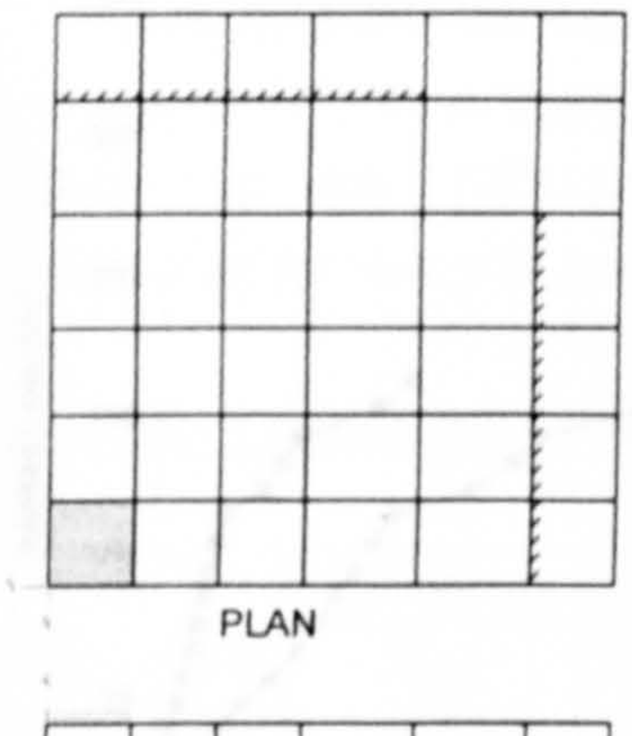

SP1

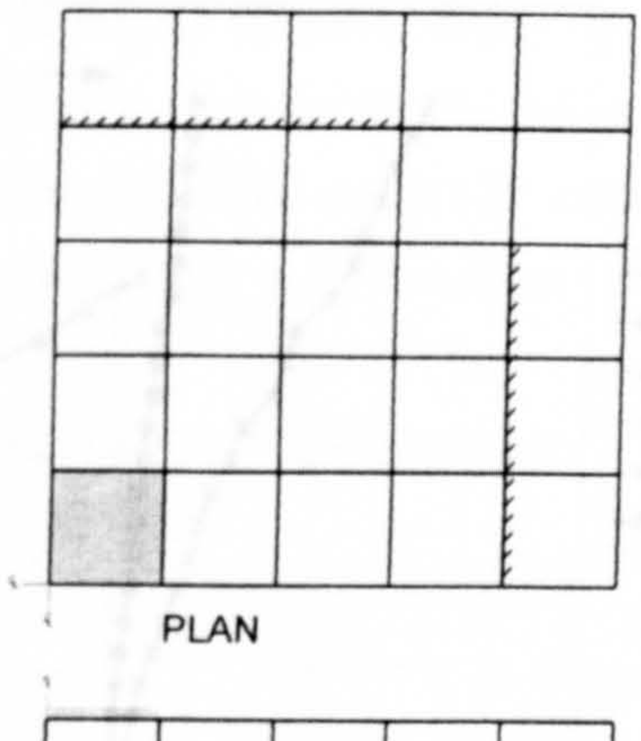

SP2

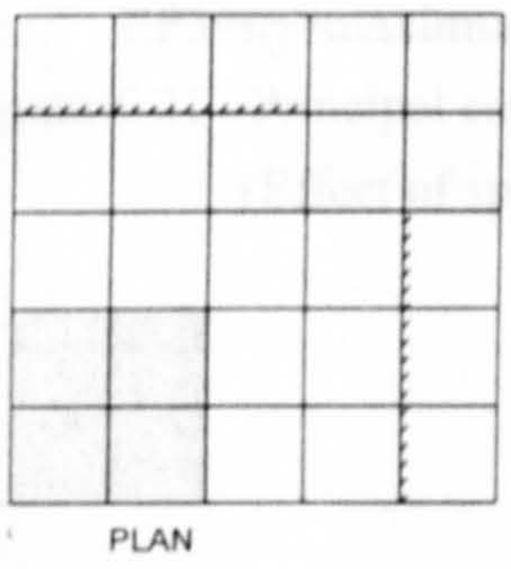

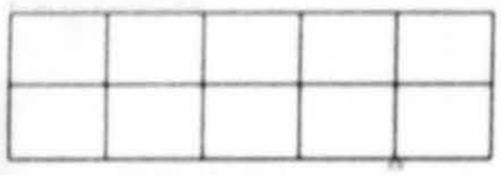

SP3,SP15

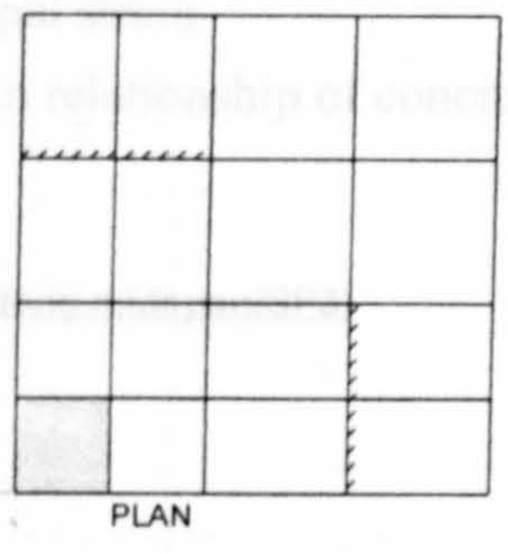

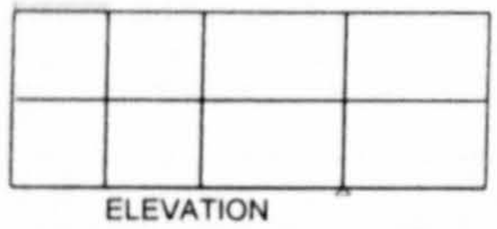

SP4,SP8,SP11,SP13

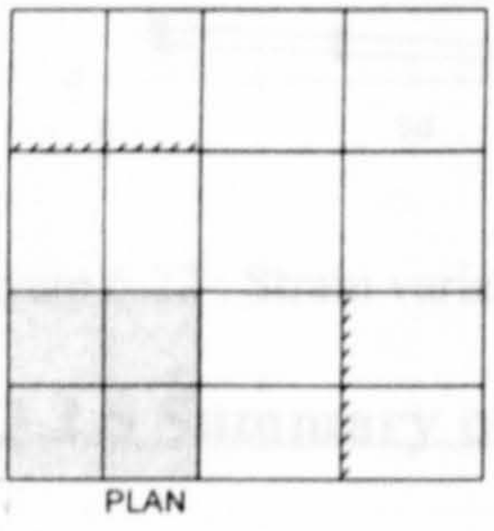

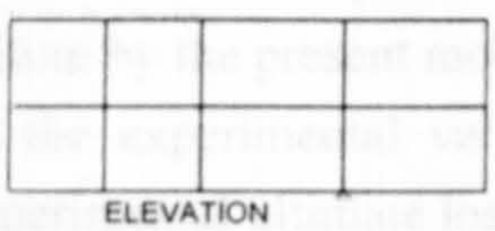

SP5,SP9,SP10,SP12,SP14,SP16

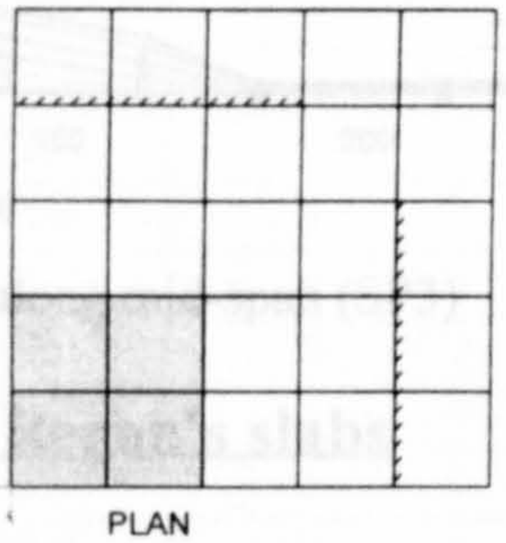

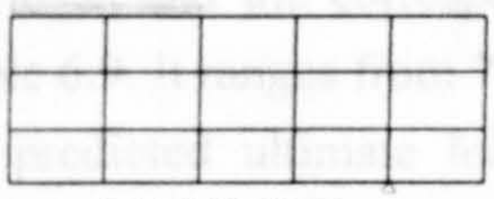

SP17,SP18

Figure 6.20 Arrangement mesh for slab SP1-SP18

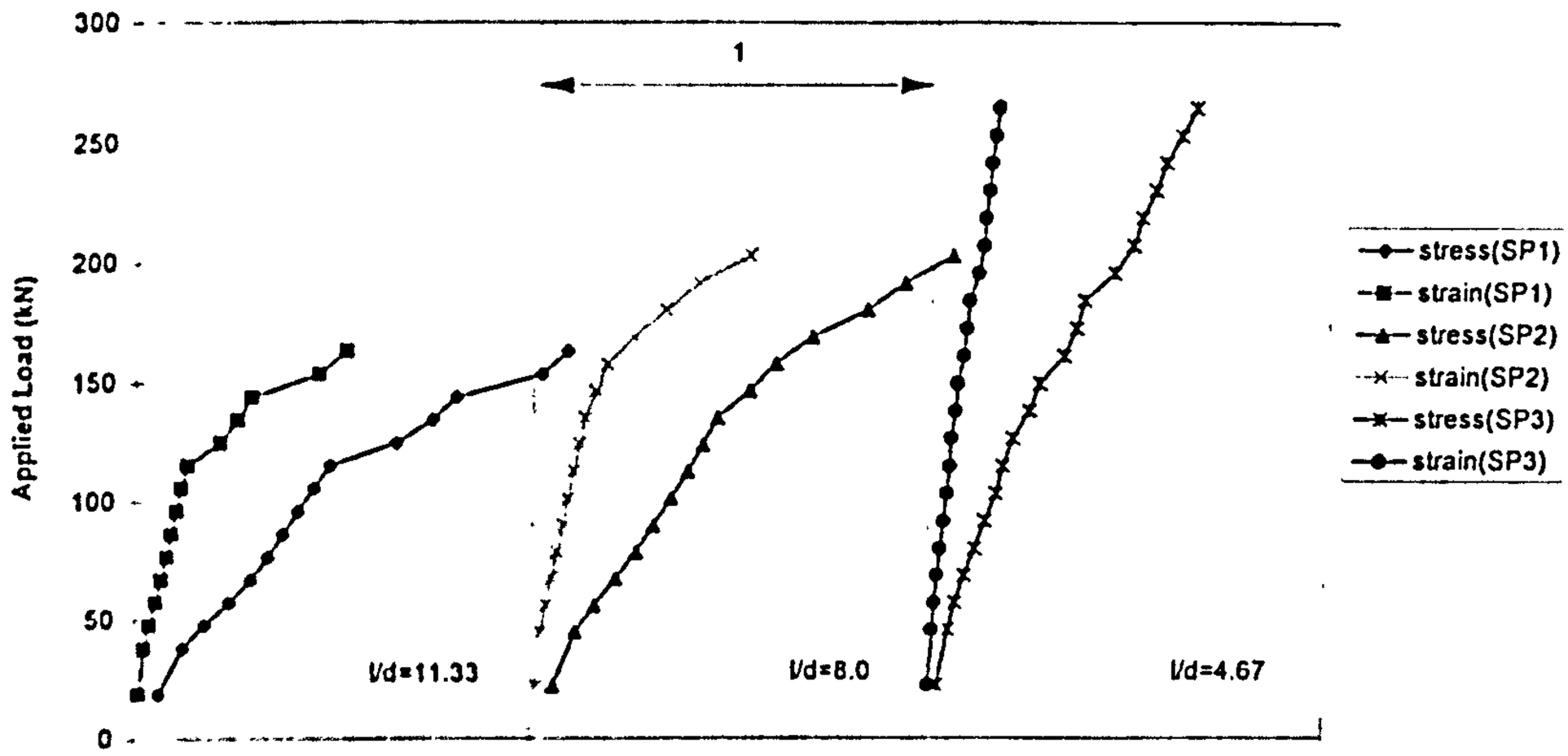

Note: SP3=σ_3=maximum compressive principal stress

EP3=ε_3=maximum compressive principal strain

Figure 6.21 : Principal compressive stress-strain relationship of concrete (Effect of span/depth ratio)

Strain profile for steel along midspan(SP3)

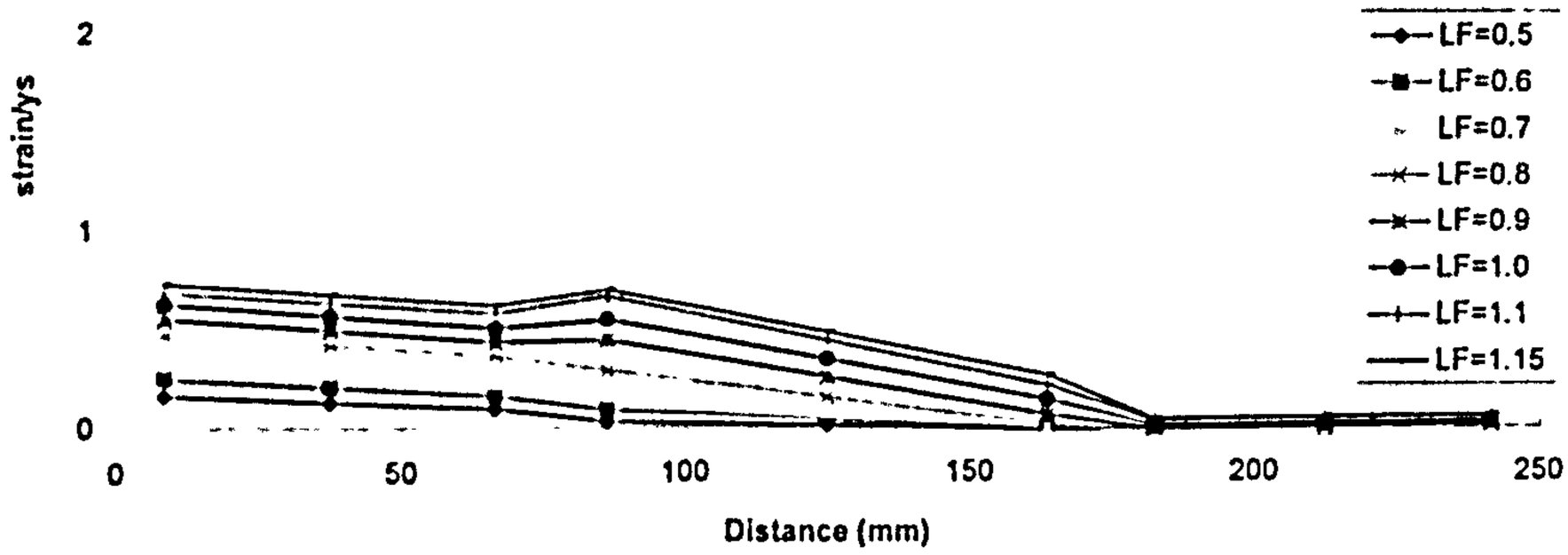

Figure 6.22 : Strain variation for flexural steel along mid-span (SP3)

6.3.2.5 Summary of predictions for Regan's slabs

A summary of the predicted ultimate loads and the corresponding mode of failure by the present model is presented in Table 6.9. It ranges from 74.2% to 125.5% of the experimental values. The average of predicted ultimate load is 94.3% of experimental ultimate load with 13.1% standard deviation. Although the ultimate load for some of the slabs was over predicted, the present model predicted correct mode of failure.

The predicted ultimate load and mode of failure by using BS8110 is presented in Table 6.10. The average of predicted ultimate load is 80.2% of experimental ultimate load with 17.0% standard of deviation. BS8110 generally underestimates ultimate load for slab with span/depth ratio less than 5 (or a_v/d less than 1.7).

Table 6.9 : Ultimate load of Regan's simply supported slab (Regan)

Slab	a_v/d	Experimental results		Numerical Predictions		P_{num}/P_{test}
		P_{test} (kN)	Failure Mode	P_{num} (kN)	Failure Mode	
SS1	10.58	194.0	s	182.6	s	0.841
SS2	10.58	176.0	s	134.5	s	0.764
SS3	10.58	194.0	s	154.0	s	0.792
SS4	10.58	194.0	s	144.0	s	0.742
SS5	10.32	165.0	s	146.9	s	0.890
SS6	10.32	165.0	s	130.5	s	0.791
SS7	10.32	186.0	y	163.1	y	0.877
SS8	6.24	825.0	s	856.0	s	1.038
SS9	6.41	390.0	s	345.6	s	0.886
SS11	6.41	117.0	s	90.0	s	0.769
V1	6.13	170.0	s	160.0	s	0.939
V2	5.64	280.0	s	245.0	s	0.874
V3	5.89	265.0	s	264.0	s	0.996
V4	5.92	285.0	s	274.0	s	0.960
V5	5.72	285.0	s	288.0	s	1.010
SP1	4.67	197.0	s	163.0	s	0.827
SP2	3.00	227.0	s	203.0	s	0.894
SP3	1.33	235.0	s	288.0	s	1.226
SP4	1.67	185.0	s	191.5	s	1.035
SP5	1:00	338.0	s	403.2	s	1.193
SP8	1.67	172.0	s	172.8	s	1.005
SP9	1.00	284.0	s	288.0	s	1.014
SP10	1.00	421.0	s	507.0	s	1.204
SP11	1.67	182.0	s	237.0	s	1.302
SP12	1.00	221.0	s	268.0	s	1.213
SP13	1.67	109.0	s	116.0	s	1.064
SP14	0.67	623.0	s	686.4	s	1.102
SP15	1.33	368.0	s	383.0	s	1.041
SP16	0.67	451.0	s	475.0	s	1.053
SP17	0.63	1099.0	s	1049.0	s	0.955
SP18	0.67	142.0	y	187.2	fp	1.318
					Average	0.988
					STDEV	0.161

y=flexural failure, s=shear failure, fp=flexural punching

Table 6.10 : Ultimate Load and Mode of failure predicted by using BS8110 (Regan)

Slab	a_v/d	Experiment results		Predictions by BS8110		P_u/P_{test}
		P_{test} (kN)	Failure Mode	P_u (kN)	Failure Mode	
SS1	10.58	194.0	s	183.2	s	0.945
SS2	10.58	176.0	s	177.4	s	1.008
SS3	10.58	194.0	s	171.1	s	0.882
SS4	10.58	194.0	s	180.1	s	0.928
SS5	10.32	165.0	s	153.8	y	0.930*
SS6	10.32	165.0	s	149.5	y	0.906*
SS7	10.32	186.0	y	163.9	y	0.881
SS8	6.24	825.0	s	742.2	s	0.900
SS9	6.41	390.0	s	339.9	s	0.871
SS11	6.41	117.0	s	100.5	c	0.864*
V1	6.13	170.0	s	125.1	c	0.736*
V2	5.64	280.0	s	287.9	s	1.028
V3	5.89	265.0	s	254.8	c	0.962*
V4	5.92	285.0	s	236.3	c	0.829*
V5	5.72	285.0	s	276.9	s	0.971
SP1	4.67	197.0	s	155.6	s	0.790
SP2	3.00	227.0	s	160.7	s	0.708
SP3	1.33	235.0	s	176.2	s	0.750
SP4	1.67	185.0	s	144.4	s	0.780
SP5	1.00	338.0	s	233.2	s	0.690
SP8	1.67	172.0	s	119.6	s	0.695
SP9	1.00	284.0	s	193.1	s	0.680
SP10	1.00	421.0	s	243.4	s	0.578
SP11	1.67	182.0	s	147.3	c	0.803*
SP12	1.00	221.0	s	189.9	s	0.859
SP13	1.67	109.0	s	102.7	c	0.942*
SP14	0.67	623.0	s	294.5	c	0.473*
SP15	1.33	368.0	s	208.6	s	0.567
SP16	0.67	451.0	s	147.3	c	0.327*
SP17	0.63	1099.0	s	616.4	c	0.561*
SP18	0.67	142.0	y	144.5	c	1.018*
					Average	0.802
					STDEV	0.170

N.B. c=local crushing

s=shear failure

y=flexure failure

* wrong mode of failure predicted

6.4 Slabs with shear reinforcement

6.4.1 Full scale slabs tested by Chana and Desai (1992)

These slabs were 3 m square, and the thicknesses were 228mm, 240mm and 250mm. The load was applied at points equally spaced along the circumference of a circle of 2.4 m diameter and supported by a square column at the centre of slab. These slabs were reinforced by stirrup as shear reinforcement, and the shear reinforcements were located at perimeters at distance of 0.5d or 1.25d from column face. Specimen 1 had no shear reinforcement. Specimen 3 had the same number and location of links as specimens 2. The difference between these two specimens is how the link was anchored. Present model assumed perfect bond between concrete and steel irrespective of the detailing of reinforcement, so specimen 3 was not analysed. The details of slabs are summarised in Table 6.11. The finite element mesh for these specimens shown in the Figure 6.23.

Table 6.11 : Details of slabs C1-C9 (Chana and Desai)

Slab	f_{cu} (N/mm^2)	d (mm)	Column size	ρ (%)	Link Diameter	No of links at	
						0.5 d	1.25 d
C1	40.3	200.0	300	0.79	T8	0	0
C2	44.4	200.0	300	0.79	T8	12	12
C3	41.1	200.0	300	0.79	T8	12	12
C4	45.4	200.0	300	0.79	T8	24	24
C5	38.3	210.0	400	0.86	T10	12	20
C6	43.4	210.0	400	0.86	T10	20	12
C7	40.4	210.0	400	0.86	T10	32	0
C8	39.7	210.0	400	0.86	T8	12	20
C9	42.5	188.0	300	0.86	T8	20	28

The predicted ultimate load for specimen 1 (slab without shear reinforcement) and Specimen 2 (slab with 24 no of links) were 686.8kN and 938.4kN respectively. Clearly there is a gain of 251.6kN due to the presence of shear reinforcement. Specimens 2 to 4 are intended to study the influence of quantities of shear reinforcement on the ultimate load of the slab. The predicted results show that slab with more shear reinforcement failed at a higher ultimate load. Specimens 5 to 7 investigated the effect of different distribution of links between the perimeters. Experimental results show that the distribution of links between the two parameters (at 0.5d and 1.25d from the column) in the first failure zone had no significant effect on the shear capacity. The predicted results also show that within the variations used,

the distribution of links generally do not affect the shear capacity. The higher ultimate load predicted for specimen 6 is mainly attributed to the higher concrete strength, and this was confirmed by re-analysis specimen 6 with the concrete strength of specimen 5. Table 6.12 shows the numerical results of Chana and Desai's slabs. Mean value of (Numerical/experimental load) is 0.885 with standard deviation of 0.090. All the slabs were predicted to fail either in flexure punching or shear mode.

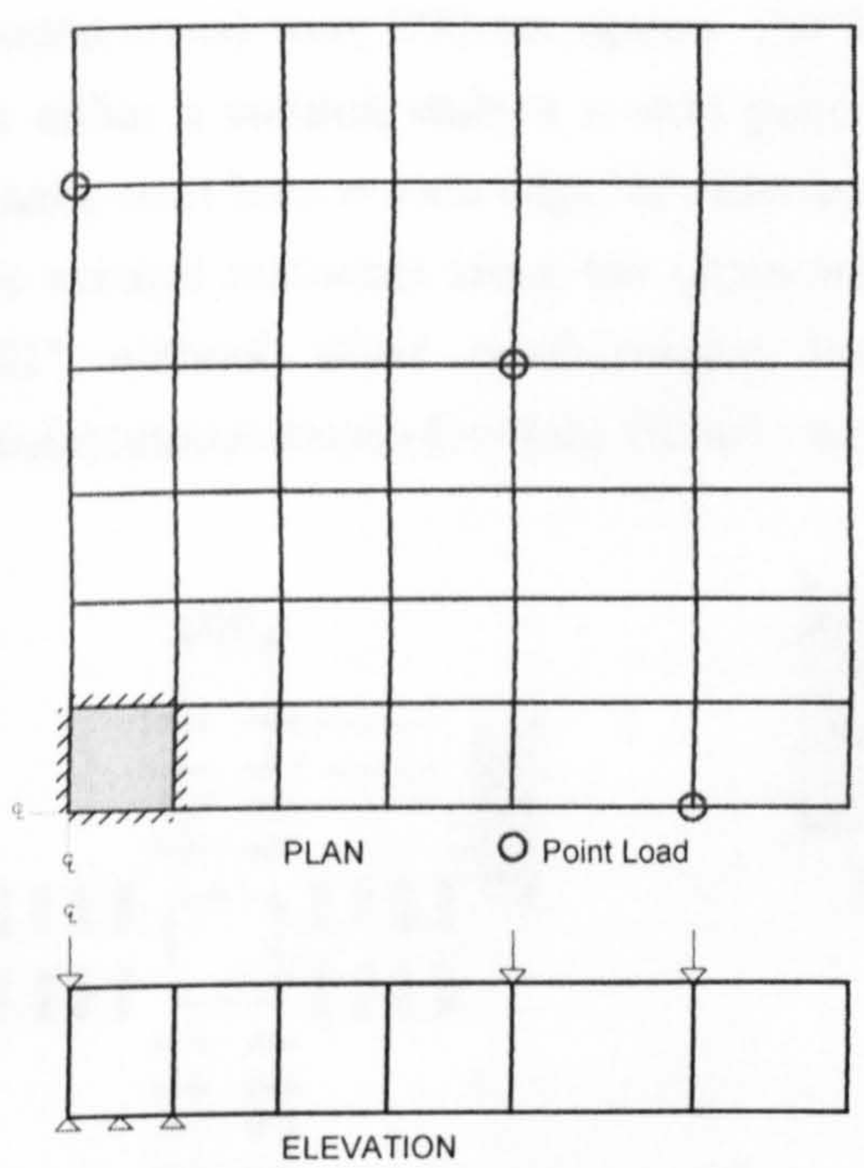

Figure 6.23 Arrangement of mesh for slabs C1-C9

Table 6.12 : Predictions for slabs C1-C9 (Chana and Desai)

Slab	Experimental results		Numerical predictions		P_{num}/P_{test}
	P_{test} (kN)	Failure Mode	P_{num} (kN)	Failure Mode	
C1	805.0	s	686.8	s	0.850
C2	1094.0	s	938.4	s	0.858
C4	1302.0	s	1142.4	fp	0.877
C5	1382.0	s	1248.0	s	0.903
C6	1283.0	s	1404.0	fp	1.094
C7	1492.0	s	1232.0	s	0.826
C8	1324.0	s	1152.0	s	0.870
C9	1135.0	s	912.0	fp	0.804
				Average	0.885
				STDEV	0.090

6.4.2 Interior slab-column connections tested by Gomes

Gomes (1991) tested a series of 10 conventional slab-column specimens with shear reinforcement. The shear reinforcement which were off-cuts from universal I beam were arranged either radially or in a cross shape on plan as shown in Figure 6.24. These specimens have the same amount of flexural steel i.e. tension steel 16mm @ 100 c/c and compression steel of T8 @ 140 c/c. The dimensions of these specimens were 200mm thick with a side length of 3000 mm. The column at the centre (or loaded areas) were 200mm square. The load was applied at the centre of slab acting on either a column stub or a steel plate. The reactions were provided by four high tensile steel bars at each edge. In order to prevent local failure at support nodal points, the vertical restraints along the edges were provided as shown in Figure 6.25. Slab "G1" without shear reinforcement was tested as a control specimen. Shear reinforcement details for slabs G2-G11 are given in Table 6.13.

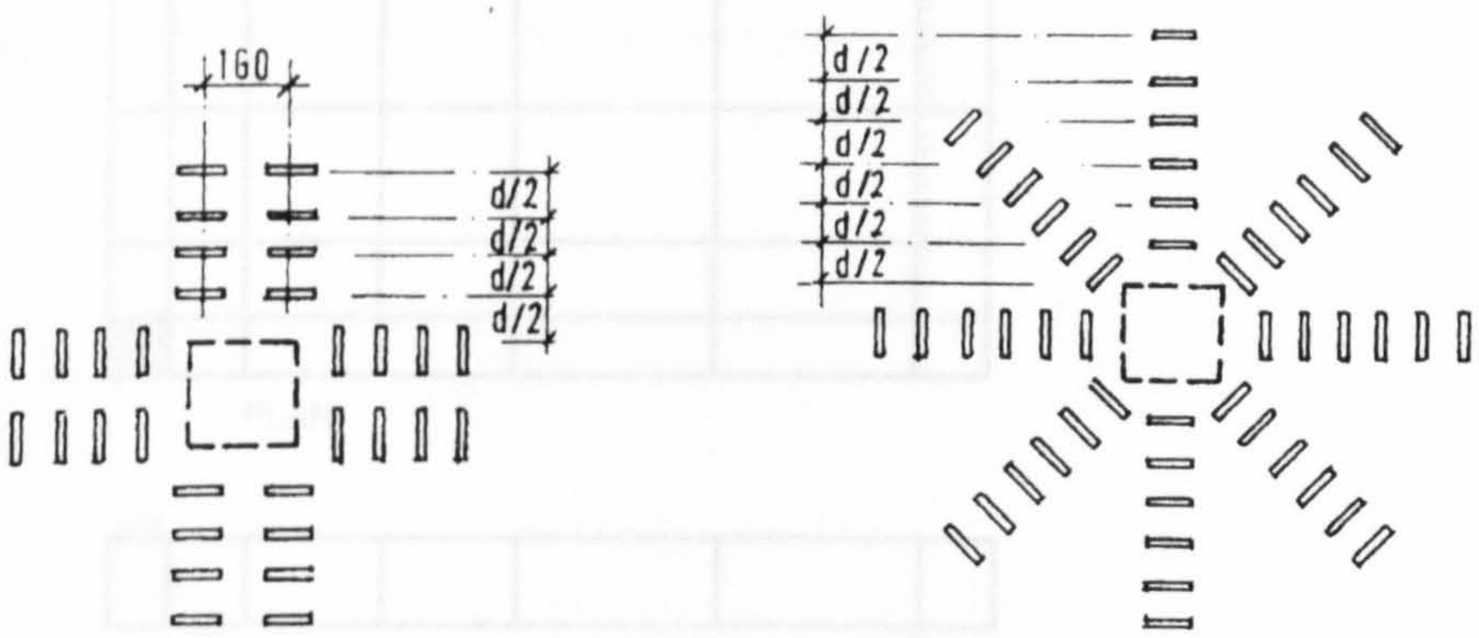

(a) Cross Pattern (b) Radial Pattern

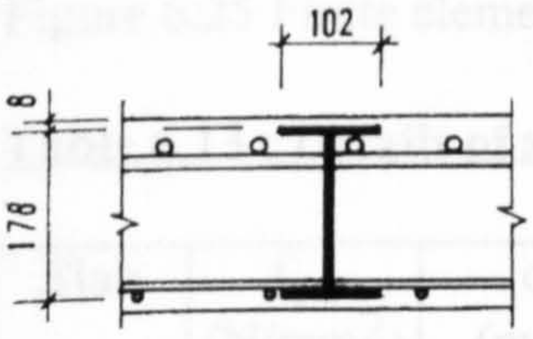

(c) Typical off-cut section

Figure 6.24 Universal I beam offcut as shear reinforcement

Figure 6.26 shows that predicted strains in shear reinforcements agree reasonably well with the experiment measurements. This figure shows that the first layer of shear reinforcement strained at 300 kN, second layer of shear reinforcement strained at 500 kN, third layer of shear reinforcement strained at 620 kN and fourth layer of shear reinforcement strained at 680 kN. This indicates that the innermost layer was the first to be strained, successive layers were strained as the load increased. As a general rule, the more remote the shear reinforcement was from the column, the higher the load needed to strain it.

Table 6.14 shows the predictions for Gomes' slabs. The mean value of numerical to experimental load is 0.876 with standard deviation of 0.091. The predicted results show that slabs with more shear reinforcement failed at higher ultimate load as observed in the experiment. Figure 6.27 shows that shear reinforcement not only increased the failure load of slabs, it also increased the ductility substantially. Analysis predicted that all slabs failed by punching. In most of the slabs, failure was accompanied by crushing of concrete (Figure 6.28).

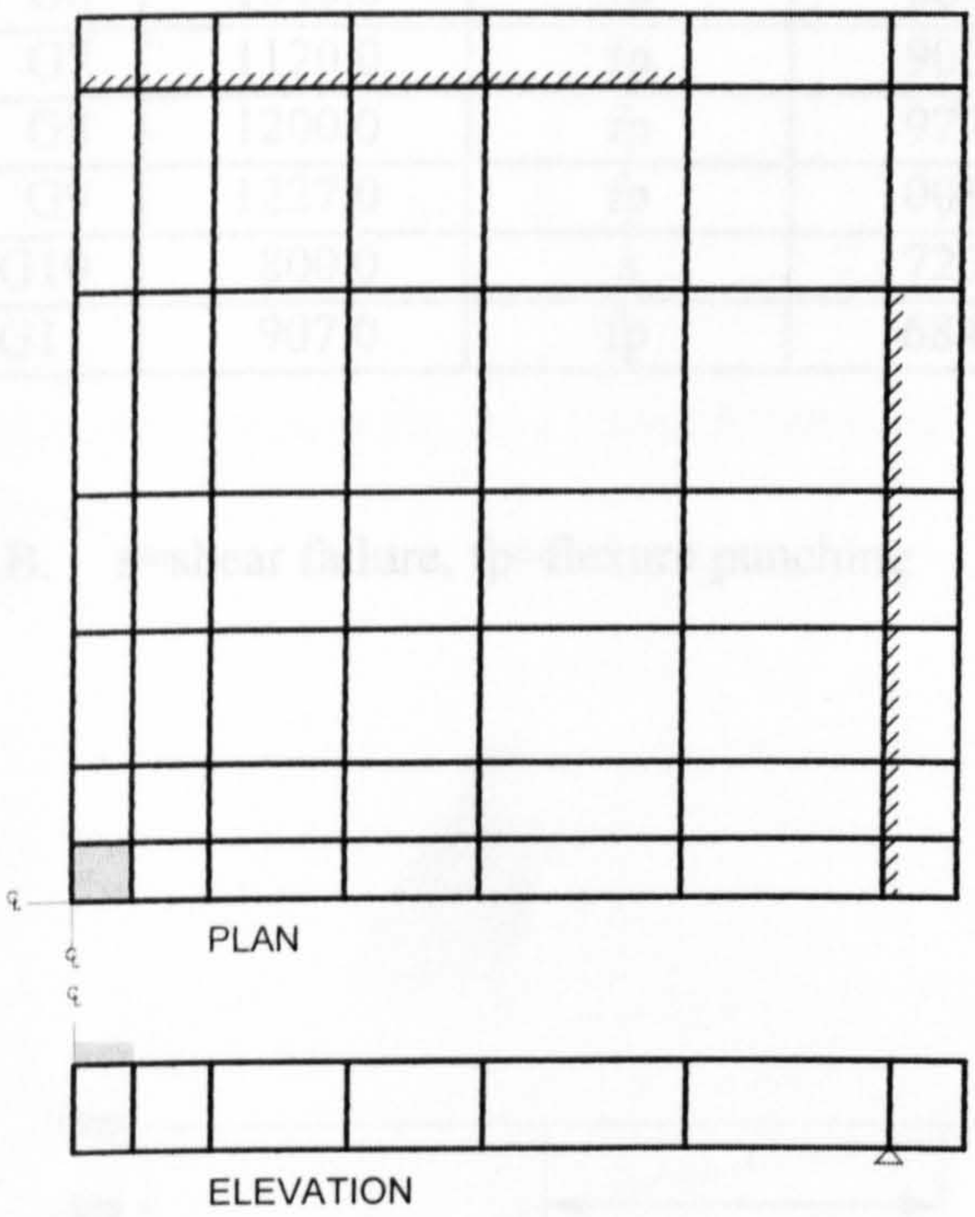

Figure 6.25 Finite element mesh for Gomes' slabs

Table 6.13 : Details of slabs G1-G11 (Gomes)

Slab	f_{cu} (N/mm^2)	d (mm)	Details of shear reinforcement		
			Pattern	layer	Area(mm^2)
G1	50.3	159.0	-	-	-
G2	43.1	153.0	cross	2	28.3
G3	49.0	158.0	cross	2	37.6
G4	40.1	159.0	cross	3	50.3
G5	43.4	159.0	cross	4	78.5
G6	46.7	159.0	radial	4	78.5
G7	42.3	159.0	radial	5	113.1
G8	42.6	159.0	radial	6	113.1
G9	50.0	159.0	radial	5	117.5
G9				4	78.5
G10	44.2	154.0	radial	5	28.3
G11	43.2	154.0	radial	5	37.6

Table 6.14 : Predictions for specimens G1-G11 (Gomes)

Slab	Test results		Numerical predictions		P_{num}/P_{test}
	P_{test} (kN)	Failure mode	P_{num} (kN)	Failure mode	
G1	560.0	s	579.6	s	1.035
G2	693.0	s	660.0	s	0.952
G3	773.0	s	690.0	s	0.893
G4	853.0	s	810.0	s	0.949
G5	853.0	s	810.0	s	0.949
G6	1040.0	fp	864.0	fp	0.831
G7	1120.0	fp	900.0	fp	0.804
G8	1200.0	fp	972.0	fp	0.810
G9	1227.0	fp	1008.0	fp	0.822
G10	800.0	s	720.0	s	0.900
G11	907.0	fp	684.0	fp	0.754
				Average	0.876
				STDEV	0.091

N.B. s=shear failure, fp=flexure punching

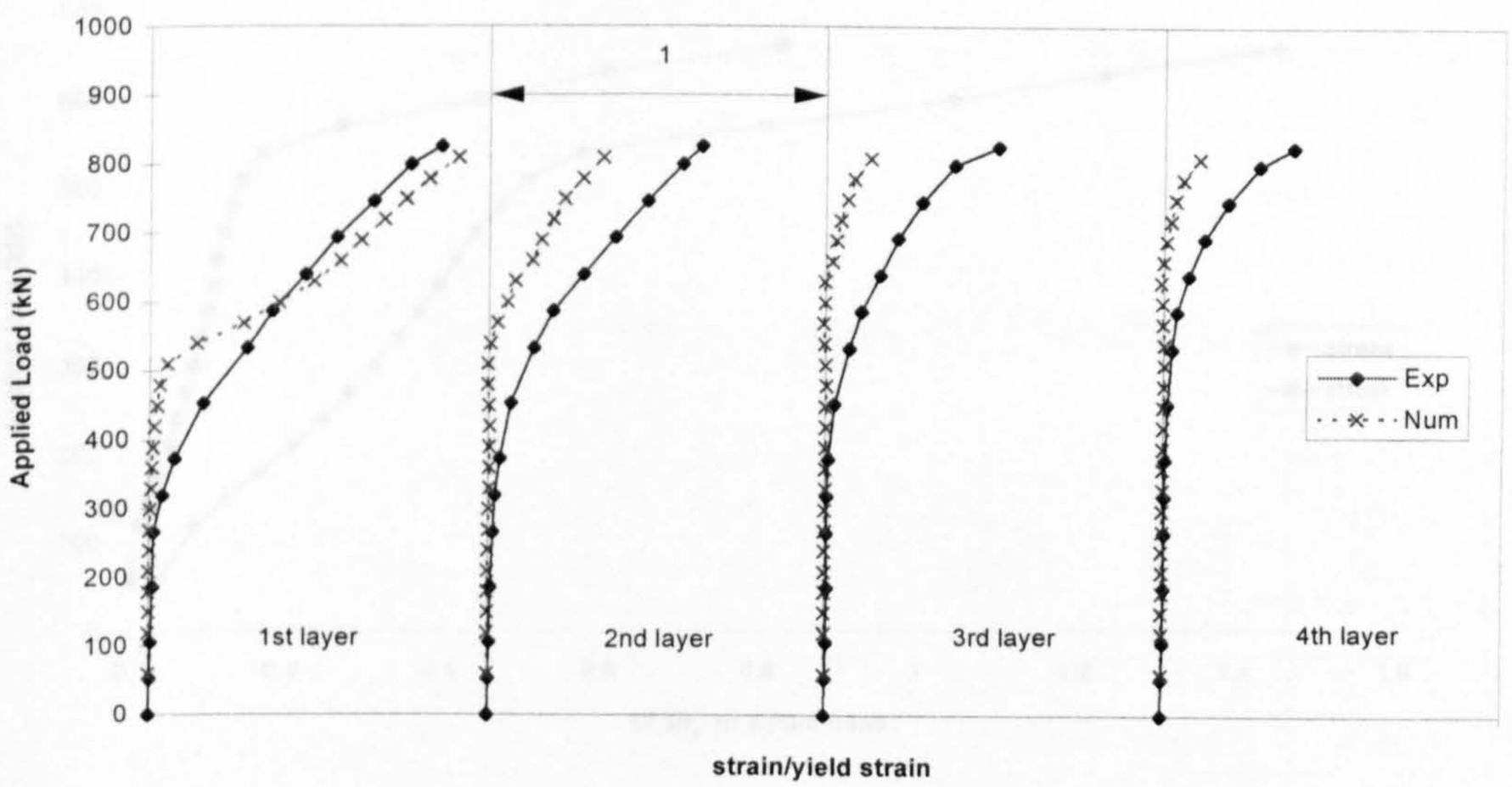

Figure 6.26 Strain in shear reinforcement (slab G5)

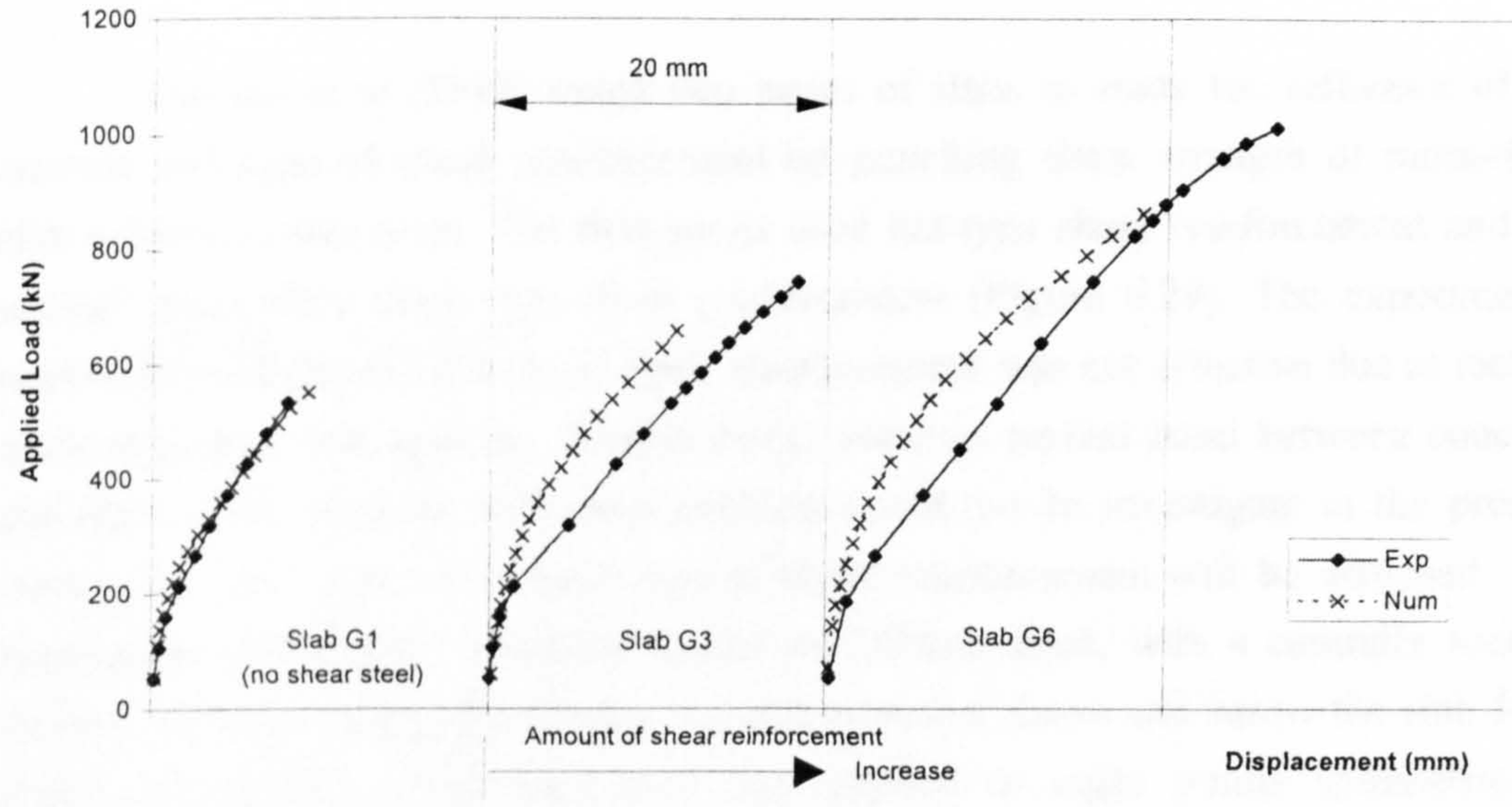

Figure 6.27 Load-deflection response for slabs "G1", "G3" and "G6"

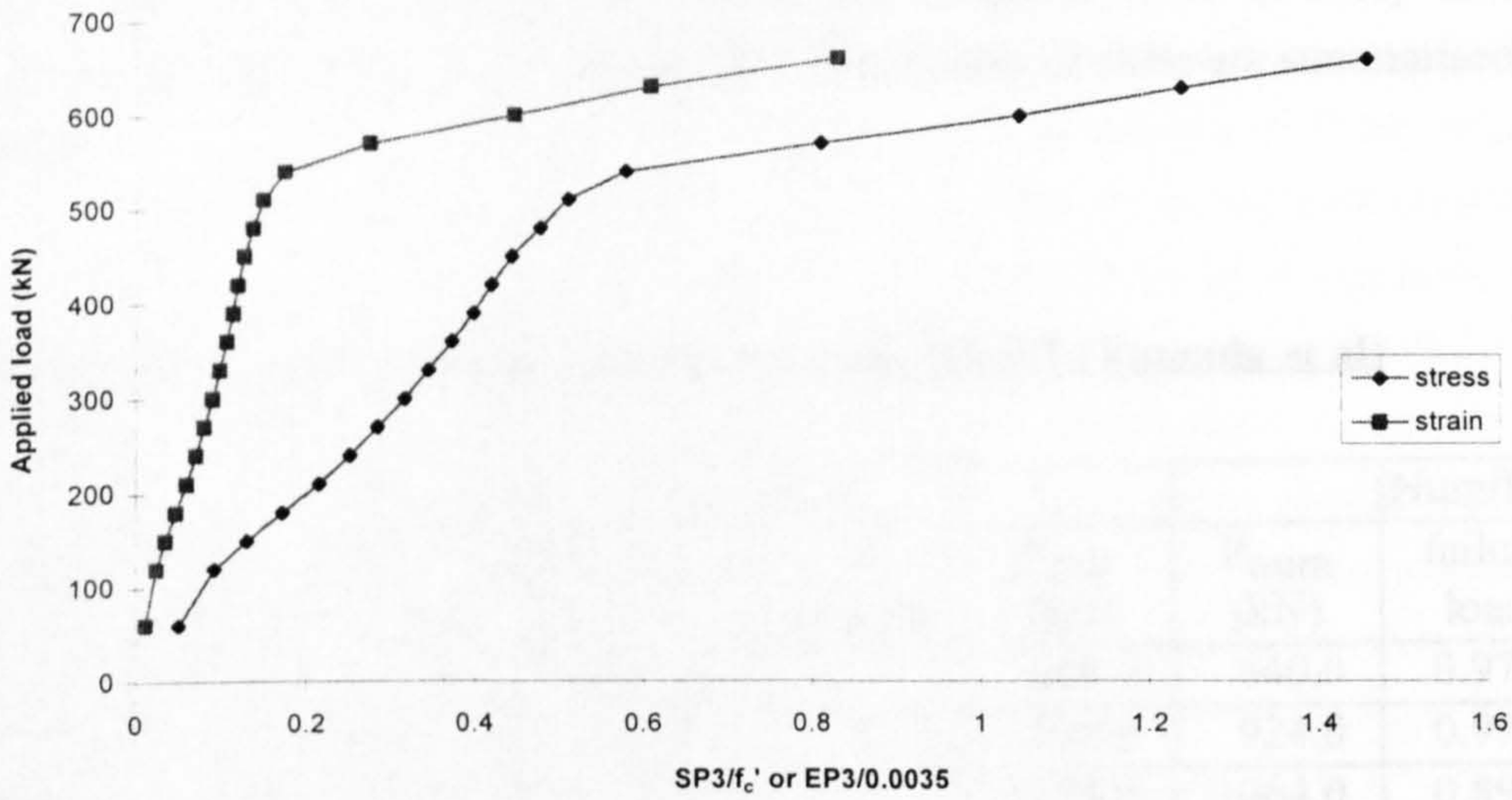

Note: $SP3=\sigma_3$=maximum compressive principal stress

$EP3=\varepsilon_3$=maximum compressive principal strain

Figure 6.28 Principal compressive stress and strain relationship of concrete (slab G2)

6.4.3 Interior slabs tested by Yamada et al (1992)

Yamada et al (1992) tested two series of slabs to study the influence of the amount and type of shear reinforcement on punching shear strength of monolithic slab-column connections. The first series used hat-type shear reinforcement and the second series used hook-type shear reinforcement (Figure 6.29). The experimental results showed that the hat-shape shear reinforcement was not effective due to lack of anchorage and wide spacing. Present model assumes perfect bond between concrete and steel. Thus possible anchorage problem could not be investigate in the present model. So, only slabs with hook-type of shear reinforcement will be analysed. The dimensions of the slabs were 2m square by 200mm thick, with a centrally located column 300mm square. The central column extended above and below the slab for a length of 300mm. Downward load was applied at eight points symmetrically distributed around the column centre at a distance of 750 mm diameter. Lower column stub acted as the reaction support. Finite element meshes for these specimens are shown in the Figure 6.30. These specimens have the same amount of flexural steel, i.e. 16mm diameter spaced at 80 mm (ρ=1.53%) in both tension and compression zone. The flexural steels were symmetrically distributed in the orthogonal X and Y directions with a minimum cover of 20mm. All the shear reinforcements were placed within a distance of 170mm (1.4 times the effective depth) from the column. Two different spacings for shear reinforcement were obtained by placing a bars at every node of the longitudinal reinforcement grid (interval=1) or at every second node (interval=2) as shown in the Figure 6.29. The details of slabs are summarised in Table 6.15.

Table 6.15 : Details and Predictions of slabs K1-K7 (Yamada et al)

		shear reinforcement					Num/Exp
Slab	f_c' (N/mm^2)	Diameter (mm)	ρ_s (%)	d Interval	P_{test} (kN)	P_{num} (kN)	failure load
K1	26.00	-	0.00	-	658.0	640.0	0.972
K2	27.17	6.0	0.25	2	950.0	924.0	0.972
K3	25.90	6.0	0.50	1	1183.0	1064.0	0.899
K4	27.37	10.0	0.55	2	1153.0	1064.0	0.923
K5	26.00	10.0	1.11	1	1440.0	1064.0	0.739
K6	26.39	13.0	0.99	2	1274.0	1080.0	0.848
K7	27.76	13.0	1.98	1	1498.0	1080.0	0.721
						Average	0.868
						STDEV	0.103

$\rho_S=100A_{sv}/bd$

A_{sv}=Total area of shear reinforcement in the slab

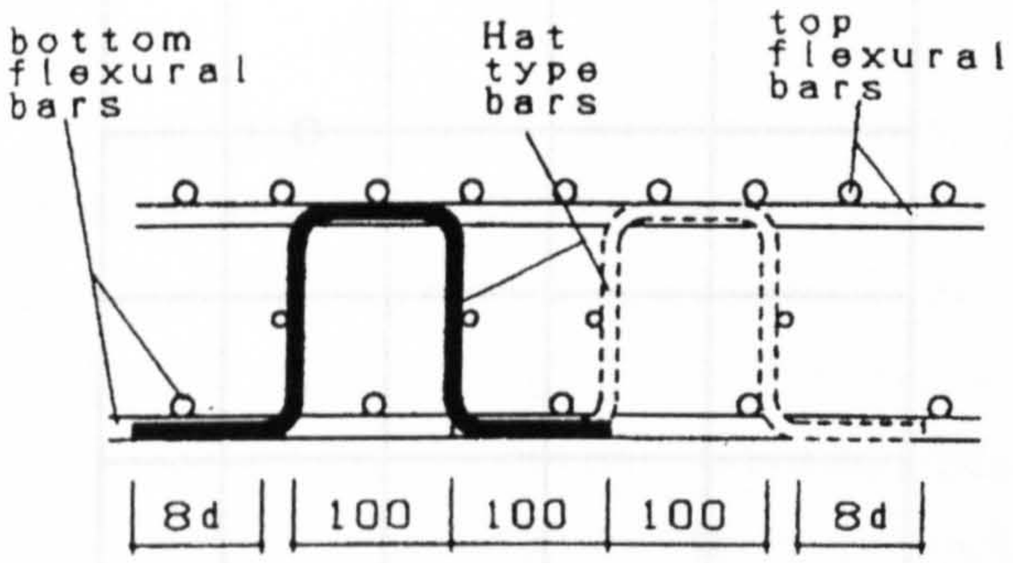

(a) Hat-type shear reinforcement

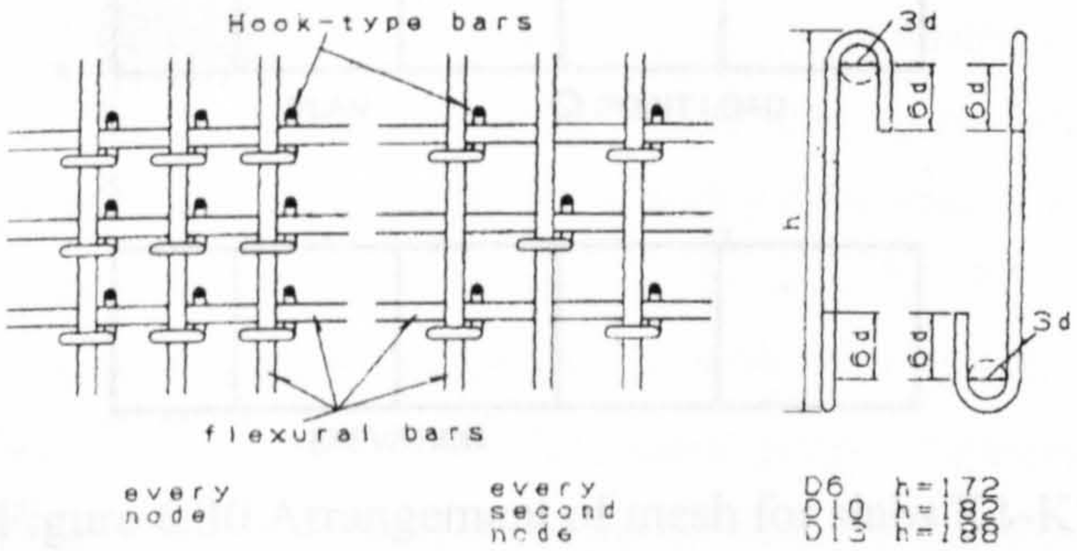

(b) Hook-type shear reinforcement

Figure 6.29 Type of shear reinforcement

The predicted ultimate load for specimen K1 (slab without shear reinforcement) and specimen K2 were 640.0kN and 924.0kN respectively. The ultimate load of the slabs increased with the increased quantity of shear reinforcement until specimen K4. For specimens K5 to K7, there was no further gain in ultimate load with the higher amount of shear reinforcement when compared to specimen K4. From the predicted structural response, there are two possible reasons for the failure of slabs K5-K7. In these slabs, either concrete failed in compression at the critical zone (Figure 6.31) or punching occurred outside the reinforcement region (Figure 6.32). Specimens K5 to K7 were then re-analysed with the cube strength increased by 50%. The predicted results were similar. Therefore, it is concluded that numerically punching occurred outside the shear reinforcement region. A stronger concrete or providing extra amount of shear reinforcement within the perimeter of 170mm would not have increased the failure load any further as the failure could always occur outside the reinforced zone. Another layer of shear reinforcement is needed to increase the failure load of the slab. Table 6.15 shows the numerical results of Yamada et al slabs. Mean value of predicted to actual failure load is 0.868 with standard deviation of 0.103. All the slabs were predicted to fail in shear mode.

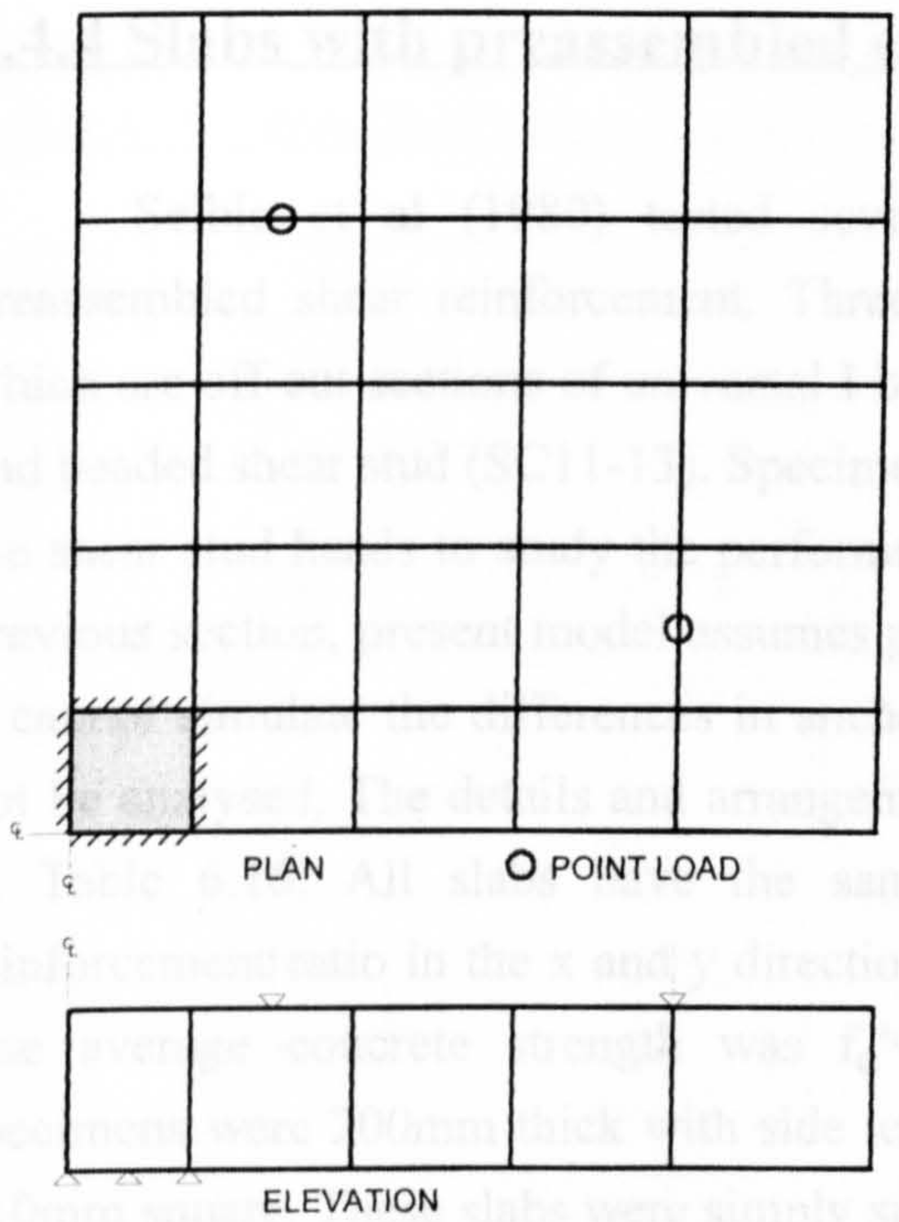

Figure 6.30 Arrangement of mesh for slabs K1-K7

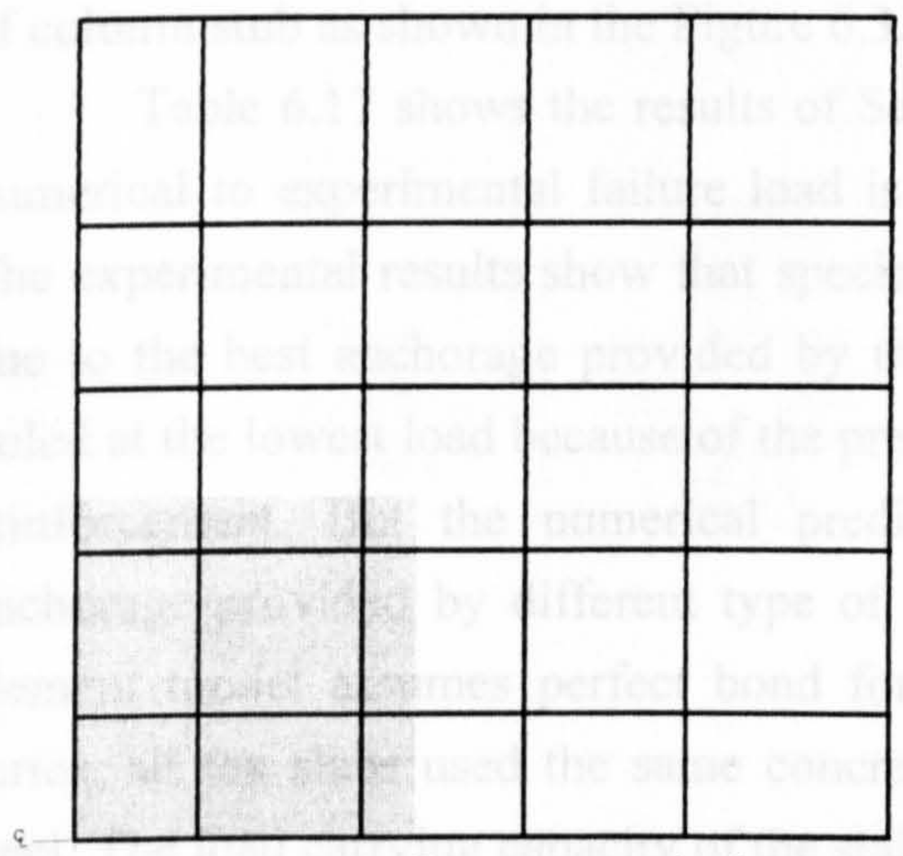

Figure 6.31 Compression failure of concrete (slab K5)

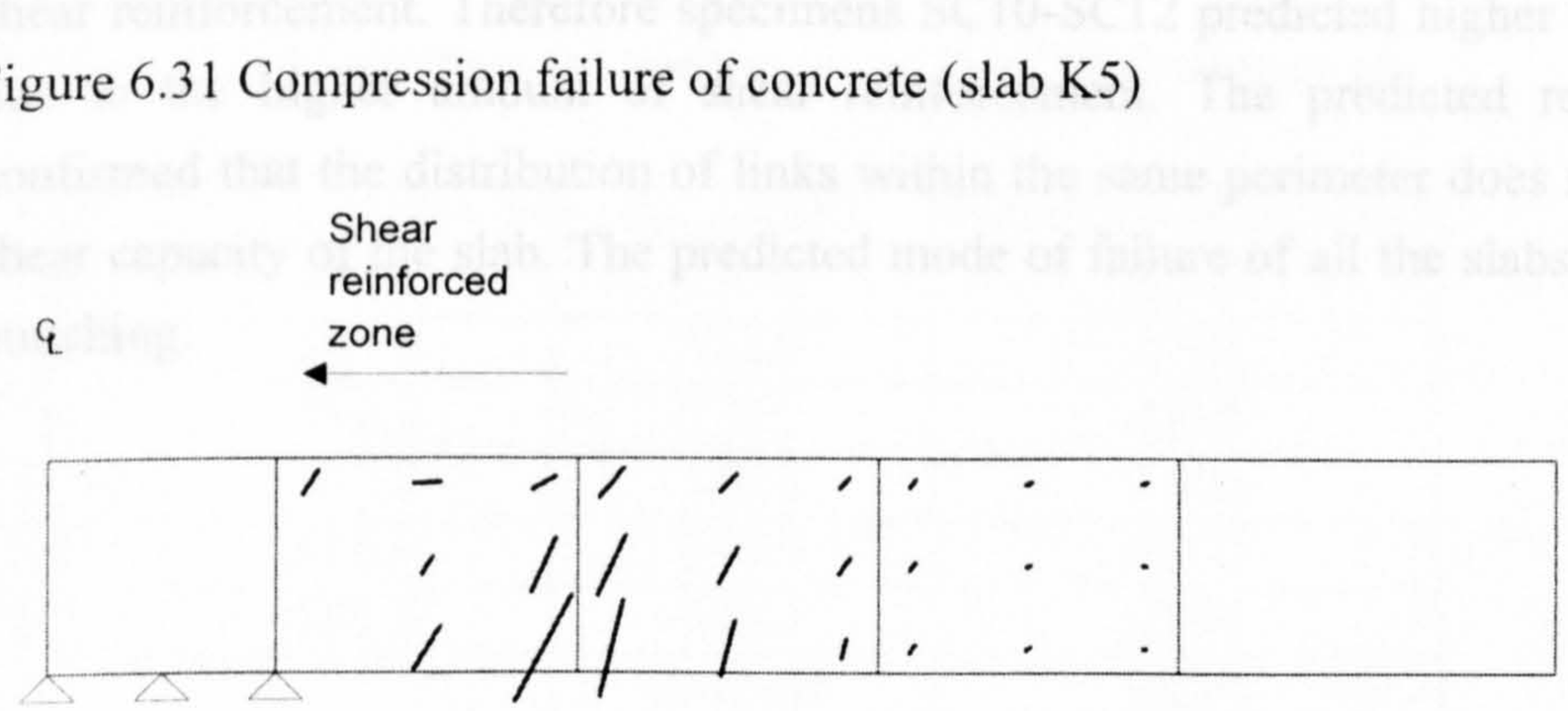

Figure 6.32 Punching occurred outside shear reinforcement region (slab K5)

6.4.4 Slabs with preassembled shear reinforcing units

Seible et al (1980) tested seven full size slab-column specimens with preassembled shear reinforcement. Three types of shear reinforcement were used, which are off-cut sections of universal I beam (SC7), welded wire fabric (SC8-SC10) and headed shear stud (SC11-13). Specimens SC12 and SC13 differ only in the size of the shear stud heads to study the performance of the anchorage. As mentioned in the previous section, present model assumes perfect bond between concrete and steel. So it cannot simulate the differences in anchorage bond. Therefore specimen SC13 will not be analysed. The details and arrangement of shear reinforcement are summarised in Table 6.16. All slabs have the same amount of flexural steel, an average reinforcement ratio in the x and y direction is ρ=1.17% using 12.7 mm diameter bar. The average concrete strength was f_c'=33.6 N/mm^2. The dimensions of these specimens were 200mm thick with side length of 1800 mm. The central column was 310mm square. These slabs were simply supported along the slab edges and subjected to a point load at the centre of slab. In the finite element idealisation, the load was simulated by a uniformly distributed load over the element representing the foot print of column stub as shown in the Figure 6.33.

Table 6.17 shows the results of Seible's slabs. The mean value of the ratio of numerical to experimental failure load is 0.893 with a standard deviation of 0.065. The experimental results show that specimen SC7 failed at the highest ultimate load due to the best anchorage provided by the flanges of I-beam, and specimens SC10 failed at the lowest load because of the premature failure of the anchorage of the shear reinforcement. But the numerical predictions do not reflect the differences in anchorage provided by different type of shear reinforcement because present finite element model assumes perfect bond for all types of shear reinforcement. In this series, all the slabs used the same concrete strength and similar amount of flexural steel. The load carrying capacity of the slab will only vary according to the quantity of shear reinforcement. Therefore specimens SC10-SC12 predicted higher ultimate load due to the higher amount of shear reinforcement. The predicted results further confirmed that the distribution of links within the same perimeter does not affect the shear capacity of the slab. The predicted mode of failure of all the slabs was flexural punching.

Table 6.16 : Details of shear reinforcement (Seible et al)

Slab	Cross Section	Top View	Type	Area/leg (mm^2)	Number
SC7	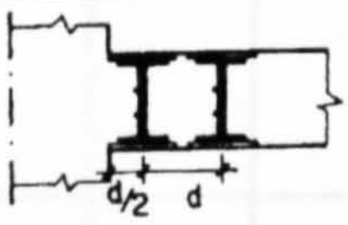	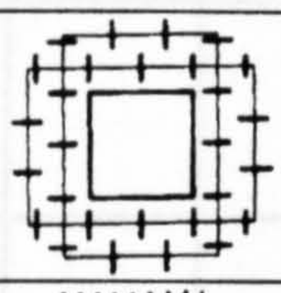	I-beam segments	62	28
SC8	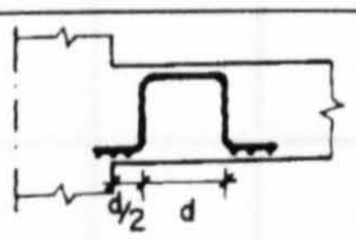	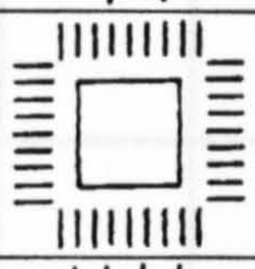	welded wire fabric	25.2	72
SC9	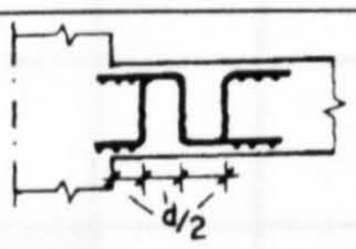	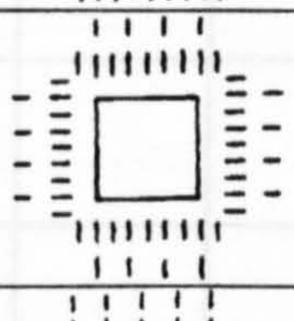	welded wire fabric	25.2	72
SC10	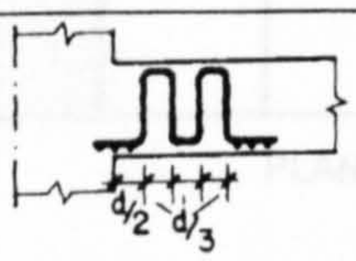	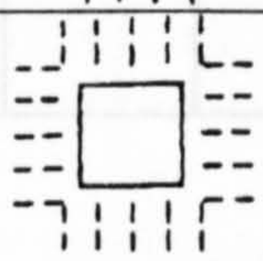	welded wire fabric	25.2	80
SC11	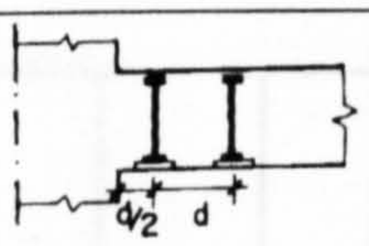	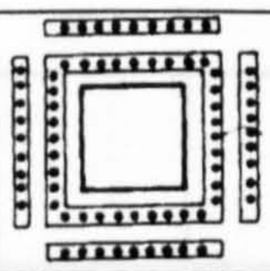	shear studs	31.0	64
SC12	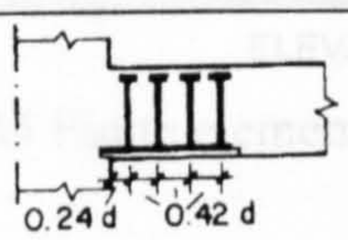	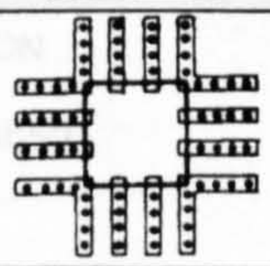	shear studs	31.0	64

Table 6.17 : Predictions for specimens SC7-SC12 (Seible et al)

Slab	P_{test} (kN)	P_{num} (kN)	Num/Exp failure load
SC7	623.0	510.0	0.819
SC8	592.0	510.0	0.861
SC9	594.0	510.0	0.859
SC10	537.0	540.0	1.006
SC11	596.0	540.0	0.906
SC12	595.0	540.0	0.908
		Average	0.893
		STDEV	0.065

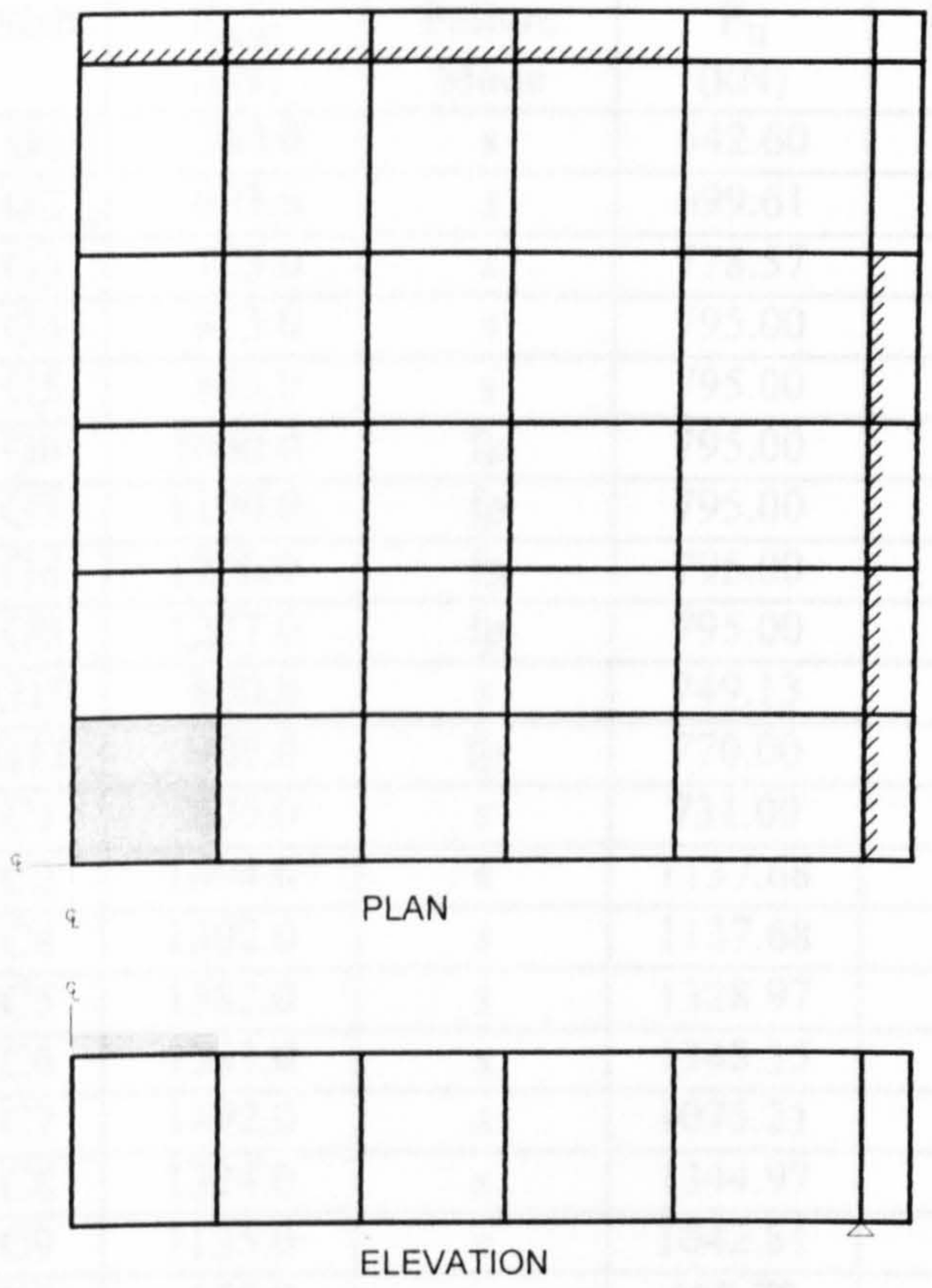

Figure 6.33 Finite element mesh

6.4.5 Code Predictions

The code BS8110 gives reasonably good predictions for slabs with shear reinforcement. Generally, for slabs which contain large quantity of shear reinforcement, the code underestimate the ultimate load of slabs due to the control of concrete crushing criterion ($\sqrt{f_{cu}}$ or 6.25 N/mm^2 whichever is less). The confinement effect and triaxial action definitely allow higher compressive stress to build up. This exercise shows that it is necessary to consider all possible failure modes to ensure a good prediction.

Table 6.18 : Ultimate Load and Mode of failure predicted by using BS8110
(Gomes, Yamada et al and Seible et al)

Slab	Test results		Predictions by BS8110		P_{test}/P_u
	P_{test} (kN)	Failure Mode	P_u (kN)	Failure Mode	
G1	560.0	s	542.60	s	0.969
G2	693.0	s	699.61	s	1.010
G3	773.0	s	778.57	s	1.007
G4	853.0	s	795.00	c	0.932*
G5	853.0	s	795.00	c	0.932*
G6	1040.0	fp	795.00	c	0.764*
G7	1120.0	fp	795.00	c	0.710*
G8	1200.0	fp	795.00	c	0.663*
G9	1227.0	fp	795.00	c	0.648*
G10	800.0	s	749.13	s	0.936
G11	907.0	fp	770.00	c	0.849*
C1	805.0	s	731.00	s	0.908
C2	1094.0	s	1137.68	out	1.040
C4	1302.0	s	1137.68	out	0.874
C5	1382.0	s	1328.97	out	0.961
C6	1283.0	s	1348.35	out	1.051
C7	1492.0	s	1075.21	out	0.721
C8	1324.0	s	1344.97	out	1.016
C9	1135.0	s	1042.81	y	0.919*
K1	658.0	s	688.78	s	1.047
K2	950.0	s	869.02	s	0.915
K3	1183.0	s	974.78	out	0.824
K4	1153.0	s	992.50	out	0.861
K5	1440.0	s	975.78	out	0.676
K6	1274.0	s	980.76	out	0.770
K7	1498.0	s	997.32	out	0.666
SC7	623.0	fp	644.05	y	1.034*
SC8	592.0	fp	644.05	y	1.088*
SC9	594.0	fp	644.05	y	1.084*
SC10	537.0	fp	644.05	y	1.199*
SC11	596.0	fp	644.05	y	1.081*
SC12	595.0	fp	644.05	y	1.082*
				Average	1.026
				STDEV	0.080

N.B. c=local crushing
s=punching occurs within shear reinforcement zone
out=punching occurs outside shear reinforcement zone
f=flexure failure

* wrong mode of failure predicted

6.5 Numerical Model and Comparisons with K&N model and BS8110

Previous sections show that the predictions by the present finite element model are close to experimental observations in terms of ultimate load, structural response and mode of failure. In terms of predictions of the ultimate load, it is useful to make a comparison between the predictions by the present model, K&N model and BS 8110. Figures 6.34 and 6.35 show the predictions by the present model for the slabs without shear reinforcement tested by Rankin and Regan. Similarly figure 6.36 shows the predictions by the present model for slabs with shear reinforcement. Figure 6.37 shows in one diagram predictions for all the slabs analysed. Similar comparison is shown in figures 6.38 for predictions by BS 8110. Figure 6.39 shows a similar comparison for K&N model. However, since K&N model does not include the effect of shear reinforcement, calculations were done assuming that there was no shear reinforcement and the failure load of slabs with shear reinforcement was calculated using the empirical formula

$$P_{shear} = P_{k\&N}\ (1+\rho_s). \qquad (6.1)$$

where $\rho_s = 100A_{sv}/bd \leq 1.0$

A_{sv} = Total area of shear reinforcement in the slab

d = effective depth

b = width of slab

Since the predictions are reasonably good, these models can be utilized to do a few numerical experiments to study the influence of different parameters (such as reinforcement ratio, effective depth etc.) on shear strength.

Results of these parametric studies shown in Figures 6.40-6.43, lead to the conclusion that the present model correlates very well with test data and gives good agreement with theoretical K&N model and code prediction. From this, it can be concluded that the present finite element model mimics realistically the structural behaviour of slab-column junctions. It should be noted that in figures 6.41 to 6.43, the experimental failures loads have been normalized for a constant cube strength of 37.1 N/mm², by multiplying the experimental failure load by $(f_{cu}/37.1)^{1/3}$.

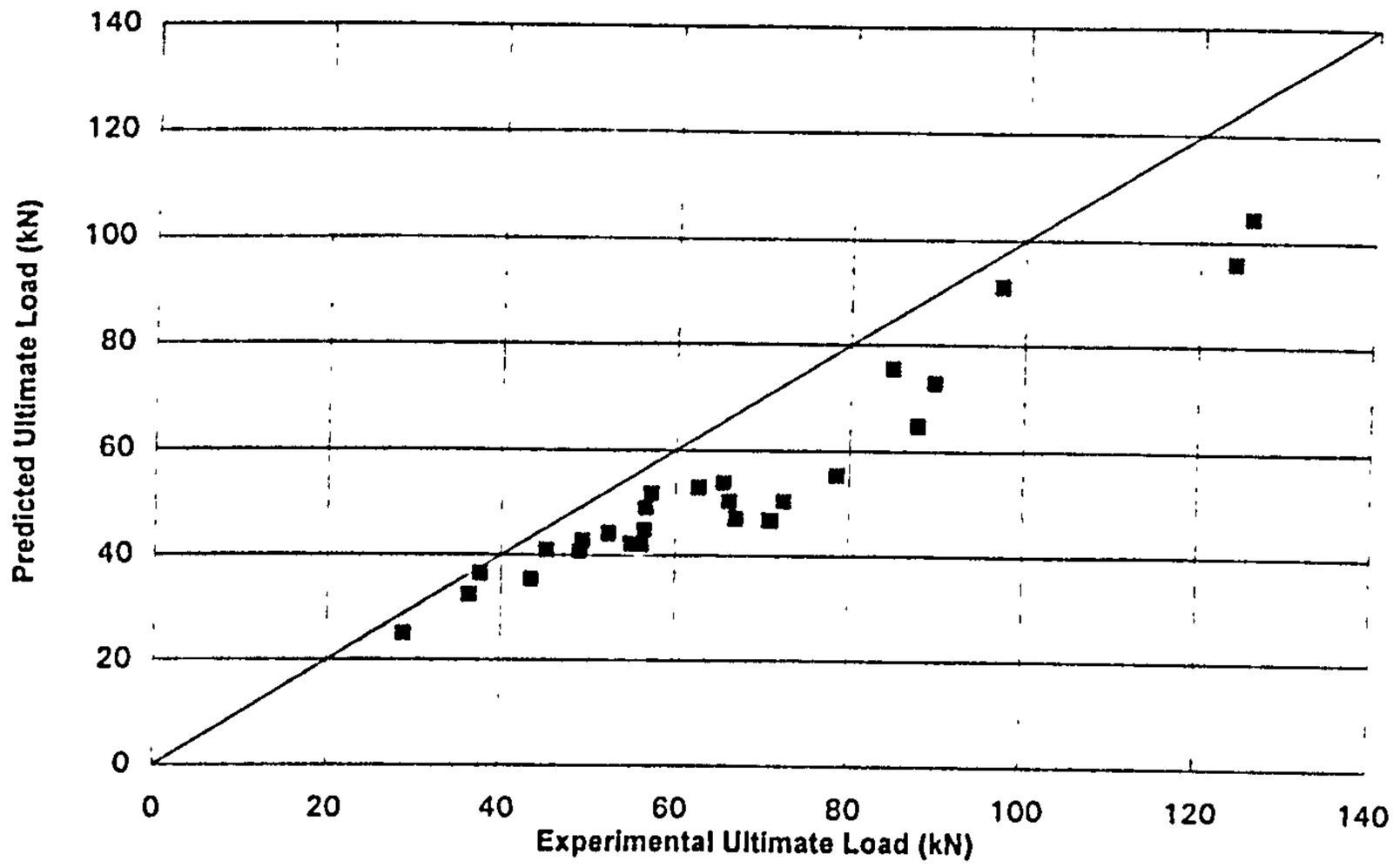

Figure 6.34 Numerical predictions for Rankin's slabs

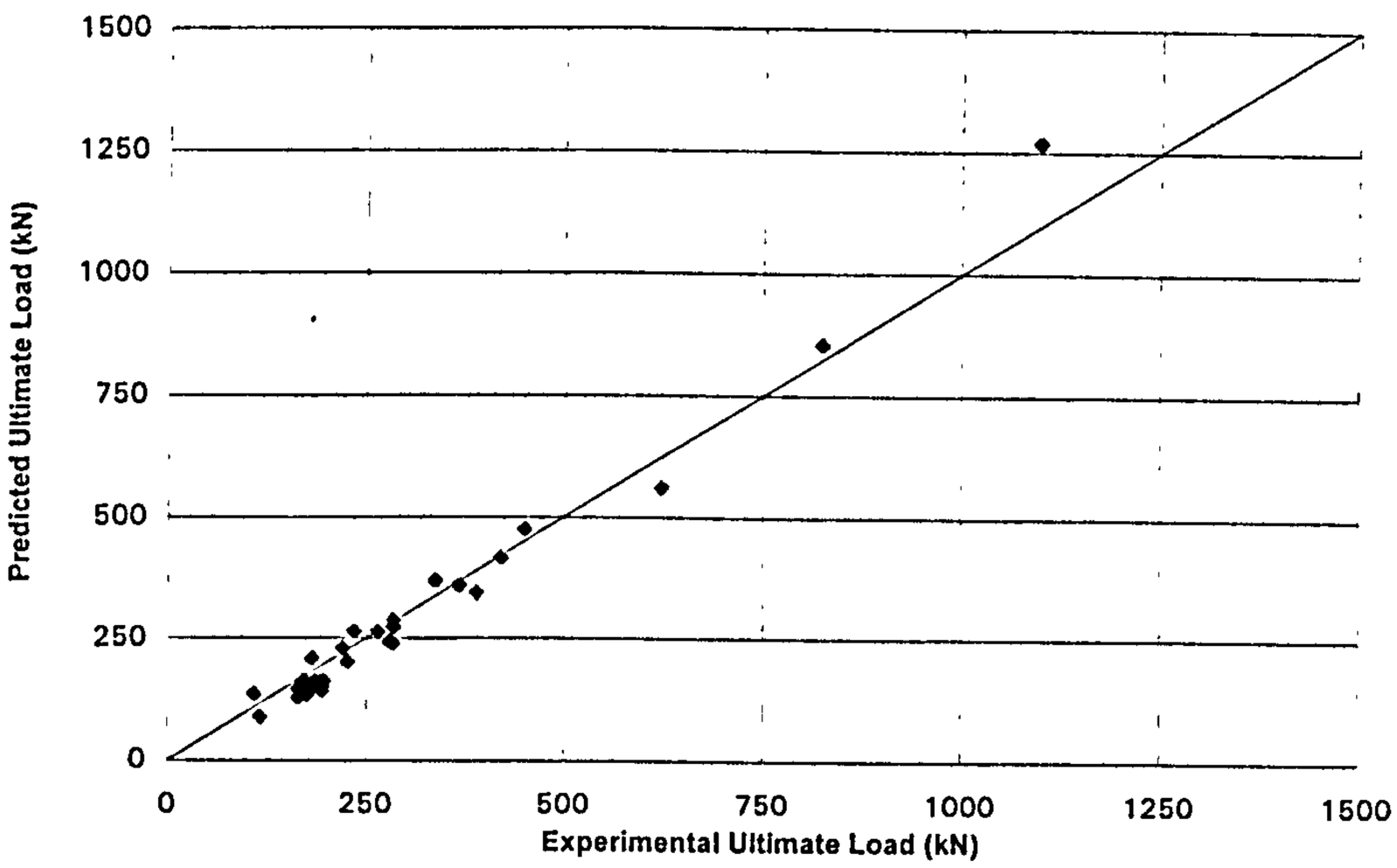

Figure 6.35 Numerical predictions for Regan's slabs

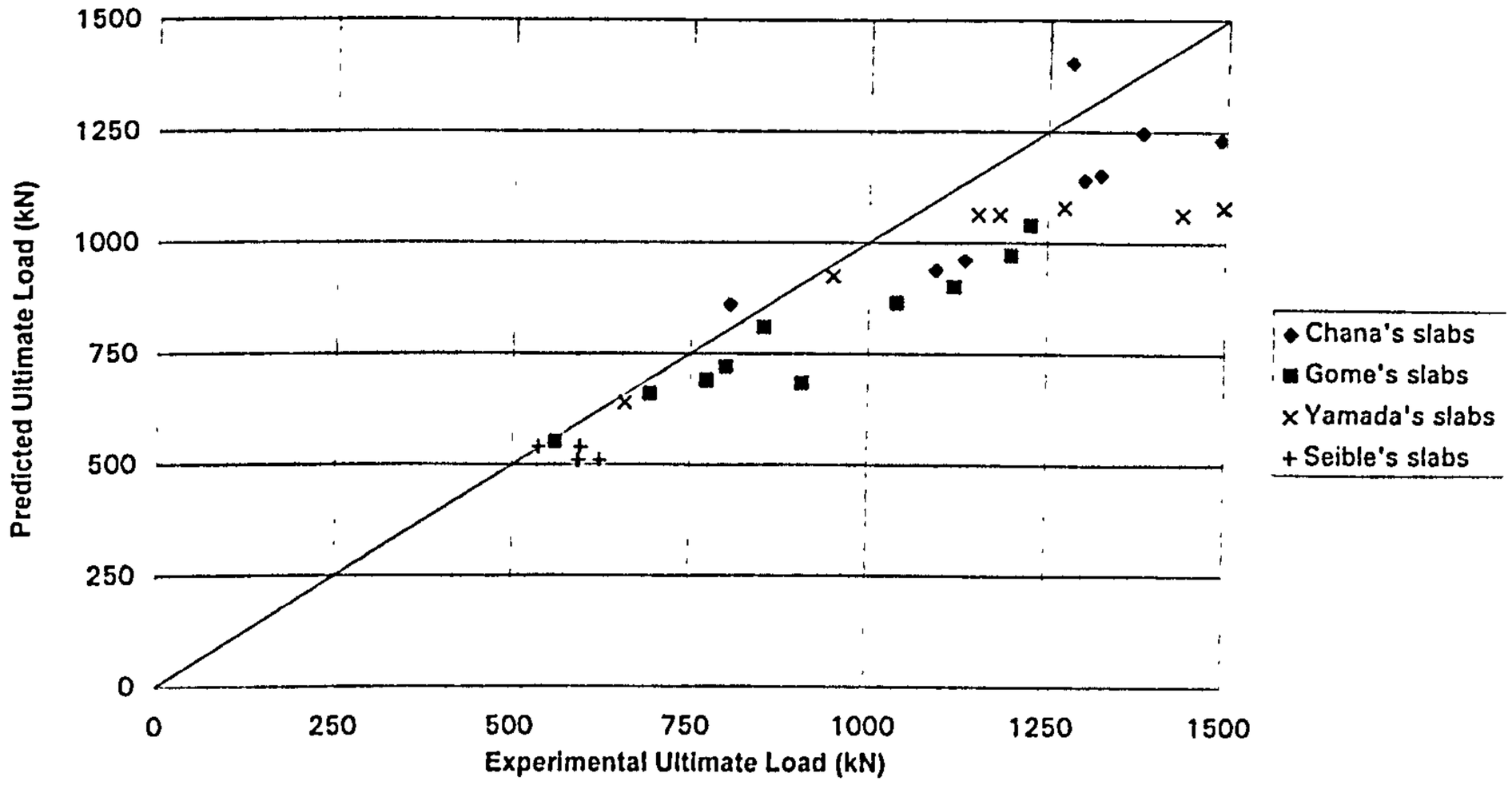

Figure 6.36 Numerical predictions for slabs with shear reinforcement

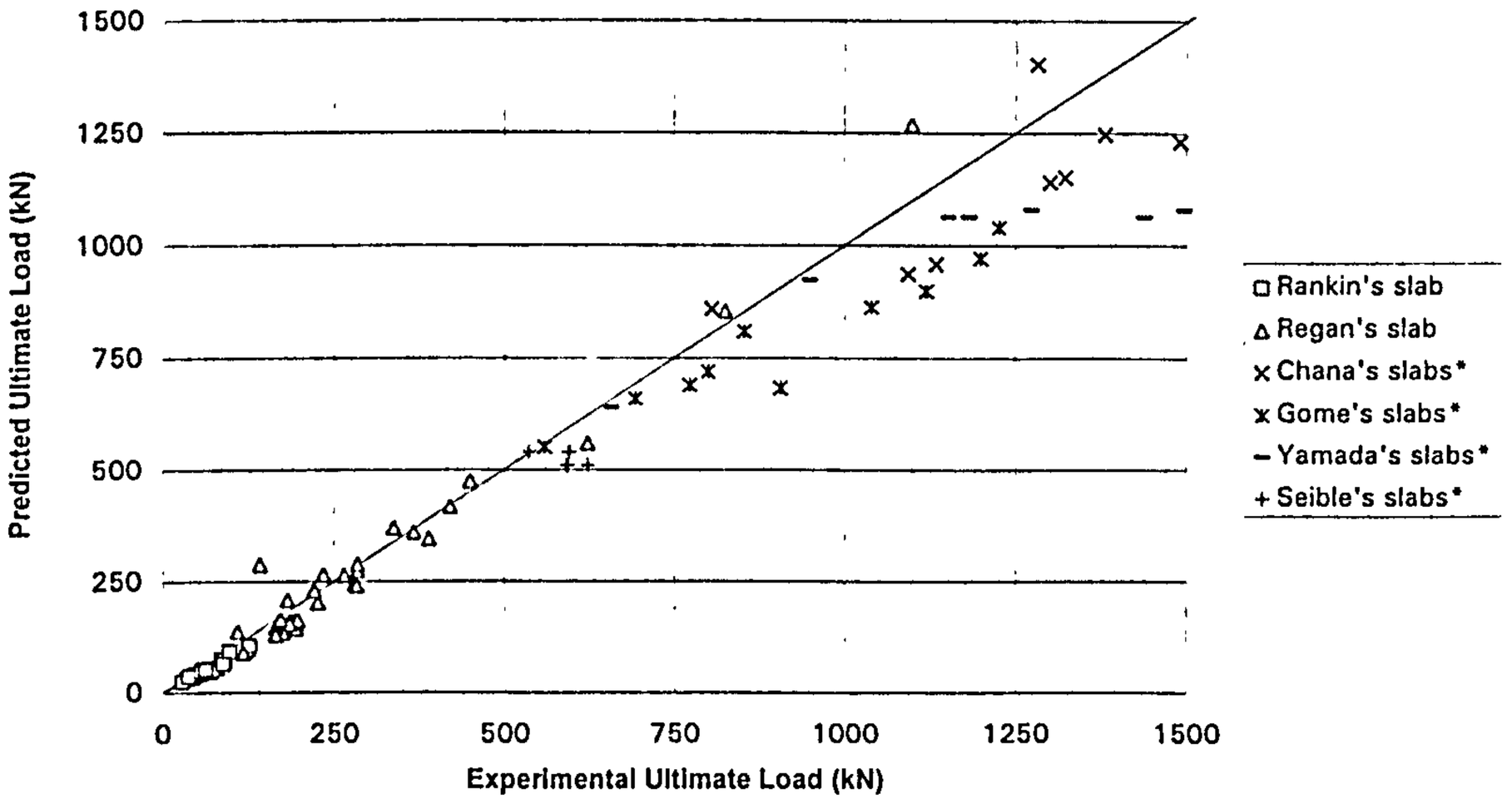

Figure 6.37 Numerical predictions for all simply supported slabs

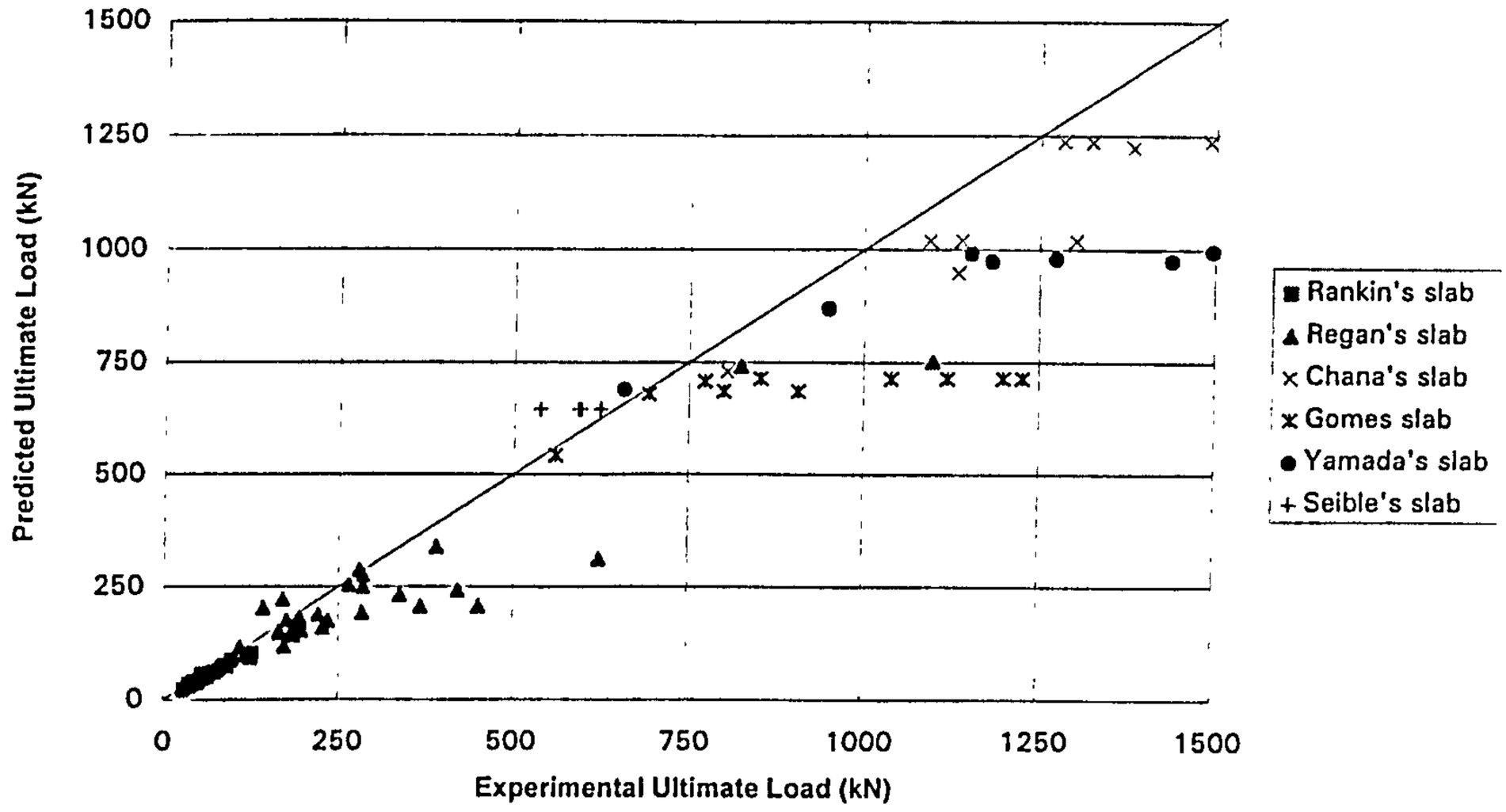

Figure 6.38 Predictions of ultimate loads by BS8110

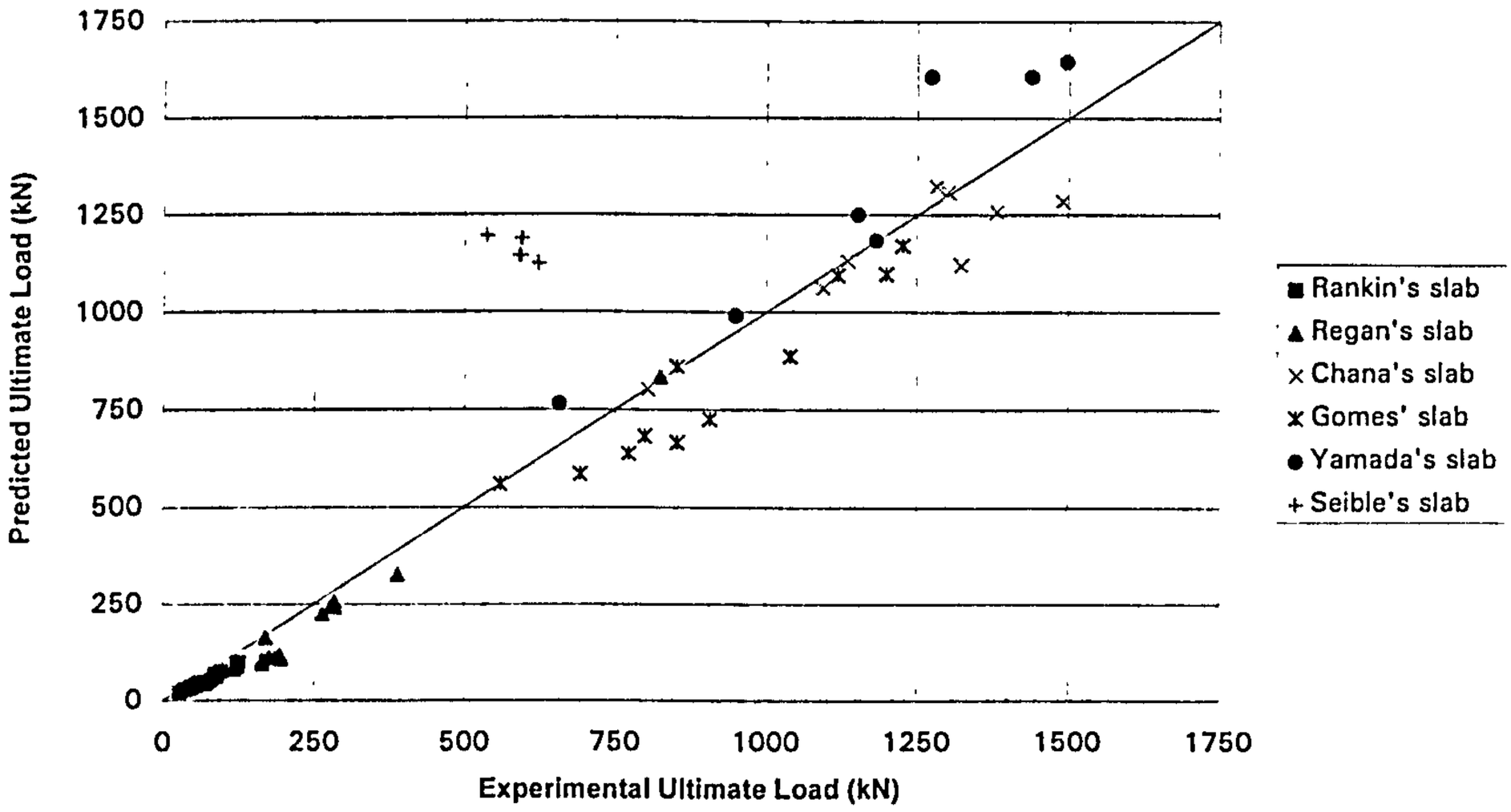

Figure 6.39 Predictions of ultimate loads by Kinnunen and Nyalnder's model

Note

(Slabs SP1-SP18 tested by Regan are not included here because K&N model is not applicable if *l/d* less than 4)

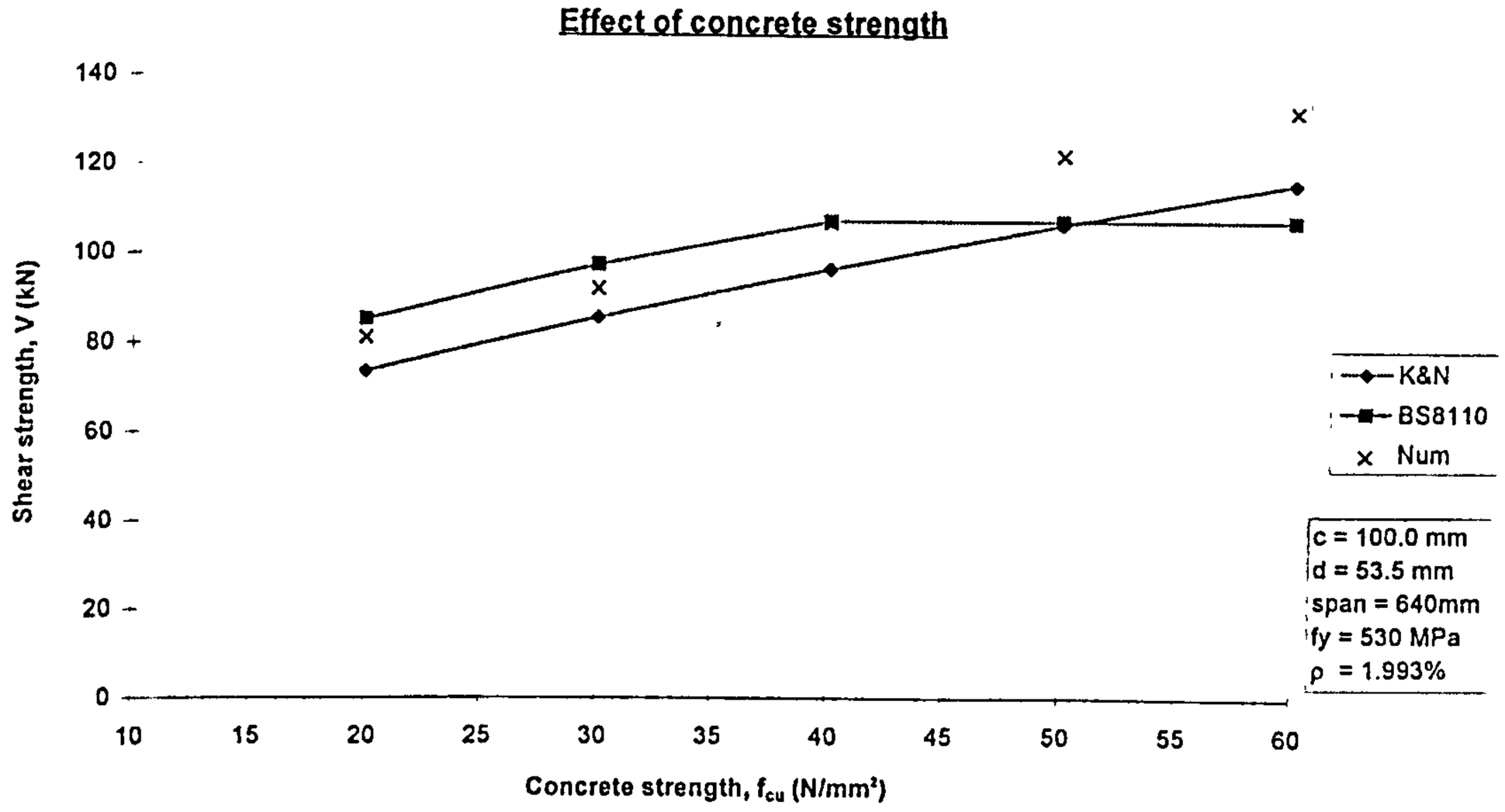

Figure 6.40 Effect of concrete strength on shear strength
(Based on details of slab "4C" tested by Rankin, section 6.3.1)

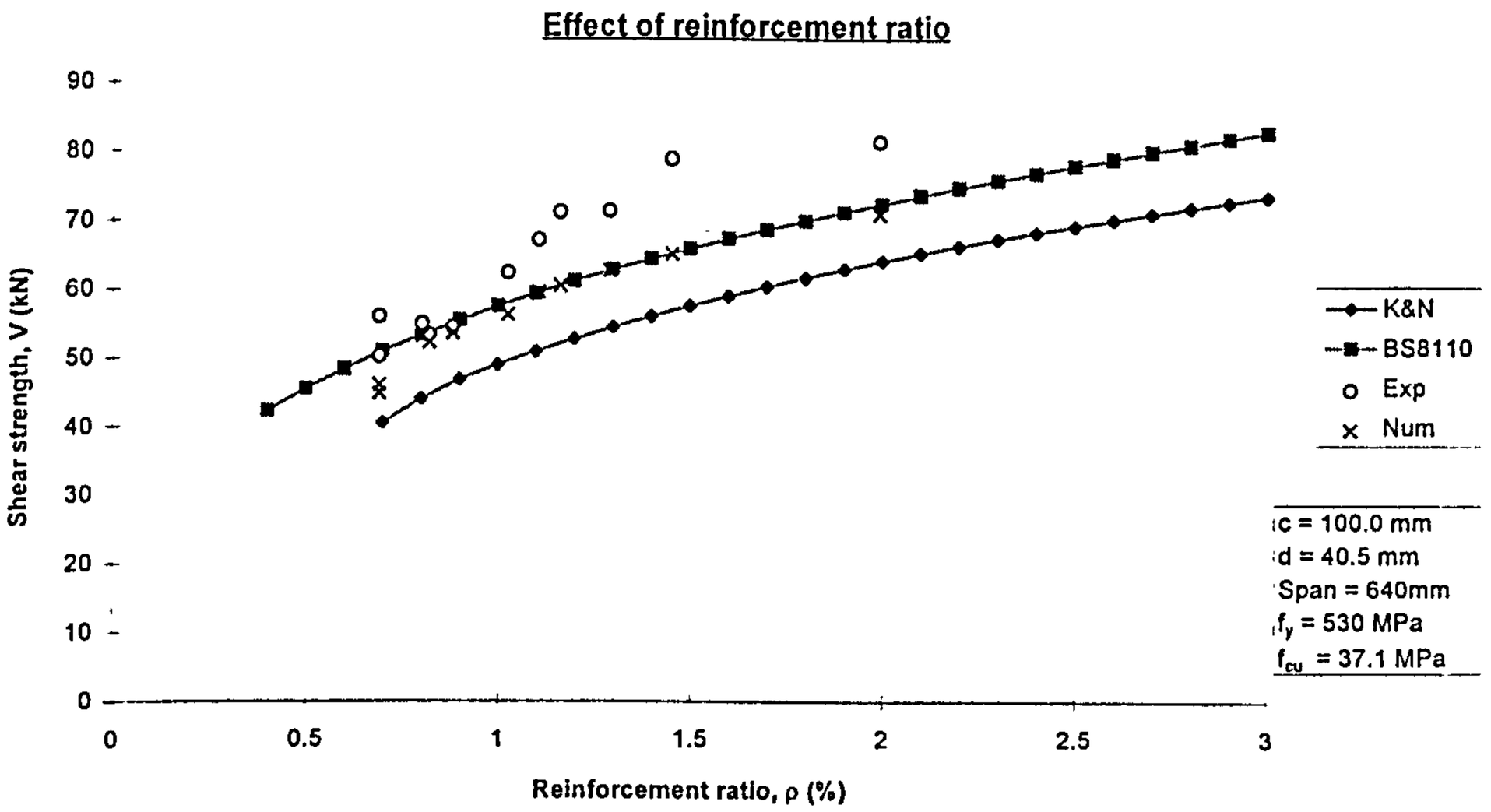

Figure 6.41 Effect of reinforcement ratio on shear strength
(compared to slabs tested by Rankin, section 6.3.1)

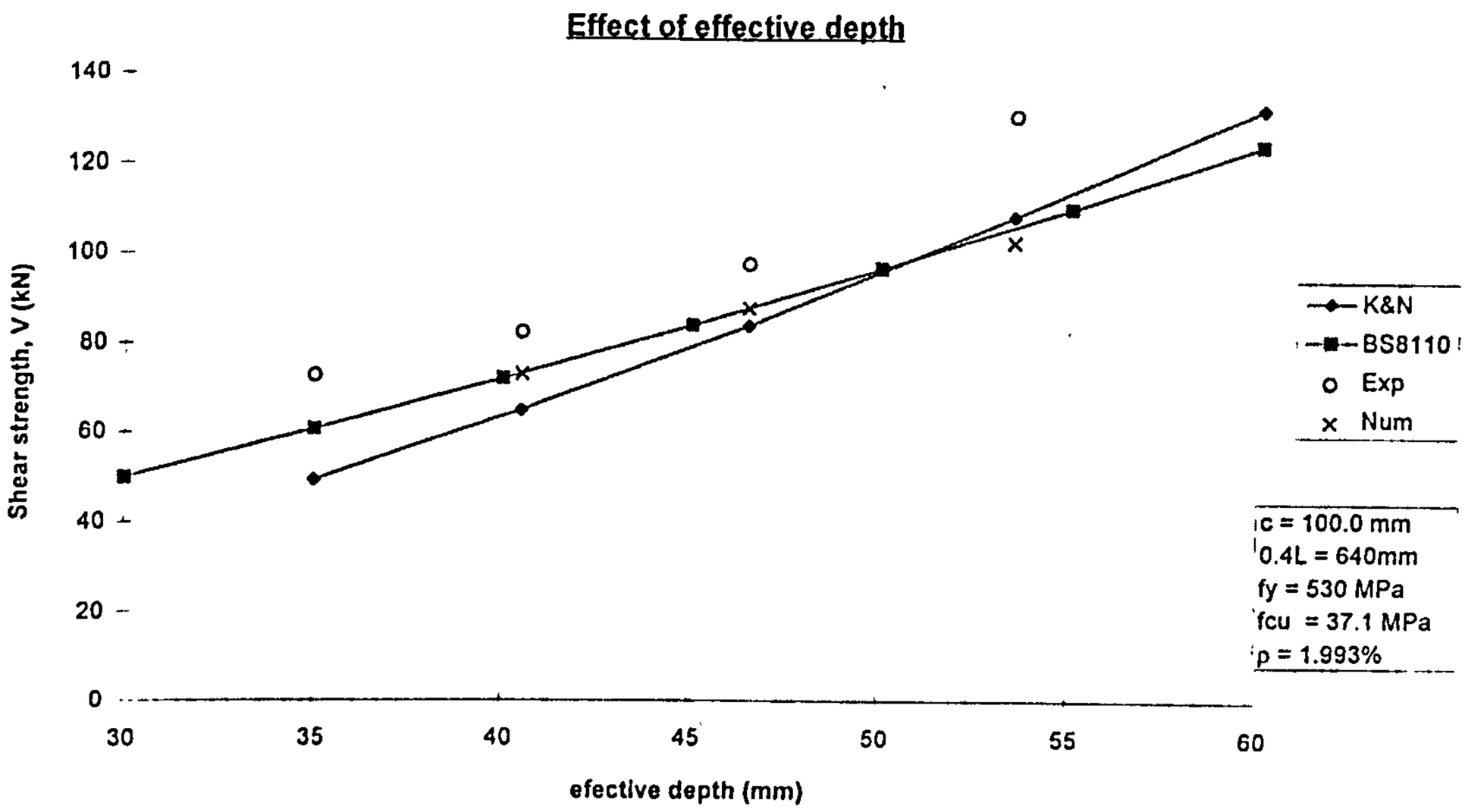

Figure 6.42 Effect of effective depth on shear strength
(compared to slabs tested by Rankin, section 6.3.1)

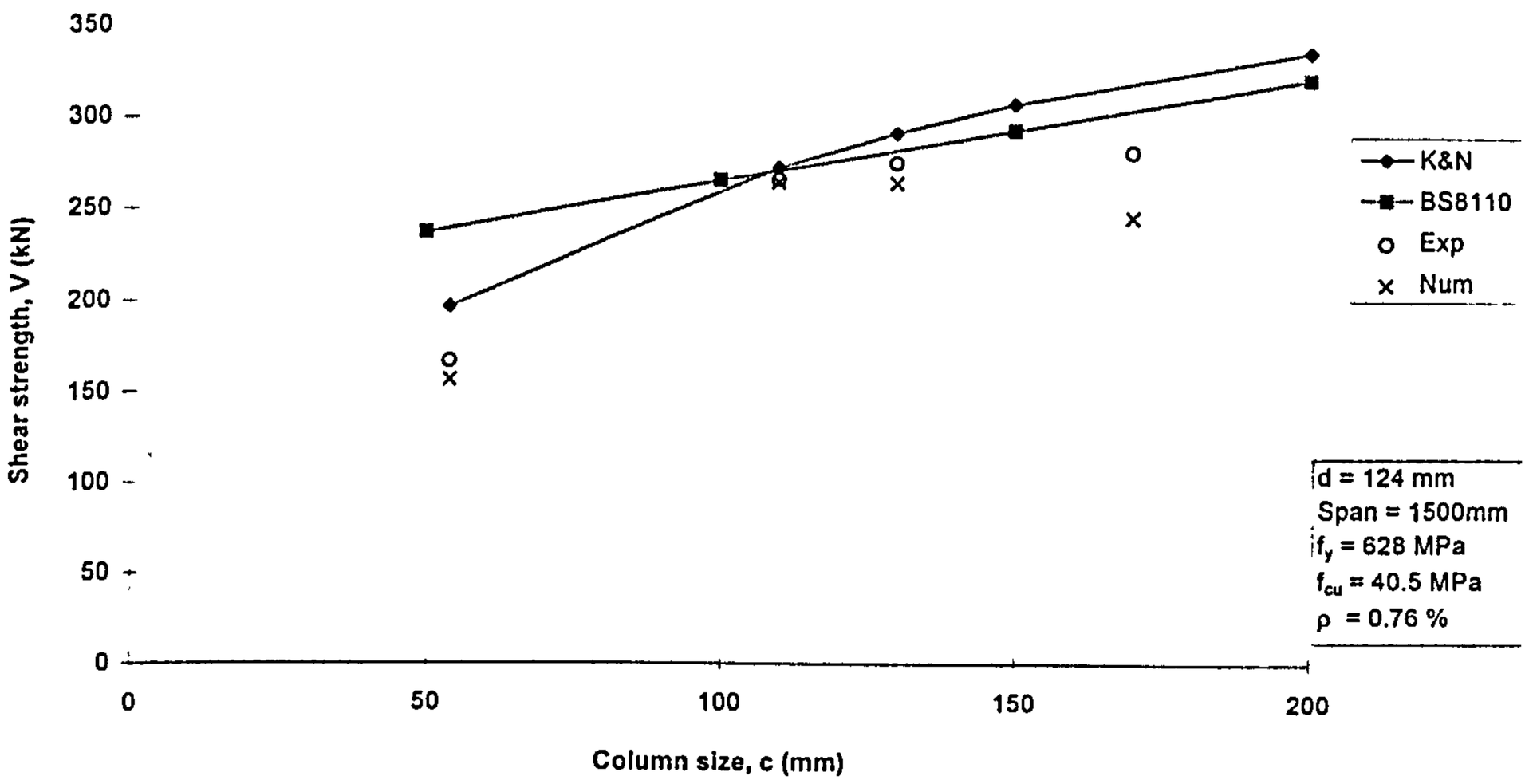

Figure 6.43 Effect of column size on shear strength
(compared to slabs tested by Regan, section 6.3.2.3)

6.6 Conclusions

Following conclusions can be drawn from the results of analysis of interior slabs subjected to shear force only from various sources :-

- Present model predicted reasonably accurate results (ultimate load, structural responses and mode of failure) for slabs with span-depth ratio more than 5 (or a_V/d more than 1.7). For slabs with span-depth ratio of 5 and lesser, present model may over predict the ultimate load of the slabs. This is because slabs with low span/depth ratio are subjected to low bending and high shear, resulting in lower principal strain in the slab. Tension stiffening model in present work is taken as a linear function of principal strain. Low principal strain means that the concrete can carry relatively high tensile stress after cracking occurs. Consequently in the analysis, stiffness deteriorates at a slower rate that what happen in real structure.

- Analysis of results for slabs with shear reinforcement further confirmed the experimental finding (Chana and desai, 1992) that the distribution of links within the same perimeters does not affect the shear strength of slabs.

- The trend of the parameters governing punching shear strength predicted by the present model correlates very well with test data, theoretical K&N model and BS8110 (Figure 6.40-6.43).

- For slabs with span-depth ratio of more than 5 (or a_V/d more than 1.7), BS8110 predicted a reasonably accurate ultimate load but in some cases it predicted incorrect mode of failure. For slabs with span-depth ratio of 5 or less, the code generally underestimates the ultimate load of slab (Figure 6.38).

- K&N model predicted a reasonably accurate ultimate load for simply supported slabs without shear reinforcement (Figure 6.39). The results also show that the empirical equation 6.1 is suitable for slabs with shear reinforcement at spacings of about 0.75d. However, it over predicted the failure load for slabs with shear reinforcement closely spaced because punching takes places outside shear reinforced region.

Chapter 7

SLAB-COLUMN CONNECTIONS WITH SHEAR AND MOMENT TRANSFER

7.1 Introduction

This chapter presents the analysed results for slabs subjected to punching shear with moment transfer such as interior slab-column junctions with moment transfer , edge column-slab junctions and corner column-slab junctions from different sources. The chosen slabs were with and without shear reinforcement. The analysis was done using a set of "constant" parameters similar to that described in section 6.1.

7.2 Interior slabs

7.2.1 Interior column-slab connections reported in CIRIA Project Report 220 (1979), SM series

These slabs were all 2.0m square and 80mm thick, with spans of 1.83m. They were generally simply supported on four edges (Figure 7.1a) but in one slab (SM6) two opposite edges were free (Figure 7.1b). Load was applied to the slab through a column stub at the centre of slab. The main flexural reinforcement was the same in all the specimens and was a simple square mesh (Y8 c/c @80) giving an average steel ratio of 1.05%. In addition to this quantity of steel, the last three specimens were provided with extra reinforcement as follows:

- SM10, a lighter compression steel mesh (Y6 c/c @80) was added.
- SM11, extra steel (6 nos of Y8) passing the column in the direction perpendicular to the unbalanced moment (see Figure 7.2).
- SM12, extra steel (6 nos of Y8) passing the column in the direction parallel to the unbalanced moment (see Figure 7.2).

The variables for this series were the size and shape of the column, steel details, load eccentricity and in one slab the arrangement of the supports. The details and test results are summarised in Table 7.1.

Owing to symmetry, only one-half of the slabs was modelled. The applied load was simulated by a uniformly distributed load over the loading stub (Figure 7.1c & 7.1d). Horizontal restraints were provided at the left hand side support to prevent rigid body movement. Finite element meshes used are shown in Figure 7.1.

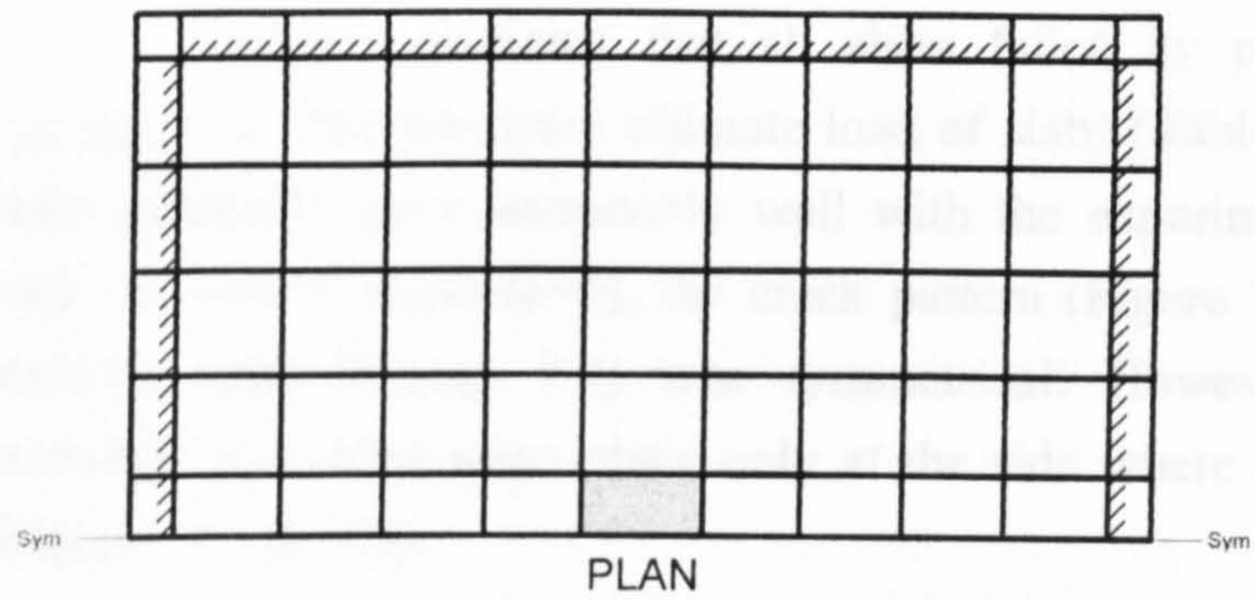

(a) SM1-SM12 except SM6

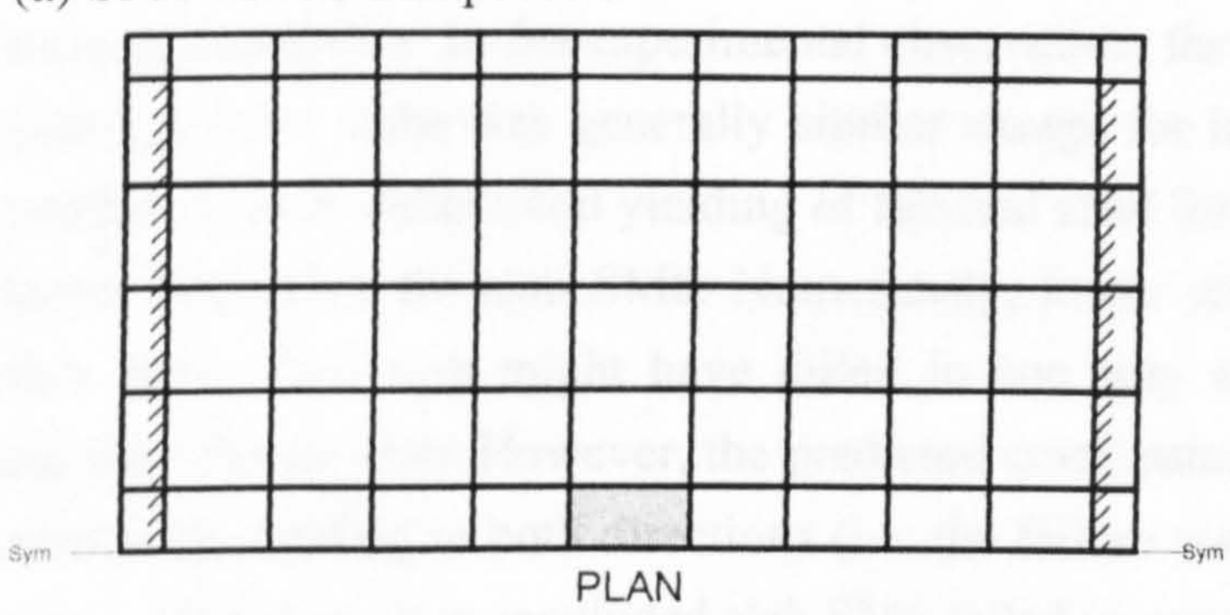

(b) SM6

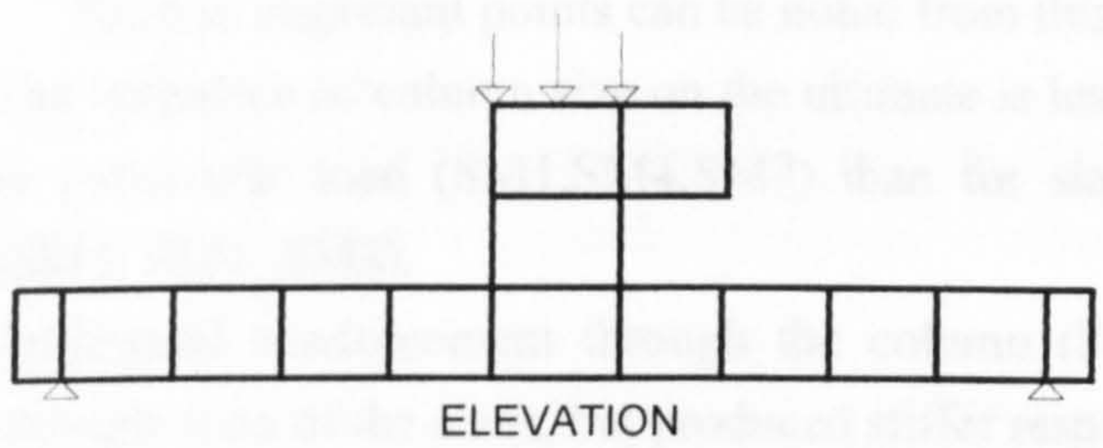

(c) Applied load <u>without</u> eccentricity (e=0)

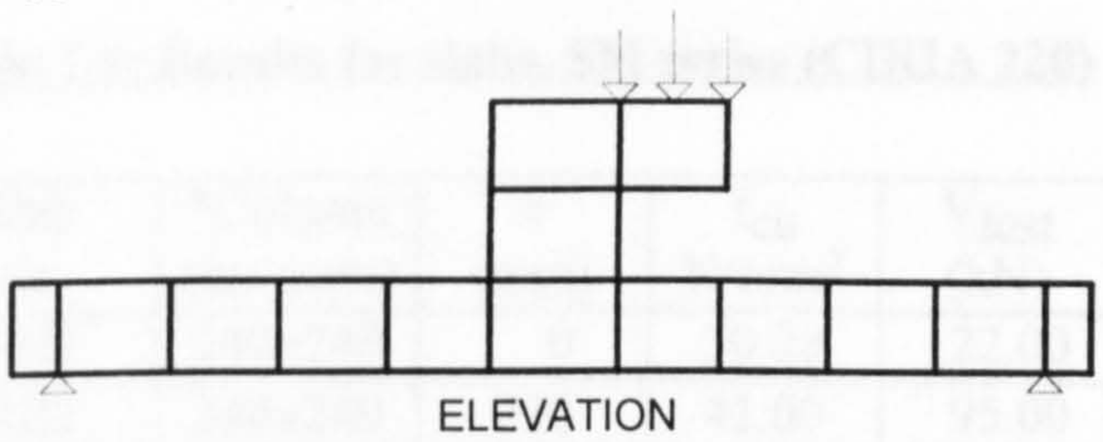

(d) Applied load <u>with</u> eccentricity

Figure 7.1 : Finite element mesh and boundary conditions

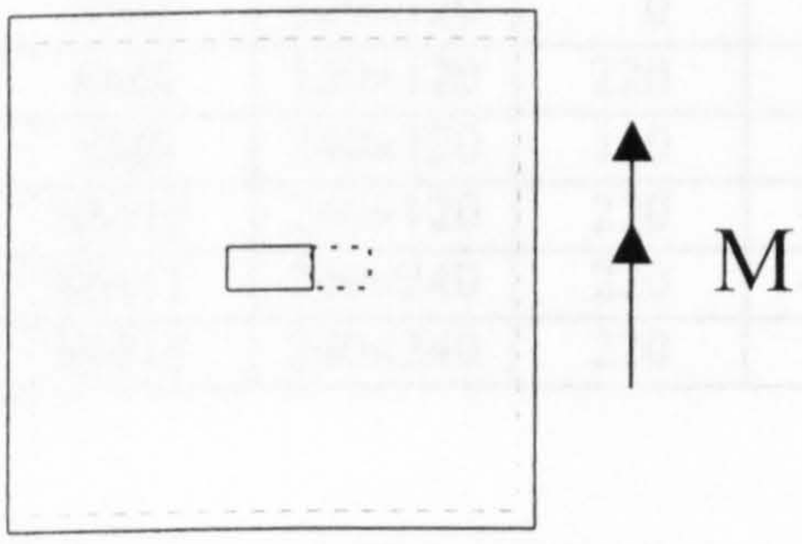

Figure 7.2 : Direction of unbalanced moment

Analysis predicted that all slabs failed by punching as observed in the experiment. The predicted ultimate load of slabs (Table 7.1) and structural response both generally agree reasonably well with the experimental observation. For slabs with concentric loads (e=0), the crack pattern (Figure 7.3) and yielding of flexural reinforcement (Figure 7.4) was symmetrical. However, when the loading was eccentric, punching takes place only at the side where shear strength was exceeded (Figures 7.5 & 7.6).

The configuration of slabs SM4 and SM6 are exactly identical except for support conditions. In the experimental observation, the pattern of failure and ultimate load for these slabs was generally similar except for larger deflection for SM6. The predicted crack pattern and yielding of flexural steel for these slabs are also similar as larger deflection for slab SM6. Numerically, lower ultimate load was predicted for slab SM6. This slab might have failed in one way shear resulting in lower shear capacity for the slab. However, the predicted crack pattern (Figure 7.8) shows that the cracks are slanting in both directions (i.e. the failure surface in the shape of truncated cone). Therefore, it is concluded slab SM6 failed in punching shear mode.

Several important points can be noted from this series of tests and analysis:

- The influence of column size on the ultimate is less significant for slabs subjected to concentric load (SM1,SM4,SM7) than for slabs subjected to eccentric load (SM3, SM5, SM8).
- Additional reinforcement through the column (SM11,SM12) does not increase ultimate load of the slabs, but produced stiffer response.

Table 7.1: Results for slabs, SM series (CIRIA 220)

Slab No	*Column size (mm)	e (mm)	f_{cu} N/mm^2	V_{test} (kN)	V_{num} (kN)	Num/Expt failure load
SM1	240×240	0	30.20	122.00	91.20	0.748
SM3	240×240	220	41.60	95.00	76.80	0.808
SM4	240×120	0	32.90	101.00	72.00	0.713
SM5	240×120	220	40.00	72.00	54.00	0.750
SM6	240×120	0	35.70	105.00	62.40	0.594
SM7	120×120	0	35.70	105.00	72.00	0.686
SM8	120×120	220	32.40	49.00	44.20	0.902
SM9	240×120	110	47.10	97.00	66.00	0.680
SM10	240×120	220	47.10	88.00	57.20	0.650
SM11	240×240	220	46.10	91.00	69.00	0.758
SM12	240×240	220	39.90	88.00	61.60	0.700
					Average	0.726
					STDEV	0.082

* dimension parallel to moment given first

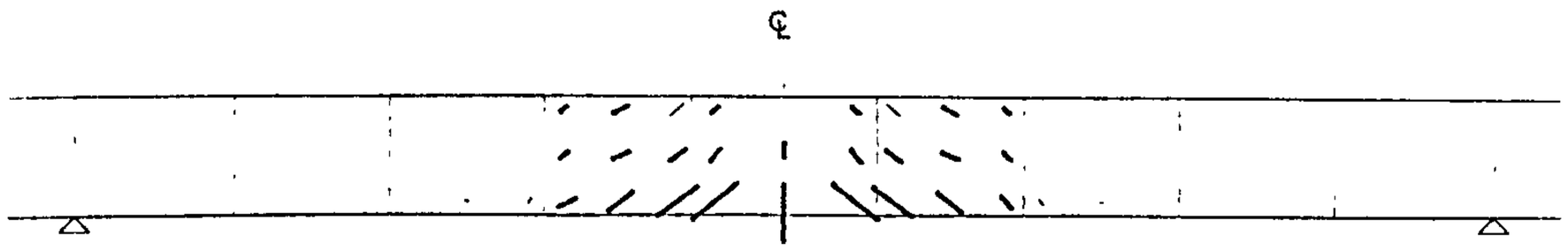

Figure 7.3 Crack pattern for slab SM1 (e=0), **symmetrical punching**

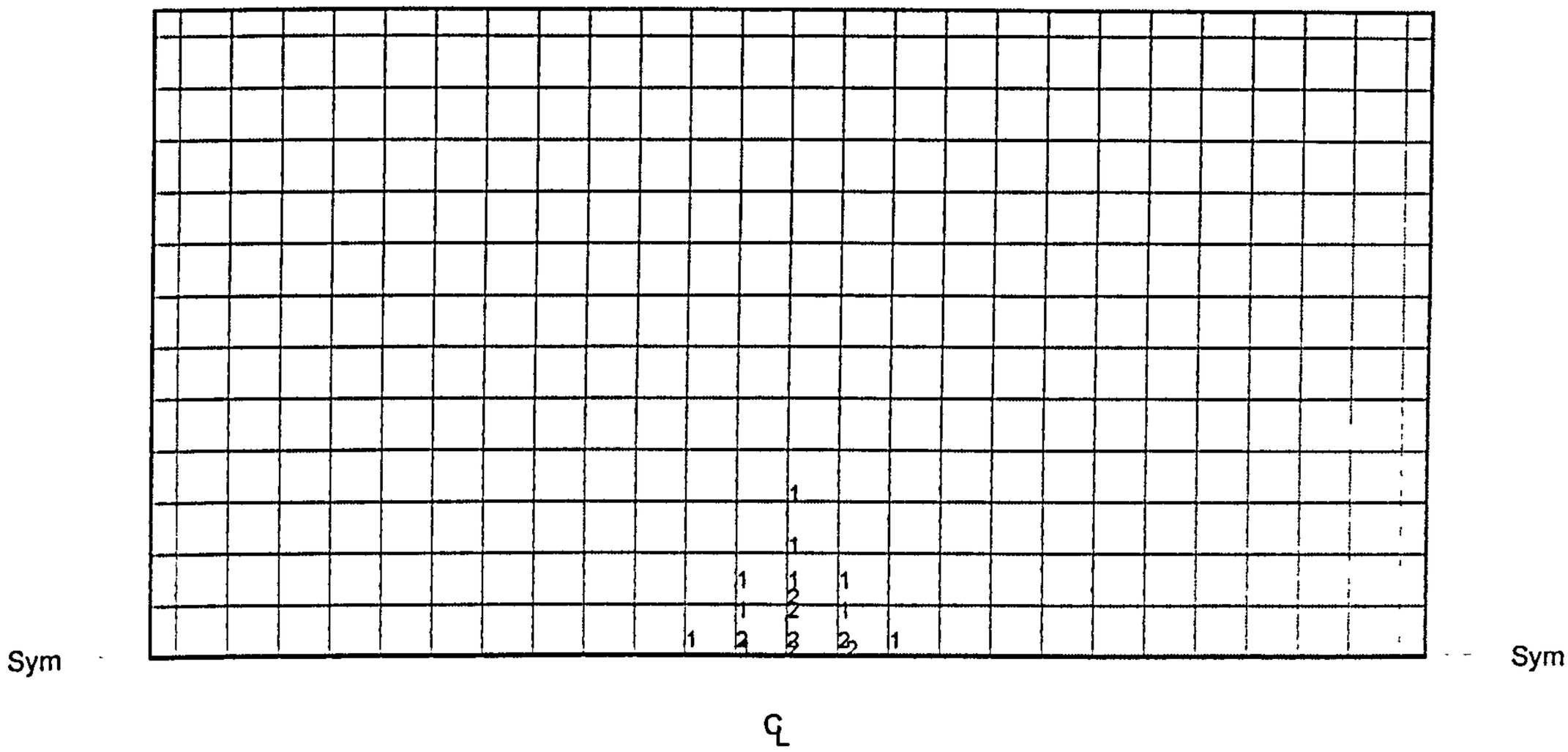

Figure 7.4 Yielding of flexural steel for slab SM1 (e=0)

NB. The numbers on the drawing indicate strain in steel at collapse expressed as a ratio of yield strain

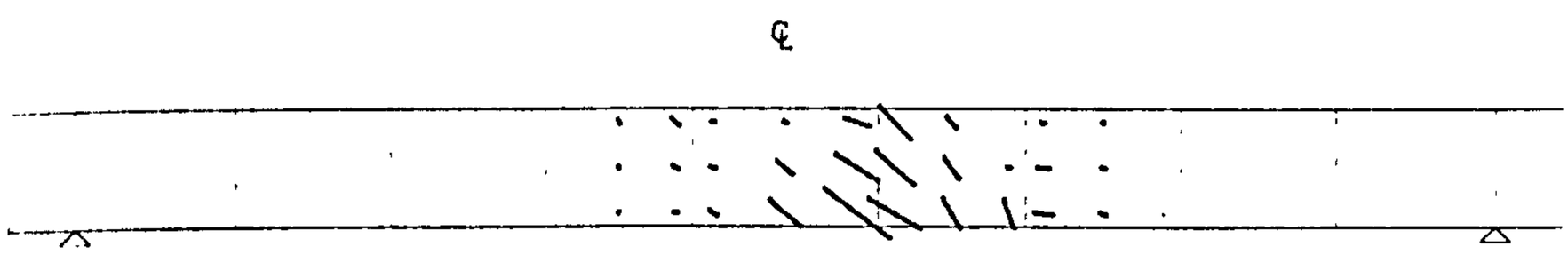

Figure 7.5 Crack pattern for slab SM3 (e=220), **punching occurs at one side only**

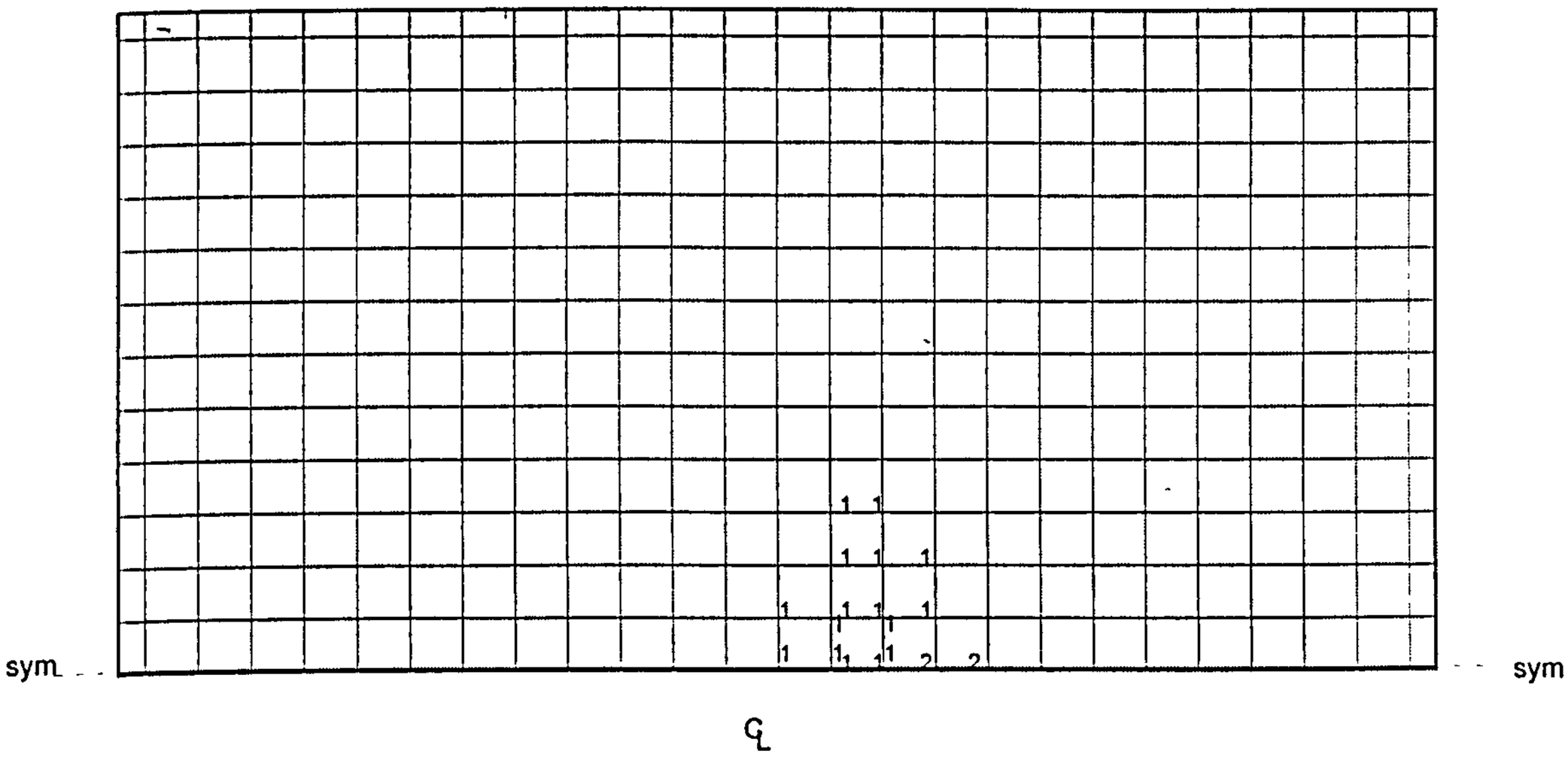

Figure 7.6 Yielding of tension steel for slab SM3 (e=220)

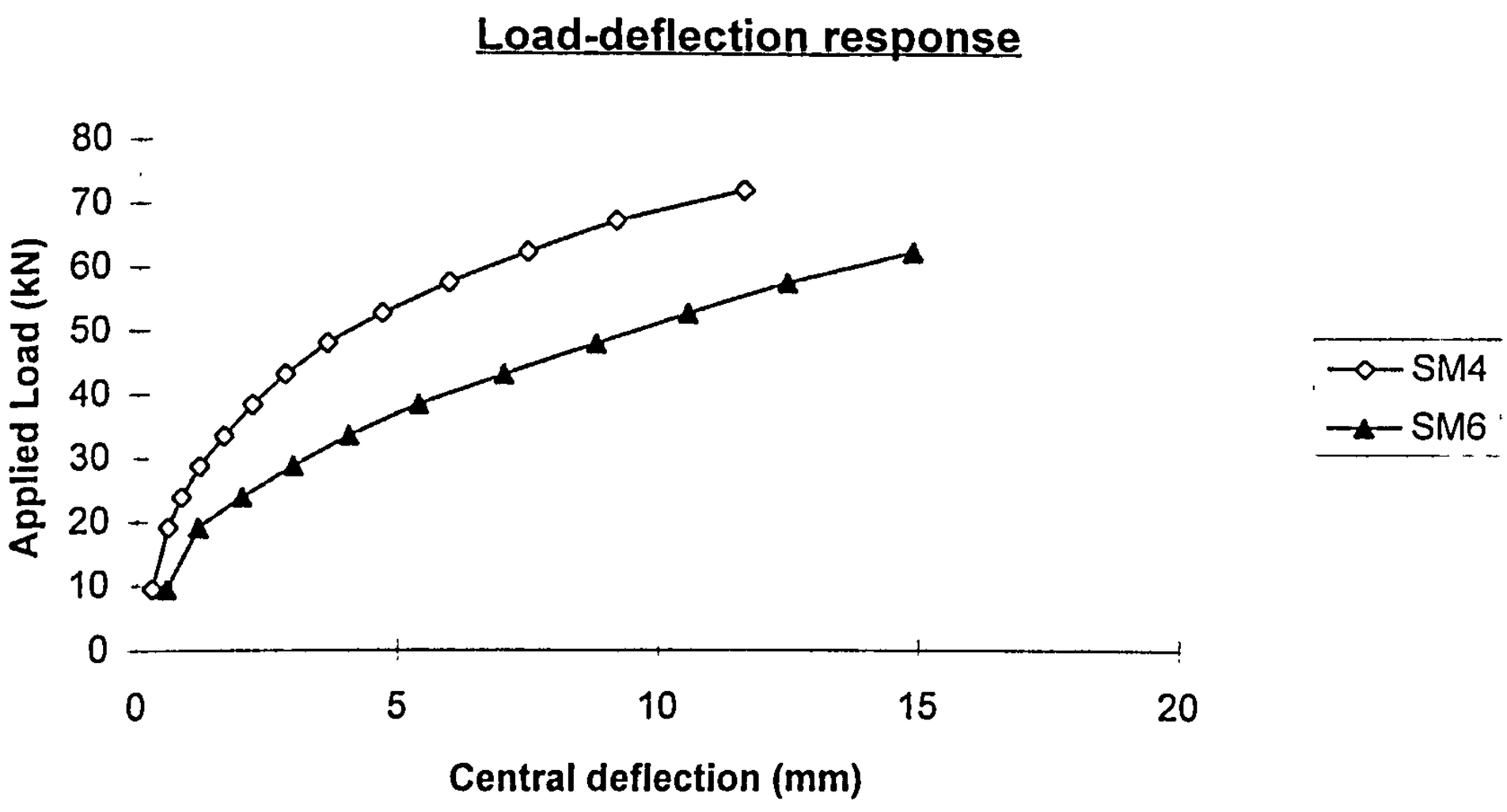

Figure 7.7 Effect of boundary conditions on deflection of slab

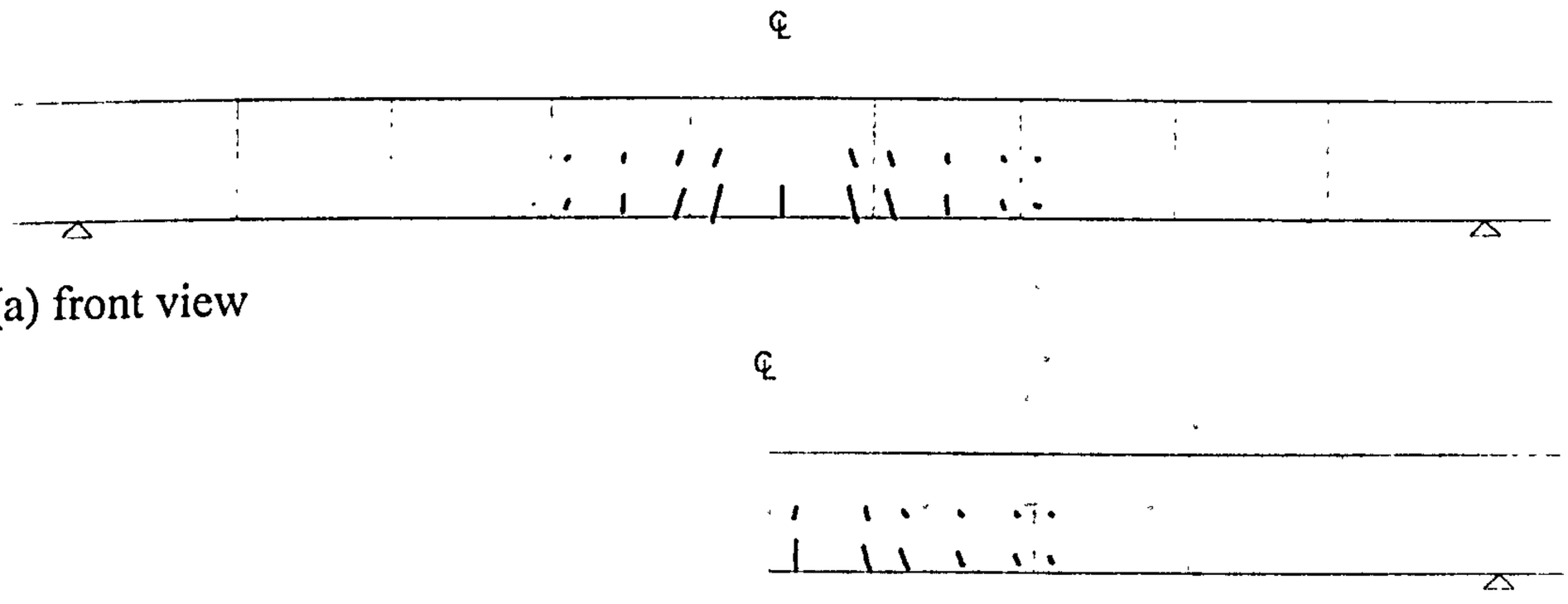

(a) front view

(b) Side view

Figure 7.8 Crack pattern for slab SM6 (e= 0)

7.2.2 Interior column-slab connections with shear reinforcement

Elgabry and Ghali (1987) conducted a series of tests on five full scale specimens of reinforced concrete interior flat slab-column connections subjected to shear and unbalanced moment. The dimensions of these slabs were 1.9m square and 150mm thick. They were all simply supported on four edges over a span of 1.8m. The shear force was applied vertically through the column and unbalanced moment was introduced by two equal and opposite horizontal loads near the column tips (Figure 7.9). The detailing of flexural reinforcement was generally similar in all the specimens (see Figure 7.9) with a slightly different steel ratio in the vicinity of the column within a distance of (column width + 3 x slab thickness).

The first slab had no shear reinforcement, while the remaining four contained various arrangements of stud shear reinforcement. The stud-shear reinforcement was arranged around the column in a cross shape on plan. The main variable for these slabs was the spacing and diameter of the shear reinforcement. Details are presented in Table 7.2.

One-half of slab was modelled with a 11×6 mesh. The vertical load was simulated by uniformly distributed load over the column while the horizontal load was simulated by a line load along the tips of column (Figure 7.10). In the experiment, vertical loads and moment were applied alternately before service load level. After reaching the service load, the unbalanced moment was cycled 10 times, then shear force was increased to V_{test} (Table 7.3) and kept constant. Subsequently the unbalanced moment was increased until failure. However, in the numerical study, these loads were applied simultaneously.

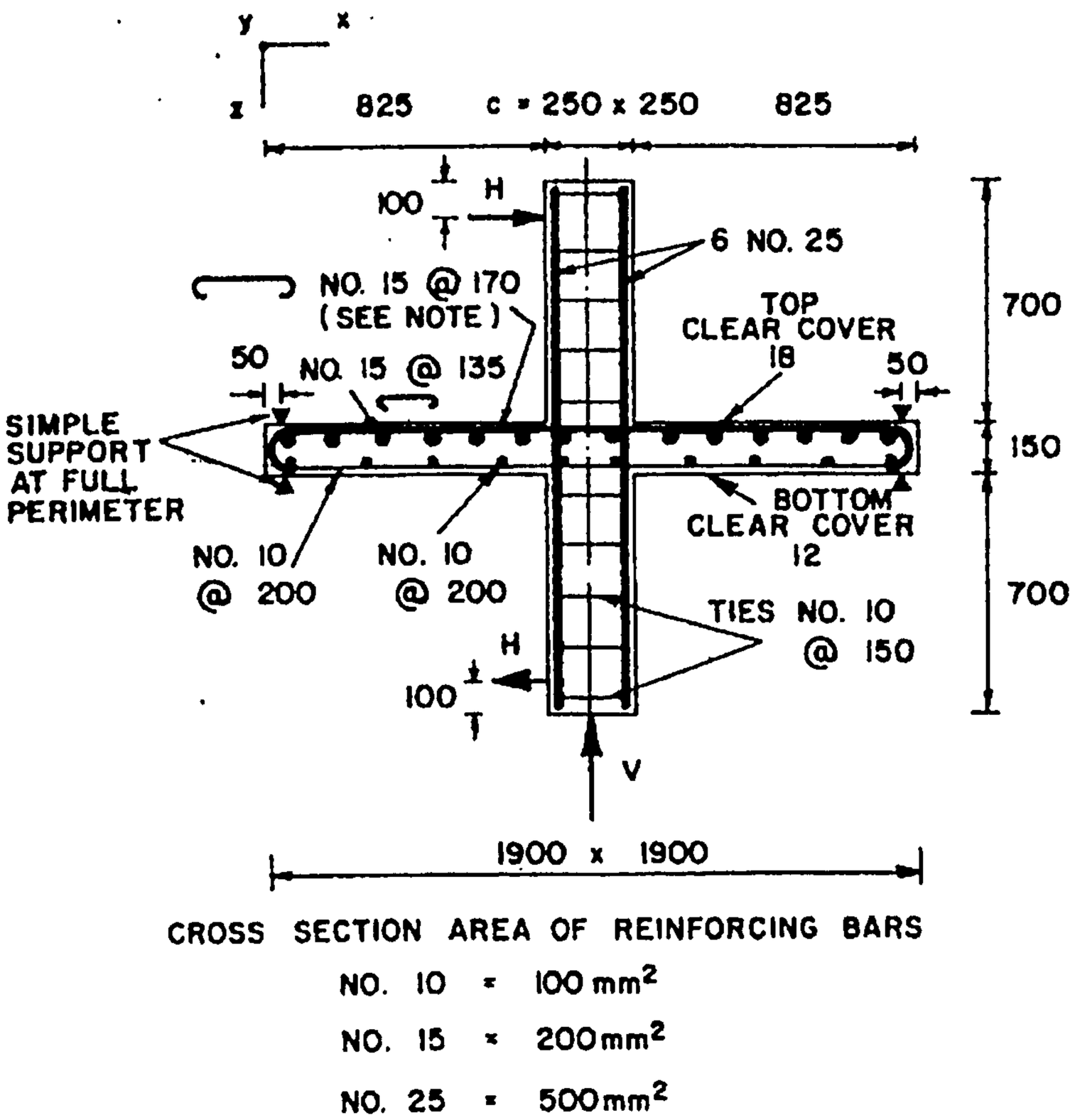

Figure 7.9 : Details and dimensions for specimens 1-5

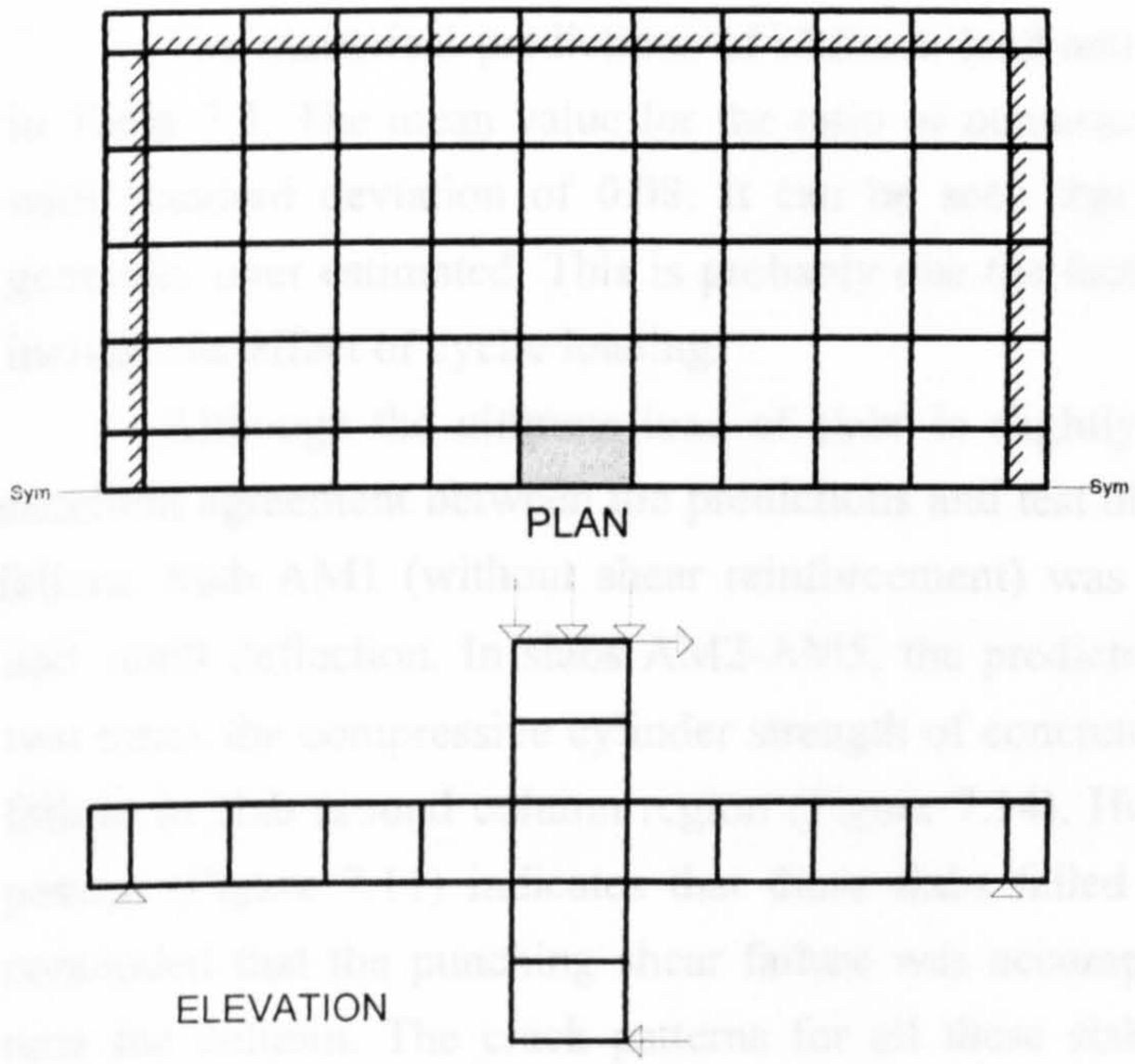

Figure 7.10 : Finite element mesh and boundary conditions

Table 7.2: Details of shear reinforcement (Elgabry and Ghali)

Slab No	Number	Diameter (mm)	f_{yv} N/mm^2	Stud row spacing
AM1	-	-	-	-
AM2	32	12.7	460	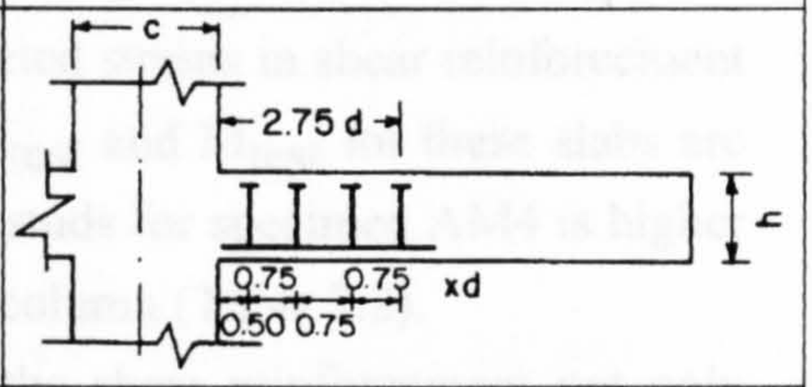
AM3	48	12.7	460	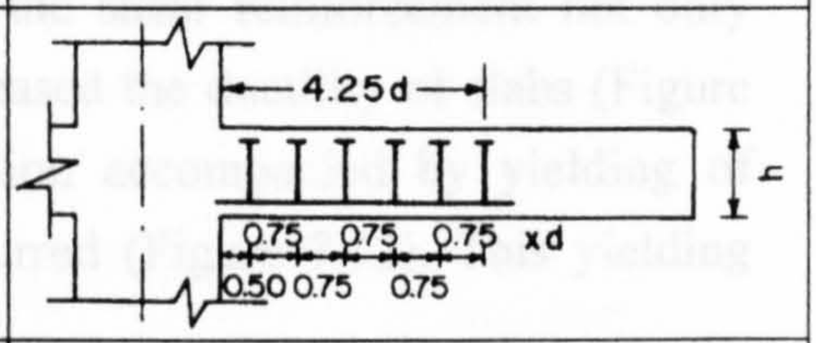
AM4	32	9.5	500	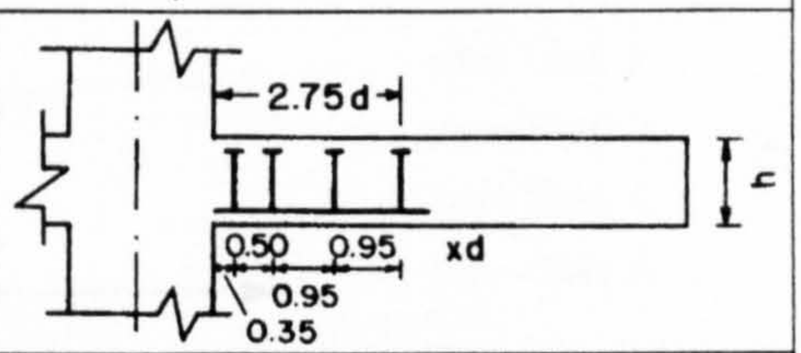
AM5	48	9.5	500	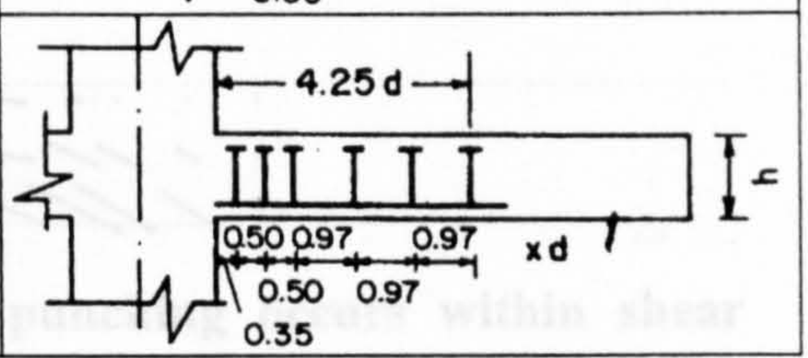

f_{yv}=yield stress of shear stud

The numerical predictions of ultimate load and mode of failure are presented in Table 7.3. The mean value for the ratio of numerical-to-experimental load is 1.05 with standard deviation of 0.08. It can be seen that the ultimate load of slabs is generally over estimated. This is probably due the fact that present analysis does not include the effect of cyclic loading.

Although the ultimate load of slabs is slightly over predicted, there was an excellent agreement between the predictions and test observation in terms of mode of failure. Slab AM1 (without shear reinforcement) was predicted to fail by punching and small deflection. In slabs AM2-AM5, the predicted compressive stress is about two times the compressive cylinder strength of concrete which indicates compression failure in slab around column region (Figure 7.14). However, a vector plot of crack pattern (Figure 7.11) indicates that these slabs failed in punching. Therefore, it is concluded that the punching shear failure was accompanied by compression failure near the column. The crack patterns for all these slabs were similar. Shear failure occurred near the column face at the right hand side, as shown in Figure 7.11. This is because unbalanced moment caused the shear stresses near face of column at right hand side to be larger than shear stresses at the other faces. There is also another indication given by the crack pattern, which is that punching shear failure in slabs AM2-AM5 took place within the shear reinforced zone as observed in the experiment.

Specimens AM2 and AM3 were over reinforced for shear. Therefore the studs in these slabs did not yield (Figure 7.15). The predicted strains in shear reinforcement for specimen AM3 and AM4 are almost similar (V_{test} and M_{test} for these slabs are also almost similar), but the corresponding strain in studs for specimen AM4 is higher at failure because the studs are located nearer to the column (Table 7.2).

This series of slabs also demonstrate that the shear reinforcement not only increased the ultimate load of slab, but it also increased the ductility of slabs (Figure 7.13). Slabs AM3-AM5 failed at a large deflection accompanied by yielding of flexural steel at the side where the punching occurred (Figure 7.12). This yielding caused a ductile failure mode.

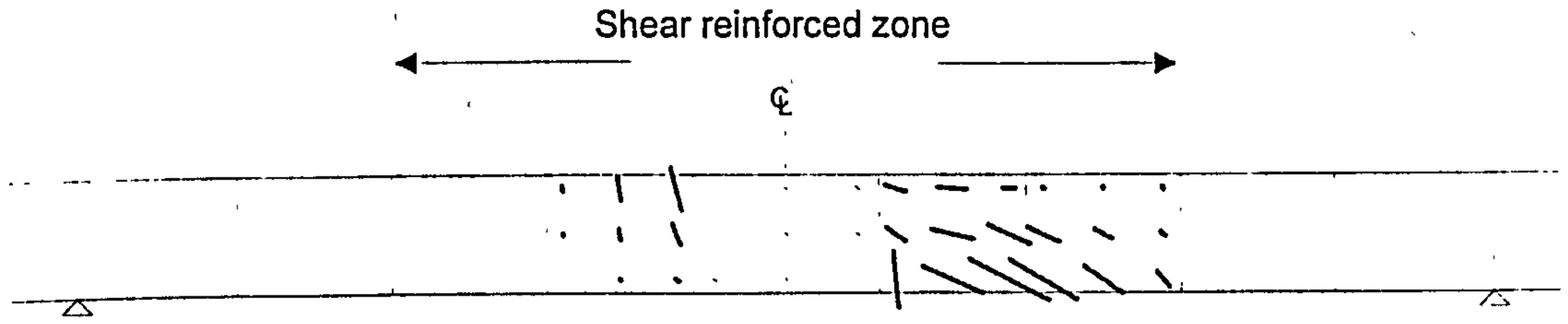

Figure 7.11 Crack pattern for Specimen AM3, **punching occurs within shear reinforced zone**

Table 7.3: Summary of test results and numerical predictions (Elgabry & Ghali)

	Test results					Numerical results	
Specimen	f_c' N/mm^2	*ρ (%)	V_{test} (kN)	M_{test} (kNm)	failure mode	Num/Exp ratio**	failure mode
AM1	35.00	1.10%	150	130	s	0.95	s
AM2	33.70	1.10%	150	162	s	1.10	s
AM3	39.00	1.23%	300	142	fp	1.15	fp
AM4	40.80	1.39%	300	150	fp	1.15	fp
AM5	55.60	1.39%	450	105	fp	1.05	fp
					Average	1.05	
					STDEV	0.084	

*the steel ratio within a distance of (column width + 3 times slab thickness) at column region

**In the numerical analysis, proportional loading was used . Therefore the quoted ratio applies to both V and M.

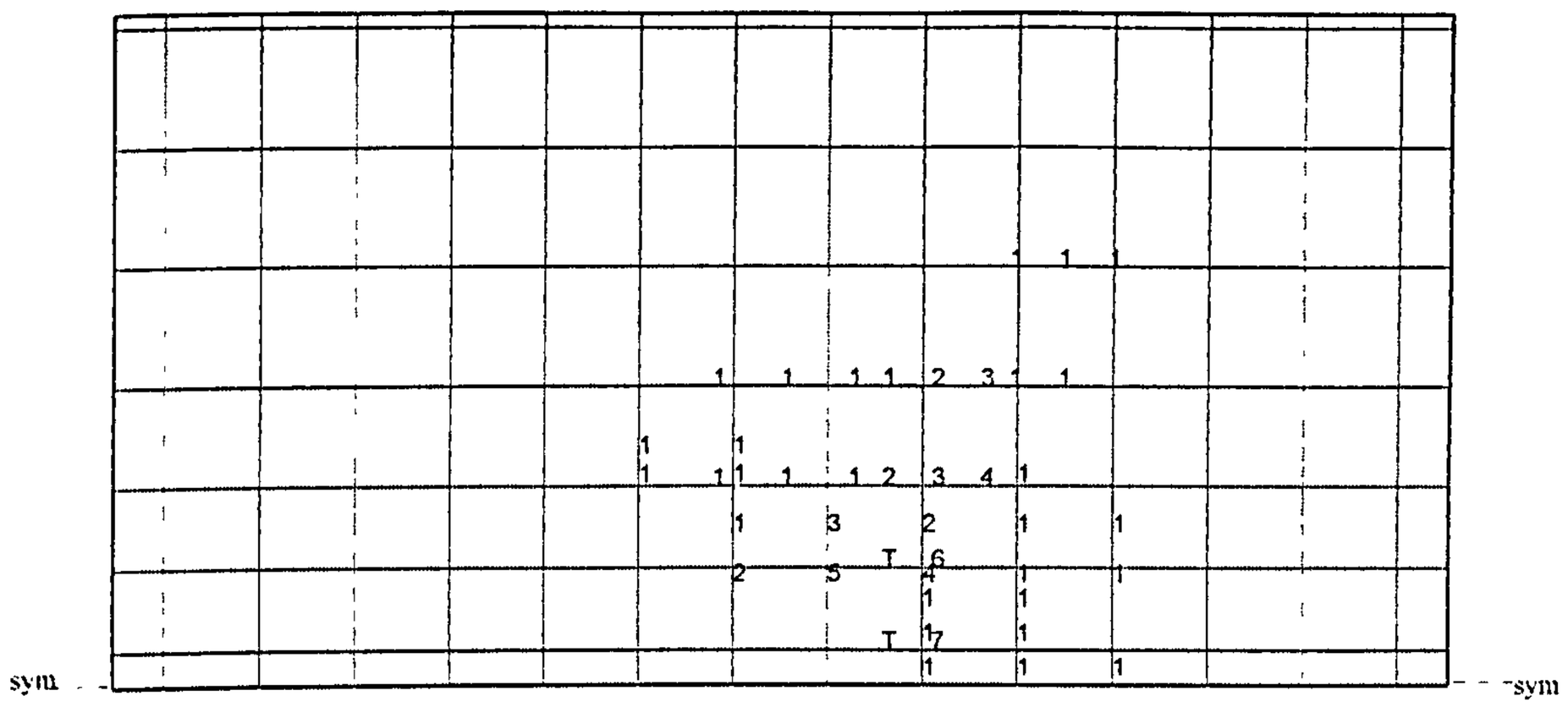

Figure 7.12 Yielding of flexural steel for Specimen AM3
(The numbers on the drawing indicate strain in steel at collapse expressed as a ratio of yield strain)

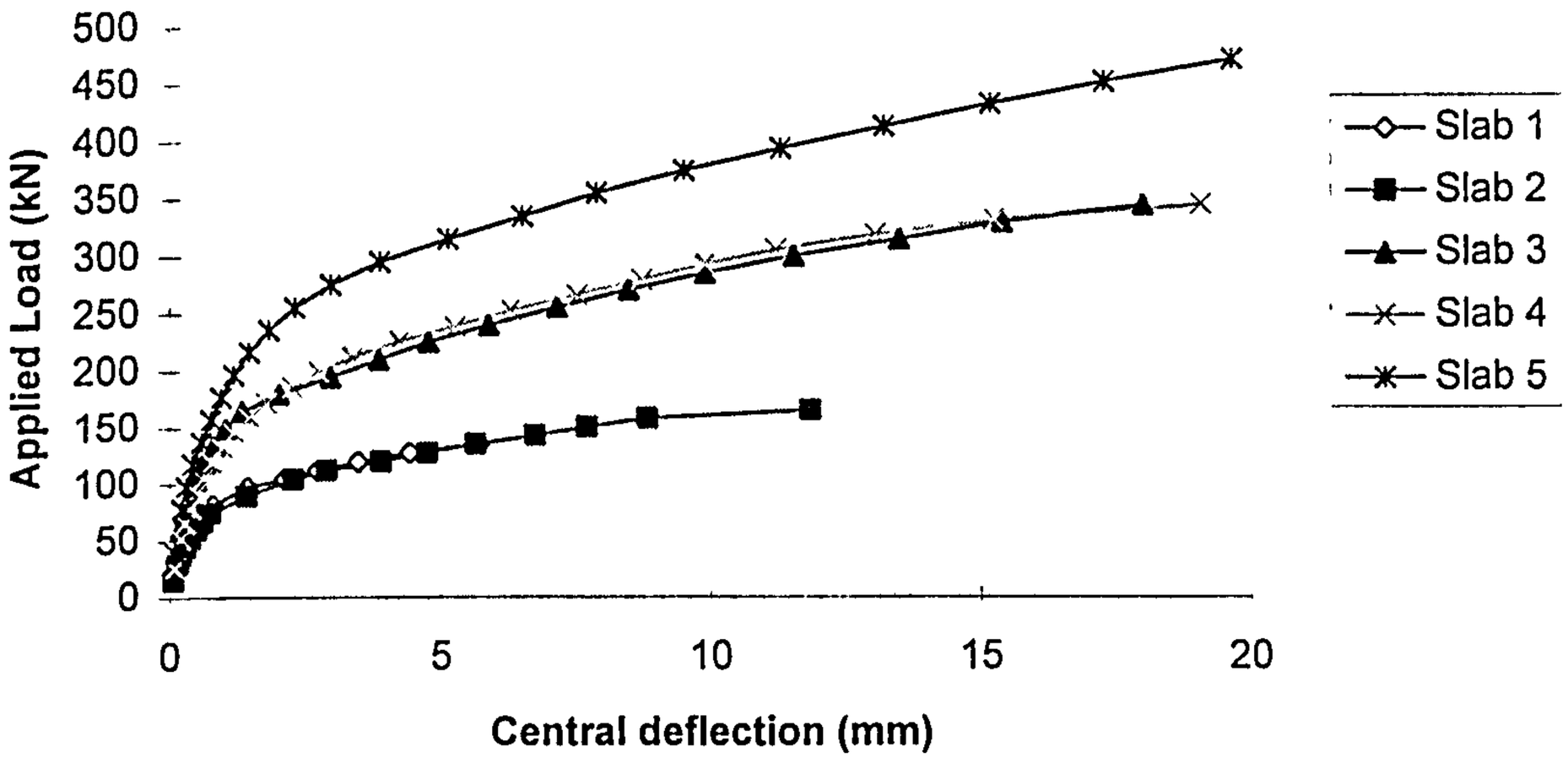

Figure 7.13 Predicted Load-deflection response for slabs AM1-AM5

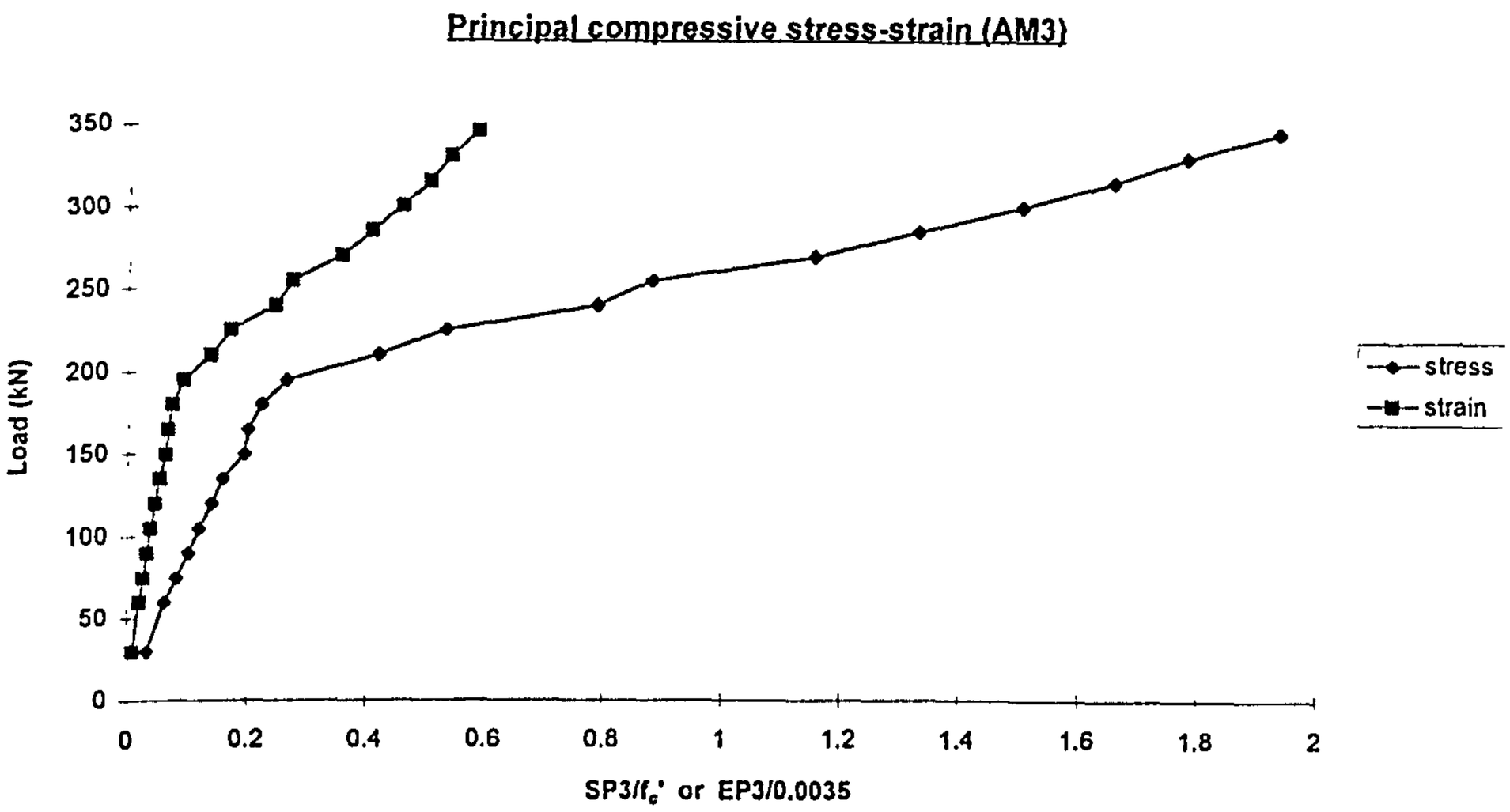

Note: SP3=σ_3=maximum compressive principal stress

EP3=ε_3=maximum compressive principal strain

Figure 7.14 Predicted principal compressive stress-strain in slab near the column

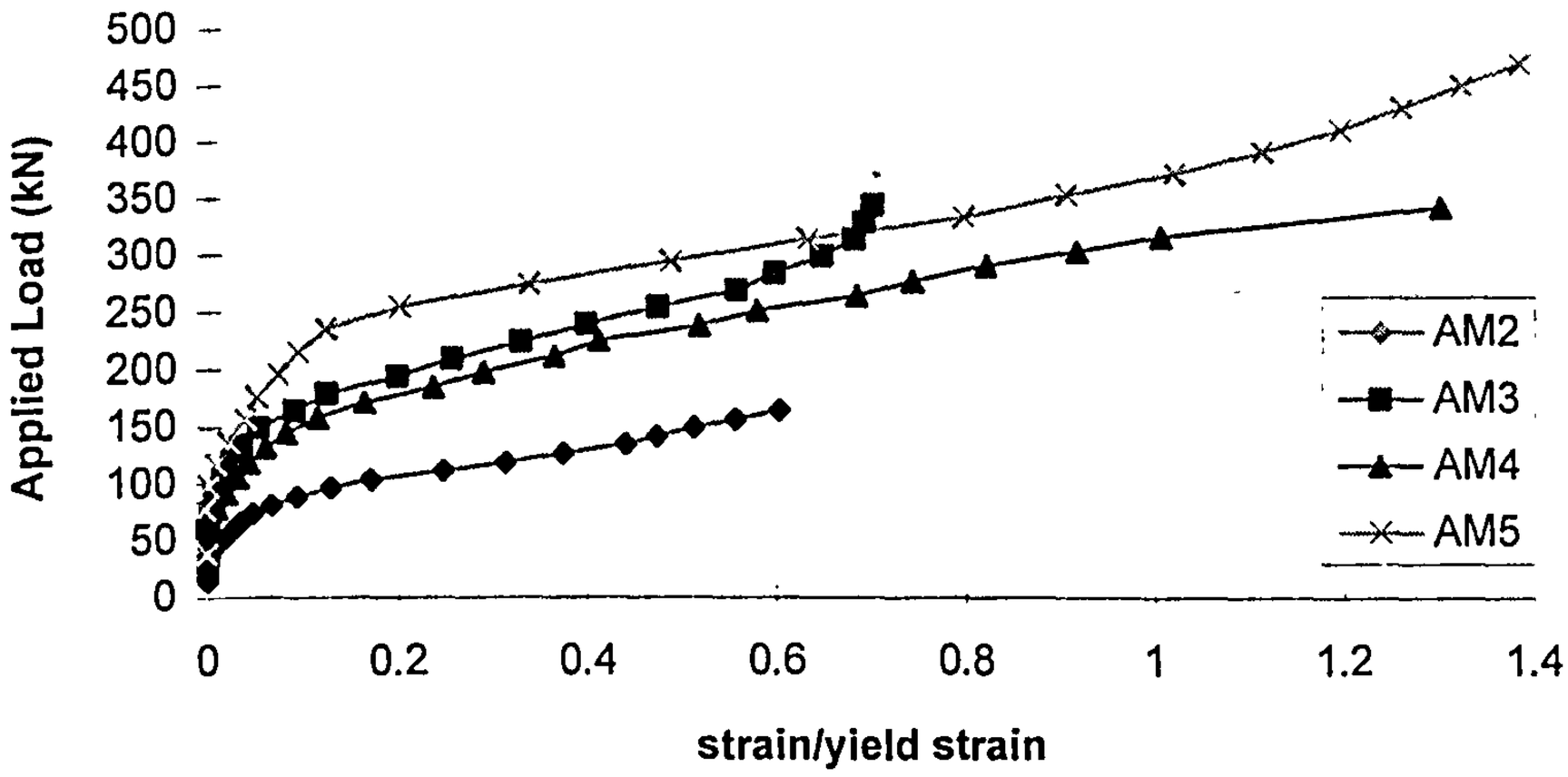

Figure 7.15 Strain in first row shear reinforcement (Predicted)

7.3 Edge column-slab connections

7.3.1 Edge column-slab connections tested by Zakaria (1978)

Eight edge column-slab specimens tested by Zakaria were analysed. These slabs were supported on two rectangular edge columns which extended above the slab, the ends of the columns were restrained by strut made of two channels (127×64 back to back) at the upper ends and by one 13mm diameter tie bar at the lower ends. Loads were applied to the slab at eight points to give a reasonably uniform distribution (Figure 7.16). This type of arrangement allows the transfer of shear and moment to develop naturally in response to the loading of slab.

The main variables for this series were : the percentage of reinforcement at the slab-column junction and the size of column. Concrete strength ranged from 34.3 to 55.2 N/mm^2. Only specimens SE3 contained shear reinforcement. The details are summarised in Table 7.4.

Owing to symmetry, only one-quarter of the slab was modelled. The applied load was simulated by concentrated load acting at a nodal point. Concrete slab was discretised by using one layer of twenty node solid elements. Column was discretised by one element on plan and four elements from upper/lower end. Vertical restraints were applied to the mid-side nodes only at the lower end of the column (Figure 7.17). The element at the lower end of the column was represented by linear elastic element to prevent local crushing. The tie and strut were represented by linear elastic element at the end of the column. The stiffness of these elements was equivalent to the stiffness of tie and strut respectively.

Table 7.4: Details and test results of Zakaria's edge slabs

Slab	*Column Size(mm)	Top steel (%)	Btm steel (%)	f_{cu} N/mm^2	V_{test} (kN)	M_{test} (kNm)	Failure Mode
SE1	300×200	1.04	1.33	44.6	198.0	39.5	s
SE2	300×200	0.58	1.33	54.6	192.0	34.0	y
SE3	300×200	0.58	1.33	45.8	256.0	32.5	y
SE4	200×300	1.04	1.33	34.3	152.0	30.5	s
SE5	200×300	0.82	0.62	55.2	164.0	38.5	fp
SE6	200×300	0.65	0.88	40.0	149.0	27.5	fp
SE7	200×300	0.75	0.37	49.5	129.0	31.7	fp
SE8	300×100	0.82	0.62	52.0	136.0	33.7	s

*First figure = dimension perpendicular to free edge

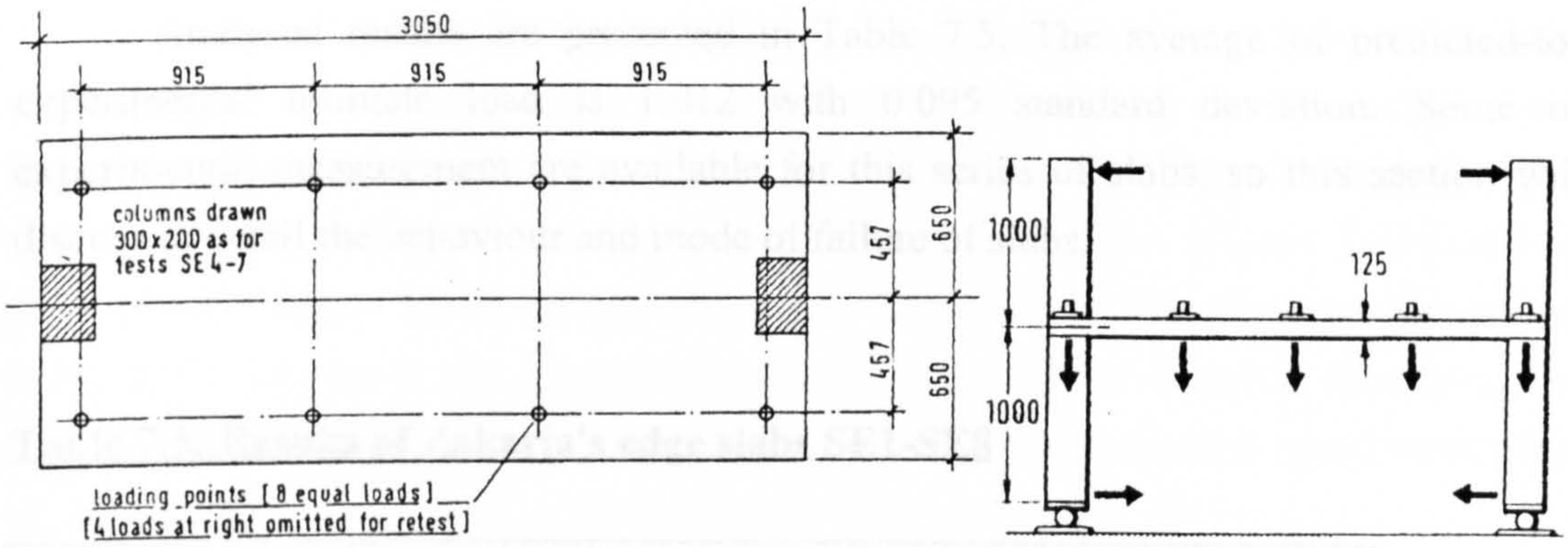

Plan Elevation

Figure 7.16 : Test arrangements for slabs SE1-SE8.

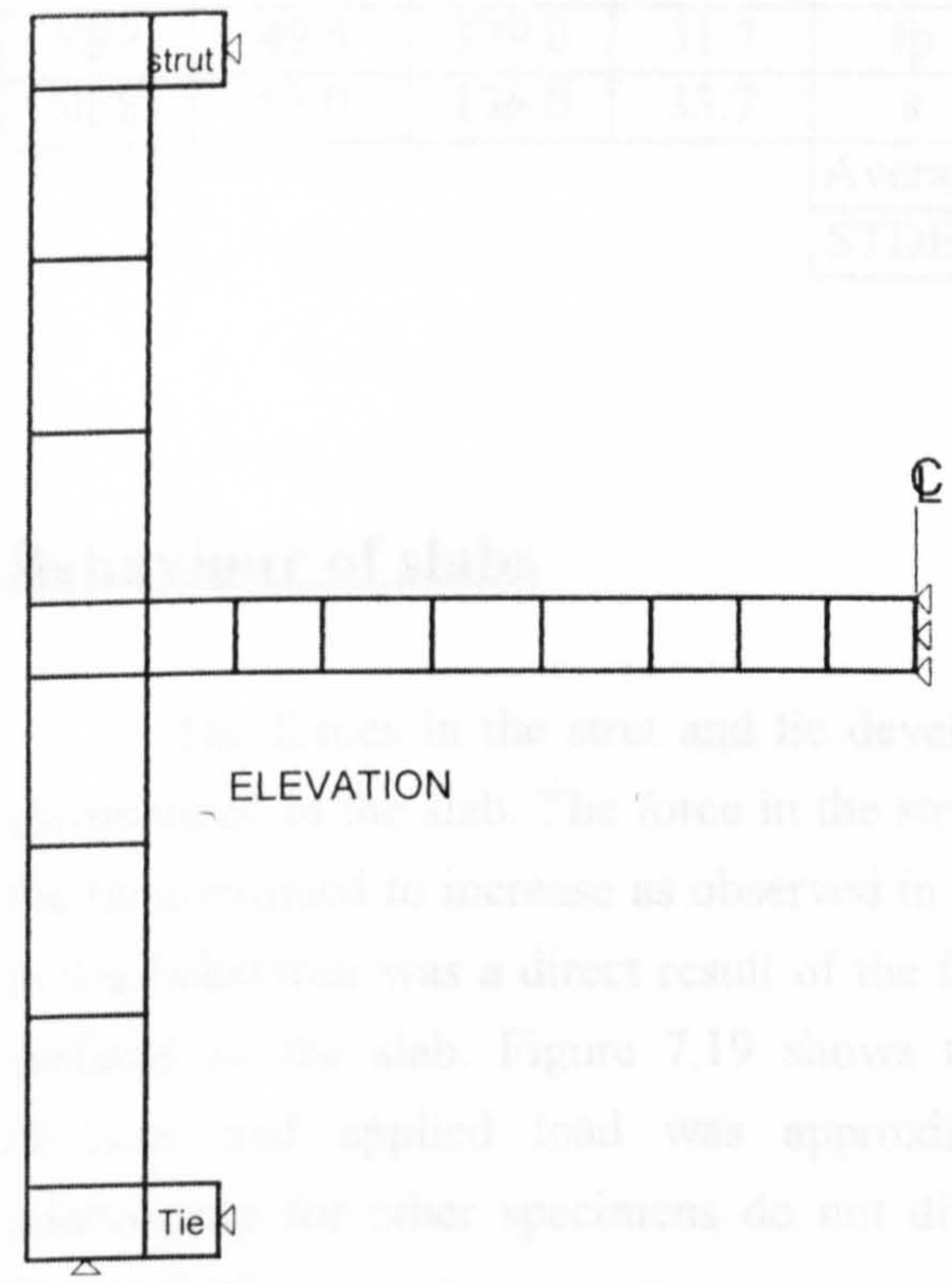

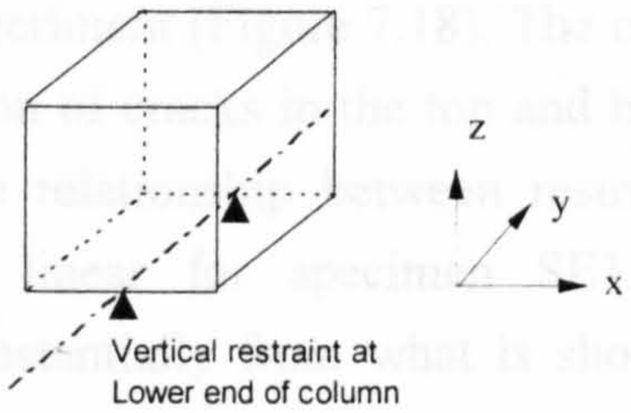

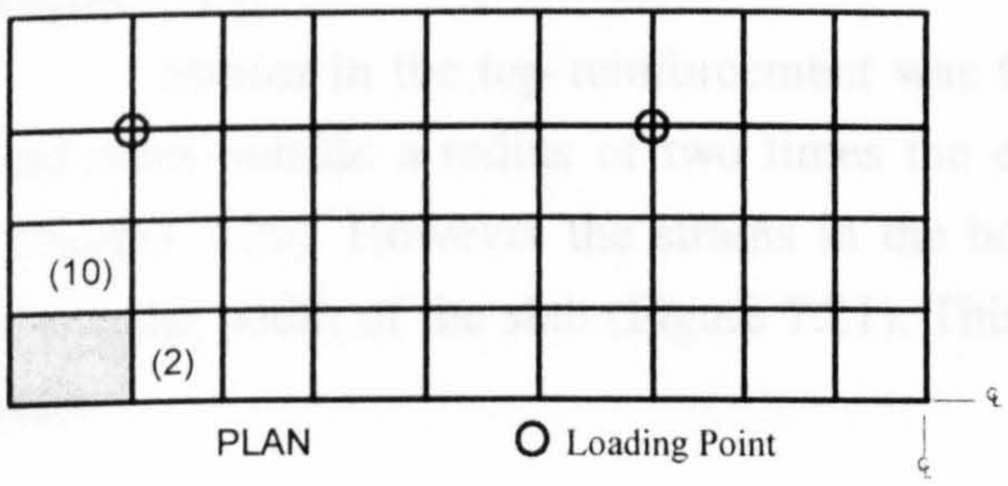

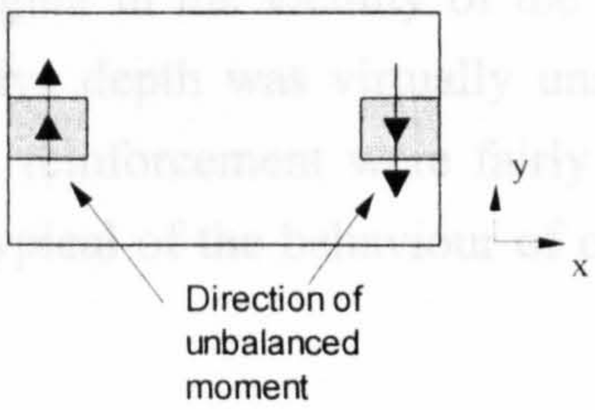

Figure 7.17 : Finite element model and boundary conditions for edge supported slabs.

Analysed results are presented in Table 7.5. The average of predicted-to-experimental ultimate load is 1.012 with 0.095 standard deviation. Some of experimental measurement are available for this series of slabs, so this section will discuss in detail the behaviour and mode of failure of slabs.

Table 7.5: Results of Zakaria's edge slabs SE1-SE8

Slab No.	f_{cu} N/mm^2	Experimental			Numerical		
		V_{test} (kN)	M_{test} (kNm)	Failure Mode	Num/Exp V	Num/Exp M	Failure Mode
SE1	44.6	198.0	39.5	s	0.859	0.958	s
SE2	54.6	192.0	34.0	y	1.128	1.001	y
SE3	45.8	256.0	32.5	y	1.000	1.158	y
SE4	34.3	152.0	30.5	s	1.000	1.102	s
SE5	55.2	164.0	38.5	fp	0.950	1.047	fp
SE6	40.0	149.0	27.5	fp	0.969	1.052	fp
SE7	49.5	129.0	31.7	fp	1.042	1.280	fp
SE8	52.0	136.0	33.7	s	1.150	1.092	s
				Average	1.012	1.086	
				STDEV	0.095	0.100	

Behaviour of slabs

The forces in the strut and tie developed at equal rate until general cracking commenced in the slab. The force in the strut then began to decrease and the force in the tie continued to increase as observed in the experiment (Figure 7.18). The change in the behaviour was a direct result of the formation of cracks in the top and bottom surfaces of the slab. Figure 7.19 shows that the relationship between restraining moment and applied load was approximately linear for specimen SE1. The relationship for other specimens do not differ substantially from what is shown in Figure 7.19.

Strains in the top reinforcement was far higher in the vicinity of the column and steel outside a radius of two times the effective depth was virtually unstrained (Figures 7.20). However the strains in the bottom reinforcement were fairly similar along the width of the slab (Figure 7.21). This is typical of the behaviour of one way slab.

The crack pattern at top surface was of elliptical shape (Figure 7.22). The crack pattern shows that punching shear failure originated near the inner face of the column and punching surface grew around the column, eventually reaching the free edge. Numerical results shows that concrete at the top surface (Figure 7.23a) and at soffit of slab (Figure 7.23b) adjacent to column had crushed. The crushing of concrete at the soffit was due to the flexural action in the longitudinal direction. However, the concrete at the top surface has crushed because of compressive membrane action (Figure 7.24).

The slab tends to expand due to the formation of cracks in the top and bottom surfaces. As the column is very stiff, it restrains element No. 2 (see Figure 7.17) from expanding. Consequently, this results in a compressive force in that section and this is known as compressive membrane action. The development of compressive membrane action was confirmed by checking the third principal strain in element No. 2. There is a very large compressive strain throughout the depth of the slab.

Shear strain along the inner face of column was fairly uniform (Figure 7.25). However, shear strain along the face of column perpendicular to the free edge is minimum at the outer corner and maximum at the inner corner (Figure 7.26). These two figures clearly show that the shear strain is the resultant of direct shear V_u and shear due to unbalanced moment M_{yy} (Figure 7.27).

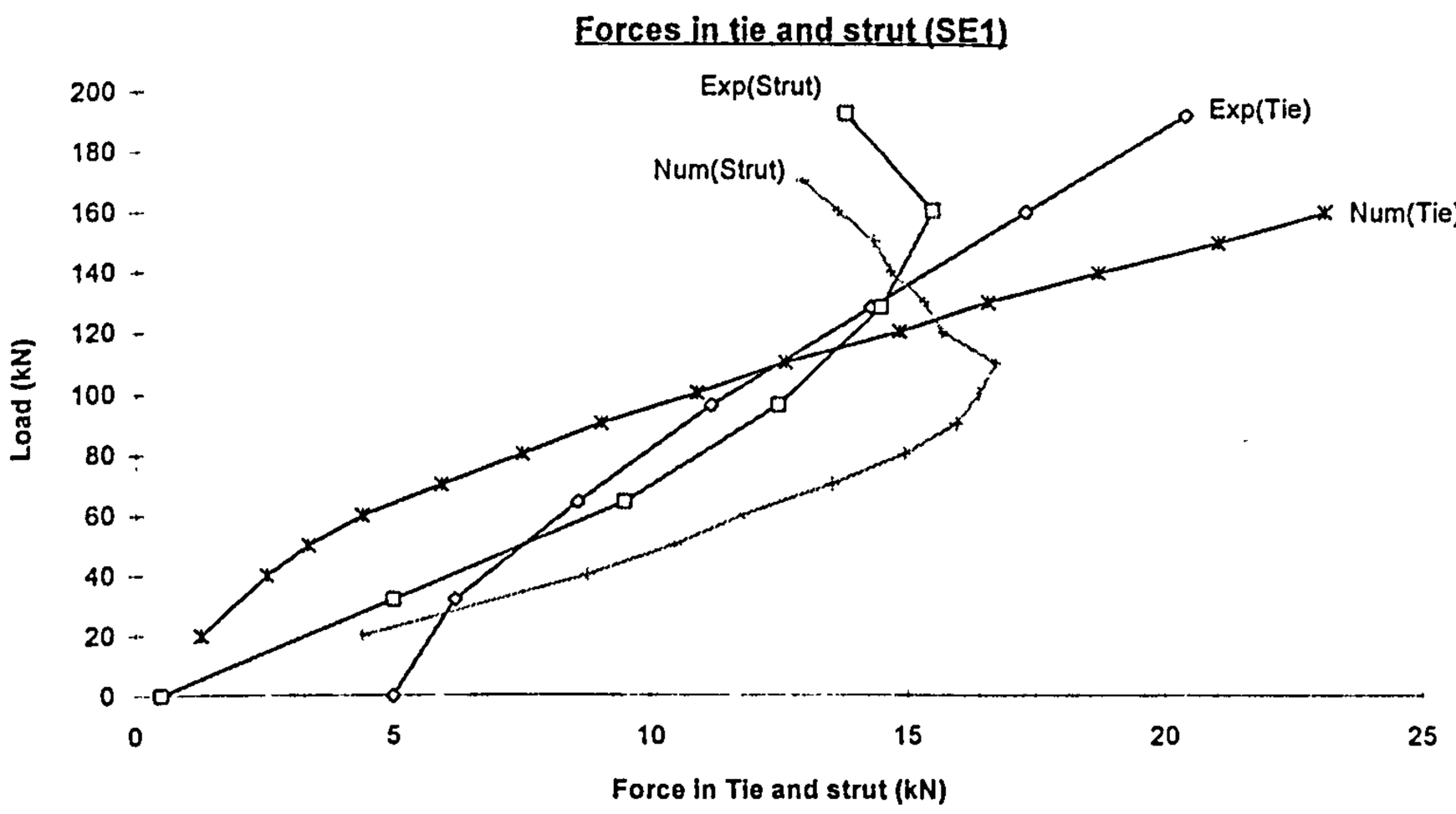

Figure 7.18 : Forces in Struts and Ties (SE1)

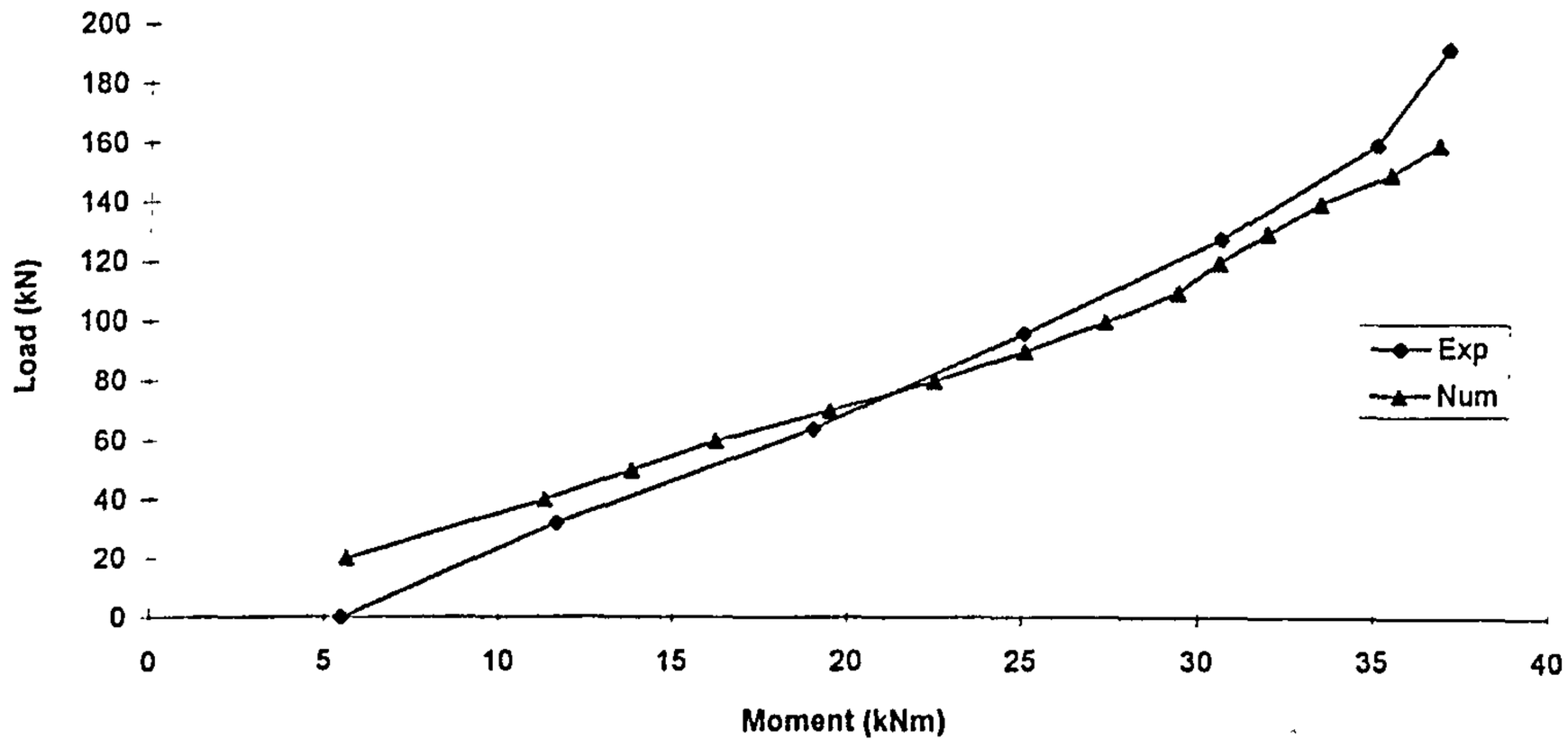

Figure 7.19 : Column's Load and moment (SE1)

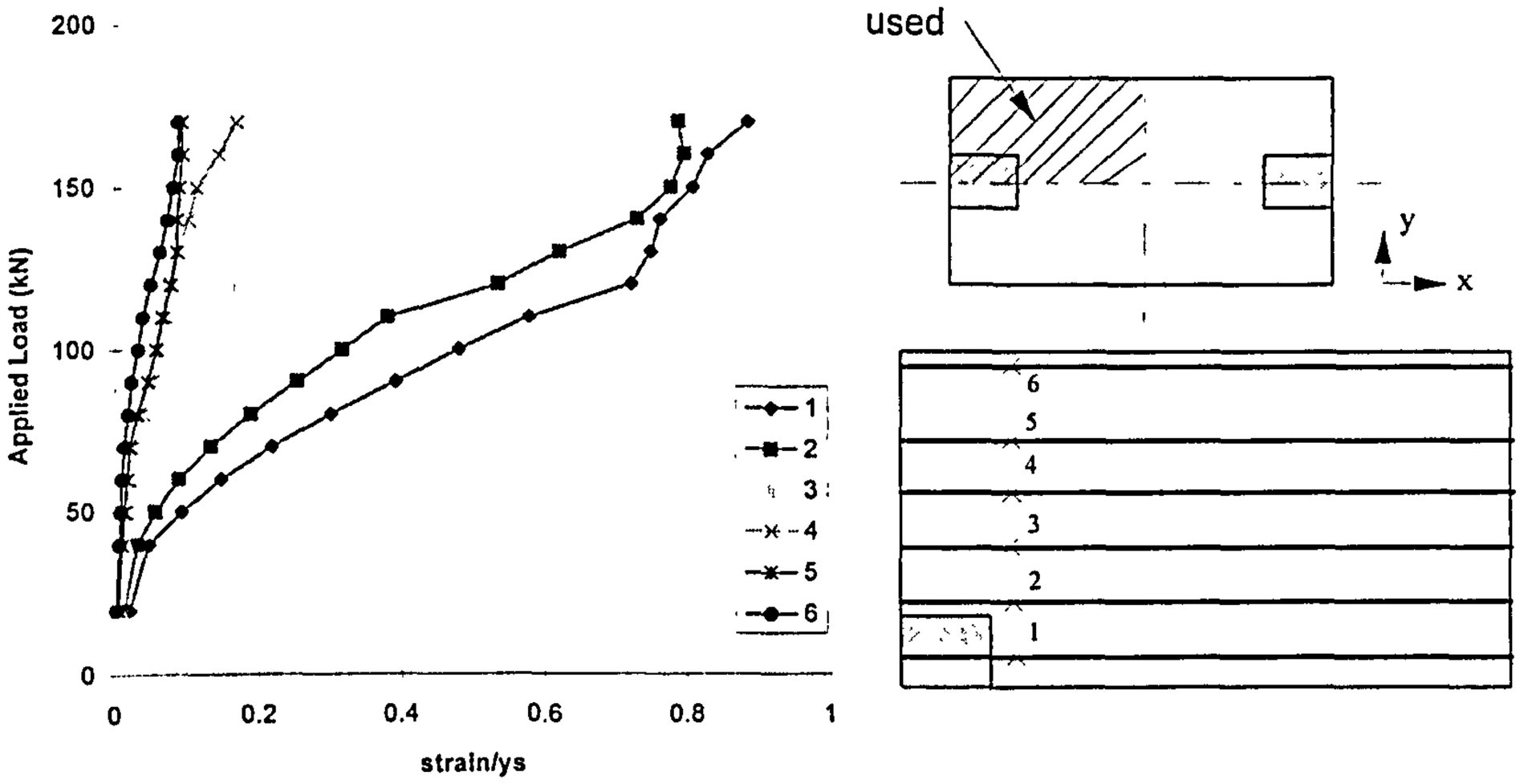

Figure 7.20 : Predicted strain in top steel in X-direction (SE1)

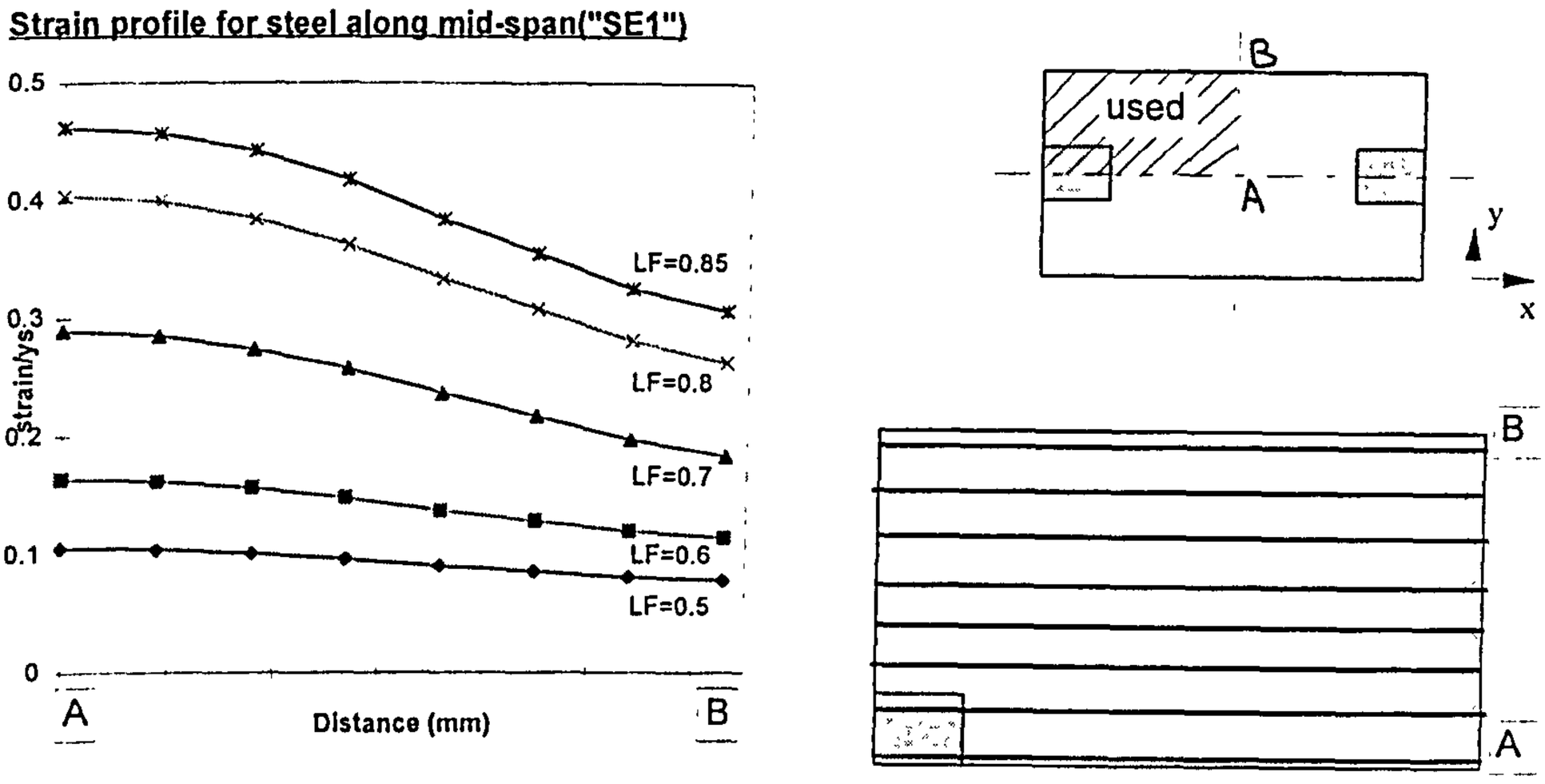

Figure 7.21 : Predicted strain profile for bottom steel at mid-span (SE1)

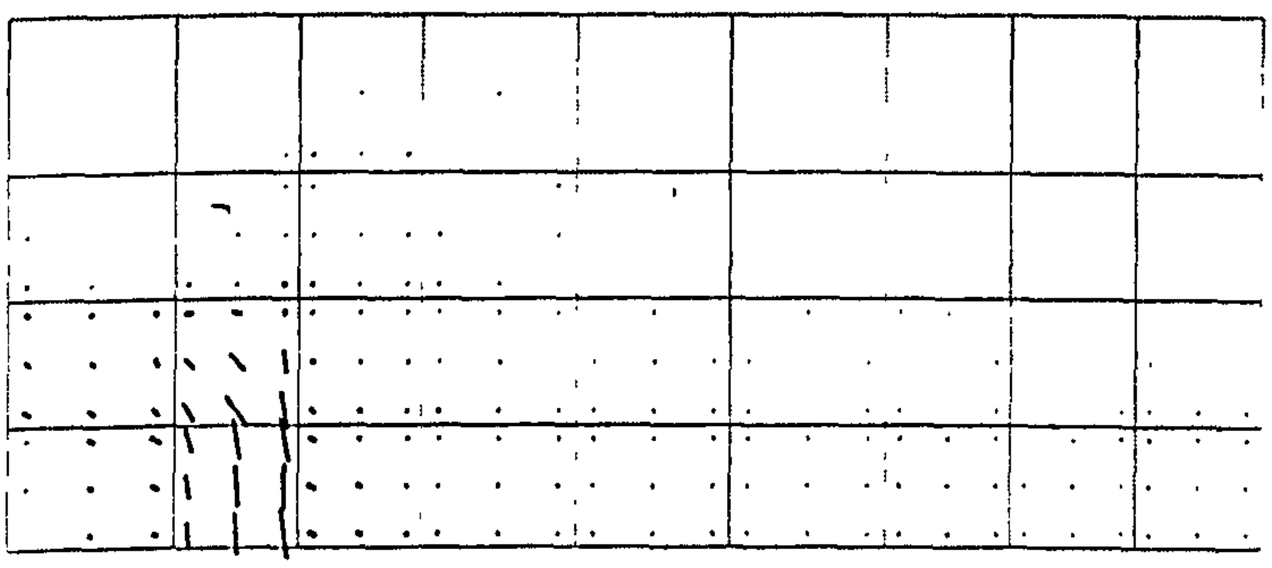

Figure 7.22 Crack pattern at top surface of slab

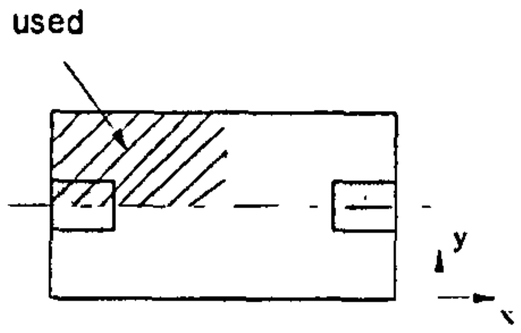

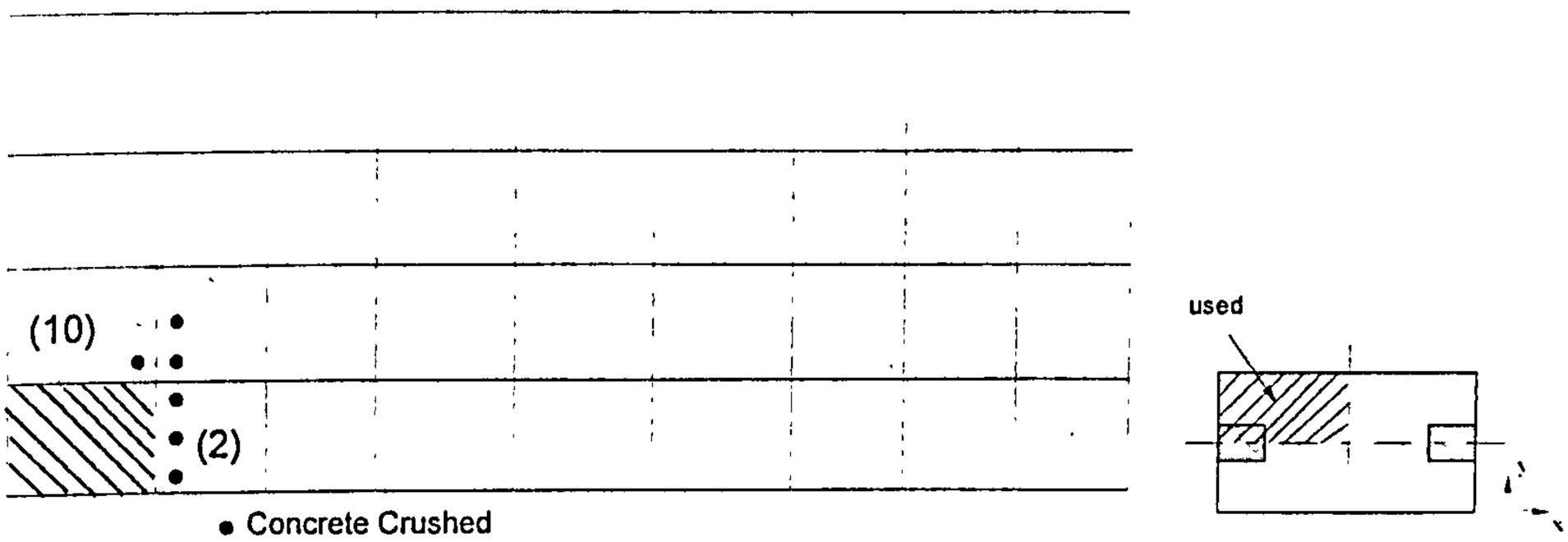

(a) Crushing at soffit of slab (SE1)

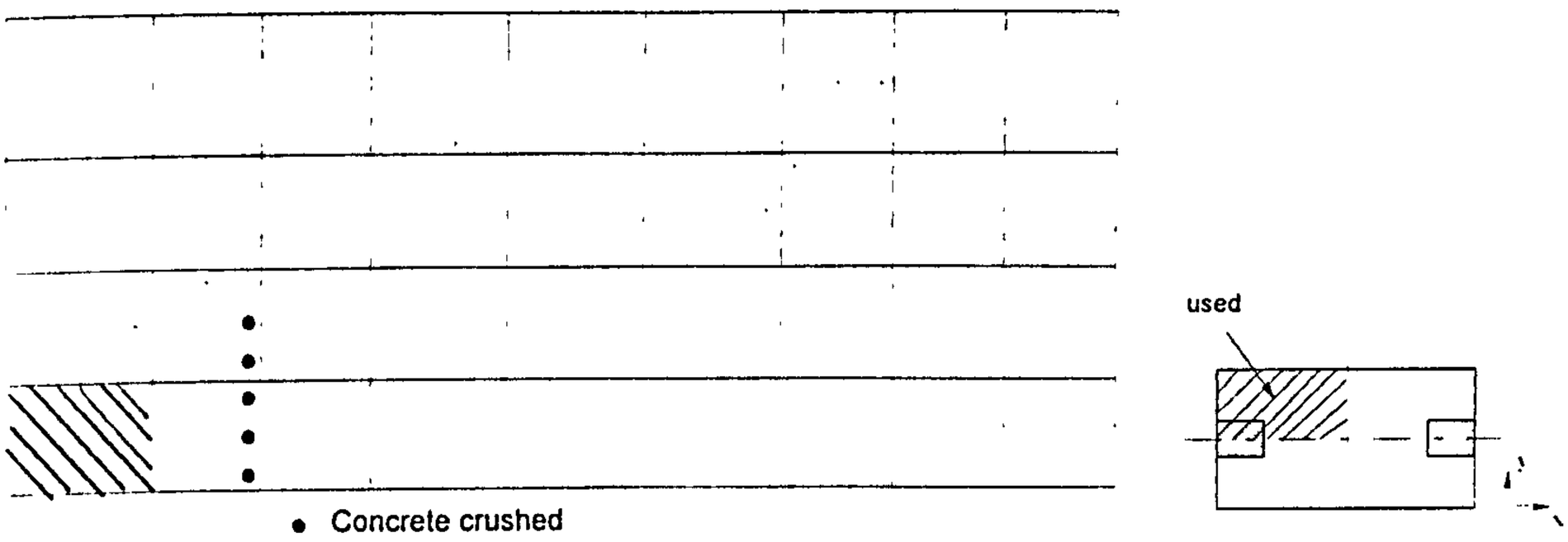

(b) Crushing at top surface of slab (SE1)

Figure 7.23 Crushing of concrete near at the slab-column junction

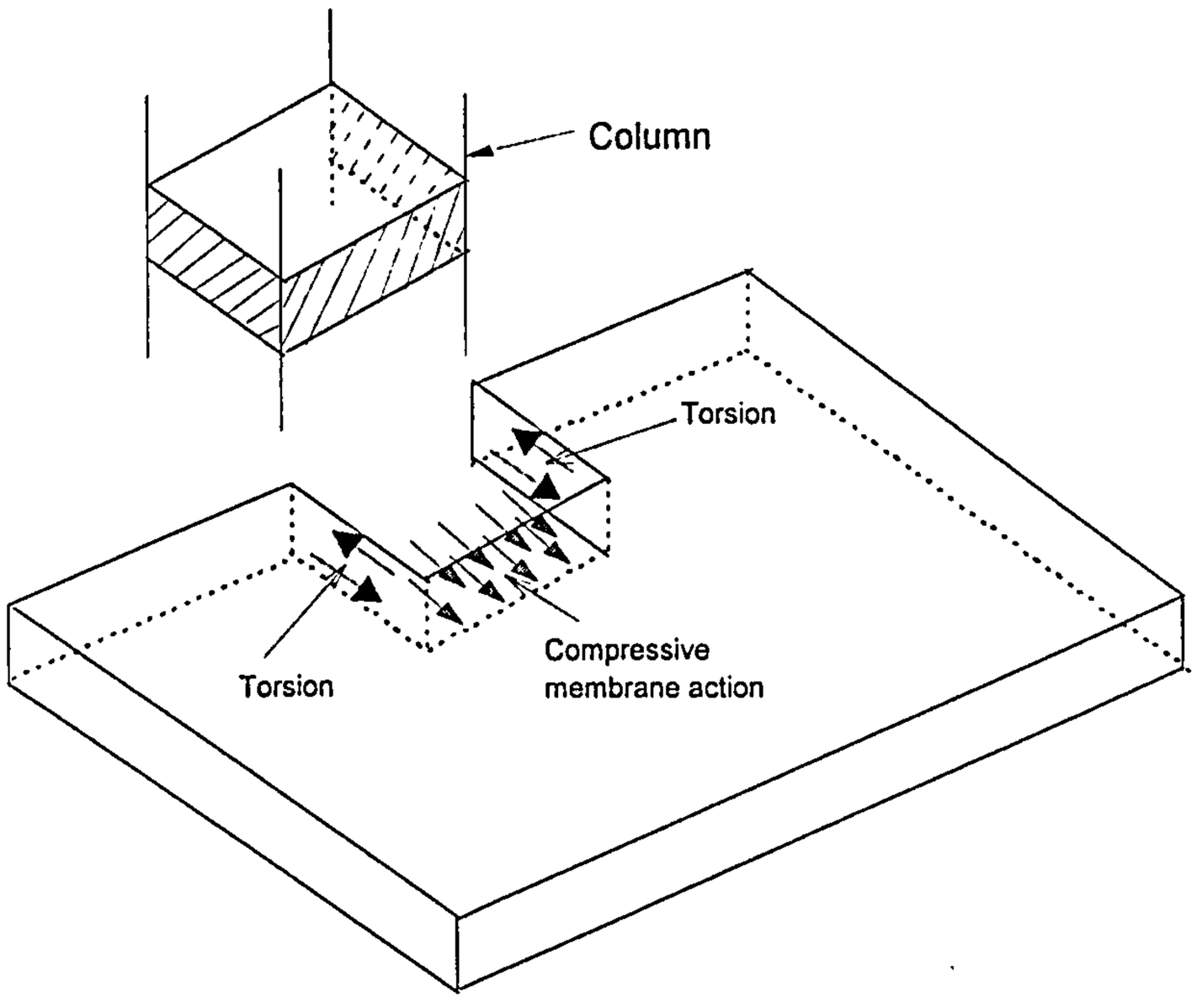

Figure 7.24 Action of torsion and membrane action

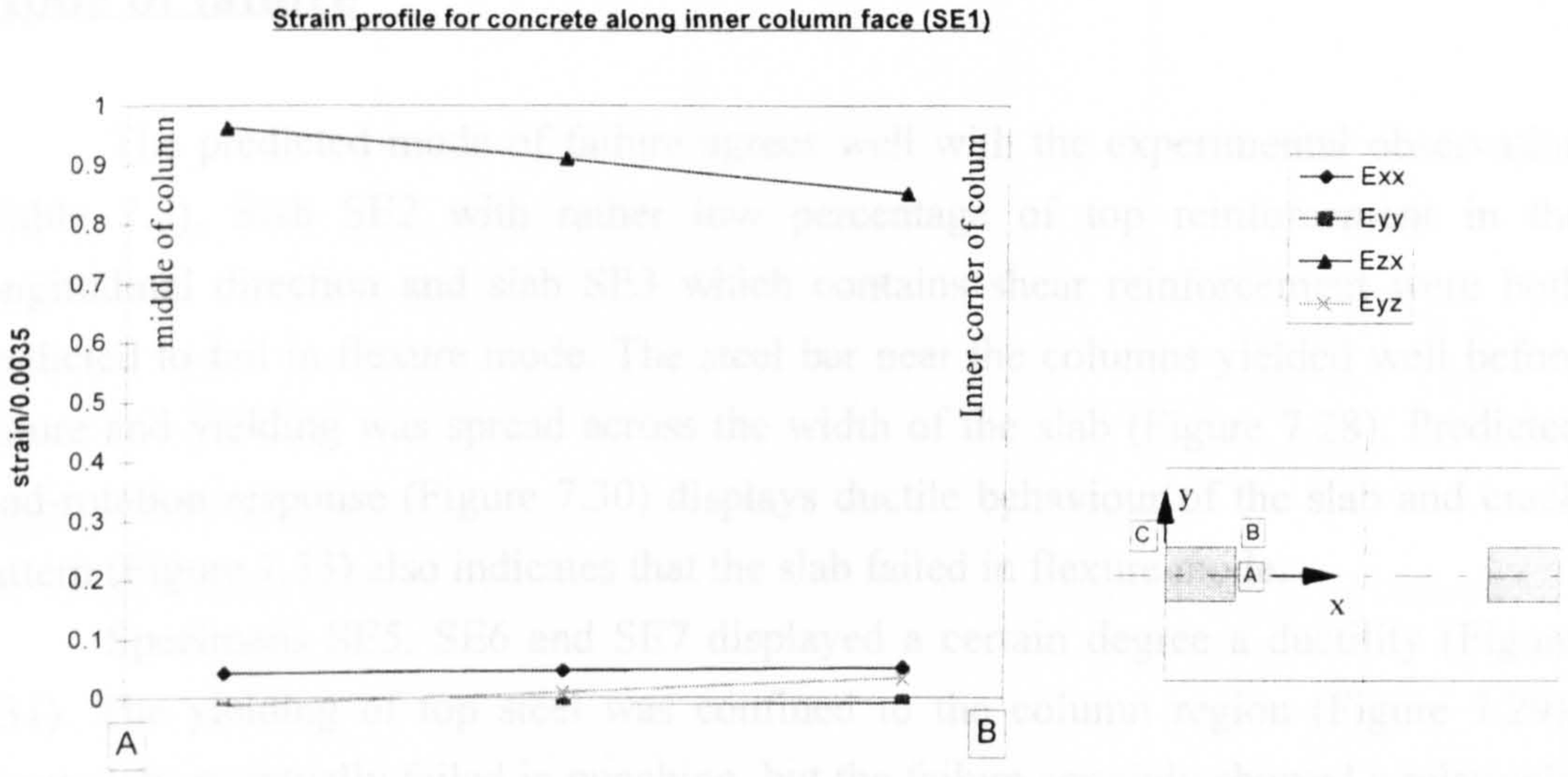

Figure 7.25 Strain profile for concrete along inner face of column (SE1)

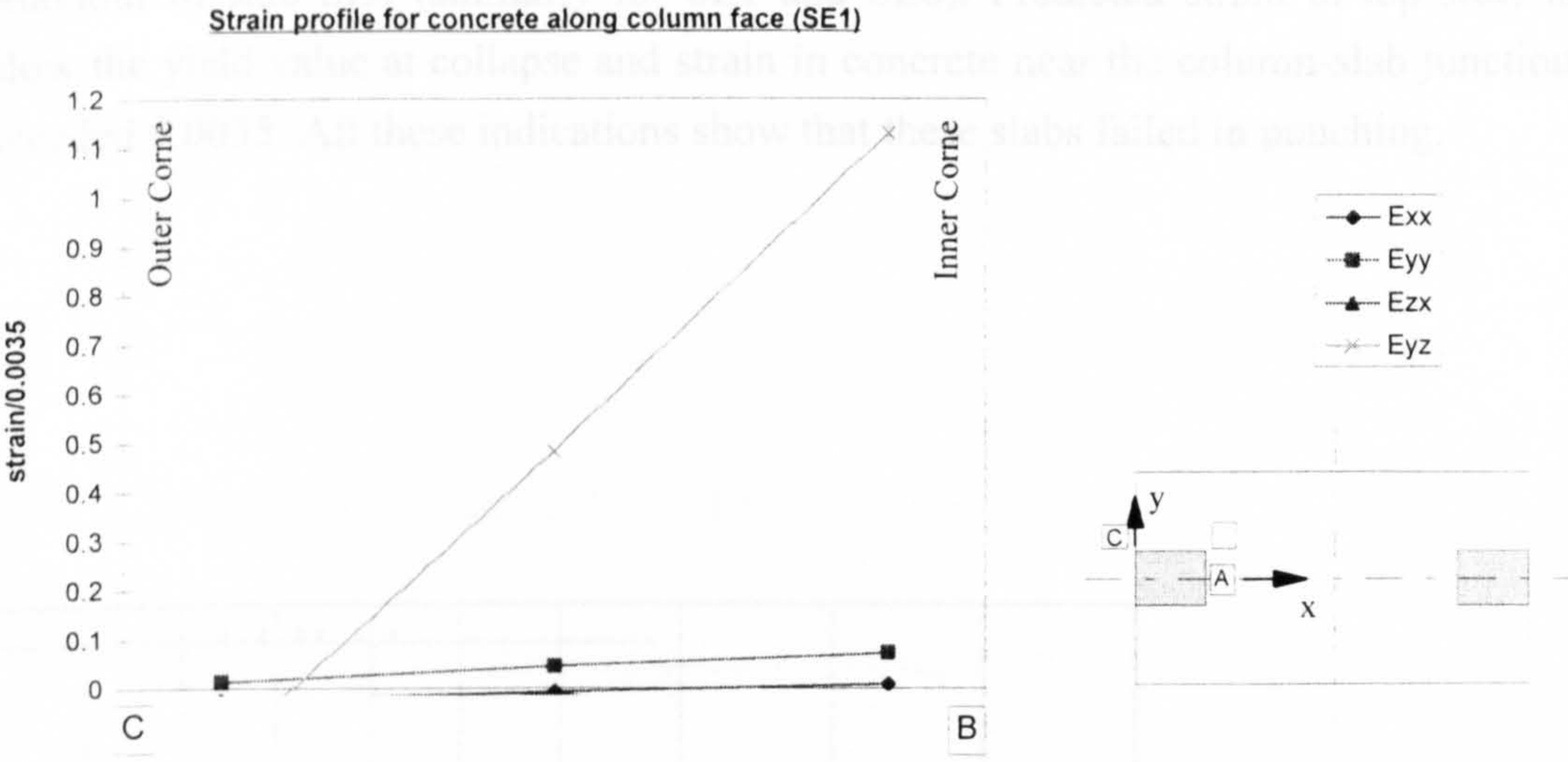

Figure 7.26 Strain profile for concrete along side column face perpendicular to free edge

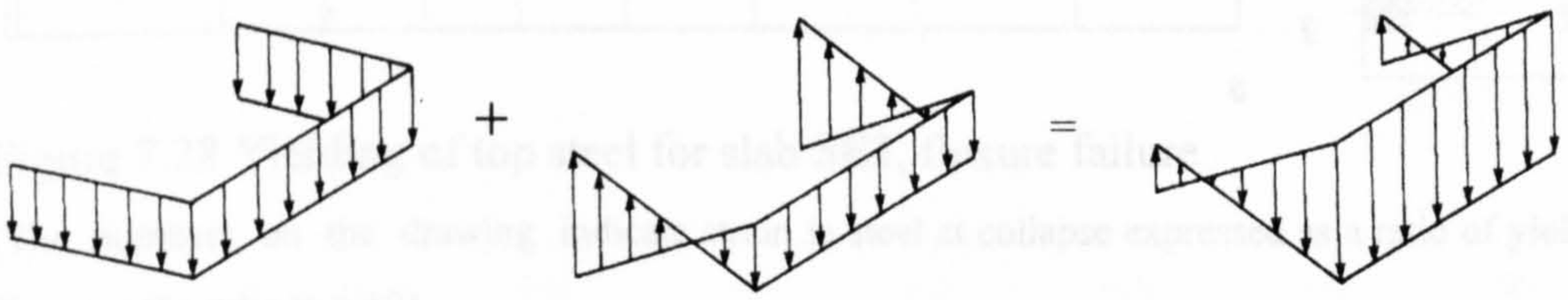

Direct shear *unbalanced moment* *Total shear strain*

Figure 7.27 Shear strain due to shear and moment transfer at edge column

Mode of failure

The predicted mode of failure agrees well with the experimental observation (Table 7.5). Slab SE2 with rather low percentage of top reinforcement in the longitudinal direction and slab SE3 which contains shear reinforcement were both predicted to fail in flexure mode. The steel bar near the columns yielded well before failure and yielding was spread across the width of the slab (Figure 7.28). Predicted load-rotation response (Figure 7.30) displays ductile behaviour of the slab and crack pattern (Figure 7.33) also indicates that the slab failed in flexure mode.

Specimens SE5, SE6 and SE7 displayed a certain degree a ductility (Figure 7.31). The yielding of top steel was confined to the column region (Figure 7.29). These slabs eventually failed in punching, but the failure certainly showed a relatively ductile behaviour. So, these slabs were categorised as having failed in flexure punching mode.

Predicted rotation in slab at the junction (Figure 7.32) displays brittle behaviour of slab SE4 (similarly for SE1 and SE8). Predicted strain in top steel is below the yield value at collapse and strain in concrete near the column-slab junction exceeded 0.0035. All these indications show that these slabs failed in punching.

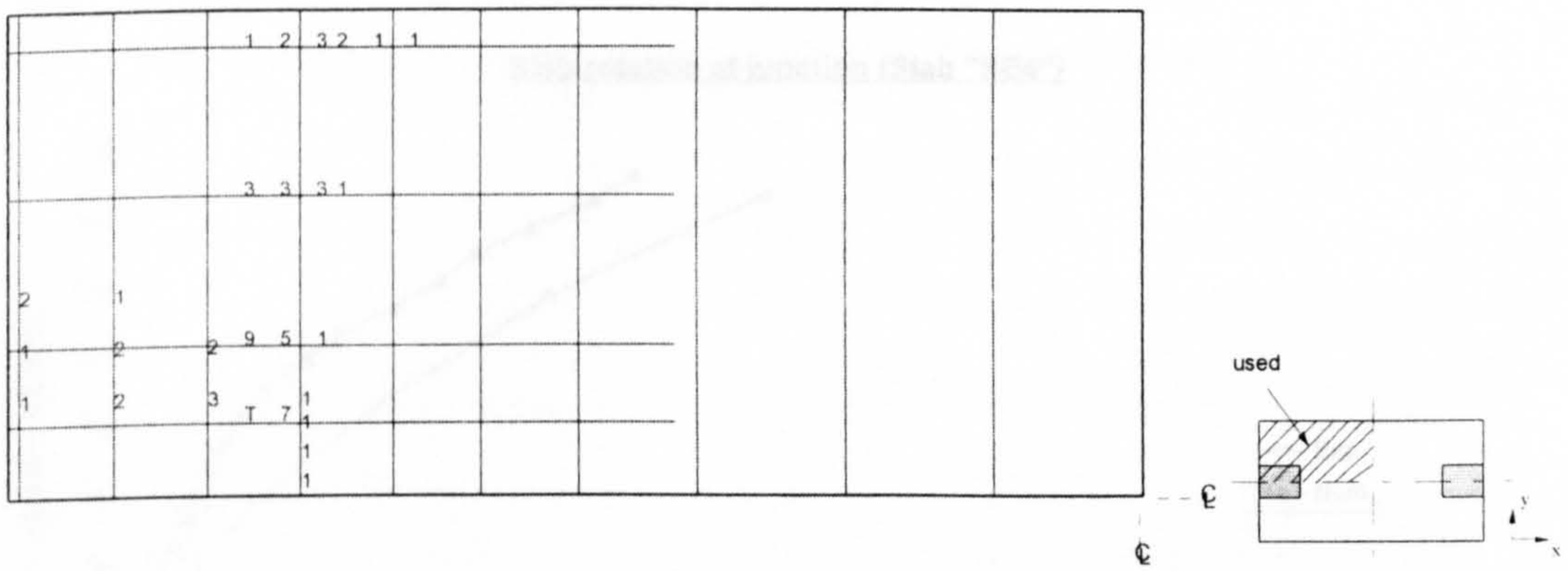

Figure 7.28 Yielding of top steel for slab SE3, flexure failure

(The numbers on the drawing indicate strain in steel at collapse expressed as a ratio of yield strain, T means the ratio is ≥ 10)

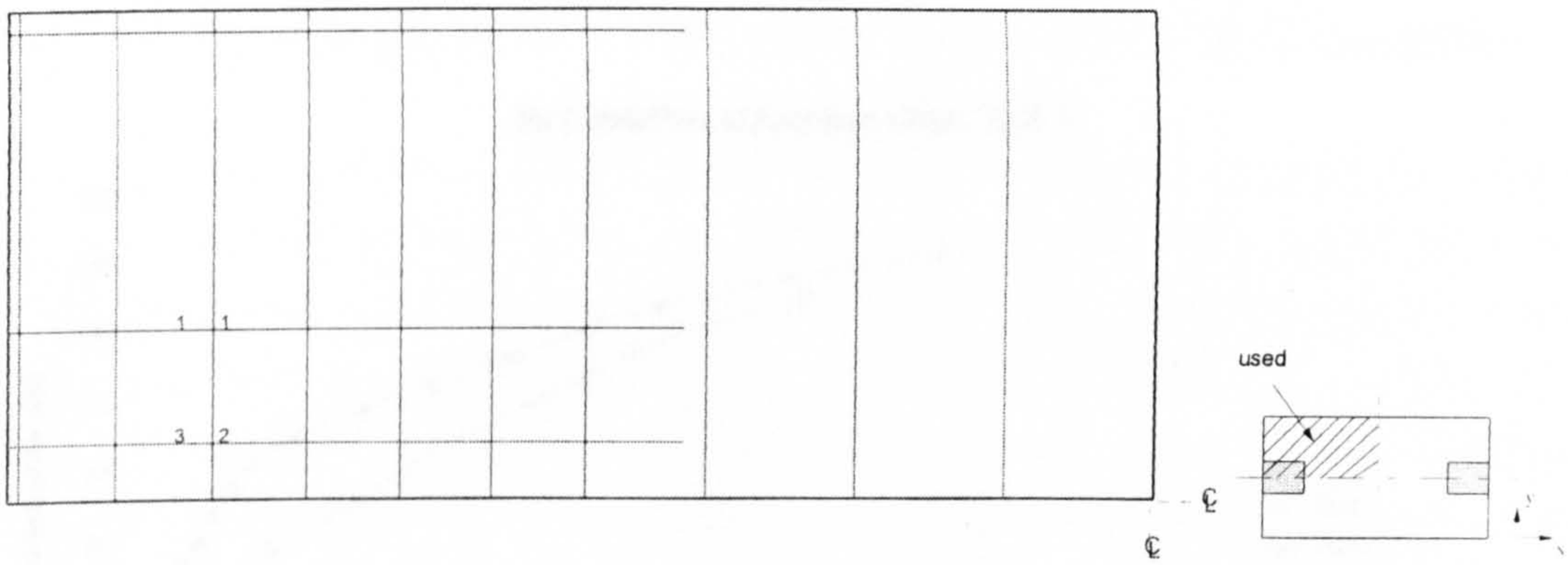

Figure 7.29 Yielding of top steel for slab SE6, flexure punching

(The numbers on the drawing indicate strain in steel at collapse expressed as a ratio of yield strain)

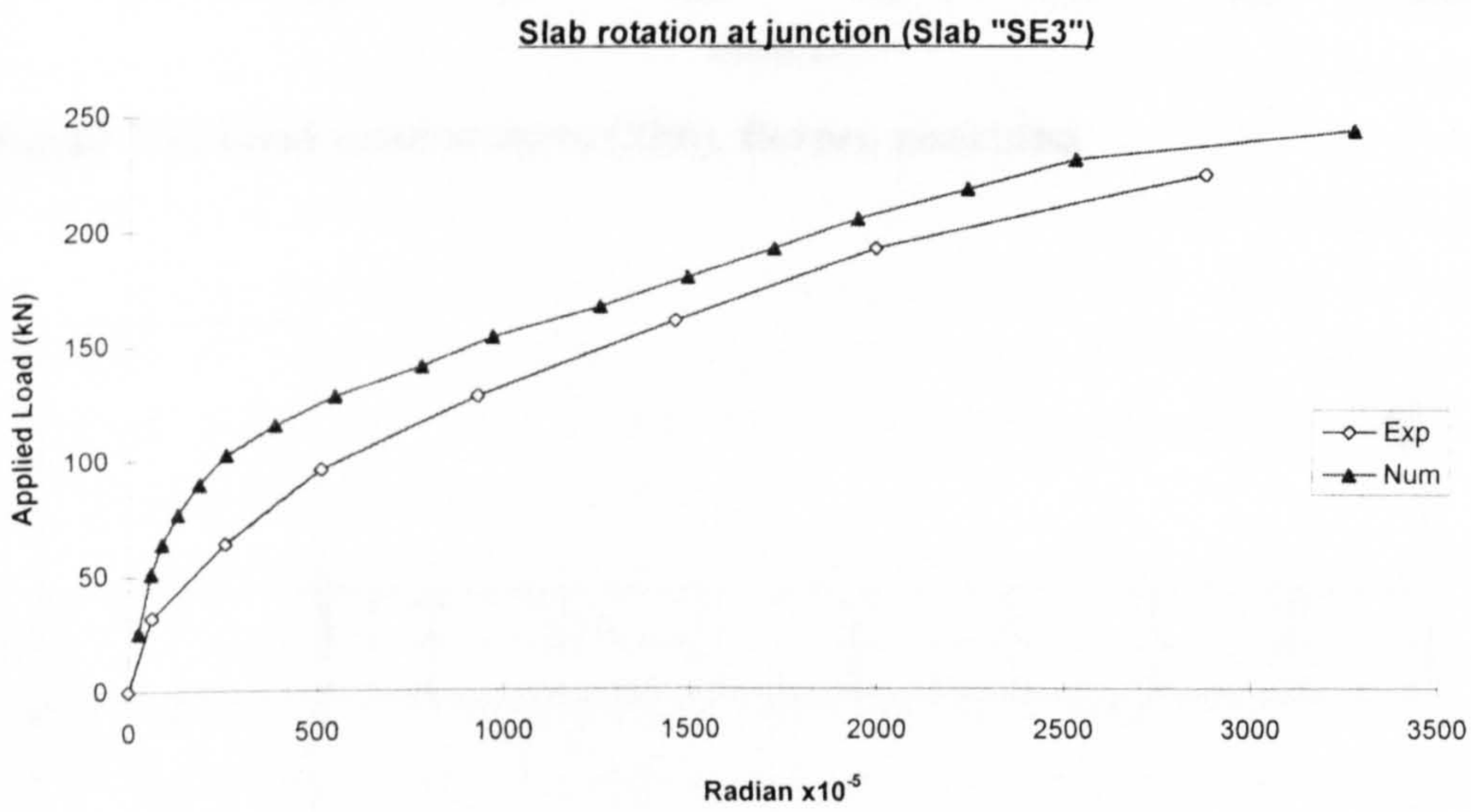

Figure 7.30 Load-rotation curve (SE3), **flexure failure**

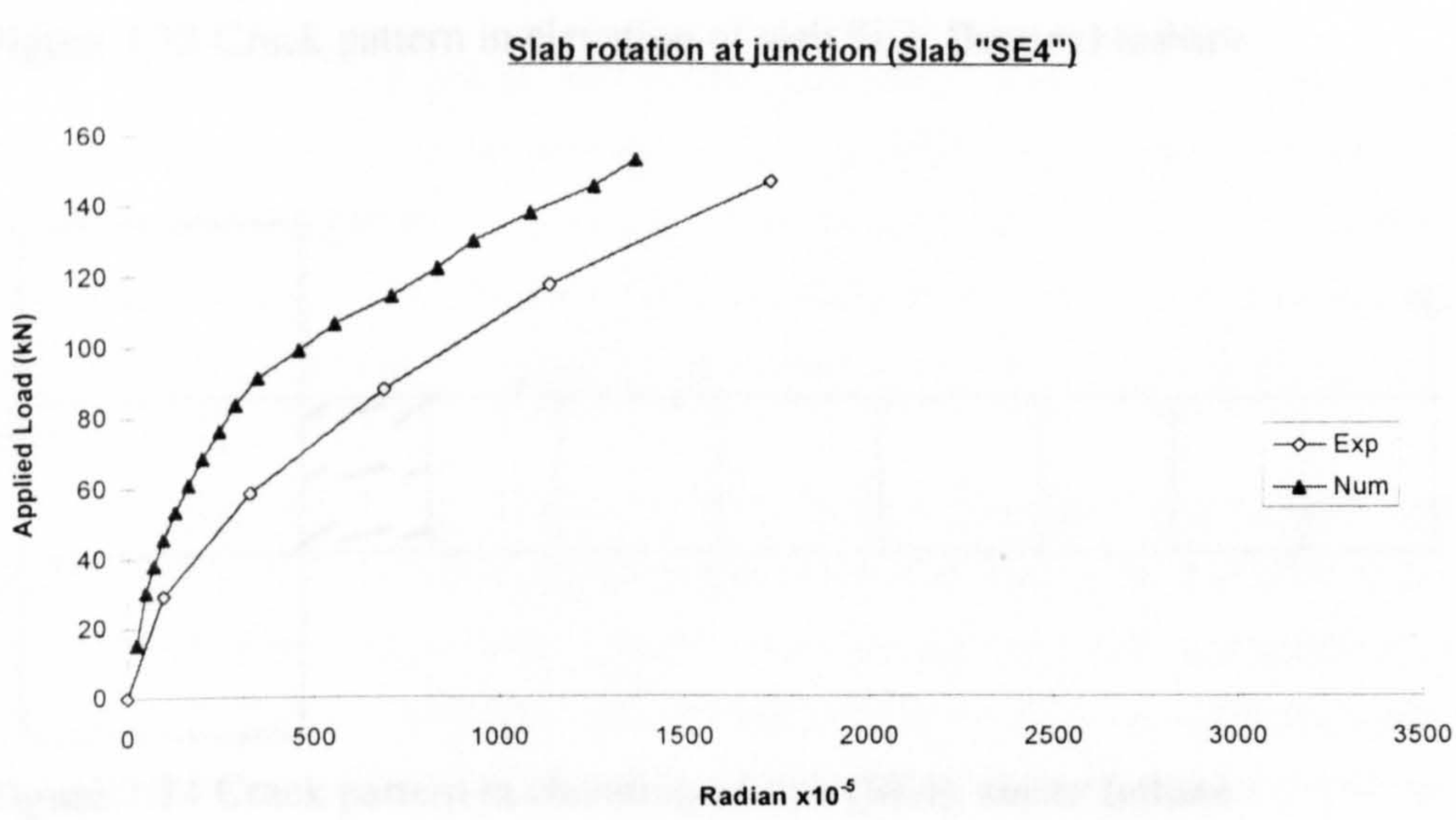

Figure 7.31 Load-rotation curve (SE4), **shear failure**

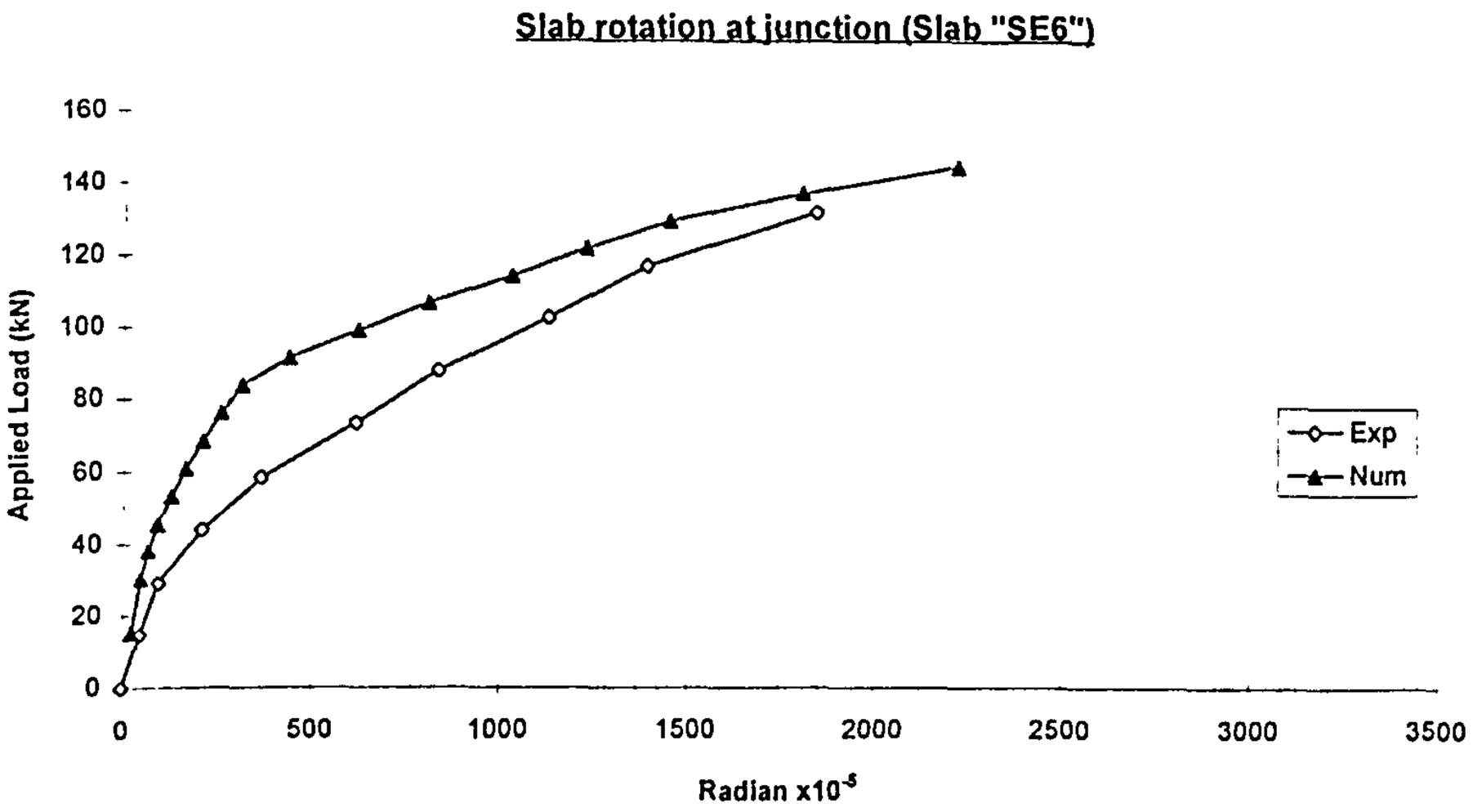

Figure 7.32 Load-rotation curve (SE6), **flexure punching**

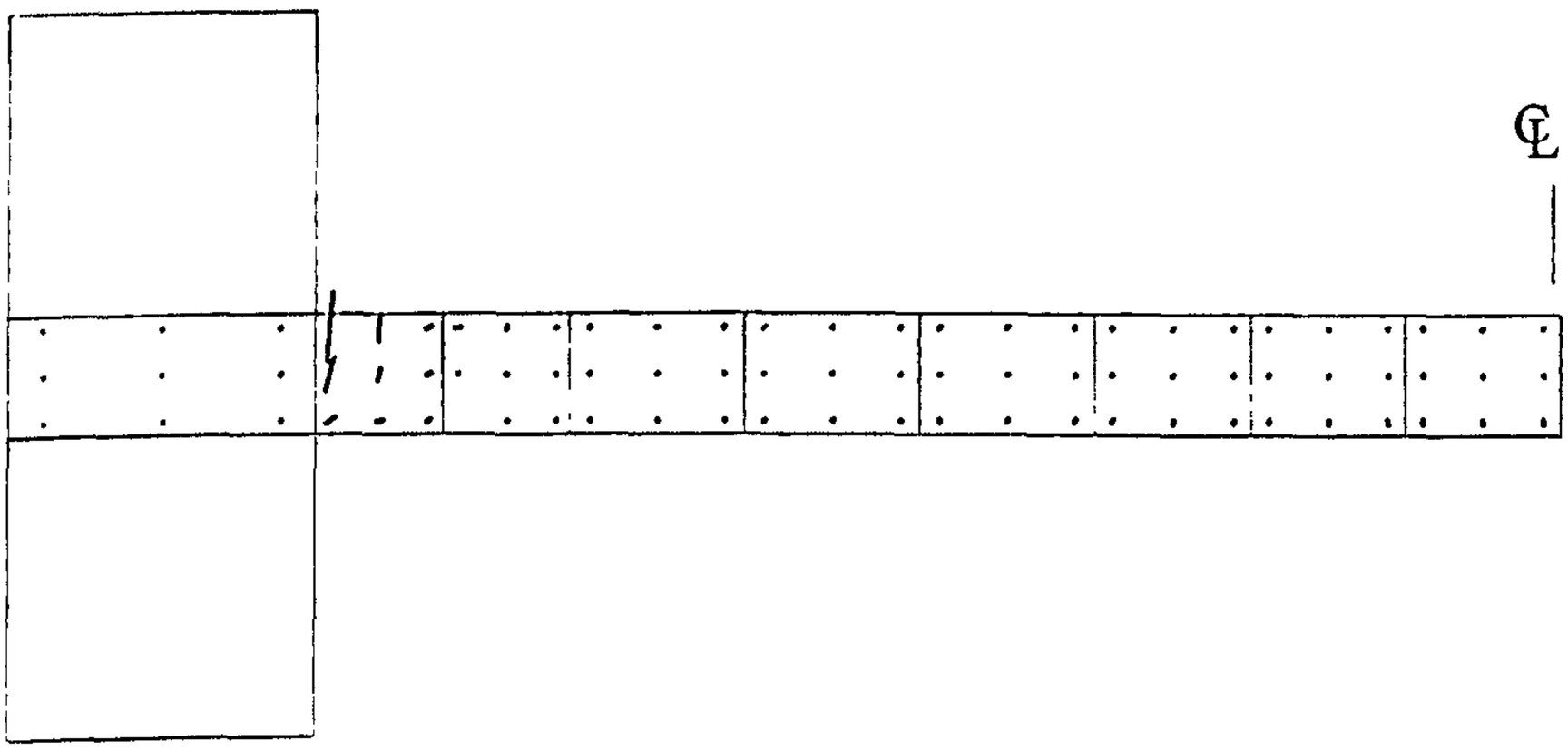

Figure 7.33 Crack pattern in elevation of slab SE3, **flexural failure**

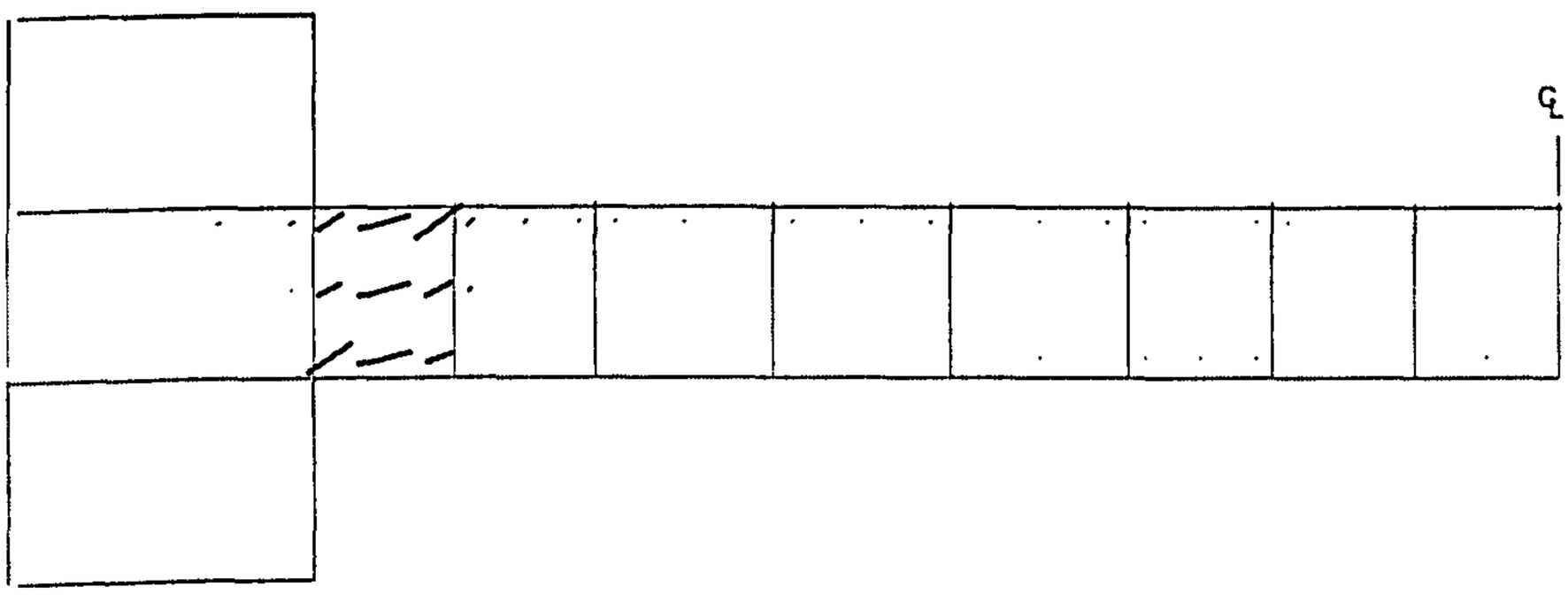

Figure 7.34 Crack pattern in elevation of slab (SE4), **shear failure**

7.3.2 Edge column-slab connections with shear reinforcement

Mortin and Ghali (1991) tested six full-scale reinforced concrete edge column flat-slab connections subjected to shear and moment transfer. These specimens were rectangular, simply supported on three sides, with a column stub located at the centre of the unsupported side (Figure 7.35). Axial force and unbalanced moment were applied to the column stub. The dimension of these specimens are shown in Figure 7.35. The top flexural reinforcement ratios parallel and perpendicular to the free edge are given in Table 7.6. The bottom reinforcement ratio was 0.4% in both direction in all specimens, with two bars passing through the column.

All specimens except JS1 and JS4 were provided with shear reinforcement. The shear reinforcement consisted of shear combs arranged in the vicinity of the column, as shown in Figure 7.37. The variables for this series were the arrangement of the studs within the spandrel strip, the number of rows of studs and size of the shear reinforced zone which varied over the range of 1.8d-2.5d, where d=effective depth.

Finite element mesh and simulation of applied loads are shown in Figure 7.38. Restraint in y and z direction were provided along the simple support and the symmetry line respectively. In order to prevent rigid body motion in x-direction, a node at the edge of slab was restrained.

Numerical failure loads and failure modes for all six specimen are given in Table 7.6. Figure 7.39 shows the applied load vs. deflection for slabs JS2 (with shear studs) and JS4 (without shear studs). Apparently, shear reinforcement increased both the strength and ductility. The stiffer response of slab JS4 must be attributed to the much higher concrete strength. This figure also highlights the fact that regardless of the amount of shear reinforcement, flexural steel yielded almost at the same load level.

The predicted mode of failure generally agrees well with experimental observation (Table 7.6). The specimens without shear studs failed in a brittle punching mode, as can be seen in the predicted crack pattern (Figure 7.41) and small deflection at failure (Figure 7.39). Those with shear studs failed in a ductile flexural mode with large deflection at failure(Figure 7.39) and the cracks were vertical at the slab near the column (Figure 7.40).

In Figure 7.42, the strains in shear studs in Specimen 2 are plotted against the applied load. The distributions of strain show that the studs near the inner face of column resisted larger shear force. This agrees with the assumption made by Kinnunen (1971) for the edge slab analysis, that part of the moment transmitted to the column is assumed to be provided by torsions at the side faces, and these torsions are assumed to create downward forces near the inner corners of the column and upward

forces near the edge (Figure 7.43). This is probably the reason why the ultimate loads of these slabs do not vary very much.

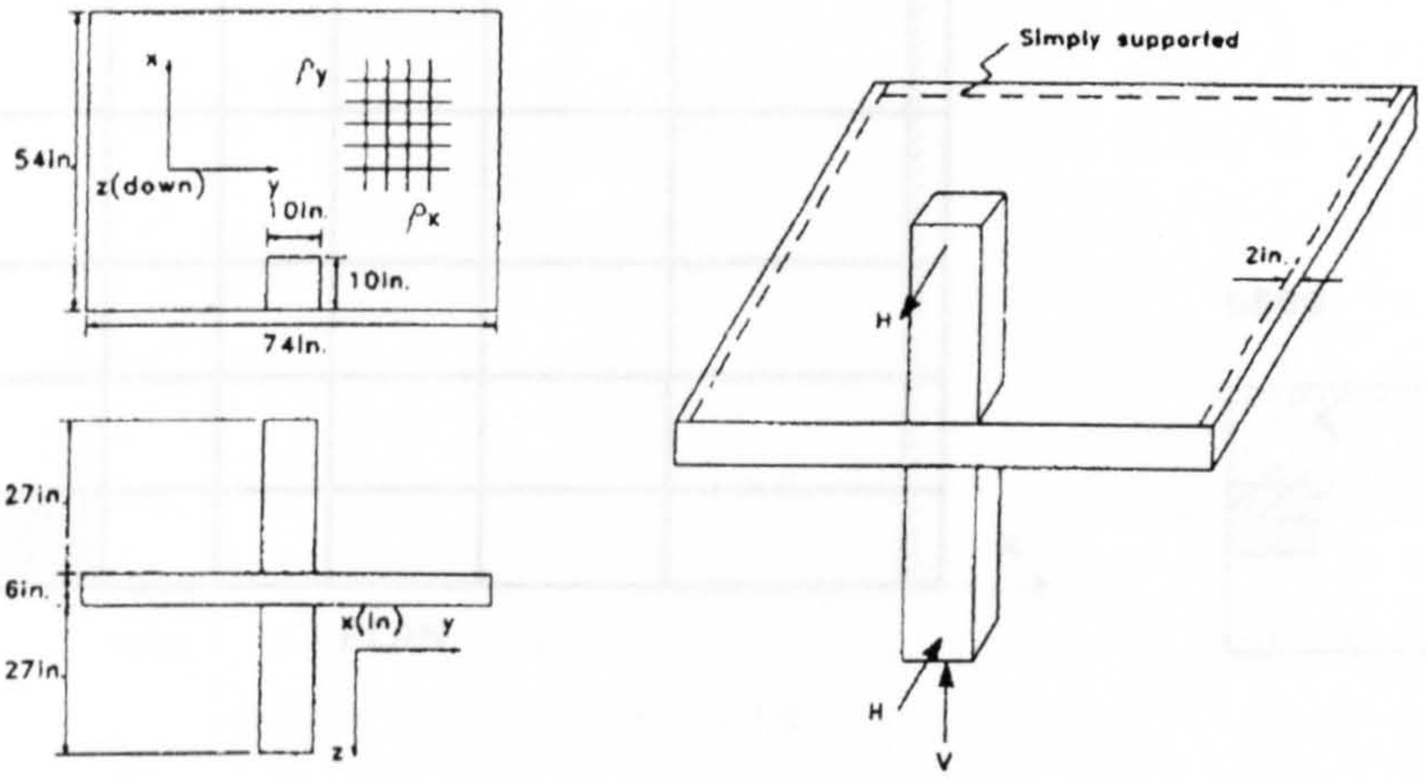

Figure 7.35 : Dimensions, loading and simple support for specimens JS1-JS6

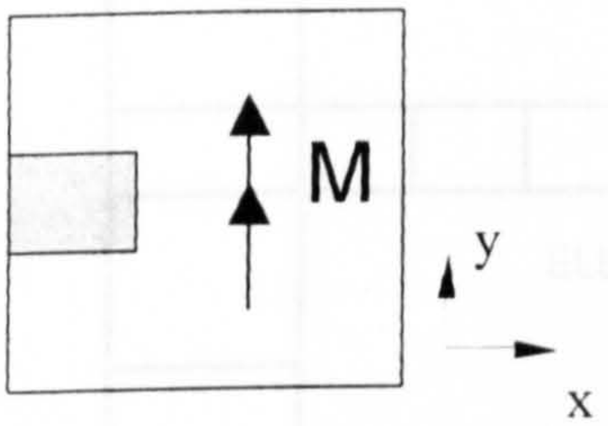

Figure 7.36 Direction of unbalanced moment

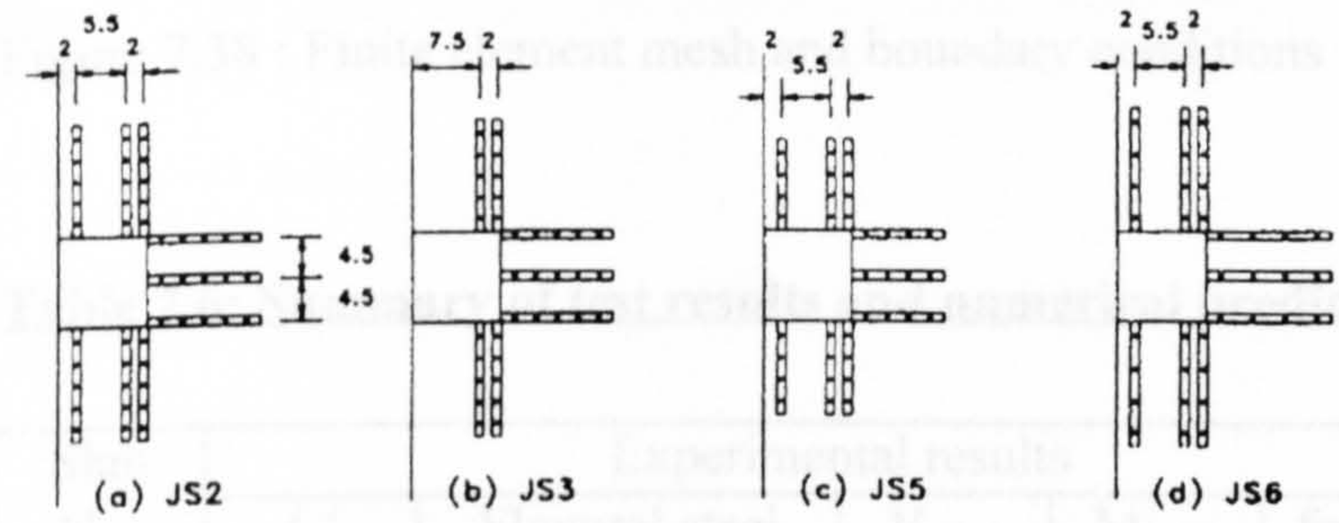

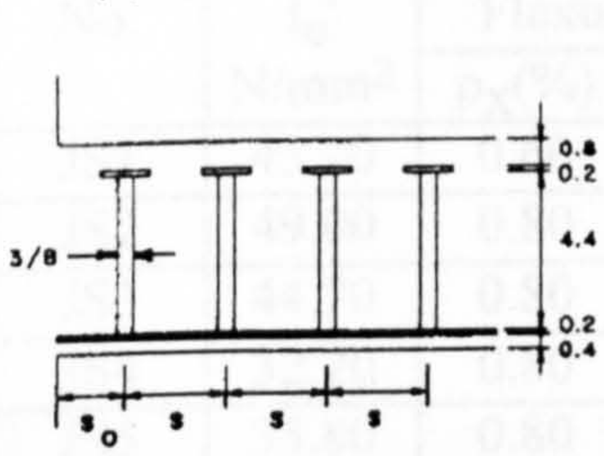

Typical section perpendicular to the three interior sides of the column.

Specimen	# of Studs per Strip	s_o (in.)	s (in.)
JS2	5	1.6	2.4
JS3	5	1.6	2.4
JS5	4	1.6	2.4
JS6	4	1.6	3.5

All dimensions are in inches.

Figure 7.37 : The arrangement of shear reinforcement

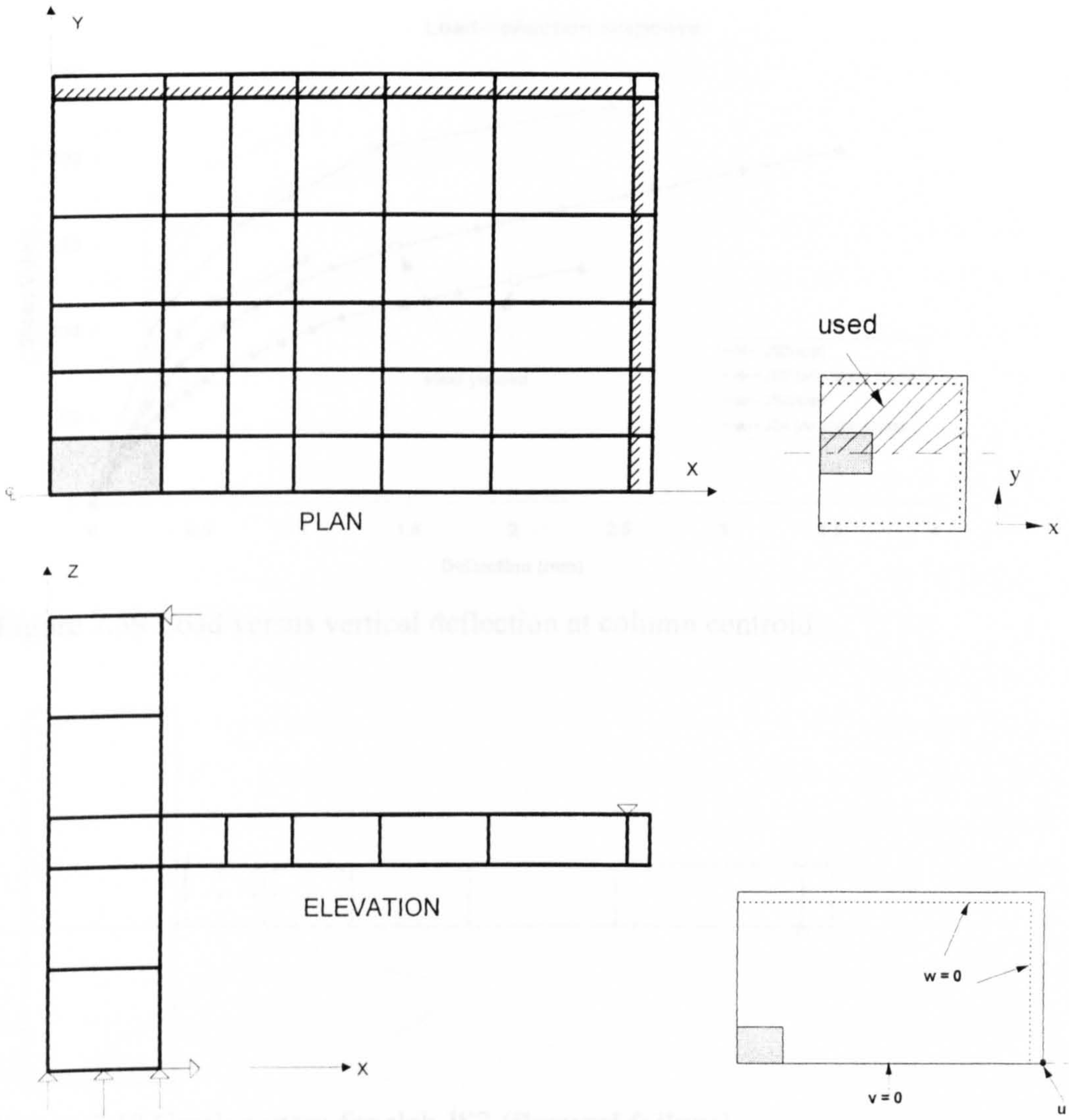

Figure 7.38 : Finite element mesh and boundary conditions

Table 7.6: Summary of test results and numerical predictions (Mortin and Ghali)

Slab No.	Experimental results						Numerical results	
	f_c' N/mm^2	Flexural steel		V_{test} (kN)	M_{test} (kNm)	failure mode	Num/Exp ratio	failure mode
		ρ_x(%)	ρ_y(%)					
JS1	43.20	0.60	0.95	140.9	60.5	s	1.05	s
JS2	49.00	0.80	1.28	231.0	95.3	y	0.89	y
JS3	44.70	0.80	1.28	212.3	89.5	y	1.00	y
JS4	32.20	0.80	1.28	141.0	60.3	s	0.97	s
JS5	35.80	0.80	1.28	212.3	86.4	fp	0.96	y
JS6	33.90	0.80	1.28	201.0	85.6	y	0.95	y
							Average = 0.970	
							STDEV = 0.053	

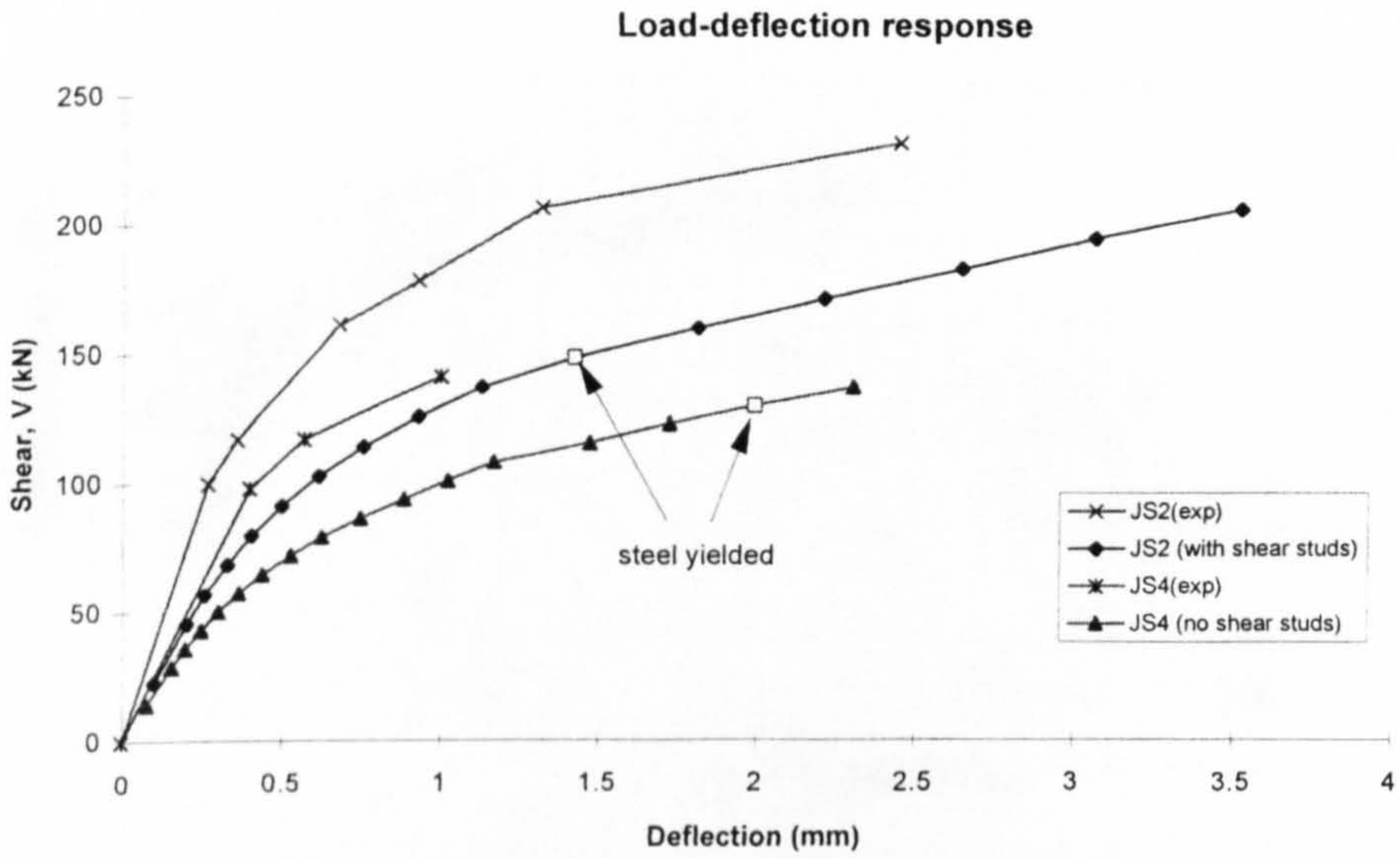

Figure 7.39 Load versus vertical deflection at column centroid

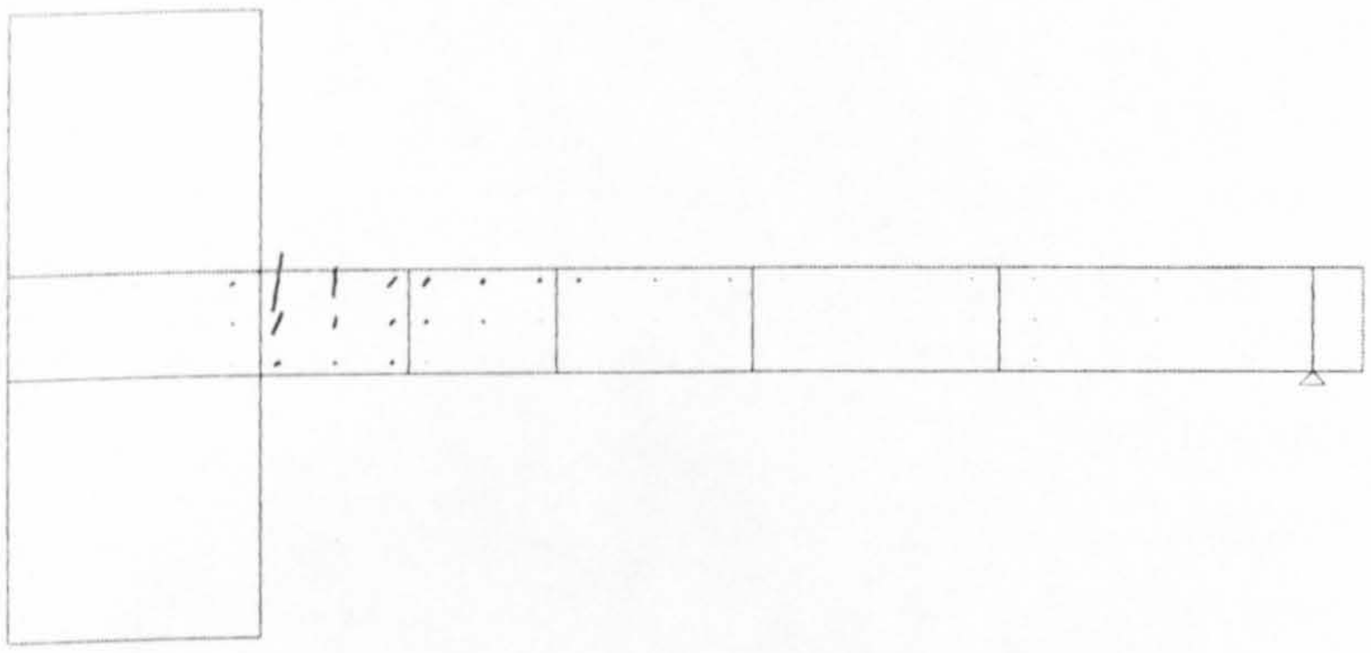

Figure 7.40 Crack pattern for slab JS2 (**flexural failure**)

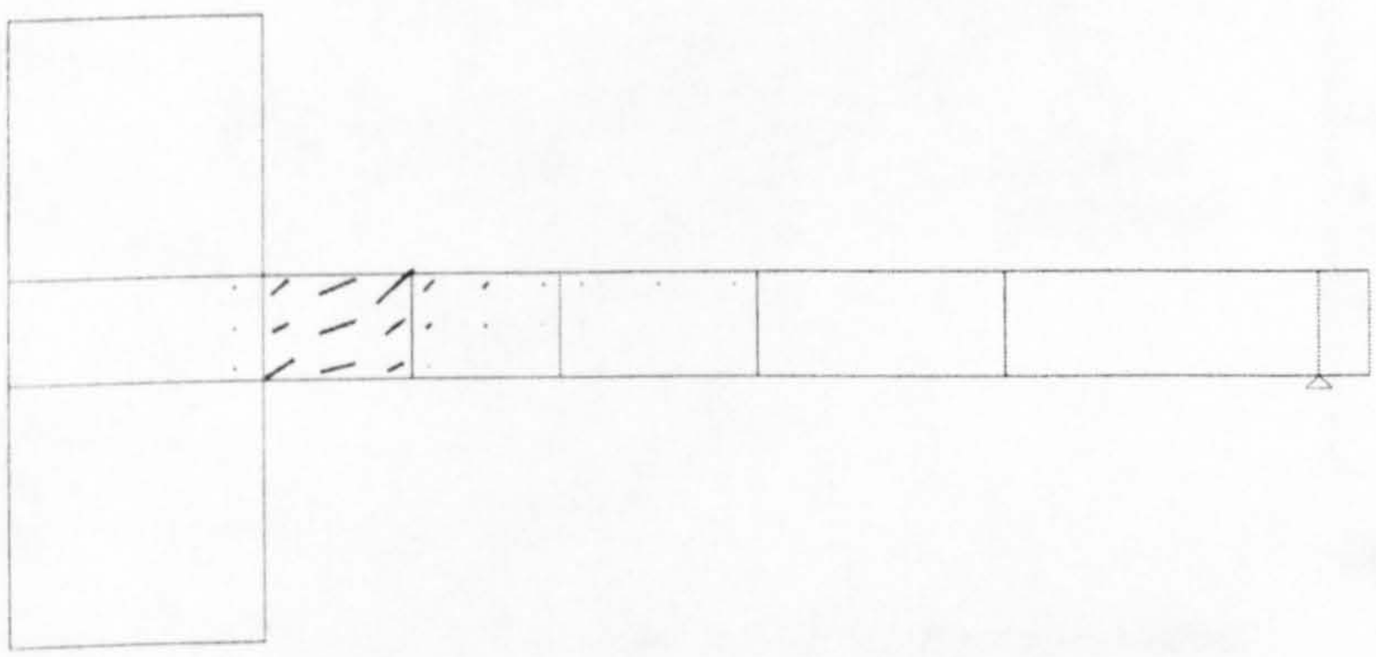

Figure 7.41 Crack pattern for slab JS4 (**shear failure**)

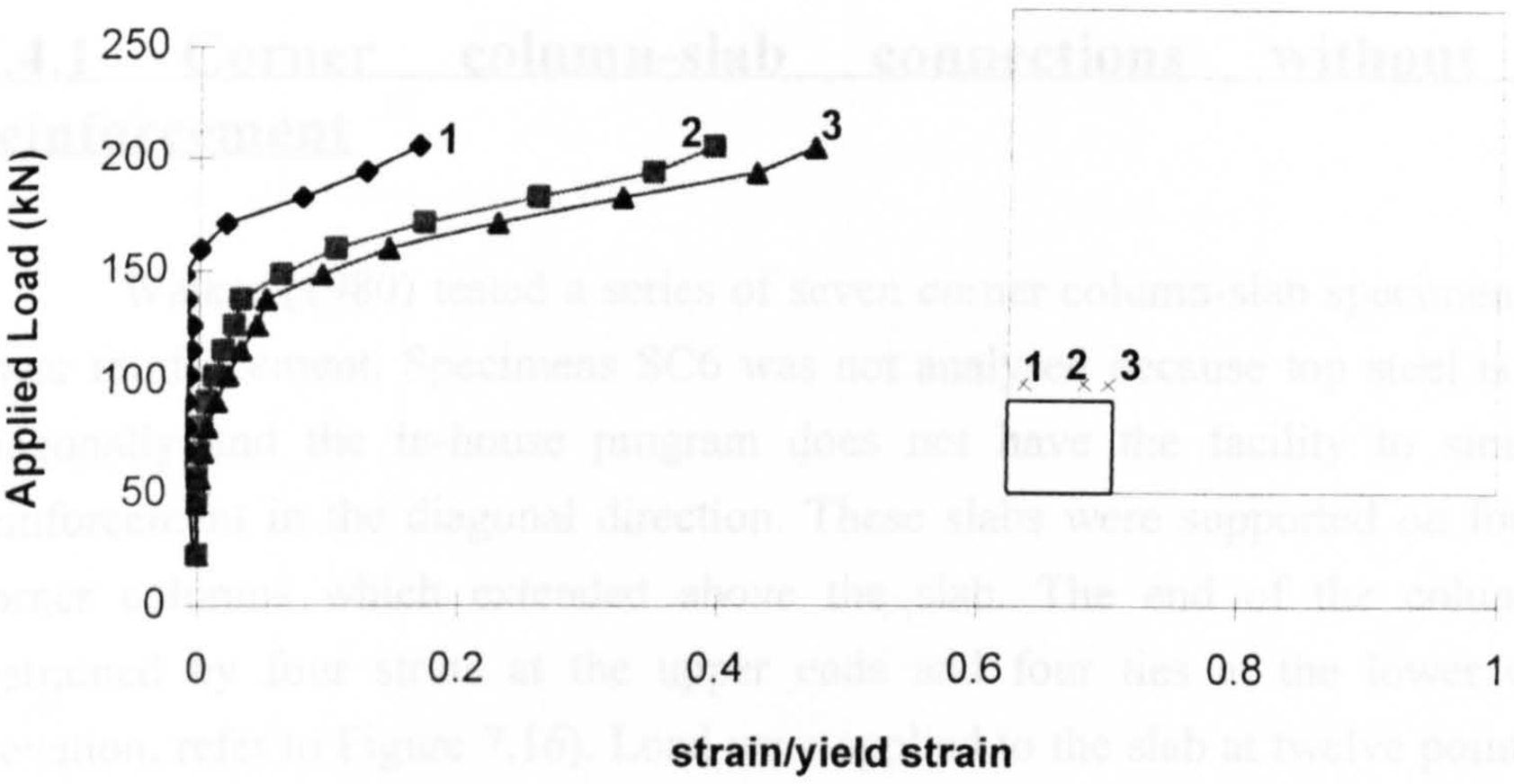

Figure 7.42 Predicted strain in shear studs for slab JS2

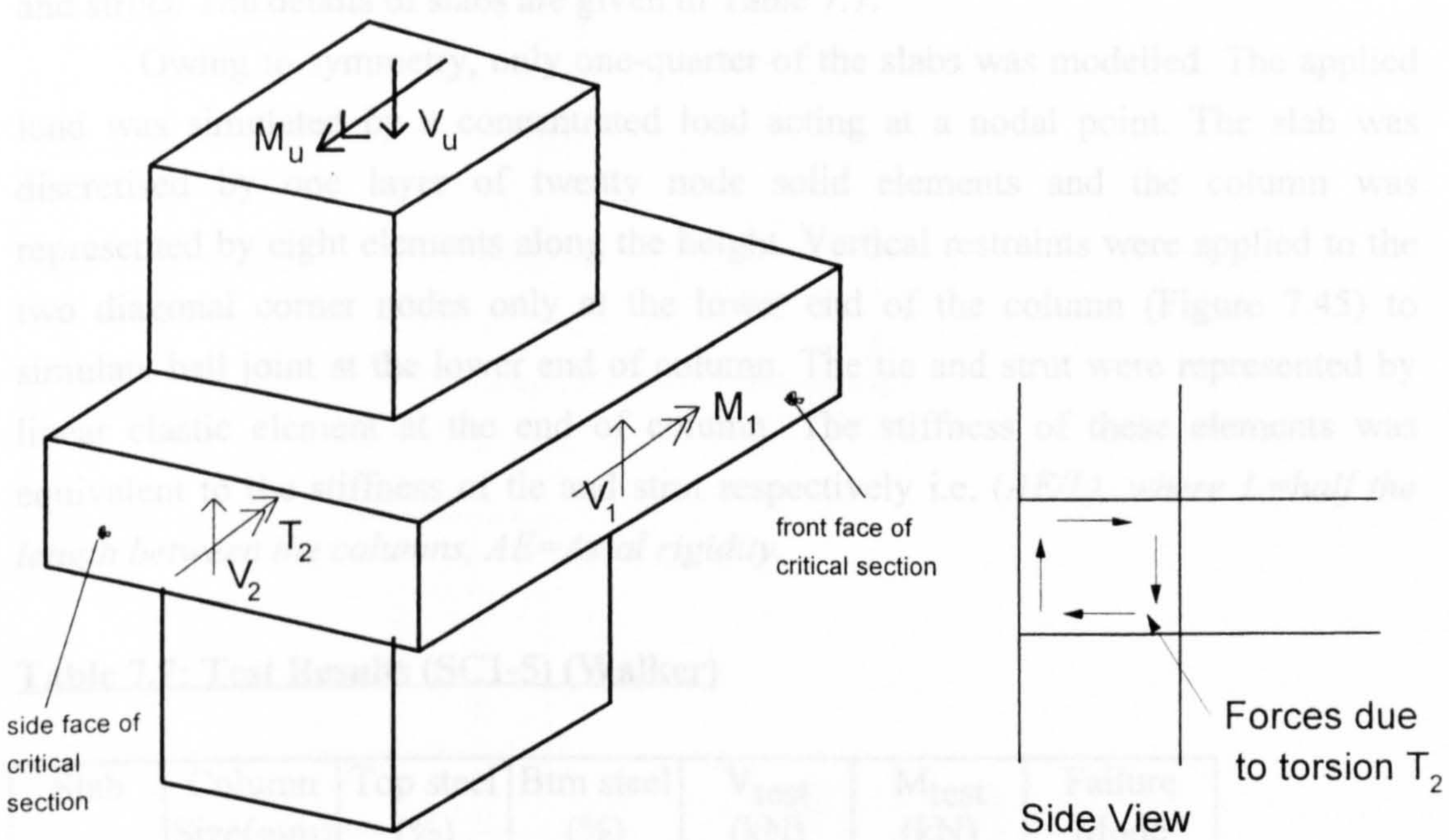

Figure 7.43 Torsion increase shear at inner face of column

7.4 Corner column-slab connections

7.4.1 Corner column-slab connections without shear reinforcement

Walker (1980) tested a series of seven corner column-slab specimens without shear reinforcement. Specimens SC6 was not analysed because top steel is arranged diagonally and the in-house program does not have the facility to simulate the reinforcement in the diagonal direction. These slabs were supported on four square corner columns which extended above the slab. The end of the columns were restrained by four struts at the upper ends and four ties at the lower ends (for elevation, refer to Figure 7.16). Load were applied to the slab at twelve points to give a reasonably uniform distribution. The loads were applied by six hydraulic jacks anchored below the floor and a system of spreader beams (Figure 7.44).

The main variables for this series were : the percentage of reinforcement at the slab-column junction and the size of column. Concrete strength ranged from 48 to 61.4 N/mm^2. Reinforcement in slab SC7 was exactly the same as for slab SC5, but the test procedure was modified so that column moments were applied externally and not allowed to developed naturally. The horizontal loads were applied by tightening ties and struts. The details of slabs are given in Table 7.7.

Owing to symmetry, only one-quarter of the slabs was modelled. The applied load was simulated by a concentrated load acting at a nodal point. The slab was discretised by one layer of twenty node solid elements and the column was represented by eight elements along the height. Vertical restraints were applied to the two diagonal corner nodes only at the lower end of the column (Figure 7.45) to simulate ball joint at the lower end of column. The tie and strut were represented by linear elastic element at the end of column. The stiffness of these elements was equivalent to the stiffness of tie and strut respectively i.e. *(AE/L), where L=half the length between the columns, AE=Axial rigidity.*

Table 7.7: Test Results (SC1-5) (Walker)

Slab	Column Size(mm)	Top steel (%)	Btm steel (%)	V_{test} (kN)	M_{test} (kN)	Failure Mode
SC1	300	0.41	0.26	81.00	36.40	fp
SC2	300	0.28	0.36	75.00	35.70	s
SC3	300	0.52	0.17	74.00	45.60	fp
SC4	220	0.41	0.26	64.00	24.00	fp
SC5	220	0.60	0.41	82.00	26.90	s
SC7	220	0.60	0.41	82.00	39.00	s

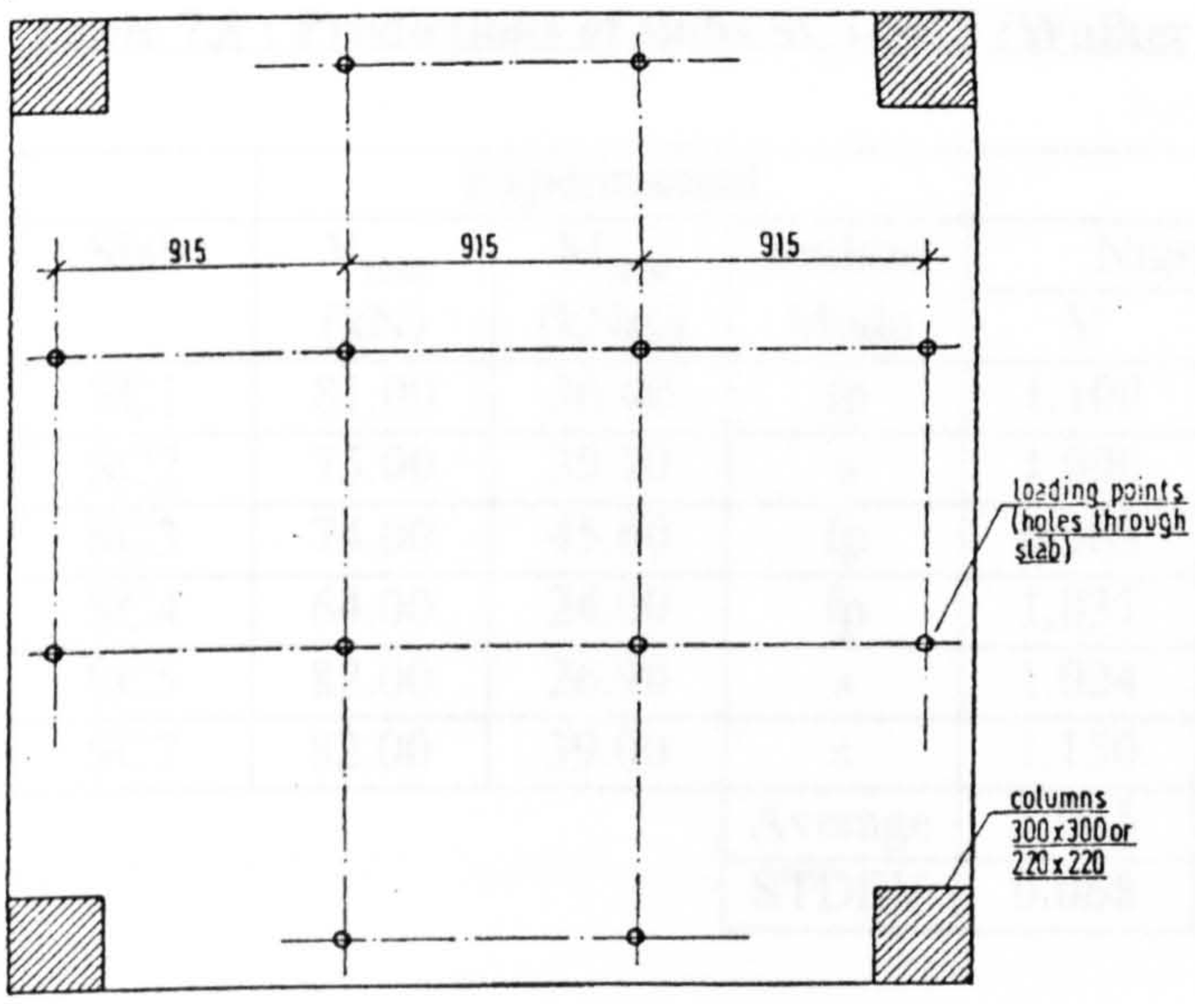

Figure 7.44 : Test arrangement for corner column supported slabs.

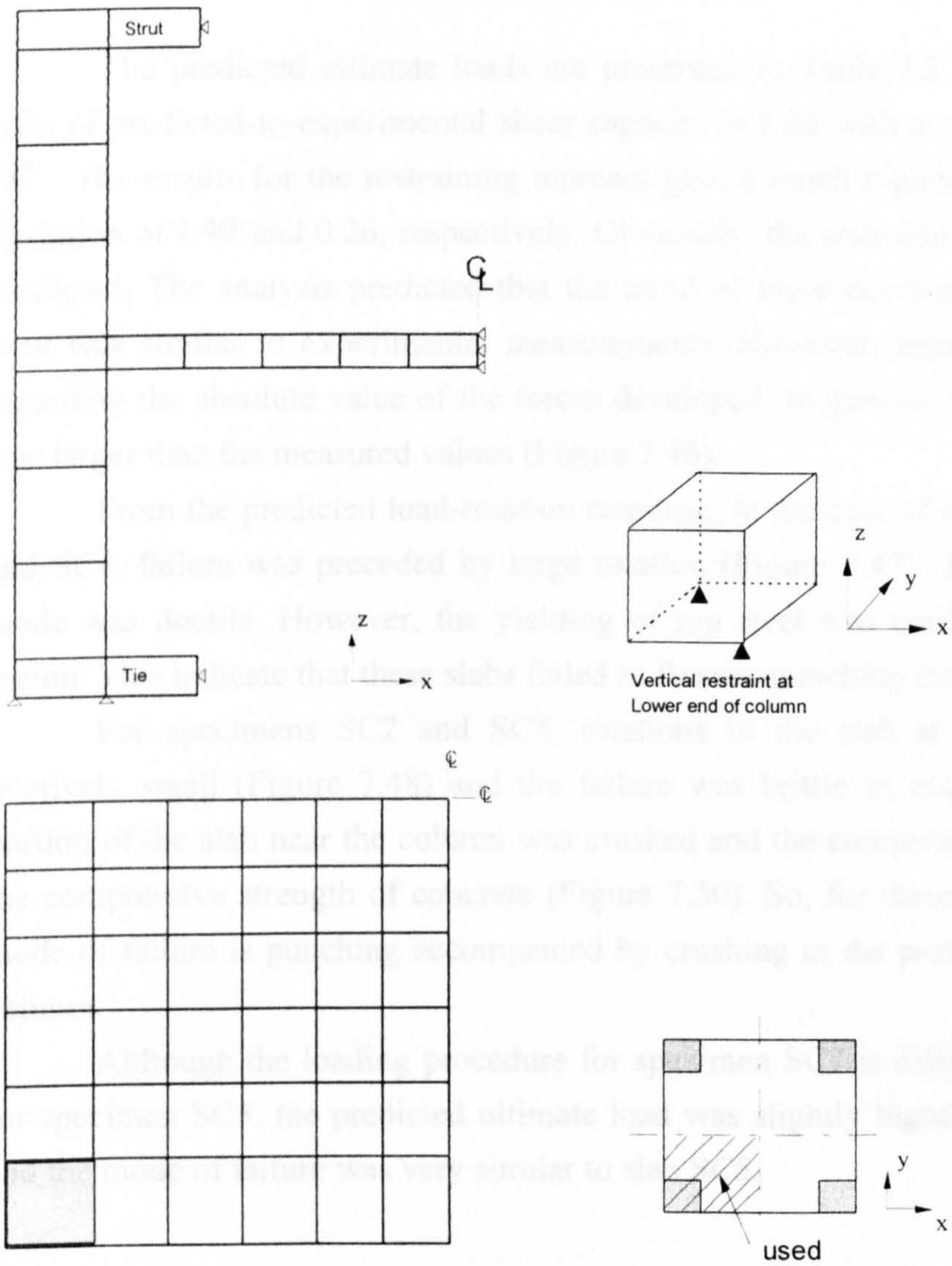

Figure 7.45 : Finite element model and boundary conditions for corner supported slabs.

Table 7.8 : Predictions of slabs SC1-SC5 (Walker)

	Experimental			Numerical		
Slab	V_{test} (kN)	M_{test} (kNm)	Failure Mode	Num/Exp V	Num/Exp M	Failure Mode
SC1	81.00	36.40	fp	1.100	1.595	fp
SC2	75.00	35.70	s	1.000	1.372	s
SC3	74.00	45.60	fp	0.963	1.038	fp
SC4	64.00	24.00	fp	1.031	1.666	fp
SC5	82.00	26.90	s	1.024	1.579	s
SC7	82.00	39.00	s	1.150	1.150	s
			Average	1.045	1.400	
			STDEV	0.068	0.260	

The predicted ultimate loads are presented in Table 7.8. The average of the ratio of predicted-to-experimental shear capacity is 1.04 with a standard deviation of 0.07 . The results for the restraining moment give a much higher mean and standard deviation of 1.40 and 0.26, respectively. Obviously, the restraining moment was over predicted. The analysis predicted that the trend of force development in the tie and strut was similar to experimental measurements. However, there was disagreement regarding the absolute value of the forces developed. In general, the predicted values was larger than the measured values (Figure 7.46).

From the predicted load-rotation response, in the case of specimens SC1, SC3 and SC4, failure was preceded by large rotation (Figure 7.47). Therefore the failure mode was ductile. However, the yielding of top steel was confined to the column region. This indicate that these slabs failed in flexure-punching mode.

For specimens SC2 and SC5, rotations in the slab at the junctions were relatively small (Figure 7.48) and the failure was brittle in nature. Furthermore, a portion of the slab near the column was crushed and the compressive stress exceeded the compressive strength of concrete (Figure 7.50). So, for these slabs the predicted mode of failure is punching accompanied by crushing in the portion of slab near the column.

Although the loading procedure for specimen SC7 is different from that used for specimen SC5, the predicted ultimate load was slightly higher for specimen SC7 and the mode of failure was very similar to slab SC5.

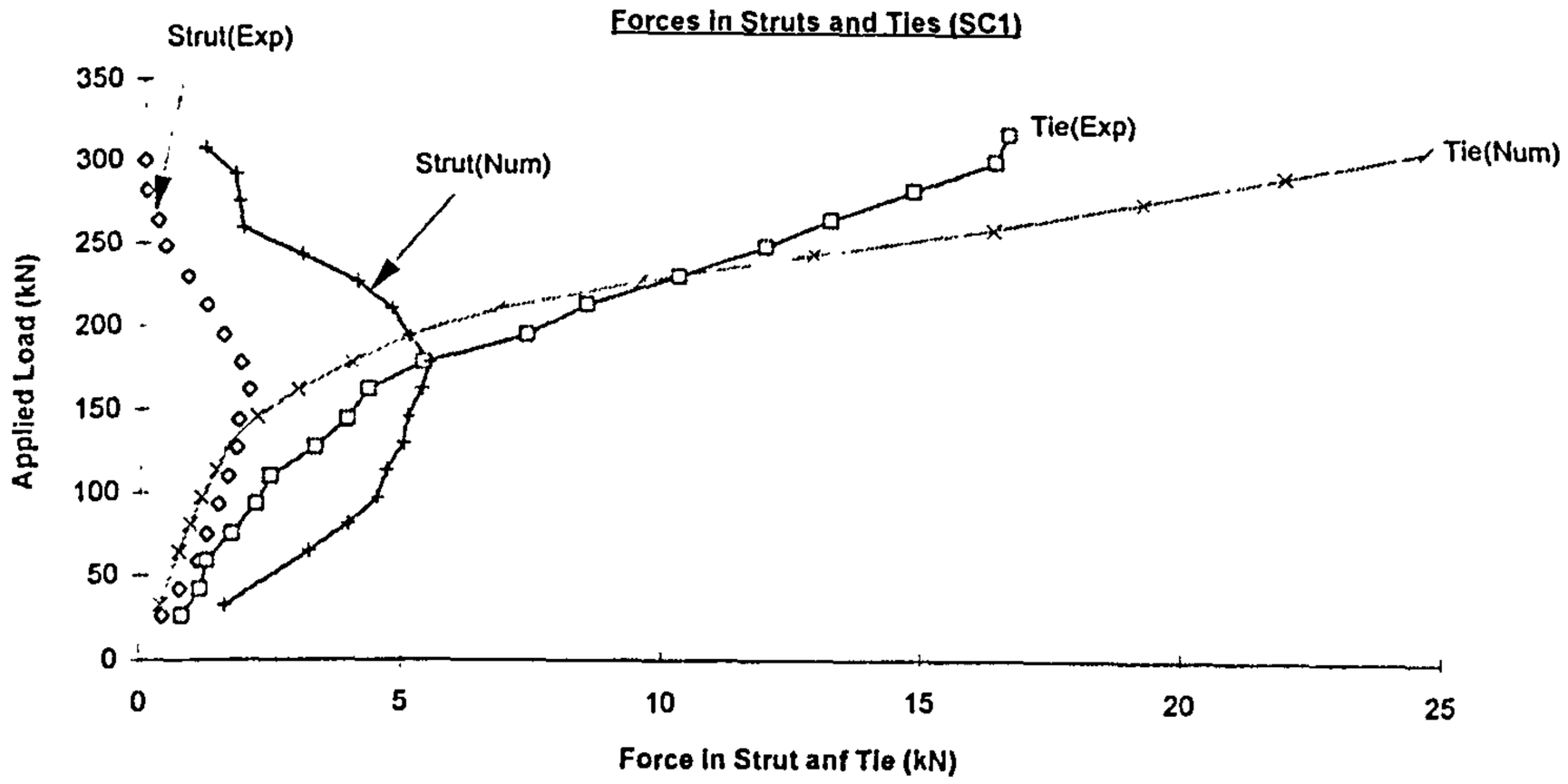

Figure 7.46 Forces in struts and Ties (SC1)

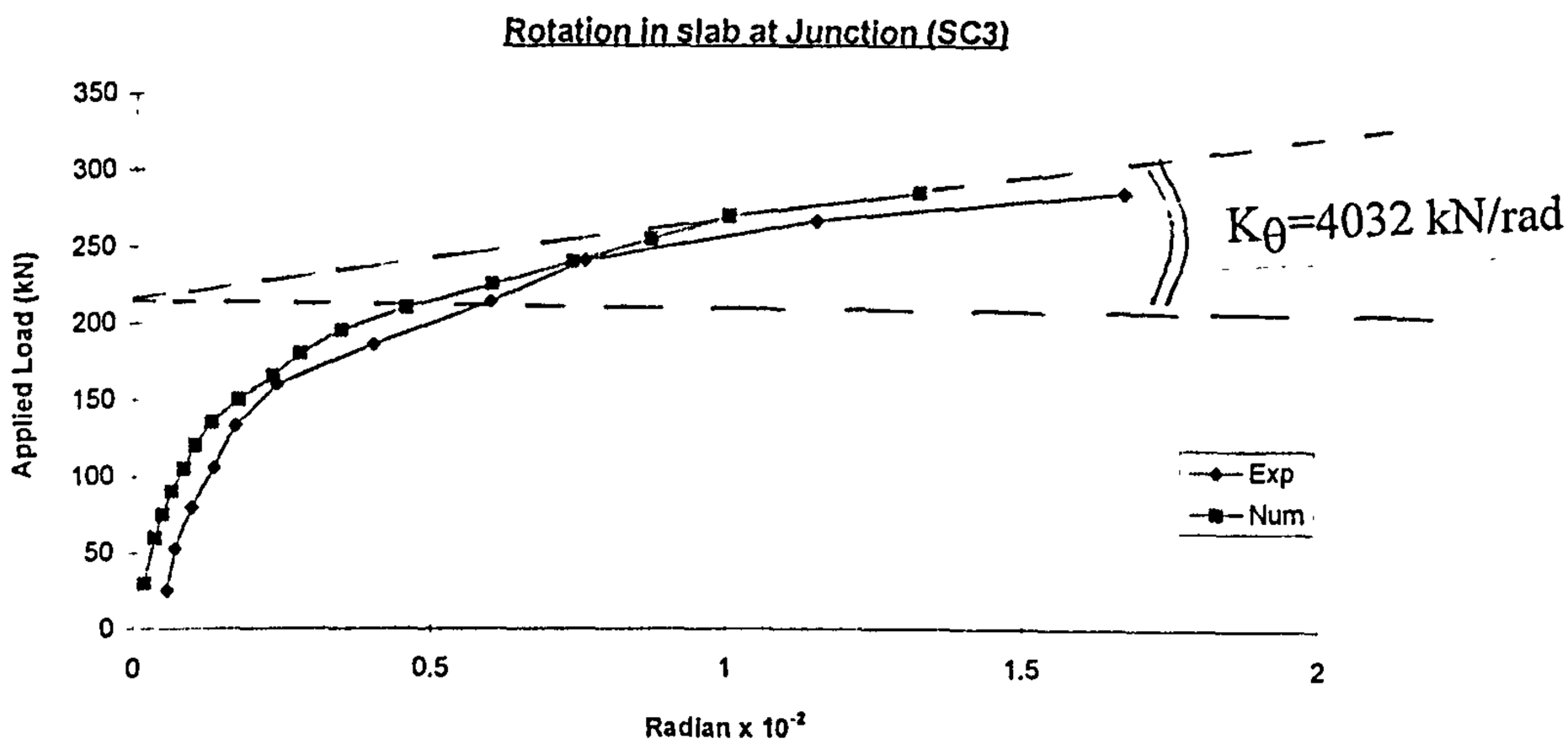

Figure 7.47 Load-rotation curve (SC3), **flexure punching**

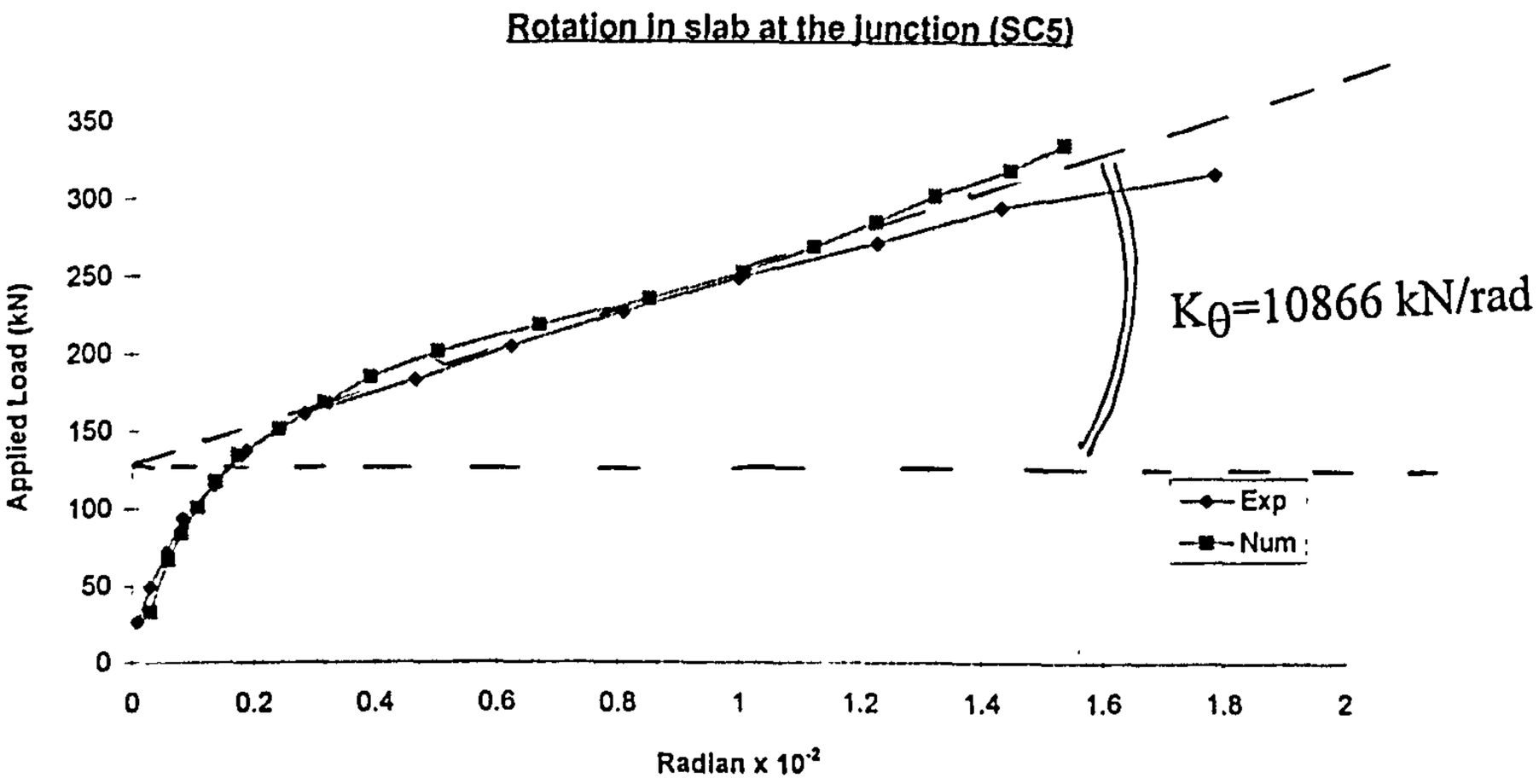

Figure 7.48 Load-rotation curve (SC5), **shear punching**

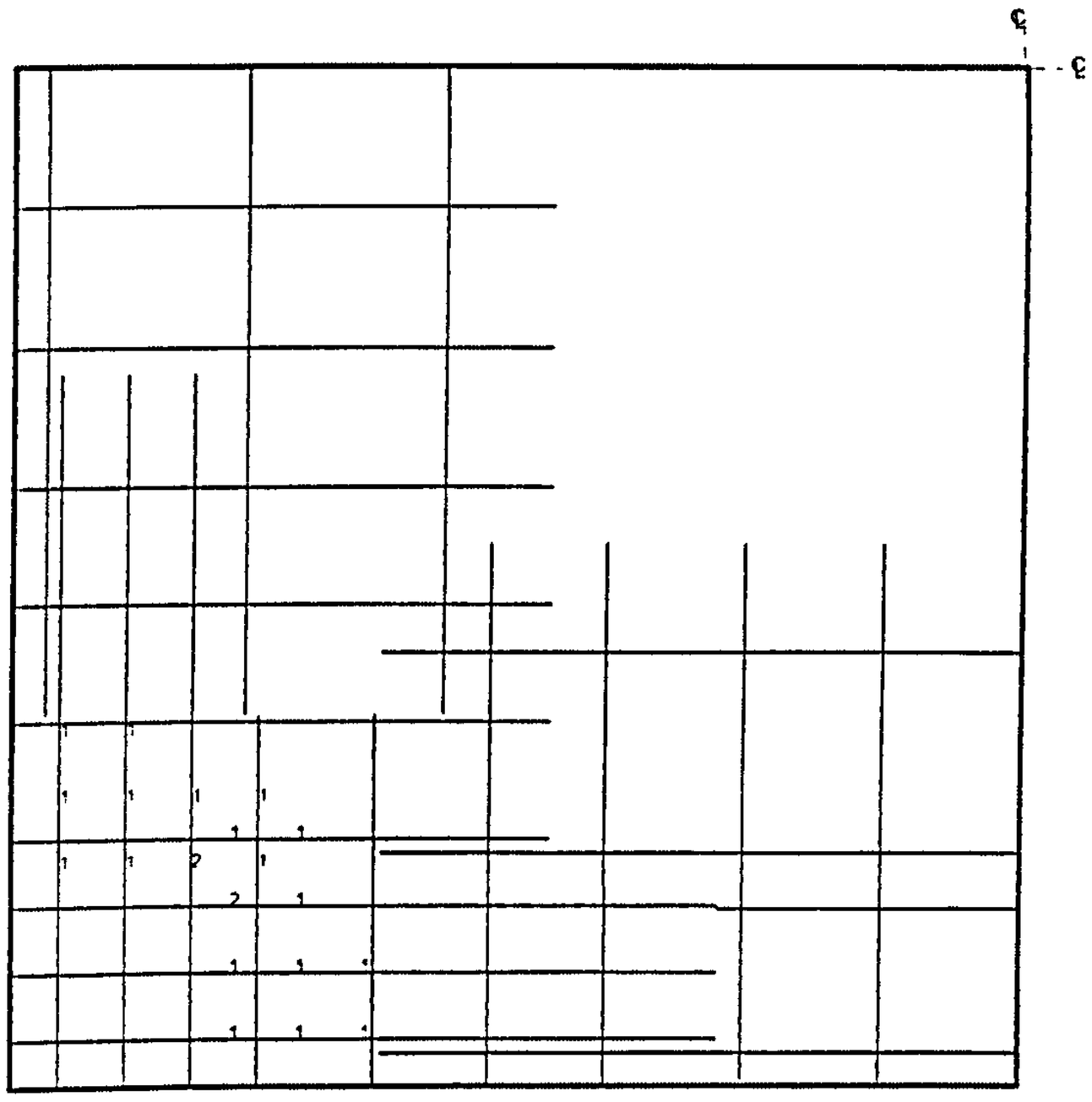

Figure 7.49 Yielding of top reinforcement (SC3), **flexure punching (yielding confined to the column region)**

(The numbers on the drawing indicate strain in steel at collapse expressed as a ratio of yield strain)

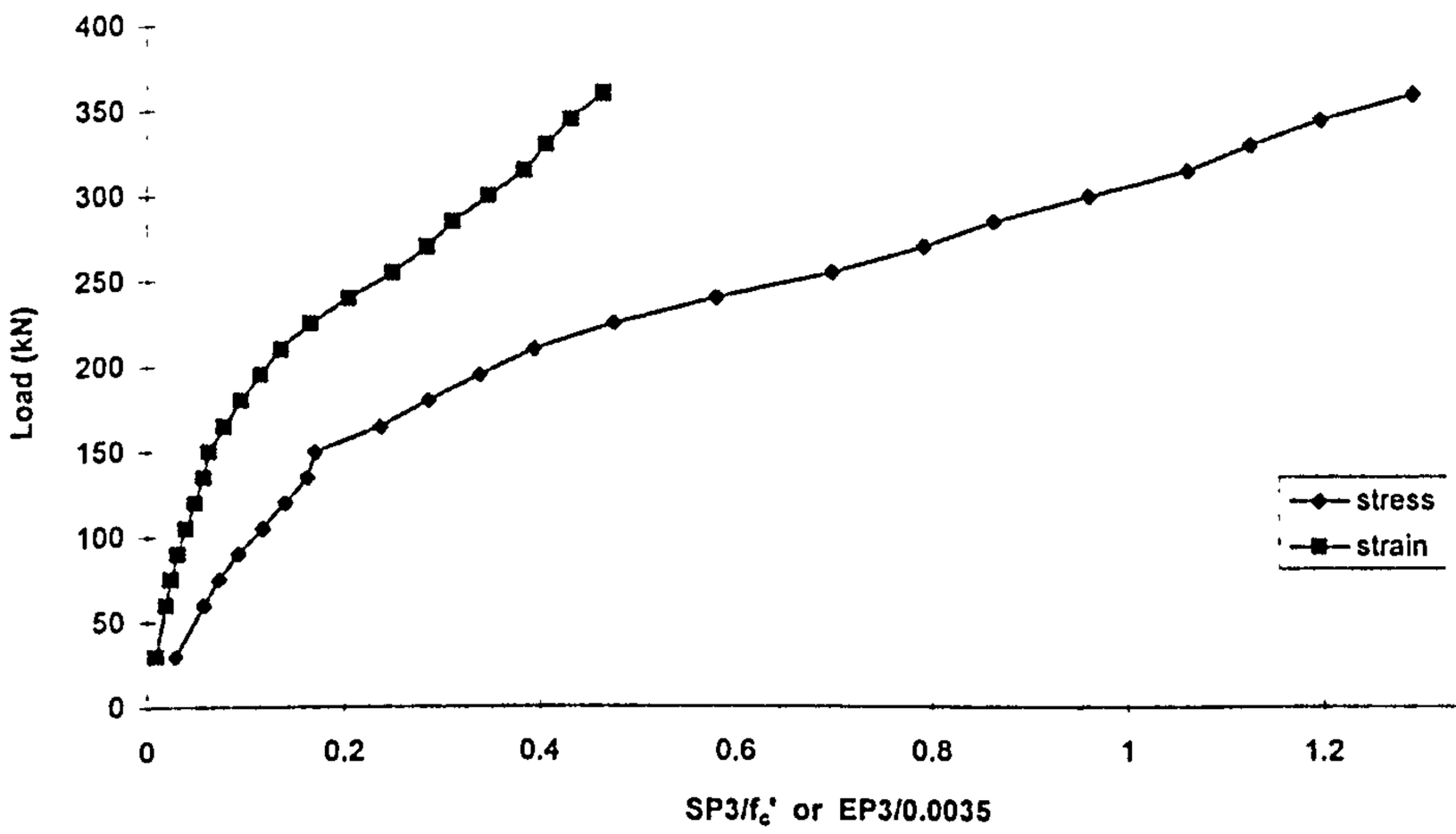

Note: SP3=σ_3=maximum compressive principal stress

EP3=ε_3=maximum compressive principal strain

Figure 7.50 Principal compressive stress and principal compressive strain of concrete for specimen SC5

7.4.2 Corner column-slab connections with shear reinforcement (Hammill and Ghali)

This section presents the results of analysis of five full scale reinforced concrete corner column-slab connections tested by Hammill and Ghali (1994). All these specimens contained identical flexural steel in slab (Figures 7.52 & 7.53) and reinforcement in column. Figure 7.51 shows the dimensions and locations of forces applied to the specimens.

The variables are the amount of shear reinforcement and the loading procedure. Only specimens NH3 and NH5 contained shear reinforcement. The layouts of shear studs are shown in Figure 7.54. The remaining three specimens had no shear reinforcement. All slabs except NH4 were subjected to both shear and unbalanced moment, while specimen NH4 was subjected to unbalanced moment only. The experimental loadings are shown in Table 7.9.

The slab was modelled with a 6×6×1 mesh. The vertical load was simulated by a uniformly distributed load over the cross section of the column, while the diagonal horizontal load was simulated by two point loads at the tips of column, as shown in Figure 7.55. Vertical restraint (z-direction) was provided along the simple support, and additional horizontal restraint (x and y direction) were provided at the two opposite corners of slab to prevent rigid body movement.

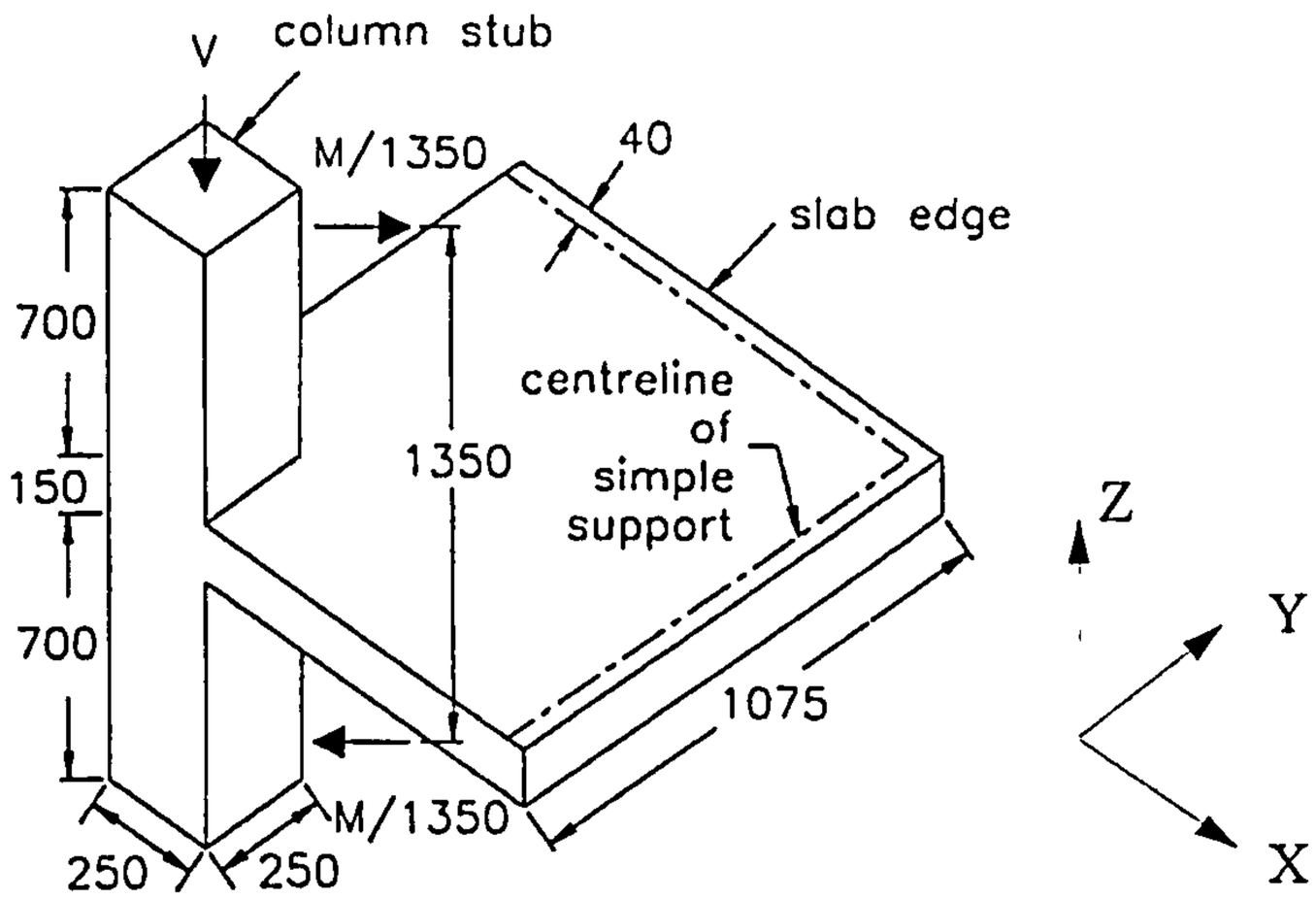

Figure 7.51 : Dimensions and loadings for Specimens NH1-NH5

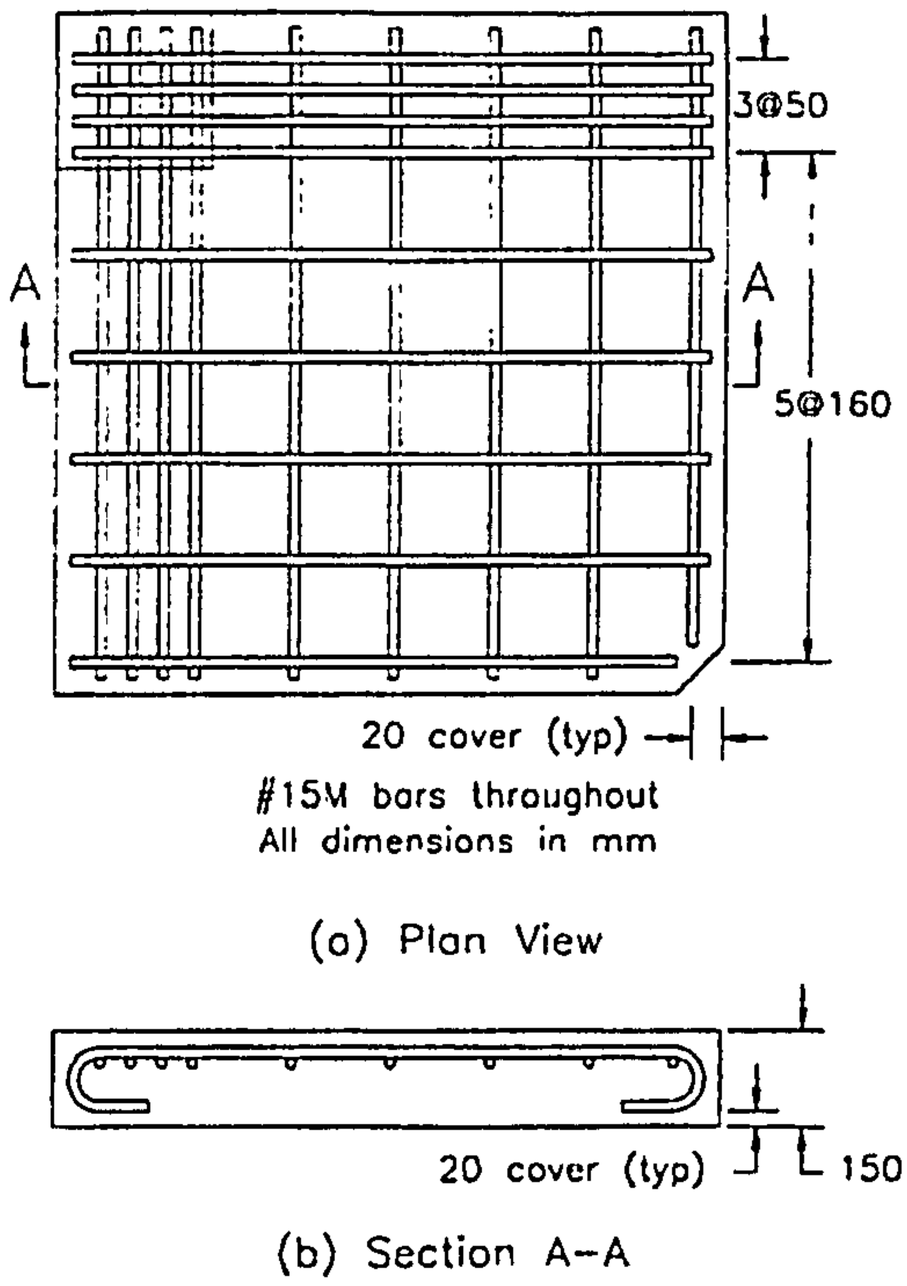

Figure 7.52 : Layout of top flexural steel

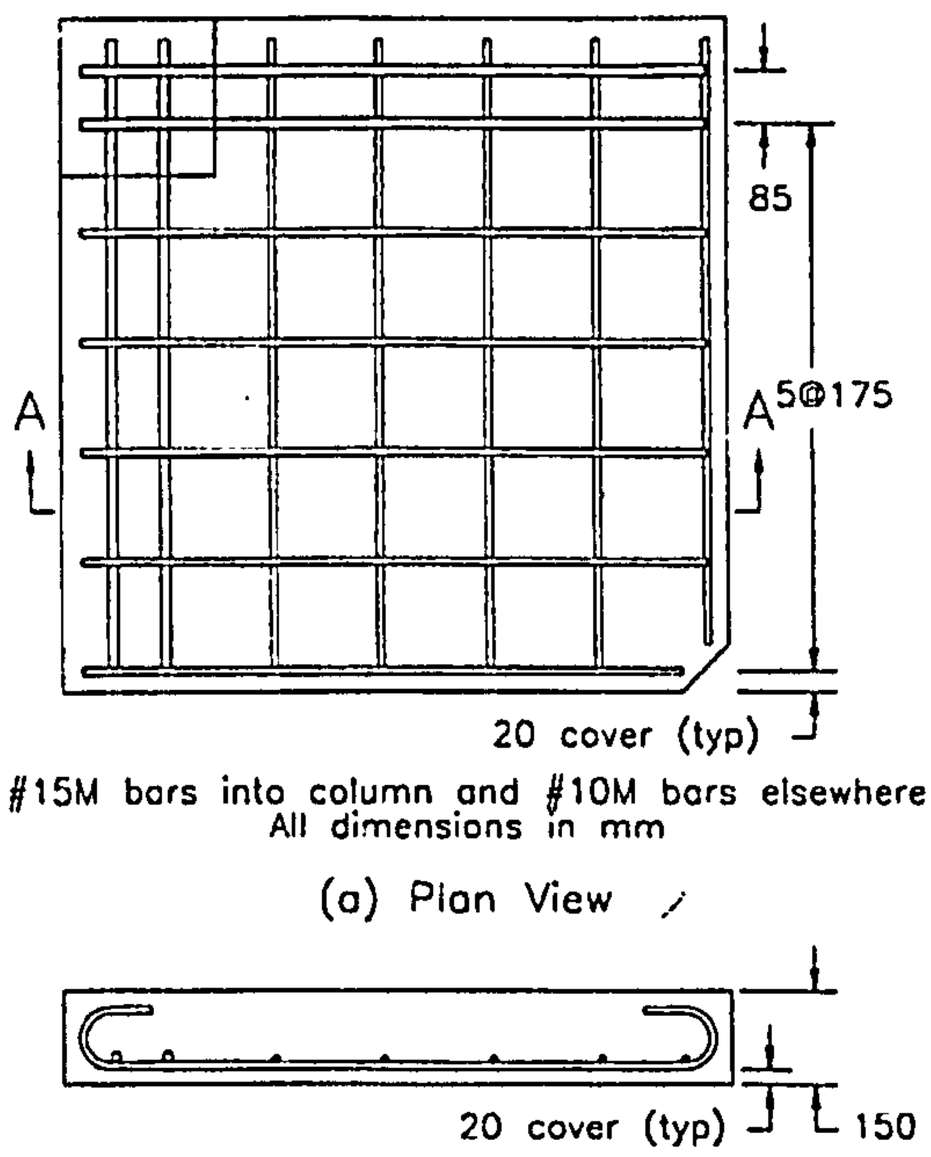

Figure 7.53 : Layout of bottom flexural steel

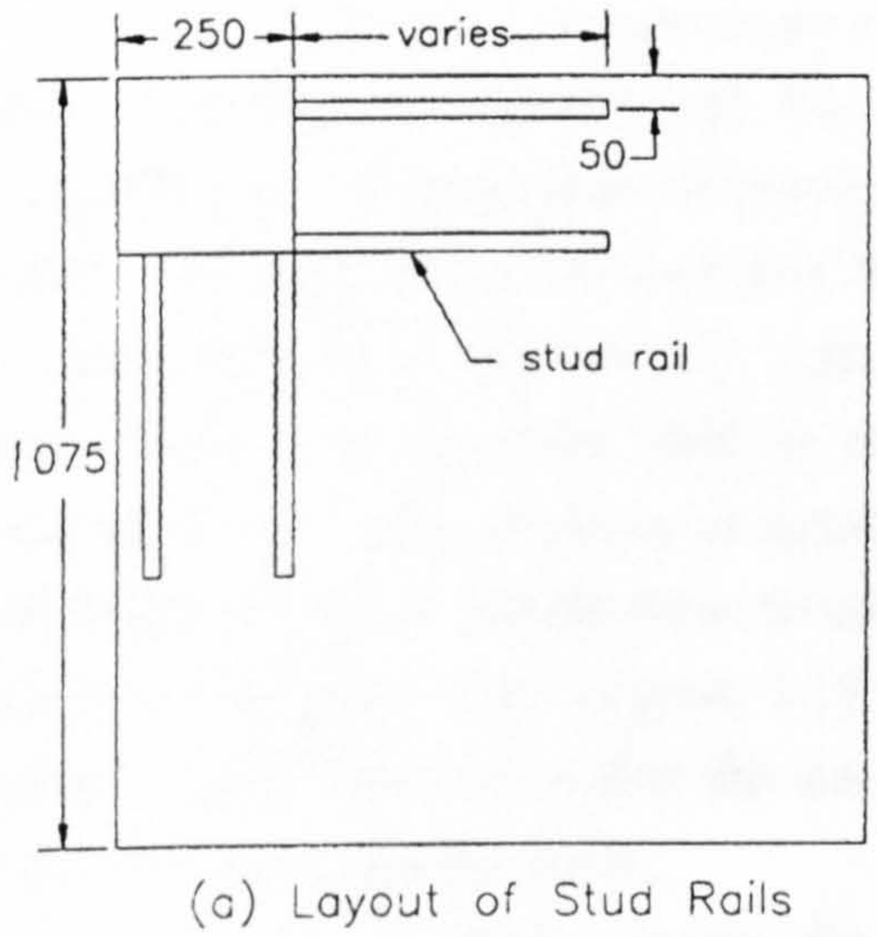

(a) Layout of Stud Rails

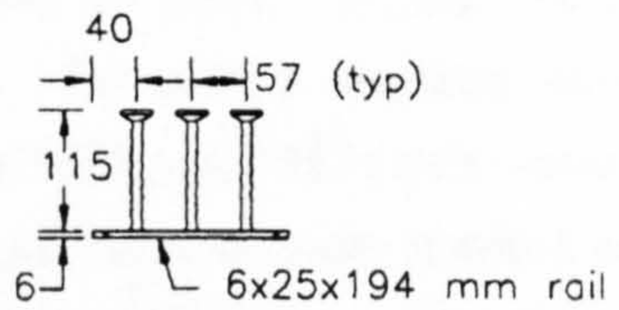

(b) NH3 Stud Rail

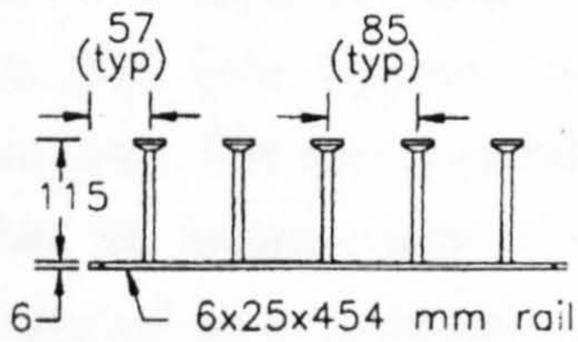

(c) NH5 Stud Rail

Figure 7.54 : Studs layouts and details for NH3 and NH5

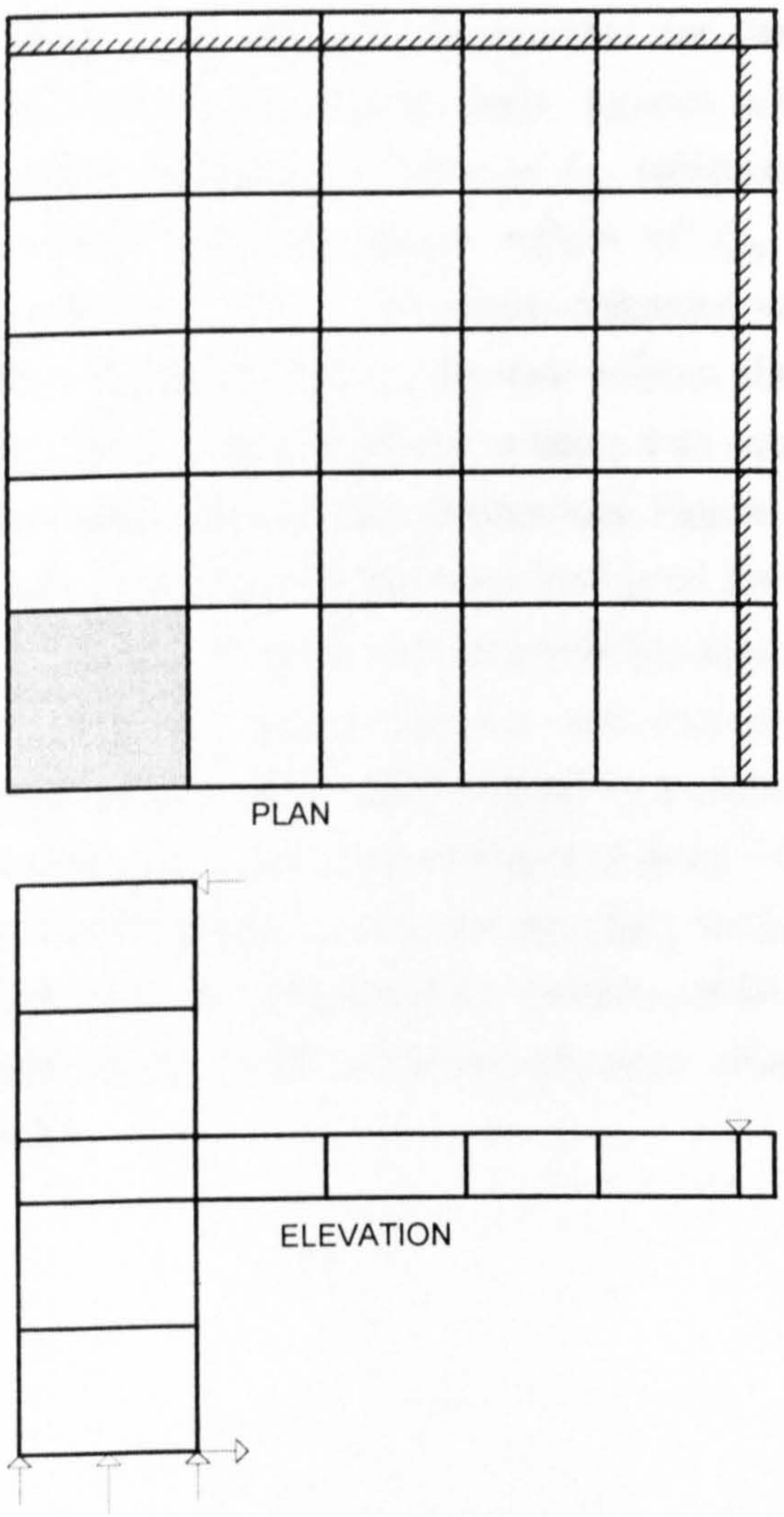

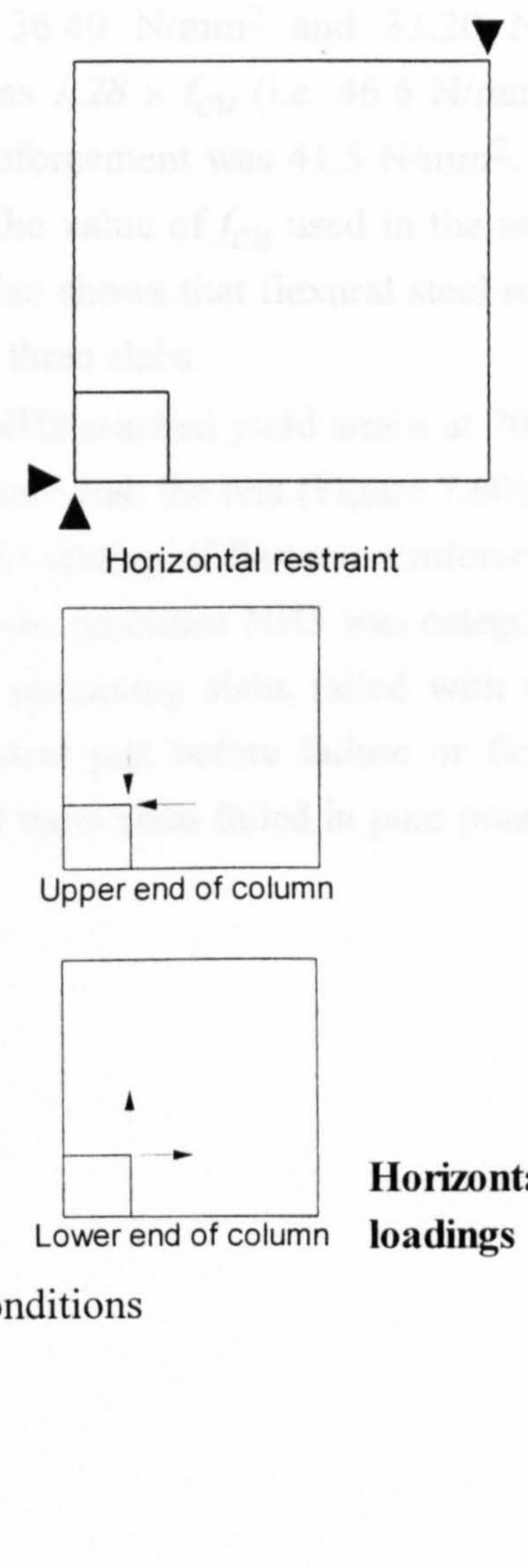

Horizontal loadings

Figure 7.55 : Finite element mesh and boundary conditions

The computed predictions are shown in Table 7.9. The mean value for the ratio of predicted-to-experimental load is 1.00 with a standard deviation of 0.13. Comparing the ultimate loads of specimens NH3 and NH5 (with shear reinforcement) to NH1 (without shear reinforcement), the addition of studs resulted in an increase in the shear capacity of 5% and 22% respectively. The reason why the enhancement of shear capacity in specimen NH3 is small is because its failure surface basically occurred at the same location as specimen NH1 (see Figures 7.56 and 7.57), i.e. punching took place outside shear reinforced zone. For specimen NH5, this area was reinforced by shear studs (Figure 7.59), thus the enhancement of shear capacity is higher. Figure 7.58 shows that the slab subjected to unbalanced moment only also failed in punching shear mode.

The main purpose of providing shear reinforcement is to enhance shear capacity and to prevent brittle failure. Figure 7.60 shows that provision of shear stud increased deflection by a small amount before collapse in all cases. The load-deflection response for these three slabs follow each other very closely because compressive strengths of concrete for these slabs used in the analysis are almost identical. In the present study, regions with shear reinforcement are assumed to be confined and have a value of f_{cu} enhanced by 28%. In the case of slab with shear reinforcement, the actual values of f_{cu} were 36.40 N/mm^2 and 33.20 N/mm^2 respectively. The confinement enhanced value was $1.28 \times f_{cu}$ (i.e. 46.6 N/mm^2 and 42.5 N/mm^2). The f_{cu} for slab without shear reinforcement was 41.5 N/mm^2. When the effect of enhancement is taken into account, the value of f_{cu} used in the analysis for these slabs are almost identical. Figure 7.60 also shows that flexural steel reached yield strain at about the same load level for all the three slabs.

The flexural reinforcement for Specimen NH5 reached yield strain at 70% of ultimate load, and displayed a more ductile behaviour than the rest (Figure 7.60). The crack pattern shows that it failed by punching and yielding of flexural reinforcement is confined to the column region (Figure 7.61). Thus, specimen NH5 was categorised as having failed in flexure punching mode. The remaining slabs failed with small deflection, accompanied by yielding of flexural steel just before failure or flexural steel did not yield. All these indications shows that these slabs failed in pure punching mode.

Table 7.9: Summary of test results and numerical predictions (Hammil and Ghali)

	Test results					Numerical results	
Specimen	f_c' N/mm^2	Applied forces	V_{test} (kN)	M_{test} (kNm)	failure mode	Num/Exp ratio	failure mode
NH1	41.50	V,M	146.9	60.8	s	0.90	s
NH2	42.20	V,M	139.1	56.9	s	1.05	s
NH3	36.40	V,M	146.1	58.4	s	0.95	s
NH4	36.90	M	0	46.6	s	1.20	s
NH5	33.20	V,M	179.0	79.0	s	0.90	s
				Average		1.00	
				STDEV		0.127	

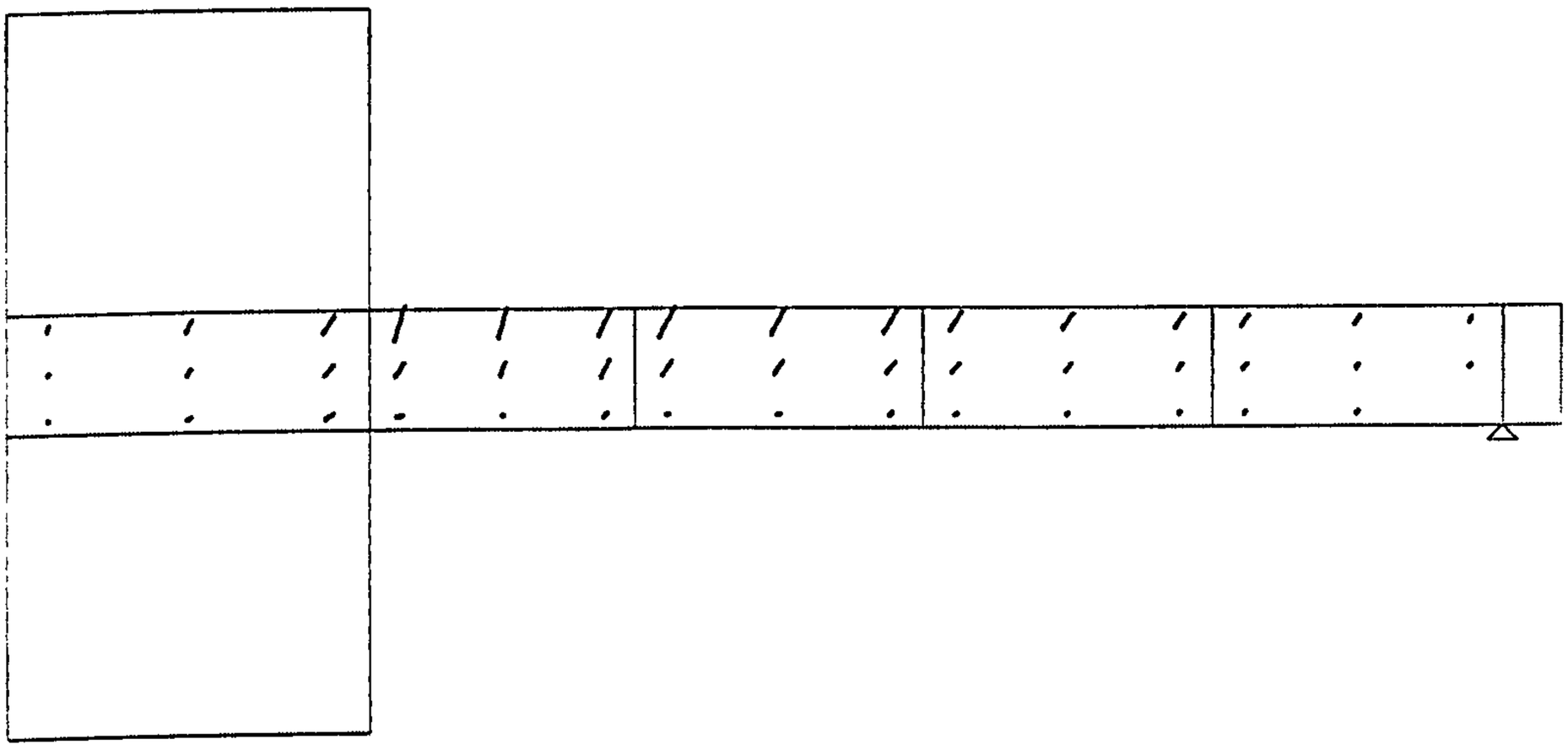

Figure 7.56 Crack pattern for Specimen NH1

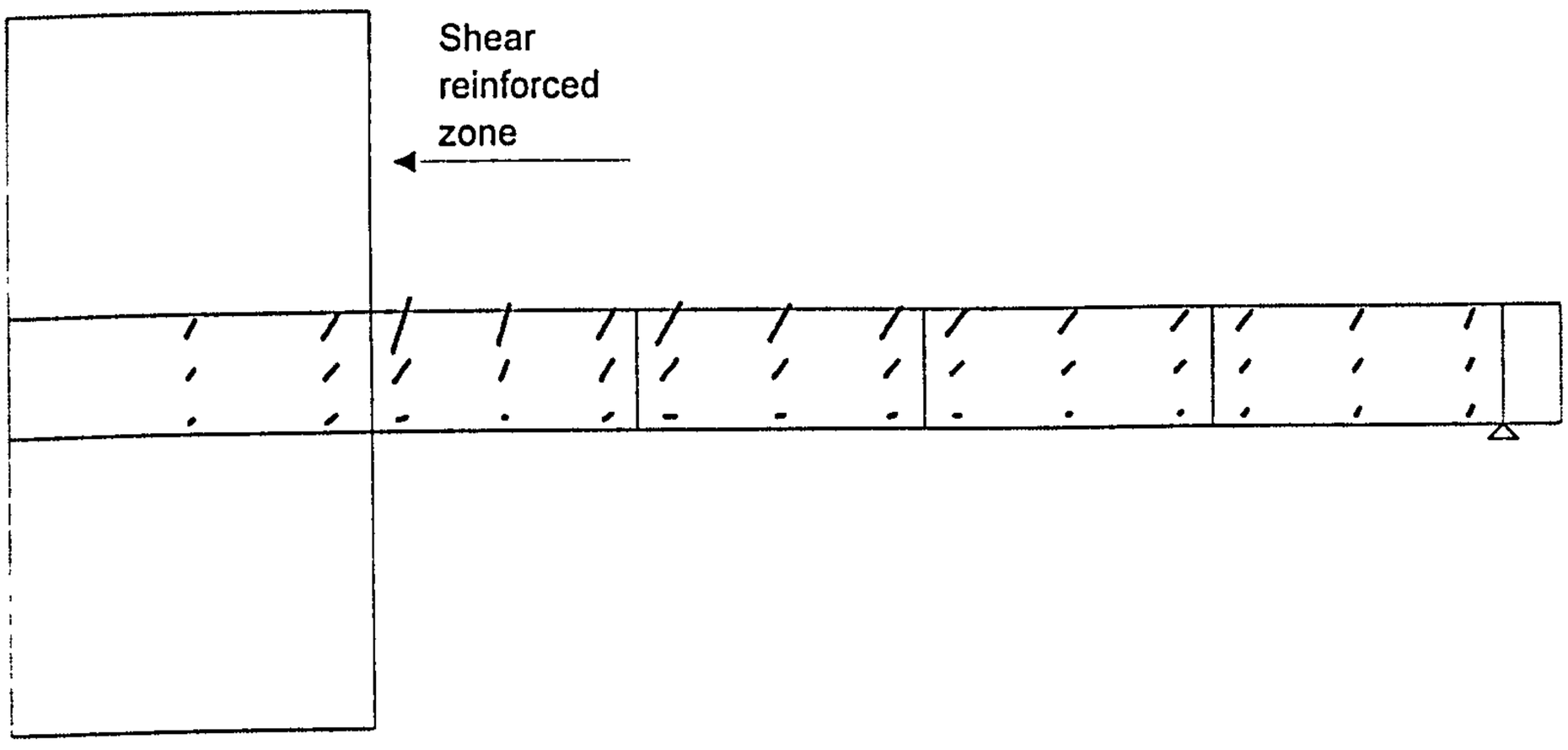

Figure 7.57 Crack pattern for Specimen NH3

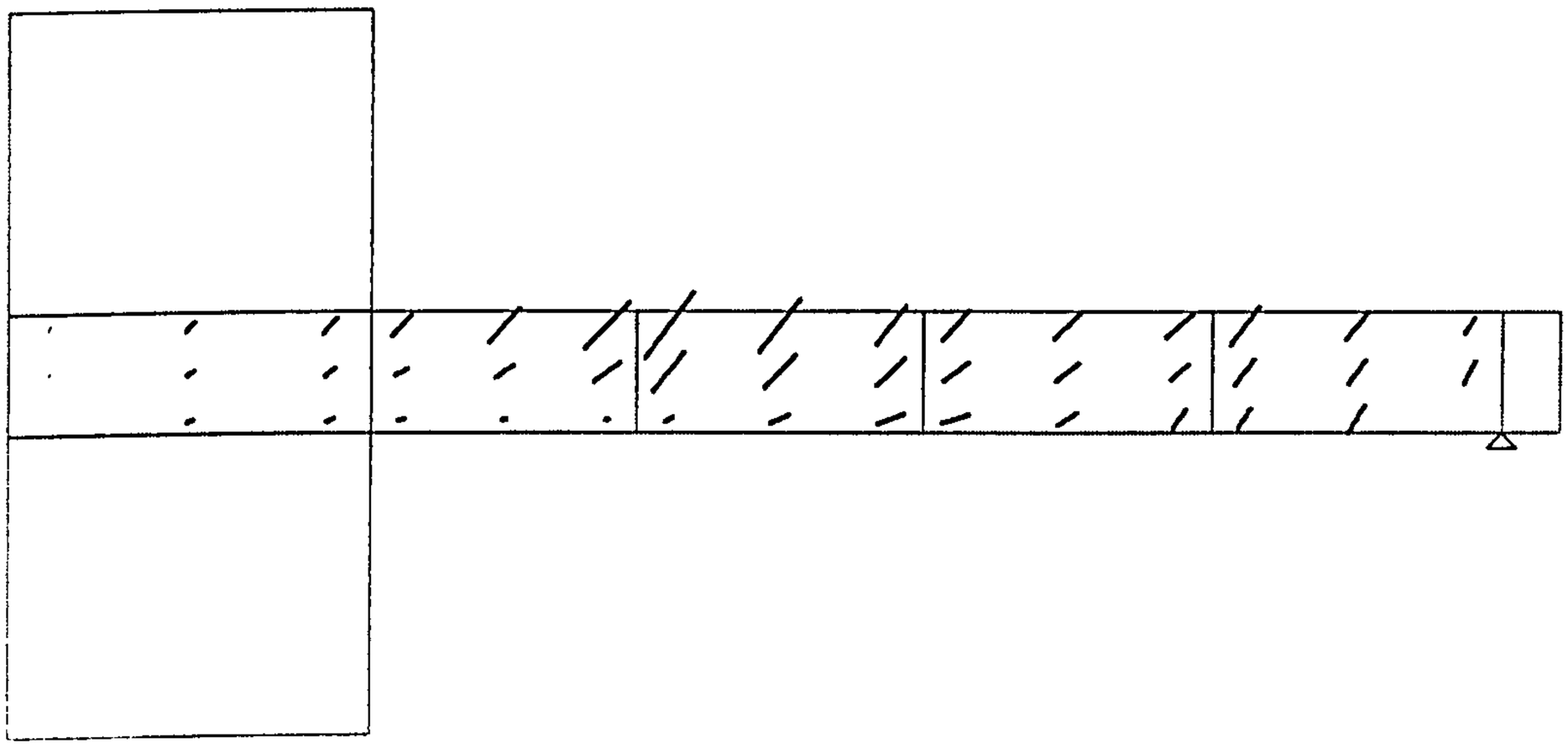

Figure 7.58 Crack pattern for Specimen NH4 (subjected to unbalanced moment only)

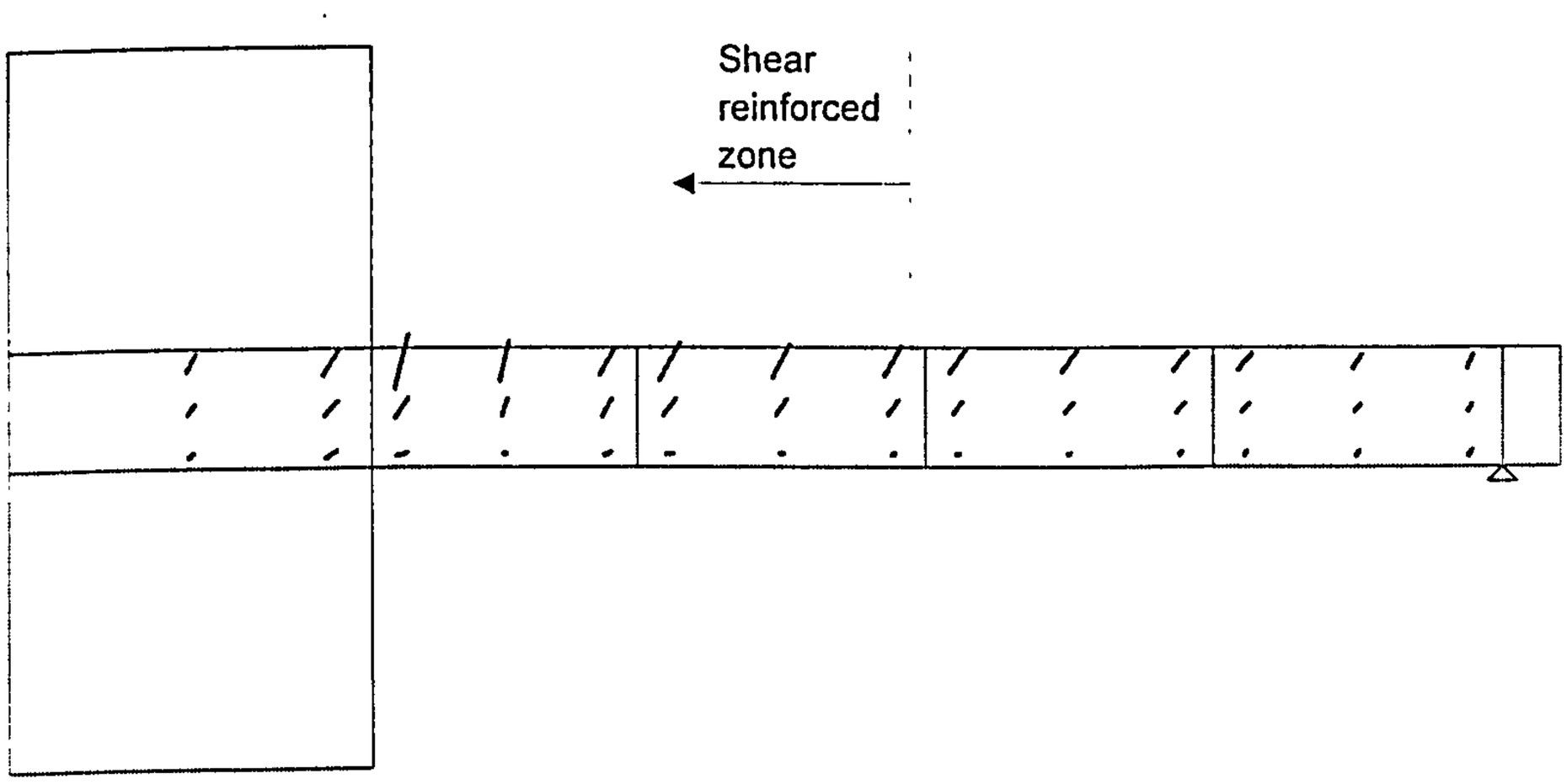

Figure 7.59 Crack pattern for Specimen NH5

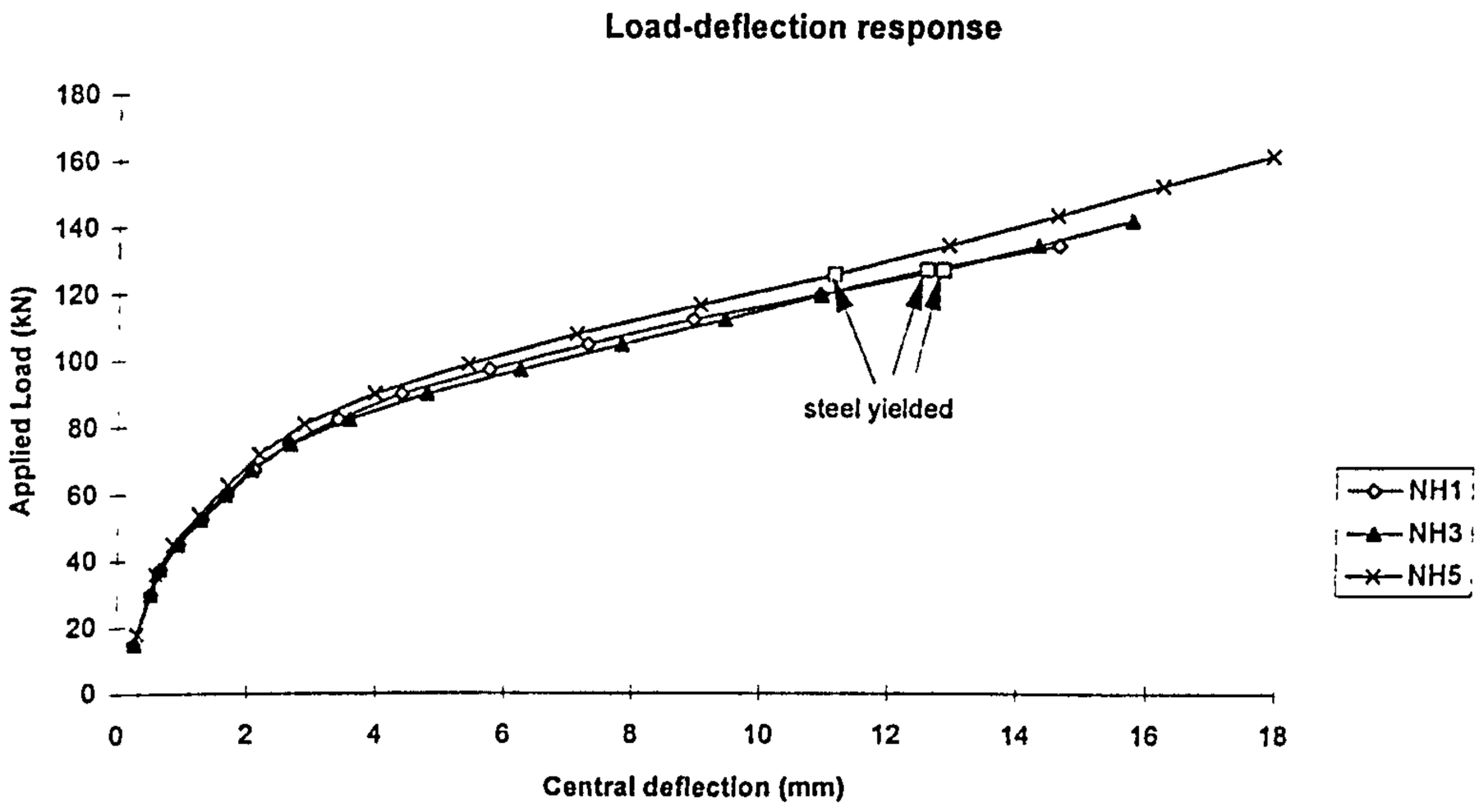

Figure 7.60 Predicted Load-deflection response for slabs NH1, NH3 and NH5

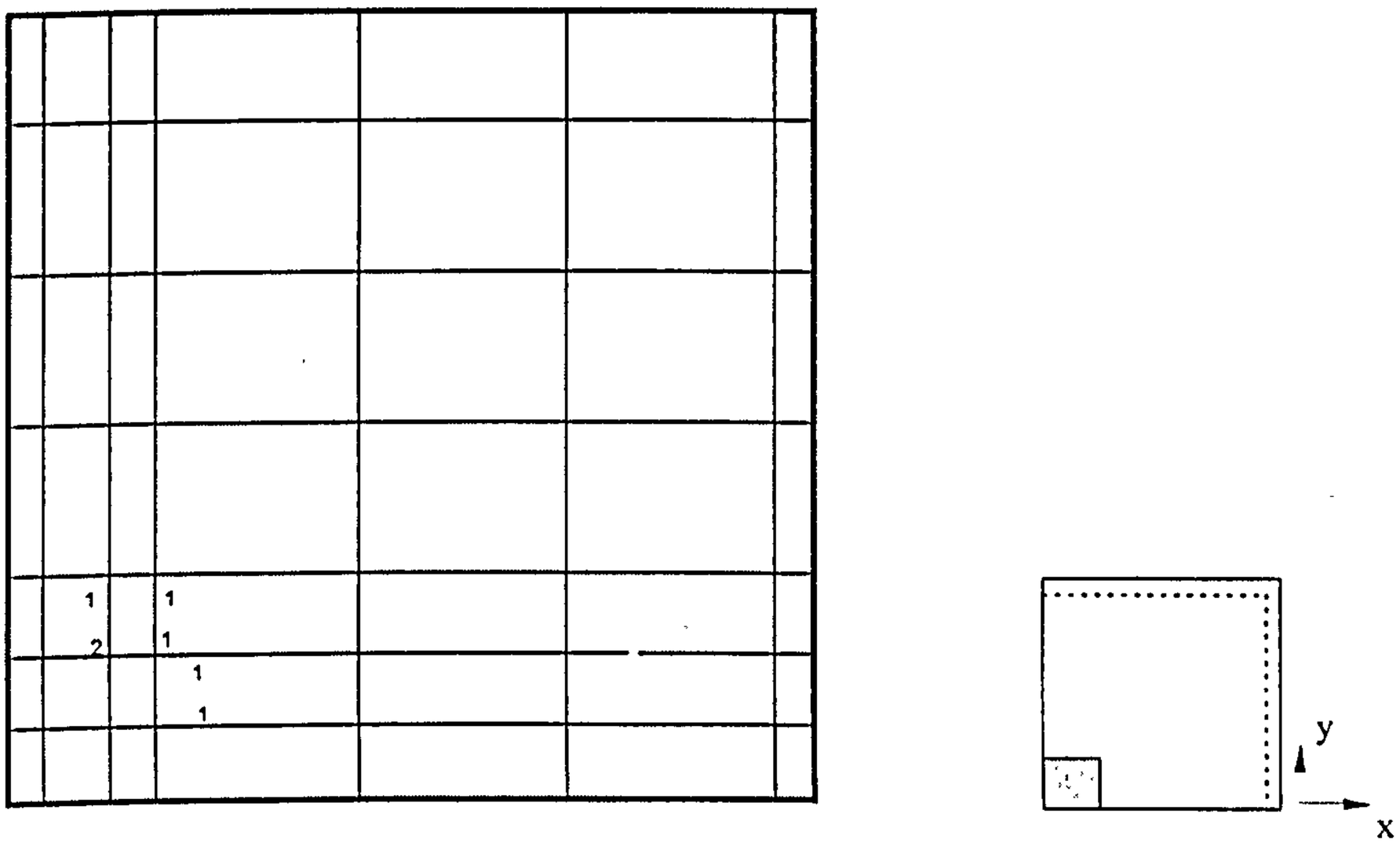

Figure 7.61 Yielding of flexural steel for Specimen NH5

(The numbers on the drawing indicate strain in steel at collapse expressed as a ratio of yield strain)

7.5 Predictions by BS8110

For slabs under a combination of shear and unbalanced moment, their shear capacity cannot be checked as for interior slabs subjected to the symmetrical punching discussed in the previous chapter. Instead, the shear and moment capacities need to be checked separately. The assumptions made for calculating the punching shear strength of slabs are similar to those in the previous chapter, but should include the effect of the unbalanced moment. The maximum shear force V_{max} from the tests are calculated as follows :

$$V_{\max} = V + \frac{M}{X}$$

where V = *Shear force transferred to the column.*

M = *The unbalanced moment*

X = *The side length of the perimeter considered parallel to the axis of bending.*

For edge and corner column-slab junction, the code also limits the amount of moment transfer from column to slab (or vice versa). The detail of the code requirement to calculate the transfer moment capacity is illustrated in sample calculations presented in Appendix A.

In order to prevent confusion (moment capacity of slab, M_u and moment transfer to slab, M_t), the notations used in the calculation are defined as follows:

M_{test} = unbalanced moment from experiments

V_{test} = shear force from experiments

$M_{elastic}$ = maximum moment per unit length in slab due to applied loads (shear force alone or the combination of shear force and unbalanced bending moment as appropriate) from linear elastic analysis using shell element. This value was obtained from the average of the moments at the Gauss points within 1m width at critical region.

M_u = moment capacity for 1m width of slab provide by flexural steel according to BS8110 with a safety factor of 1.0.

M_t = transfer moment capacity based on the effective width (see Appendix A) provide by flexural steel according to BS8110 with a safety factor of 1.0.

For **moment capacity of slab,** compare M_u to $M_{elastic}$

For **moment transferred to slab,** compare M_t to M_{test}.

7.5.1 Interior slab-column connections

All specimens considered were subjected to the unbalanced moment about one axis only. Therefore the value of X is defined as

$$X = Cy + 3d$$

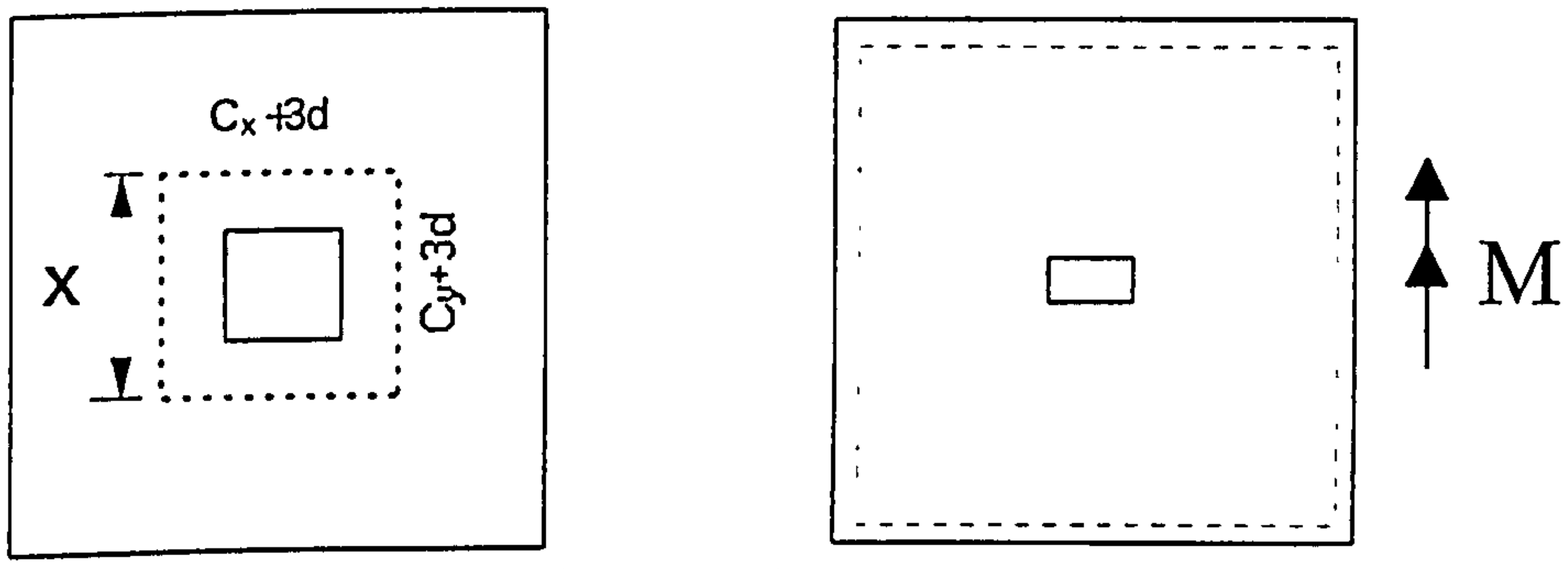

Figure 7.62 : Control perimeter and direction of unbalanced moment

Table 7.10 : Predicted moment capacity for interior slabs

(CIRIA 220, Elgabry and Ghali)

Slab	M_{test} (kNm)	V_{test} (kN)	$M_{elastic}$ (kNm)	M_u (kNm)	$M_u/M_{elastic}$
SM1	0	122.00	19.60	15.86	0.81
SM3	20.90	95.00	20.92	16.47	0.79
SM4	0	101.00	16.23	16.04	0.99
SM5	15.84	72.00	22.31	16.41	0.74
SM6	0	105.00	30.69	16.20	0.53
SM7	0	105.00	23.67	16.20	0.68
SM8	10.78	49.00	20.30	16.01	0.79
SM9	10.67	97.00	23.73	16.66	0.70
SM10	19.36	88.00	30.47	16.66	0.55
SM11	20.02	91.00	22.60	16.63	0.74
SM12	19.36	88.00	21.83	16.40	0.75
AM1	130.00	150	82.70	69.97	0.85
AM2	162.00	150	98.30	69.72	0.71
AM3	142.00	300	108.50	78.20	0.72
AM4	150.00	300	112.30	86.69	0.77
AM5	105.00	450	113.80	89.00	0.78
				Average	0.74
				STDEV	0.11

Table 7.11 : Predicted shear capacities and mode of failure for interior slabs
(CIRIA 220, Elgabry and Ghali)

Slab	Test results		Predictions by BS8110		$P_u/V_{max(test)}$
	$V_{max(test)}$ (kN)	Failure Mode	P_u (kN)	Failure Mode	
SM1	122.00	s	138.51	s	1.135
SM3	144.76	s	152.11	s	1.051
SM4	101.00	s	142.52	s	1.411
SM5	109.71	s	130.38	s	1.188
SM6	105.00	s	125.53	s	1.196
SM7	105.00	s	104.61	s	0.996
SM8	84.93	s	101.28	s	1.192
SM9	122.40	s	130.38	s	1.065
SM10	134.10	s	130.38	s	0.972
SM11	138.67	s	152.11	s	1.097
SM12	134.10	s	151.99	s	1.133
AM1	359.00	s	404.84	s	1.128
AM2	410.45	s	581.25	c	1.416*
AM3	528.30	fp	581.25	c	1.100*
AM4	541.16	fp	581.25	c	1.074*
AM5	618.81	fp	581.25	c	0.939*
				Average	1.131
				STDEV	0.133

* wrong mode of failure predicted

Table 7.10 shows that BS8110 under estimated the flexural capacity for all the slabs. However, this is to be expected because the comparison is made with the elastic moment and as slab is a statically indeterminate structure, and redistribution of moment will take place, i.e. the moment at the critical areas are reduced by redistribution of stresses to the neighbouring areas which are less stressed. BS8110 over predicted the shear capacity for almost all the slabs. This shows that it is necessary to include the coefficient of 1.5 in $V_{eff} = V + \frac{1.5M}{X}$ (see Chapter 2, equation 2.20, page 32) to ensure a safe design.

7.5.2 Edge column-slab connections

All specimens studied were subjected to an unbalanced moment parallel to the free edge only. Therefore the value of X is defined as $X = C_y + 3d$ (Figure 7.63).

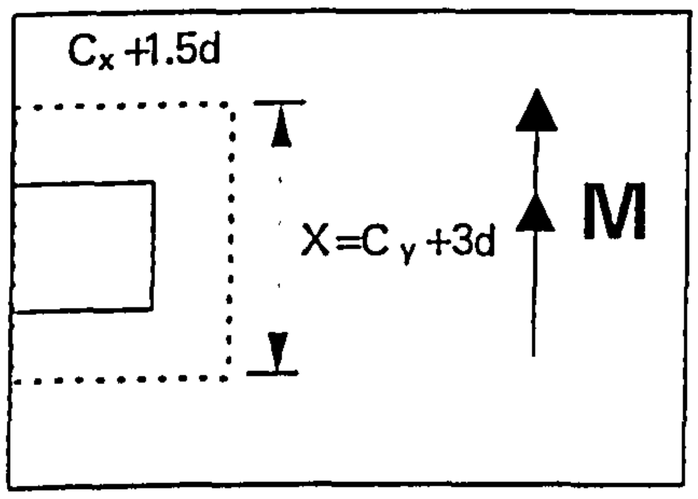

Figure 7.63 : Control perimeter for edge column-slab connections

Table 7.12 shows that moment capacity of slabs predicted by BS8110 are inconsistent. It over predicted the moment capacity of some of Zakaria's slabs and gave very poor prediction for the remaining slabs (SE2 and SE3) where the top reinforcement perpendicular to the free edge was extremely light. The capacity of all slabs tested by Mortin and Ghali (1991) were under estimated. The reason for the difference between these two group of slabs must be due to the test configuration. The slabs tested by Zakaria consists of a pair of edge columns connected to a slab where the other two edges are not supported (Figure 7.64a). On the other hand, the slabs tested by Mortin consists of a single edge where the slabs are simple support in the other three edge edges (Figure 7.64b).

Figures in Table 7.13 show that the moment transferred to the slabs, particularly for slabs which were poorly detailed (e.g. SE2 and SE3 with very low amount of top reinforcement) is underestimated. This implies that the effective width b_e imposed by the code is restrictive (For example, from both numerical and experimental observation for specimen SE2, the area of slab where steel yielded spread over the full width of slab. So, the actual width for transfer of moment must be greater than b_e. Conversely, for specimen SE4, yielding of steel confined was to a small area around the column. Thus, the width transfer the moment must be smaller).

Generally, the shear capacities predicted by BS8110 (Table 7.14) agree well with the experimental results.

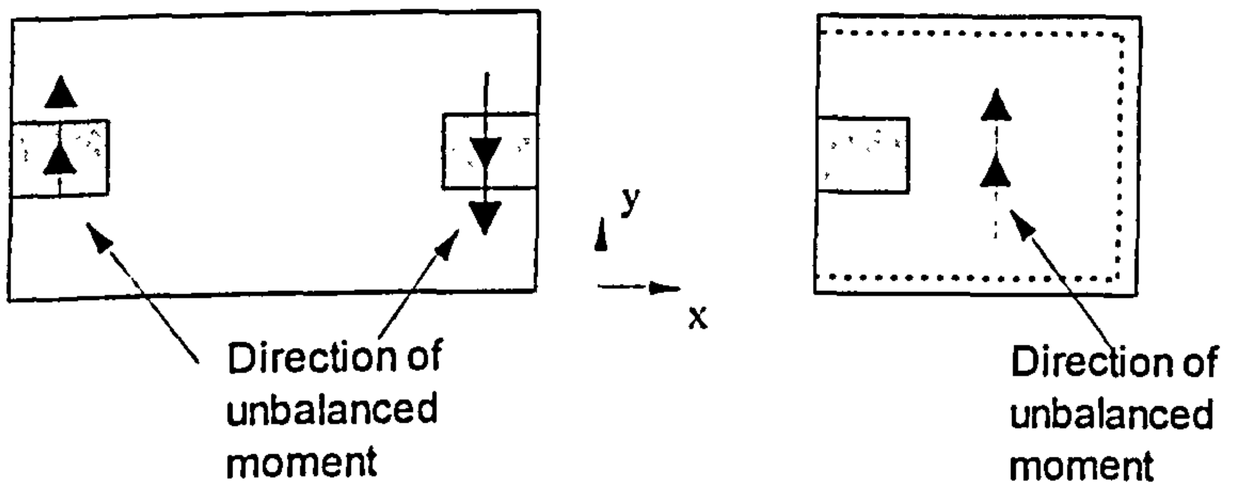

(a) Zakaria's slabs (b) Mortin and Ghali's slabs

Figure 7.64 : Support conditions for edge column-slabs

Table 7.12 : Predicted moment capacity for edge column-slab connections

(Zakaria, Mortin and Ghali)

Slab	M_{test} (kNm)	V_{test} (kN)	$M_{elastic}$ (kNm)	M_u (kNm)	$M_u/M_{elastic}$
SE1	39.50	198.0	32.5	37.1	1.14
SE2	34.00	192.0	31.5	8.6	0.27
SE3	32.50	256.0	42.0	8.6	0.21
SE4	30.50	152.0	25.8	40.9	1.58
SE5	38.50	164.0	27.8	35.9	1.29
SE6	27.50	149.0	25.3	20.3	0.80
SE7	31.70	129.0	21.9	30.4	1.39
SE8	33.70	136.0	26.4	35.8	1.36
JS1	60.50	140.9	49.4	35.6	0.72
JS2	95.30	231.0	78.1	47.5	0.61
JS3	89.50	212.3	71.7	47.5	0.66
JS4	60.30	141.0	49.4	46.9	0.95
JS5	86.40	212.3	71.0	47.2	0.67
JS6	85.60	201.0	67.9	47.1	0.69
				Average	0.88
				STDEV	0.42

Table 7.13 : Predicted transfer moment capacity for edge column-slab connections (Zakaria, Mortin and Ghali)

Slab	M_{test} (kNm)	M_t (kNm)	M_t/M_{test}
SE1	39.50	29.68	0.75
SE2	34.00	6.91	0.20
SE3	32.50	6.91	0.21
SE4	30.50	24.71	0.81
SE5	38.50	25.16	0.65
SE6	27.50	14.18	0.52
SE7	31.70	21.26	0.67
SE8	33.70	25.07	0.74
JS1	60.50	27.16	0.45
JS2	95.30	36.22	0.38
JS3	89.50	36.22	0.40
JS4	60.30	34.42	0.57
JS5	86.40	35.99	0.42
JS6	85.60	35.87	0.42
		Average	0.51
		STDEV	0.193

Table 7.14 : Predicted shear capacity and mode of failure for edge column-slab connections (Zakaria, Mortin and Ghali)

Slab	Test results		Predictions by BS8110		$P_u/V_{max(test)}$
	$V_{max(test)}$ (kN)	Failure Mode	P_u (kN)	Failure Mode	
SE1	277.96	s	175.12	s	0.630
SE2	259.59	s	153.79	s	0.592
SE3	320.61	s	234.00	out	0.730
SE4	203.35	s	154.39	s	0.759
SE5	228.81	s	157.83	s	0.690
SE6	195.06	s	147.16	s	0.754
SE7	182.10	s	156.24	s	0.858
SE8	221.53	s	160.88	s	0.726
JS1	238.48	s	208.16	s	0.873
JS2	384.71	out	292.00	out	0.759
JS3	356.65	out	292.00	out	0.819
JS4	238.26	s	229.60	s	0.964
JS5	351.65	out	292.00	out	0.830
JS6	339.06	out	306.05	out	0.903
				Average	0.778
				STDEV	0.104

7.5.3 Corner column-slab connections

For corner column-slab junctions, the unbalanced moment exists about both axis. Therefore the X is defined as

$$X = \sqrt{(C_x + 1.5d)(C_y + 1.5d)}$$

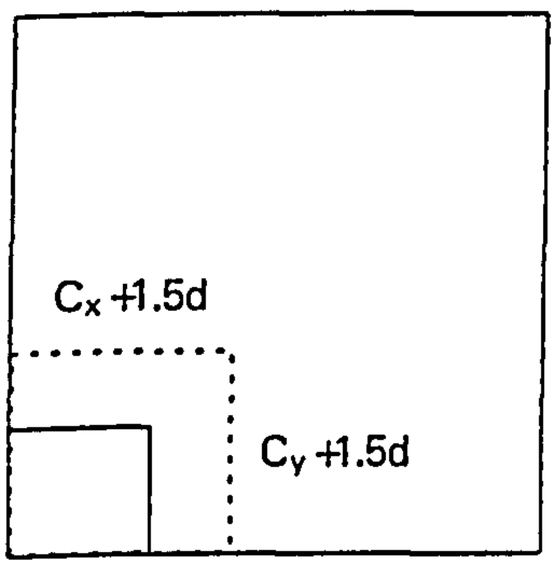

Figure 7.65 : Control perimeter for corner column-slab connections

Table 7.15 shows that BS8110 generally over predicted the moment capacity of slabs. This may be due to the fact that the length considered is larger than the possible yield line which can develope in the corner slabs (Figure 7.66). However, it under-estimates the moment transfer to slab as in the case of edge slab-column connection (Table 7.16).

Table 7.17 shows that the shear strength for all the slabs except specimen NH4 (subjected to unbalanced moment only) is underestimated.

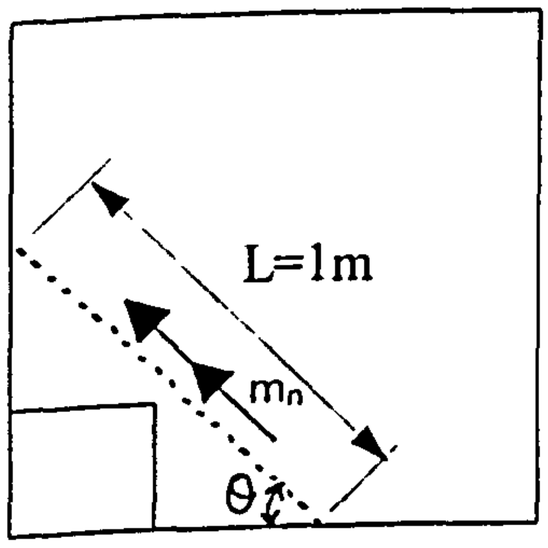

Figure 7.66 : moment resistance for corner column-slab connections

Table 7.15 : Predicted moment capacity for corner column-slab connections
(Walker, Hammil and Ghali)

Slab	M_{test} (kNm)	V_{test} (kN)	$M_{elastic}$ (kNm)	*M_u (kNm)	$M_u/M_{elastic}$ load
SC1	36.40	81.00	37.6	31.1	0.83
SC2	35.70	75.00	34.8	19.5	0.56
SC3	45.60	74.00	34.3	36.9	1.08
SC4	24.00	64.00	31.4	33.9	1.08
SC5	26.90	82.00	30.3	47.0	1.55
SC7	39.00	82.00	38.0	47.0	1.24
NH1	19.36	60.80	48.1	59.4	1.23
NH2	20.02	56.90	45.5	59.5	1.31
NH3	19.36	58.40	45.1	59.5	1.32
NH4	130.00	46.60	55.7	59.5	1.07
NH5	105.00	79.00	58.7	59.6	1.02
				Average	1.12
				STDEV	0.27

*Note

$M_u = m_n = m_x\cos^2\theta + m_y\sin^2\theta$ (for orthotropically reinforced slab)

m_x, m_y = flexural resistance moments in x and y directions

Table 7.16 : Predicted transfer moment capacity for corner column-slab connections (Walker, Hammil and Ghali)

Slab	M_{test} (kNm)	M_t (kNm)	M_t/M_{test}
SC1	36.40	26.40	0.73
SC2	35.70	16.58	0.46
SC3	45.60	31.32	0.69
SC4	24.00	21.09	0.88
SC5	26.90	28.29	1.05
SC7	39.00	28.29	0.73
NH1	19.36	42.00	0.69
NH2	20.02	42.04	0.74
NH3	19.36	42.08	0.72
NH4	130.00	42.11	0.90
NH5	105.00	42.15	0.53
		Average	0.740
		STDEV	0.172

Table 7.17 : Predicted punching shear strength and mode of failure for corner column-slab connections (Walker, Hammil and Ghali)

Slab	Test results		Predictions by BS8110		$P_u/V_{max(test)}$
	$V_{max(test)}$ (kN)	Failure Mode	P_u (kN)	Failure Mode	
SC1	138.20	s	104.37	s	0.755
SC2	130.73	s	91.11	s	0.697
SC3	146.13	s	111.71	s	0.764
SC4	109.87	s	83.16	s	0.757
SC5	133.83	s	92.64	s	0.692
SC7	157.14	s	92.64	s	0.590
NH1	247.23	s	126.78	s	0.513
NH2	233.00	s	126.78	s	0.544
NH3	242.47	out	126.78	out	0.523
NH4	76.90	s	126.78	s	1.649
NH5	309.37	out	191.43	out	0.619
				Average	0.737
				STDEV	0.317

7.6 Conclusions

Following conclusions can be drawn from the analysis of slabs subjected to shear and unbalanced moment :-

- In this chapter, interior slab-column junctions subjected to shear and unbalanced moment, edge and corner column-slab junctions have been analysed. The results of predictions of the ultimate loads (Figure 7.67) and mode of failure are in good agreement with experimental observations.

- Predictions of the moment capacity of slab by BS8110 is not consistent because the comparison is made with the elastic moment. In real structure, redistribution of moment will alter the moment distribution from elastic value.

- BS8110 generally underestimates the transfer moment capacity of slabs (Table 7.10,7.12 and 7.14), particularly for slabs which are poorly detailed (e.g. SE2 and SE3 with very low amount of top reinforcement). This implied that the width of moment transfer may depends on the amount of tension reinforcement. Using the value effective width b_e as prescribe in BS8110, the value M_t compared to test value is very low. This implies that the value b_e as prescribed is too small.

- BS8110 generally over predicted the punching shear strength of interior slabs with unbalanced moment. However, the shear capacities for edge and corner column-slabs junction were underestimated except specimen for NH4 (subjected to unbalanced moment only).

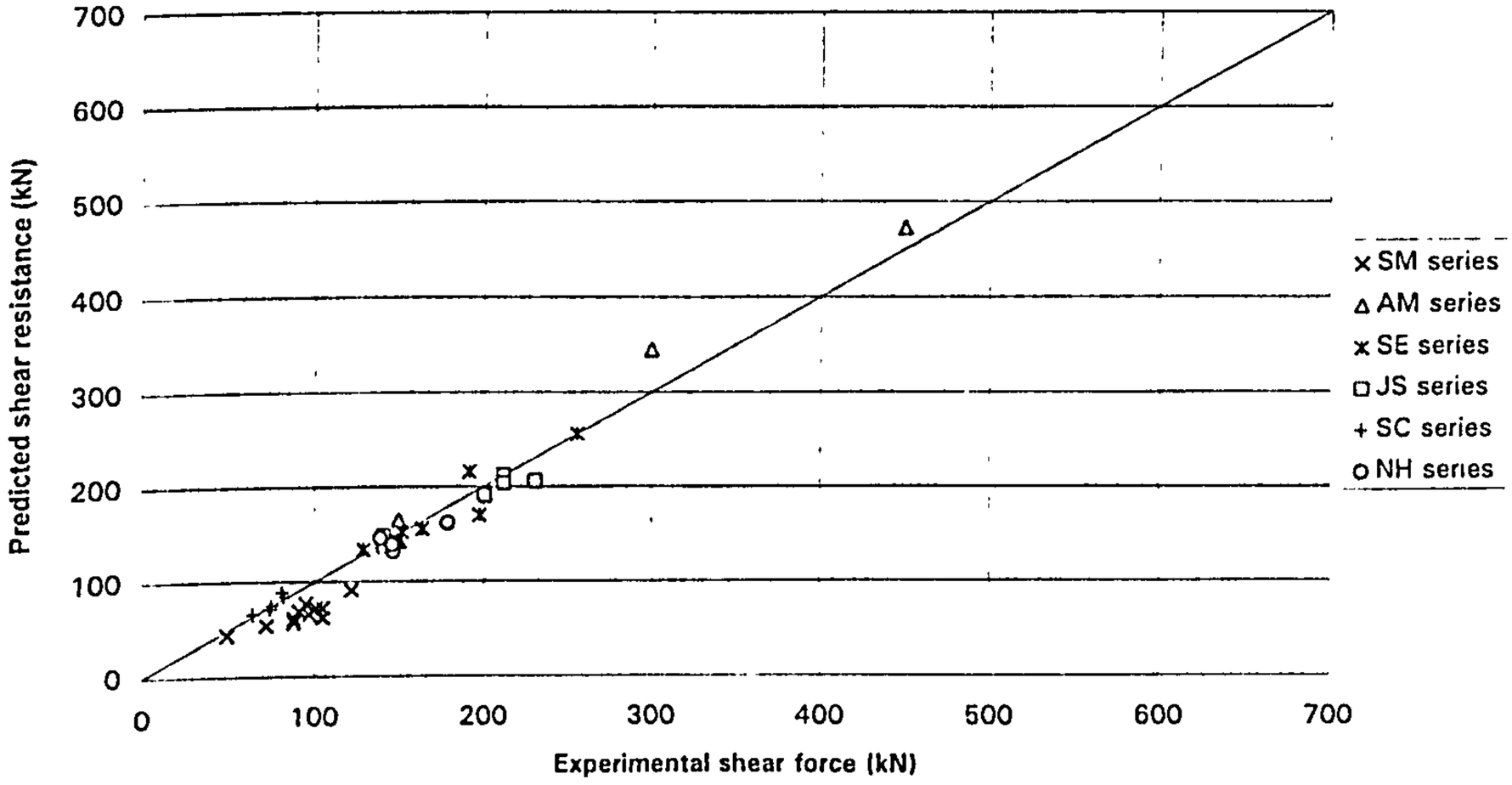

Figure 7.67 : Numerical predictions for slab-column junction subjected to shear and unbalanced moment

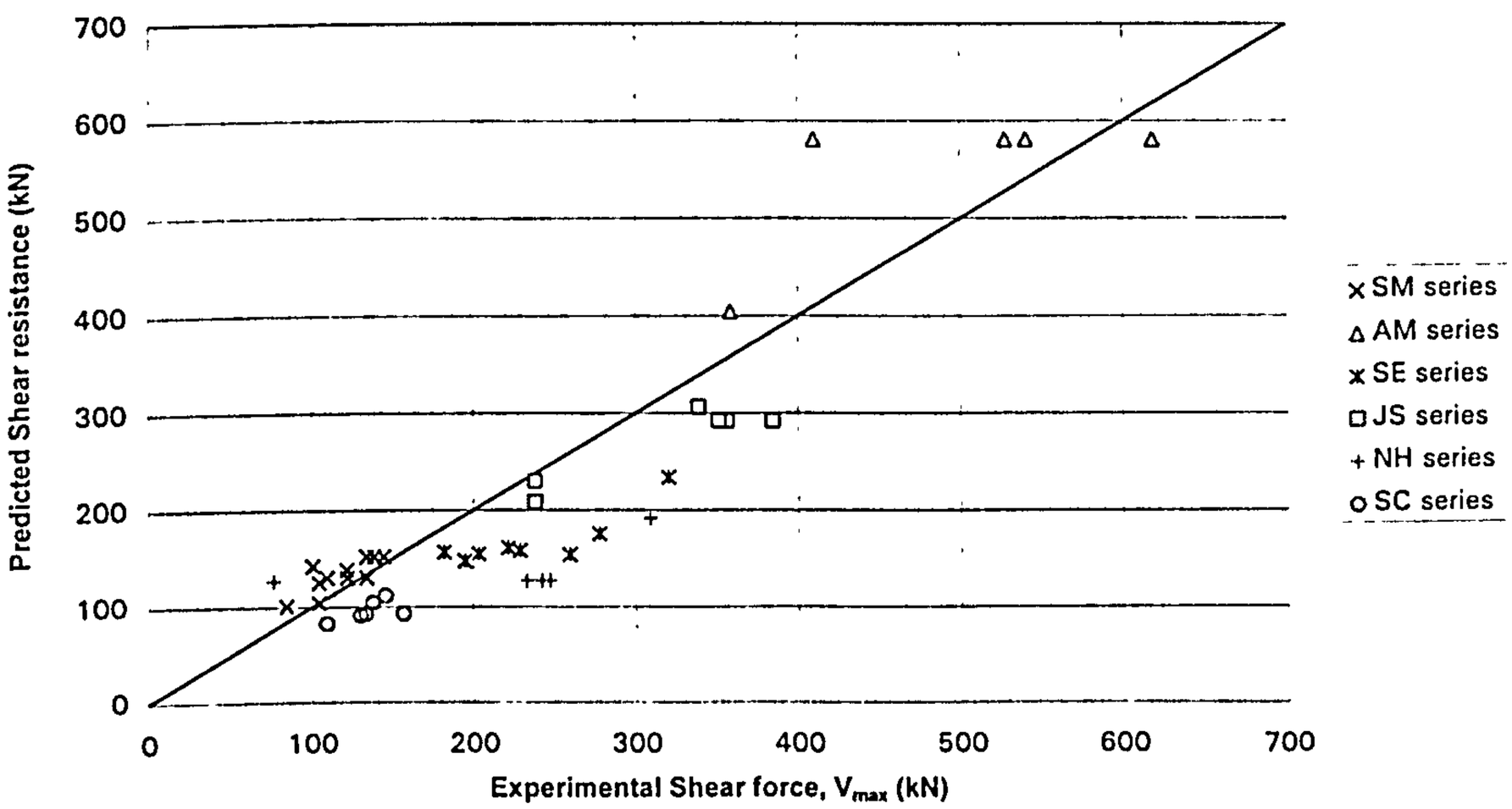

Figure 7.68 : Shear resistance for slab-column junction subjected to shear and unbalanced moment predicted by BS8110

Chapter 8

Restrained slabs

8.1 Introduction

This chapter presents the results of analysis of slabs with different degrees of in-plane restraint (partially or fully restrained). The restraint was provided either by the surrounding slab beyond support or by edge beams. To the author's knowledge, no information on the study of punching shear for restrained slabs with shear reinforcement is available in the literature. Therefore, only slabs without shear reinforcement were analysed. The analysis used same set of "constant" parameters described previously in section 6.1.

8.2. Full panel slab-column specimens tested by Rankin

In addition to the conventional specimens described in section 6.2.1, Rankin (1987) extended the test to a series of full panel slab-column specimens (see Figure 8.1) to include the effect of compressive membrane action. These slabs were simply supported along the four edges with corners free to lift and subjected to a concentrated load at the centre of slab.

The main variable in these slabs was the degree of in-plane restraint which depends on the length of the portion of slab beyond the support. The slabs had constant span of 640mm, but the size of slabs ranged from 800mm to 1600mm. Others variable included, thickness of slab (45.5-64mm), flexural reinforcement ratio (0.517%-1.107%) and concrete strength. The details are summarised in Table 8.1.

Owing to symmetry, only one-quarter of the slab was modelled as shown in Figure 8.2. The applied load was simulated by uniformly distributed load over the element representing the loading stub. Concrete slab was discretised by using one layer of twenty node solid elements.

Predicted ultimate loads are shown in Table 8.2. It ranges from 69.7% to 106.8% of the experimental values. The average of predicted ultimate load is 86.9% of experimental ultimate load with 10.2% standard deviation.

All slabs were predicted to fail either in flexure punching mode or pure punching mode (see Table 8.2). For slabs with relatively low reinforcement ratio (0.5%), the conventional specimen (slab 10, Table 6.3) failed in pure flexure mode. However, the large panel specimens (R3-05 and R5-05, Table 8.2) were predicted to fail by punching. This shows that lateral restraint not only increased the punching

shear capacity, it also changed the mode of failure. Figure 8.3 shows that the higher the degree of restraint (longer the portion of slab beyond support, higher the restraint), stiffer the response and higher the ultimate load. Slab R5-08 (size=1600) was predicted to behave with a much stiffer response and higher ultimate load than the rest of slabs. This is because its concrete strength was very much higher than the rest. Although the predicted ultimate load of slabs was generally lower than the actual ultimate load, the rate of increase in strength with restraint as predicted from numerical analysis was higher than that from experimental results (Figure 8.4).

In order to trace the development of membrane action, vector plot for third principal strain shows that the slabs were subjected compressive stress throughout the depth of slab (Figure 8.5).

The predicted ultimate load and mode of failure by using BS8110 are presented in Table 8.3. Predictions of ultimate load by BS8110 were much lower than the actual ultimate load (71.2% of experimental ultimate load with 7.9% standard deviation) and in addition showed incorrect mode of failure for some of the slabs. This table also shows that higher the restraint, poorer the predictions because the code does not include the effect of membrane action.

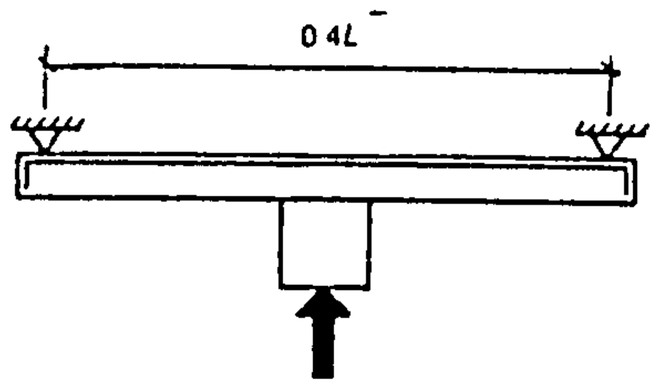

(a) Conventional specimen

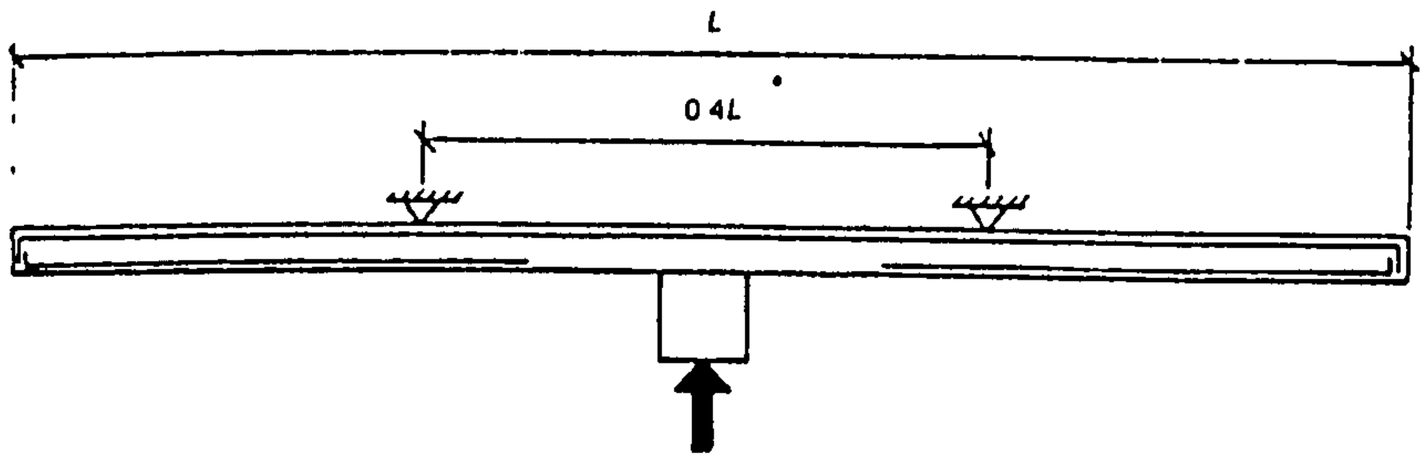

(b) Full panel specimen

Figure 8.1 Loading and support conditions

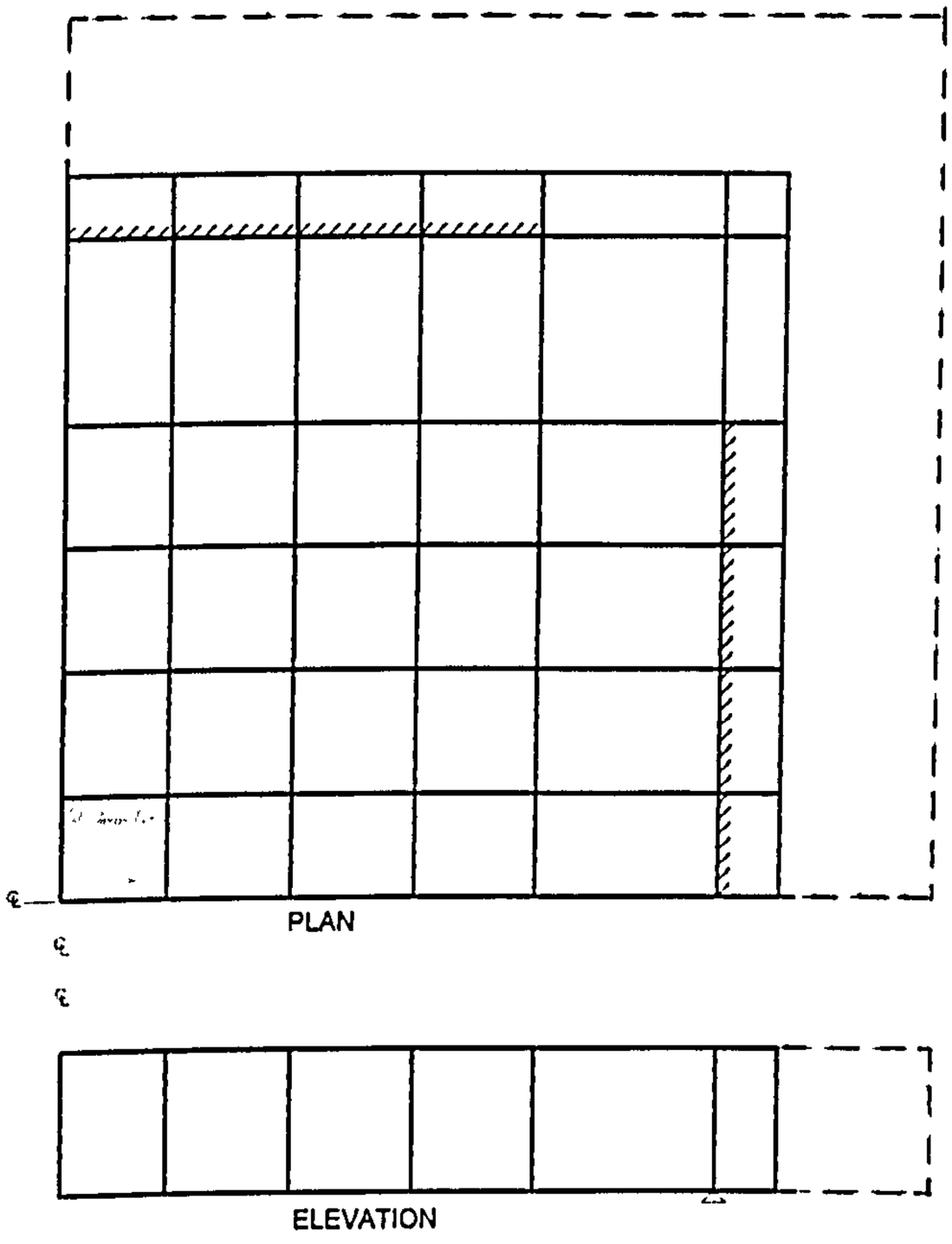

Figure 8.2 Finite element mesh

Table 8.1 : Details of large panel specimens (Rankin)

Slab	Size (mm)	h (mm)	d (mm)	f_{cu} (N/mm^2)	ρ (%)	P_{test} (kN)
R1-08	800	51.00	40.50	37.70	0.802	65.22
R2-08	1000	51.00	40.50	38.90	0.802	64.81
R3-08	1200	51.00	40.50	41.10	0.802	69.66
R4-08	1400	51.00	40.50	33.50	0.802	71.47
R5-08	1600	51.00	40.50	53.80	0.802	77.84
R2-11	1000	51.00	40.50	40.10	1.107	69.73
R4-11	1400	51.00	40.50	43.60	1.107	81.59
R5-11	1600	51.00	40.50	38.90	1.107	87.89
R3-05	1200	51.00	40.50	38.50	0.517	56.16
R5-05	1600	51.00	40.50	38.50	0.517	62.51
R3A-08	1200	57.00	46.50	38.30	0.800	96.41
R5A-08	1600	57.00	46.50	39.60	0.800	95.34
R3B-08	1200	45.50	35.00	36.90	0.799	55.22
R5B-08	1600	45.50	35.00	39.40	0.799	60.34
R3C-08	1200	64.00	53.50	41.30	0.800	112.47
R5C-08	1600	64.00	53.50	44.10	0.800	126.27

Table 8.2 : Comparisons between experimental results and numerical predictions (Rankin)

Slab	Test results		Numerical Predictions		P_{num}/P_{test}
	P_{test} (kN)	*Failure Mode	P_{num} (kN)	Failure mode	
R1-08	65.22	s	47.04	fp	0.721
R2-08	64.81	s	50.40	fp	0.778
R3-08	69.66	s	62.64	s	0.899
R4-08	71.47	s	57.60	s	0.806
R5-08	77.84	s	83.16	s	1.068
R2-11	69.73	s	55.68	s	0.800
R4-11	81.59	s	73.44	s	0.900
R5-11	87.89	s	74.66	s	0.849
R3-05	56.16	s	54.72	fp	0.974
R5-05	62.51	s	62.40	s	0.998
R3A-08	96.41	s	67.20	s	0.697
R5A-08	95.34	s	81.60	s	0.856
R3B-08	55.22	s	44.93	s	0.814
R5B-08	60.34	s	51.00	s	0.845
R3C-08	112.47	s	101.52	s	0.903
R5C-08	126.27	s	124.80	s	0.988
				Average	0.869
				STDEV	0.102

*no detail of failure mode is given in the paper, it only stated that all the slabs failed by punching.

Table 8.3 : Ultimate Load and Mode of failure predicted by using BS8110 (Rankin)

Slab	Experiment		Predictions by BS8110		P_u/P_{test}
	P_{test} (kN)	Failure Mode	P_u (kN)	Failure Mode	
R1-08	65.22	s	53.28	y*	0.817
R2-08	64.81	s	53.43	y*	0.824
R3-08	69.66	s	53.68	y*	0.771
R4-08	71.47	s	51.47	s	0.720
R5-08	77.84	s	54.61	s	0.702
R2-11	69.73	s	60.80	s	0.872
R4-11	81.59	s	60.80	s	0.745
R5-11	87.89	s	60.24	s	0.685
R3-05	56.16	s	35.51	s	0.632
R5-05	62.51	s	35.51	y*	0.568
R3A-08	96.41	s	64.50	y*	0.669
R5A-08	95.34	s	65.22	s	0.684
R3B-08	55.22	s	39.58	y*	0.717
R5B-08	60.34	s	39.81	y*	0.660
R3C-08	112.47	s	79.07	s	0.703
R5C-08	126.27	s	79.07	y*	0.626
				Average	0.712
				STDEV	0.079

* wrong mode of failure predicted

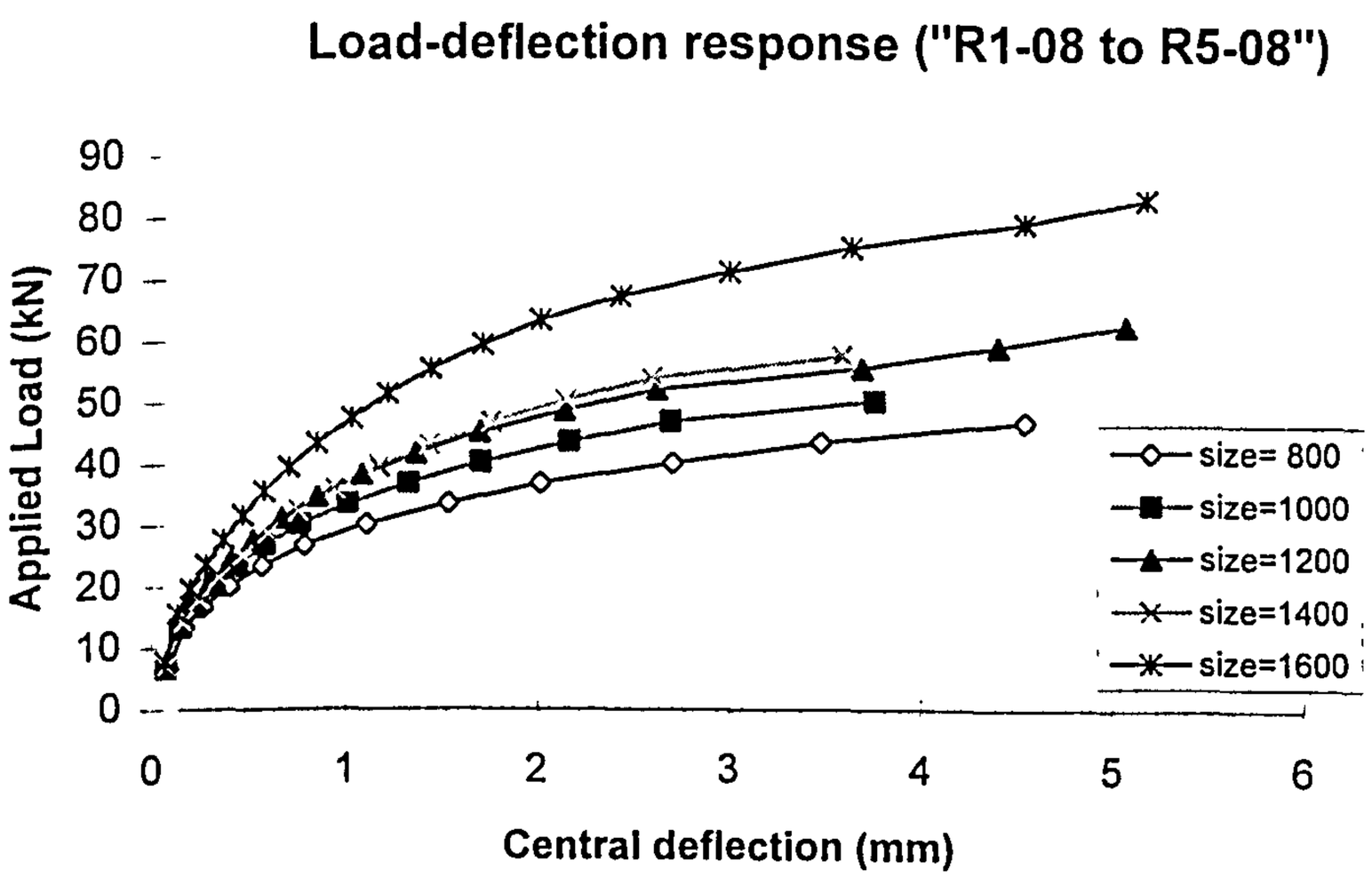

Figure 8.3 Predicted load deflection response for constant slab thickness, reinforcement ratio and varying slab size

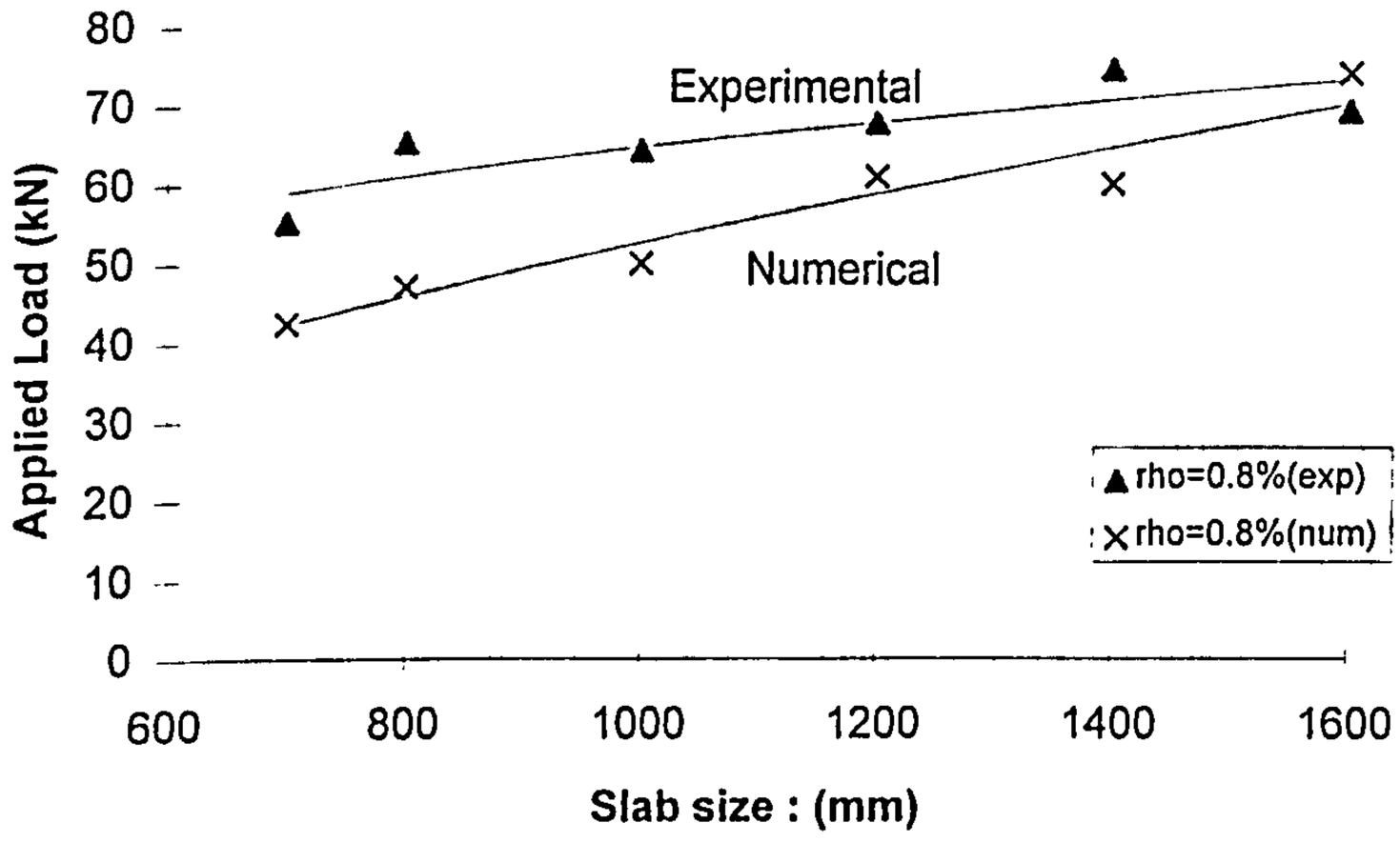

Figure 8.4 Predicted load against slab size for constant slab thickness, reinforcement ratio and varying slab size

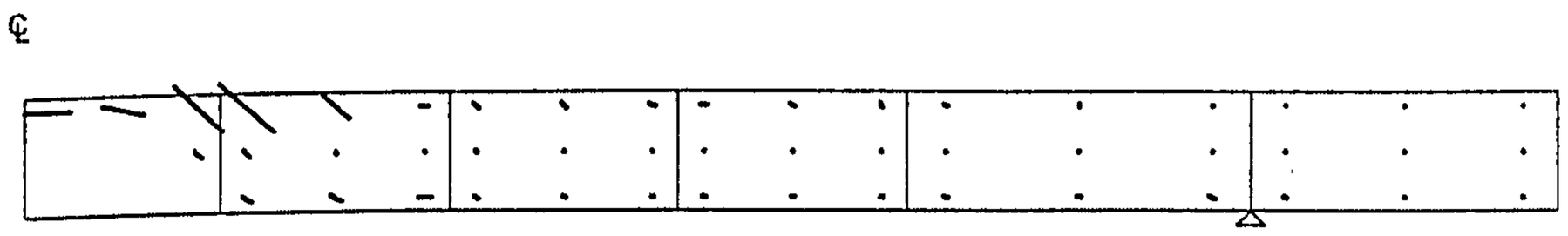

(a) Compression flow for R1-08 (size=800) at ultimate load

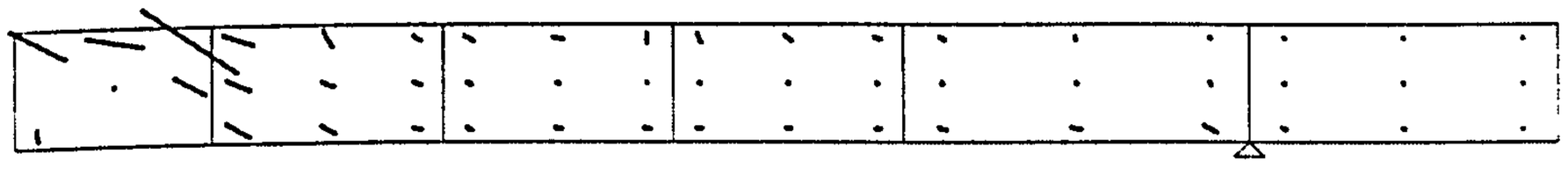

(b) Compression flow for R5-08 (size=1600) at ultimate load

Figure 8.5 Vector plot for third principal strain

8.3 Slab-beam panels

Kuang and Morley (1994) tested slabs supported by integral edge beams simply supported at the ends. Inplane restrain was provided by edge beams. For all these specimens, the clear span of the slab panel was constant at 1.2m. Slab thicknesses were 60 and 40 mm. Three levels of reinforcement were used for the slabs, i.e. 0.3, 1, and 1.6 percent in both directions. The different degree of edge restraint imposed at the slab surrounds were provided by different width of the edge beams. Details of slabs are summarised in Table 8.4.

The specimen was placed on four separate pedestals to simulate simple support condition for the edge beams (Figure 8.6) and the corners were prevented from lifting. The specimens were loaded at their geometric centre through a 120 mm square plate, simulating a concentrated load. Owing to symmetry, only one-quarter of the slab was modelled (Figure 8.7).

Predicted ultimate load is shown in Table 8.4. It ranges from 69.8% to 104.8% of the experimental values. The average of predicted ultimate load is 83.3% of experimental ultimate load with 12.6% standard deviation. All the slabs were predicted to fail by punching. A summary of the numerical predictions is presented in Table 8.5.

Inplane restraint has little effect on early behaviour. Deflections are almost same at a load level of 20kN as shown Figure 8.8. However, restraint clearly affected subsequent behaviour of the slabs. Slabs with higher degree of restraint (with a wider beam) display stiffer response and higher ultimate load. Therefore, it appears that compressive membrane action plays an important part in the deflection and ultimate load of slabs. Figure 8.9 shows that tension developed at the junction between the slab and the beam because rotation of slabs was restrained by the edge beam.

Load carrying capacity of slabs and mode of failure predicted by using BS8110 are presented in Table 8.6. The average of predicted ultimate load is 44.8% of experimental ultimate load with 19.8% standard deviation. It can be seen that in all cases the experimental failure loads are much higher than those predicted by BS8110. When the reinforcement ratio is 0.3%, the values of experimental failure load are approximately 4.4 to 5.3 times higher than those predicted by the code. However, this is not suprising because the code does not include the effect of in-plane restraint and it is not suitable for analysing restrained slab with low reinforcement ratio where the membrane action can have a relatively large effect. For slabs with reinforcement ratio of 1% and 1.6% (more likely to fail in shear mode), the actual failure loads are about 1.4-2.4 times higher than the values predicted by the code. This implies that the

influence of restraint is less significant for slabs with high percentage of steel. The code gave incorrect mode of failure for almost all the slabs.

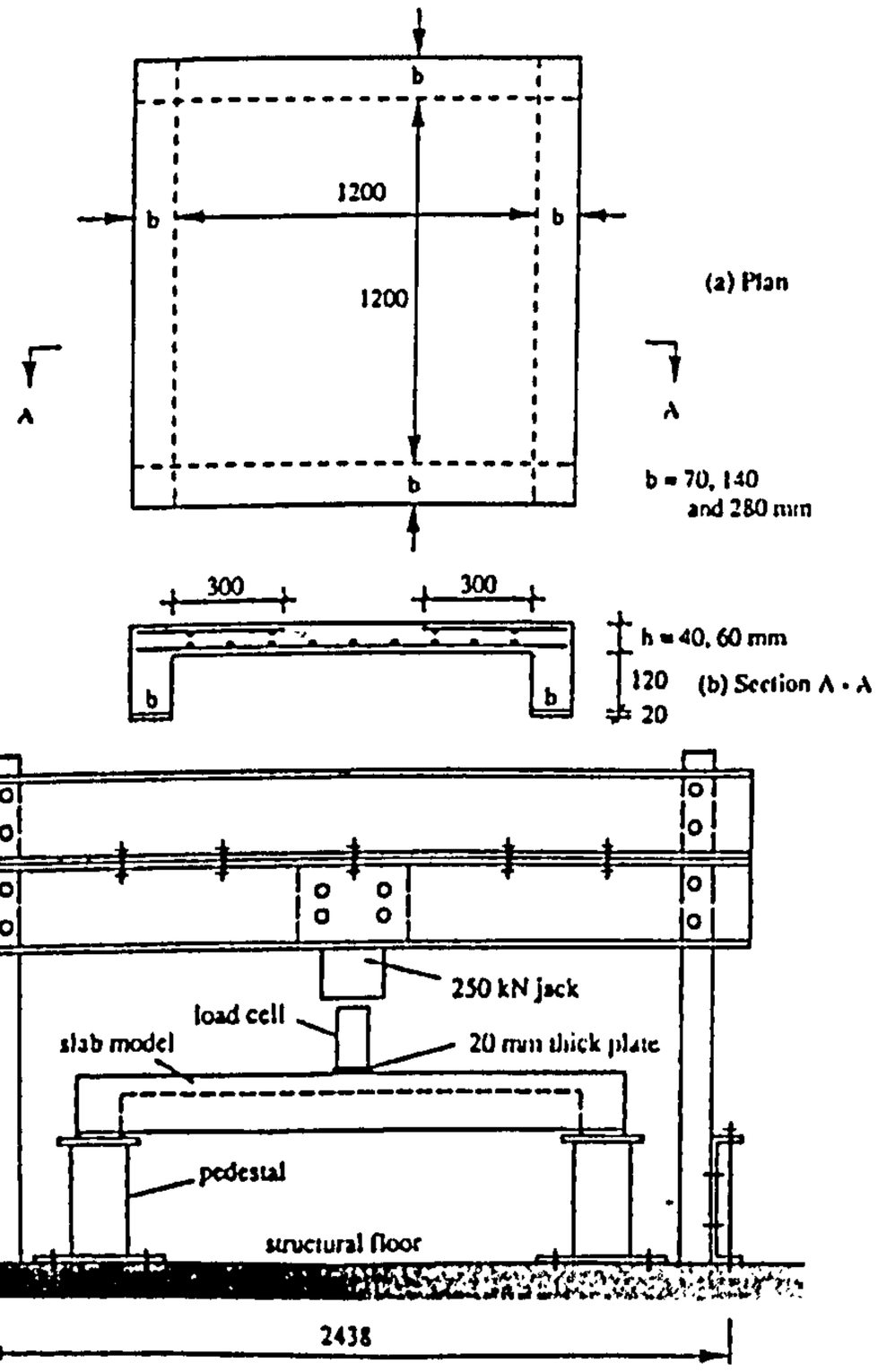

Figure 8.6 Dimensions and support conditions.

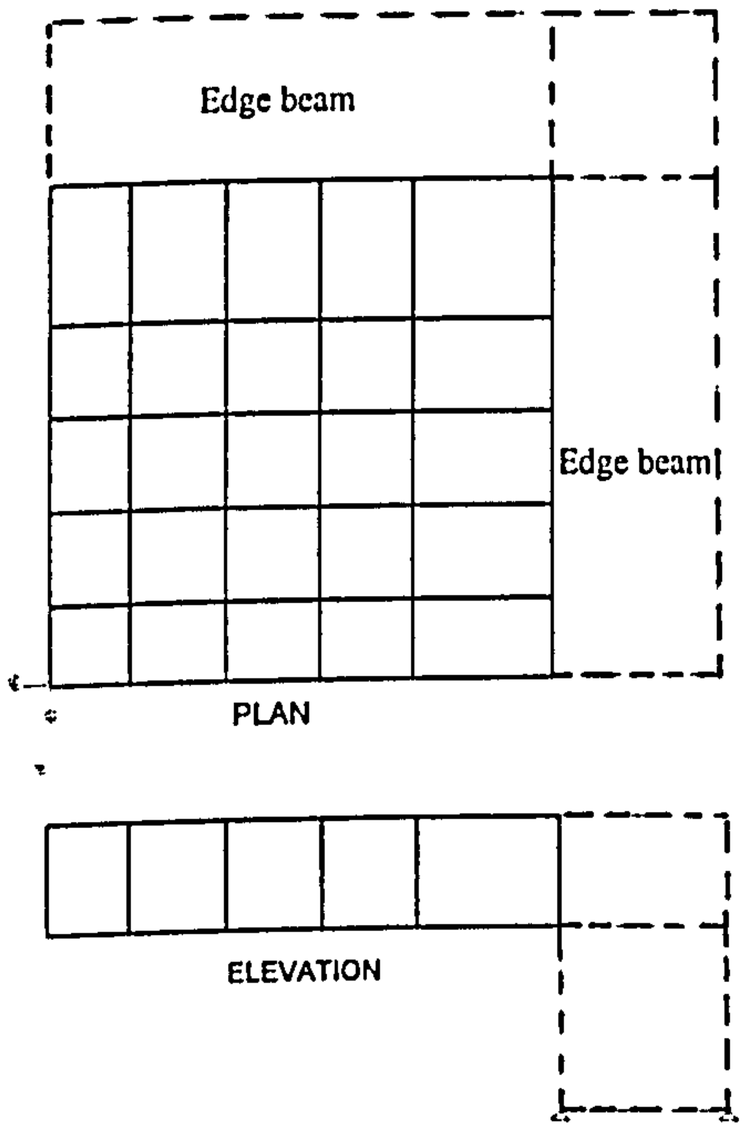

Figure 8.7 Finite element discretization

Table 8.4 ; Details of slab-beam panels (Kuang and Morley)

Slab	b (mm)	h (mm)	d (mm)	f_{cu} (N/mm^2)	ρ (%)	P_{test} (kN)
S1-C03	280	60.0	49.0	48.7	0.3	101.0
S1-C10	280	60.0	49.0	33.8	1.0	118.0
S1-C16	280	60.0	49.0	41.2	1.6	149.0
S2-C03	280	40.0	31.0	48.1	0.3	49.0
S2-C10	280	40.0	31.0	45.8	1.0	70.0
S2-C16	280	40.0	31.0	42.6	1.6	68.0
S1-B10	140	60.0	49.0	45.9	1.0	116.0
S2-B03	140	40.0	31.0	50.8	0.3	42.0
S2-B10	140	40.0	31.0	59.5	1.0	69.0
S1-A10	70	60.0	49.0	46.5	1.0	99.0
S2-A03	70	40.0	31.0	47.8	0.3	43.0
S2-A10	70	40.0	31.0	60.3	1.0	63.0

b = width of edges beams

Table 8.5 ; Comparison between experimental results and numerical predictions (Kuang and Morley)

Slab	Experimental		Numerical		P_{num}/P_{test}
	P_{test} (kN)	*failure Mode	P_{num} (kN)	failure Mode	
S1-C03	101.0	s	105.8	fp	1.048
S1-C10	118.0	s	82.3	s	0.698
S1-C16	149.0	s	104.2	s	0.699
S2-C03	49.0	s	49.0	fp	1.000
S2-C10	70.0	s	52.2	s	0.746
S2-C16	68.0	s	47.1	s	0.692
S1-B10	116.0	s	94.1	s	0.811
S2-B03	42.0	s	39.9	fp	0.950
S2-B10	69.0	s	59.2	fp	0.858
S1-A10	99.0	s	93.5	fp	0.944
S2-A03	43.0	s	34.6	fp	0.804
S2-A10	63.0	s	46.8	fp	0.743
				Average	0.833
				STDEV	0.126

* All the slabs were broadly classified as failing in punching shear mode.

Table 8.6 : Ultimate Load and Mode of failure predicted by using BS8110 (Kuang and Morley)

Slab	Experiment		Predictions by BS8110		P_u/P_{test}
	P_{test} (kN)	Failure Mode	P_u (kN)	Failure Mode	
S1-C03	101.0	s	22.84	y*	0.226
S1-C10	118.0	s	70.76	y*	0.600
S1-C16	149.0	s	88.44	s	0.594
S2-C03	49.0	s	9.14	y*	0.187
S2-C10	70.0	s	29.30	y*	0.419
S2-C16	68.0	s	43.69	y*	0.643
S1-B10	116.0	s	73.23	y*	0.631
S2-B03	42.0	s	9.14	y*	0.218
S2-B10	69.0	s	29.94	y*	0.434
S1-A10	99.0	s	73.32	y*	0.741
S2-A03	43.0	s	9.14	y*	0.213
S2-A10	63.0	s	29.97	y*	0.476
				Average	0.448
				STDEV	0.198

*wrong mode of failure predicted

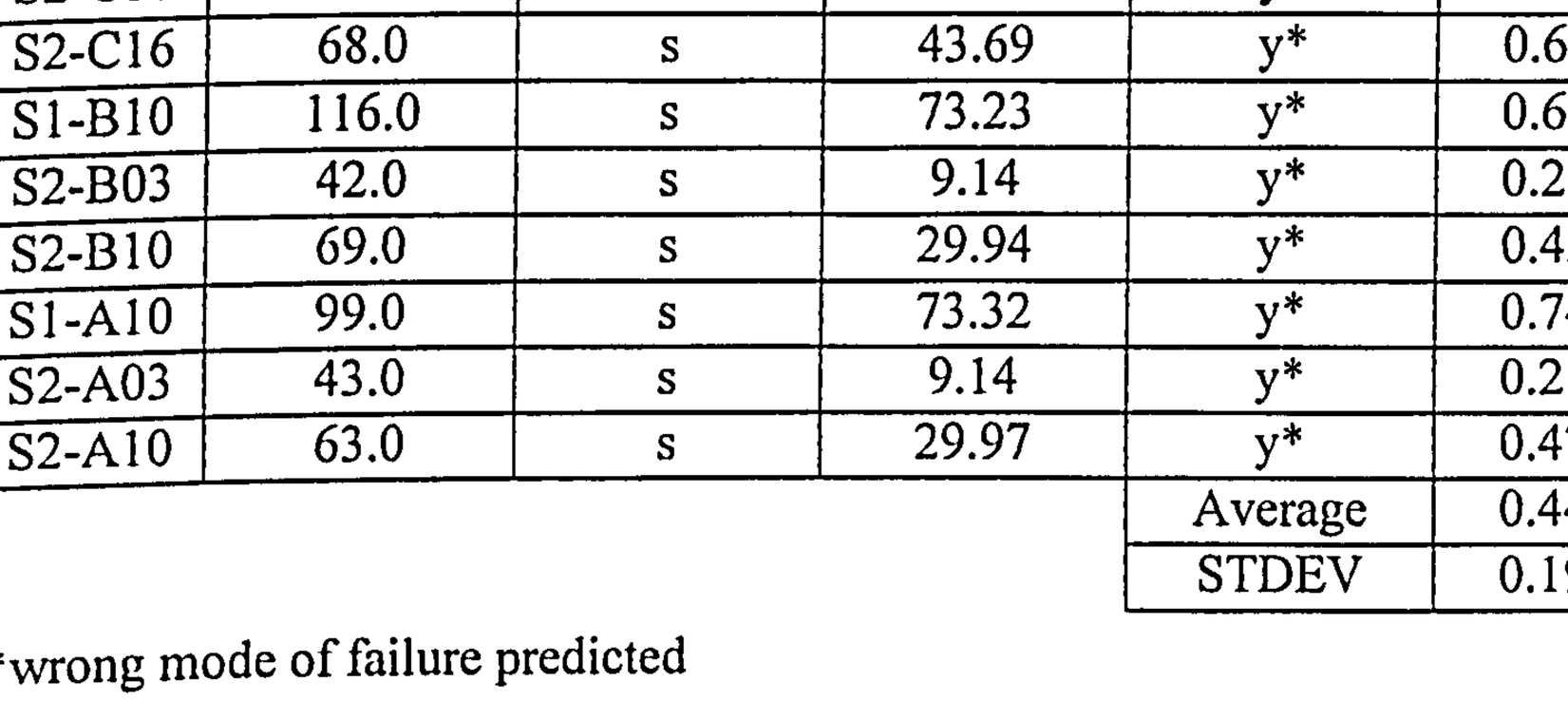

Figure 8.8 Load-deflection for slabs with same thickness, reinforcement ratio and different width of edge beam (S2-C03, S2-B03 and S2-A03)

Figure 8.9 Crack pattern for specimen S2-B03 at ultimate load

8.4 Fully restrained slab

Taylor and Hayes (1965) tested a series of fully restrained slabs subjected to punching shear. The slabs, which were 890 square and 76mm thick, were loaded at the centre by square plates with side length varying between 51 and 152 mm. These slabs were supported at their edges on roller bearing giving spans of 864mm. The slabs were tested in pairs - in one group lateral expansion was effectively prevented by a massive steel frame, while in the other the slabs were free to expand. The flexural steels were distributed equally in two directions. The details of slabs are shown in Table 8.7.

Table 8.7 : Details of slabs and test results (Taylor and hayes)

Series	Slab	ρ (%)	size of loaded area (mm)	f_{cu} (N/mm^2)	support condition	P_{test} (kN)
2	2S2	1.57	51.0	32.40	simple	71.1
	2R2		51.0	32.40	restrained	82.2
	2S3		76.0	30.70	simple	91.2
	2R3		76.0	30.70	restrained	112.8
	2S4		102.0	29.00	simple	85.8
	2R4		102.0	29.00	restrained	136.8
	2S5		127.0	27.60	simple	96.6
	2R5		127.0	27.60	restrained	142.2
	2S6		152.0	23.00	simple	96.6
	2R6		152.0	23.00	restrained	154.5
3	3S2	3.14	51.0	28.50	simple	78.5
	3R2		51.0	28.50	restrained	78.5
	3S4		102.0	28.30	simple	115.2
	3R4		102.0	28.30	restrained	132.4
	3S6		152.0	27.10	simple	150.1
	3R6		152.0	27.10	restrained	169.2

The slab geometry and finite element discretization is shown in Figure 5.2. The applied load was simulated by uniformly distributed load over the element representing the loading plate. Concrete slab was discretised by using one layer of twenty node solid elements. For restrained slabs, the lateral movement at slab edges were prevented (Figure 8.10b).

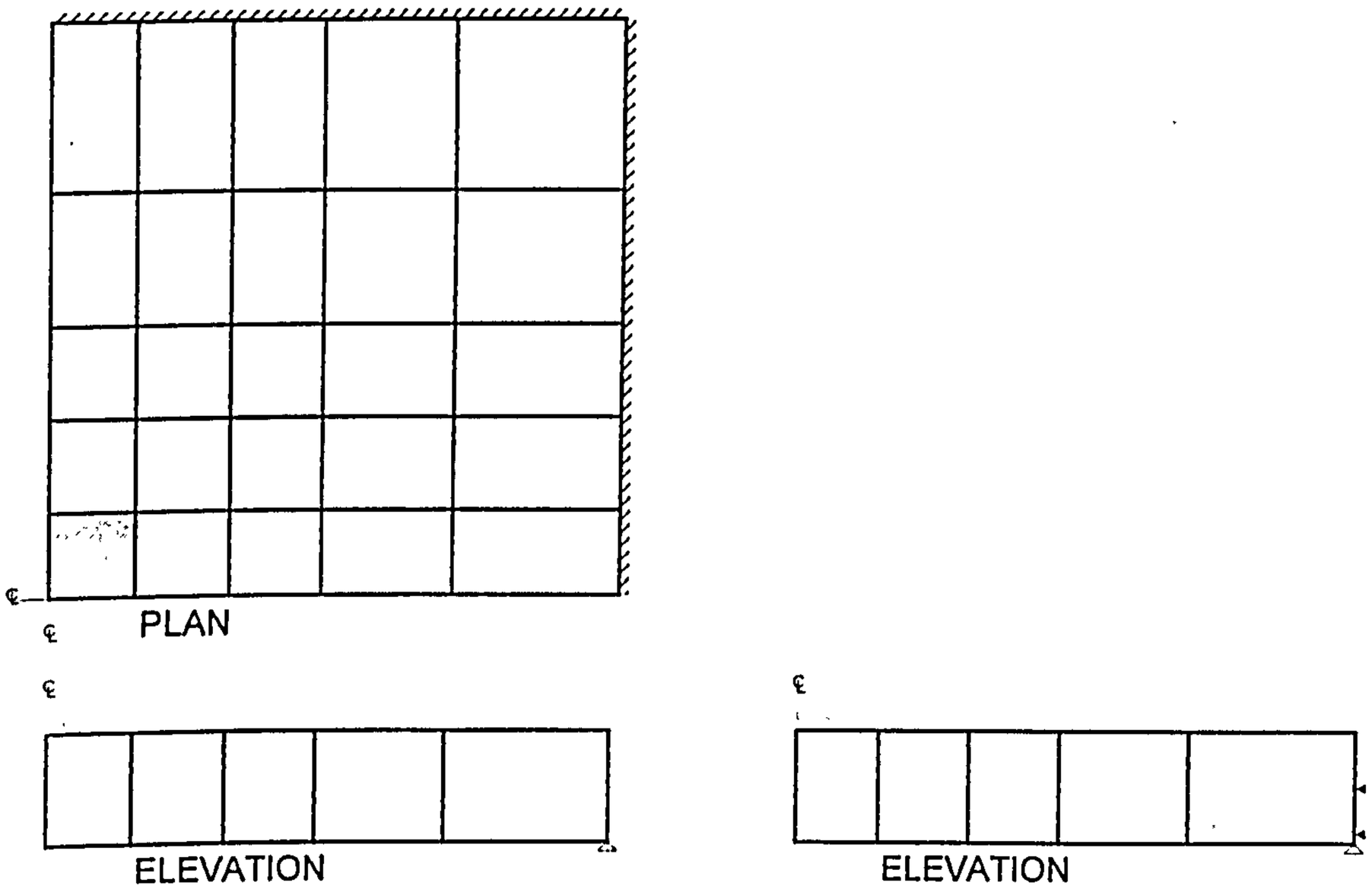

(a) Simply supported (b) Restrained slab

Figure 8.10 Finite element mesh and boundary conditions

A summary of numerical predictions is presented in Table 8.8. The ultimate loads of all the restrained slabs were over estimated. It is believed that this was due to the assumption made in the analysis, that the lateral movement at edge of slabs were prevented. But in reality, bowing of steel frame will occur. Thus the lateral movement will never be 100% prevented. The average of predicted ultimate load is 100.4% of experimental ultimate load with 23.8% standard deviation. This seem like a rather poor prediction, but if simply supported slabs are analysed separately, the corresponding values are 83.3% and 10.4%. For restrained slabs an average of 124.8% with standard deviation of 11.1% are obtained.

Most of the simply supported slabs were predicted to fail by punching. However, crushing of concrete occurred over a wide area of all the restrained slabs and the flexural steel of these slabs either did not yield or the yielding of steel was concentrated near the loading plate. Therefore, all the restrained slab were categorised as failing by crushing of concrete.

Figure 8.11 shows that tensile strain at mid span was very small which means the cracks were fine for restrained slab, where as the tensile strain are large (wider crack) for simply supported slab. This indicates that compressive membrane action plays an important part in the control of cracking in slabs. Similarly, the values of deflection were smaller for the restrained slabs than for simply supported slabs(Figure 8.12). The experimental results shows that the restraint had little effect on failure load for heavily reinforced slabs (ρ=3.14%). Numerical results also exhibited similar trend,

but due to the difficulty of simulating real boundary conditions, the increase in failure load due to restraint for this series is slightly higher than the experimental values. The increase of load carrying capacity due to restraint is more significant for slabs with lower amount of flexural reinforcement (ρ=1.57%), particularly for those slabs loaded through larger loading plate.

The predicted ultimate load and mode of failure by using BS8110 presented in Table 8.9. The average of predicted ultimate load is 101.3% of experimental ultimate load with 20.0% standard deviation. The code predicted a reasonably accurate ultimate load because most of slabs failed by crushing (i.e. controlled by $\sqrt{f_{cu}} \leq 6.25\,\mathrm{N/mm^2}$) and the effect of restraint is less significant for heavily reinforced slab.

Table 8.8 : Comparison between experimental results and numerical predictions (Taylor and Hayes)

Series	Slab Marking	Experimental results		Numerical predictions		P_{num}/P_{test}
		P_{test} (kN)	Failure Mode	P_{num} (kN)	Failure Mode	
2	2S2	71.1	s	64.8	fp	0.911*
	2R2	82.2	s	102.0	s	1.240
	2S3	91.2	s	68.4	fp	0.750*
	2R3	112.8	s	141.0	s	1.250
	2S4	85.8	s	69.1	fp	0.805*
	2R4	136.8	s	157.3	s	1.150
	2S5	96.6	s	81.6	y	0.845*
	2R5	142.2	s	155.8	s	1.095
	2S6	96.6	s	67.2	fp	0.696*
	2R6	154.5	s	184.3	s	1.193
3	3S2	78.5	s	79.2	s	1.009*
	3R2	78.5	s	110.9	s	1.413
	3S4	115.2	s	103.7	s	0.900*
	3R4	132.4	s	184.8	s	1.400
	3S6	150.1	s	111.6	fp	0.744*
	3R6	169.2	s	210.0	s	1.241
					Average	1.040
					STDEV	0.238

* Simply supported

N.B. : No detail of mode of failure is given in the paper, it only mentioned that most slabs failed by punching, and extensive yielding of flexural reinforcement occurred in some slabs.

Note For simply supported slabs Average=83.3%, STDEV=10.4%

For restrained slabs Average=124.8%, STDEV=11.1%

Table 8.9 : Ultimate Load and Mode of failure predicted by using BS8110 (Taylor and hayes)

Slab	Test results		Predictions by BS8110		P_u/P_{test}
	P_{test} (kN)	Failure Mode	P_u (kN)	Failure Mode	
2S2	71.1	s	76.40	c	1.075
2R2	82.2	s	76.40	c	0.929
2S3	91.2	s	111.17	c	1.219
2R3	112.8	s	111.17	c	0.986
2S4	85.8	s	119.09	s	1.388
2R4	136.8	s	119.09	s	0.871
2S5	96.6	s	117.14	s	1.213
2R5	142.2	s	117.14	s	0.824
2S6	96.6	s	110.23	s	1.141
2R6	154.5	s	110.23	s	0.713
3S2	78.5	s	71.88	c	0.916
3R2	78.5	s	71.88	c	0.916
3S4	115.2	s	143.25	c	1.243
3R4	132.4	s	143.25	c	1.082
3S6	150.1	s	146.69	s	0.977
3R6	169.2	s	146.69	s	0.867
				Average	1.013
				STDEV	0.200

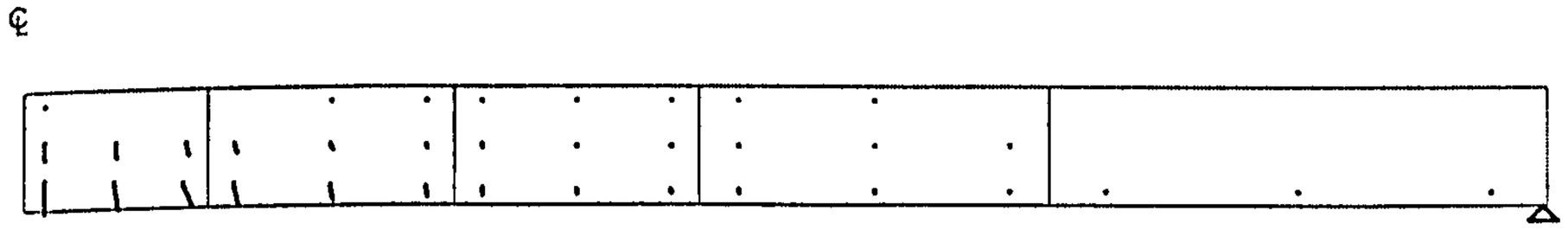

(a) 2S4, **simply supported**

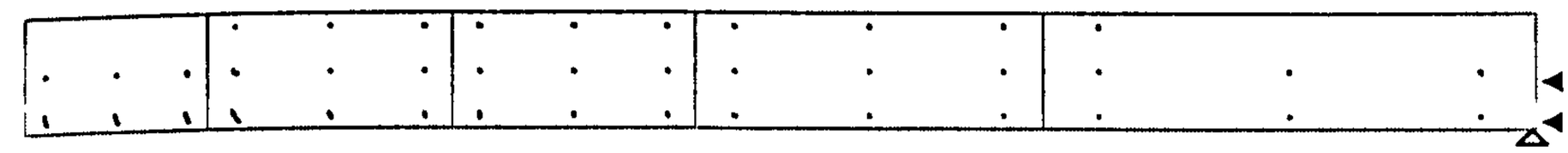

(b) 2R4, **restrained**

Figure 8.11 Crack pattern for slabs 2S4 and 2R4 at failure

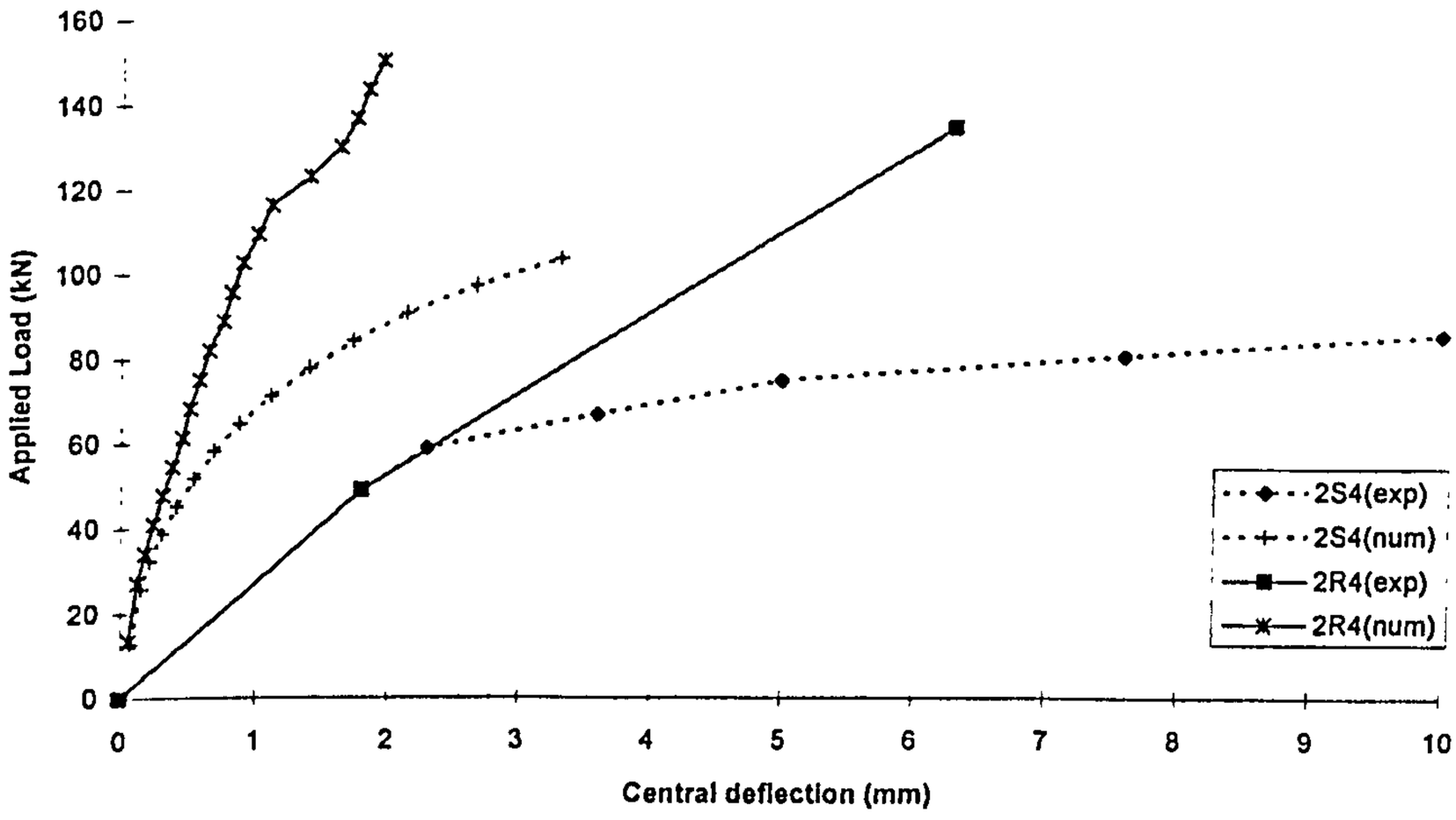

Figure 8.12 Load-deflection response for slabs 2S4 and 2R4

8.5. Punching with in-plane restraint

Previous sections show that in-plane restraint will increase the load carrying capacity of the slabs. However, those tests only cover the parameters over a certain range. Since the present finite element model can mimic the behaviour of restrained slabs reasonably well, the influence of the in-plane restraint was studied numerically over the full range (i.e. increase the lateral stiffness until there is no further increase in ultimate load of slabs). The full panel slab-column specimens (Figure 8.1) tested by Rankin (1987) were used for this purpose. The increase of lateral stiffness was achieved by increasing the length of portion of slab beyond the support.

Figure 8.13 shows that punching capacity of slabs were increased due in-plane restraint in all cases. However, the enhancement is more significant for lightly reinforced slabs and less significant for heavily reinforced slabs. This figure also indicates that the maximum enhancement of shear capacity was achieved at a length of portion of slabs beyond the support of about 700mm. For further increase in length, the beneficial effect is low due to crushing of concrete.

The effect of thickness of slab for restrained slab (length of the portion of slab beyond the support=680mm) is shown in Figure 8.14. It shows that the reinforcement ratio has little influence on the ultimate punching capacity for thin slabs since the

most likely failure mode is crushing of concrete. However, the influence of reinforcement ratio is significant for thicker slabs. Figure 8.15 shows that the higher concrete strength, the higher the ultimate load for restrained slabs because the failure mode is controlled by crushing of concrete.

From the above observation, the enhancement of punching capacity due to in-plane restraint highly depends on the ductility of slabs (e.g. low reinforcement ratio and thin slab). Therefore, it is recommended to provide shear reinforcement for flat slab structure to ensure a ductile behaviour. Consequently the enhancement due to membrane action can be guaranteed.

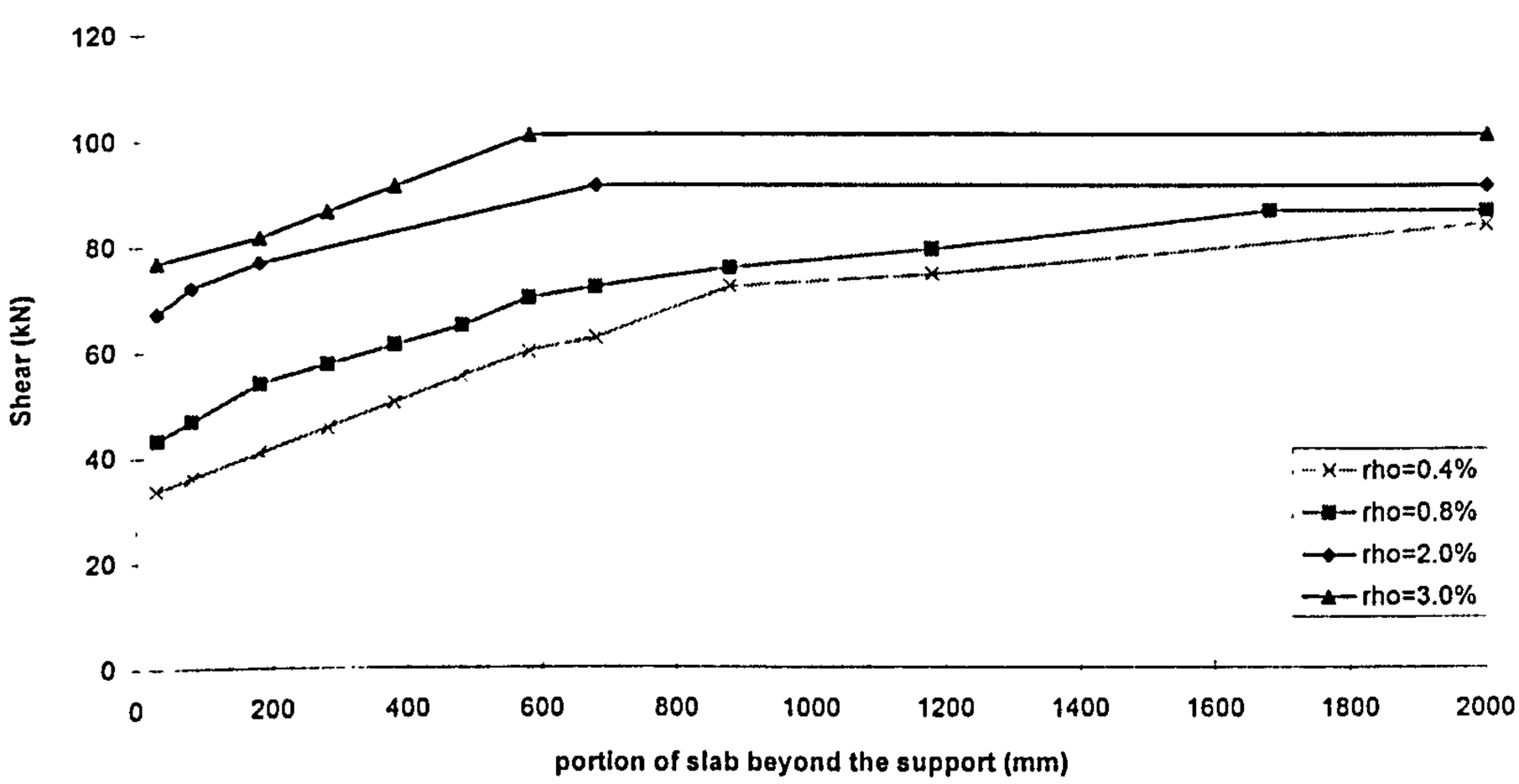

Figure 8.13 Effect of in-plane restraint on ultimate punching capacity for slabs with constant span/depth ratio, concrete strength and varying reinforcement ratio
(h=51mm, span=640mm, f_{cu}=40 N/mm^2)

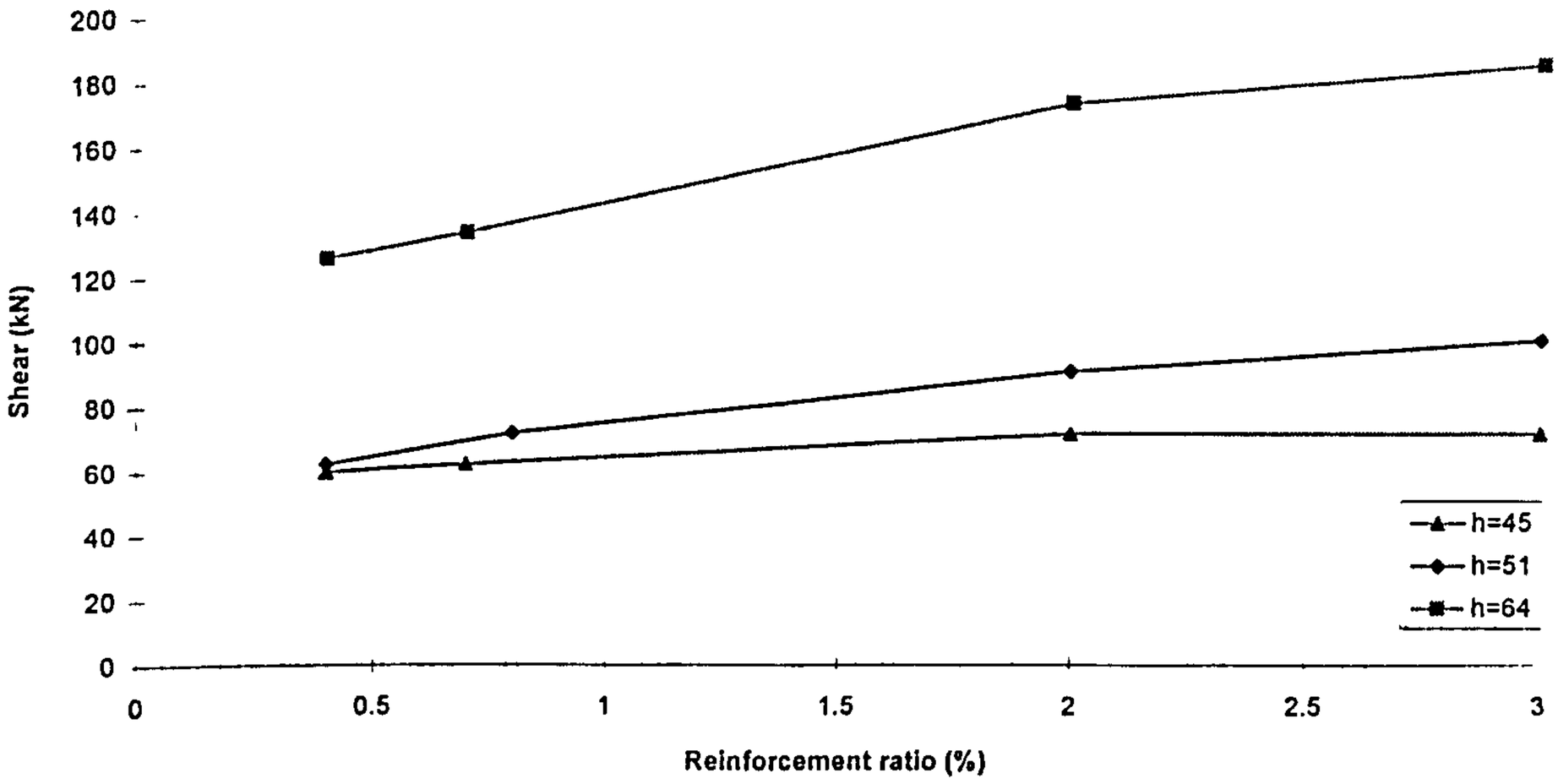

Figure 8.14 Effect of thickness of slab on punching shear capacity for restrained slabs

(span=640mm, f_{cu}=40 N/mm^2, length of the portion of slab beyond support=680mm)

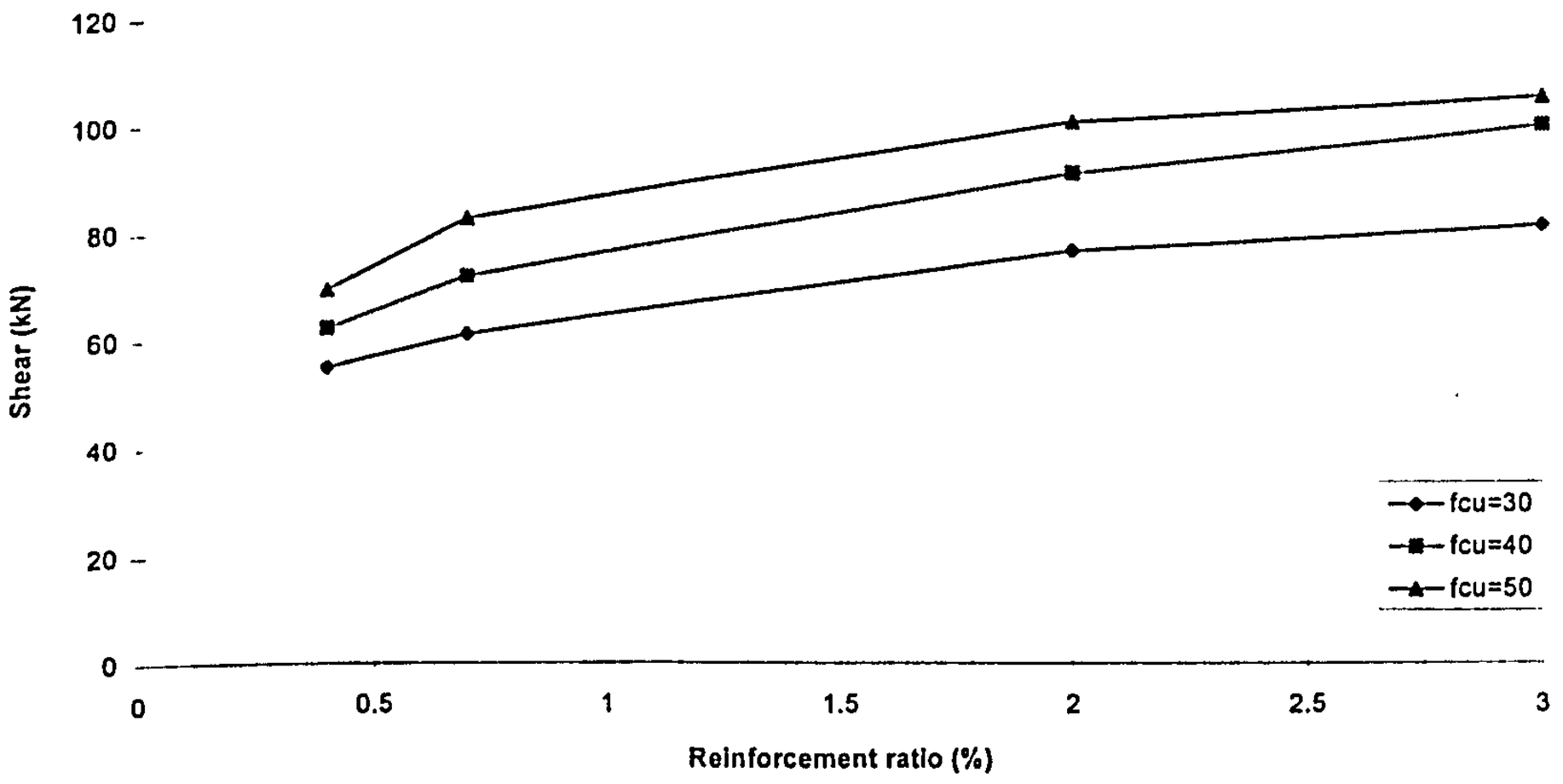

Figure 8.15 Effect of concrete strength on punching shear capacity for restrained slabs

(h=51mm, span=640mm, length of the portion of slab beyond support=680mm)

8.6 Conclusions

Following conclusions can be drawn from the results of analysis of restrained slabs :-

- Generally, the present model predicted correct mode of failure for all restrained slabs. However, it slightly over predicted the ultimate load for all fully restrained slabs (Figure 8.16).

- The enhancement of punching capacity due to in-plane restraint highly depends on the ductility of slabs. If a design is to include the effect of compressive membrane action, it is recommended to provide shear reinforcement, so that ductile behaviour can be guaranteed.

- BS8110 generally underestimates the failure load of slabs (Figure 8.17) and predicted incorrect mode of failure because the code does not include the effect of in-plane restraint.

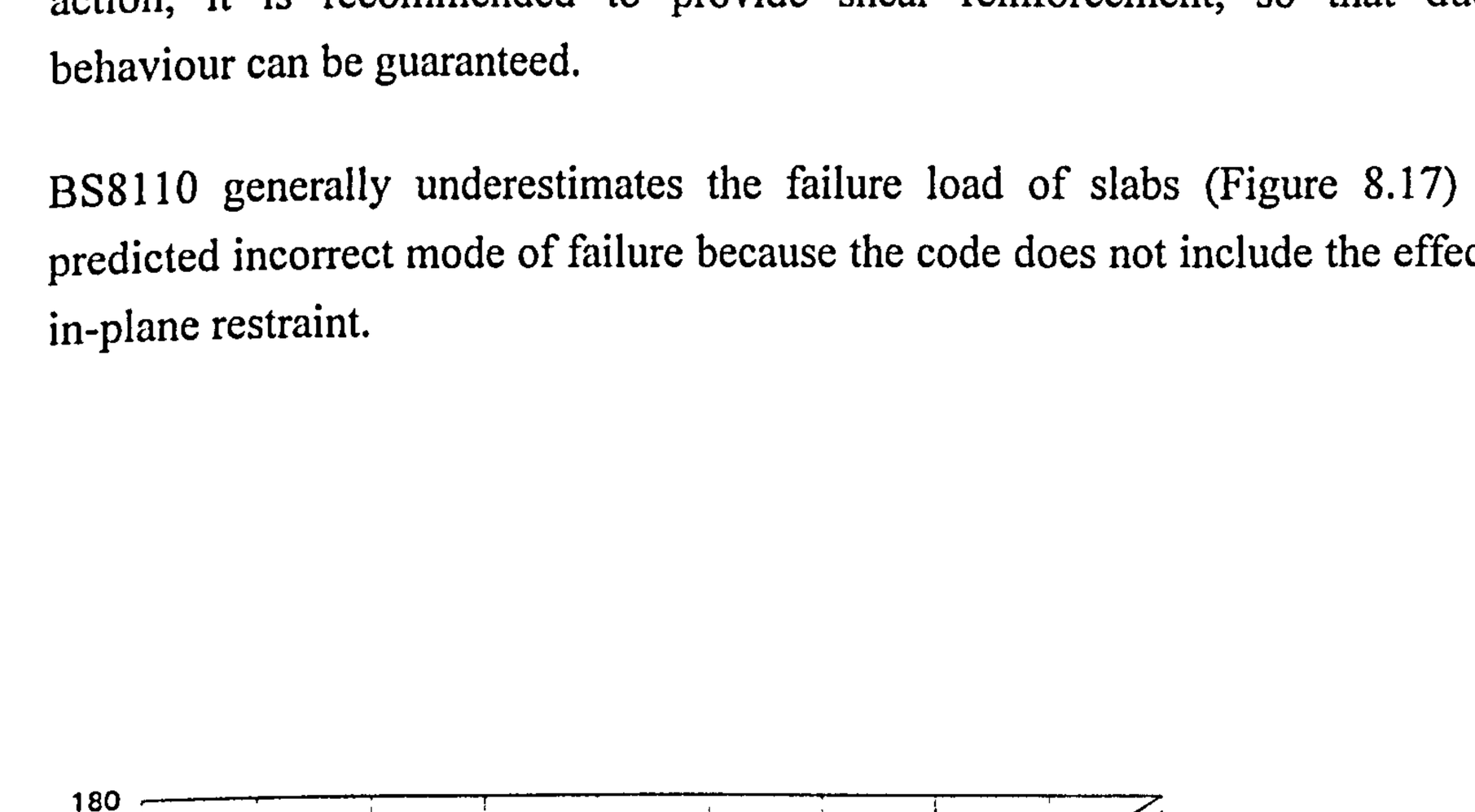

Figure 8.16 Numerical predictions of ultimate load for restrained slabs

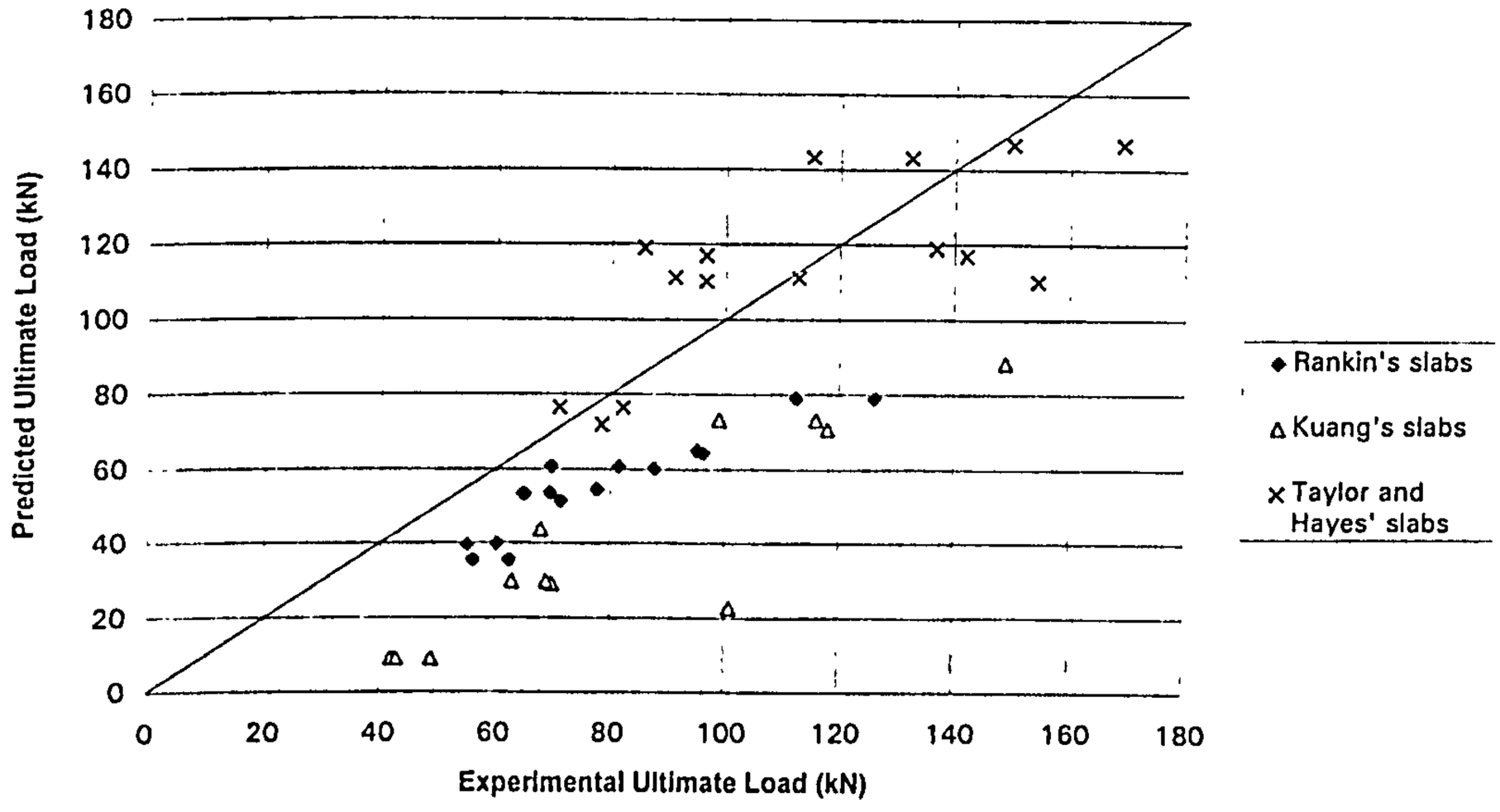

Figure 8.17 Ultimate load for restrained slabs predicted by BS8110

Chapter 9

Conclusions and Recommendations

9.1 General conclusions

This thesis presents a study of punching shear capacity of Flat slab-column connections. The main conclusion from the work is that the current model gives a good prediction of the behaviour of slabs failing in punching shear and can be used with confidence in practice. From the results of analysis, the following detailed conclusions can be drawn :

1. From this study, it was concluded that Kotsovos' model is a good model for three dimensional analysis of punching shear problem. However, with the limited amount of analysis done using ABAQUS, the predictions were poor; more work needs to be done before drawing firm conclusions.

2. Computational cost can be reduced substantially by using suitable values for the following numerical parameters:
   - Convergence tolerance generally does not greatly affect the ultimate load and behaviour of slabs, but smaller value increase the computational cost tremendously. 5% tolerance deemed acceptable.
   - Applying small load increments for highly non-linear parts and large load increments at early stage of loading gave reasonably good results.
   - Within limits, the predictions are not mesh dependent. So, a finer mesh arrangement near the critical zone and coarser mesh for elements further away from failure region is recommended.
   - Generally, using one element through the thickness of slab predicted reasonably good results.

3. The following conclusions can be drawn from the parametric study for material parameters :
   - Within limits, the effect of tensile strength of concrete on ultimate load of slabs is insignificant, but it will influence deflection and strain in steel for lightly reinforced slabs. A low tensile strength of concrete may cause divergence of the solution.
   - Tension stiffening has a more significant effect on the structural response of lightly reinforced slabs than on the response of heavily reinforced slabs.

Reducing the tensile strength immediately after cracking can better reflect the loss of stiffness due to cracking of concrete.

- Shear retention factor generally does not affect the paths of responses vs. load. However, a smaller value of shear retention factor is preferable because too large a value may lead to overestimation of failure load and also lead to the predicted mode of failure of slabs being flexural where as the actual failure of the slabs is by punching shear.
- Different types of shear reinforcement provide different degrees of confinement. Shear reinforcement, such as off cuts of I-sections and shear studs provide a higher degree of confinement than stirrup. It is necessary to include the confinement effect of concrete for slabs with shear reinforcement to ensure good predictions.

4. Predictions by the present finite element model generally agree with the experimental results in terms of mode of failure and behaviour for various type of connections (including restrained slabs) with and without shear under different load combinations. But it overestimates the failure load although it predicted the correct mode of failure for slabs with shear span-depth ratio (a_v/d) less than 1.7 and fully restrained slabs.

5. The trend of the parameters governing punching shear strength predicted by present model correlates very well with test data, Kinnunen-Nylander model and BS8110.

6. Finally, Figure 9.1 shows the predicted failure load and the corresponding experimental load for one hundred and seventy eight slabs. Clearly, if $P_{pred}=0.8\ P_{exp}$ gives a good lower bound and can be used with confidence in design. Correlation between experimental and numerical prediction with 95% confidence limits are shown in Figures 9.2 and 9.3.

9.2. Recommendations for future work

This section recommends further research in this field as follows :

1. Softening behaviour of concrete in tension for short span slabs.

2. Influence of in-plane restraint for slabs with shear reinforcement subjected to punching shear.

3. Extension of the investigation to flat slabs with opening and perforated slabs.

4. There is plenty information on the factors governing punching shear strength for interior slabs subjected to shear only. However, no systematic study of the factors governing punching shear for slab-column junction subjected to a combination of shear and unbalanced moment especially for edge and corner column-slab junctions has been undertaken. The in-house program provides a useful tool for this task.

5. The work can clearly be extended to the analysis of prestressed slabs particularly for slabs with unbonded cables which are most commonly used in practice.

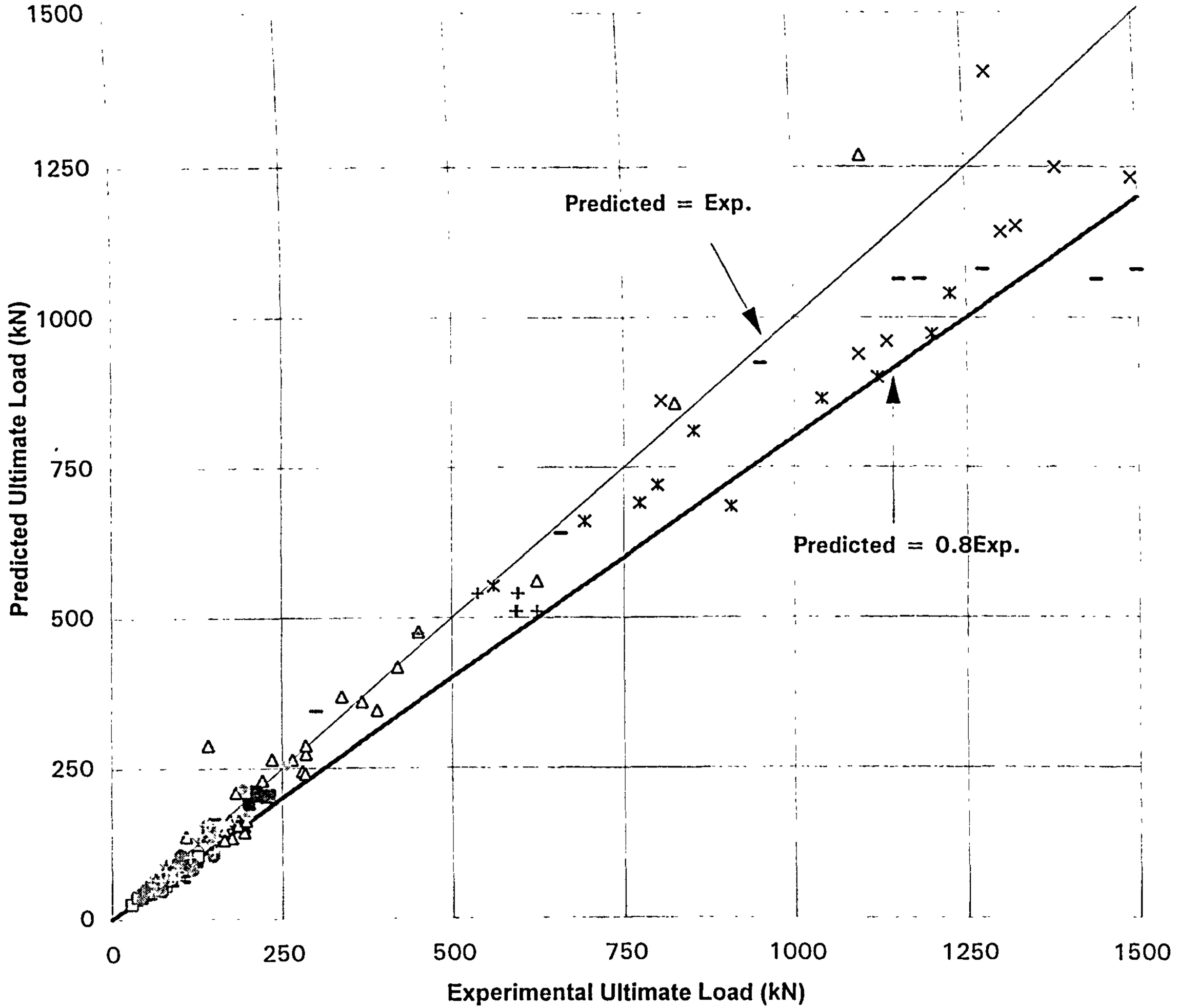

□ Rankin's slab △ Regan's slab × Chana's slabs* ✳ Gome's slabs* – Yamada's slabs* + Seible's slabs*	Simply supported slabs
- SM series – AM series* ◇ SE series ■ JS series* ▲ SC series × NH series*	Slabs subjected to shear-moment transfer
✳ Rankin's slab ● Kuang's slabs + Taylor's slab	Restrained slabs

Note

* slabs with shear reinforcement

Figure 9.1 Numerical predictions for all the slabs

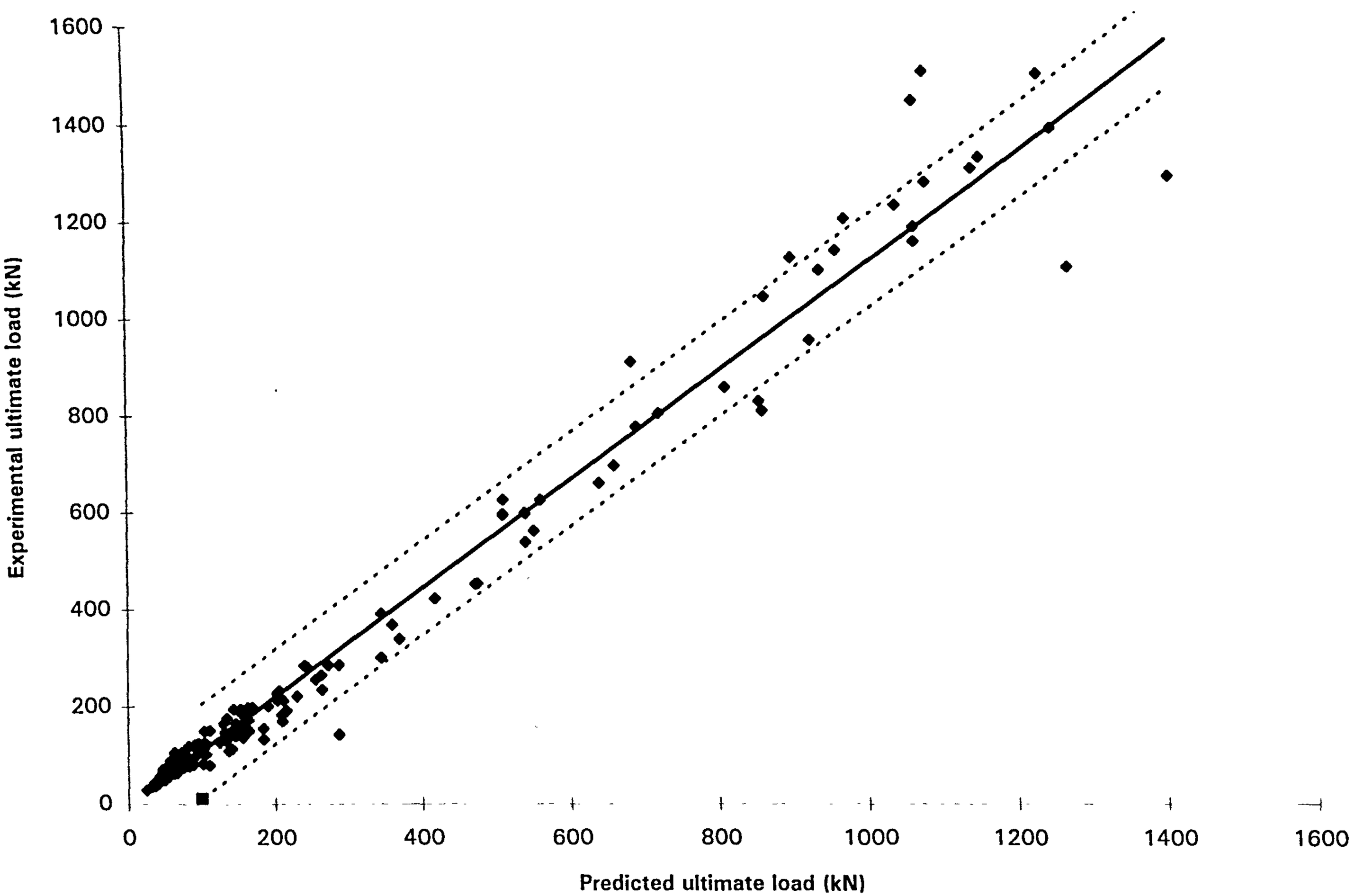

Figure 9.3 : 95% of Confidence limit on Numerical predictions (Range : 0-1600 kN)

References

Abbasi M.S.A., Baluch M.H., Azad A.K. and Abdel Rahman H.H. (1992)
Nonlinear finite element modelling of failure modes in RC slabs
Computers and Structures, Vol. 42, No. 5, pp 815-823

Abdel-Kader M.M.A. (1993)
Prediction of shear strength of reinforced and prestressed concrete beams by Finite Element method
Ph.D. thesis, University of Glasgow

ACI 318-89, (1989)
"Building Code Requirements for reinforced Concrete"
American Concrete Institute, Detroit

Alexander S.D.B. and Simmonds S.H. (1992)
Tests of column flat plate connections
ACI Structural Journal, Vol. 89, No. 5, pp 495-502

Anis.N.N. (1970)
Shear strength of reinforced concrete flat slabs with shear reinforcement
PhD thesis, Imperial College, London.

Aoki.Y. and Seki.H. (1971)
Shearing strength and cracking in two-way slabs subjected to concentrated load
ACI Publication SP-30, pp 104-127

Attard M.M. and Setunge S. (1996)
Stress-strain relationship of confined and unconfined concrete
ACI Materials Journal, Vol. 93, No. 5, pp 432-442

Bangash M.Y.H. (1989)
Concrete and Concrete Structures : Numerical Modelling and Applications
Elsevier Science Publishers Ltd

Bathe K-J. (1996)
Finite Element Procedures
Prentice-Hall, Inc

Baumann, T. and Rusch,H. (1970)
Tests studying the dowel action of flexural tensile reinforcement in reinforced concrete beam
Berlin, Deutscher Ausschuss für Stahlbeton,Heft 210
[Quoted by Regan, 1974]

Broms.C.E. (1990)
Punching of flat plates-A Question of concrete properties in Biaxial compression and size effect
ACI Structural Journal, Vol. 87, No. 3, pp 292-304

BSI. 1985.
Structural use of concrete. Standard BS-8110,
British Standard Institution, London, United Kingdom

Chana.P.S. and Desai.S.B. (1992)
Design of shear reinforcement against punching
The Structural Engineer, Vol. 70, No. 9, pp 159-164

Chen A.C.T. and Chen W.F. (1975)
Constitutive Relations for Concrete
Journal of the Engineering Mechanics Division
ASCE, Vol. 101, EM4, Proc. Paper 11529, pp465-481

Chen W.F. (1982)
Plasticity in Reinforced Concrete
McGraw-Hill Book Company

Criswell M.E., (1974a)
Shear strength of slabs: Basic principle and their relation to current method of analysis
Publication SP-42, Vol 2, ACI, 1974, pp 641-676

Criswell M.E., (1974b)
Static and Dynamic response of reinforced concrete slab-column connections
Publication SP-42, Vol 2, ACI, 1974, pp 721-746

de Borst. R. and Nauta. P. (1984)
Smeared Crack Analysis of Reinforced Concrete beams and slabs failing in shear
Proceedings of International Conference on Computer Aided Analysis and Design of Concrete Structure- Part I, Split, Yugoslavia, pp. 261-273

Elgabry, A. A. and Ghali, A. (1987)
Tests on concrete slab-column connections with stud-shear reinforcement subjected to shear-moment transfer
ACI Structural Journal, Vol. 84, No. 5, pp 433-442

Elstner, R. C. and Hognestad, E. (1956)
Shearing strength of Reinforced concrete slabs
ACI Journal Proceedings, Vol. 53, No. 1, pp 29-58

Fang I. K., Lee J. H. and Chen C.R. (1994)
Behaviour of Partially Restrained Slabs under Concentrated Load
ACI Structural Journal, Vol. 91, No. 2, pp 133-139

Gilbert R.I. and Warner R.F. (1978)
Tension Stiffening concept based on bond slip
J of structural Div., ASCE, Vol 104, No. 12, pp 1885-1900

Gomes R.B. (1991)
Punching resistance of reinforced concrete flat slabs with shear reinforcement
Ph.D. thesis, Polytechnic of Central London

Gonzalez.V.F, Kotsovos.M.D, and Pavlovic.M.N. (1988)
Symmetrical punching of Reinforced concrete slab: An analytical Investigation Based on Nonlinear Finite element Modelling
ACI Structural Journal, Vol.85, No. 3, pp 241-250

Gonzalez.V.F, Kotsovos.M.D, and Pavlovic.M.N. (1991)
Three-dimensional non-linear finite element model for structural concrete.
Part 2 : generality study
Proc. Inst. Civ. Engrs, Vol 91, Part 2, pp545-560

Gupta A.K. and Maestrini S.R. (1990)
Tension-Stiffness Model for Reinforced concrete bars
J of structural Div., ASCE, Vol. 116, No. 3, pp 769-790

Hammil, N. and Ghali, A. (1994)
Punching shear resistance of corner slab-column connections
ACI Structural Journal, Vol. 91, No. 6, pp 697-707

Hawkins, N.M. (1971a)
Progress Report on NSF Grant No. Gk-16375
Shear and moment transfer between concrete flat plates and columns
Department of Civil Engineering, University of Washington

Hawkins, N.M., Fallsen H.B., Hinojosa R.C. (1971b)
Influence of column rectangularity on the behaviour of flat plate structures
Publication SP-30, ACI, 1971, pp 127-146

Hawkins, N.M., Criswell M.E. and Roll F. (1974a)
Shear strength of slabs without shear reinforcement
Publication SP-42 Vol. 2, ACI, 1974, pp 677-720

Hawkins, N.M. (1974b)
Shear strength of slabs with moments transferred to columns
Publication SP-42 Vol. 2, ACI, 1974, pp 817-846

Hewitt.B.E. and Batchelor.D.deV. (1975)
Punching Shear strength of restrained slabs
ASCE Journal of the structural division, Vol. 101, No. ST9, pp 1837-1853

Hibbit, Karlsson, and Sorenson (1989)
ABAQUS Vers. 5.3, HKS Corporation, Providence.

Hinton E, and Owen D.R.J. (1989)
Finite Element Programming
Academic Press

Hobbs D.W., Pomeroy C.D. and Newman J.B. (1977)
Design stresses for concrete structures subjected to multi-axial stresses
The Structural Engineer, Vol. 55, No. 4, pp 151-164

Jofriet J.C, and McNeice.G.M. (1971)
Finite element analysis of Reinforced concrete slabs
Journal of the Structural Division, Proc. of ASCE, Vol. 97, No. ST3, pp 785-806

John S.L. and David I.L. (1990)
Punching shear behaviour of slabs with varying span-depth ratios
ACI Structural Journal, Vol. 87, No. 5, pp 507-511

Kinnunen.S. and Nylander.H. (1960)
Punching of concrete slabs without shear reinforcement
Meddelande Nr 38, Institutionen for Byggnadsstatik,
KTH, Stockholm
[Quoted by Regan, 1985]

Kinnunen.S. (1971)
Försok med betongplattor understödda av pelare vid fri kant,
Rapport R2 : 1972, Statens Institut för Byggnadsforskning,
Stockholm

Kinnunen.S., Nylander.H. and Tolf.P. (1978)
Investigation of punching at the building statics institute KTH
Nordisk Betong, pp 25-27
[Quoted by Regan, 1985]

Kirpartrick.J, Rankin.G.I.B. and Long.A.E. (1984)
Strength evaluation of M-beam bridge deck slab
The Structural Engineer, Vol. 62B, No. 2, pp 60-68

Kirpartrick.J, Rankin.G.I.B. and Long.A.E. (1986)
The influence of compressive membrane action on the serviceability of beam and bridge deck slab
The Structural Engineer, Vol. 64B, No. 2, pp 8-12

Kotsovos M.D. and Newman J.B. (1979a)
A mathematical description of the deformational behaviour of concrete under complex loading
Magazine of Concrete Research, Vol. 31, No. 107, pp 77-90

Kotsovos M.D. (1979b)
A mathematical description of the strength properties of concrete under generalised stress
Magazine of Concrete Research, Vol. 31, No. 108, pp 151-158

Kotsovos M.D. and Palvlovic M.N. (1995)
Structural Concrete : Finite Element analysis for limit state design
Thomas Telford Publications

Kuang.J.S. and Morley.C.T. (1992)
Punching shear behaviour of restrained concrete slabs
ACI Structural Journal, Vol. 89, No. 1, pp 13-19

Kupfer H., Hilsdorf H.K. and Rusch H. (1969)
Behaviour of concrete under Biaxial stresses
ACI Journal, August, Vol. 66, No.8, pp 656-666

Lahlouh E. H. and Waldron P. (1992)
Membrane action in one way slab strips
Proc. Inst. Civil Engr, Vol. 9466, pp 419-428

Langhor P.H., Ghali. A., and Dilger W. H. (1976)
Special shear reinforcement for concrete flat plates
ACI Journal Proceedings, Vol. 73, No. 3, pp 141-146

Lin C.S. and Scordelis A.C. (1975)
Non-linear analysis of RC shell of General form
J of structural Div., ASCE, Vol. 111, No. 3, pp 523-538

Malvar.L.J. (1992)
Punching shear failure of a Reinforced concrete pier deck model
ACI Structural Journal, Vol. 89, No. 5, pp 569-576

Manterola.M.J. (1966)
Poinconnement de Dalles sans Armature d'Effort Tranchant
CEB Bulletin, No. 58, October , pp 2-36
[Quoted by Hawkins, 1974a]

Marzouk.H.M. and Hussein A.(1991a)
Experimental Investigation on the behaviour of High strength concrete slabs
ACI Structural Journal, Vol. 88, No. 6, pp 505-513

Marzouk.H.M. and Hussein A.(1991b)
Punching shear analysis of reinforced high-strength concrete slabs
Canadian Journal of Civil Engineering, Vol.18, pp 954-963

Marzouk.H.M. and Chen Z.(1993)
Finite element Analysis of High strength concrete slab
ACI Structural Journal, Vol. 90, No. 5, pp 505-513

Marzouk.H.M. and Jiang D.(1996)
Finite element evaluation of shear enhancement of High strength concrete plate
ACI Structural Journal , Vol. 93, No. 6, pp 667-673

Millard S.G. and Johnson R.P. (1985)
Shear transfer in cracked reinforced concrete
Magazine of Concrete Research : Vol. 37, No. 130, pp 3-15

Moe J.(1961)
Shearing strength of reinforced concrete slabs and footings under concentrated load
Bulletin D47, Portland Cement Association,
Research and Development Laboratories, Skokie, Illinois

Mortin J.D., and Ghali A. (1991)
Connection of flat plates to edge columns
ACI Structural Journal, V.88, No. 2, pp 191-198

Pan A.D., and Mochle.J.P (1992)
An experimental study of slab-column connections
ACI Structural Journal, Vol. 89, No. 6, pp 626-638

Rankin.G.I.B. (1982)
Punching failure and compressive membrane action in reinforced concrete slabs
PhD thesis, The Queen's University of Belfast

Rankin.G.I.B. and Long.A.E. (1987)
Predicting the enhanced punching strength of interior slab-column connection
Proc. Inst. Civ. Engr, Part 1, Vol.82, pp 1165-1186

Rankin.G.I.B, Niblock.R.A, Skates.A.S. and Long.A.E. (1991)
Compressive membrane action strength enhancement in uniformly loaded, laterally restrained slabs
The Structural Engineer, Vol. 69, No. 16, pp 287-295

Regan. P.E. (1974)
Design for punching shear
The Structural Engineer, No. 6, Volume 52, pp. 197-207

Regan. P.E, Walker.P.R. and Zakaria.K.A.A. (1979)
Tests of reinforced concrete flat slab
CIRIA Project Report 220

Regan. P.E. (1984)
The dependence of punching resistance upon the geometry of the failure surface,
Magazine of concrete research, Volume 36, No. 126, pp. 3-8

Regan. P.E. and Braestrup M. W. (1985)
Punching shear in Reinforced concrete : A State of the Art Report,
Bulletin d'Information No. 168,
Comité Euro-International du Béton, Lausane

Regan. P.E. (1986)
Symmetric punching of reinforced concrete slabs
Magazine of concrete research, Volume 38, No. 136, pp. 115-128

Regan. P.E. (1987)
Shear combs, reinforcement against punching
The Structural Engineer, No. 4, Volume 63B, pp. 76-84

Roberts.E.H. (1969)
Load-carrying capacity of slab-strips restrained against longitudinal expansion
Concrete, Vol. 3(9), pp. 369-378.

Salami.A.T. (1994)
Equation for predicting the strength of fully-clamped two-way reinforced concrete slabs
Proc. Inst. Civ. Engr, Vol. 104, pp 101-107

Scanlon A. and Murray D.W. (1974)
Time dependent Reinforced concrete slab deflection
J of structural Div., ASCE, Vol. 100 No 9, May, pp 1911-1924

Seible F., Ghali A., and Dilger W.H. (1980)
Preassembled Shear Reinforcing Units for flat plates
ACI Journal Proceedings, Vol. 77, No. 1, pp 28-35

Shehata. I.M., and Regan. P. (1989)
Punching in Reinforced Concrete slabs
J of structural Div., ASCE, Vol. 115, No. 7, pp 1726-1740

Soroushian P., Obaseki K., Rojas, M.C. and Sim J. (1986)
Analysis of Dowel bars acting against concrete core
ACI Journal, Vol. 83, pp 642-649

Stevens, N. J., Uzumeri S.M., Rojas M.C., and Will G.T.J. (1991)
Constitutive model for Reinforced Concrete Finite Element Analysis
ACI Journal, Vol. 88, No. 1, pp 49-59

Taylor.R. and Hayes.B. (1965)
Some tests on the effect of edge restraint on punching shear in reinforced concrete slabs
Magazine of Concrete Research: Vol. 17, No. 50, pp 39-44

Tong.P.Y. and Batchelor.D.deV. (1971)
Compressive membrane enhancement in two-way bridge slabs
ACI Publication SP-30, pp 271-286

Vanderbilt M.D. (1972)
Shear strength of continuous slabs
Proceedings ASCE, Vol. 98, No. ST5, pp 961-973

Vintzeleou E.N. and Tassios T.P. (1986)
Mathematical models for dowel action under monotonic and cyclic conditions
Magazine of Concrete Research: Vol. 38, No. 134 : March , pp. 13-22

Vecchio.F.J. and Tang K. (1990)
Membrane action in reinforced concrete slabs
Canadian Journal of Civil Engineering, Vol. 17, pp 686-697

Vecchio.F.J. (1992)
Finite Element modelling of Concrete expansion and confinement
J. of Struc. Eng., ASCE, Vol. 118, No. 9, pp 2390-2406

Walker P.R. (1980)
An investigation into moment and shear transfer at corner columns in flat slab construction
Ph.D. thesis, Polytechnic of Central London

Yamada T., Nanni A. and Endo K. (1992)
Punching shear resistance of flat slabs : Influence of reinforcement type and ratio
ACI Structural Journal, Vol. 88, No. 4, pp. 555-563

Zakaria K.A.A. (1978)
Shear and moment resistance at edge columns in flat slab structures
Ph.D. thesis, Polytechnic of Central London

Zienkiiewicz O.C. and Taylor R.L. (1989)
The Finite Element Method
McGraw-Hill Book Company

Appendix A : Sample calculations using BS8110

A1 Interior Slab

Example : Specimen G5

A1.1 Shear capacity

Dimensions and Material Properties	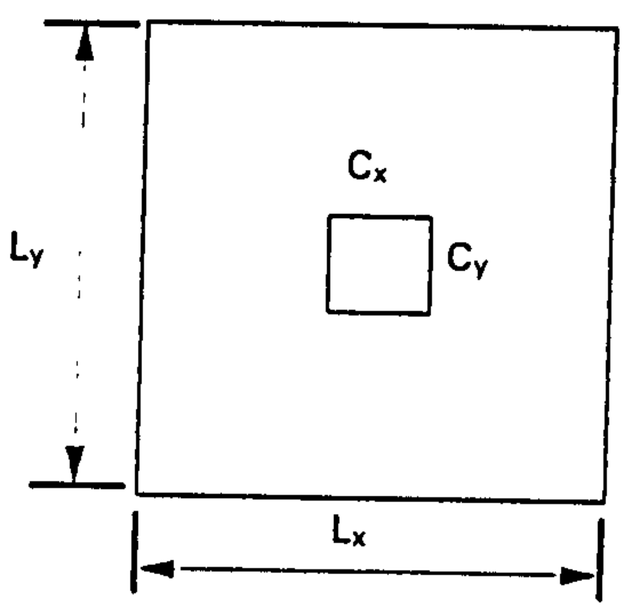	d = 159 mm L_x = 3000 mm L_y = 3000 mm C_x = 200 mm C_y = 200 mm f_{cu} = 43.4 N/mm^2 f_y = 670.0 N/mm^2 f_{yv} = 400.0 N/mm^2
Shear force at column face, P_c	$P_c = v_{max}.u_o d$ $v_{max} = \sqrt{f_{cu}} \leq 6.25 N/mm^2$	u_o = 800 mm v_{max} = 6.25 N/mm^2 P_c = 795.0 kN
First perimeter, **u**	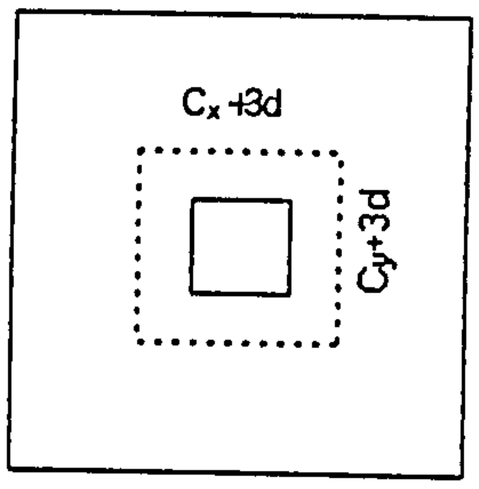	C_x+3d = 677.0 mm C_y+3d = 677.0 mm u = 2708.0 mm ρ_x = 1.31% ρ_y = 1.31% ρ_{avg} = 1.31% A_{sv} = 1256.0 mm^2
Shear force at first perimeter, $P_{v(in)}$	$P_{v(in)} = V_c + V_s$ $V_c = v_c.ud$ $V_s = f_{yv}.A_{sv}$ $v_c = 0.79\rho^{1/3}\left(\frac{400}{d}\right)^{1/4}\left(\frac{f_{cu}}{25}\right)^{1/3}$	v_c = 1.26 N/mm^2 V_c = 542.5 kN V_s = 502.4 kN $P_{v(in)}$ = 1044.9 kN
Shear force at a perimeter outside shear reinforcement region, $P_{v(out)}$	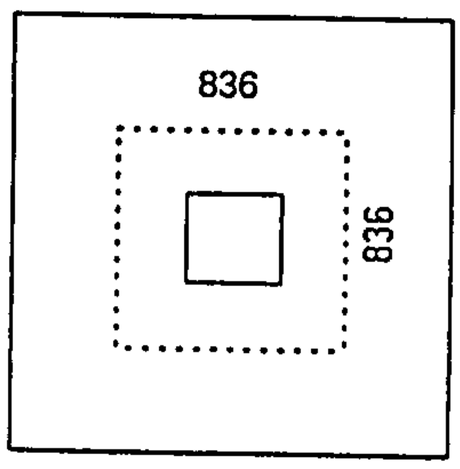	u_{sv} = 3344.0 mm $P_{v(out)} = v_c.u_{sv}d$ $P_{v(out)}$ = 670.0 kN
Shear Capacity, P_u	Smaller of [P_c, $P_{v(in)}$, $P_{v(out)}$]	P_u = 670.0 kN

A1.2 Moment capacity

Moment capacity, **M**	$0.9x = \dfrac{f_y A_s}{0.67 f_{cu} b}$ Take b=1000 mm $z = d - 0.45x \leq 0.95d$ $M_{xx} = f_y A_s . z$	0.9x = 46.5 mm z = 135.8 mm $M_{XX} = M_{yy}$ M_{XX} = 183.6 kNm/m

A2 Edge Slab

Example : Specimen JS2

A2.1 Shear capacity

Dimensions and Material Properties	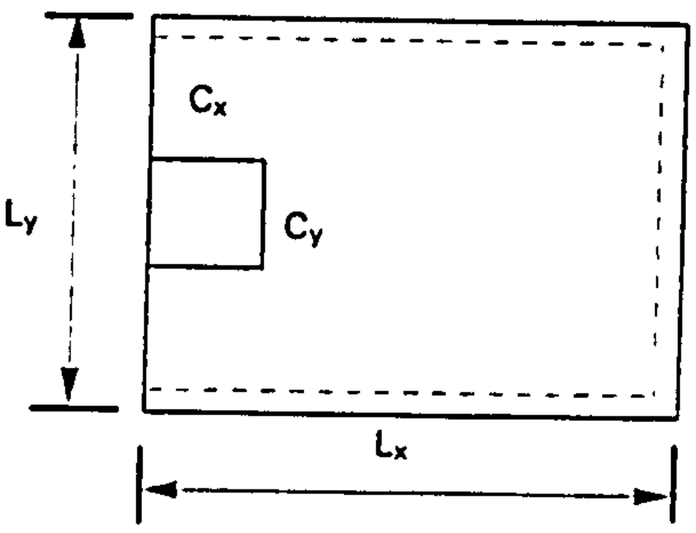	d = 122 mm L_x = 1372 mm L_y = 1880 mm C_x = 254 mm C_y = 254 mm f_{cu} = 61.2 N/mm2 f_y = 420.0 N/mm2 f_{yv} = 480.0 N/mm2
Shear force at column face, **P_c**	$P_c = v_{max}.u_o d$ $v_{max} = \sqrt{f_{cu}} \le 6.25 N/mm^2$	u_o = 762 mm v_{max} = 6.25 N/mm2 P_c = 581.0 kN
First perimeter, **u**	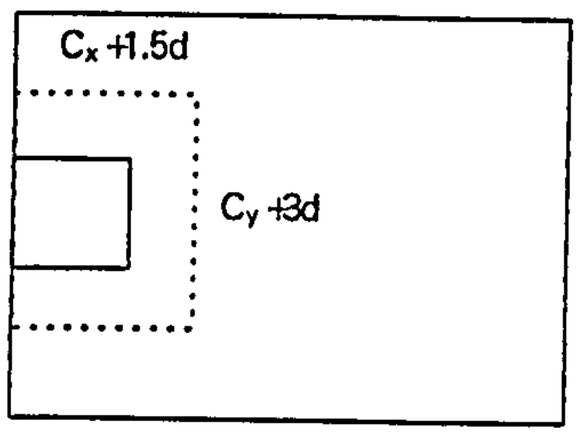	C_x+1.5d = 437.0 mm C_y+3.0d = 620.0 mm u = 1494.0 mm ρ_x = 0.80% ρ_y = 1.28% ρ_{avg} = 1.04% A_{sv} = 1914.0 mm2
Shear force at first perimeter, **$P_{v(in)}$**	$P_{v(in)} = V_c + V_s$ $V_c = v_c.ud$ $V_s = f_{yv}.A_{sv}$ $v_c = 0.79\rho^{1/3}\left(\frac{400}{d}\right)^{1/4}\left(\frac{f_{cu}}{25}\right)^{1/3}$	v_c = 1.26 N/mm2 V_c = 229.6 kN V_s = 918.0 kN $P_{v(in)}$ = 1147.6 kN
Shear force at a perimeter outside shear reinforcement region, **$P_{v(out)}$**	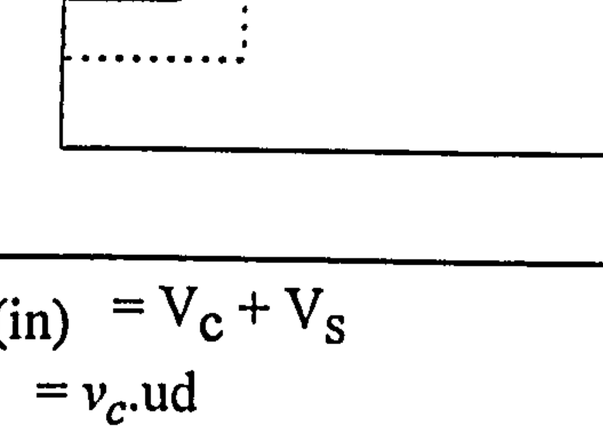	u_{sv} = 1900.0 mm $P_{v(out)} = v_c.u_{sv}d$ = 292.0 kN
Shear Capacity, **P_u**	Smaller of [P_c, $P_{v(in)}$, $P_{v(out)}$]	P_u = 191.40 kN

A2.2 Moment capacity

Width of slab for transfer of moment by steel	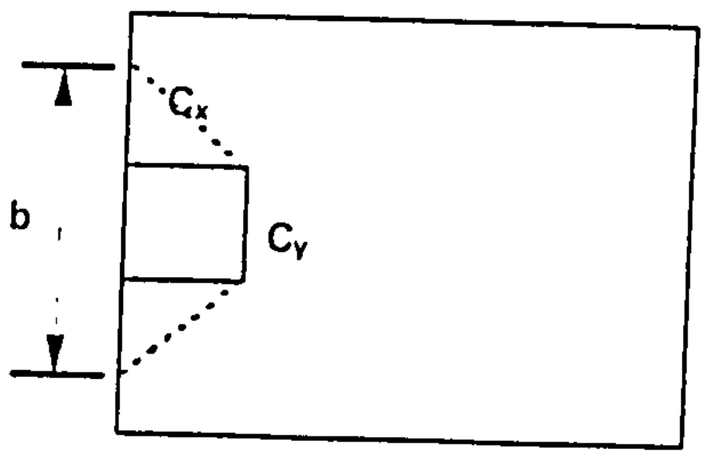	b $= C_y + 2C_x$ $= 762$ mm
Moment transfer by steel, $\mathbf{M_t}$	$0.9x = \frac{f_y A_s}{0.67 f_{cu} b_1}$ $z = d - 0.45x \le 0.95d$ $M_t = f_y A_s z$	0.9x = 10.0 mm z = 115.9 mm M_t = 36.2 kNm
Effective width of slab for maximum allowable moment capacity.	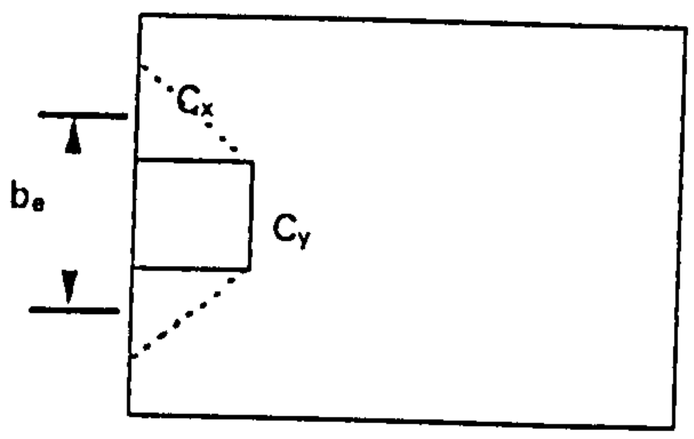	$b_e = C_y + C_x$ $= 508.0$ mm
Maximum allowable moment capacity, $\mathbf{M_{t.max}}$	$M_{t.max} = 0.15 b_e d^2 f_{cu}$	$M_{t.max}$ = 52.1 kNm
Moment transfered to column, **M**		M = 36.2 kNm

A3 Corner Slab

Example : Specimen NH5

A3.1 Shear capacity

Dimensions and Material Properties	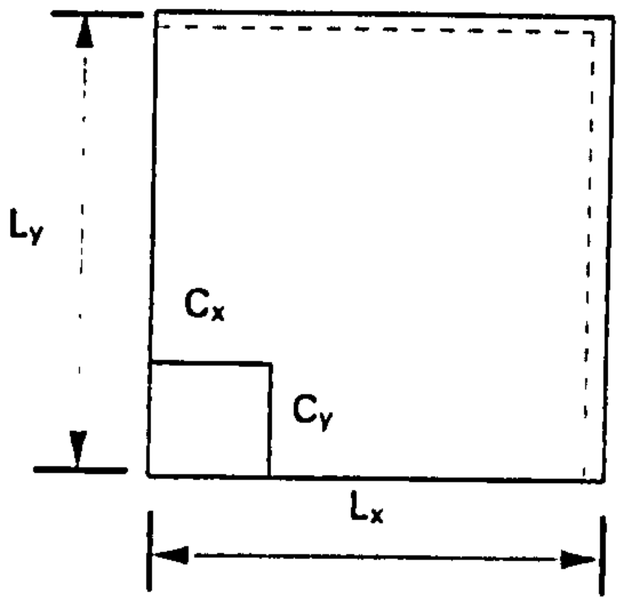	d = 119 mm L_x = 1075 mm L_y = 1075 mm C_x = 250 mm C_y = 250 mm f_{cu} = 64.5 N/mm^2 f_y = 440.0 N/mm^2 f_{yv} = 480.0 N/mm^2
Shear force at column face, P_c	$P_c = v_{max}.u_o d$ $v_{max} = \sqrt{f_{cu}} \leq 6.25 N/mm^2$	u_o = 500 mm v_{max} = 6.25 N/mm^2 P_c = 371.9 kN
First perimeter, **u**	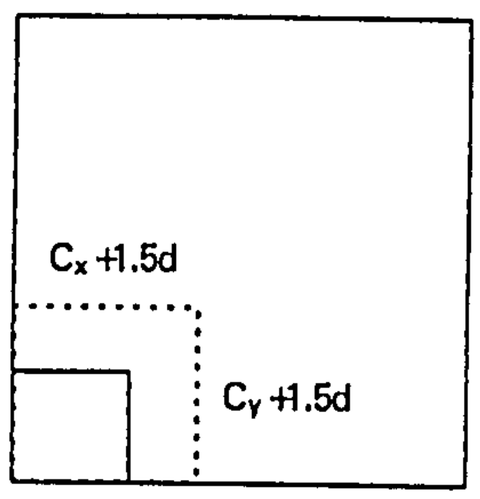	C_x+1.5d = 428.5 mm C_y+1.5d = 428.5 mm u = 857.0 mm ρ_x = 0.981% ρ_y = 0.981% ρ_{avg} = 0.981% A_{sv} = 567.0 mm^2
Shear force at first perimeter, $P_{v(in)}$	$P_{v(in)} = V_c + V_s$ $V_c = v_c.ud$ $V_s = f_{yv}.A_{sv}$ $v_c = 0.79\rho^{1/3}\left(\frac{400}{d}\right)^{1/4}\left(\frac{f_{cu}}{25}\right)^{1/3}$	v_c = 1.24 N/mm^2 V_c = 126.8 kN V_s = 272.2 kN $P_{v(in)}$ = 399.00 kN
Shear force at a perimeter outside shear reinforcement region, $P_{v(out)}$	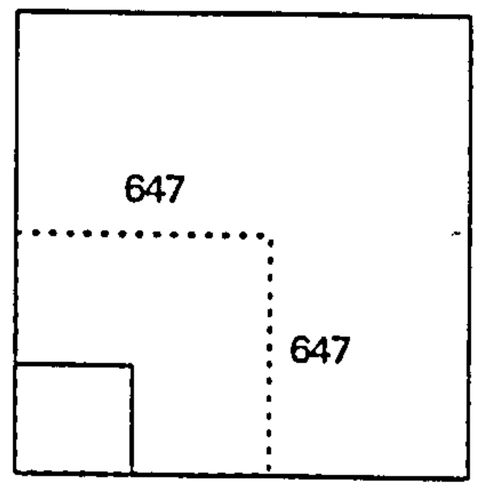	u_{sv} = 1294.0 mm $P_{v(out)} = v_c.u_{sv}d$ = 191.4 kN
Shear Capacity, P_u	Smaller of [P_c, $P_{v(in)}$, $P_{v(out)}$]	P_u = 191.40 kN

A3.2 Moment capacity

Width of slab for transfer of moment by steel	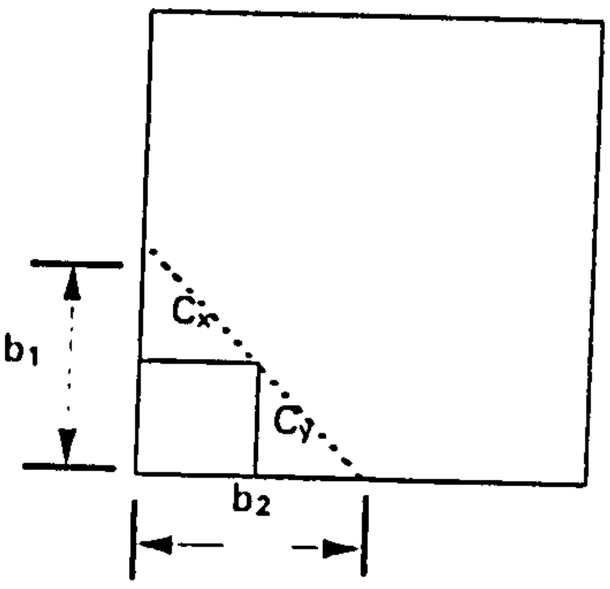	For slab with square column, $b_1 = b_2$ $= C_x + C_y$ $= 500$ mm $M_{xx} = M_{yy}$
Moment transfer by steel, $\mathbf{M_t}$	$0.9x = \frac{f_y A_s}{0.67 f_{cu} b_1}$ $z = d - 0.45x \le 0.95d$ $M_{xx} = f_y A_s . z$ $M_t = \sqrt{M_{xx} + M_{yy}}$	$0.9x = 12.2$ mm $z = 112.9$ mm $M_{xx} = 29.8$ kNm $M_t = 42.2$ kNm
Effective width of slab for maximum allowable moment capacity.	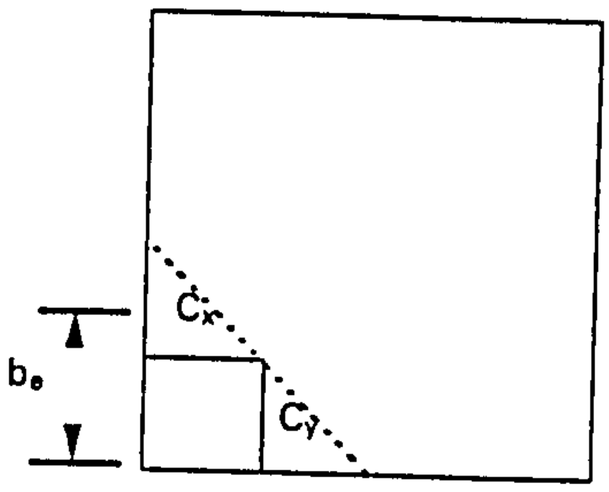	$b_e = C_y + (C_x/2)$ $= 375.0$ mm
Maximum allowable moment capacity, $\mathbf{M_{t.max}}$	$M_{t.max} = 0.15 b_e d^2 f_{cu}$	$M_{t.max} = 51.4$ kNm
Moment transfered to column, **M**		M = 42.2 kNm

Appendix B

Flow chart for the computer program for Kinnunen and Nylander's model

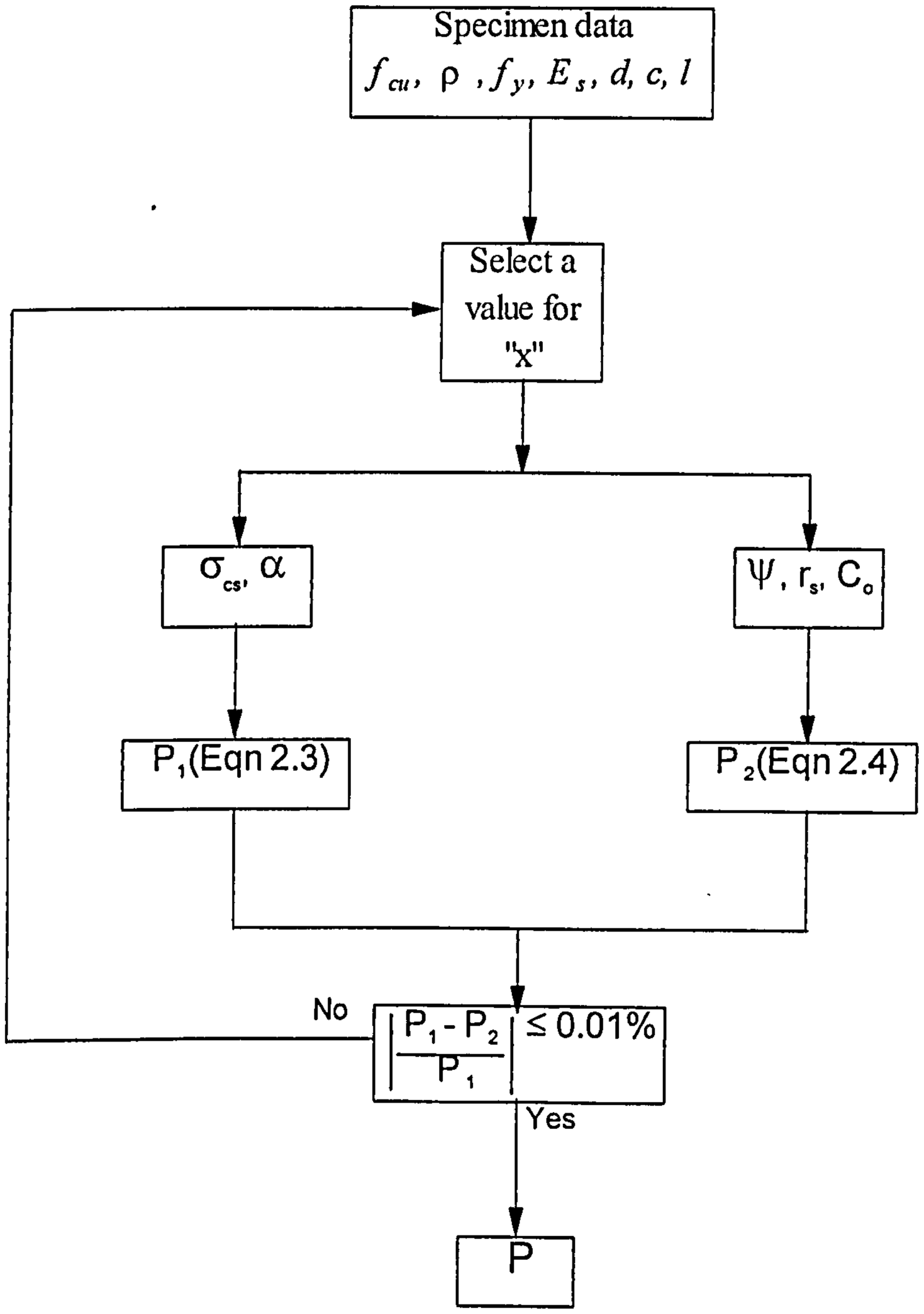

For the definition of notation, please refer to Figure 2.9 (page 10).
Details of Equations 2.3 and 2.4 are given in pages 11 and 12.

Appendix C

Numerical results

This section presents following numerical predictions for all slabs following :

- Ultimate load of slabs
- mode of failures
- Load-deflection response
- Principal compressive stress and strain in concrete
- Yielding of flexural steel
- Crack pattern

All computed crack pattern and yielding of flexural steel is shown at the last converged increment.

C1 Simply supported slabs

This section presents numerical results for internal slab-column connections subjected to shear only.

For yielding of flexural steel, only shaded area is shown.

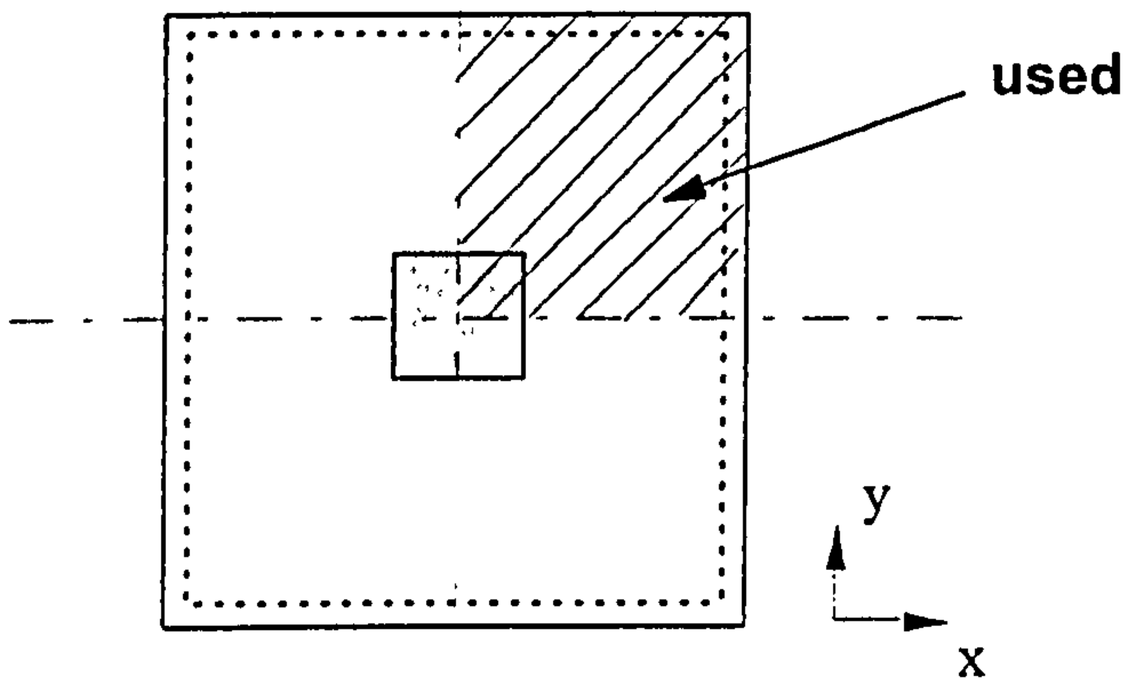

For crack pattern,

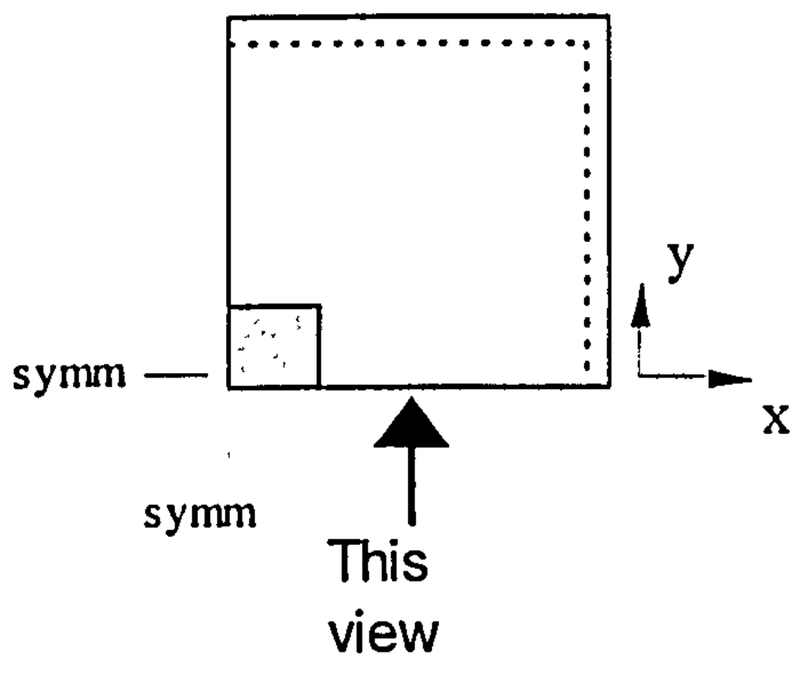

Rankin's conventional slabs

C1.1 Rankin's conventional slab-column specimens (without shear reinforcement)

Slab	Experimental results		Numerical Predictions		P_{num}/P_{test}
	P_{test} (kN)	Failure Mode	P_{num} (kN)	Failure Mode	
1	36.42	y	32.40	y	0.890
2	49.08	y	40.79	y	0.831
3	56.55	y	44.90	y	0.794
4	56.18	y	42.14	y	0.750
5	57.27	y	51.83	y	0.905
6	65.58	s	53.78	fp	0.820
7	70.94	s	46.82	s	0.660
8	71.09	s	46.78	s	0.658
9	78.60	s	55.41	s	0.705
10	43.59	y	35.52	y	0.815
11	55.00	y	42.24	y	0.768
12	67.06	s	47.08	s	0.702
13	49.39	y	42.82	y	0.867
14	52.45	y	44.16	y	0.842
15	84.84	s	75.60	s	0.891
1A	45.19	y	41.03	y	0.908
2A	66.24	y	50.41	y	0.761
3A	89.72	s	72.94	s	0.813
4A	97.43	s	91.20	s	0.936
1B	28.85	y	24.96	y	0.865
2B	37.63	y	36.50	y	0.969
3B	56.67	y	49.00	s	0.864
4B	72.52	s	50.40	s	0.695
1C	62.74	y	34.80	y	0.845
2C	87.86	s	53.02	fp	0.738
3C	124.14	s	95.96	s	0.773
4C	125.94	s	102.10	s	0.810
				Average	0.810
				STDEV	0.083

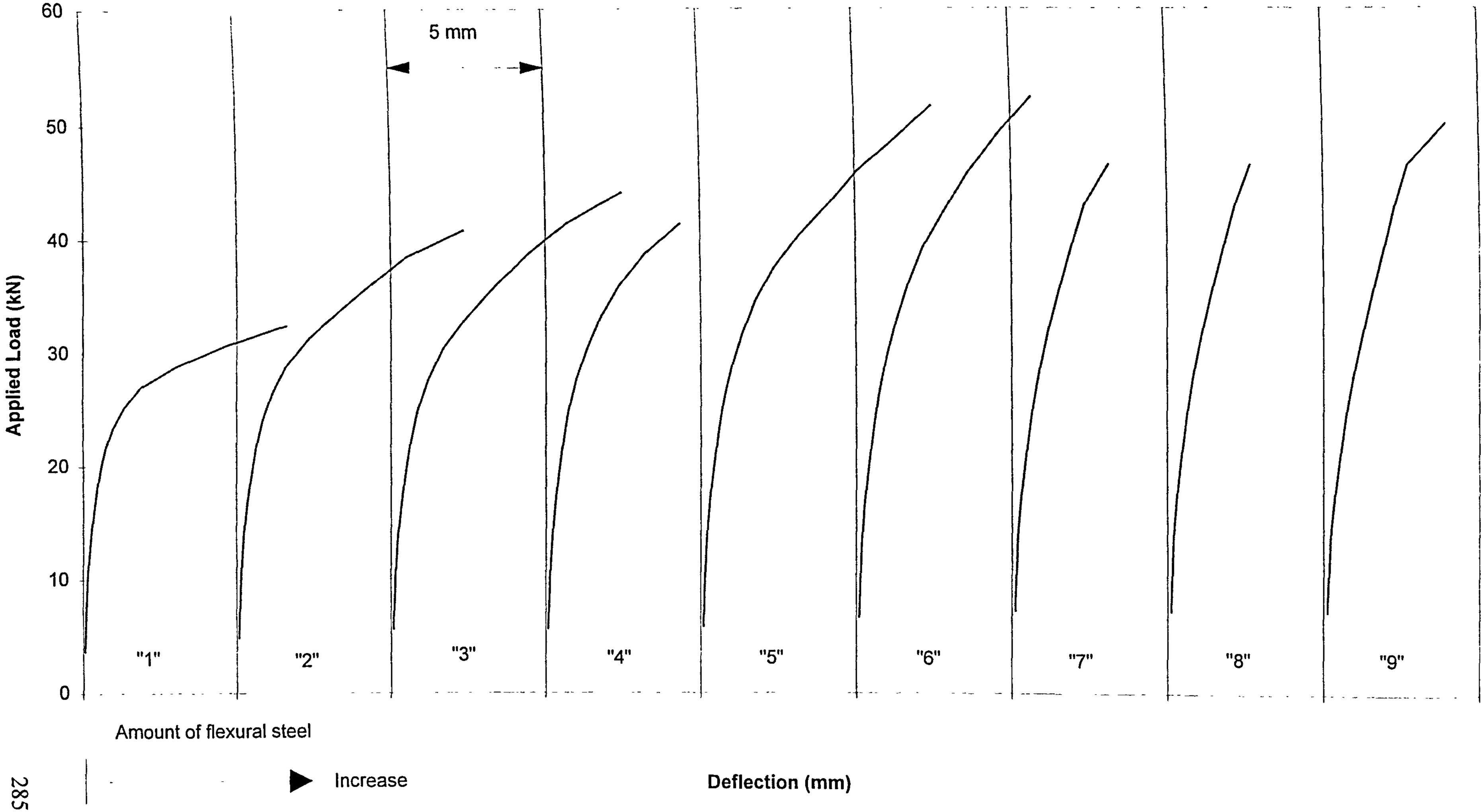

Predicted load-deflection response for slabs 1-9

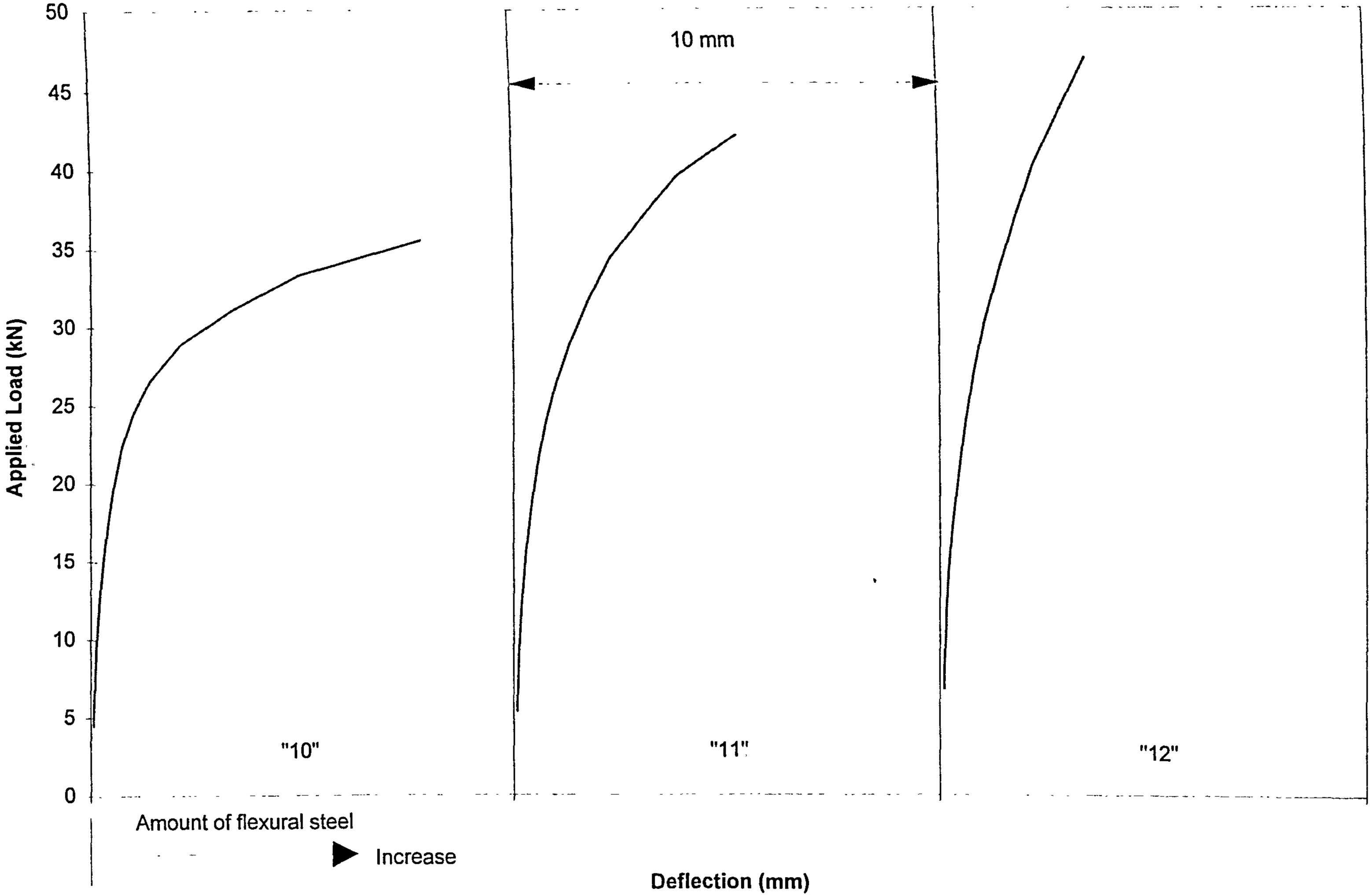

Predicted load-deflection response for slabs 10-12

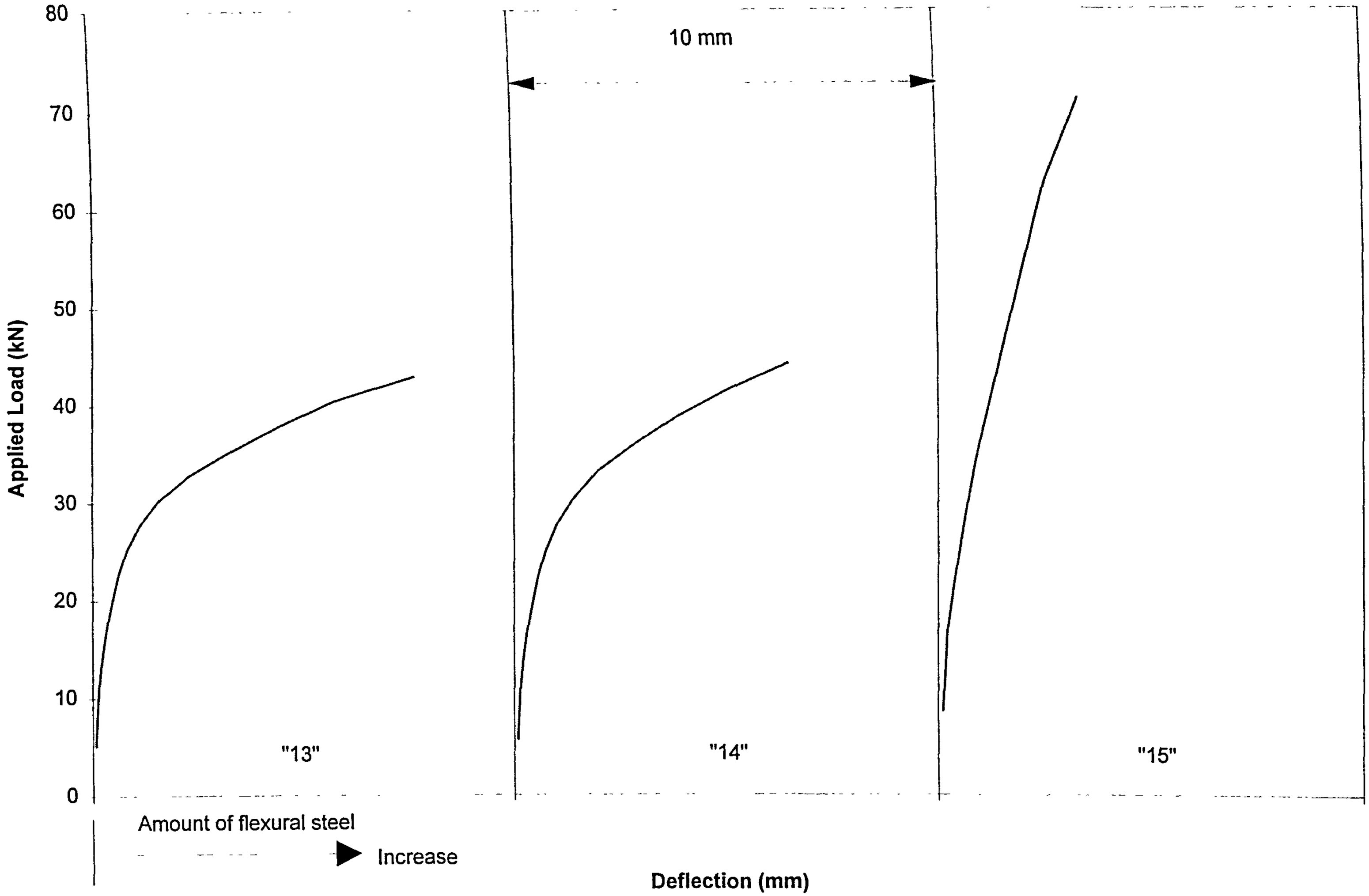

Predicted load-deflection response for slabs 13-15

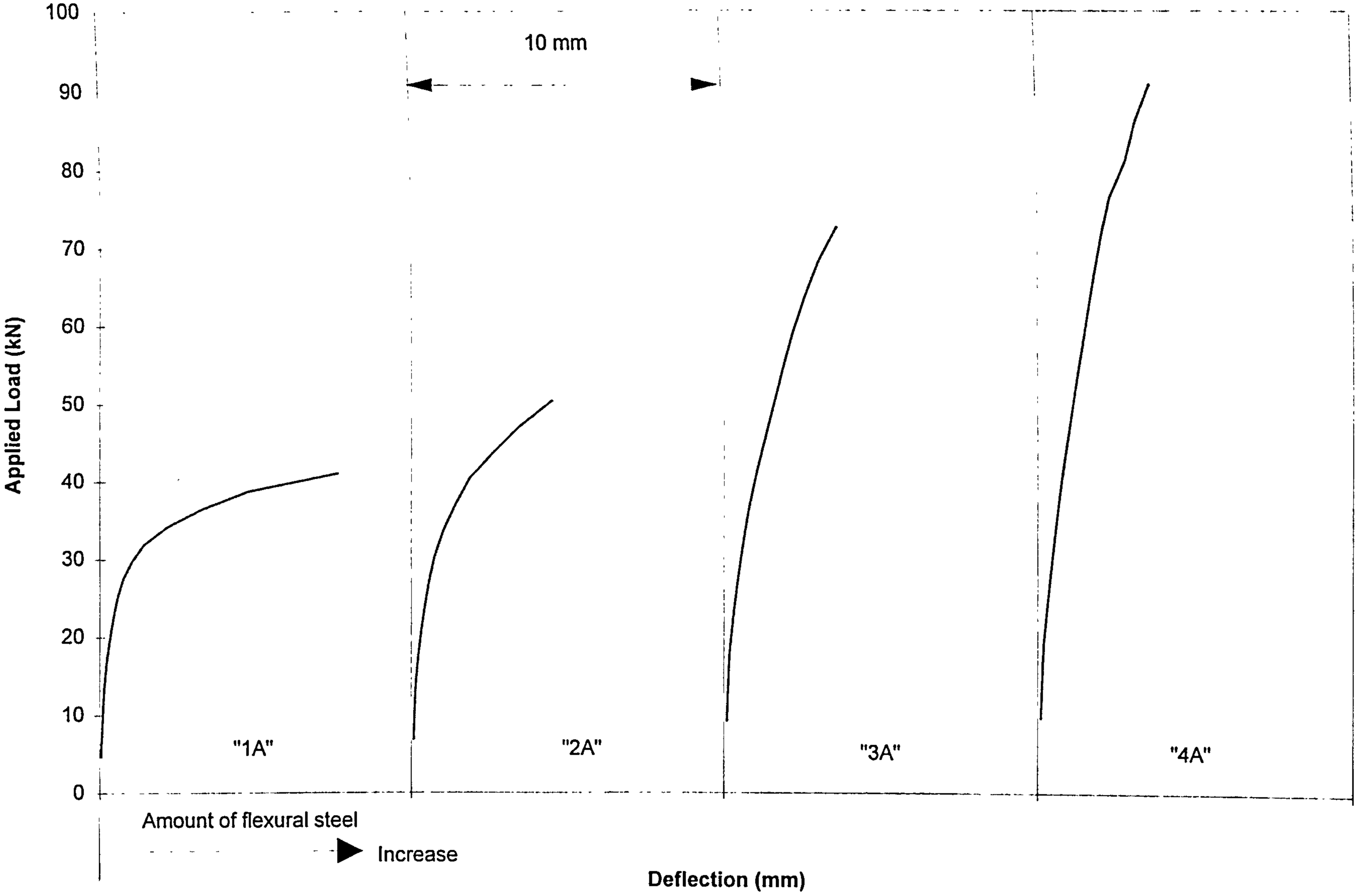

Predicted load-deflection response for slabs 1A-4A

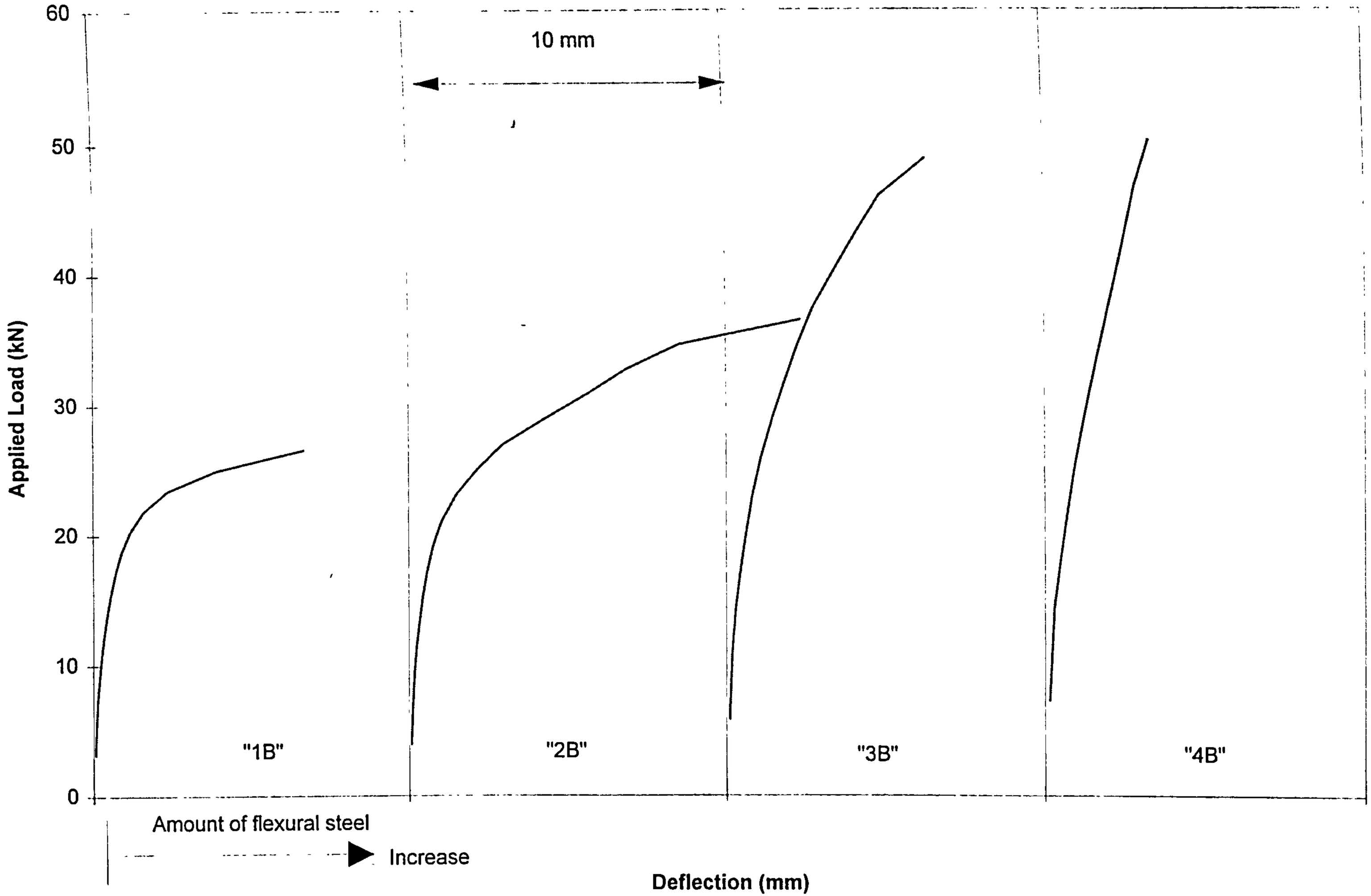

Predicted load-deflection response for slabs 1B-4B

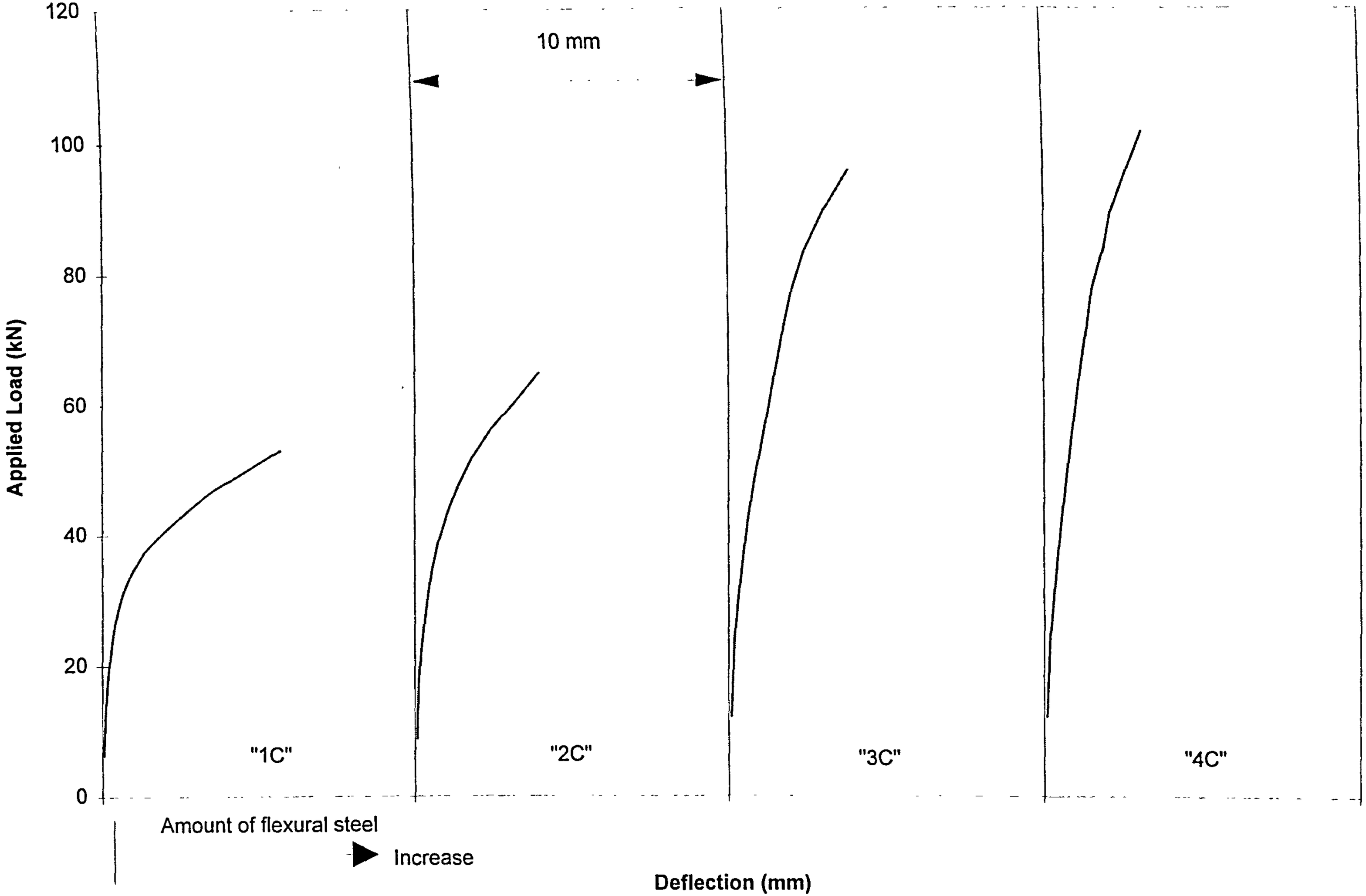

Predicted load-deflection response for slabs 1C-4C

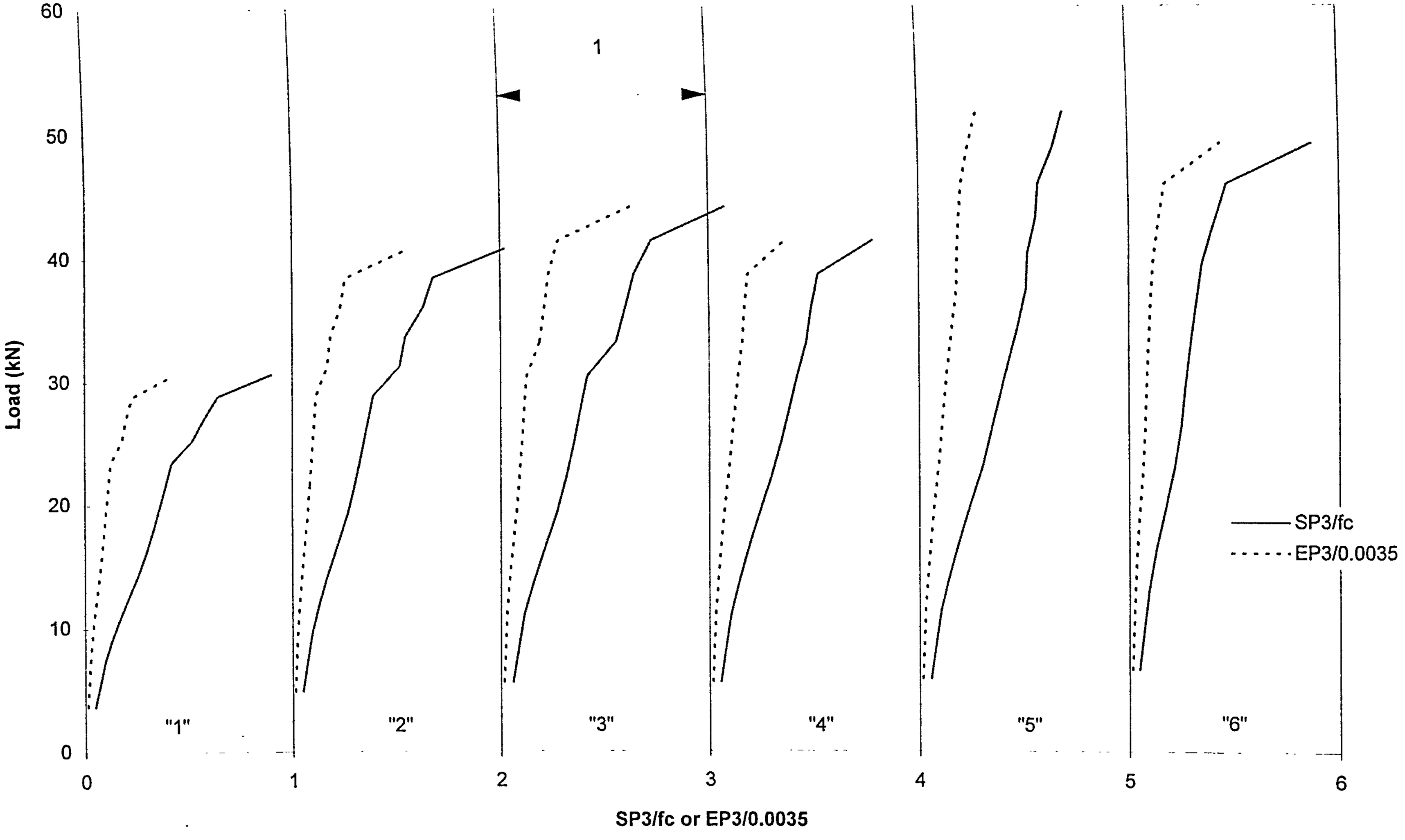

Predicted principal compressive stress and strain in concrete (slabs "1" - "6")

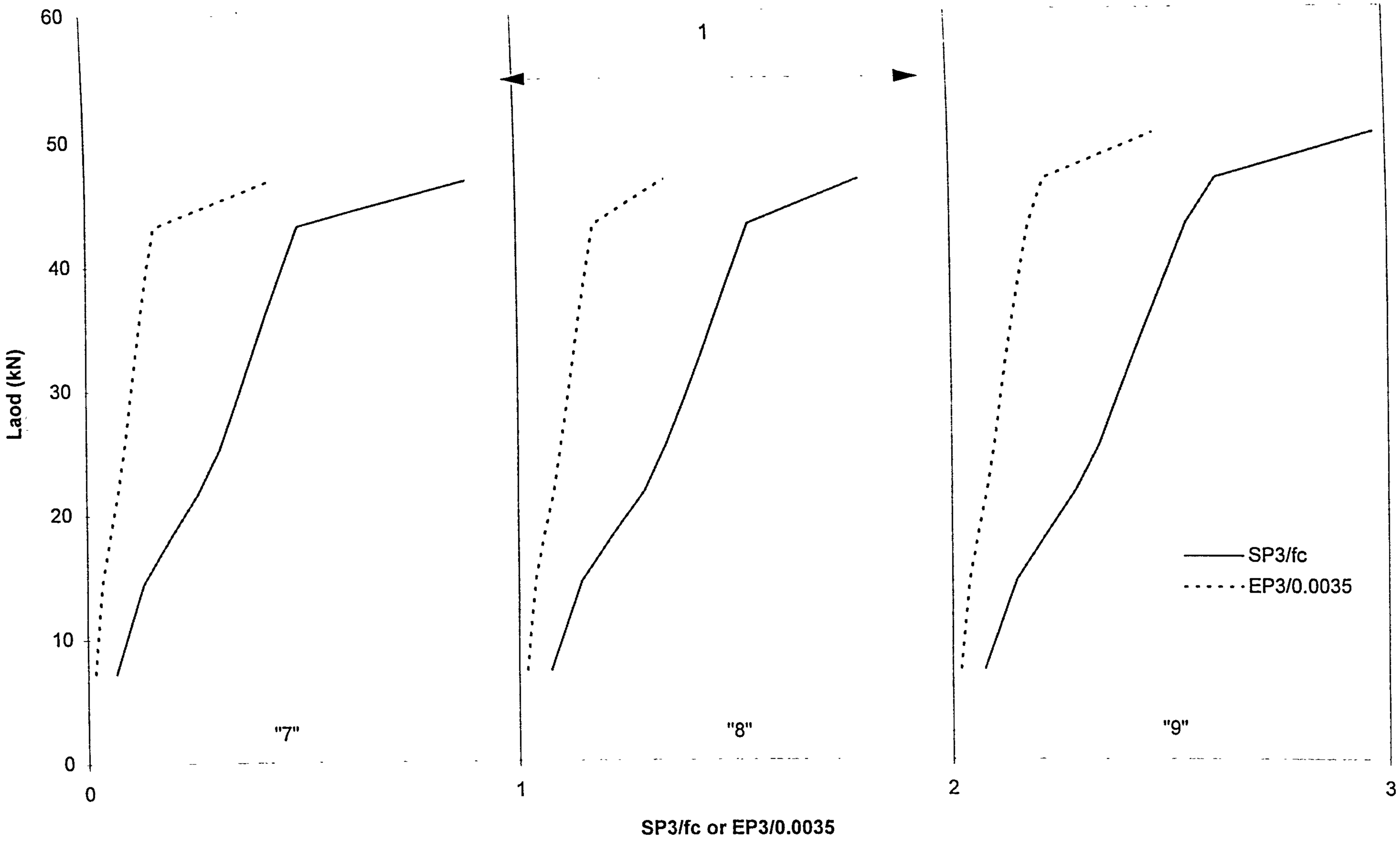

Predicted principal compressive stress and strain in concrete (slabs "7" - "9")

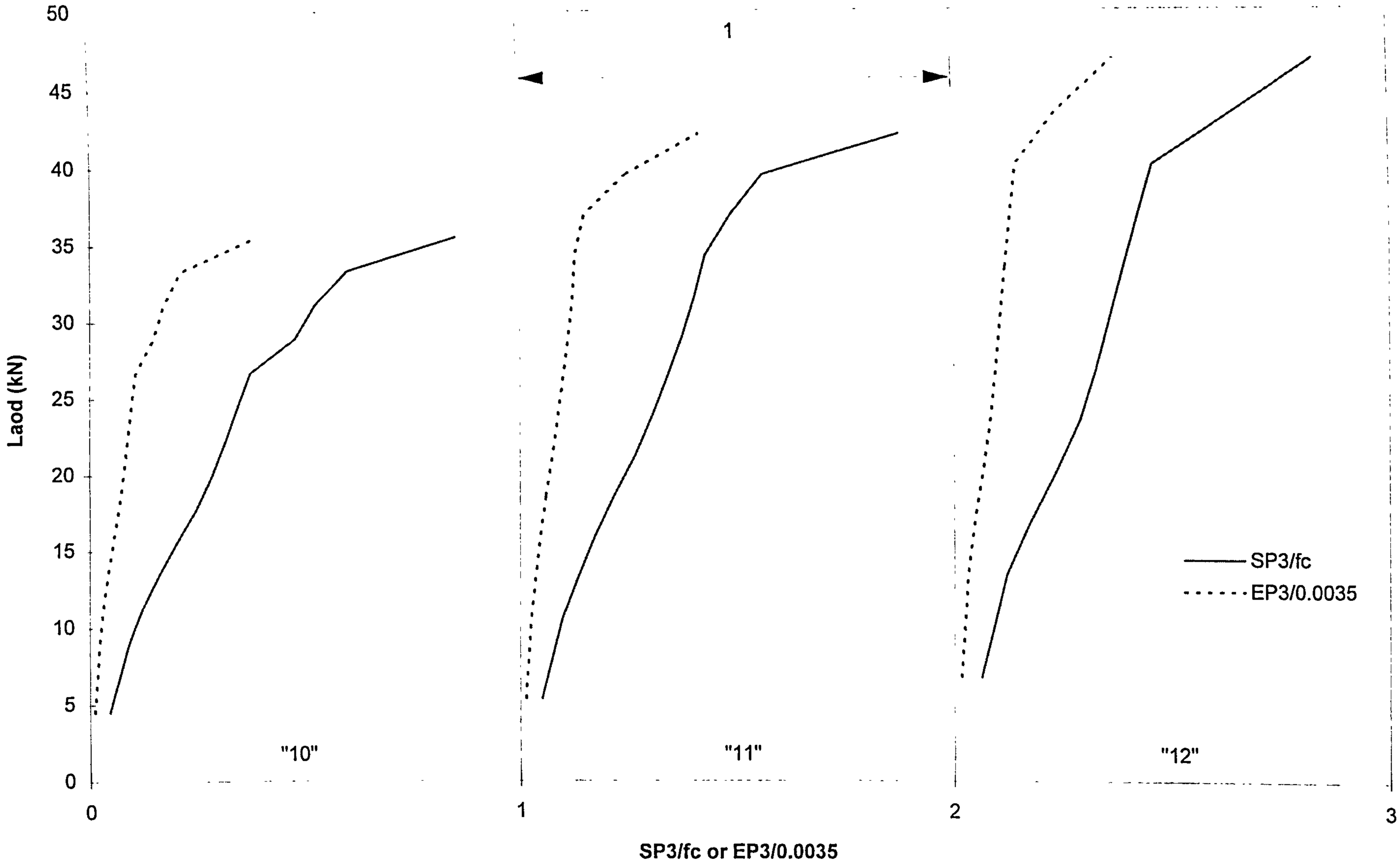

Predicted principal compressive stress and strain in concrete (slabs "10" - "12")

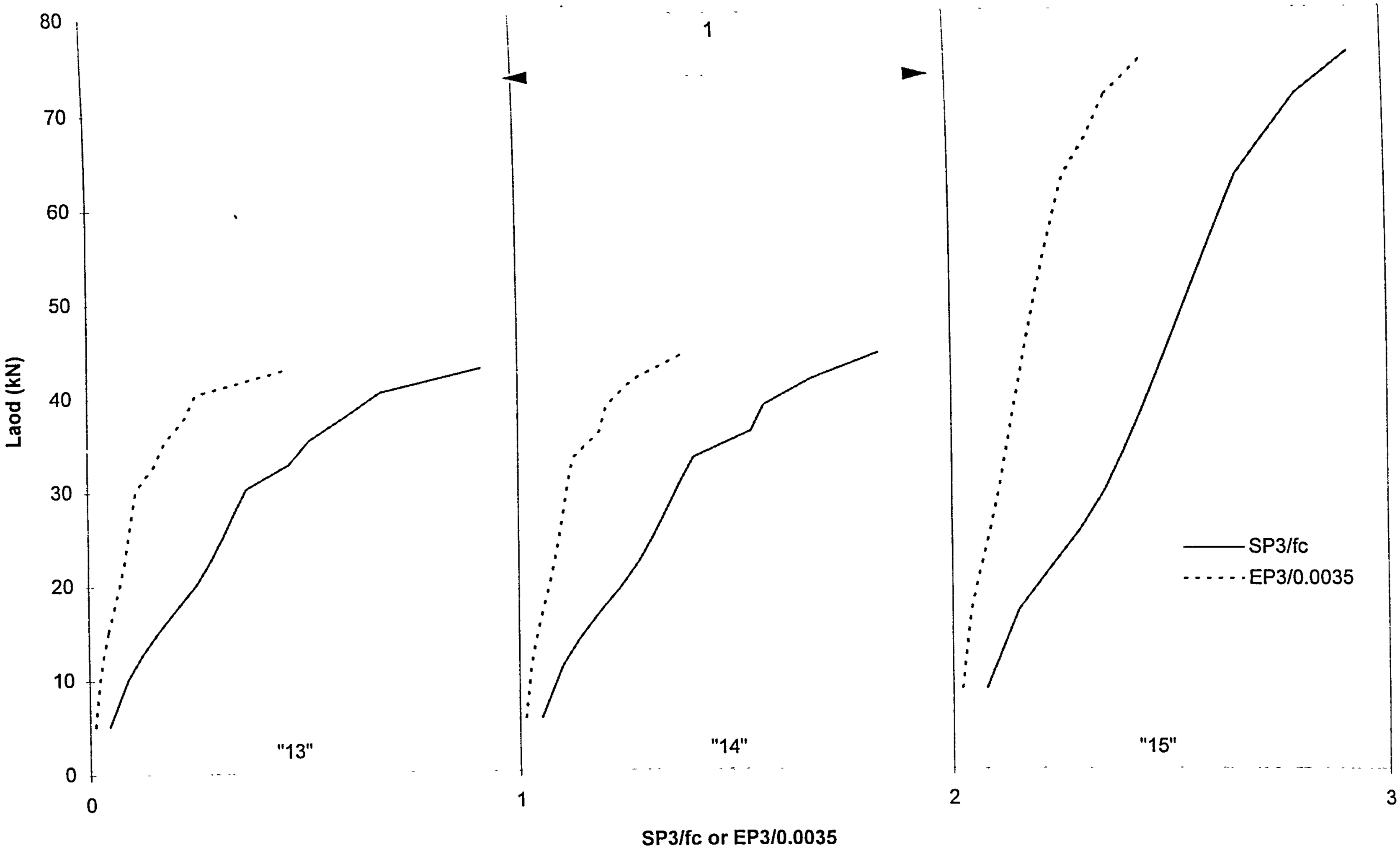

Predicted principal compressive stress and strain in concrete (slabs "13" - "15")

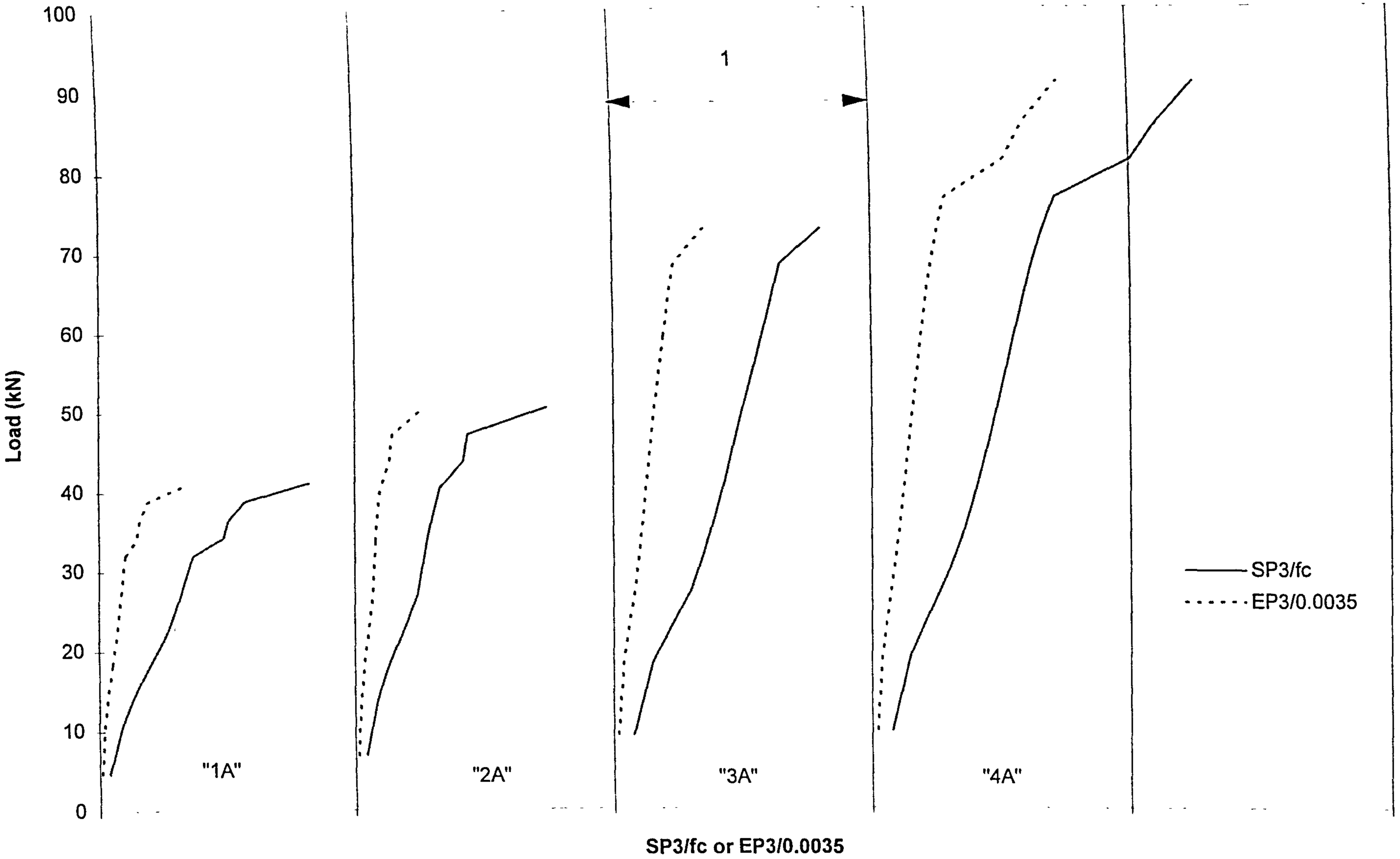

Predicted principal compressive stress and strain in concrete (slabs "1A" - "4A")

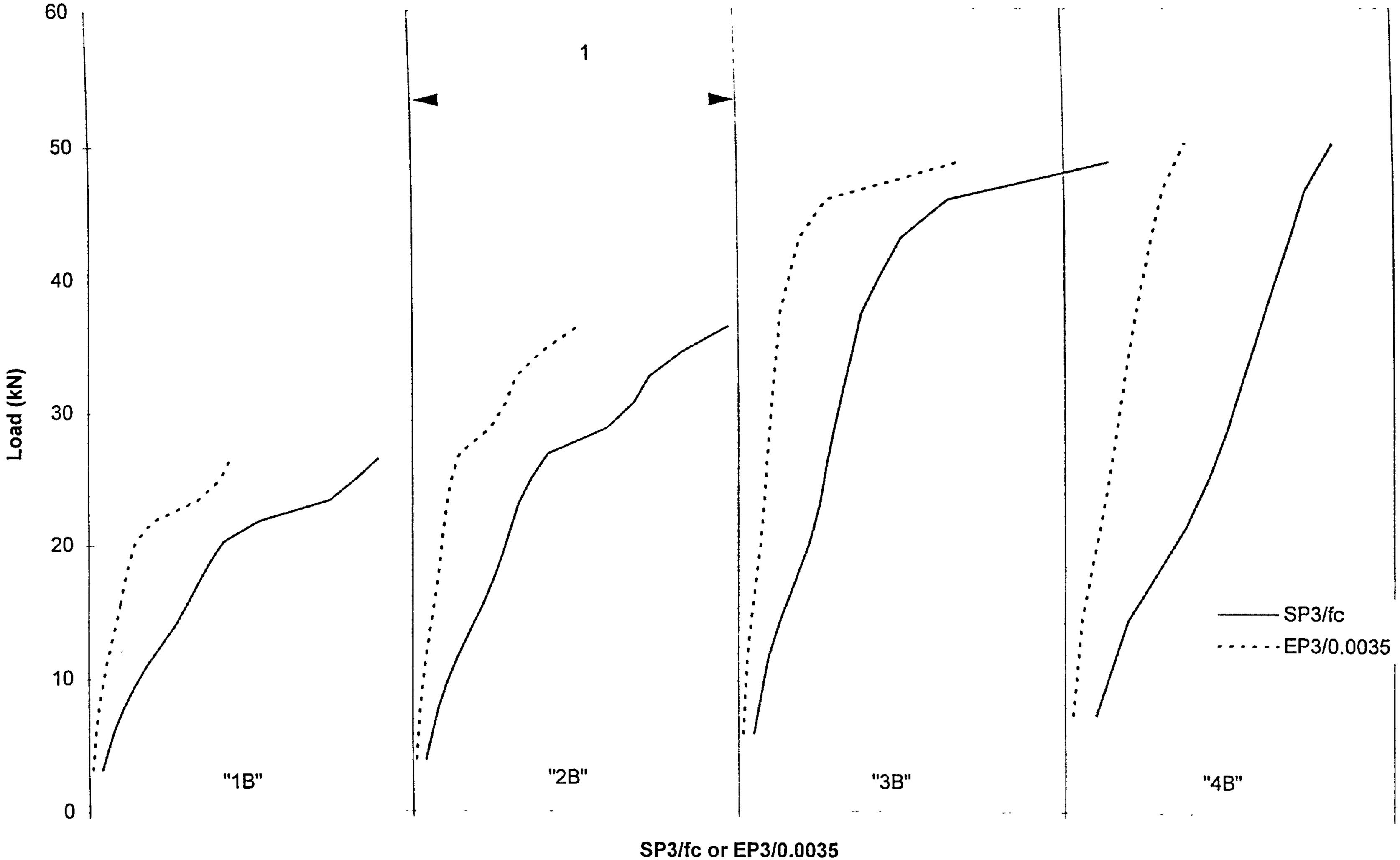

Predicted principal compressive stress and strain in concrete (slabs "1B" - "4B")

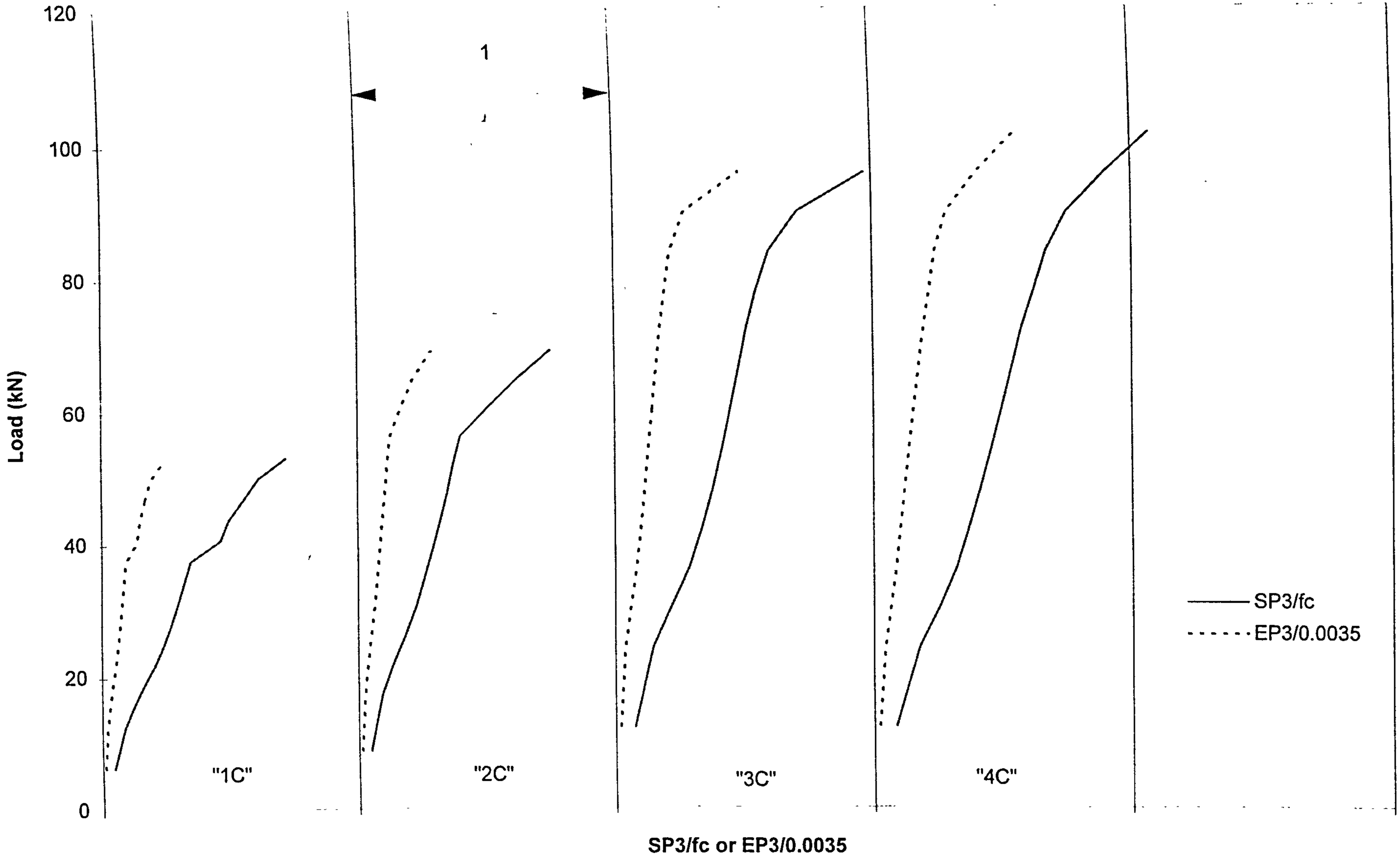

Predicted principal compressive stress and strain in concrete (slabs "1C" - "4C")

Yielding of flexural steel for conventinal slabs tested by Rankin

NB. : The numbers on the drawing indicate strain in steel at collapse expressed as a ratio of yield strain

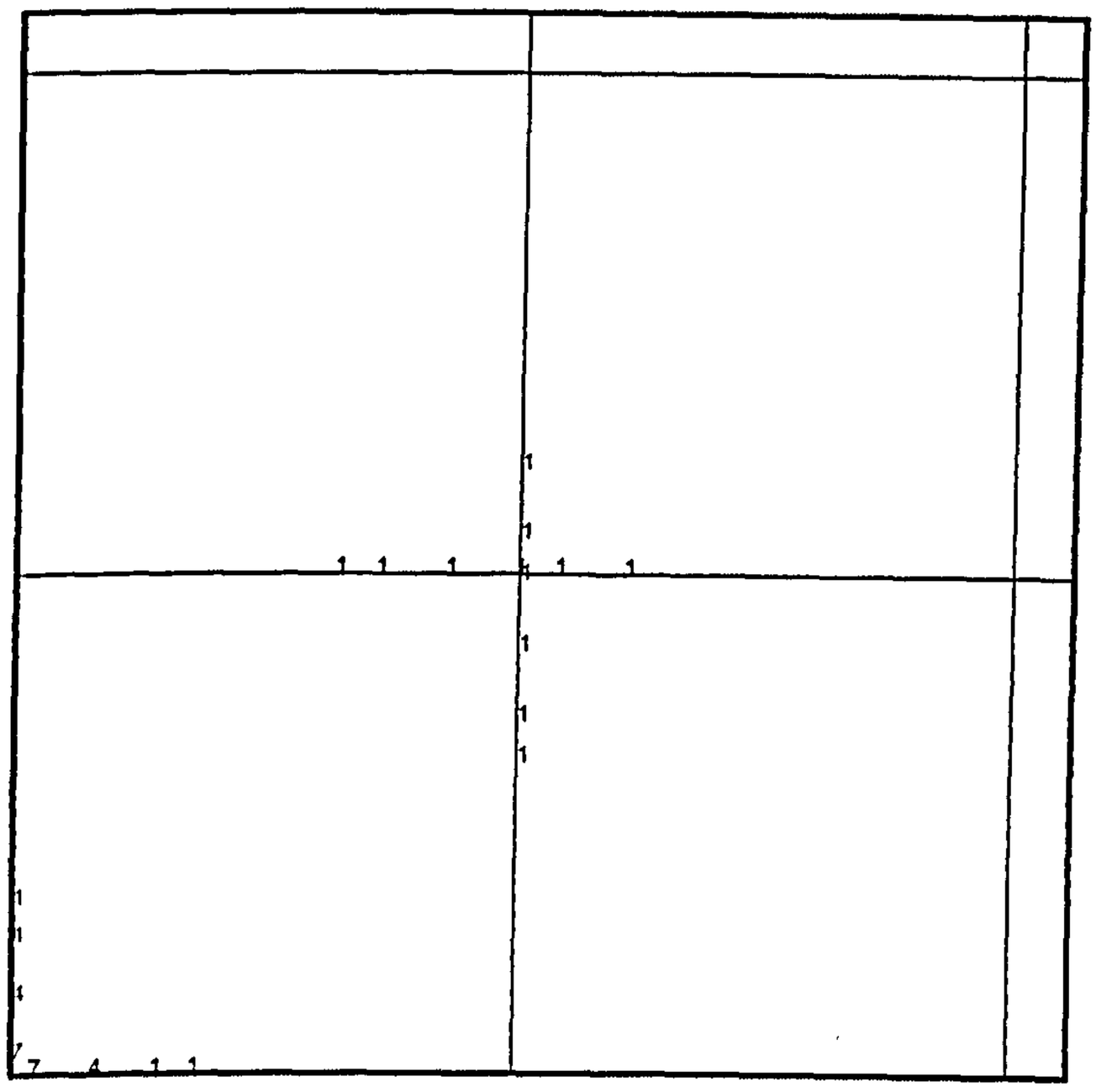

Slab " 1 "

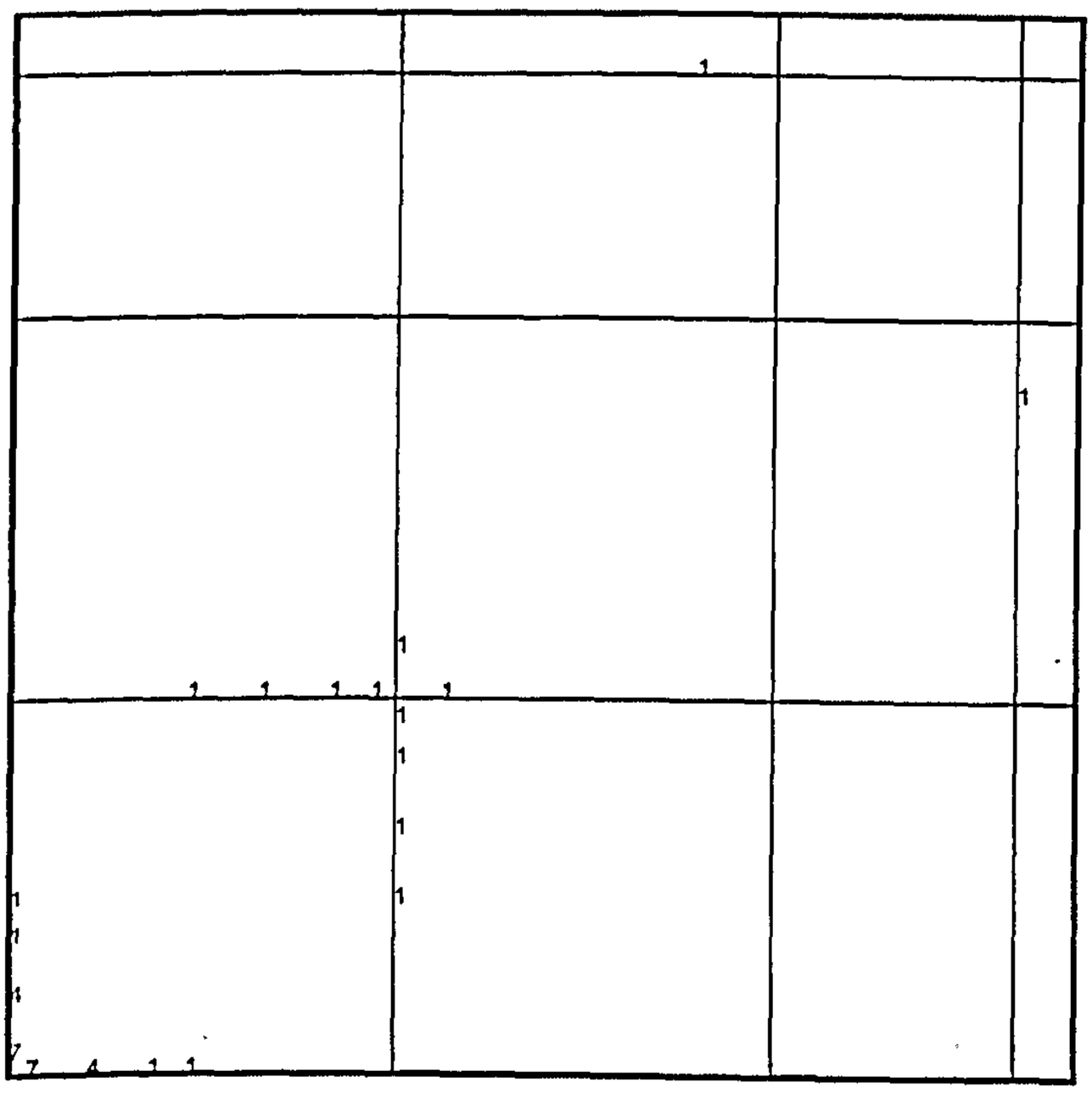

Slab " 2 "

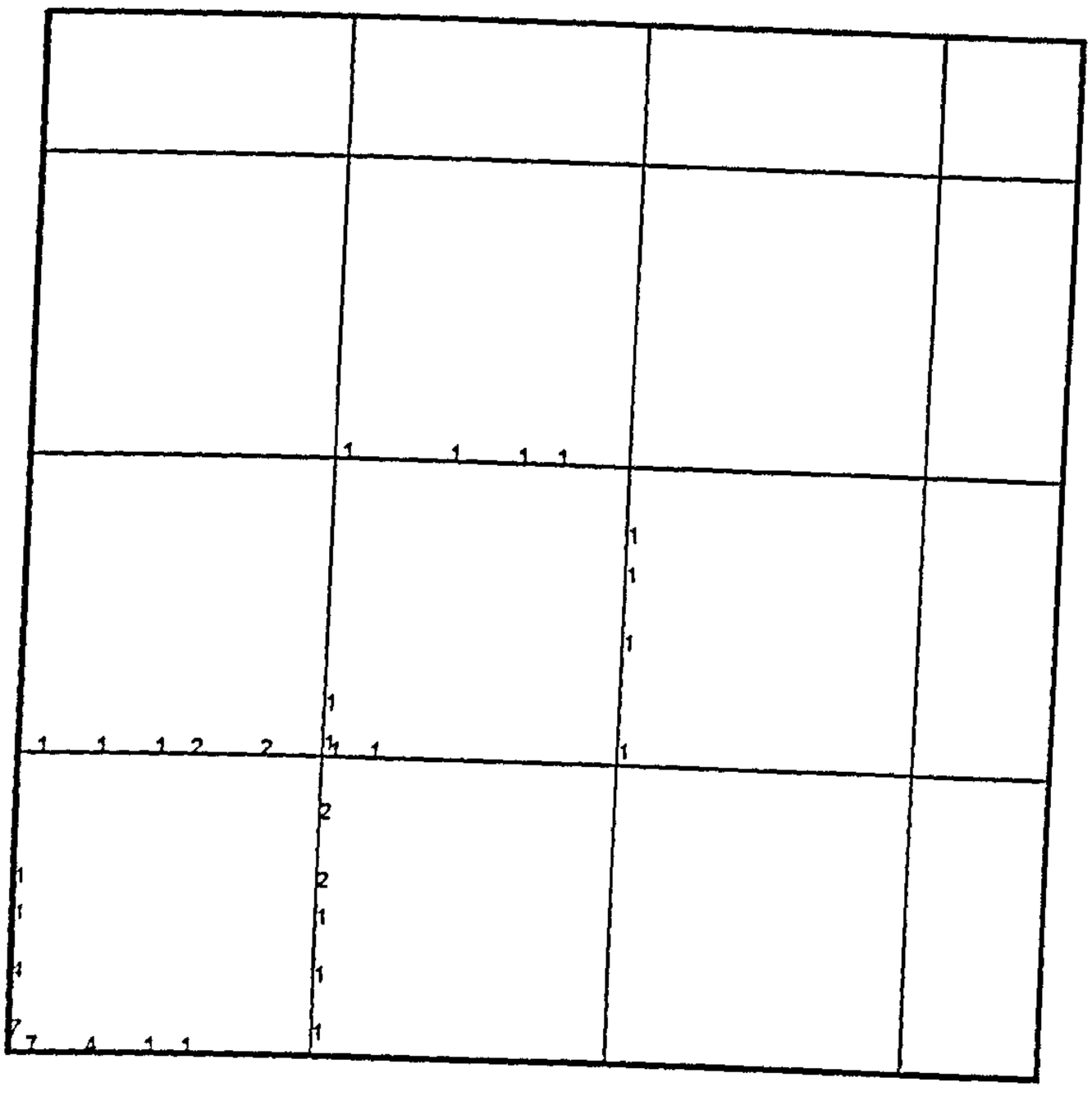

Slab " 3 "

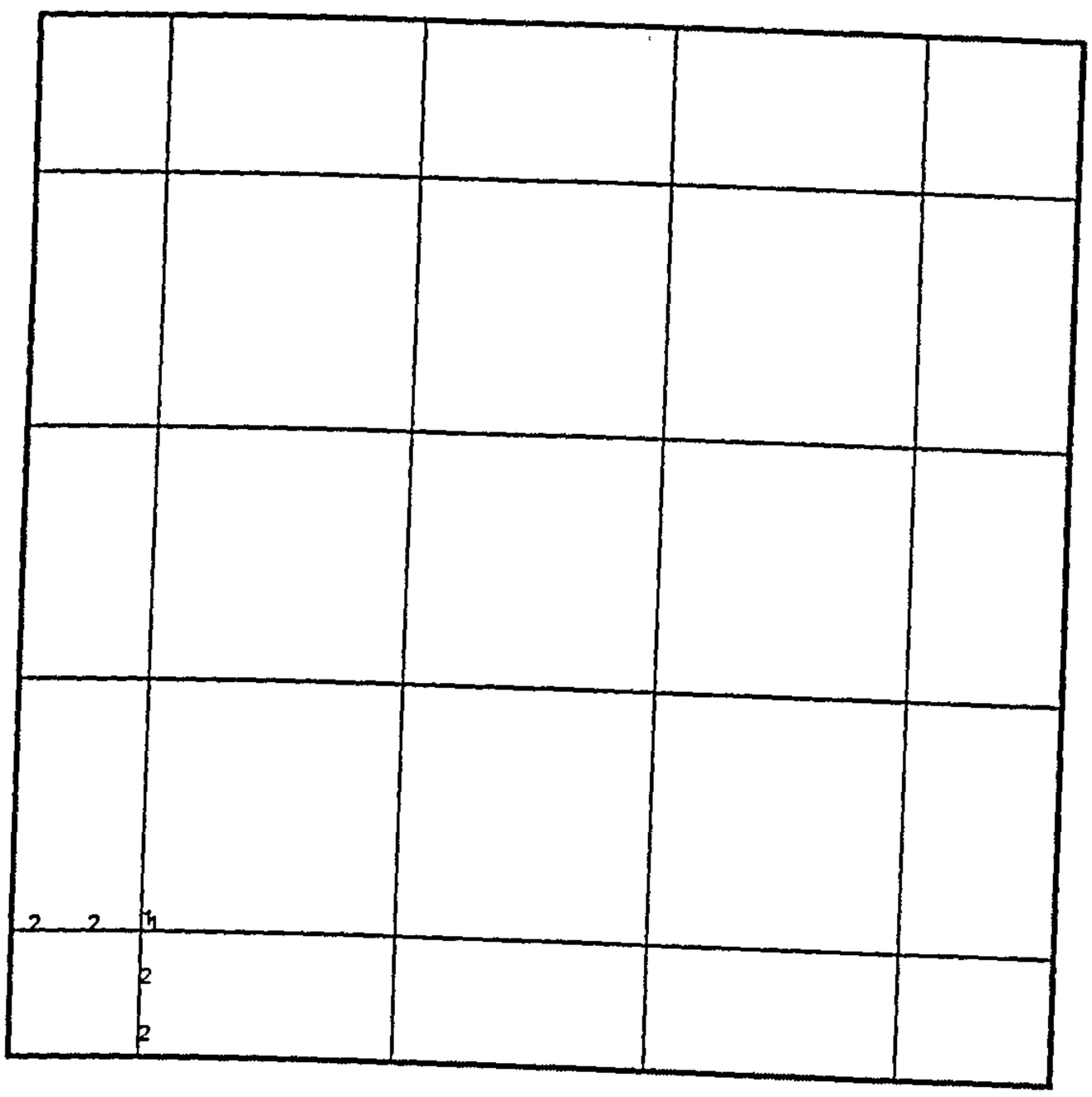

Slab " 4 "

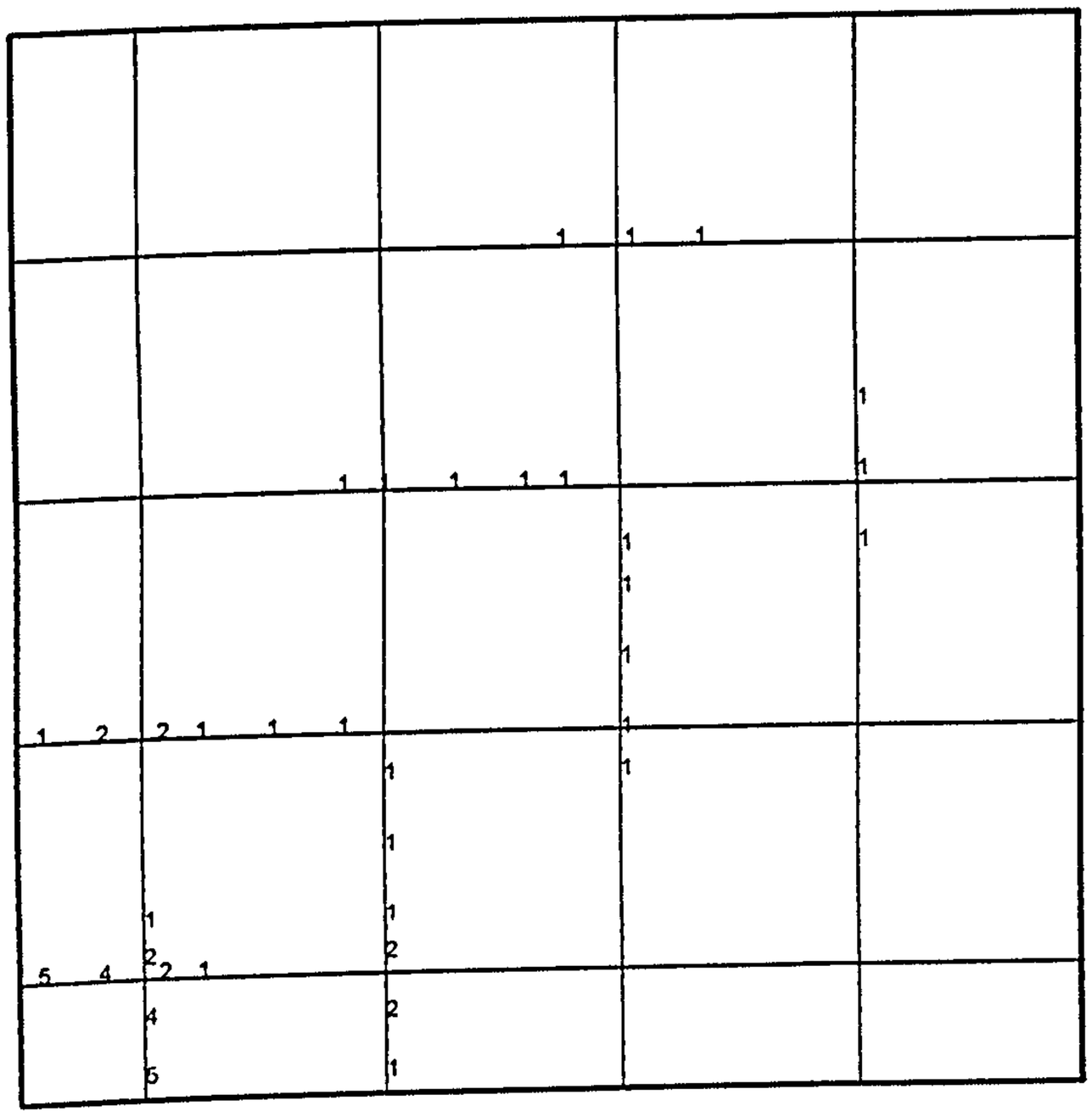

Slab " 5 "

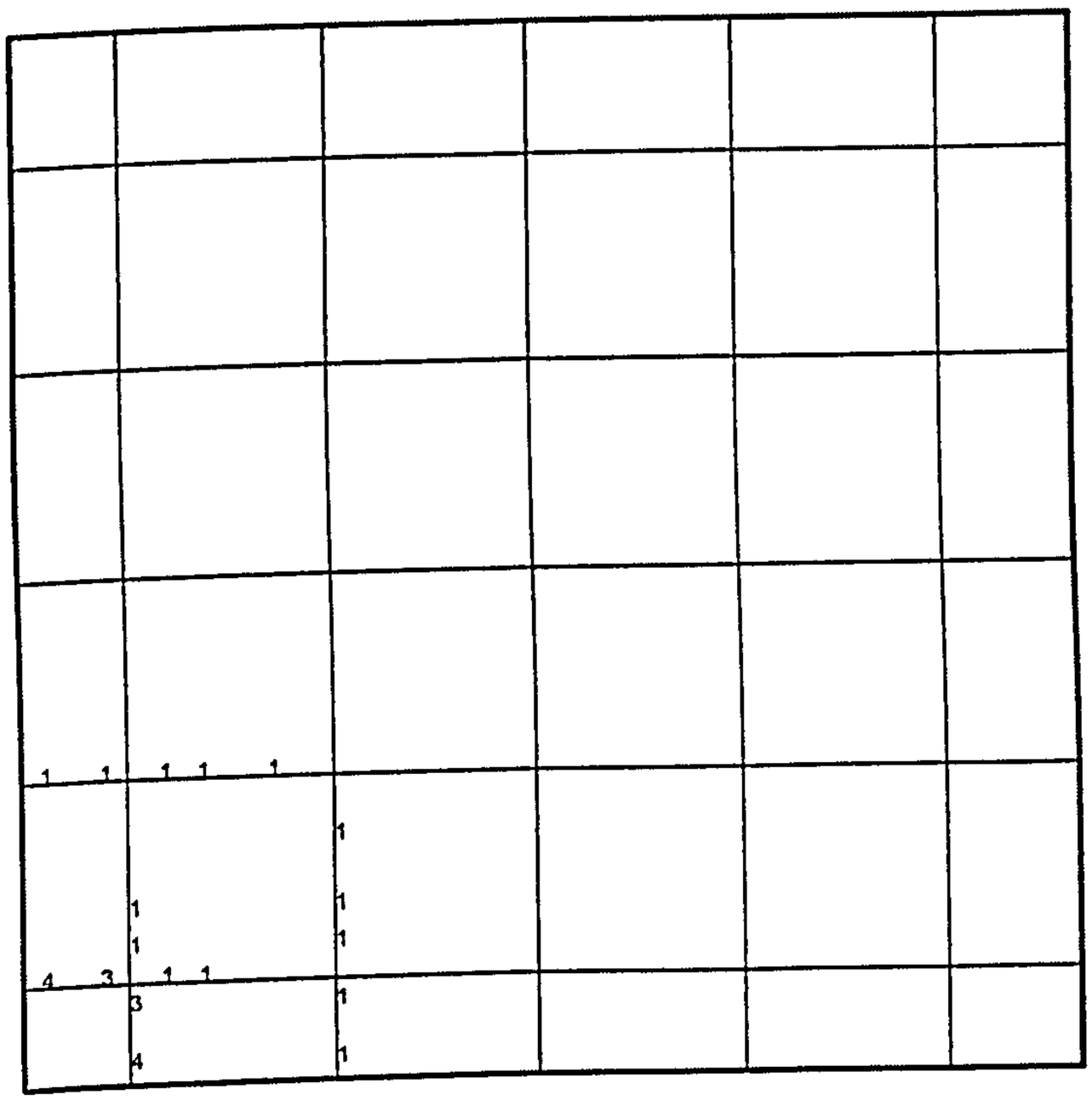

Slab " 6 "

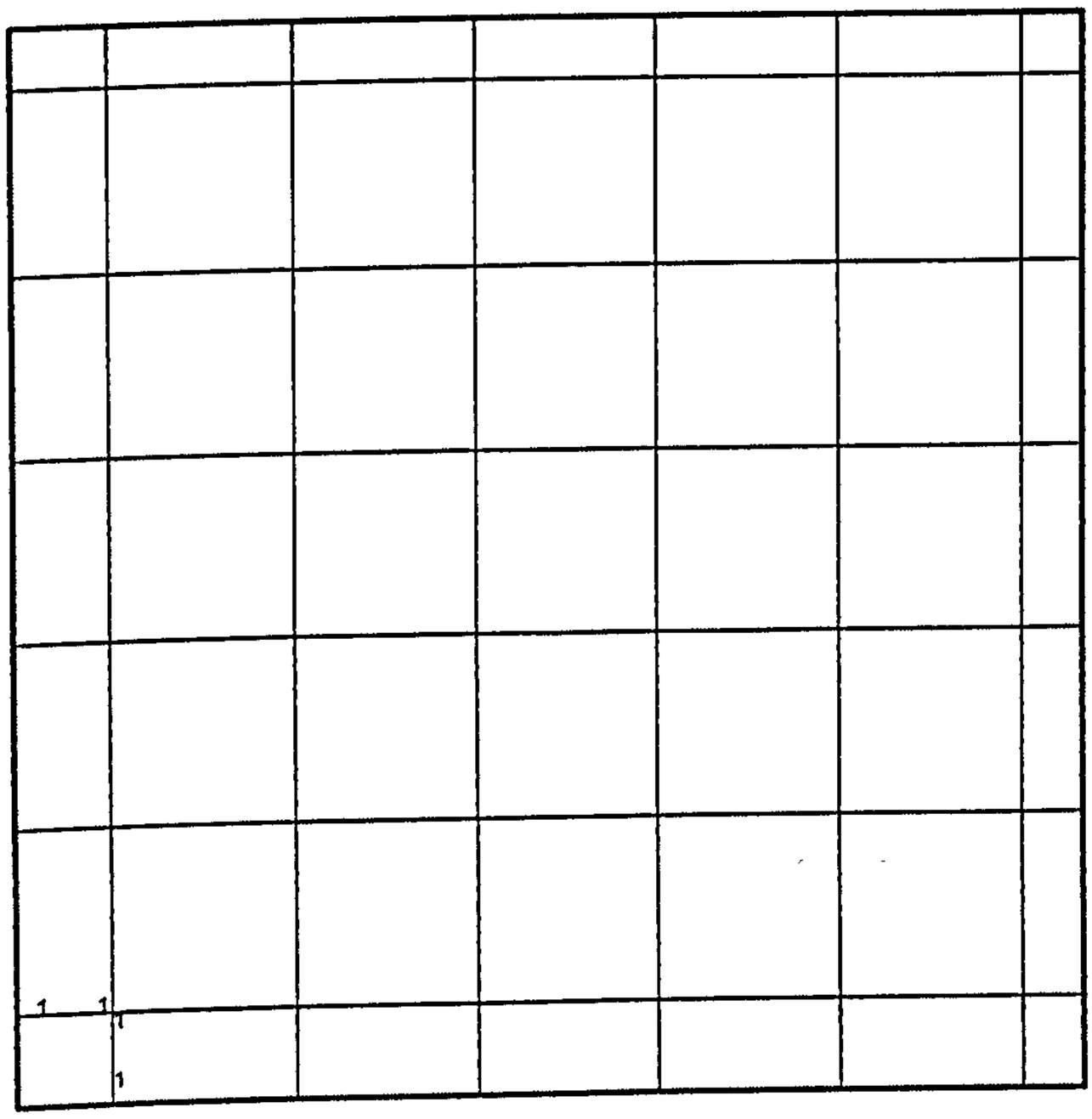

Slab " 7 "

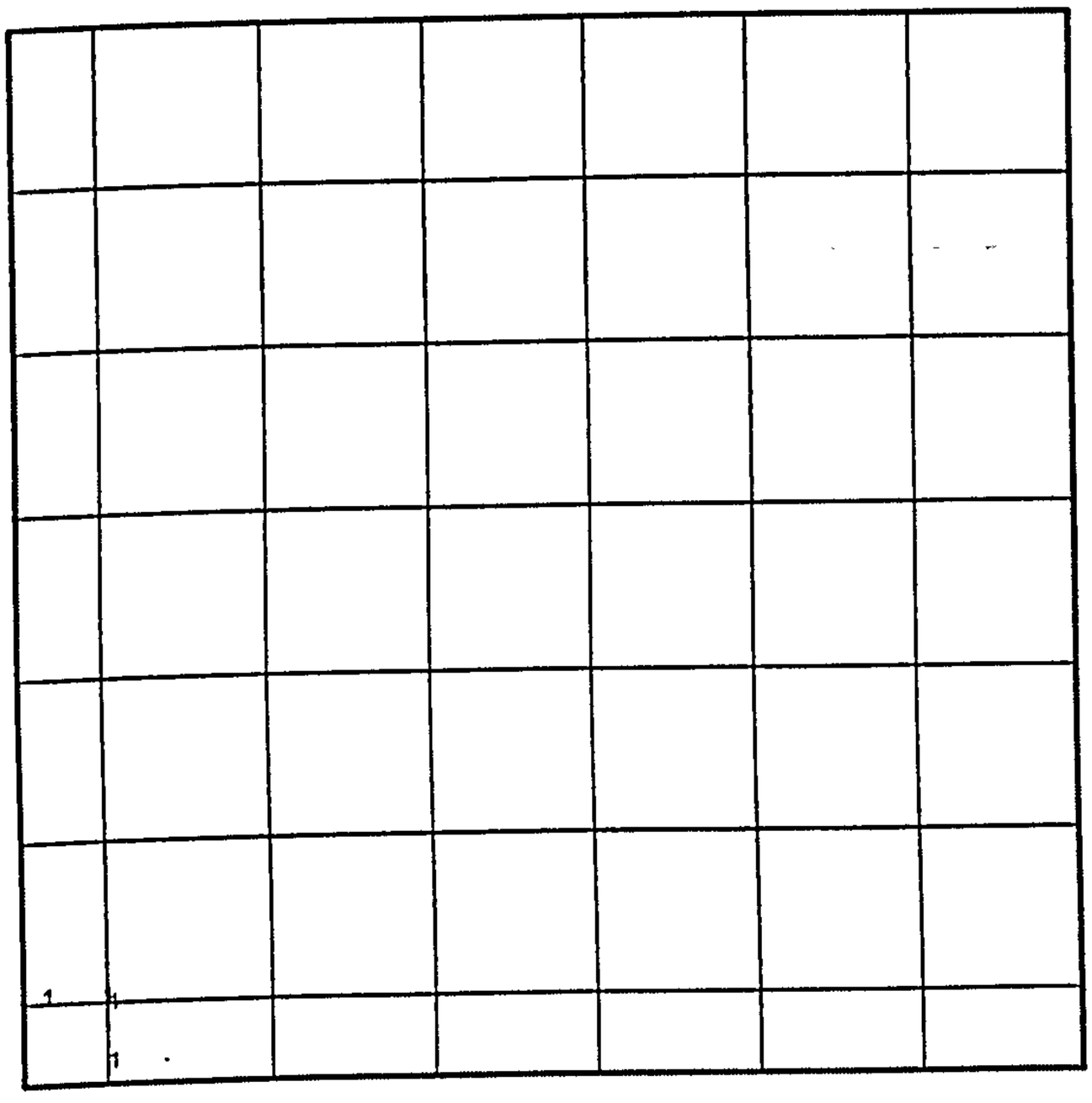

Slab " 8 "

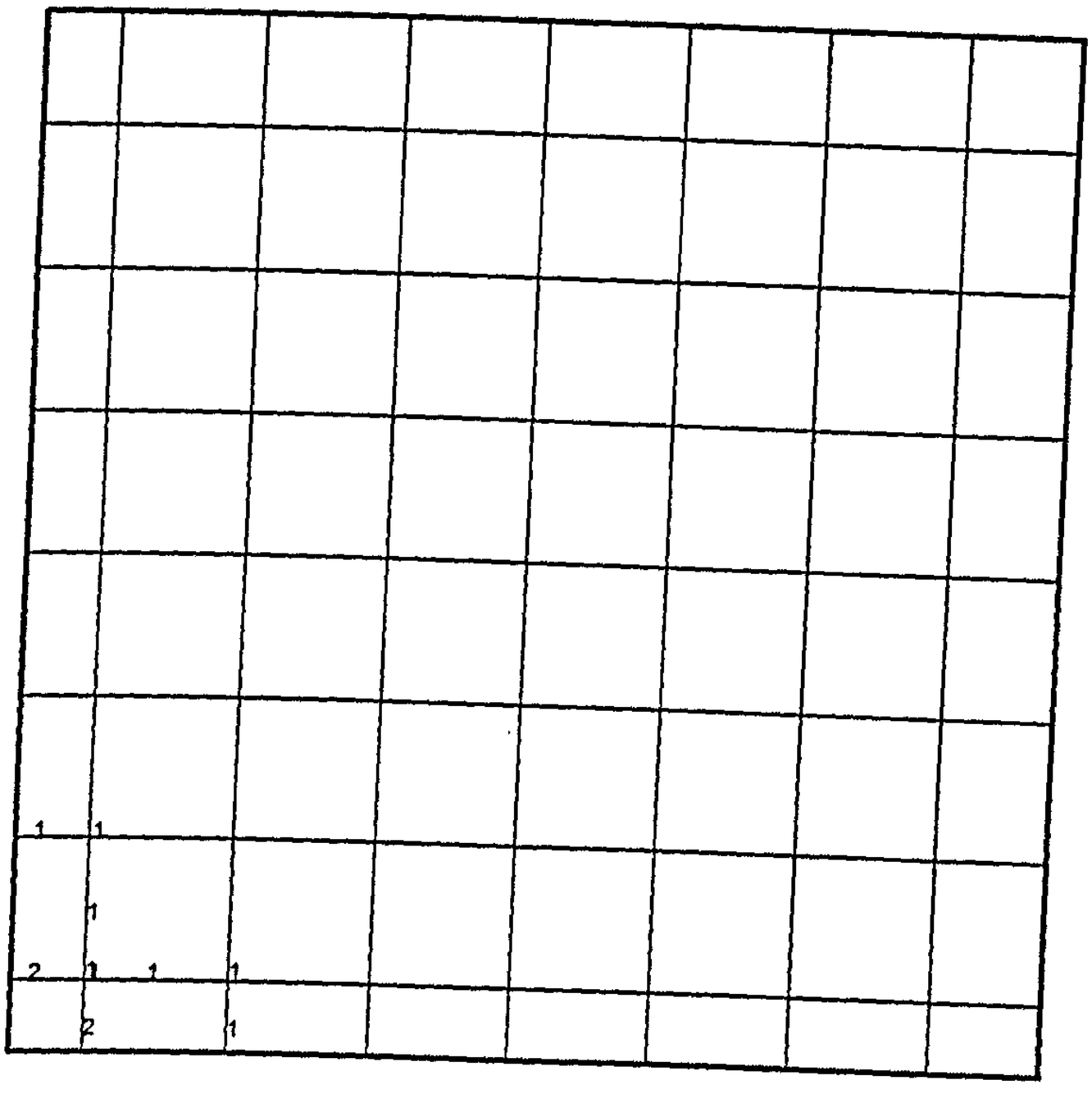

Slab " 9 "

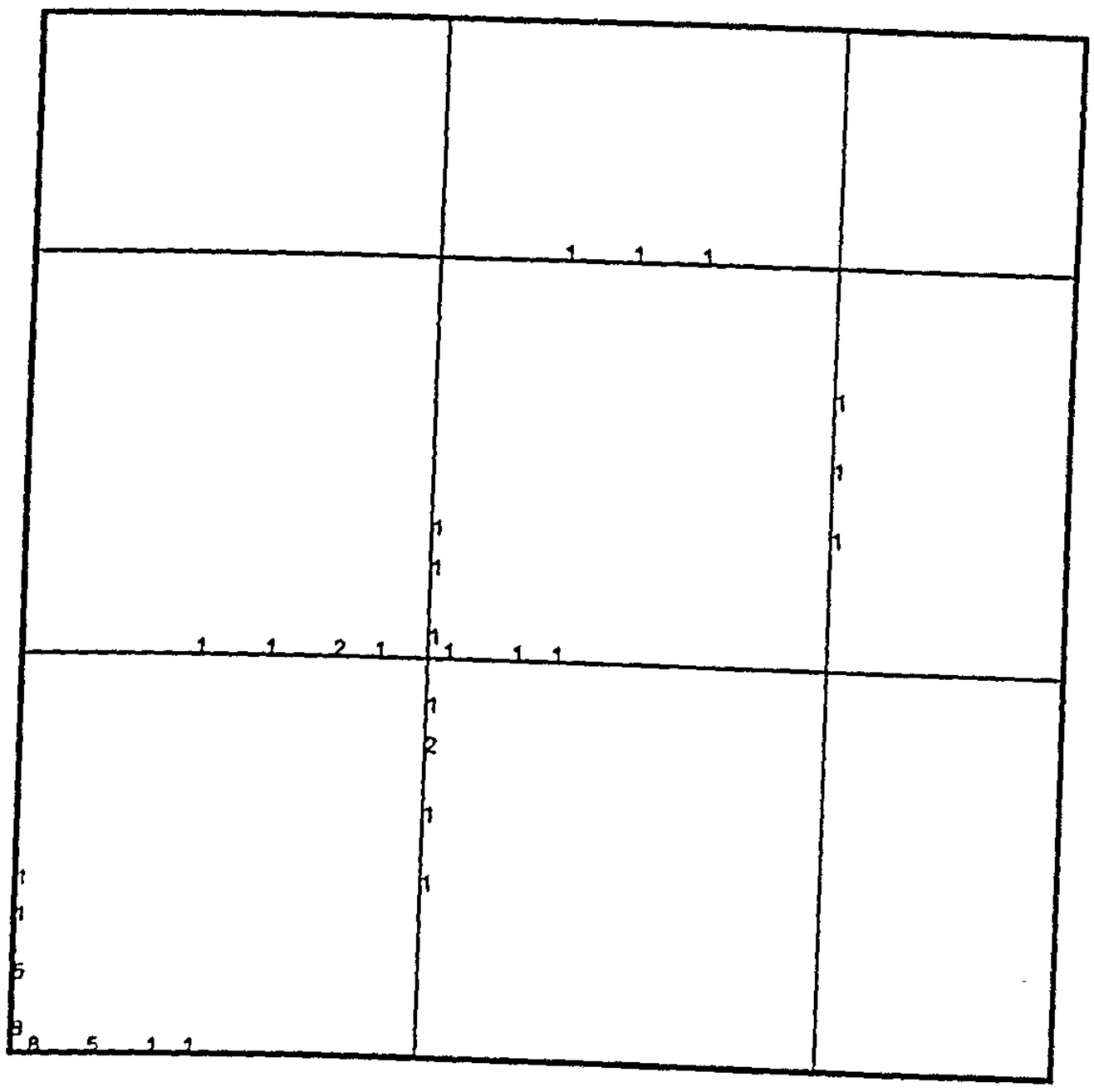

Slab " 10 "

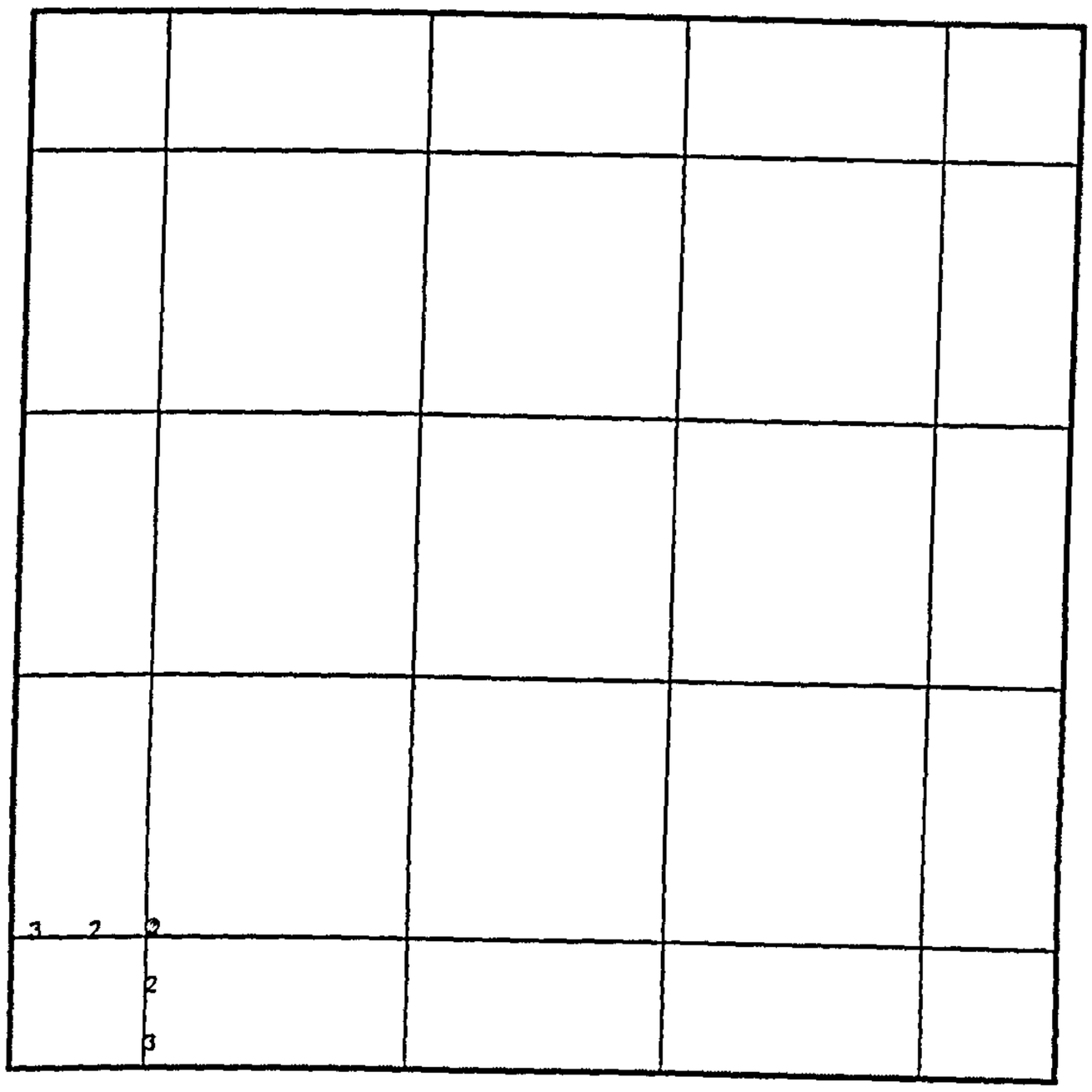

Slab " 11 "

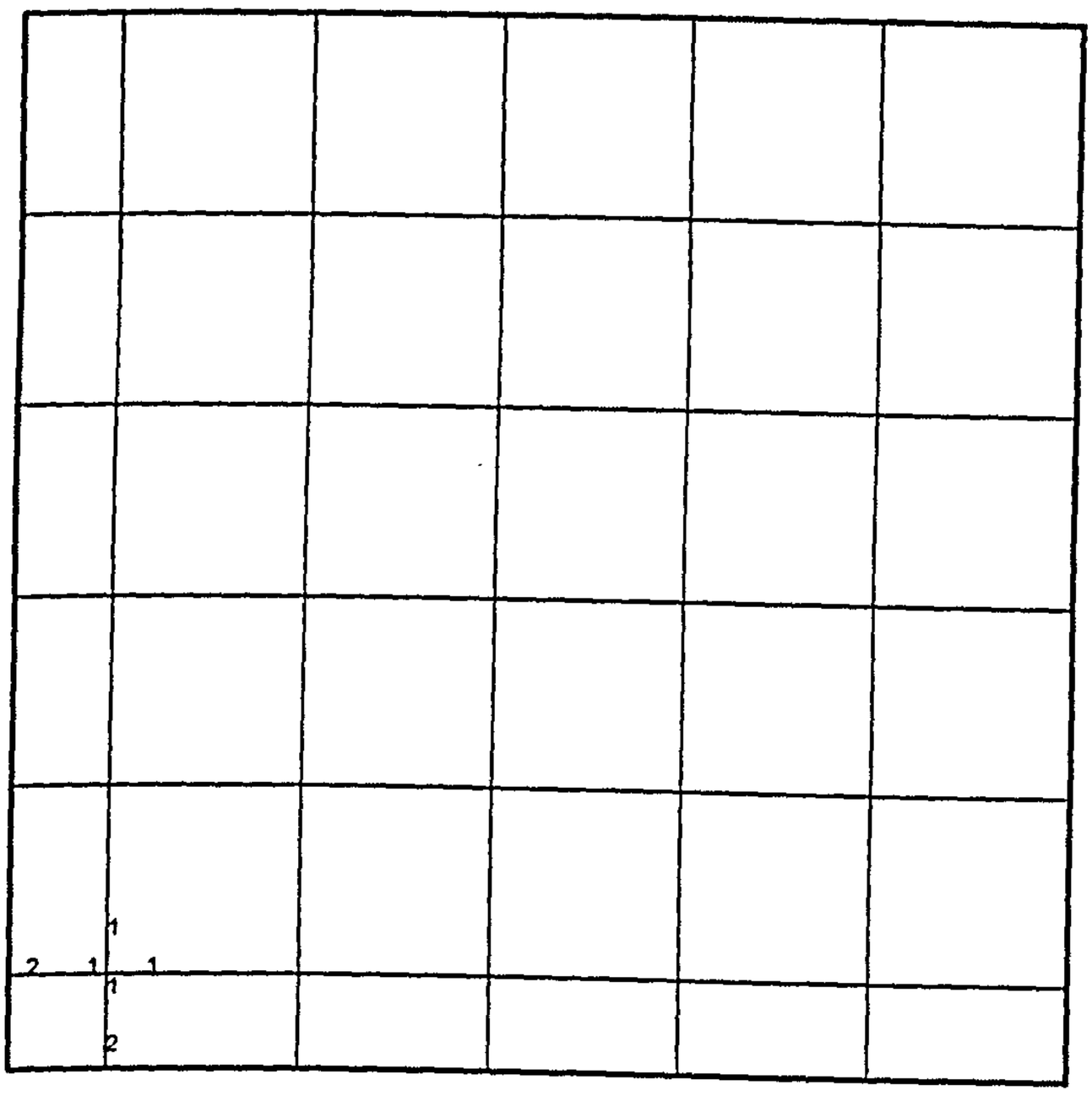

Slab " 12 "

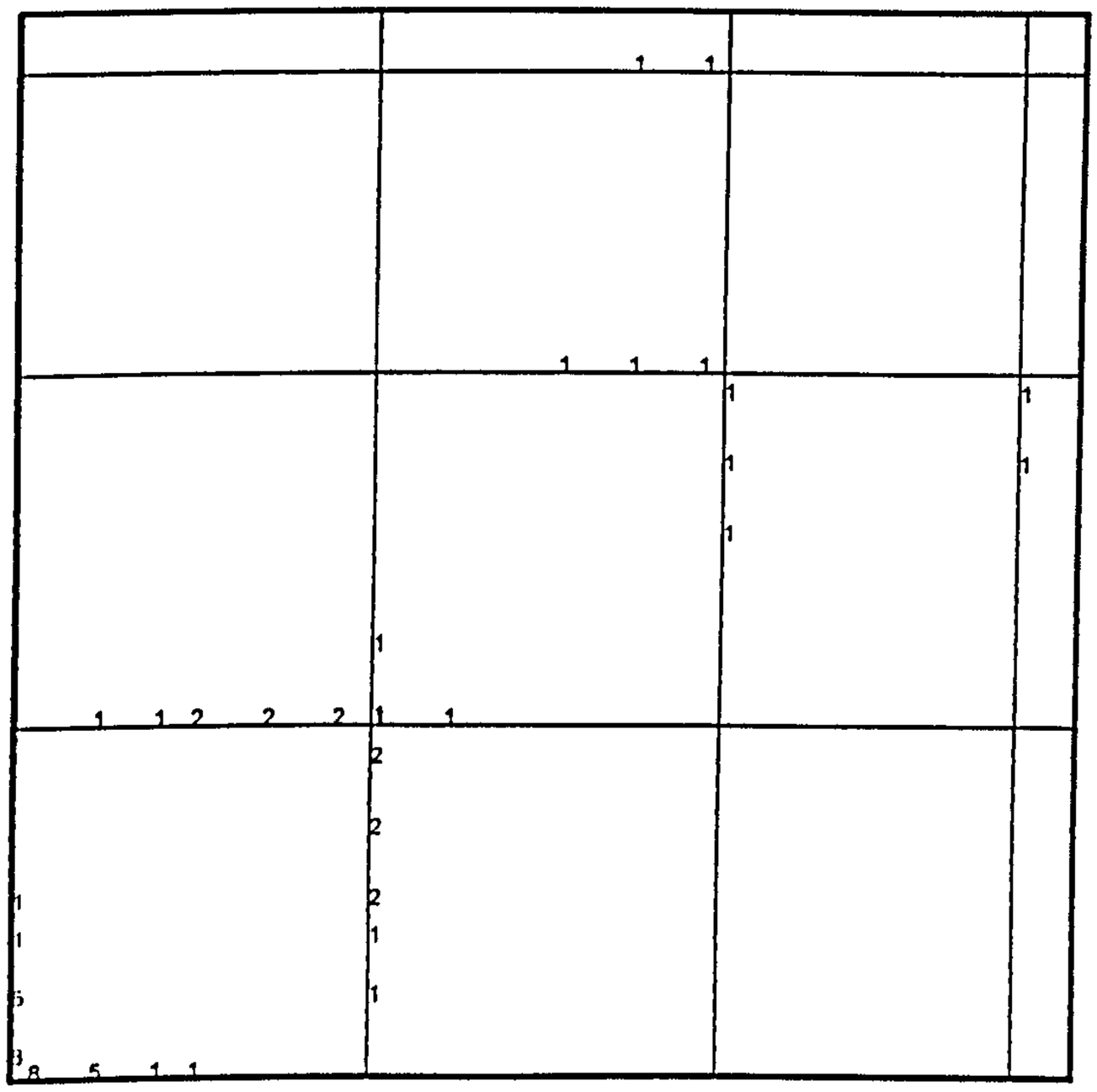

Slab " 13 "

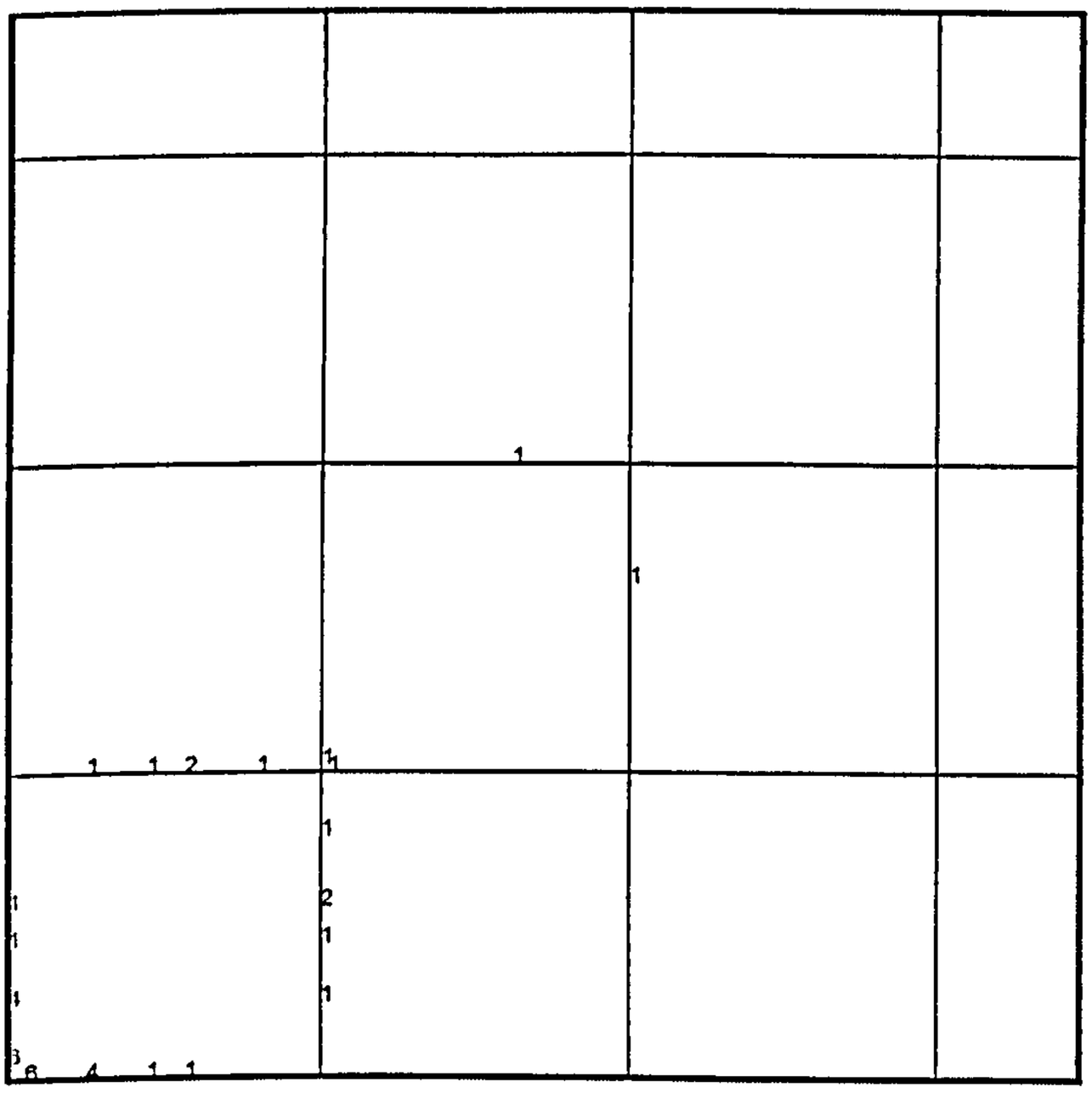

Slab " 14 "

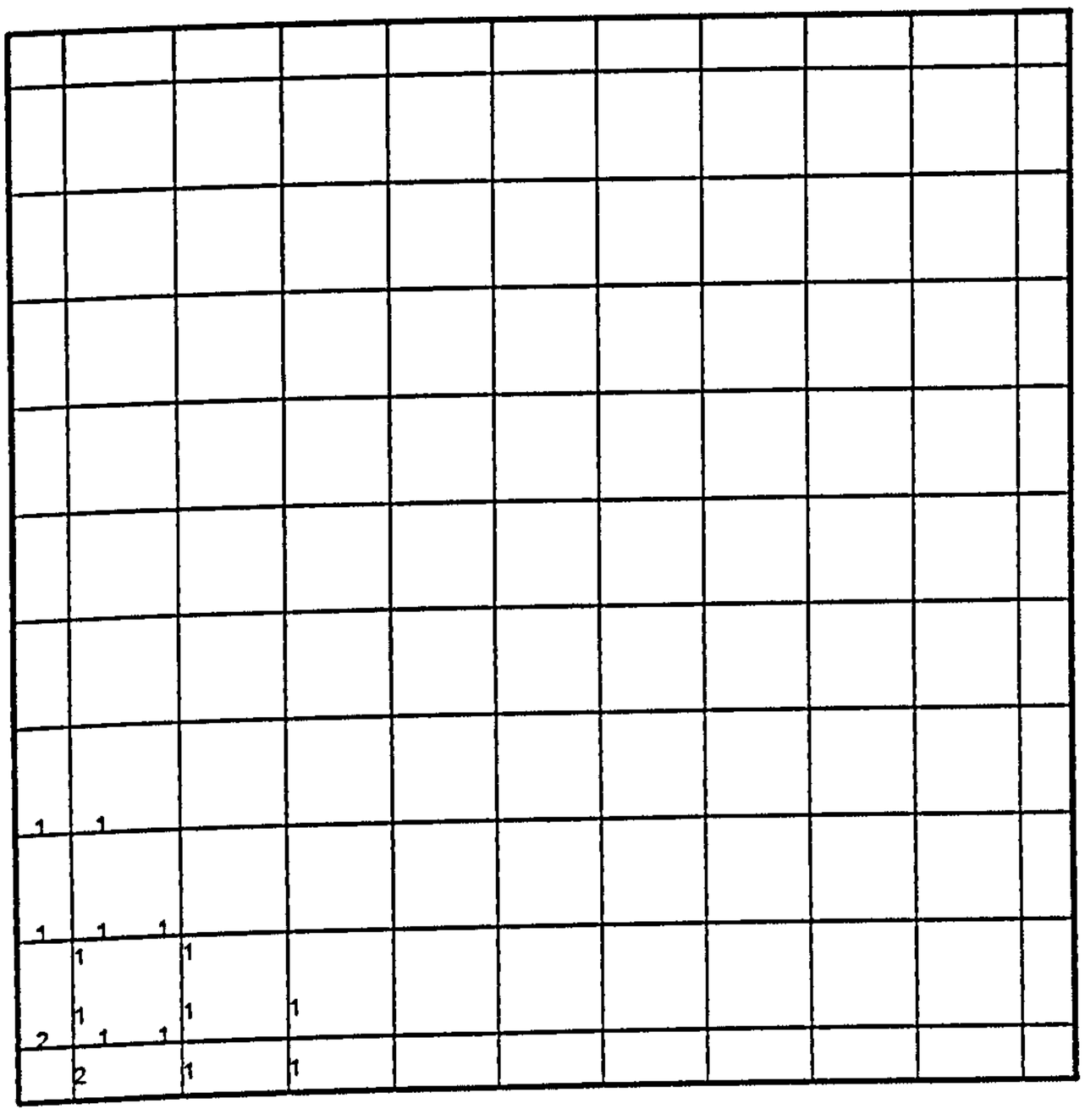

Slab " 15 "

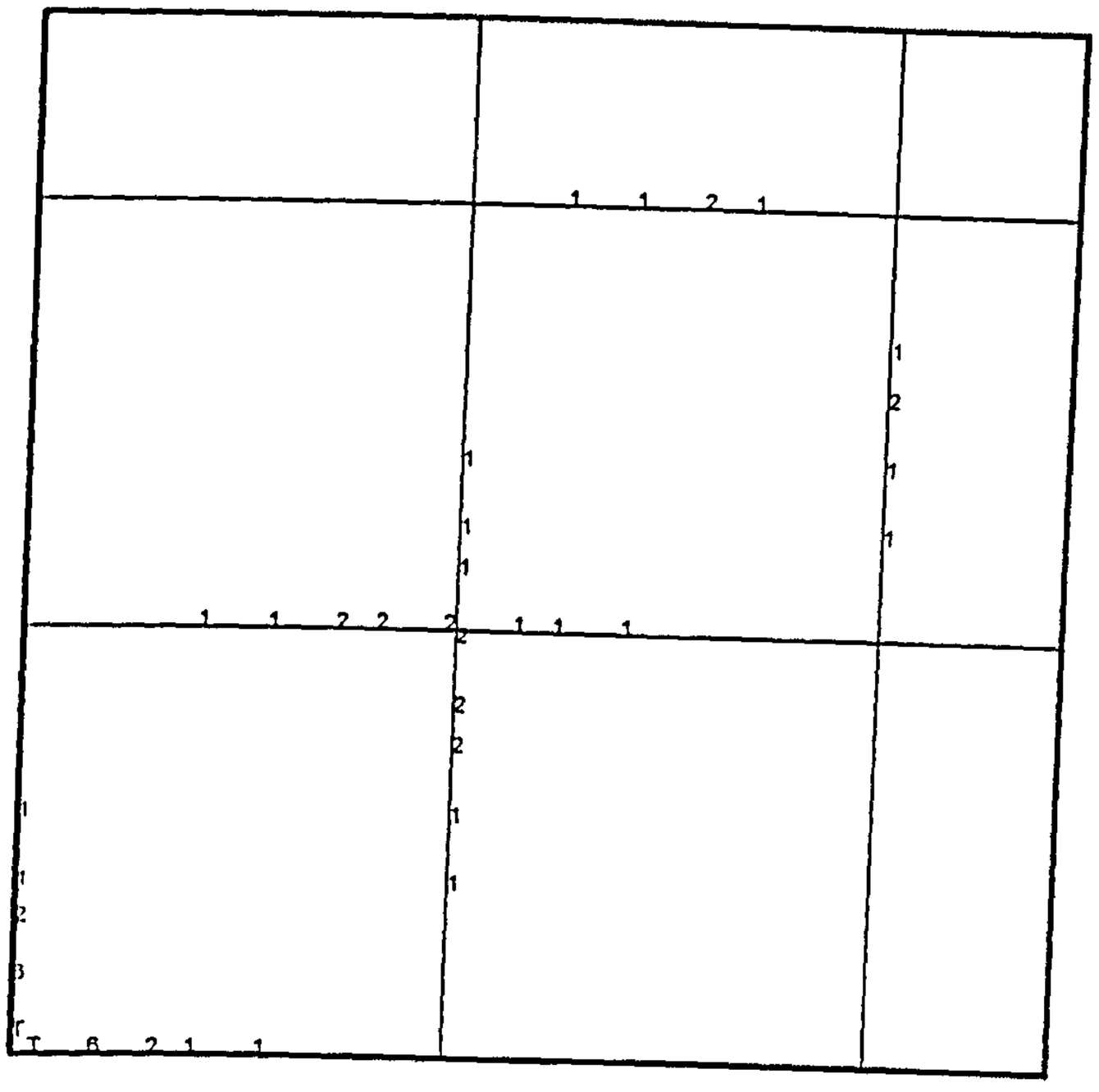

Slab "1A"

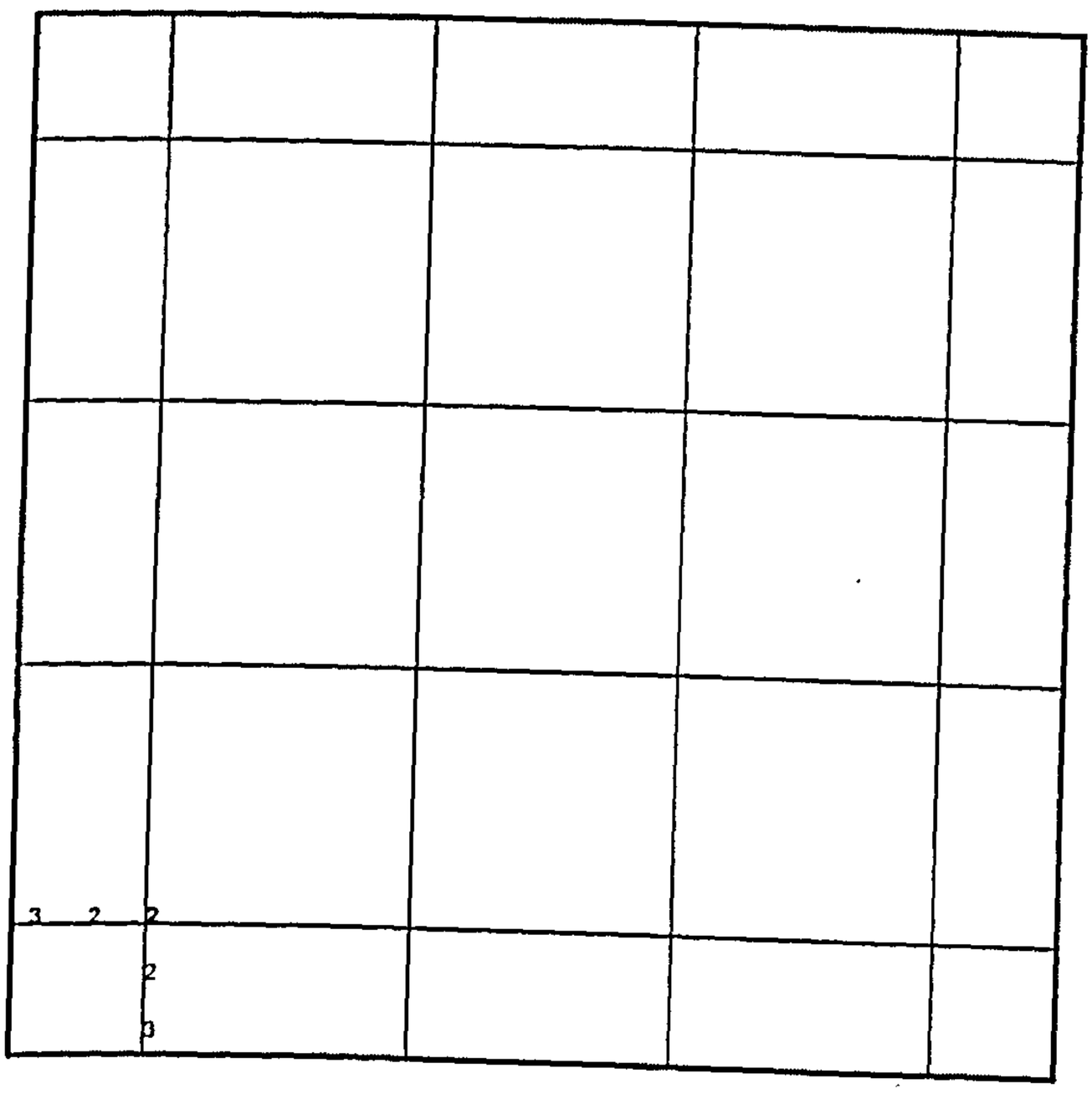

Slab "2A"

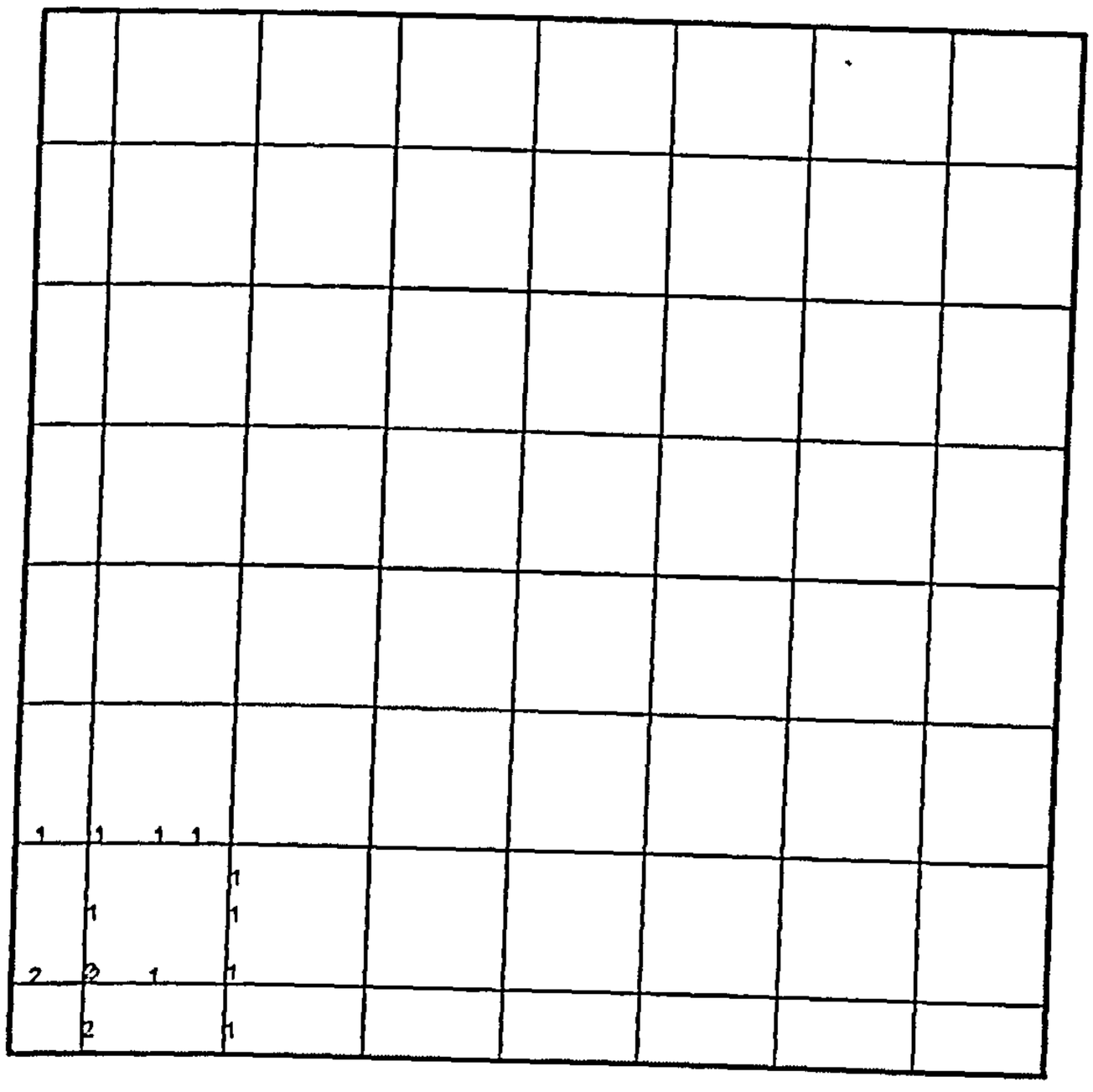

Slab "3A"

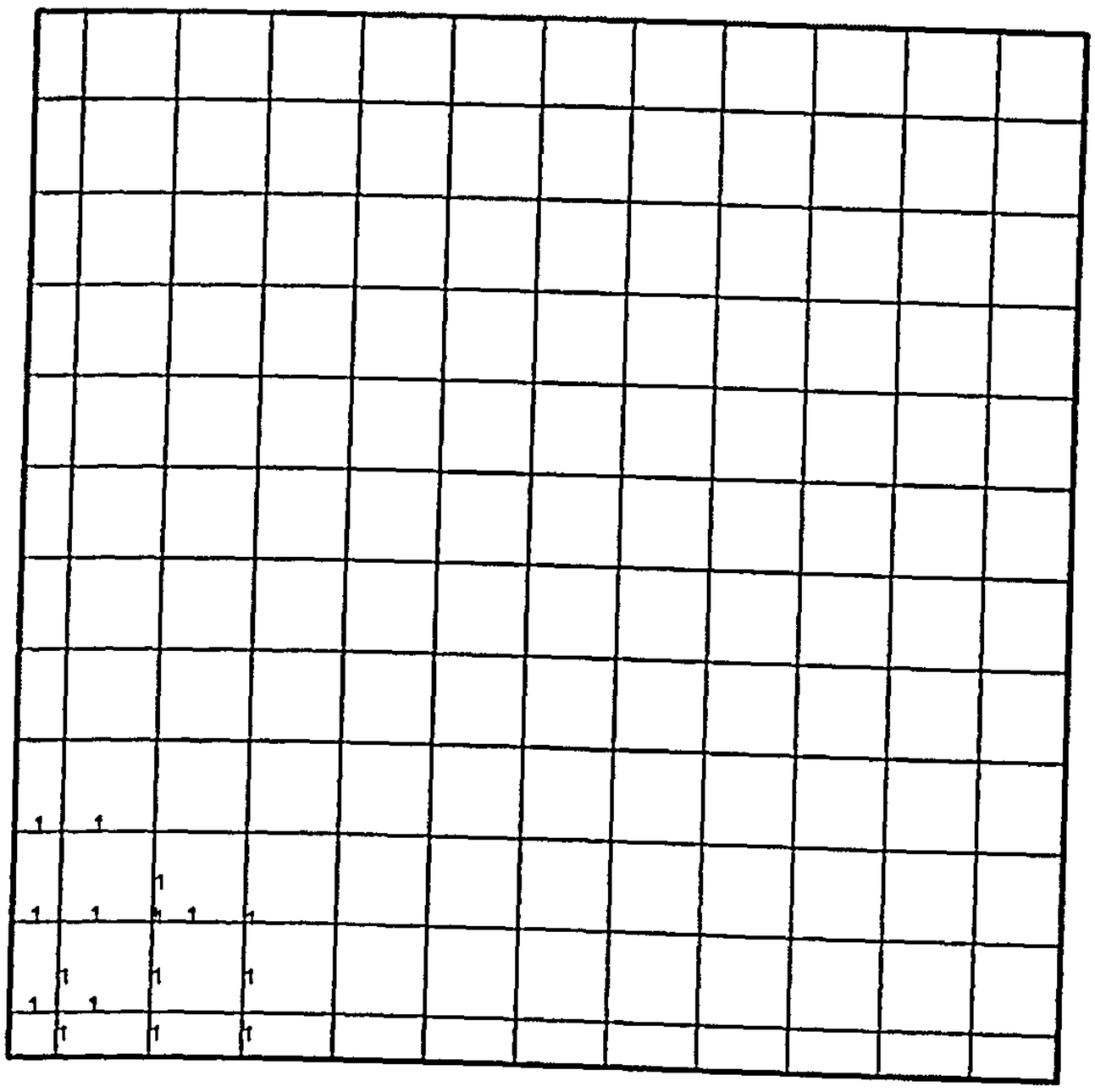

Slab "4A"

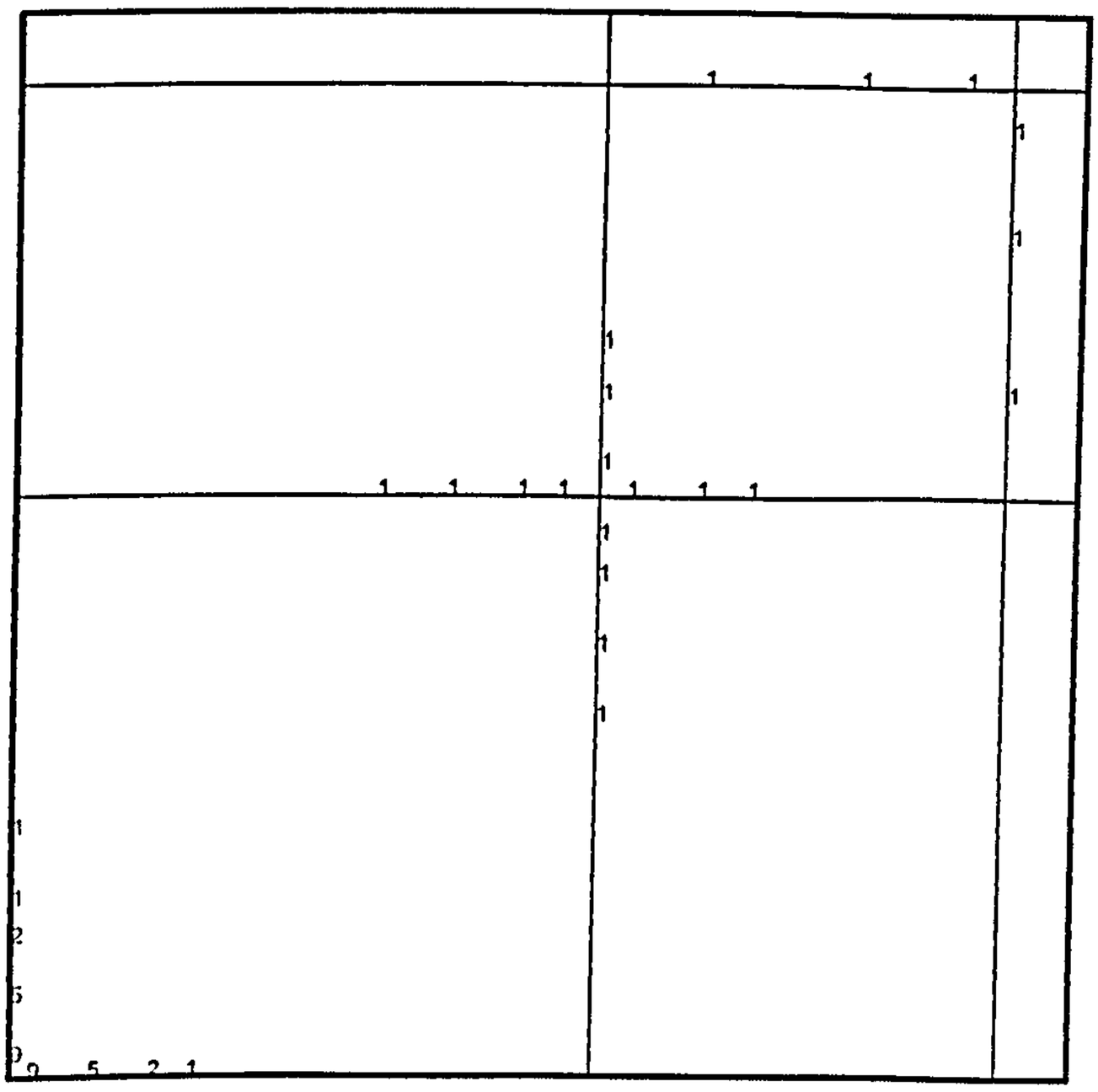

Slab "1B"

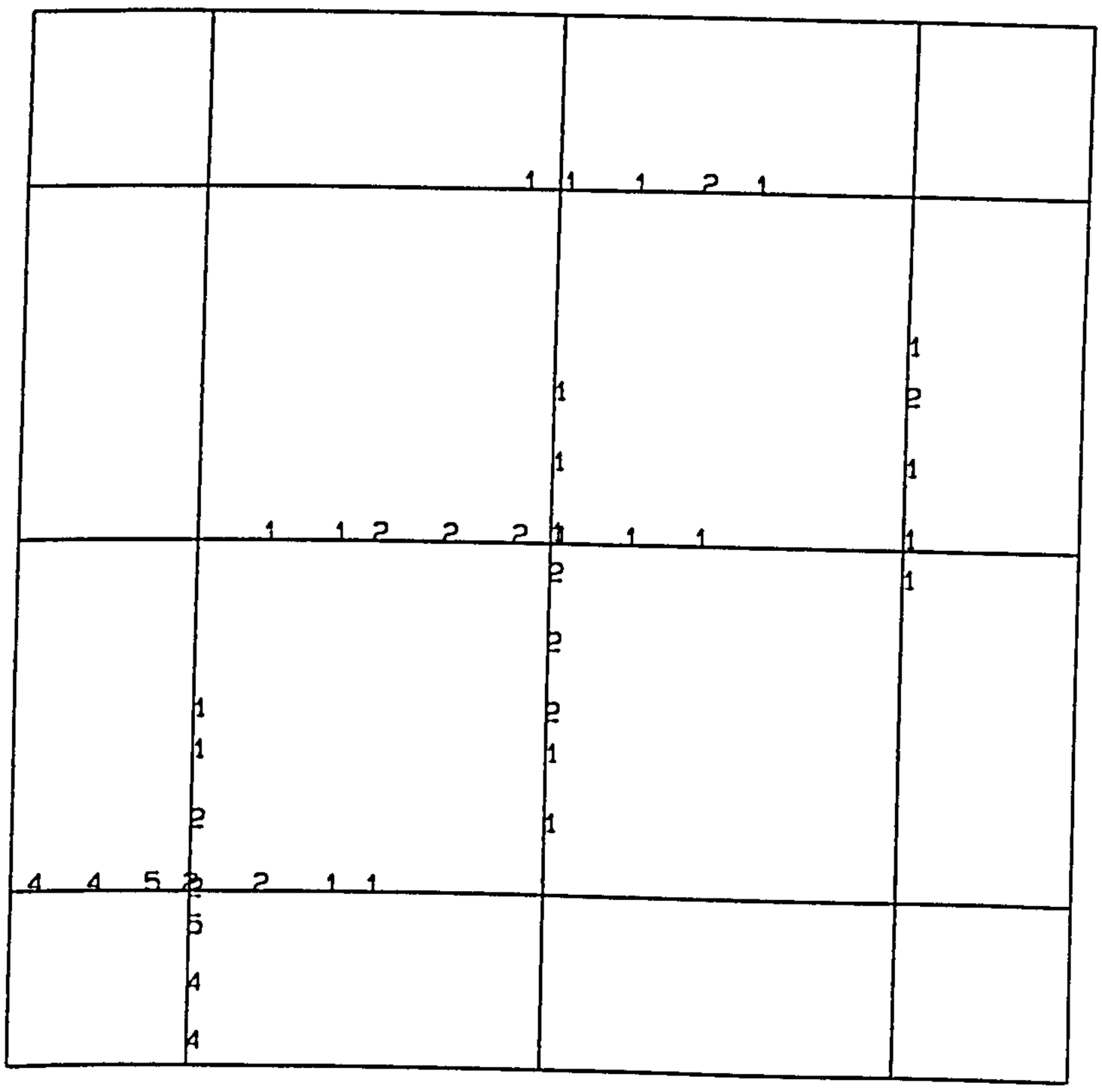

Slab "2B"

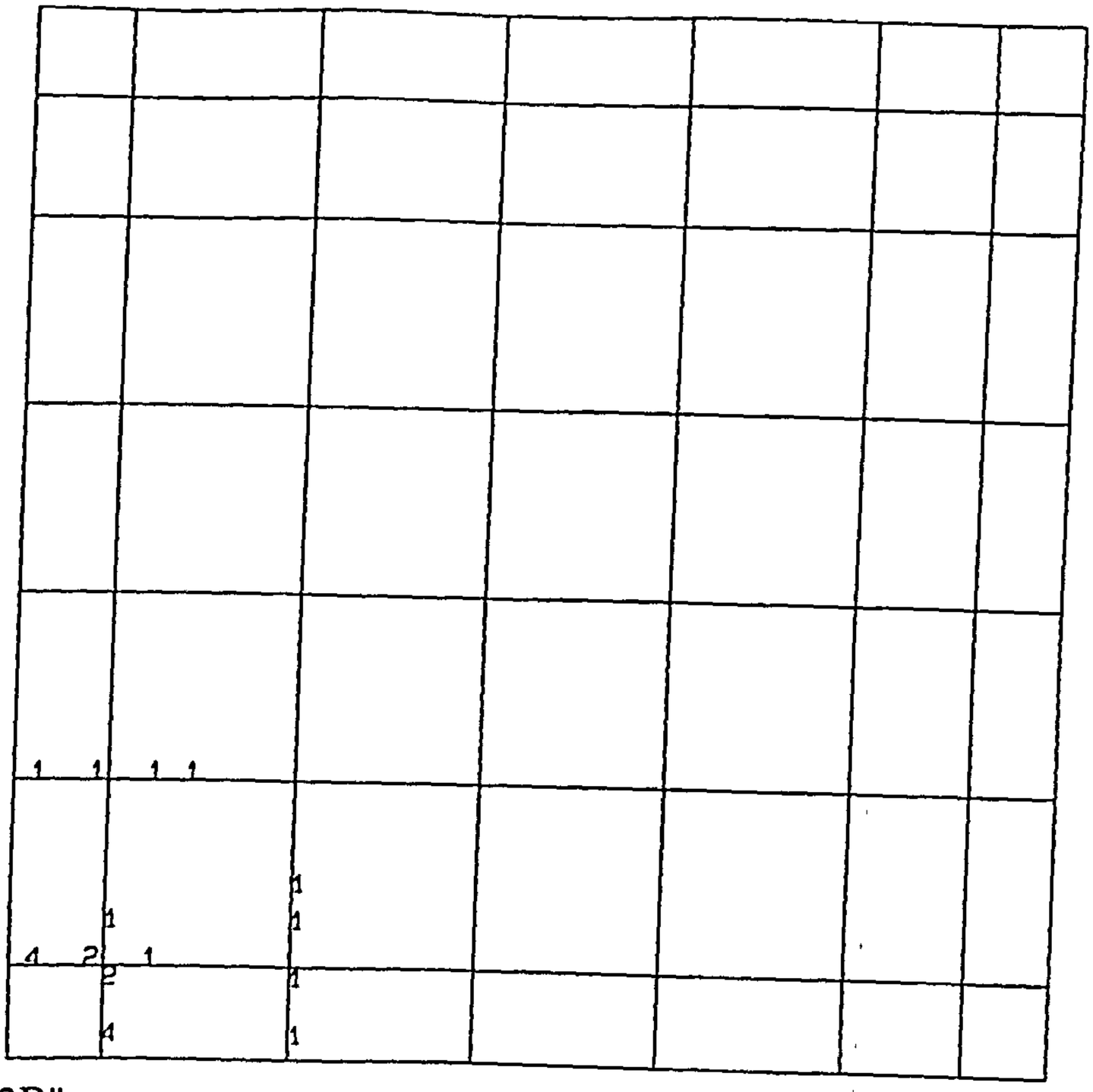

Slab "3B"

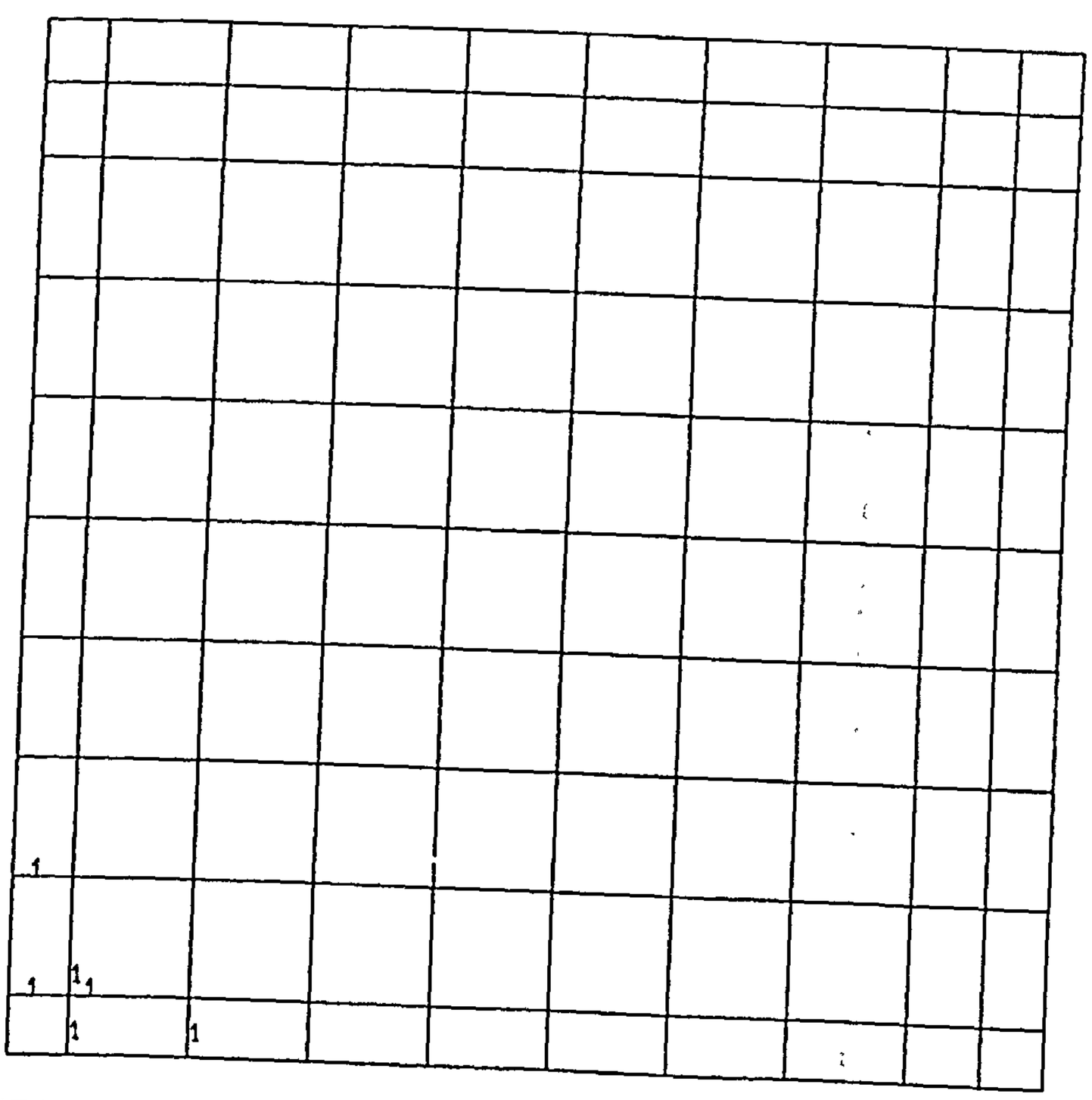

Slab "4B"

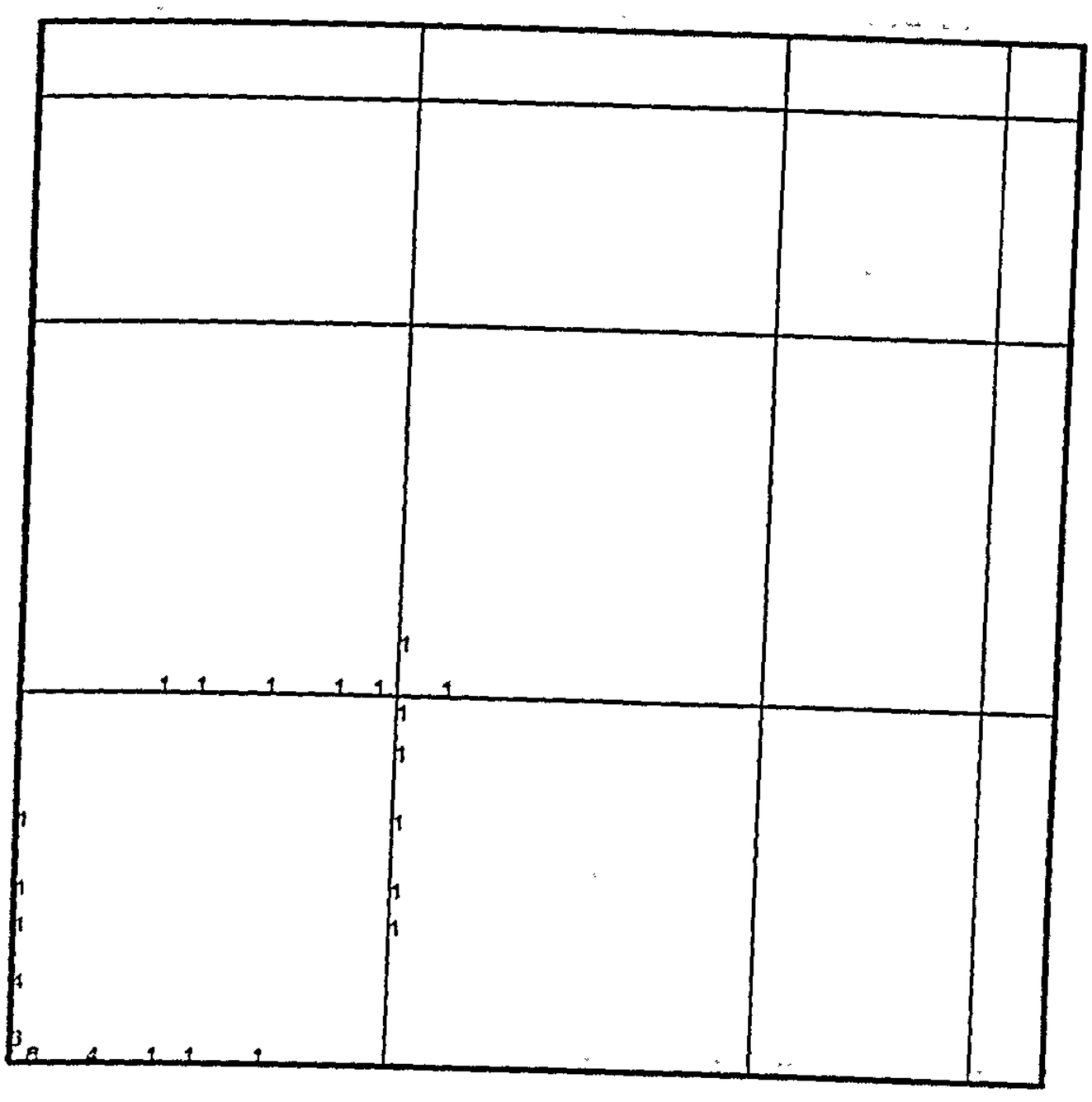

Slab "1C"

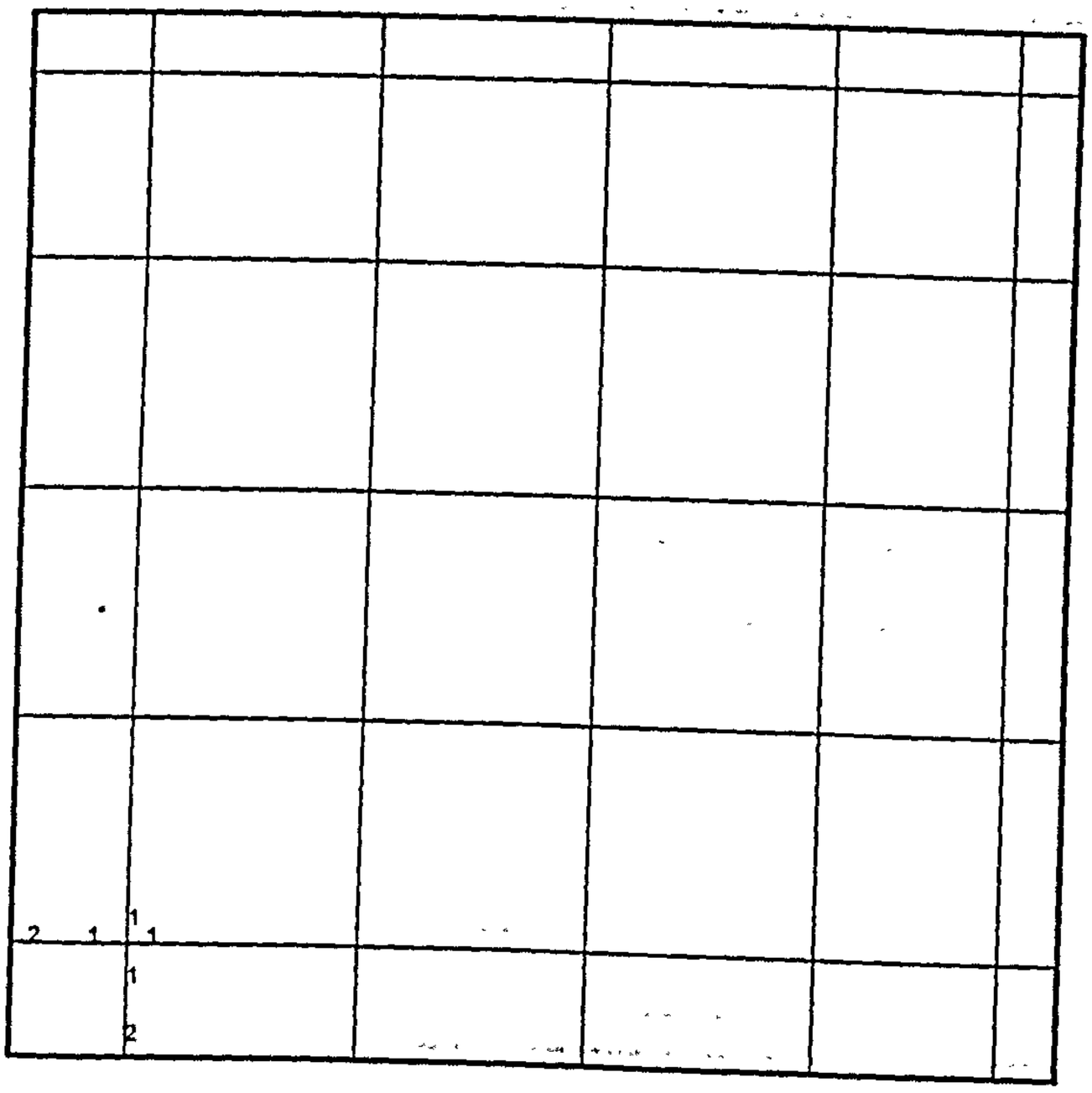

Slab "2C"

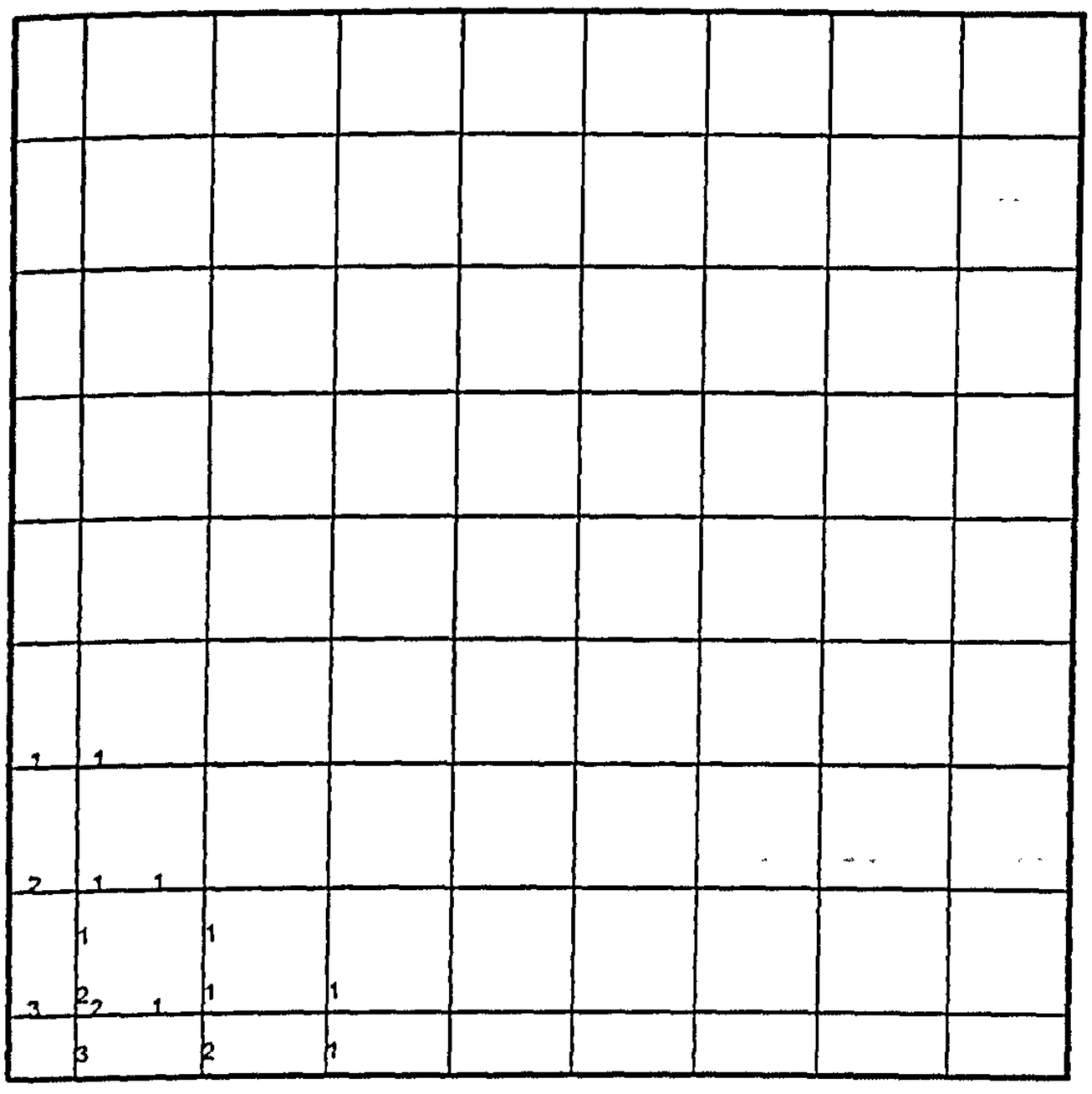

Slab "3C"

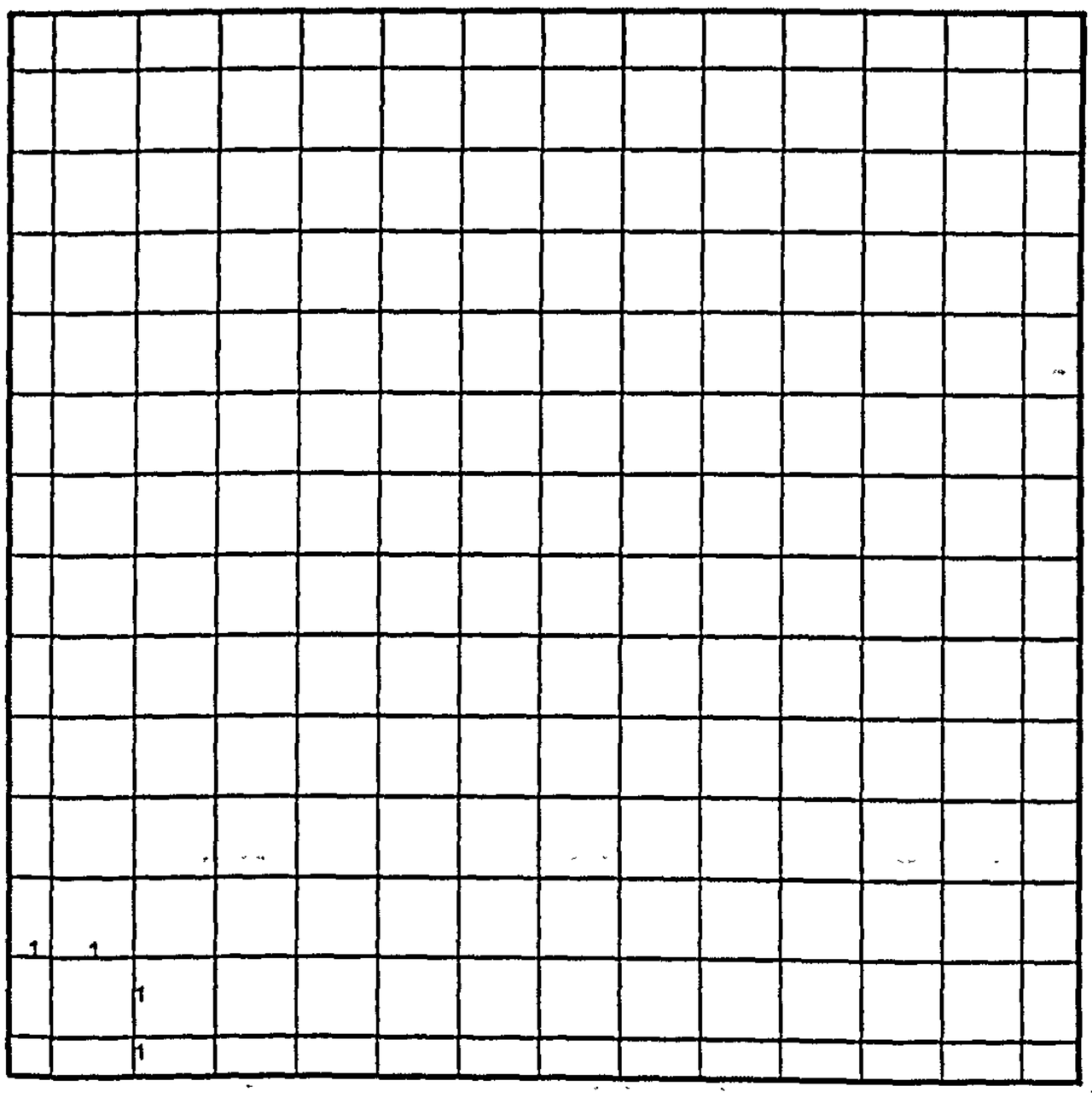

Slab "4C"

Conventional slabs tested by Rankin

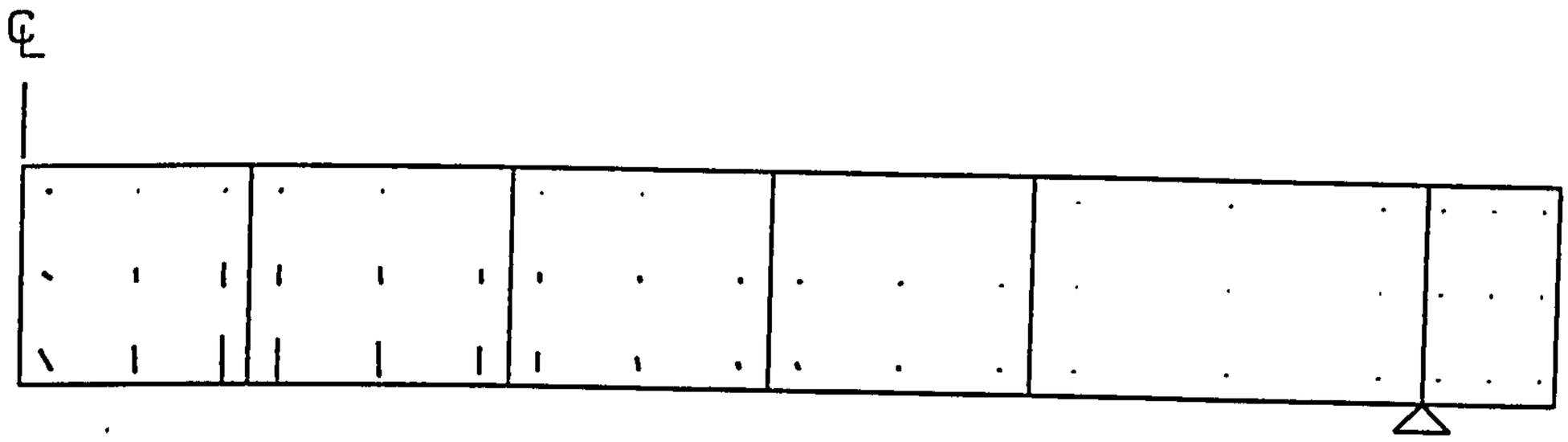

"1"

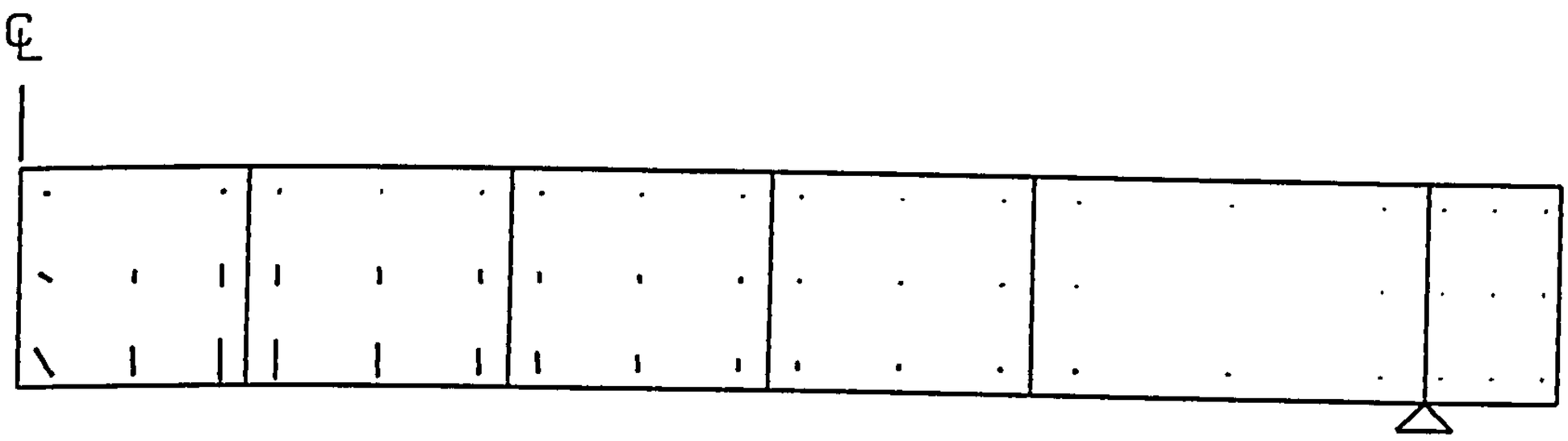

"2"

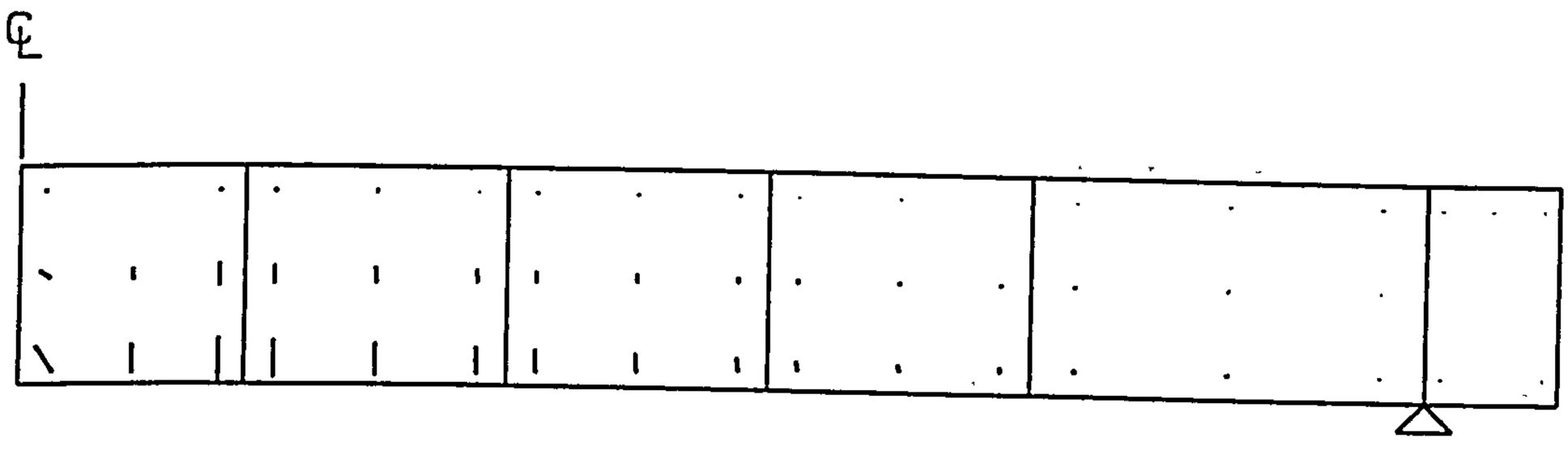

"3"

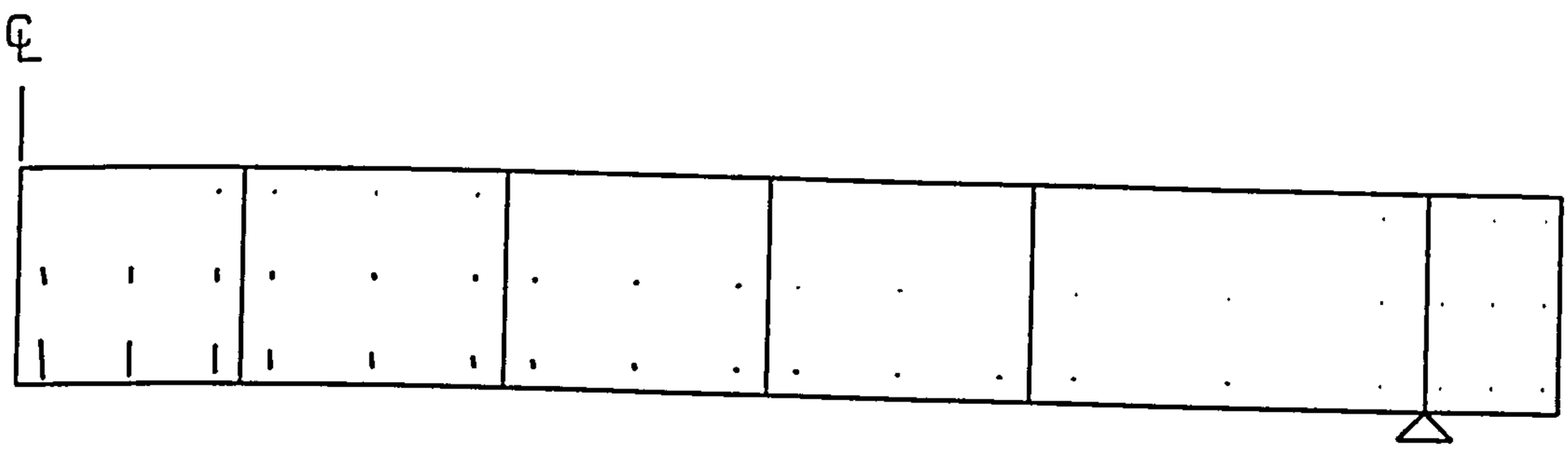

"4"

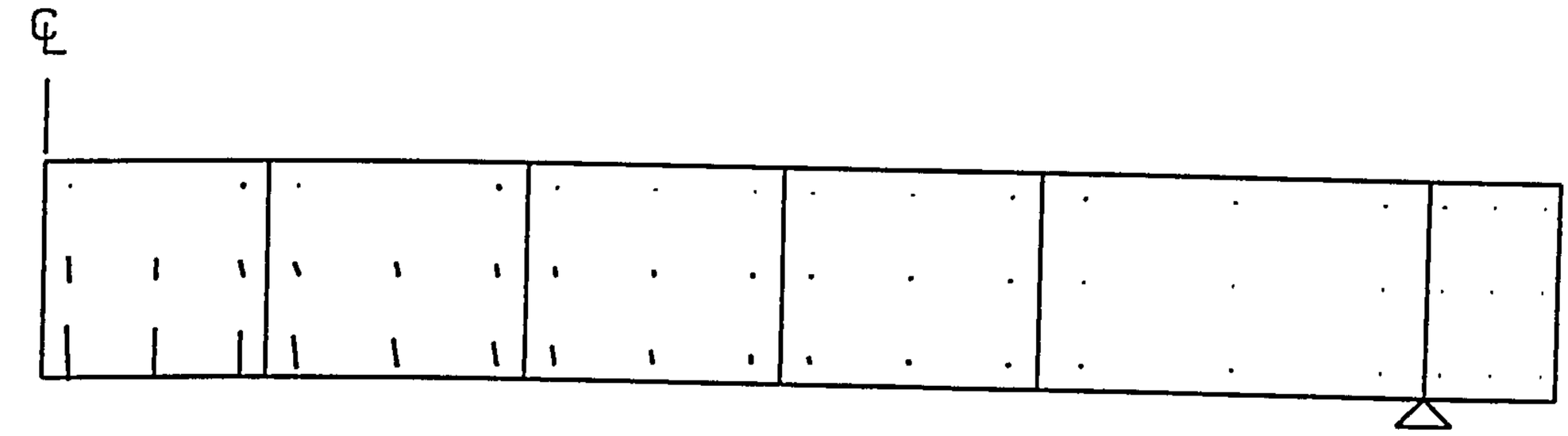

"5"

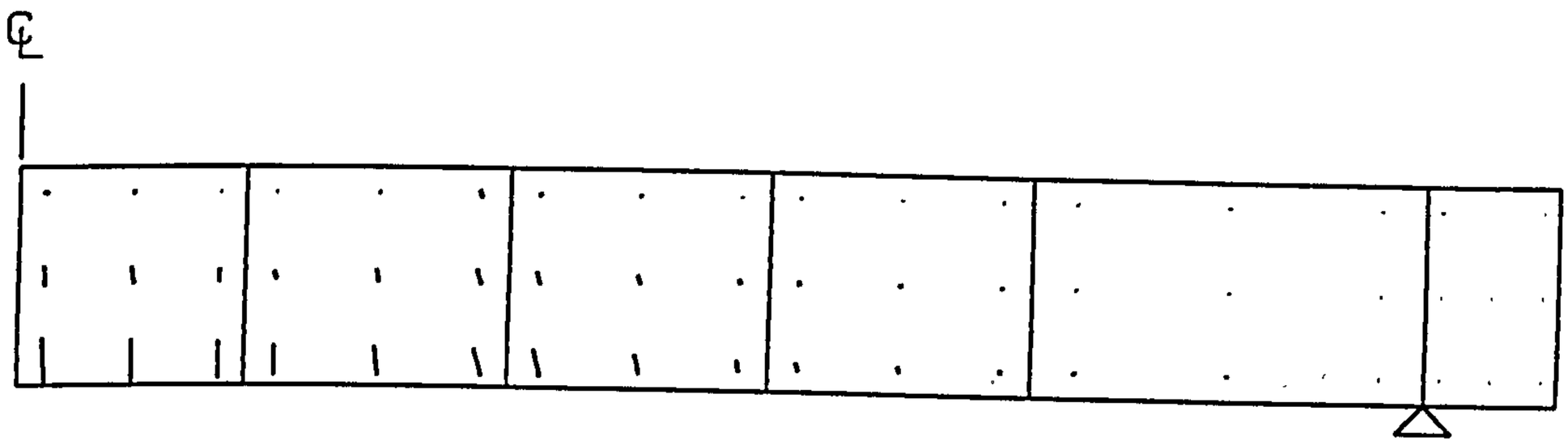

"6"

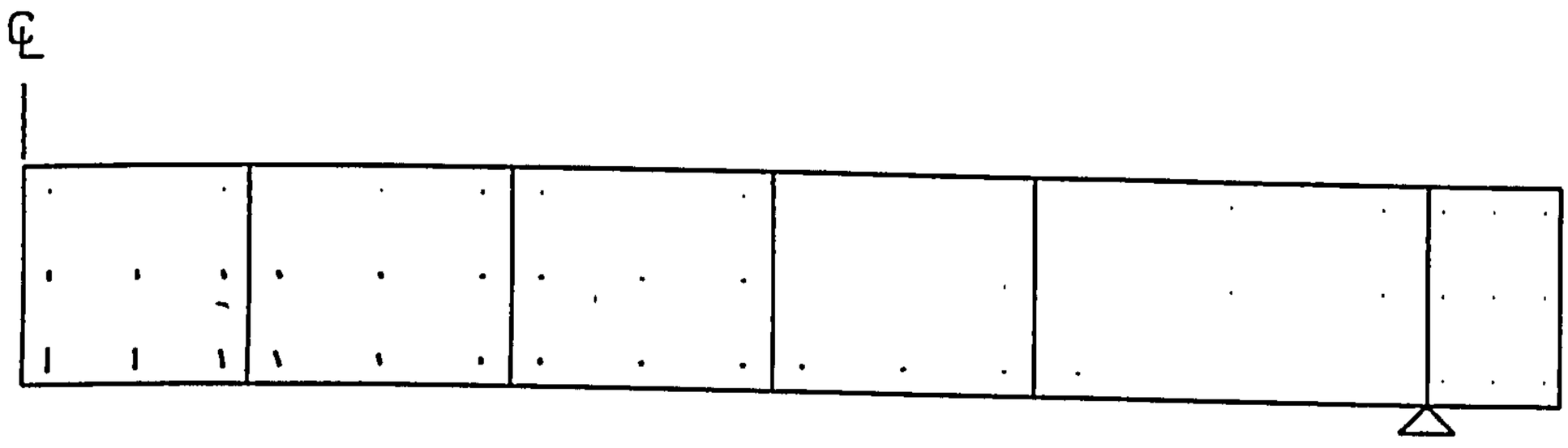

"7"

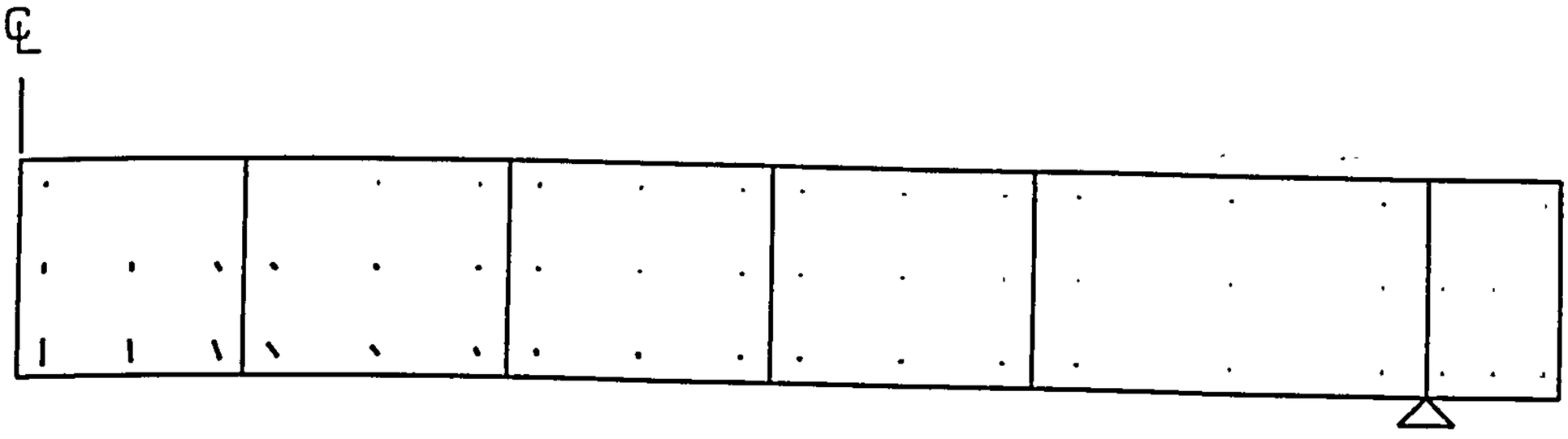

"8"

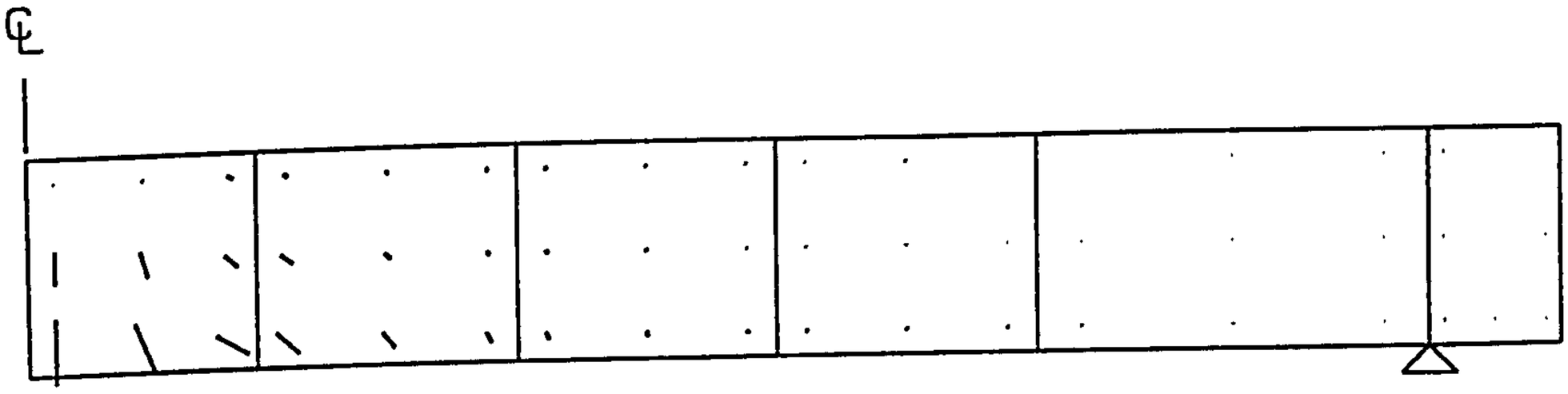

" 9 "

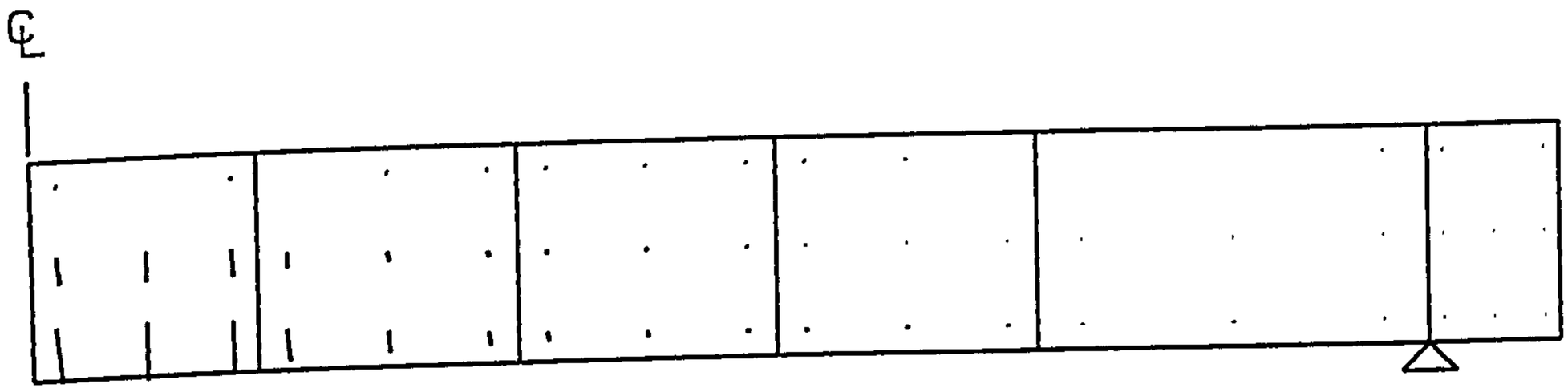

" 10 "

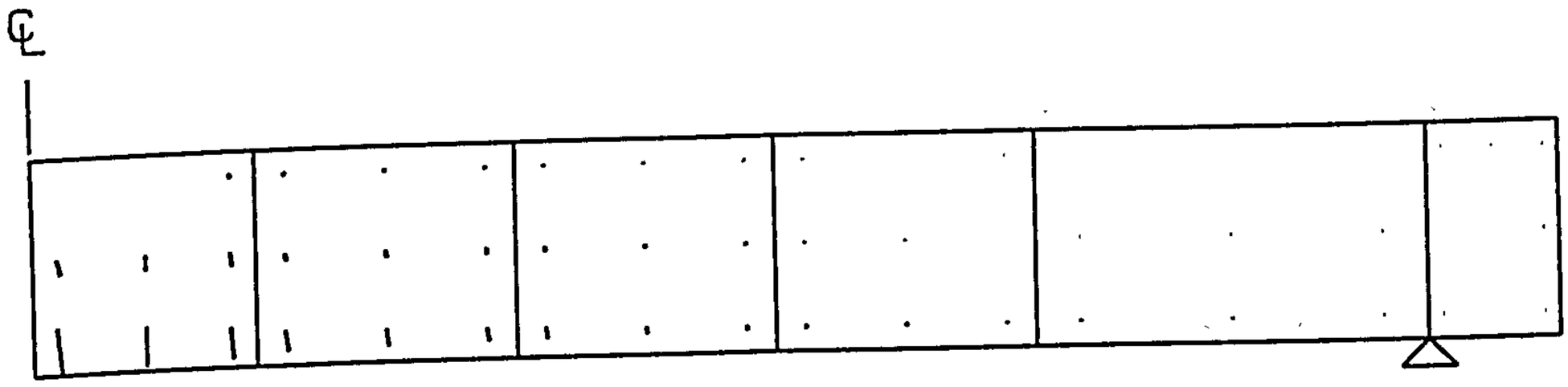

" 11 "

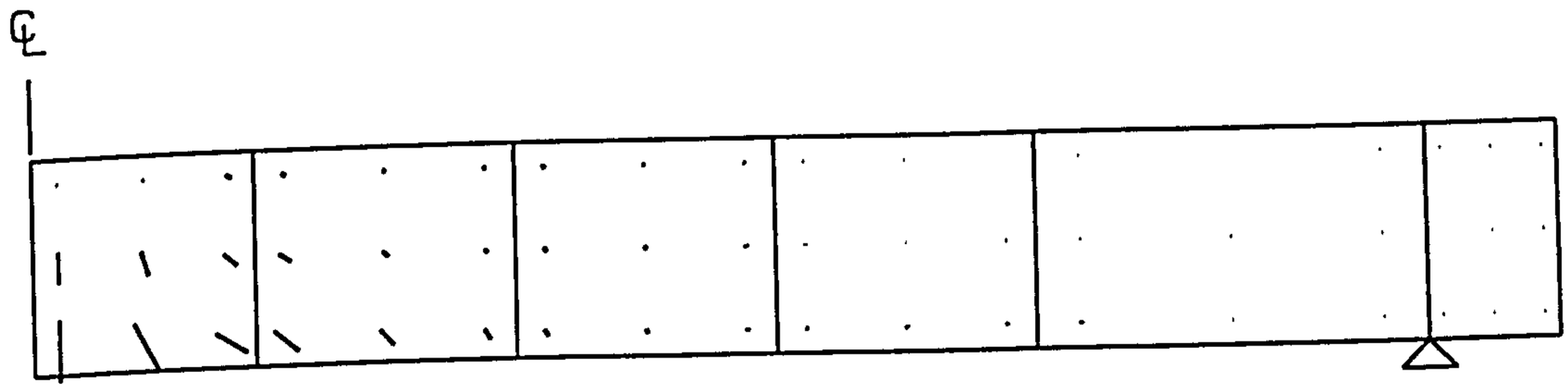

" 12 "

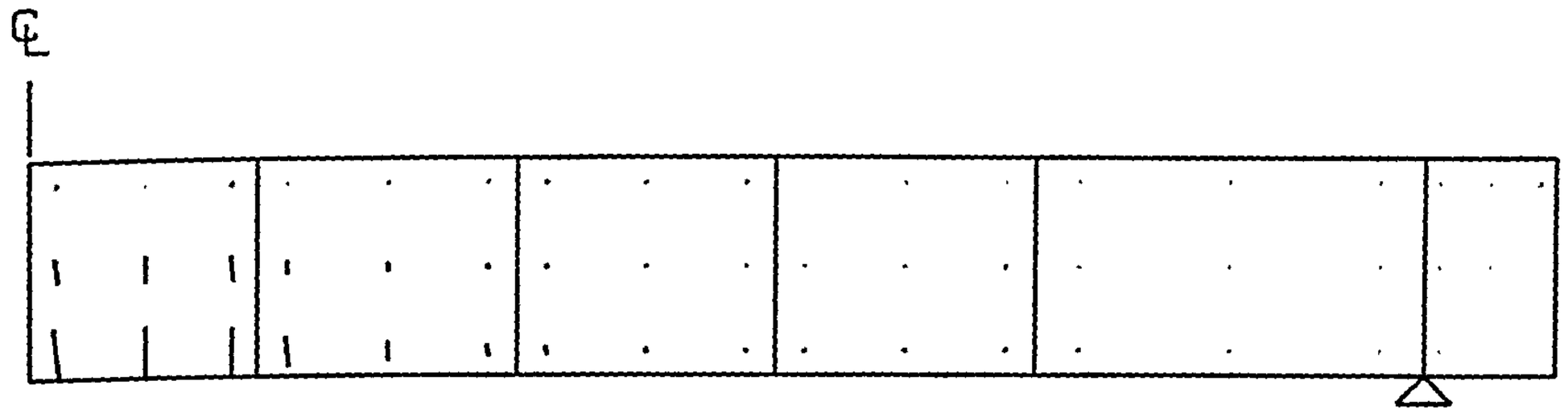

" 13 "

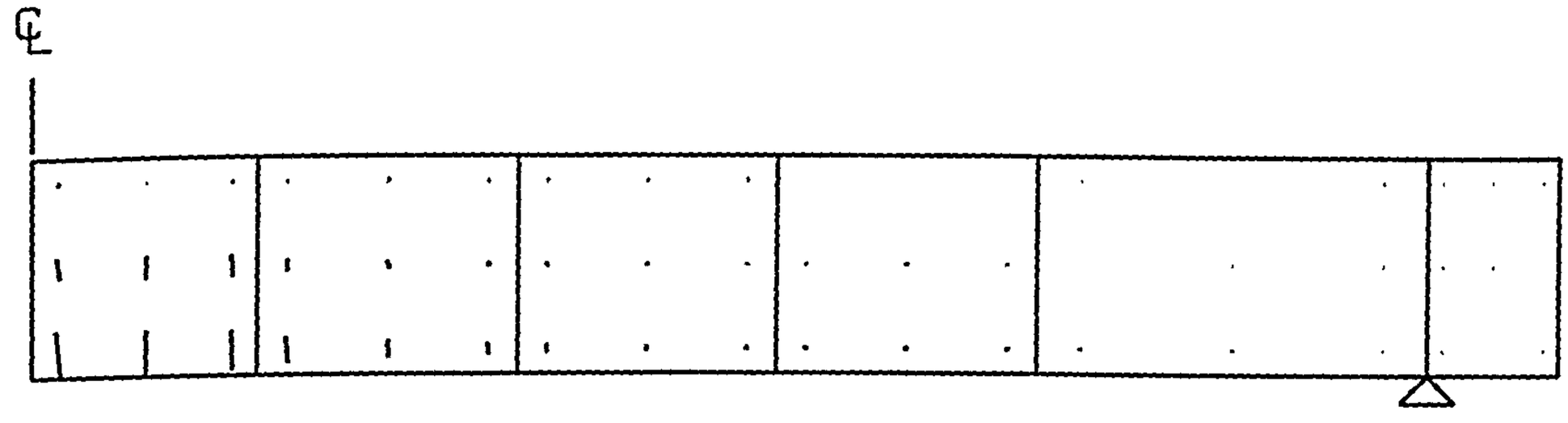

" 14 "

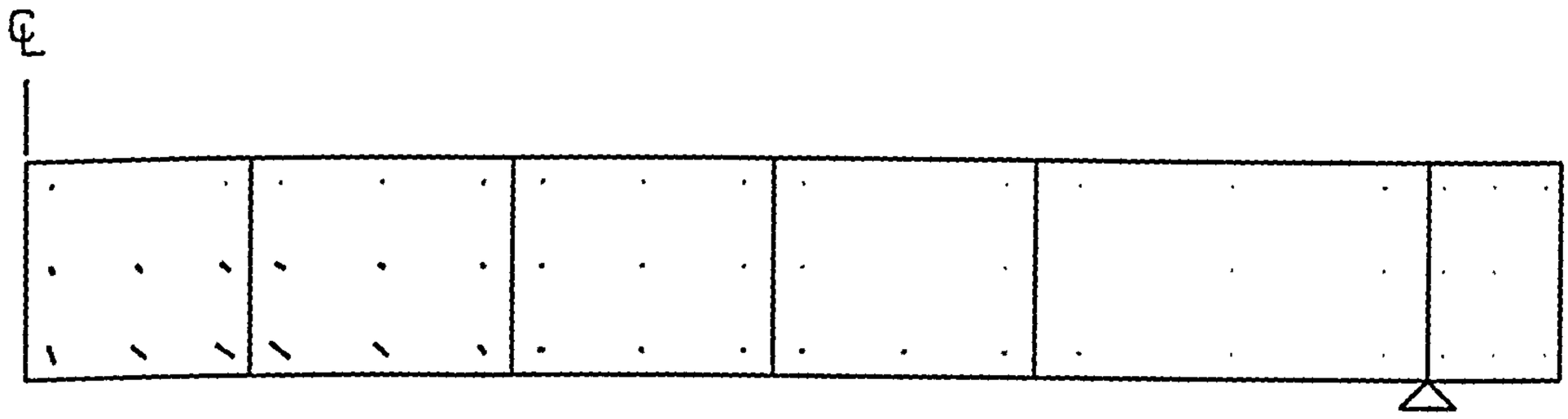

" 15 "

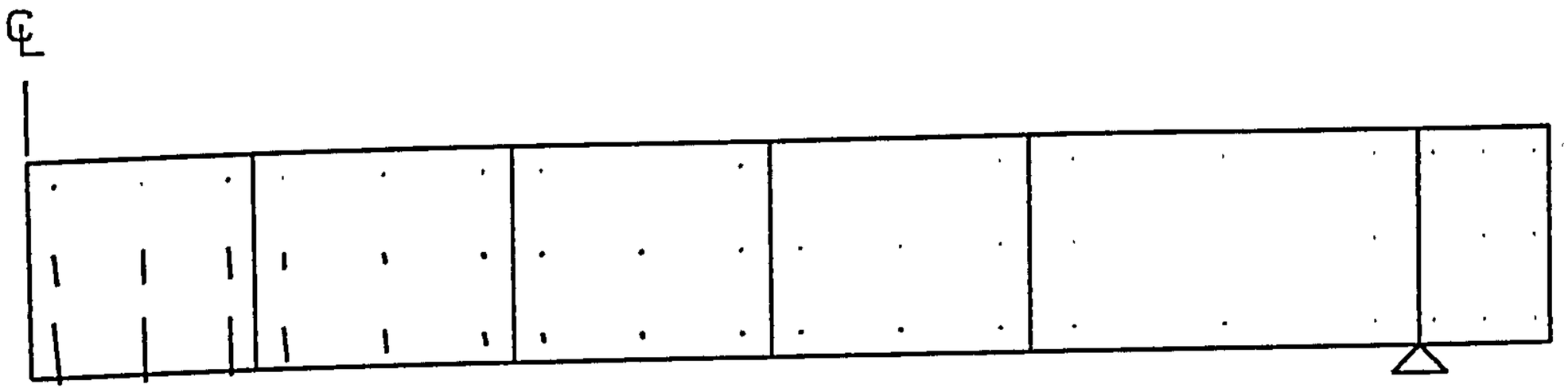

" 1A "

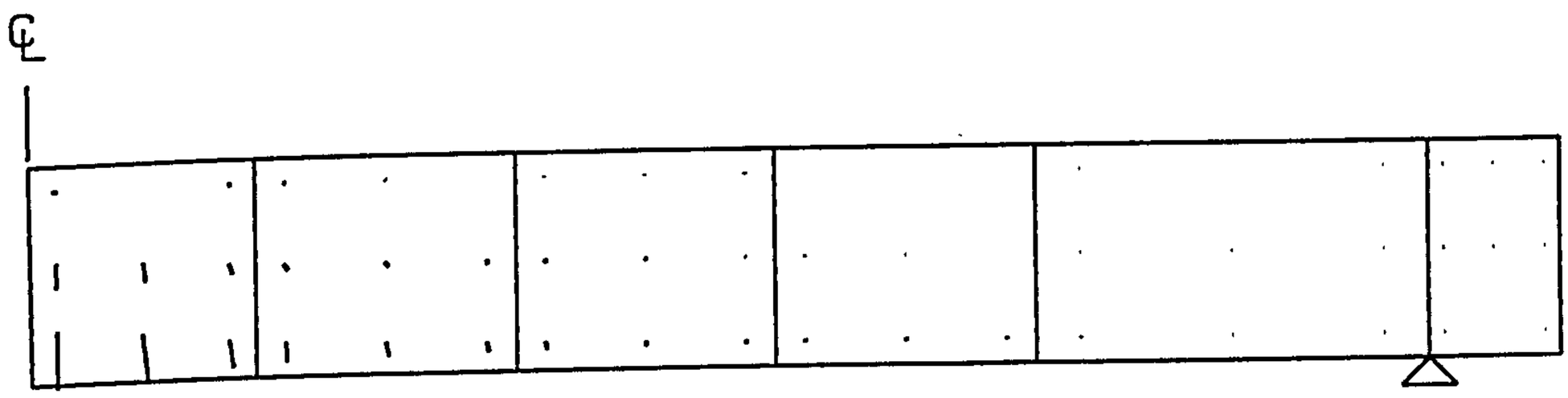

" 2A "

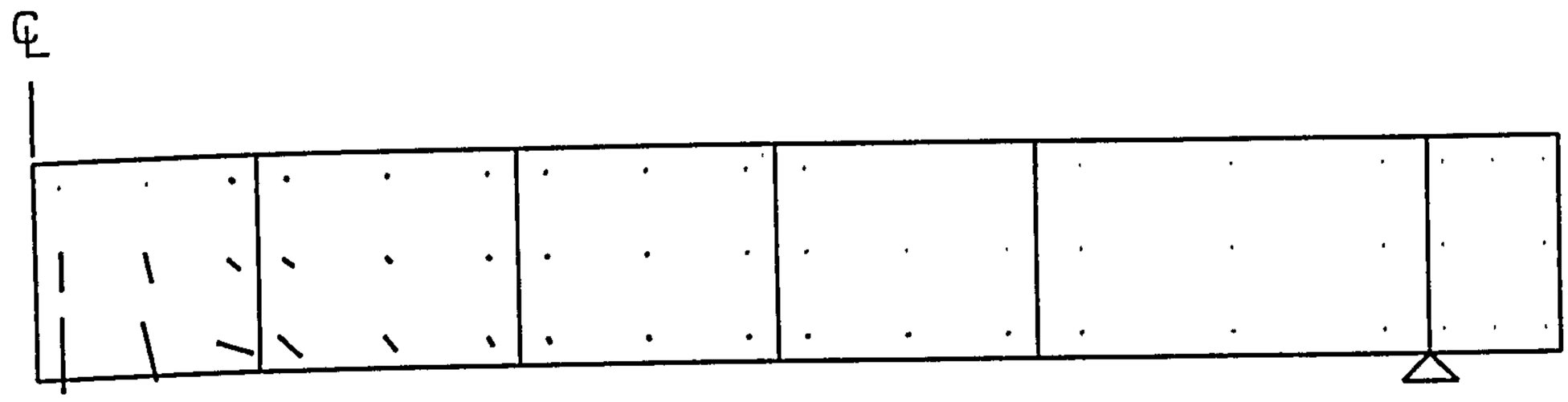

" 3A "

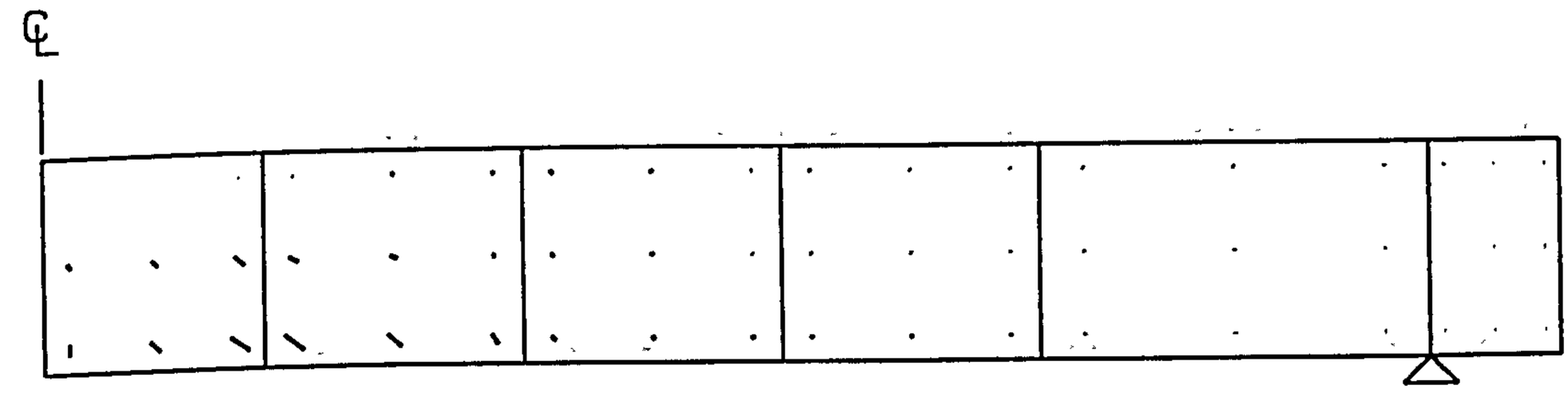

" 4A "

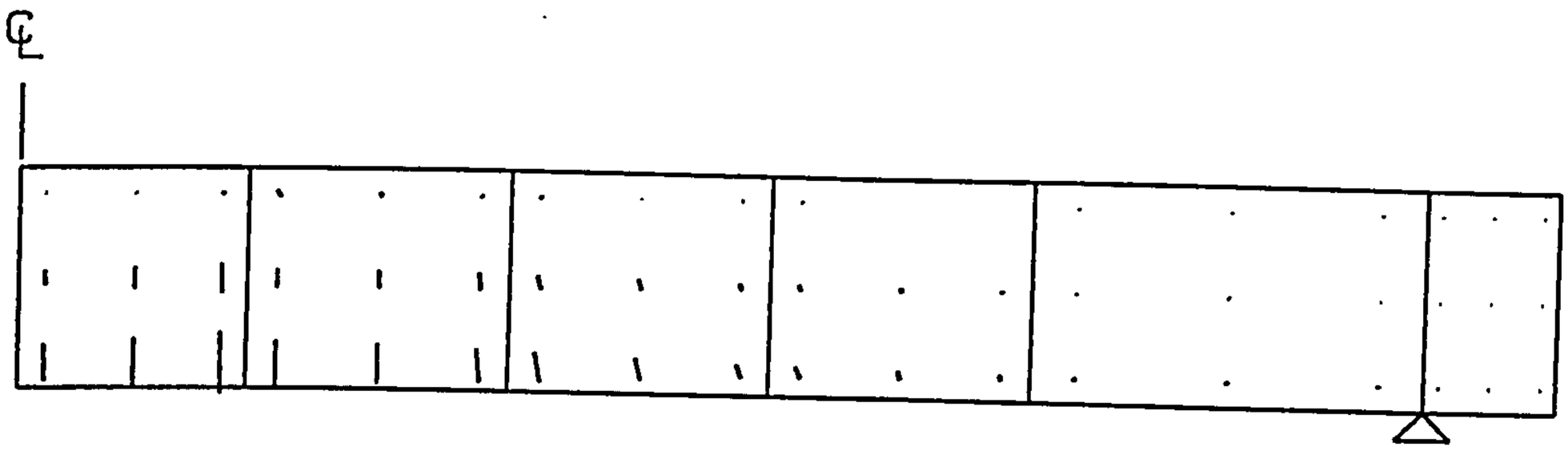

" 1B "

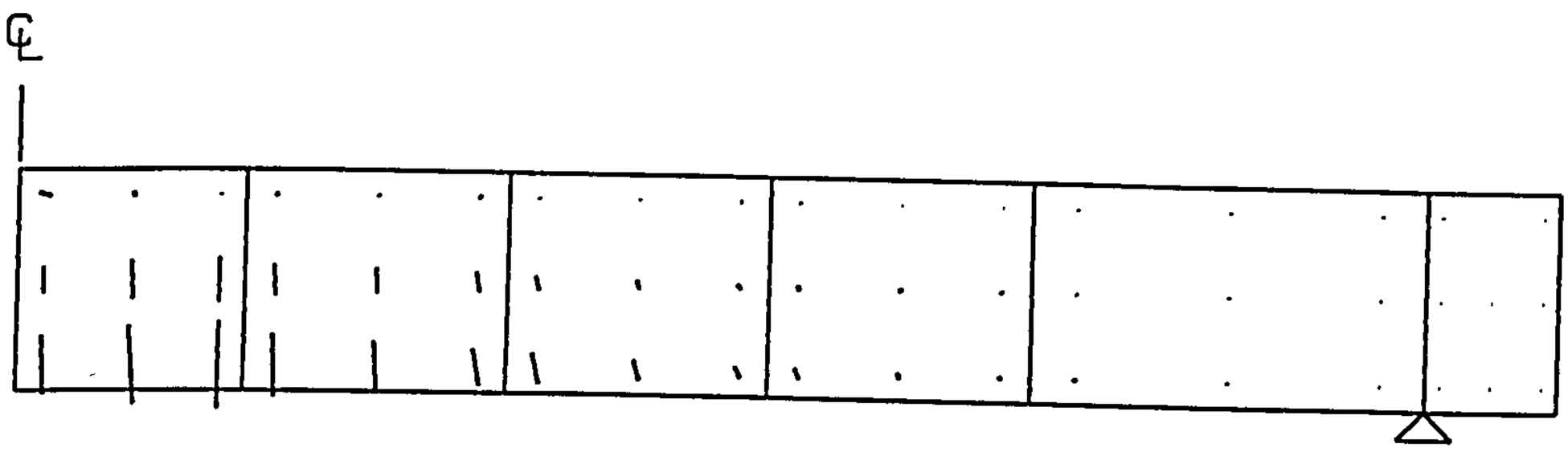

" 2B "

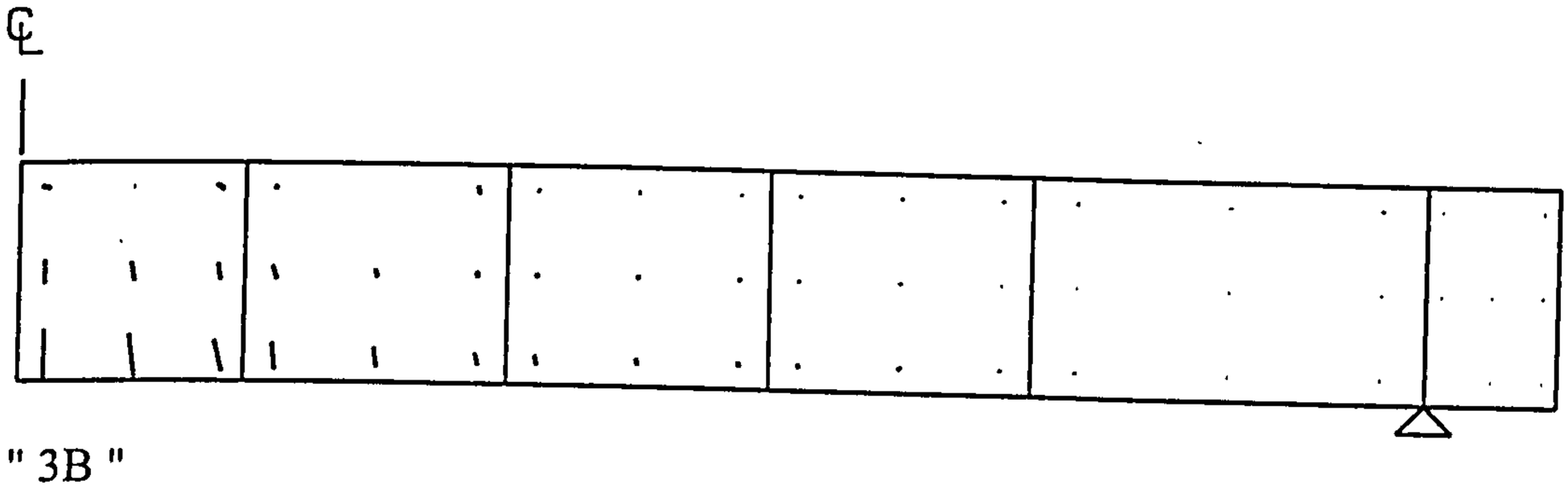

" 3B "

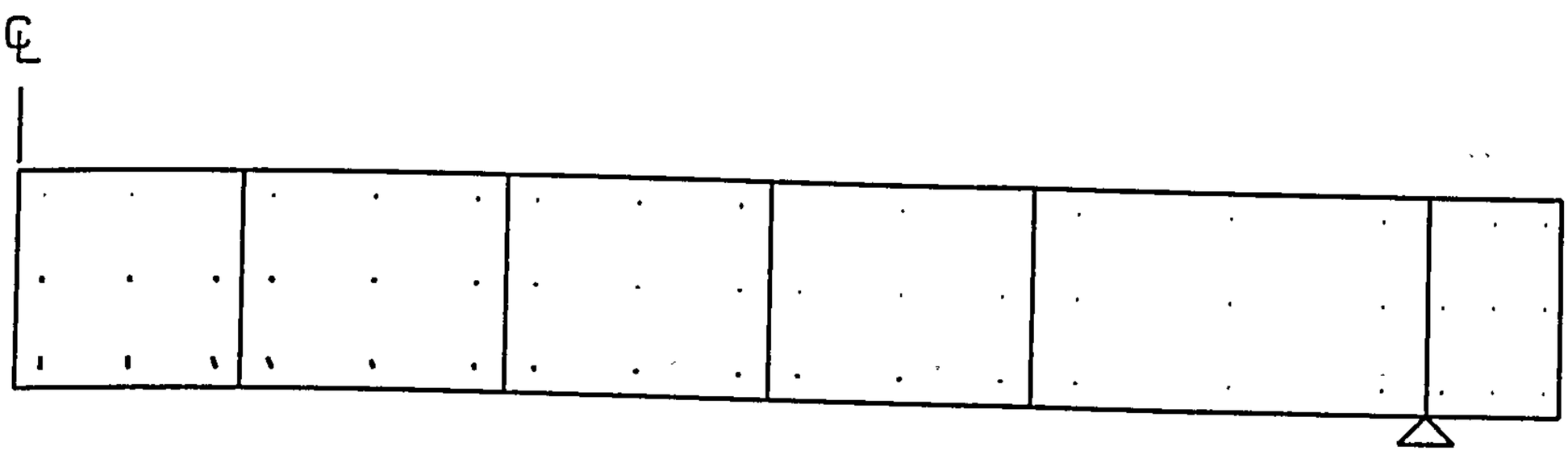

" 4B "

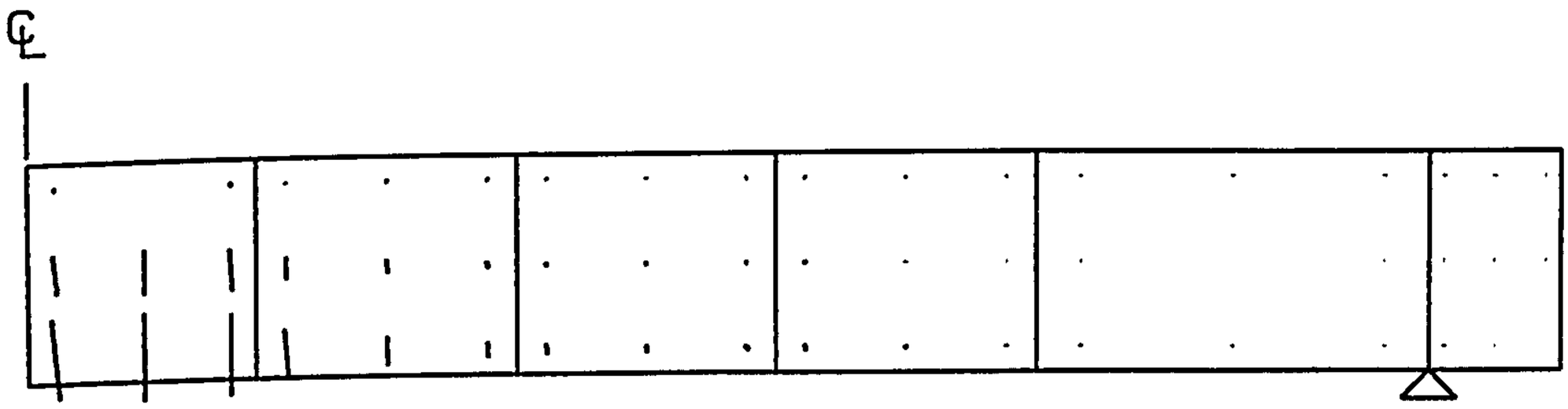

" 1C "

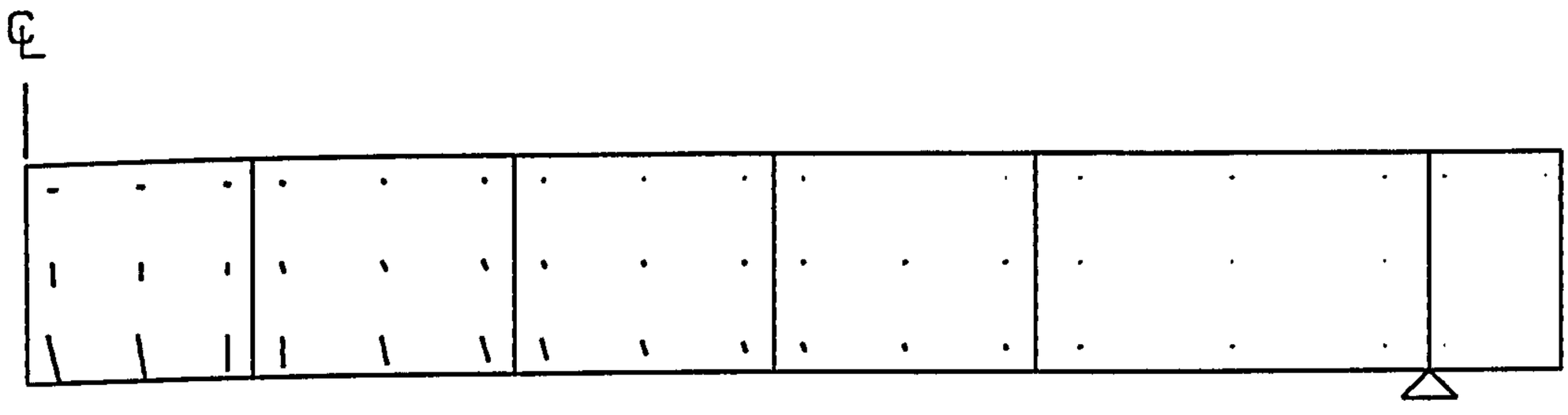

" 2C "

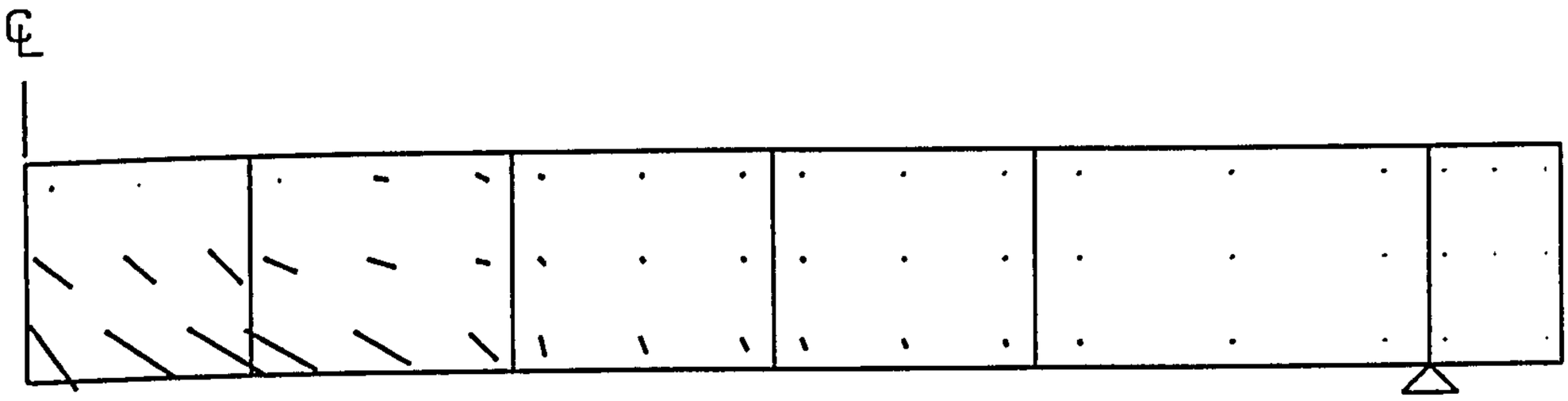

" 3C "

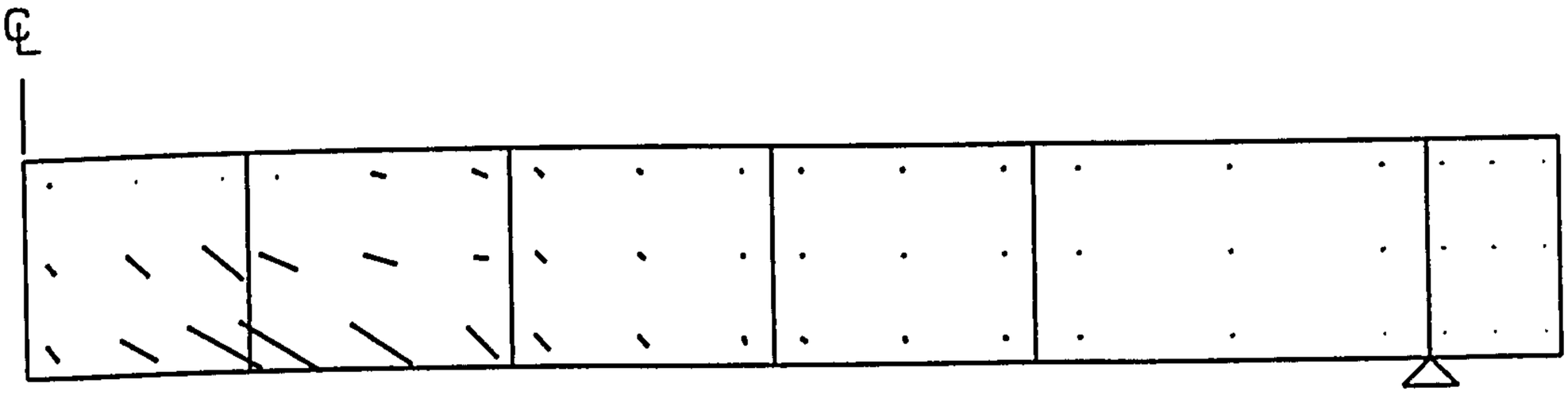

" 4C "

Regan's slabs

C1.2 Regan's slabs (without shear reinforcement)

Slab	a_V/d	Experimental results		Numerical Predictions		P_{num}/P_{test}
		P_{test} (kN)	Failure Mode	P_{num} (kN)	Failure Mode	
SS1	10.58	194.0	s	182.6	s	0.841
SS2	10.58	176.0	s	134.5	s	0.764
SS3	10.58	194.0	s	154.0	s	0.792
SS4	10.58	194.0	s	144.0	s	0.742
SS5	10.32	165.0	s	146.9	s	0.890
SS6	10.32	165.0	s	130.5	s	0.791
SS7	10.32	186.0	y	163.1	y	0.877
SS8	6.24	825.0	s	856.0	s	1.038
SS9	6.41	390.0	s	345.6	s	0.886
SS11	6.41	117.0	s	90.0	s	0.769
V1	6.13	170.0	s	160.0	s	0.939
V2	5.64	280.0	s	245.0	s	0.874
V3	5.89	265.0	s	264.0	s	0.996
V4	5.92	285.0	s	274.0	s	0.960
V5	5.72	285.0	s	288.0	s	1.010
SP1	4.67	197.0	s	163.0	s	0.827
SP2	3.00	227.0	s	203.0	s	0.894
SP3	1.33	235.0	s	288.0	s	1.226
SP4	1.67	185.0	s	191.5	s	1.035
SP5	1.00	338.0	s	403.2	s	1.193
SP8	1.67	172.0	s	172.8	s	1.005
SP9	1.00	284.0	s	288.0	s	1.014
SP10	1.00	421.0	s	507.0	s	1.204
SP11	1.67	182.0	s	237.0	s	1.302
SP12	1.00	221.0	s	268.0	s	1.213
SP13	1.67	109.0	s	116.0	s	1.064
SP14	0.67	623.0	s	686.4	s	1.102
SP15	1.33	368.0	s	383.0	s	1.041
SP16	0.67	451.0	s	475.0	s	1.053
SP17	0.63	1099.0	s	1049.0	s	0.955
SP18	0.67	142.0	y	187.2	fp	1.318
					Average	0.988
					STDEV	0.161

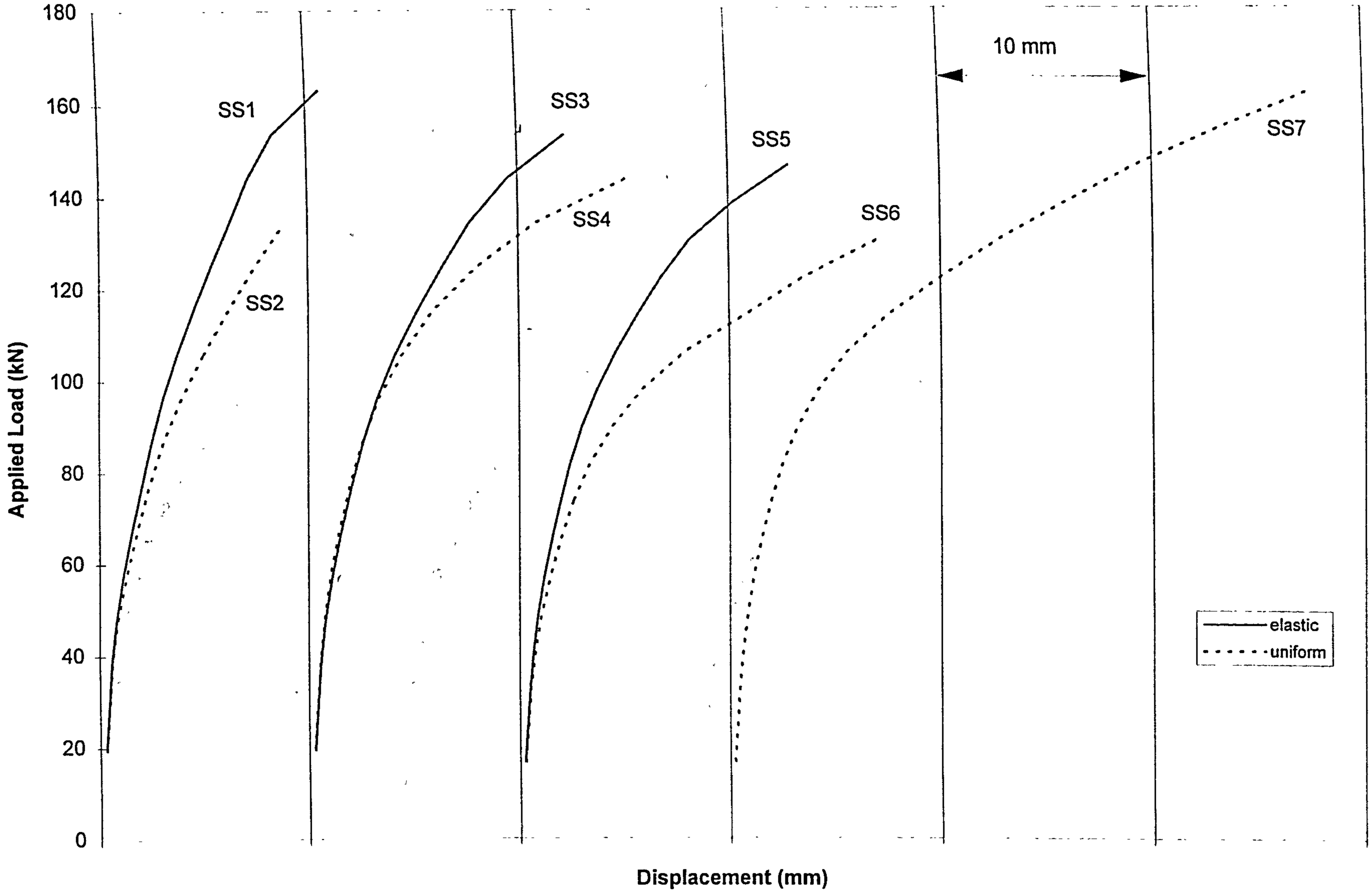

Predicted Load-deflection response for slabs SS1-SS7

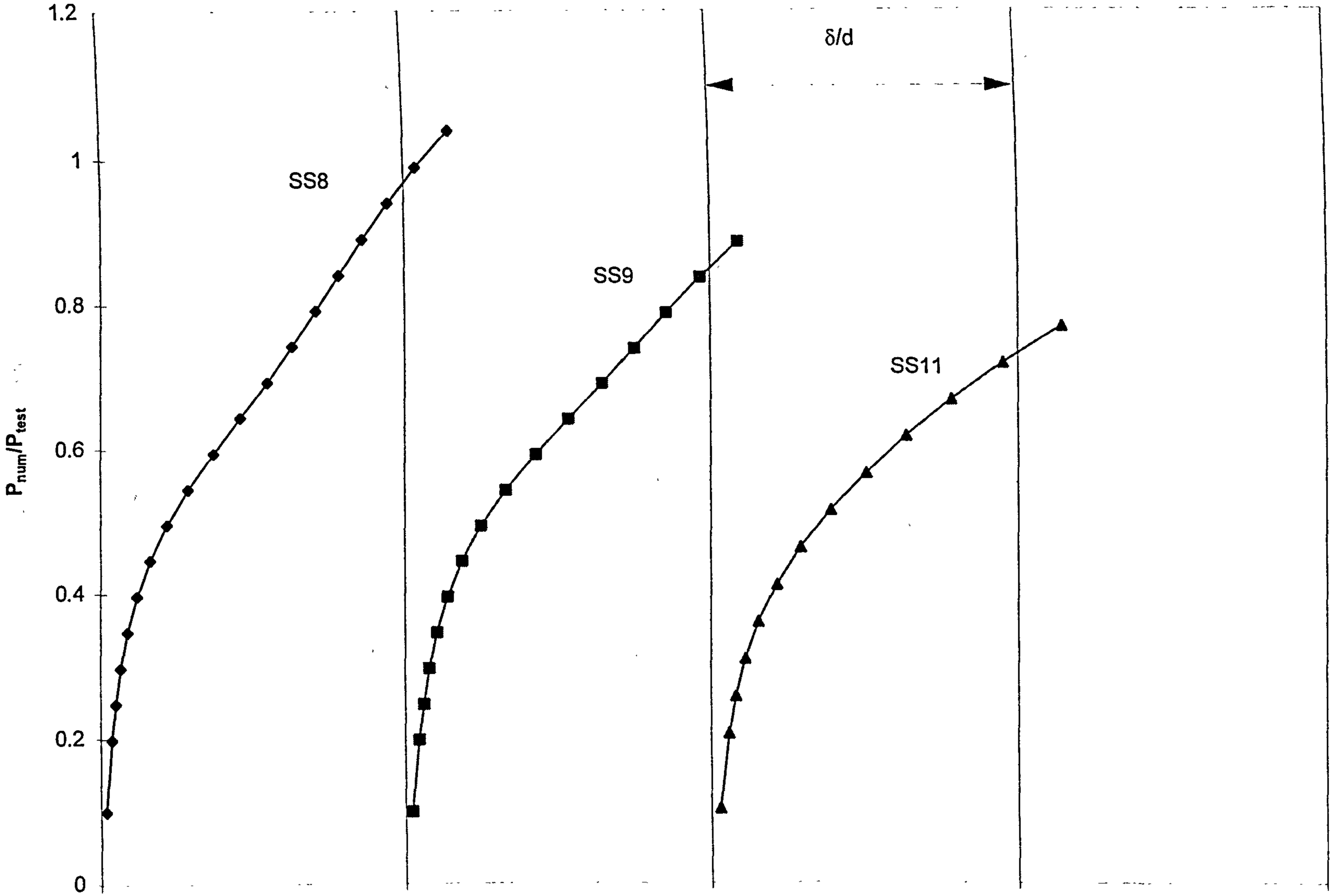

Predicted load-deflection response for slabs SS8-SS11

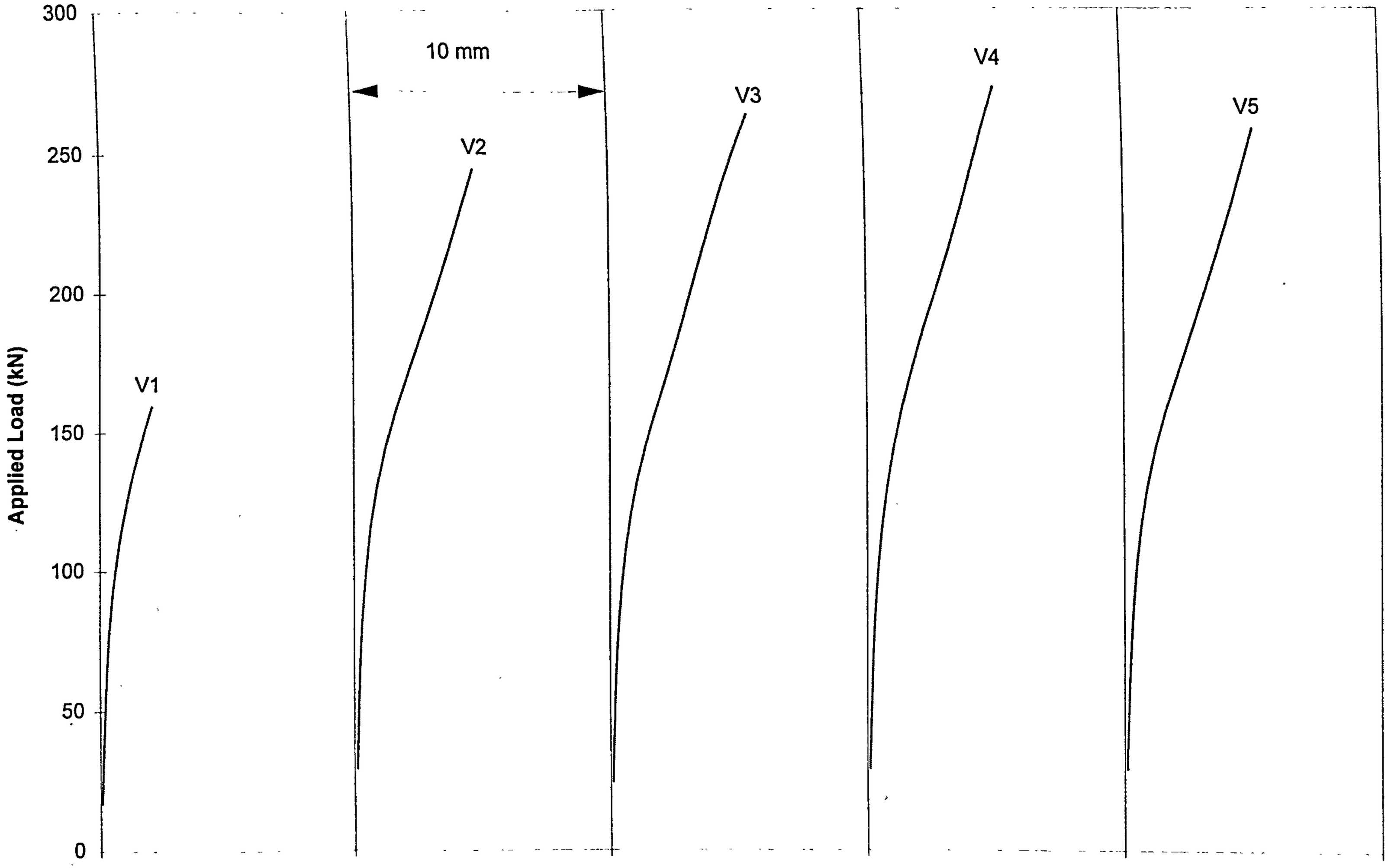

Predicted Load-deflection response for slabs V1-V5

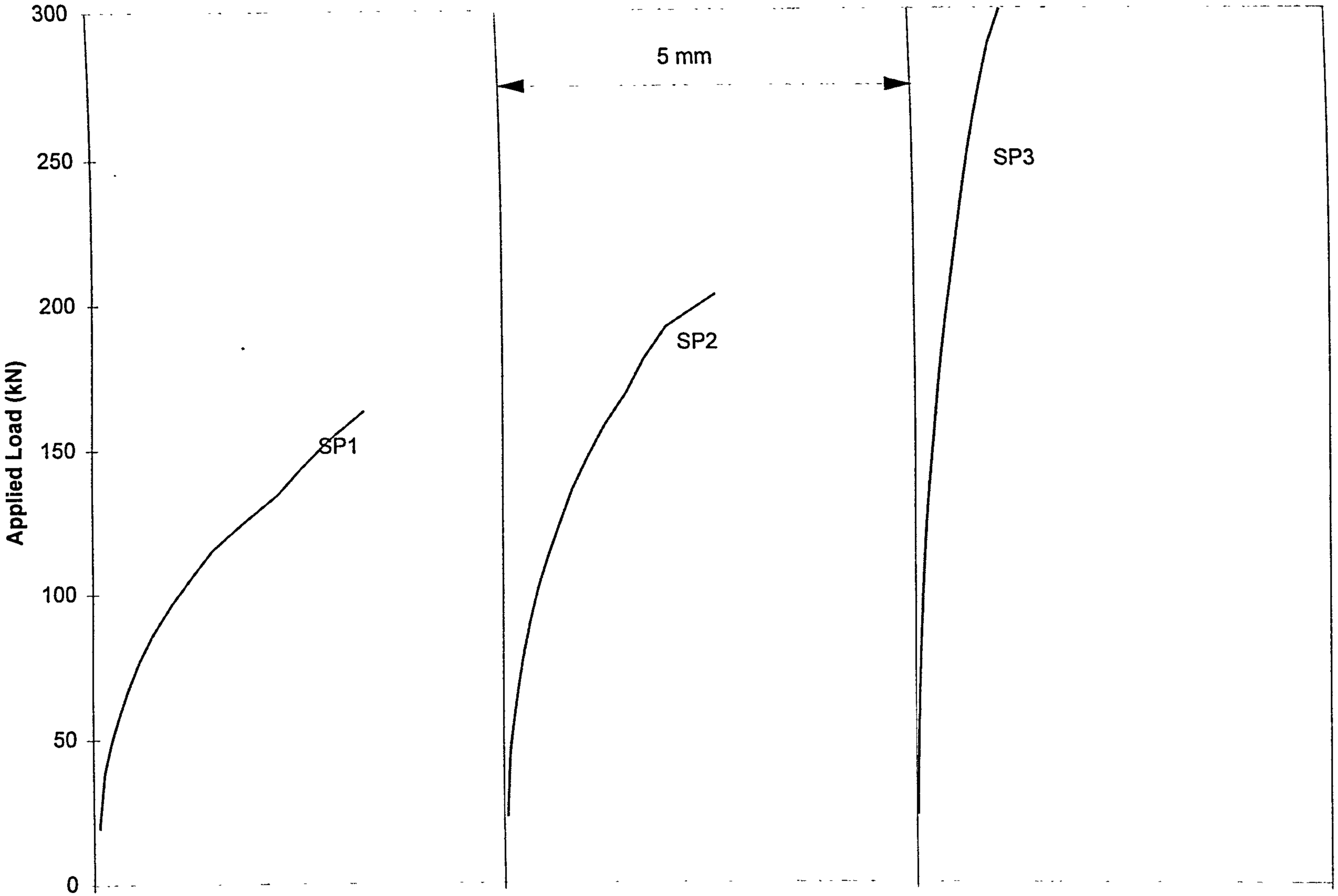

Predicted load-deflection response for slabs SP1-SP3

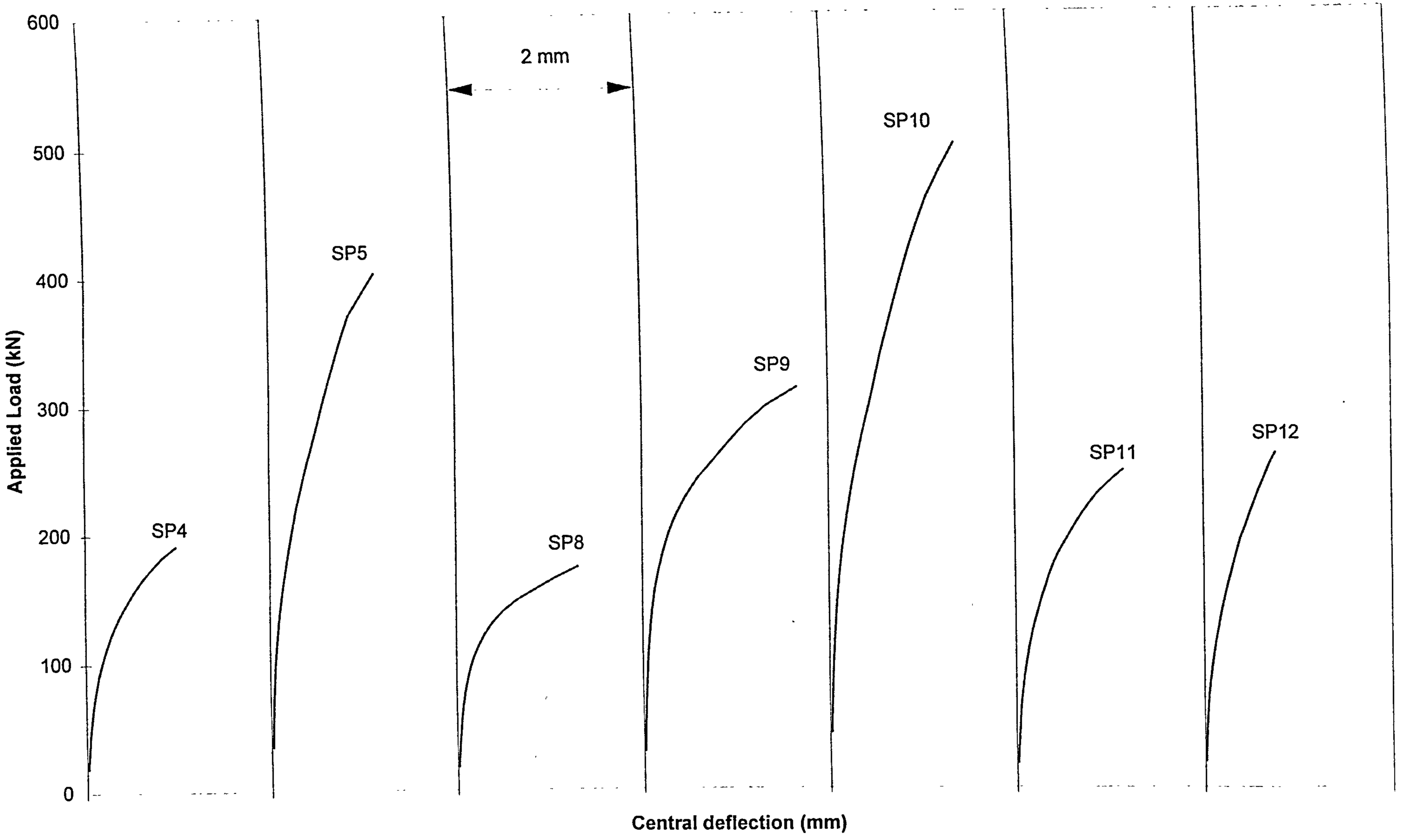

Predicted load-deflection response for slabs SP4-SP12

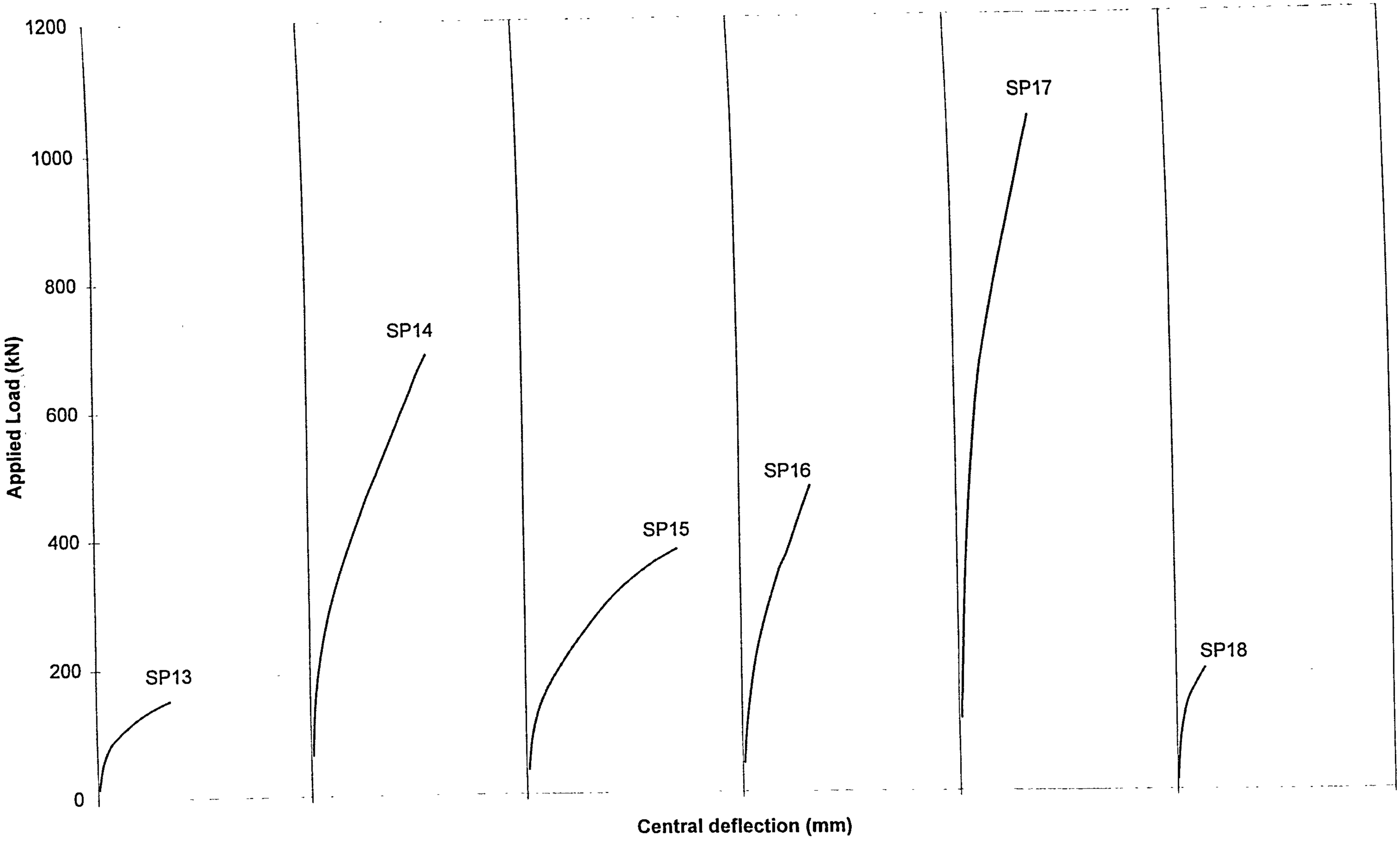

Predicted load-deflection response for slabs SP13-SP18

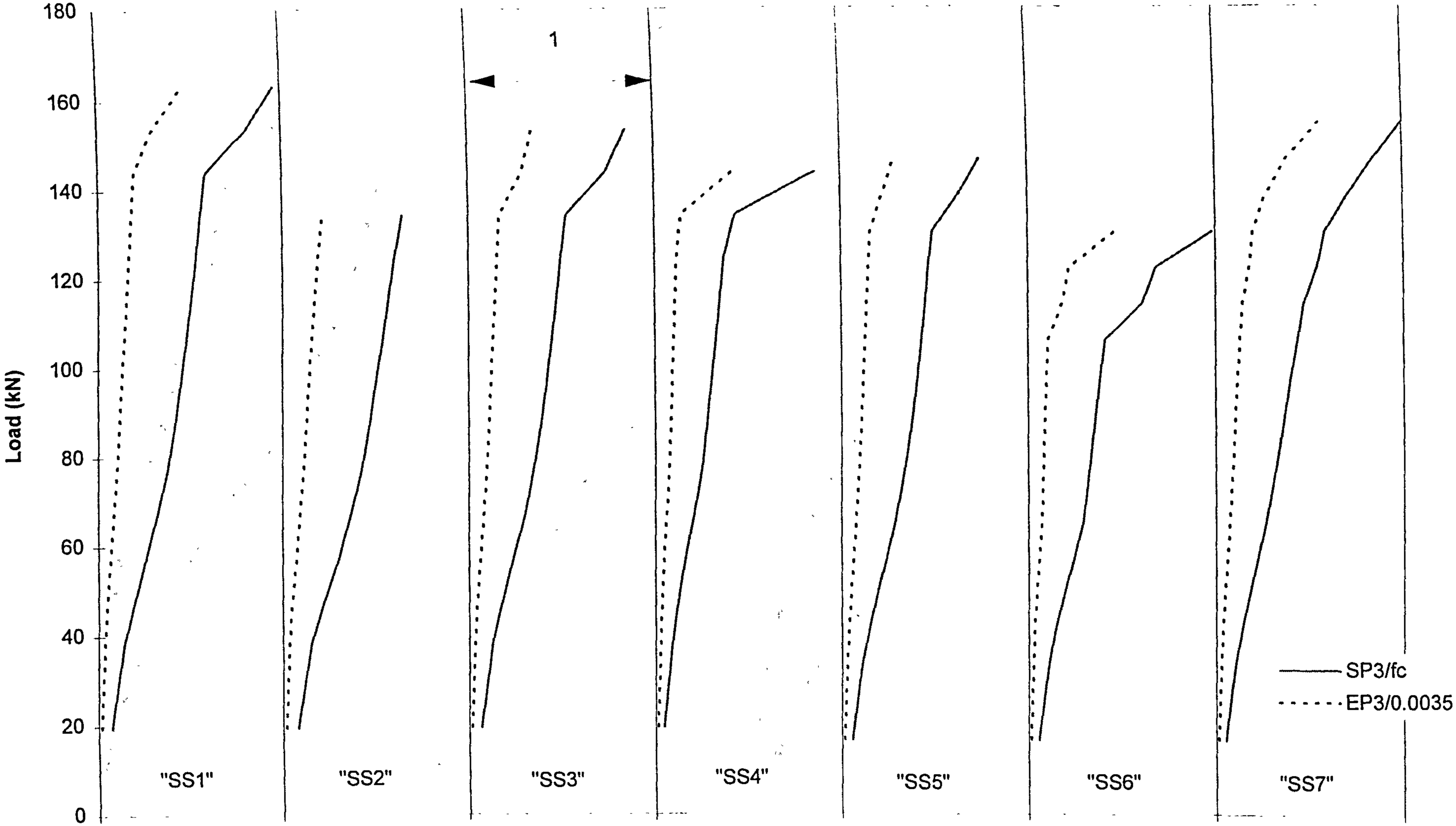

Predicted principal compressive stress and strain in concrete (slabs "SS1" - "SS7")

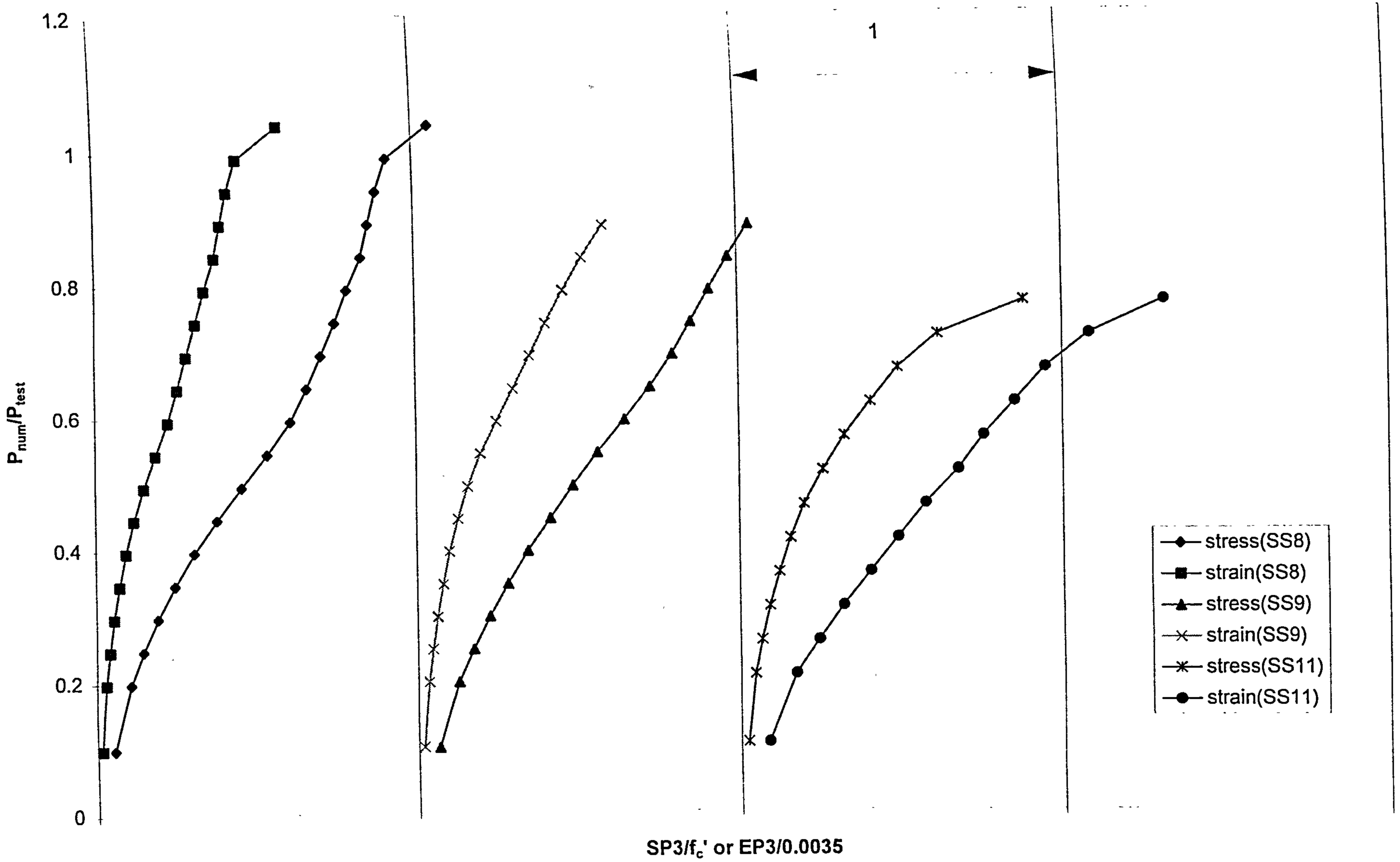

Predicted principal compressive stress and strain in concrete for slabs SS8-SS11

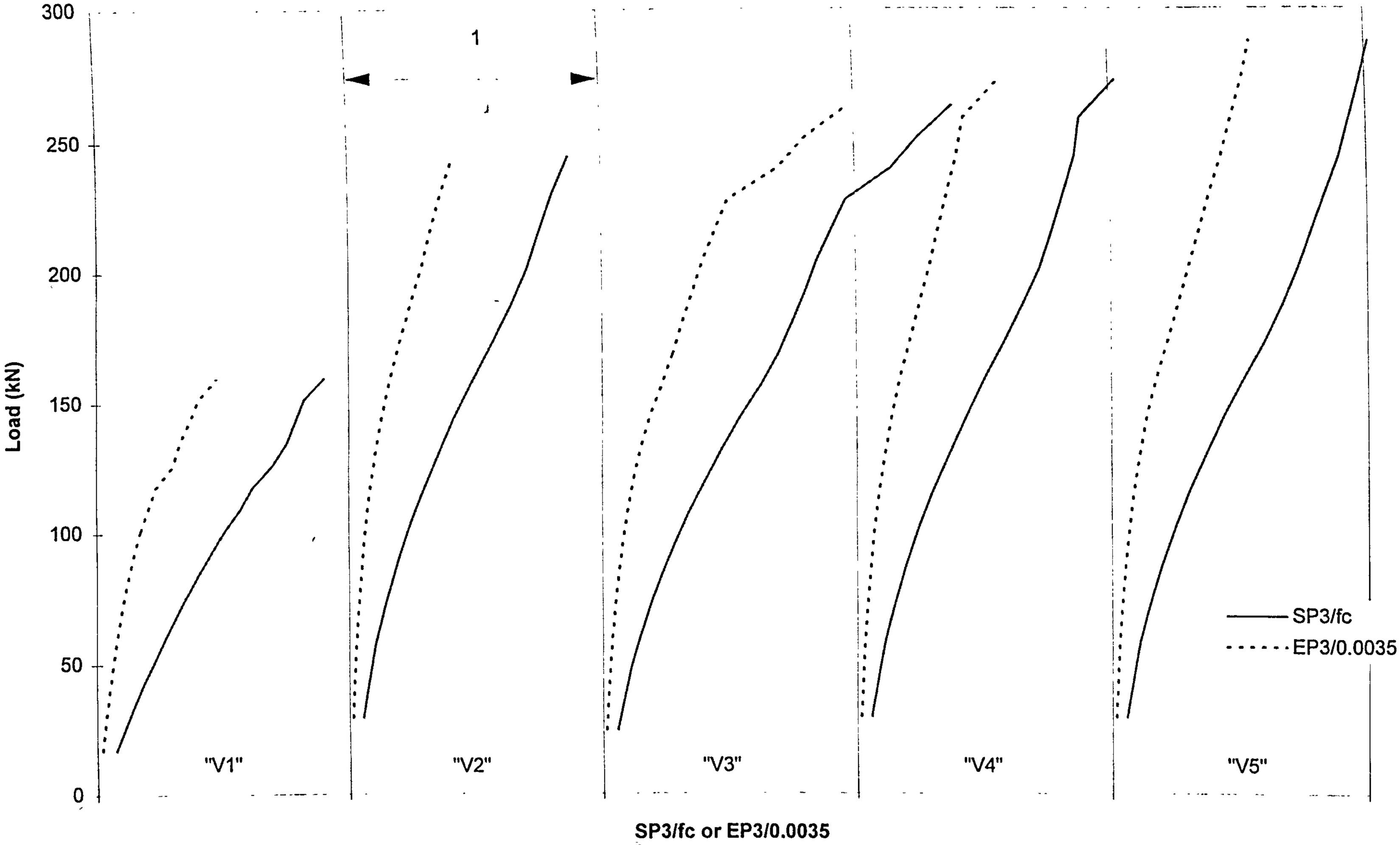

Predicted principal compressive stress and strain in concrete (slabs "V1" - "V5")

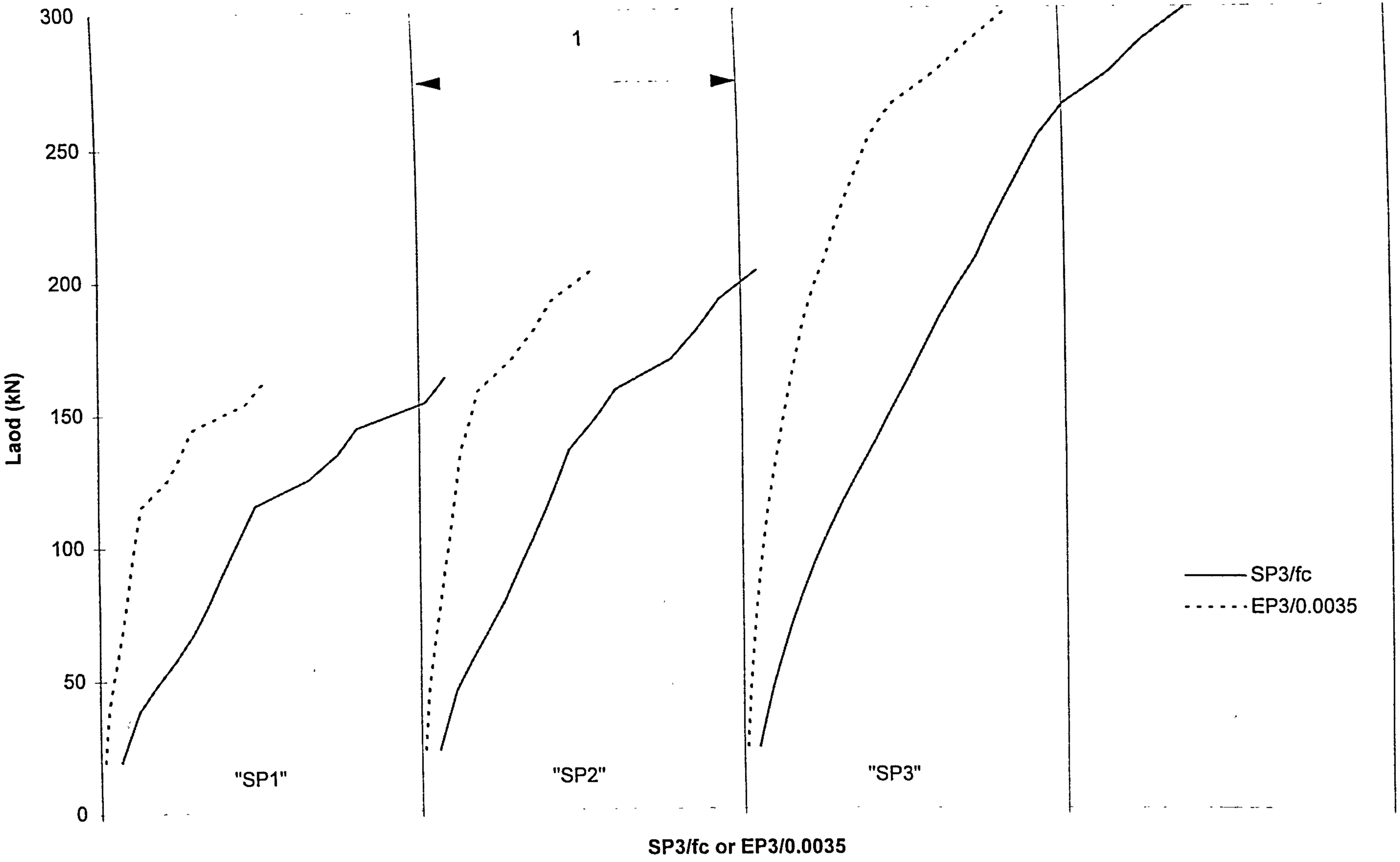

Predicted principal compressive stress and strain in concrete (slabs "SP1" - "SP3")

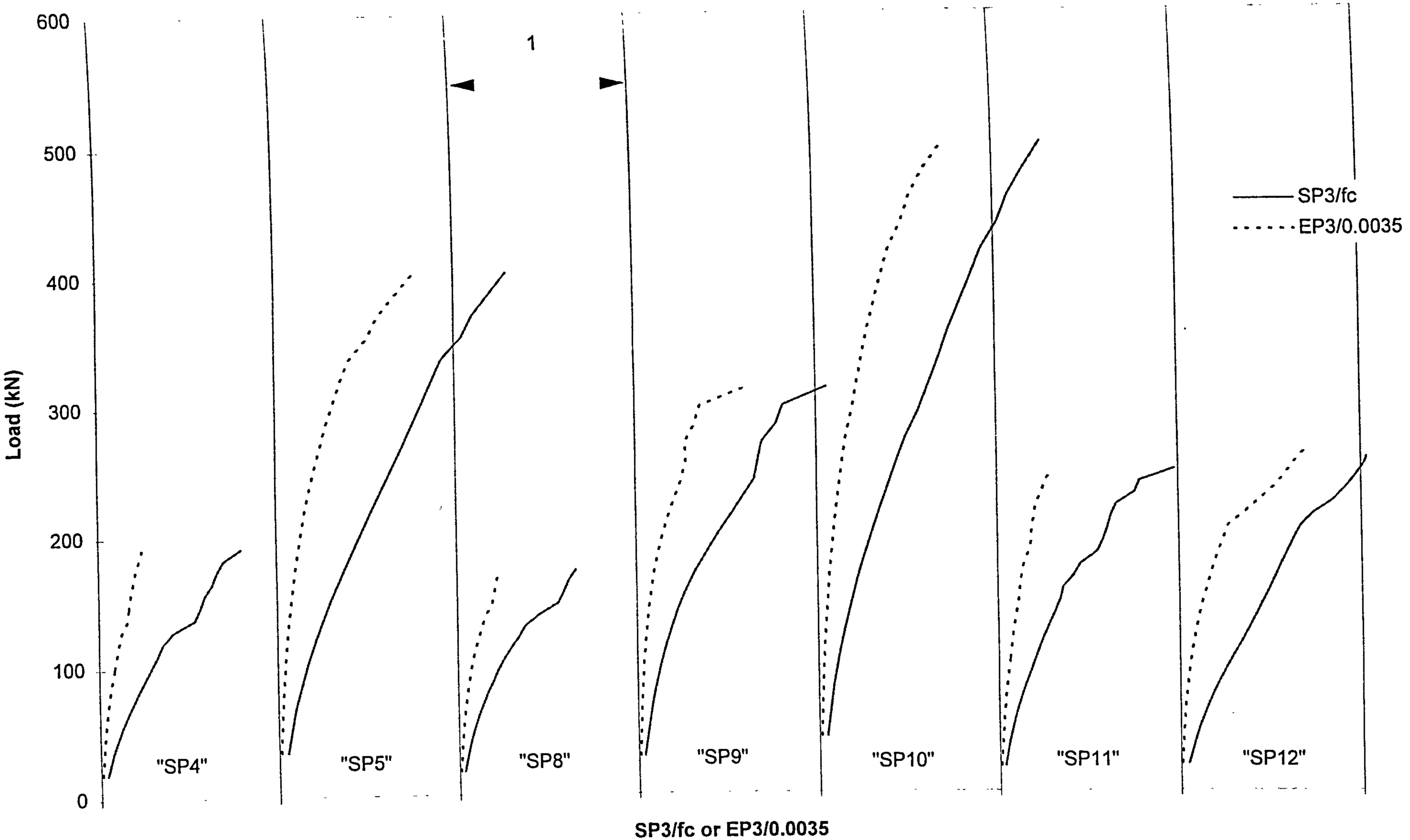

Predicted principal compressive stress and strain in concrete (slabs "SP4" - "SP12")

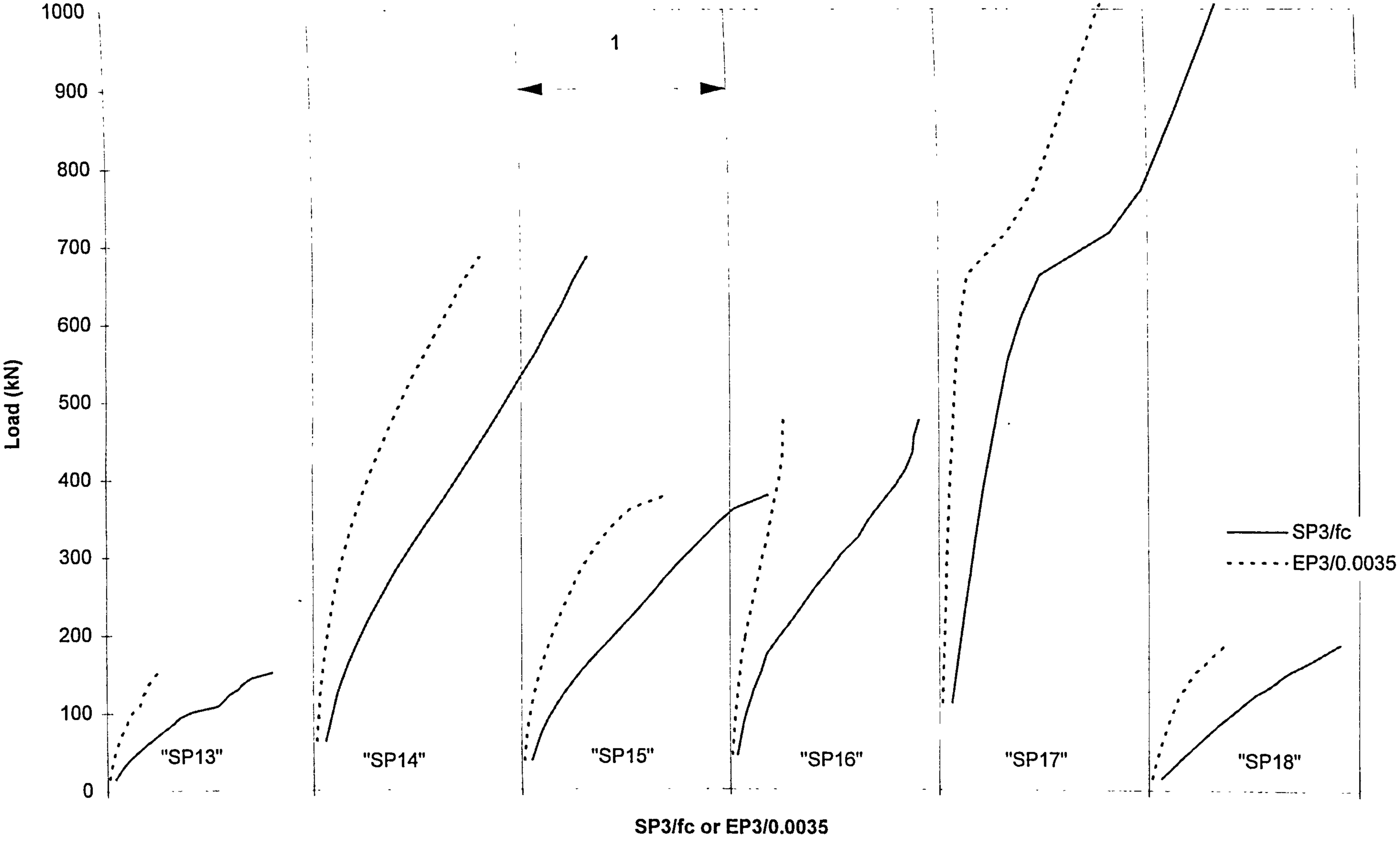

Predicted principal compressive stress and strain in concrete (slabs "SP13" - "SP18")

Yielding of tension steel, Specimens SS1-SS7 (Regan)

NB. : The numbers on the drawing indicate strain in steel at collapse expressed as a ratio of yield strain

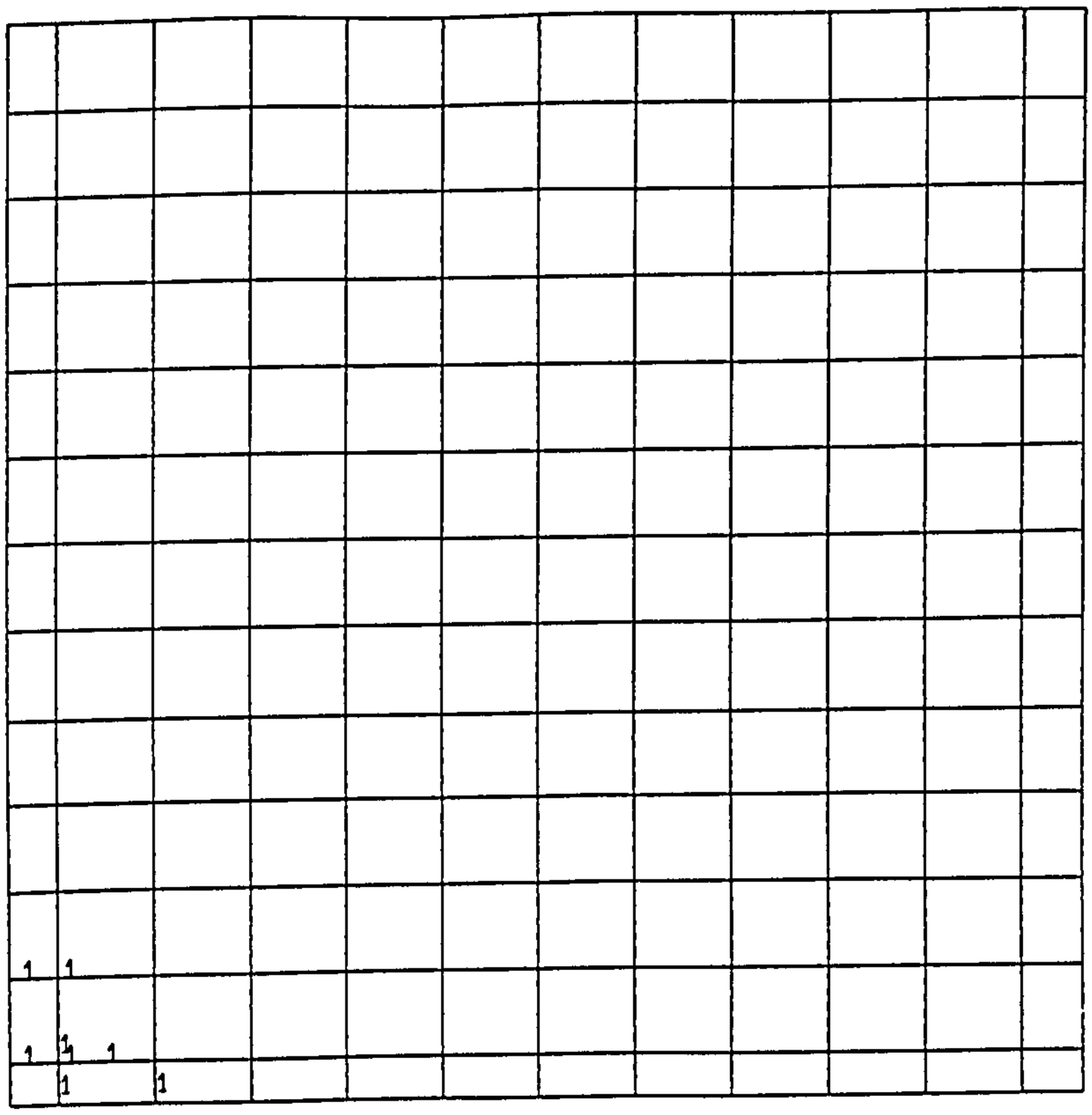

SS2

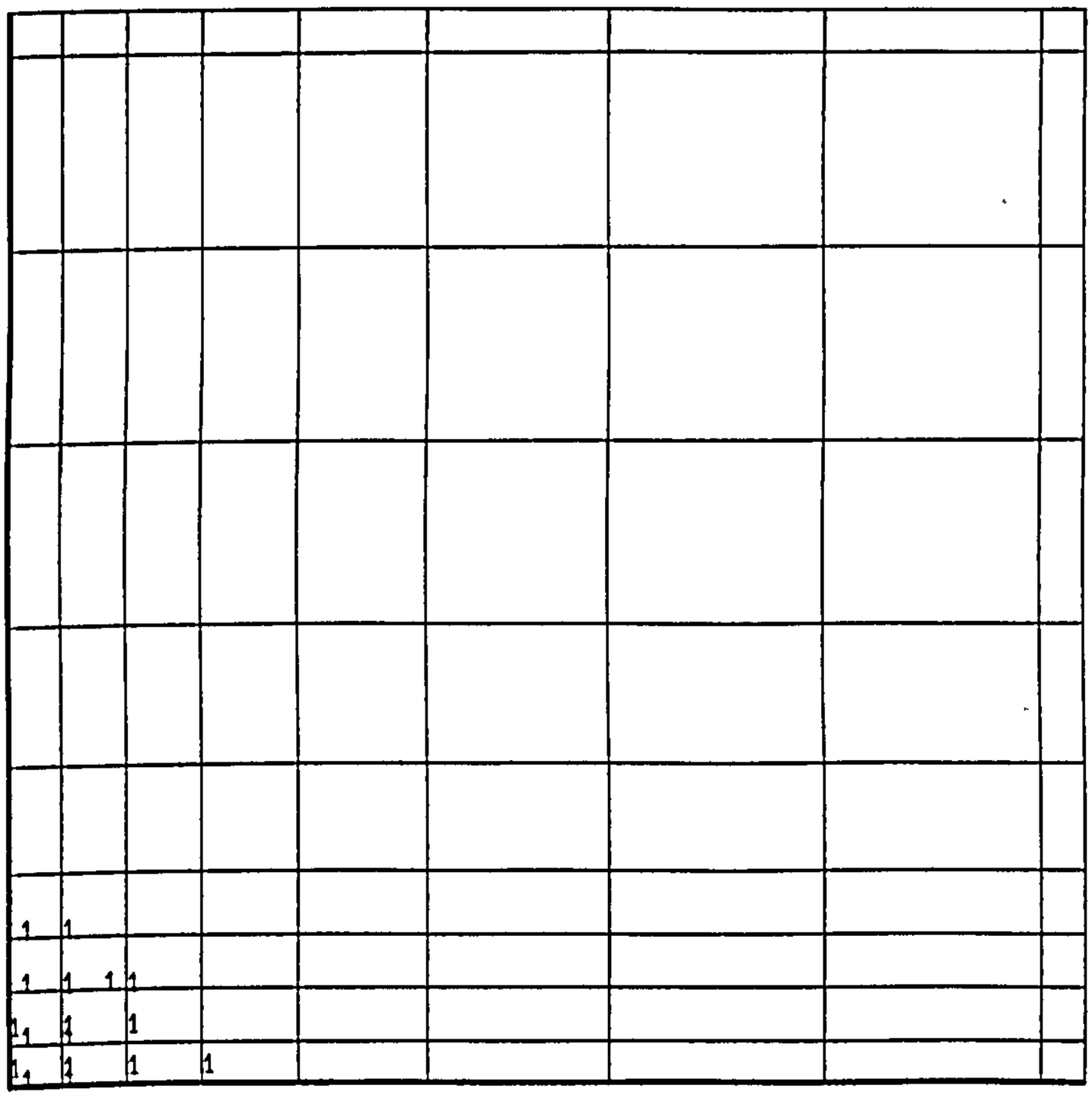

SS3

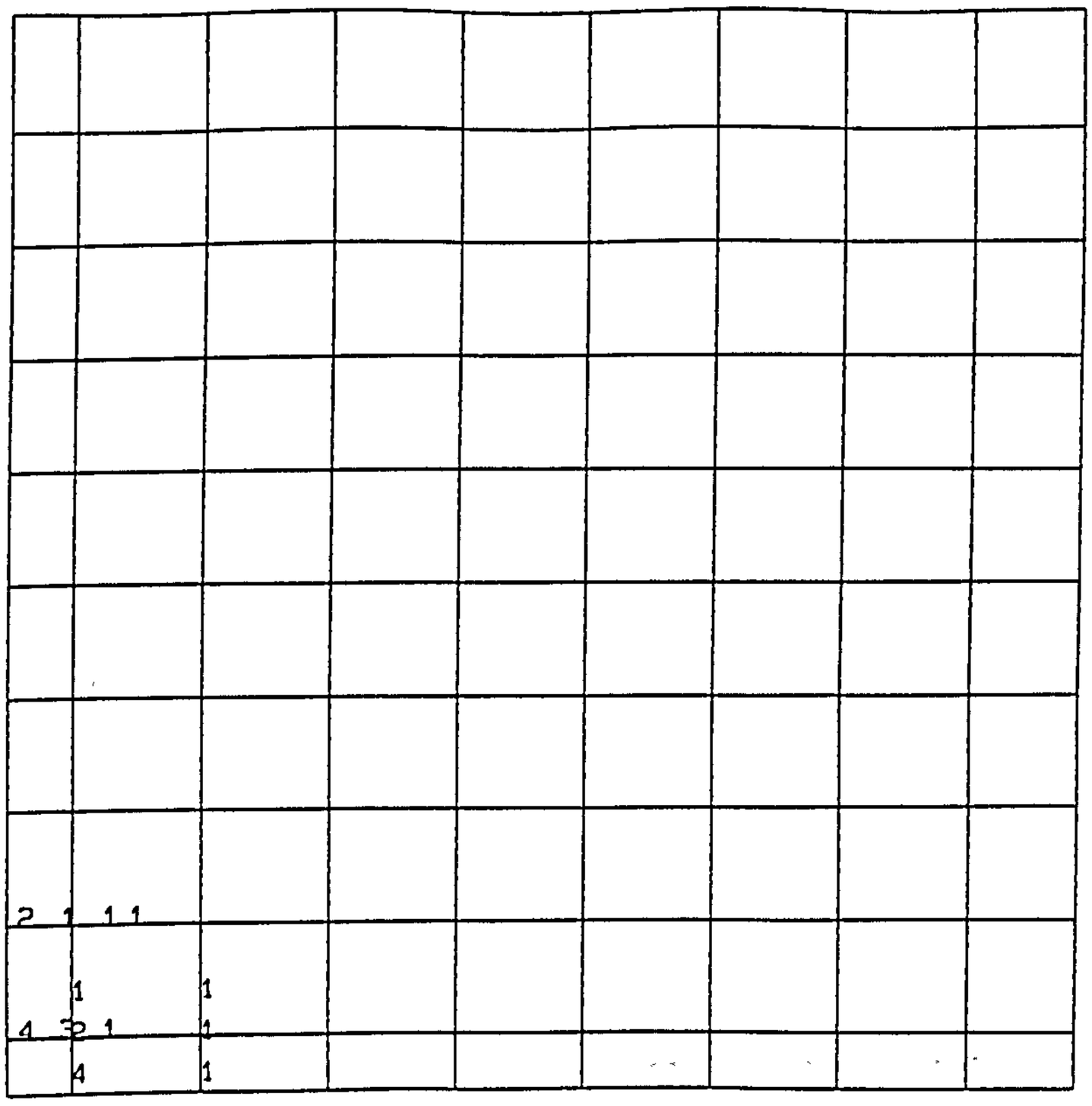

SS4

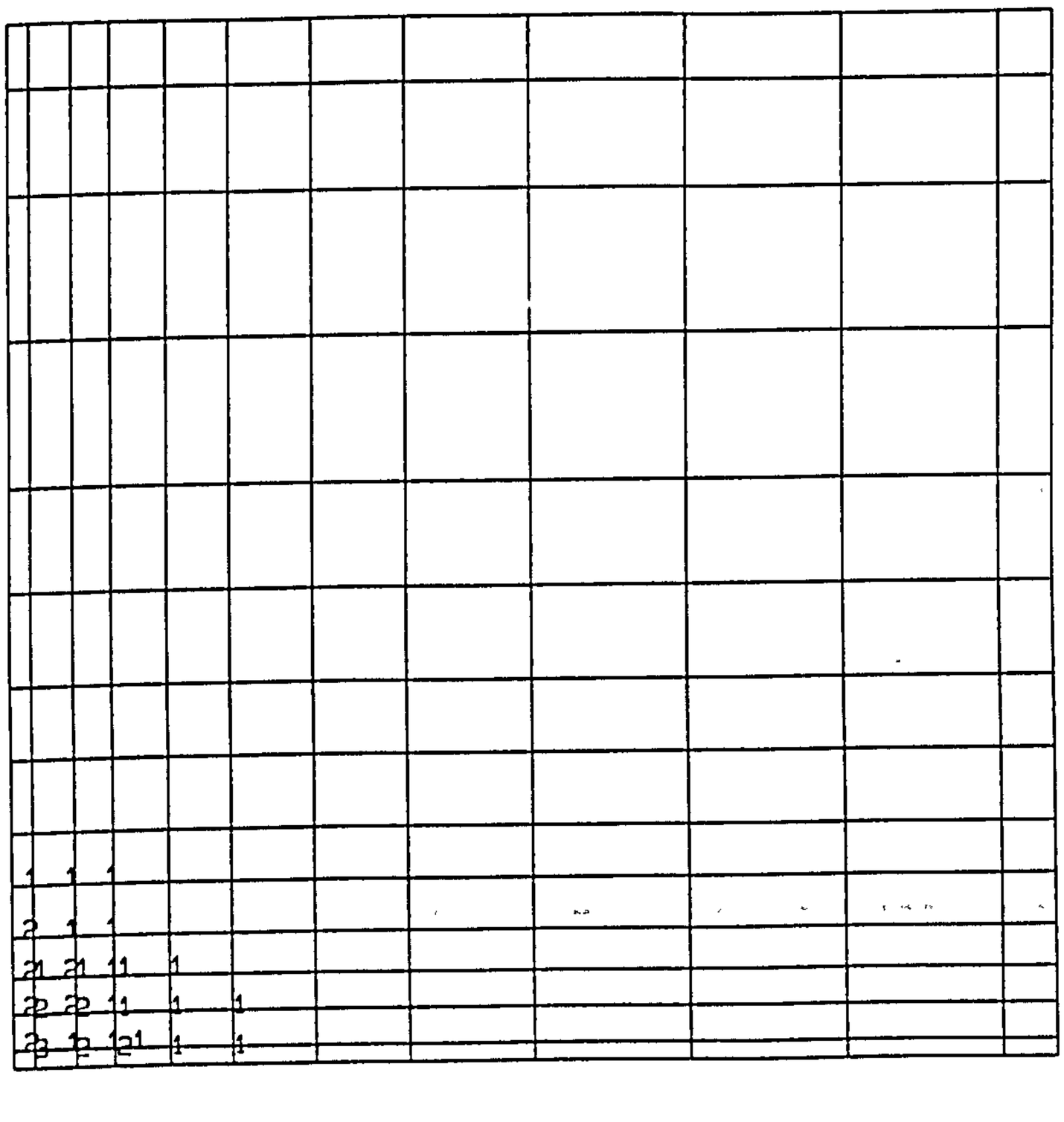

SS5

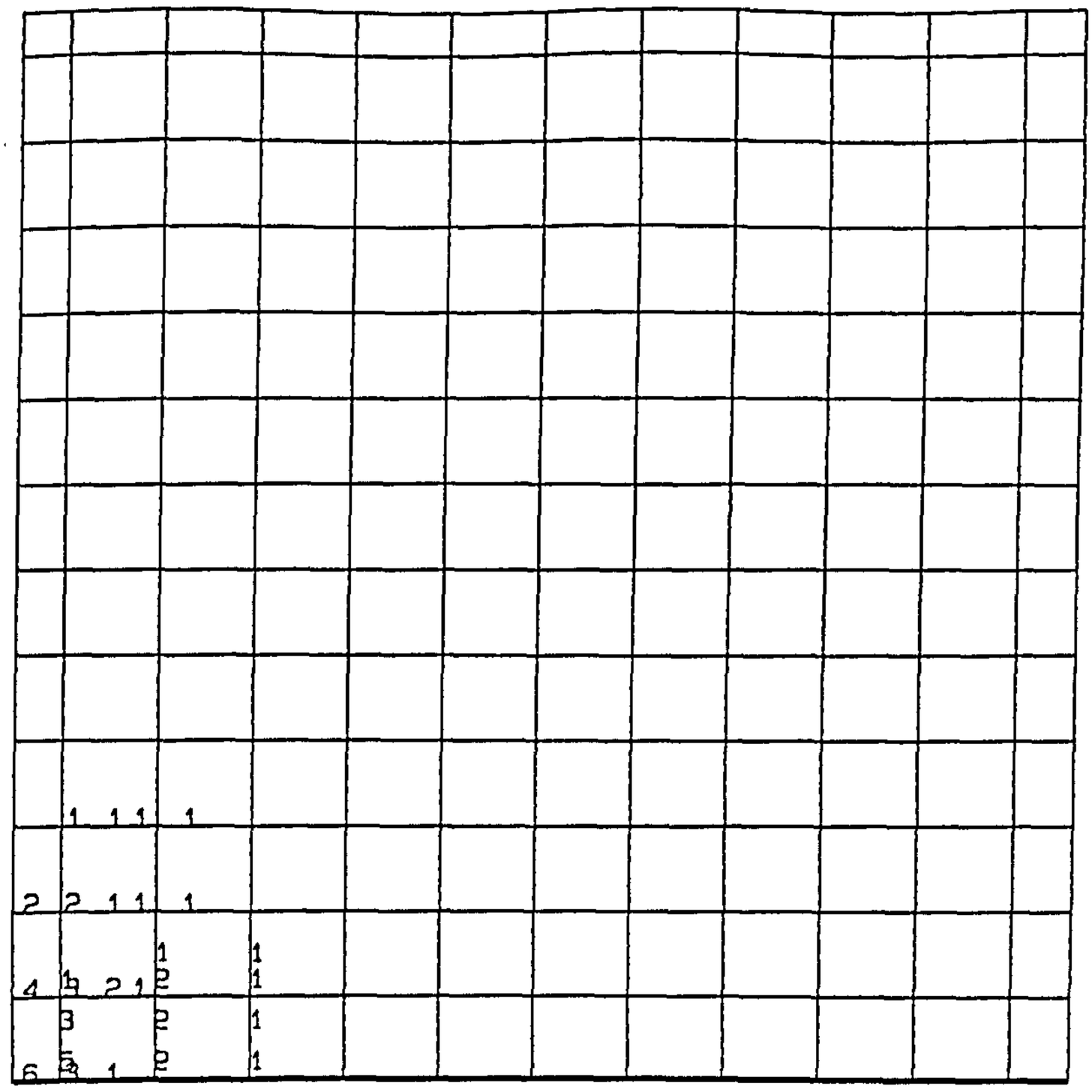

SS6

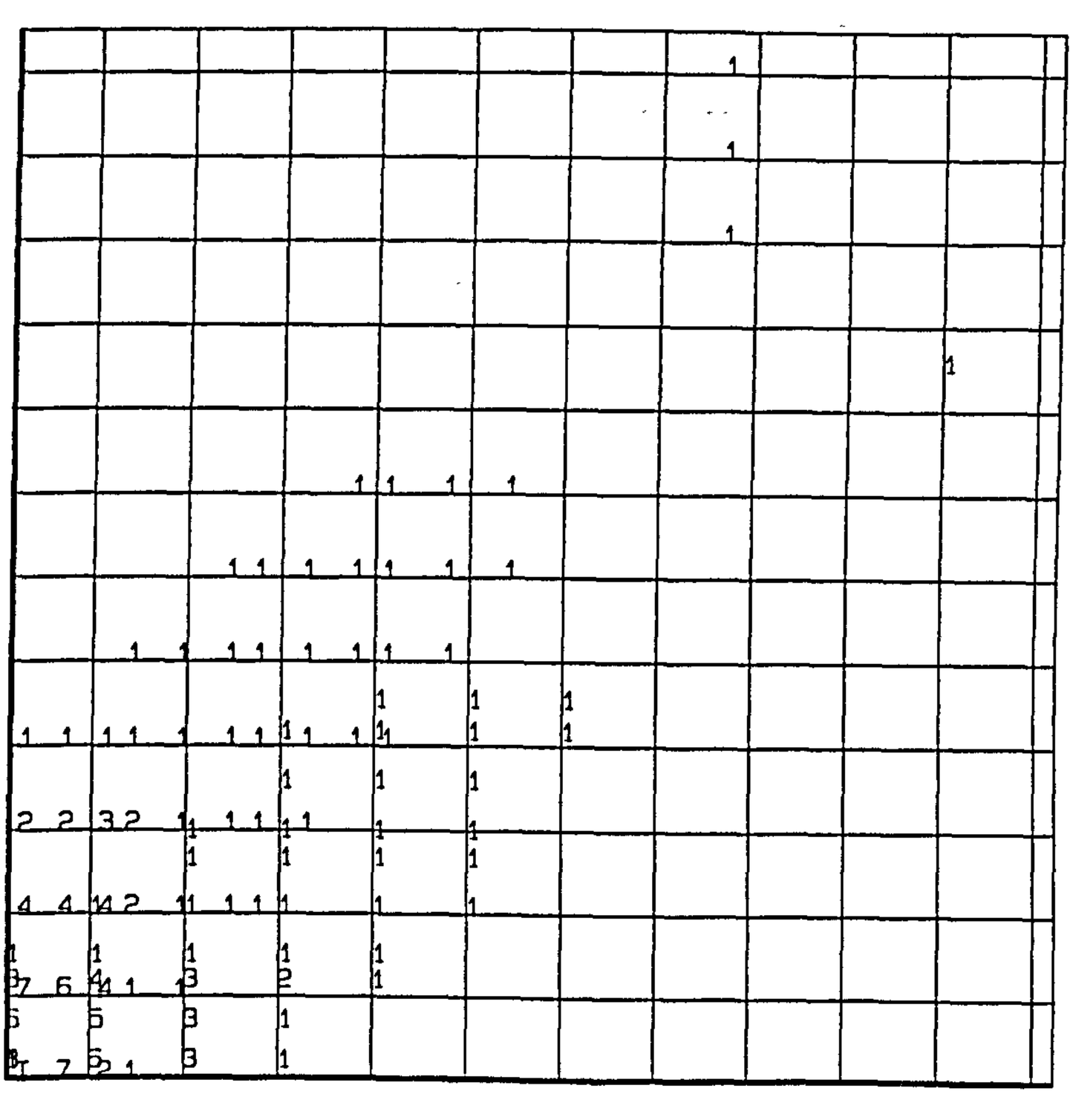

SS7

Note

Flexural steel in slab "**SS1**" did not yield.

Yielding of tension steel, Specimens SS8-SS11 (Regan)

NB. : The numbers on the drawing indicate strain in steel at collapse expressed as a ratio of yield strain

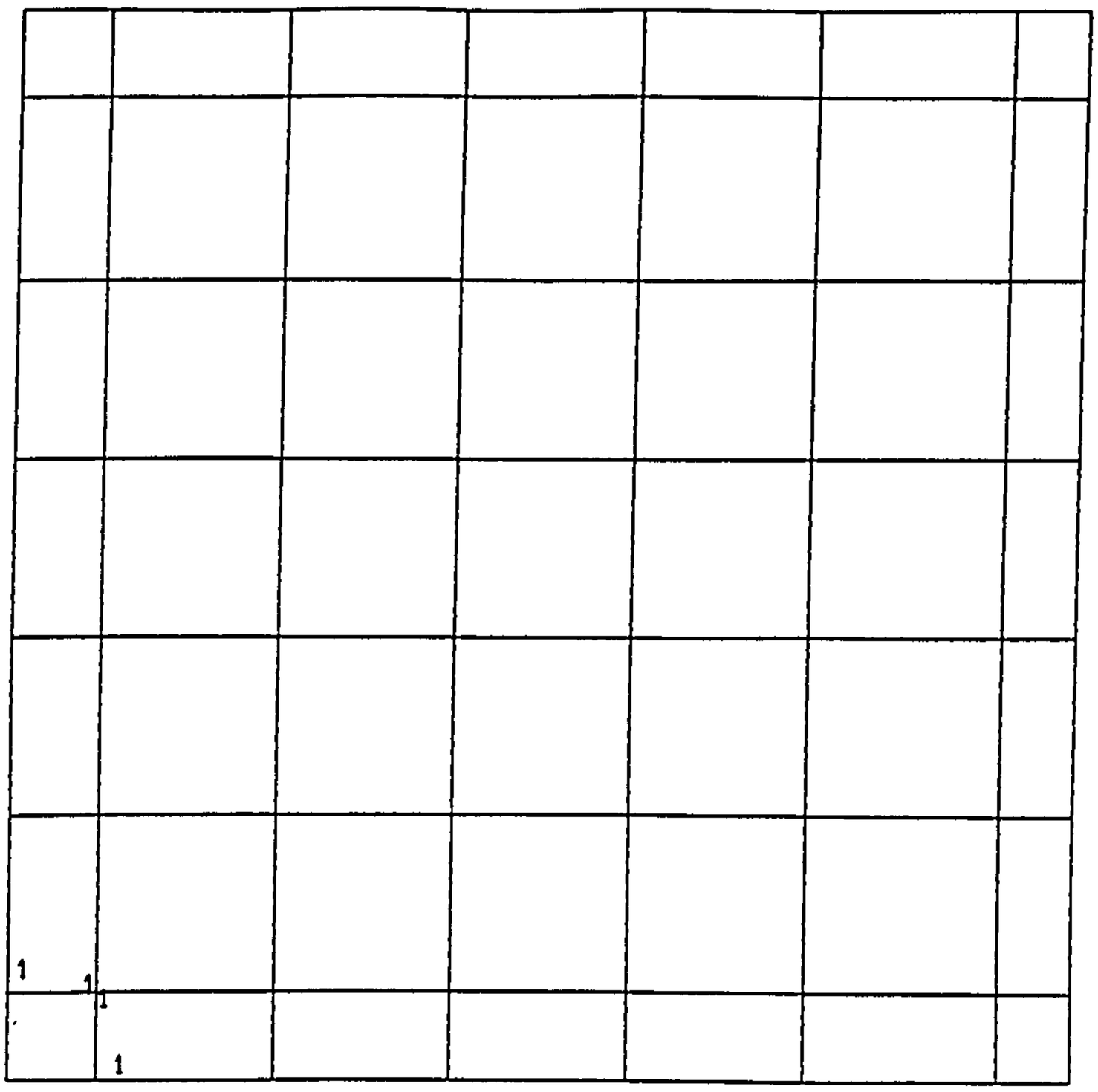

SS8

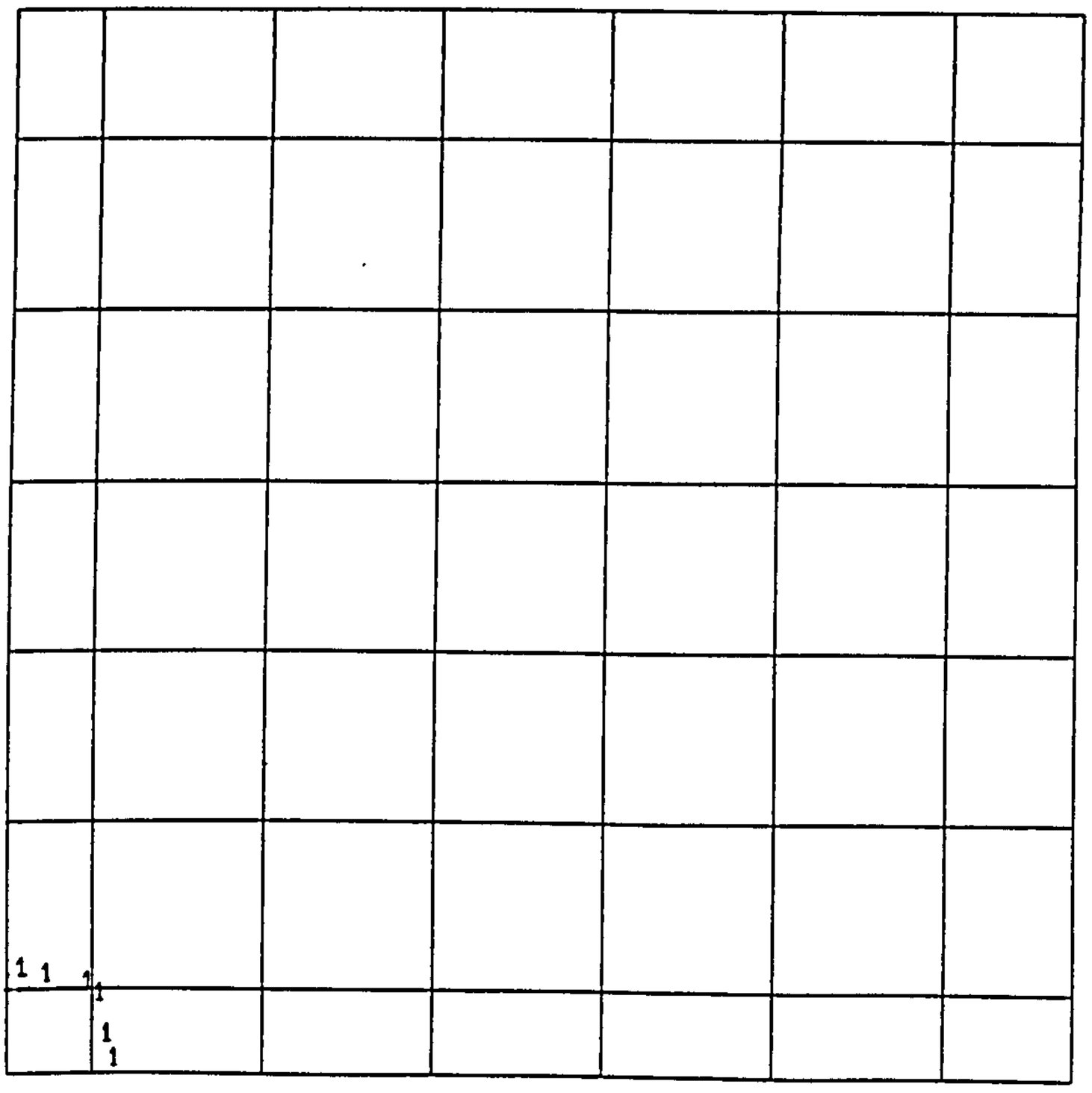

SS9

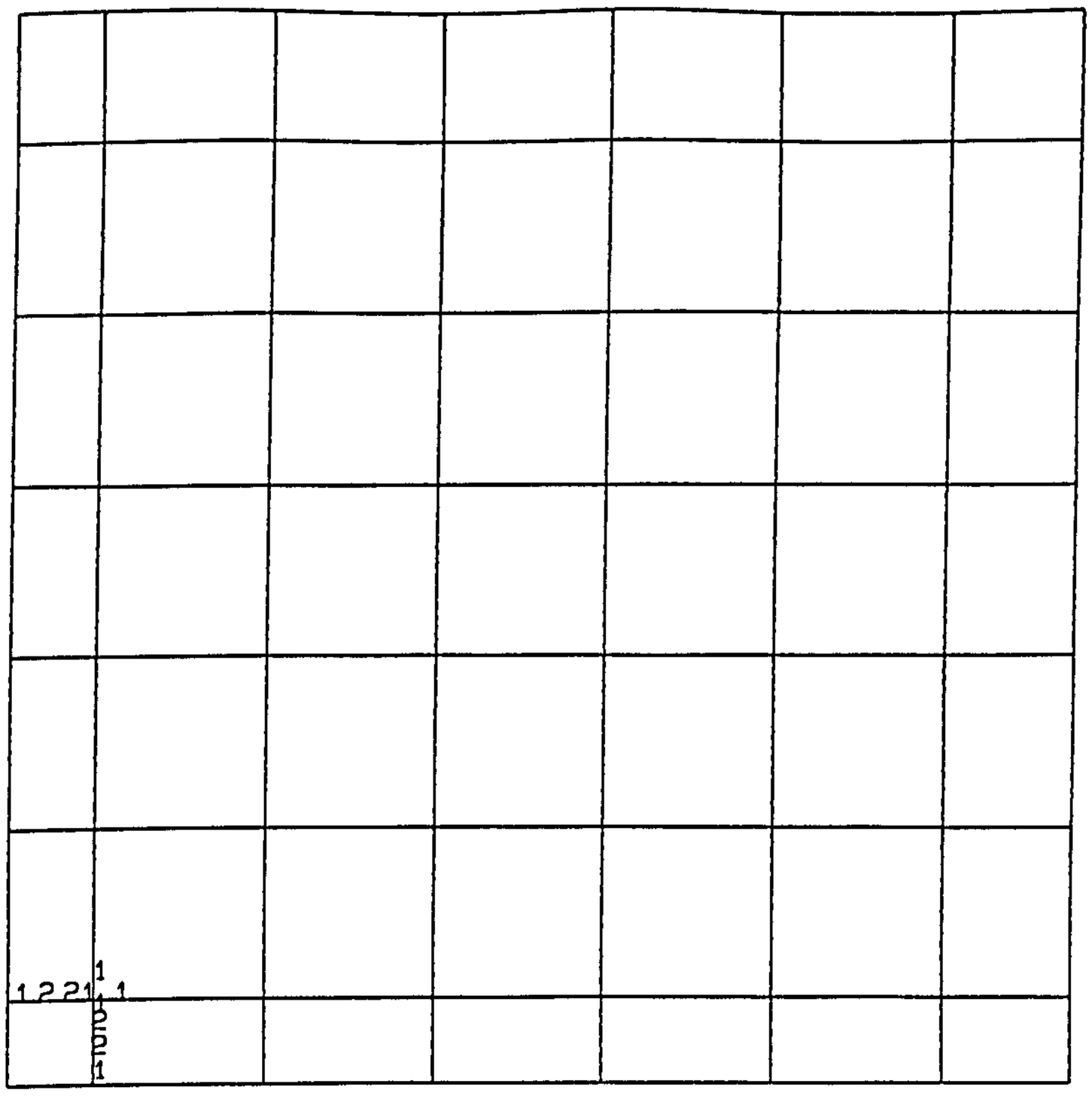

SS11

Yielding of tension steel, Specimens V1-V5 (Regan)

NB. : The numbers on the drawing indicate strain in steel at collapse expressed as a ratio of yield strain

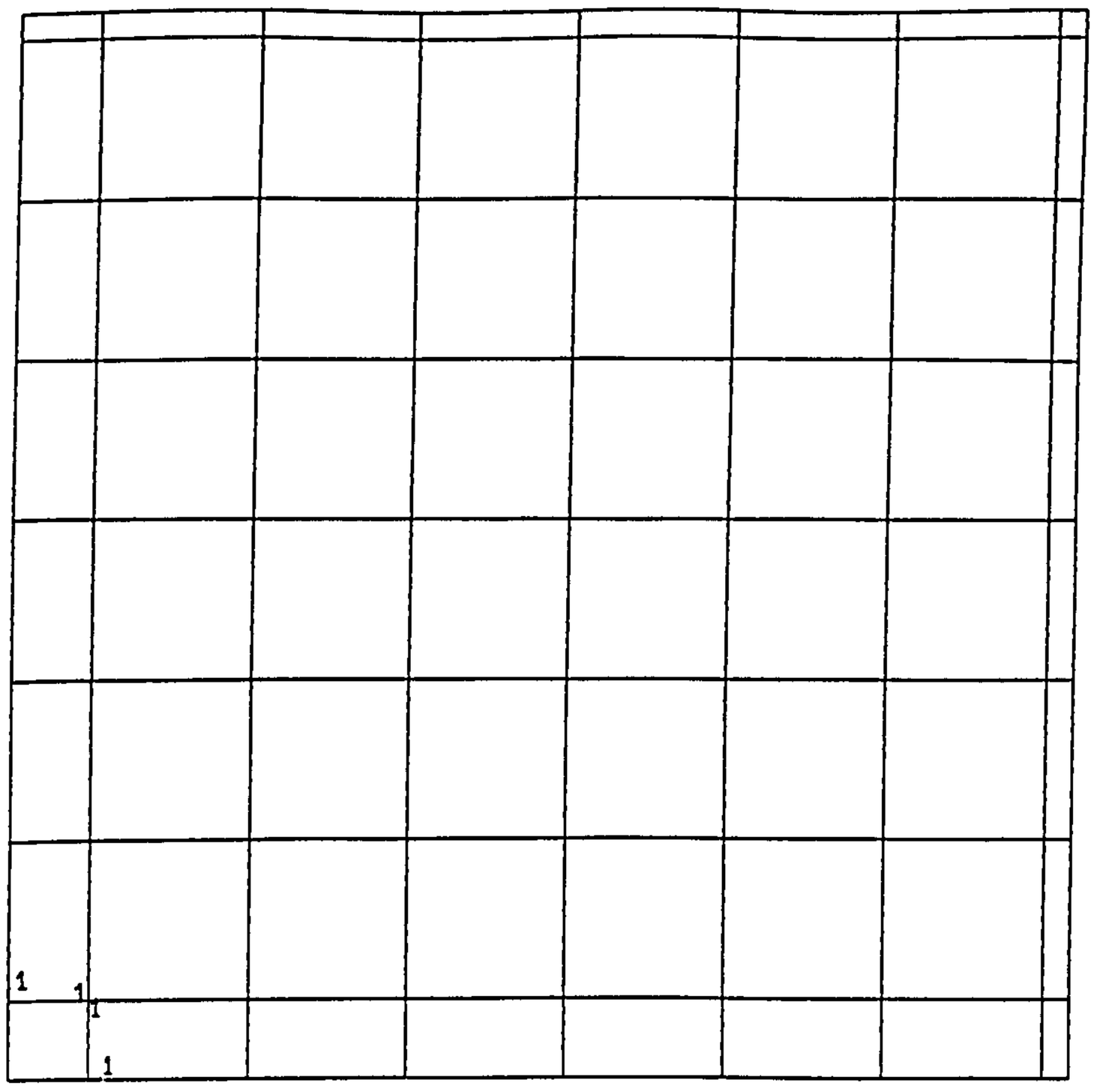

V3

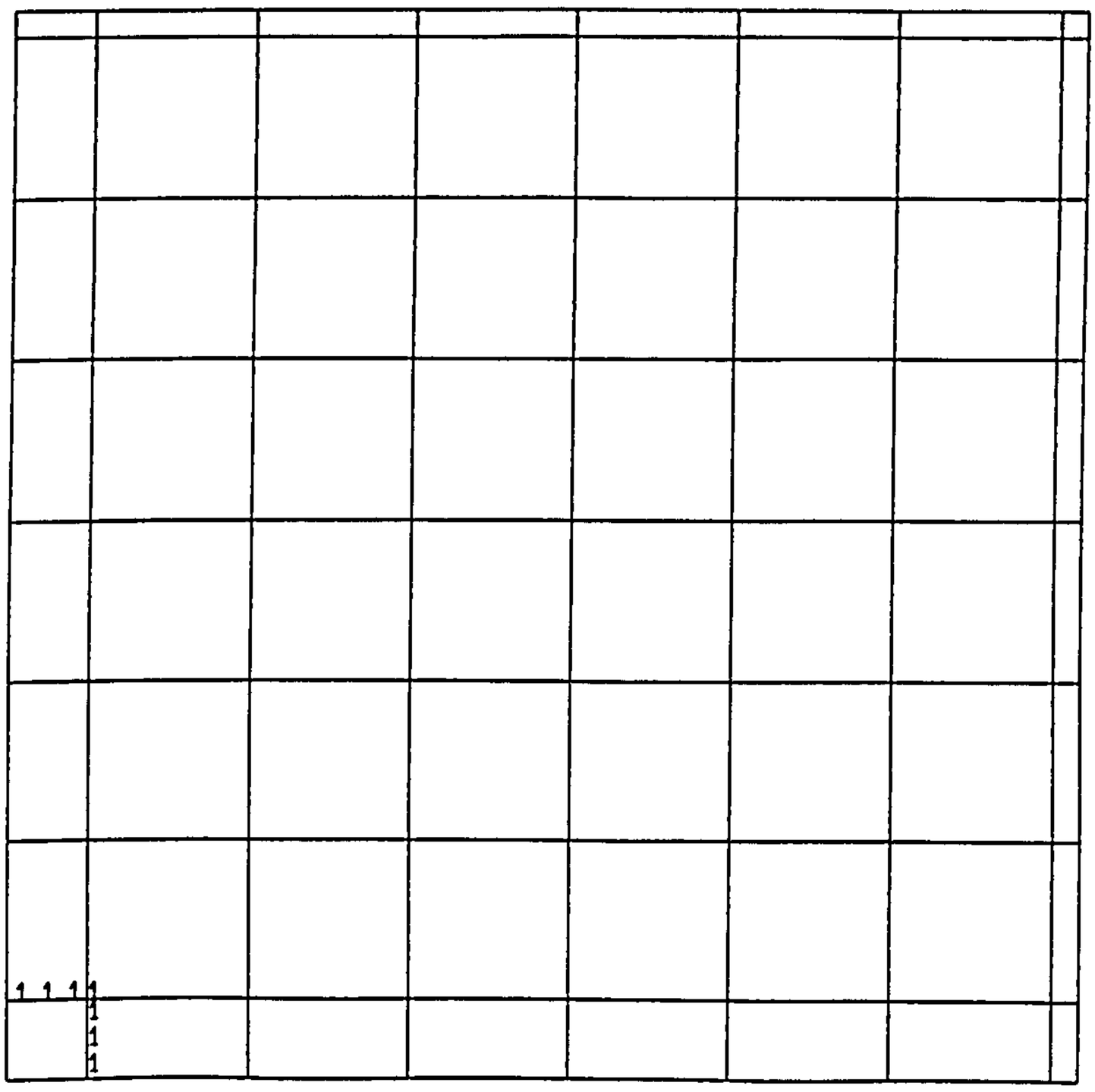

V4

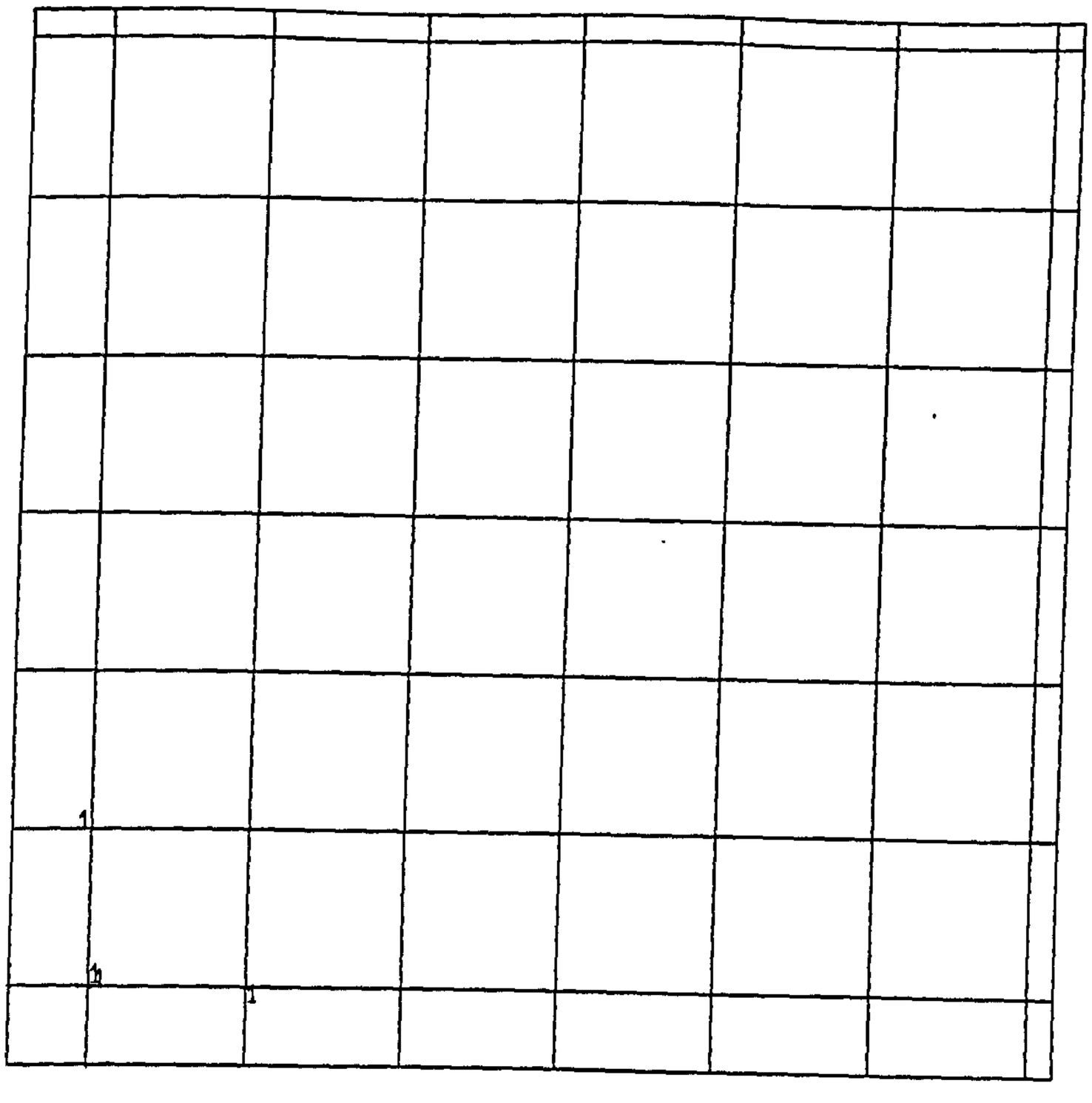

V5

Note

Flexural steel in slab "**V1**" and "**V2**" did not yield.

Yielding of flexural steel for specimens SP1-SP18 (Regan)

NB. : The numbers on the drawing indicate strain in steel at collapse expressed as a ratio of yield strain

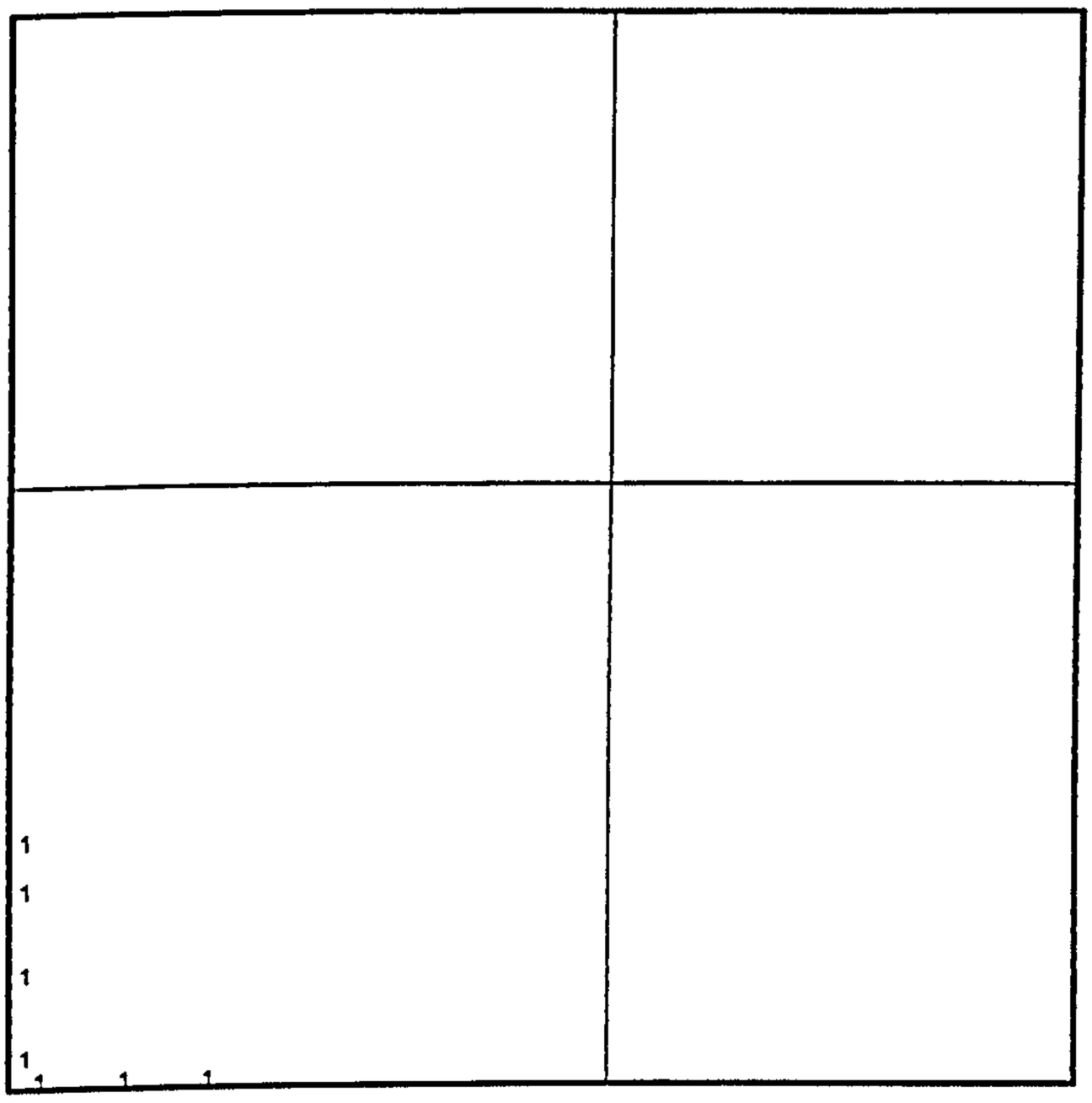

SP8

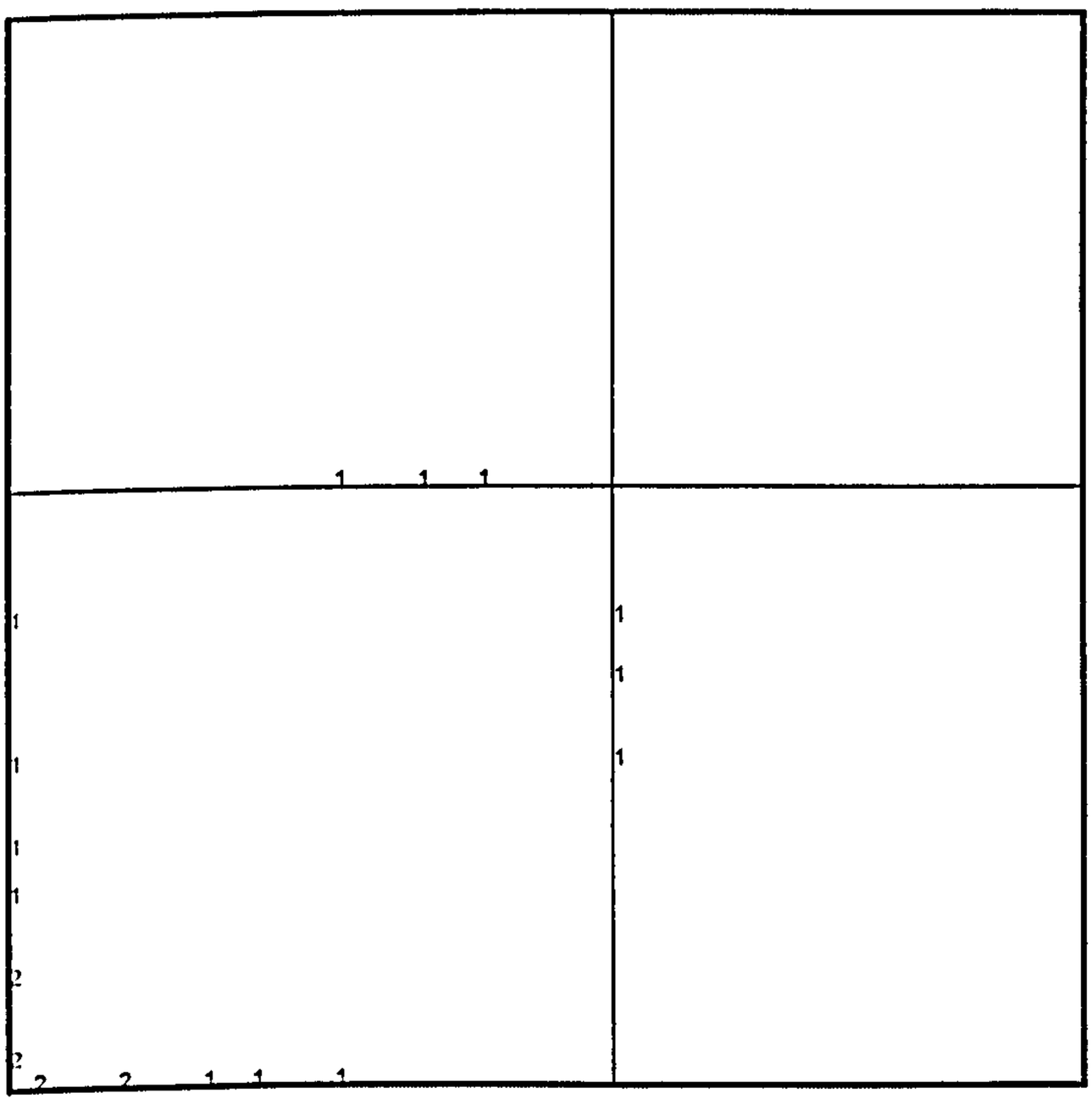

SP9

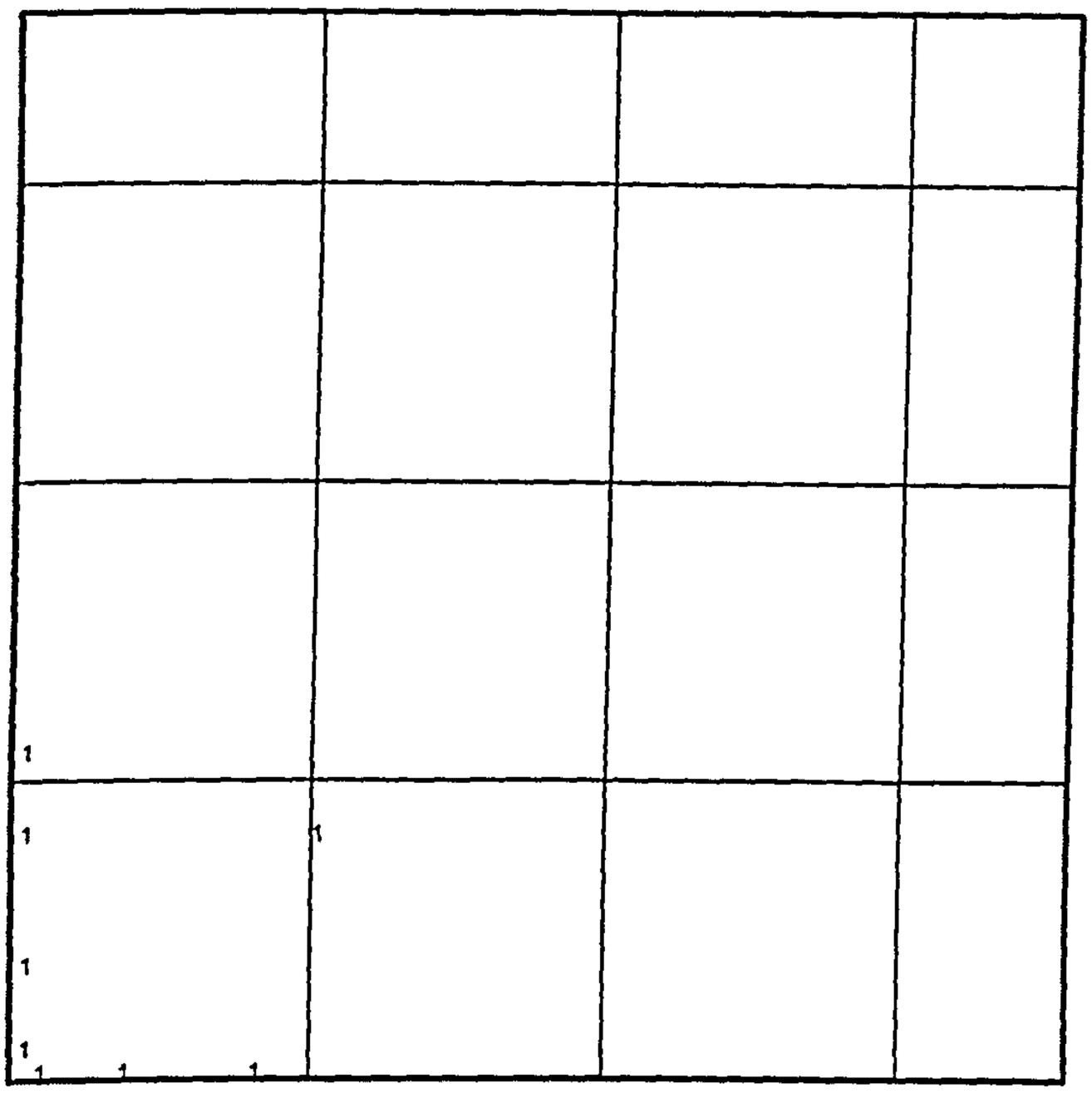

SP14

Note

Flexural steel in following slabs did not yield :

SP1, SP2, SP3, SP4, SP5, SP6, SP7, SP10, SP11, SP12, SP13, SP15, SP16, SP17, SP18.

Predicted crack pattern for slabs SS1-SS7 (CIRIA 220)

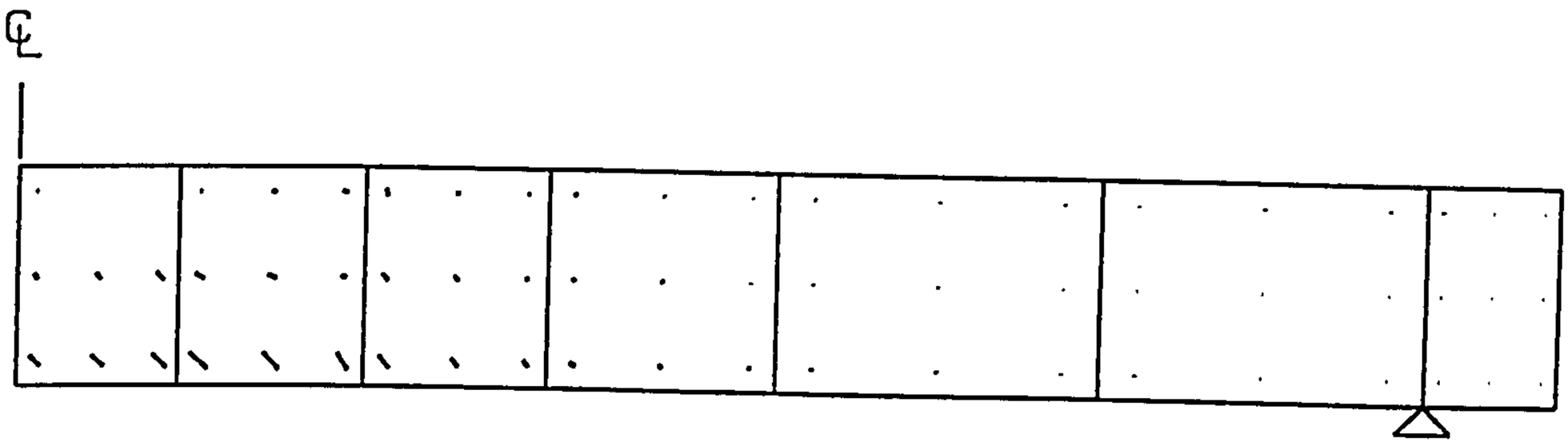

" SS1 "

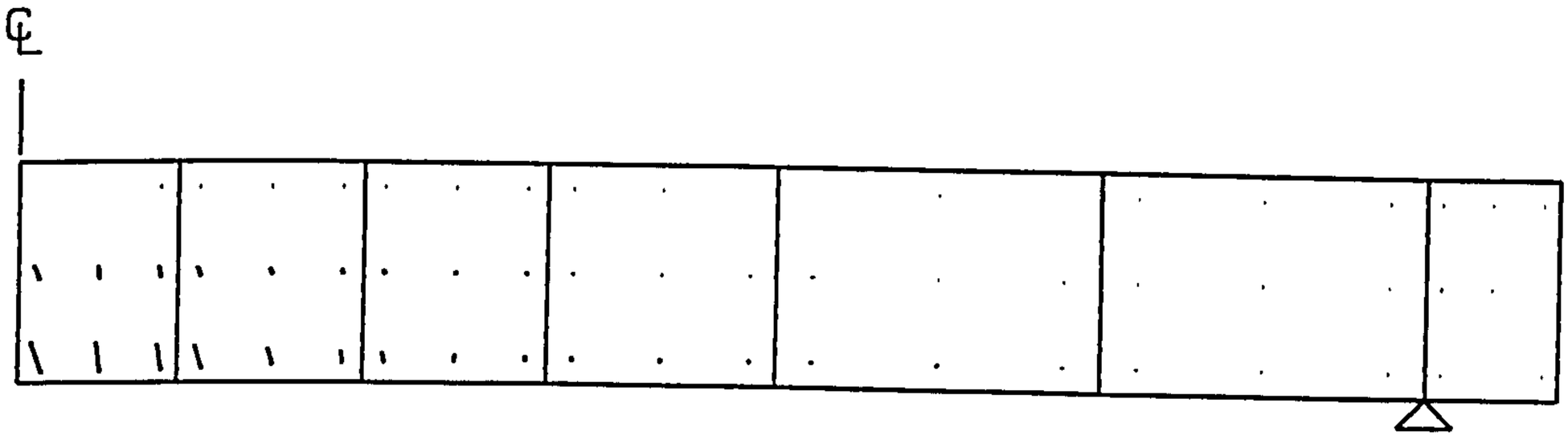

" SS2 "

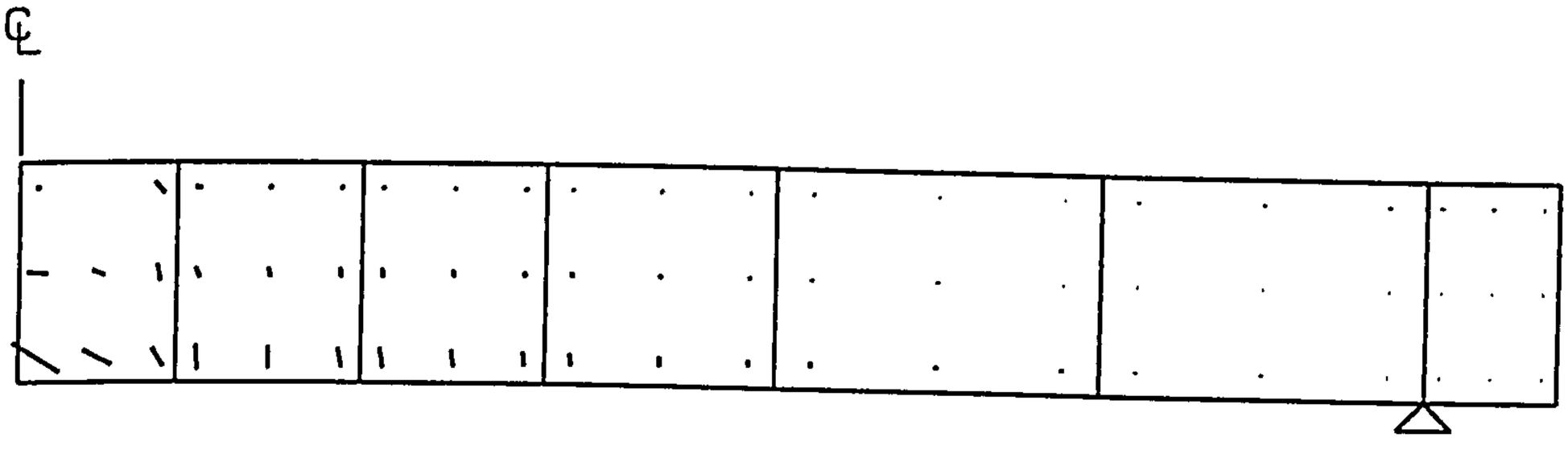

" SS3 "

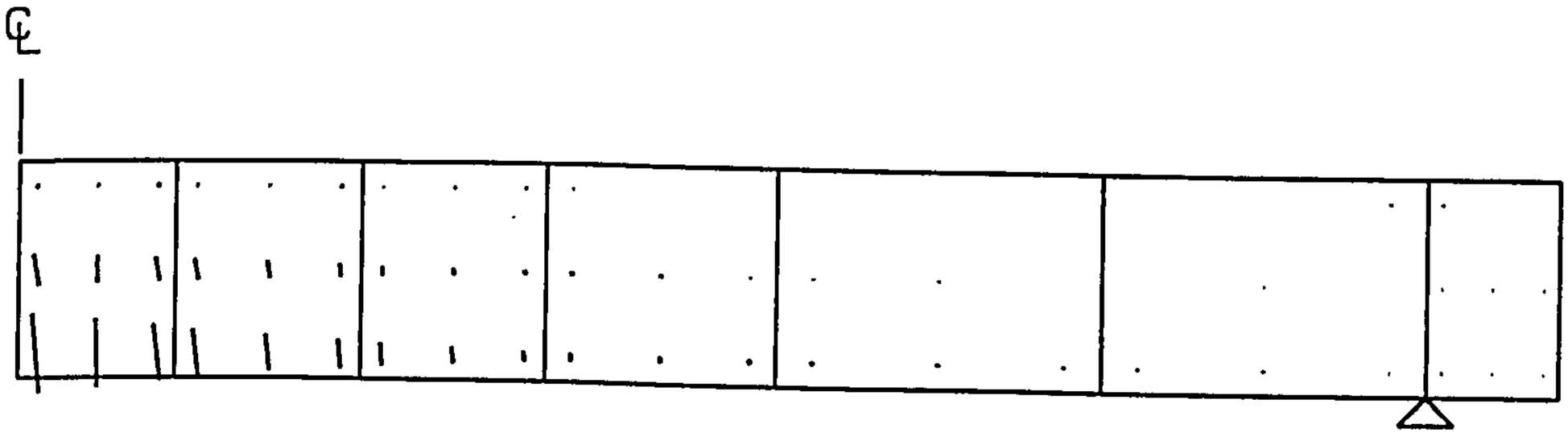

" SS4 "

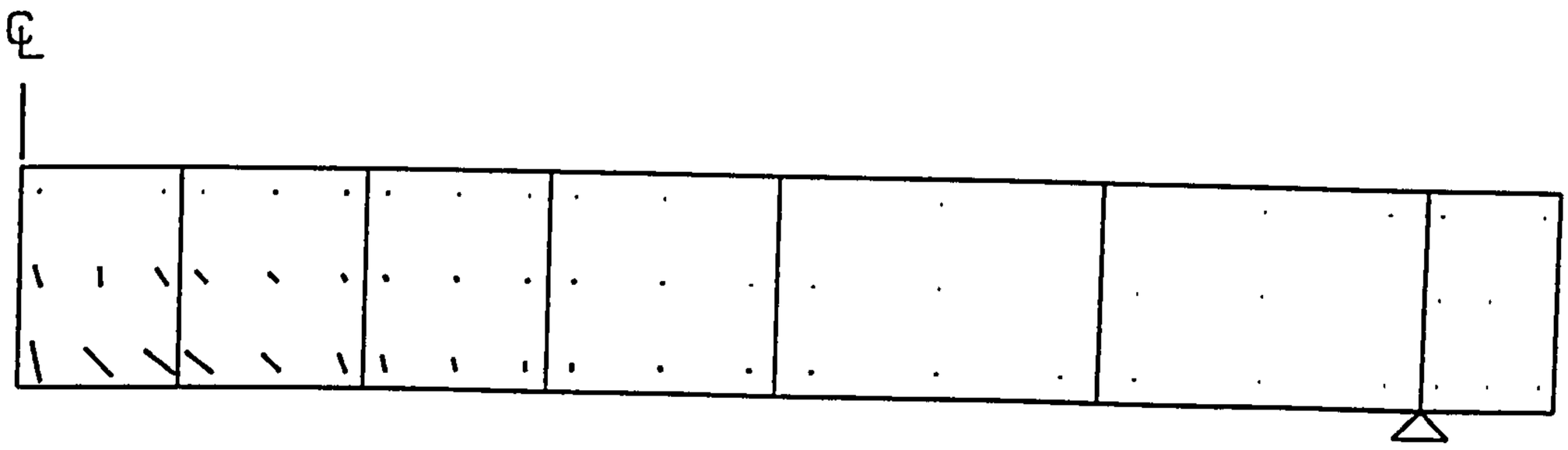

" SS5 "

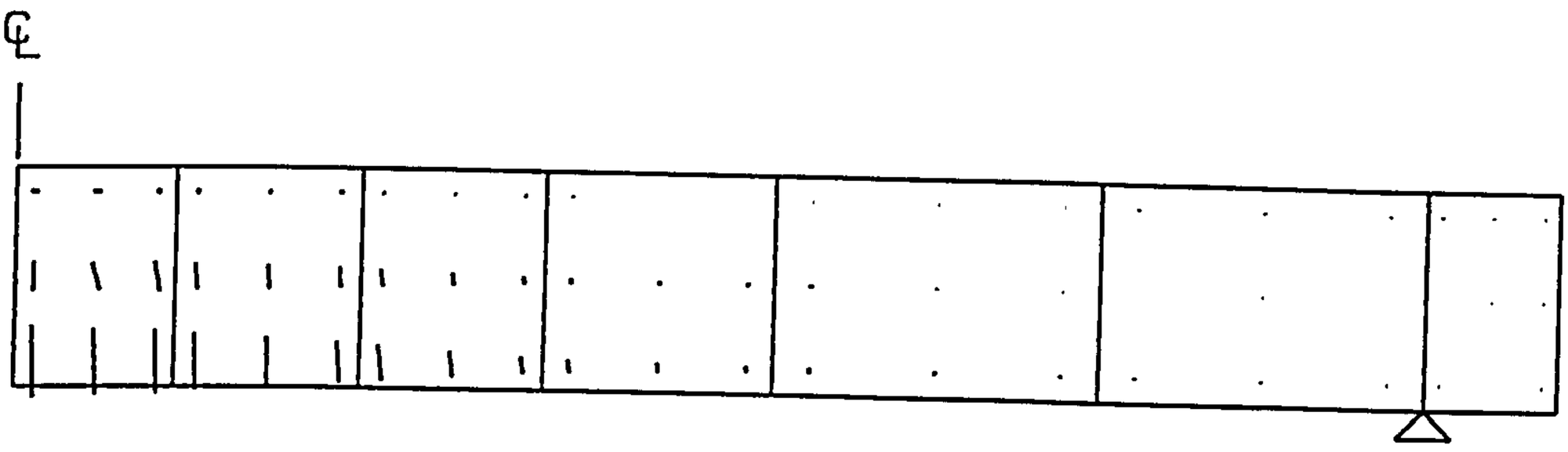

" SS6 "

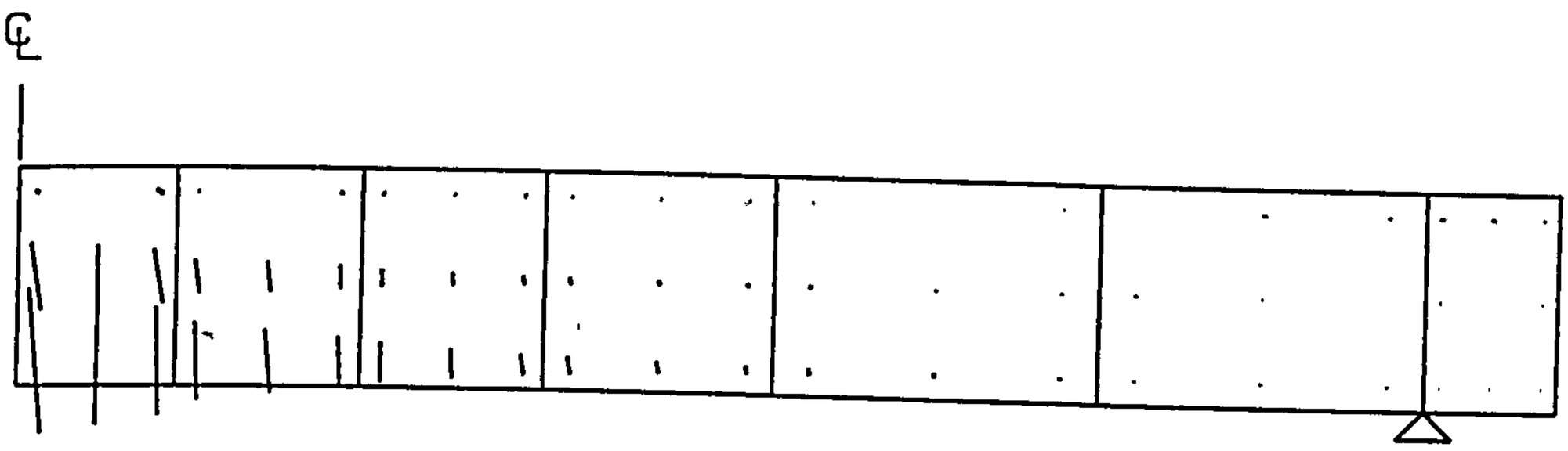

" SS7 "

Predicted crack pattern for slabs SS8-SS13 (CIRIA 220)

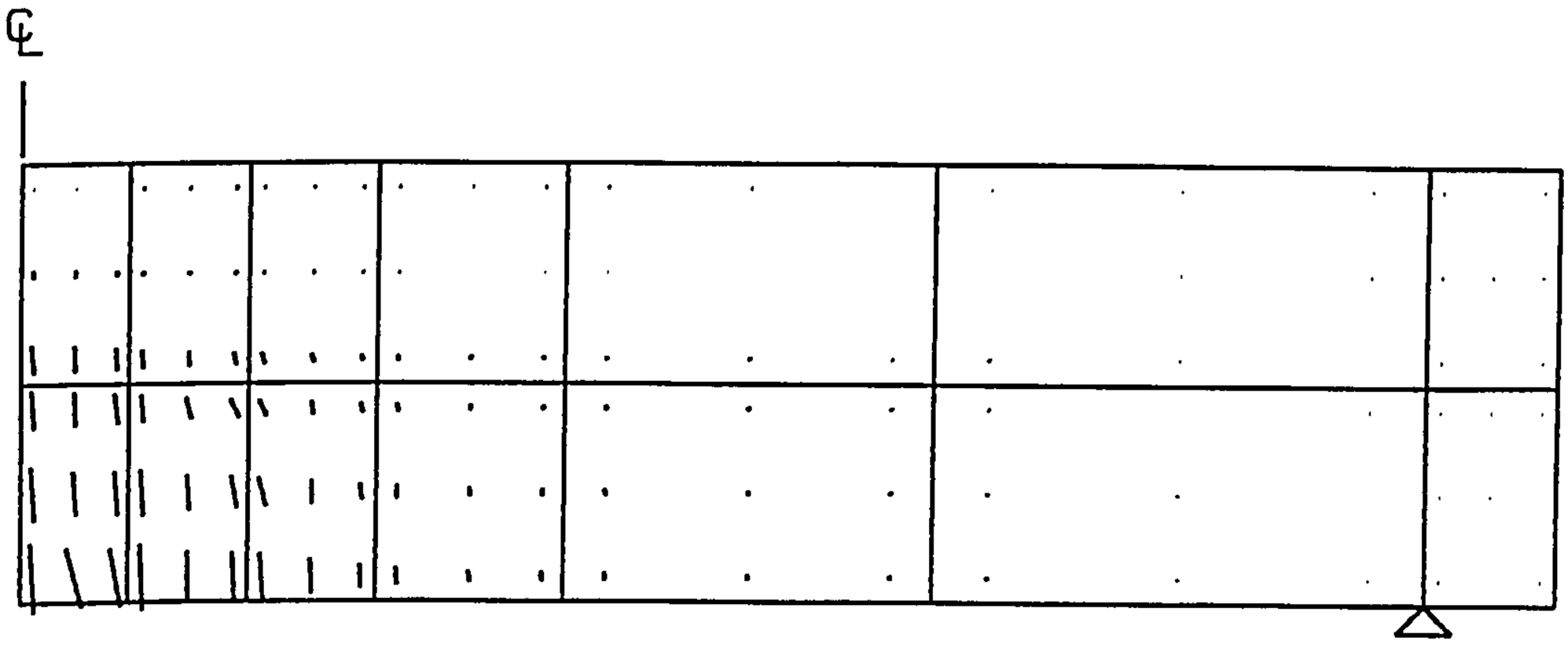

" SS8 "

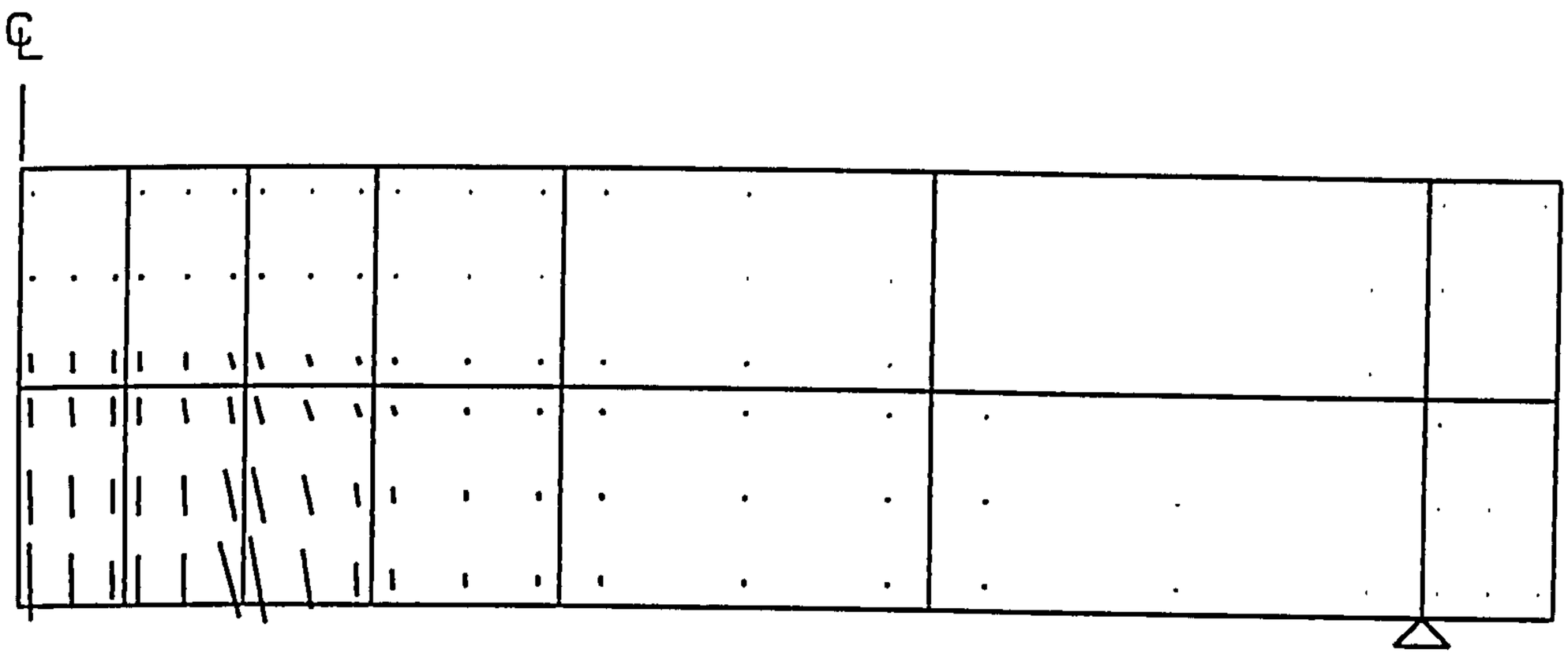

" SS9 "

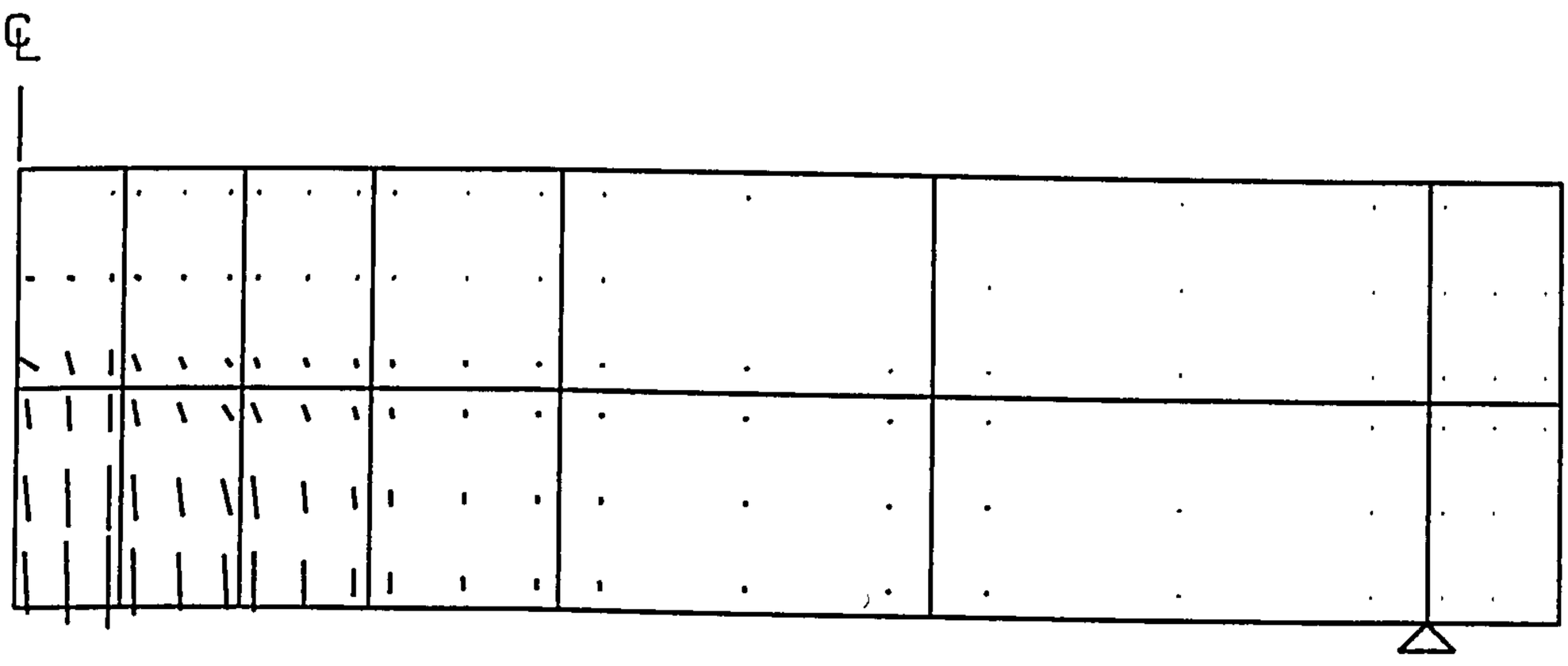

" SS11 "

Predicted crack pattern for slabs V1-V5 (Regan)

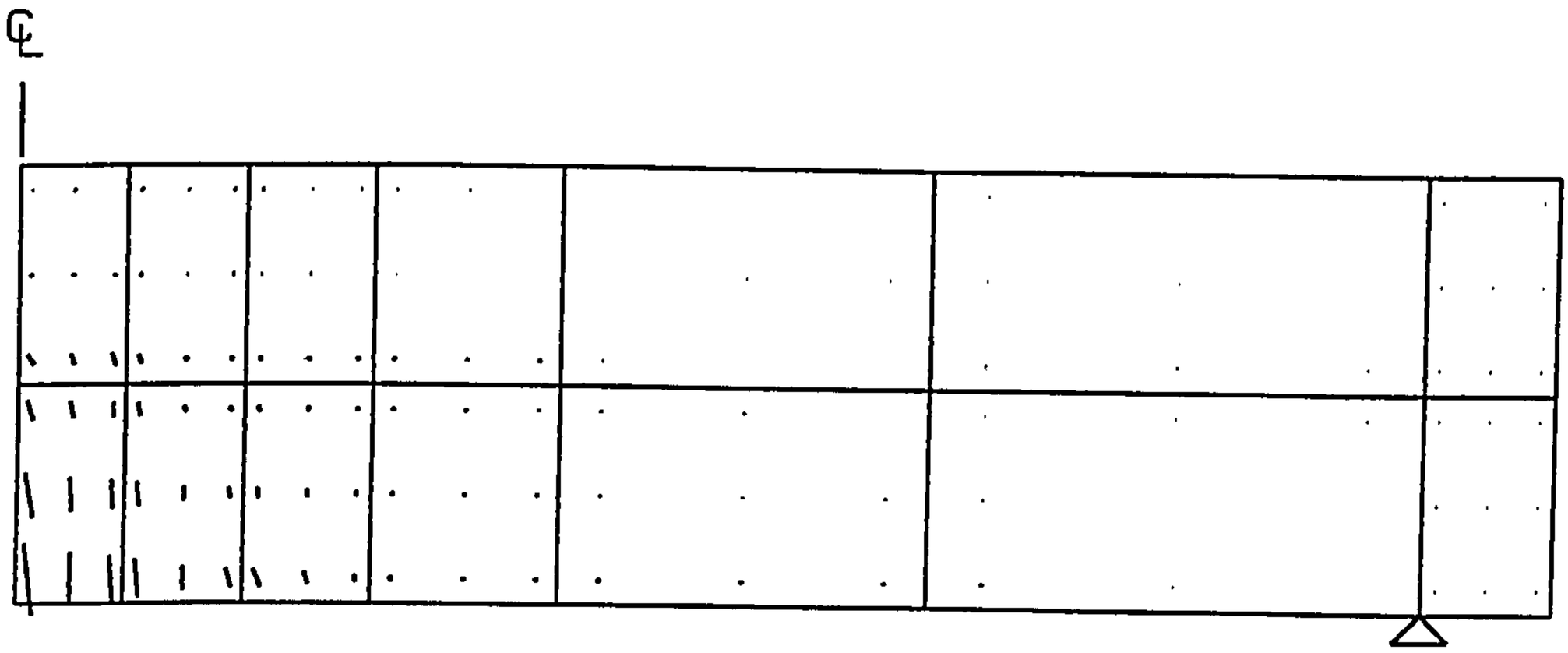

" V1 "

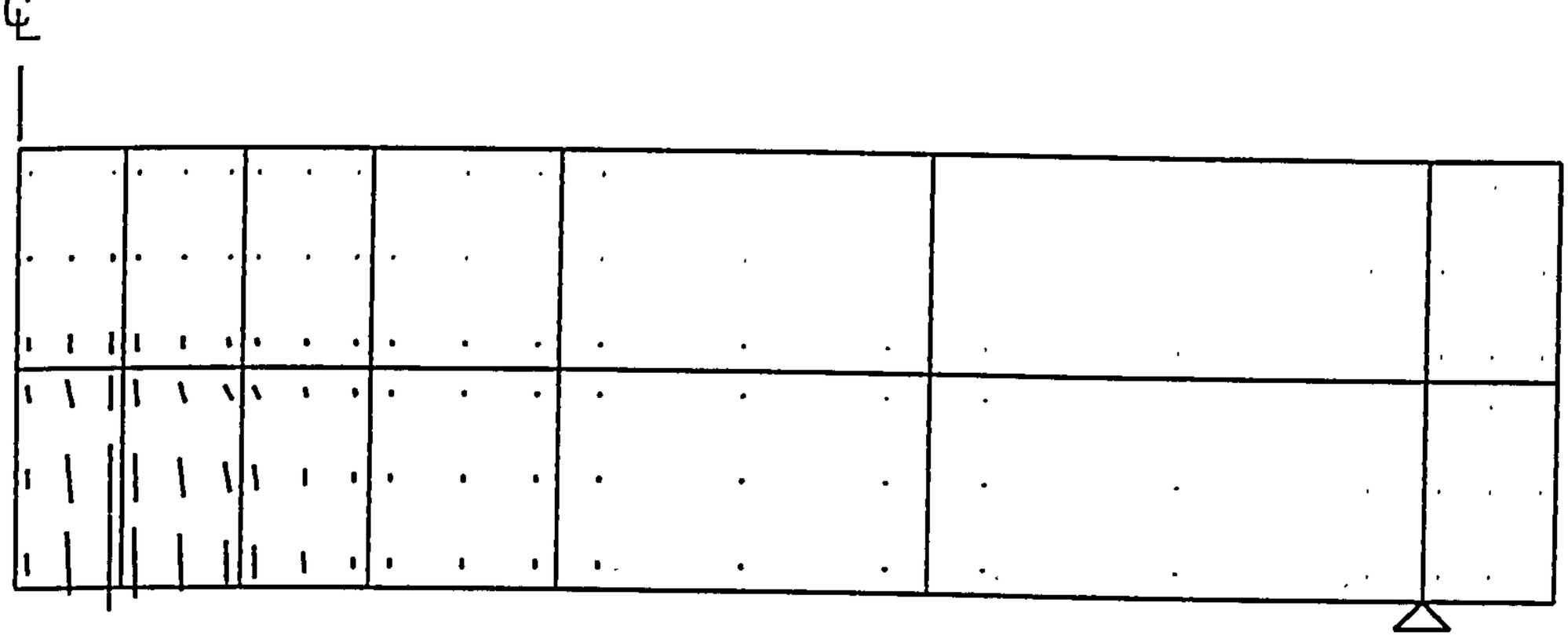

" V2 "

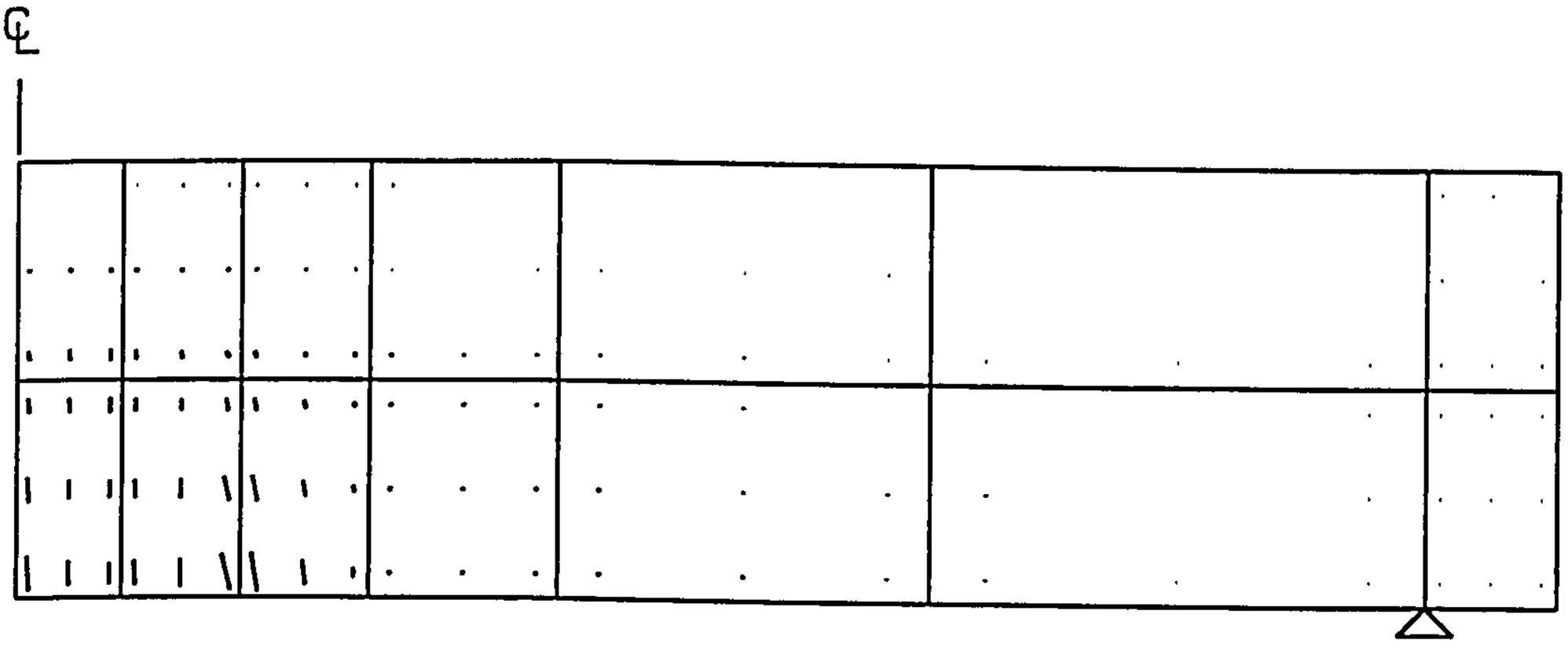

" V3 "

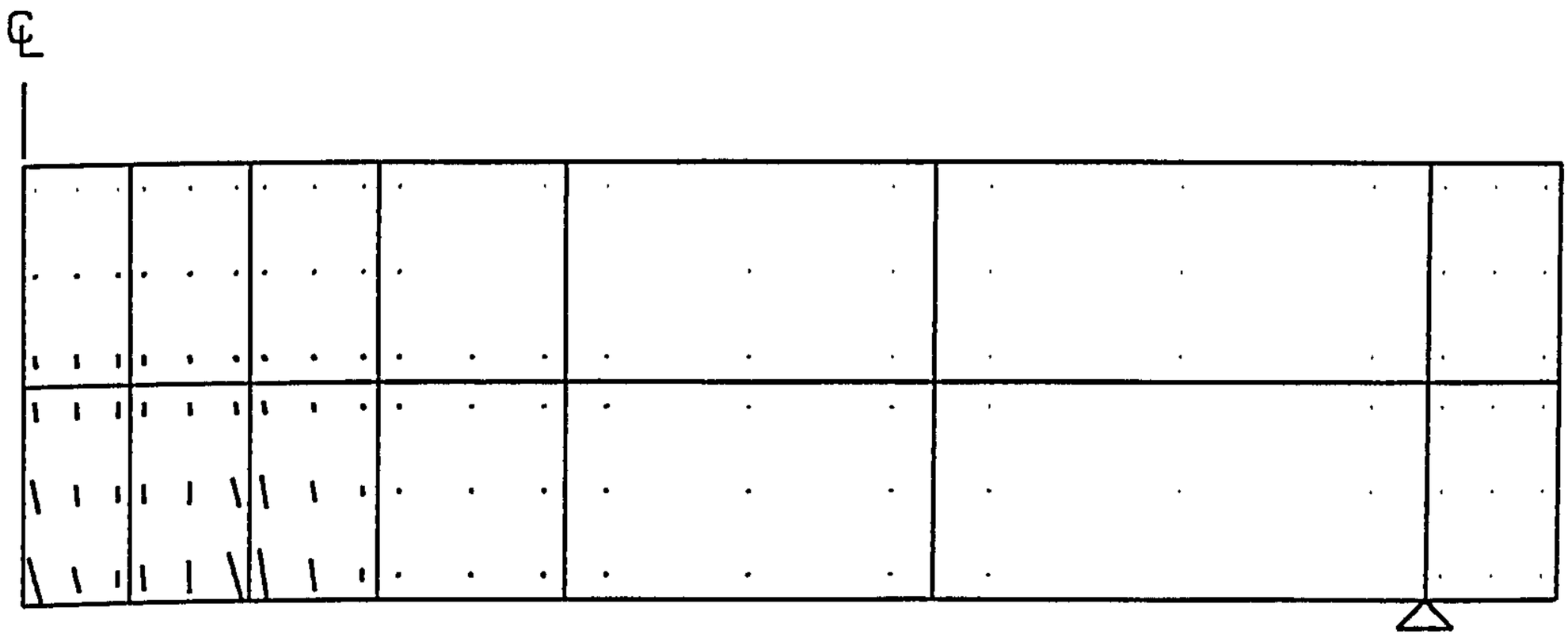

" V4 "

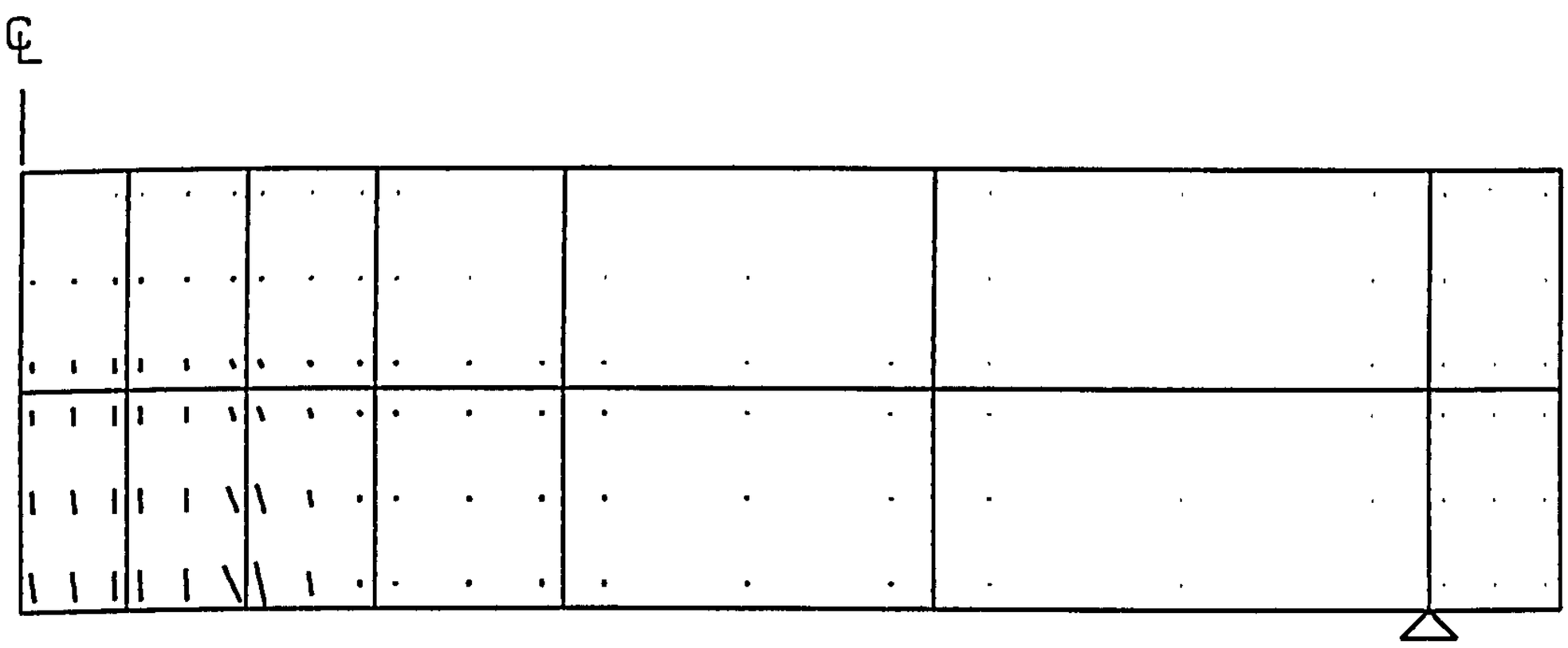

" V5 "

Predicted crack pattern for specimens SP1-SP18 (Regan)

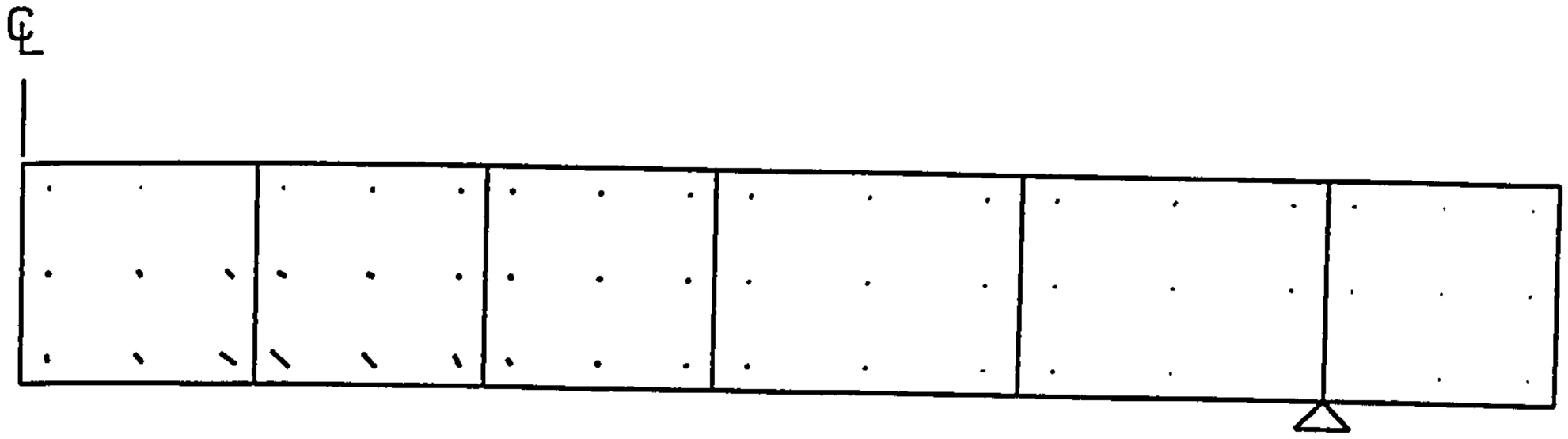

SP1

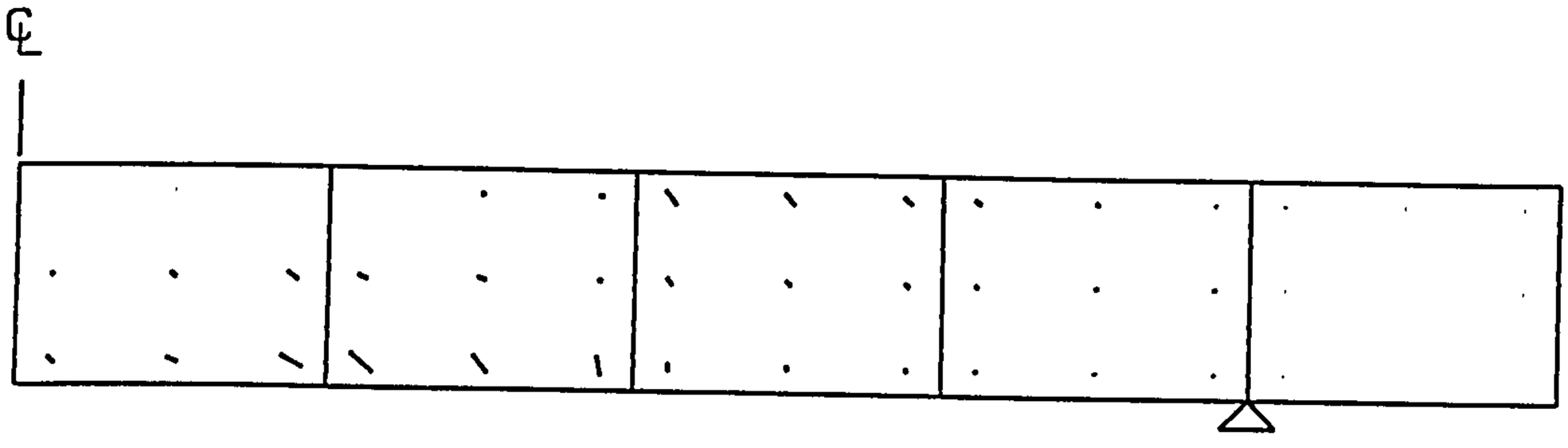

SP2

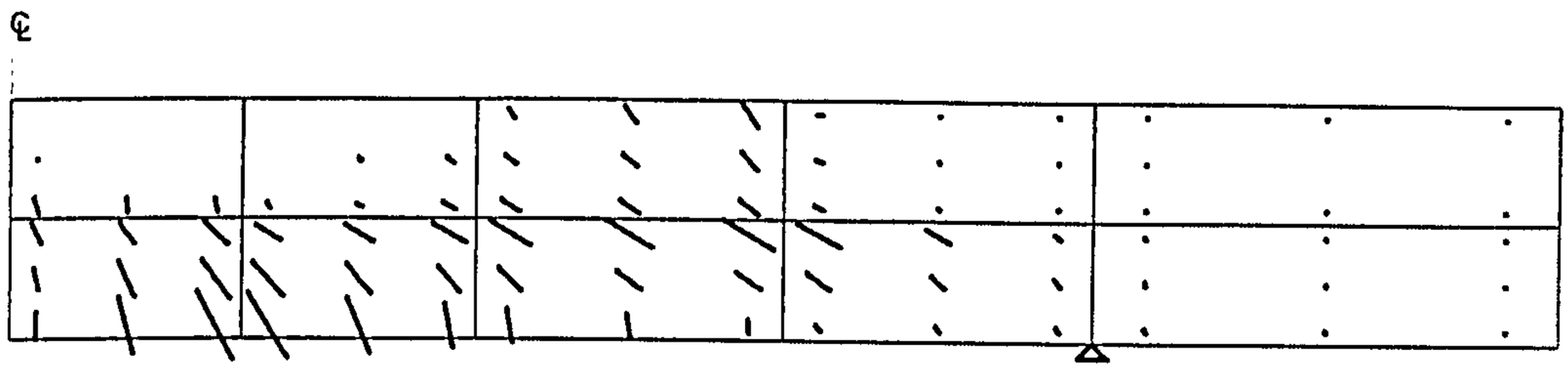

SP3

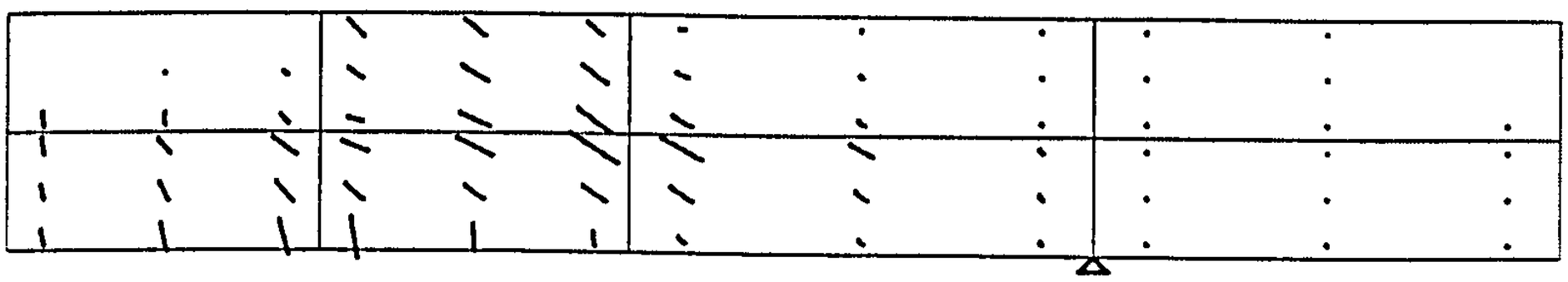

SP4

SP5

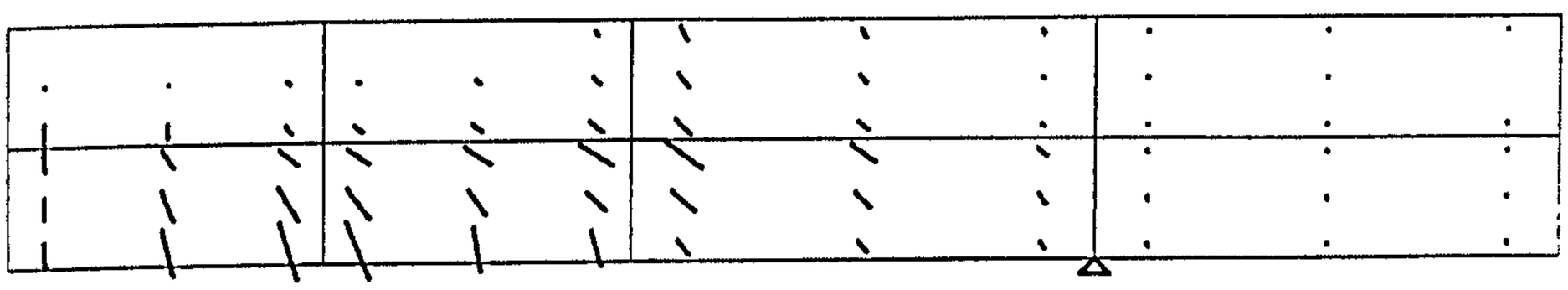

SP8

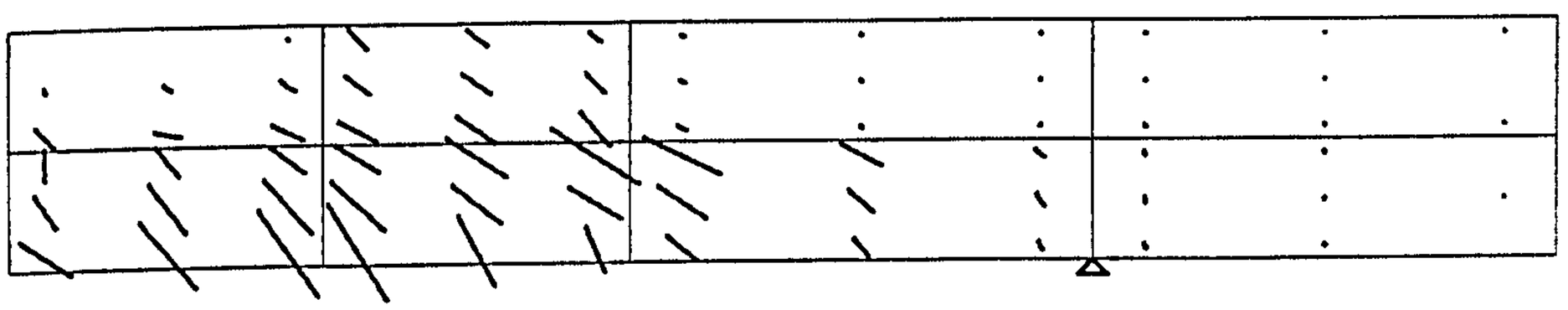

SP9

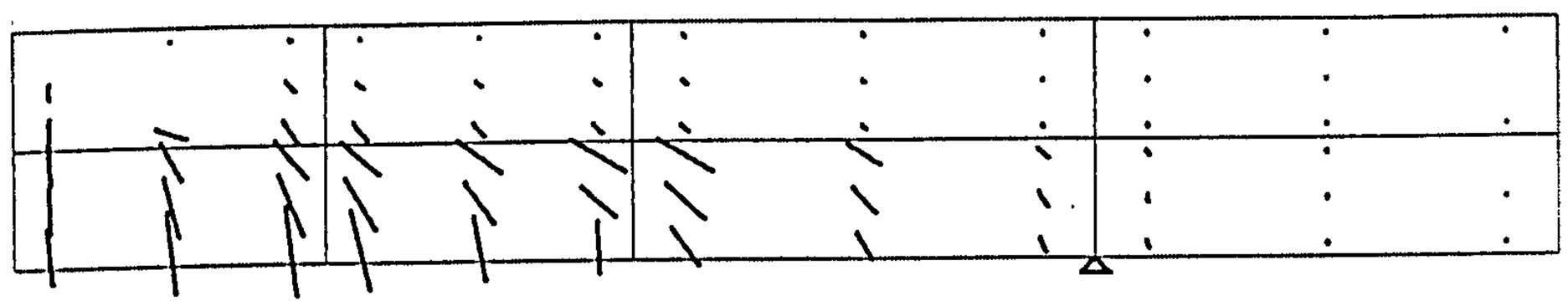

SP10

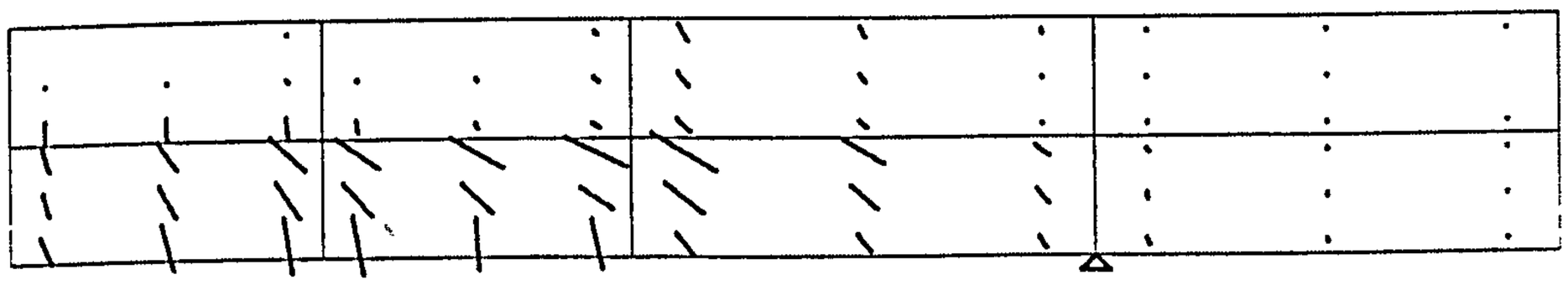

℄

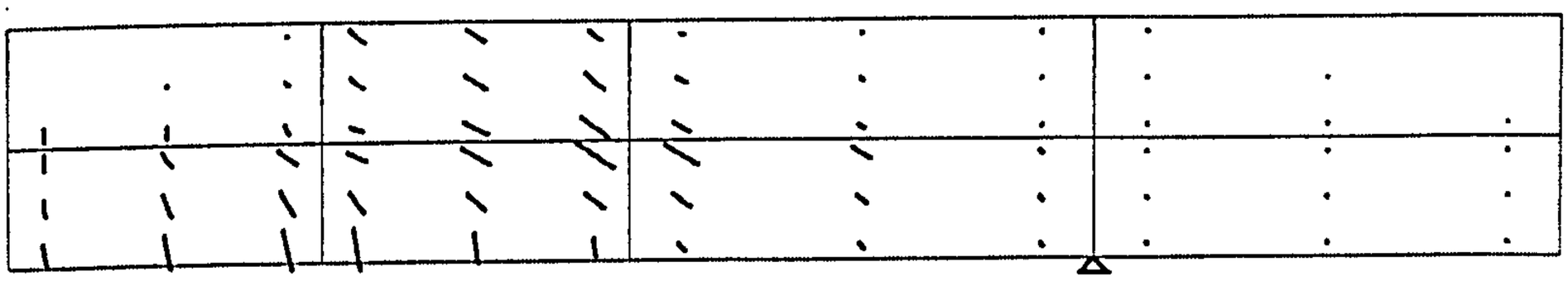

SP11

℄

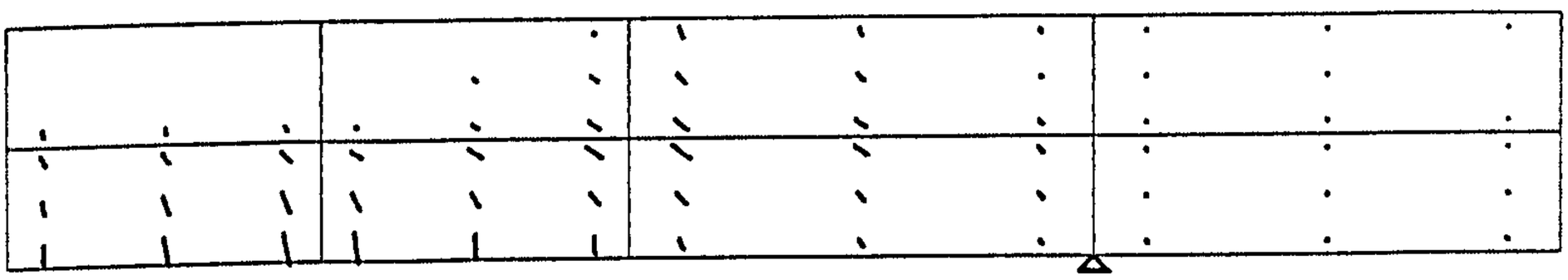

SP12

℄

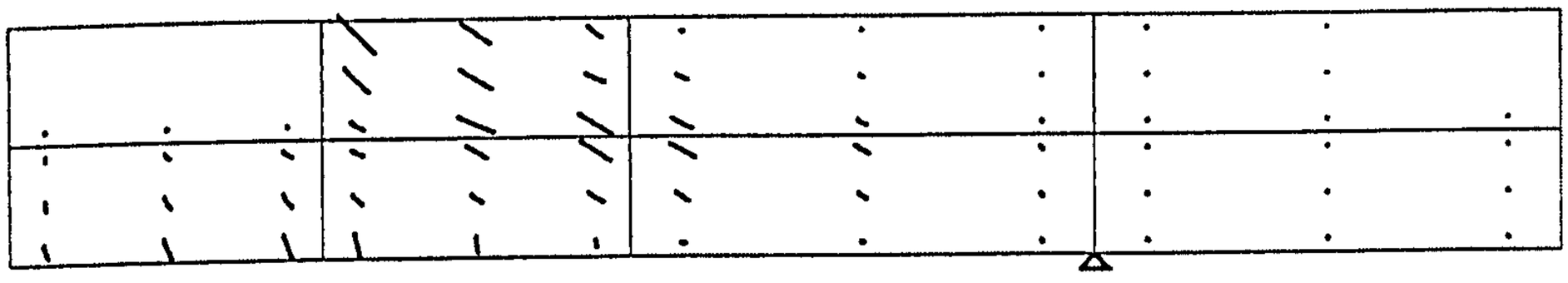

SP13

℄

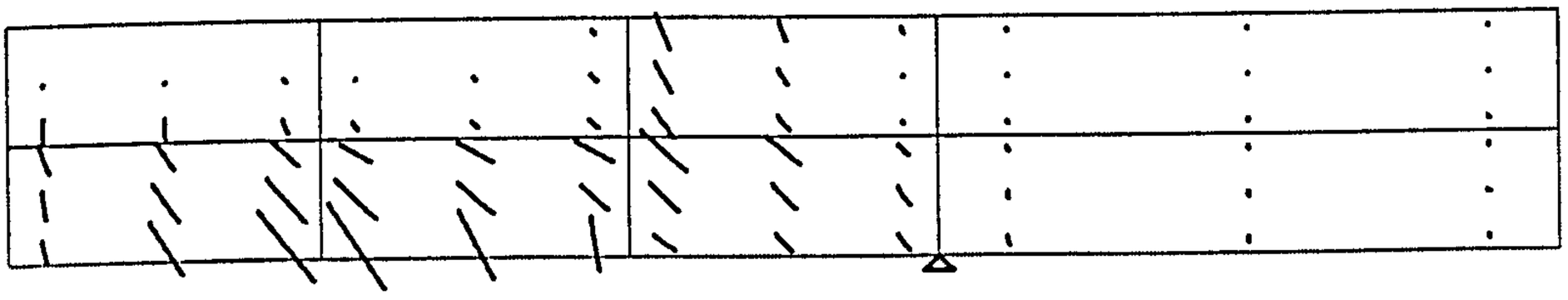

SP14

℄

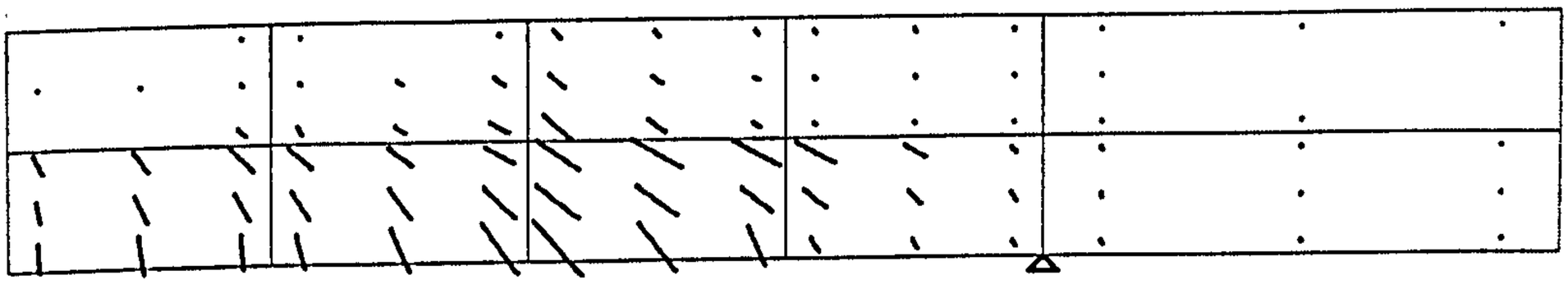

SP15

℄

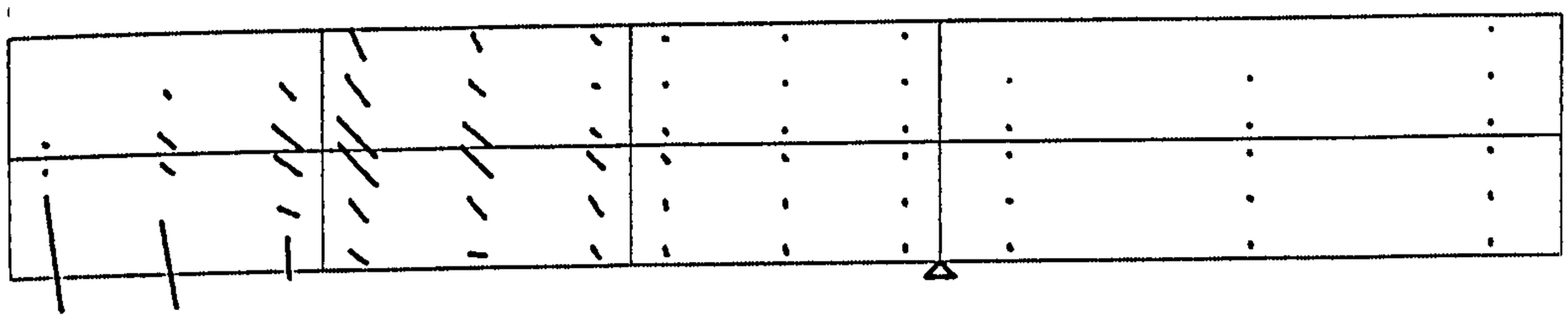

SP16

℄

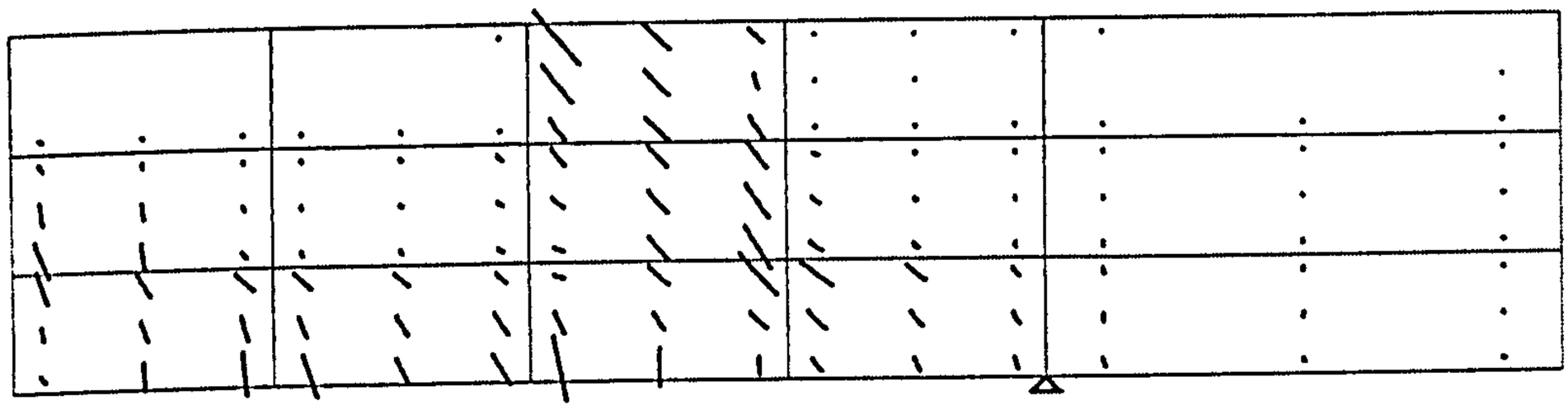

SP17

℄

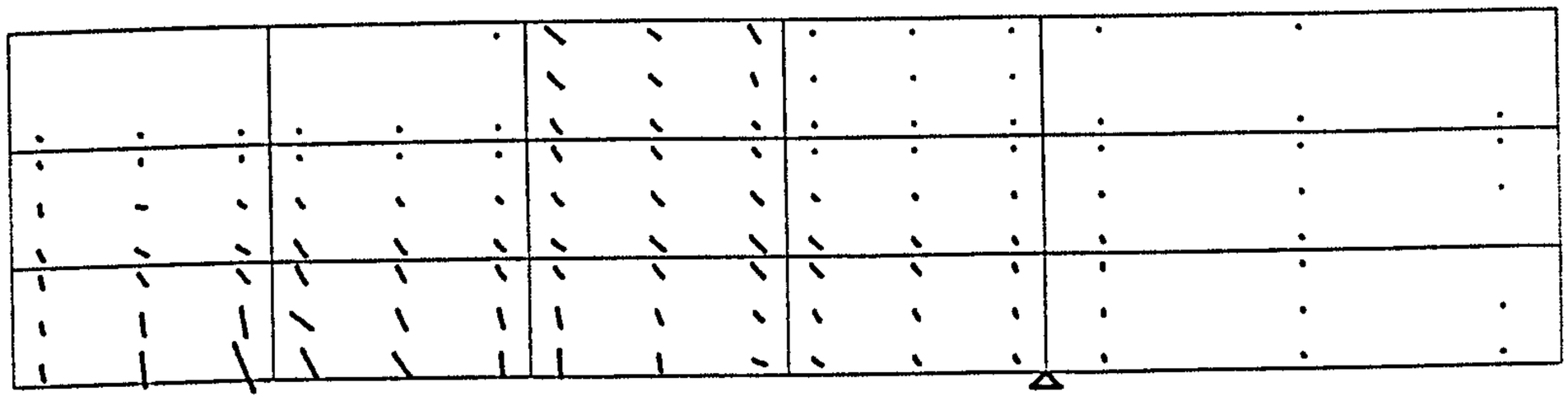

SP18

Chana and Desai's slabs

C1.3 Chana and Desai's slabs (with shear reinforcement)

Slab	Experimental results		Numerical predictions		P_{num}/P_{test}
	P_{test} (kN)	Failure Mode	P_{num} (kN)	Failure Mode	
C1	805.0	s	686.8	s	0.850
C2	1094.0	s	938.4	s	0.858
C4	1302.0	s	1142.4	fp	0.877
C5	1382.0	s	1248.0	s	0.903
C6	1283.0	s	1404.0	fp	1.094
C7	1492.0	s	1232.0	s	0.826
C8	1324.0	s	1152.0	s	0.870
C9	1135.0	s	912.0	fp	0.804
				Average	0.885
				STDEV	0.090

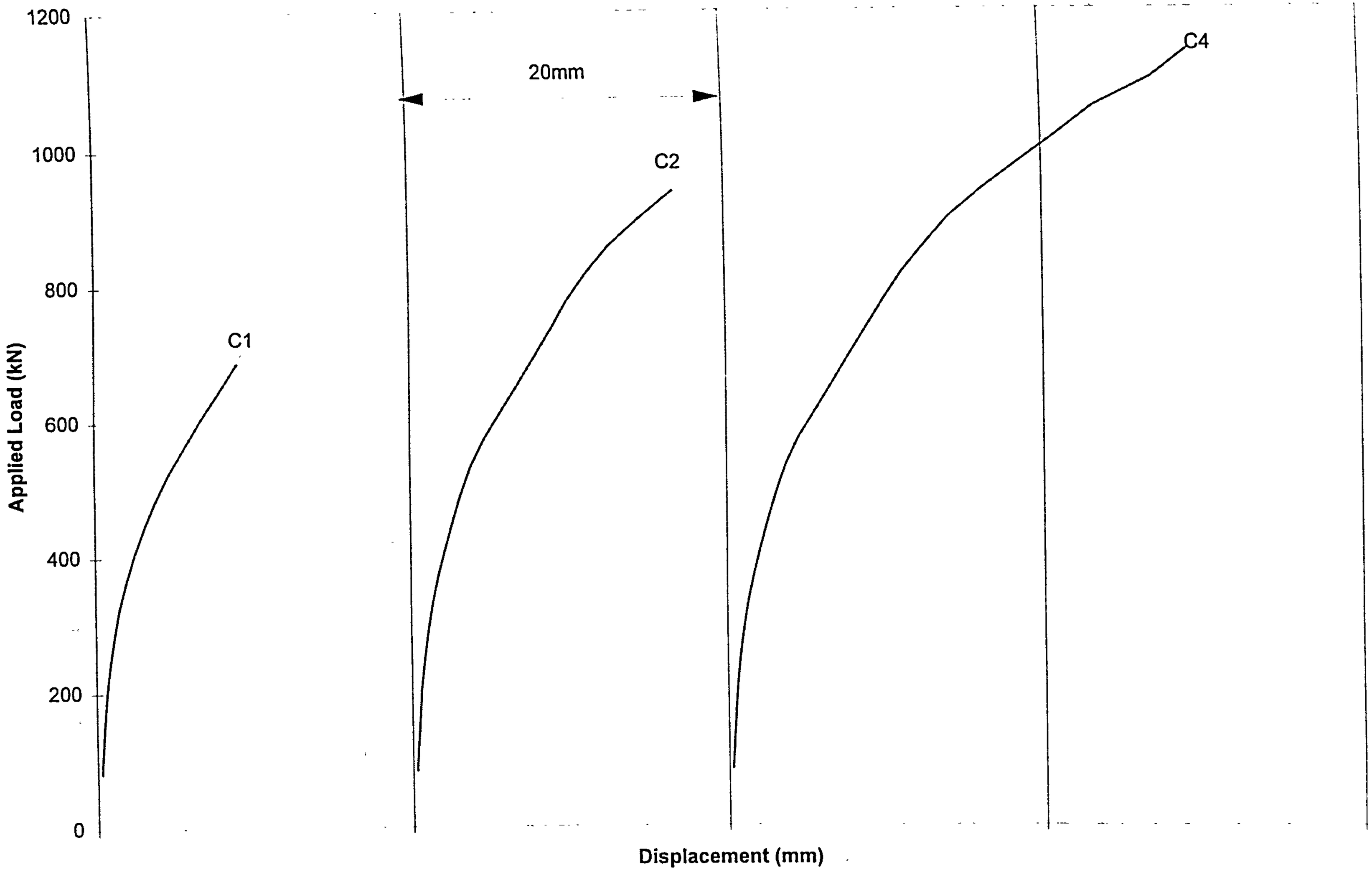

Predicted load-deflection response for slabs C1-C4

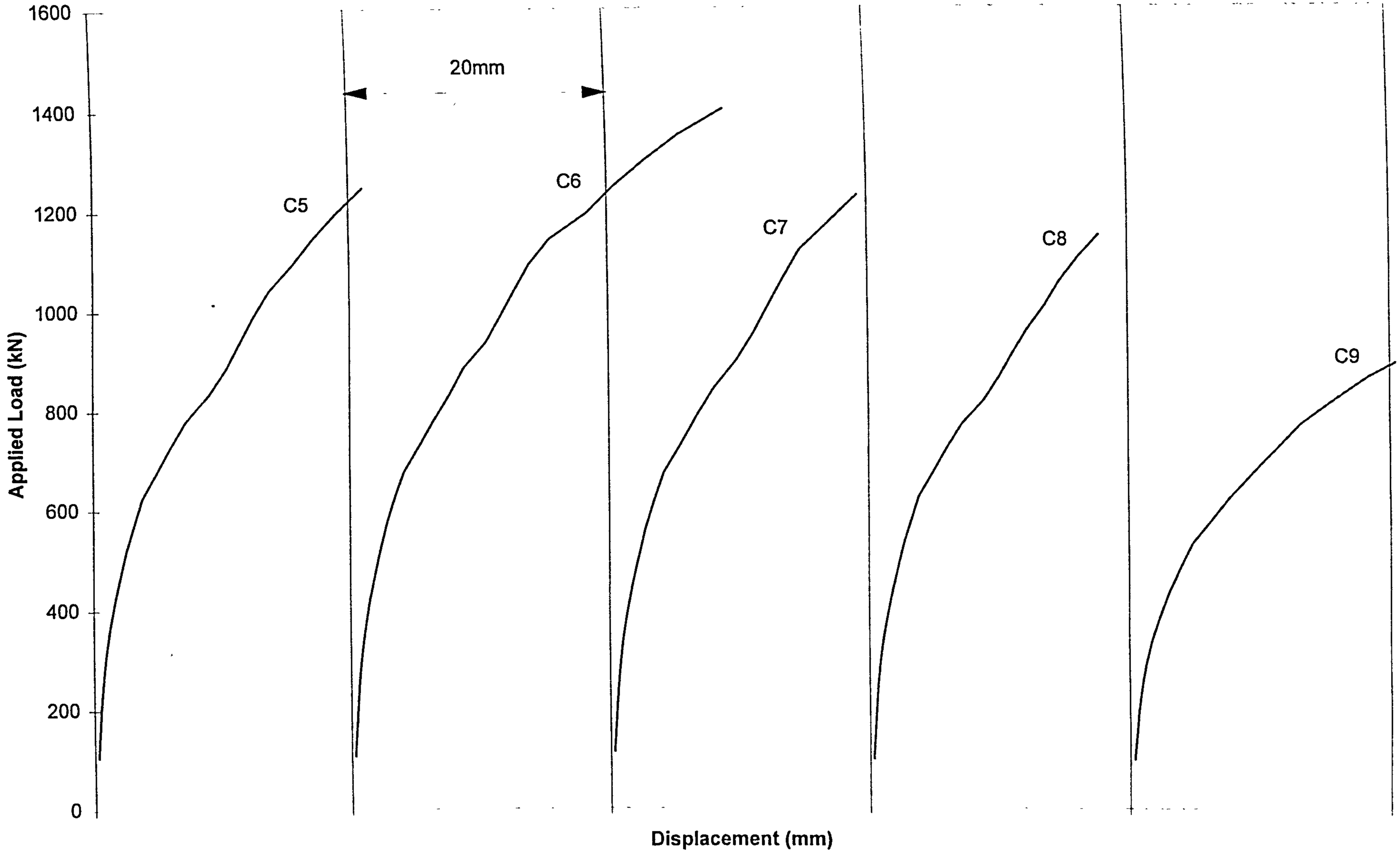

Predicted load-deflection response for slabs C5-C9

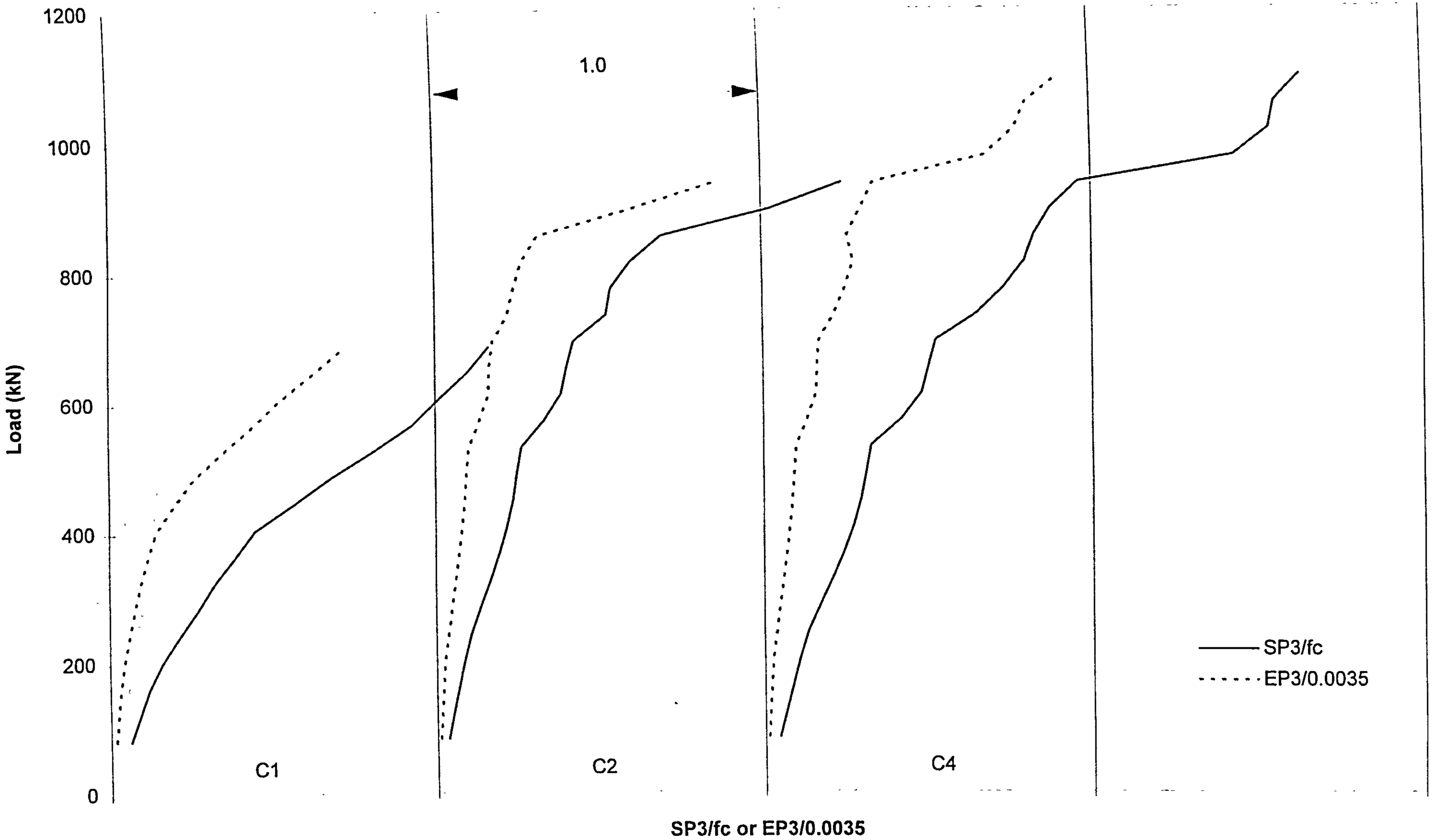

Predicted principal compressive stress and strain in concrete (slabs C1-C4)

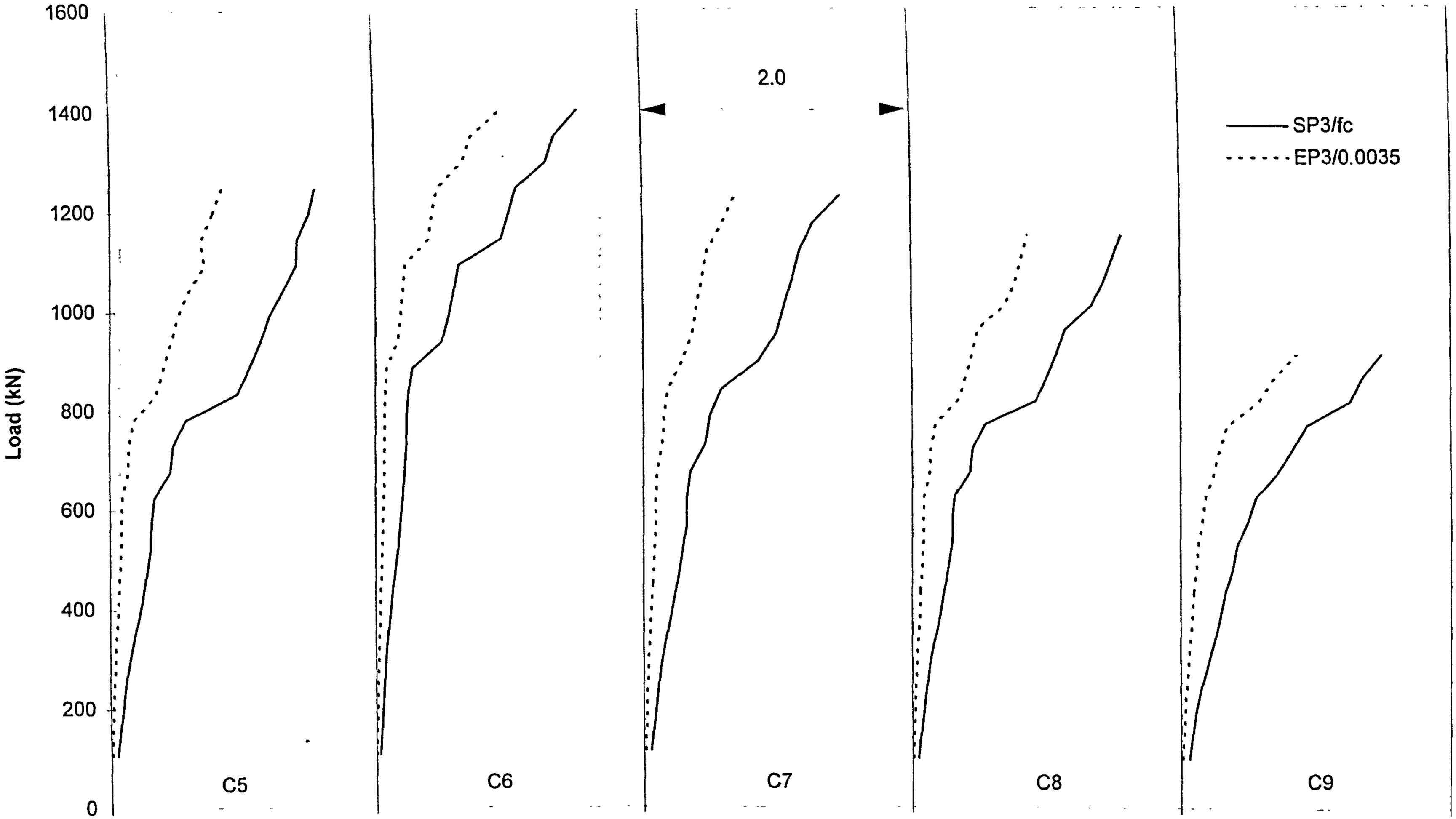

Predicted principal compressive stress and strain in concrete (slabs C5-C9)

Yielding of flexural steel for specimens C1-C9 (Chana and Desai)

NB. : The numbers on the drawing indicate strain in steel at collapse expressed as a ratio of yield strain

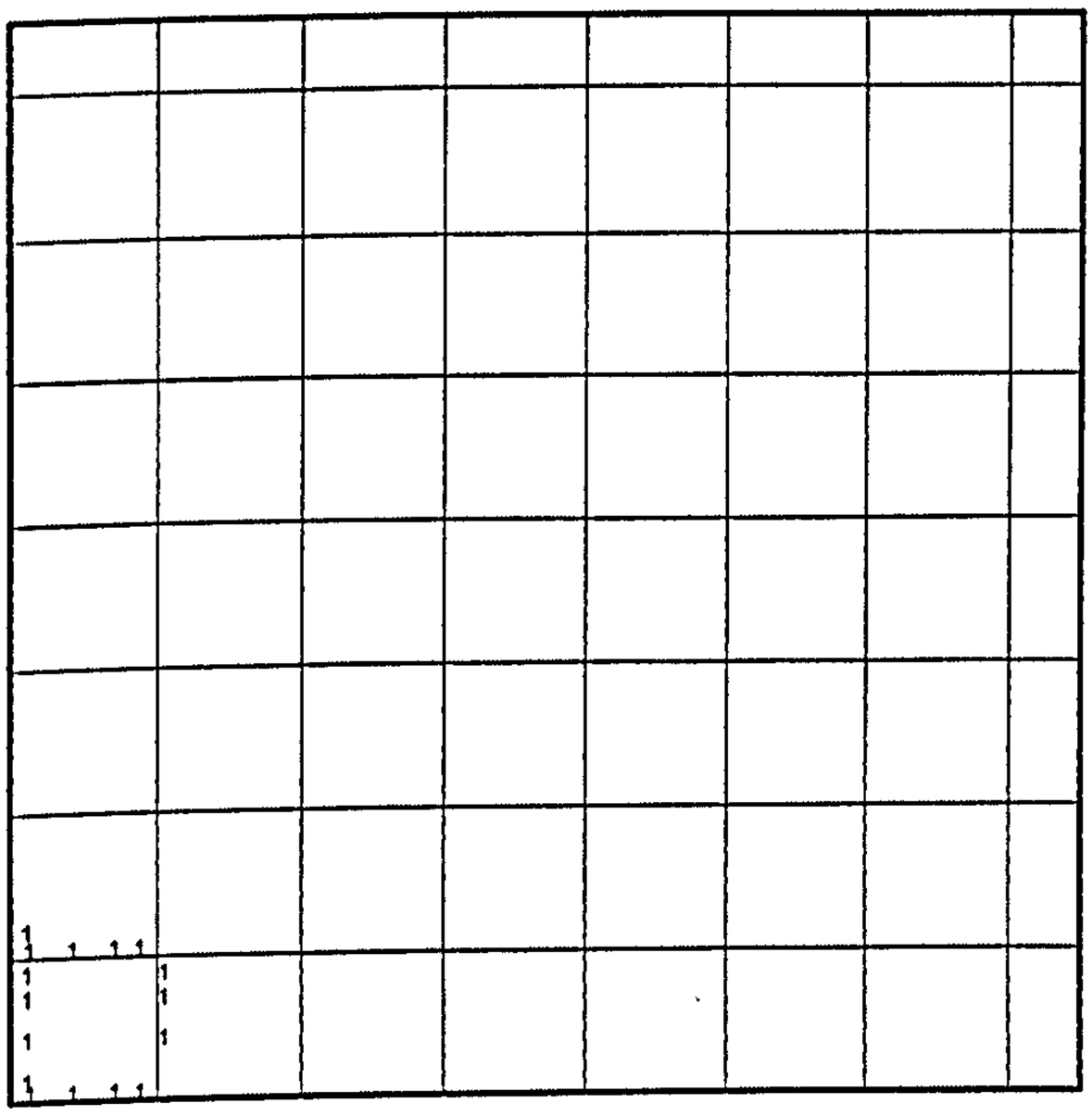

" C2"

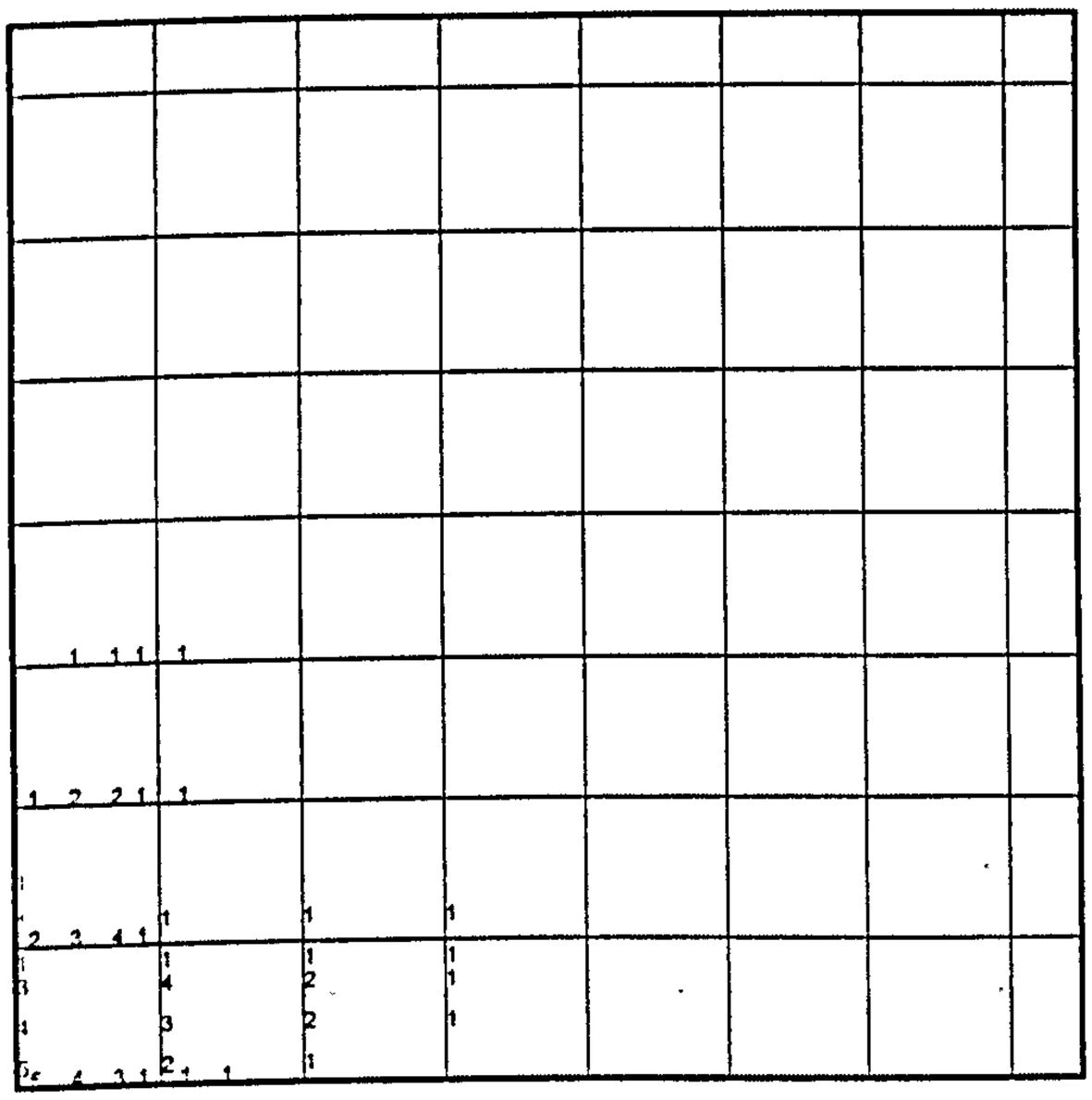

" C4 "

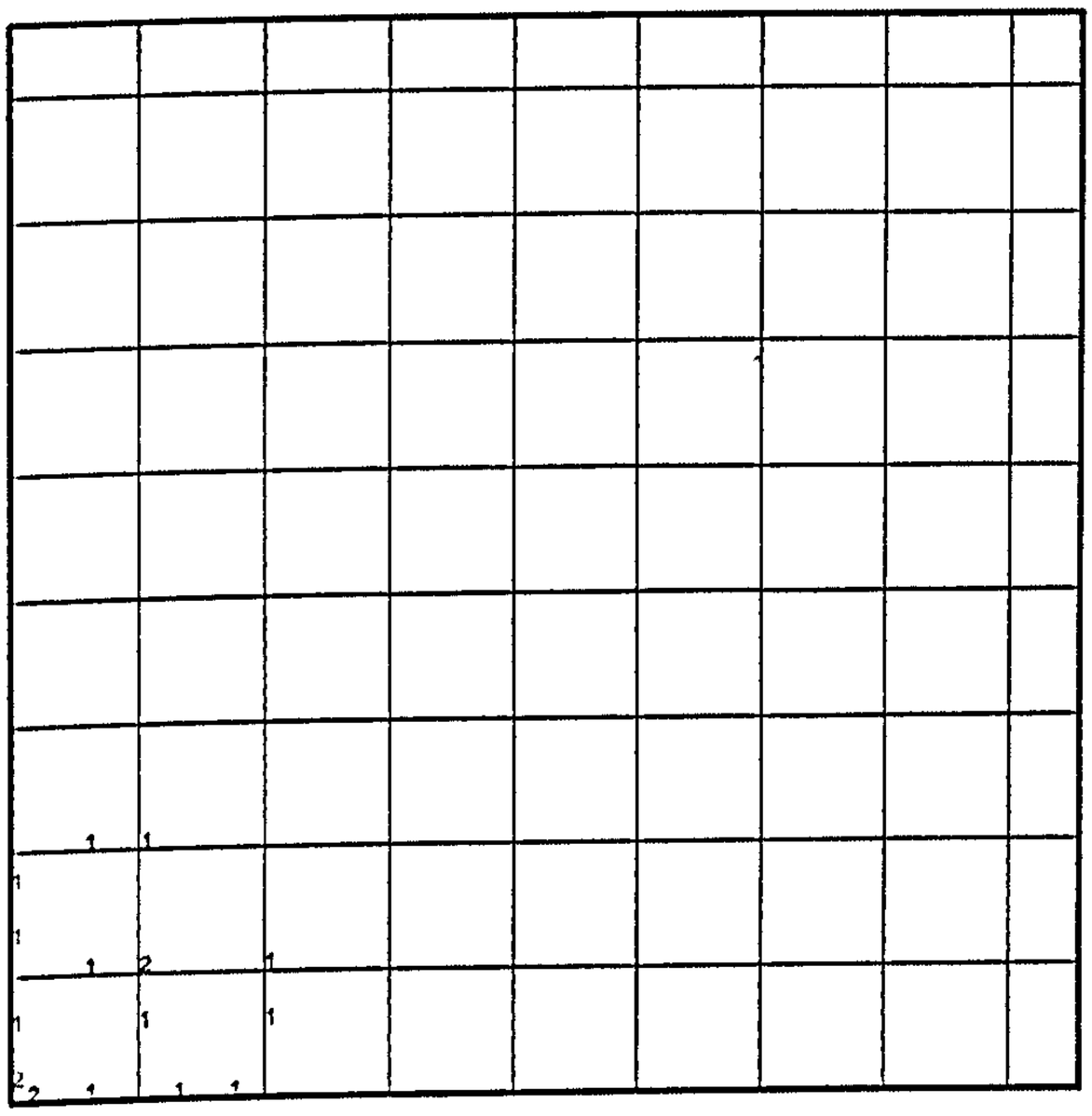

" C5 "

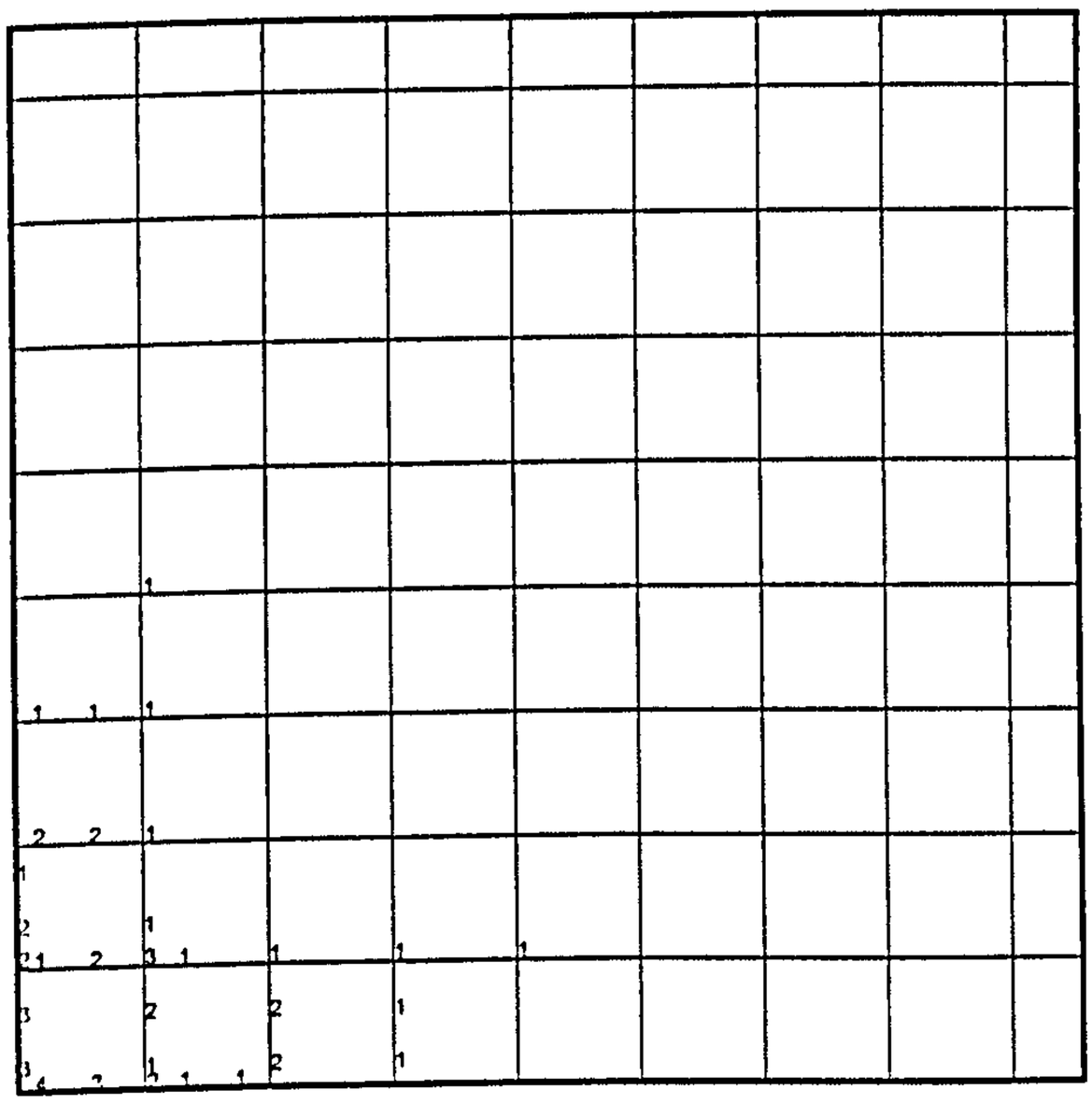

" C6 "

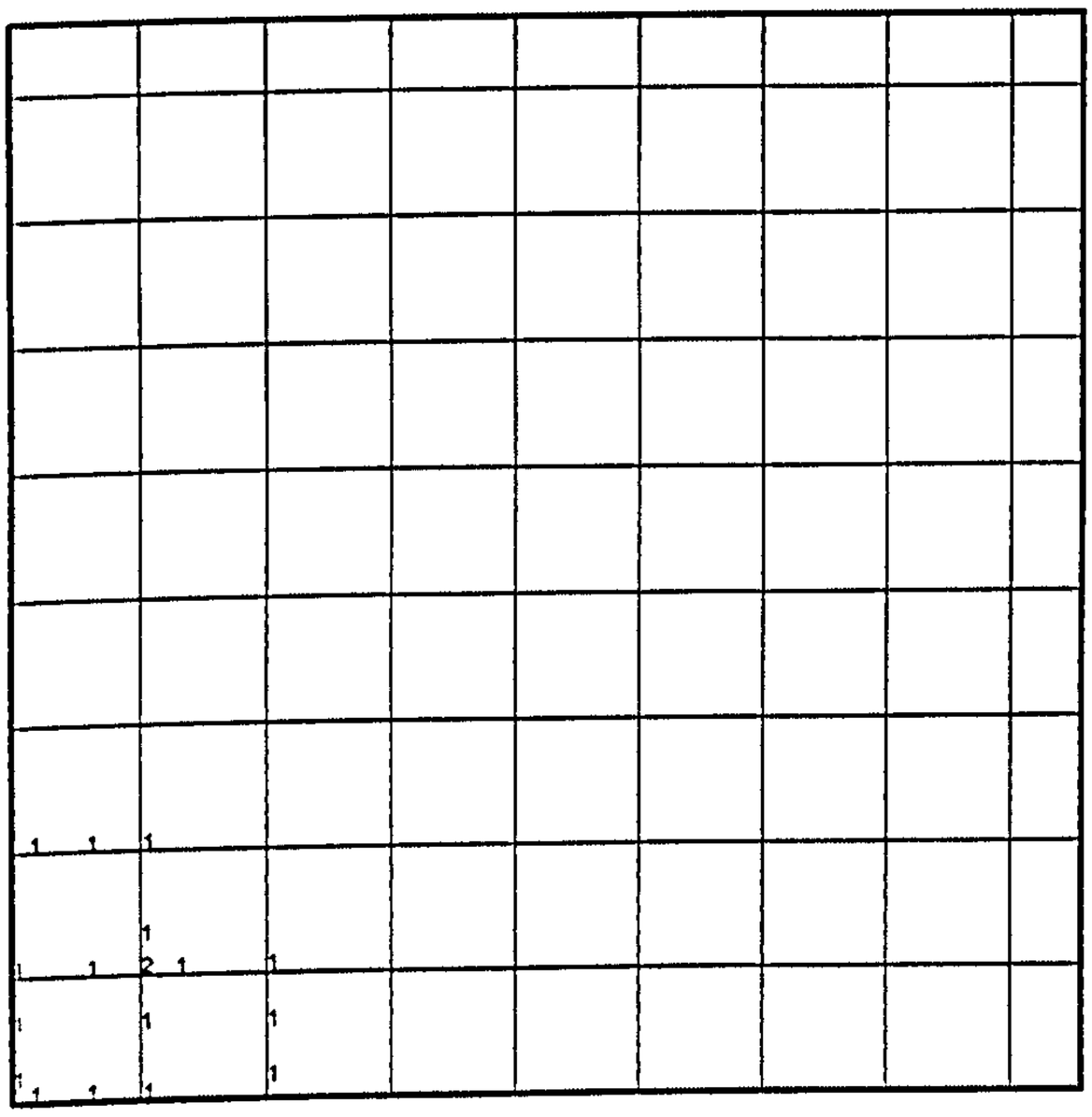

" C7 "

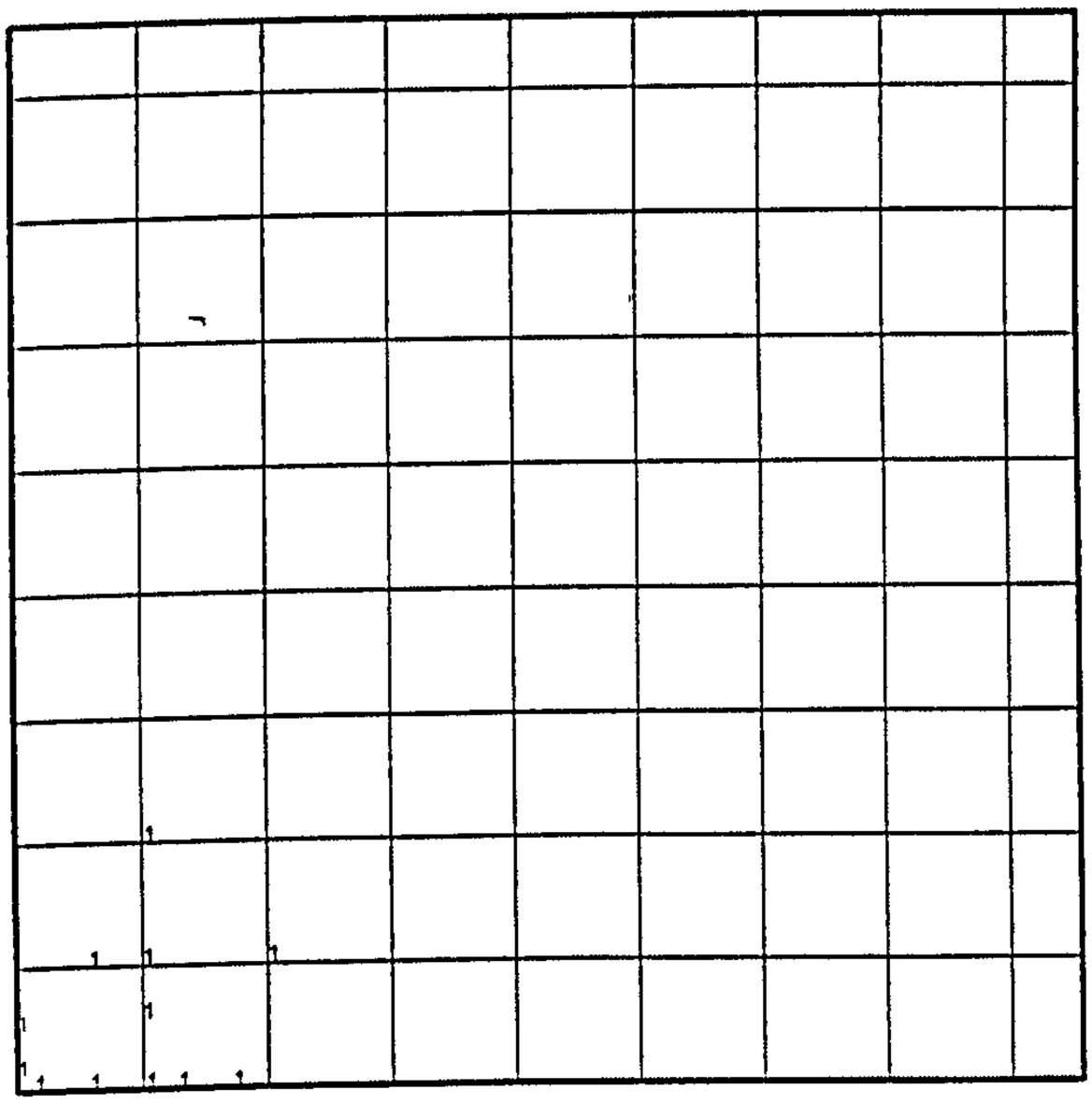

" C8 "

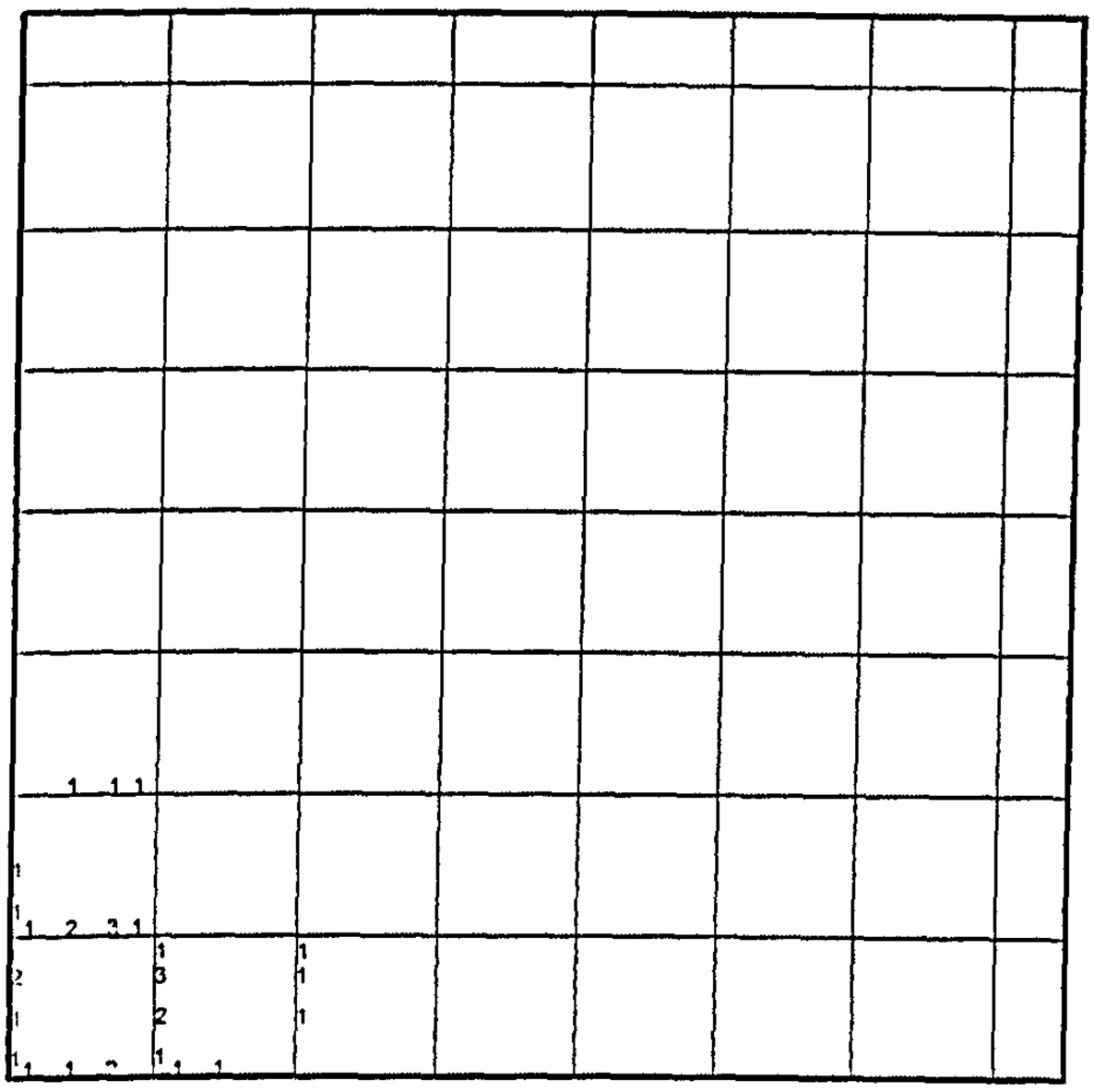

" C9 "

Note

Flexural steel in slab "C1" did not yield.

Predicted crack pattern for specimens C1-C9 (Chana and Desai)

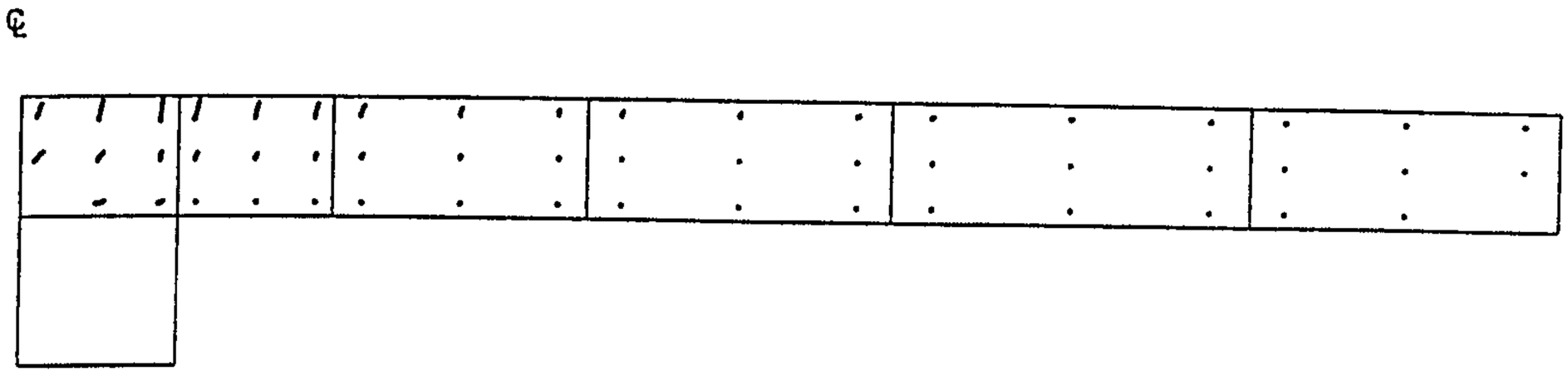

" C1 "

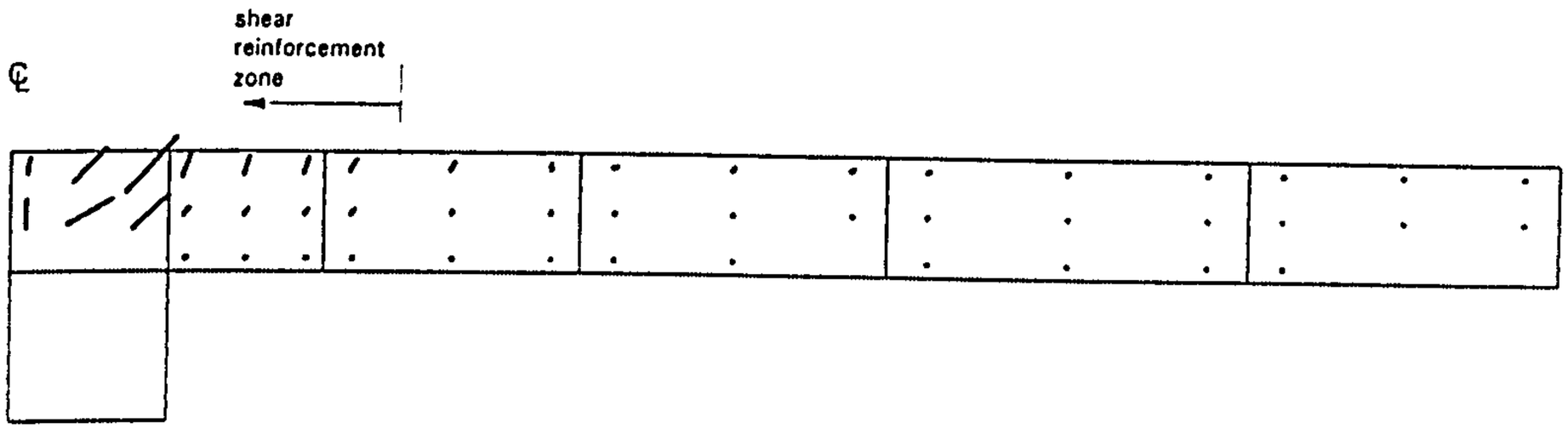

" C2 "

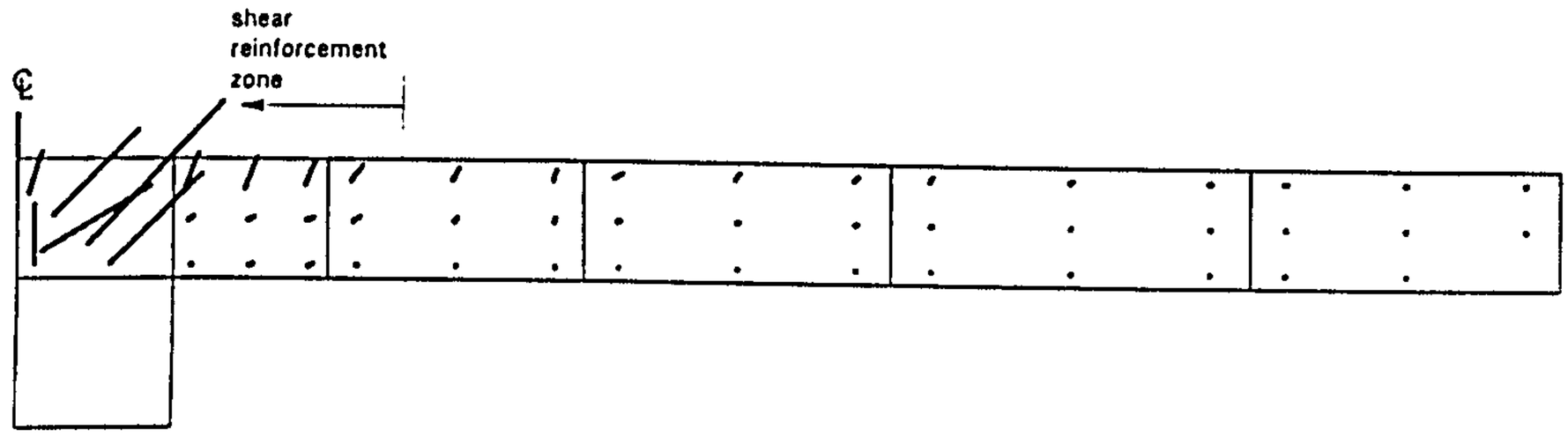

" C4 "

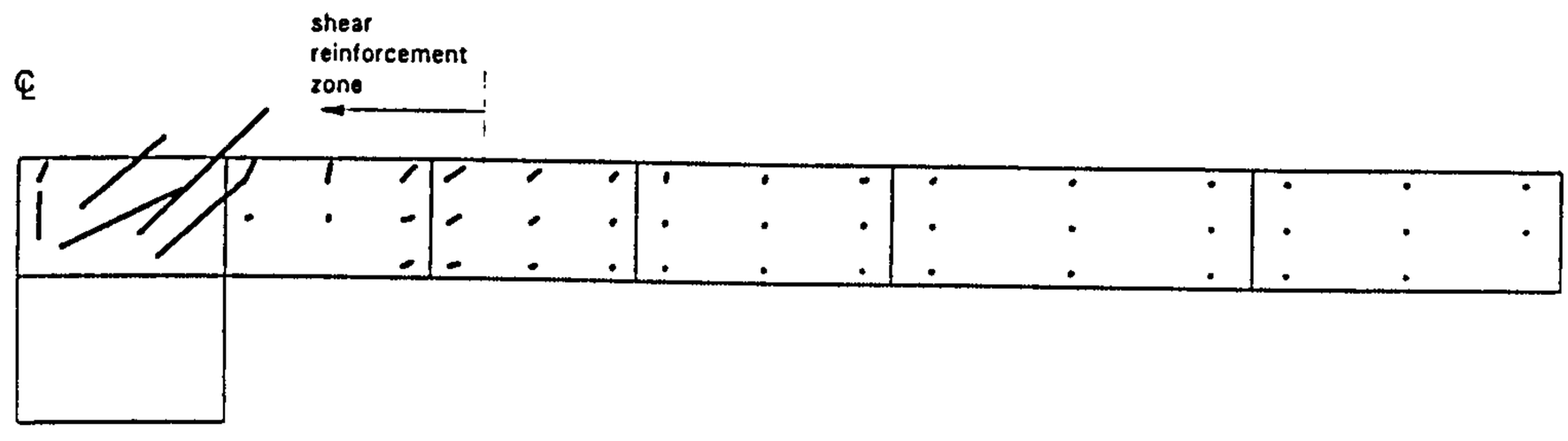

" C5 "

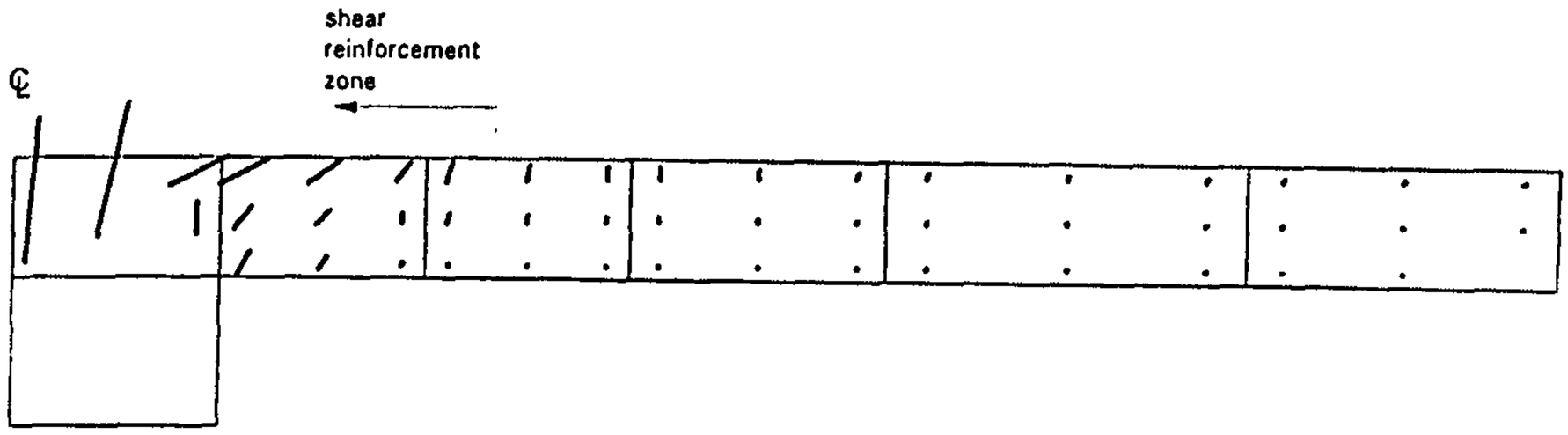
shear
reinforcement
zone
℄

" C6 "

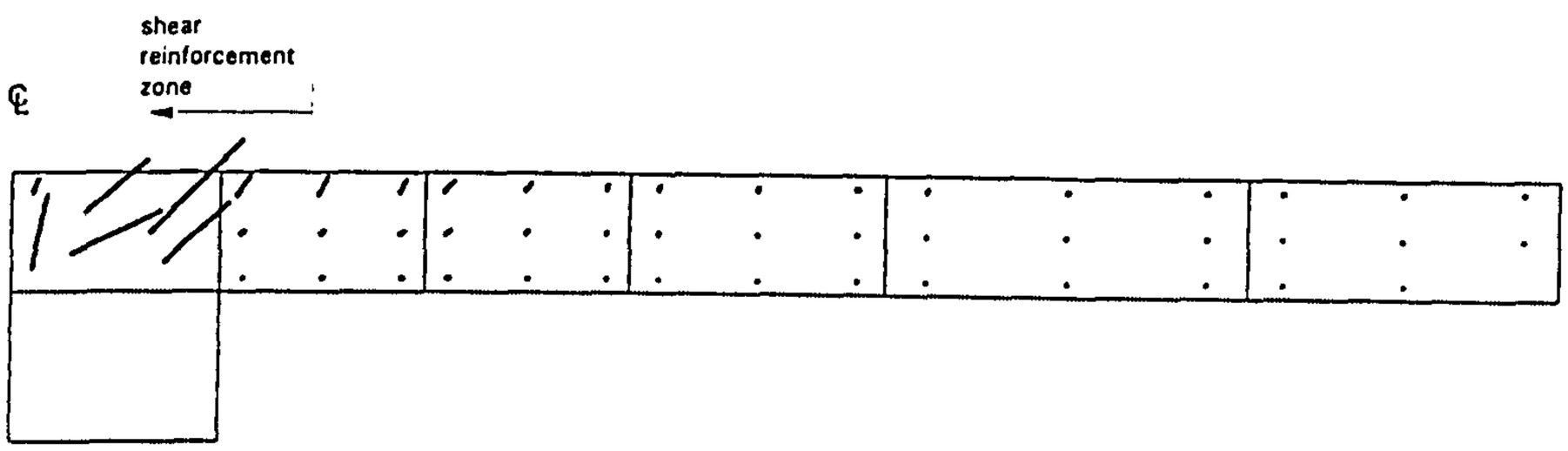
shear
reinforcement
zone
℄

" C7 "

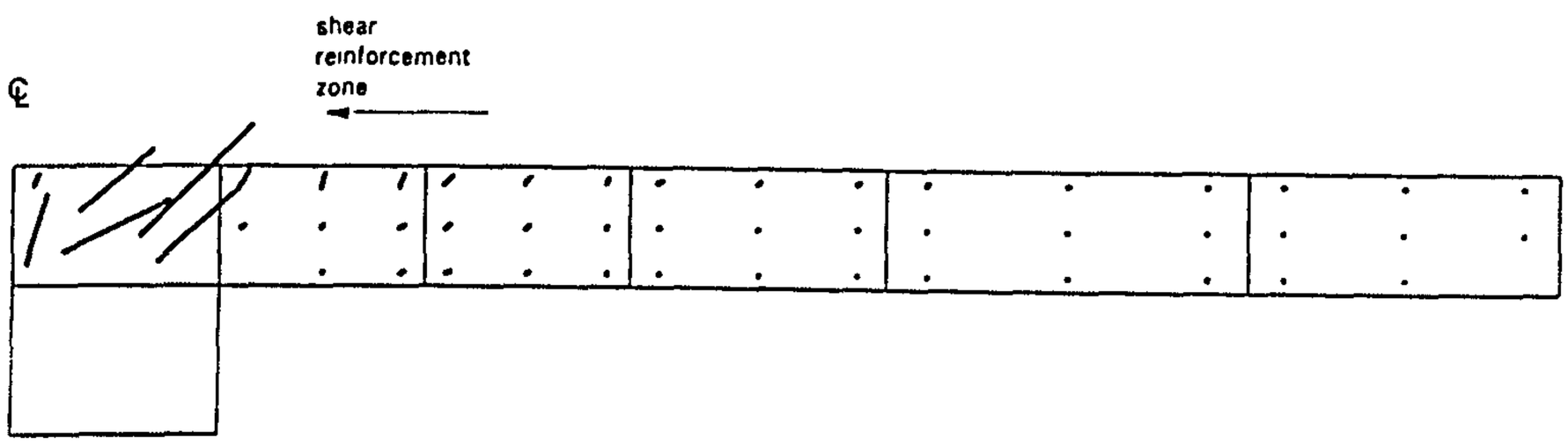
shear
reinforcement
zone
℄

" C8 "

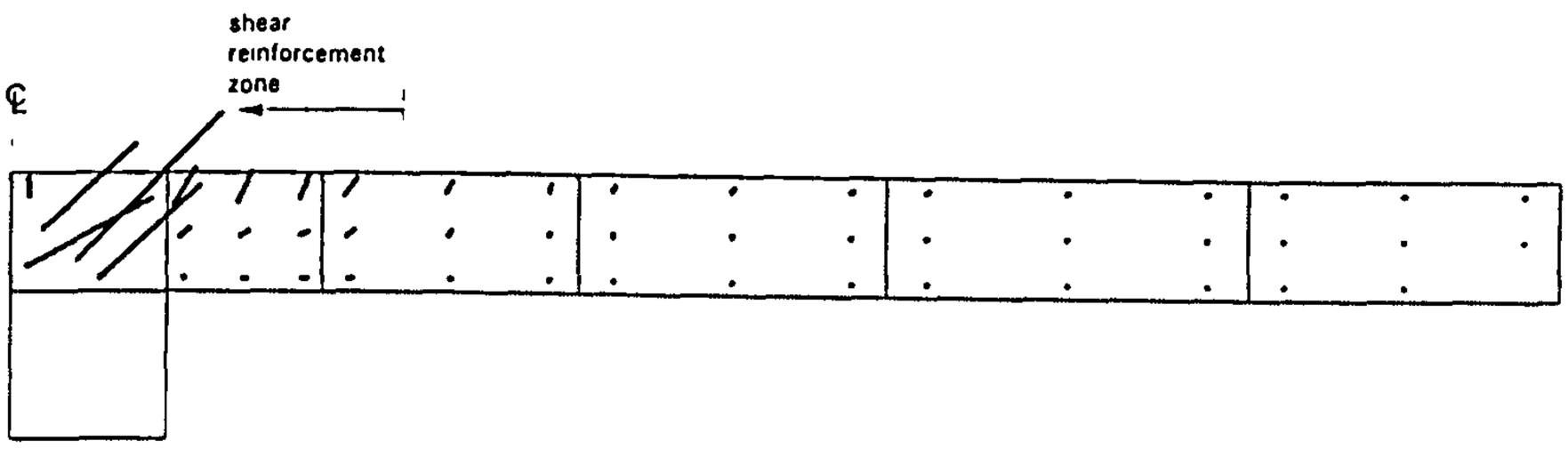
shear
reinforcement
zone
℄

" C9 "

Gomes' slabs

C1.4 Gomes' slabs (with shear reinforcement)

Slab	Test results		Numerical predictions		P_{num}/P_{test}
	P_{test} (kN)	Failure mode	P_{num} (kN)	Failure mode	
G1	560.0	s	579.6	s	1.035
G2	693.0	s	660.0	s	0.952
G3	773.0	s	690.0	s	0.893
G4	853.0	s	810.0	s	0.949
G5	853.0	s	810.0	s	0.949
G6	1040.0	fp	864.0	fp	0.831
G7	1120.0	fp	900.0	fp	0.804
G8	1200.0	fp	972.0	fp	0.810
G9	1227.0	fp	1008.0	fp	0.822
G10	800.0	s	720.0	s	0.900
G11	907.0	fp	684.0	fp	0.754
				Average	0.876
				STDEV	0.091

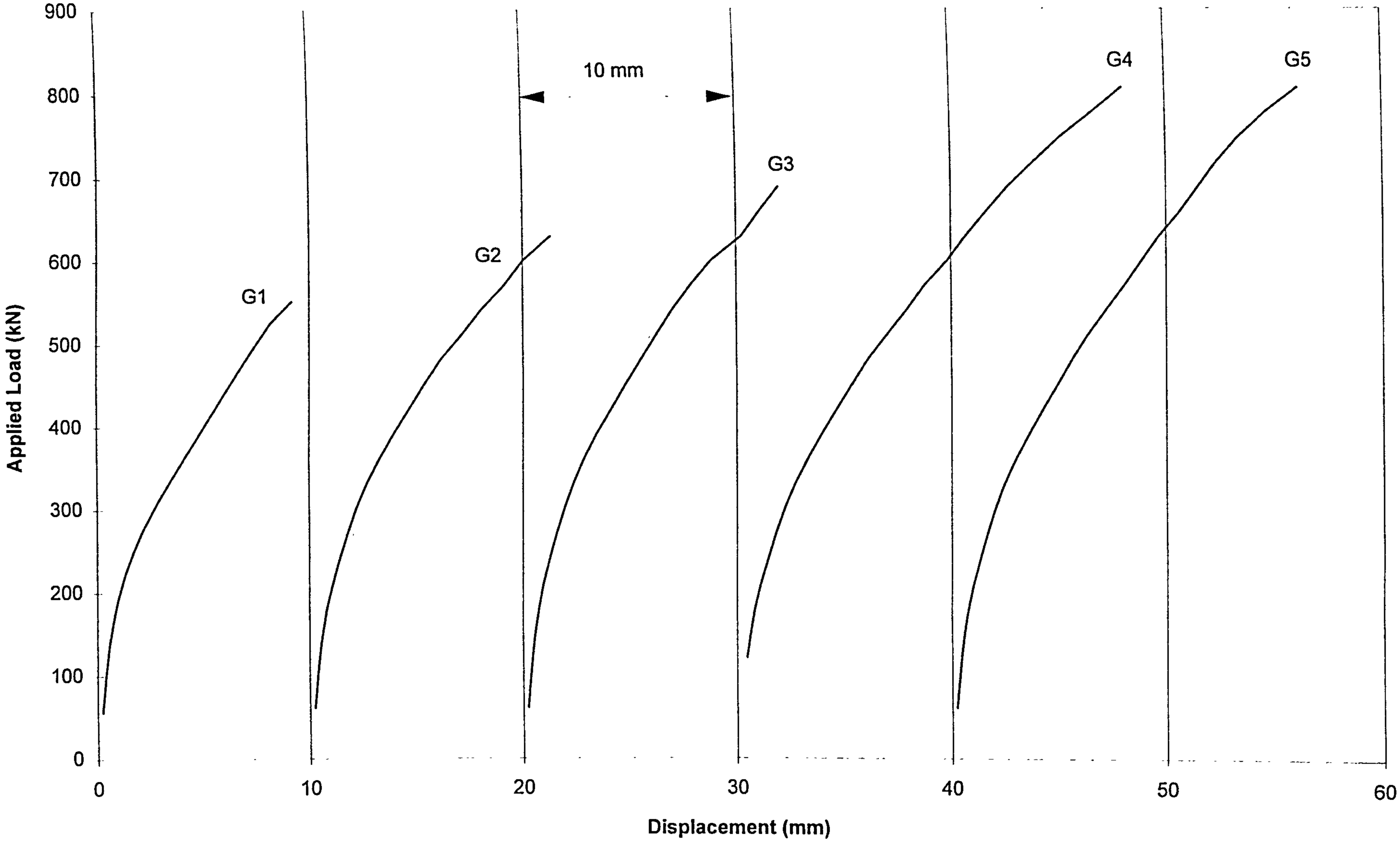

Predicted load-deflection response for slabs G1-G5

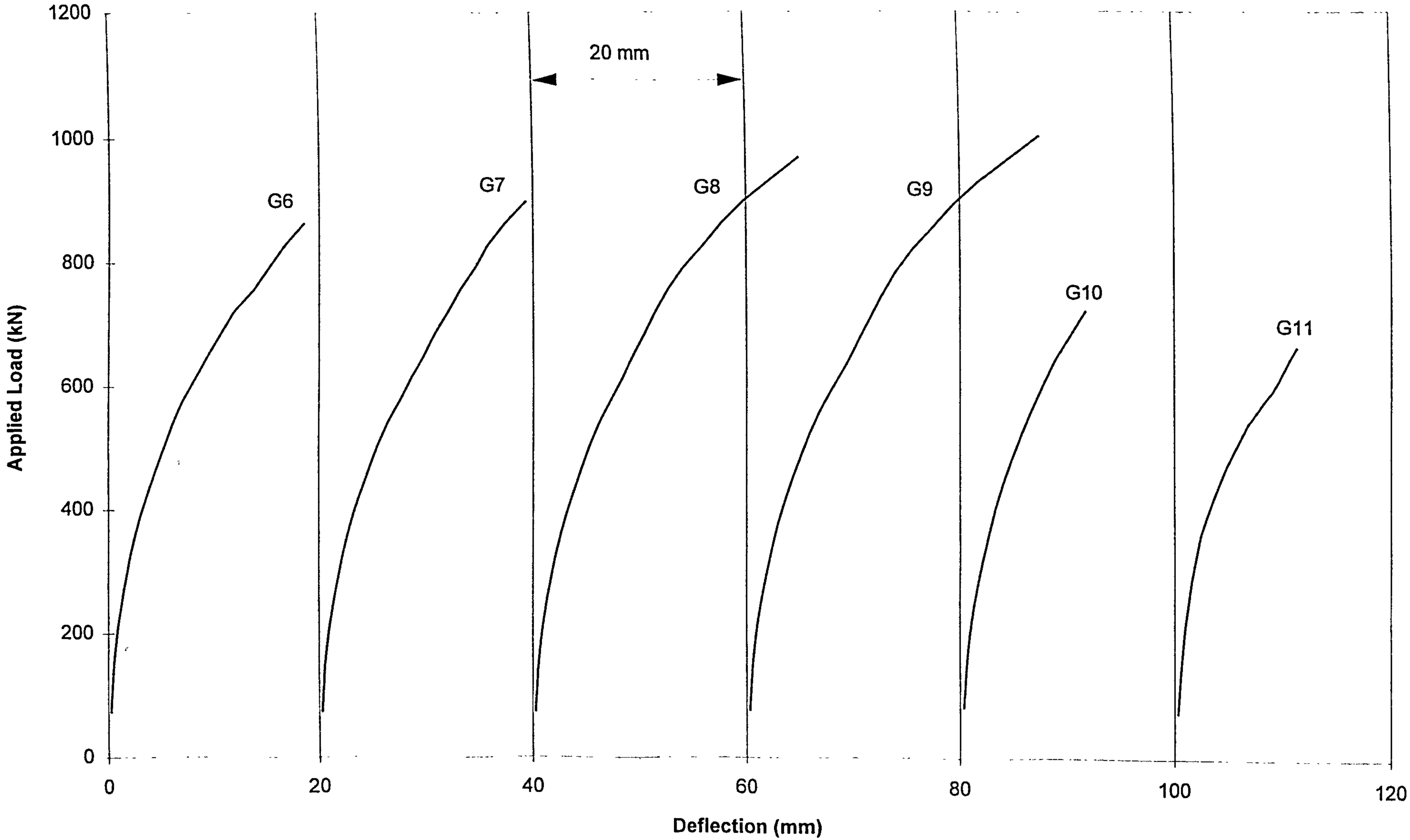

Predicted load-deflection response for slabs G6-G11

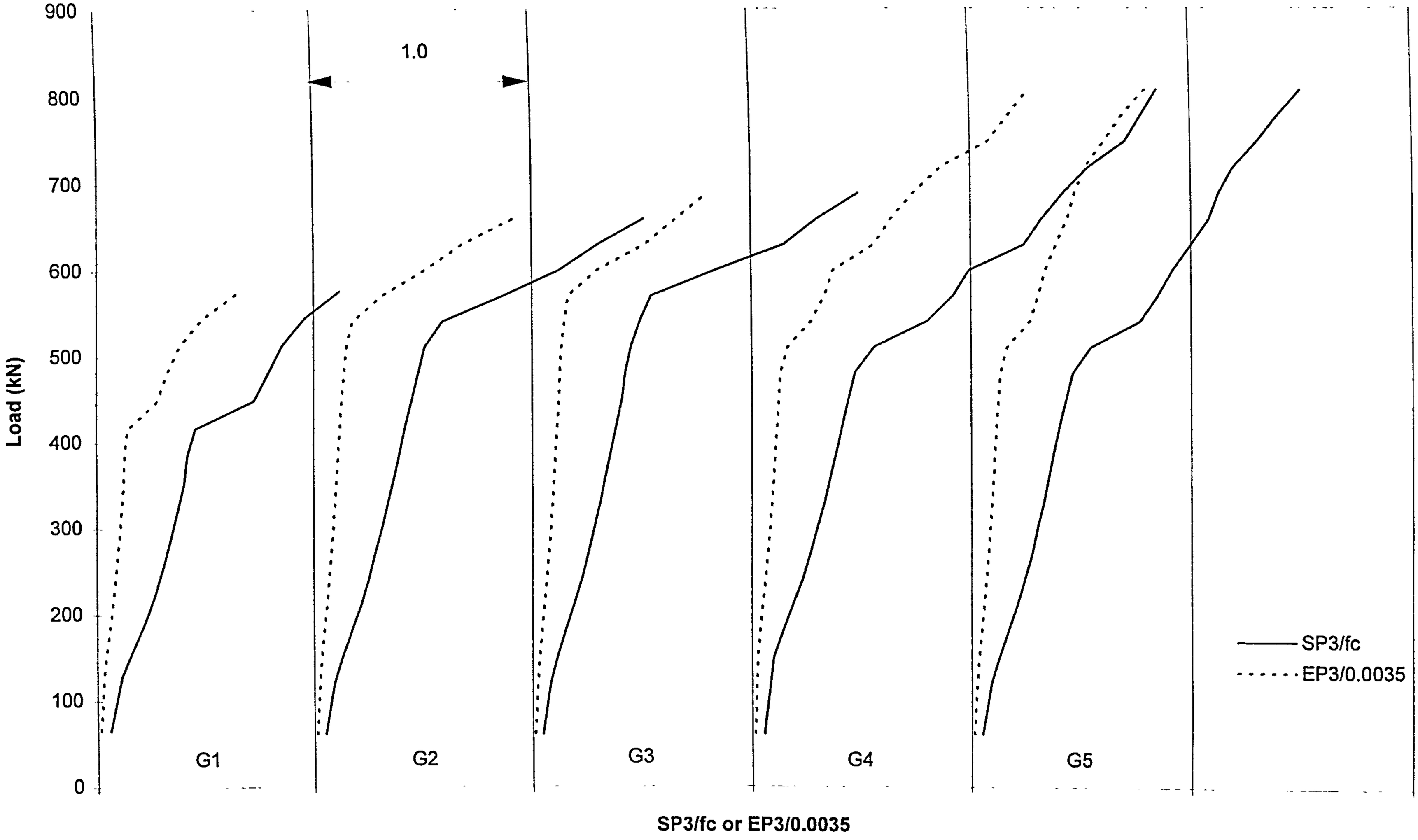

Predicted principal compressive stress and strain in concrete (slabs G1-G5)

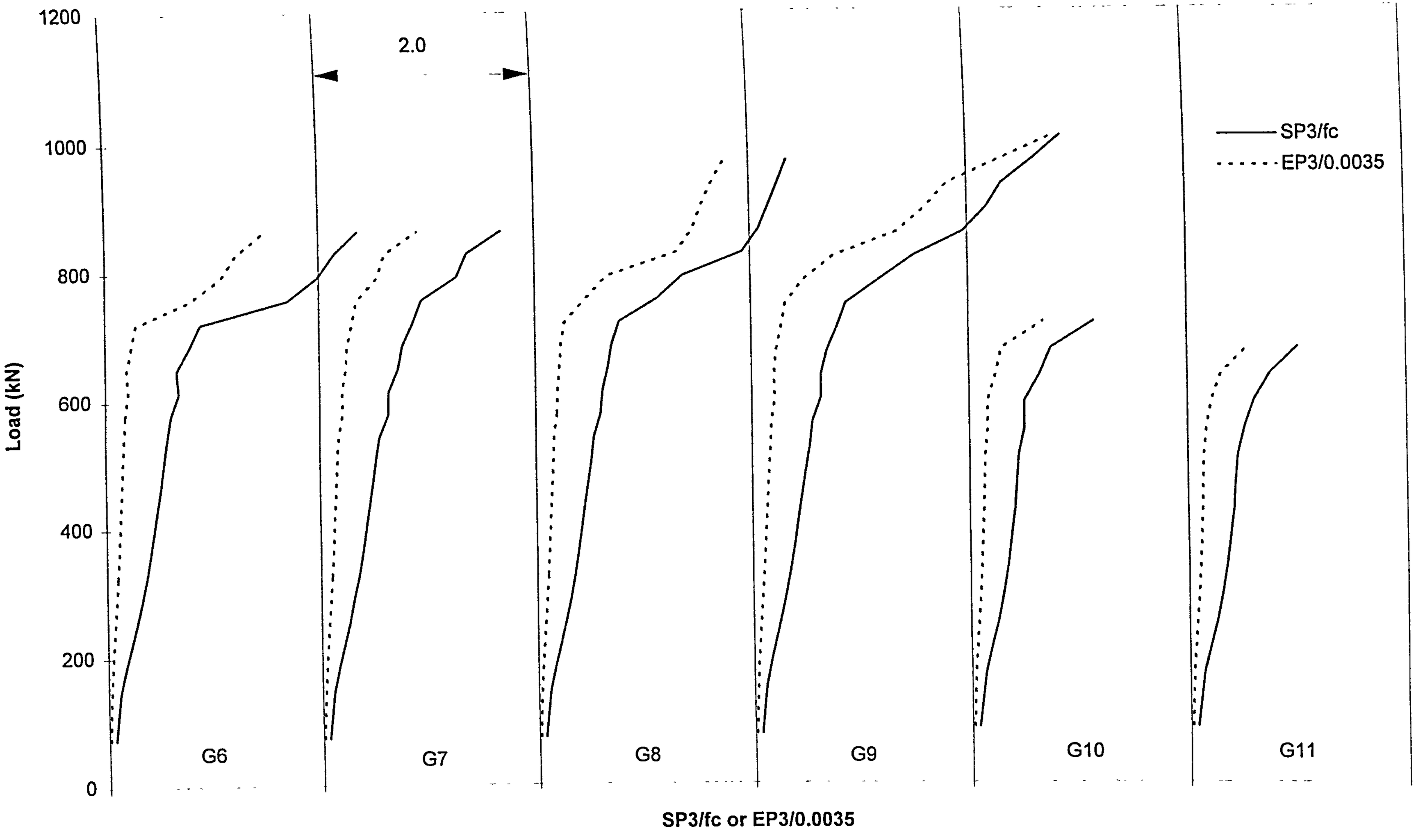

Predicted principal compressive stress and strain in concrete (slabs G6-G11)

Yielding of flexural steel for specimens G1-G11 (Gomes)

NB. : The numbers on the drawing indicate strain in steel at collapse expressed as a ratio of yield strain

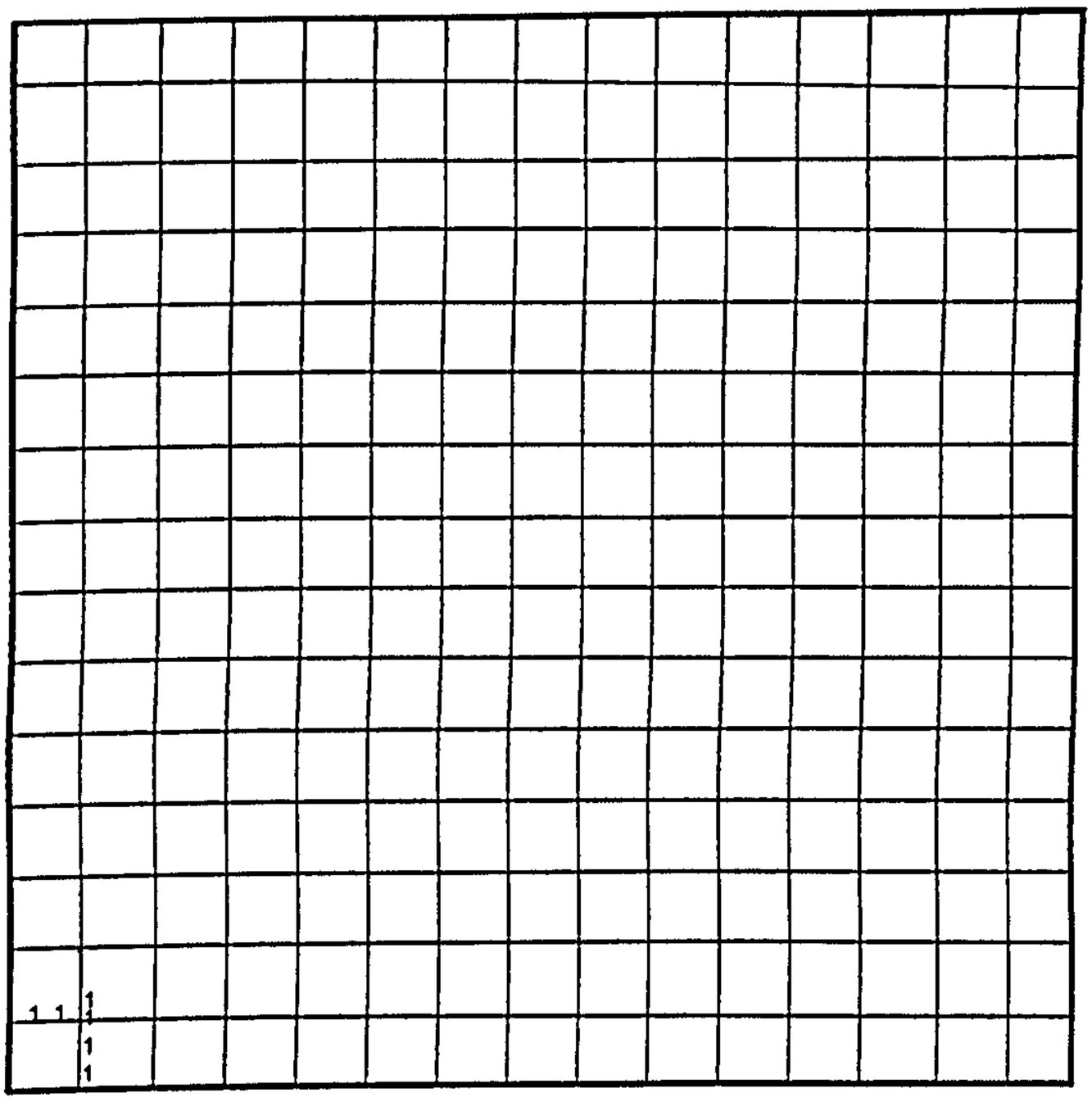

" G2 "

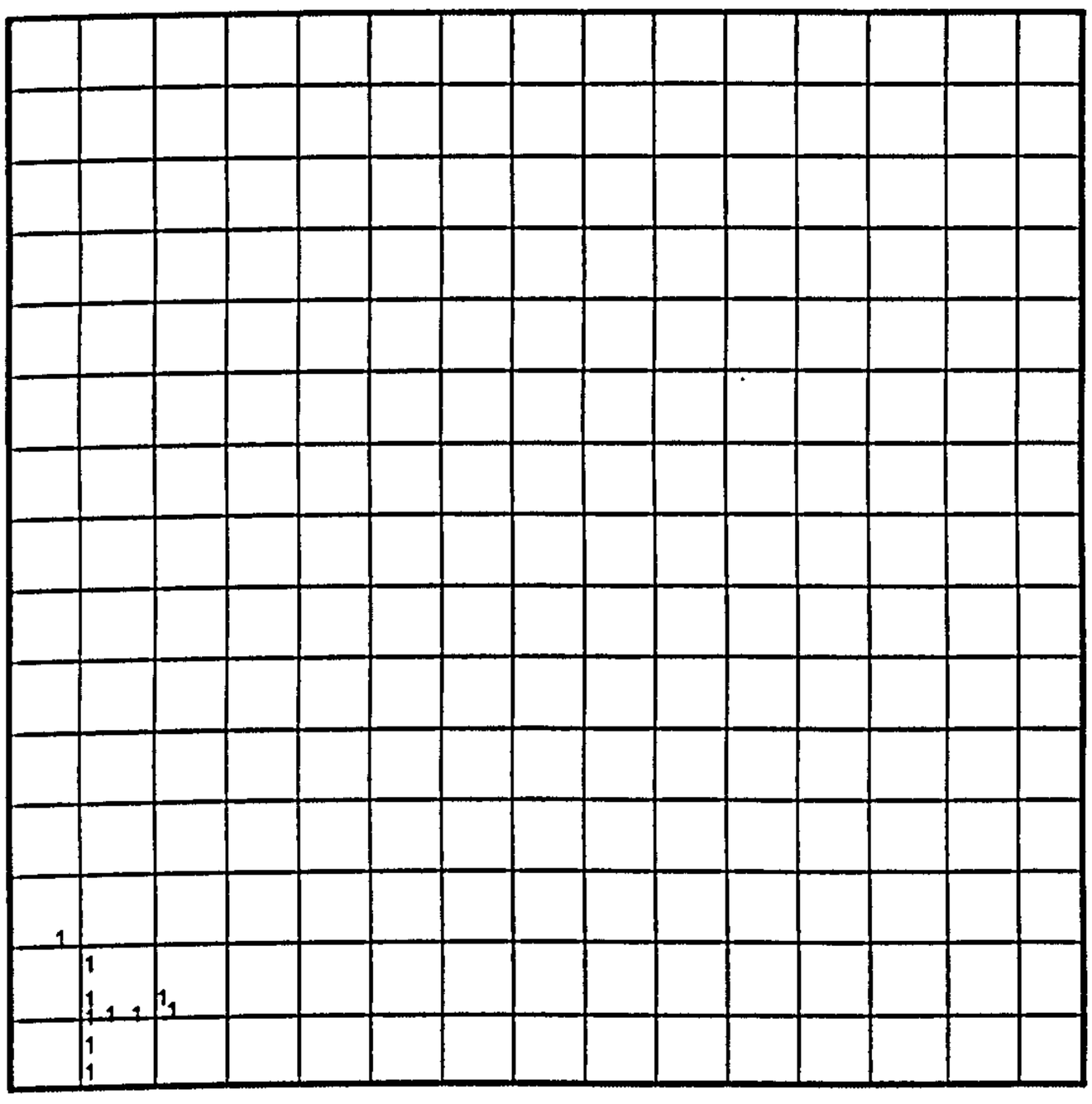

" G3 "

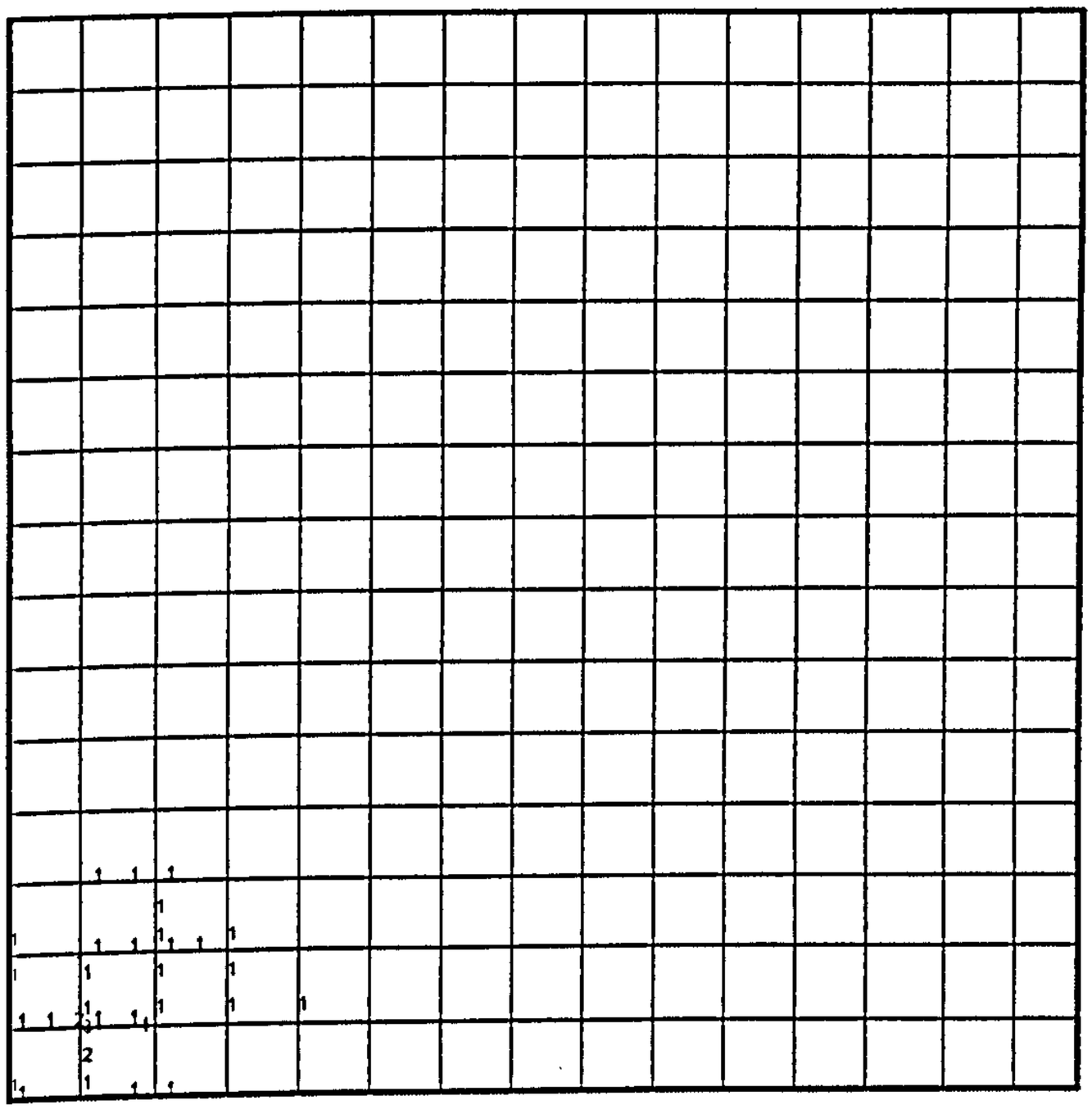

" G4 "

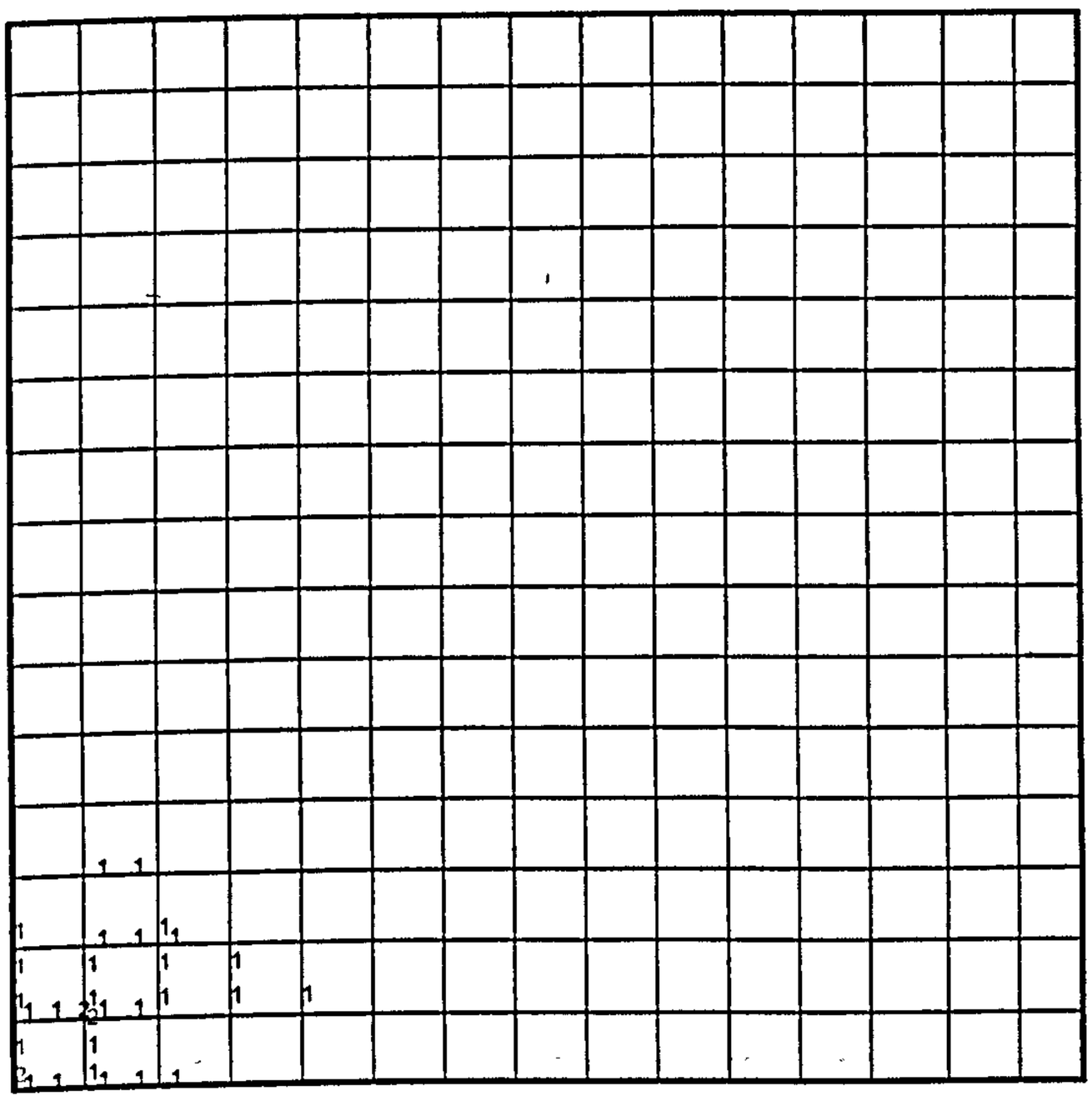

" G5 "

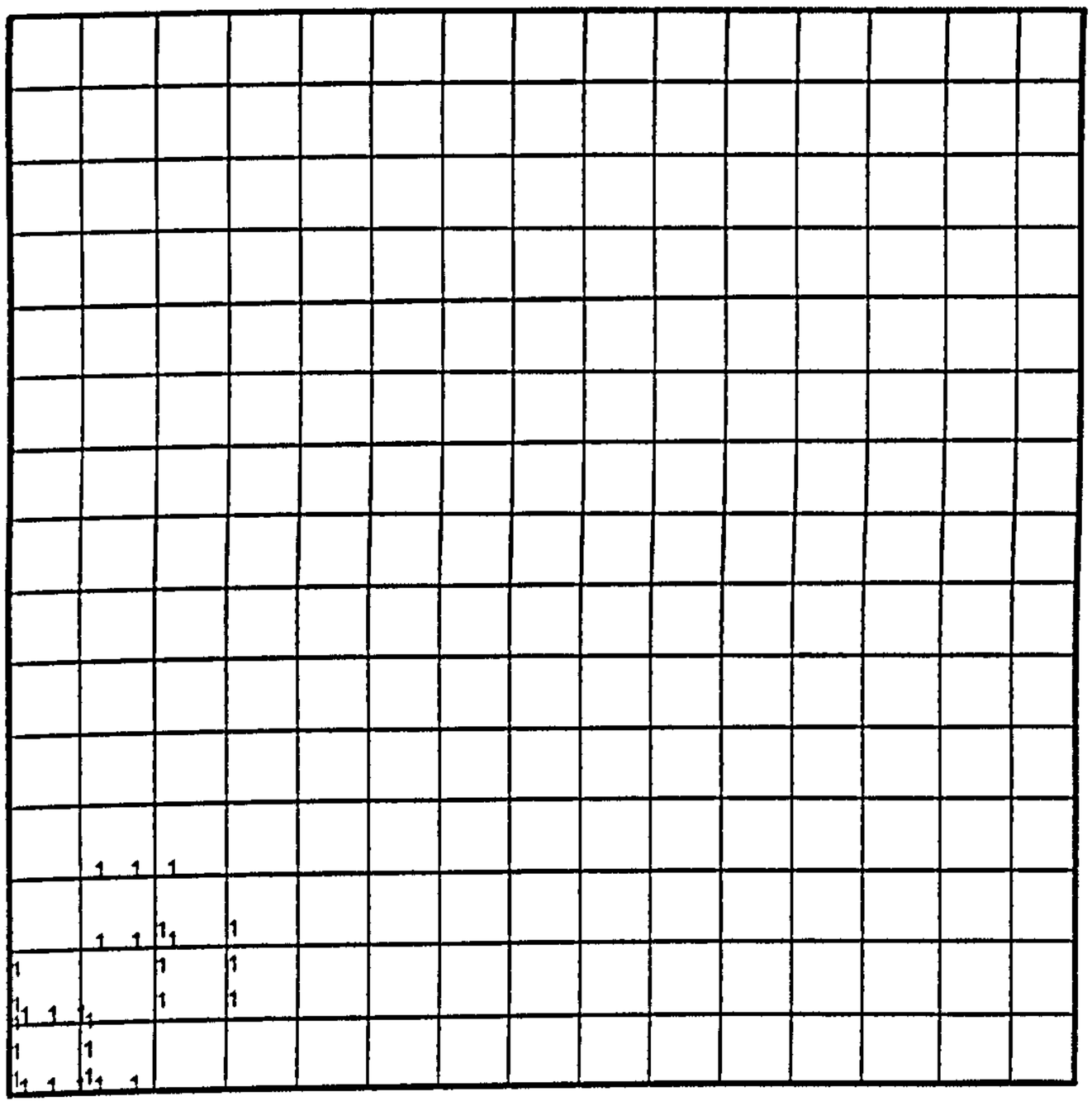

" G6 "

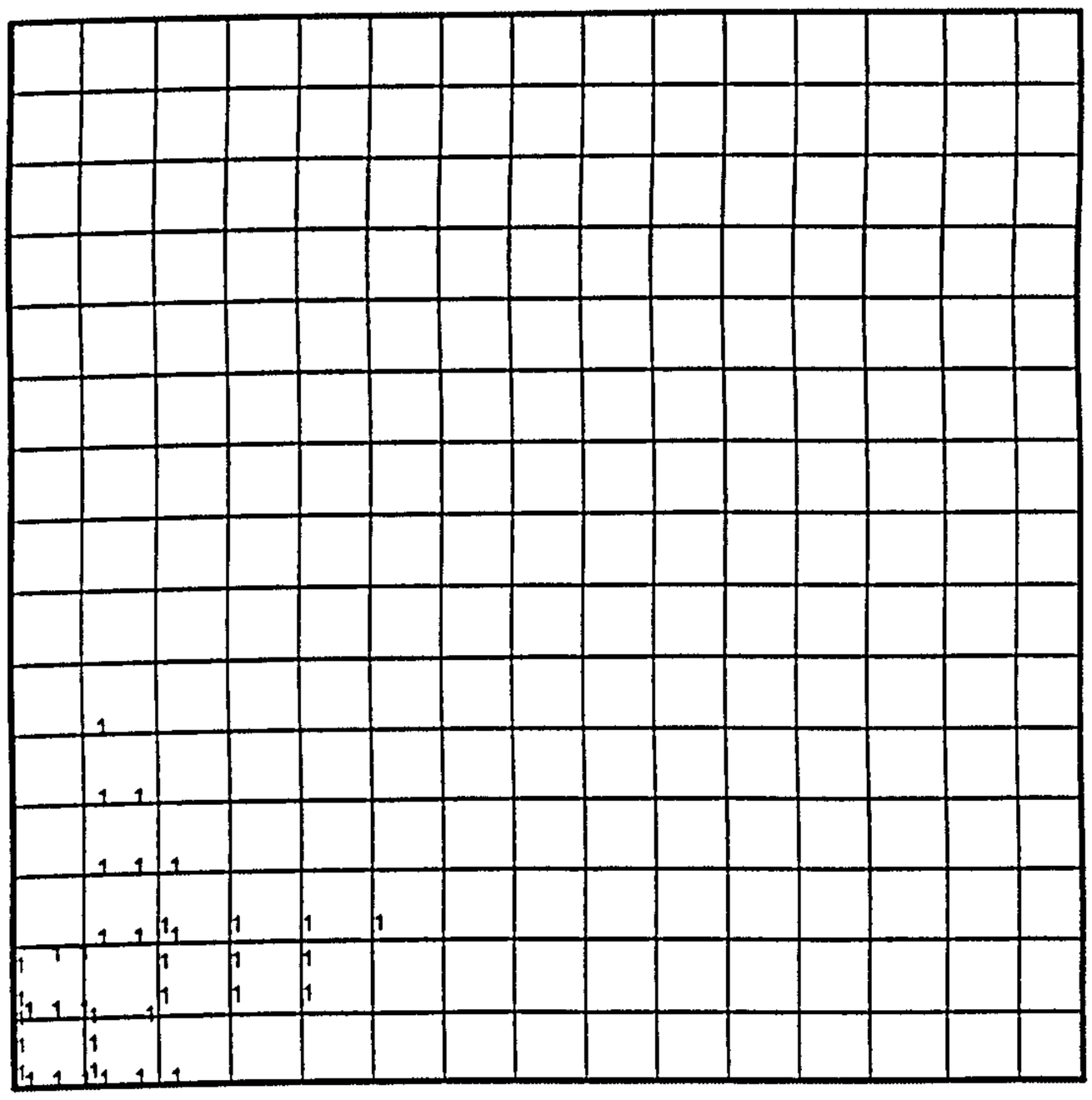

" G7 "

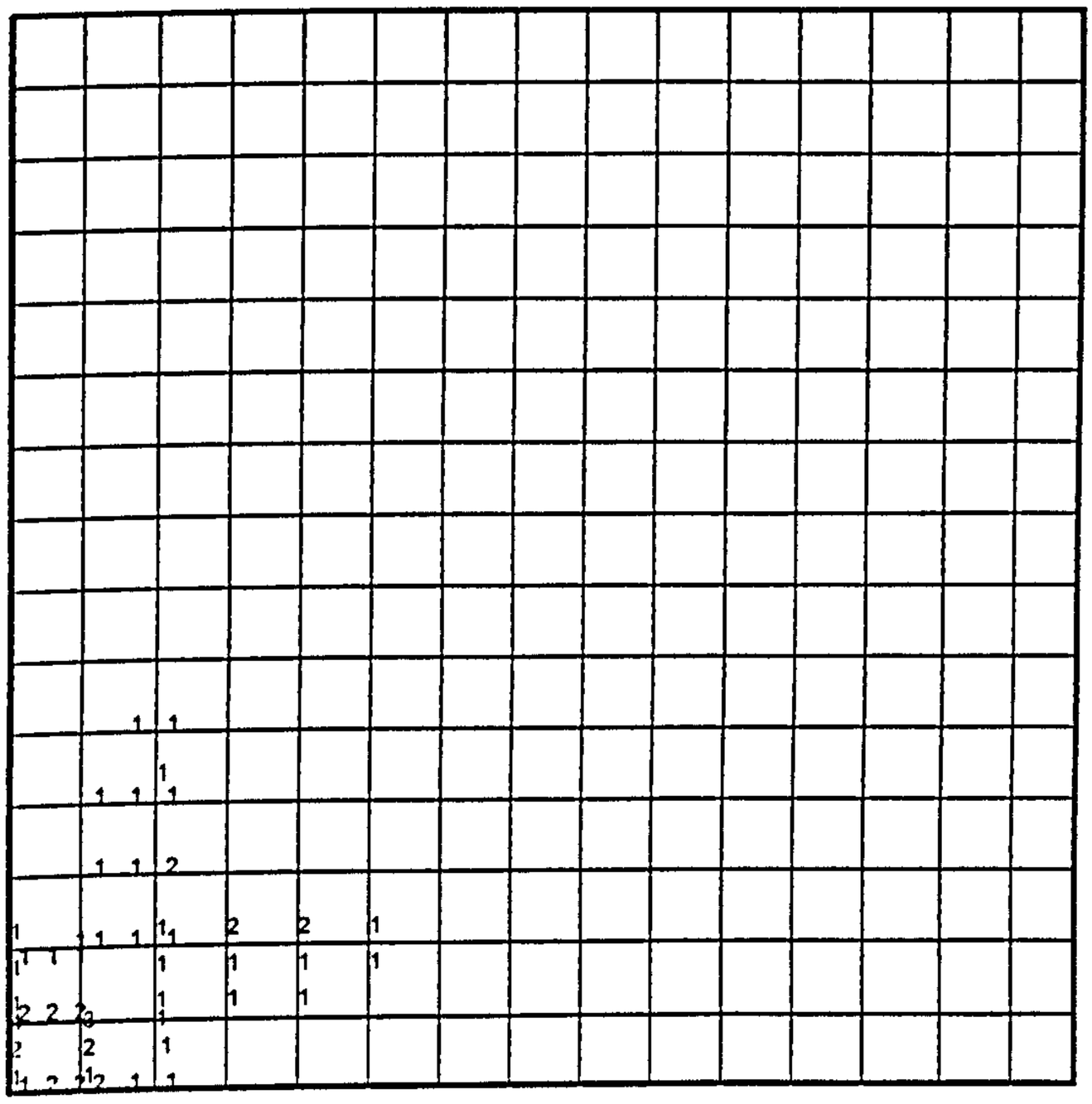

" G8 "

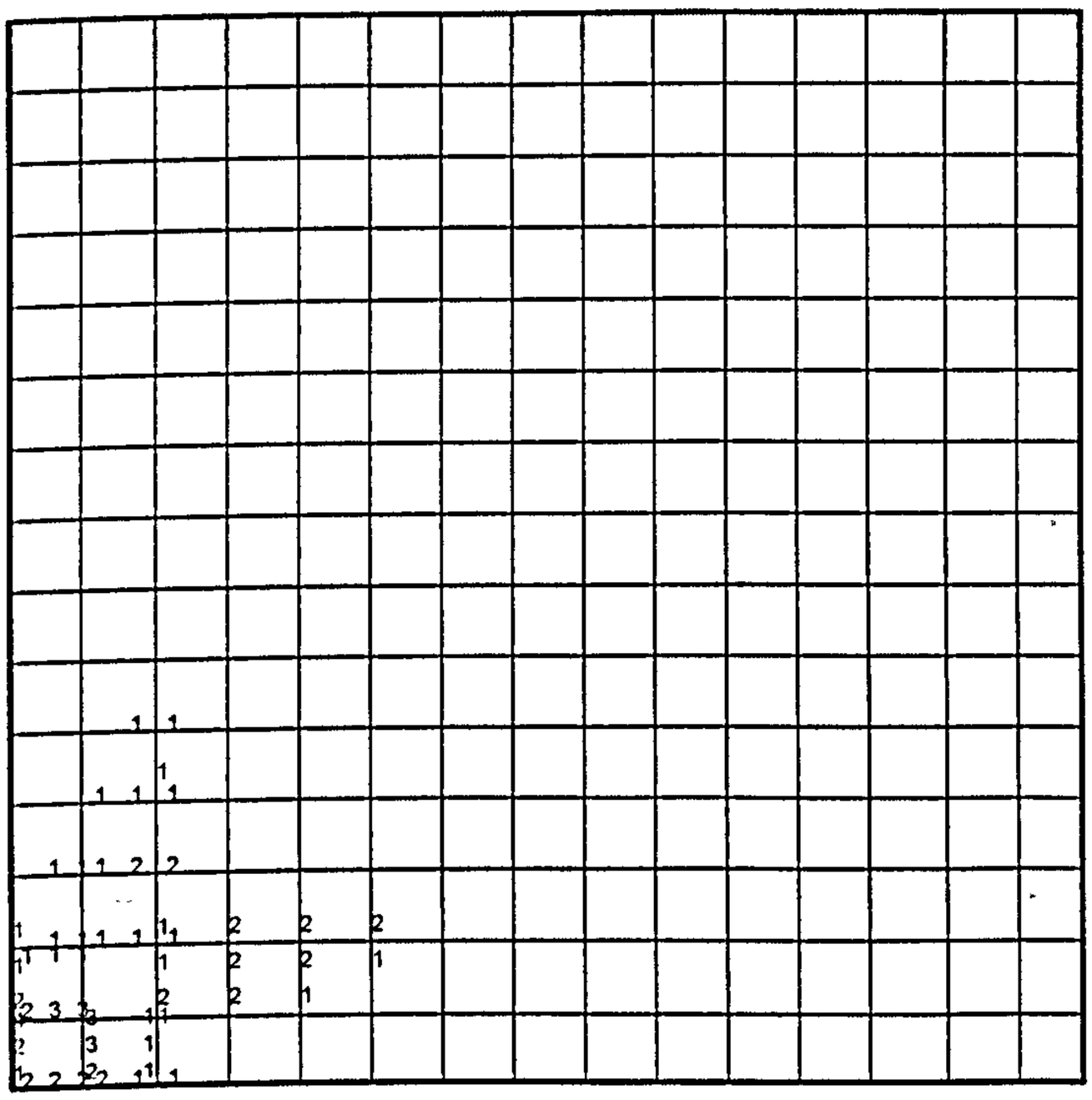

" G9 "

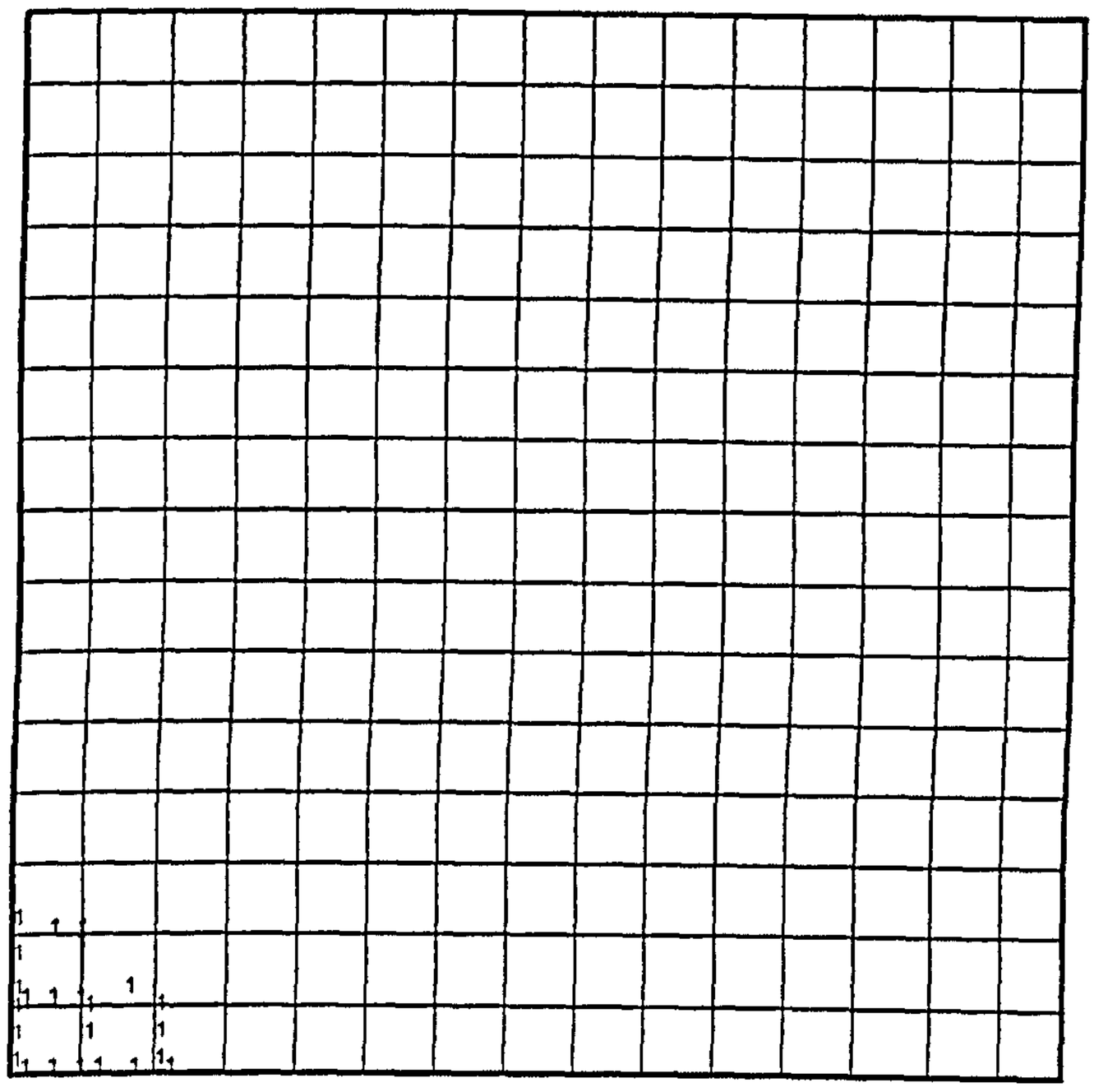

" G10 "

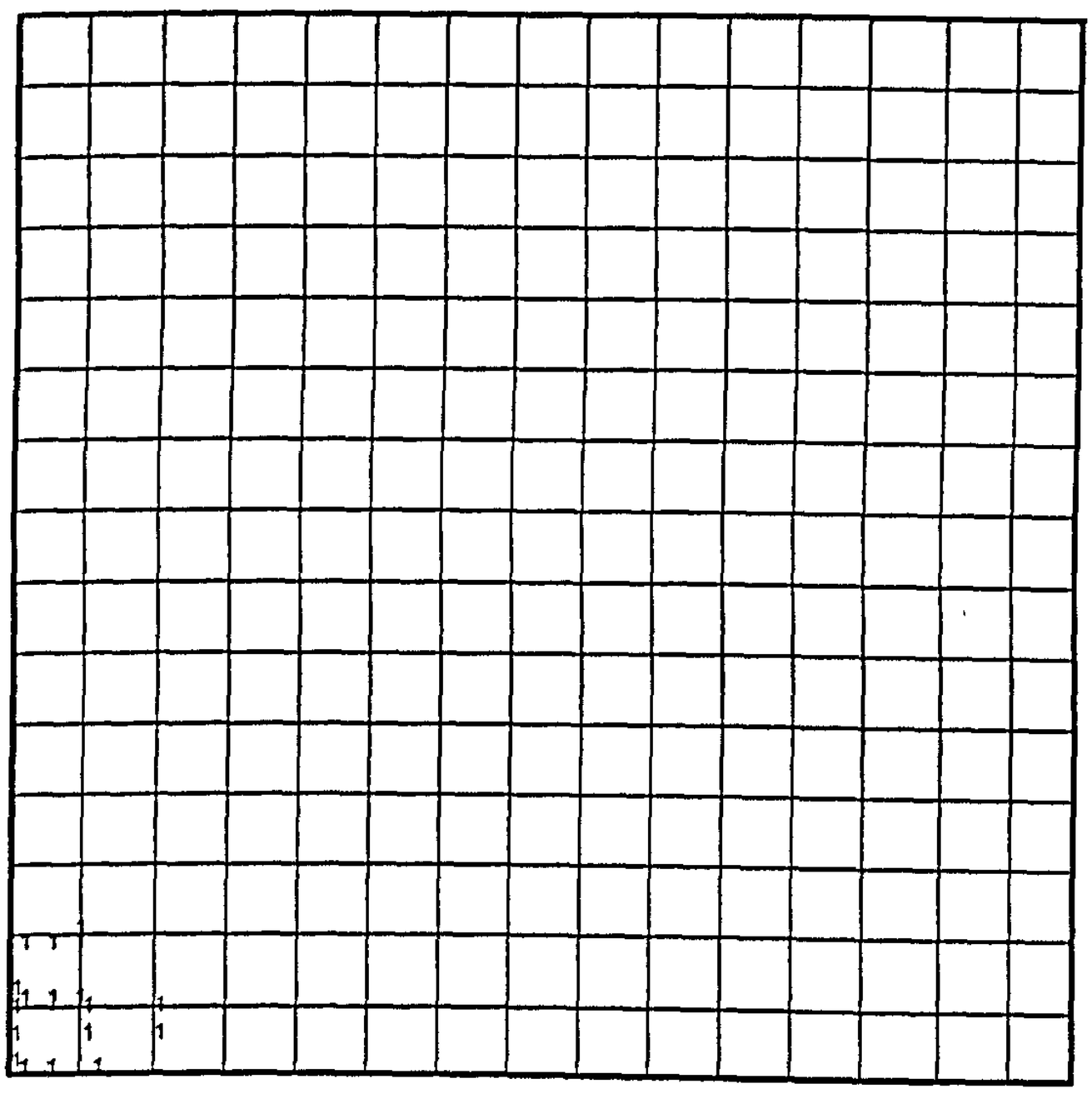

" G11 "

Note

Flexural steel in slab "**G1**" did not yield.

Interior slabs with shear reinforcement tested by Gomes

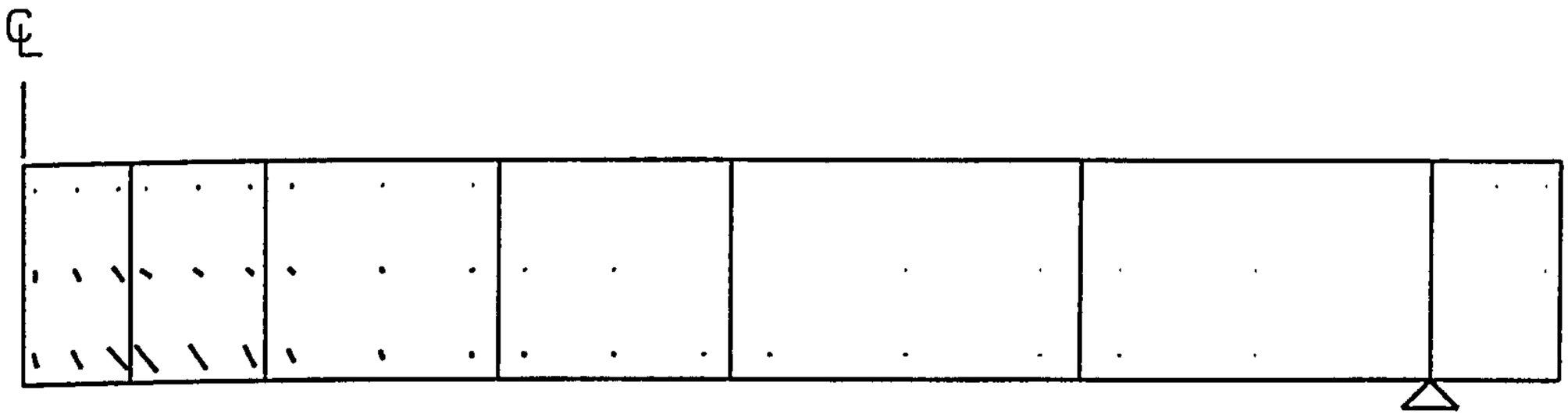

G1

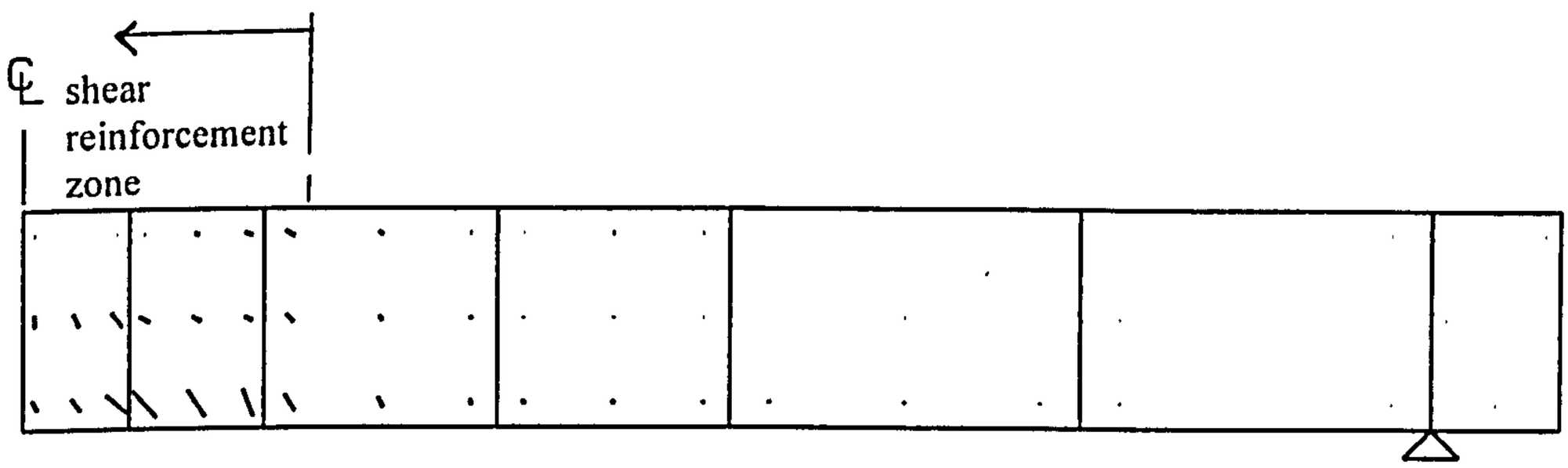

G2

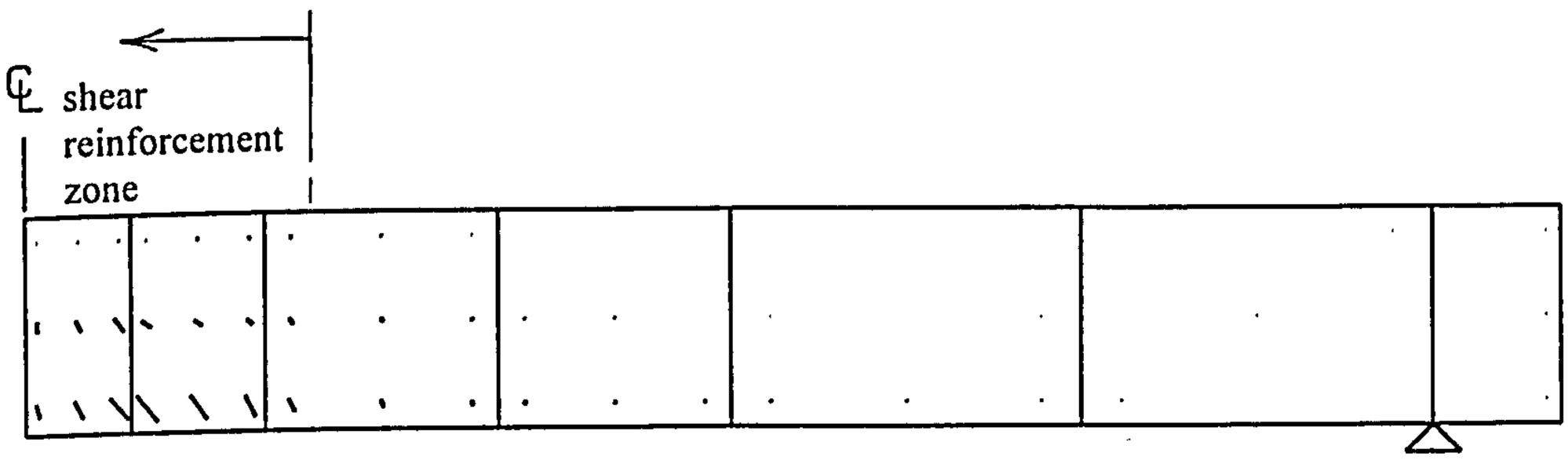

G3

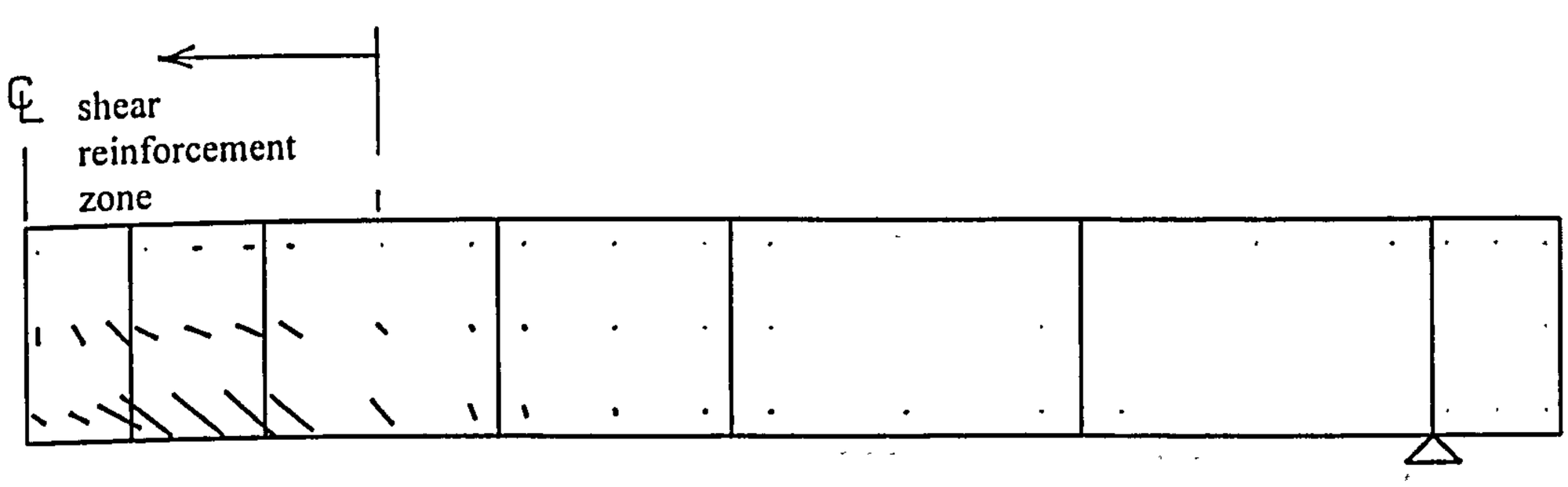

G4

Interior slabs with shear reinforcement tested by Gomes

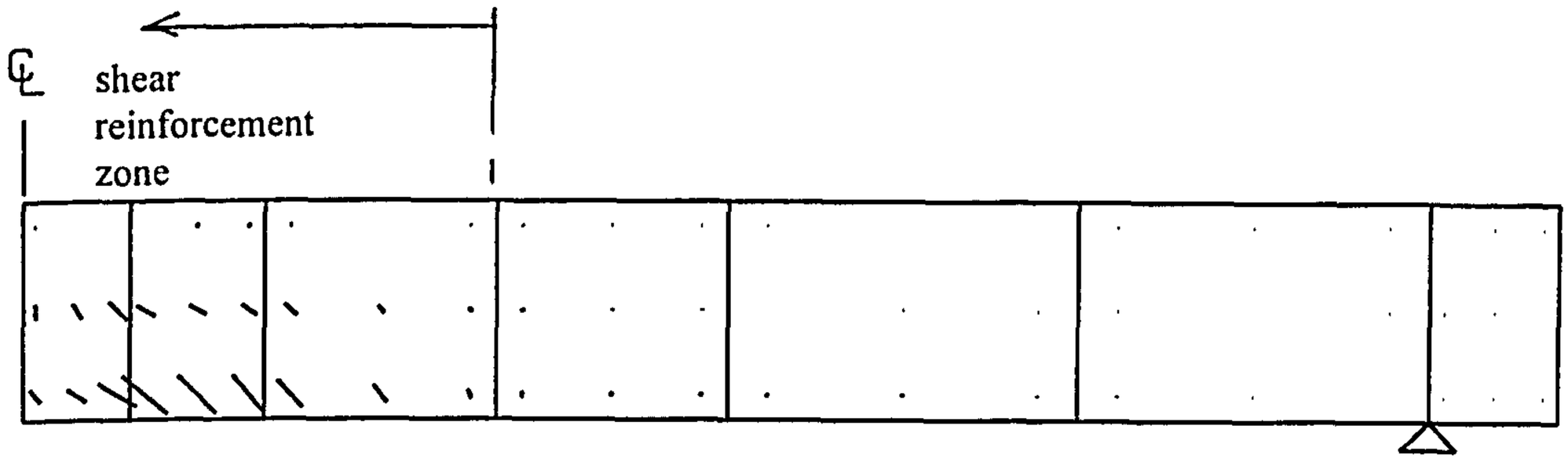

G5

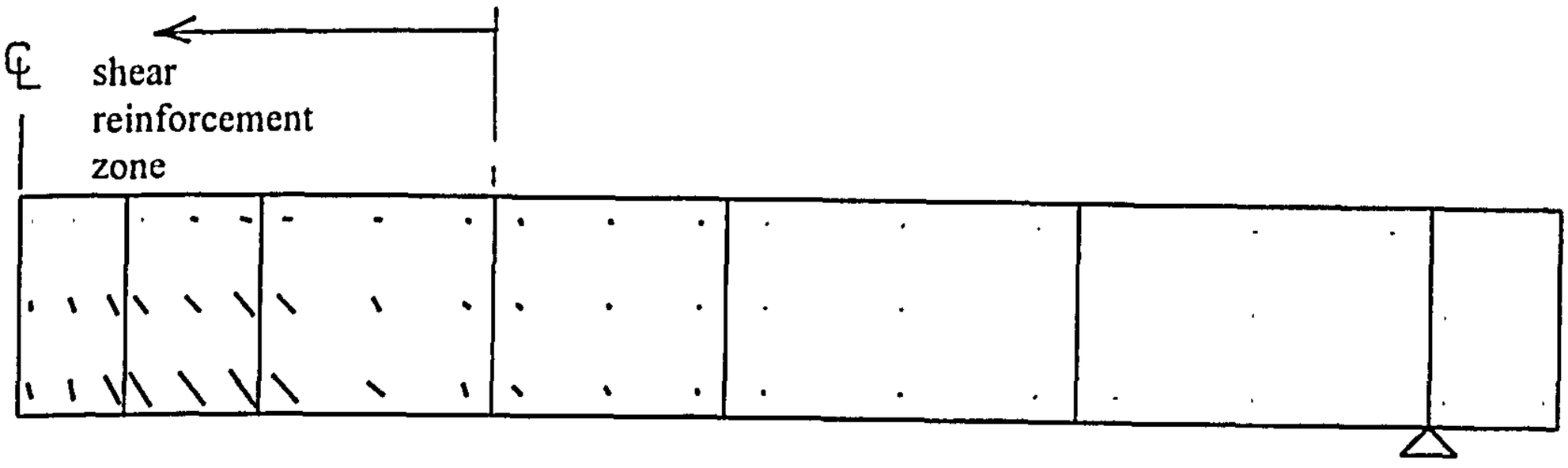

G6

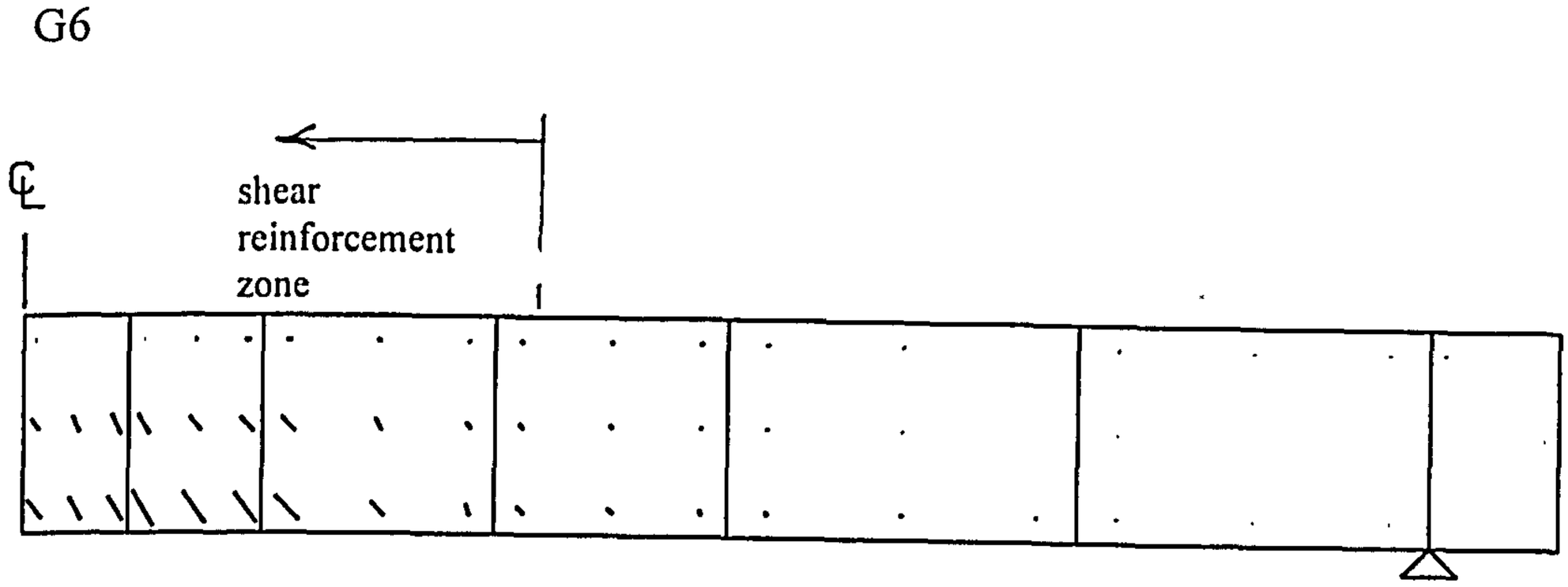

G7

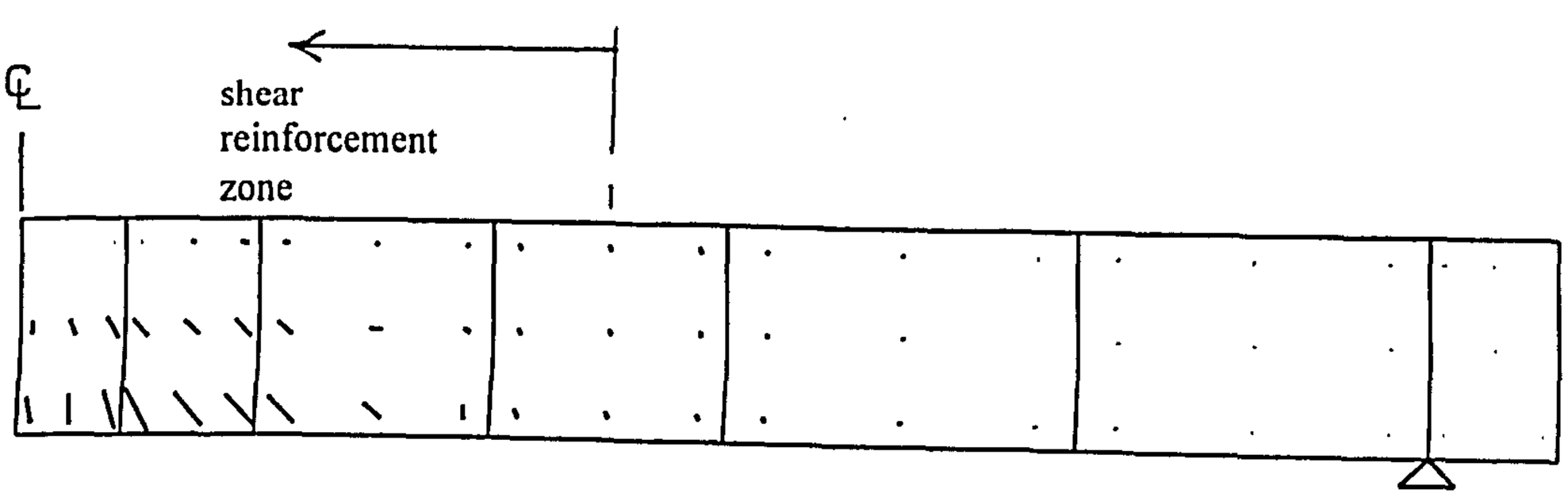

G8

Interior slabs with shear reinforcement tested by Gomes

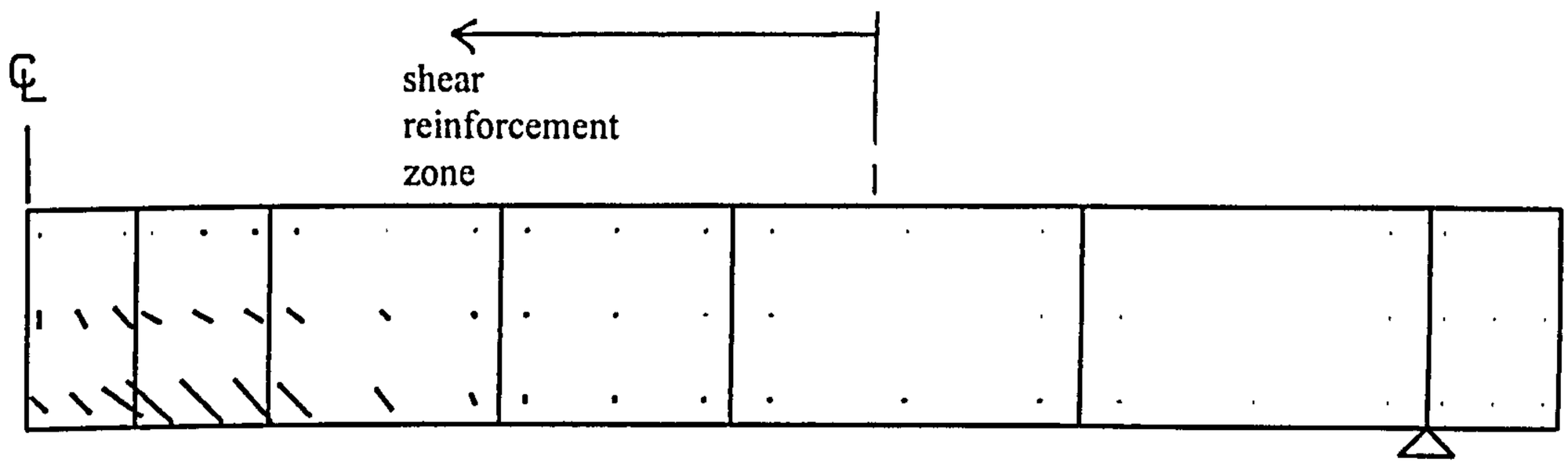

G9

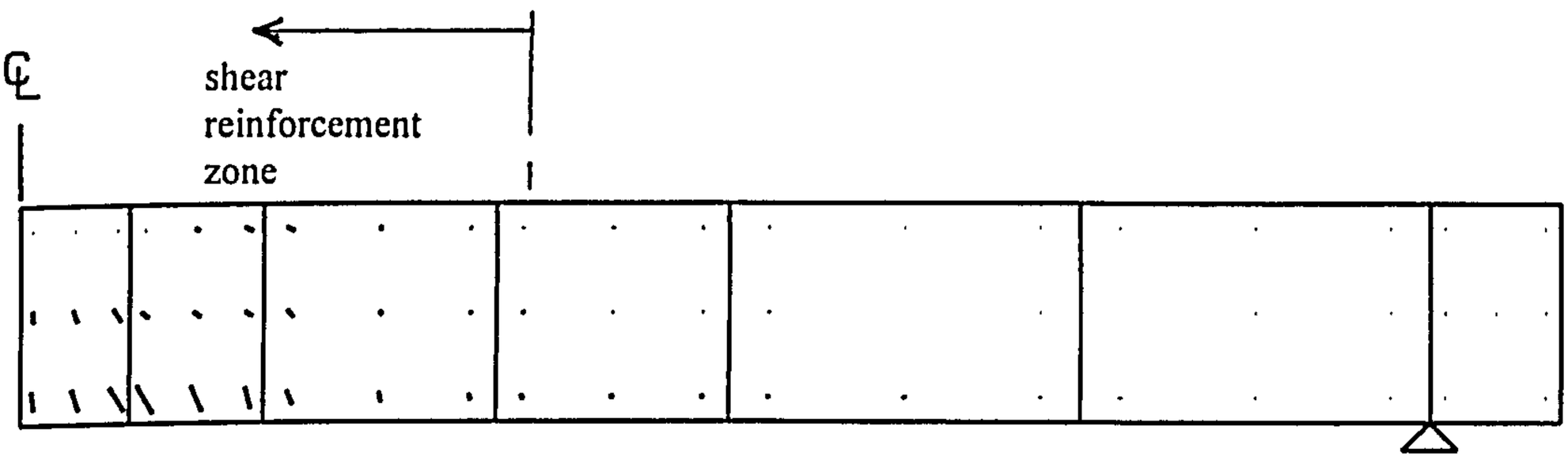

G10

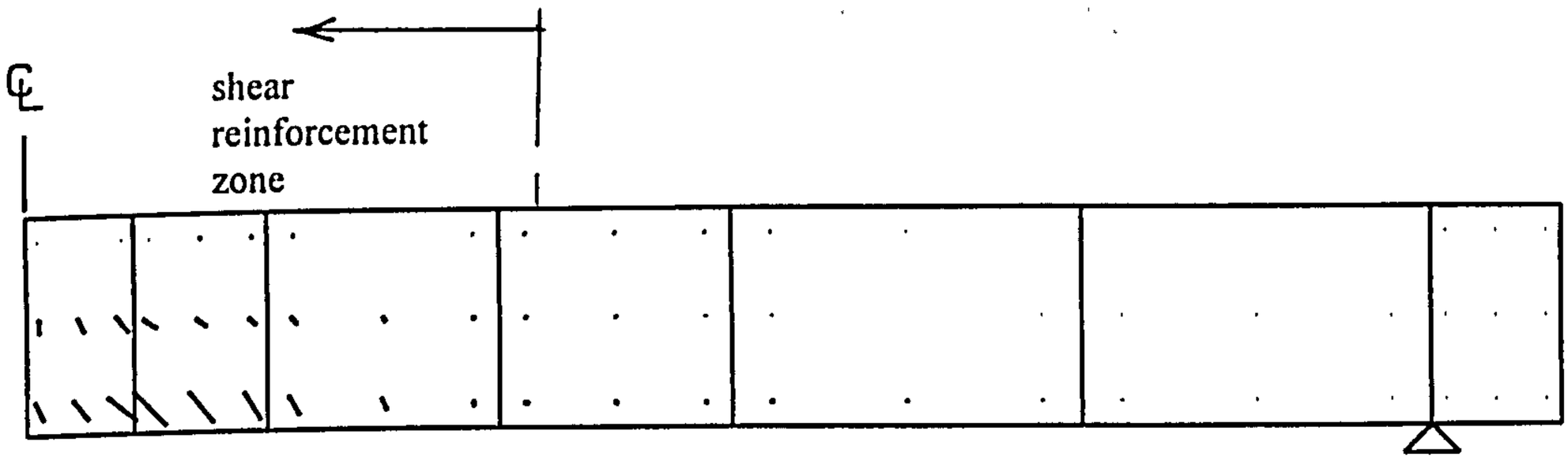

G11

Yamada's slabs

C1.5 Yamada's slabs (with shear reinforcement)

Slab	Test results		Numerical predictions		P_{num}/P_{test}
	P_{test} (kN)	Failure mode	P_{num} (kN)	Failure mode	
K1	658.0	s	640.0	s	0.972
K2	950.0	s	924.0	s	0.972
K3	1183.0	s	1064.0	s	0.899
K4	1153.0	s	1064.0	s	0.923
K5	1440.0	s	1064.0	s	0.739
K6	1274.0	s	1080.0	s	0.848
K7	1498.0	s	1080.0	s	0.721
				Average	0.868
				STDEV	0.103

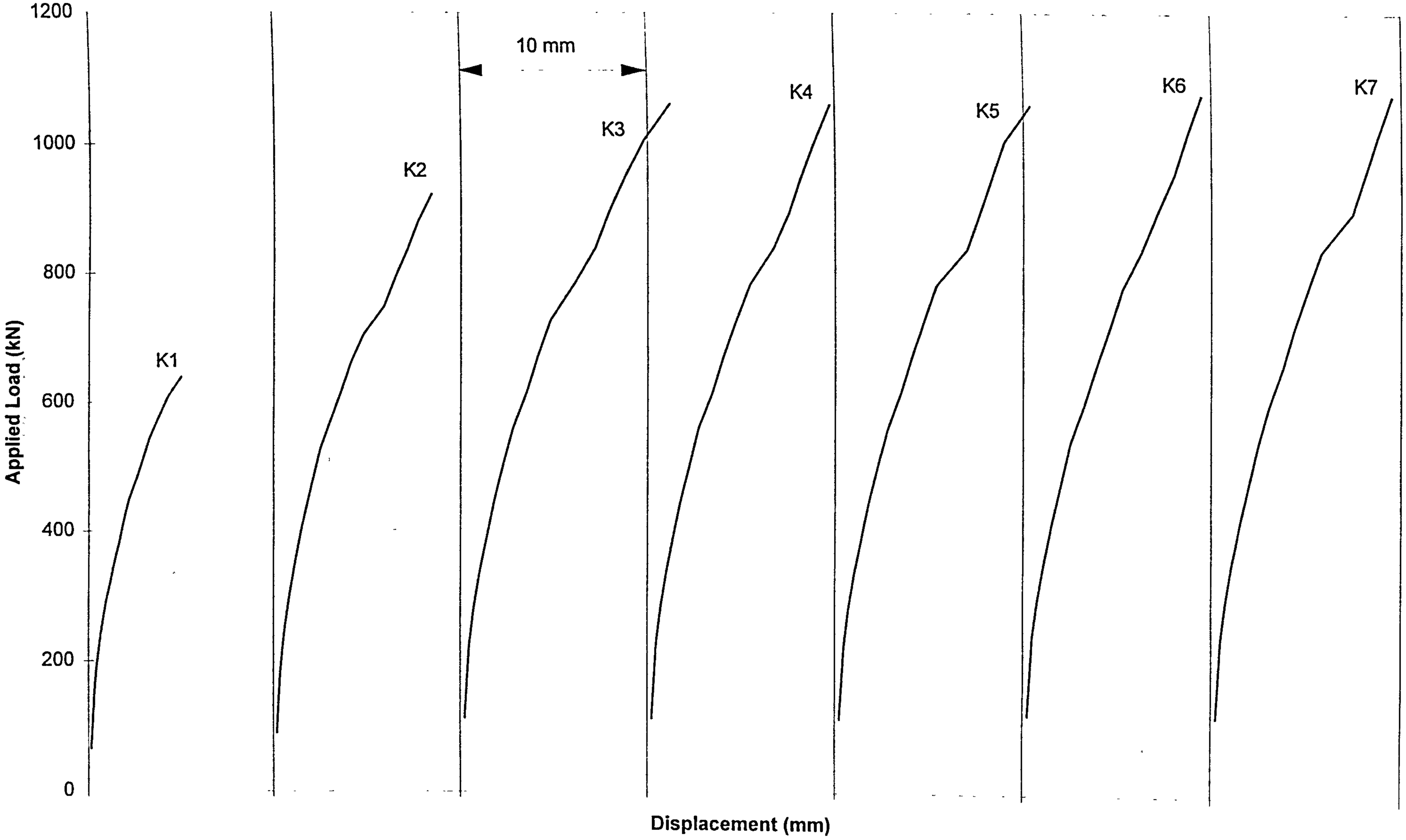

Predicted load-deflection response for slabs K1-K7

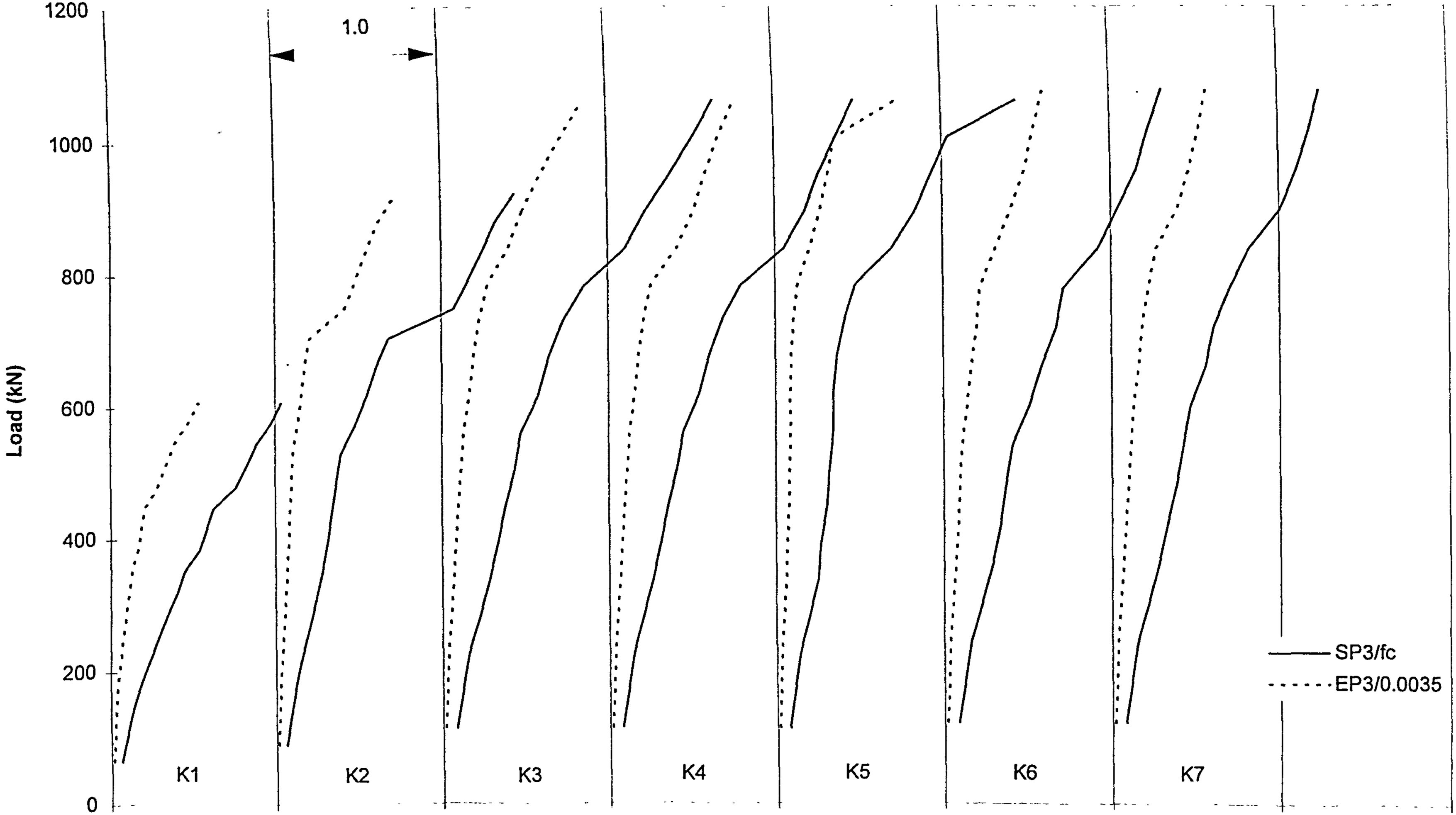

Predicted principal compressive stress and strain in concrete (slabs K1-K7)

Yielding of flexural steel for specimens K1-K7 (Yamada et al)

NB. : The numbers on the drawing indicate strain in steel at collapse expressed as a ratio of yield strain

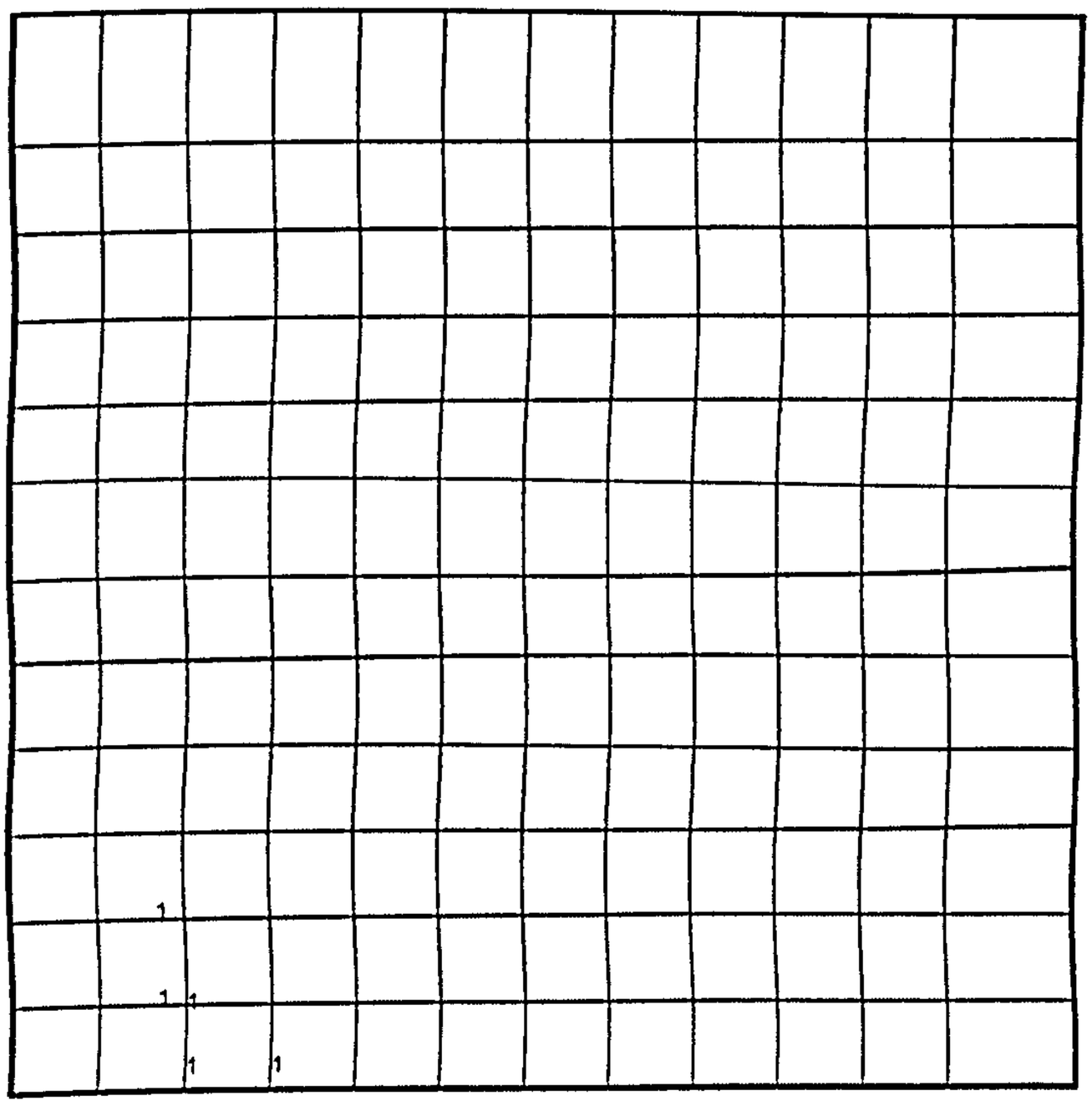

" K3 "

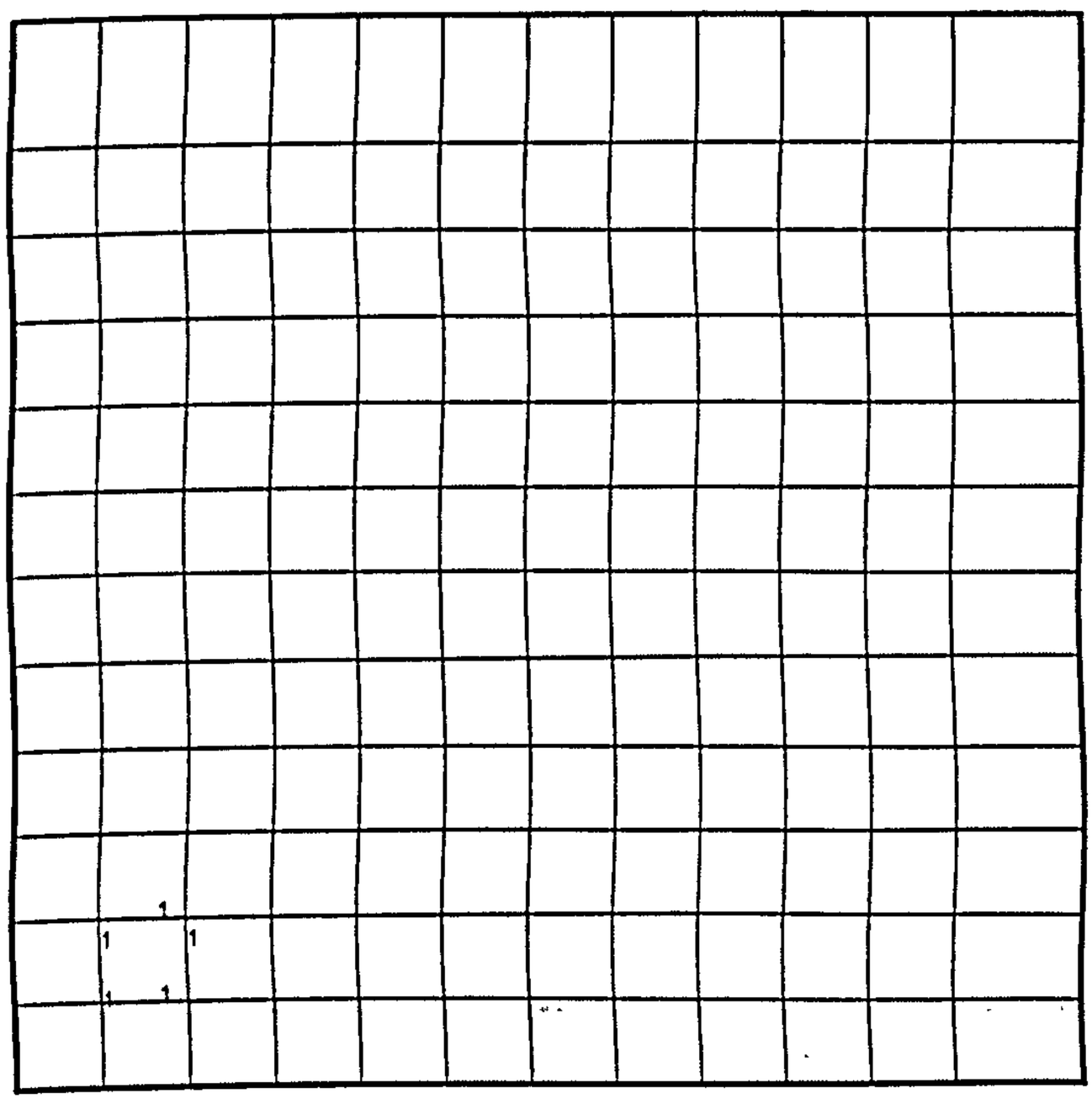

" K4 "

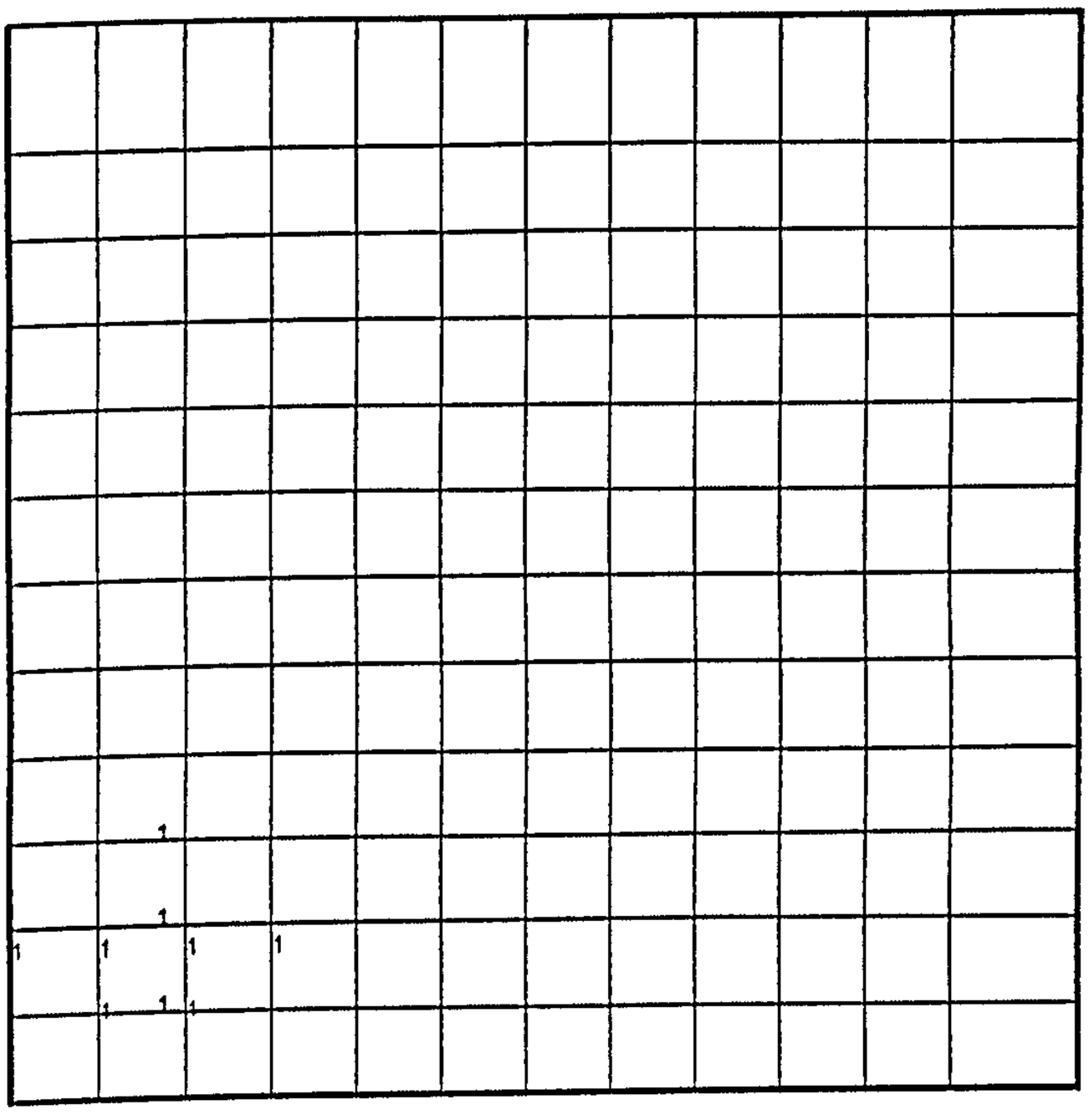

" K5 "

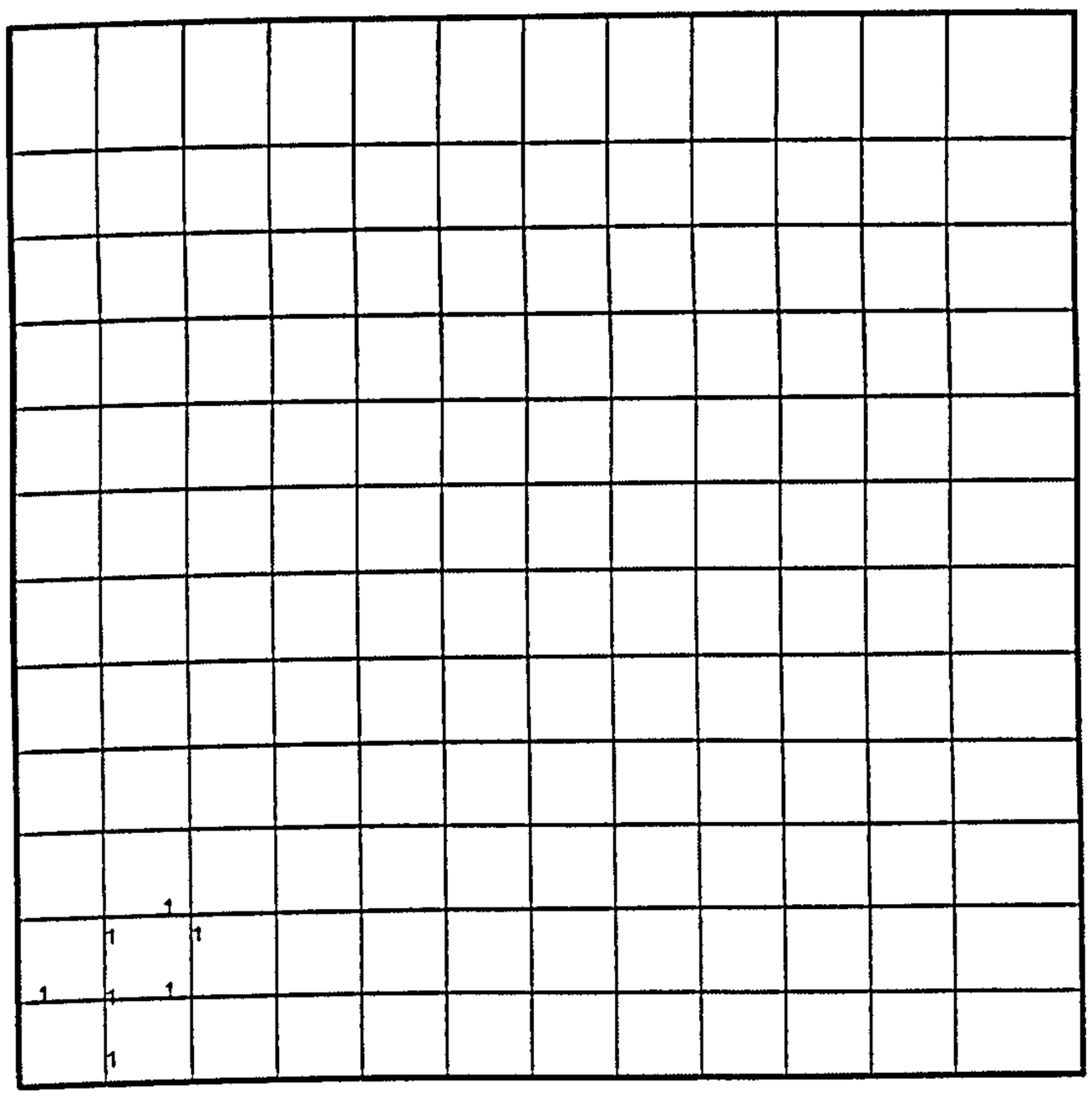

" K6 "

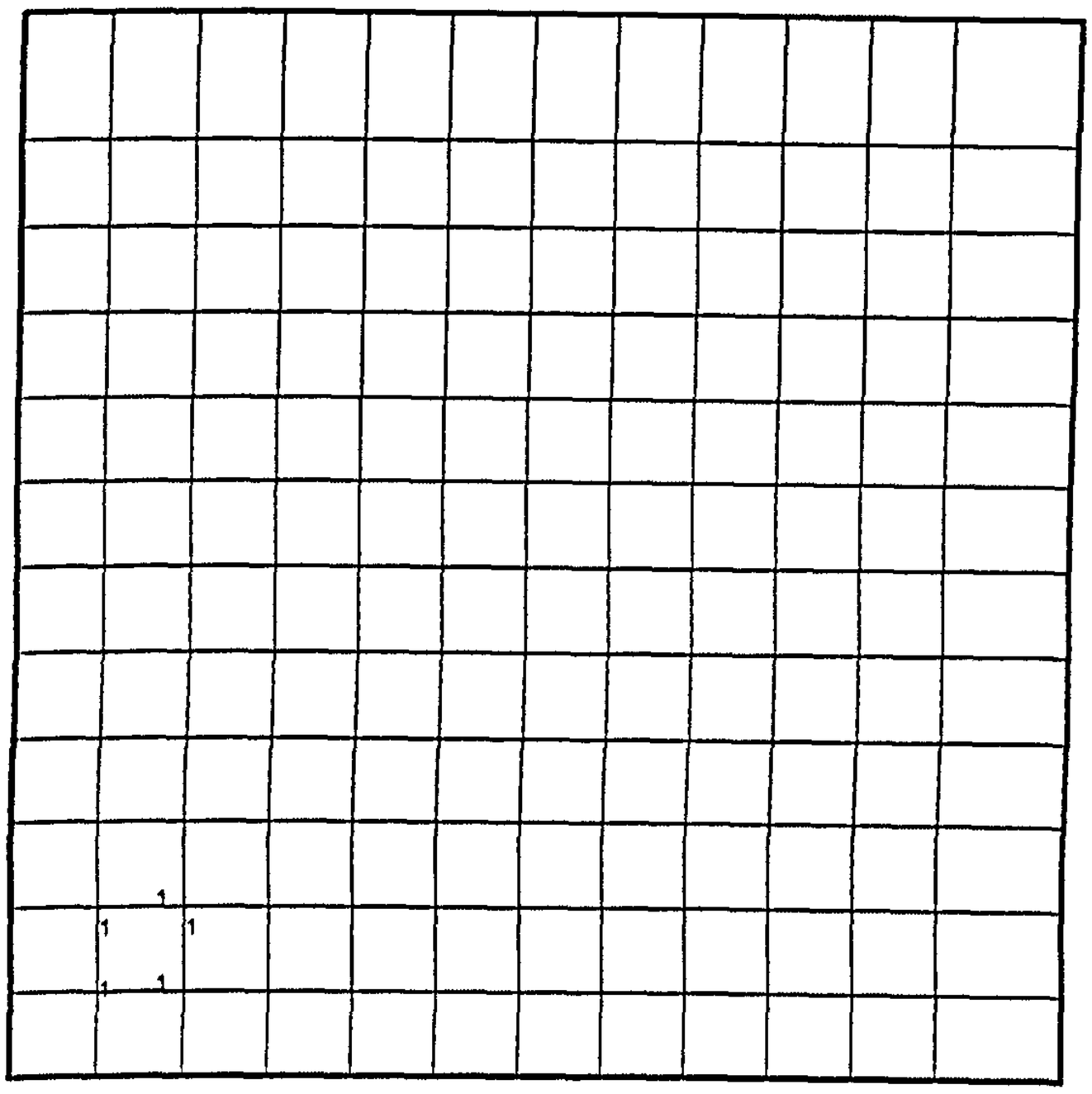

" K7 "

Note

Flexural steel in slabs "K1"and "K2" did not yield.

Predicted crack pattern for specimens K1-K7 (Yamada et al)

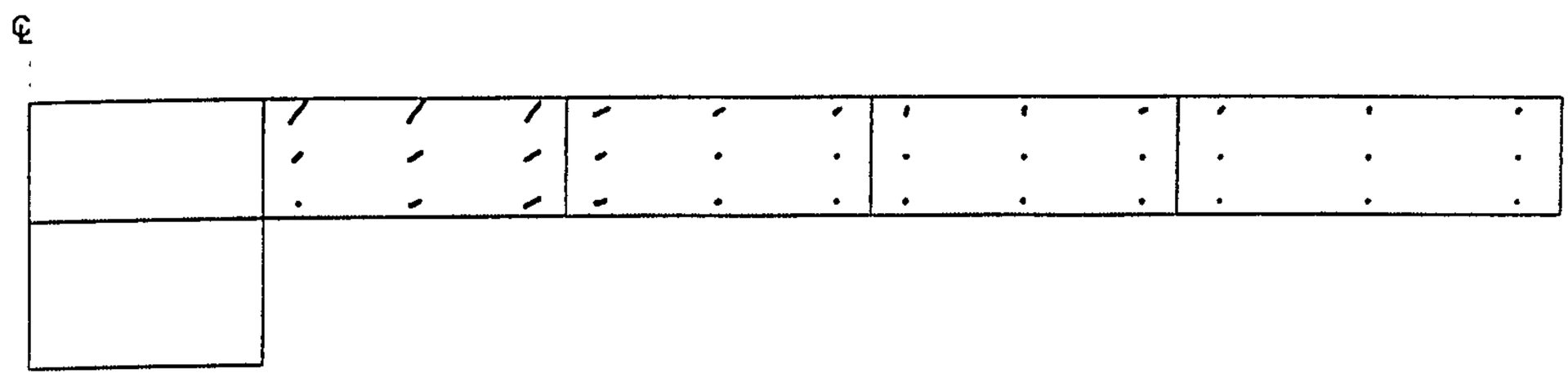

" K1 "

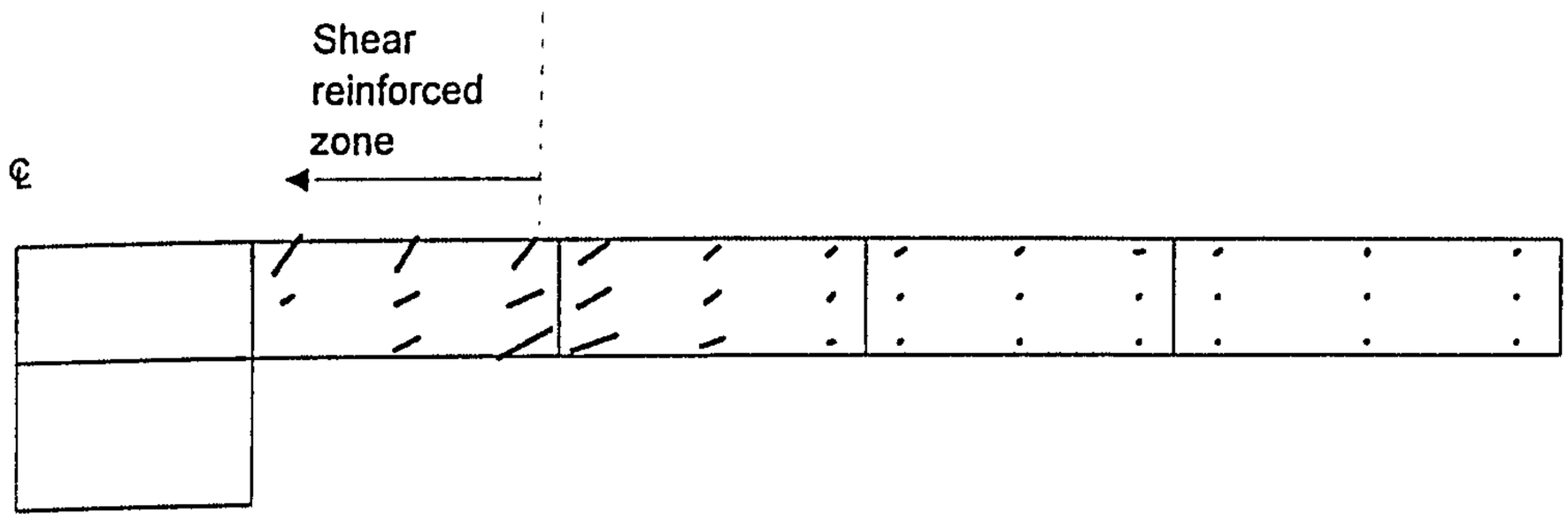

" K2 "

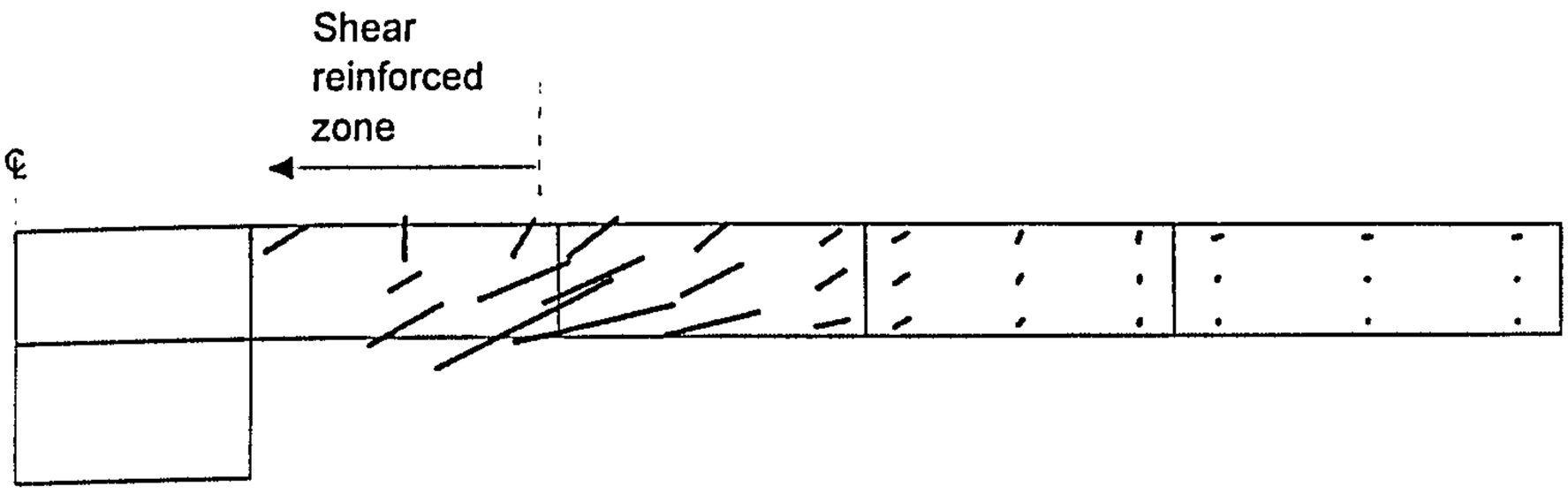

" K3 "

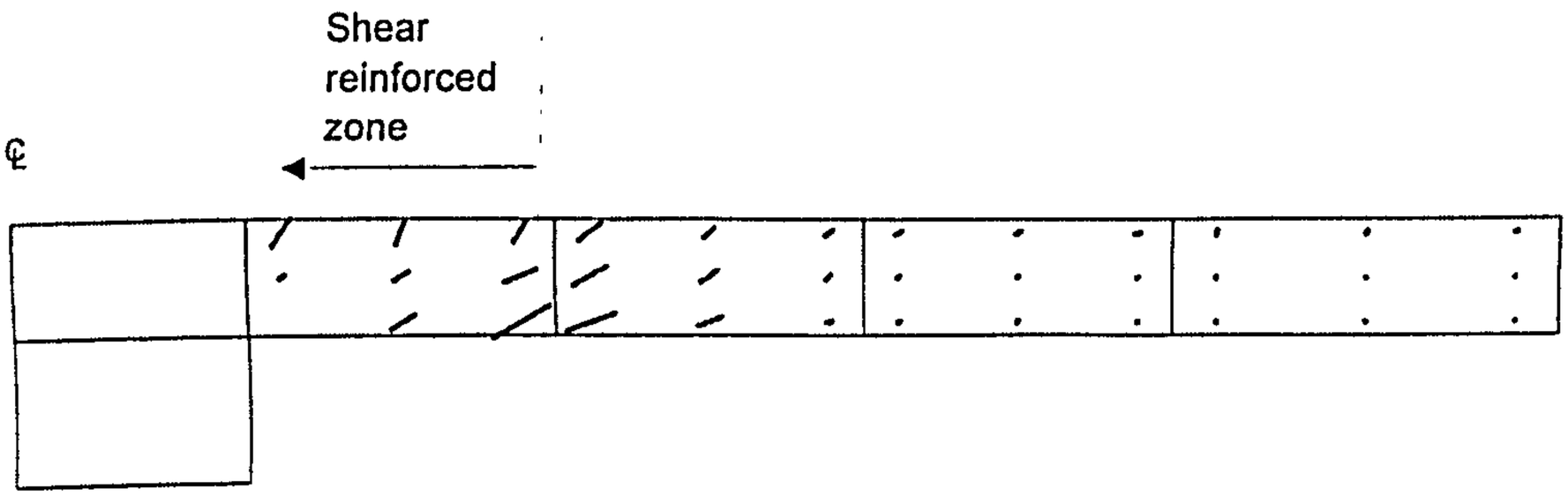

" K4 "

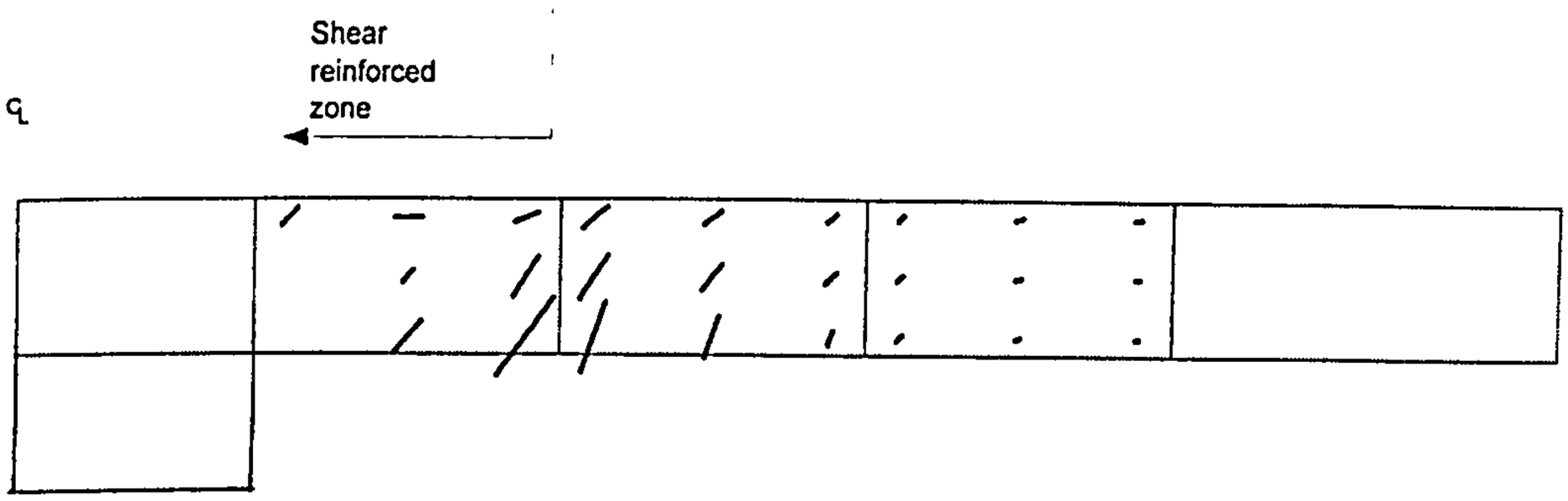
Shear
reinforced
zone
℄

" K5 "

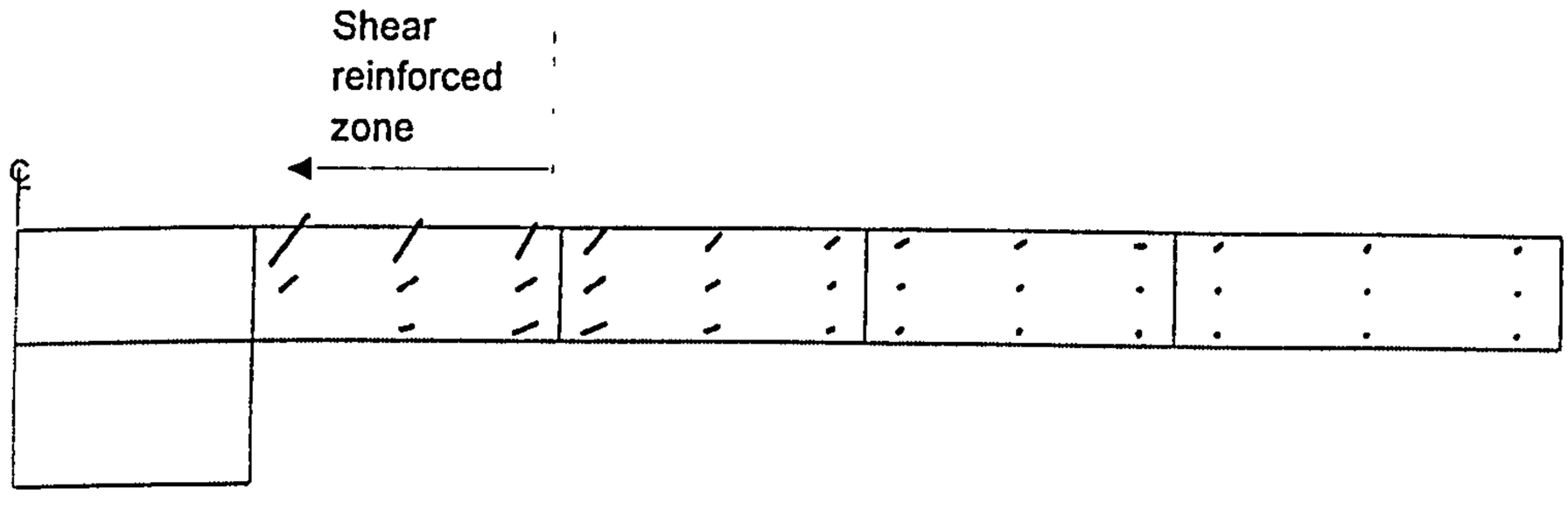
Shear
reinforced
zone
℄

" K6 "

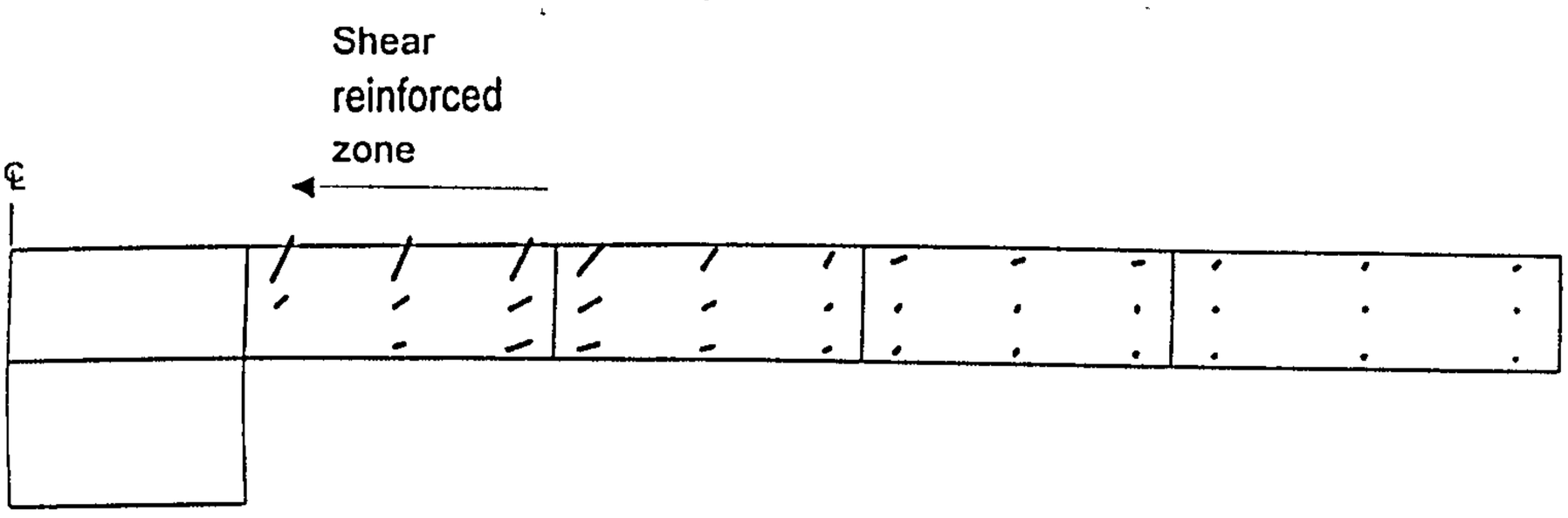
Shear
reinforced
zone
℄

" K7 "

Seible's slabs

C1.6 Seible's slabs (with shear reinforcement)

Slab	Test results		Numerical predictions		P_{num}/P_{test}
	P_{test} (kN)	Failure mode	P_{num} (kN)	Failure mode	
SC7	623.0	fp	510.0	fp	0.819
SC8	592.0	fp	510.0	fp	0.861
SC9	594.0	fp	510.0	fp	0.859
SC10	537.0	fp	540.0	fp	1.006
SC11	596.0	fp	540.0	fp	0.906
SC12	595.0	fp	540.0	fp	0.908
				Average	0.893
				STDEV	0.065

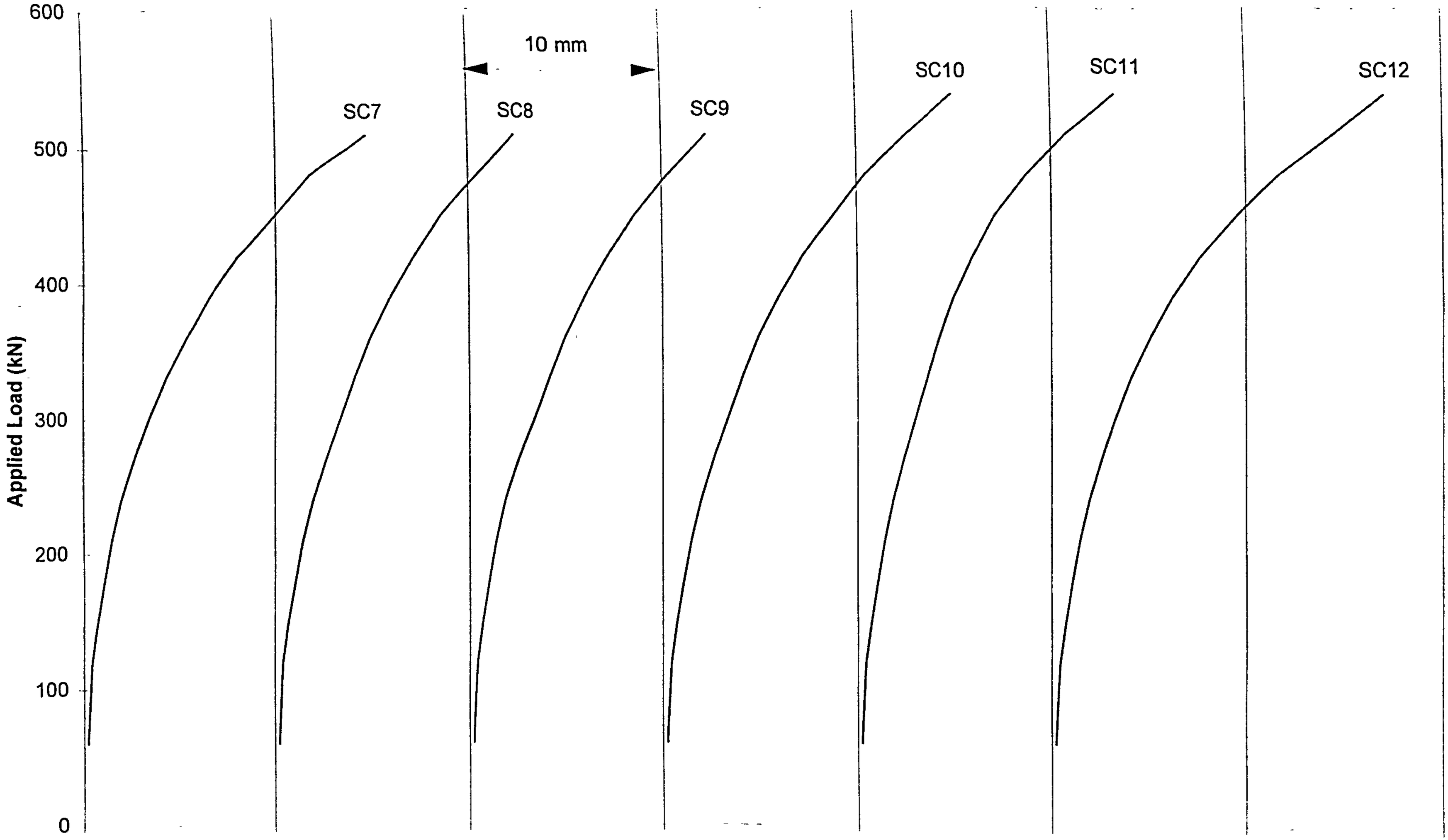

Predicted load-deflection response for slabs SC7-SC12

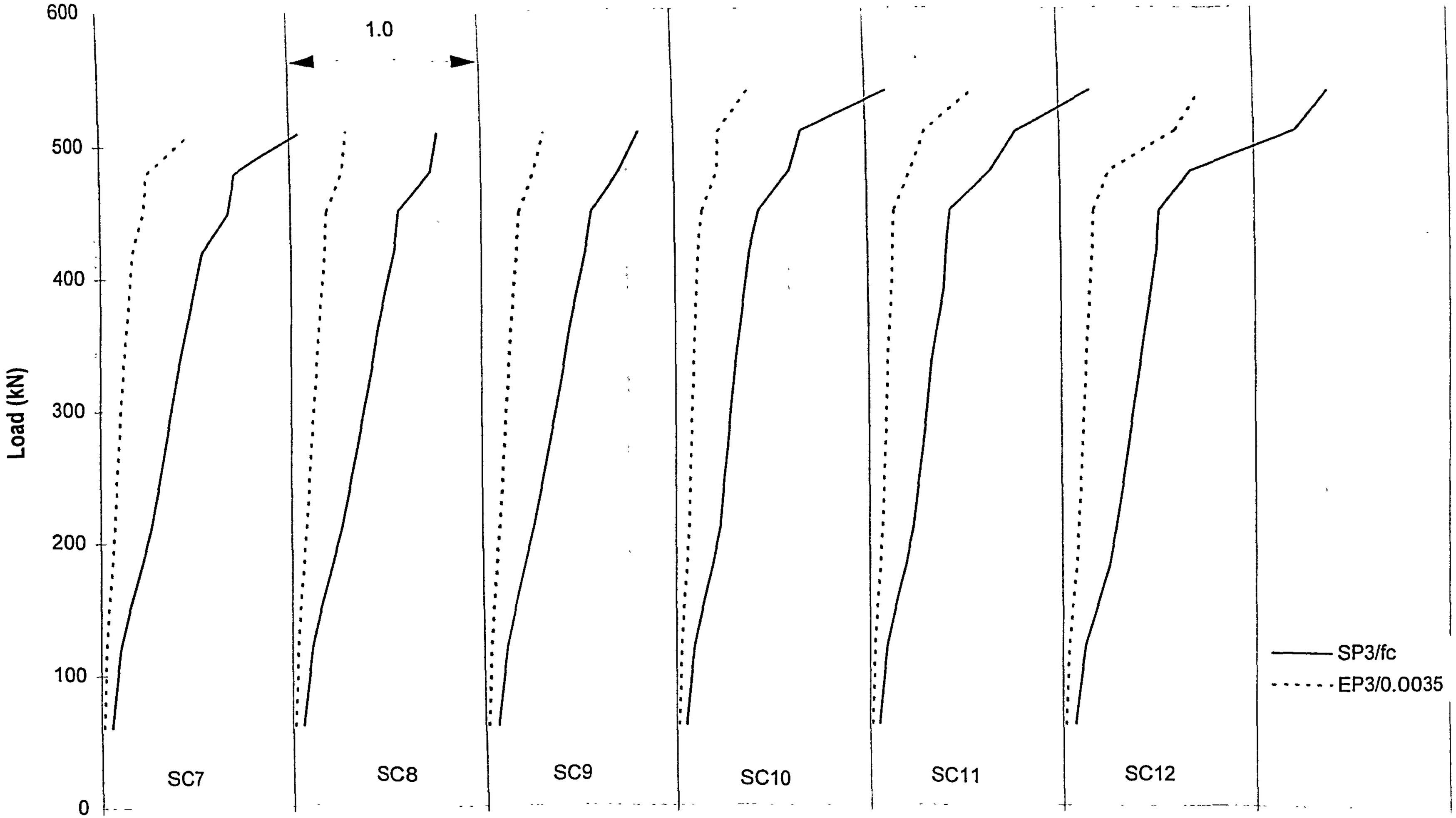

Predicted principal compressive stress and strain in concrete (slabs SC7-SC10)

Yielding of flexural steel for specimens SC7-SC12 (Seible et al)

NB. : The numbers on the drawing indicate strain in steel at collapse expressed as a ratio of yield strain

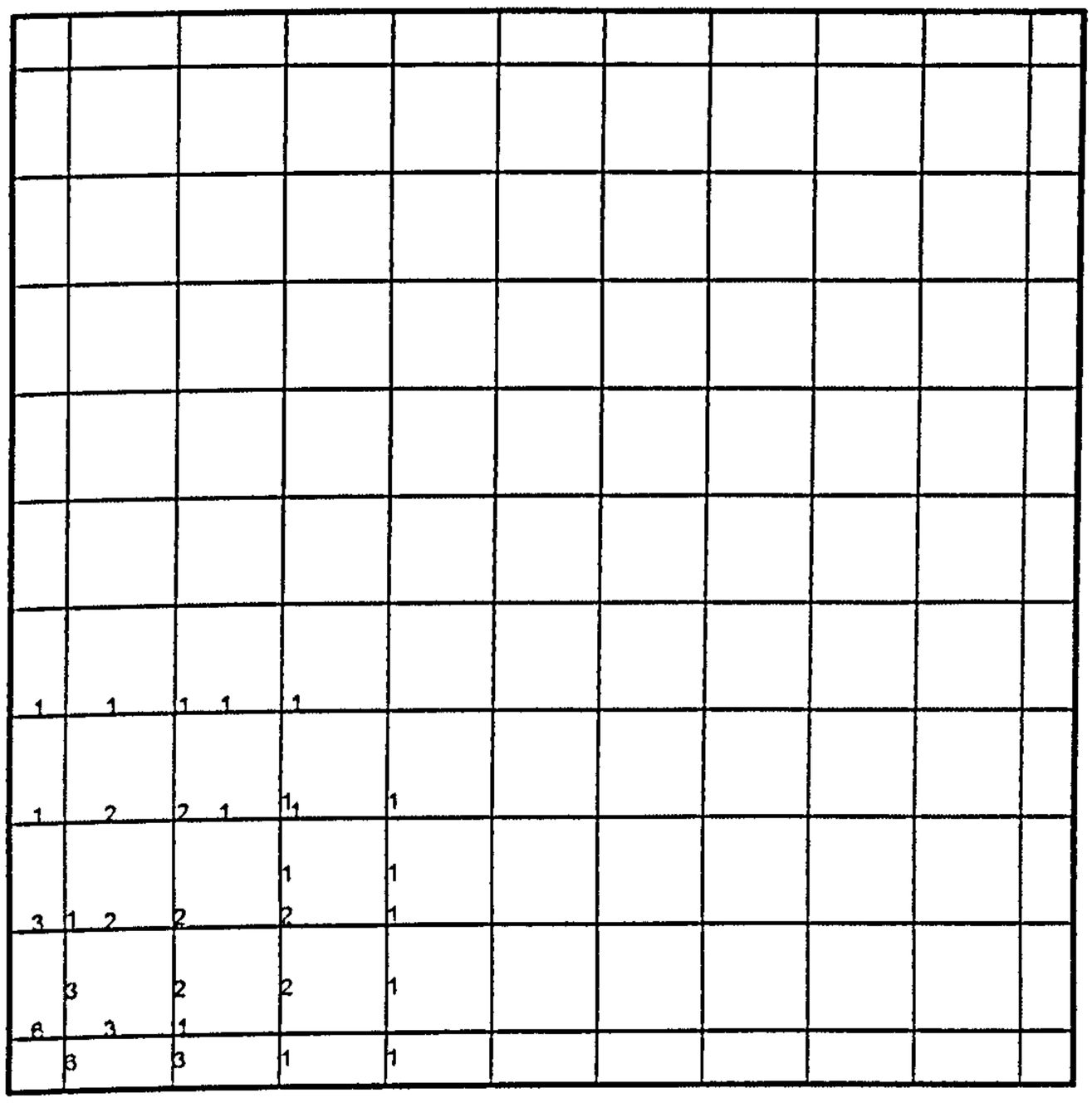

" SC7 "

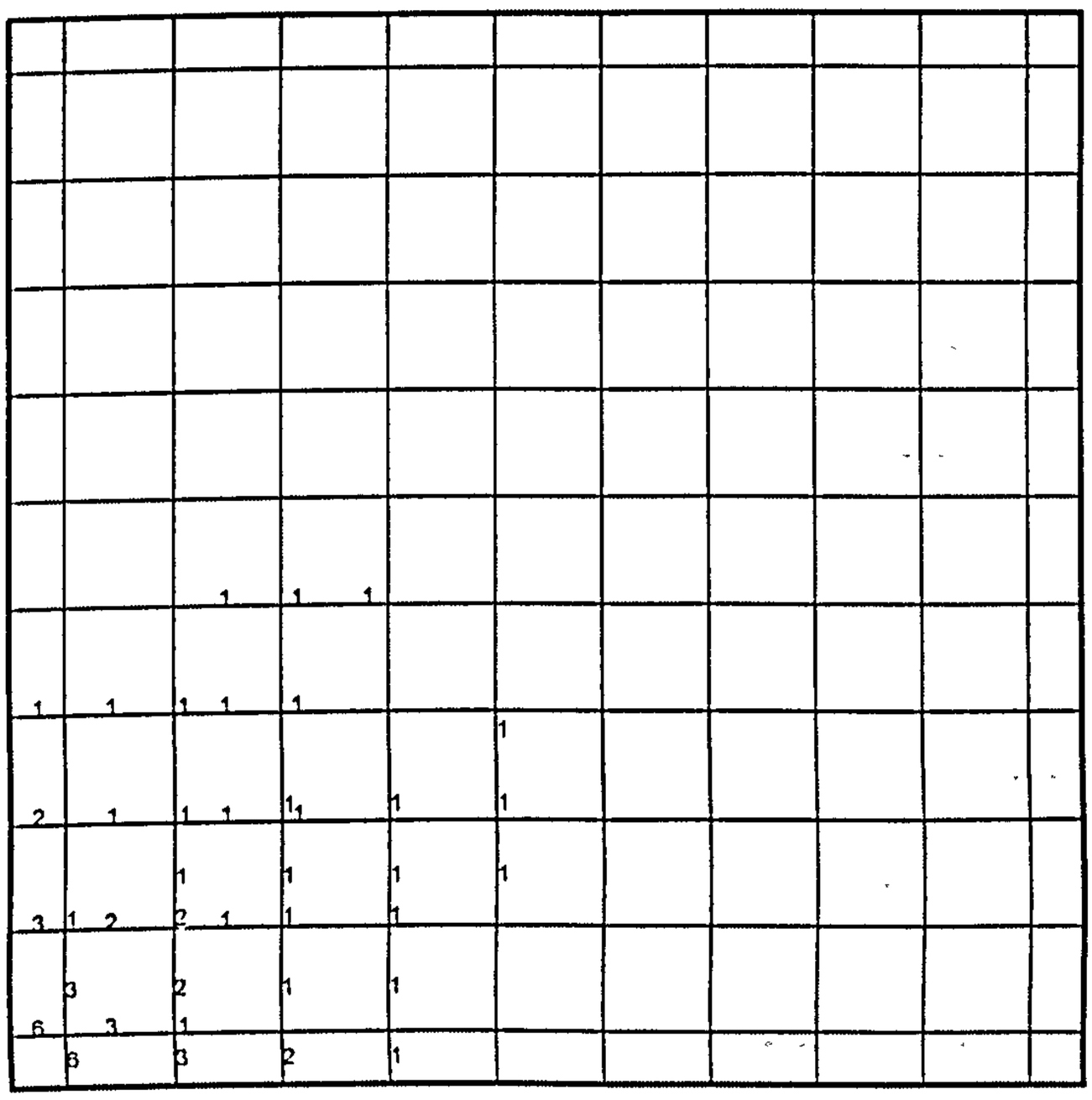

" SC8 "

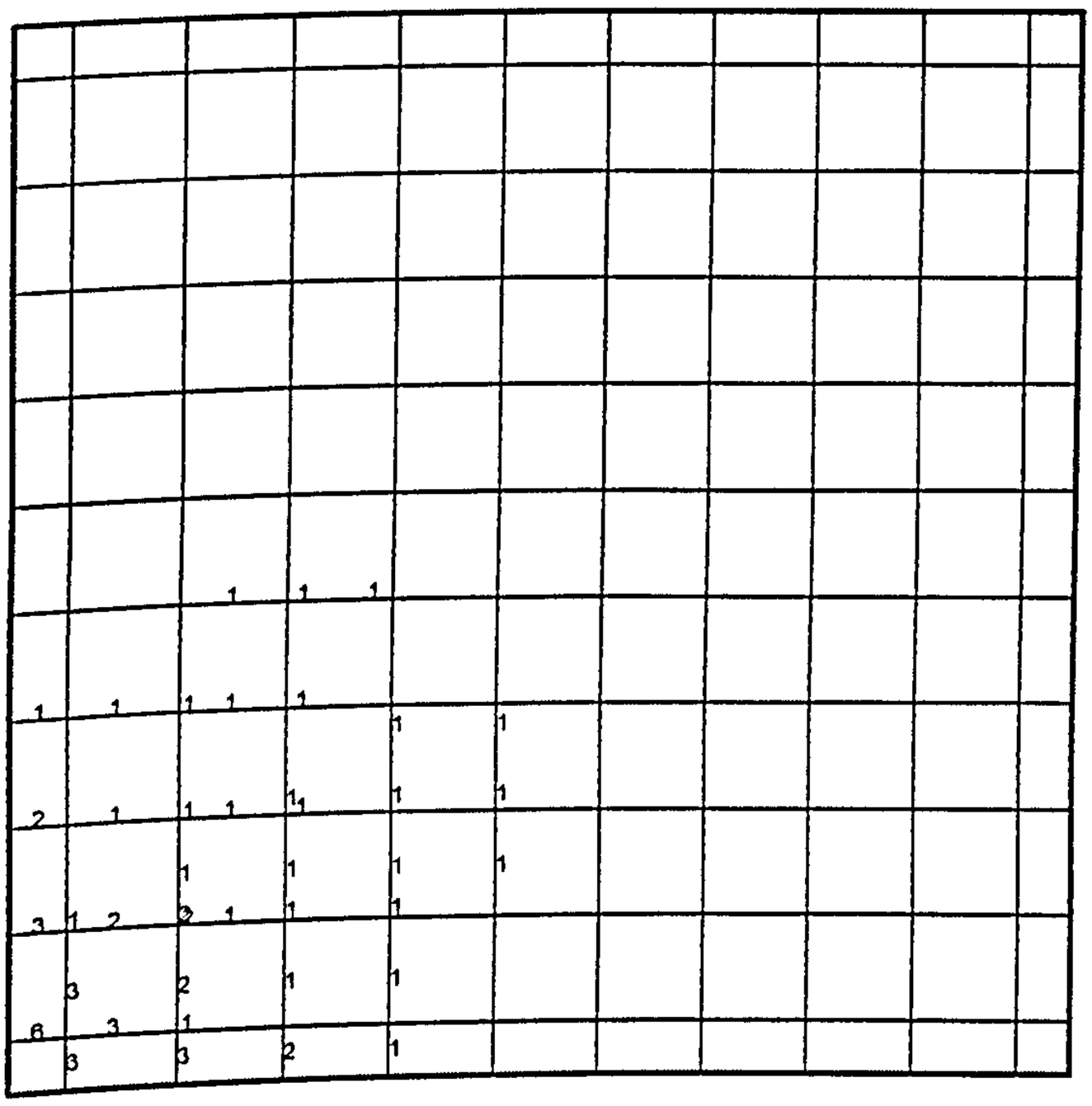

" SC9 "

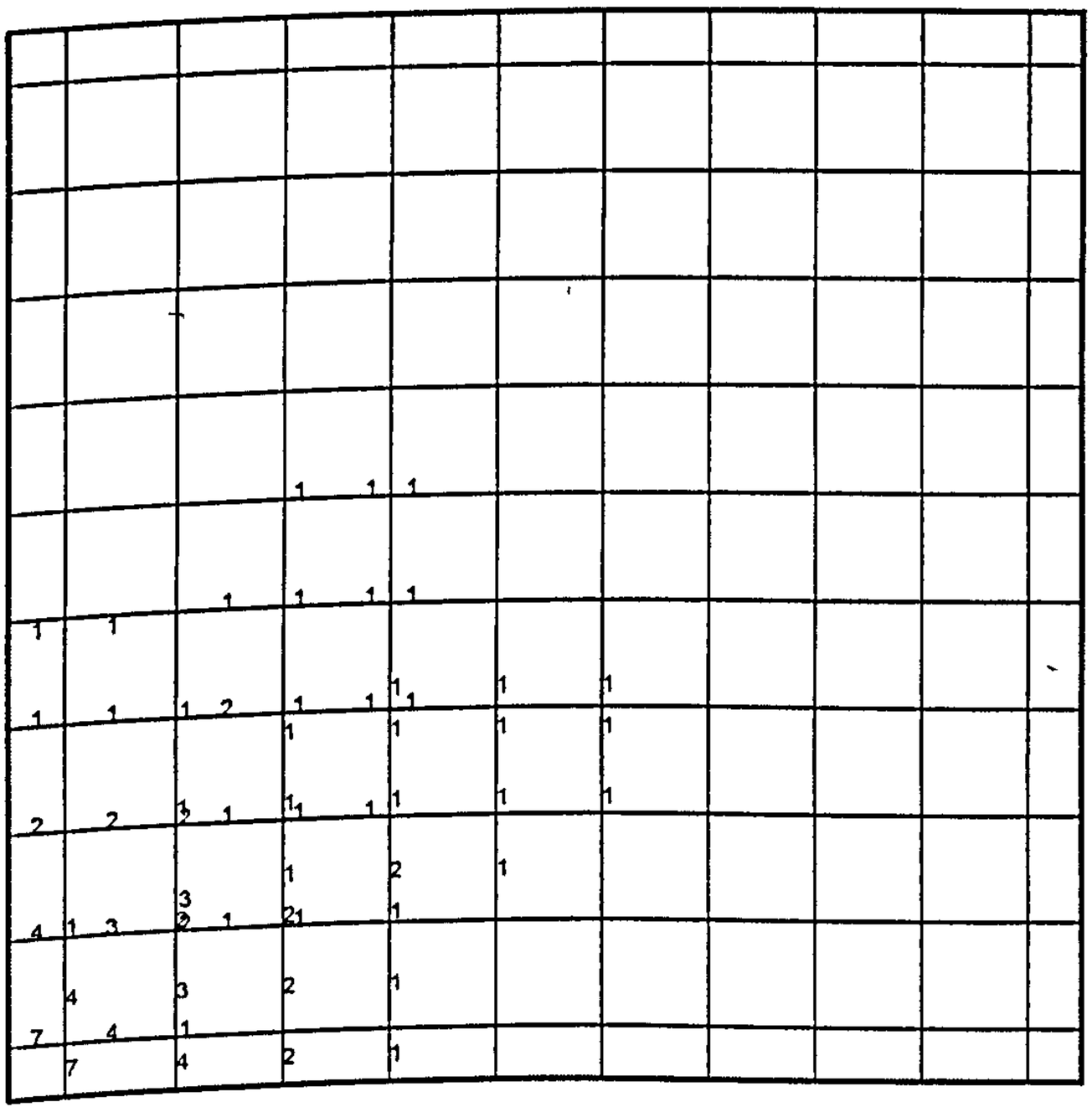

" SC10 "

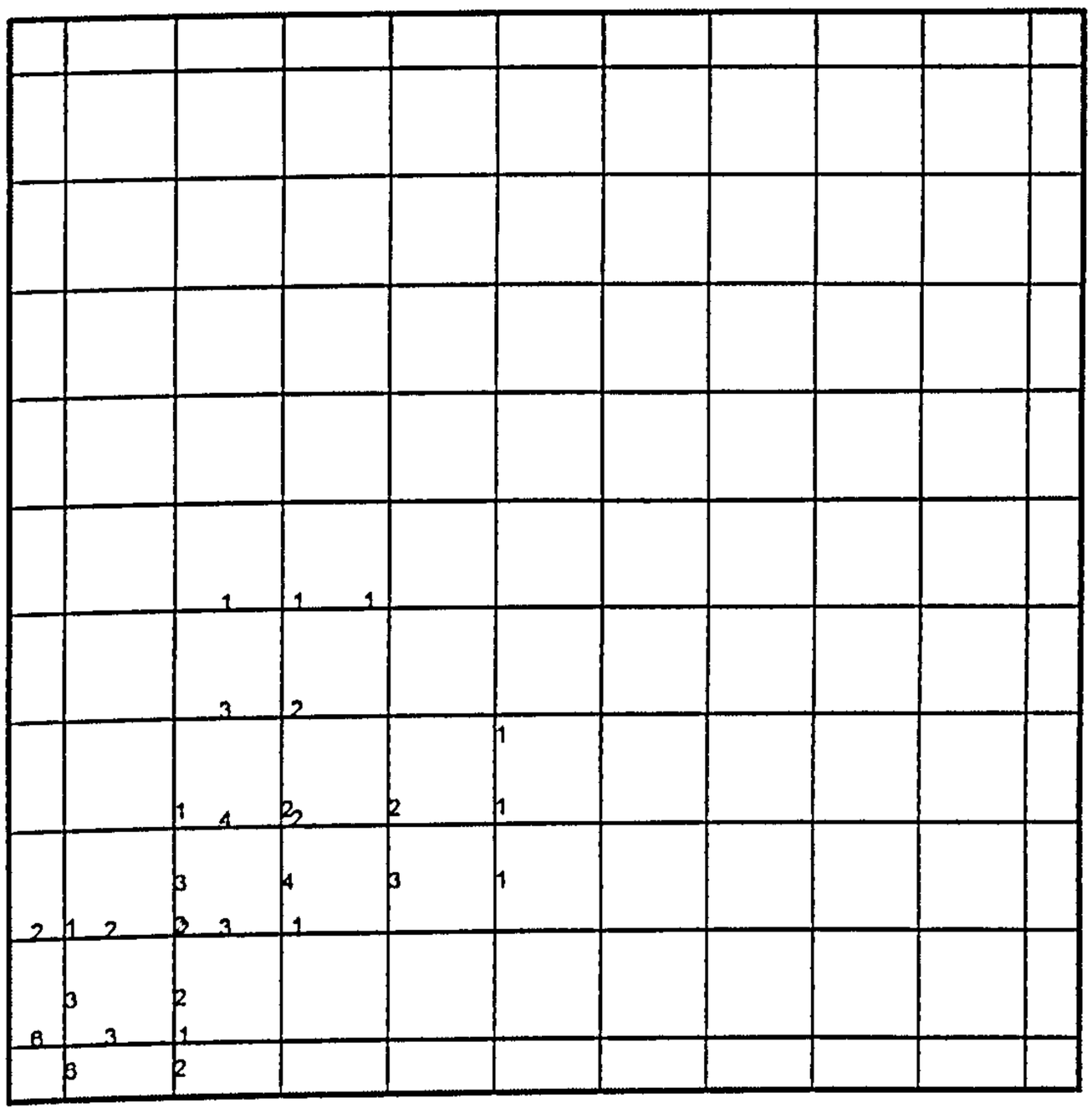

" SC11 "

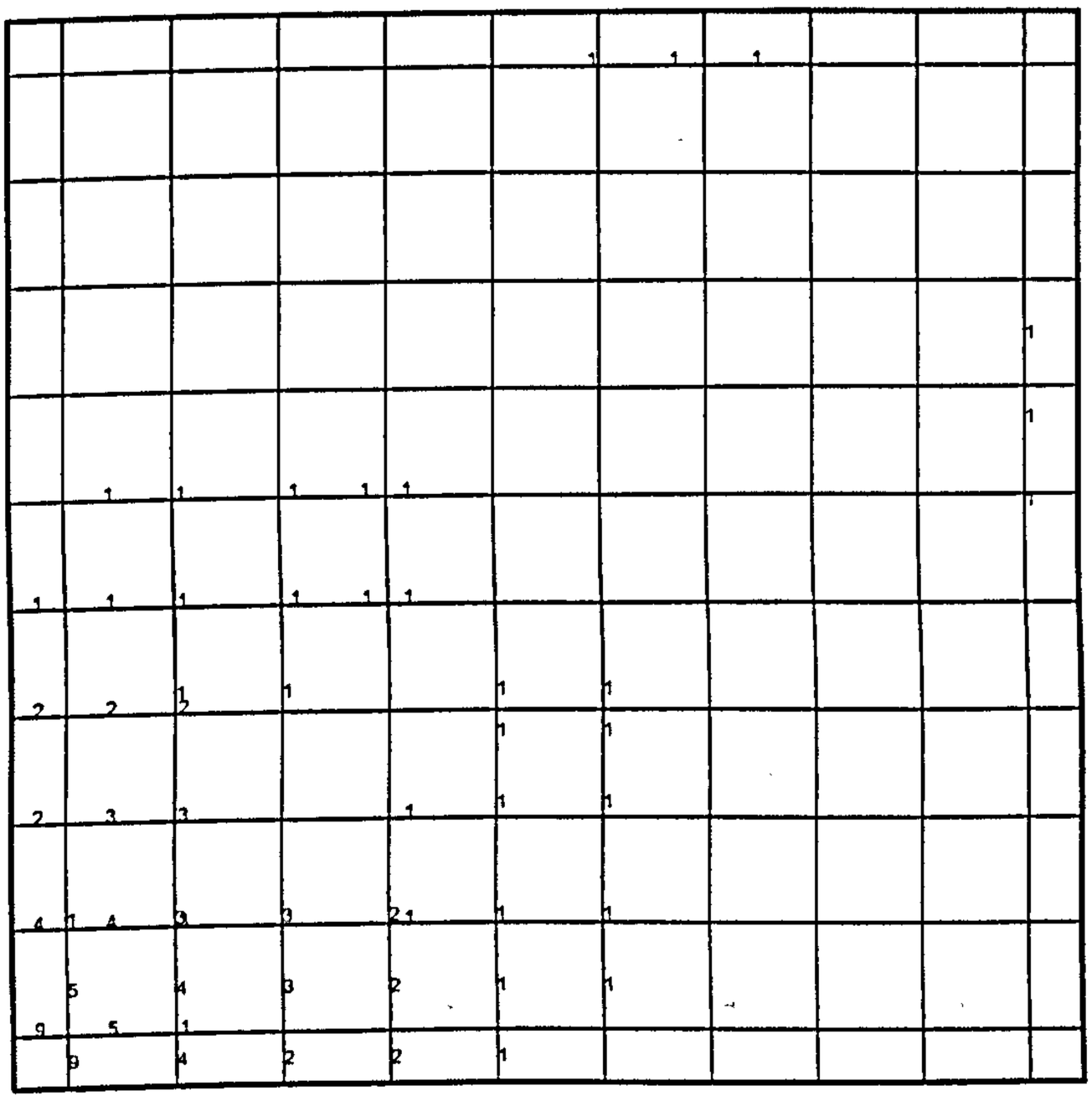

" SC12 "

Predicted crack pattern for slabs SC7-SC12 (Seible et al)

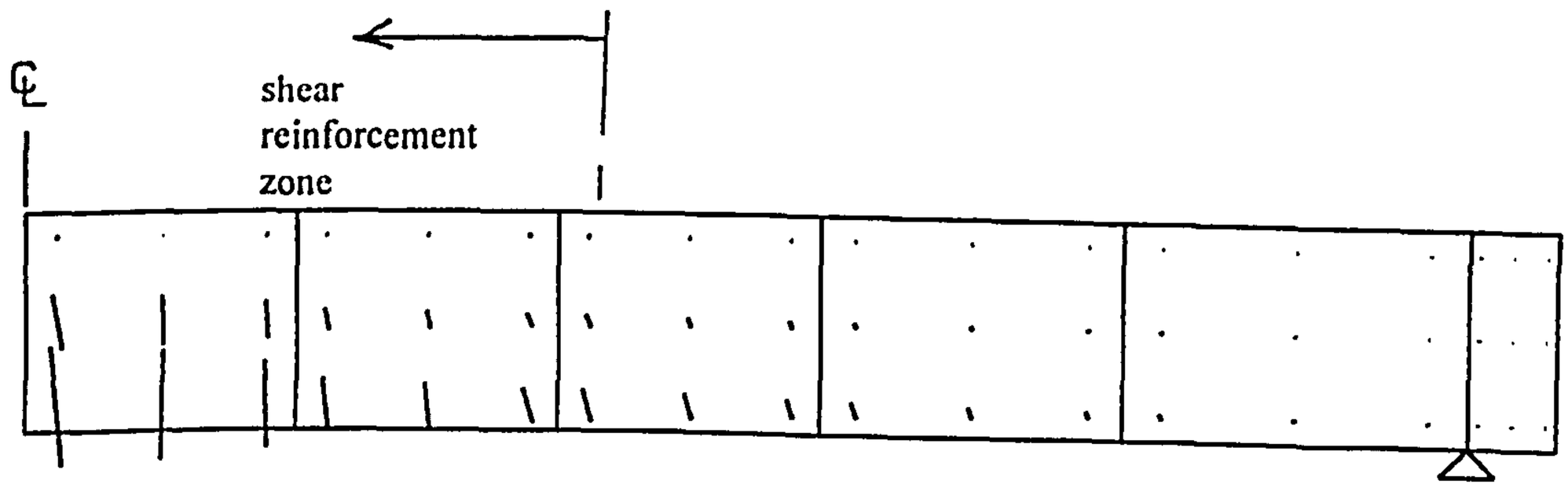

" SC7 "

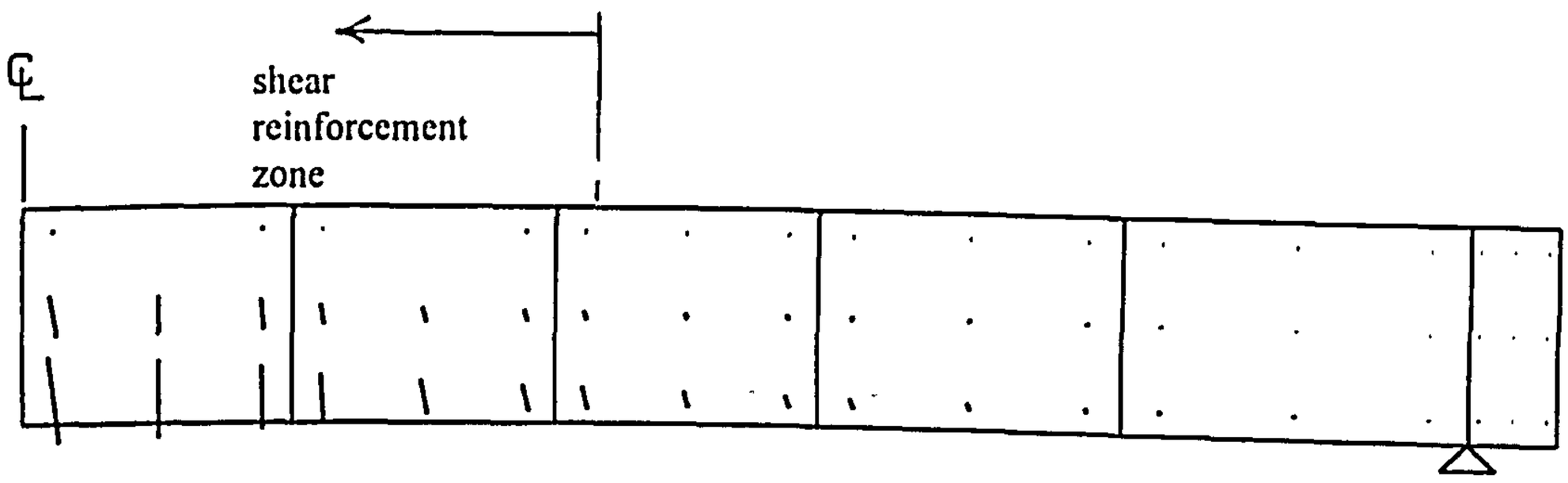

" SC8 "

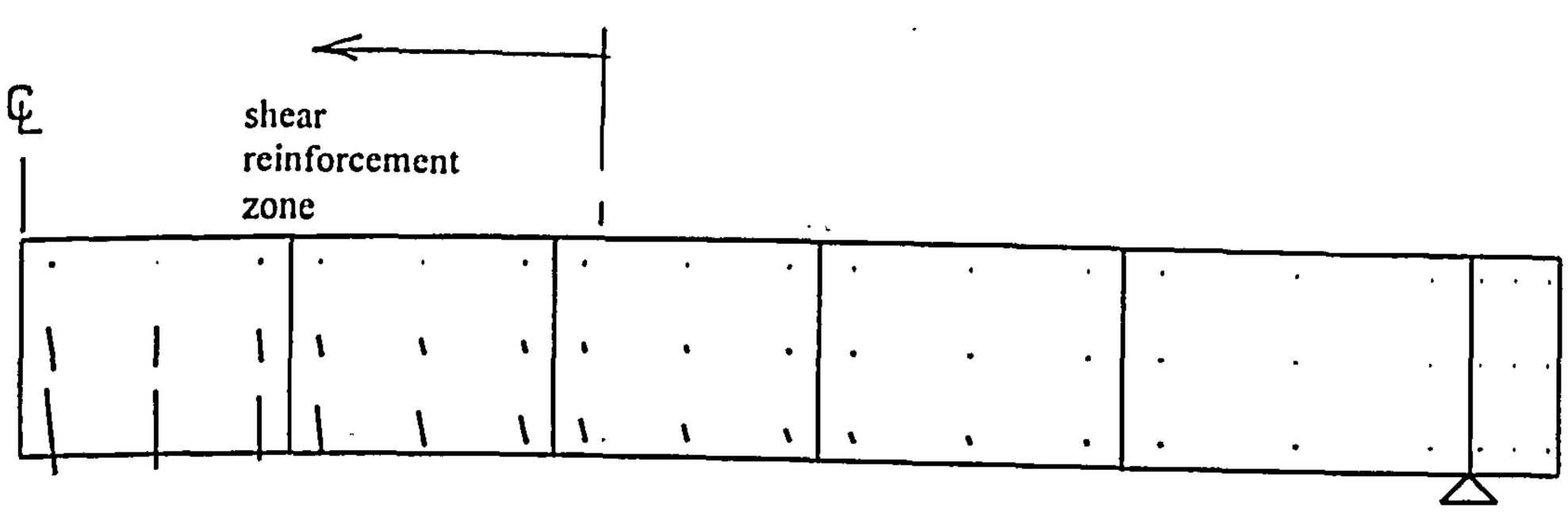

" SC9 "

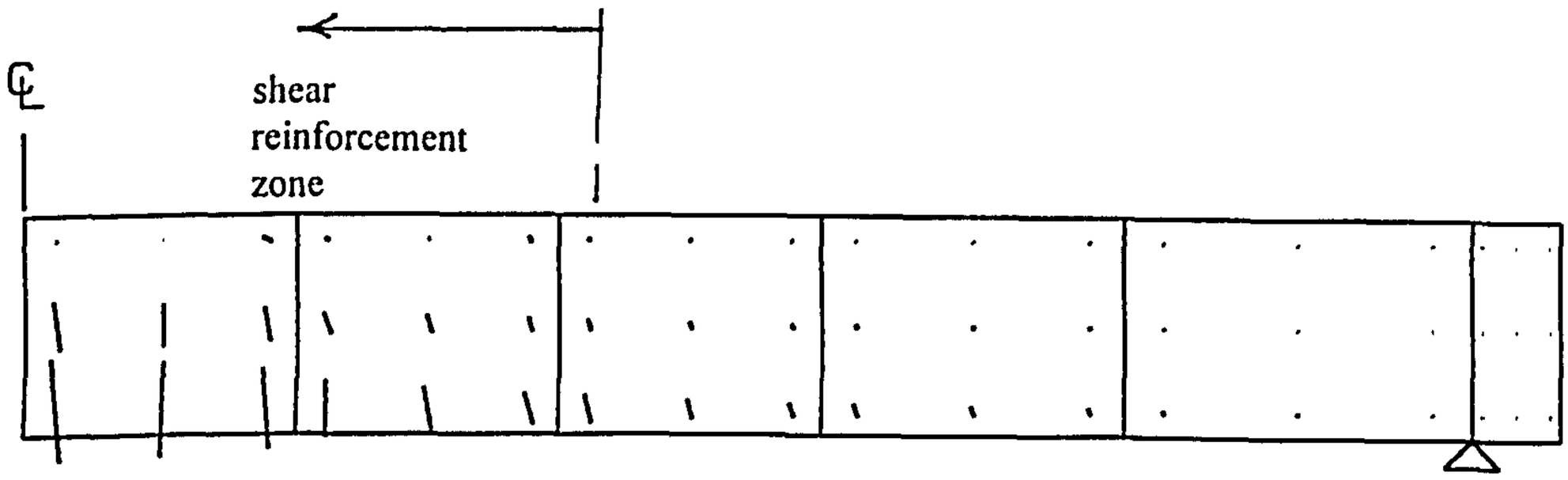

" SC10 "

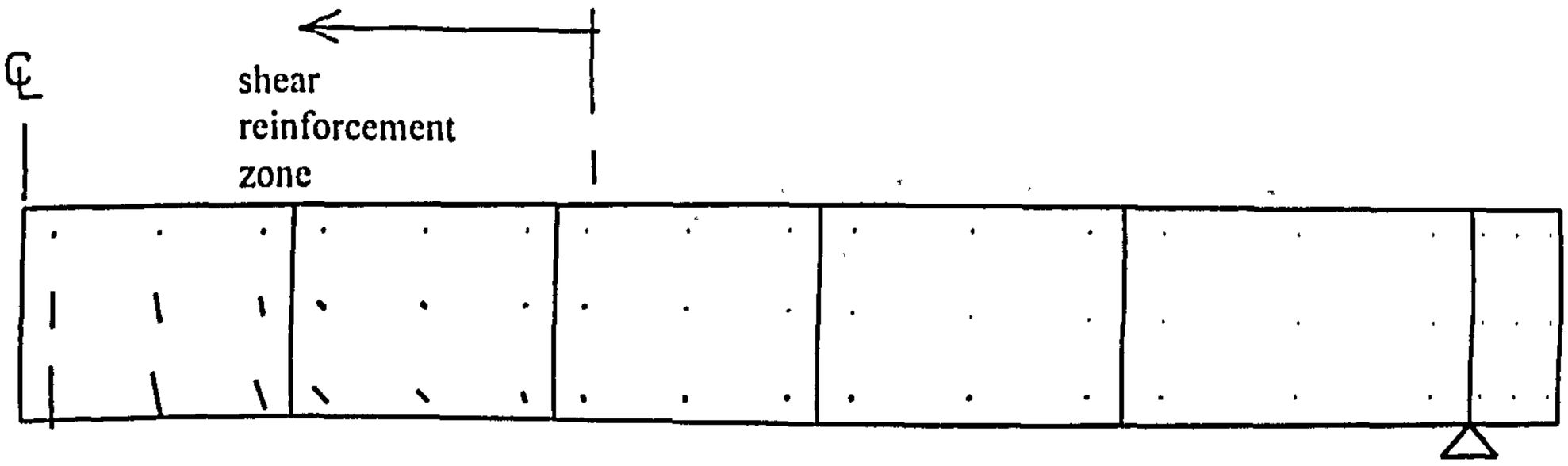

" SC11 "

" SC12 "

SM series (CIRIA 220)

C2 Slab-column connections with shear and moment transfer

C2.1 Interior slab-column connections without shear reinforcement (CIRIA 220)

Slab	Test results		Numerical predictions		P_{num}/P_{test}
	V_{test} (kN)	Failure mode	V_{num} (kN)	Failure mode	
SM1	122.00	s	91.20	s	0.748
SM3	95.00	s	76.80	s	0.808
SM4	101.00	s	72.00	s	0.713
SM5	72.00	s	54.00	s	0.750
SM6	105.00	s	62.40	s	0.594
SM7	105.00	s	72.00	s	0.686
SM8	49.00	s	44.20	s	0.902
SM9	97.00	s	66.00	s	0.680
SM10	88.00	s	57.20	s	0.650
SM11	91.00	s	69.00	s	0.758
SM12	88.00	s	61.60	s	0.700
				Average	0.726
				STDEV	0.082

For yielding of flexural reinforcement,

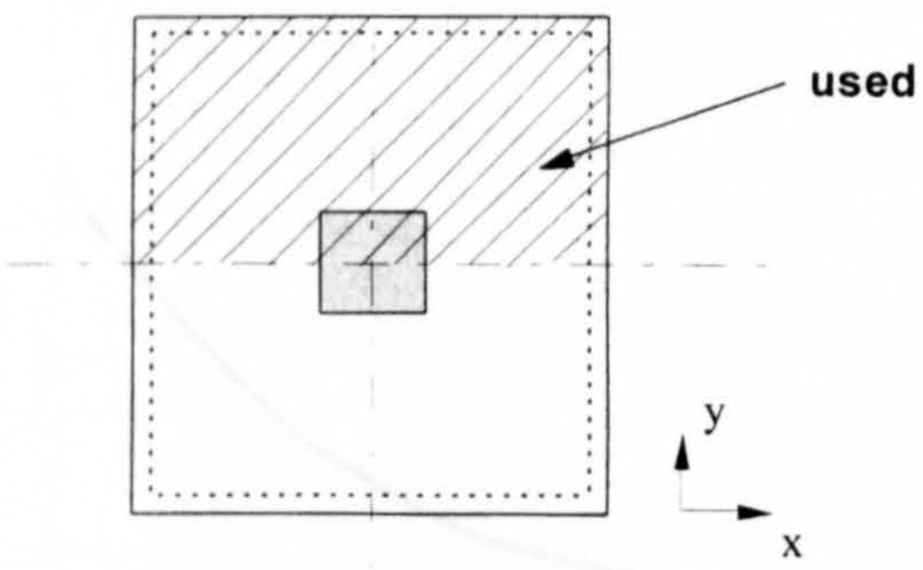

For crack pattern,

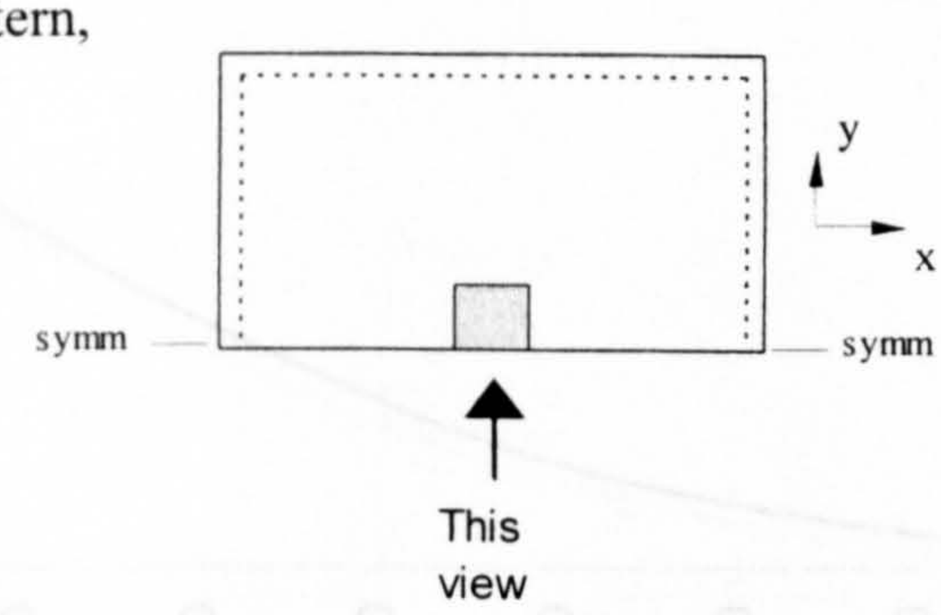

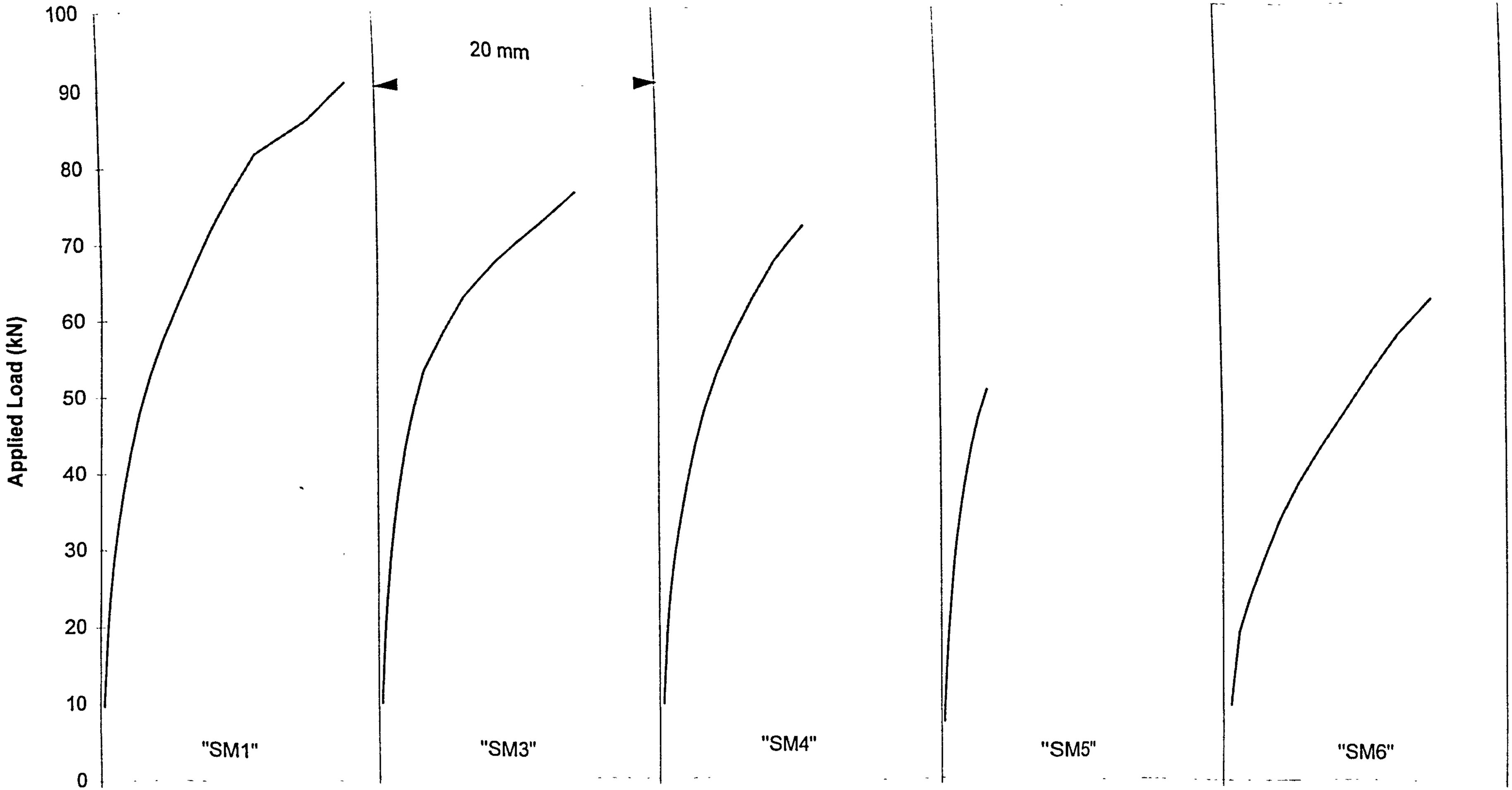

Predicted load-deflection response for slabs SM1-SM6

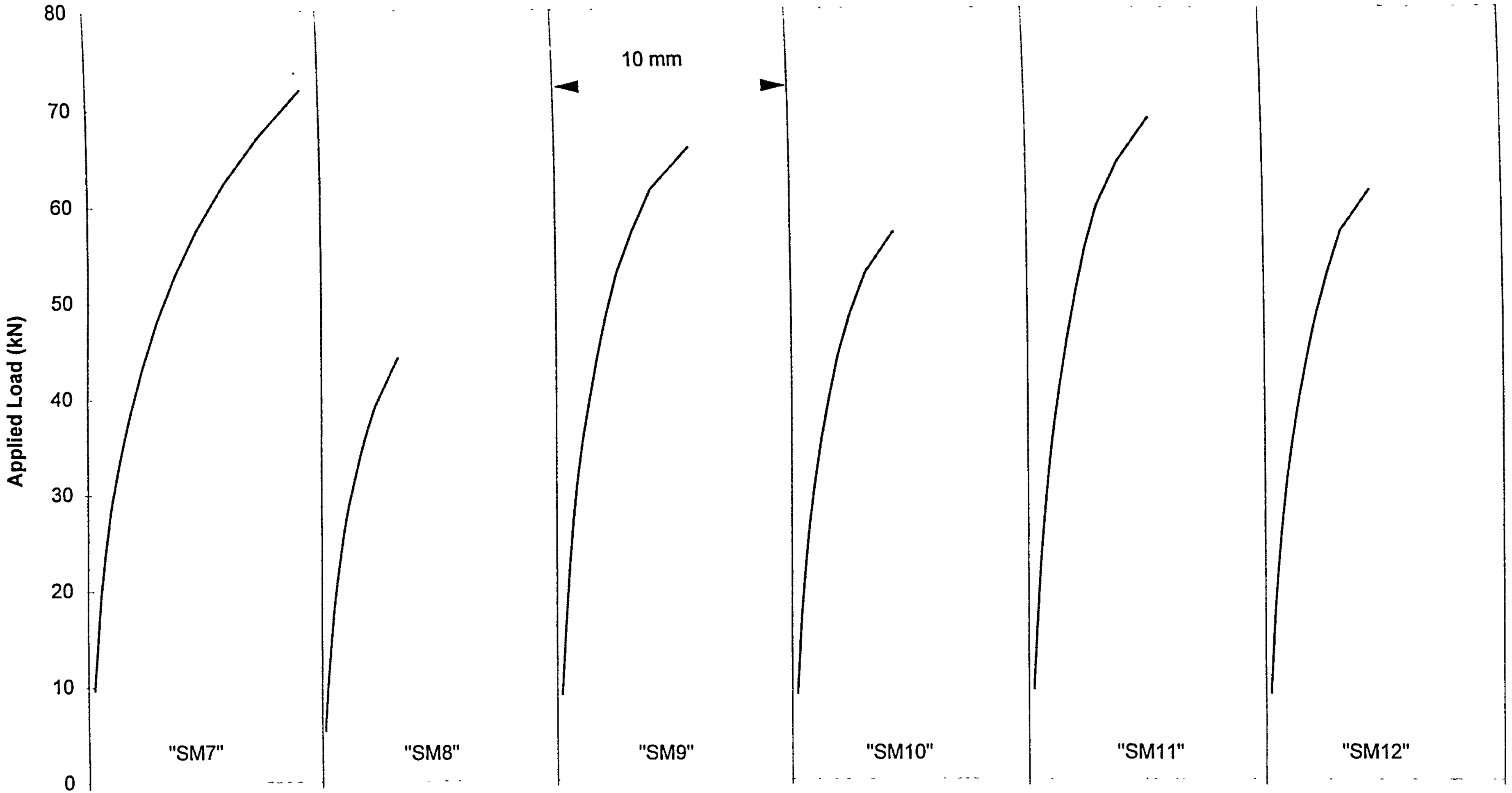

Predicted load-deflection response for slabs SM7-SM12

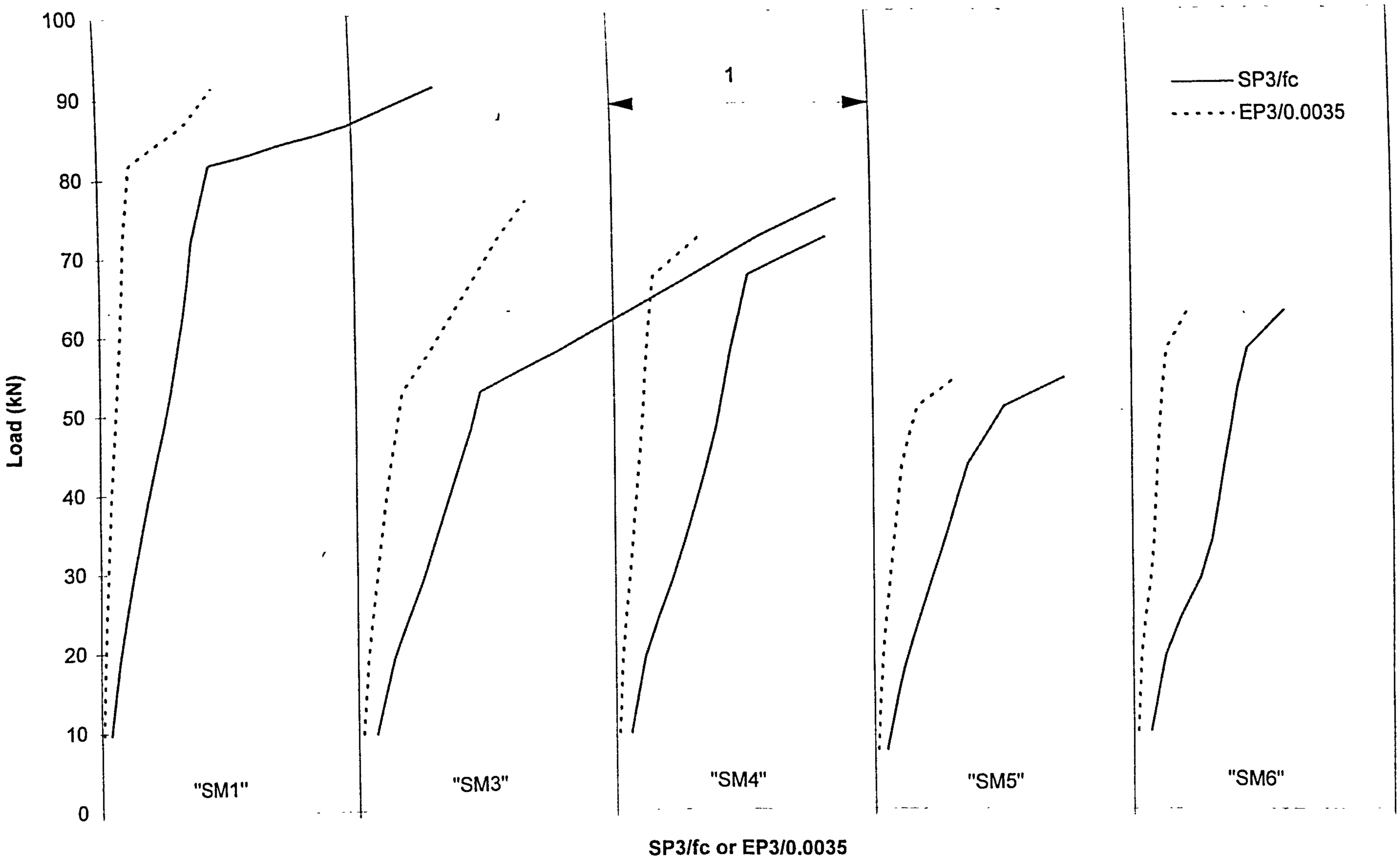

Predicted principal compressive stress and strain in concrete (slabs "SM1" - "SM6")

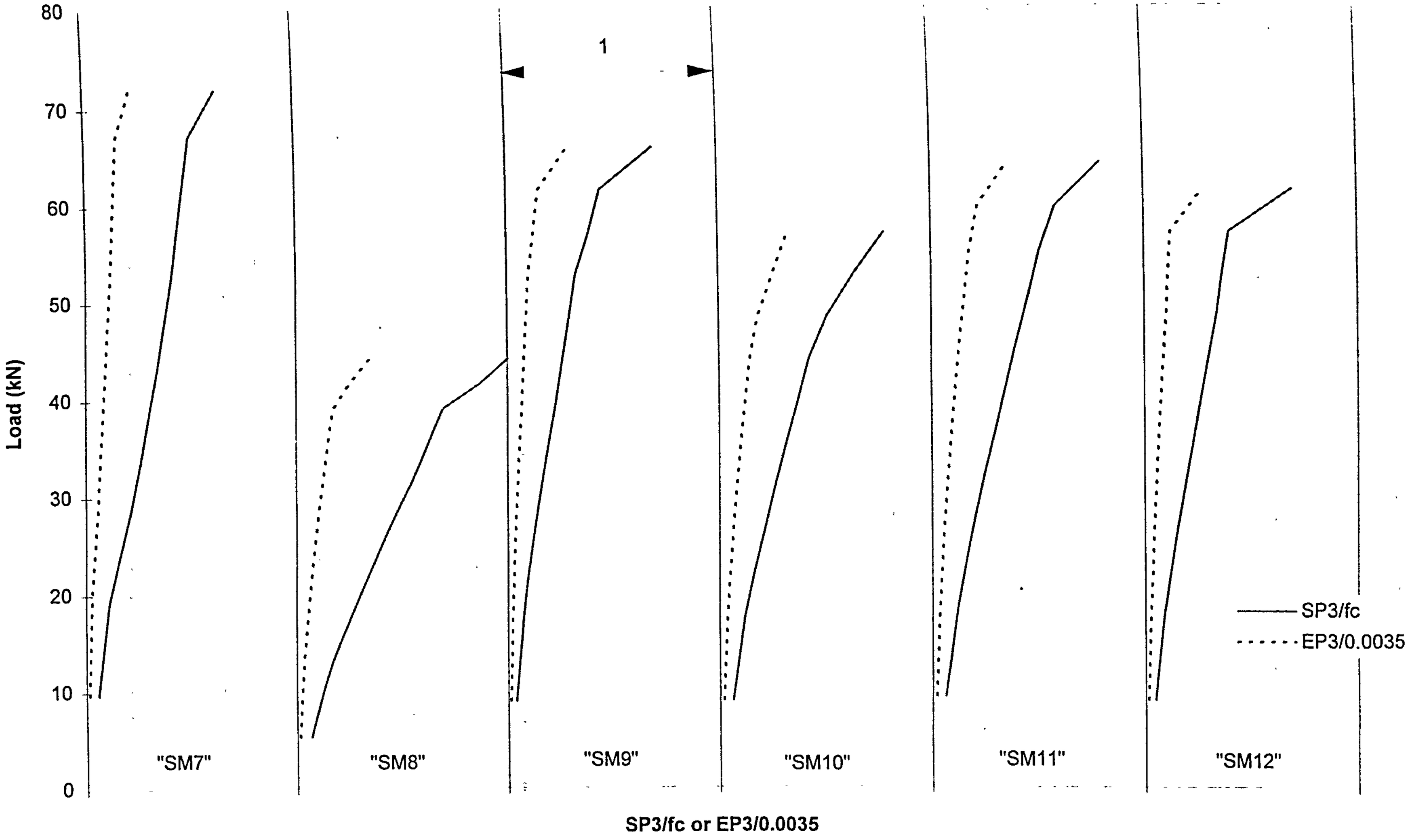

Predicted principal compressive stress and strain in concrete (slabs "SM7" - "SM12")

Yielding of tension steel, SM series (CIRIA 220)

NB. : The numbers on the drawing indicate strain in steel at collapse expressed as a ratio of yield strain

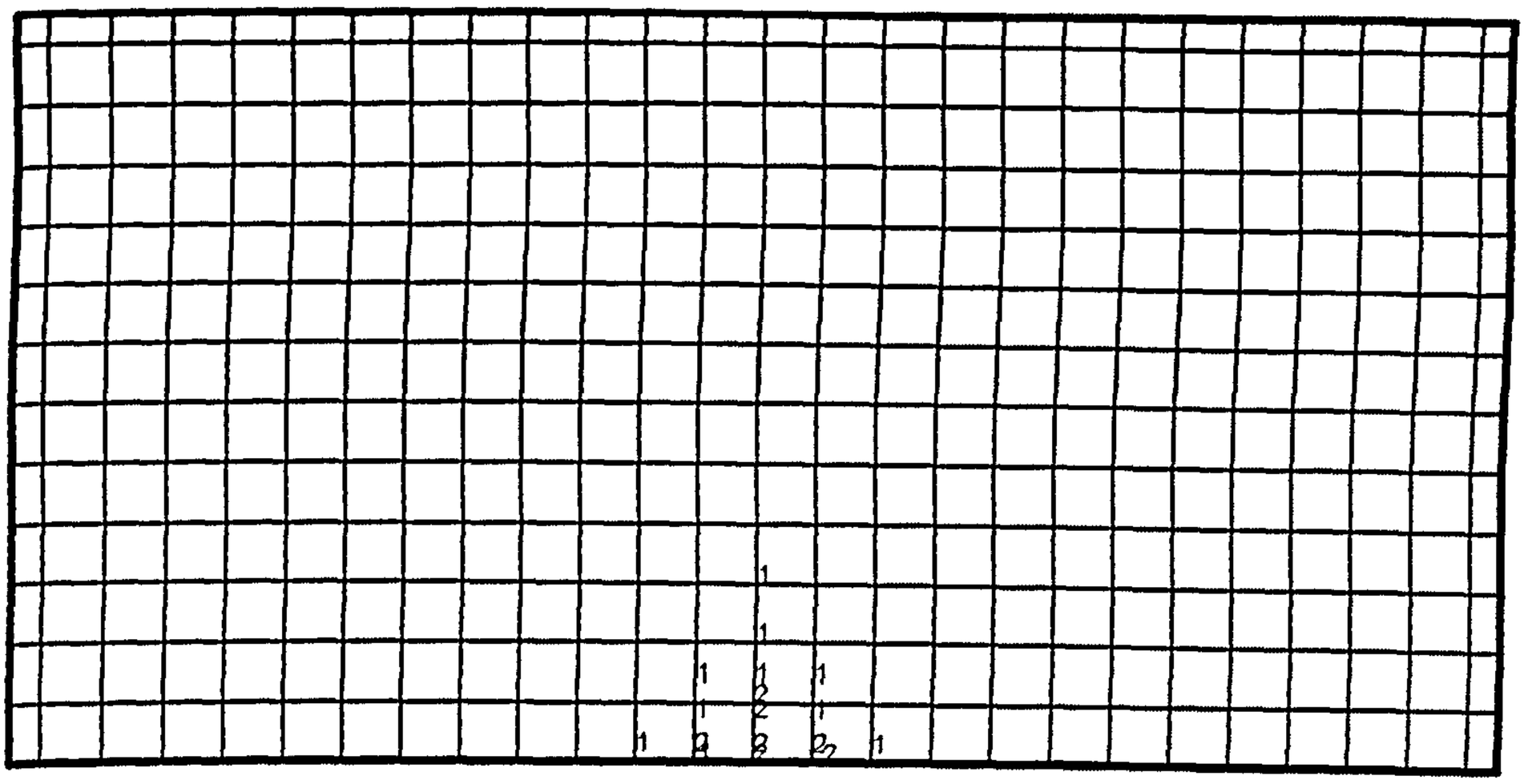

Slab SM1

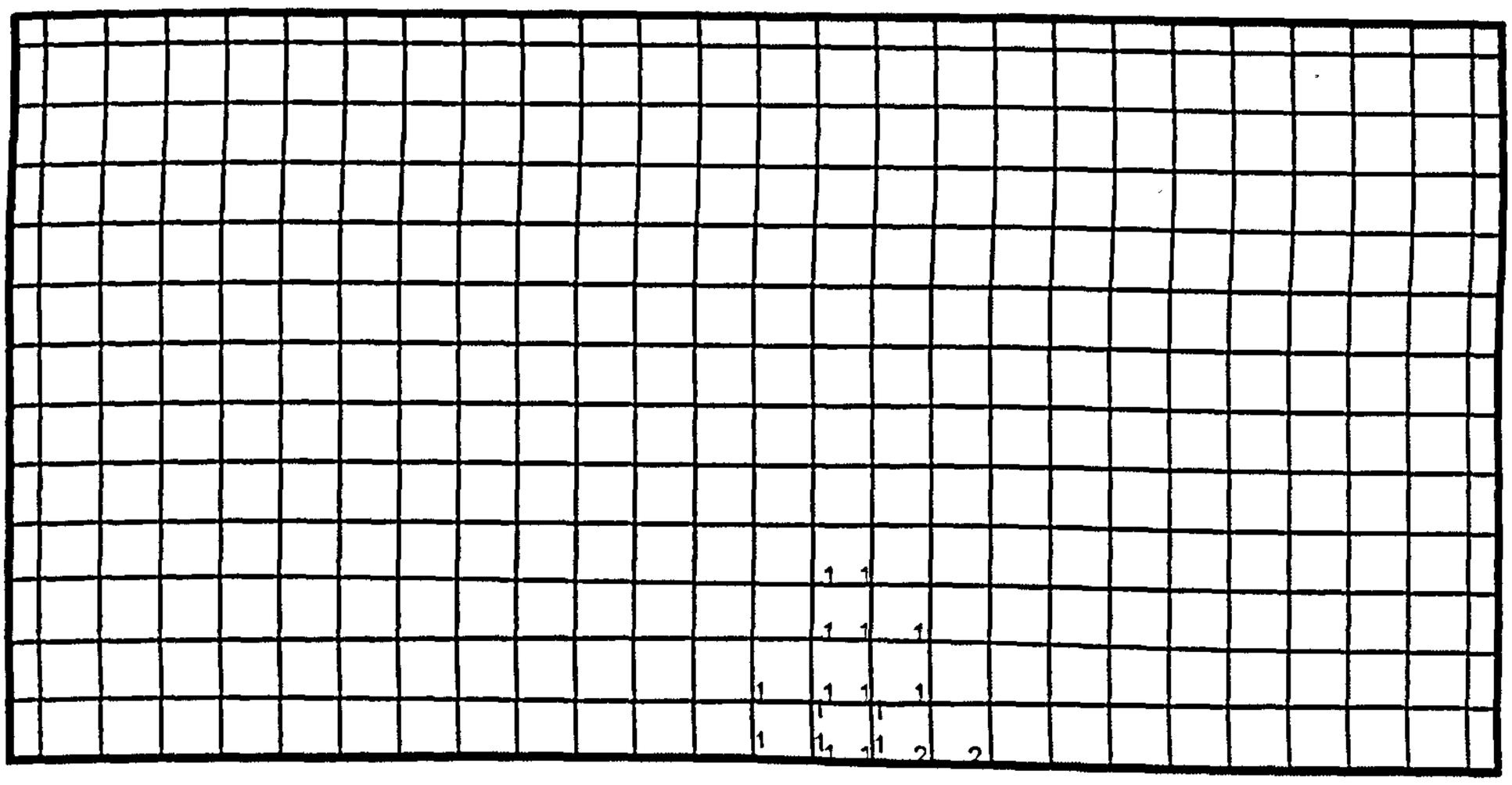

Slab SM3

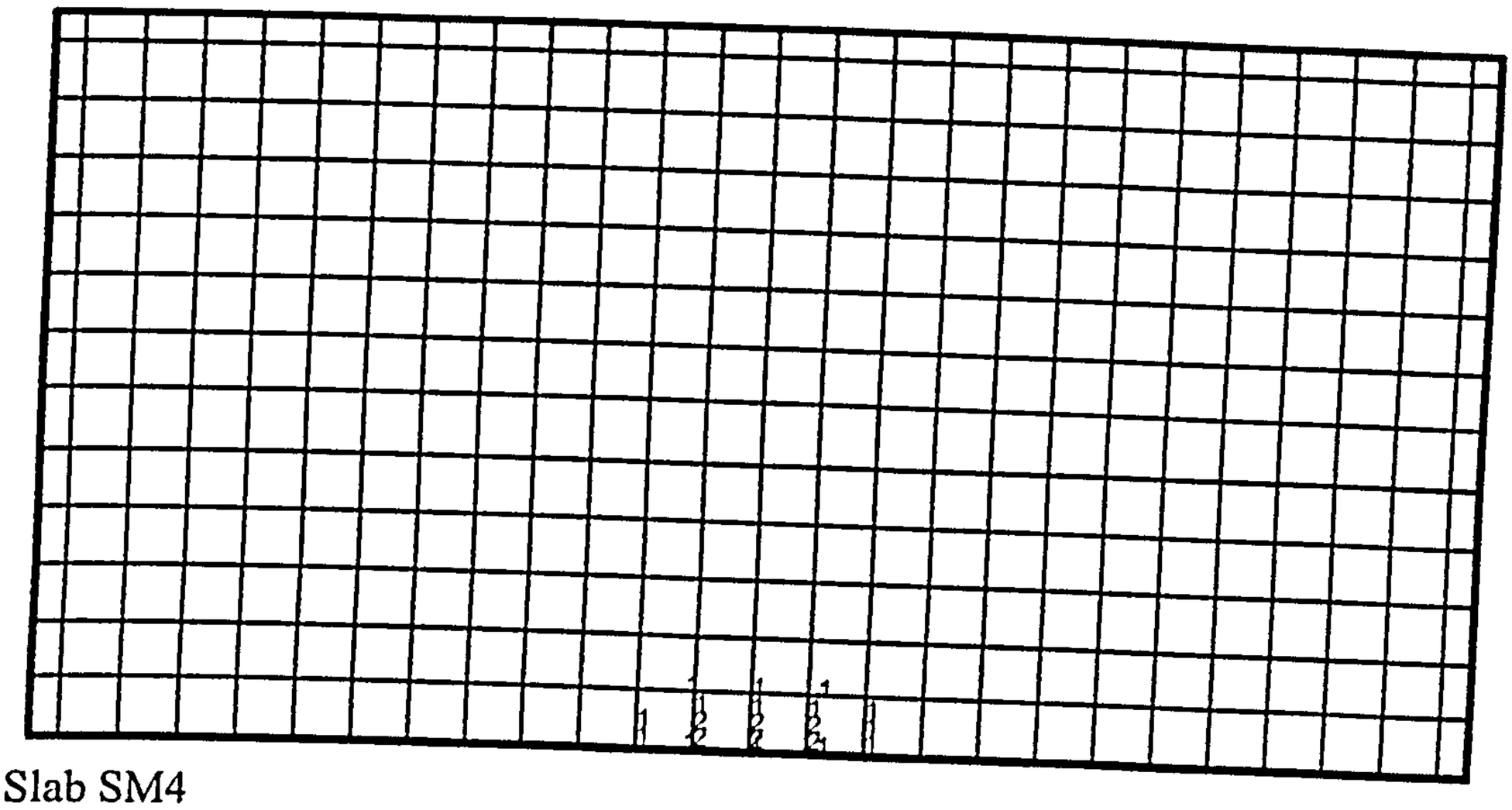

Slab SM4

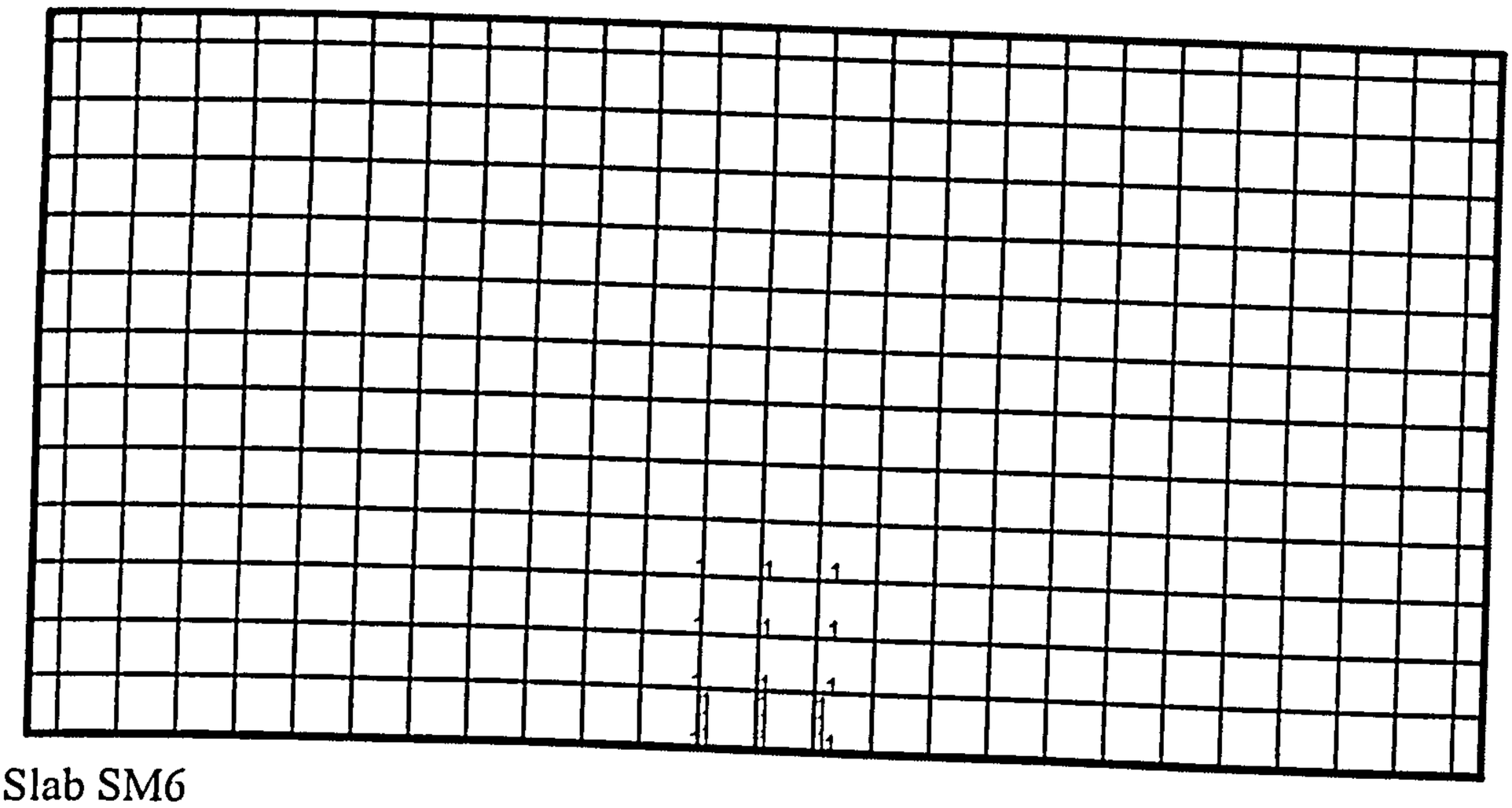

Slab SM6

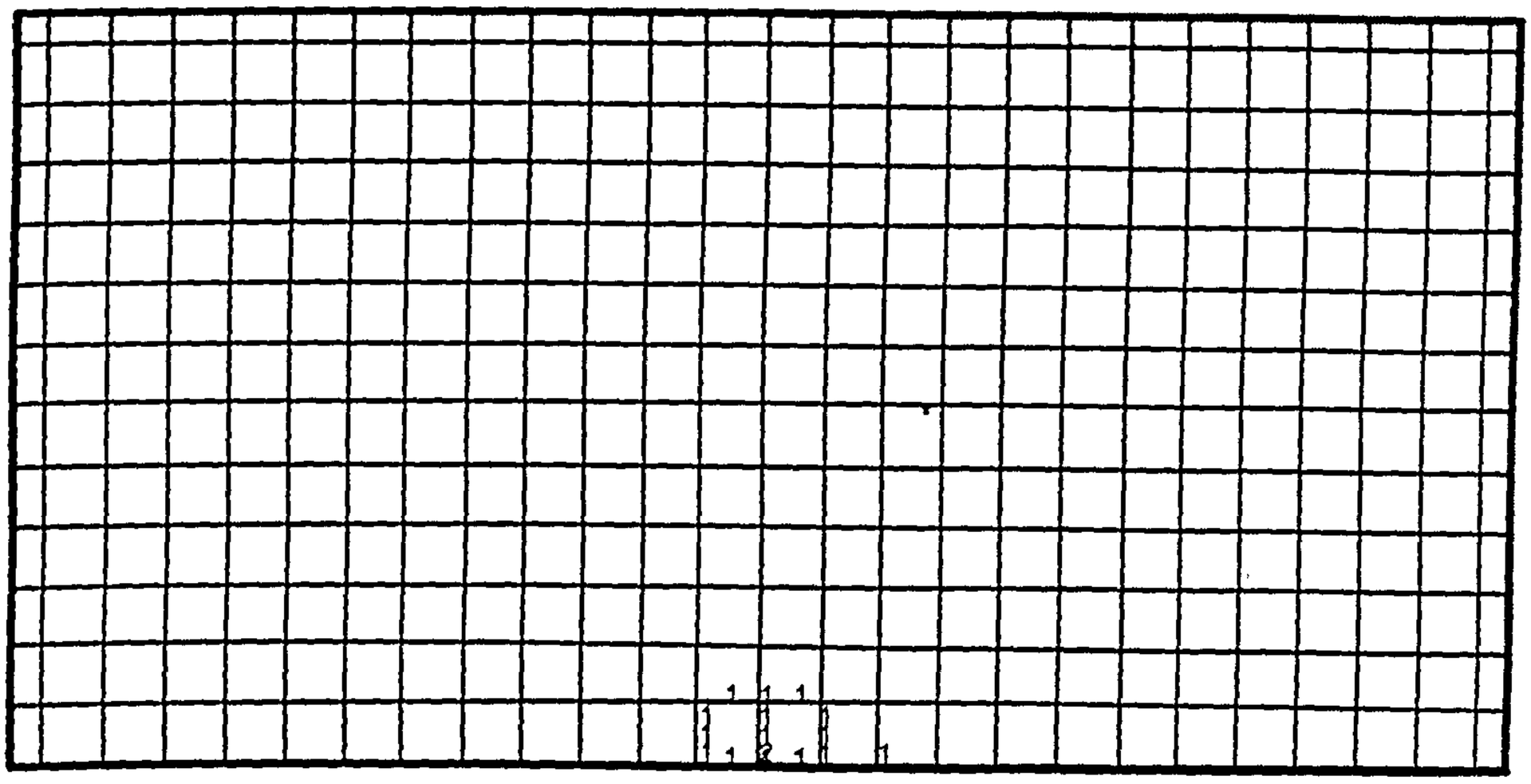

Slab SM7, LF=0.69

Note

Flexural steel in slabs **SM5, SM8, SM9, SM10, SM11** and **SM12** did not yield.

Predicted crack pattern for SM series (CIRIA 220)

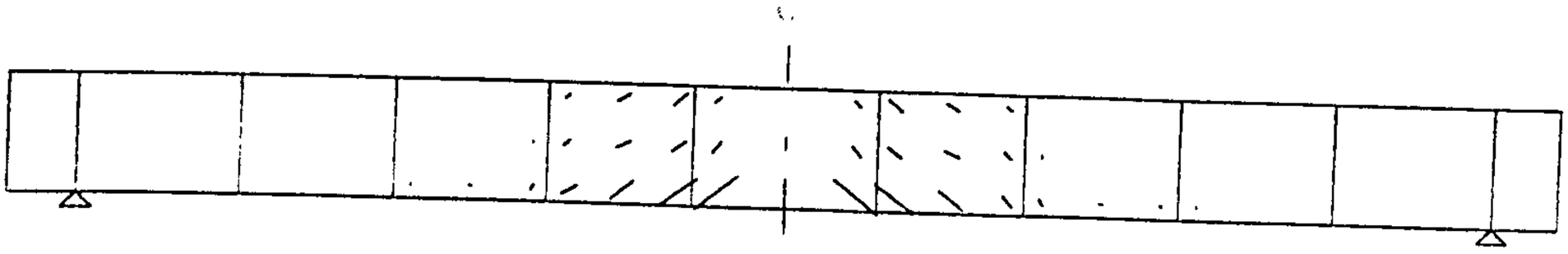

SM1

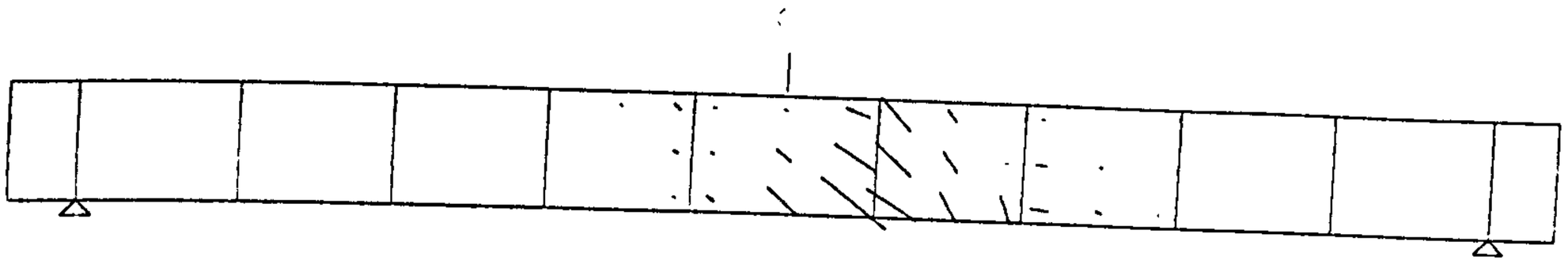

SM3

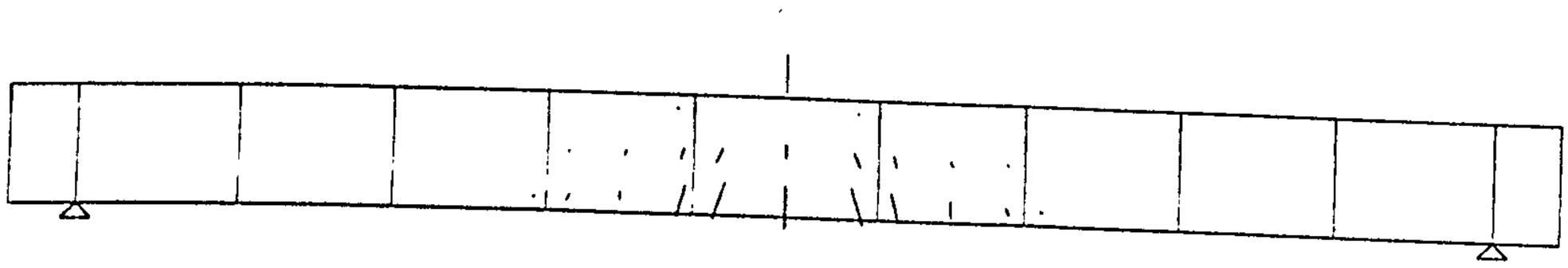

SM4

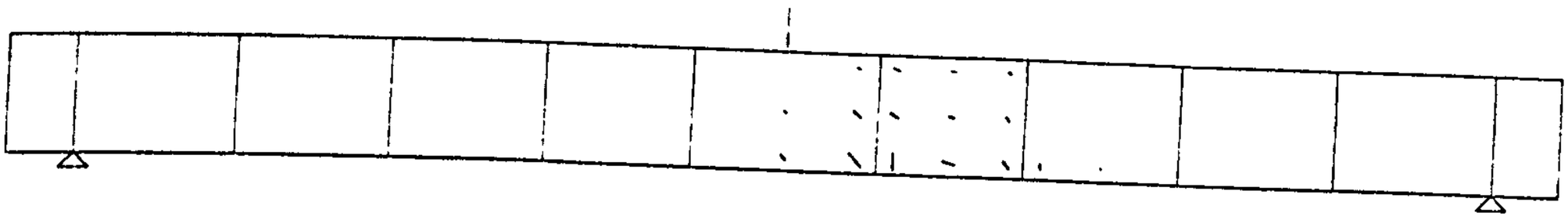

SM5

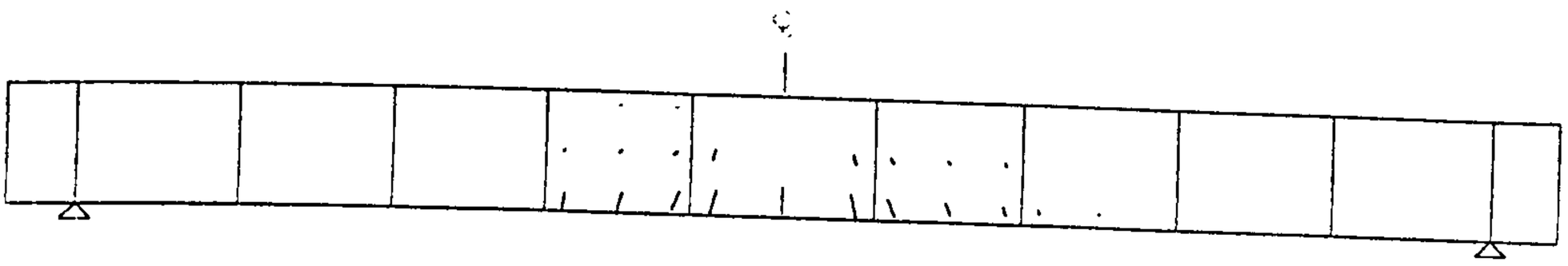

SM6

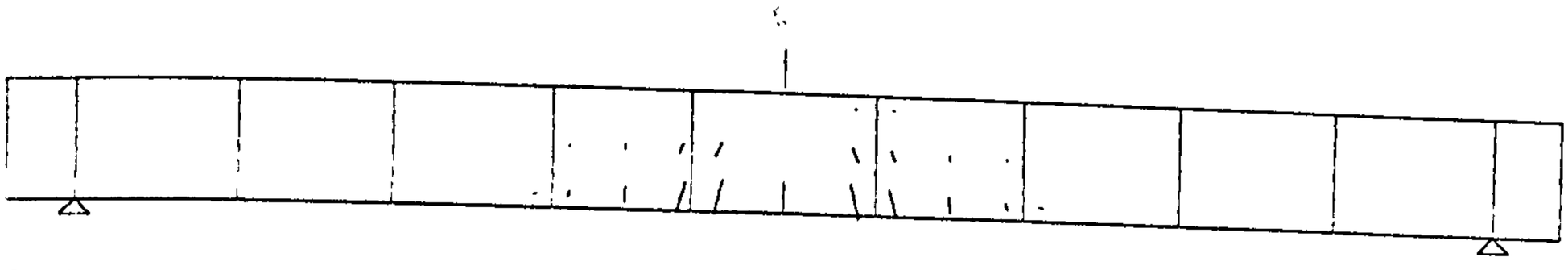

SM7

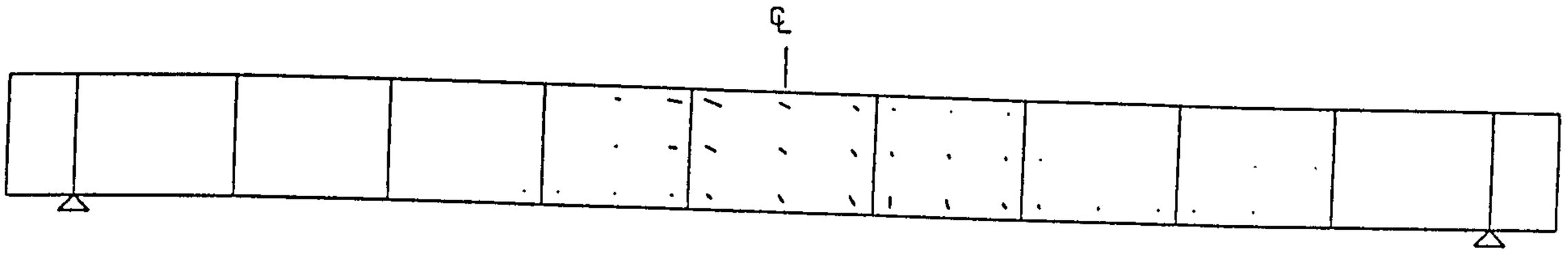

SM8

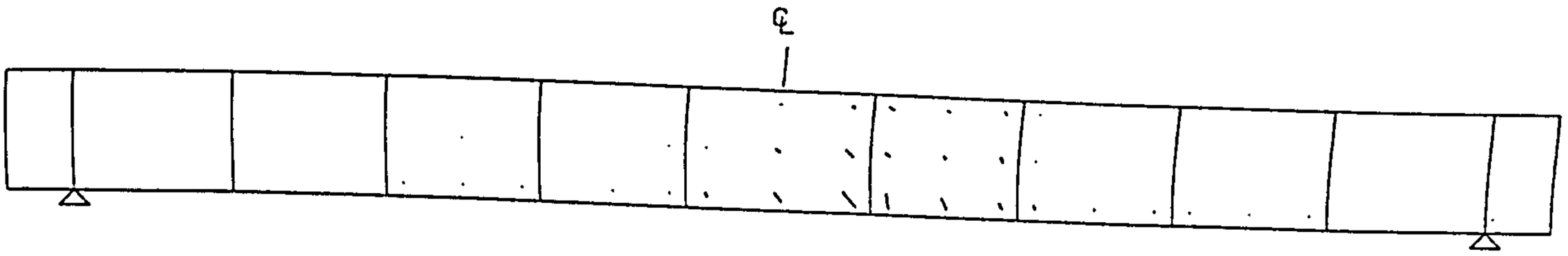

SM9

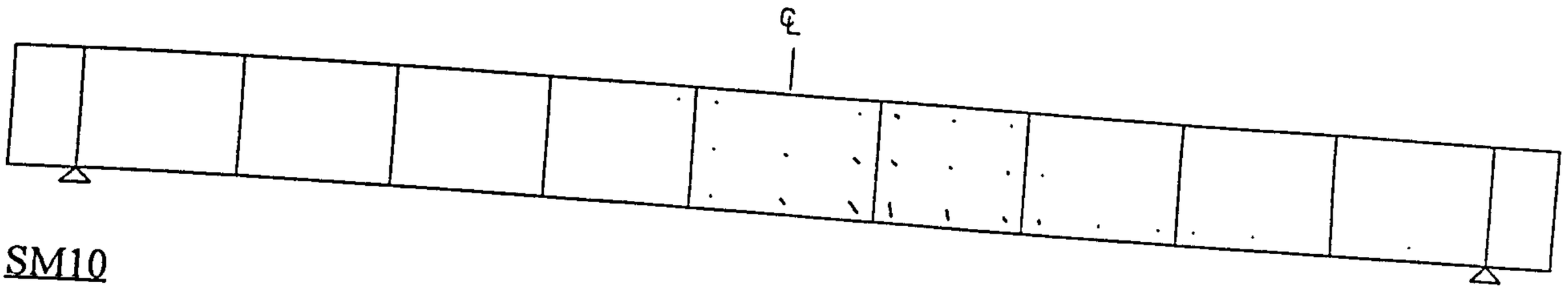

SM10

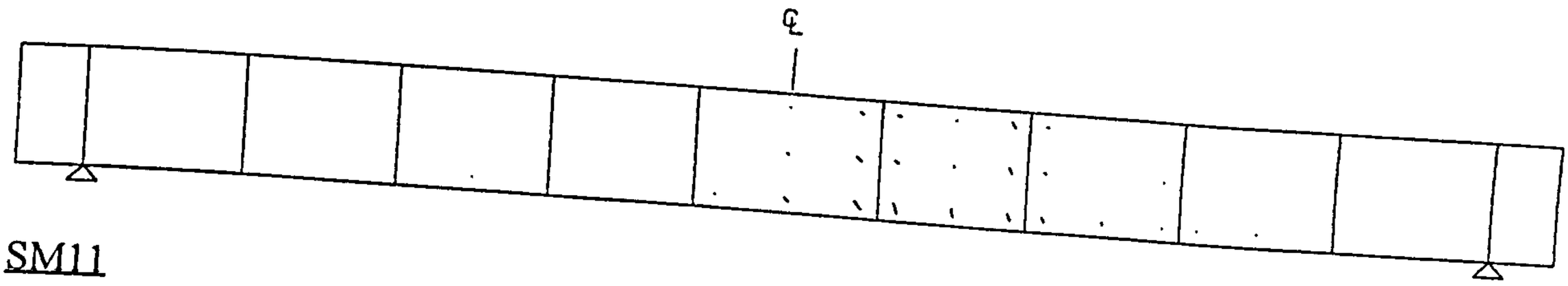

SM11

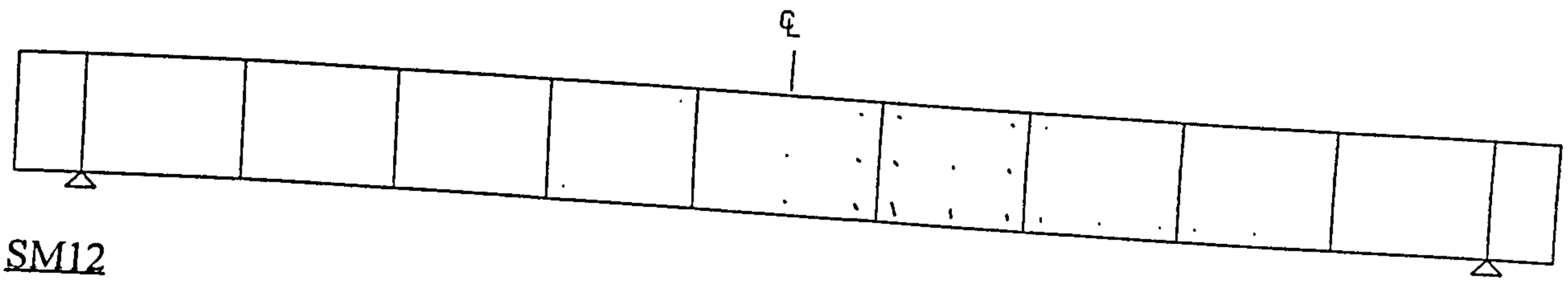

SM12

AM series (Elgabry and Ghali)

C2.2 Interior slab-column connections with shear reinforcement (Elgabry and Ghali)

	Test results					Numerical results	
Specimen	f_c' N/mm^2	*ρ (%)	V_{test} (kN)	M_{test} (kNm)	failure mode	Num/Exp ratio**	failure mode
AM1	35.00	1.10%	150	130	s	0.95	s
AM2	33.70	1.10%	150	162	s	1.10	s
AM3	39.00	1.23%	300	142	fp	1.15	fp
AM4	40.80	1.39%	300	150	fp	1.15	fp
AM5	55.60	1.39%	450	105	fp	1.05	fp
					Average	1.05	
					STDEV	0.084	

For yielding of flexural reinforcement,

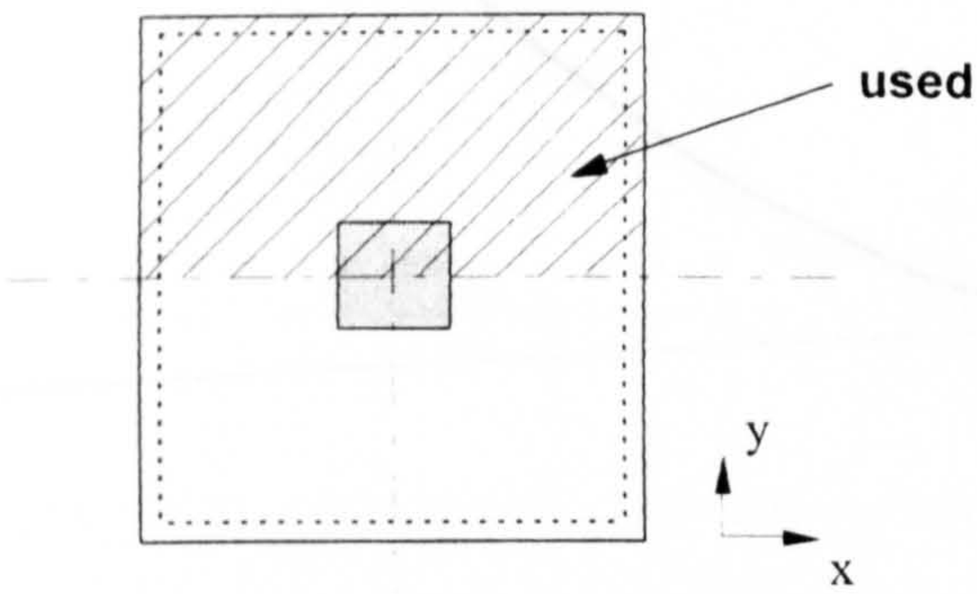

For crack pattern,

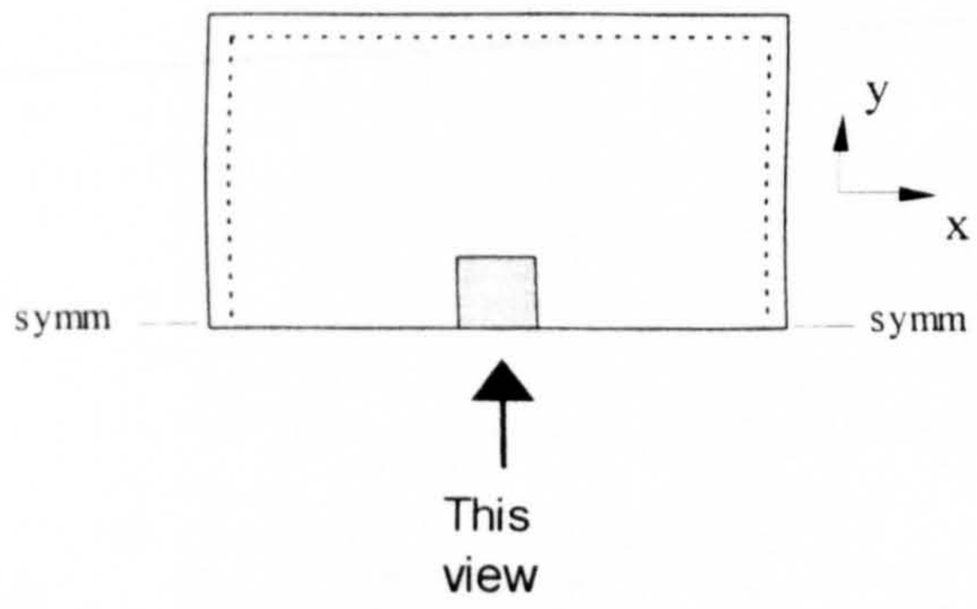

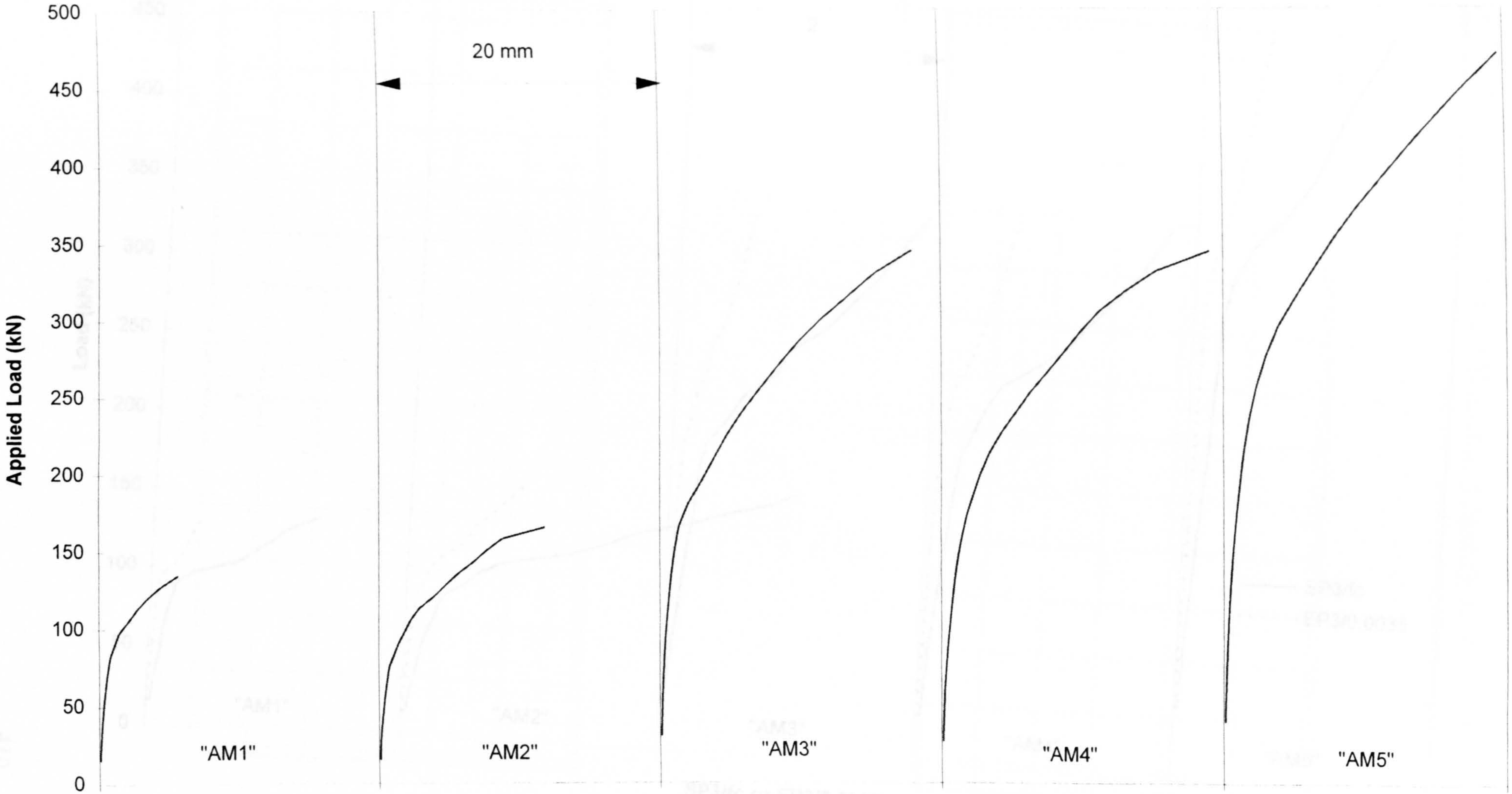

Predicted load-deflection response for slabs AM1-AM5

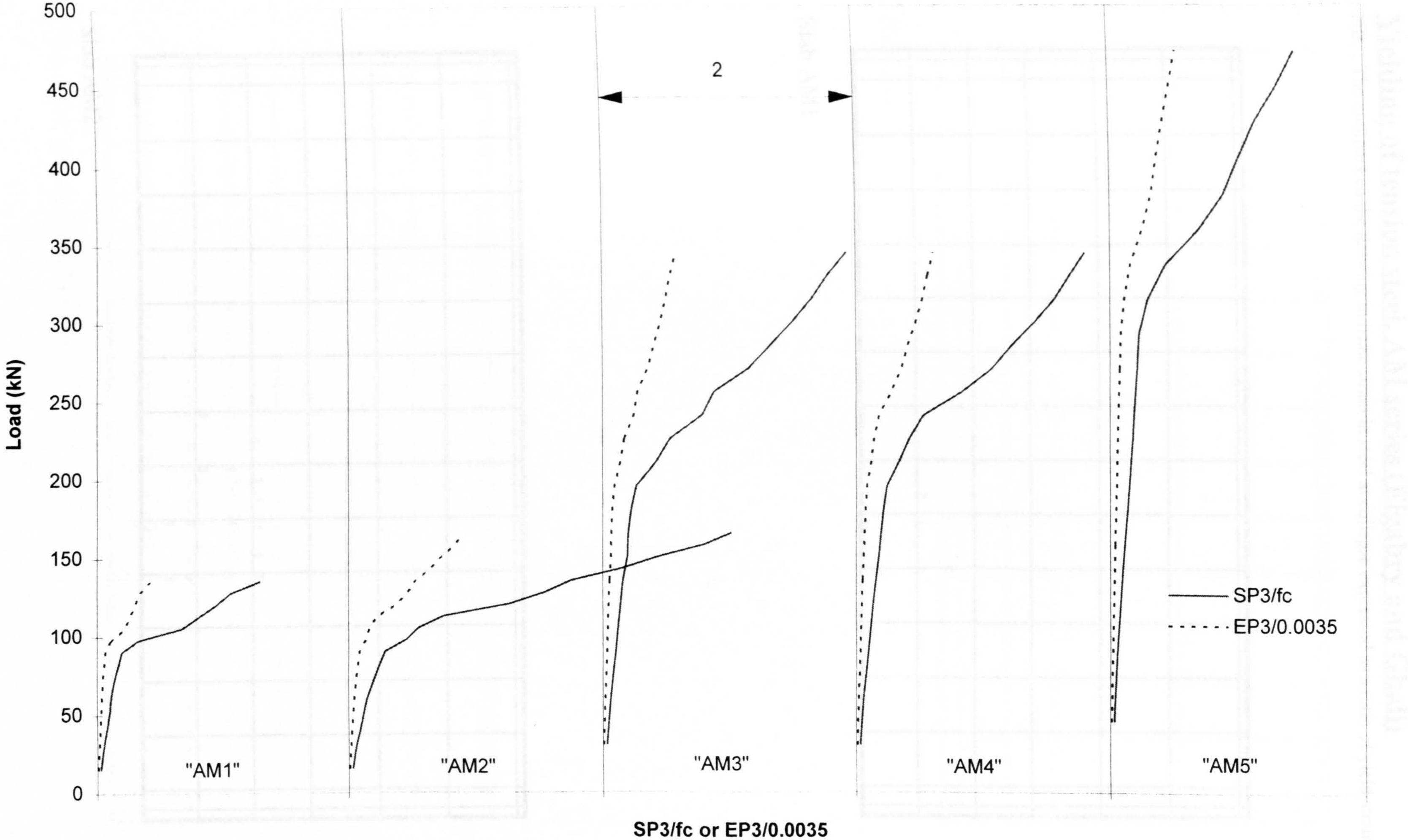

Predicted principal compressive stress and strain in concrete (slabs "AM1" - "AM5")

Yielding of tension steel, AM series (Elgabry and Ghali)

NB. : The numbers on the drawing indicate strain in steel at collapse expressed as a ratio of yield strain

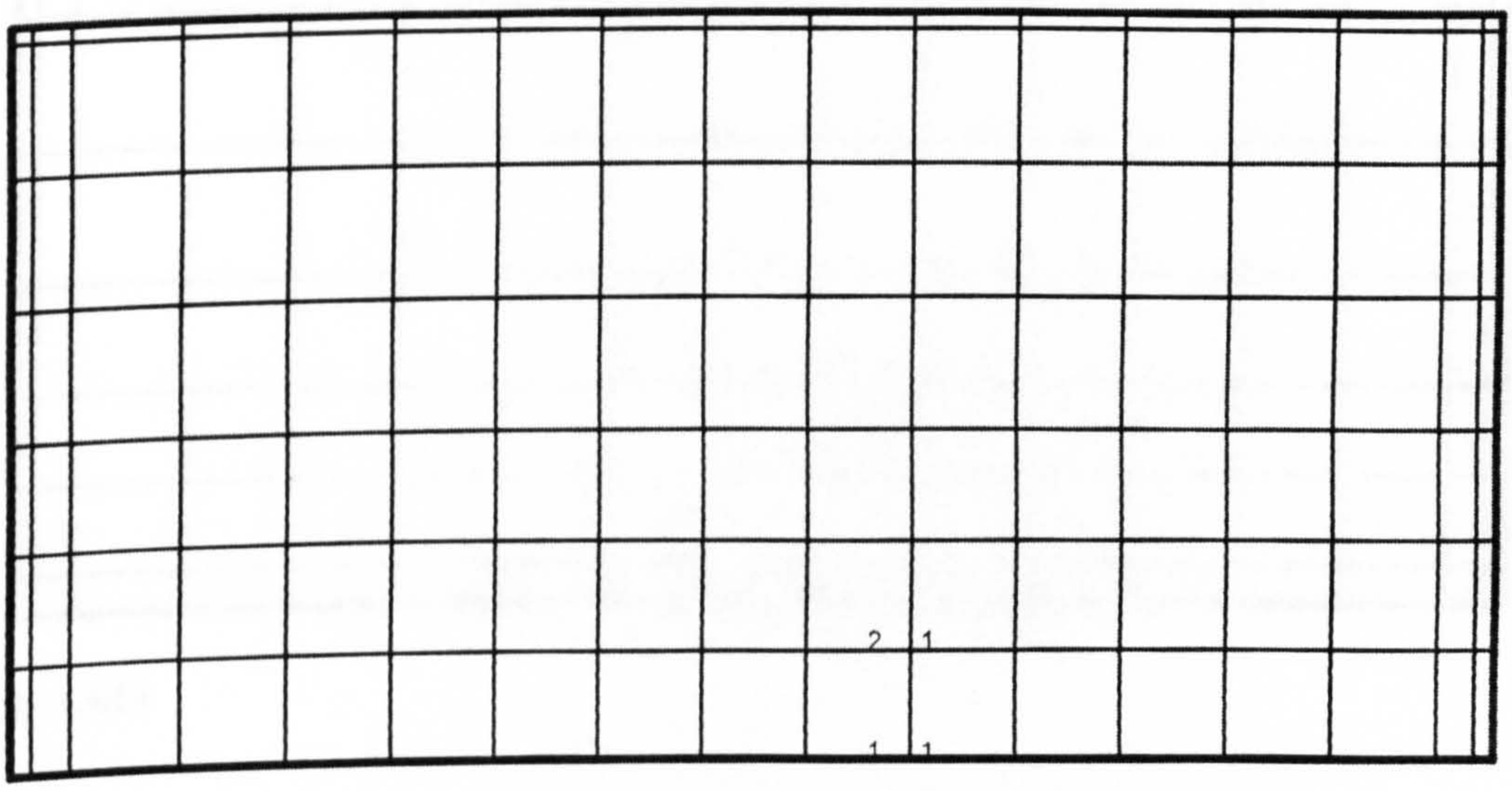

Slab AM1

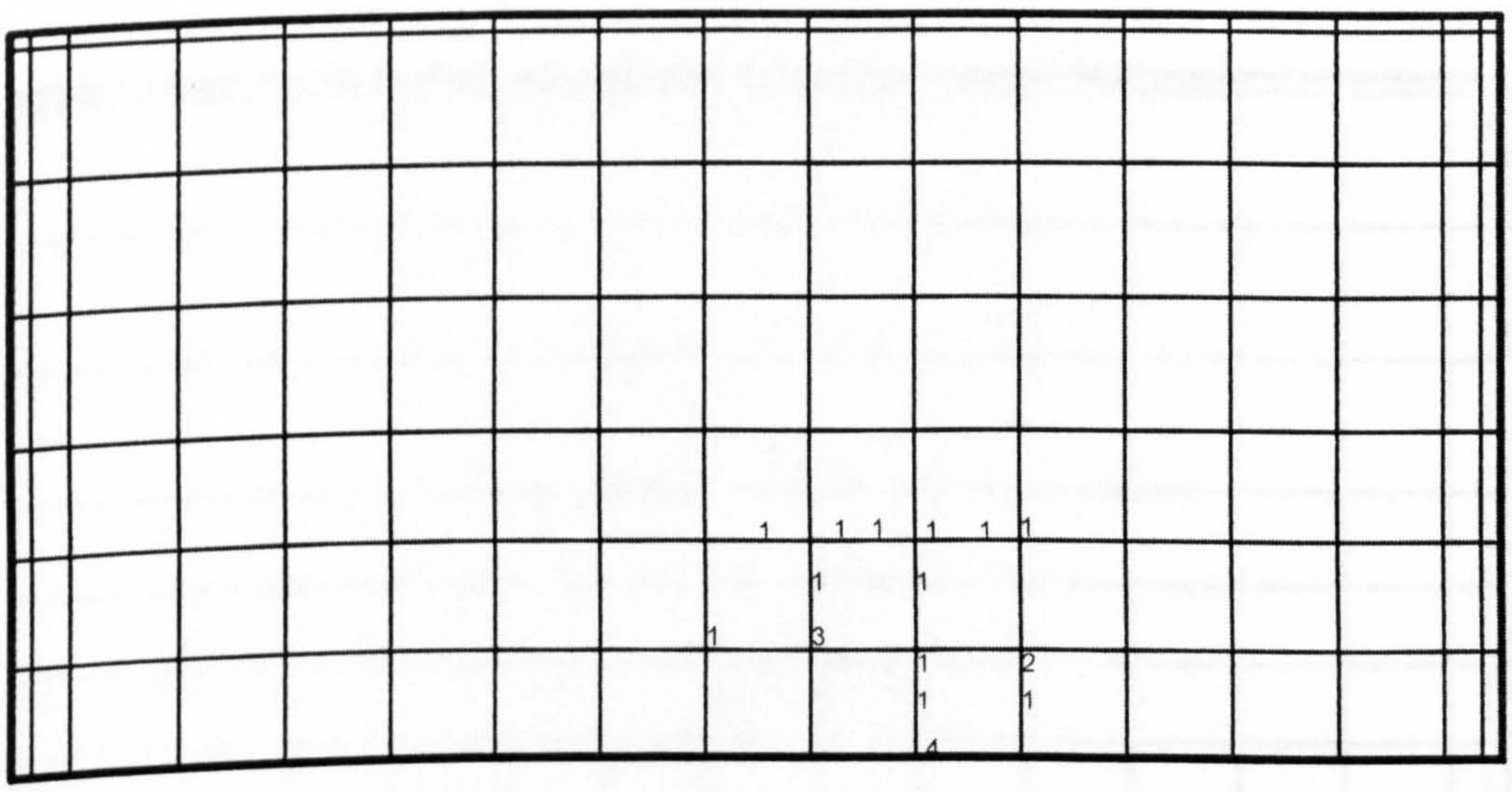

Slab AM2

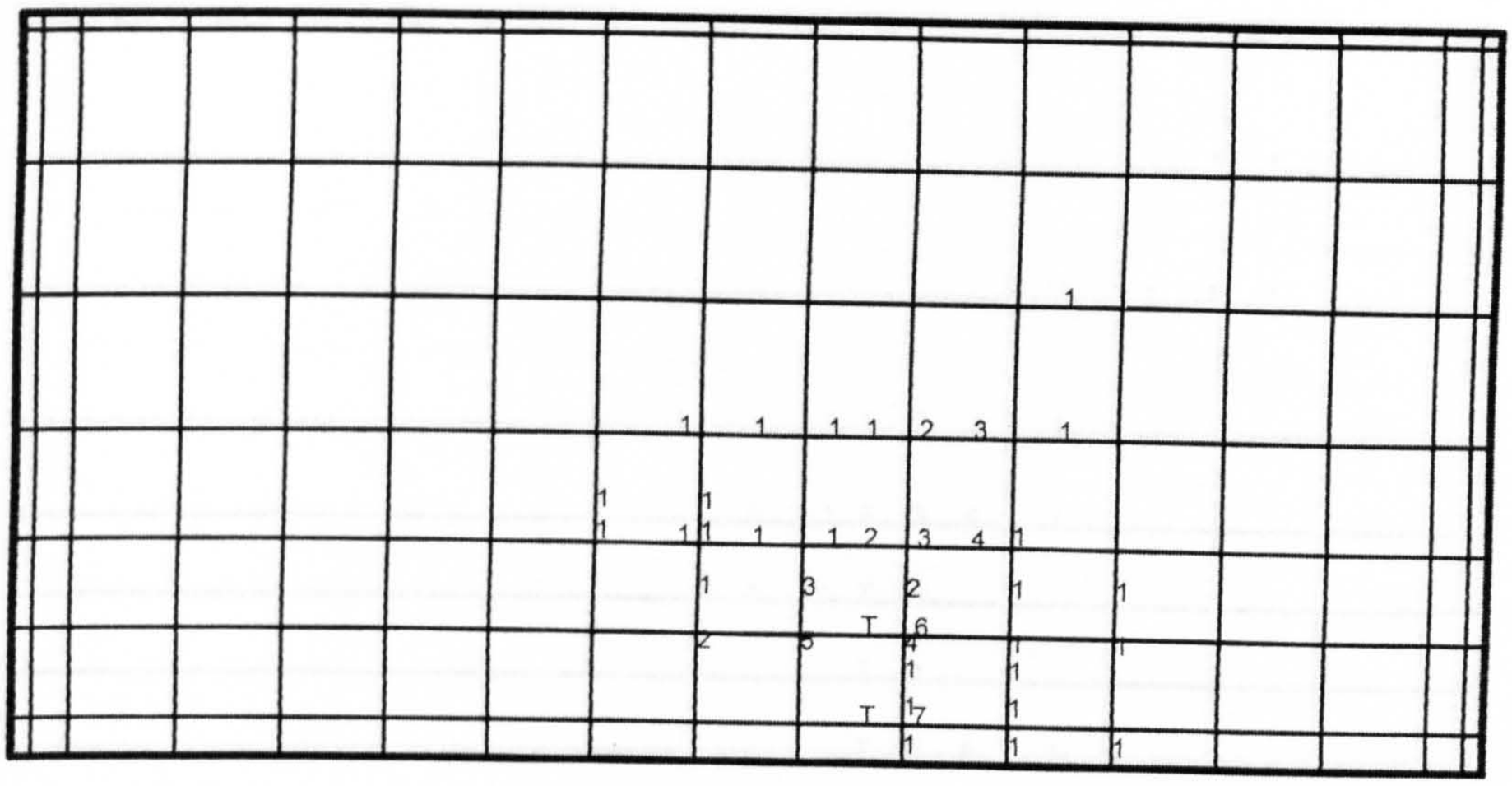

Slab AM3

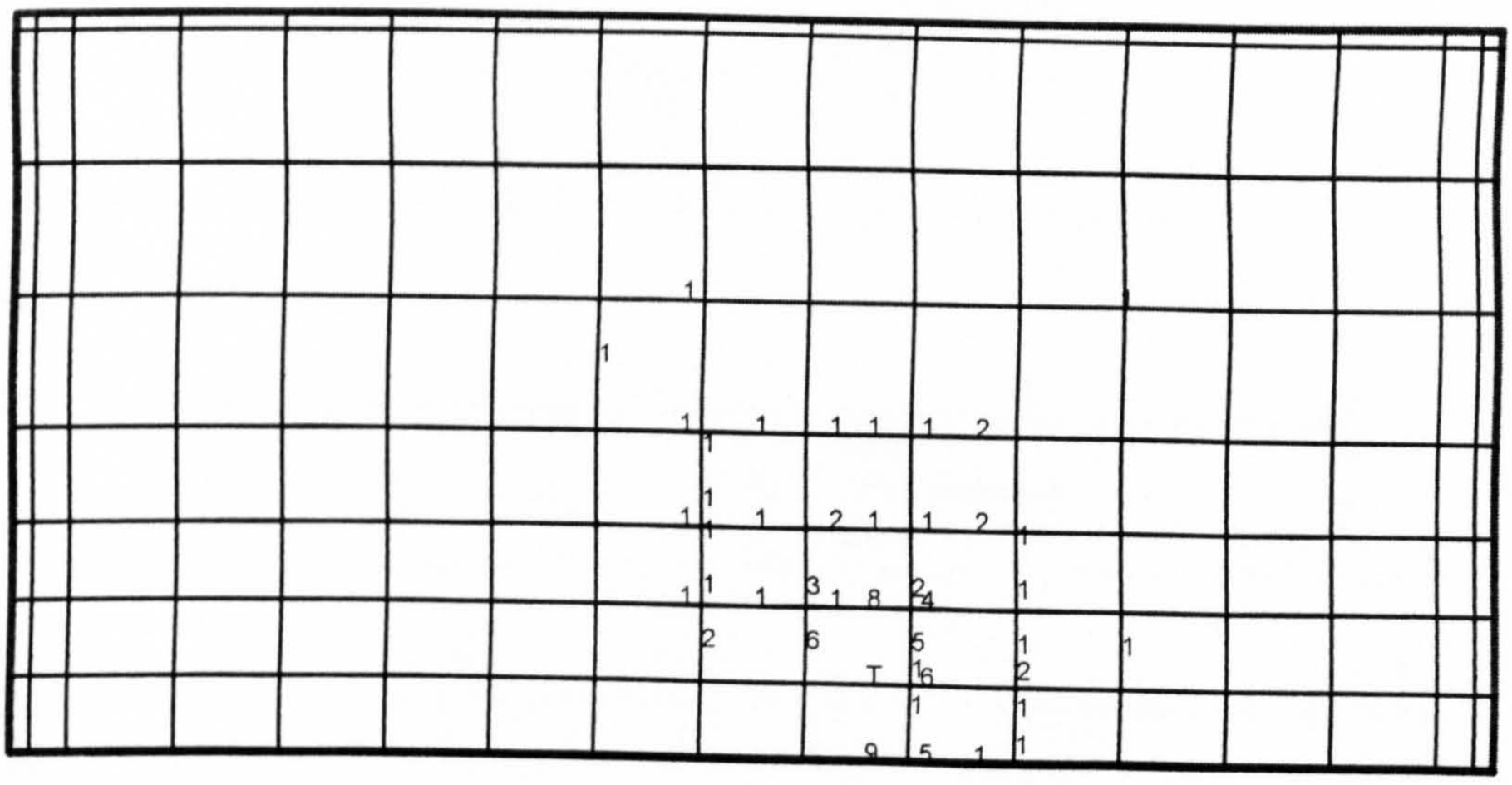

Slab AM4, tension steel, LF=1.30

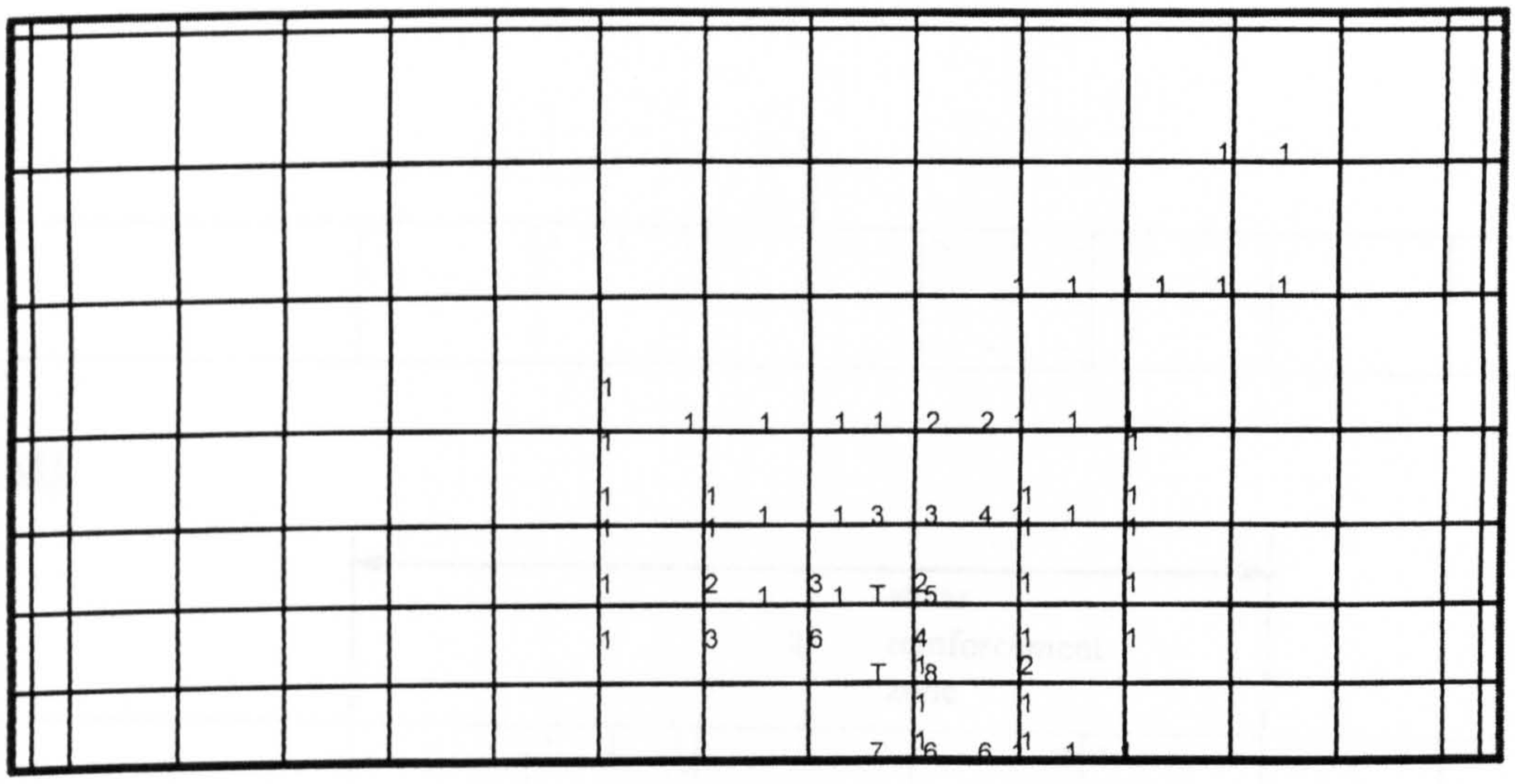

Slab AM5

Predicted crack pattern for AM series (Elgabry and Amin)

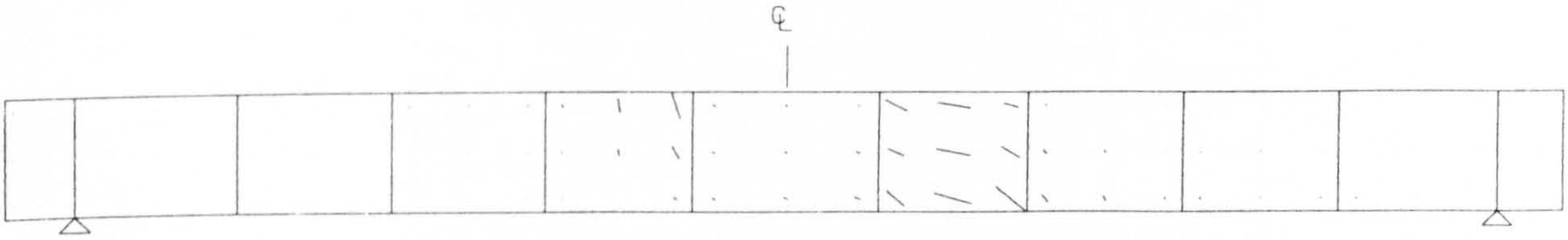

AM1

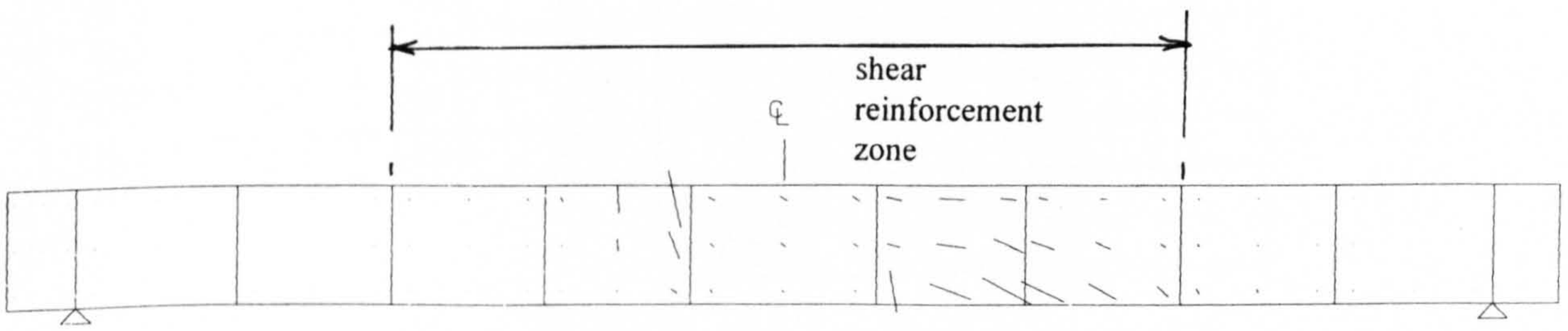

AM2

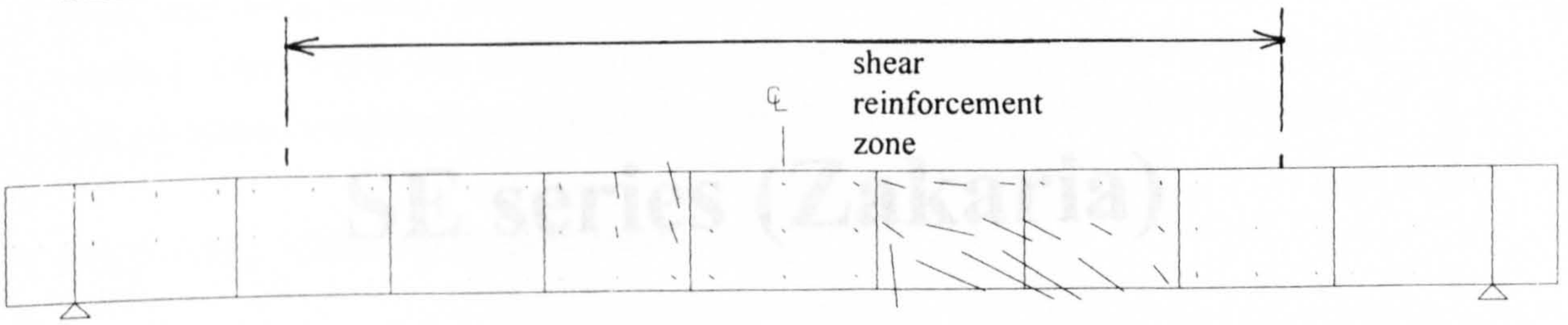

AM3

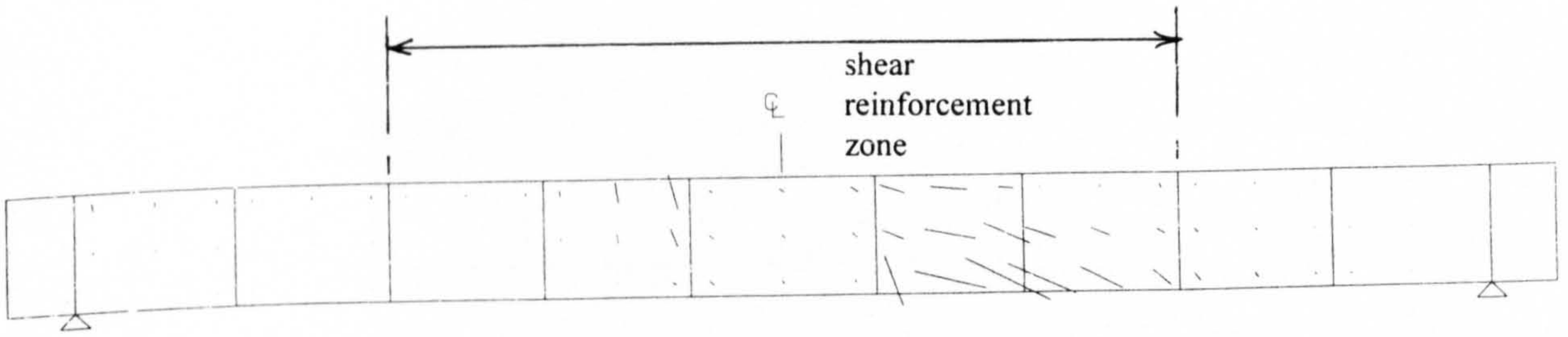

AM4

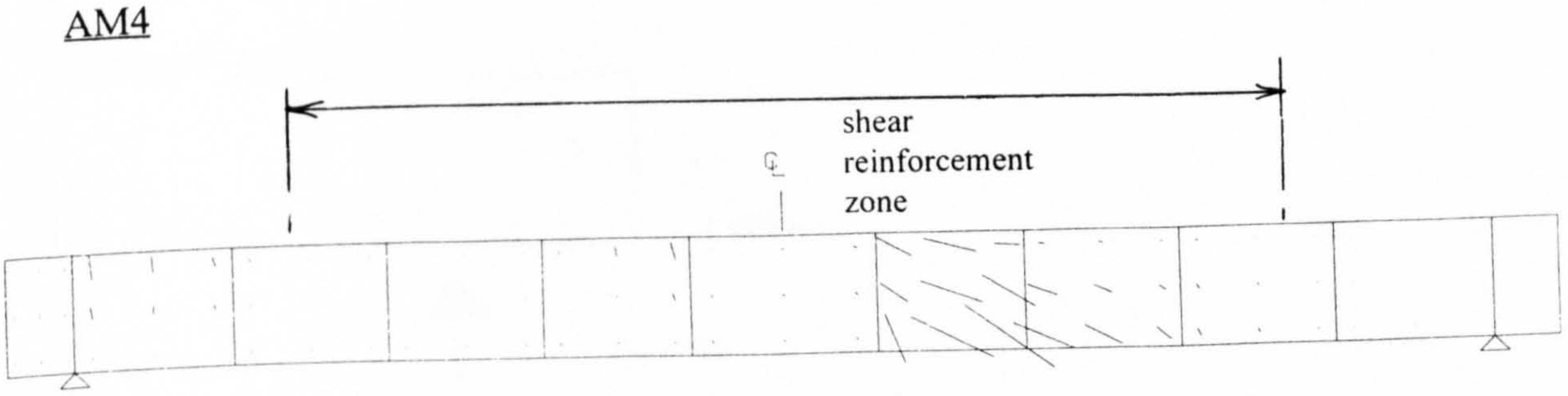

AM5

SE series (Zakaria)

C2.3 Edge column-slab connections tested by Zakaria (without shear reinforcement)

Slab No.	f_{cu} N/mm^2	Experimental			Numerical		
		V_{test} (kN)	M_{test} (kNm)	Failure Mode	Num/Exp V	Num/Exp M	Failure Mode
SE1	44.6	198.0	39.5	s	0.859	0.958	s
SE2	54.6	192.0	34.0	y	1.128	1.001	y
SE3	45.8	256.0	32.5	y	1.000	1.158	y
SE4	34.3	152.0	30.5	s	1.000	1.102	s
SE5	55.2	164.0	38.5	fp	0.950	1.047	fp
SE6	40.0	149.0	27.5	fp	0.969	1.052	fp
SE7	49.5	129.0	31.7	fp	1.042	1.280	fp
SE8	52.0	136.0	33.7	s	1.150	1.092	s
				Average	1.012	1.086	
				STDEV	0.095	0.100	

Note

From numerical results, concrete at most of gauss point near column-slab junction had crushed. Therefore it was not possible to plot the principal compressive stress. The plot principal compressive strain here was based on the calculation of six strains.

For yielding of flexural reinforcement

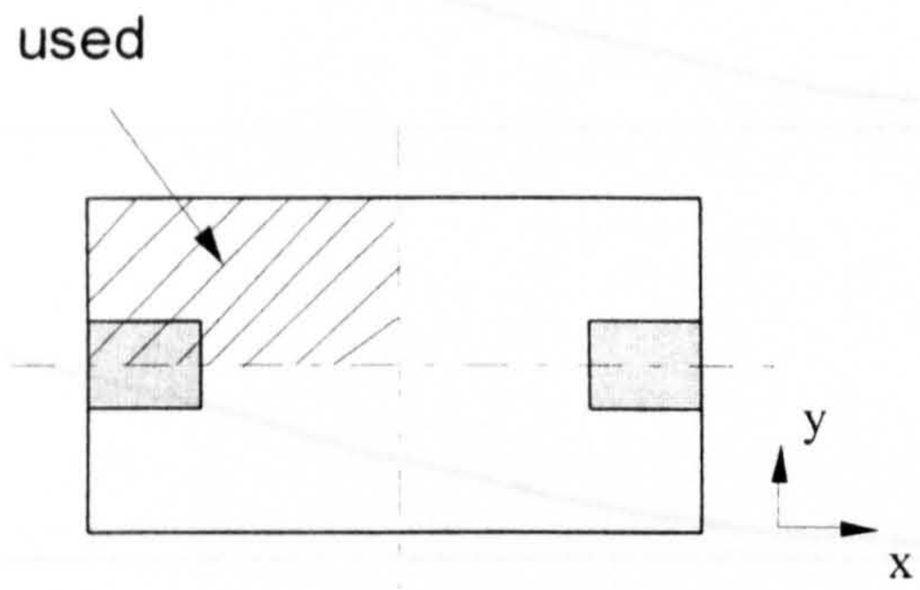

For crack pattern,

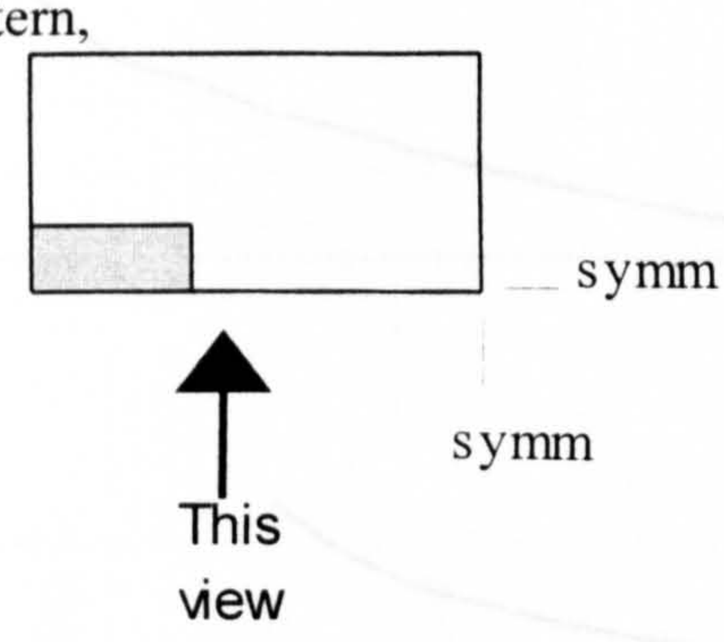

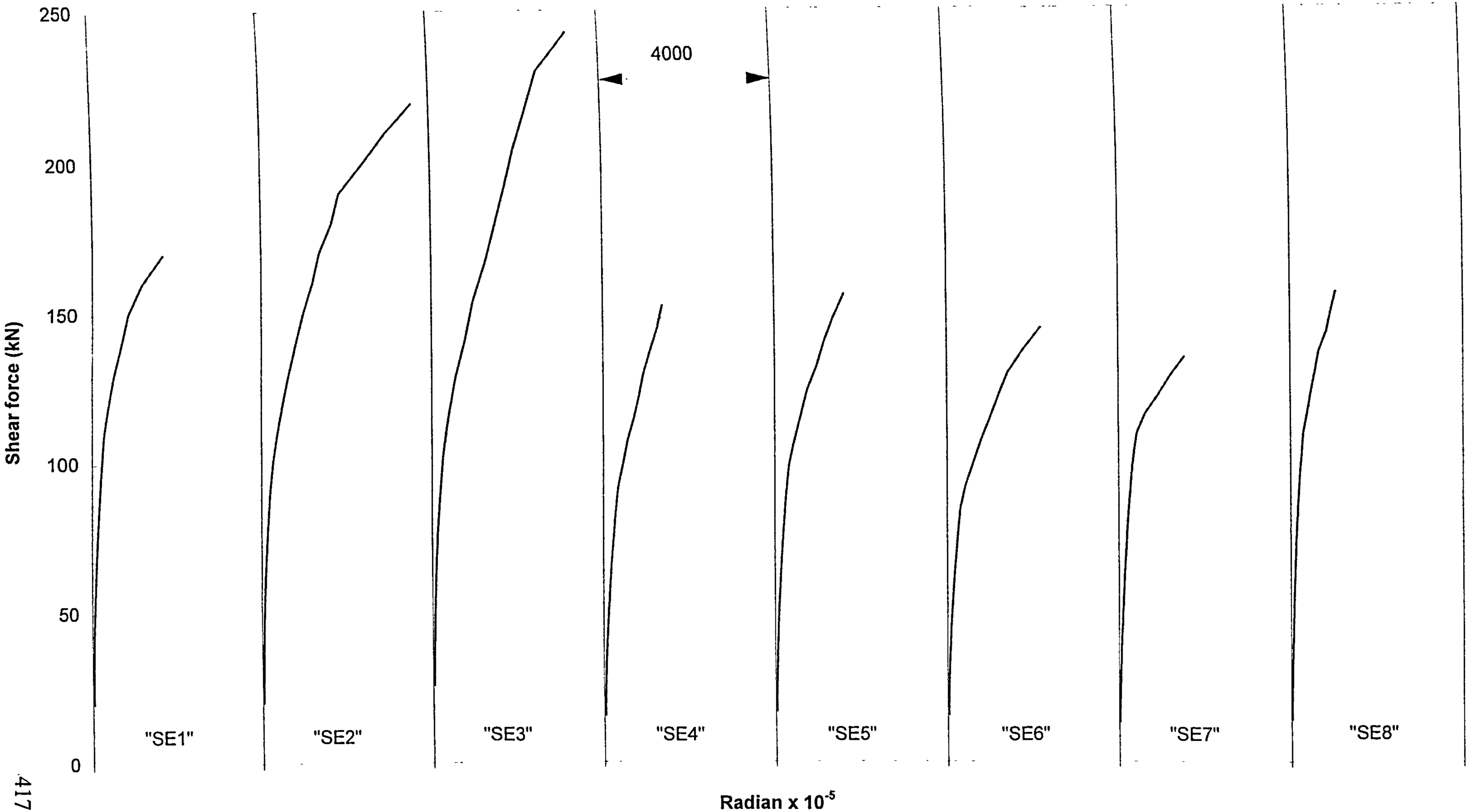

Predicted load-rotation response for slabs SE1-SE8

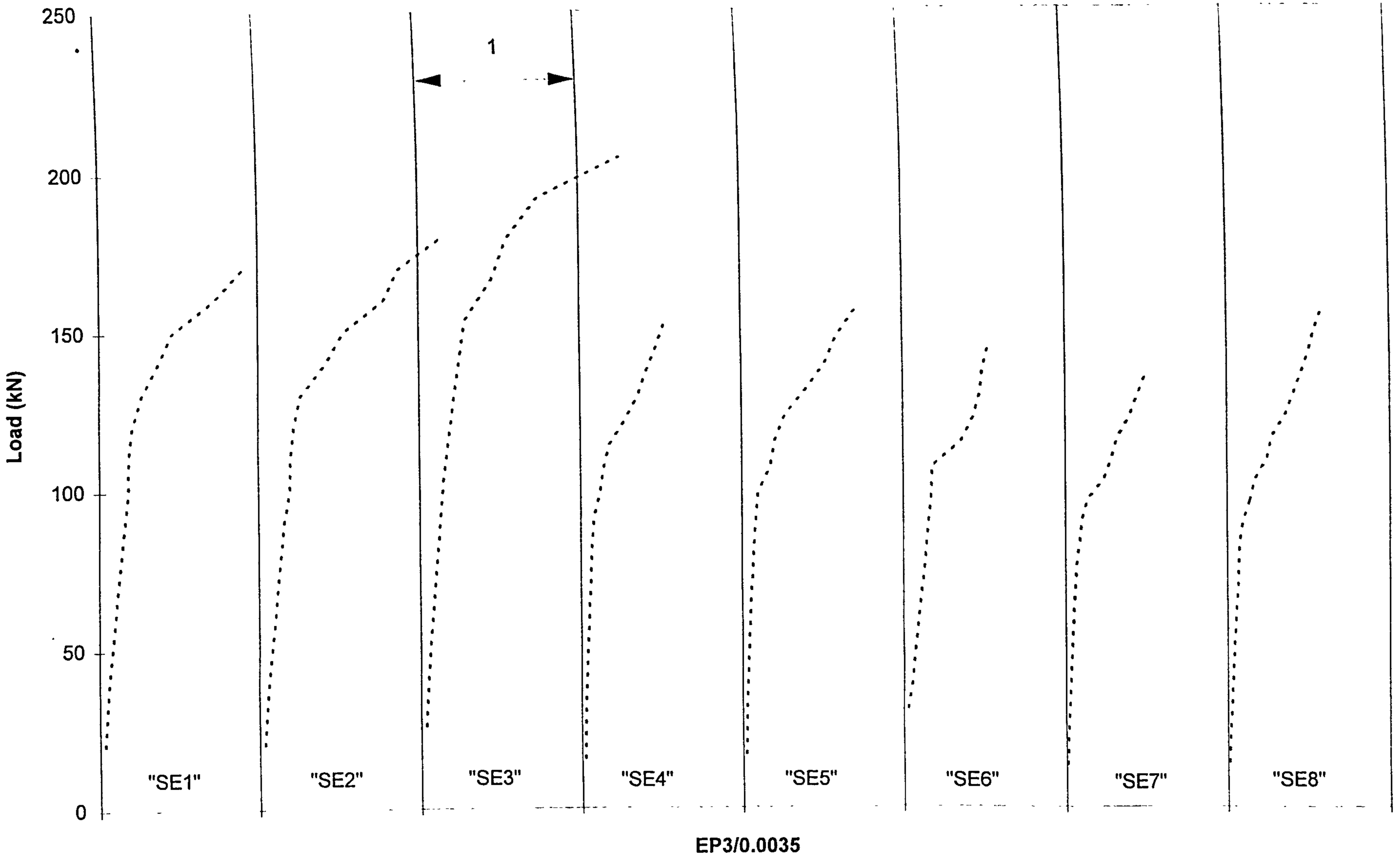

Predicted principal compressive strain in concrete (slabs "SE1" - "SE8")

Yielding of tension steel, SE series (Zakaria)

NB. : The numbers on the drawing indicate strain in steel at collapse expressed as a ratio of yield strain

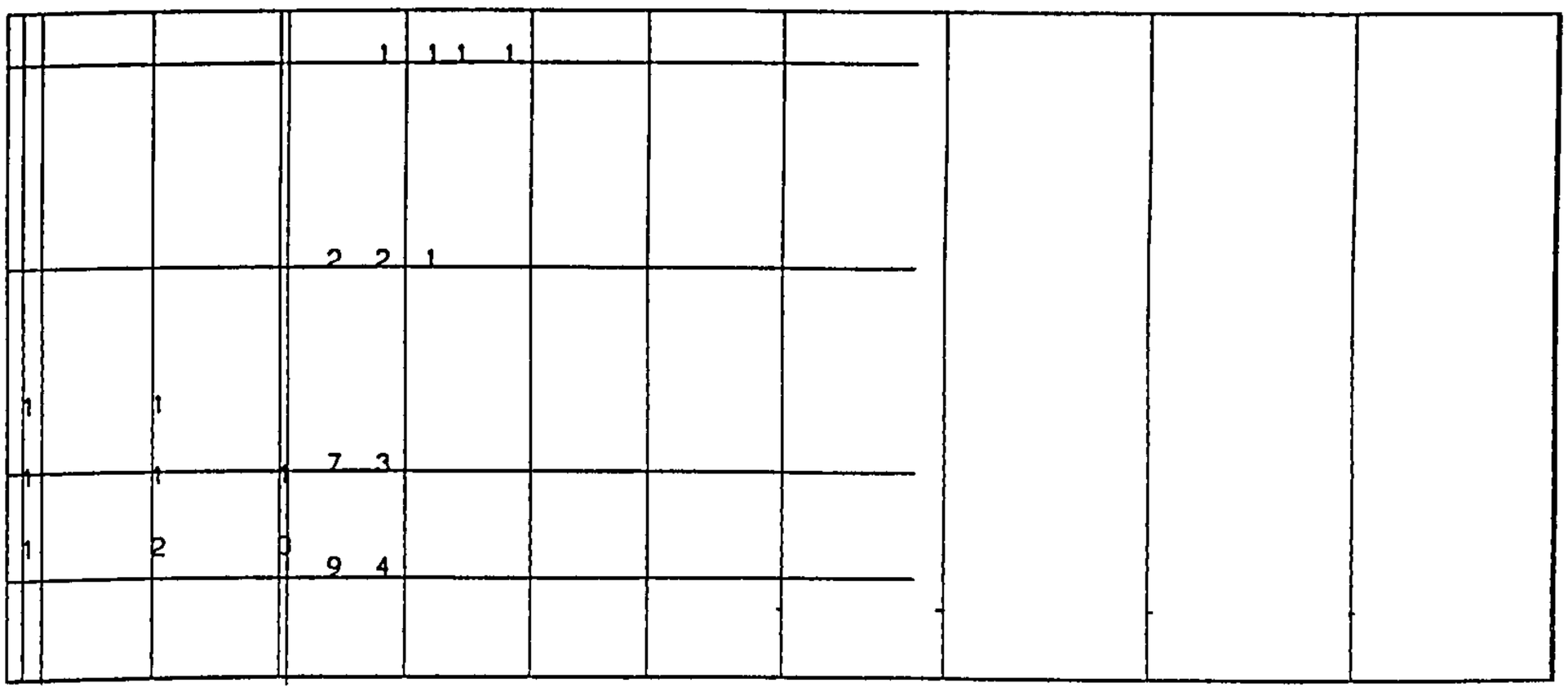

SE2

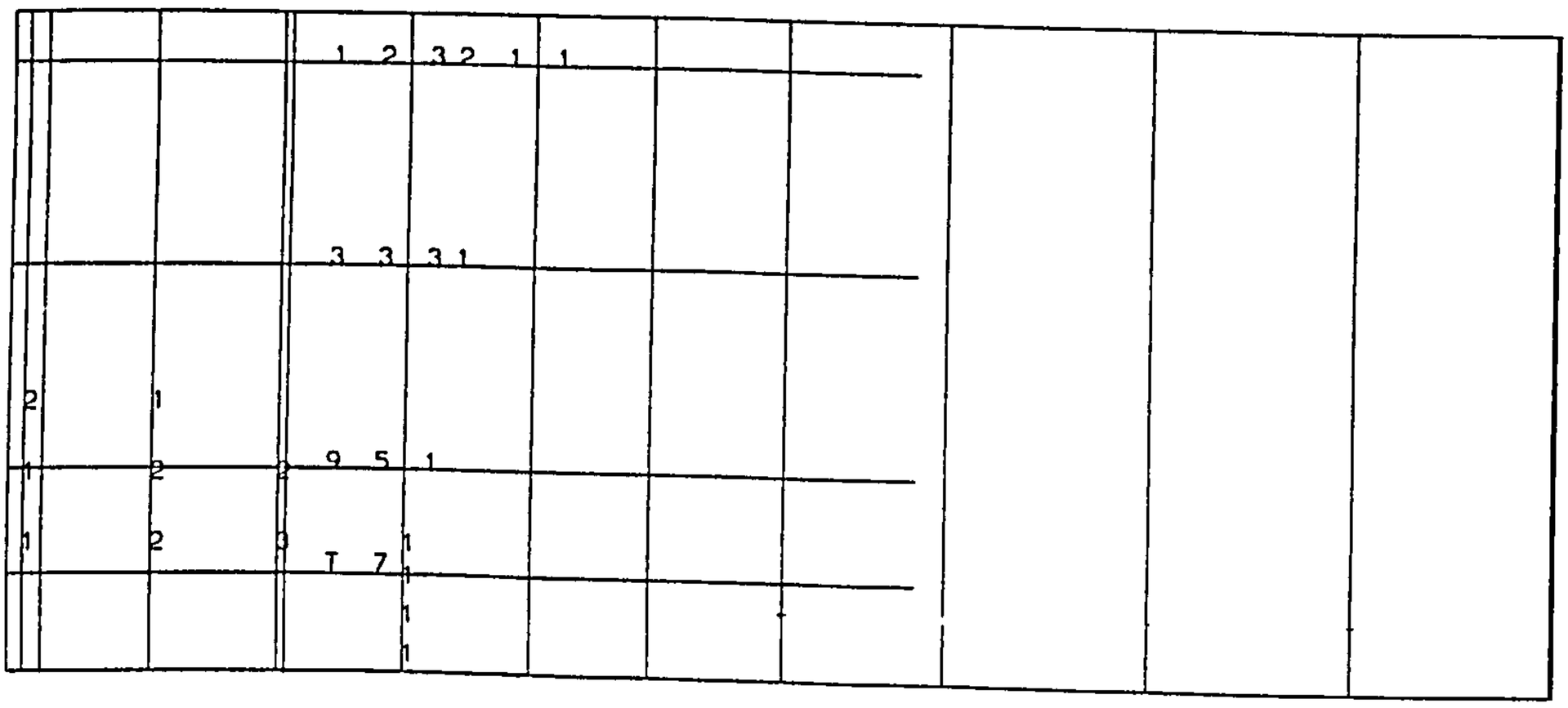

SE3

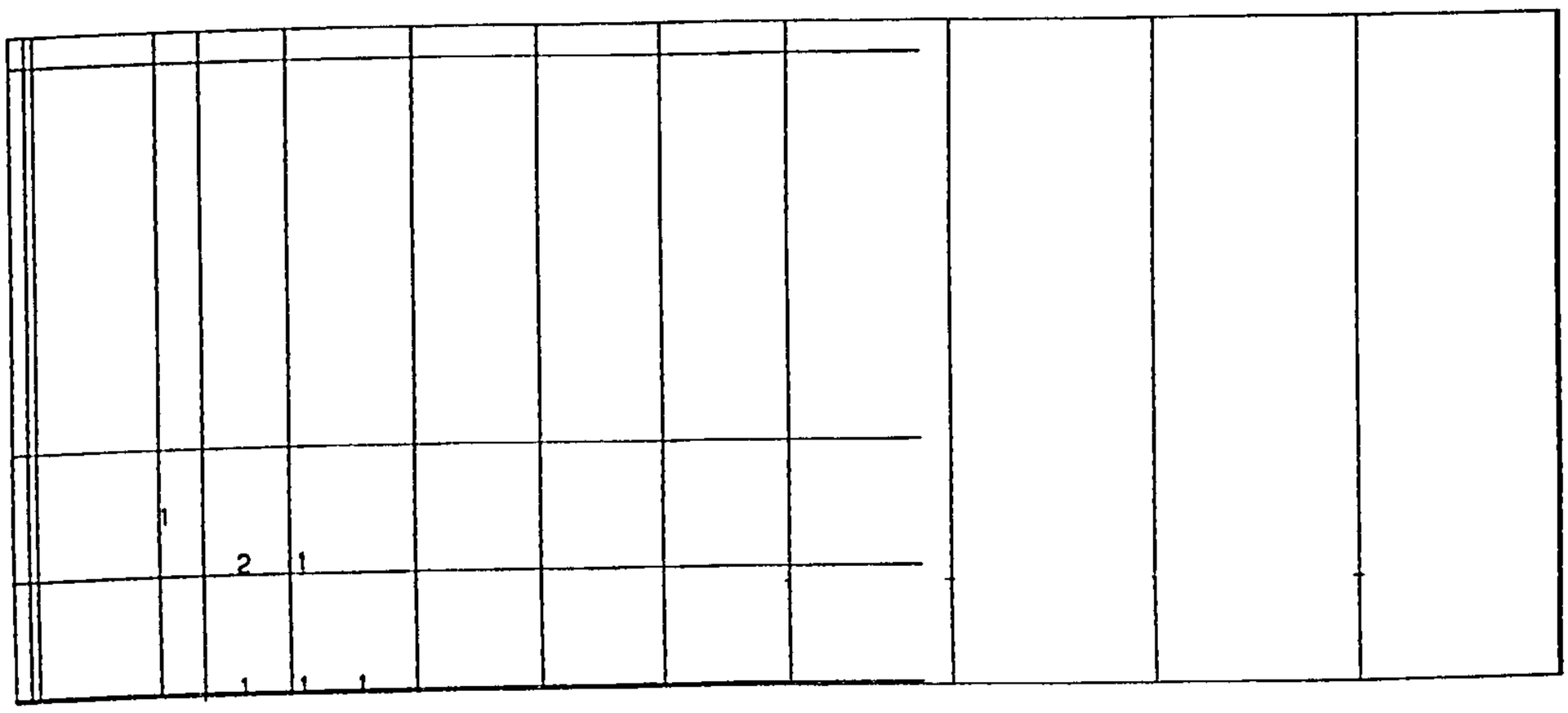

SE5

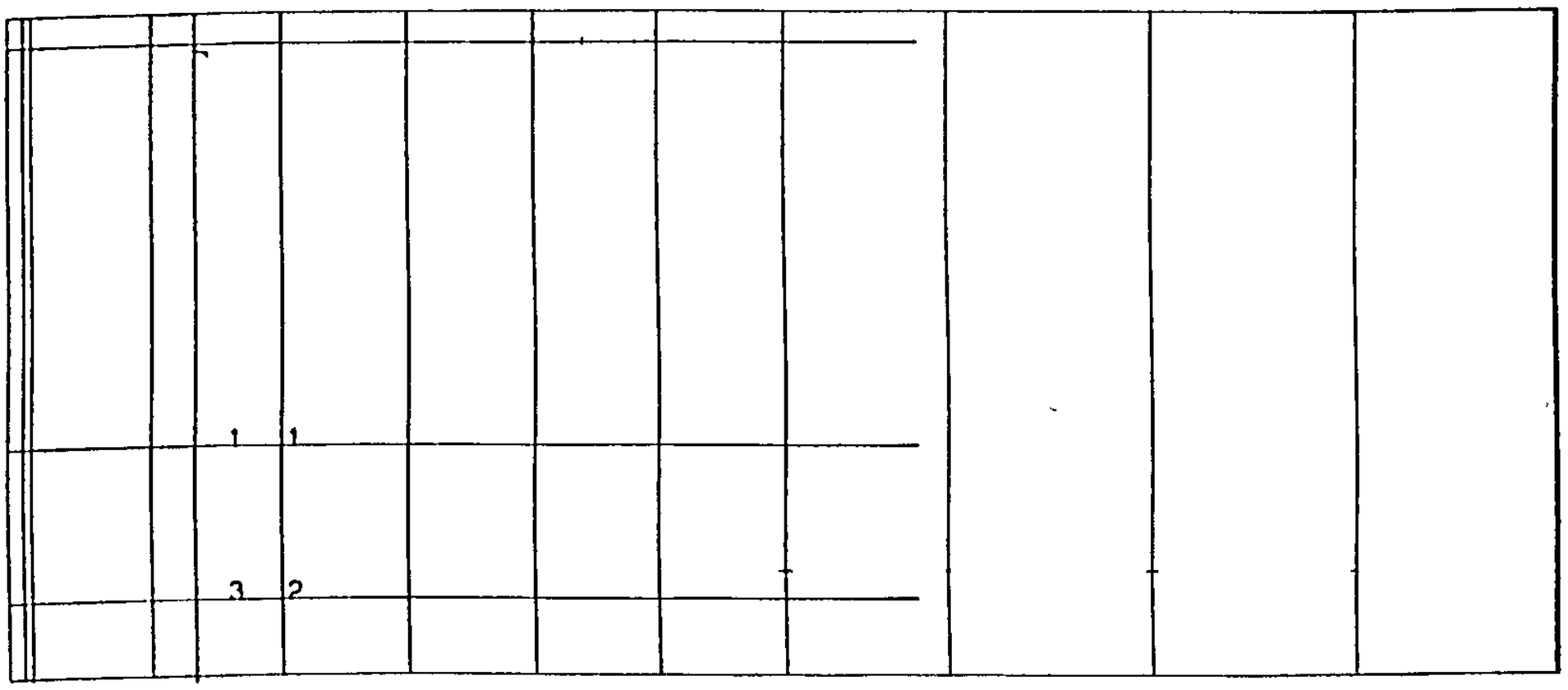

SE6

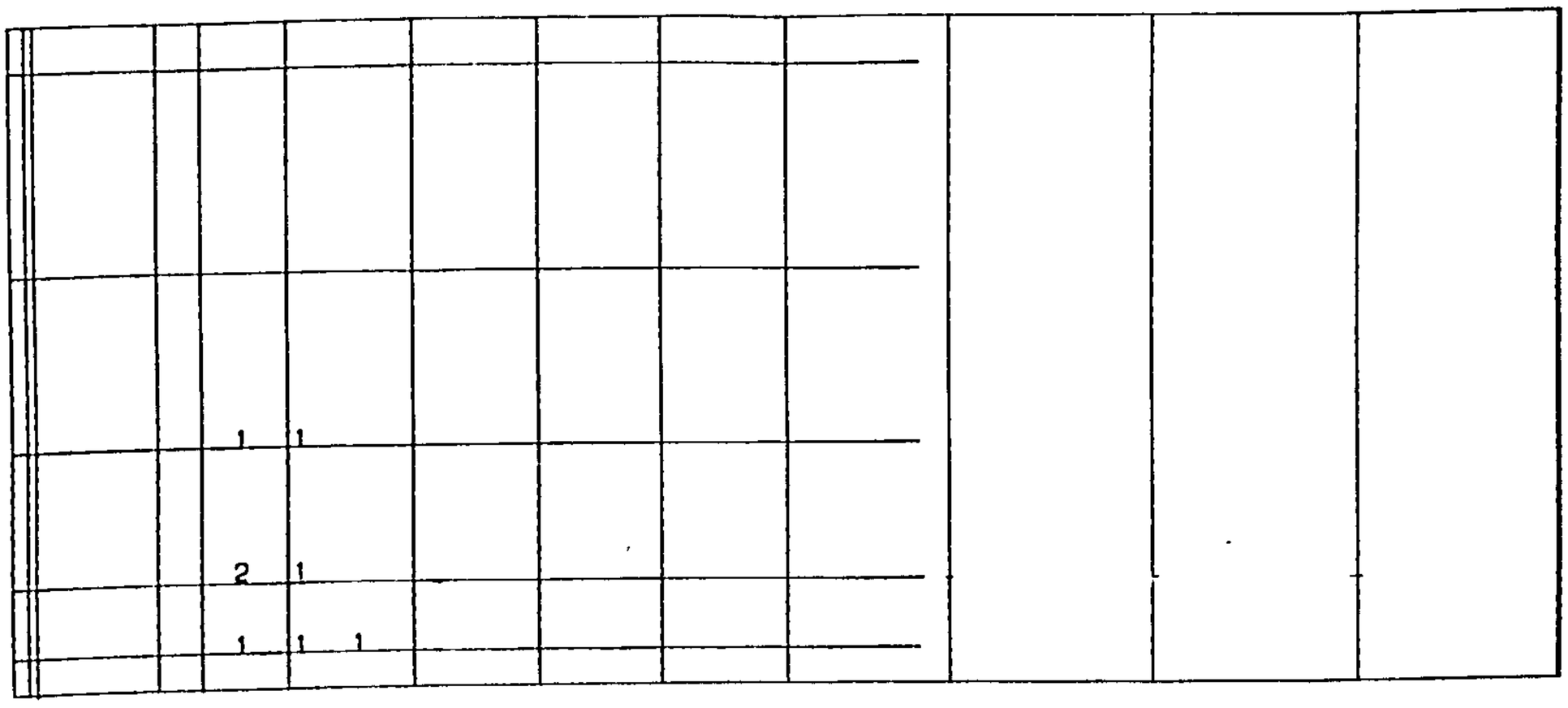

SE7

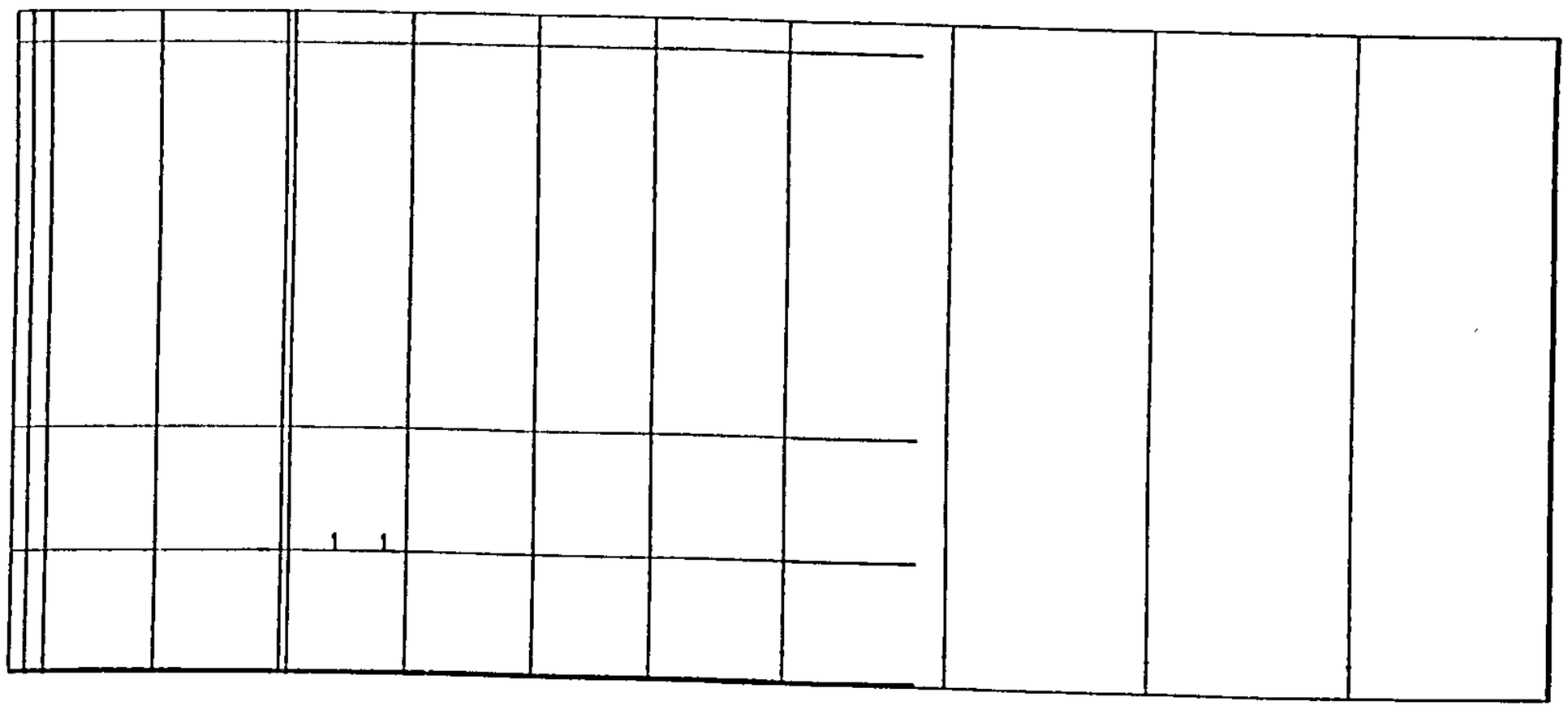

SE8

Note

Flexural steel in slabs **SE1** and **SE4** did not yield.

Predicted crack pattern for SE series (Zakaria)

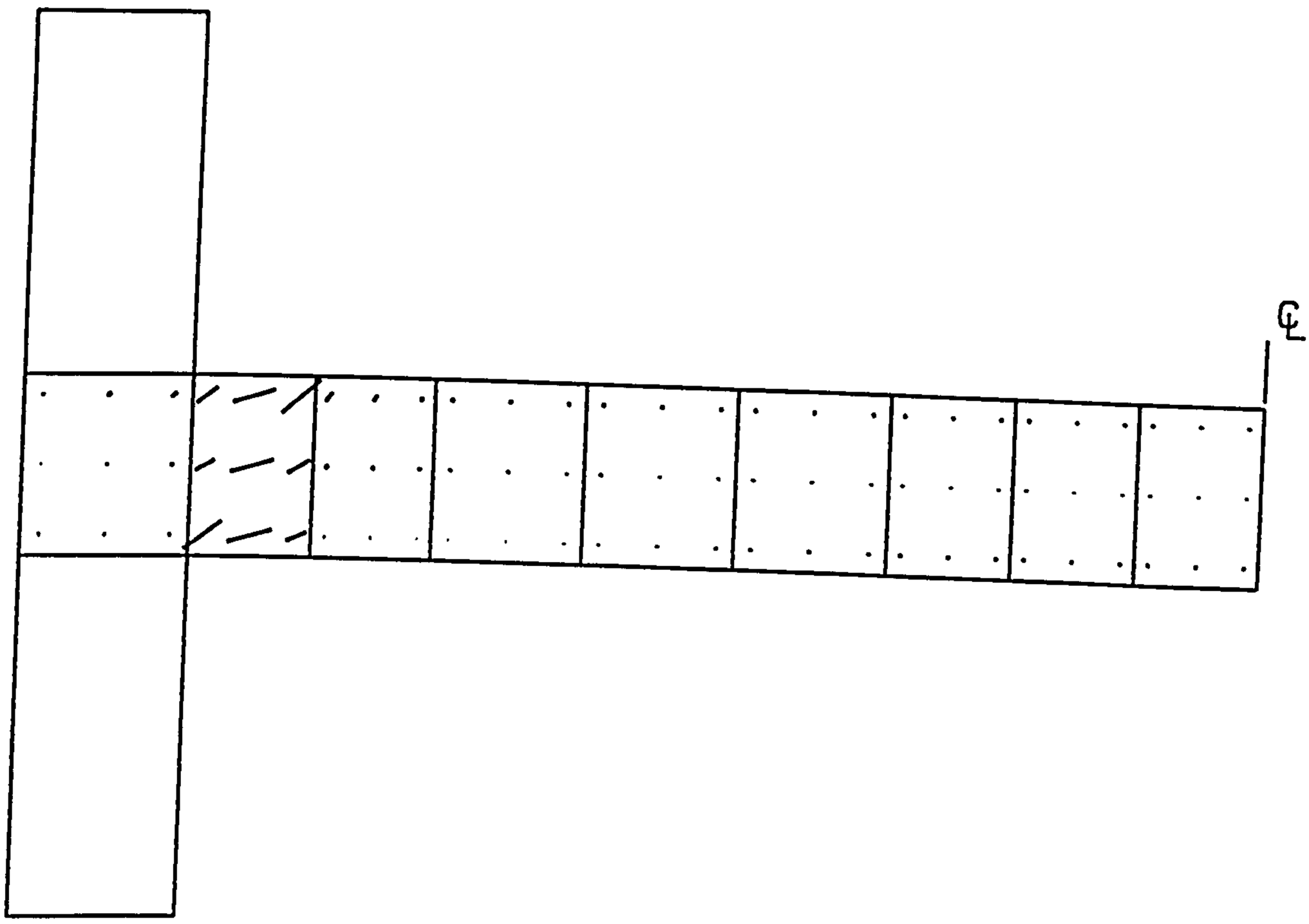

SE1

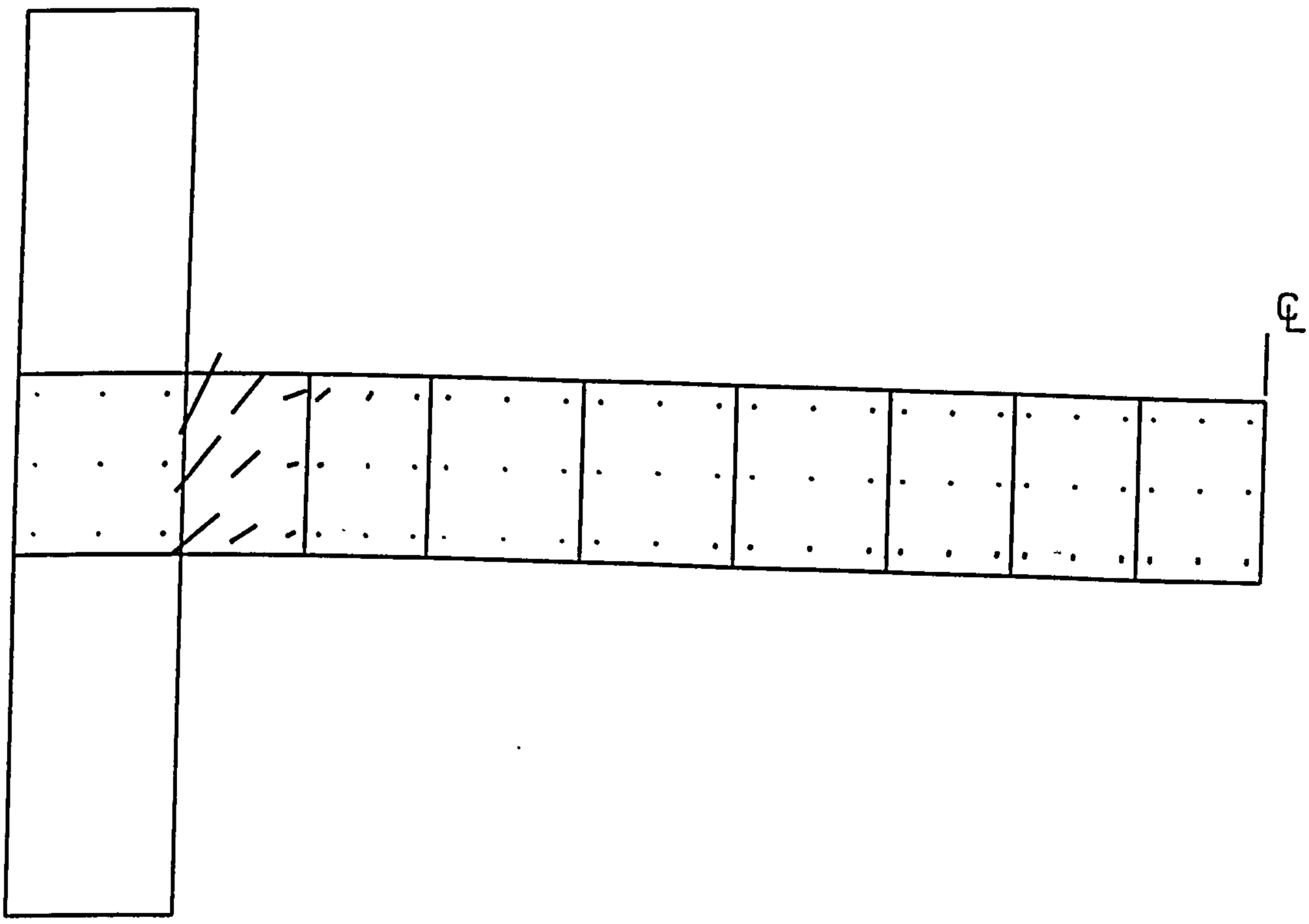

SE2

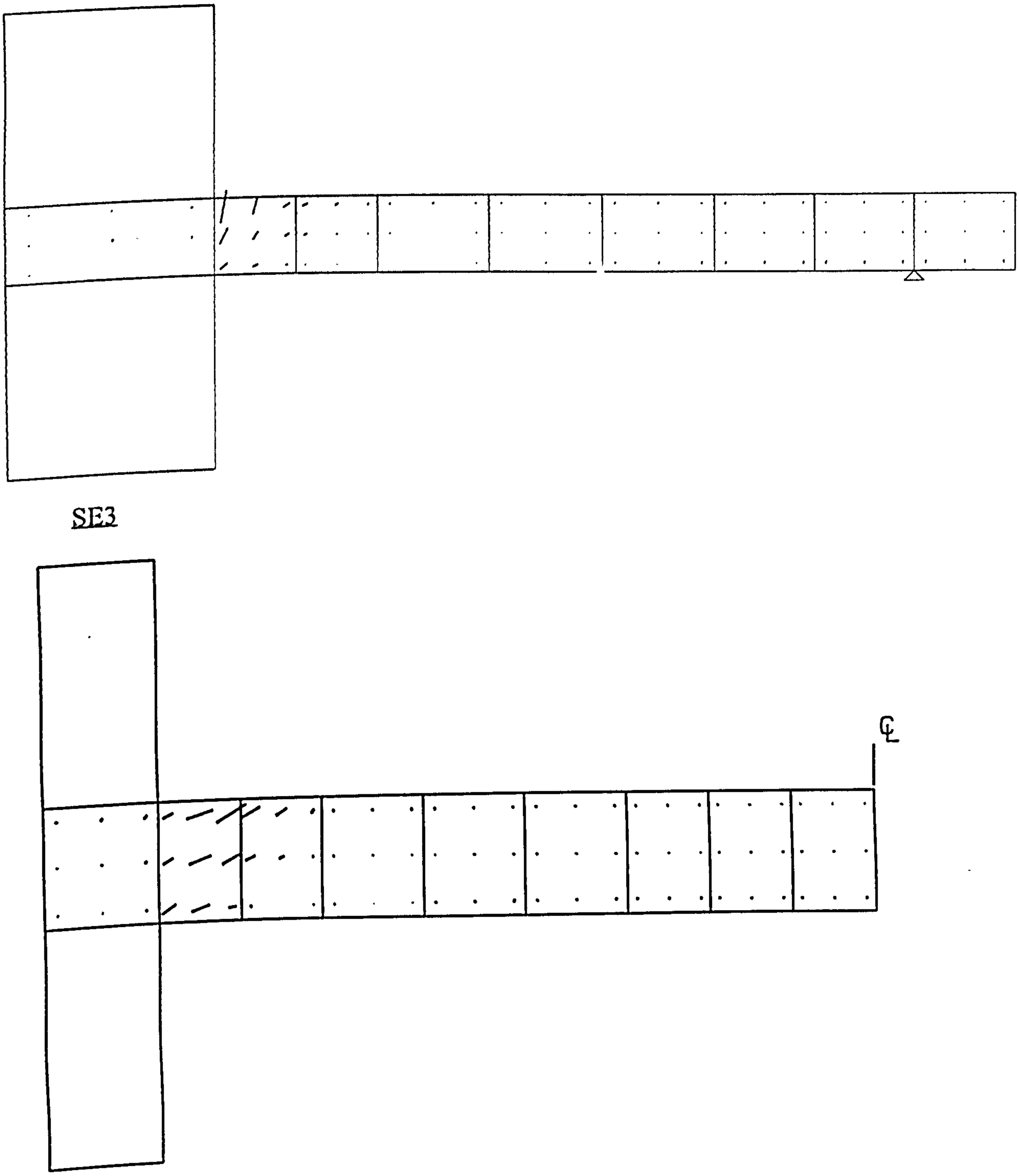
SE3
SE4
℄

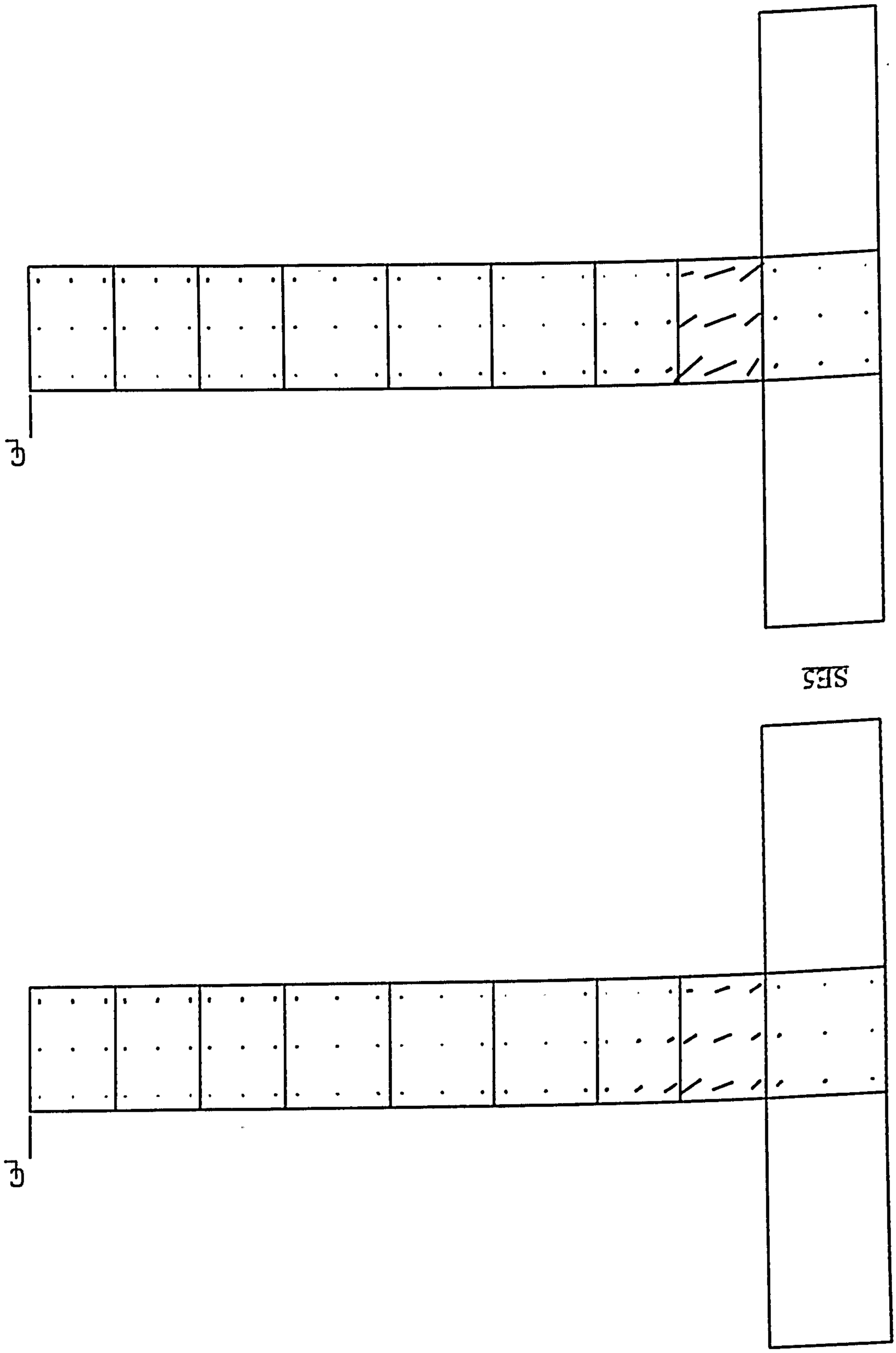
SE6
SE5
E
E

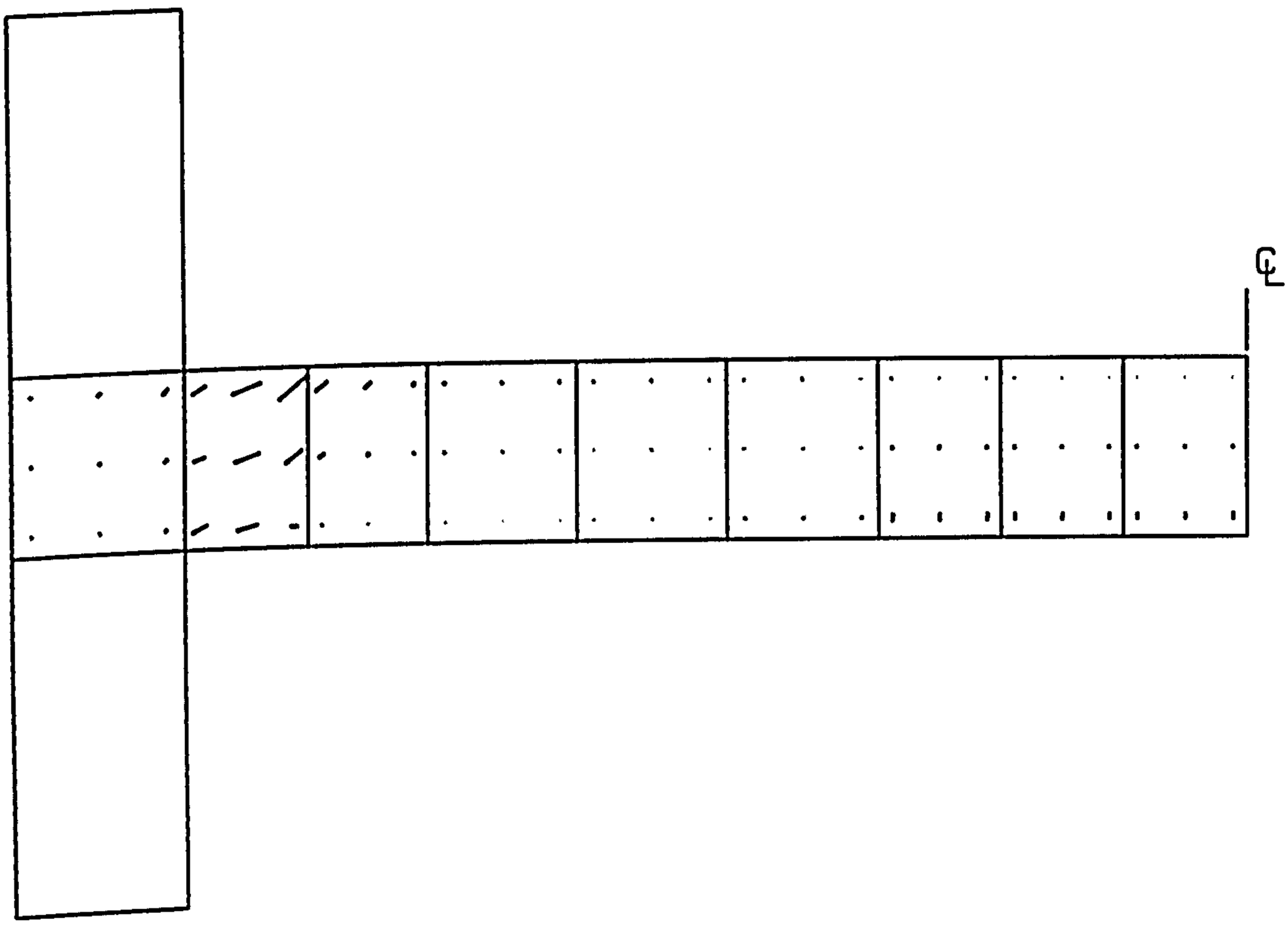

SE7

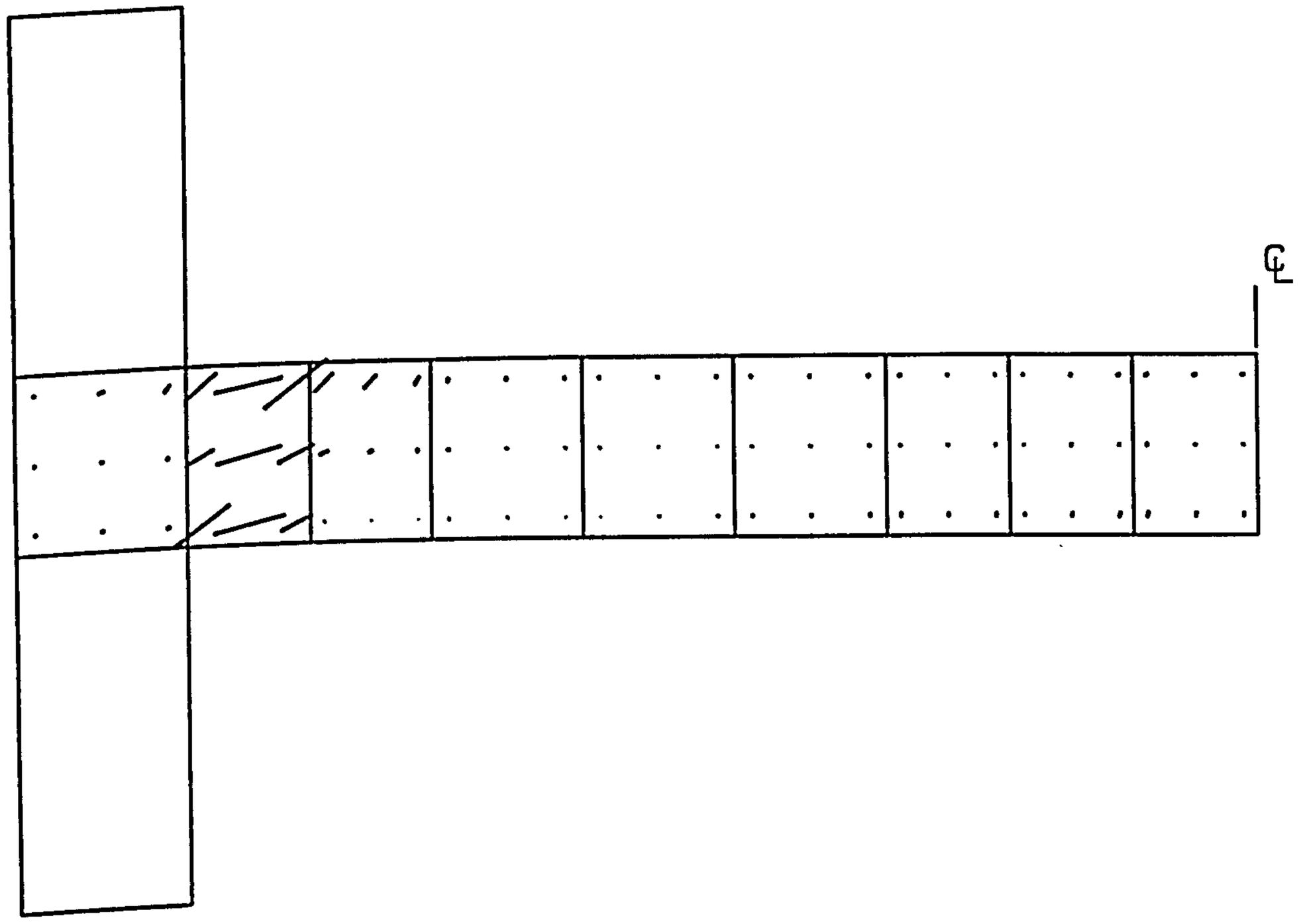

SE8

JS series (Mortin and Ghali)

C2.4 Edge column-slab connections with shear reinforcement (Mortin and Ghali)

Slab No.	Experimental results						Numerical results	
	f_c' N/mm^2	Flexural steel		V_{test} (kN)	M_{test} (kNm)	failure mode	Num/Exp ratio	failure mode
		ρ_x(%)	ρ_y(%)					
JS1	43.20	0.60	0.95	140.9	60.5	s	1.05	s
JS2	49.00	0.80	1.28	231.0	95.3	y	0.89	y
JS3	44.70	0.80	1.28	212.3	89.5	y	1.00	y
JS4	32.20	0.80	1.28	141.0	60.3	s	0.97	s
JS5	35.80	0.80	1.28	212.3	86.4	fp	0.96	y
JS6	33.90	0.80	1.28	201.0	85.6	y	0.95	y
							Average = 0.970	
							STDEV = 0.053	

For yielding of flexural reinforcement

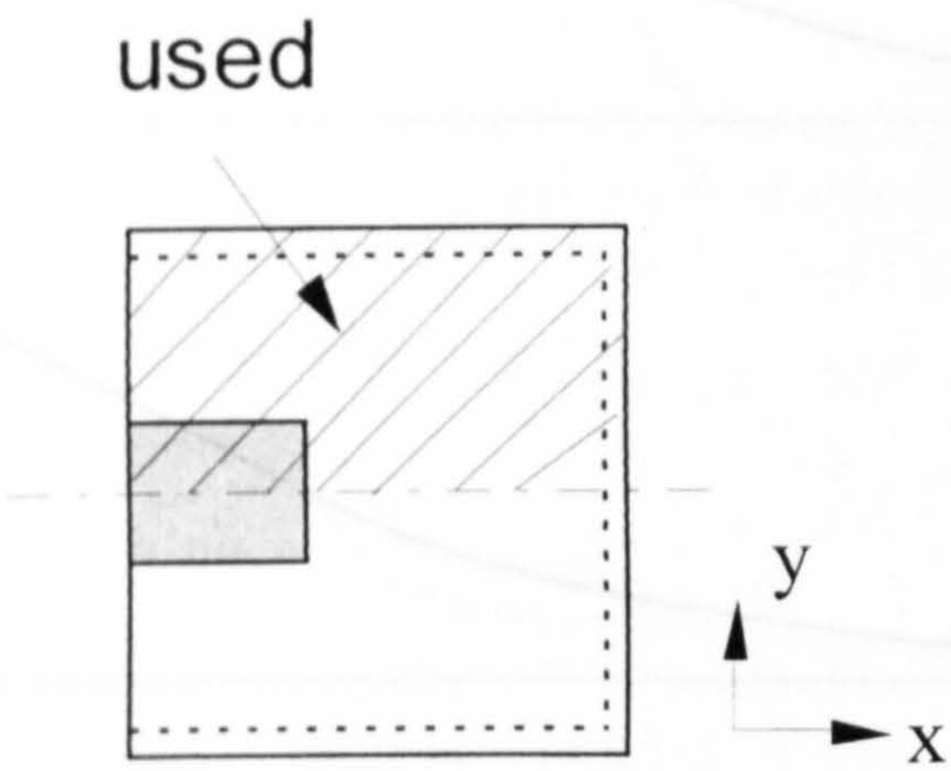

For crack pattern,

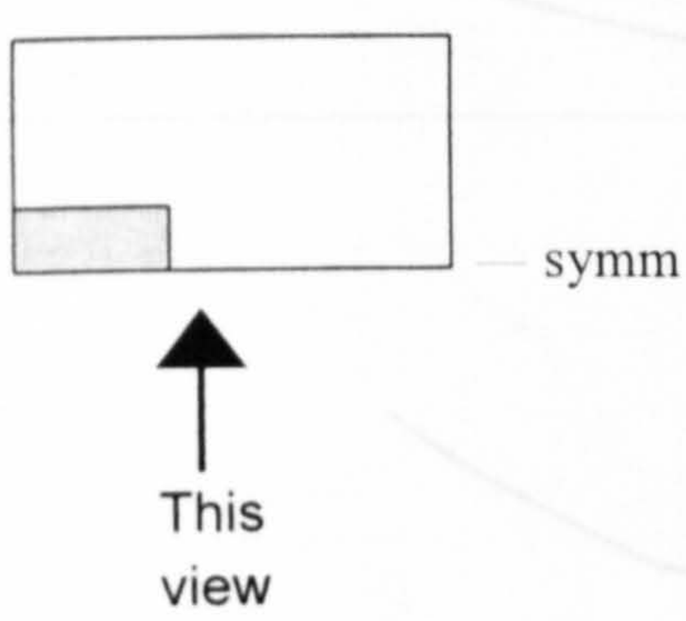

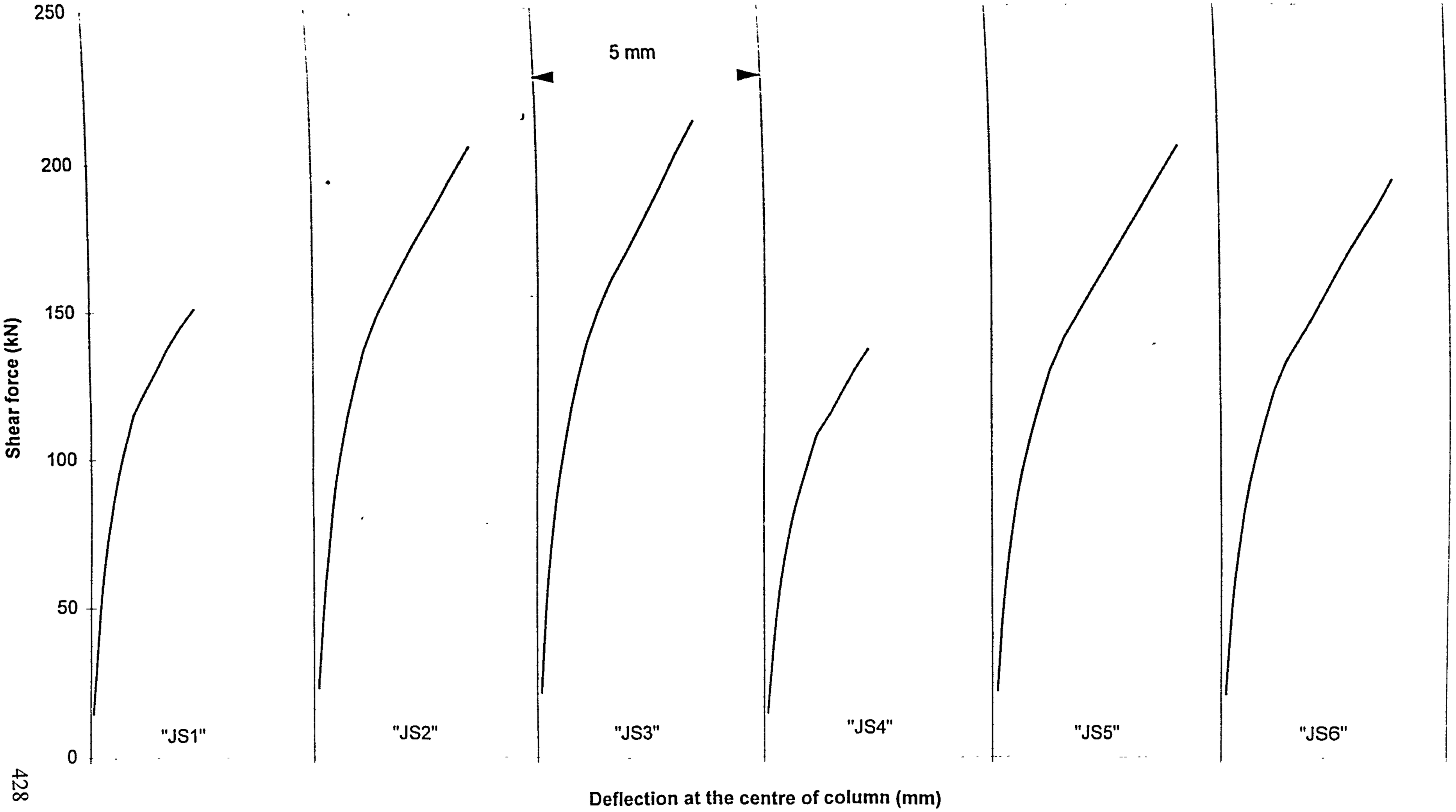

Predicted load-deflection response for slabs JS1-JS6

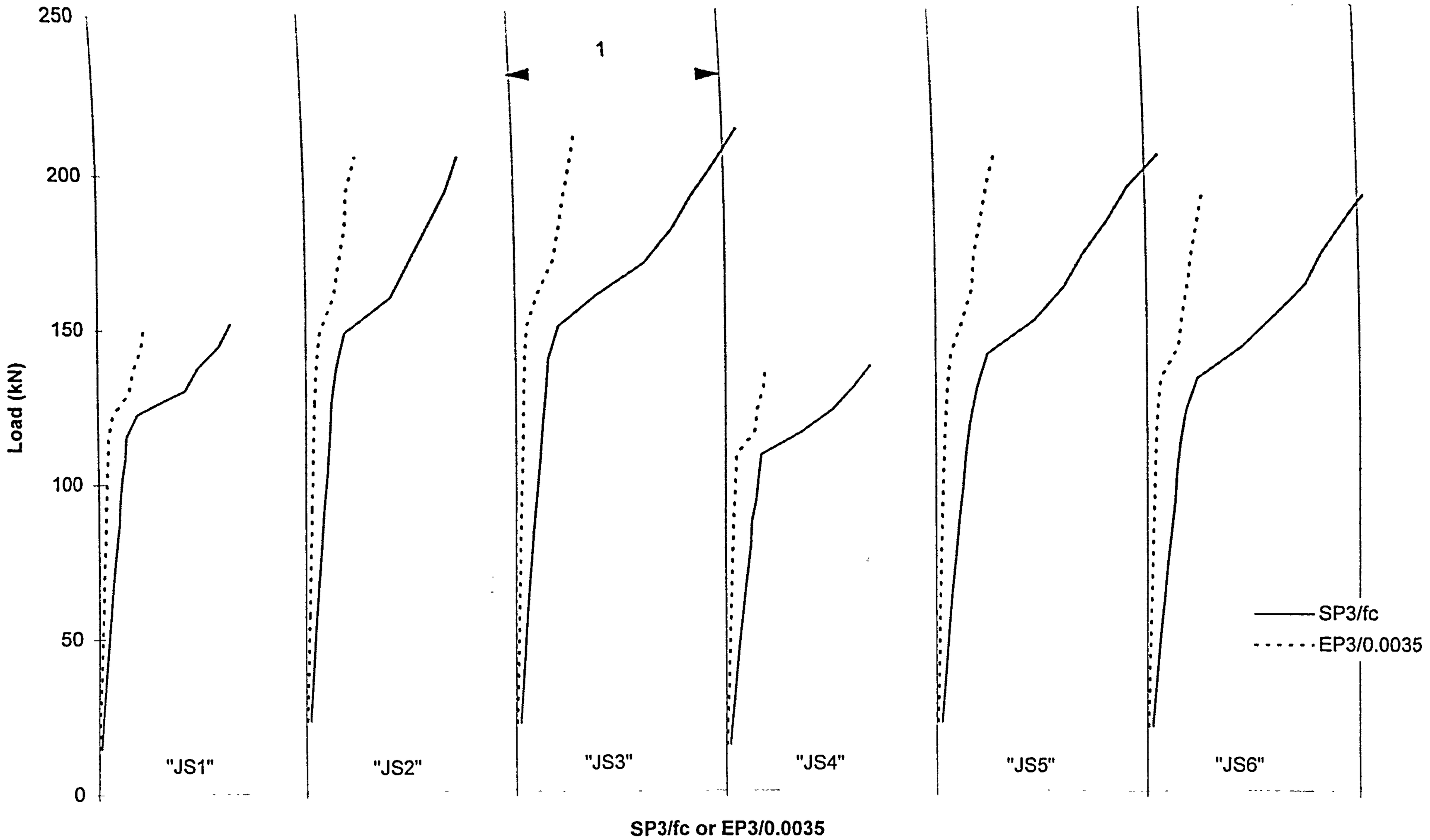

Predicted principal compressive stress and strain in concrete (slabs "JS1" - "JS6")

Yielding of tension steel, JS series (Mortin and Ghali)

NB. : The numbers on the drawing indicate strain in steel at collapse expressed as a ratio of yield strain

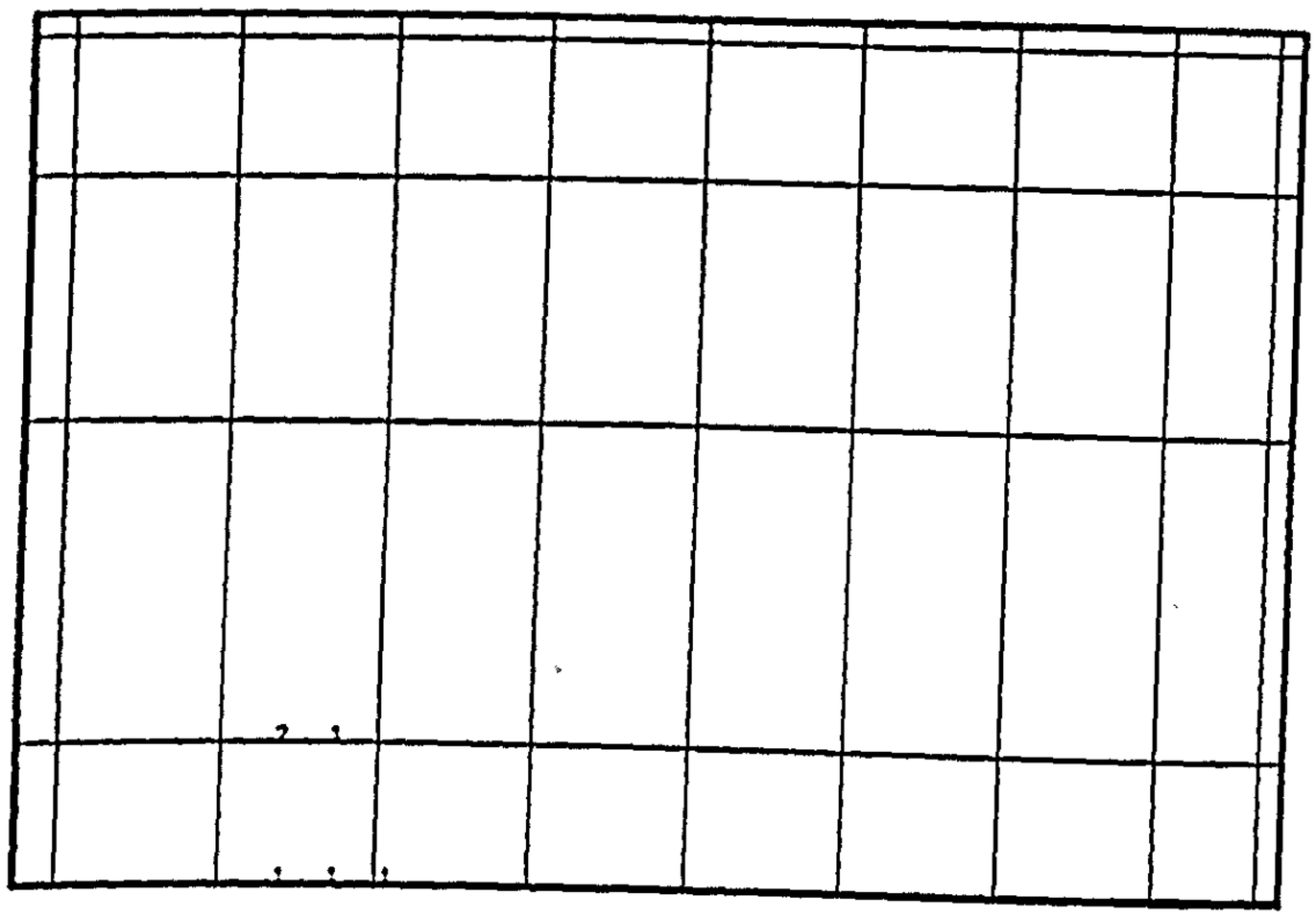

Slab JS1

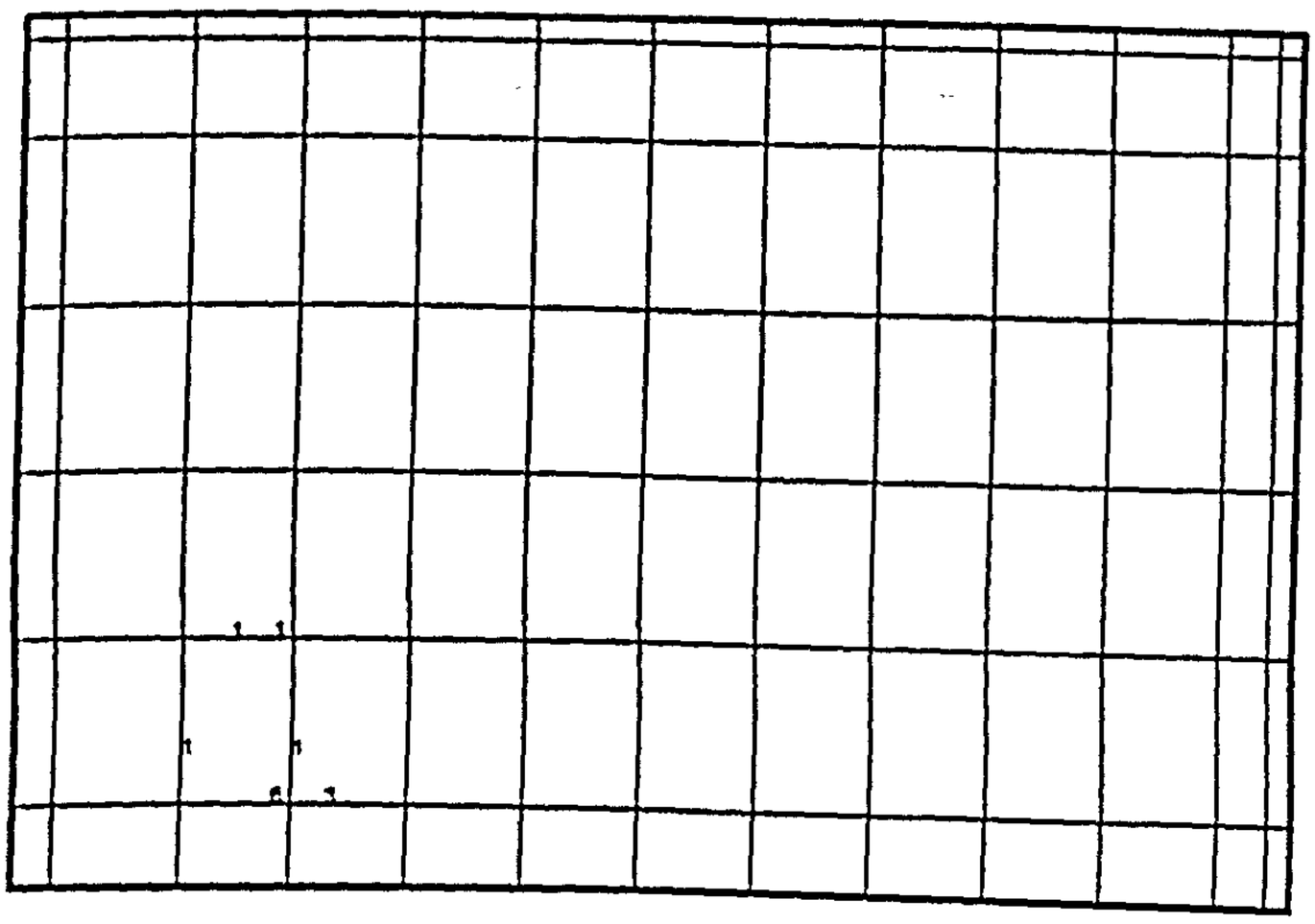

Slab JS2

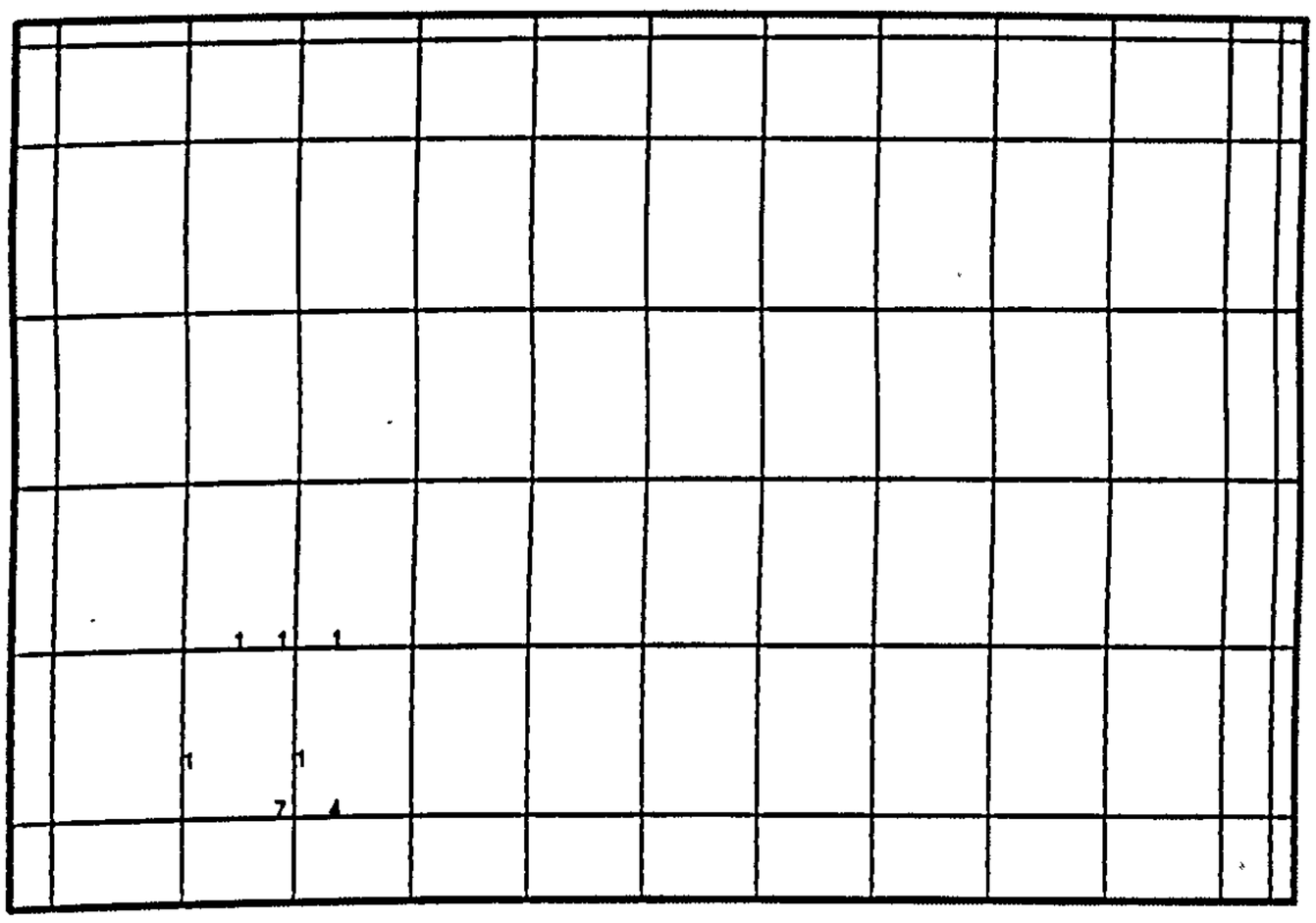

Slab JS3

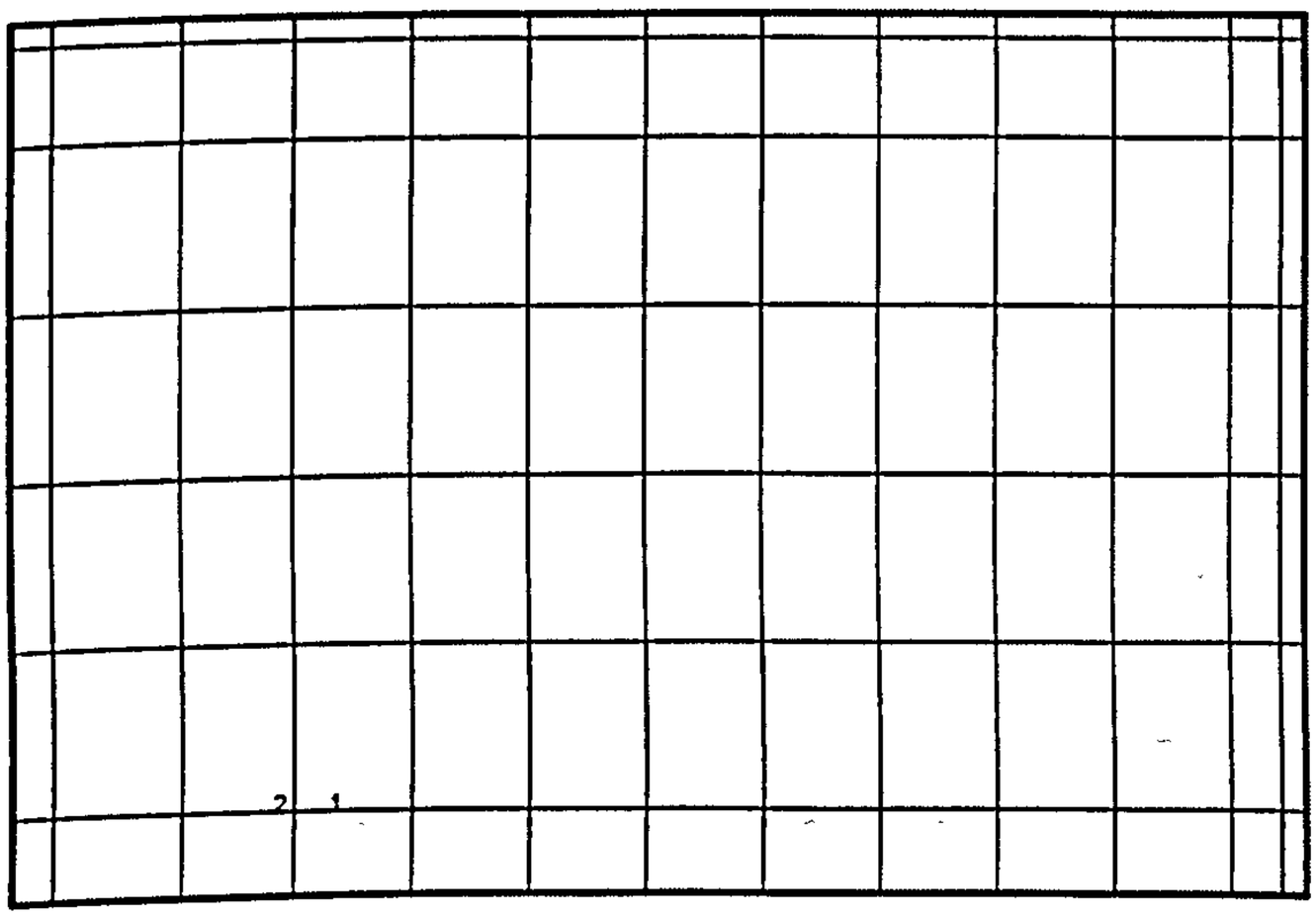

Slab JS4

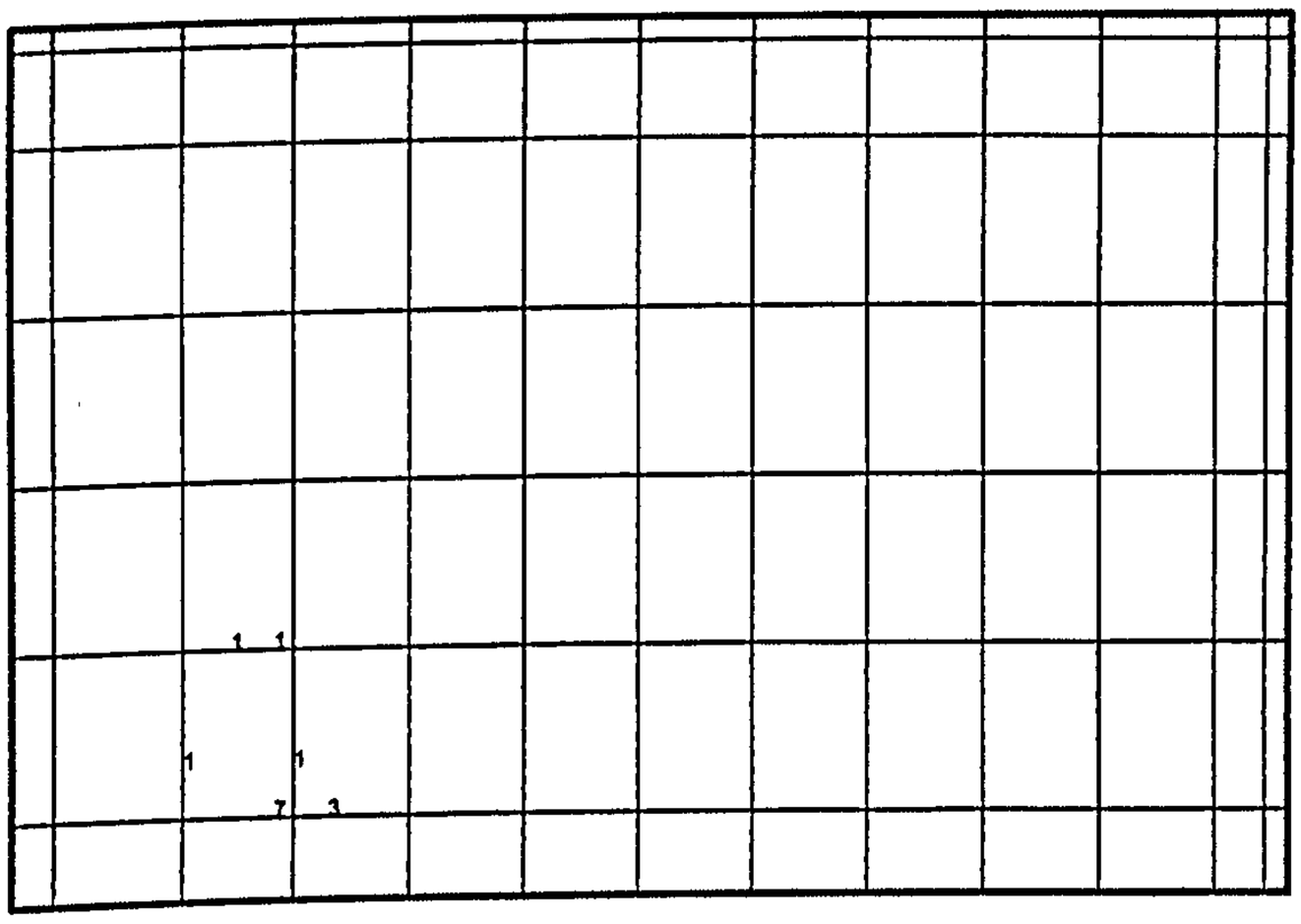

Slab JS5

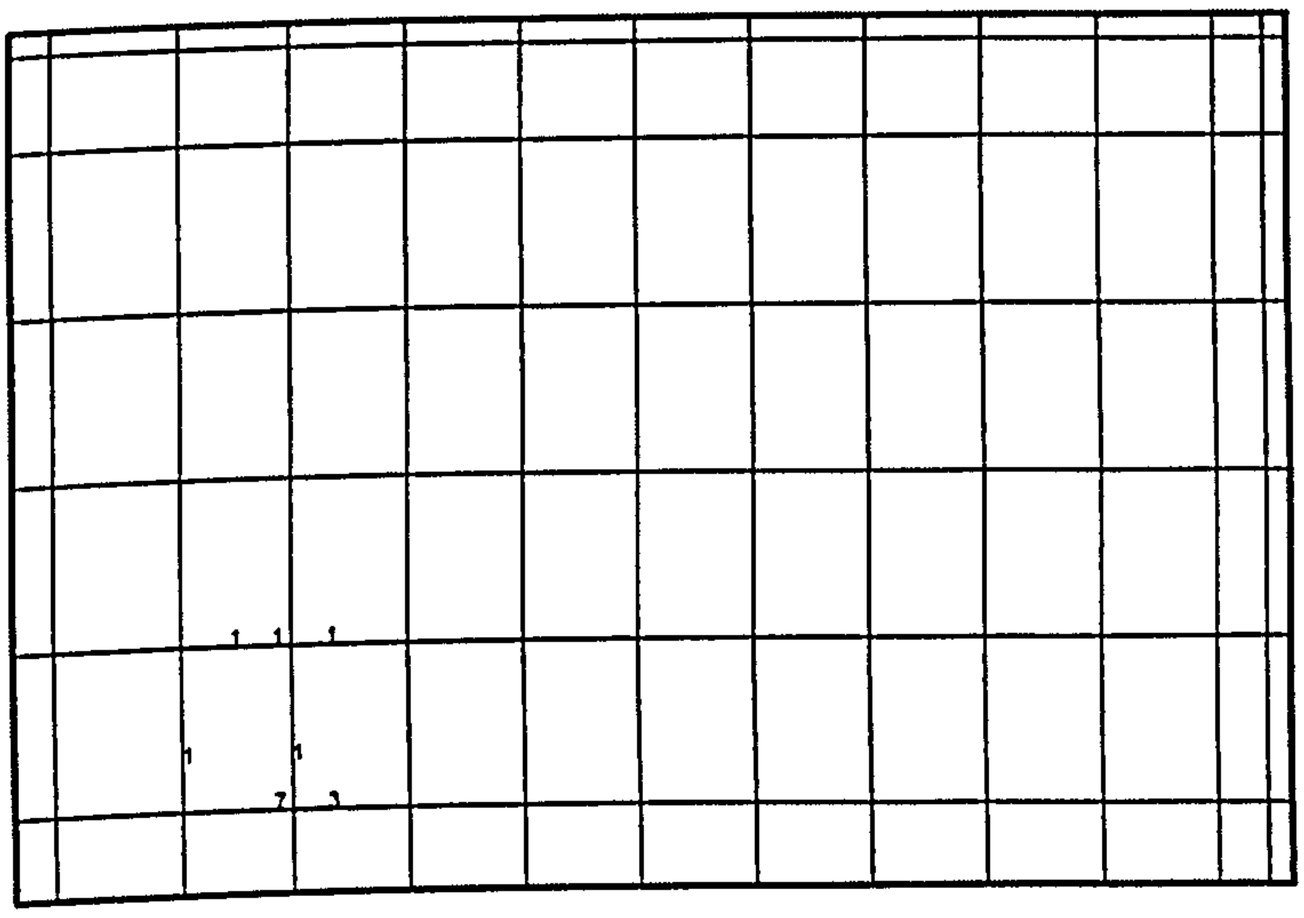

Slab JS6

Predicted crack pattern for JS series (Mortin and Ghali)

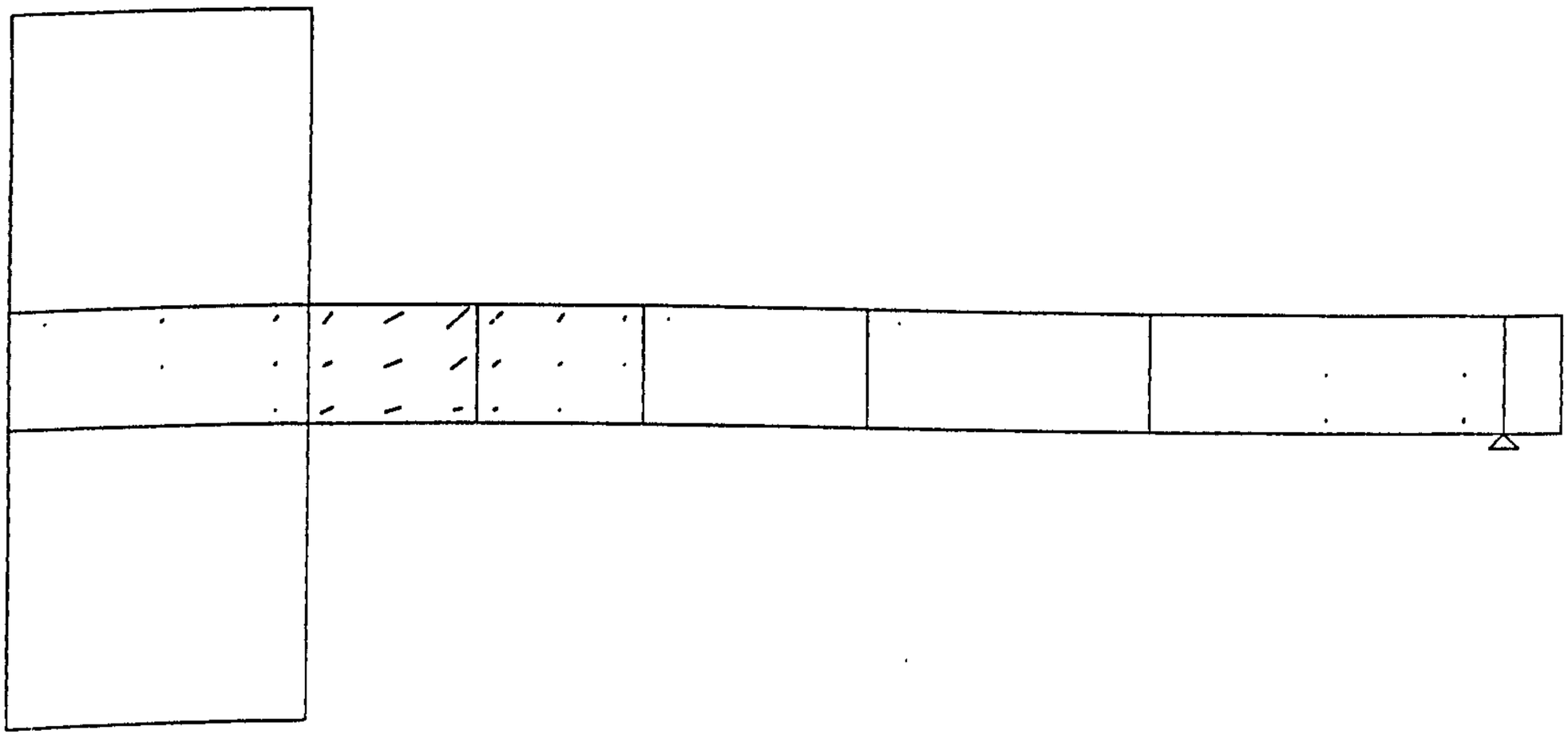

JS1

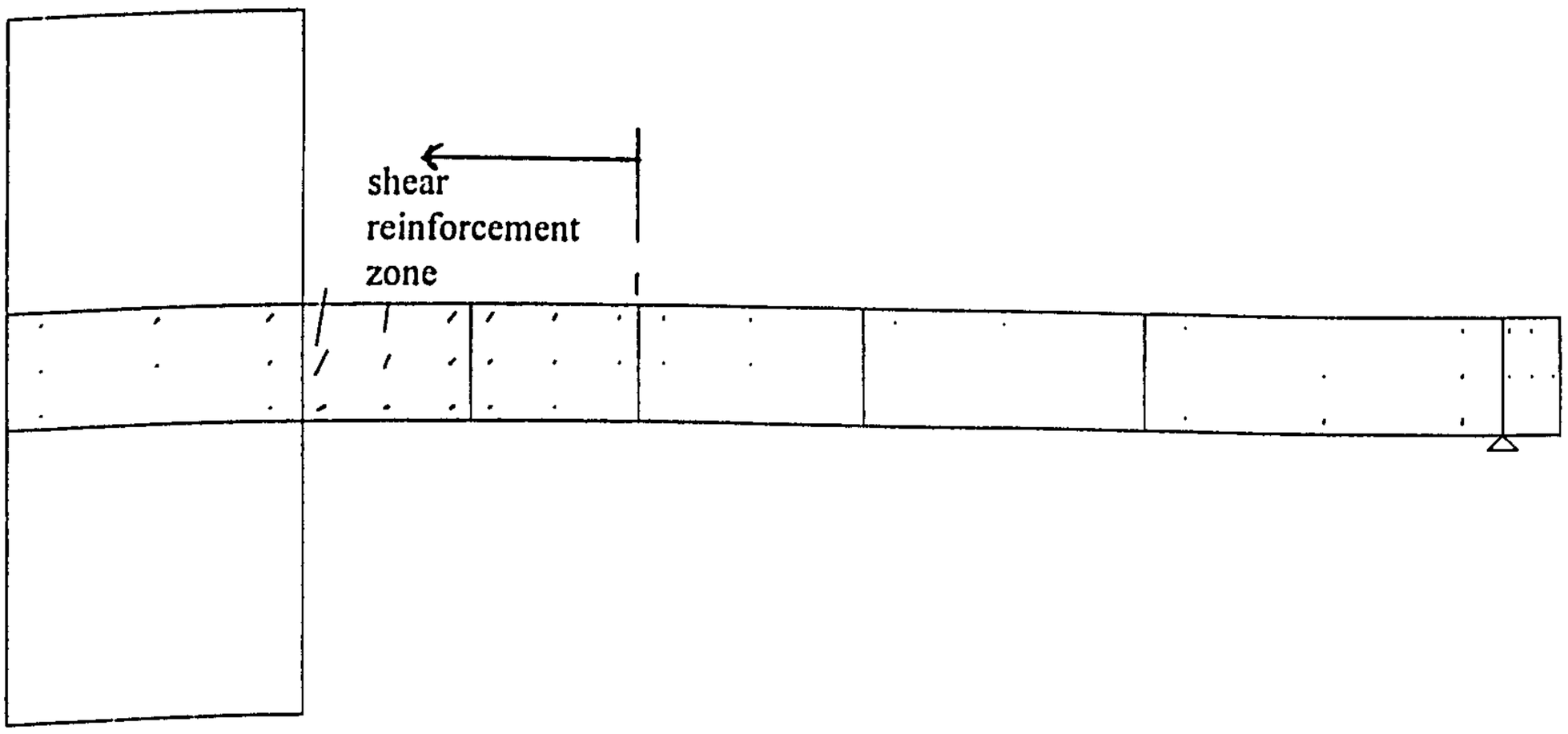

JS2

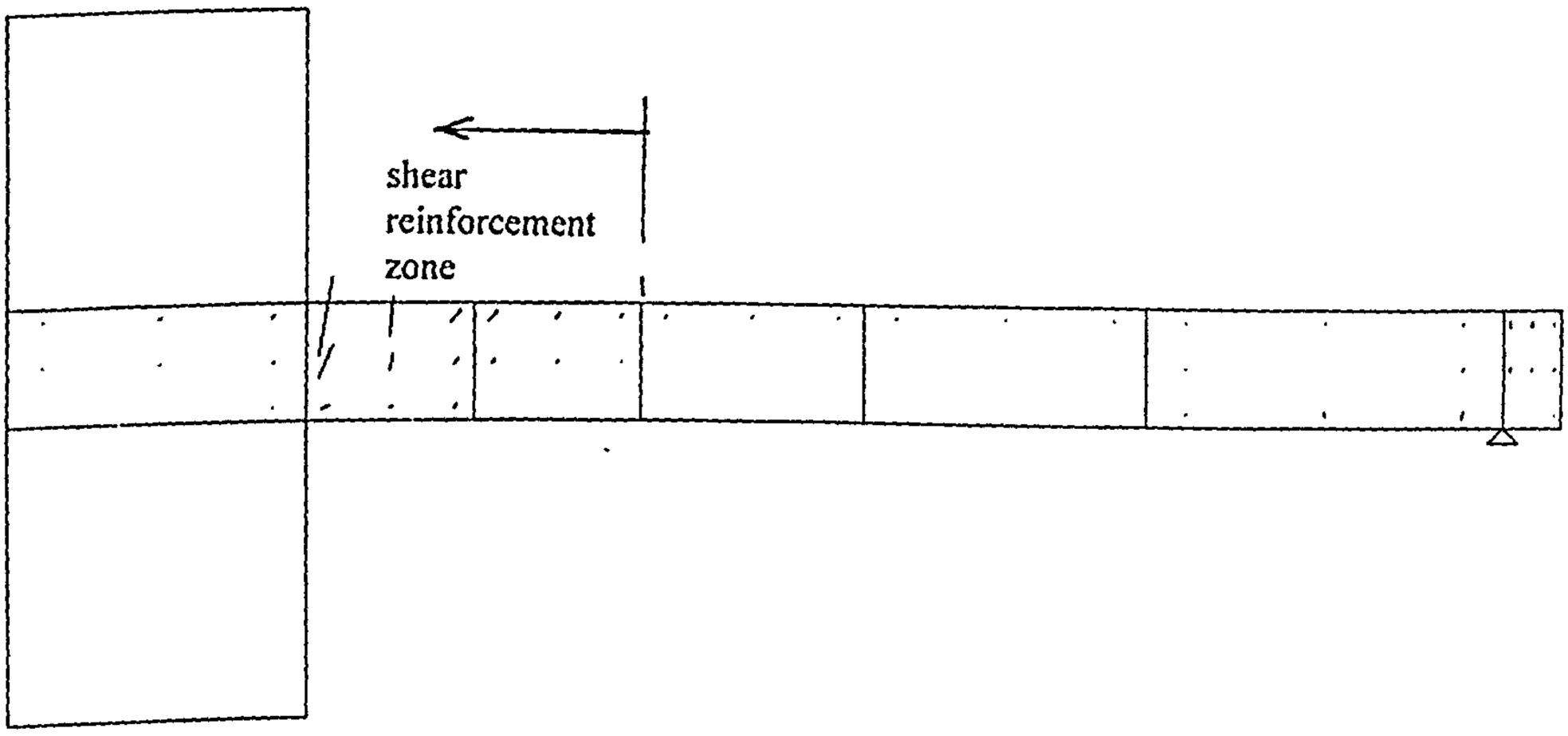

JS3

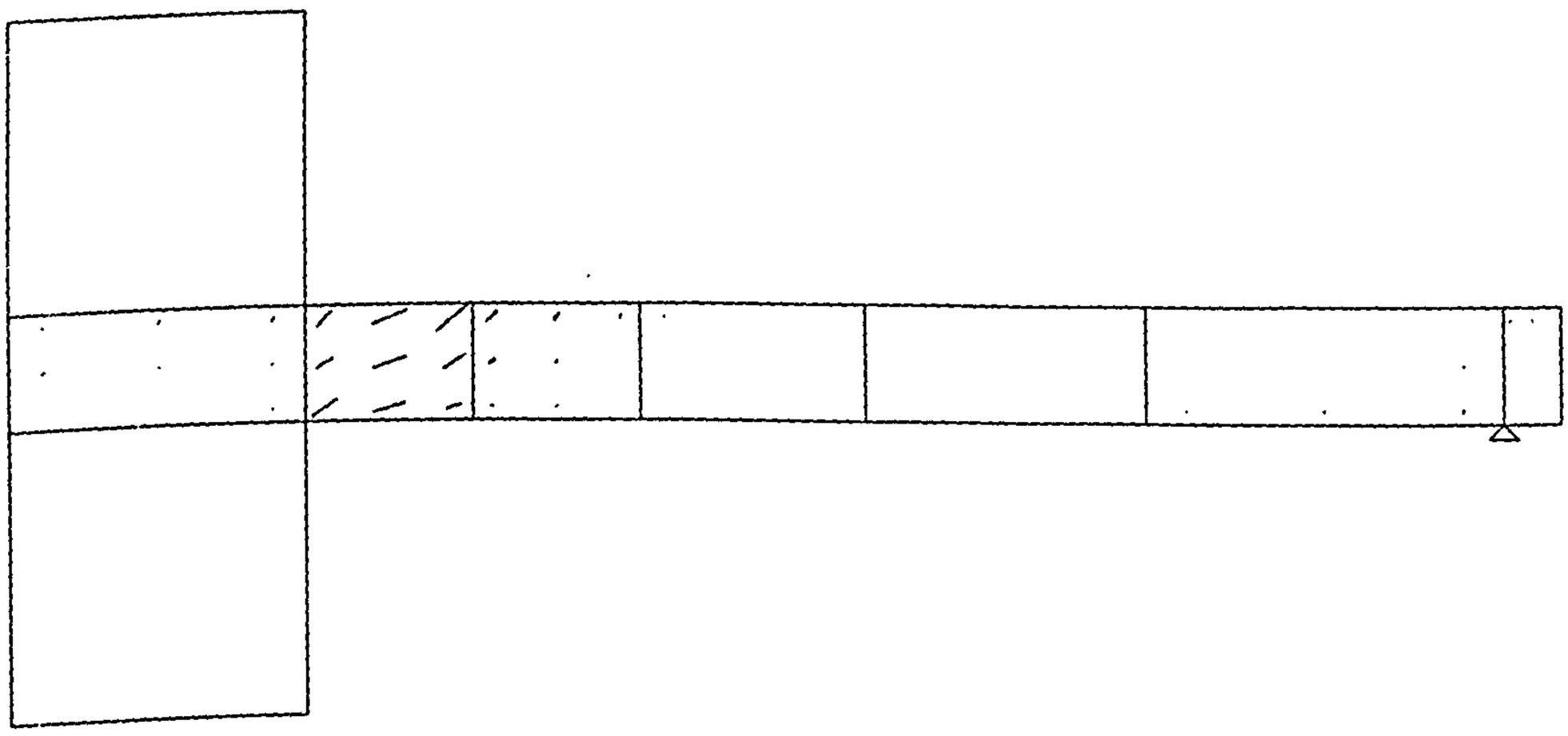

JS4

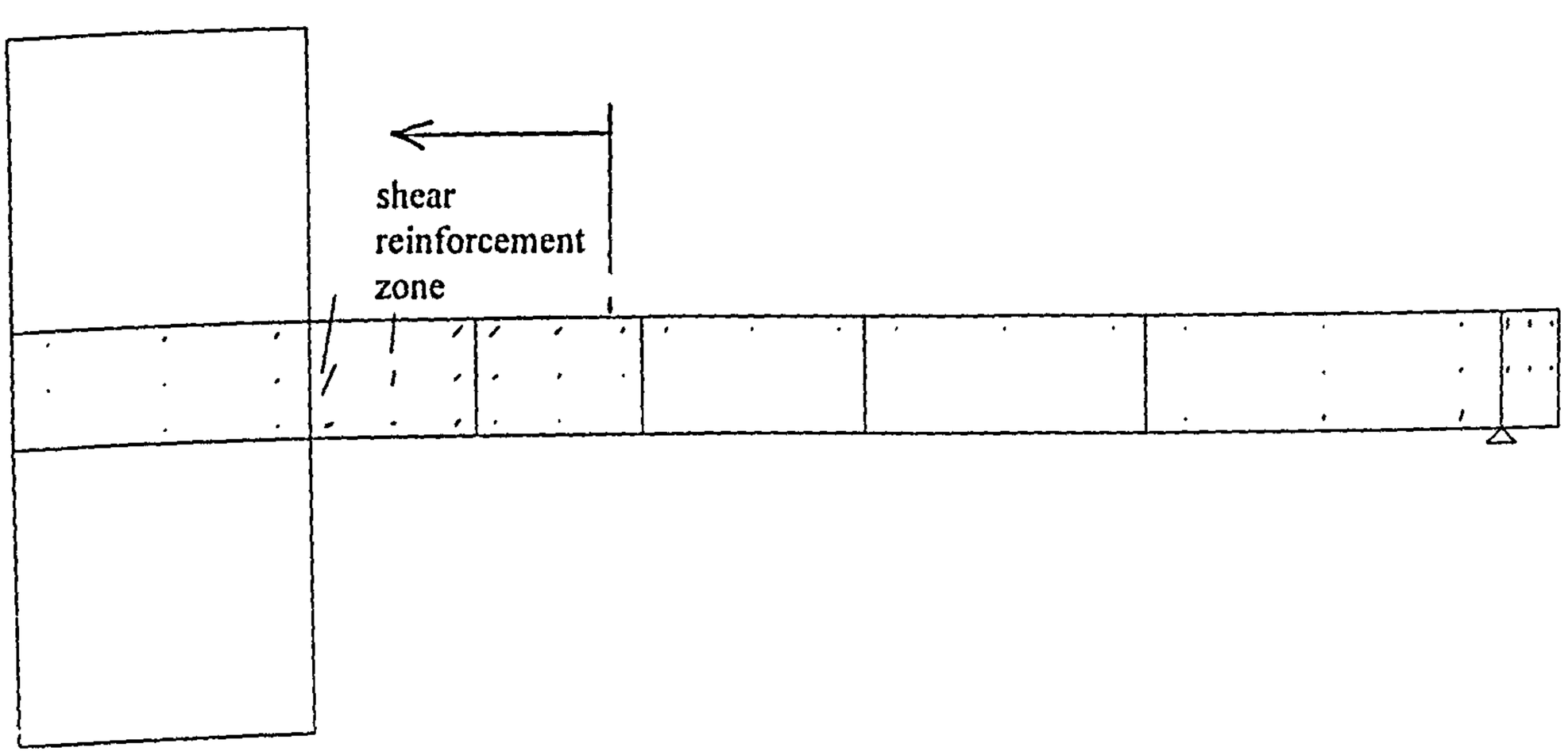

JS5

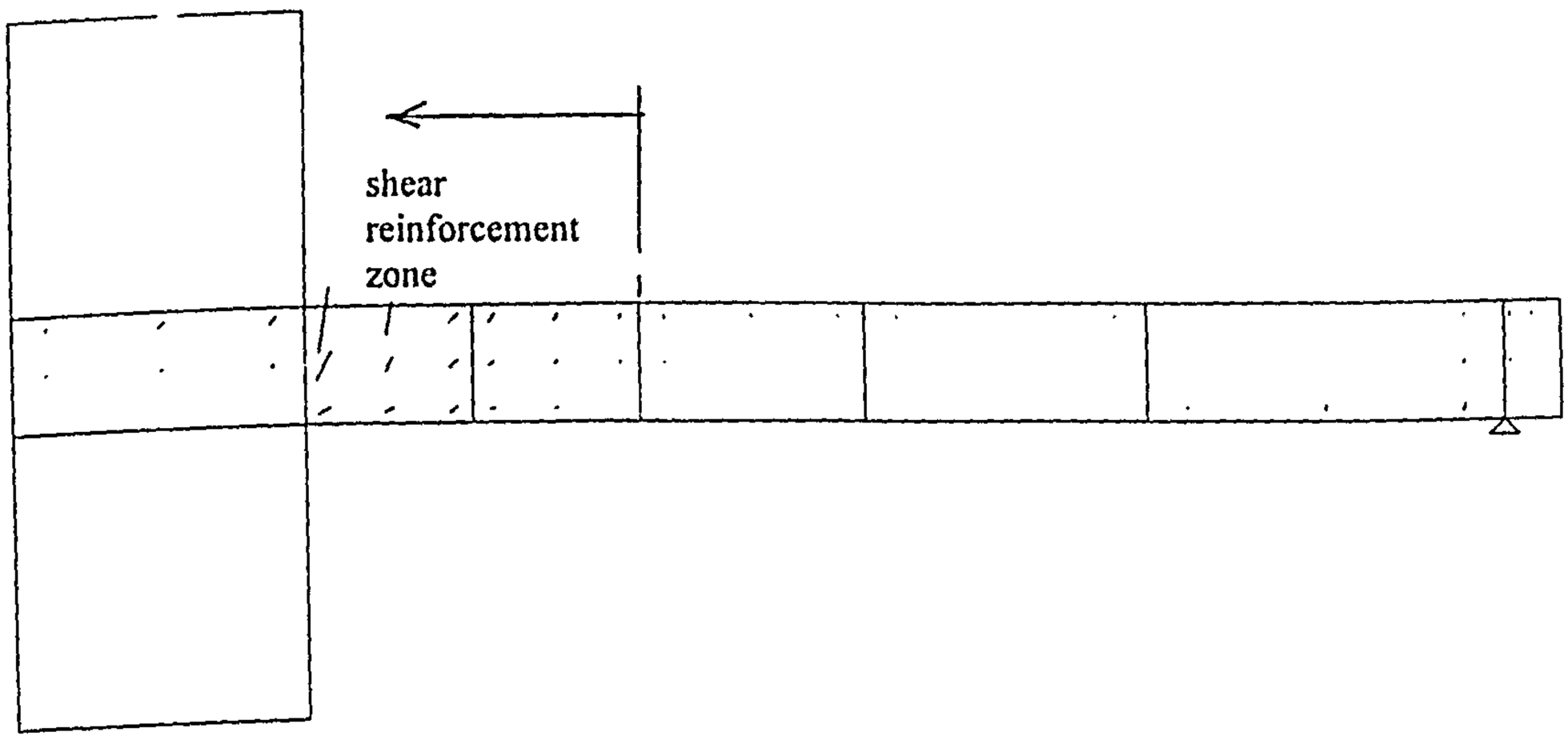

JS6

SC series (Walker)

C2.5 Corner column-slab connections tested by Walker (without shear reinforcement)

	Experimental			Numerical		
Slab	V_{test} (kN)	M_{test} (kNm)	Failure Mode	Num/Exp		Failure Mode
				V	M	
SC1	81.00	36.40	fp	1.100	1.595	fp
SC2	75.00	35.70	s	1.000	1.372	s
SC3	74.00	45.60	fp	0.963	1.038	fp
SC4	64.00	24.00	fp	1.031	1.666	fp
SC5	82.00	26.90	s	1.024	1.579	s
SC7	82.00	39.00	s	1.150	1.150	s
			Average	1.045	1.400	
			STDEV	0.680	0.260	

For yielding of flexural reinforcement

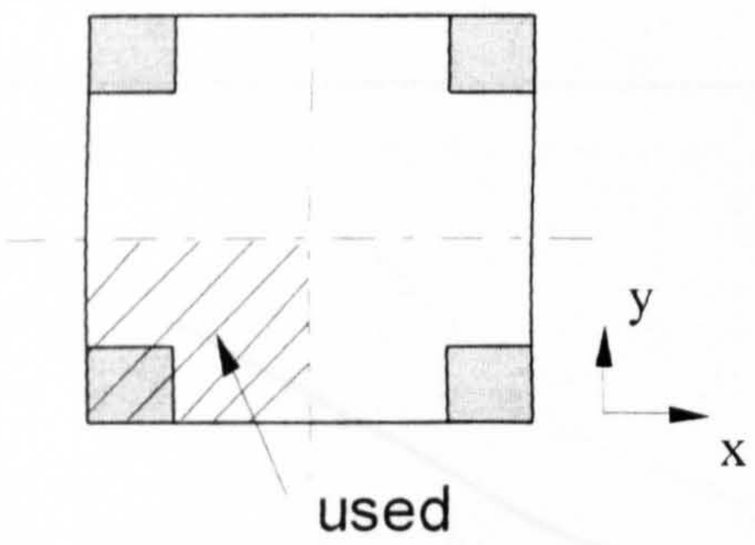

For crack pattern,

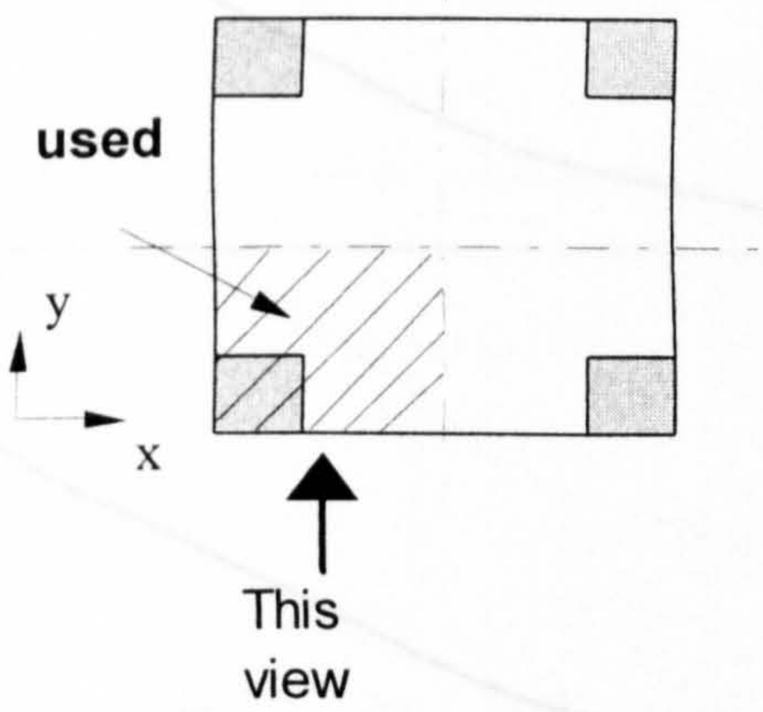

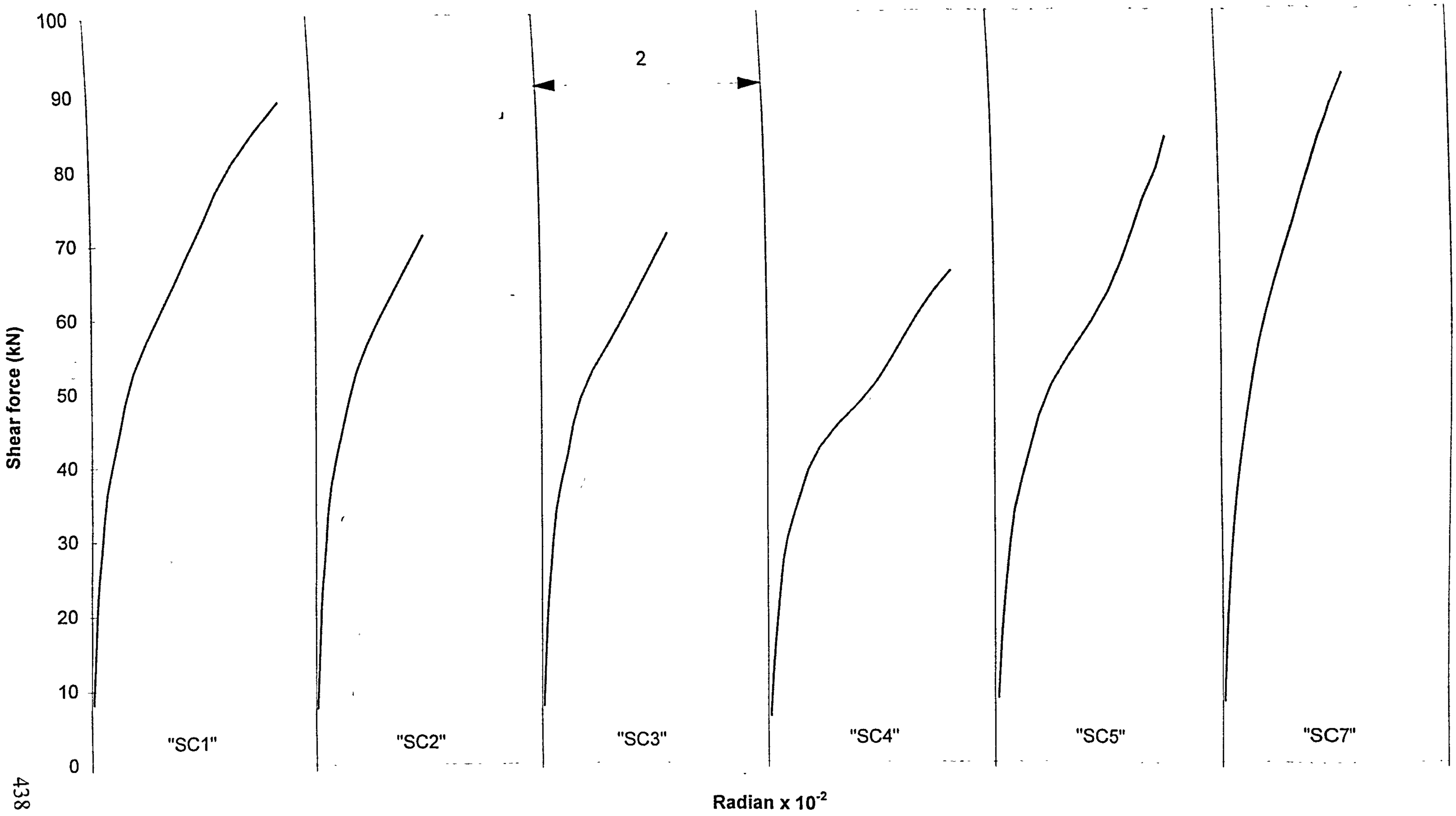

Predicted load-rotation response for slabs SC1-SC7

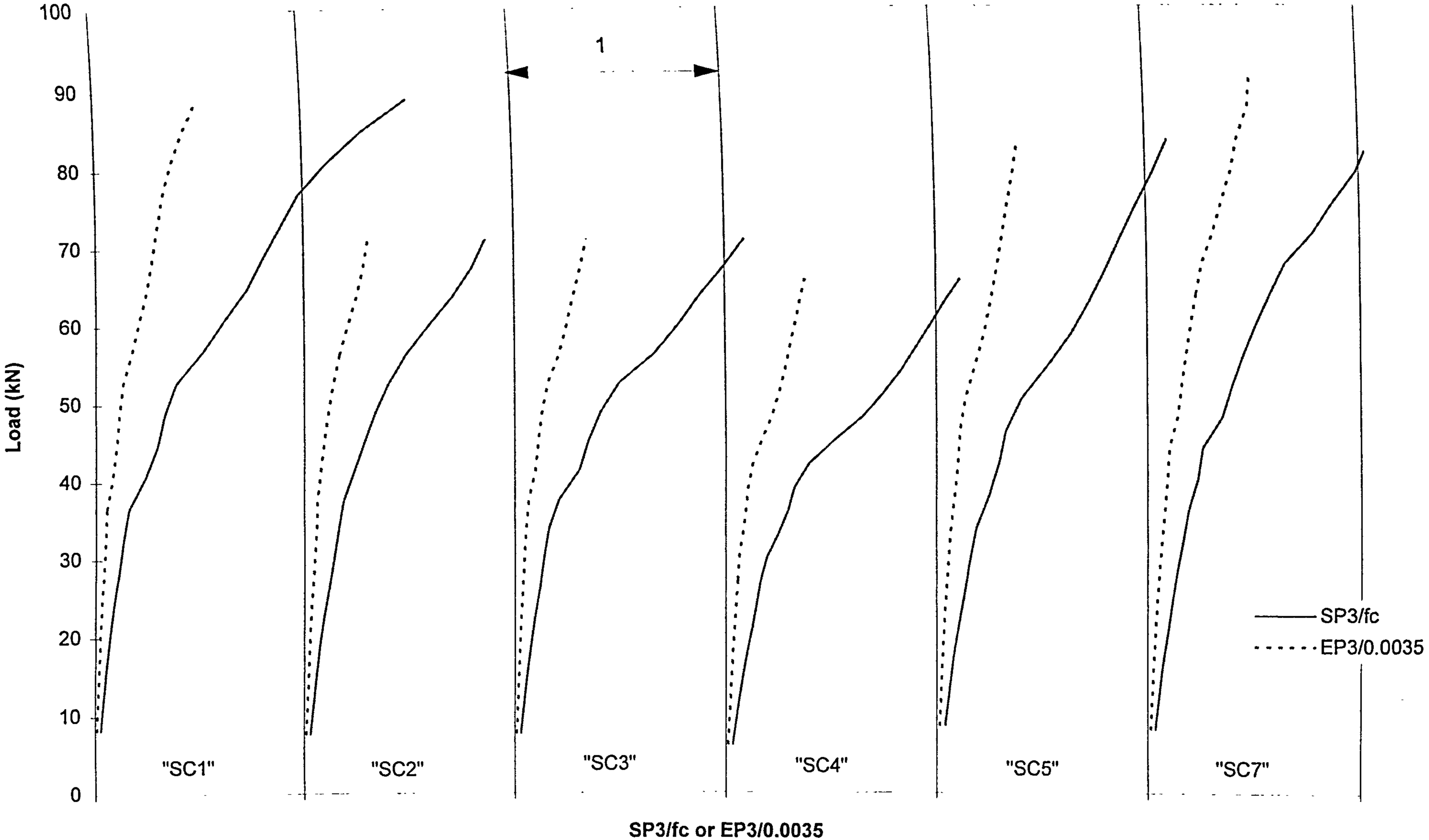

Predicted principal compressive stress and strain in concrete (slabs "SC1" - "SC7")

Yielding of tension steel, SC series (Walker)

NB. : The numbers on the drawing indicate strain in steel at collapse expressed as a ratio of yield strain

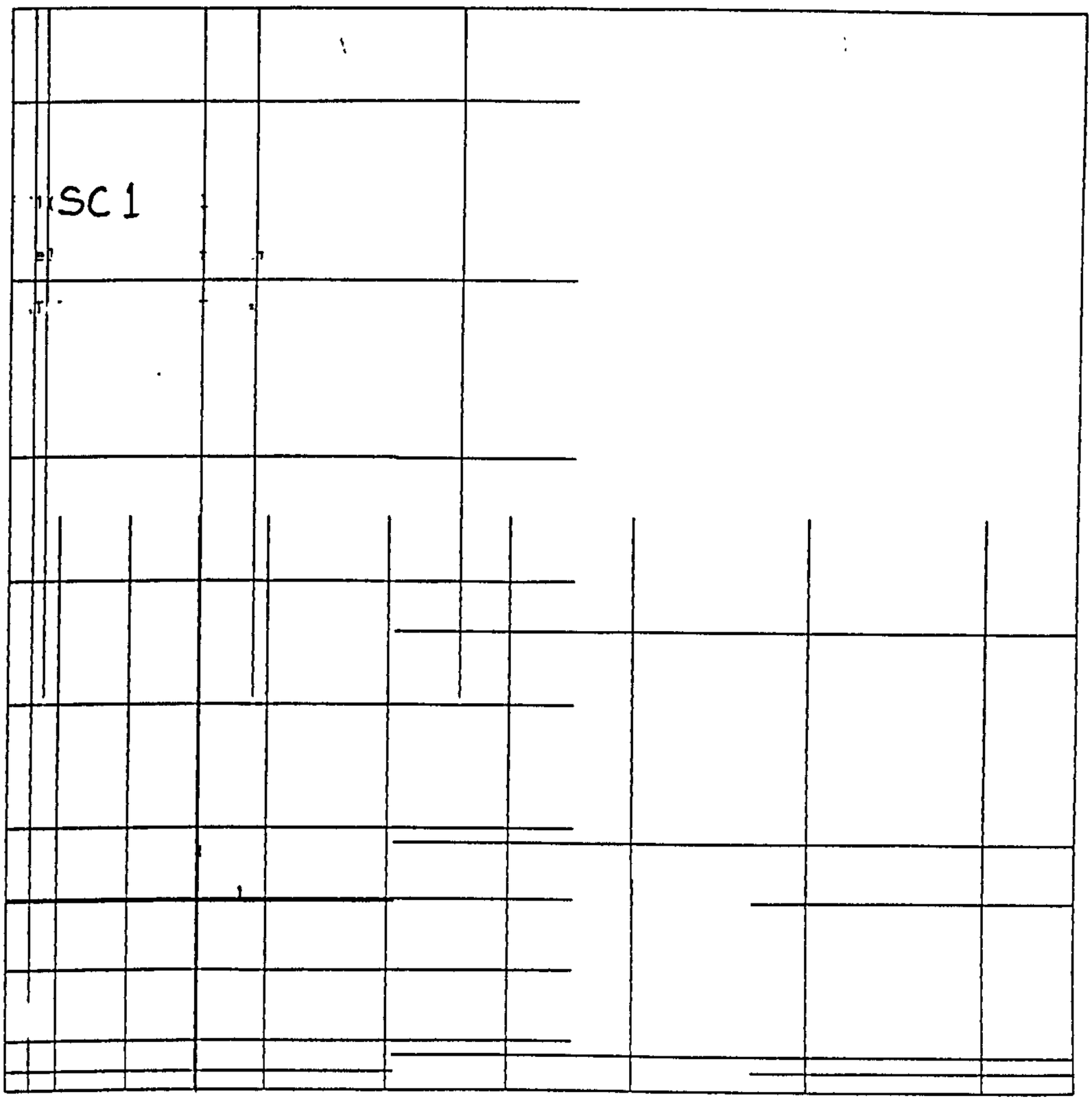

SC1

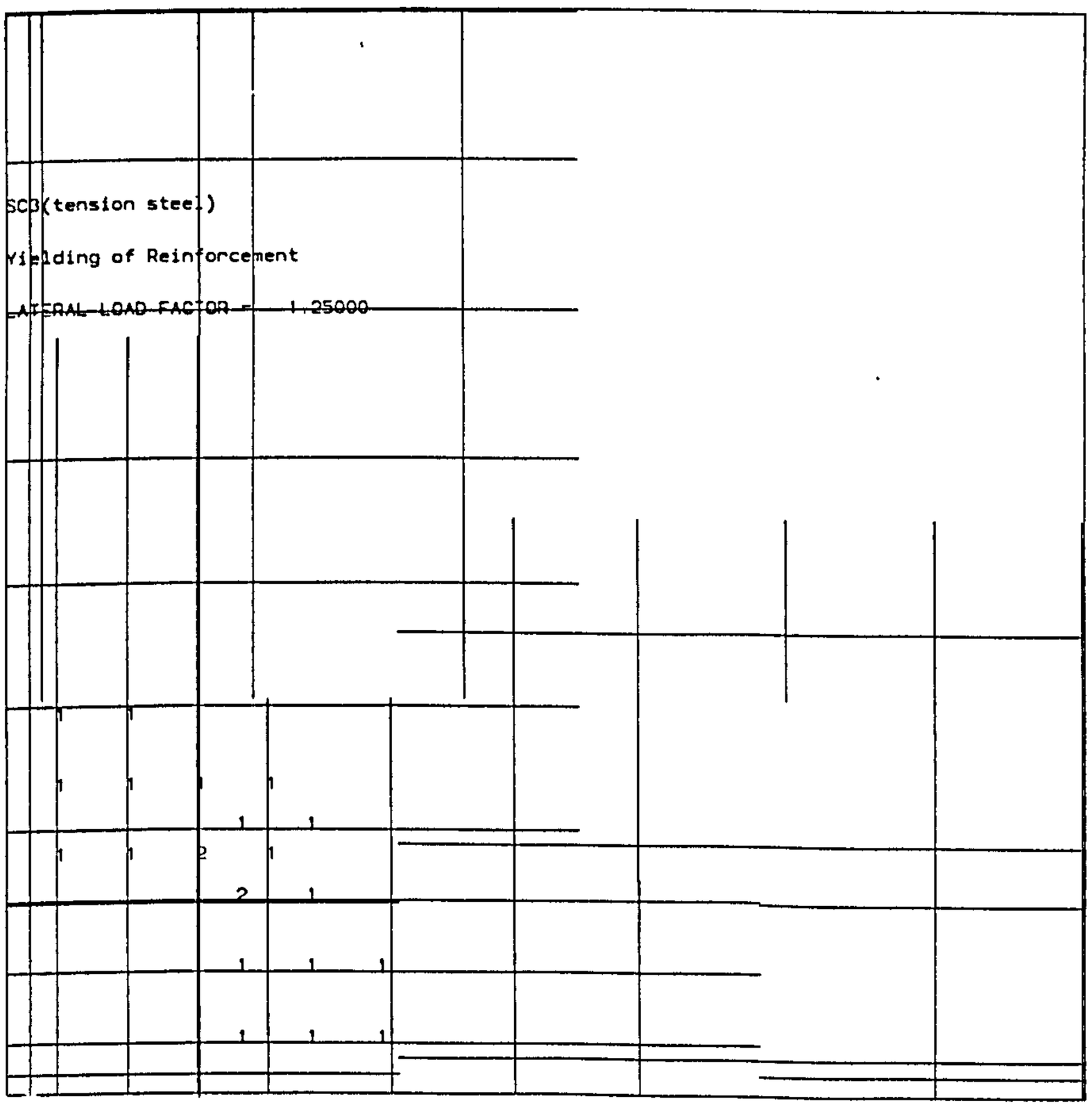

SC3

"SC4"(tension steel)

Yielding of Reinforcement

LATERAL J

SC4

SC5 (tension steel)

Yielding of Reinforcement

LATERAL LOAD FACTOR = 0 95000

SC5

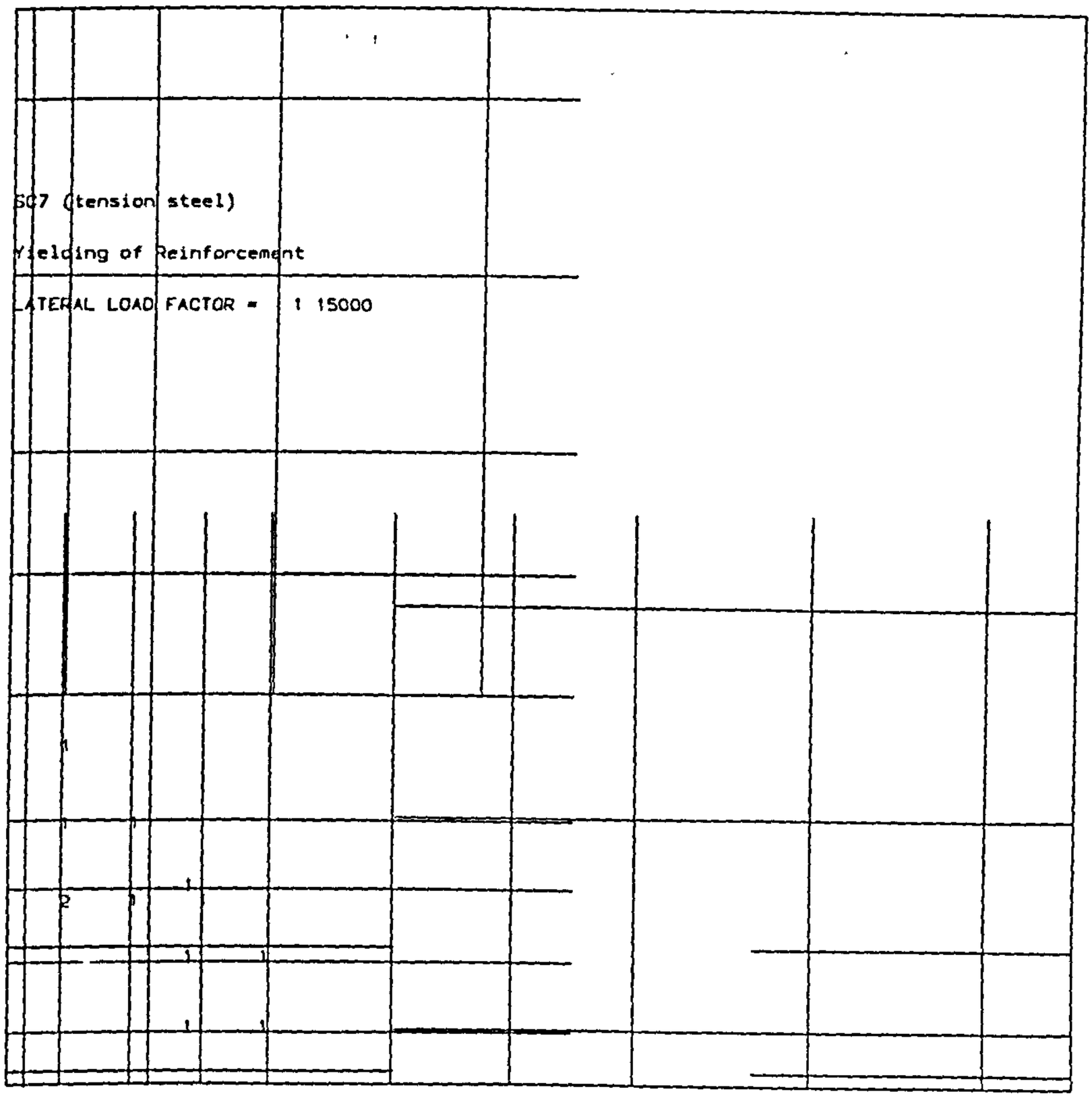

SC7

Note

Tension steel in slab **SC2** did not yield.

Predicted crack pattern for SC series (Walker)

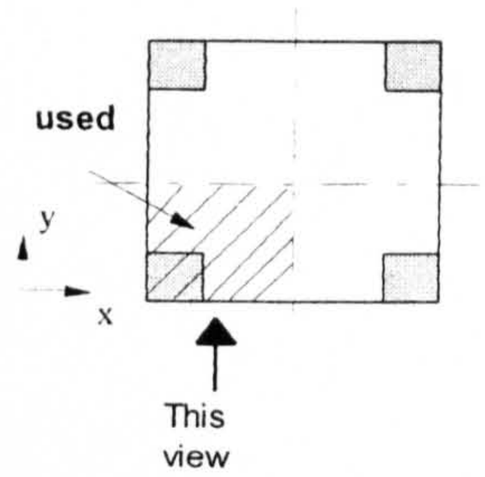

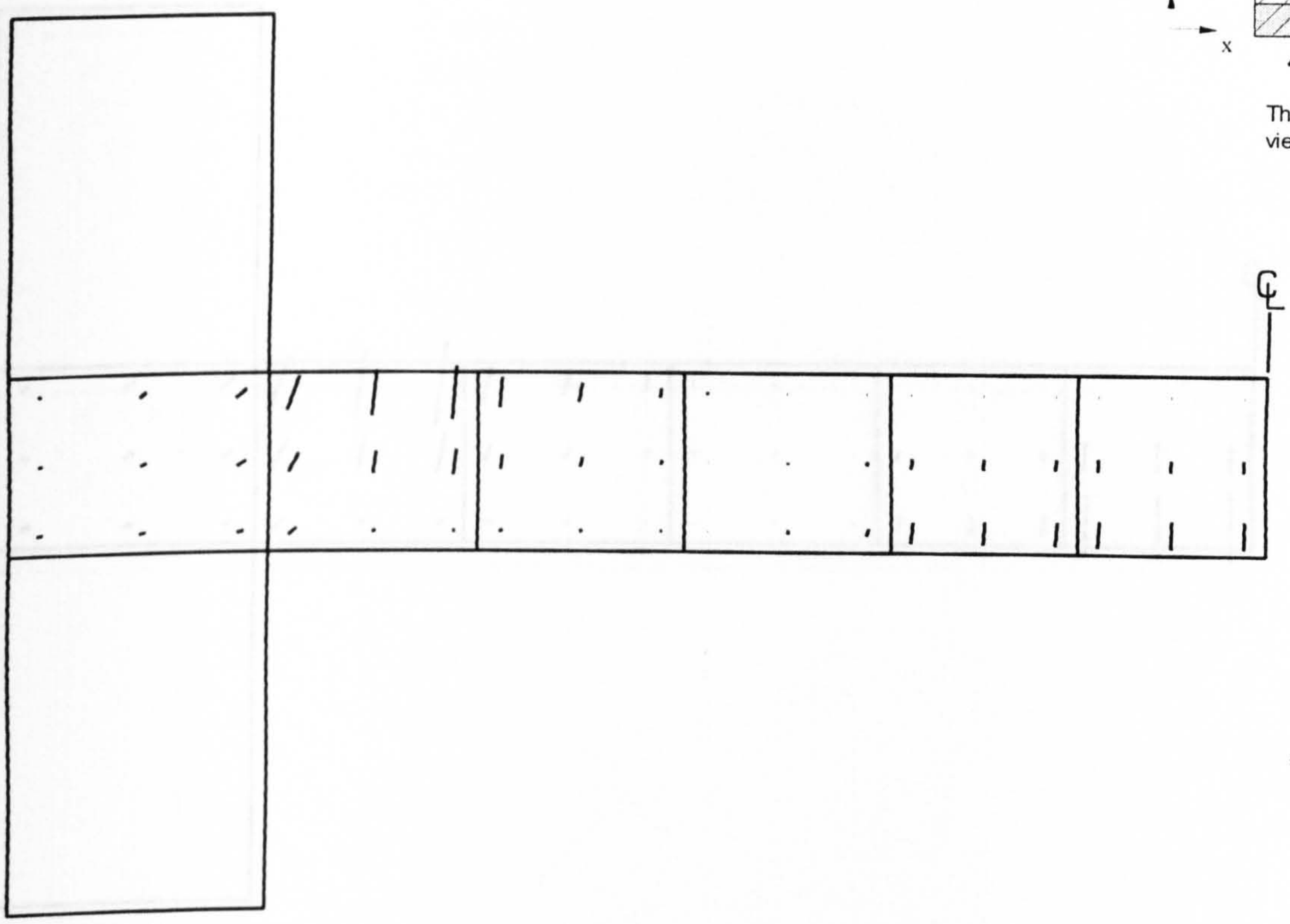

SC1

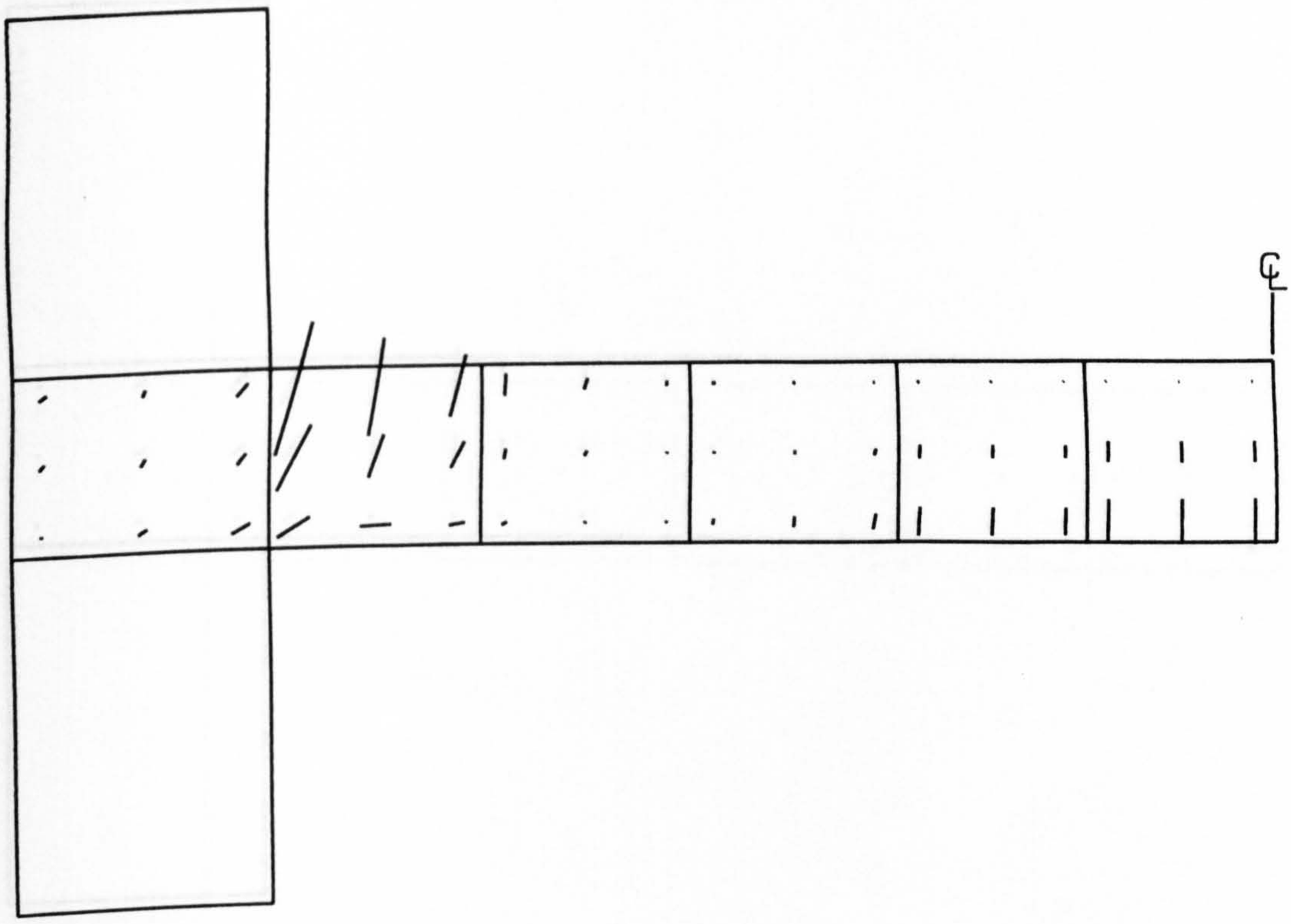

SC2

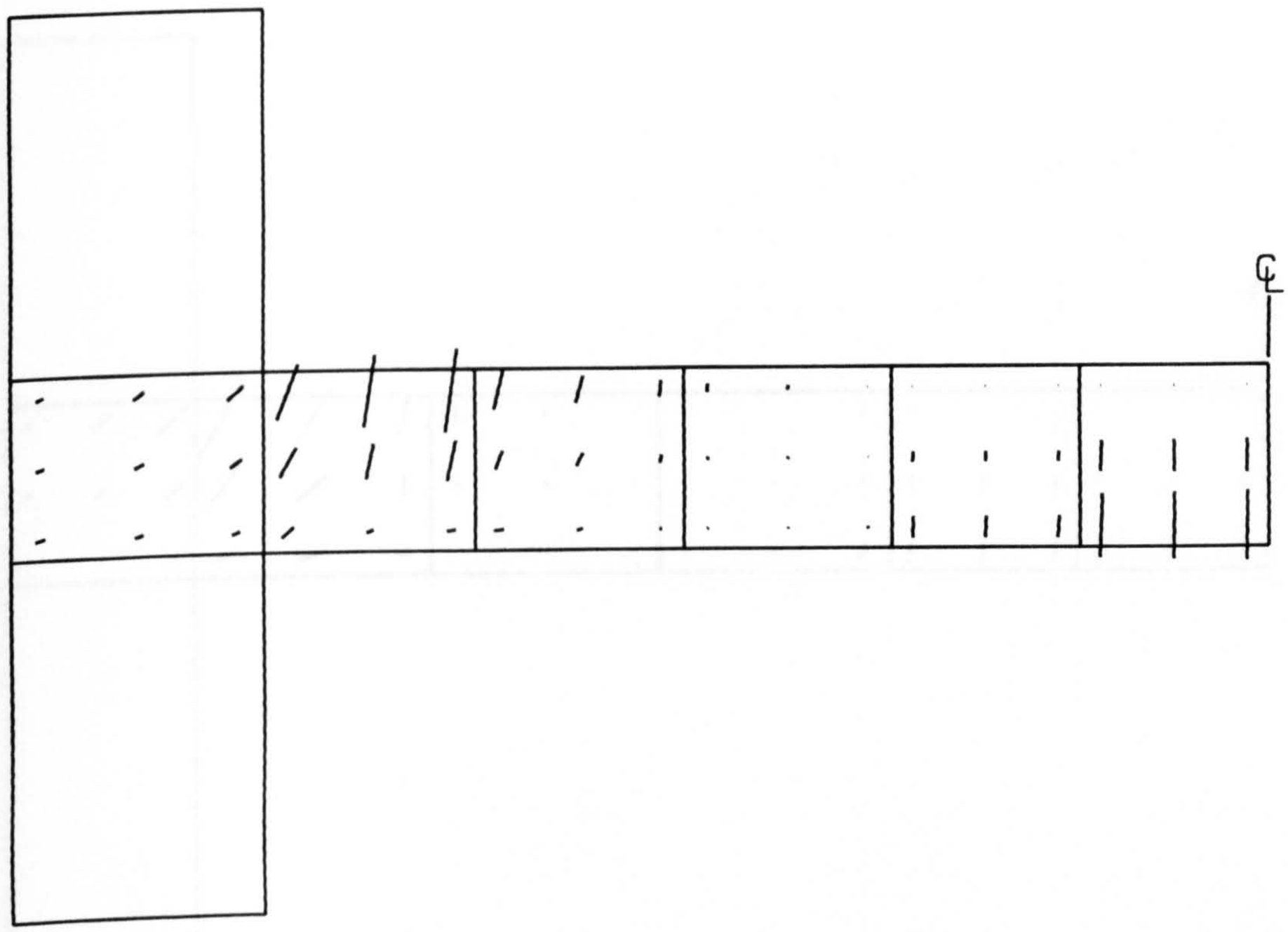

SC3

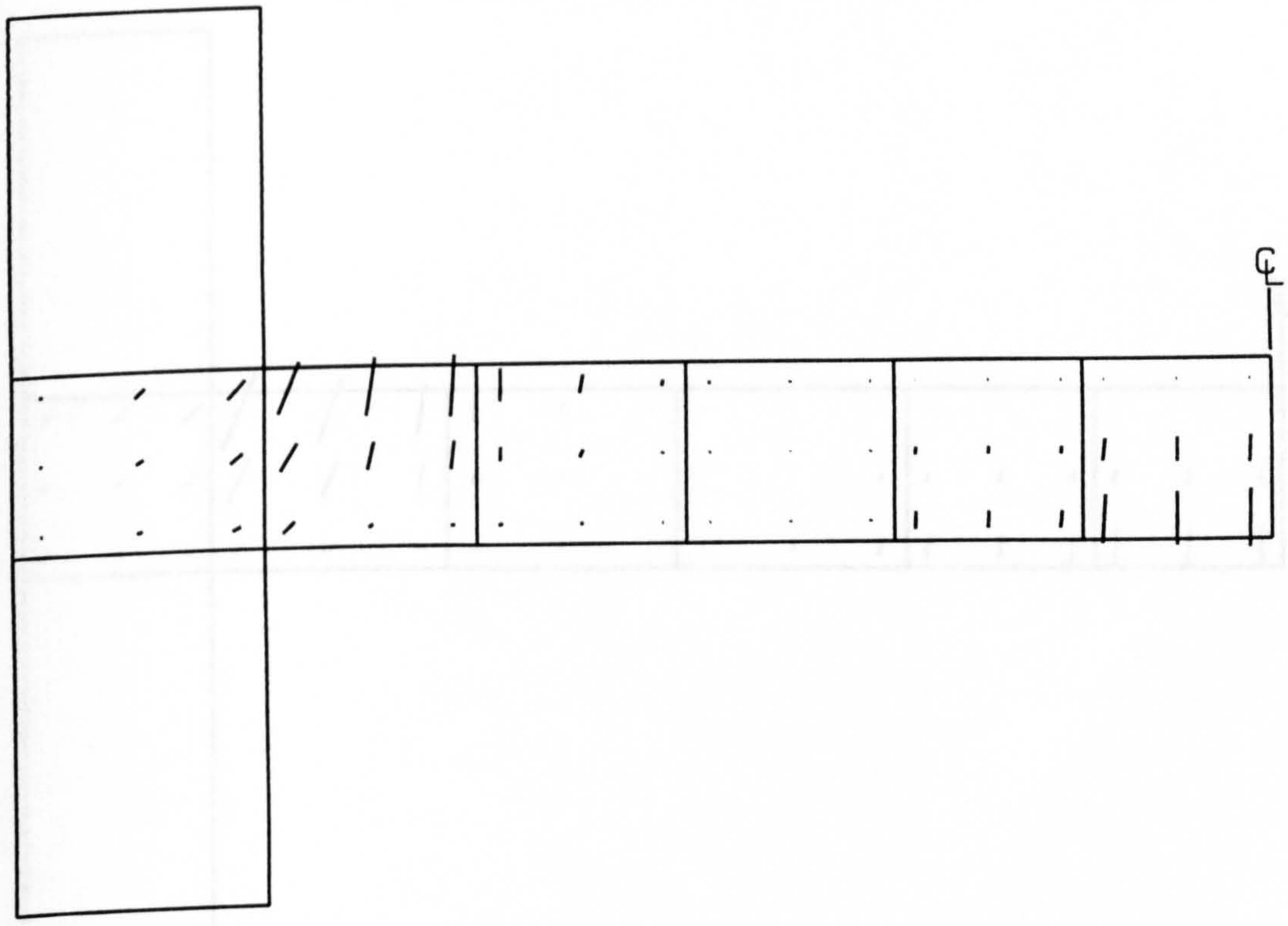

SC4

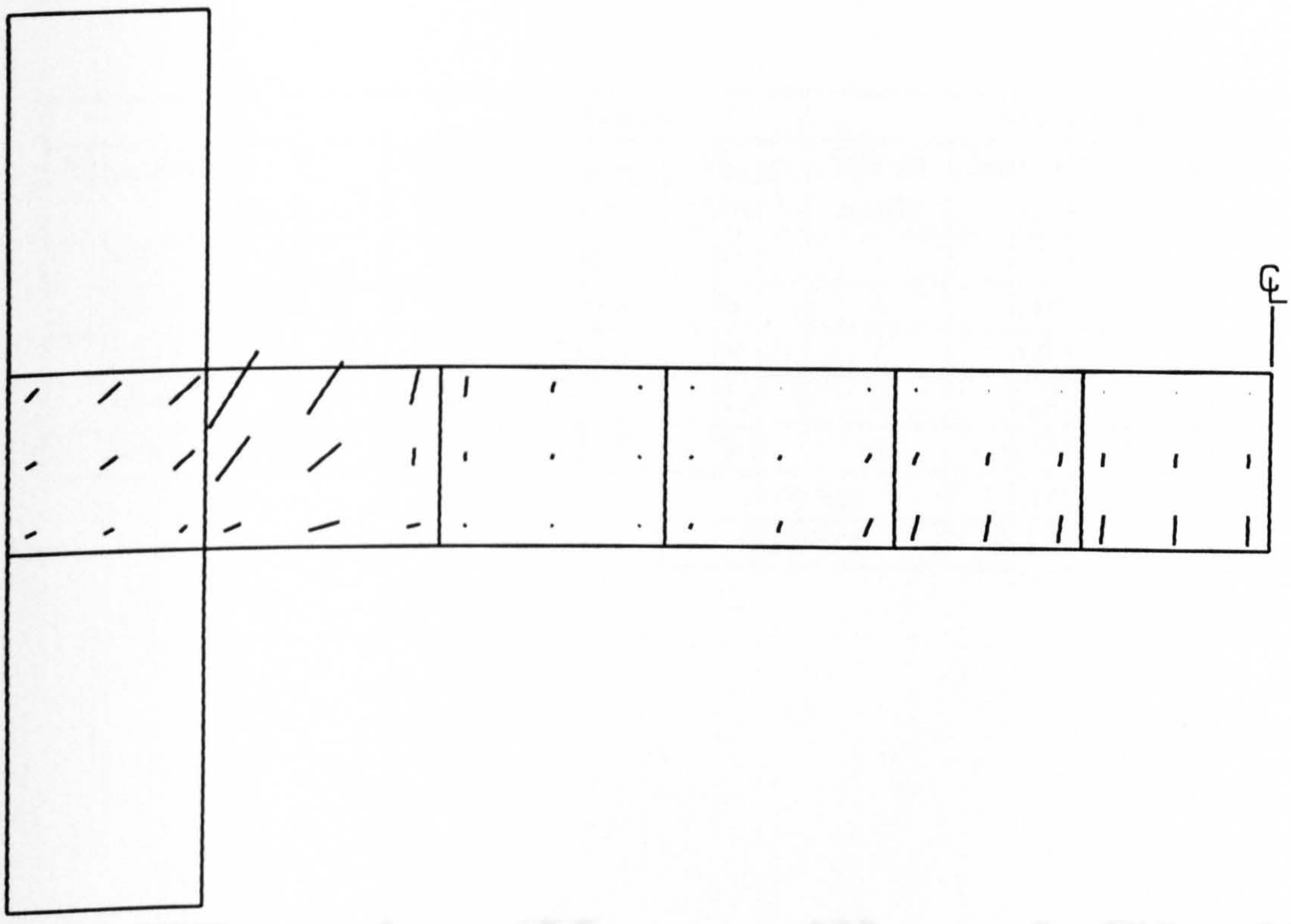

SC5

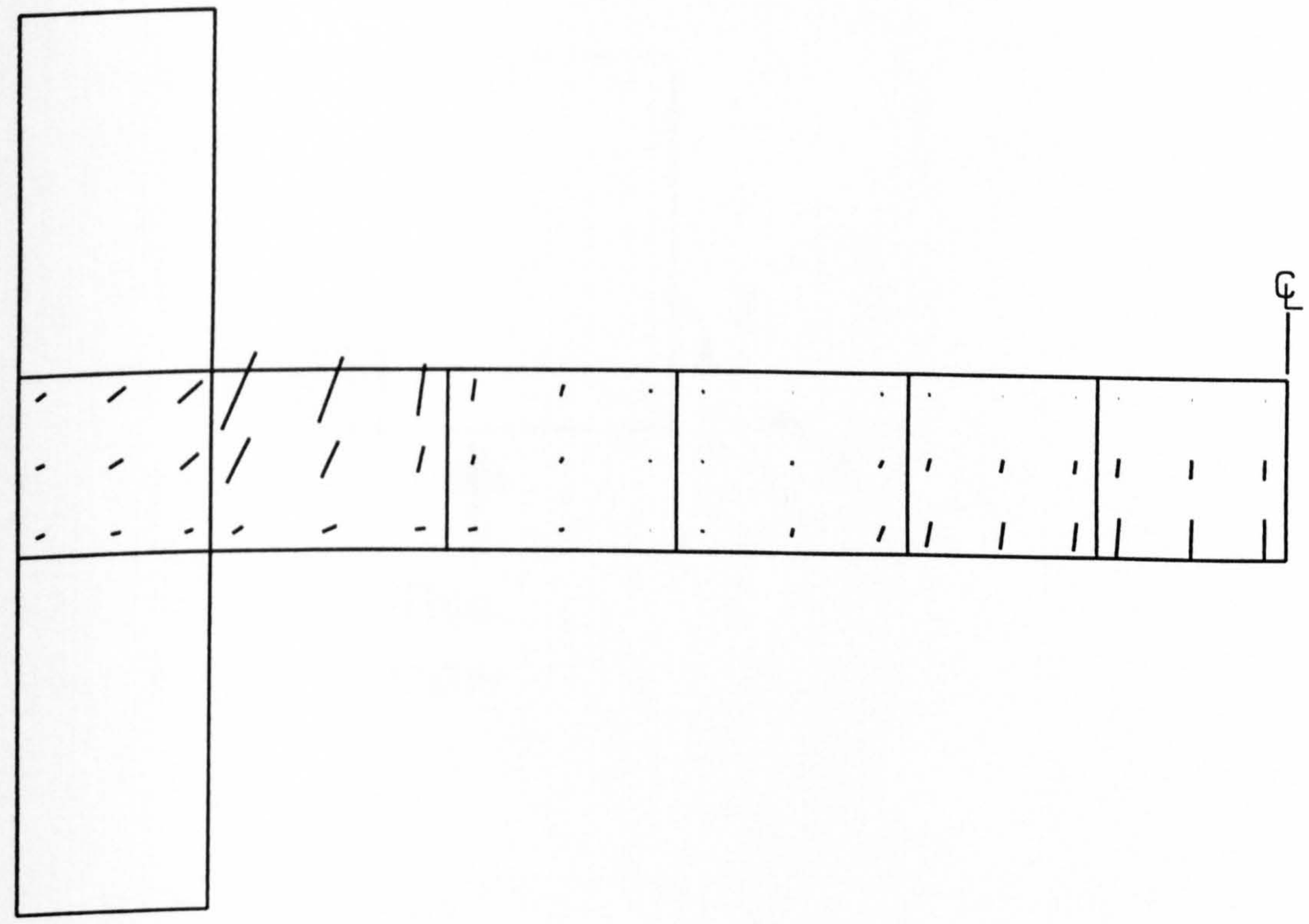

SC7

NH series (Hammill and Ghali)

C2.6 Corner column-slab connections with shear reinforcement (Hammill and Ghali)

	Test results					Numerical results	
Specimen	f_c' N/mm^2	Applied forces	V_{test} (kN)	M_{test} (kNm)	failure mode	Num/Exp ratio	failure mode
NH1	41.50	V,M	146.9	60.8	s	0.90	s
NH2	42.20	V,M	139.1	56.9	s	1.05	s
NH3	36.40	V,M	146.1	58.4	s	0.95	s
NH4	36.90	M	0	46.6	s	1.20	s
NH5	33.20	V,M	179.0	79.0	s	0.90	s
				Average		1.00	
				STDEV		0.127	

For yielding of flexural reinforcement and crack pattern,

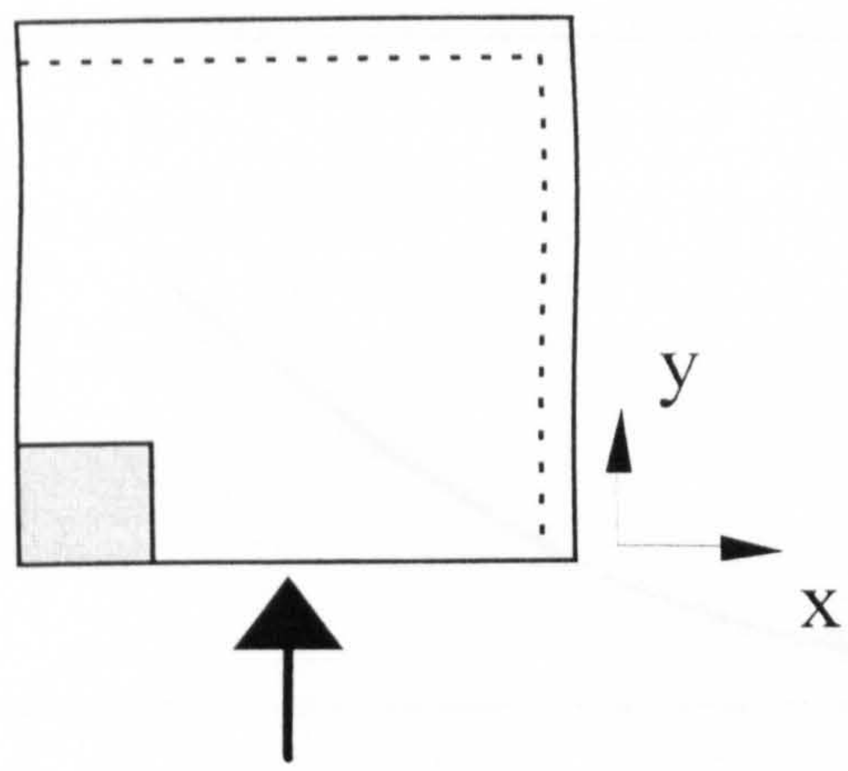

This
view

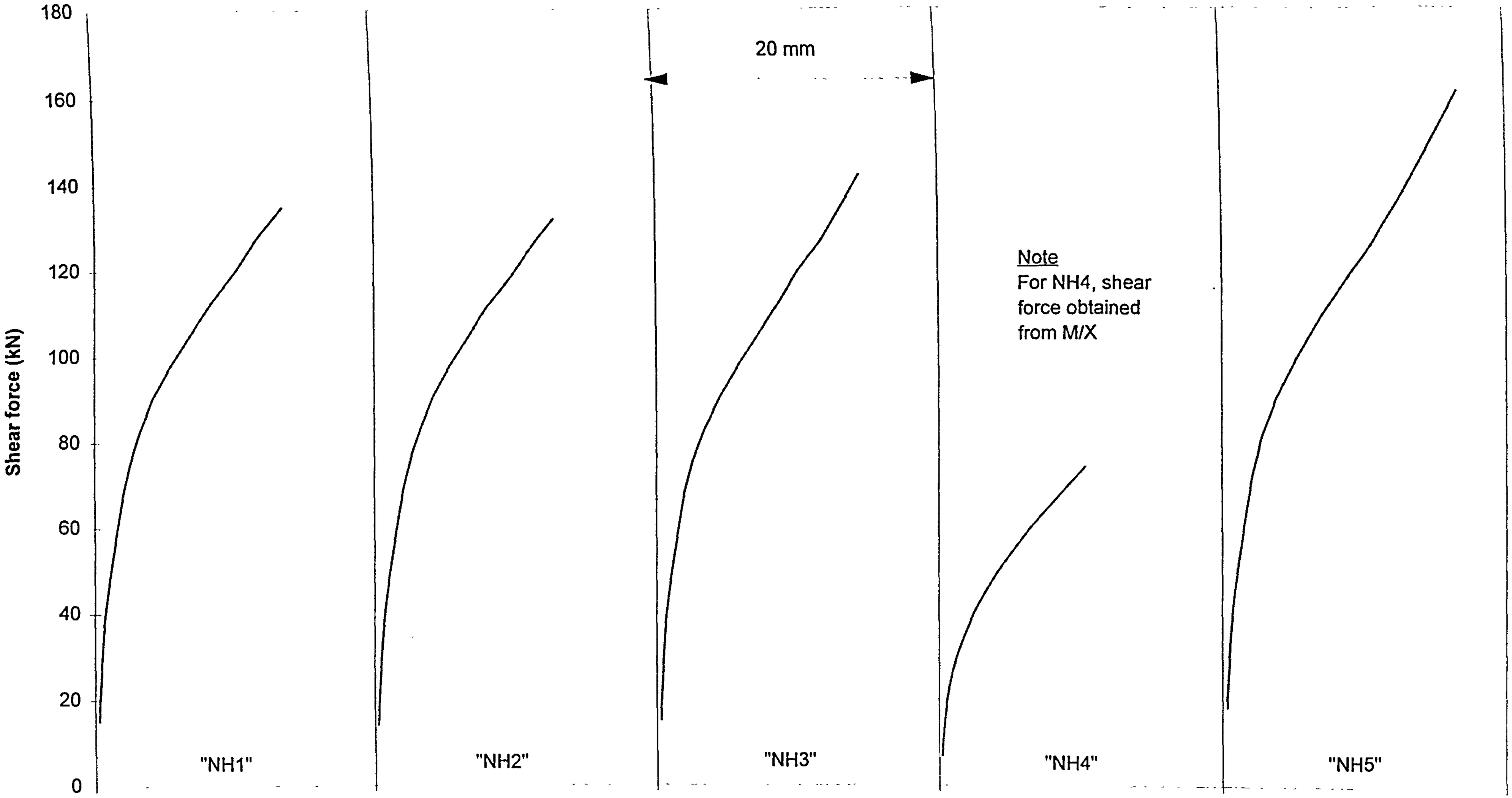

Predicted load-deflection response for slabs NH1-NH5

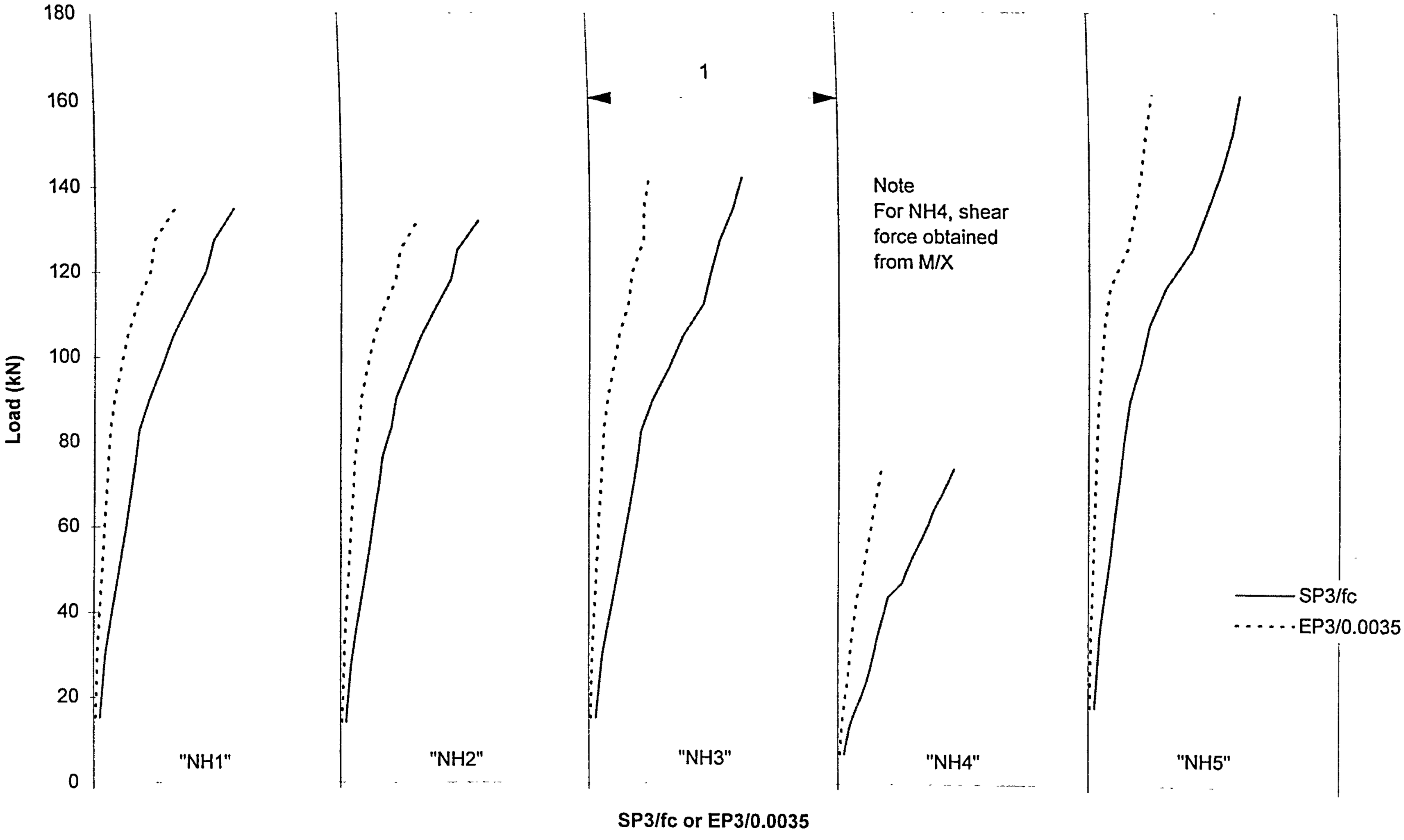

Predicted principal compressive stress and strain in concrete (slabs "NH1" - "NH5")

Yielding of tension steel, NH series (Hammil and Ghali)

NB. : The numbers on the drawing indicate strain in steel at collapse expressed as a ratio of yield strain

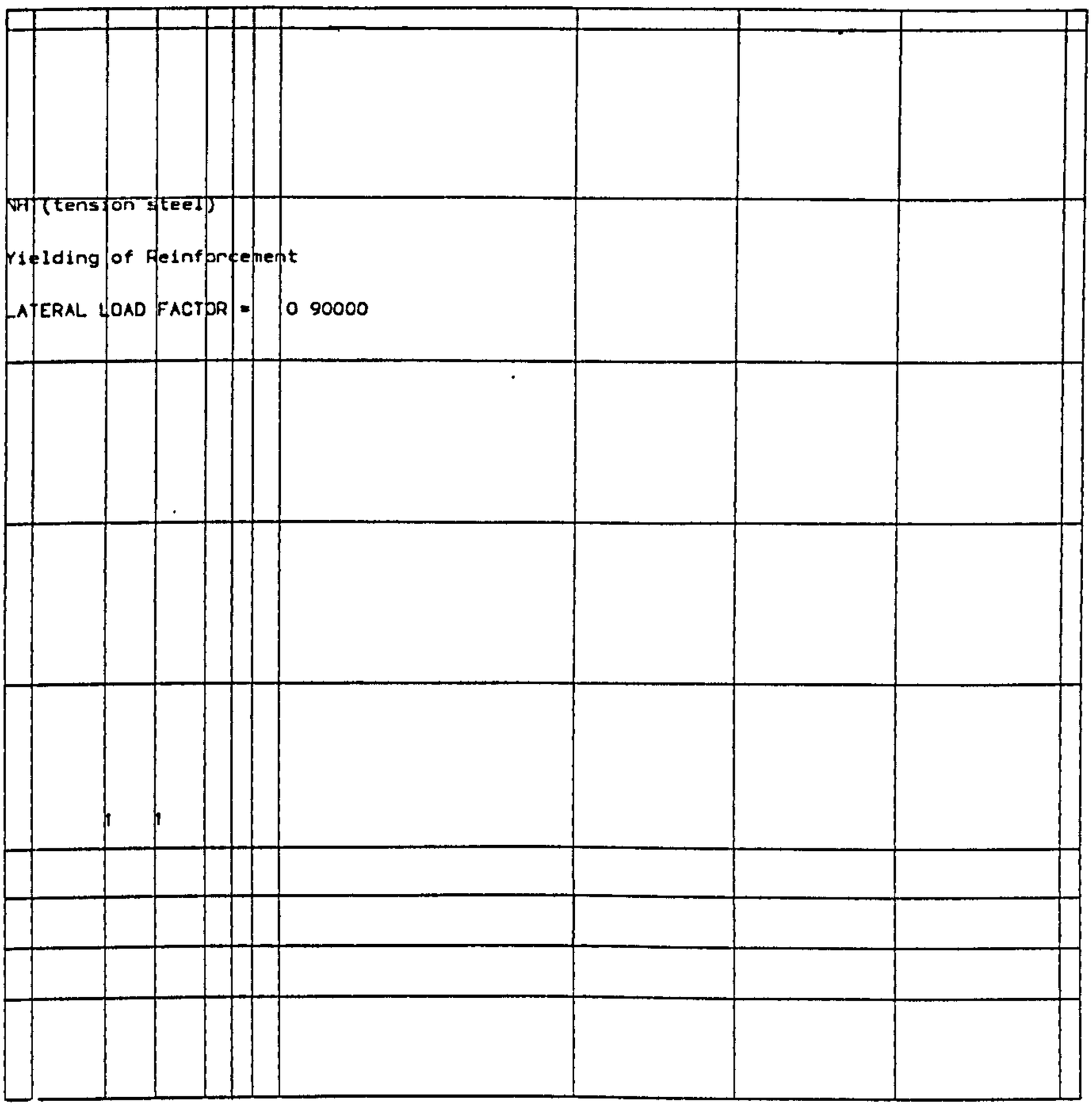

NH1

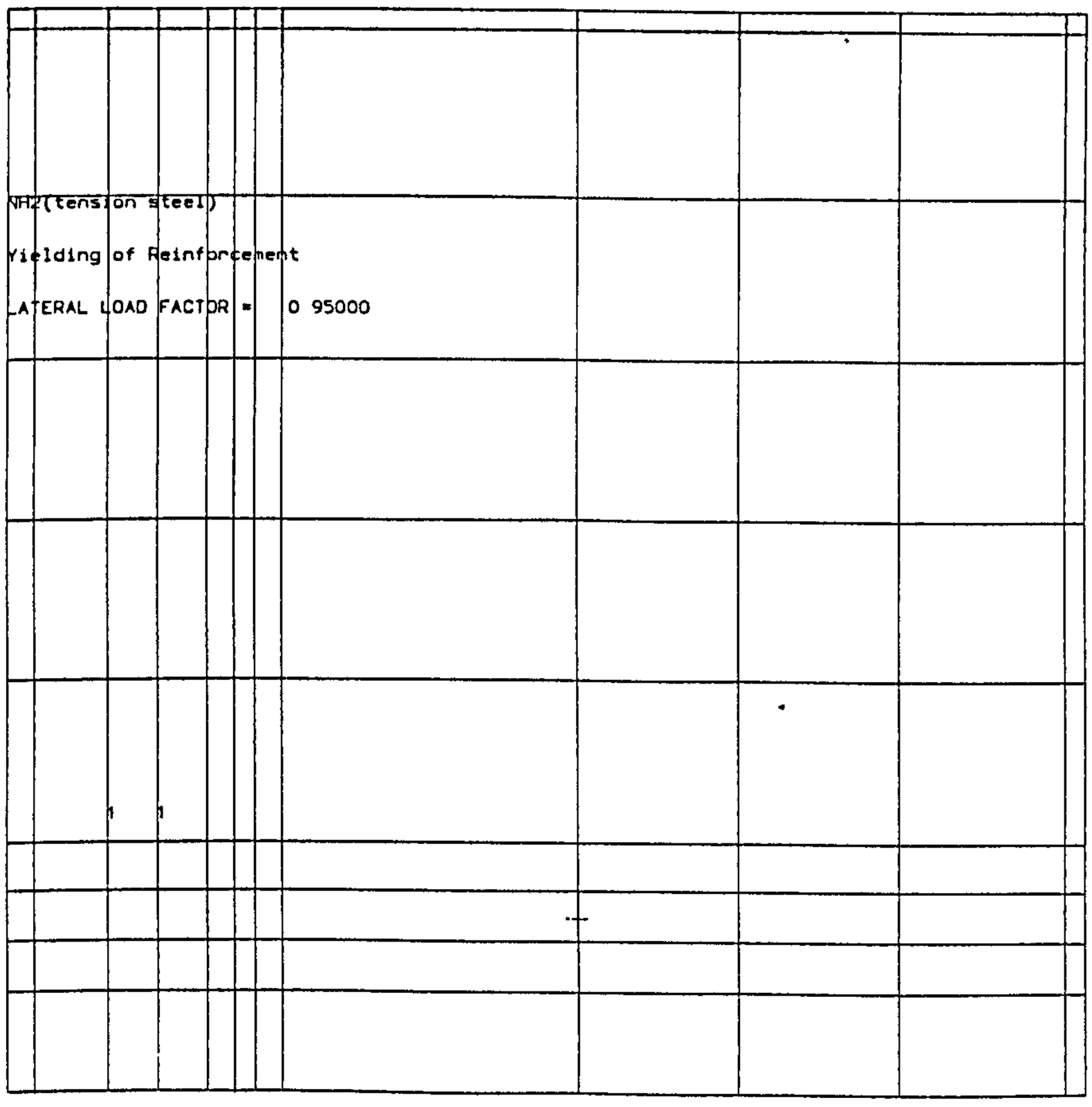

NH2

NH3(tension steel)

Yielding of Reinforcement

LATERAL LOAD FACTOR = 1 05000

NH3

NH4(tension steel)

Yielding of Reinforcement

LATERAL LOAD FACTOR = 1 20000

NH4

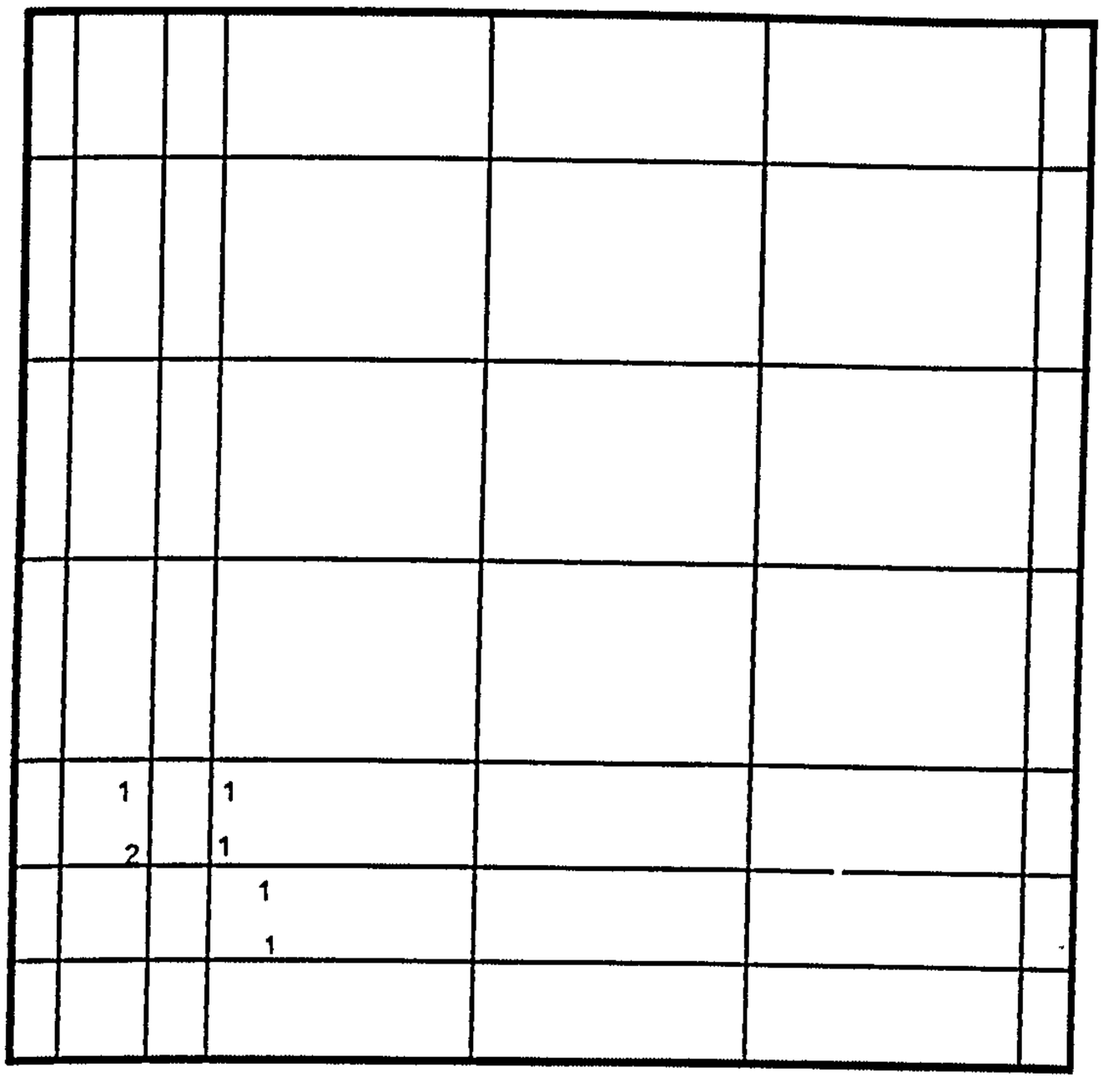

NH5

Predicted crack pattern for NH series (Hammill and Amin)

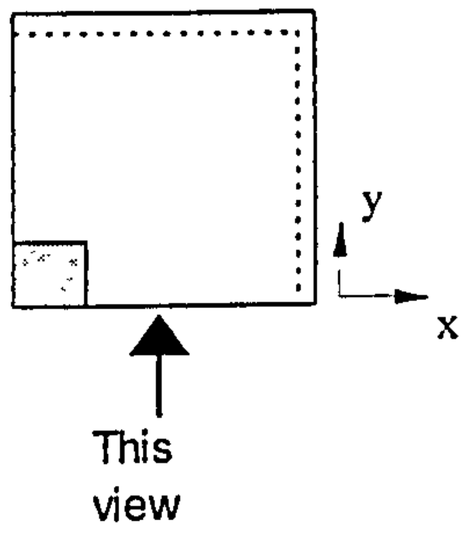

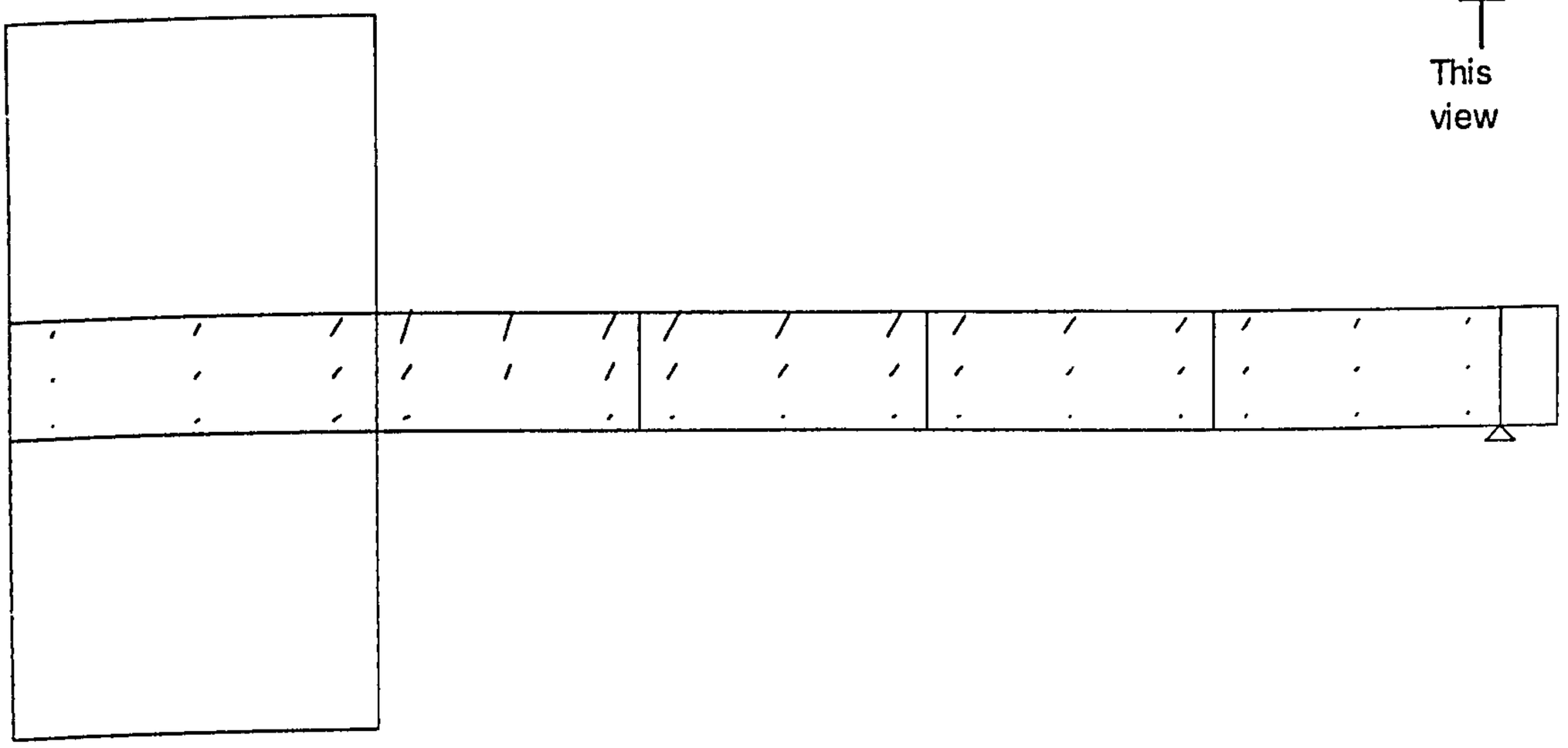

NH1

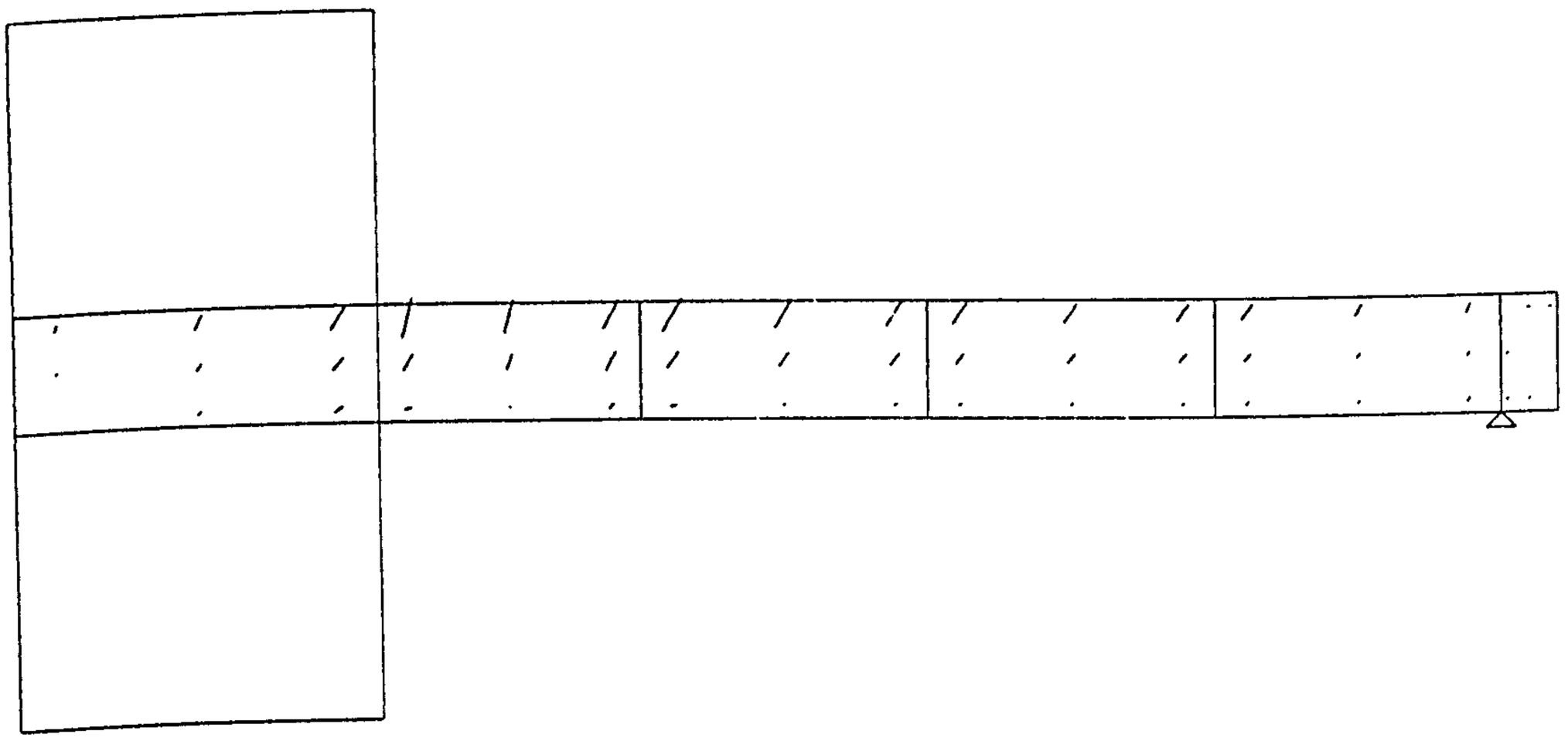

NH2

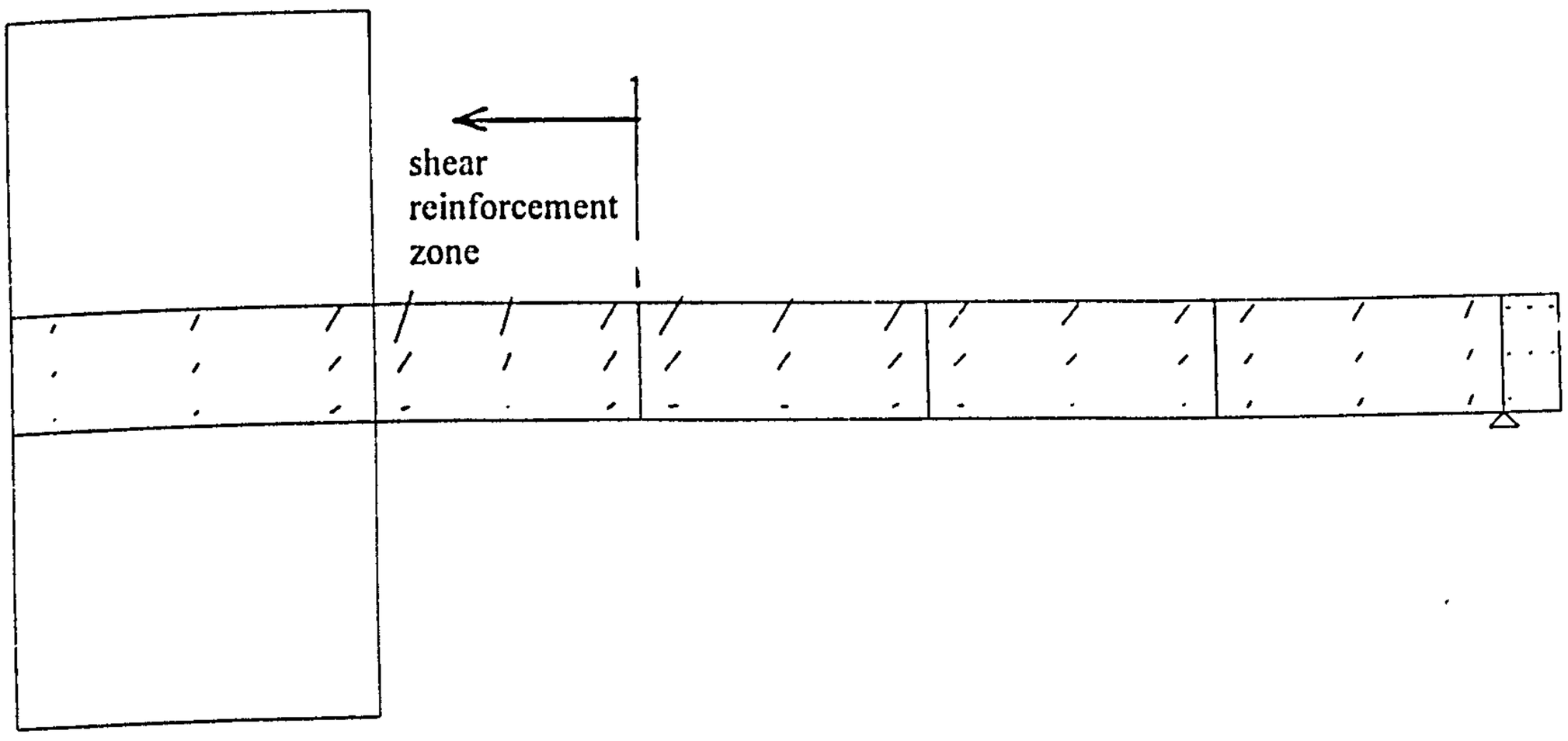

NH3

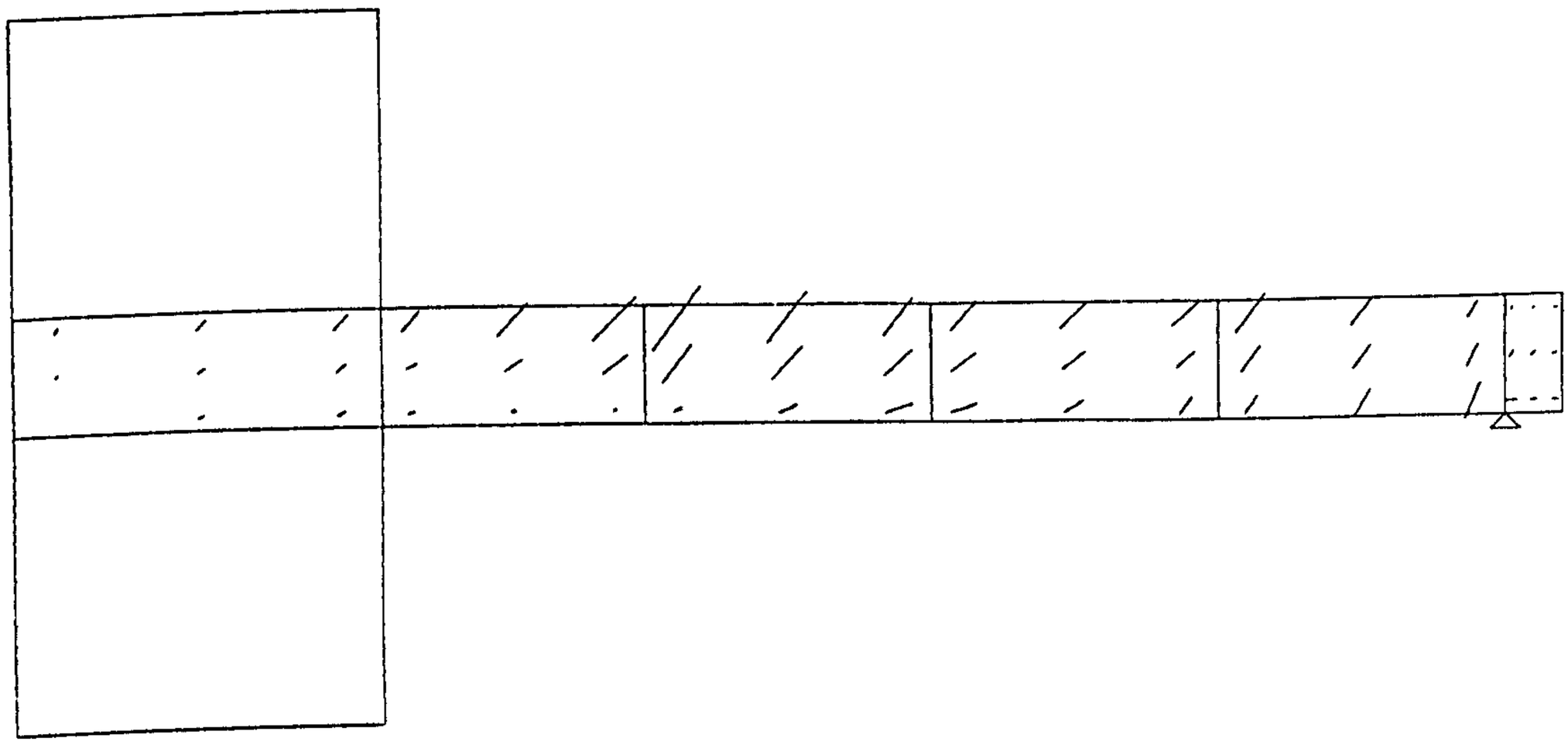

NH4

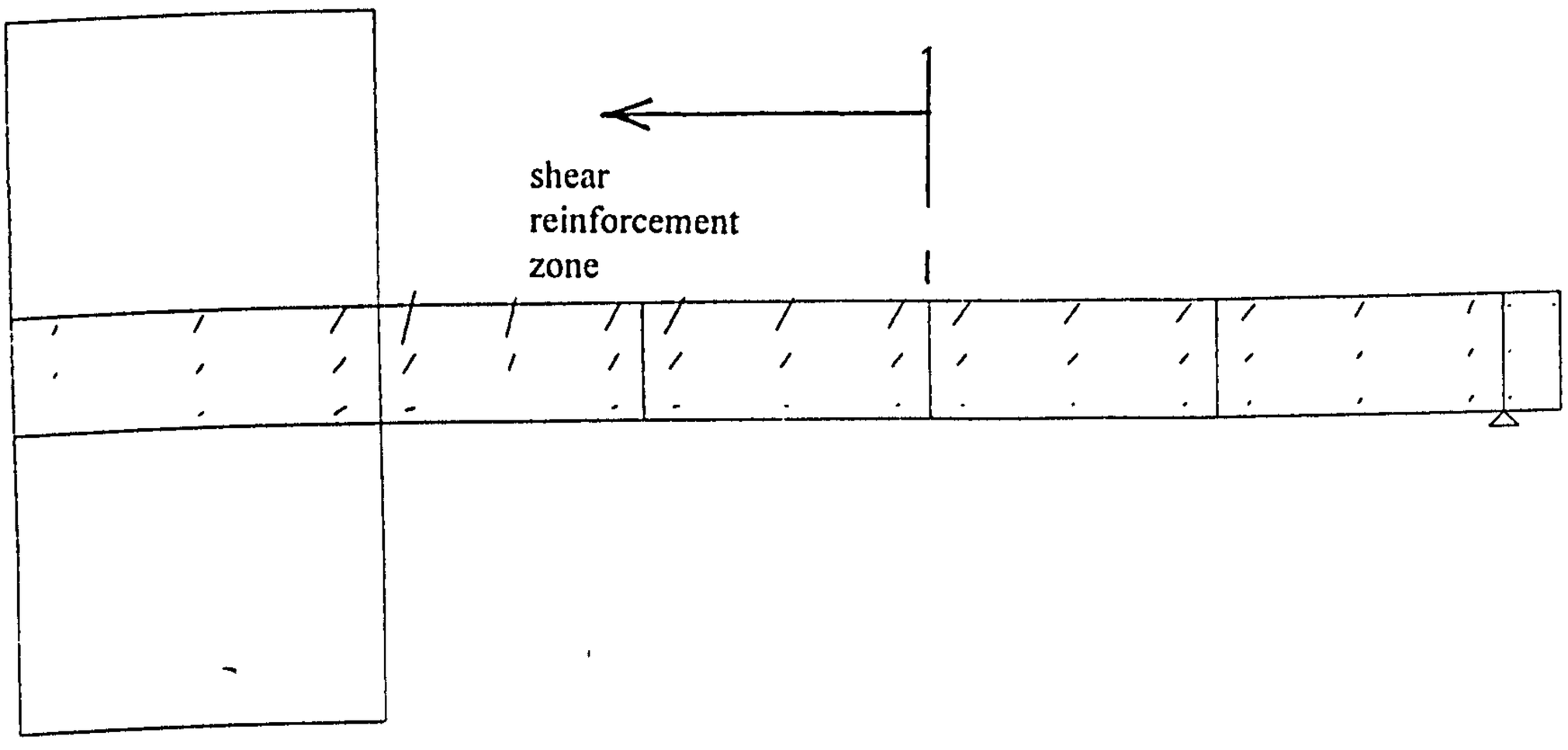

NH5

C3 Restrained slabs

This section presents numerical results for restrained slabs.

For yielding of flexural steel, only shaded area is shown.

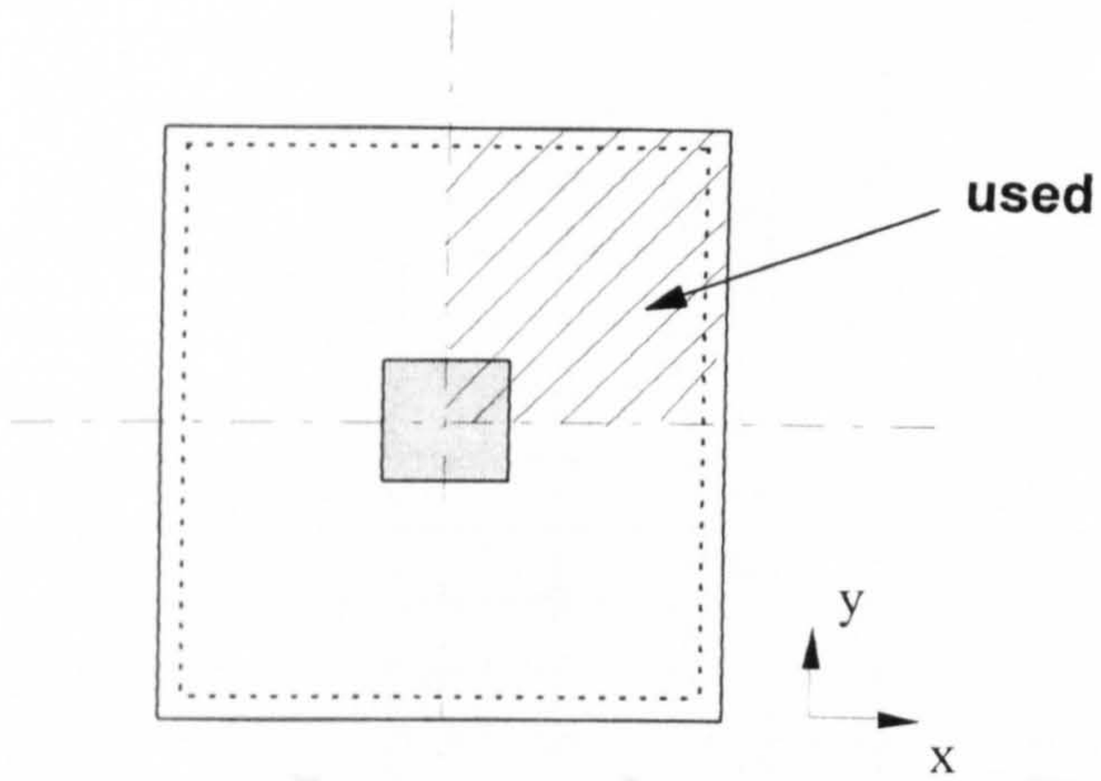

For crack pattern,

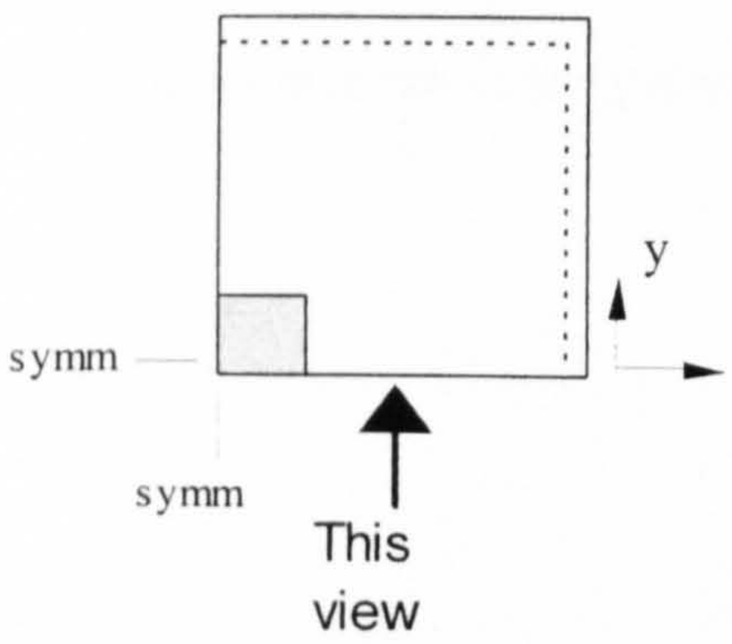

Full panel specimens (Rankin)

C3.1 Full panel slab-column specimens tested by Rankin

Slab	Test results		Numerical Predictions		P_{num}/P_{test}
	P_{test} (kN)	*Failure Mode	P_{num} (kN)	Failure mode	
R1-08	65.22	s	47.04	fp	0.721
R2-08	64.81	s	50.40	fp	0.778
R3-08	69.66	s	62.64	s	0.899
R4-08	71.47	s	57.60	s	0.806
R5-08	77.84	s	83.16	s	1.068
R2-11	69.73	s	55.68	s	0.800
R4-11	81.59	s	73.44	s	0.900
R5-11	87.89	s	74.66	s	0.849
R3-05	56.16	s	54.72	fp	0.974
R5-05	62.51	s	62.40	s	0.998
R3A-08	96.41	s	67.20	s	0.697
R5A-08	95.34	s	81.60	s	0.856
R3B-08	55.22	s	44.93	s	0.814
R5B-08	60.34	s	51.00	s	0.845
R3C-08	112.47	s	101.52	s	0.903
R5C-08	126.27	s	124.80	s	0.988
				Average	0.869
				STDEV	0.102

*no detail of failure mode is given in the paper, it only stated that all the slabs failed by punching.

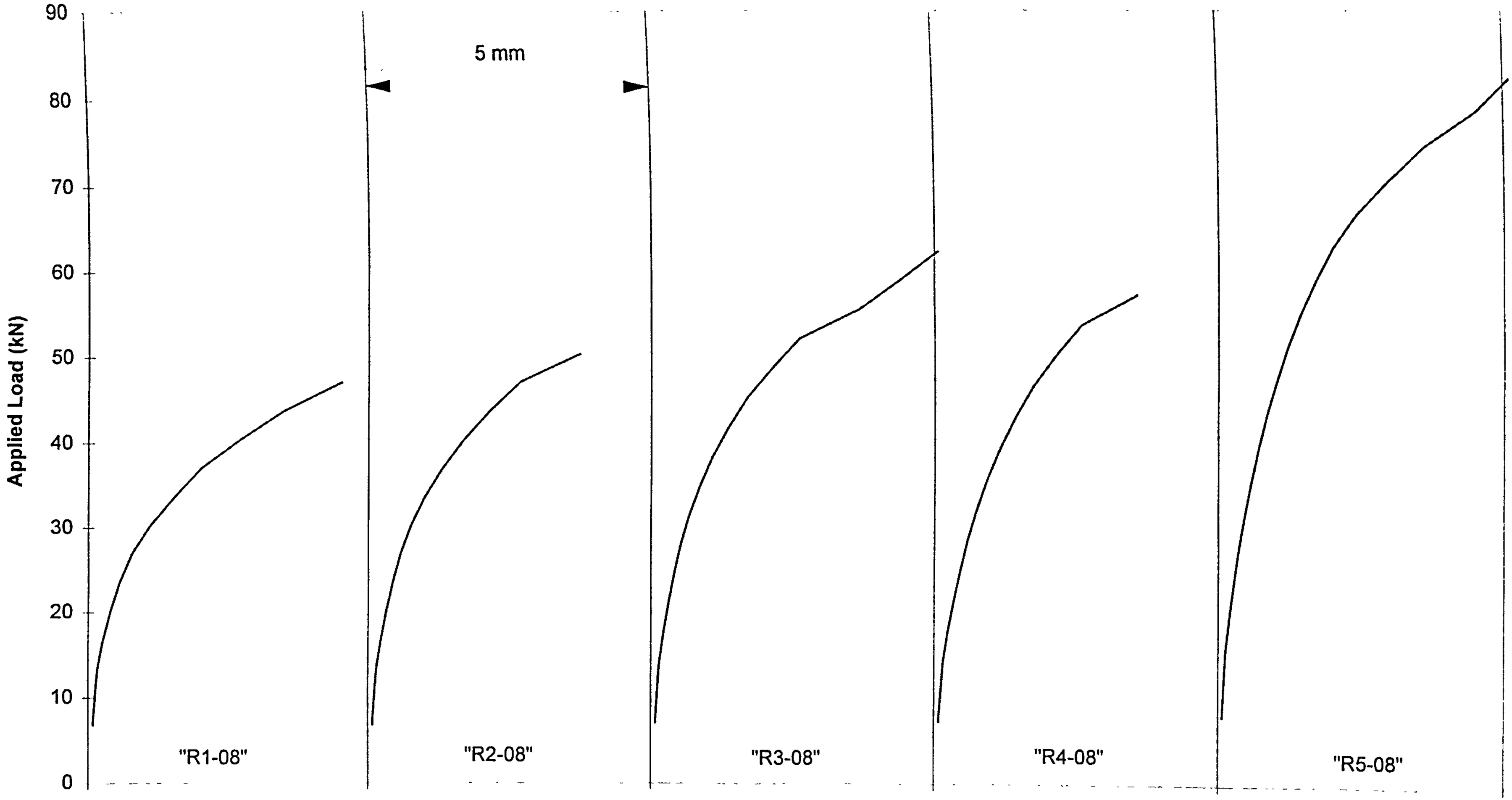

Predicted load-deflection response for slabs R1-08 to R5-08

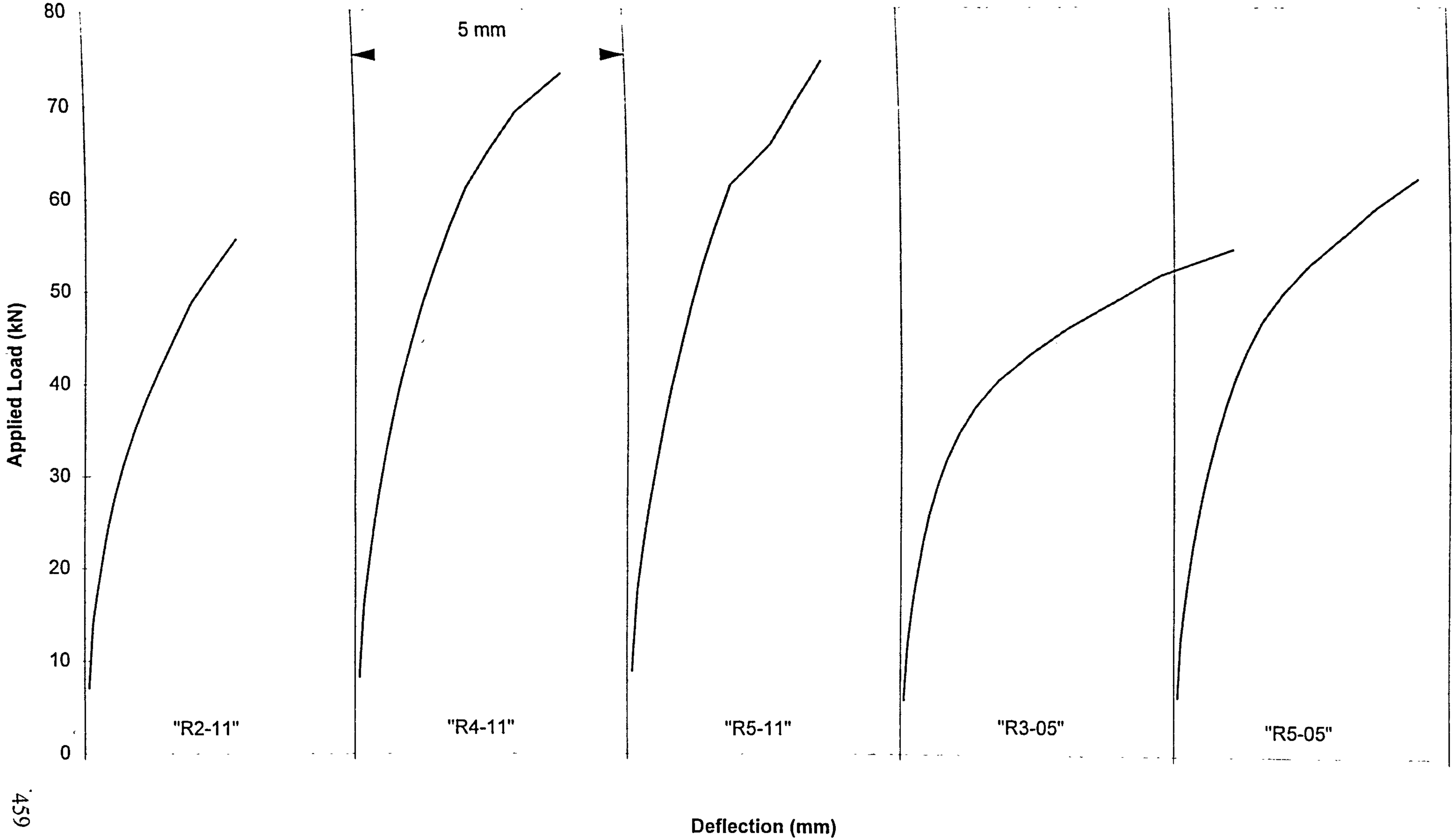

459

Predicted load-deflection response for slabs R2-11 to R5-11, R3-05 and R5-05

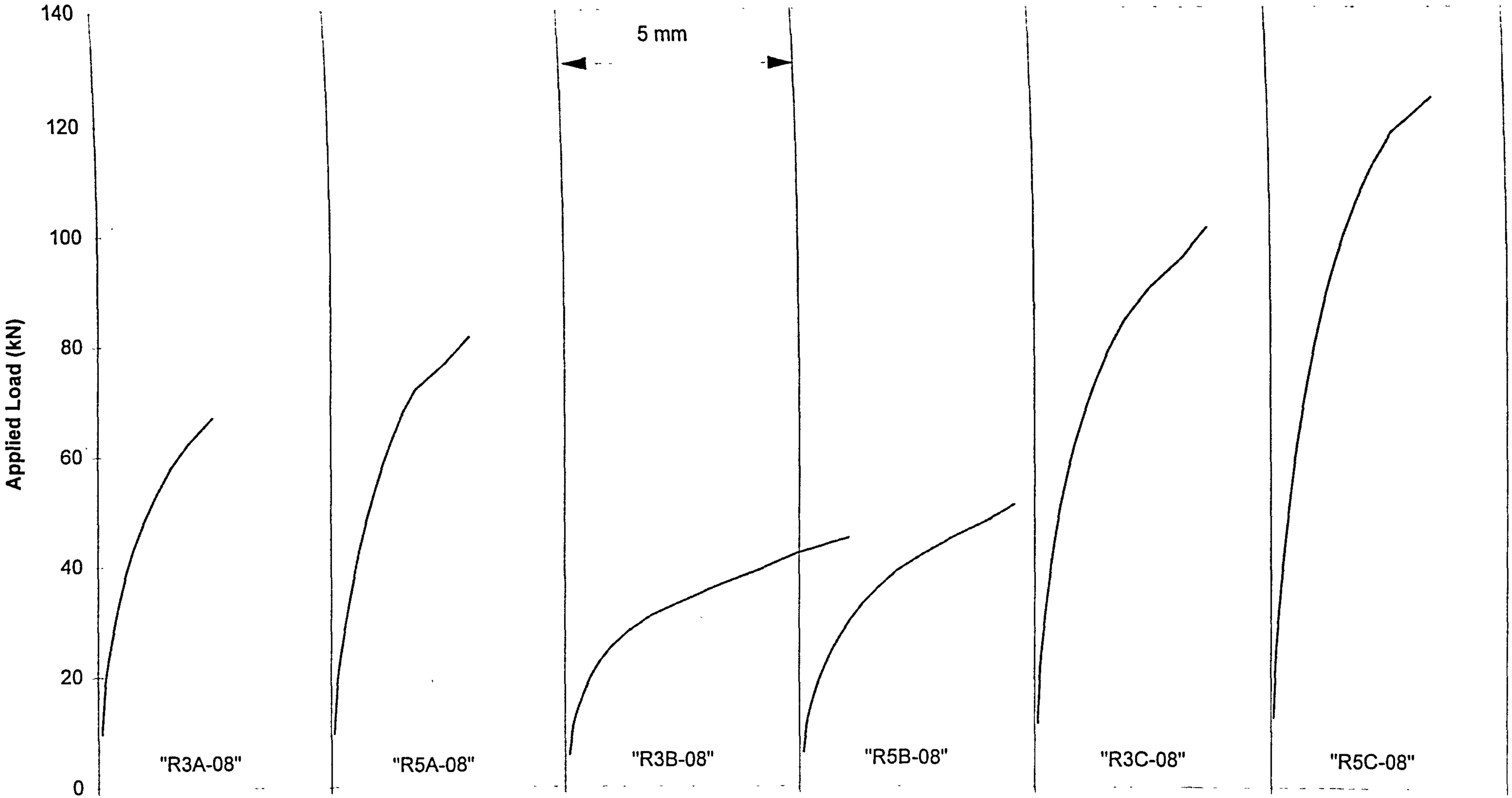

460

Predicted load-deflection response for slabs R3A-08, R5A-08, R3B-08, R5B-08, R3C-08 and R5C-08

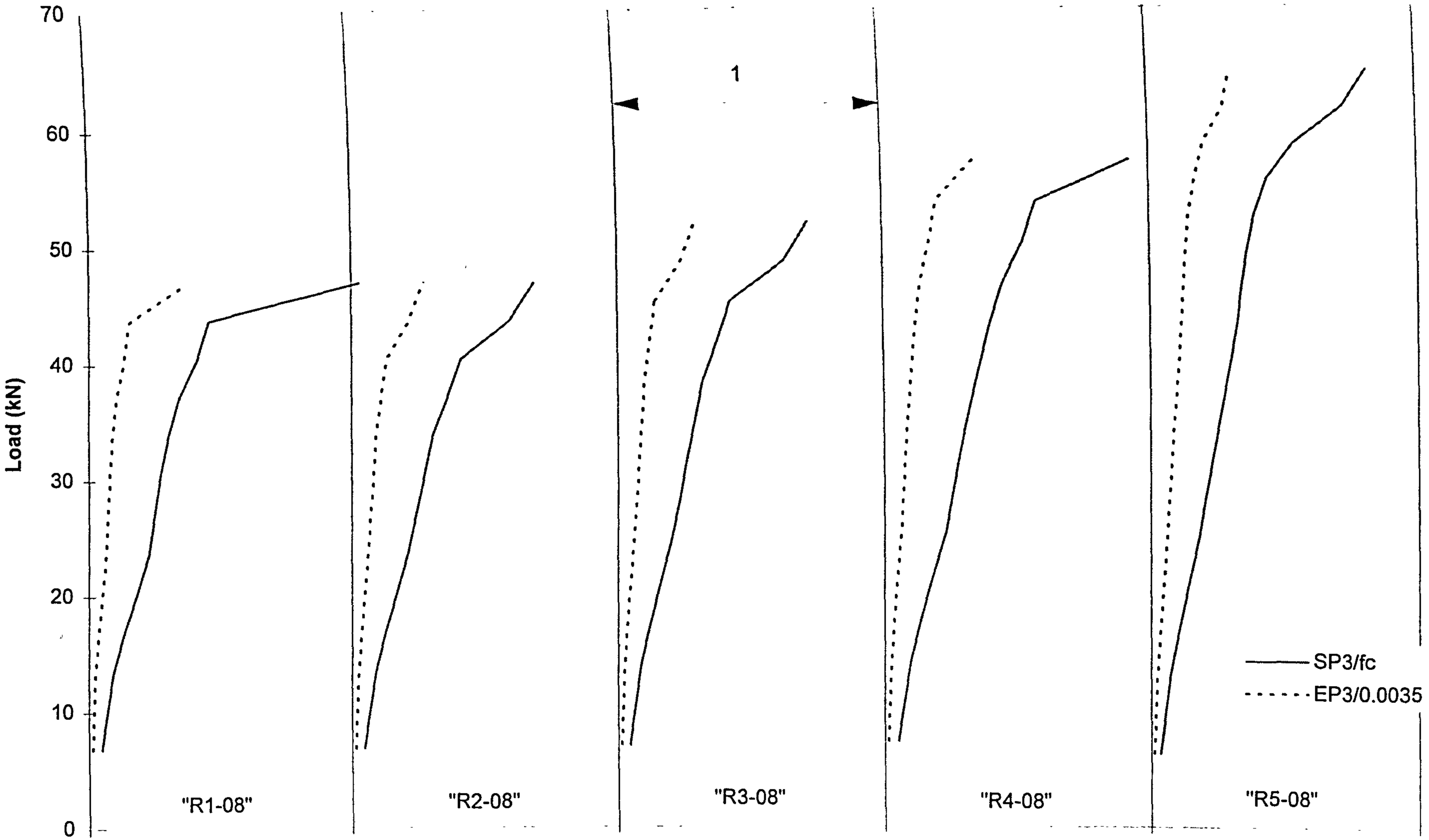

Predicted principal compressive stress and strain in concrete (slabs "R1-08" - "R5-08")

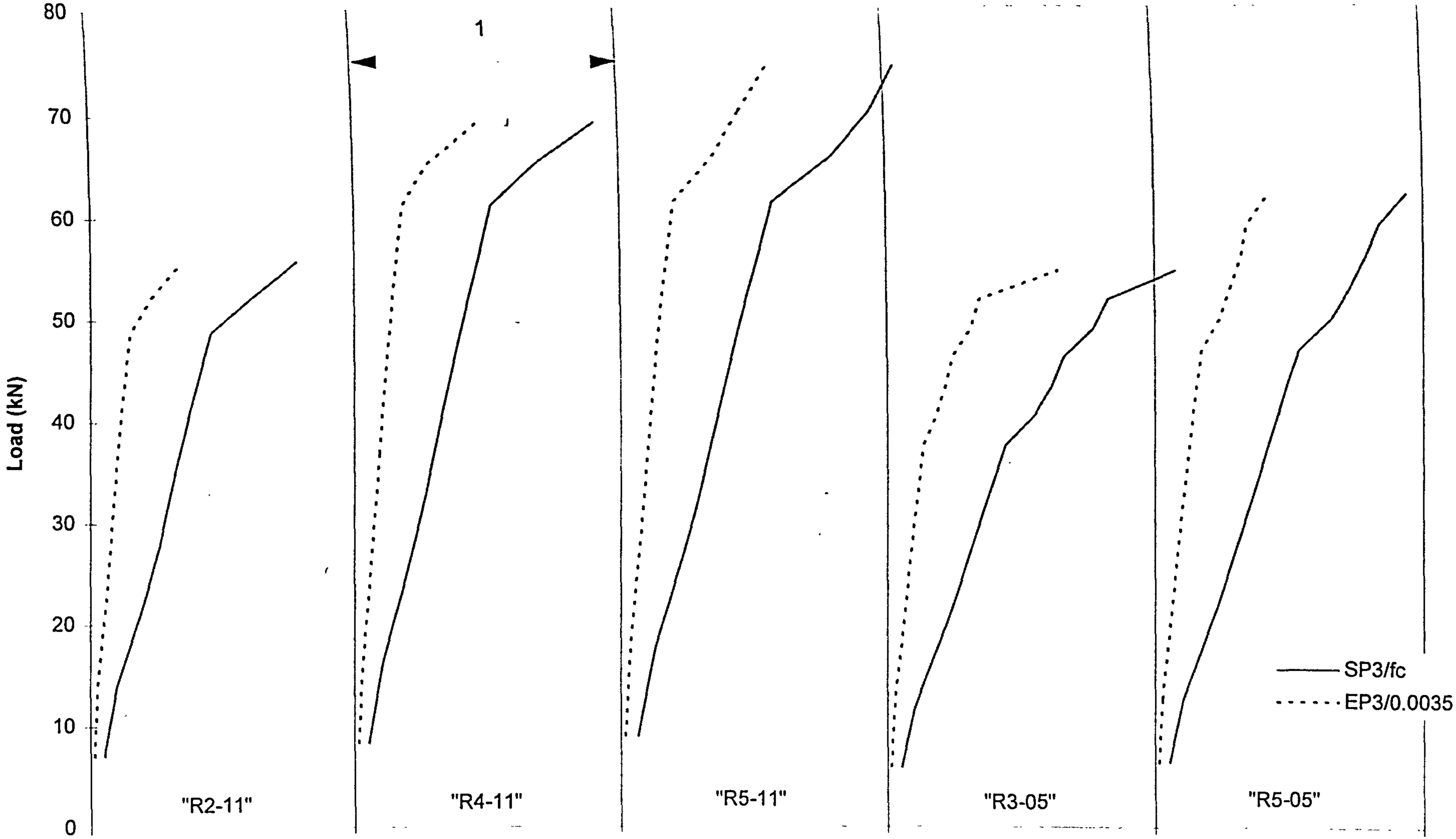

Predicted principal compressive stress and strain in concrete (slabs "R2-11" to "R5-11", R3-05 and R5-05)

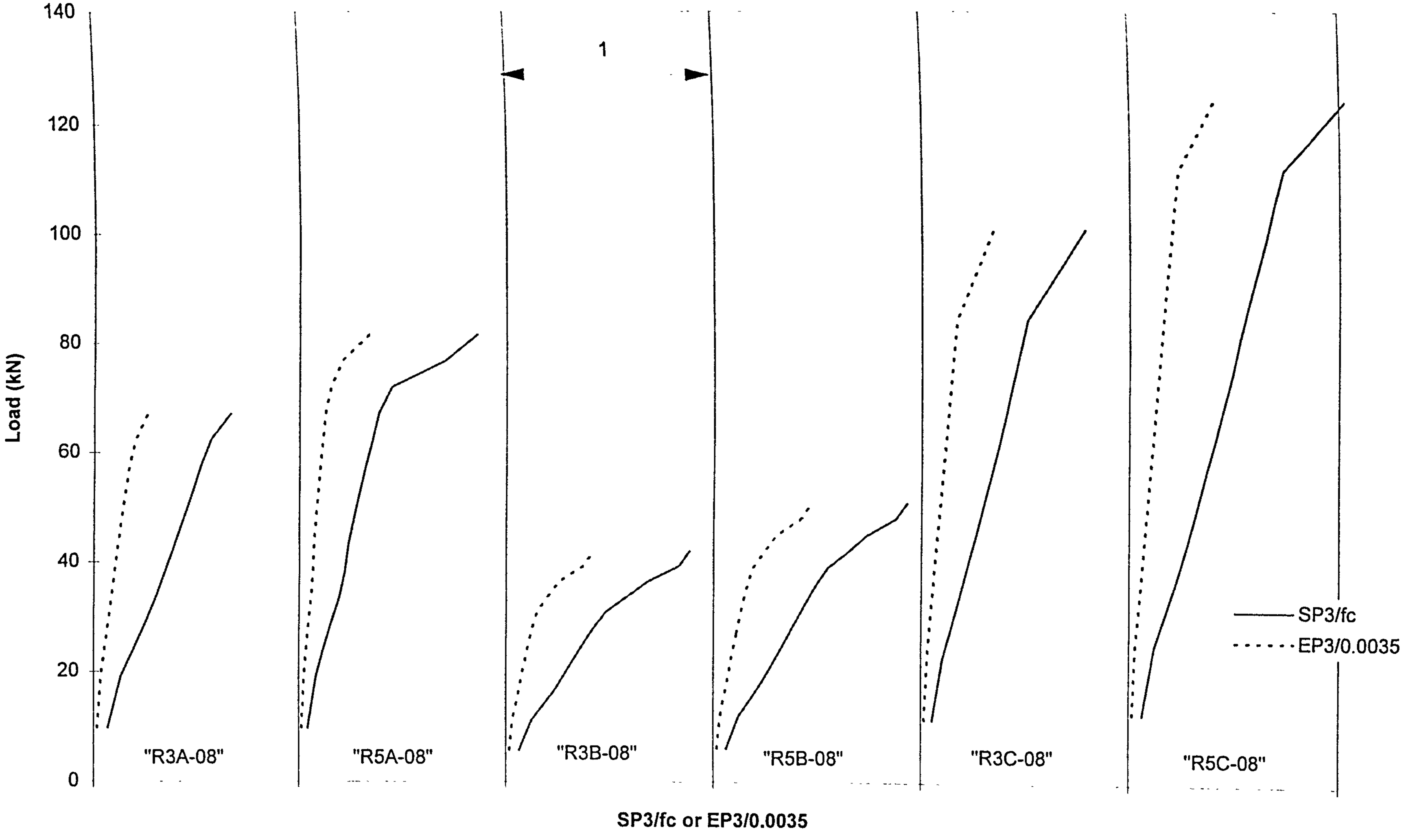

Predicted principal compressive stress and strain in concrete (slabs "R3A-08, R5A-08, R3B-08", "R5B-08", R3C-08 and R5C-08)

Yielding of tension steel, Large panel tested by Rankin

NB. : The numbers on the drawing indicate strain in steel at collapse expressed as a ratio of yield strain

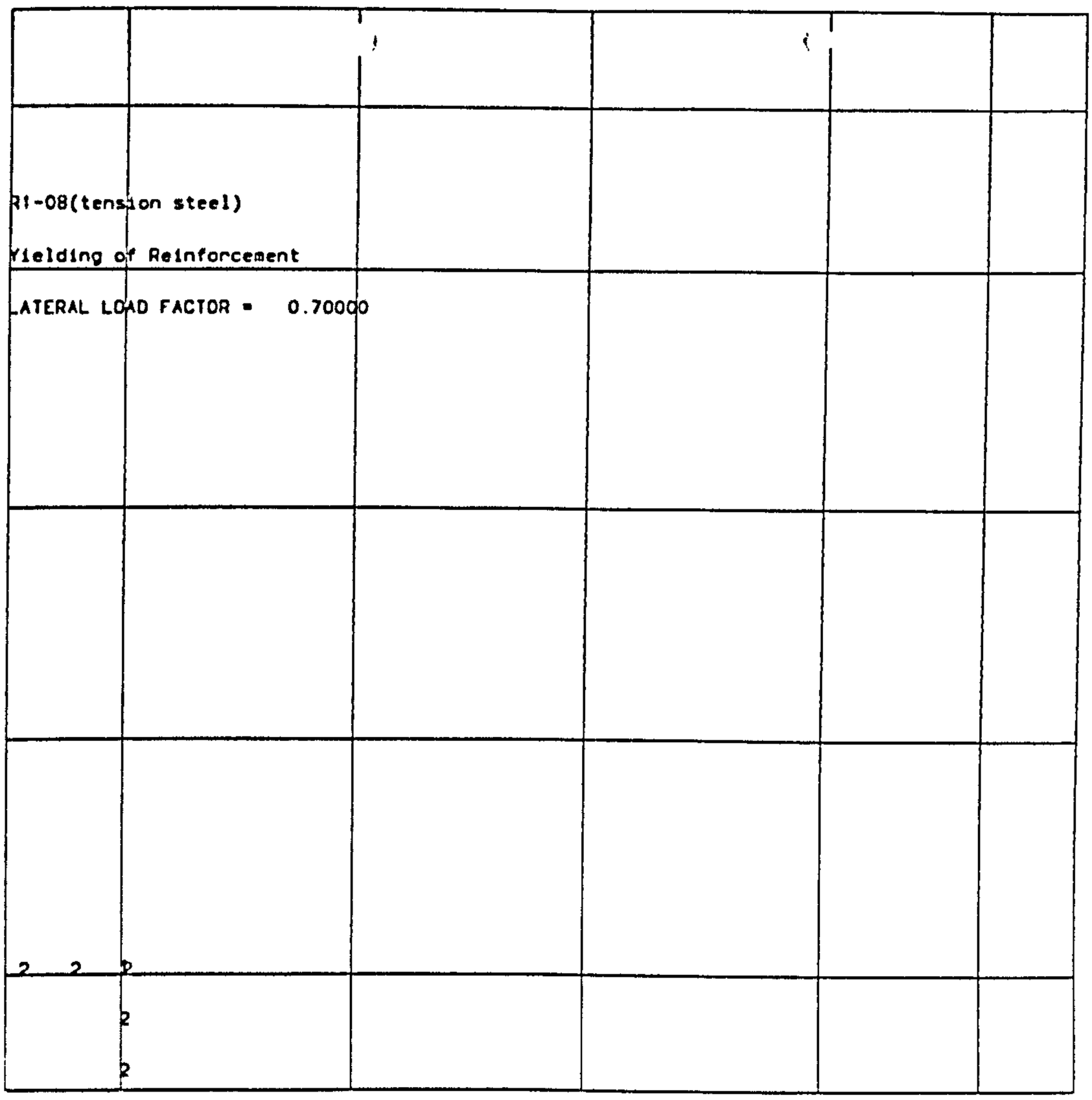

R1-08

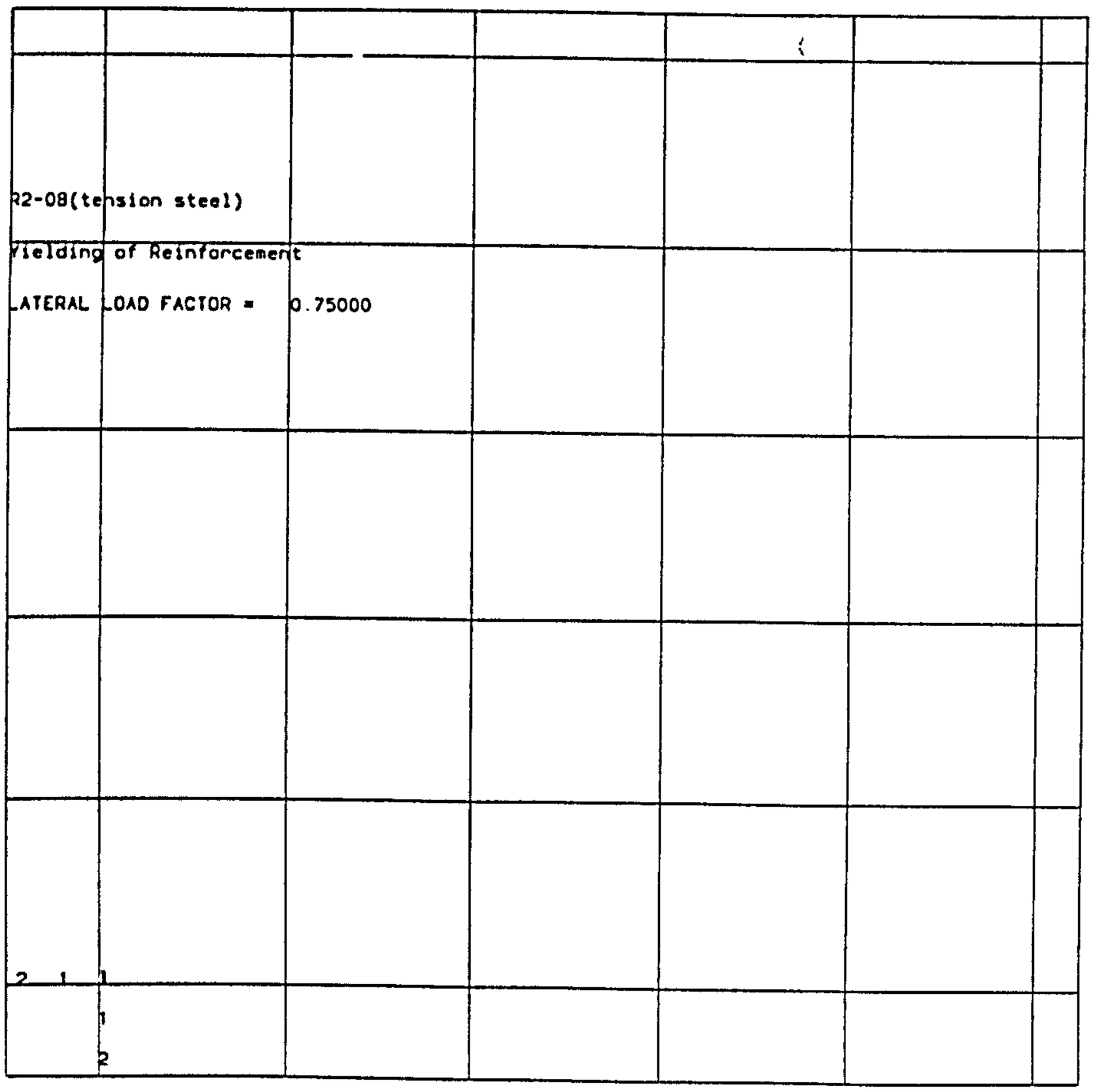

R2-08

R3-08(tension steel)

Yielding of Reinforcement

LATERAL LOAD FACTOR = 0 90000

R3-08

R4-08(tension steel)

Yielding of Reinforcement

LATERAL LOAD FACTOR = 0 80000

R4-08

R5-08(tension steel)

Yielding of Reinforcement

LATERAL LOAD FACTOR = 1.05000

R5-08

R2-11(tension steel)

Yielding of Reinforcement

LATERAL LOAD FACTOR = 0.80000

R2-11

R4-11(tension steel)

Yielding of Reinforcement

LATERAL LOAD FACTOR = 0.90000

R4-11

R5-11(tension steel)

Yielding of Reinforcement

LATERAL LOAD FACTOR = 0.85000

R5-11

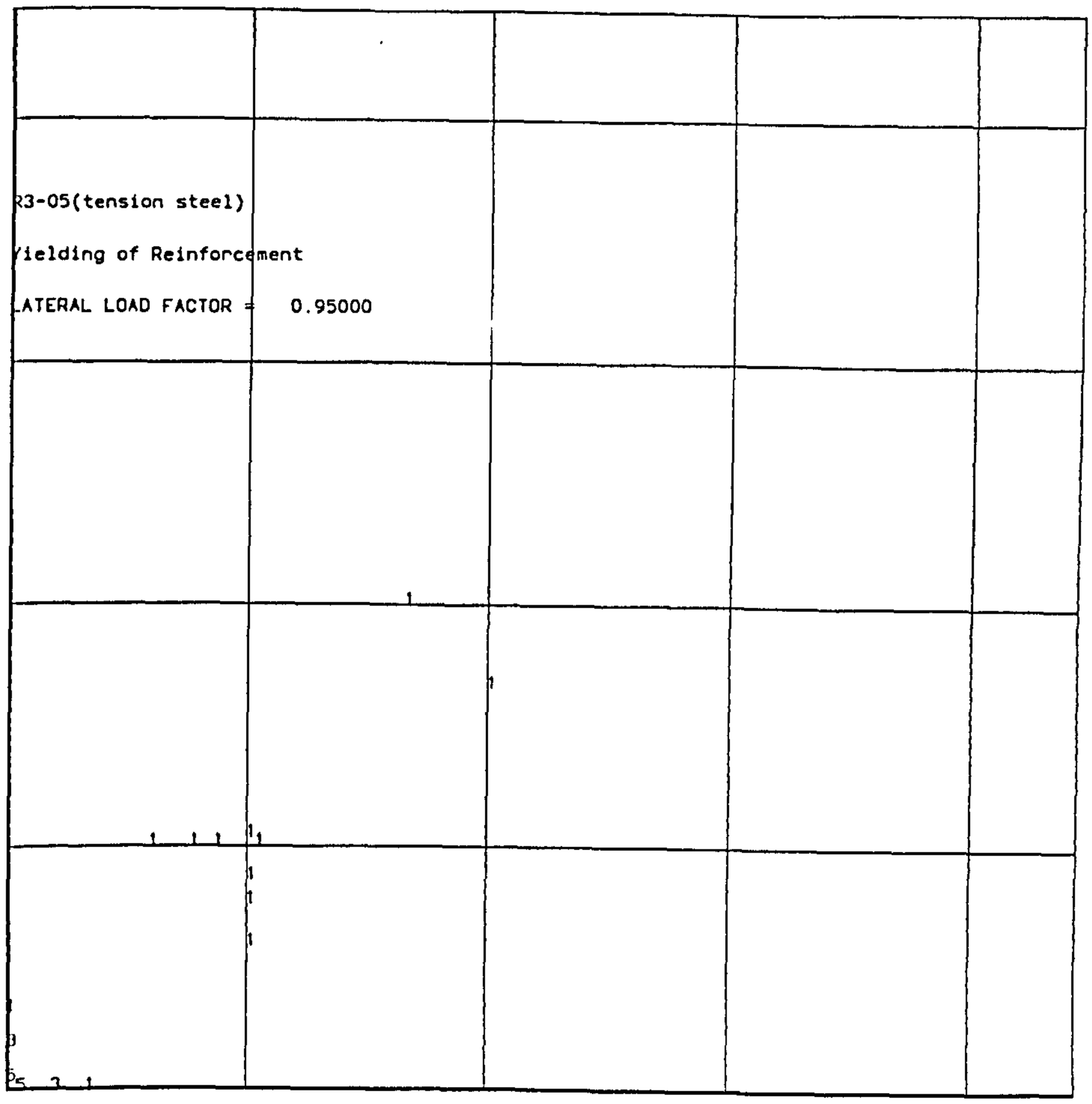
R3-05(tension steel)
Yielding of Reinforcement
LATERAL LOAD FACTOR = 0.95000

R3-05

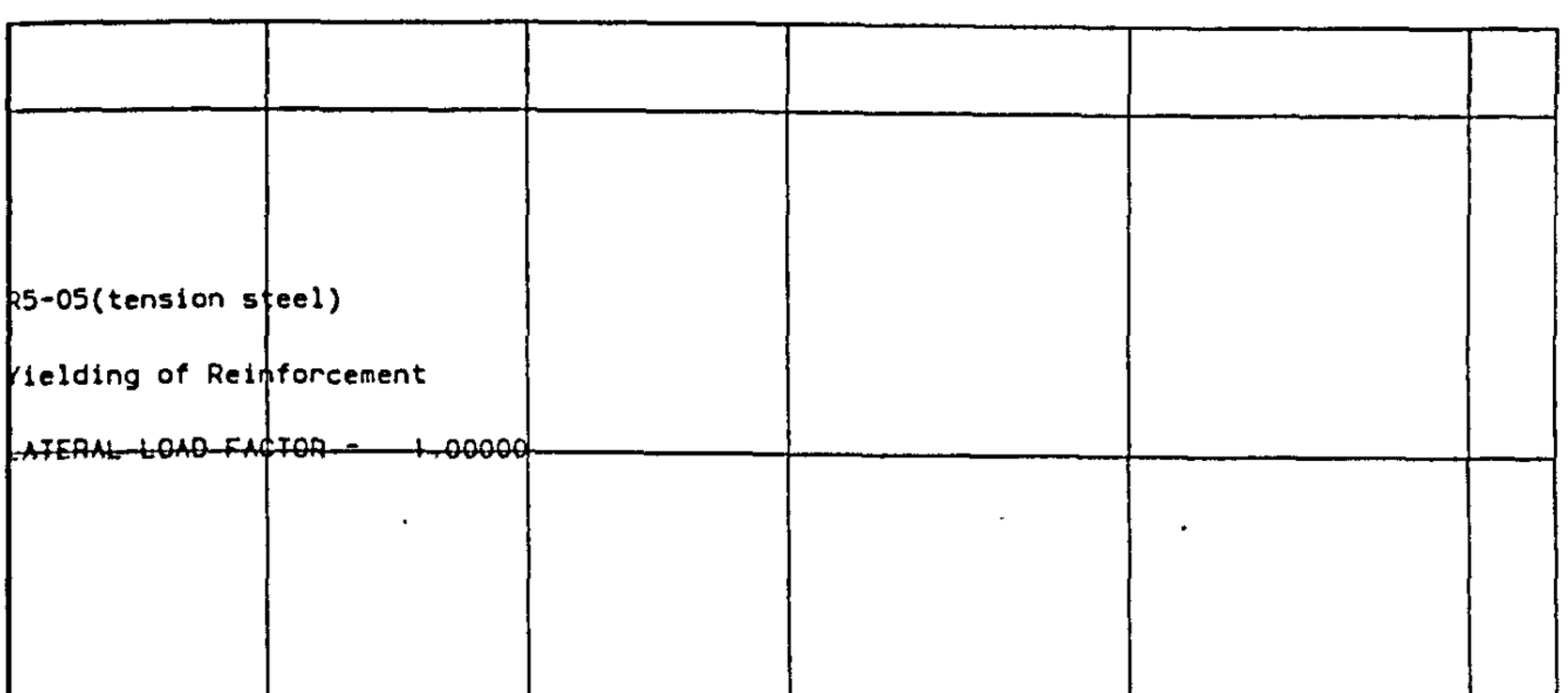
R5-05(tension steel)
Yielding of Reinforcement
LATERAL LOAD FACTOR = 1.00000

R5-05

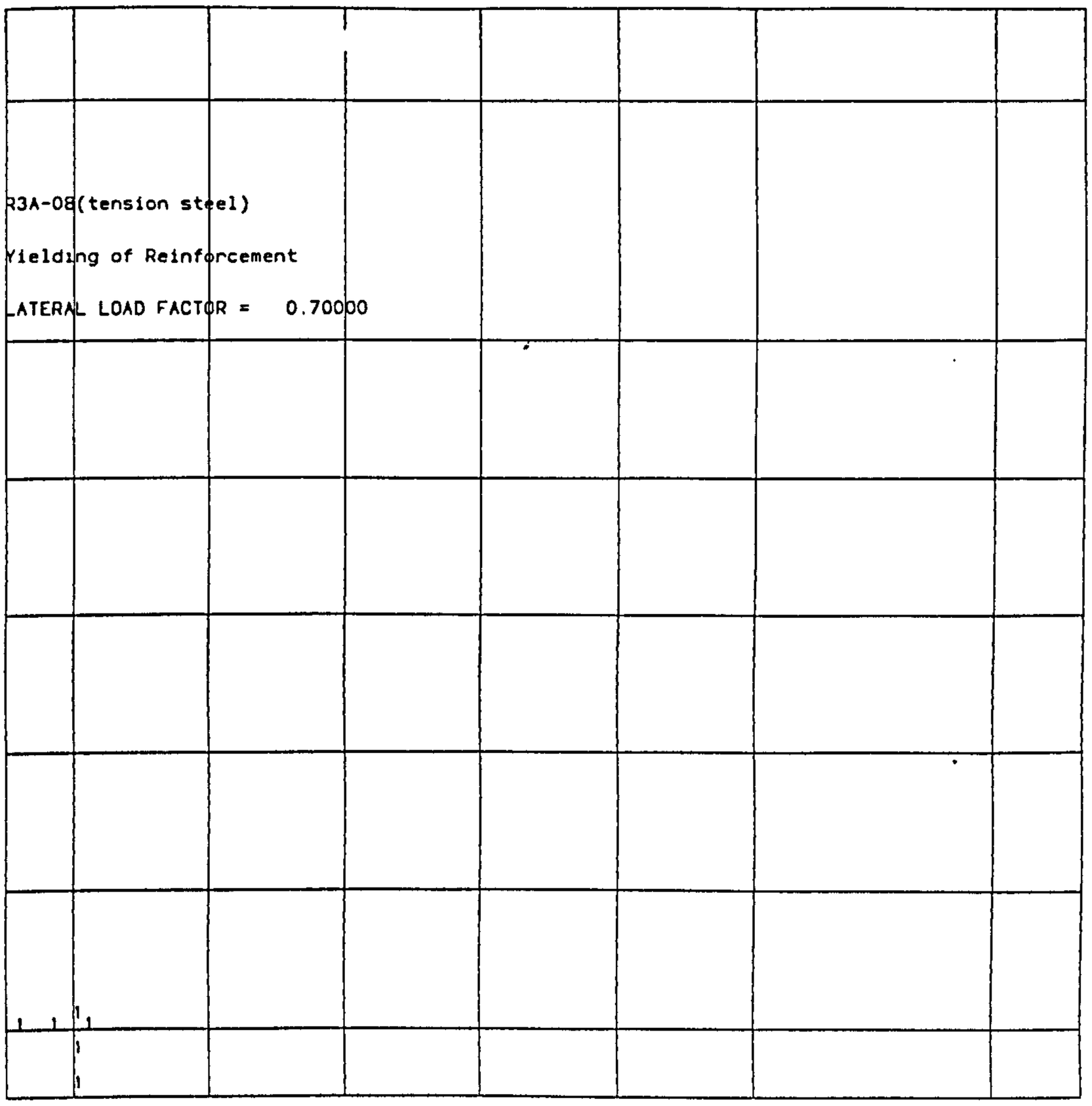
R3A-08(tension steel)
Yielding of Reinforcement
LATERAL LOAD FACTOR = 0.70000

R3A-08

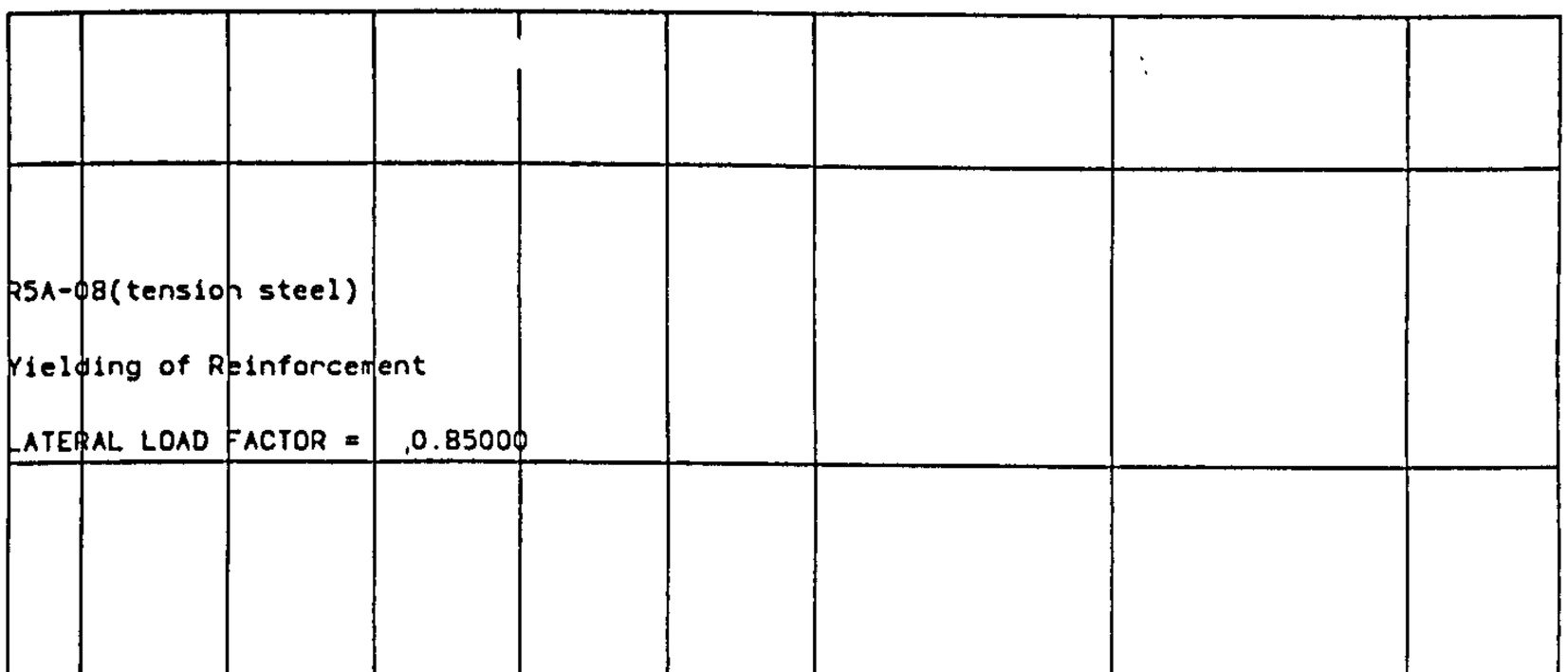
R5A-08(tension steel)
Yielding of Reinforcement
LATERAL LOAD FACTOR = ,0.85000

R5A-08

R38-08(tension steel)

Yielding of Reinforcement

LATERAL LOAD FACTOR = 0.80000

R3B-08

R5B-08(tension steel)

Yielding of Reinforcement

LATERAL LOAD FACTOR = 0.85000 ((st yield))

R5B-08

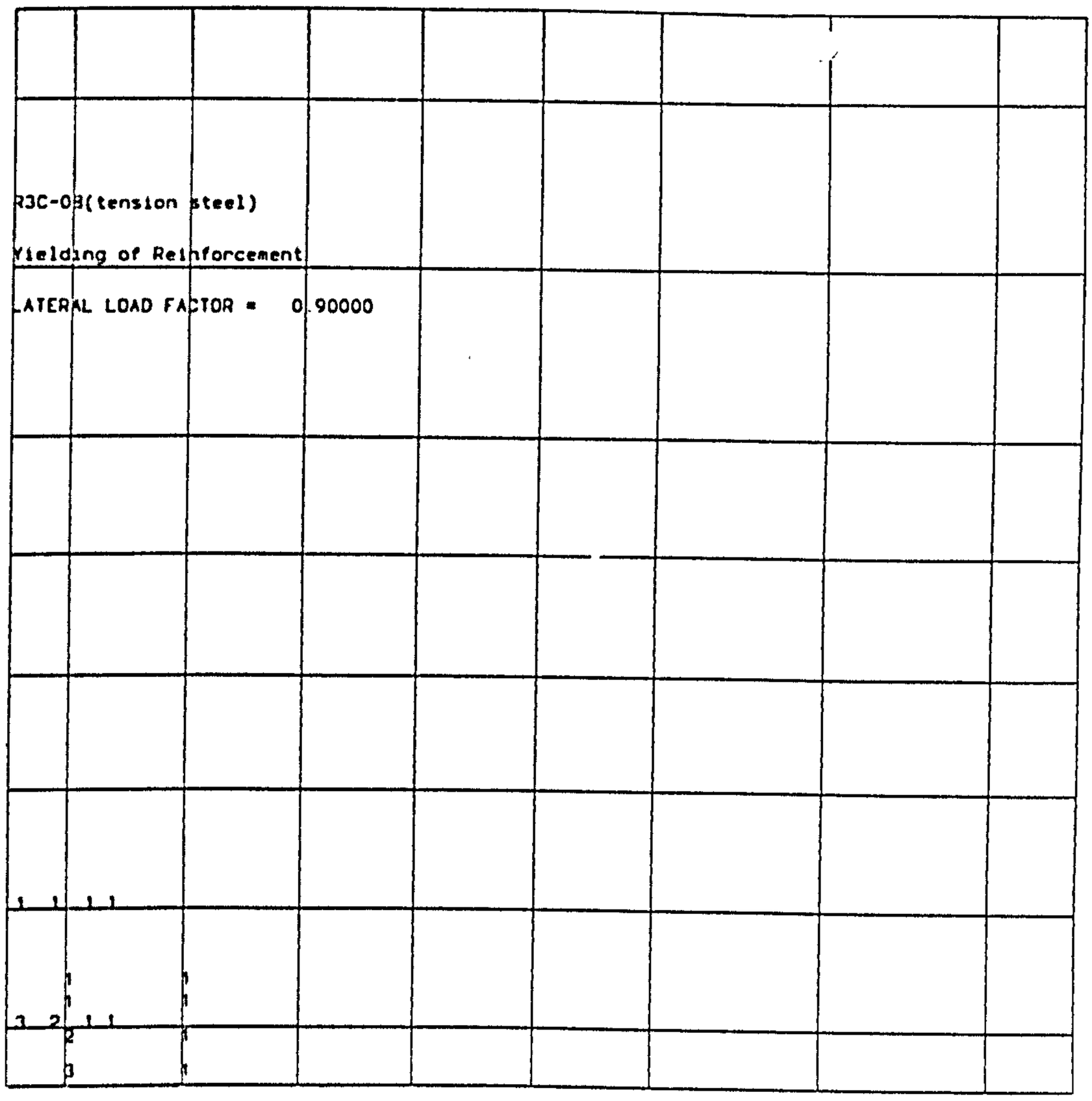
R3C-08(tension steel)
Yielding of Reinforcement
LATERAL LOAD FACTOR = 0.90000

R3C-08

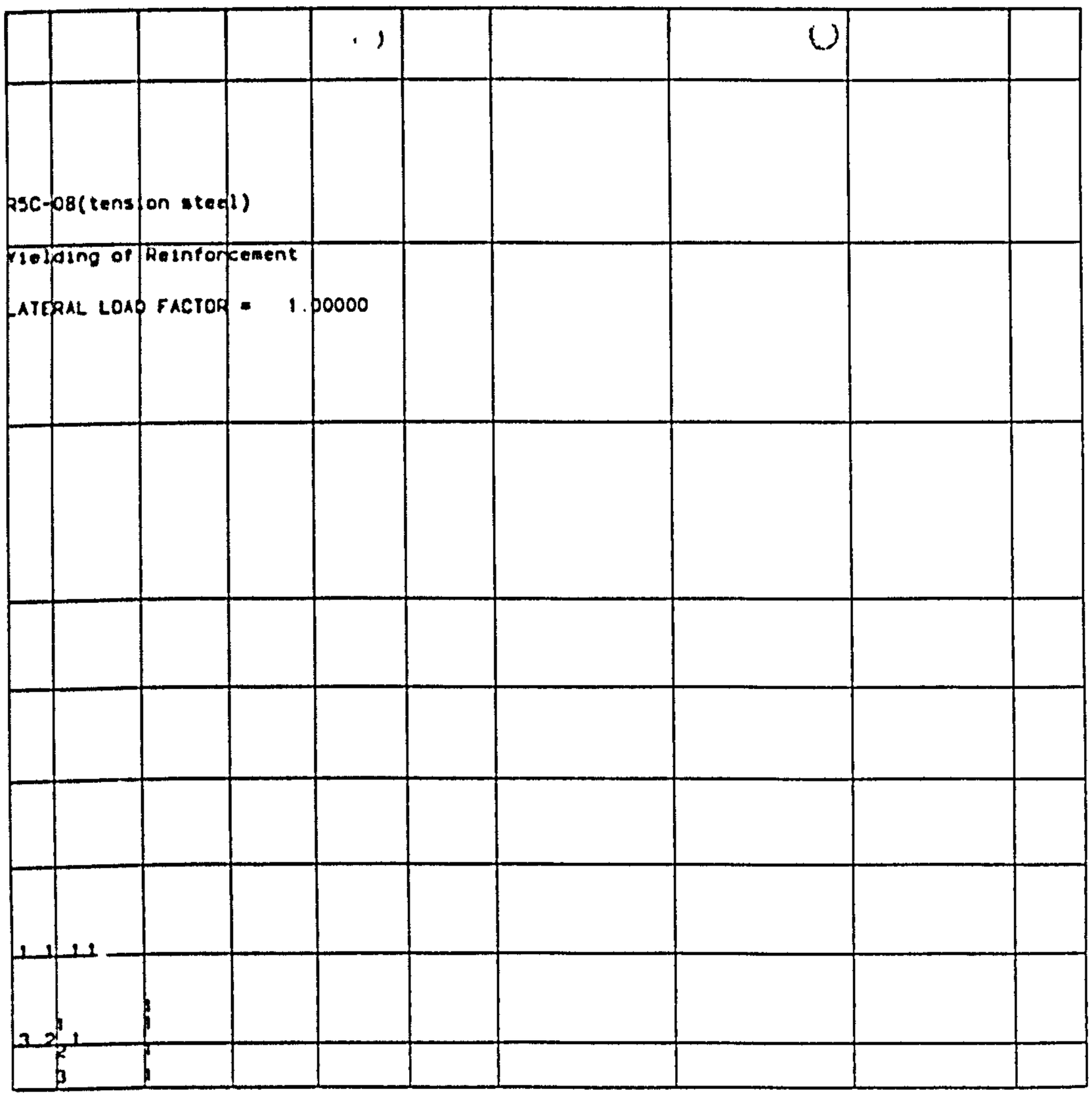
R5C-08(tension steel)
Yielding of Reinforcement
LATERAL LOAD FACTOR = 1.00000

R5C-08

Predicted crack pattern for large panel specimen (Rankin)

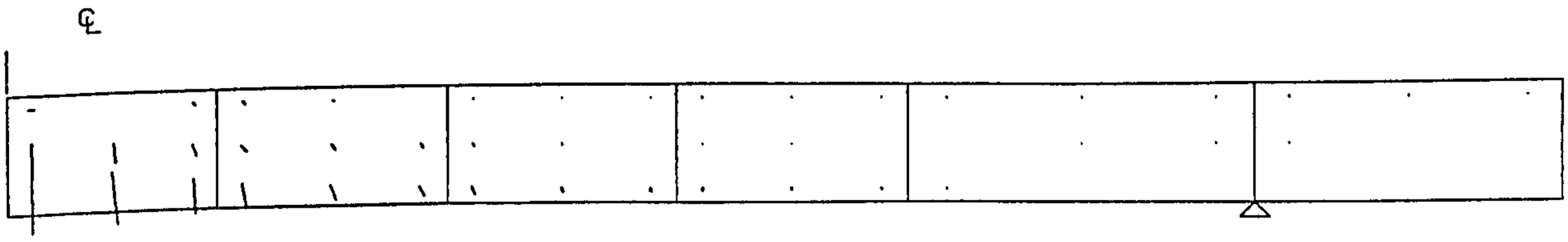

R1-08

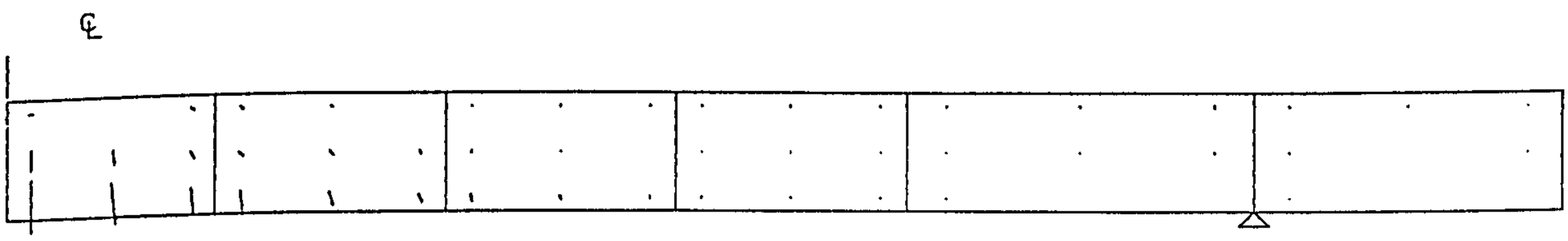

R2-08

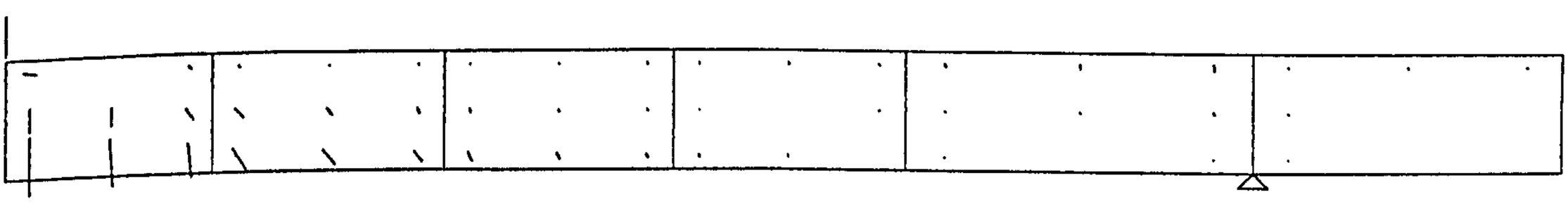

R3-08

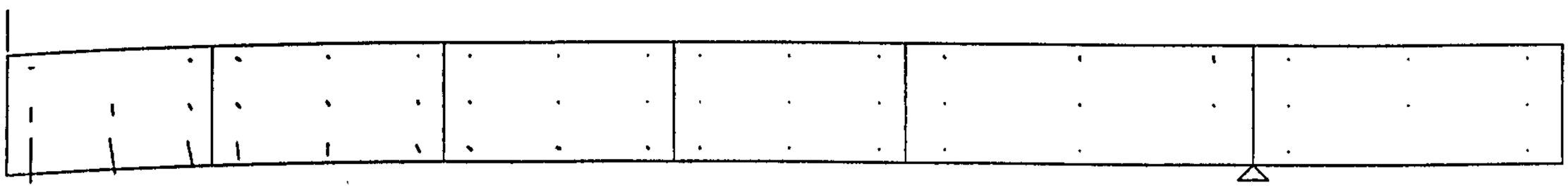

R4-08

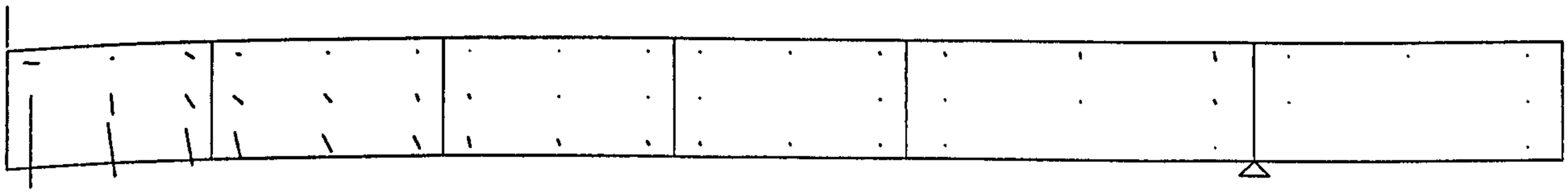

R5-08

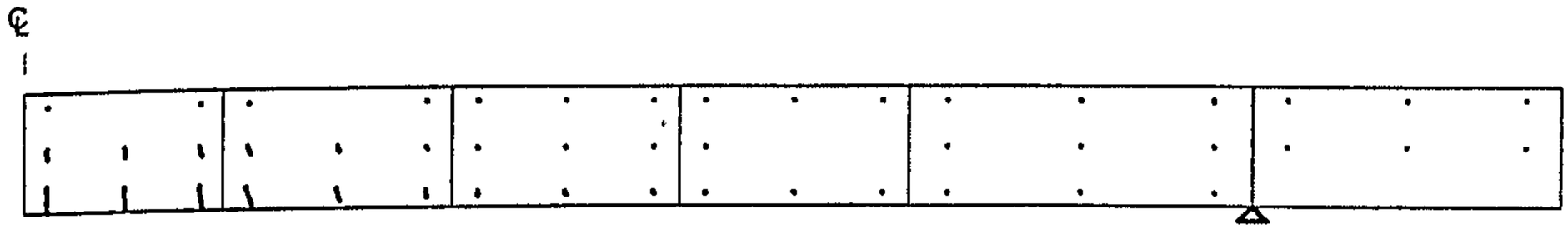

R2-11

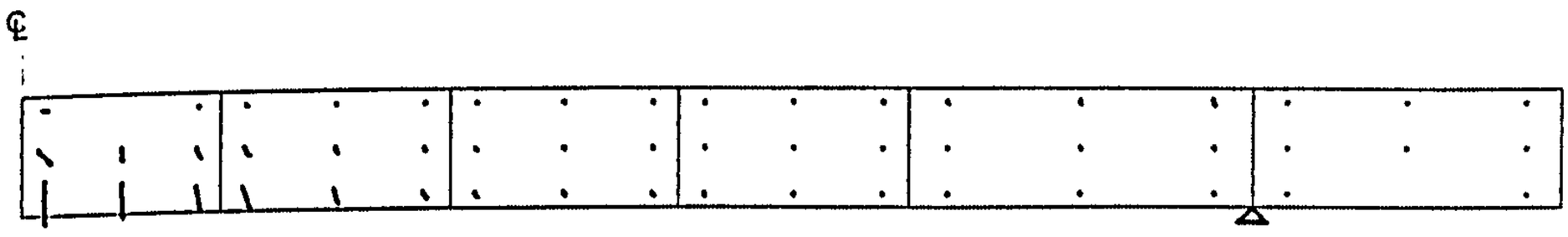

R4-11

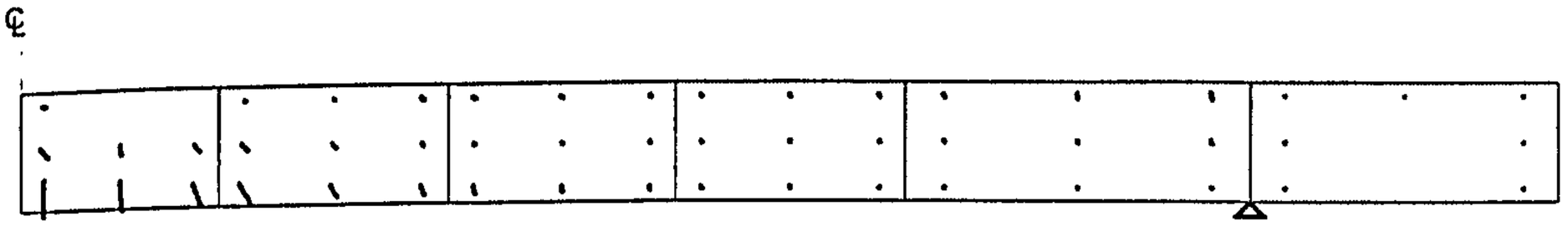

R5-11

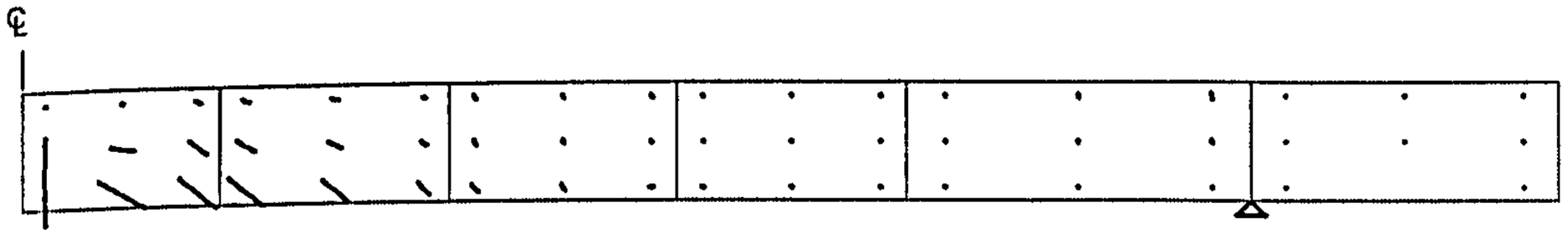

R3-05

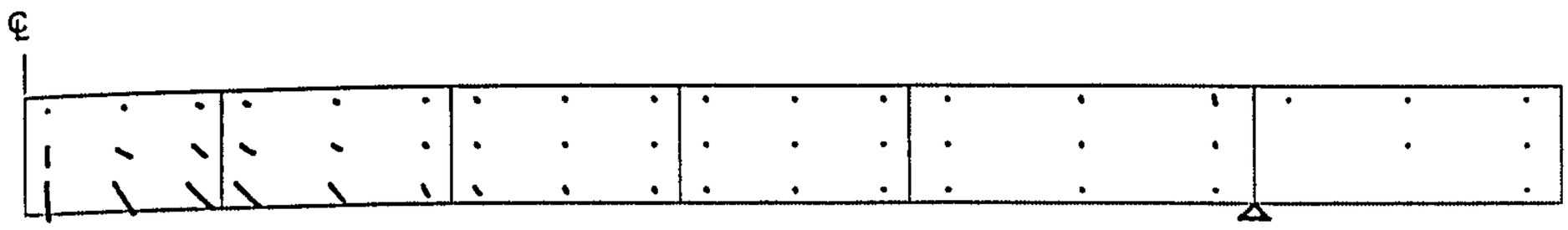

R5-05

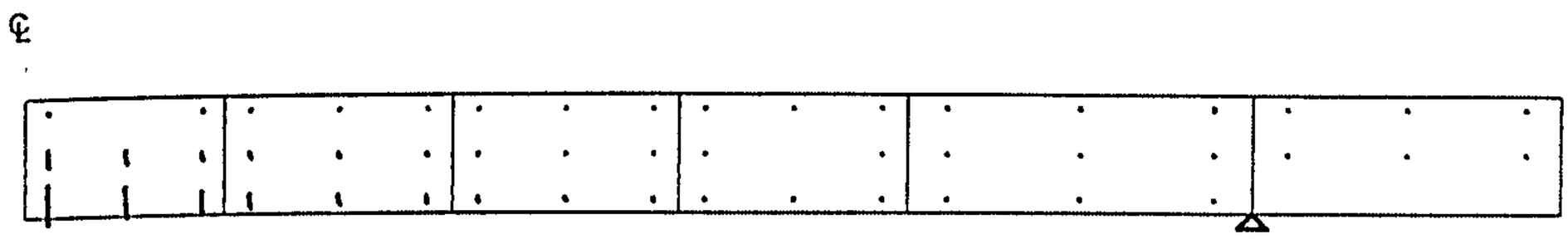

R3A-08

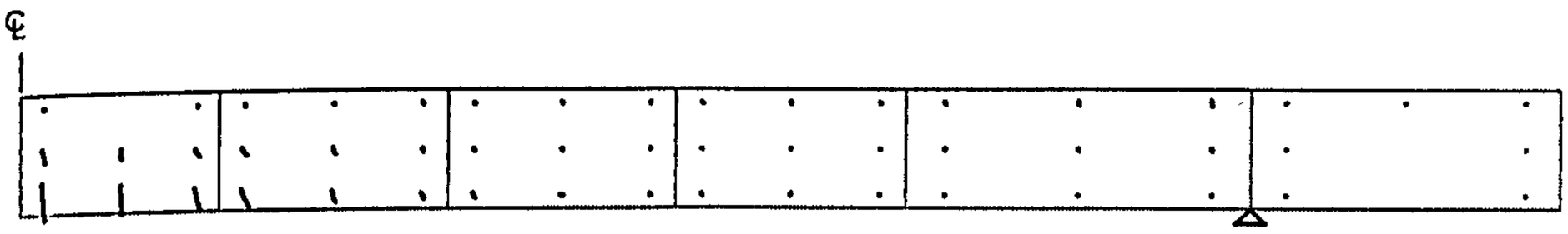

R5A-08

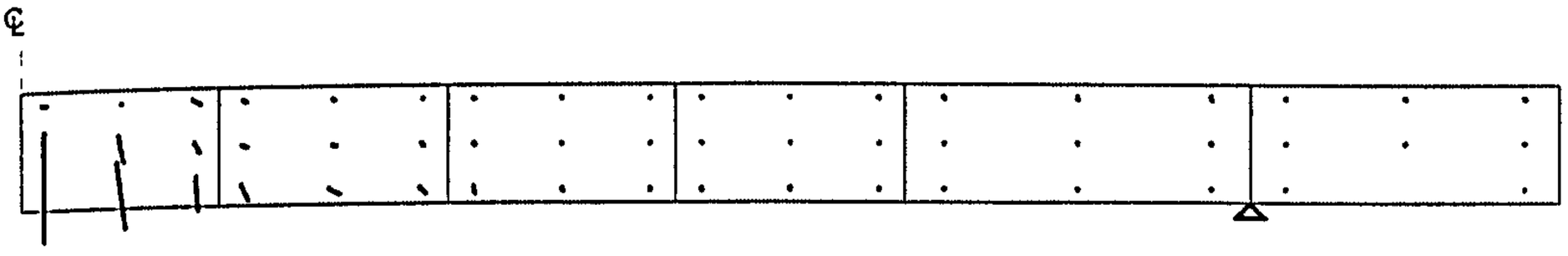

R3B-08

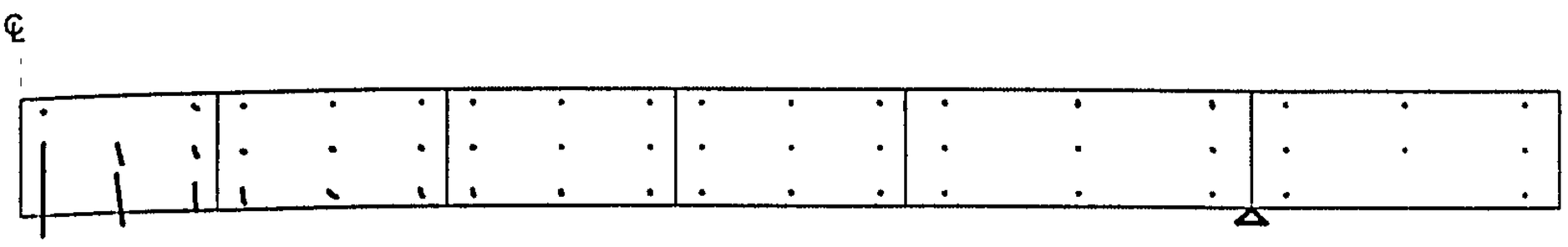

R5B-08

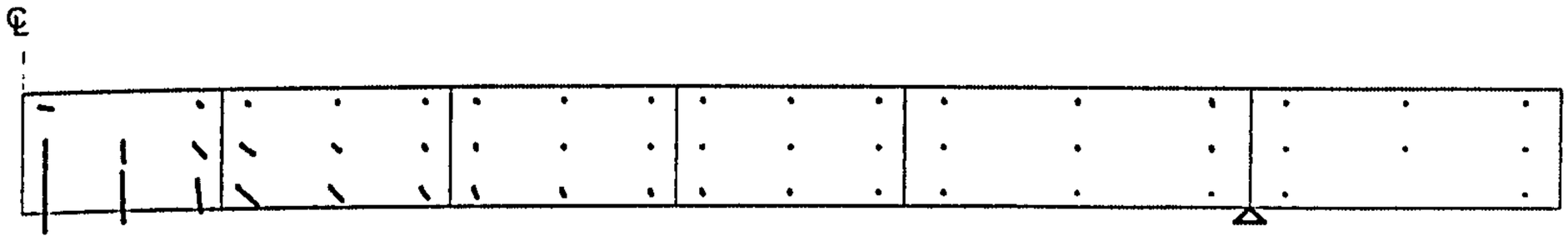

R3C-08,

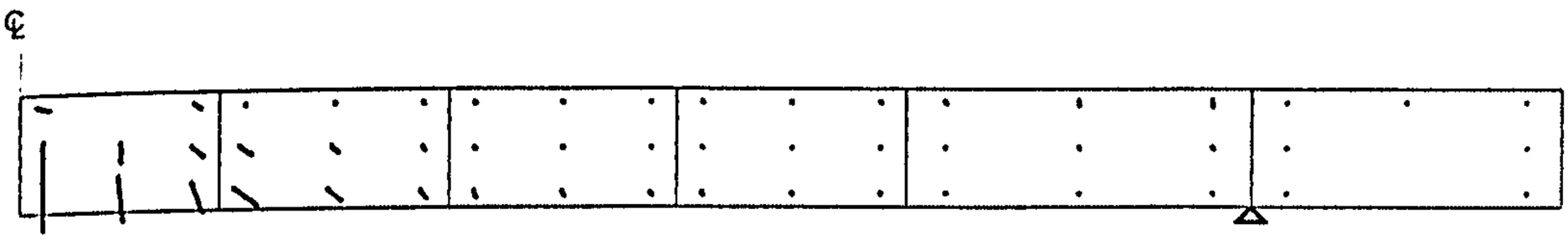

R5C-08,

Slab-beam panels
(Kuang and Morley)

C3.2 Slab-beam panels (Kuang and Morley)

Slab	Experimental		Numerical		P_{num}/P_{test}
	P_{test} (kN)	*failure Mode	P_{num} (kN)	failure Mode	
S1-C03	101.0	s	105.8	fp	1.048
S1-C10	118.0	s	82.3	s	0.698
S1-C16	149.0	s	104.2	s	0.699
S2-C03	49.0	s	49.0	fp	1.000
S2-C10	70.0	s	52.2	s	0.746
S2-C16	68.0	s	47.1	s	0.692
S1-B10	116.0	s	94.1	s	0.811
S2-B03	42.0	s	39.9	fp	0.950
S2-B10	69.0	s	59.2	fp	0.858
S1-A10	99.0	s	93.5	fp	0.944
S2-A03	43.0	s	34.6	fp	0.804
S2-A10	63.0	s	46.8	fp	0.743
				Average	0.833
				STDEV	0.126

* All the slabs were broadly classified as failing in punching shear mode.

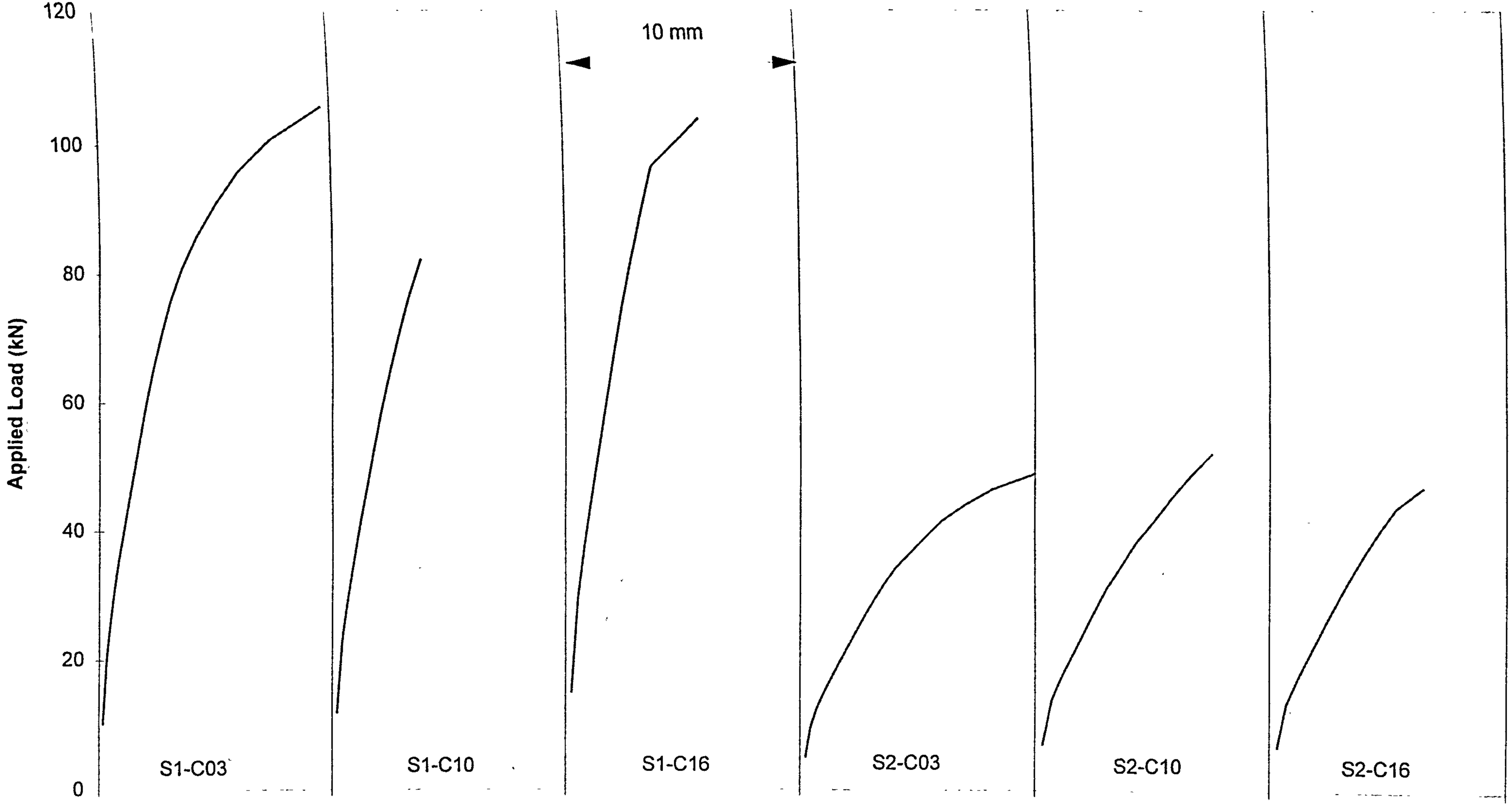

Predicted load-deflection response for slabs S1-C03,S1-C10, S1-C16, S2-C03, S2-C10 and S2-C16

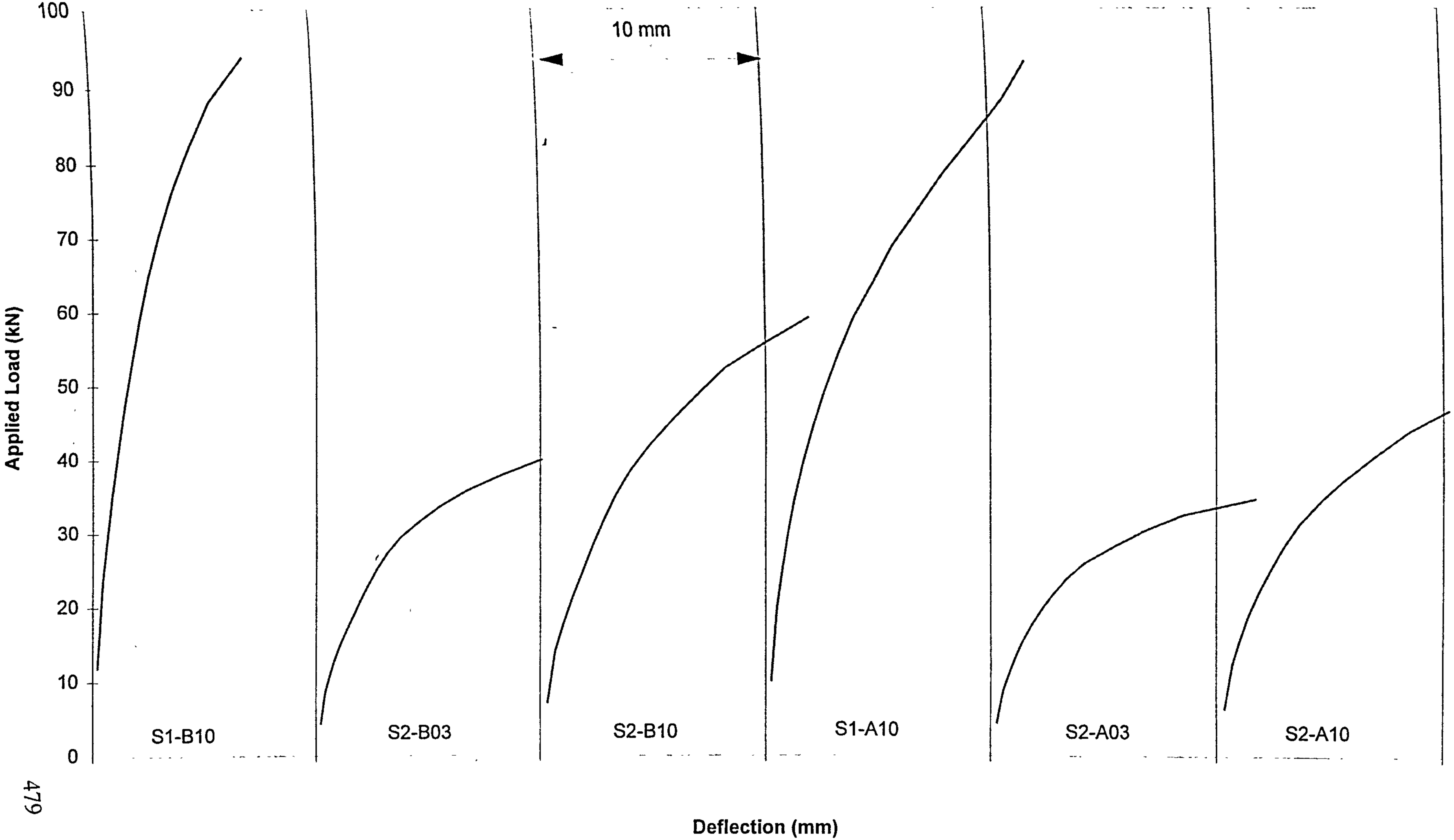

Predicted load-deflection response for slabs S1-B10,S2-B03, S2-B10, S1-A10, S2-A03 and S2-A10

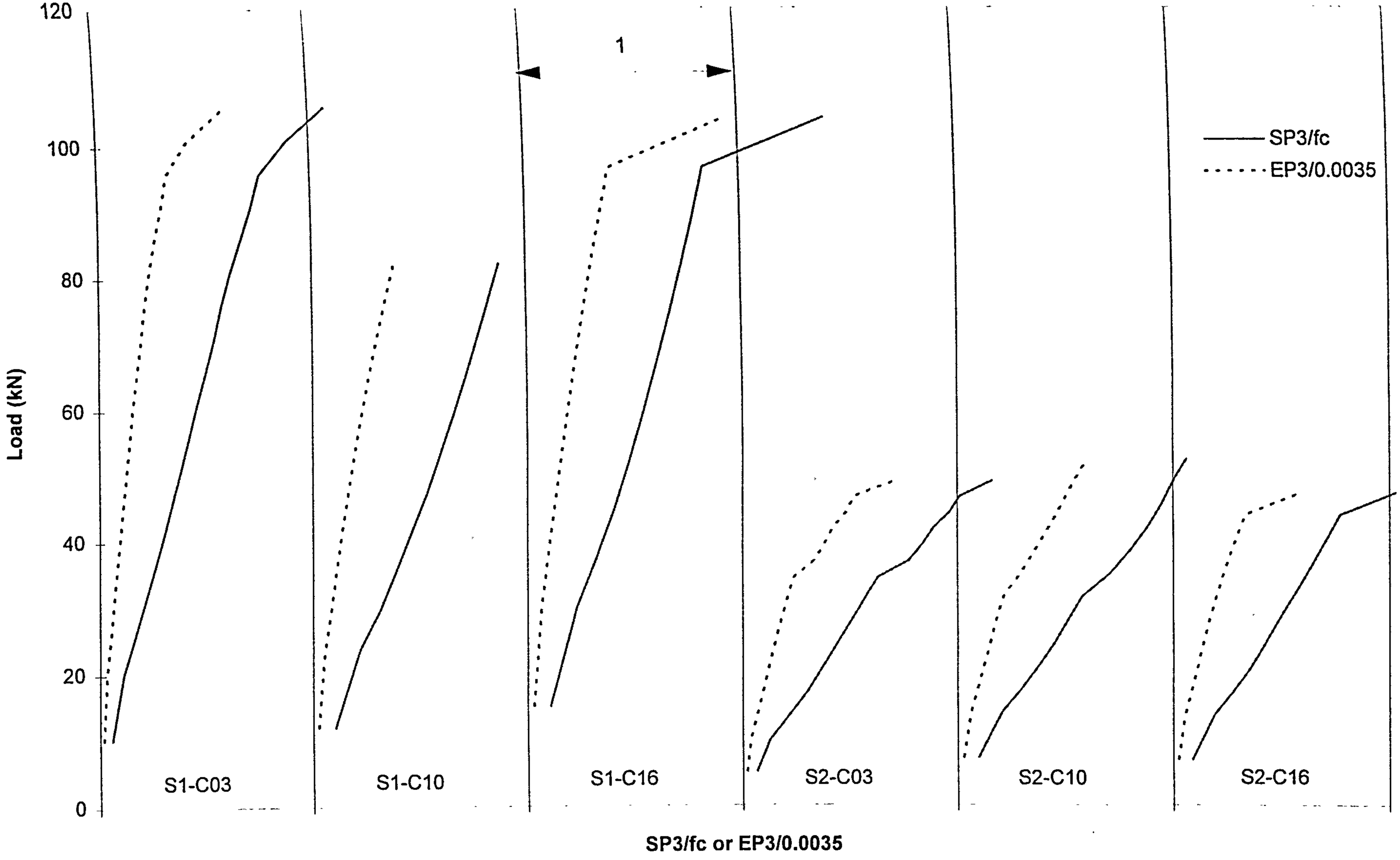

Predicted principal compressive stress and strain in concrete (slabs "S1-C03, S1-C10, S1-C16", "S1-C03", S1-C10 and S1-C16)

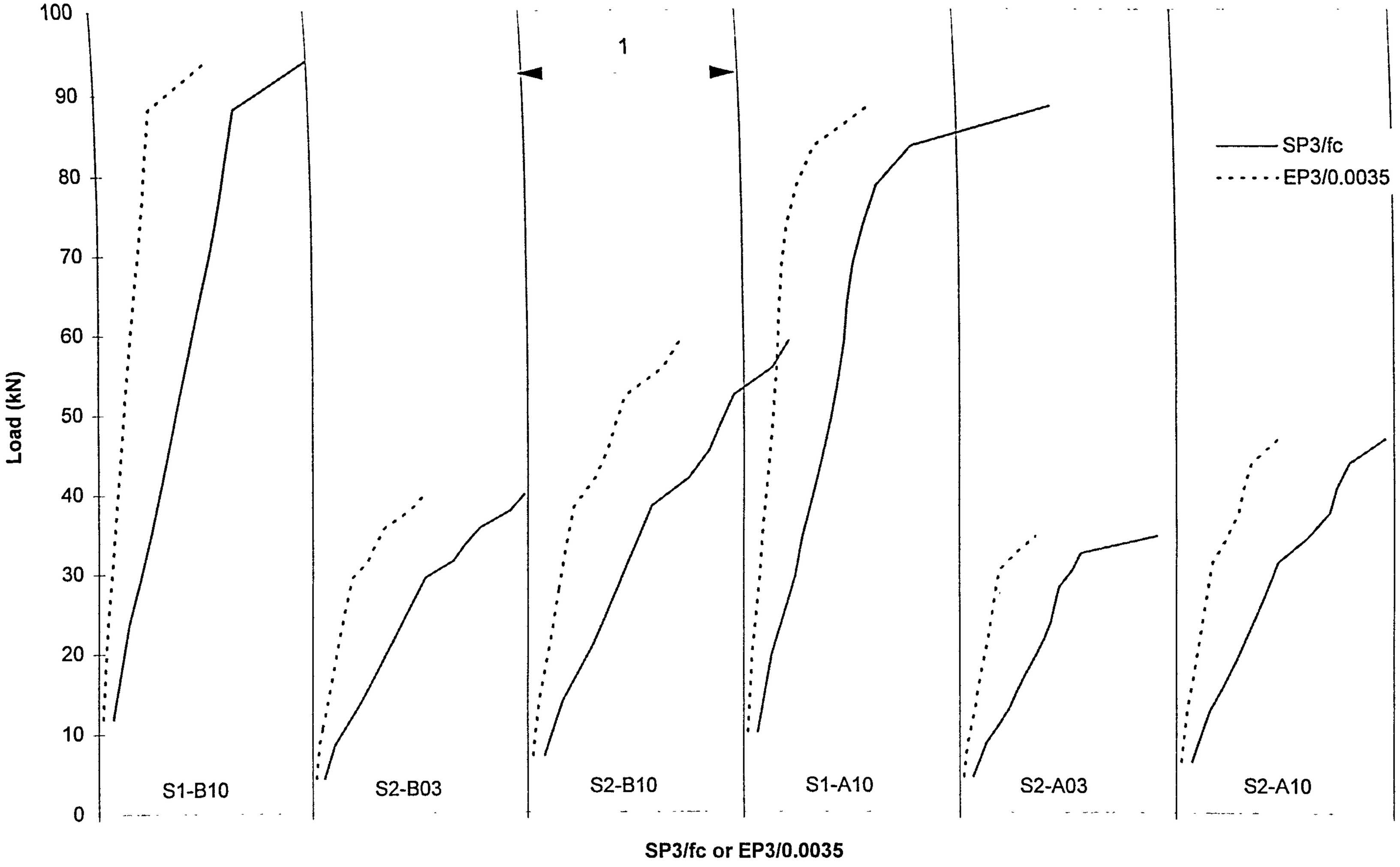

Predicted principal compressive stress and strain in concrete (slabs "S1-B10, S2-B03, S2-B10", "S1-A10", S2-A03 and S2-A10)

Yielding of tension steel, Slab-beam panels tested by Kuang

NB. : The numbers on the drawing indicate strain in steel at collapse expressed as a ratio of yield strain

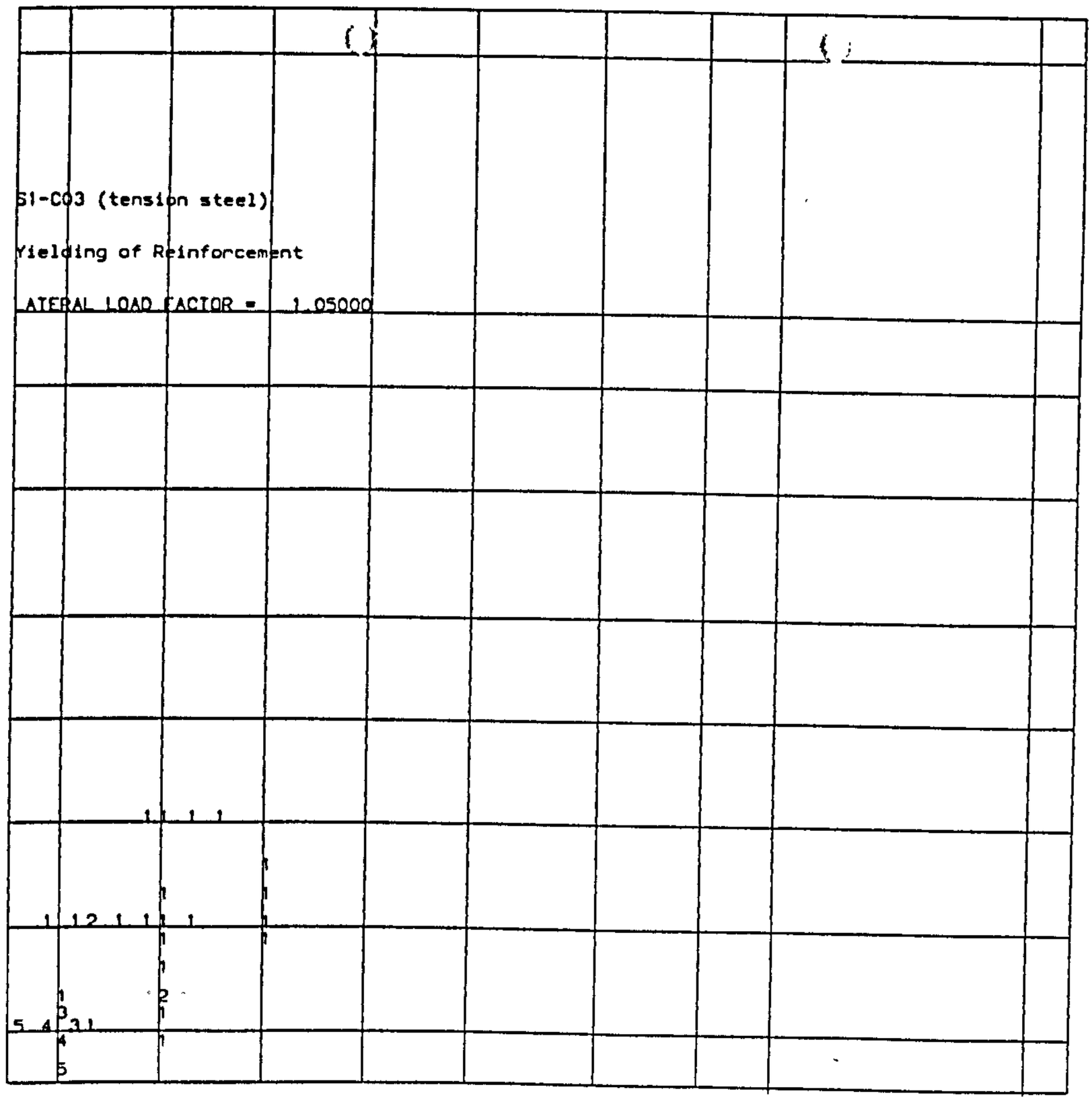

S1-C03

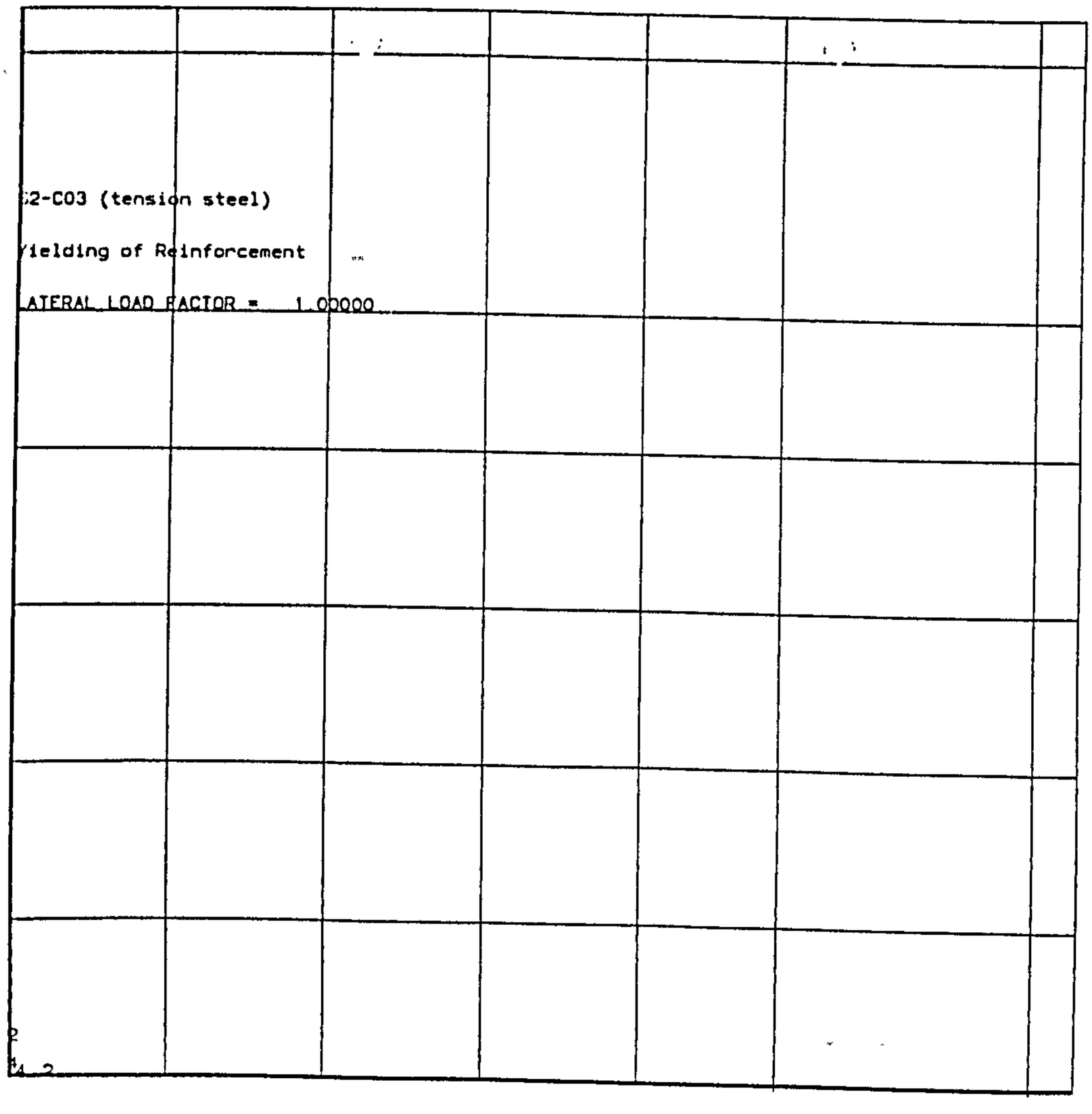

S2-C03

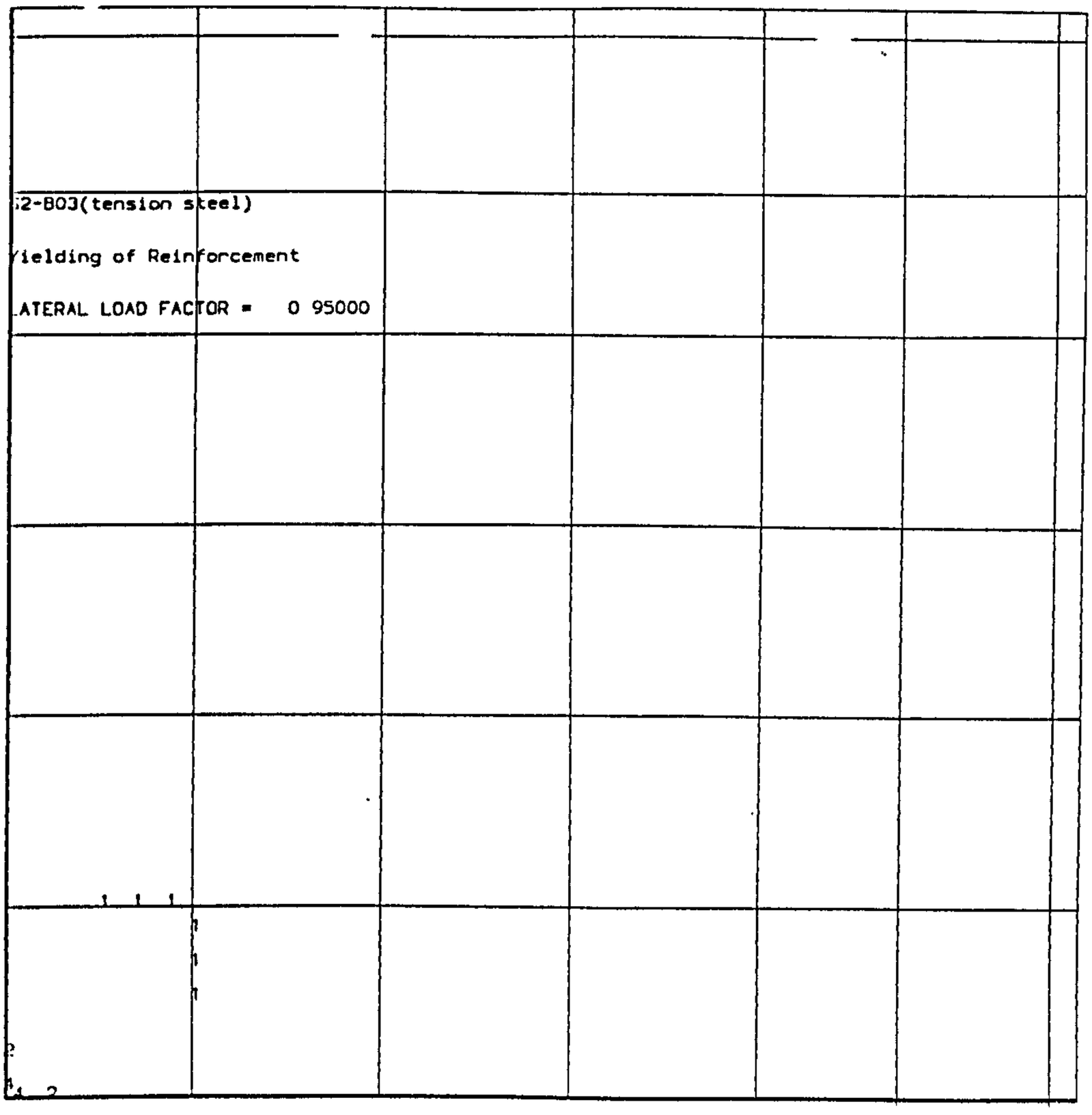
S2-B03(tension steel)
Yielding of Reinforcement
LATERAL LOAD FACTOR = 0 95000

S2-B03

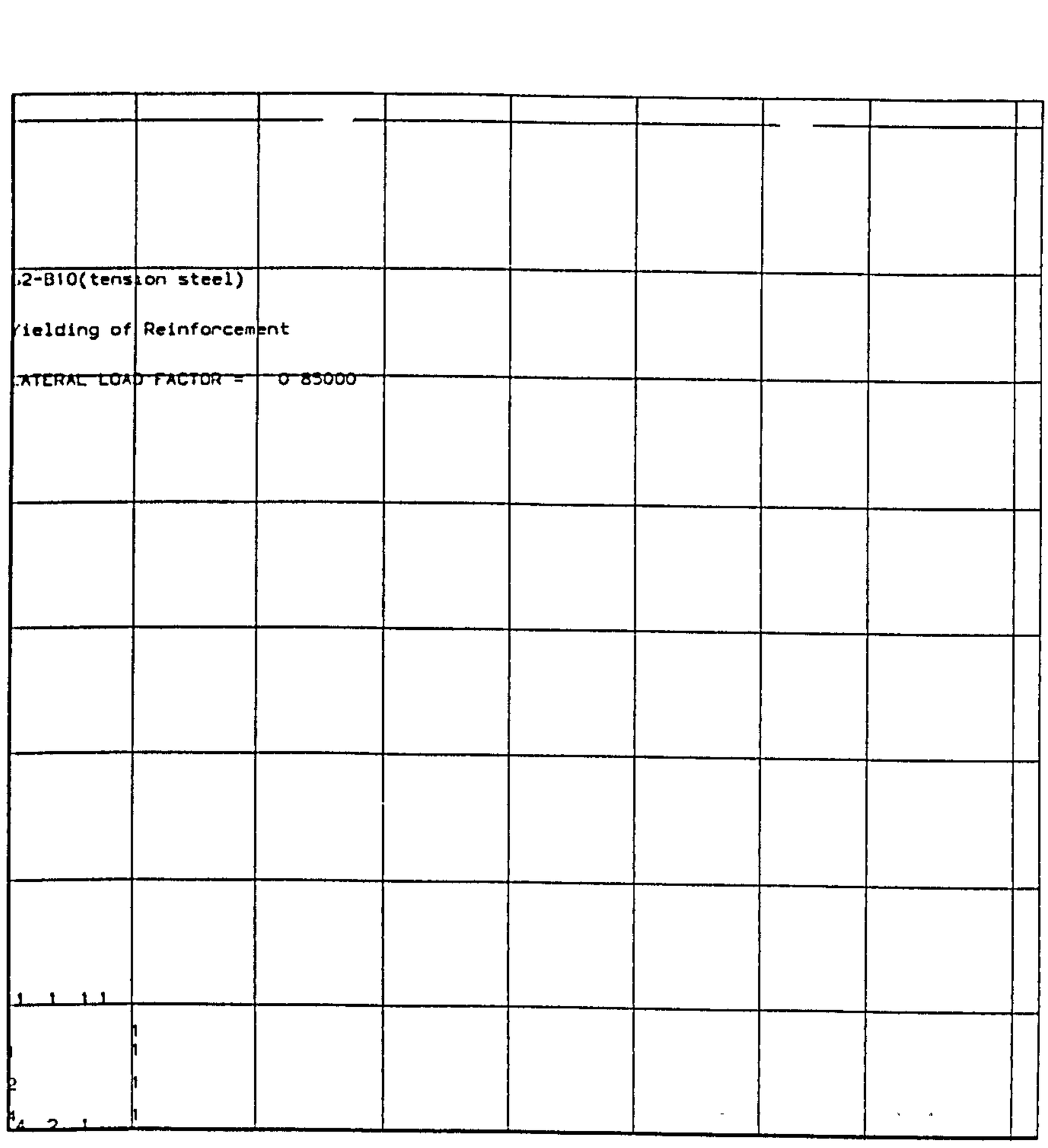
S2-B10(tension steel)
Yielding of Reinforcement
LATERAL LOAD FACTOR = 0 85000

S2-B10

S1-A10(tension steel)

Yielding of Reinforcement

LATERAL LOAD FACTOR = 0 95000

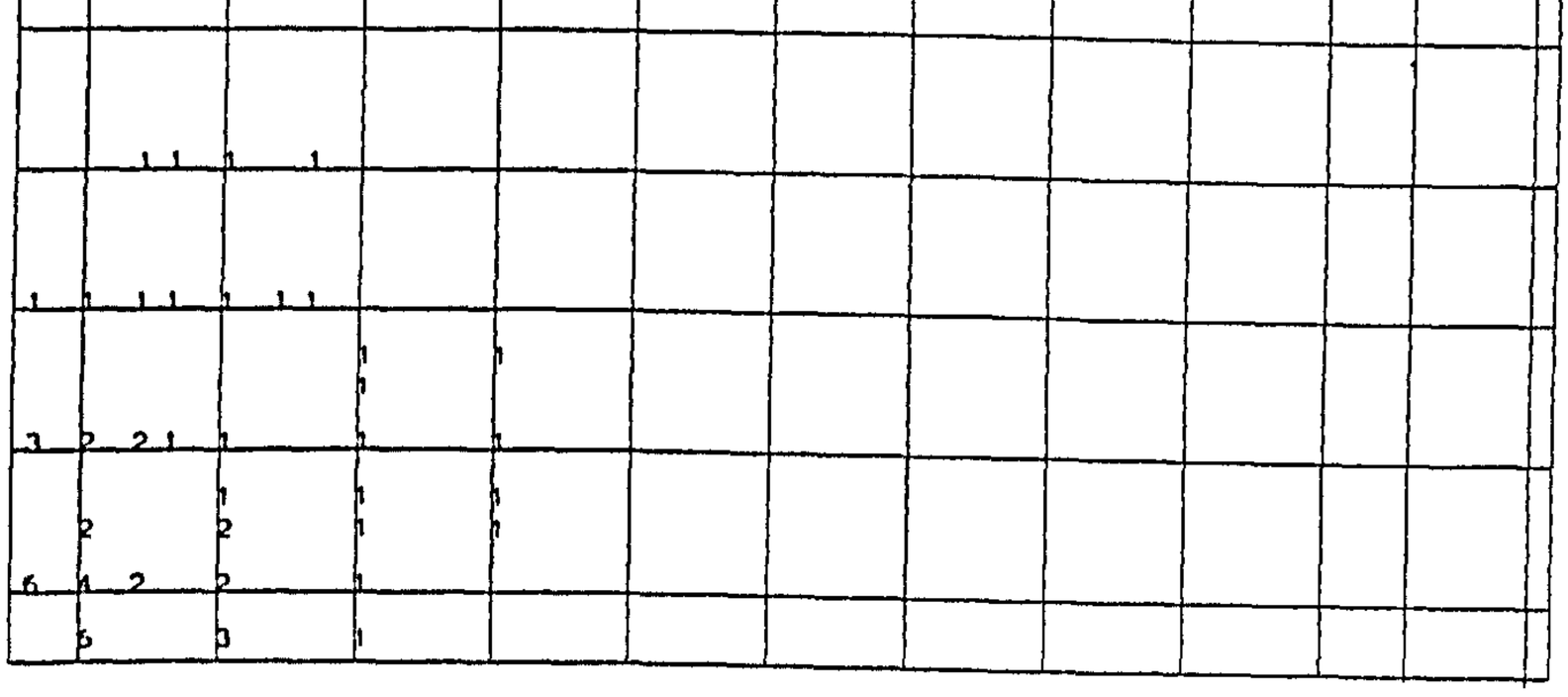

S1-A10

S2-A03(tension steel)

Yielding of Reinforcement

LATERAL LOAD FACTOR = 0 80000

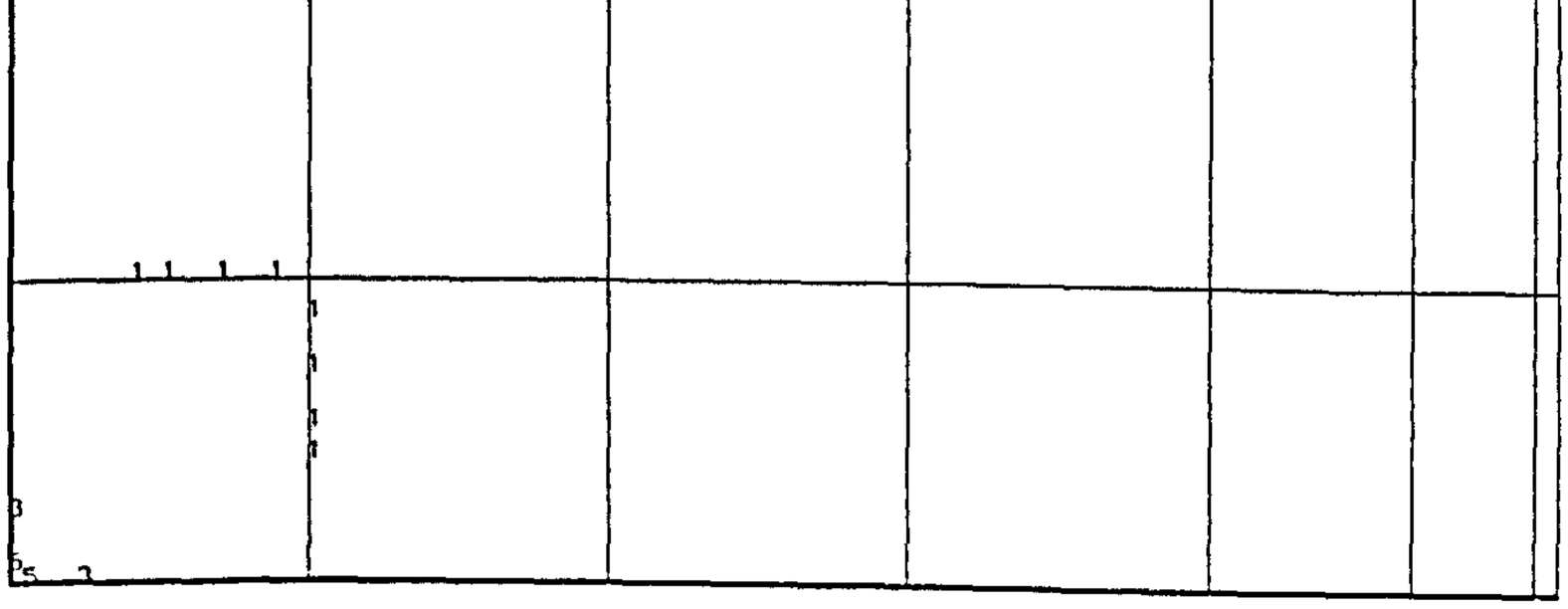

S2-A03

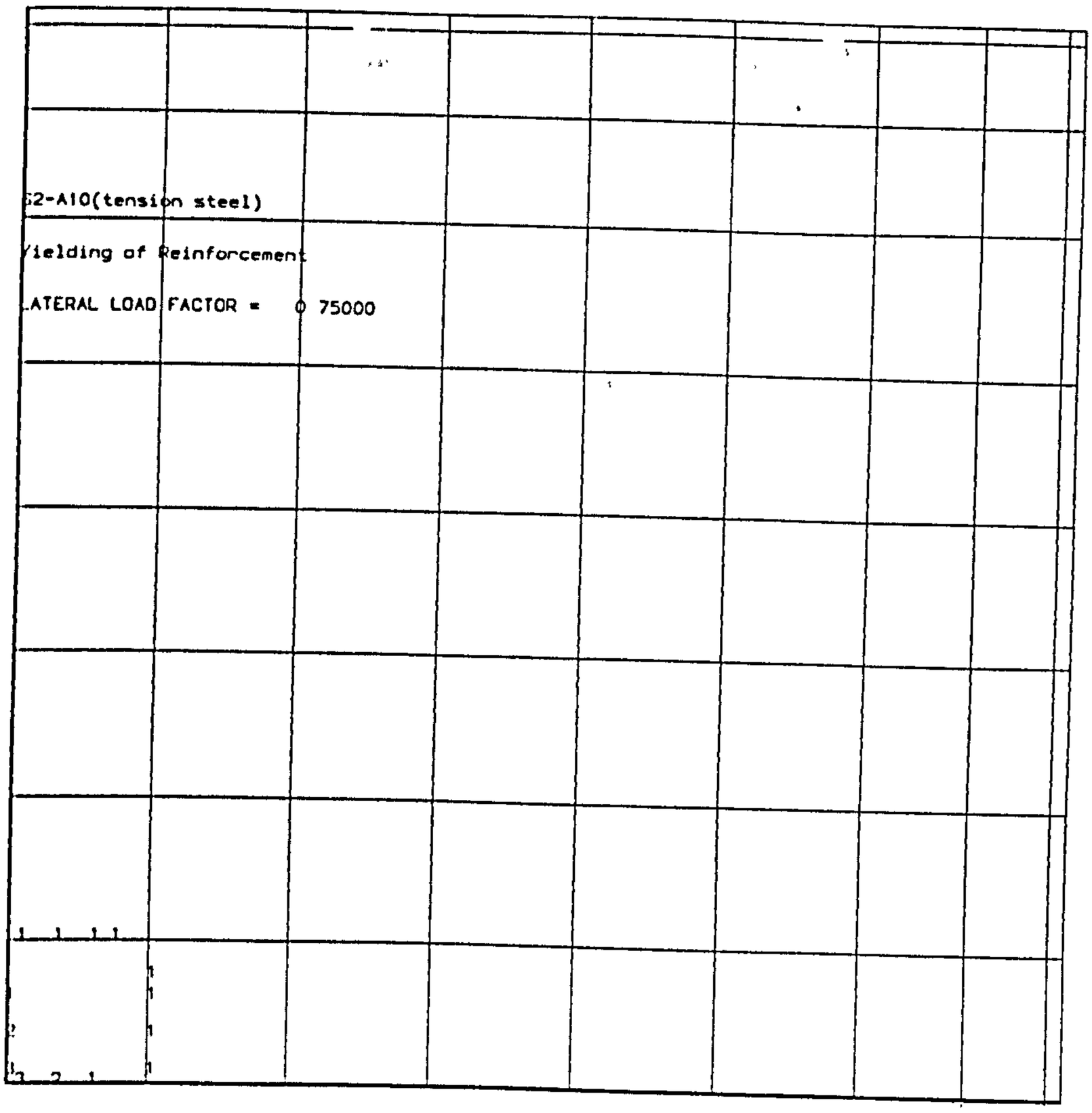

S2-A10

Note

Flexural steel in slabs **S1-C10, S1-C16, S2-C10, S2-C16** and **S1-B10** did not yield.

Predicted crack pattern for slab-beam panels (Kuang and Morley)

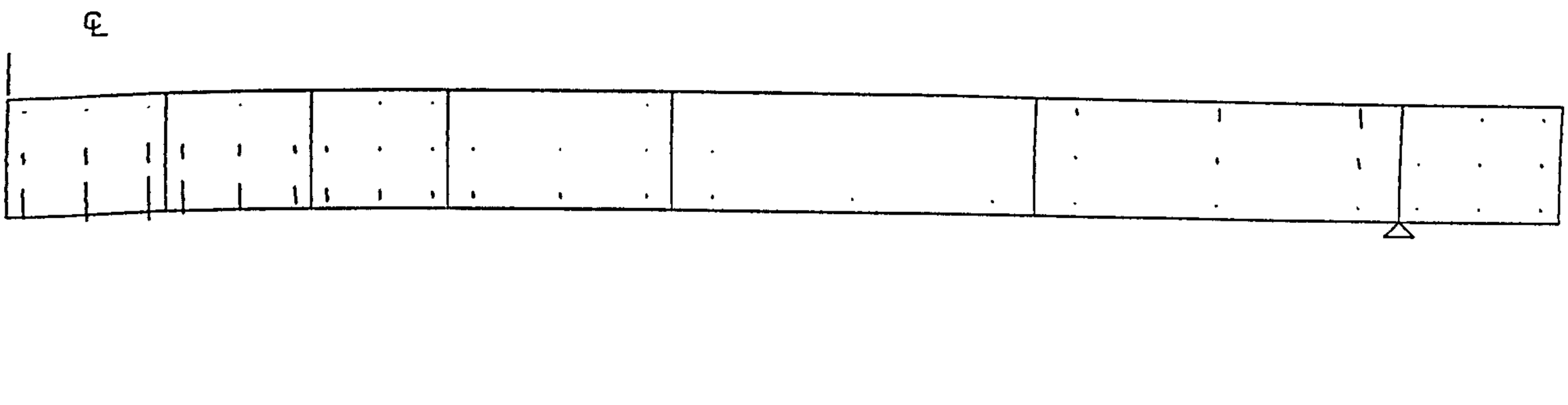

" S1-C03 "

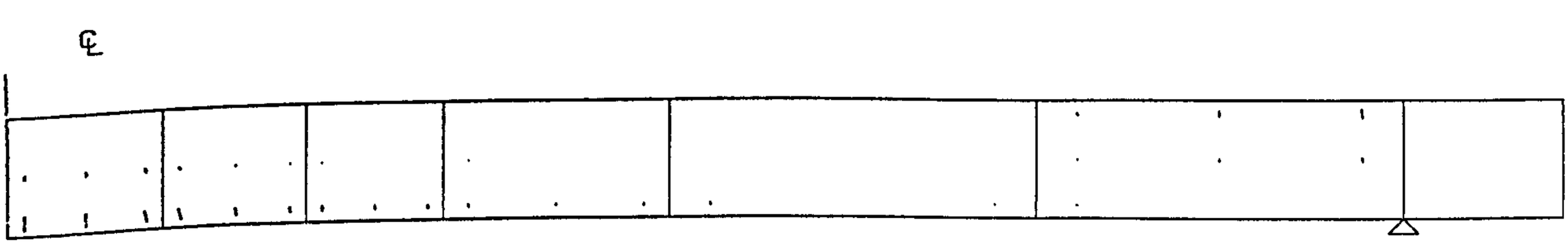

" S1-C10 "

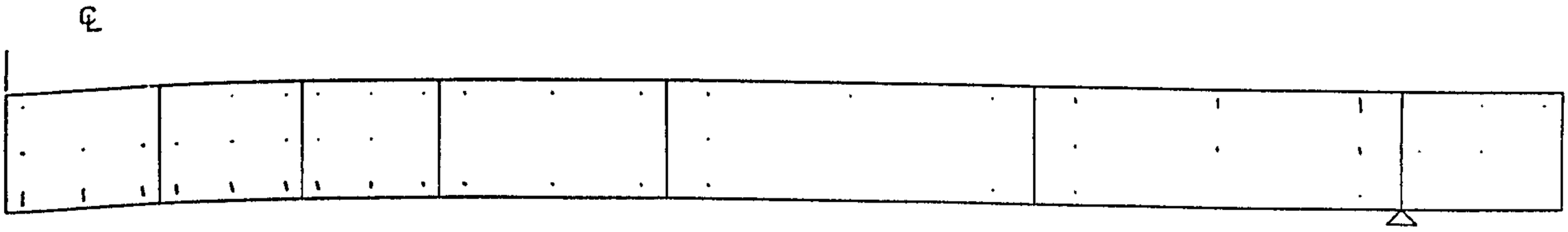

" S1-C16 "

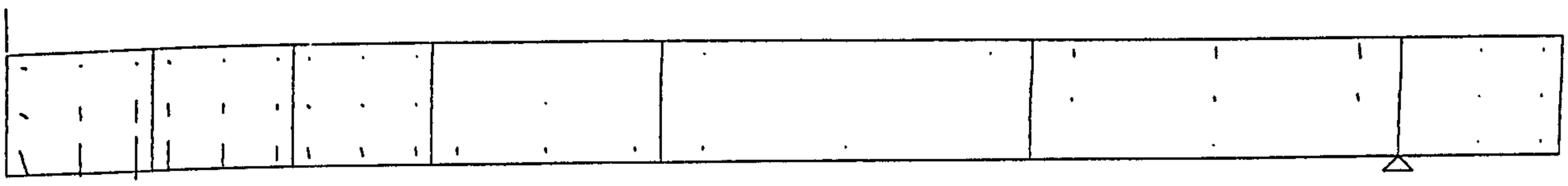

" S2-C03 "

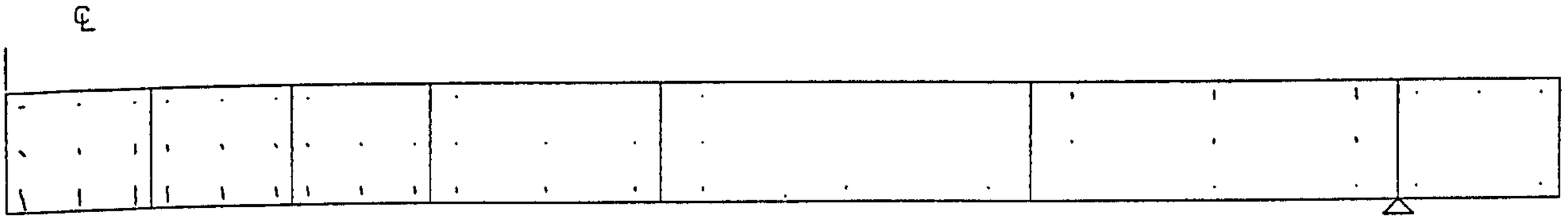

" S2-C10 "

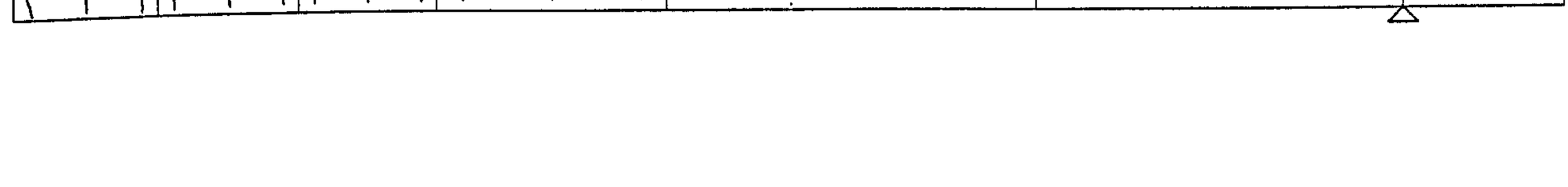

" S2-C16 "

℄

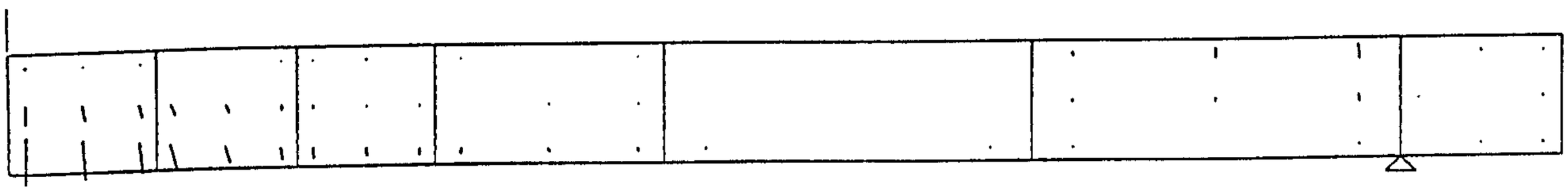

" S1-B10 "

℄

" S2-B03 "

℄

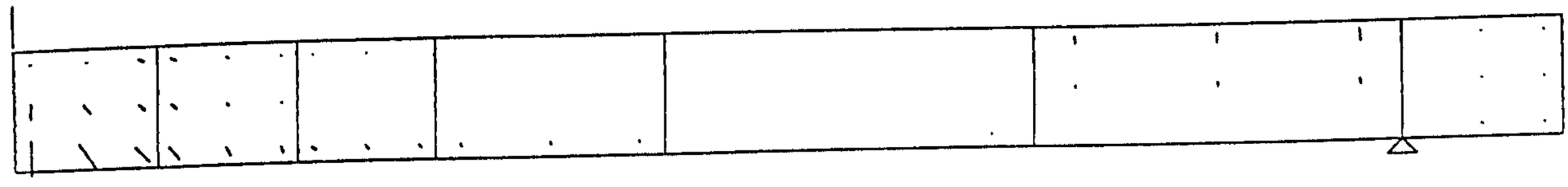

" S2-B10 "

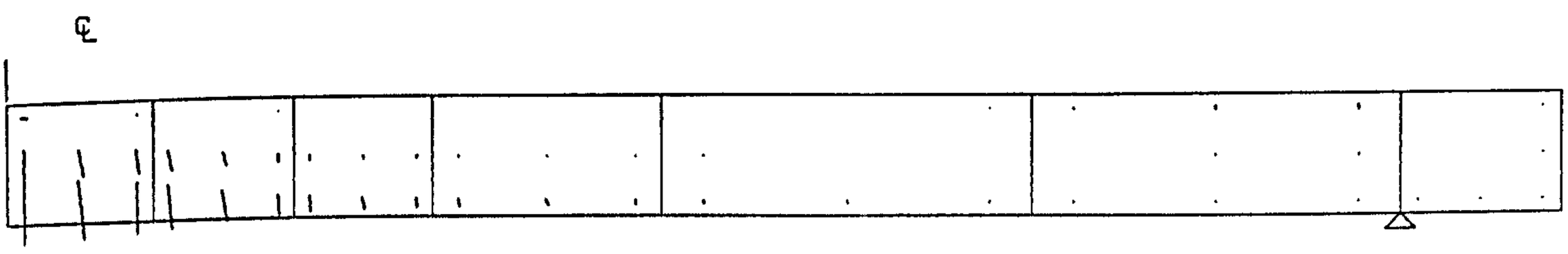

" S1-A10 "

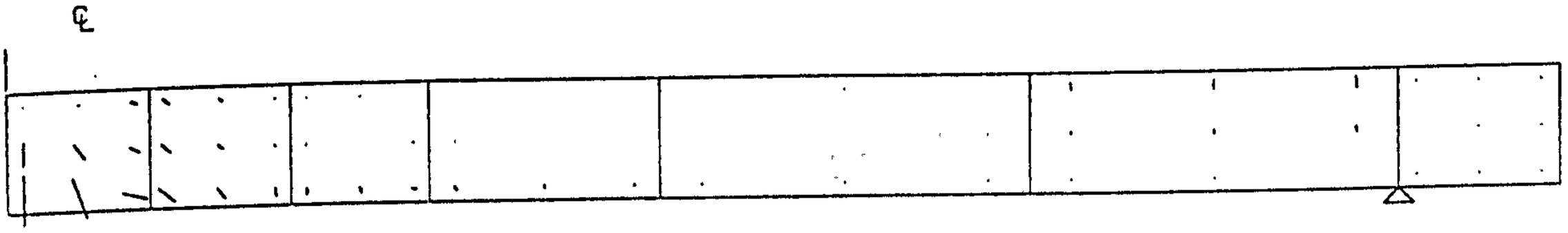

" S2-A03 "

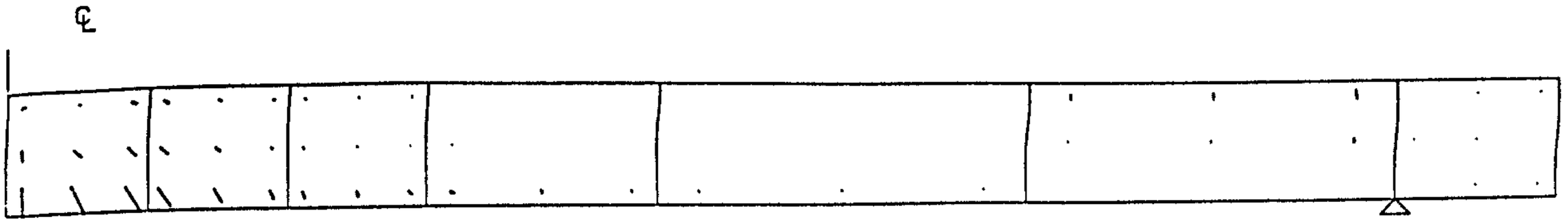

" S2-A10 "

Fully restrained slabs
(Taylor and Hayes)

C3.3 Fully restrained slabs (Taylorand Hayes)

Series	Slab Marking	Experimental results		Numerical predictions		P_{num}/P_{test}
		P_{test} (kN)	Failure Mode	P_{num} (kN)	Failure Mode	
2	2S2	71.1	s	64.8	fp	0.911*
	2R2	82.2	s	102.0	s	1.240
	2S3	91.2	s	68.4	fp	0.750*
	2R3	112.8	s	141.0	s	1.250
	2S4	85.8	s	69.1	fp	0.805*
	2R4	136.8	s	157.3	s	1.150
	2S5	96.6	s	81.6	y	0.845*
	2R5	142.2	s	155.8	s	1.095
	2S6	96.6	s	67.2	fp	0.696*
	2R6	154.5	s	184.3	s	1.193
3	3S2	78.5	s	79.2	s	1.009*
	3R2	78.5	s	110.9	s	1.413
	3S4	115.2	s	103.7	s	0.900*
	3R4	132.4	s	184.8	s	1.400
	3S6	150.1	s	111.6	fp	0.744*
	3R6	169.2	s	210.0	s	1.241
* Simply supported					Average	1.040
					STDEV	0.238

N.B. : No detail of mode of failure is given in the paper, it only mentioned that most slabs failed by punching, and extensive yielding of flexural reinforcement occurred in some slabs.

Note For simply supported slabs Average=83.3%, STDEV=10.4%

For restrained slabs Average=124.8%, STDEV=11.1%

Predicted strain in flexural steel for all restrained slabs below yield value.
i.e. flexural steel in slabs 2R2-2R6, 3R2-3R6 did not yield.

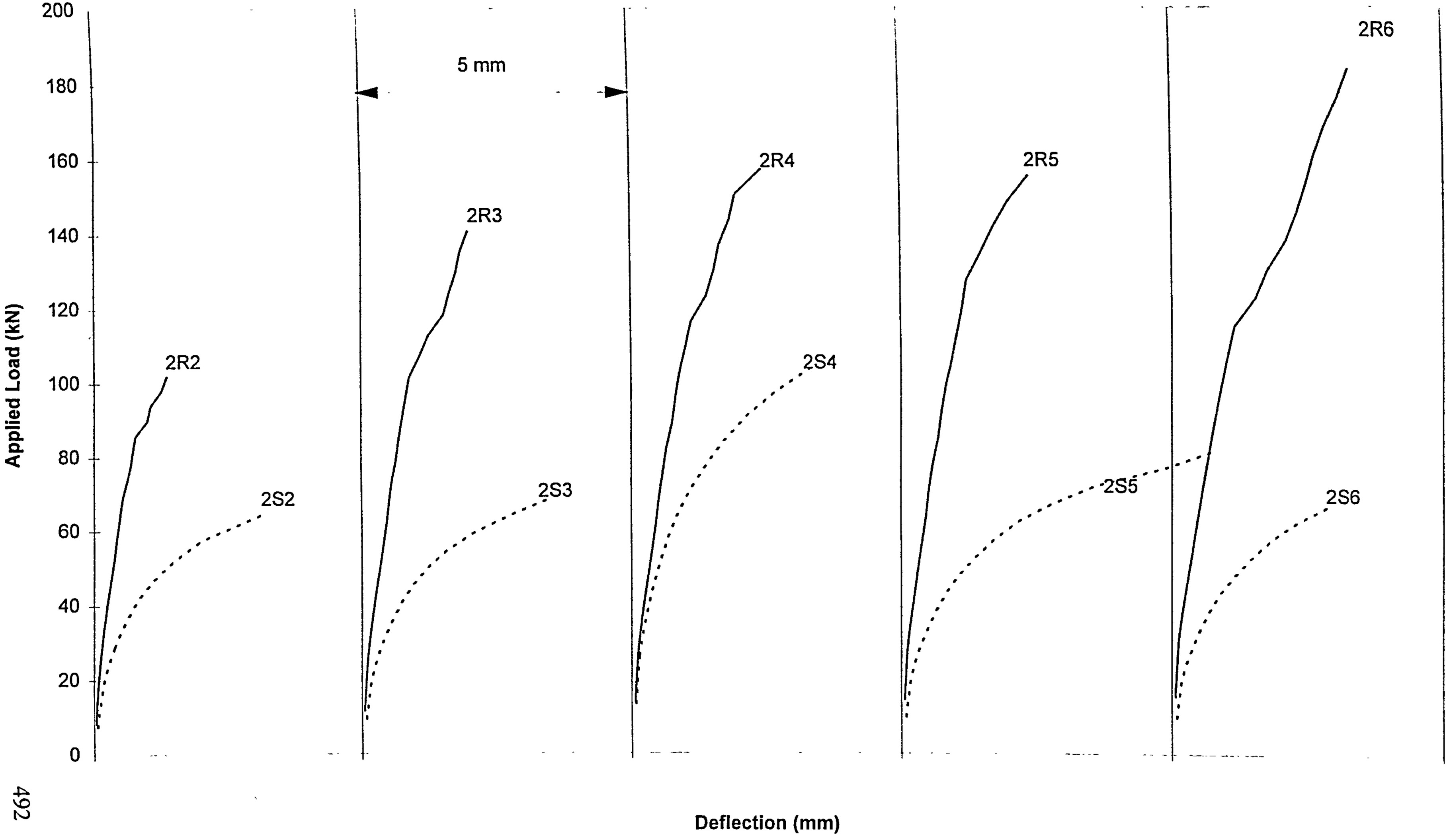

Predicted load-deflection response for slabs 2S2-2S6 and 2R2-2R6

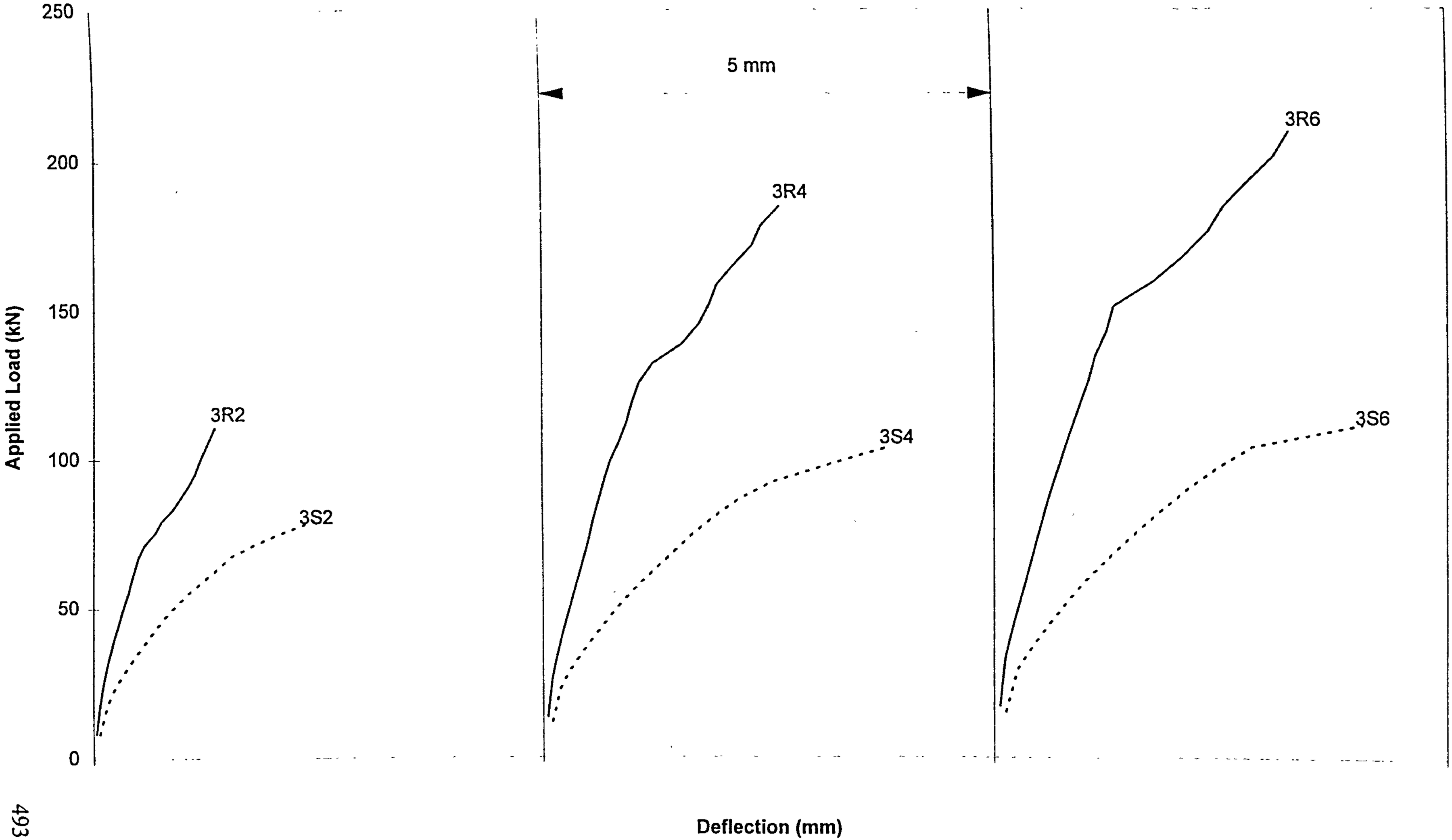

Predicted load-deflection response for slabs 3S2-3S6 and 3R2-3R6

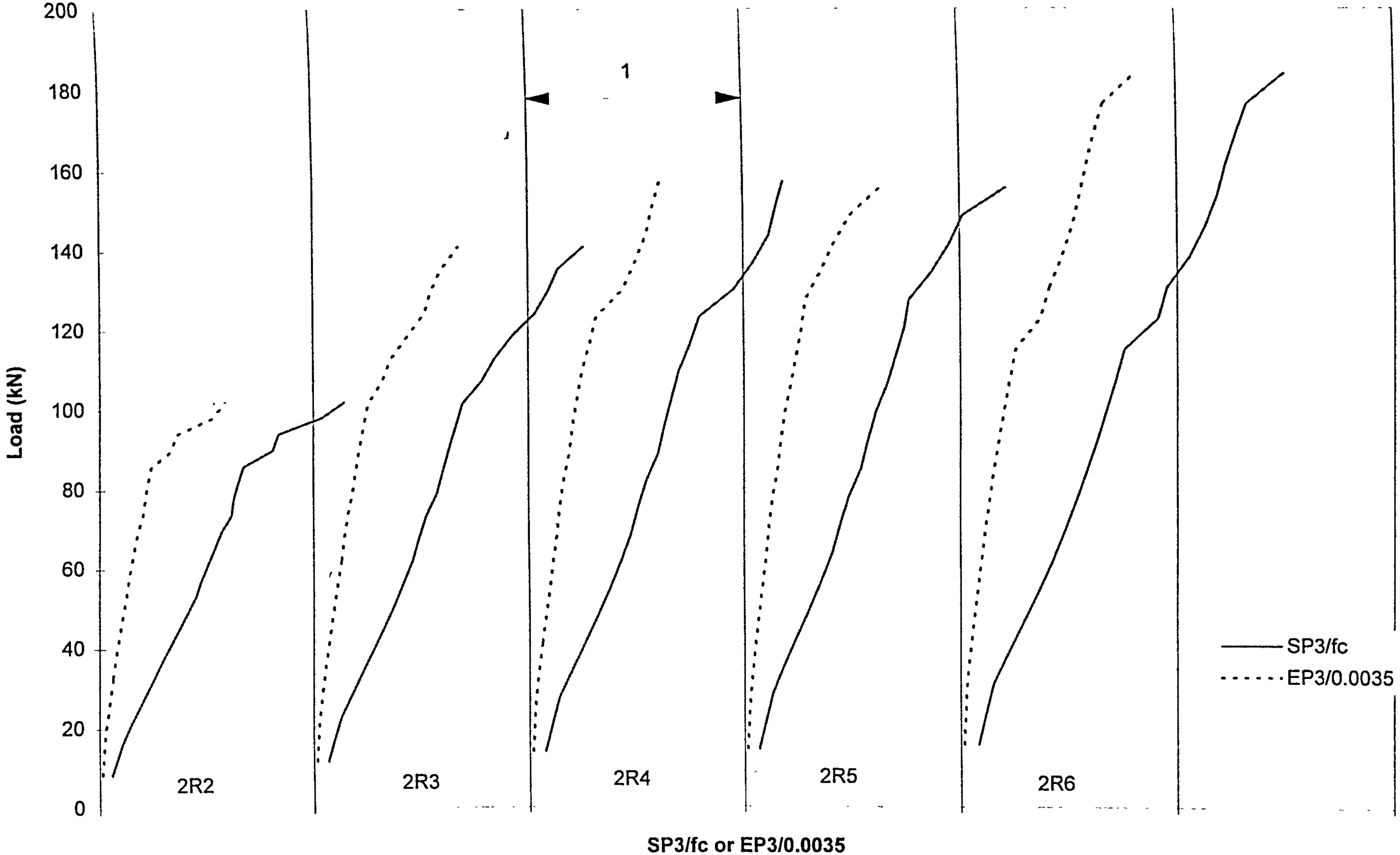

Predicted principal compressive stress and strain in concrete (slabs "2R2" - "2R6")

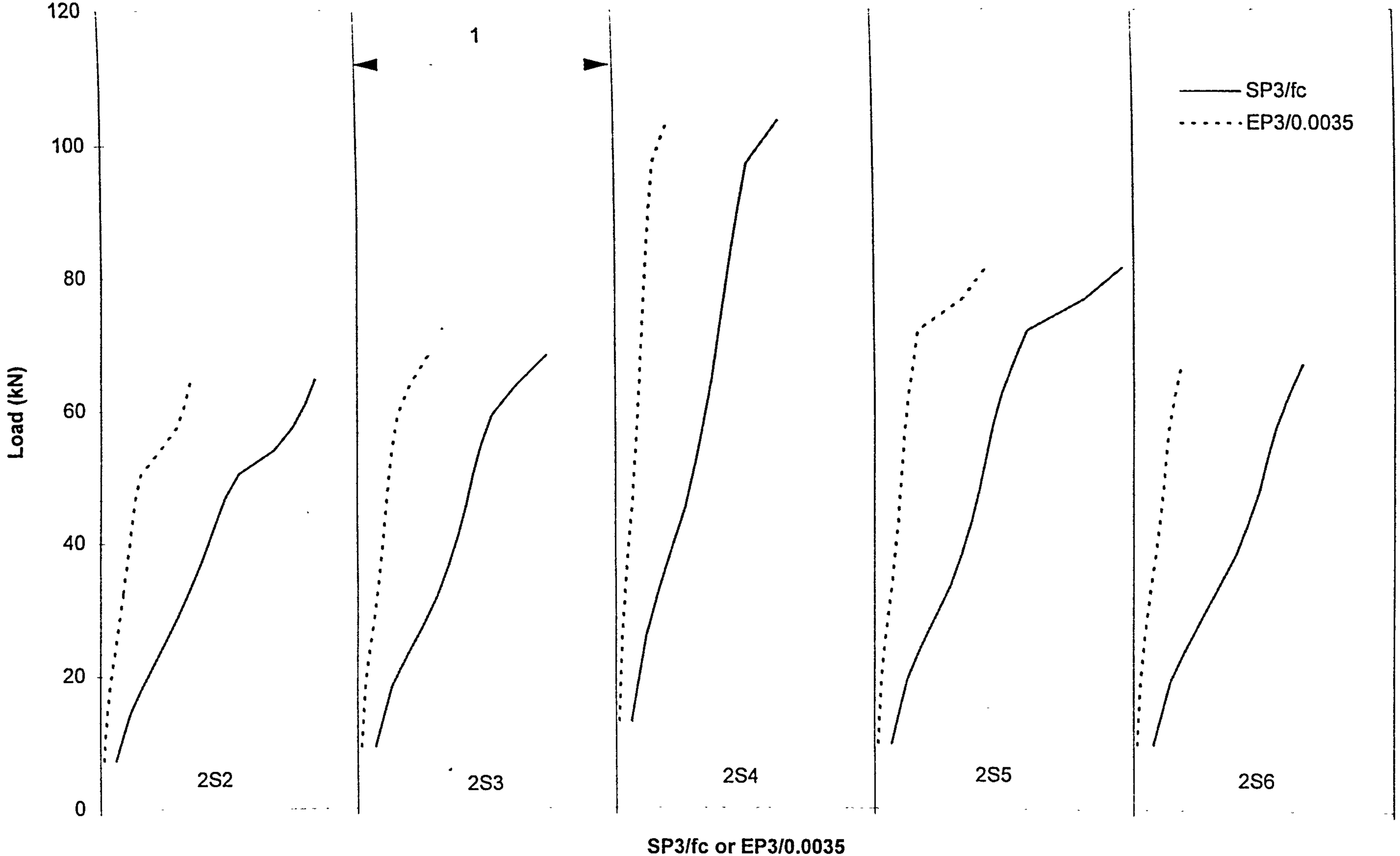

Predicted principal compressive stress and strain in concrete (slabs "2S2" - "2S6")

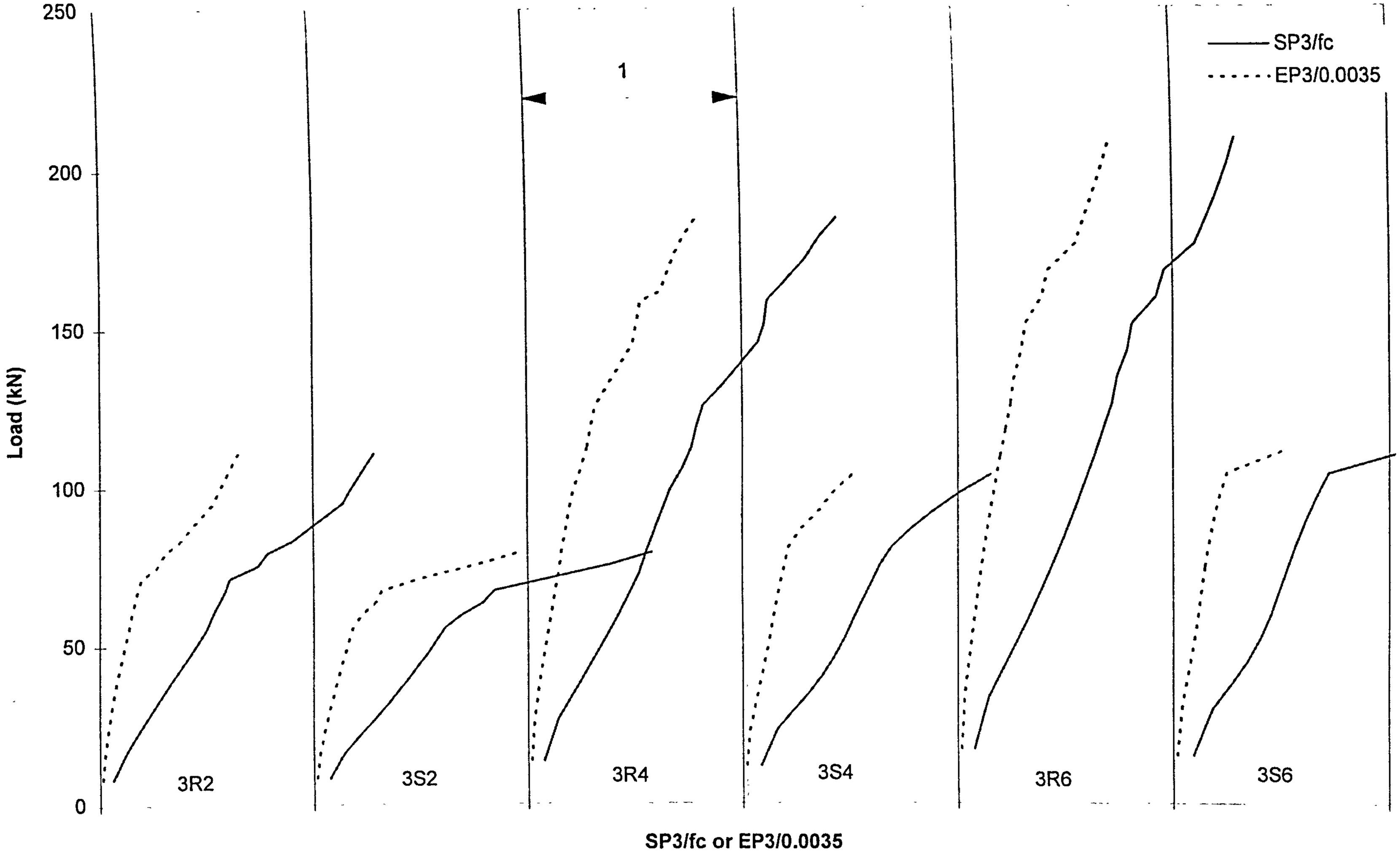

Predicted principal compressive stress and strain in concrete (slabs 3R2 - 3R6 and 3S2-3S6)

Yielding of tension steel, Restrained slab tested by Taylor and Hayes

NB. : The numbers on the drawing indicate strain in steel at collapse expressed as a ratio of yield strain

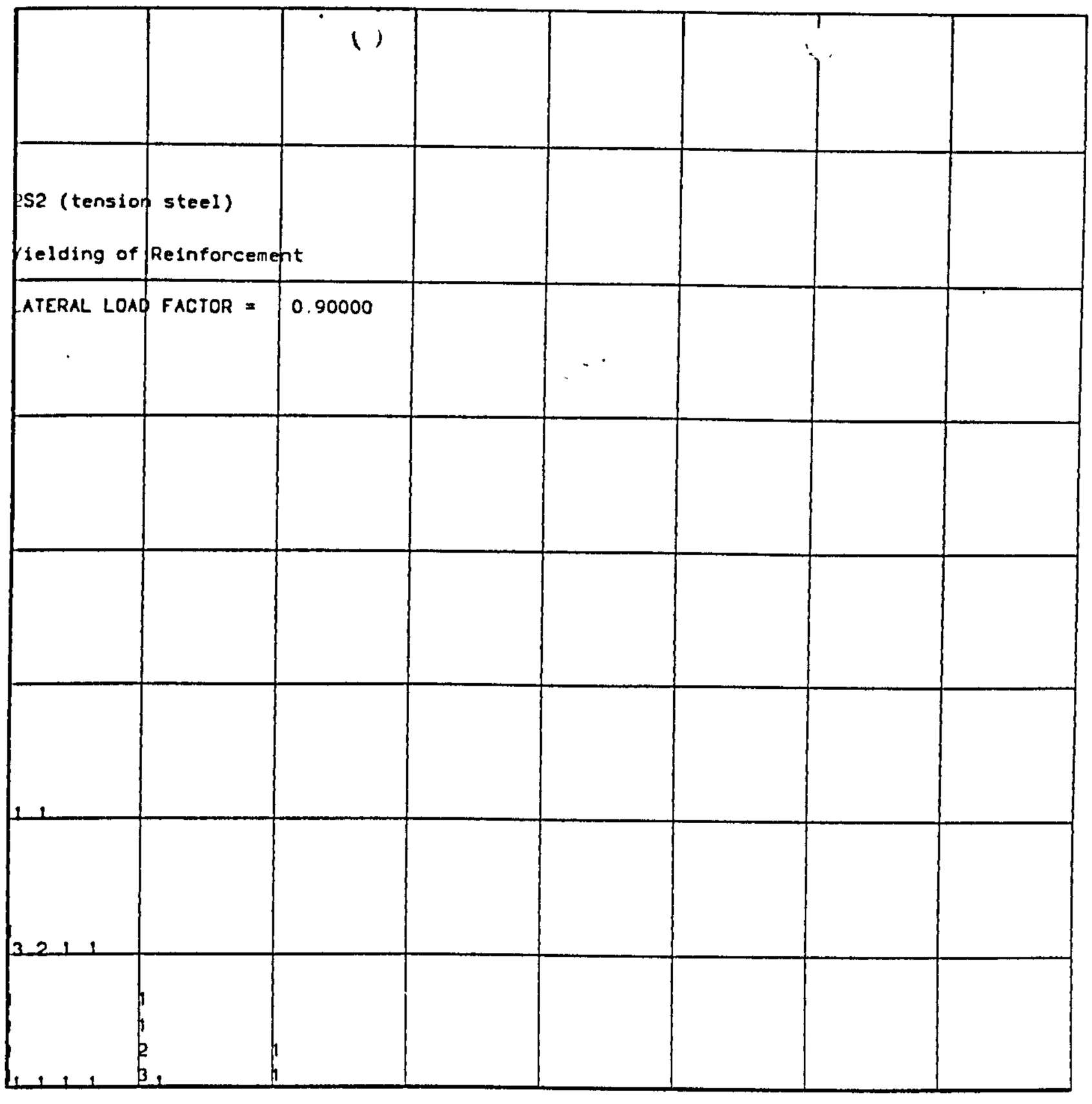

2S2

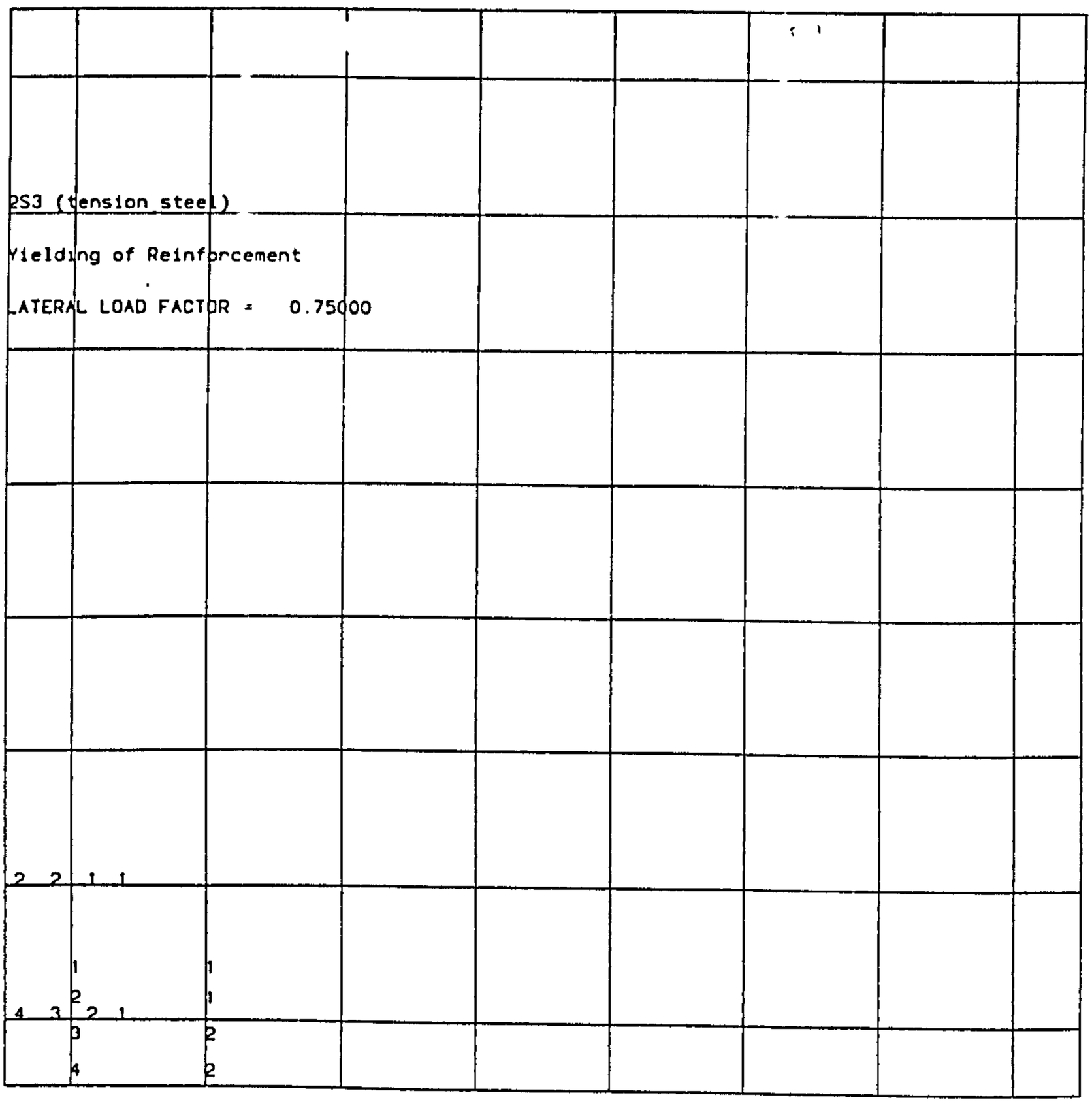

2S3

2S4 (tension steel)

Yielding of Reinforcement

LATERAL LOAD FACTOR = 0.80000

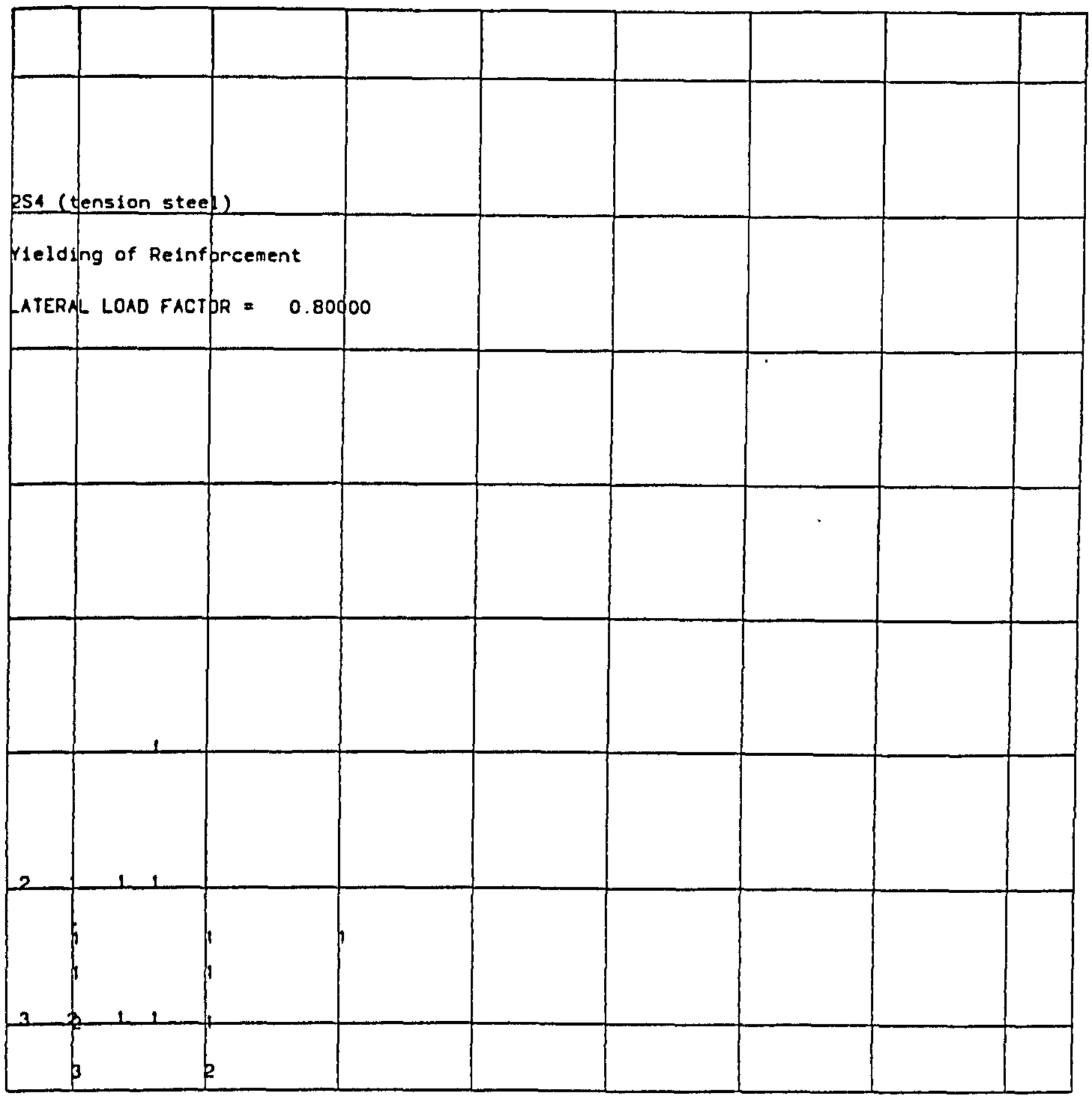

2S4

2S5 (tension steel)

Yielding of Reinforcement

LATERAL LOAD FACTOR = 0 85000

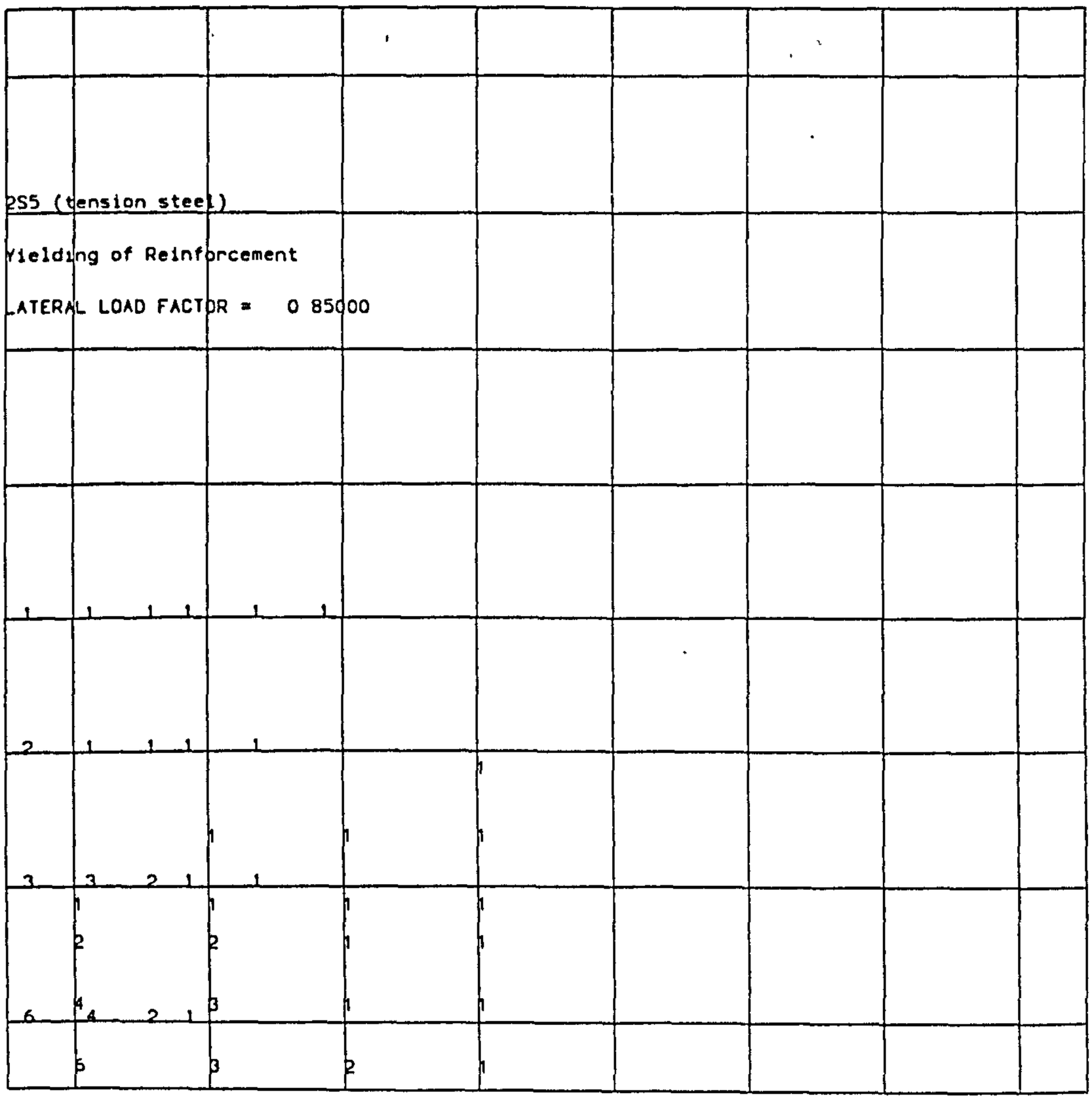

2S5

2S6 (tension steel)

Yielding of Reinforcement

LATERAL LOAD FACTOR = 0.70000

2S6

3S2 (tension steel)

Yielding of Reinforcement

LATERAL LOAD FACTOR = 1.00000

3S2

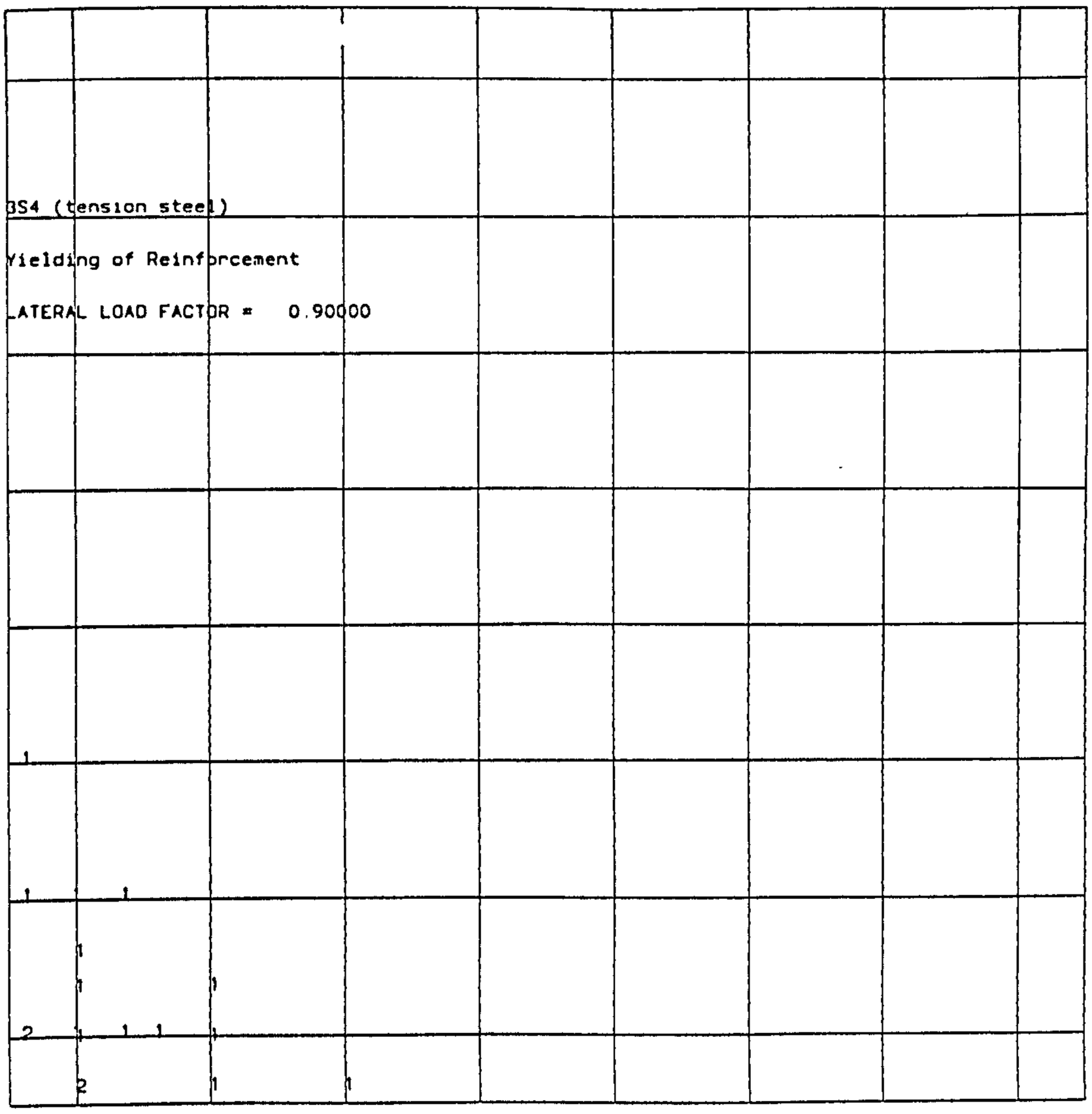
3S4 (tension steel)
Yielding of Reinforcement
LATERAL LOAD FACTOR = 0.90000

3S4

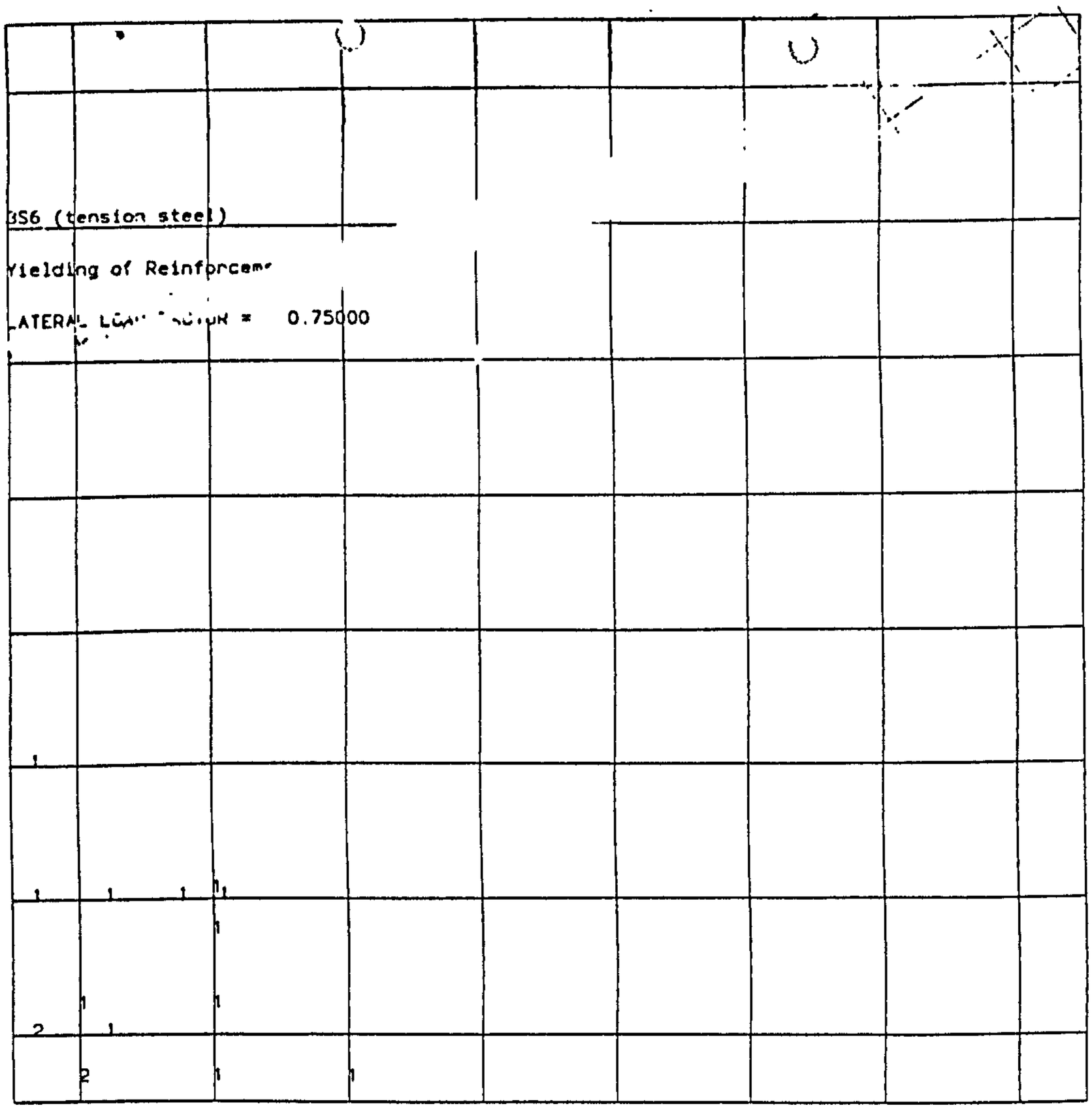
3S6 (tension steel)
Yielding of Reinforcem
LATERAL LOAD FACTOR = 0.75000

3S6

500

Predicted crack pattern for restrained slabs (Taylor and Hayes)

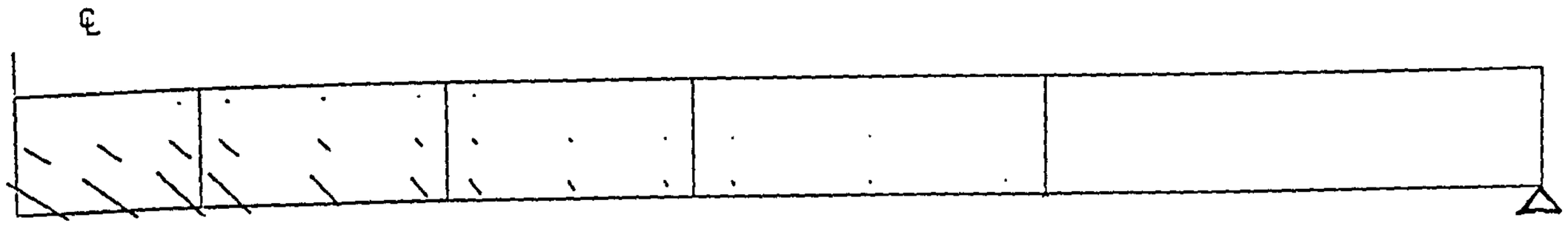

" 2S2 "

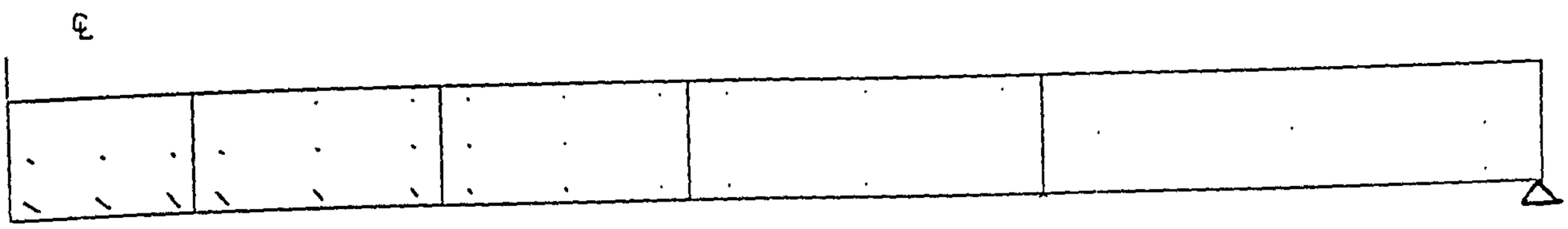

" 2R2 "

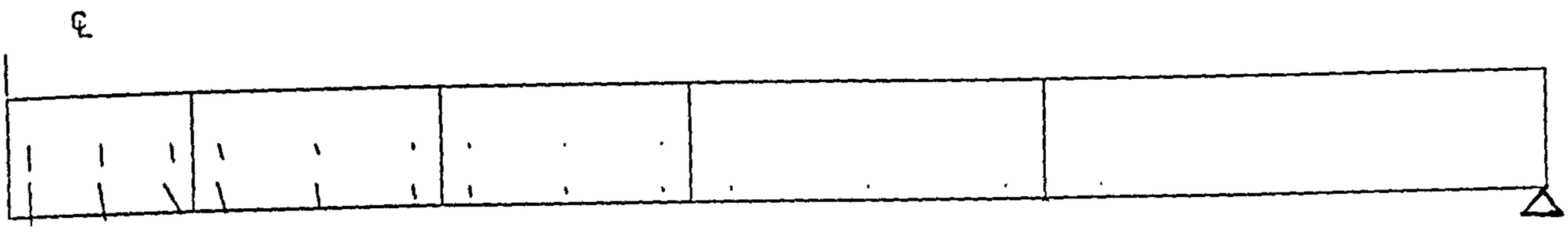

" 2S3 "

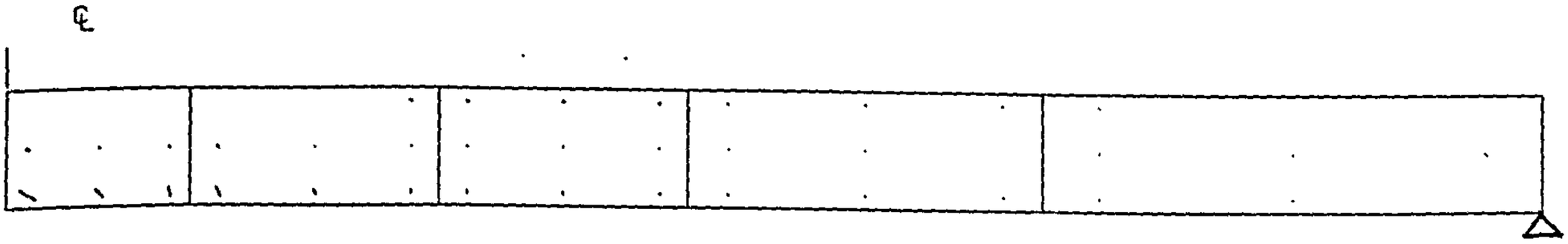

" 2R3 "

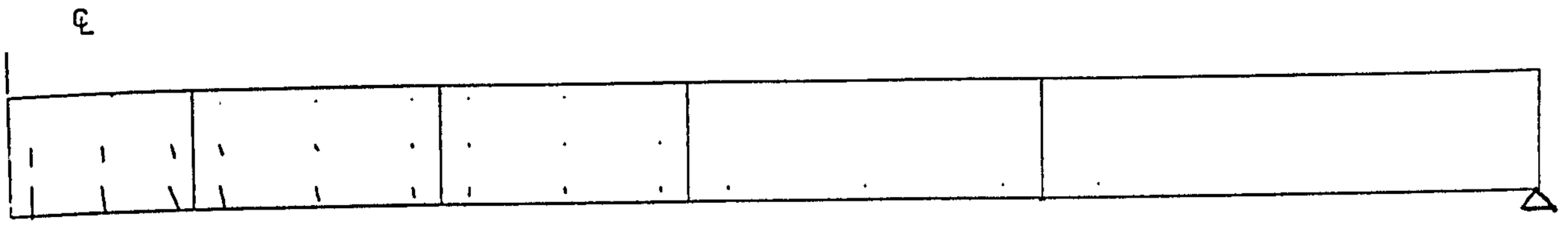

" 2S4 "

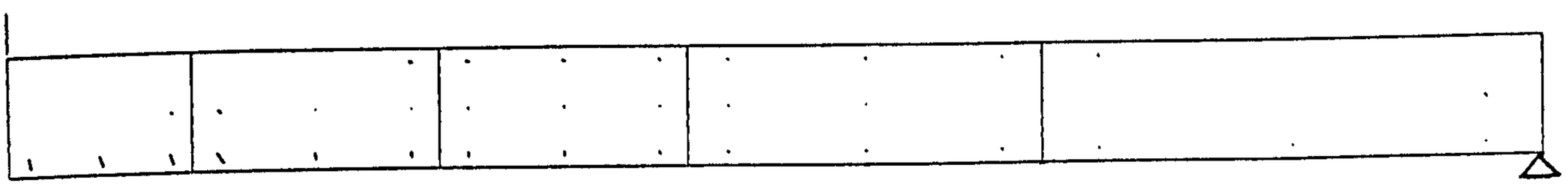

" 2R4 "

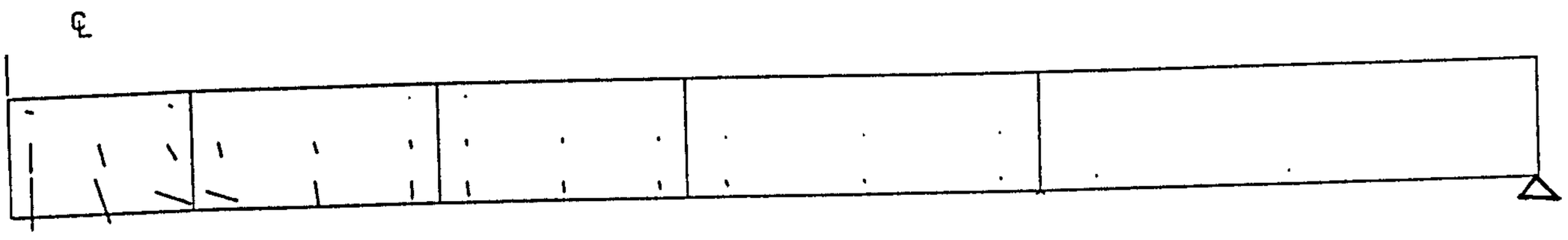

" 2S5 "

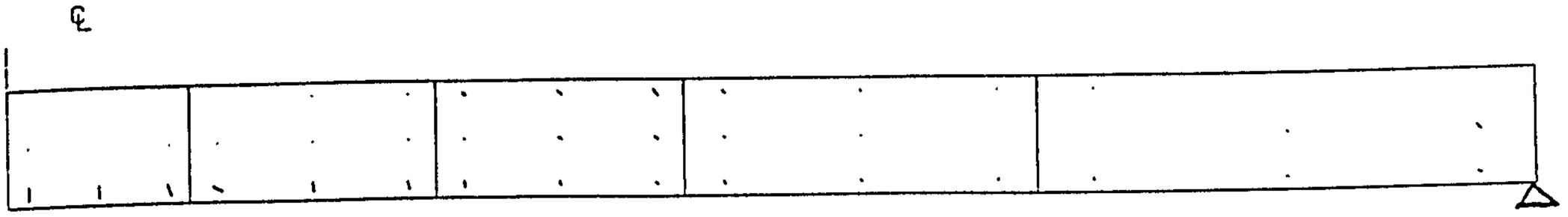

" 2R5 "

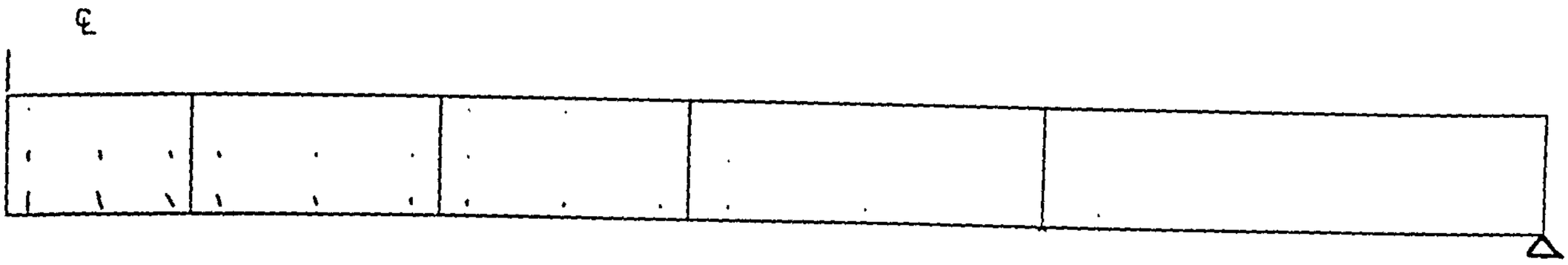

" 2S6 "

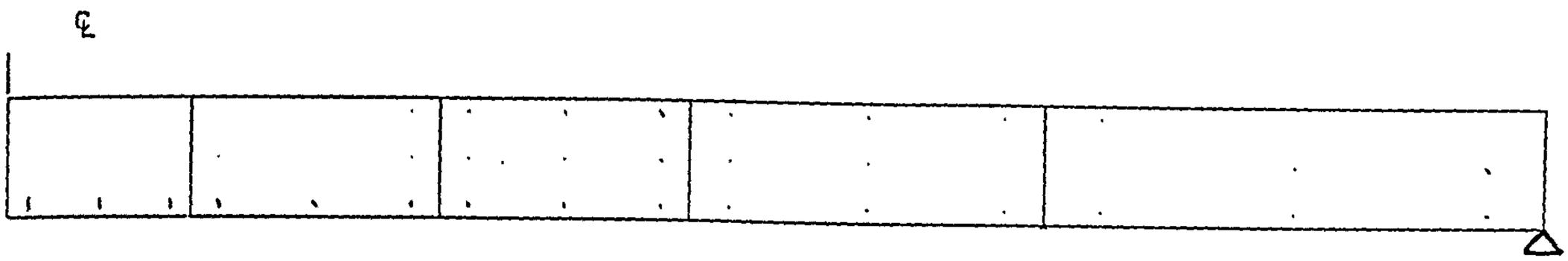

" 2R6 "

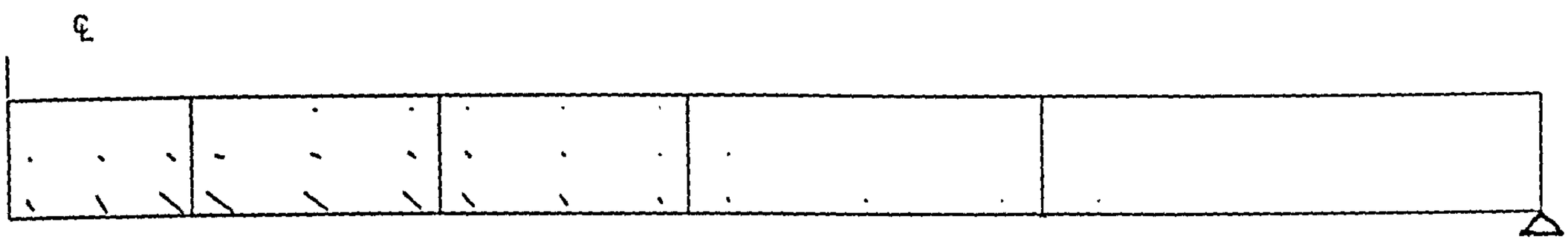

" 3S2 "

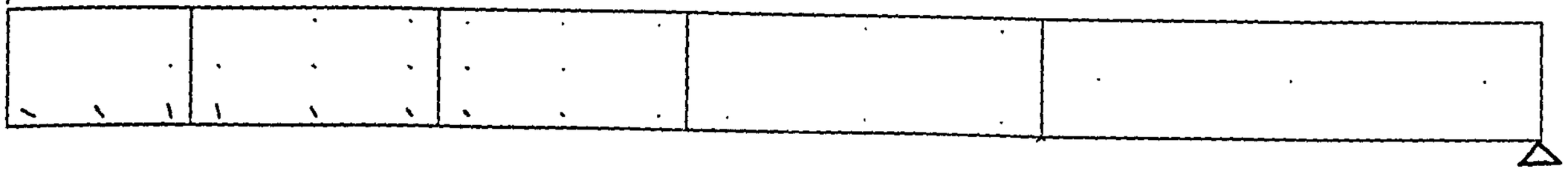

" 3R2 "

„ 3R6 "

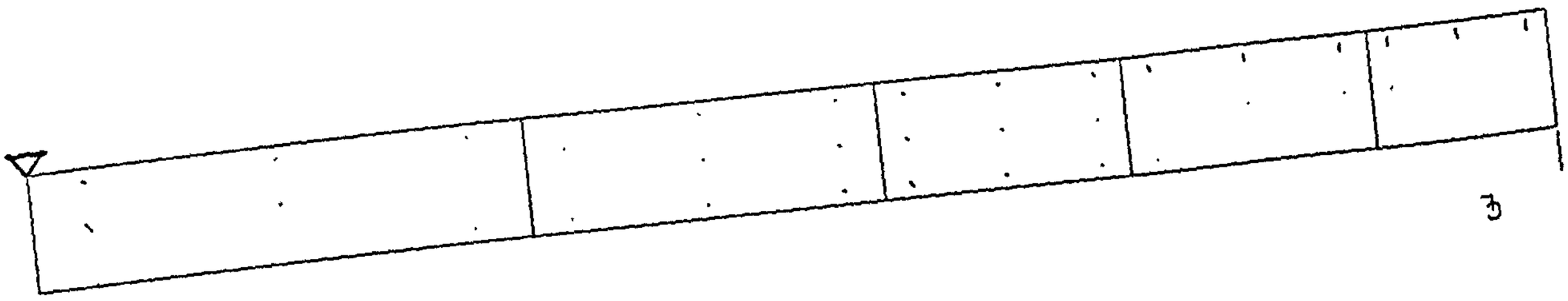

„ 3S6 "

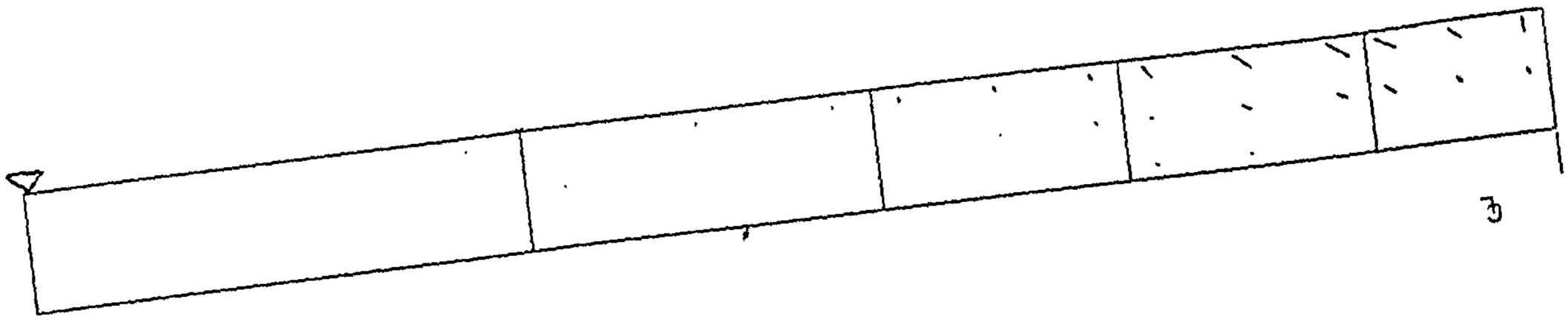

„ 3R4 "

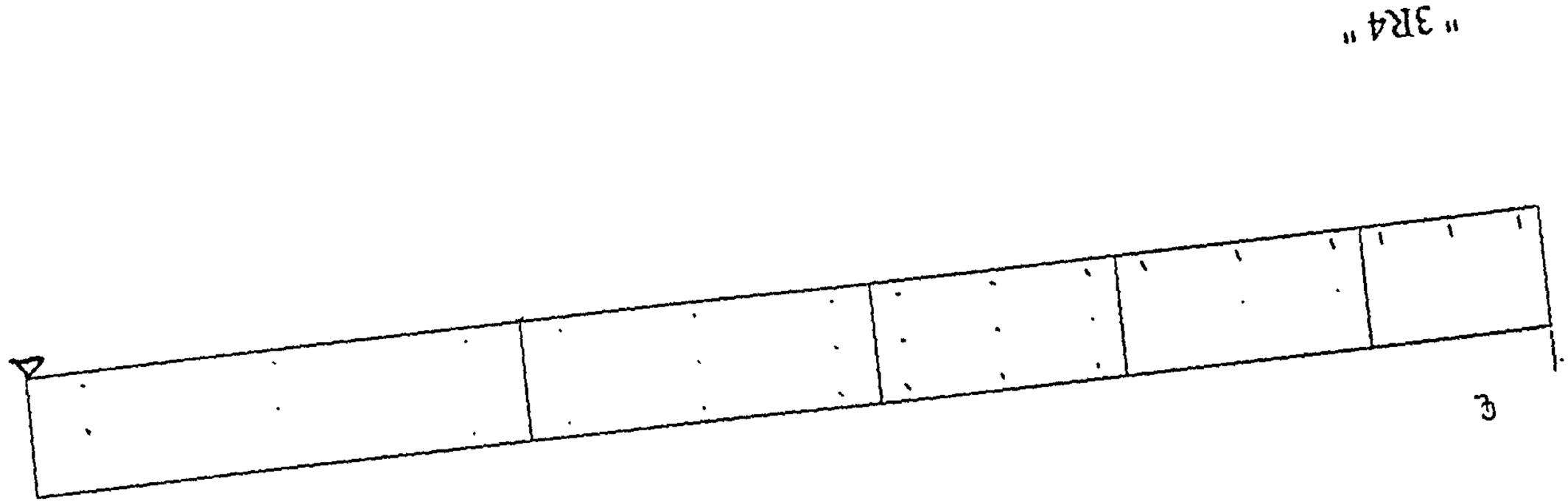

„ 3S4 "